INDC SPECiAL 3

SECOND IAEA SYMPOSIUM ON PHYSICS AND CHEMISTRY OF FISSION

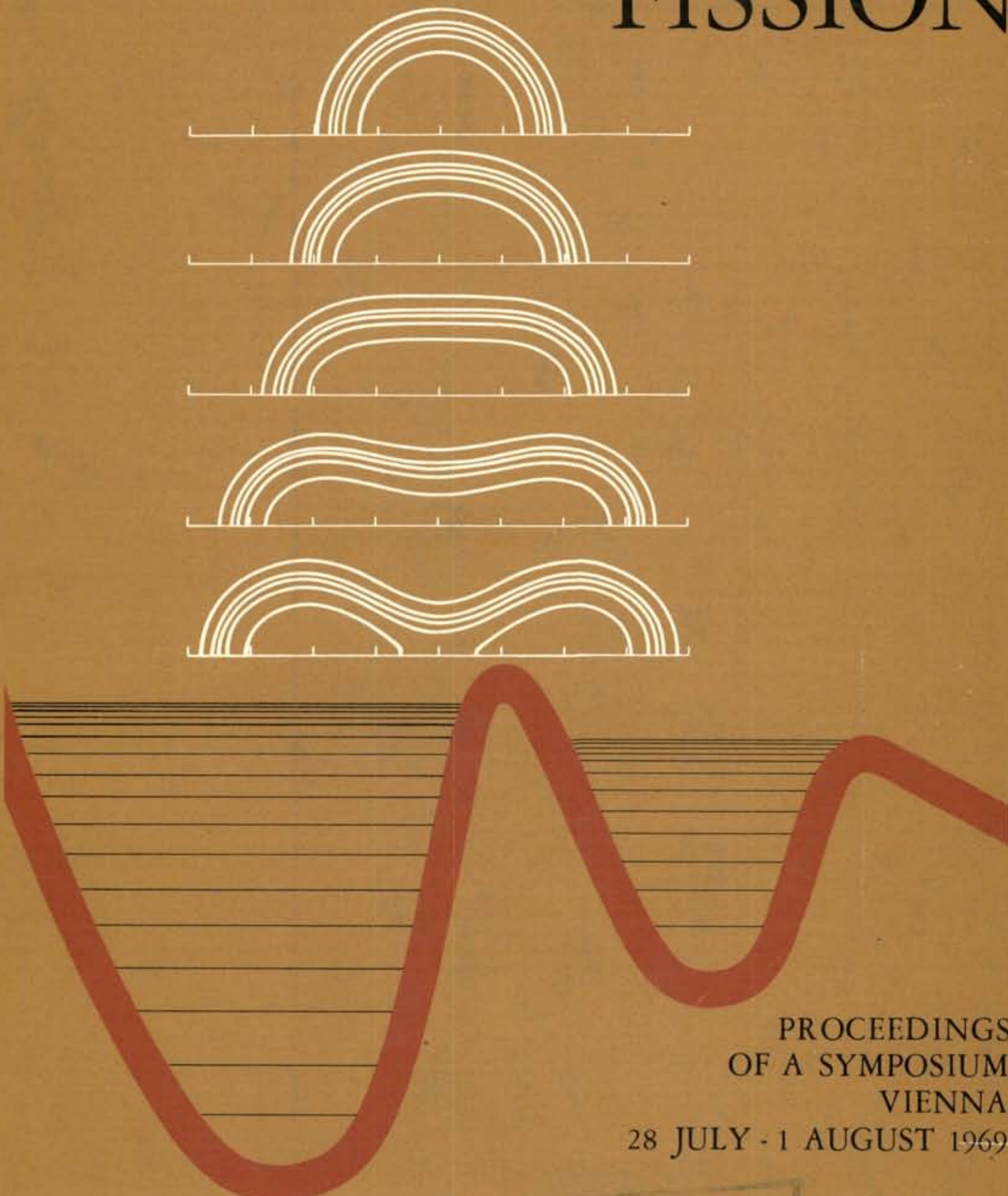

PROCEEDINGS
OF A SYMPOSIUM
VIENNA,
28 JULY - 1 AUGUST 1969

INTERNATIONAL ATOMIC ENERGY AGENCY, VIENNA, 1969

PHYSICS AND CHEMISTRY OF FISSION

The following States are Members of the International Atomic Energy Agency:

AFGHANISTAN
ALBANIA
ALGERIA
ARGENTINA
AUSTRALIA
AUSTRIA
BELGIUM
BOLIVIA
BRAZIL
BULGARIA
BURMA
BYELORUSSIAN SOVIET SOCIALIST REPUBLIC
CAMBODIA
CAMEROON
CANADA
CEYLON
CHILE
CHINA
COLOMBIA
CONGO, DEMOCRATIC REPUBLIC OF
COSTA RICA
CUBA
CYPRUS
CZECHOSLOVAK SOCIALIST REPUBLIC
DENMARK
DOMINICAN REPUBLIC
ECUADOR
EL SALVADOR
ETHIOPIA
FINLAND
FRANCE
GABON
GERMANY, FEDERAL REPUBLIC OF
GHANA
GREECE
GUATEMALA
HAITI
HOLY SEE
HUNGARY
ICELAND
INDIA
INDONESIA
IRAN
IRAQ
ISRAEL
ITALY
IVORY COAST
JAMAICA
JAPAN
JORDAN
KENYA
KOREA, REPUBLIC OF
KUWAIT
LEBANON
LIBERIA
LIBYA
LIECHTENSTEIN
LUXEMBOURG
MADAGASCAR
MALAYSIA
MALI
MEXICO
MONACO
MOROCCO
NETHERLANDS
NEW ZEALAND
NICARAGUA
NIGER
NIGERIA
NORWAY
PAKISTAN
PANAMA
PARAGUAY
PERU
PHILIPPINES
POLAND
PORTUGAL
ROMANIA
SAUDI ARABIA
SENEGAL
SIERRA LEONE
SINGAPORE
SOUTH AFRICA
SPAIN
SUDAN
SWEDEN
SWITZERLAND
SYRIAN ARAB REPUBLIC
THAILAND
TUNISIA
TURKEY
UGANDA
UKRAINIAN SOVIET SOCIALIST REPUBLIC
UNION OF SOVIET SOCIALIST REPUBLICS
UNITED ARAB REPUBLIC
UNITED KINGDOM OF GREAT BRITAIN AND NORTHERN IRELAND
UNITED STATES OF AMERICA
URUGUAY
VENEZUELA
VIET-NAM
YUGOSLAVIA
ZAMBIA

The Agency's Statute was approved on 23 October 1956 by the Conference on the Statute of the IAEA held at United Nations Headquarters, New York; it entered into force on 29 July 1957. The Headquarters of the Agency are situated in Vienna. Its principal objective is "to accelerate and enlarge the contribution of atomic energy to peace, health and prosperity throughout the world".

Printed by the IAEA in Austria
December 1969

PROCEEDINGS SERIES

PHYSICS AND CHEMISTRY OF FISSION

PROCEEDINGS OF THE SECOND IAEA SYMPOSIUM
ON THE
PHYSICS AND CHEMISTRY OF FISSION
HELD BY THE
INTERNATIONAL ATOMIC ENERGY AGENCY
IN VIENNA, 28 JULY - 1 AUGUST 1969

INTERNATIONAL ATOMIC ENERGY AGENCY
VIENNA, 1969

PHYSICS AND CHEMISTRY OF FISSION
IAEA, VIENNA, 1969
STI/PUB/234

FOREWORD

Fission studies have developed rapidly and significantly since the first IAEA Symposium on the Physics and Chemistry of Fission, held in 1965 in Salzburg. Several surprising discoveries and some excellent experimental results have given rise to many new theoretical investigations. From the individual theoretical models, laboriously improved and carefully fitted to the experimental data, a more general theoretical picture has begun to take shape and this has provided fresh ideas for experimental work.

The Second Symposium on the Physics and Chemistry of Fission, held at the IAEA Headquarters in Vienna from 28 July to 1 August 1969, was a short pause in the rapid flow of developing theoretical concepts and new experimental investigations; it was devoted to the discussion, comparison and analysis of the recent achievements, and to a glance at the way fission studies are likely to develop in the near future. Two facts, the emphasis on theory and the important interplay of theory and experiment, left a strong mark on the contributions and discussions. The number of papers dealing with theoretical aspects is substantially larger than at the earlier symposium; this points to the fact that with increased efforts the theoreticians have succeeded in narrowing the wide gap between the large amount of empirical data and the theoretical understanding of it.

The titles of individual sessions indicate the new trends in fission research. Theories of fragment distribution, shell structure effects in fissioning nuclei, intermediate structure, and isomeric fission are topics which were discussed with a great deal of uncertainty at the Salzburg symposium. At the present meeting, they were far more prominent and they were argued with great confidence and with the intensity and enthusiasm that only such exciting ideas can arouse.

From the extensiveness of the discussion records the vivid interest of the participants is clearly seen; the pertinent problems still to be solved are also revealed. These problems are a challenge for the coming years.

A considerable amount of work originally submitted for consideration for inclusion in the Symposium could not be presented orally. The main reasons for this were the obvious time limitations imposed by a week-long symposium, and the need to keep the Proceedings down to a reasonable size. However, abstracts of this work - sometimes in slightly extended form - are included at the end of this book, and readers interested in the work summarized in this section should apply to the individual authors for further details.

EDITORIAL NOTE

The papers and discussions incorporated in the proceedings published by the International Atomic Energy Agency are edited by the Agency's editorial staff to the extent considered necessary for the reader's assistance. The views expressed and the general style adopted remain, however, the responsibility of the named authors or participants.

For the sake of speed of publication the present Proceedings have been printed by composition typing and photo-offset lithography. Within the limitations imposed by this method, every effort has been made to maintain a high editorial standard; in particular, the units and symbols employed are to the fullest practicable extent those standardized or recommended by the competent international scientific bodies.

The affiliations of authors are those given at the time of nomination.

The use in these Proceedings of particular designations of countries or territories does not imply any judgement by the Agency as to the legal status of such countries or territories, of their authorities and institutions or of the delimitation of their boundaries.

The mention of specific companies or of their products or brand-names does not imply any endorsement or recommendation on the part of the International Atomic Energy Agency.

CONTENTS

SHELL-STRUCTURE EFFECTS IN FISSIONING NUCLEI (Session C)

INTERMEDIATE STRUCTURE IN FISSION (Session D)

DELAYED NEUTRONS AND GAMMA RAYS (Session G)

ENERGY, MASS AND CHARGE DISTRIBUTION (Session H)

THEORIES OF FRAGMENT DISTRIBUTION

(Session A)

Chairman: E.R. Rae

THE PRINCIPLE OF KINETIC DOMINANCE FOR RAPID COLLECTIVE MOTION*

A Review

J.J. GRIFFIN
University of Maryland,
College Park, Maryland,
United States of America

Abstract

THE PRINCIPLE OF KINETIC DOMINANCE FOR RAPID COLLECTIVE MOTION. Rapid collective motion during the late stages of fission is proposed as the means whereby the nucleus can "remember" saddle-point properties, such as the angular distribution of its symmetry axis. It is argued that for very rapid collective motion a principle of kinetic dominance prevails, under which the collective inertia determines the trajectory of the motion. The author shows that collective inertia may vary by an order of magnitude among various trajectories, and that nucleonic adjustment to independent particle level crossings is a major source of this variation. The author shows also that the minimal trajectory which kinetic dominance selects can lead to scission mass ratios of the magnitude observed in heavy element fission.

1. Collective Motion Towards Fission: Rapid or Slow ?

A basic assumption which divides into two groups all attempts to calculate the properties of fission fragment distributions is whether or not the motion proceeds slowly enough that statistical equilibrium prevails (at least approximately) during the motion. Indeed, "Statistical Theories" of fission assume explicitly that the probability distributions of all the various properties of fragments (e.g. masses, excitation energies, etc.) mirror directly the equilibrium state at scission.[1] Other studies aim at the calculation of more limited information, such as excitation energy (to compute the number of neutrons) vs. fragment mass,[2] to [6] by assuming at scission an equilibrium described by several selected parameters. Finally, we note that with a few recent exceptions[6][7], studies of the classical liquid drop implicitly restrict themselves to slow collective motion, by considering only the potential energy of deformation, and neglecting the kinetic energy associated with the fluid flow.

Difficulties with the Equilibrium Assumption

It should be emphasized that the equilibrium assumptions often achieve a remarkable measure of success. So much so that the ultimate theoretical description of fission, if it should turn out to involve rapid collective motion, must certainly provide also an explanation of how the equilibrium assumption is able in some respects to provide such good agreement with observation. One can think of possibilities for such an explanation, such as partial equilibrium within subset(s) of coordinates or strong effects of level densities which might be stimulated by equilibrium distributions. It is much more difficult to understand how a description based upon equilibrium at the scission point can allow a "memory" of saddle point properties,

* Research supported in part by the US Atomic Energy Commission.

as the fission fragment angular distributions seem to do in reflecting K_0^2 values which correspond to excitation energy in excess of the saddle point energy.

This single case of "memory" of a saddle point property exhibits the unhappy lose or no-win choice which the question of equilibrium offers to equilibrists: A scission equilibrium strictly precludes any memory of an earlier stage, whereas a lack of memory fails to verify the equilibrium. For this reason, the fragment angular distribution data provides a serious problem for the assumption that total equilibrium prevails at scission. One is therefore led to consider the possibility that the collective motion, at least during (the latter) part of the fission process, is so rapid as to prevent the realization of equilibrium.

Rapid Collective Motion and Collective Inertia

Such a viewpoint has been proposed by the author[9] as a basis for incorporating the effects of reflection symmetry[10][11] into a description of the post-barrier fission process. We review this proposal in the next section, and then discuss the interpolation of collective dynamics between the extremes of slow and rapid collective motion. From this discussion the collective inertia is identified as the crucial parameter for rapid motion, and the following principal of Kinetic Dominance emerges as the basis for predicting rapid collective motion: In the limit of high collective velocity, nuclear shape changes are described by a potential energy surface defined by the energies of nuclear configurations which are deformed into one another with a minimal collective inertia.

2. Implications of Reflection Symmetry for Rapid Collective Motion

Collective Velocity and Level Crossings

Zener[12] first provided the complete solution[13] (See Appendix I) to the problem (See Fig. 1) of a system (here, a nucleus) involving an external parameter, (shape: α) driven at a constant rate of change ($\dot{\alpha}$) through a value (α=0) at which the levels would cross, except for a small constant coupling between the two levels. The result provides a basic distinction between slow and rapid collective motion: When the shape changes through the value where a filled independent particle level is crossed by an unfilled level, the excitation of nucleons (to the excited orbit E_a) has a probability of one if the shape changes very rapidly and zero (particles remain in E_{low}) if the shape change is slow.

Distinct Potential Surfaces for Slow or Rapid Motion

In the extreme of rapid motion, then, one can obtain a very simple description of the nuclear energy after any shape change away from that at which the lowest energy state last had been realized. The nuclear energy, $V_{Rapid}(\alpha)$, exceeds the Liquid Drop (1) energy,

(1) By "Liquid Drop" energy surface, we mean here simply the surface describing the energy of the lowest energy nuclear configurations vs shape, including all suitable improvements over the simplest liquid drop description, e.g. shell effects, both spherical and generalized, pairing correlations, etc. Also, for the remainder of the discussion V_{Rapid} and V_{Slow} will be simplified to V_R and V_S.

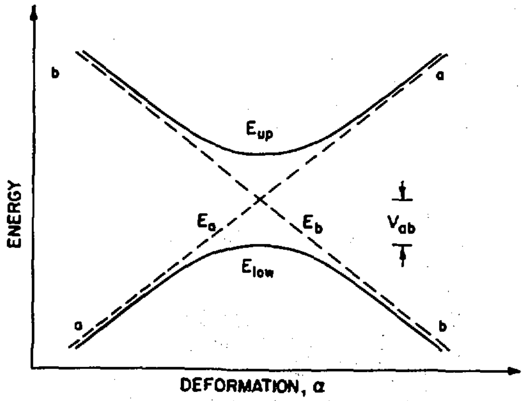

FIG. 1. A level crossing split by a non-diagonal interaction, V, leads to eigenvalues E_{low} and E_{up} which depend on the external parameter, α, as shown. If α varies slowly with time then a system in E_a at $\alpha = -\infty$ will follow E_{low} into E_b at $+\infty$. For rapid motion, however, the system will "jump" and arrive at $\alpha = +\infty$ *still in the level* E_a (see Appendix I for a more detailed discussion).

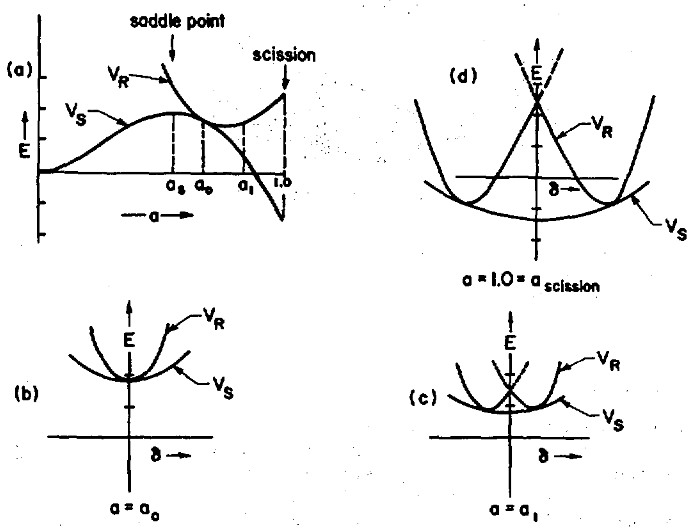

FIG. 2. The study of the potential surface for rapid motion, V_R, which applies when the "jump" probability in Fig. 1 is unity, is especially simple for reflection symmetric shapes, Fig. 2a, and for scission (disjoint) shapes, Fig. 2d. Fig. 2c shows an intermediate cut of the potential surface which is conjectured from the behaviour at a_0 and $a_{scission}$. The liquid drop surface, V_S, on which reflection symmetric shapes have always the least energy, is shown for comparison (the figure is schematic only.)

$V_{Slow}(\alpha)$, by the total excitation energy associated with all the level crossings which occurred during the motion. This difference may (and does) vary with shape, with the result that a valley in $V_{Slow}(\alpha)$ may be a ridge in $V_{Rapid}(\alpha)$. Then rapid motion proceeds over paths quite unpredictable from a knowledge of $V_{Slow}(\alpha)$ alone.

Reflection Symmetry

In particular, in previous discussions one has focussed on the spatial reflection symmetry of the nucleonic orbitals as the property which is expected to determine the fission mass distribution, and overlooked all other details of these orbitals.

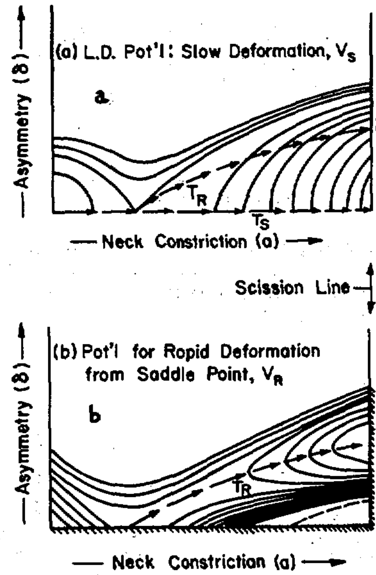

FIG. 3. Schematic contour plots of V_R and V_S are shown together with the trajectories, T_R and T_S, which follow their respective valleys. As in Fig. 2, the properties of the surfaces are conjectured from their behaviour along the line $\alpha=0$, and along the scission line, $a=1.0$.

Mass Ratio Implied

Then it is easy to calculate $V_R(\alpha)$ for a simple statistical nucleus along a line of reflection symmetric shapes and also along a line of scission shapes of varying degrees of reflection asymmetry (i.e. varying right-left volume ratios). In this way the value of $V_R(\alpha)$ is traced out along a line and an edge of a two dimensional shape-parameter space. (See Fig. 2 and Fig. 3.)

One assumes that the rapid motion commences at the fission barrier shape and proceeds to the lowest energy scission point on V_R, which occurs at the mass ratio given by

$$M_{Heavy} / M_{Light} = N_+ / N_- \qquad (1)$$

where N_+ (N_-) is the number reflection symmetric (asymmetric) orbitals occupied at the (saddle point) shape where the collective motion first became rapid. (For slow collective motion, of course, the liquid drop potential exhibits a valley leading to a symmetric scission shape as indicated in Fig. 3a.) The ratio (1) is plotted vs Z^2/A in Fig. 4.

We note that the minimum energy scission configuration is also a ground state configuration, and so the surface V_R is tangent to the surface V_S at the scission point, at the saddle point and (presumably) along a curve joining these two points. That is, the valley trajectory, T_R of V_R lies in both surfaces, V_R and V_S.

3. Connection Between Trajectories Favored by Slow Motion and by Rapid Motion; Kinetic Dominance

In the above description, two separate and distinct potential surfaces occur for the two extremes of slow and rapid collective motion. On each surface there exists a maximum gradient trajectory from saddle point to scission which would describe the most probable path for a classical motion. An interesting question is then how to understand the change from the slow trajectory (Fig. 3a) to the rapid trajectory (Fig. 3b) as the collective velocity increases from zero to a large value. The answer to this question is not completely available as yet. Nevertheless, we would like to suggest the general outlines which that answer is likely to take, and to present some partial results.

Role of Kinetic Energy

In the first place we consider the situation from the point of view of V_S. In this limit the collective kinetic energy in the Hamiltonian,

$$H_{coll} = \sum_{ij} M_{ij}\, \dot{\alpha}_i\, \dot{\alpha}_j + V(\vec{\alpha}) \qquad (2)$$

is zero since $\dot{\alpha}=0$. As one considers the effect of gradually increasing $\dot{\alpha}$, the variation occurs in just this kinetic energy term, focusing the attention upon the collective inertia tensor, M_{ij}, which summarizes all the influences of the internal nucleonic dynamics upon the collective motion. In particular, if the trajectory, T_S, along the line of symmetric shapes is to lose its preferred status as the collective velocity increases then it must be the collective inertia which introduces the requisite effects via the Hamiltonian, (2).

Structure of the Inertial Parameter

Specifically, we suggest (on the basis of the discussion to follow) that T_S is a trajectory along which the inertia is great, whereas the valley trajectory of V_R, T_R, viewed as a trajectory in V_S is a trajectory of minimal inertia. Thus one is able to understand from the point of view of the liquid drop potential surface, V_S, why the preferred trajectory shifts away from T_S towards T_R as the collective velocity increases: The inertia decreases with such shifts, so that for any fixed finite collective velocity the energy is less along some path intermediate between T_S and T_R than it is along T_S. For very rapid collective motion, T_R is the preferred trajectory. In that limit, from the point of view of the liquid drop potential, we have realized V_S, the limit of Kinetic Dominance wherein the physical trajectory is dictated entirely by the properties of the collective inertia and the influence of liquid drop potential energy is negligible.

From the viewpoint of the rapid motion, on the other hand, we suggest below that the potential surface, V_R, is everywhere a surface of minimal inertia. As such, it is the appropriate replacement in the limit of Kinetic Dominance for the liquid drop surface, V_S, which is the surface of minimal potential energy and describes the motion in the limit of what we might now call Potential Dominance (i.e. negligible kinetic energy). The difference V_R-V_S is then a measure of the internal nuclear excitation energy which it costs to maintain throughout the motion a nuclear configuration with a minimal collective inertia, as compared with allowing the nucleons to readjust to the lowest energy configuration and accepting the increase in the inertia which such adjustments imply.

4. Collective Inertial Parameters

Hill and Wheeler[10] display an approximate solution of the time dependent Schrödinger equation which describes the collective motion of a nucleon whose wave function adjusts continuously and without topological alteration of its nodal surfaces to the changing shape of the nucleus. This discussion is reviewed in Appendix I, and it is suggested in addition that such distortions are those which occur under rapid nuclear shape changes. On these grounds we propose that the collective inertia appropriate for motion on V_R, and, in particular, along the trajectory, T_R, is roughly equal to the inertia associated with irrotational motion of a classical fluid of the same density.

In contrast, motion on the potential surface V_S generally involves a continual readjustment of nucleons so that the lowest energy orbitals remain occupied at every shape. It is shown in Appendix I that the level crossings which dictate such readjustments involve also a significant contribution to the collective inertia, as calculated by the cranking model. Indeed, the average contribution to the inertia from such crossings may, along some paths, exceed the irrotational value by a large factor.

Thus, we conclude that paths with many crossings (such as the symmetric path T_S, favored by V_S) will involve inertial parameters far exceeding the irrotational value which is expected for minimal inertia paths (such as T_R). This conclusion, in turn, forces a reassessment of the predictions of fragment mass ratios made on the basis of the reflection symmetry of nucleonic orbits, which we discuss in the following section.

5. Mass Ratio Predictions: Minimal Inertia vs Reflection Symmetry

In the earlier discussions [9] of fragment mass ratios and reflection symmetry of nucleonic orbitals, all the properties of the orbitals were suppressed except for the reflection symmetry. Thus, it was assumed in obtaining the trace of the potential surface, V_R, along the line of symmetric shapes only that the number of nucleons in reflection symmetric orbits was conserved, and that the lowest energy configuration consistent with this value would be realized. Although natural enough when the emphasis is upon the symmetry property, these assumptions are oversimplified for a description which identifies the minimal inertial path as that expected in the limit of Kinetic Dominance.

Indeed, minimal inertia requires that at <u>every</u> crossing the evolution of the nucleonic configuration preserve its spatial topological properties, whereas the restriction to $N+$=constant imposes this condition only at crossings of levels with different reflection symmetry, and allows the system to follow E_{low} at any crossing of two levels of the same symmetry. In Appendix II, we consider a crude model to describe this effect and obtain the estimates summarized in Fig. 4 for the mass ratio M_H/M_L.

Comparison of Results

One sees in Fig. 4 that the "Minimal Inertia" mass ratios are higher than the "Reflection-Symmetry" mass ratios for all Z^2/A, and in much better agreement with the values observed in the heavier nuclei. On the other hand, the trend towards symmetric fission at lower Z^2/A which was a significant basis for encouragement in the earlier results has practically disappeared.

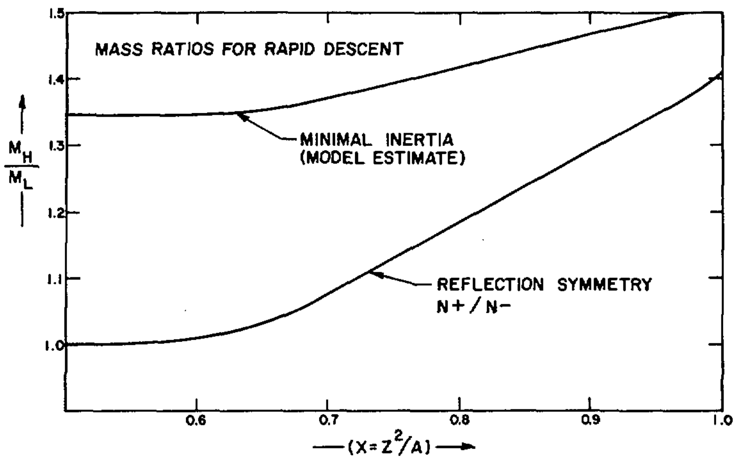

FIG. 4. The mass ratio at the lowest energy scission configuration is exhibited as a function of Z^2/A for the "Reflection-Symmetric" trajectory, T_R, and for the "Minimal-Inertia" path, T_M. The former is appropriate when "jumps" are assumed to occur whenever levels of different symmetry cross; the latter applies when "jumps" are assumed to occur at every crossing. The "Minimal Inertia" mass ratios are based on a very schematized model (Appendix II) and should be considered semi-quantitative at best.

Another feature of the "Minimal Inertia" path is that it leads at scission not to a ground state configuration but to a configuration involving many particles and holes. Whereas the lowest energy "Reflection Symmetry" path, T_R, lay in the liquid drop surface, the lowest energy minimal inertial path, T_M, is realized only by moving off the liquid drop potential surface into excited configurations. The question of whether motion along such a path might require potential energy in excess of that available in low or moderate energy fission requires here even more emphasis than in the "Reflection Symmetry" case. For both trajectories, this question is, so far, unanswered. In seeking an answer to it, the influence of the generalized shell effects discussed by Strutinsky, et al[14] might play an important part. One might also find that the sudden shift to symmetric fission, which occurs for nuclei below Thorium sets in when the potential energy along the minimal inertial path begins to increase from saddle to scission.

It must be emphasized, however, that there is no theoretical freedom to choose between the "Reflection Symmetric" and the "Minimal Inertial" descriptions of the process. The latter is merely a more detailed inference based on the same physical principles. Within the framework of present knowledge there exist no grounds on which to reject "minimum inertia" without also rejections the "reflection symmetric" description.

6. Overview

One can summarize by stating the basic principle of kinetic dominance which we here propose: That the differences in the collective inertia along various trajectories to scission play a dominant role in determining the properties of fission fragments.

This paper, however, provides no conclusive defense of this proposition. It does provide some supporting arguments: (a) that the magnitude of collective inertia is strongly influenced by level crossings, (b) that its variation among various trajectory may span an order of magnitude, and (c) that the minimal inertial path which kinetic dominance predicts exhibits a mass ratio of the rough magnitude observed for heavy element fission.

The development discussed here seems, on the other hand, to lose one promising feature of the earlier (narrower) focus on reflection symmetry; viz. a built-in tendency for symmetric fission at lower Z^2/A.

APPENDIX I. Irrotational and Level-Crossing Contributions to Collective Inertia

Irrotational Inertia Applies on V_R

Hill and Wheeler [10] consider the effect of a time dependent nuclear shape on a wave function which distorts continuously as the deformation proceeds. Consider the irrotational motion of a classical fluid inside a container of the same shape. That motion can be described by a velocity potential ψ, such that

$$\vec{v} = -\nabla\psi, \tag{I-1}$$

$$\nabla^2\psi = 0, \tag{I-2}$$

$$\frac{\partial\psi}{\partial t} = 1/2(\nabla\psi)^2 + \frac{p}{\rho} \tag{I-3}$$

and

$$\frac{\partial B}{\partial t} + \vec{v} \cdot \nabla B = 0 \tag{I-4}$$

where

$$B[\alpha(t), \vec{r}] = 0 \tag{I-5}$$

describes the moving boundary. And let

$$H_o(\alpha)\ U_i(\alpha) = \varepsilon_i(\alpha)\ U_i(\alpha) \tag{I-6}$$

describe for fixed α an eigenfunction of the independent particle Hamiltonian

$$H_o(\alpha) = T + V(\alpha). \tag{I-7}$$

Then, if $\ddot{p}/\rho$ (proportional to acceleration $\ddot{\alpha}$) is negligible, the wave function

$$\Psi_i(t) = U_i[\alpha(t)] \exp - \frac{i}{\hbar} [\int^t \varepsilon_i[\alpha(t)]\, dt - M\psi] \qquad \text{(I-8)}$$

satisfies the time dependent Schrödinger equation

$$i\hbar\dot{\Psi} = H_o\Psi \qquad \text{(I-9)}$$

if only the total derivative approximation

$$DU_i(\alpha)/Dt = 0 \qquad \text{(I-10)}$$

i.e.
$$\dot{\alpha}\frac{\partial}{\partial\alpha} U_i = \nabla\psi \cdot \nabla U_i \qquad \text{(I-10a)}$$

is valid.

The energy of the nucleon described by (I-8) is equal to

$$\langle U_i(\alpha) \mid \frac{m}{2} (\frac{\vec{p}}{m} + \vec{v})^2 + V(\alpha) \mid U_i(\alpha)\rangle = \varepsilon_i(\alpha) + \frac{m}{2} \langle\vec{v}^2\rangle \qquad \text{(I-11)}$$

where $\vec{p}$ is the nucleon momentum operator and $\vec{v}$ is the classical irrotational fluid velocity. For the entire nucleus, therefore, the collective kinetic energy is equal simply to the energy of irrotational flow for a classical fluid of the nuclear density $\rho=\Sigma|U_i|^2$:

$$\frac{m}{2} \sum_{i=1}^{A} \int(\nabla\psi)^2 \, |U_i|^2 \, d\tau = \frac{m}{2} \int(\nabla\psi)^2 \rho d\tau \qquad \text{(I-12)}$$

It follows that the inertia also has the classical irrotational value.

Then when is (I-10) a good approximation? One can see at once that for an infinite square well potential (I-10) is always satisfied exactly at the nuclear boundary: An acceptable choice for the boundary function B would be simply $B=U_i$; then Eq. (I-4) specifying the boundary condition on ψ becomes identical to Eq. (I-10). This argument extends also to the interior nodal surfaces of U_i, if only the integrated probability of finding the nucleon in each of the elementary volumes enclosed by the nodal surfaces of U_i remains constant with deformation.

The approximation (I-10) can also be shown to be exactly true for the ellipsoidal deformations of a 3-dimensional oscillator potential.

<u>Total Derivative Approximation Invalid for E_{low} at Level Crossing</u>

On the other hand, it is manifestly inaccurate whenever the topology of the nodal surfaces of an independent particle state changes in the course of the motion, as happens when E_{low} is followed at the level crossing in Fig. 1. We therefore assume that Eq. (I-10) is a good approximation whenever the nuclear configuration follows the shape change by retaining the occupation of the "same" single particle orbitals (i.e. the single particle orbitals which evolve continuously in such a way as to maintain the nodal topology of those originally occupied). But this is exactly the response which occurs in rapid collective motion when the "jump" probability of Fig. 1 approaches unity. Thus, we conclude that the potential surface V_R is a surface on which the irrotational value of the collective inertia, M_{irrot}, is everywhere approximately the correct value. Moreover, motion on any potential surface other than V_R must involve the re-adjustment of independent particle orbitals at level crossings, and their consequent positive contributions to the collective inertia, as discussed below. It follows, therefore, that the collective inertia is minimal for motion on the surface V_R.

Adjustment at Level Crossings Implies Large Inertia Increases

We turn now to consider the effect on M of the nuclear configuration's following E_{low} of Fig. 1. The idea here is essentially the same as that proposed by Primack[15] in his discussion of the inertial parameters for the calculation of spontaneous fission lifetimes.

Zener - Landau Problem

Consider in Fig. 1 the topmost filled level, E_a, being crossed at the point α=0 by the downsloping level E_b. Each line is meant to represent a degenerate pair of nucleonic orbitals related to one another by time reversal. If a residual two-body interaction, V_{ab}=V, exists which mixes the two levels, then the eigenvalues of the system for fixed $\dot{\alpha}$ will follow the arcs E_{low} and E_{up} rather than the crossing which would apply in the absence of residual interactions. Zener[12] and Hill and Wheeler[10] calculate the probability that a system in which level E_a is occupied at $\alpha= -\infty$ with a probability of 1 and for which $\dot{\alpha}$=constant will arrive at $\alpha= +\infty$ with the system in the lower of the two levels E_b and the complementary probability that the system will have made the jump to the higher of the two levels, E_a, at $\alpha= +\infty$. The latter jump probability is equal to

$$J = \exp - 2\pi\gamma \qquad \text{(I-13)}$$

where

$$\gamma = |V|^2 \,/\, \hbar\dot{\alpha}\ [d|\varepsilon_a - \varepsilon_b|/d\alpha] \qquad \text{(I-14)}$$

Correction to Inertia for Level Crossing

We wish to calculate the collective inertia M when the nucleons remain in the lowest eigenvalue, E_{low}. For this purpose we shall use the cranking model formula and assume for simplicity that the cranking perturbation matrix element between levels a and b vanishes:

$$\langle a \mid \frac{\partial}{\partial\alpha} \mid b\rangle \equiv 0 \qquad \text{(I-15)}$$

We first write down the inertia for the large $\dot{\alpha}$ situation where level a remains occupied rather than E_{low} (that is, where the jump is made from the eigenvalue E_{low} to the eigenvalue E_{up}). The inertia is then

$$M_R = 2h^2 \sum_{\substack{j\geq b \\ i\leq a}} \frac{|<j|\frac{\partial}{\partial\alpha}|i>|^2}{\varepsilon_i-\varepsilon_j} \approx M_{irrot} \quad \text{(I-16)}$$

We have inserted here the result already argued above that this sum is approximately equal to the classical irrotational inertia.

We now consider the inertial parameter appropriate to the situation where the level E_{low} remains filled and no jump occurs to the level E_{up} for $\alpha=\infty$. The inertial parameter in this case is identical to that in Eq. (I-16) except for the terms involving i=a or j=b, since the levels a and b are now replaced by the levels E_{low} and E_{up}. These have wave functions (for fixed α), as follows:

$$|low> = A(\alpha)|a> + B(\alpha)|b> \quad \text{(I-17a)}$$

$$|up> = B(\alpha)|a> - A(\alpha)|b> \quad \text{(I-17b)}$$

where

$$A(\alpha) = -V/[(\varepsilon_a - E_{low})^2 + V^2]^{1/2} \quad \text{(I-18a)}$$

$$B(\alpha) = (\varepsilon_a - E_{low})/[(\varepsilon_a - E_{low})^2 + V^2]^{1/2} \quad \text{(I-18b)}$$

and

$$E_{low} - \frac{\varepsilon_a+\varepsilon_b}{2} - [\left(\frac{\varepsilon_a-\varepsilon_b}{2}\right)^2 + V^2]^{1/2} \quad \text{(I-19)}$$

We note that in the cranking model expression, Eq. (I-16), a term with i=a, j=b has been assumed in Eq. (I-15) to vanish identically. However, when levels a and b are mixed by an interaction, V, and when E_{low} remains occupied during the collective motion then the corresponding term no longer vanishes, but assumes the value

$$\Delta(\alpha) = 2\hbar^2 \frac{|<up|\frac{\partial}{\partial\alpha}|low>|^2}{E_{up} - E_{low}} = 2\hbar^2 \frac{|B\frac{\partial A}{\partial\alpha} - A\frac{\partial B}{\partial\alpha}|^2}{E_{up} - E_{low}} \quad \text{(I-20)}$$

<u>Average Value of Crossing Contribution, $\overline{\Delta M}$</u>

For two levels which vary linearly with α, and which cross at $\alpha=0$ with relative slope c, one can evaluate (I-20) to obtain

$$\frac{\Delta}{2\hbar^2} = \frac{c^2}{8V^3}[1 - \frac{5}{2}\frac{c^2}{V^2}\alpha^2 + \ldots] \quad \text{(I-21)}$$

If we neglect higher terms and assume that the (positive definite) quantity, Δ, vanishes when the approximation (I-21) would give a negative value, then the following underestimate of the average value of Δ results

$$\bar{\Delta} = 2\hbar^2 \frac{2}{3} \cdot \frac{c^2}{8V^3} \text{ for } -\sqrt{\frac{2V^2}{5c^2}} < \alpha < \sqrt{\frac{2V^2}{5c^2}} \qquad \text{(I-22)}$$

If along an extended deformation path, ρ_c level crossings occur per unit α, then one expects an average contribution to the collective inertia equal to

$$\overline{\Delta M} = \bar{\Delta}\,\rho_c \cdot 2\sqrt{\frac{2V^2}{5c^2}} = \frac{1}{3}\sqrt{\frac{2}{5}}\,\frac{c}{V^2}\,\rho_c \hbar^2 \qquad \text{(I=23)}$$

For quadrupole deformations, as described e.g. by the Nilsson model with $\alpha=\varepsilon=0.95\beta$, one can estimate $c\simeq 20$ MeV, and $\rho_c \approx 10^2$ per unit ε. If $V\approx 0.1$ (a typical value for a nuclear pairing force matrix element) then

$$\overline{\Delta M} \approx (4\times 10^4)\hbar^2 \approx 10^3\, M_{irrot} \qquad \text{(I-24)}$$

Other Corrections are Unimportant

Besides the contribution (I-20), the mixing of levels a and b also effects modifications in other terms of the cranking model sum (I-16). On the average the changes are due to increases in the energy denominators when ε_a, ε_b are replaced respectively by E_{low} and E_{up}. In general, such corrections are expected to result in at most 50% changes in the terms concerned, and, therefore, to perhaps ~10% changes in the estimate of M_{irrot}. Since nowhere in our present discussion are we concerned with such small effects as this, we shall omit further discussion of these additional corrections.

One sees, therefore, that the single term in the cranking model formula associated with the two-level mixing far exceeds(1) the entire remaining sum of Eq. (I-16). Moreover, Eq. (I-24) shows that the possible range of values for M along different paths may cover several orders of magnitude.

Estimation of Pairing Effects

It is also true, however, that the pure independent particle estimate, (I-24), is not very realistic because nuclear pairing forces act coherently to mix together the several single particle states near the Fermi surface and to generate a pairing gap of the order of 1 MeV in heavy even-even nuclei. We turn now to the consideration of such effects in terms of an idealized model.

---

(1) This result agrees with the similar conclusion of Primack, reference [15]

The model for pairing which we wish to consider is the following: N pairs of orbitals, ($i=1, \ldots N$), degenerate at the Fermi energy (taken as the energy scale zero for this discussion), interact with constant matrix elements $-V$. Then the ground state is the coherent equal amplitude superposition of these with energy $-NV$, and $N-1$ excited states are degenerate at energy 0.

We consider the analog of a two-level crossing to occur when one of the N levels (e.g. $i=1$) increases rapidly in energy out of degeneracy with the ground state group while a new level ($i=0$) decreases rapidly to replace it. Then one can estimate crudely the factors which must be applied to the expression (I-22) to describe the following modifications: (a) only a fraction $1/\sqrt{N}$ of the ground state amplitude is involved in the variation with α, and (b) the energy denominator is increased to NV instead of V. The resulting estimate is

$$\Delta \rightarrow \Delta' = [(\frac{1}{\sqrt{N}})^2 \cdot \frac{1}{N}]\Delta \approx \Delta/N^2 \qquad \text{(I-25)}$$

Likewise

$$\overline{\Delta M} \rightarrow \overline{\Delta M}' = [(\frac{1}{\sqrt{N}})^2 \cdot \frac{1}{N}]\ \overline{\Delta M} \approx \overline{\Delta M}/N^2 \qquad \text{(I-26)}$$

We therefore estimate roughly that a pairing correlation among, say, $N=10$, levels with pairing matrix elements $|V|=0.1$ MeV which describes an energy gap equal to $NV \approx 1$ MeV, would diminish the contribution (I-24) of level crossings to the collective inertia by a factor of $N^2=100$ to the value

$$\overline{\Delta M}' \approx (4 \times 10^3)h^2 \approx 10\ M_{irrot} \qquad \text{(I-27)}$$

We conclude, therefore, that pairing effects, although they seriously complicate the problem technically, and effect quantitative modifications, are insufficient to destroy the predominance of the level crossing contributions to the collective inertia for paths involving many level crossings.

APPENDIX II. Mass Ratios for Minimal Inertial Path

In this Appendix, we attempt to estimate the effect on the mass ratio of considering every level crossing in tracing out the surface V, instead of just crossings of levels of different reflection symmetry. The latter procedure results naturally when attention is limited only to the reflection symmetry of the nucleonic orbitals, as in previous discussions[9] of this problem, but must be considered somewhat arbitrary from the viewpoint of the minimal inertial path.

Trajectory, T_M, Does Not Lie in V_S

We note in the first place that the present considerations will surely lead to particle-hole excitations among both the reflection symmetric and the reflection anti-symmetric subsets of orbitals. In general, therefore, one cannot expect the minimal energy scission configuration any longer to represent a ground state configuration; nor will the maximum gradient trajectory, T_M, in V_M lie in the liquid drop surface, V_S.

Potential Energy of Excitation Not Considered Here

This circumstance emphasizes the possible importance of the corresponding increase in potential energy for moderate energy fission of this type. This question is not discussed in this paper. Instead, we focus our attention on the limit of high collective velocity, assuming that the available energy is adequate to follow the Kinetically Dominated path.

Excitations Increase M_H/M_L

We note also that, in general, particle-hole excitations will increase the mass ratio of the lowest energy scission configuration. This is an immediate consequence of the expansion of Symmetric-Asymmetric independent particle orbitals into localized Right-Left orbitals at the scission shape. For any scission configuration, every reflection-symmetric (+) orbital is exactly degenerate with a "partner" reflection-asymmetric (-) orbital. If both (+) and (-) partners are filled, then the expansion in localized Right (R)-Left (L) orbitals certainly leads to one nucleon in each fragment. But if only one of the (+) and (-) partners is filled, then the independent probability at the reflection-symmetric shape is 1/2 that the nucleon appears in either fragment. This is true whether the vacancy of the partner orbital results from a scarcity of nucleons in (-) orbitals (i.e. $N_+ > N_-$), from a hole state of either type or from a particle of either symmetry excited to an orbital.

Loose Particles Go into Heavy Fragment

Also independent of how one partner state came to be vacant is the result that the lowest energy volume-asymmetric configuration occurs when every particle not certainly localized either R or L is placed into the Heavy fragment. This conclusion follows at once by

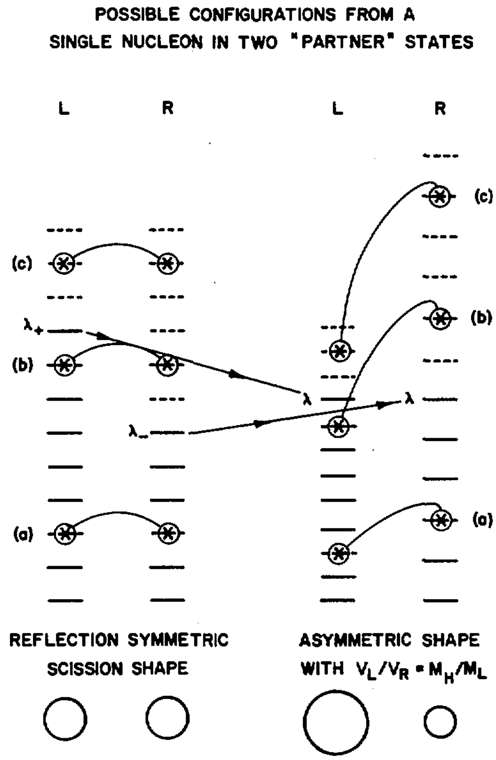

FIG. 5. This figure illustrates the statement that for any singly occupied pair of partner states in a reflection symmetric well, a lower energy will result at the asymmetric scission shape if the particle is placed into the heavy fragment, and the hole excitation, if any, into the light fragment (see text for more detail.)

inspection of Fig. 5. Consider a single nucleon in a pair of partner levels which (a) is below the Fermi energy λ for both the Heavy and the Light fragments, (b) is below λ_H, but above λ_L, or (c) is above both λ_H and λ_L. Case (a) offers the choice of a hole excitation in L or H. Clearly, when the R/L volume ratio has been allowed to shift to M_H/M_L the excitation energy of the light hole will be less on the average than that of the heavy. For case (b) one can choose either a particle excitation in L <u>and</u> a hole in H, or neither. Again, the energy is less if the particle goes into H. Finally, case (c) offers the choice between a particle excitation in H or a more highly excited one in L, and also favors placing the particle into H.

<u>Model to Estimate Crossing Excitation</u>

We consider a smoothed model of the nuclear level scheme to estimate the number of crossings which result from a quadrupole deformation of the order of those involved in fission ($\Delta\varepsilon \approx 0.3$), and

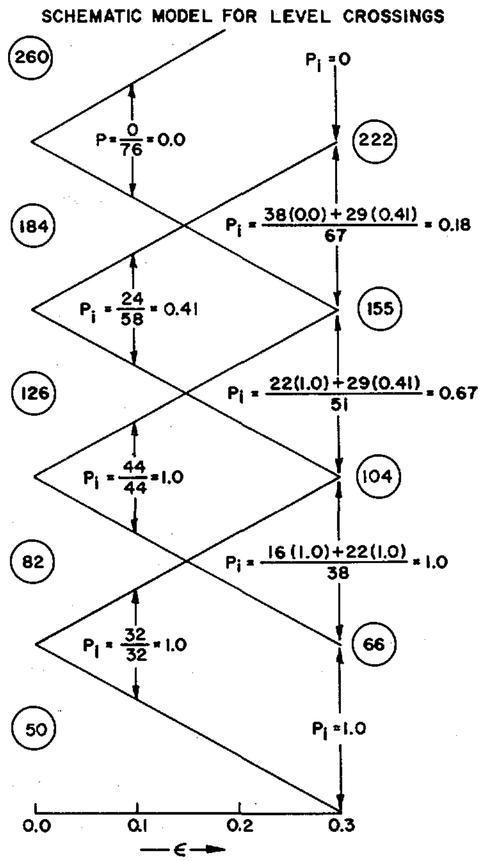

FIG. 6. Schematic model used in Appendix II to estimate the average occupation probabilities, P_i, which might result from a rapid quadrupole deformation, such as that which occurs between saddle point and scission (see text for more detail.)

a distribution of the excitation energies of the resulting particles and holes. In this model, each major shell is considered a continuum of states which spreads out from degeneracy at spherical to a width of $2\hbar w_o$ at $\varepsilon \approx 0.3$. (See Figure 6). The number, N, of nucleons in each major shell fixes the occupation probability $P_i(o)$, for each level in that shell at the spherical shape. Then at larger values of the deformation the continua of the major shells overlap and an occupation probability can be calculated for the various regions of the combined continuum from the occupations and relative weights of the constituents.

Figure 6 exhibits the model for N=150. At spherical the 82 and 126 shells have occupation probability 1.0, the 184 shell has

24 neutrons in 58 levels for a probability of 0.41. At ε=0.3 we assume each shell has spread out over $2\hbar\omega_o$ of energy. The weighted occupation probabilities at ε=0.3 are then as indicated on the graph. In this way, we have generated, as blindly as possible, an estimate of the occupation probabilities of the single particle levels which might result if a spherical ground state were deformed to ε=0.3 in such a way (rapidly!) as to make all the particles "jump" at each level crossing.

This estimate is assumed to be "typical"; specifically, we assume that the same occupation probabilities would describe both the (+) and (-) level sets for the reflection-symmetric scission shape if the rapid motion had begun in the ground state at the saddle point shape.

N_+/N_- Specified

Having thus estimated occupation probabilities, we now incorporate reflection symmetry by the straightforward assumption that in every interval, the levels divide into (+) and (-) in the proportion defined by N_+/N_- at the saddle point. (This assumption guarantees e.g. that the no particle - no hole state at scission would have the ratio N_+/N_-.)

Thus e.g. for N_+/N_- = 1.21, the first 104 levels would include 57 (+) levels and 47 (-) levels, occupied with a probability of 1.0. The next 51 levels include 28 (+) and 23 (-), occupied with a probability of 0.67. And the last 67 levels include 38 (+) and 29 (-), occupied with a probability of 0.18.

Calculation of M_H, M_L

We can now calculate the lowest energy mass ratio, since the light fragment mass is given by the number of (+-) "partners" both occupied.

$$M_L = \Sigma \; P_i^+ P_i^-$$

Here P_i^+ is the probability that the (+) partner of the i^{th} pair is occupied. The heavy fragment mass is equal to the number of level pairs in which both partners are occupied, plus the number in which only one partner is occupied:

$$M_H = \Sigma_i [P_i^+ P_i^- + P_i^+(1 - P_i^-) + (1 - P_i^+)P_i^-] = N - M_L$$

In this way we obtain a rough indication of the Minimal Inertial mass ratio M_H/M_L for each value of N_+/N_-.

Clearly this is the crudest kind of estimate and should not be taken quantitatively. On the other hand, it does indicate that mass ratios sufficiently larger than N_+/N_- to fit the data on high Z^2/A fission might be obtained from the principle of Kinetic Dominance. It also suggests that the explanation for the symmetric fission of elements of lower Z^2/A is not contained in the present simplified discussion.

REFERENCES

[1] FONG, P., Statistical Theory of Nuclear Fission, Gordon and Breach, Inc., New York (1968).
[2] VANDENBOSCH, R., Nuclear Phys. 46 (1963) 129.
[3] ARMBRUSTER, P., Proc. Int'l Symp. on Physics and Chemistry of Fission, Salzburg, Austria 1965 (I.A.E.A., Vienna).
[4] (blank)
[5] SCHMITT, H. W., (Proc. Int'l Symp. on "Why and How ... Nuclides Far Off the Stability Line", Lysekil, Sweden, 1966) Almquist U. Wiksell, Stockholm (1967).
[6] DICKMANN, F. and DIETRICH, K., to be published in Nuclear Phys.
[7] LAWRENCE, J. N. P., Symmetric Fission of a Two Parameter Liquid Drop (Ph.D. Thesis, Vanderbilt Univ., Nashville, Tenn., September 1967), Los Alamos Scientific Laboratory (New Mexico, U.S.A.) Report LA-3774 (1967).
[8] HASSE, R. W., et al, Nuclear Phys. A106 (1968) 117, and Nuclear Phys. A118 (1968) 577.
[9] GRIFFIN, J. J., Phys. Rev. Letters 21 (1968) 826. See also Proc. Second Conf. on Neutron Cross Sections and Technology, Wash., D.C., 1968 (GOLDMAN, D. T., Ed.) U.S. Gov't Printing Office (1968).
[10] HILL, D. L. and WHEELER, J. A., Phys. Rev. 89 (1953) 1102. Cf especially pp 1115 and 1128, Fig.'s 19 through 22. Other references are made herein to Fig.'s 33, 34, 8 and 10.
[11] KELSON, I., Phys. Rev. Letters 20 (1968) 867.
[12] ZENER, C., Proc. Roy. Soc. A137 (1932) 696. Fig.'s 33 and 34 of reference [10] summarize Zener's calculation.
[13] NEUMAN, J. von and WIGNER, E. P., Physik. Z. 30 (1929) 467 describe the behaviour for the limiting cases and the dimensionless parameter which characterizes them.
[14] STRUTINSKY, V. M., Nuclear Phys. A95 (1967) 420 and A122 (1968) 1.
[15] PRIMAK, J., Phys. Rev. Letters 17 (1968) 539 and B.S. Thesis, "Unified Model Calculations in Fission Theory", Princeton Univ. 1966.

DISCUSSION

L. WILETS: I have a few comments. First, the qualitative behaviour of the mass yield presented is in disagreement with experiment. The ratio is 1 for small Z^2/A, is discontinuous and then decreases with $A(Z^2/A)$. Second, adiabaticity also leads to asymmetry. The liquid-drop model is irrelevant, and one should talk about the adiabatic model. Third, angular distributions do preserve the quantum number K (as you implied), but this does not mean that other quantum numbers could not be destroyed. Fourth, pairing (which implies superfluidity) should have a very large effect in reducing mass parameter. Can you offer any numerical estimates? Fifth, the placing of degenerate unpaired particles on one side is not self-consistent. Indeed, this implies too high a density in terms of the original well.

J.J. GRIFFIN: In regard to your first comment, I agree. As to the second, if by "adiabaticity" you mean "liquid drop plus shell corrections", then that is what I called "liquid drop", so that I was talking about the adiabatic model when I used the words "liquid drop". I consider it an open question whether slow motion over such a potential surface does lead to asymmetry, as you claim. It may indeed, but it may also develop that the energy lowering due to shell effects provides only a local depression in the potential surface, which might never be reached during a slow collective motion from the saddle point. In reply to your third comment, I know no reason in principle why K should be preserved. Moreover, I would expect that in a slow enough collective motion, it would not, in fact, be preserved. I agree that different aspects of the saddle point situation may require different degrees of rapidity for their memory, i.e. a given collective velocity may be fast enough for some properties to be remembered and too slow for others. My reply to your fourth question is yes. The estimate (described in the Appendix to my paper) is that pairing reduces the level crossing contribution to the inertia by a factor of about 10^2, from 10^3 times to 10 times the irrotational value. Lastly, much of the excitation energy (V_R - V_S in Fig. 2 of the paper) along the line of reflection symmetric shapes ($\delta = 0$) is due to density fluctuations away from the average density, which arise because some nucleons are free to pass back and forth between the two fragments. It is just this energy which is regained by allowing more particles to be in one fragment and allowing as well a larger volume for this fragment, i.e. by moving to a reflection-asymmetric shape.

J.R. NIX: I agree with the author that in principle it is necessary to consider the kinetic-energy term in the Hamiltonian. However, recent considerations of the effect of single particles on the potential energy suggest that between the saddle point and scission there are ridges and valleys in the potential energy as a function of over-all distortion and mass asymmetry. I find it more reasonable to consider that the experimental mass distribution is determined primarily by the system evolving along the valleys of the potential energy.

J.J. GRIFFIN: I was not aware that anyone had traced out a valley in the potential surface leading all the way from saddle point to scission. So long as such depressions as shells (and generalized shells) imply are localized, one still has to verify that they can be reached during a slow deformation process, before being certain that they suffice to explain the mass asymmetry. Furthermore, I did not intend to suggest that the potential energy surface is unimportant in the actual fission processes but merely that the "gedanken" limit where the collective velocity is so large that the kinetic energy dominates is a useful limit conceptually.

C.Y. WONG: I think I can throw some light on the problem of mass asymmetry. I have calculated the single-particle states for two overlapping ellipsoids of different sizes and shapes at various separations, including the spin-orbit interaction. This can be done very easily by making use of the cylinder parabolic functions and matching the wave functions at the plane where the two ellipsoids meet. It is found that there are groupings of single-particle states at an asymmetry of about 1.4. These groupings give rise to the formation of generalized shells in the sense of Strutinsky. Whether a shell occurs with a particular nucleon number at this asymmetry depends on the shapes of the two fissioning parts. At a separation of 14 fm and with the ratios of the major to minor axis for both ellipsoids equal to 1.7, we find a shell at an asymmetry of 1.3 to 1.4 for the neutron number N ~ 146-148. It is, therefore, quite evident that the single-particle structure effects can give rise to a potential minimum at large asymmetry. Consequently, an adiabatic model will predict asymmetry.

J.J. GRIFFIN: I would agree entirely if only the word "will" in the last sentence were replaced by "may". After it has been shown that generalized shell effects give such a minimum for an asymmetric configuration near scission, there still remains the question whether that minimum will, in fact, be reached by a slow collective motion which starts at the saddle point. A valley which runs from scission all the way back to the saddle point would be much more convincing than the more restricted property you describe.

C. SYROS: We have heard two different points of view: the kinetic dominance theory and the dynamic dominance theory. I would like to mention a third point of view, which takes account of these two theories. Dr. Griffin's Fig. 1 reminds us of the predissociation theory of diatomic molecules. We went a step further and considered the nucleus in the scissioning state as a system of two clusters moving in a Morse potential. The results relating to the mass distributions agree well with the data on the assumption that the range of the collective forces depends on the fragment masses. As regards the shell effects on mass distribution, I would like to point out that the nucleus of the scissioning state has a good memory and also a vision of its future. This is expressed by the difference between the initial- and final-state energies, which gives the mass distribution the well-known fine structure.

A.C. PAPPAS: My question concerns Fig. 4 where you plot $X = (Z^2/A)/(Z^2/A)_{crit}$. We know that the mass ratios of the observed mass distributions decrease with increasing X, i.e. go in the direction opposite to that shown in your figure. How do you explain this?

J.J. GRIFFIN: This description is certainly not able, at this stage, to give the kind of detail you mention.

S. BJØRNHOLM: In connection with the applicability of Prof. Griffin's views, I would like to call attention to the experiments on heavy-ion fission by Yu. C. Oganessian et al. at JINR. They suggest, as I understand them, that for fission at high temperatures the transition point from adiabatic to rapid fission lies <u>beyond</u> the scission point, if $Z^2/A \lesssim 37$. As Z^2/A rises above $Z^2/A \approx 37$, the transition point (a_1 in Fig. 2) begins to move in from the scission point towards the saddle point. This is based on the observed steep rise in the width of the mass (and charge) distributions.

J.J. GRIFFIN: I really do not know the work you mention well enough to comment. If it provides an experimental basis for measuring whether the late stages of fission are fast or slow, then it is certainly very important. I do not know of any other experimental data which give such information unambiguously.

S.A. KARAMYAN: I do not quite understand why Dr. Griffin places the emphasis on the very high velocity of the fission process. If, indeed, the process occurs very fast, then the collision approximation should operate - the approximation assuming a sudden switch-on of the interaction, in which event the potential energy may not play any part and the final mass of the fission fragments will be determined exclusively by the initial conditions - the initial momentum of deformation of one or other type. So far as our results at Dubna are concerned, we did not confirm that at some Z^2/A values the process became very fast. We only noted that the conditions of statistical equilibrium may differ if we take account of different aspects of the process. The process may be fast in respect of rotation but slow, let us say, in respect of dipole oscillations, which are responsible for the establishment of equilibrium in charge distribution. This is treated in detail in my paper (SM-122/130).

J. J. GRIFFIN: Dr. Karamyan points out that my "gedanken" extrapolation to very high collective velocities would, if it were actualized, require a reassessment of the nuclear dynamical assumptions underlying the whole description. Of course, I do not wish to consider collective motions so rapid as that. "Rapid" here actually means that $J \approx 1$ (Eq. I.13) in the Zener-Landau problem and "kinetic dominance" means that changes in the liquid-drop potential energy have a negligible effect compared with charges in the inertial parameters. Either or both may or may not be realized in actual fission processes.

I agree entirely that the time scales to distinguish "fast" and "slow" may differ for different nuclear properties such as reflection symmetry, rotation, etc. Such differences will come into the problem via differences in the dimensionless parameter, $\gamma = |V|^2/\hbar\alpha c$, of the Zener-Landau problem (see Eqs I.14 and I.21).

AN ADIABATIC MODEL OF ASYMMETRIC FISSION

F. DICKMANN
Kernforschungszentrum Karlsruhe,
Federal Republic of Germany
and
K. DIETRICH
Institut für Theoretische Physik,
University of Heidelberg
and
Kernforschungszentrum Karlsruhe,
Federal Republic of Germany

Abstract

AN ADIABATIC MODEL OF ASYMMETRIC FISSION. It is assumed that, in the process of fission, a potential barrier develops at a position $Z=Z_0$ (the symmetry axis of the nucleus is chosen as Z-axis). Consequently, a neck is formed in the nuclear shape which leads to the final separation of the fragments. We represent the barrier by a repulsive δ-function which is added to the single-particle potential. We determine the position z_0 of the neck by requiring that the energy E(Z) needed to insert the barrier should have its smallest value. This picture presupposes an adiabatic fission process at the time of neck formation.

Preliminary calculations have been performed for the nuclei ^{246}Cf, ^{236}U, and ^{226}Ra using a cylindrical box as a highly simplified single-particle potential. For ^{246}Cf and ^{236}U the absolute minima of E(Z) were located at asymmetric positions z corresponding to the mass ratios 1.33 and 1.43, respectively. For ^{226}Ra, the absolute minimum of E(Z) was obtained for symmetric fission. However, a secondary minimum, only slightly larger in energy, was observed for the mass ratio 1.55. The ratio of the diameter to the length of the cylindrical box was 0.35 for the case of the above-mentioned results.

1. FORMULATION OF THE MODEL

Recently, one of the authors (K.D.) proposed a simple model [1] for the explanation of symmetric and asymmetric fission:

1) It is assumed that the division of the nucleus is connected with the formation of a potential barrier between the nascent fragments. For simplicity, this barrier is described by a repulsive δ-potential $C_0\,\delta(Z-Z_0)$ which is added to the average shell-model potential $U^{(s)}(X, Y, Z)$. We choose the Z-axis to be the nuclear symmetry axis and the origin at the centre of the nucleus. The variables Z_0 and $C_0 > 0$ give the location and the weight of the δ-function. The set of shape parameters is designated by s.

As the nucleus passes from the saddle to the scission point the barrier increases from an initially small perturbation to a large barrier which separates the fragments.

2) The process leading from the saddle (or possibly some shape isomer near the saddle) to the scission point is believed to be adiabatic to a fair extent so that the coupling between collective and intrinsic degrees of freedom can be omitted in a first approximation. Following this adiabatic picture, we determine the location Z_0 of the barrier by the require-

ment that the increase $E(Z_0)$ of total intrinsic energy due to the barrier $C_0\delta(Z-Z_0)$ should be a minimum:

$$\frac{\partial E}{\partial Z_0} = 0; \qquad \frac{\partial^2 E}{\partial Z_0^2} > 0 \tag{1}$$

3) Furthermore, we assume that the location Z_0 of the barrier is to be determined with the nucleus at its saddle point or possibly at some shape-isomeric state near the saddle point. In this way, the parameters s of the shell-model potential $U^{(s)}$ are, in principle, well-defined quantities.
4) Finally, it is assumed that the location Z_0 should be determined from relations (1) for the case of a small barrier $C_0\delta(Z-Z_0)$ which can be treated in lowest order of perturbation theory. Then Z_0 turns out to be independent[1] of the strength parameter C_0.

On the basis of a single-particle model, the energy increase $E(Z_0)$ for a nucleus of A nucleons is given by

$$E(Z_0) = \left\langle \Psi^{(s)} \left| \sum_{i=1}^{A} C_0\delta(Z_i - Z_0) \right| \Psi^{(s)} \right\rangle \tag{2}$$

where $\Psi^{(s)}$ is a Slater determinant of the A lowest occupied single-particle states $\varphi_i^{(s)}$.

Equation (2) can be rewritten in the form

$$E(Z_0) = C_0 \sum_{i=1}^{A} \rho_i^{(s)}(Z_0) \tag{3}$$

where the single-particle density $\rho_i^{(s)}$ is defined by

$$\rho_i^{(s)}(Z_0) = \iint dX\, dY \varphi_i^{(s)*}(X, Y, Z_0)\, \varphi_i^{(s)}(X, Y, Z_0) \tag{4}$$

The expression $\sum_{i=1}^{A} \rho_i^{(s)}(Z_0)$ can be interpreted as the number of nucleons in a disc perpendicular to the Z-axis with thickness 1 around $Z = Z_0$.

The prediction of the model is thus that the barrier is formed at a local minimum of the density distribution. A closer discussion (see Ref. [1]) shows that the solution Z_0 of Eq. (1) is determined by the number of occupied even ("gerade") and odd ("ungerade") single-particle states. In the case of a cylindrical box the density $\rho_i^{(s)}$ of an odd single-particle state $\varphi_i^{(s)}$ is zero at the centre $Z_0 = 0$, the density of an even state is at its maximum at the centre $Z_0 = 0$. Therefore, in our model, the odd states favour symmetrical, the even states asymmetrical fission. The outcome of this competition depends on the number of occupied even and odd states.

[1] Calculations for larger barriers without the use of perturbation theory have shown that the dependence of Z_0 on C_0 is small.

Once the location Z_0 of the barrier is given, the most probable ratio of the heavy to the light mass $f = m_H/m_L$ is obtained from the ratio of nuclear volumes at both sides of the barrier

$$f(Z_0) = \frac{m_H}{m_L} = \frac{\sum\limits_{i=1}^{A} \int\limits_{-\infty}^{Z_0} dZ\, \rho_i^{(s)}(Z)}{\sum\limits_{i=1}^{A} \int\limits_{Z_0}^{+\infty} dZ\, \rho_i^{(s)}(Z)} \qquad (Z_0 > 0) \tag{5}$$

At present, we cannot answer the delicate question of whether our assumptions are justified. We only present results obtained from the model in specific examples.

2. RESULTS

The liquid-drop model (LDM) predicts nearly cylindrical nuclear shapes at the saddle point for nuclei heavier than about Ra and dumbbell shapes for nuclei lighter than Ra [2]. Therefore, we choose as a single-particle potential $U^{(s)}$ a cylindrical box for the nuclei $\geqq$ Ra and a cylindrical box with a reduced central depth for nuclei < Ra (see Fig. 1). We performed calculations with infinitely high and finite walls of the cylindrical wells.

Figure 2 shows the energy difference

$$\Delta E(Z_0) = E(Z_0) - E(0) \tag{6}$$

as a function of the mass-ratio $f(Z_0) = m_H/m_L$ which corresponds to the location Z_0 of the δ-function (see Eq. (5)). We show the result for three

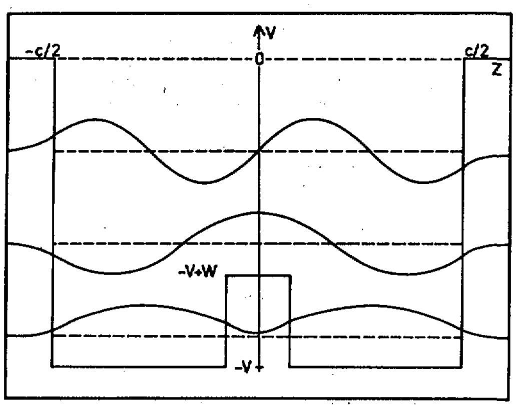

FIG. 1. The nuclear potential used for calculating the Z-components of the single-particle wave functions. Even ("gerade") wave functions for energies below and above the central barrier W and an odd ("ungerade") wave function for an energy above the barrier are shown.

representative nuclei. A cylindrical box potential is used with infinitely high walls. It is determined by the ratio $q = a/c$ of diameter a and length c of the cylinder and by the volume of the box. The value of q is kept fixed for the various nuclei of Fig. 2; the volume is chosen to be proportional to the mass number A.

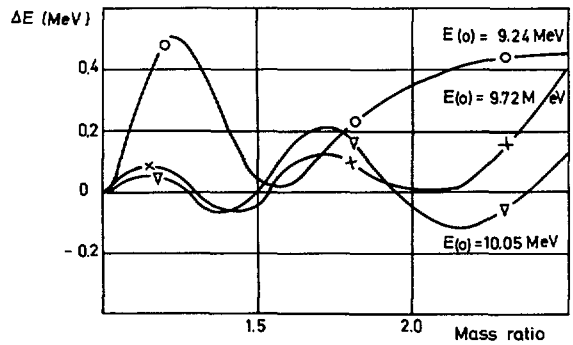

FIG.2. Difference $\Delta E = E(Z_0) - E(0)$ of the energies required to insert a small δ-barrier at the location $Z = Z_0$ and the central location $Z = 0$. Instead of Z_0, we plot the mass ratio $f(Z_0)$ on the abscissa. Curves are shown for ^{226}Ra (O), ^{236}U (×), and ^{246}Cf (∇). The single-particle potential $U^{(s)}$ is chosen to be a cylindrical box with infinitely high walls and $q = a/c = 0.354$. The energy E(0), i.e. number of particles in a central disc of thickness 1, is shown in the plot.

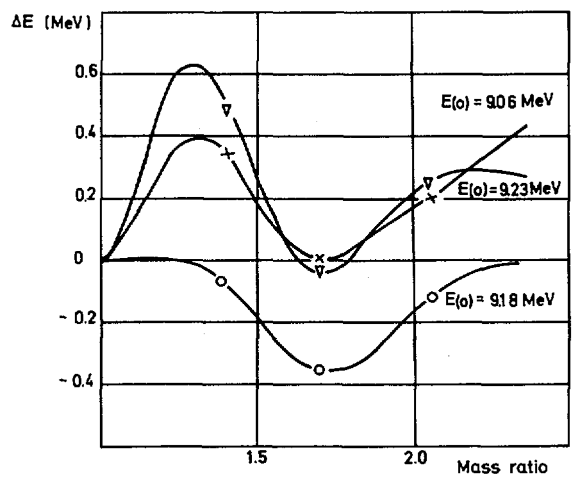

FIG.3. The same as Fig. 2, but for a cylindrical well of finite depth V = 45 MeV.

Figure 3 shows the same function for the case of a finite cylindrical well. The depth of the potential was chosen to be 45 MeV.

Figure 4 shows $\Delta E(Z_0)$ for the one nucleus (^{236}U) but for different shapes q of a finite cylindrical box. The value E(0) is given for each curve in the figure.

In all our plots the strength constant C_0 is equal to 1 MeV $\cdot 10^{-13}$ cm. As a consequence, the quantity $E(Z_0)$ is directly equal to the average number of nucleons in a disc perpendicular to the Z-axis and of thickness of 10^{-13} cm around Z_0. $\Delta E(Z_0)$ gives the difference between the average number of particles in a disc at Z_0 compared to a disc at the nuclear centre $Z_0 = 0$.

The results show generally a competition between a symmetrical ($Z_0 = 0$) and an asymmetrical ($Z_0 \neq 0$) solution. The results of the model depend strongly on the shape q of the potential and less strongly on the particle number A. This is to be expected, because the number of "gerade" and "ungerade" states is a function of the nuclear shape.

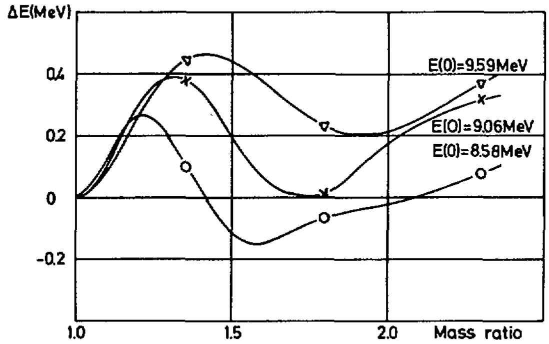

FIG. 4. Difference $\Delta E = E(Z_0) - E(0)$ as a function of the mass ratio $f(Z_0)$ for different shapes q of a finite cylindrical well (V = 45 MeV): g = 0.316 (O), 0.354 (X), 0.388 (∇). The mass number (^{236}U) is kept fixed.

For a potential with infinitely high walls the density fluctuates more strongly as a function of Z than in the case of a finite potential. As a consequence, our model may exhibit more than one asymmetric solution. This undesirable feature disappears for the case of the finite potential (compare Figs 3 and 2).

The mass ratios predicted by the model are of reasonable magnitude. The shape q of the cylindrical potential could, of course, be adjusted for each nucleus so as to give the correct value of the most probable mass division (see Fig. 4). This would not be meaningful as long as we discuss a primitive box potential without spin-orbit coupling.

If the nucleus at the saddle point or at a strongly deformed metastable state is dumb-bell shaped, we describe the central neck by reducing the depth of the potential by a quantity W in the central region. The single-particle densities $\rho_i^{(s)}(Z)$ of odd states continue to be zero at $Z = 0$. If the energy $\epsilon_{\nu_1}^Z$ of an even single-particle state is lower than the height W of the barrier the corresponding single-particle density $\rho_{\nu_1}^{(s)}(Z)$ has a minimum at $Z = 0$ (see Fig. 1). Therefore, not only the odd single-particle states but also the even states with $\epsilon_{\nu_1}^Z < W$ favour symmetrical mass division [1]. The total single-particle energies ϵ_ν for a cylindrical box potential are composed of the contribution $\epsilon_{\nu_1}^Z$ in Z-direction and the energy $\epsilon_{\nu_2,\Lambda}$ in the ρ and φ-directions (Z, ρ, φ = cylindrical co-ordinates)

$$\epsilon_\nu = \epsilon_{\nu_1}^Z + \epsilon_{\nu_2,\Lambda}$$

The quantum number Λ is the Z-component of the orbital angular momentum and ν_2 counts the number of nodes in ρ-direction.

The smaller the energy $\epsilon^Z_{\nu_1}$ in Z-direction, the more frequently it occurs as a contribution to an occupied level ϵ_ν. Thus, because of the high degeneracy of low-lying $\epsilon^Z_{\nu_1}$, even a small reduction W of the central depth should have a strong influence on the results of our model.

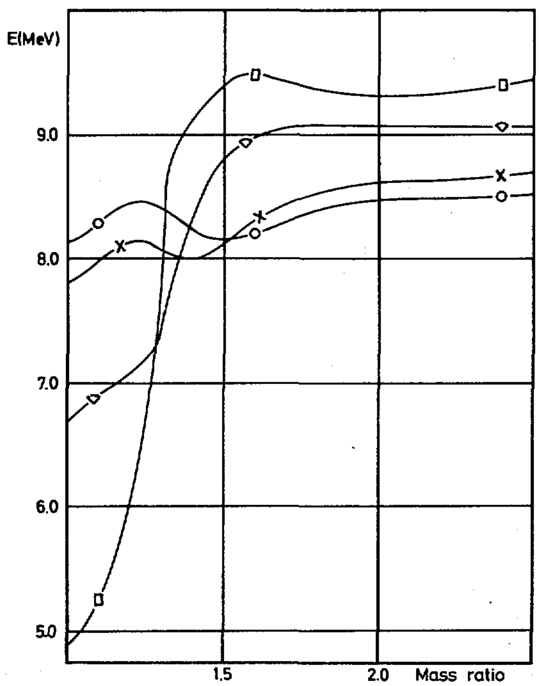

FIG.5. Energy $E(Z_0)$ as a function of the mass ratio $f(Z_0)$ for a finite cylindrical well (V = 45 MeV) with its central depth reduced by different amounts W. The curves have been calculated for q = 0.316 and ^{226}Ra. The following values of W were used: W = 0 (○), W = 1 MeV (×), W = 5 MeV (♡) and W = 10 MeV (□). The width of the central barrier was 0.2 · c i.e. 20% of the length of the nucleus.

This is indeed borne out by the numerical results presented in Fig. 5. Here, the energy $E(Z_0)$ for ^{226}Ra is shown as a function of the mass ratio $f(Z_0)$ for different values W of the central depth. The ratio q is kept fixed: Even a small reduction of the central depth leads to a strong preference of symmetric mass division.

Let us summarize the results: For the case of simple cylindrical wells, our model predicts in general a competition between symmetric and asymmetric mass division. The mass ratios depend rather sensitively on the nuclear shape and have a reasonable magnitude.

For the case of dumb-bell-shaped nuclei, our model predicts symmetric fission, even for rather gentle central necks. It thus offers a simple explanation for the sudden transition from asymmetric to symmetric fission as one passes from cylindrical to dumb-bell-shaped nuclei.

A very important feature of asymmetric fission is the stability of the heavy mass peak near m_H = 135. So far, we have applied the model only for potentials without spin-orbit coupling which therefore do not predict the correct magic numbers. Furthermore, we chose the potentials to be symmetric against reflection at a central plane perpendicular to the nuclear symmetric axis. In this simple case, we cannot hope to obtain quantitatively meaningful mass ratios.

The validity of our model, therefore, depends upon what it will predict when more realistic shell-model potentials are available for the description of the saddle point or a metastable shape isomer near the saddle point.

It is very likely that the model can only predict a strong preference for asymmetric fission if the nucleus displays already a certain asymmetry at the saddle point or at some metastable state close to it.

REFERENCES

[1] DIETRICH, K., Z. Phys. 214 (1968) 503.
[2] COHEN, S., SWIATECKI, W.J., Ann. Phys. (N.Y.) 22 (1963) 406.

DISCUSSION

C. SYROS: I would like to observe that a very important feature of your model is the δ-function barrier. This barrier has the peculiar property of actually attracting all nucleons in a plane perpendicular to the Z-axis at the point $Z = Z_0$. Furthermore, this density distribution (disk) does not change if you take a positive or negative δ-function barrier. There are also other similar models, for example, Professor Greiner's model, which, however, assumes a break of the "disk" rather than division of it by a plane perpendicular to the Z-axis. Can you please comment on this?

K. DIETRICH: When I spoke of the average number of particles in a disk of unit thickness around Z_0 and perpendicular to the symmetry axis, I just wanted to interpret formula (3).

The fact that the wave-functions are not affected by the δ-barrier is due to our treating the δ-barrier in the lowest order of perturbation theory.

U. MOSEL: As a comment on Professor Dietrich's paper, I would like to mention that, as indicated by Dr. Syros, a similar calculation but with a barrier of finite dimensions has been performed by P. Holzer, W. Greiner and myself (to be published). Our model consists of two touching oscillator potentials which just lead to this energy barrier at the Z = 0 plane. In an an earlier paper (Z. Physik 222 (1969) 261, section 5) we have shown that the difficulties which arise in the pure microscopical Nilsson- type single-particle calculations, namely the increase of the total energy at large deformations, come from the strong increase of the quantum-mechanical zero-point energy at large deformations. This is a direct consequence of the restriction to one-centre potentials only. A barrier at Z = 0 in the potential changes this quite drastically and, we have, in fact, shown that our two-centre potential gives the right qualitative behaviour of the potential-energy surface at large deformations. A two-centre potential has, furthermore, the advantage that it can describe the ground state of the fissioning nucleus as well as that of the two separated fragments and has, therefore, the correct physical boundary conditions for the whole fission process. In our model we obtain the wave functions analytically by a matching procedure. These two-centre functions can therefore serve as an excellent basis for further studies of the more refined (Saxon-Wood type) two-centre potentials.

INFLUENCE OF SHELL ENERGY ON THE DYNAMIC MODEL OF ASYMMETRIC FISSION

R.W. HASSE *
Physikalisches Institut der Universität Würzburg,
Würzburg, Federal Republic of Germany

(Presented by E. Hilf)

Abstract

INFLUENCE OF SHELL ENERGY ON THE DYNAMIC MODEL OF ASYMMETRIC FISSION. The recently investigated dynamic model with a shell correction added to the liquid-drop potential allows the low-energy fission process of heavy nuclei to be described. The shell-correction term was taken to be the sum of the Myers and Swiatecki shell energies of two clusters in the compound nucleus undergoing fission, multiplied by an arbitrary attenuation factor which is equal to unity at the scission point and vanishes approximately at the saddle point.

In this paper, the influence of the shell-energy correction term is studied, with special reference to the effect of its attenuation factor on results such as the mass distribution. For a vanishing shell correction the mass distribution is symmetric, whereas a full shell correction (attenuation factor equal to unity everywhere) yields the most asymmetric mass distribution.

DESCRIPTION OF THE MODEL

In a paper entitled "Studies in the Liquid-Drop Theory of Nuclear Fission," Nix and Swiatecki [1] have shown how to calculate some experimentally well known fission distributions, such as fragment mass and kinetic energy distributions. In their method, it is necessary to parametrize the nuclear surface, and to construct a liquid-drop potential, which, in general, consists of surface and Coulomb energies. A liquid-drop kinetic energy is also required, and is obtained by the assumption of ideal hydrodynamic flow of nuclear matter. The classical Hamiltonian of the system (consisting of the sum of the potential and the kinetic energies) is constructed, and the equations of motion are solved. The calculations are carried out with various initial values of the generalized coordinates (which specify the nuclear surface) and their time derivatives. The way in which the system reaches the saddle point from the ground state is not relevant and it is sufficient to follow the motion from the saddle point to the scission point and to configurations of widely separated fragments. If the potential energy is sufficiently smooth in its dependence on the various coordinates, the final distributions can be obtained by solving equations of motion for some particular values of the generalized coordinates, and by using the results to determine correlations between initial and final values of the coordinates. With such correlations it is possible to transform initial distributions into final ones.

Unfortunately, however, the calculations predict mass distributions peaked at symmetry, and the method is, therefore, applicable only to symmetric fission cases, i.e., to the fission of nuclei lighter than

* Present address: Oak Ridge National Laboratory, Physics Division, Oak Ridge, Tenn., USA.

radium or to the fission of heavier nuclei at high excitation energies. This limitation is due to the fact that the liquid-drop model intrinsically favors symmetric configurations [2] and it is likely that asymmetric fission results from shell structure effects [3].

To make this dynamic model also applicable to the low energy fission of heavy elements, we have added a simple shell-energy term to the liquid-drop potential and carried out the calculations [4] as described above. In addition to the shell energy term, we have also included a curvature energy [5] in the liquid drop potential. Unfortunately, shell energies based on single particle levels in highly deformed nuclear potentials are now known. We have, therefore, made use of a modified form of the Myers and Swiatecki [6] shell energy which is based on the sequence of magic numbers. It also contains a phenomenological attenuation factor to allow for nonspherical ground states.

Our modification consists of making the Myers and Swiatecki shell energy, which vanishes near the saddle point, applicable to the region beyond the saddle and to the vicinity of the scission point. This was achieved by defining two "clusters" in the nucleus undergoing fission. The proton and neutron numbers of the clusters are Z_H, Z_L and N_H, N_L respectively, where subscripts H and L refer to heavy and light clusters. We now have assumed that in the region between the saddle and the scission point, the sum of the shell energies of the clusters applies, multiplied by an arbitrary attenuation factor. Thus the definition of the total shell energy is as follows:

$$E_{shell} = \left\{ E_{MS}(N_H, Z_H) + E_{MS}(N_L, Z_L) \right\} \begin{cases} \exp(-bZ_2/R_o) & \text{pre-scission} \\ 1 & \text{post-scission} \end{cases}$$

In this equation the attenuation factor, $\exp(-bZ_2/R_o)$, contains the constriction coordinate Z_2 of the parametrization of the nuclear surface in cylindrical coordinates, and a semiempirical constant b which is discussed below, $R_o = r_o A^{-1/3}$ is the radius of a sphere of equal volume. The cylindrical parametrization of the nuclear surface is given by [4] :

$$F^2(Z) = R_o^3 \lambda \left\{ Z_o^2 - (Z+Z_s)^2 \right\} \left\{ Z_2|Z_2| + (Z+Z_S-Z_1)^2 \right\}$$

where Z_o is the elongation coordinate (half of the total length), and Z_1 the asymmetry coordinate which describes deviations from reflection symmetry about the plane Z = 0 and is related to the mass ratio of the fragments. The constriction coordinate Z_2 was mentioned above, the factor λ guarantees volume conservation, and Z_S shifts the center of mass to Z = 0. The total shell energy defined above also vanishes approximately at the saddle point ($Z_2 \approx 1.5\ R_o$). It includes the Myers and Swiatecki shell energies of the scission point fragments ($Z_2 = 0$) and of separated fragments ($Z_2 < 0$).

RESULTS AND DISCUSSION

In our case, the potential energy surface has too much structure to allow the establishment of simple correlations between initial and final coordinates. We have, therefore, applied the Monte-Carlo method by starting at the saddle point with random initial values and then generating the required final distributions. At the saddle point, the three modes of elongation, constriction, and asymmetry are converted into normal modes by means of the method of small oscillations. This yields two oscillator modes, <u>asymmetry</u> and <u>vibration</u>, and one <u>fission</u> exponential mode arising from the fission barrier; their normal coordinates are called η_A, η_V, and η_F, respectively [4].

Let us first review the results for the reaction $^{235}U(n_{th},f)$ with an intermediate value of the attenuation constant b = 1. The mass distribution of 100 events can be seen in Fig. 1. It shows a clear peak in the neighborhood of the doubly magic heavy fragment $^{132}_{82}Sn_{50}$. This nucleus is energetically favored by the Myers and Swiatecki shell energy. The shell energy used in this calculation (i.e., the sum of the Myers and Swiatecki shell energies of the clusters or fragments) does not take any interaction between the nuclear potential wells of the clusters or of the fragments into account. Maybe, this is the reason that not the experimental most probable mass A_H = 140 is yielded. We hence see that calculations involving a realistic potential of a highly deformed nucleus (which automatically includes the interaction between the two clusters or fragments) are of great importance at present.

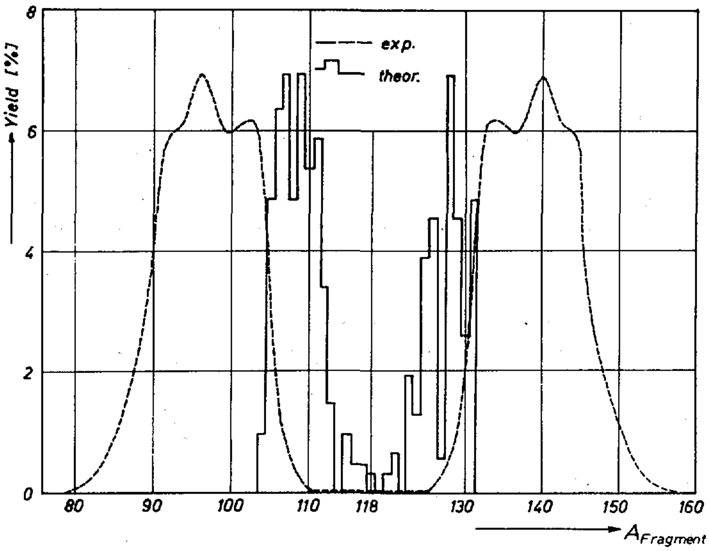

FIG. 1. Theoretical (solid line) and experimental [7] (dashed line) mass yield curves of the fission of ^{235}U with thermal neutrons. The histogram in the light-fragment region was obtained by rounding off the resulting A values to the nearest whole number, while the histogram in the heavy-fragment region was obtained by rounding the proton and neutron numbers individually. The theoretical distributions have been normalized to equal peak height with the experimental distribution. The attenuation constant is b = 1.

In Fig. 2, the total and individual fragment kinetic energies are shown as a function of fragment mass. These have been obtained in the usual way: After the integration is stopped a short time following scission, the kinetic energy of motion is divided into translational kinetic energy of the center-of-mass and the vibrational kinetic energy of the fragments. The total kinetic energy of the fragments at infinite separation is then obtained by adding the fragment translational kinetic energy obtained above to the Coulomb-interaction energy. The calculated distributions agree rather well with the experimental results [7].

Let us now discuss the dependence of the most probable mass on the arbitrary attenuation constant b. In Fig. 3, the attenuation factors, exp $(-b\,\zeta_2)$, are plotted for various values of b. The parameter ζ_2 is defined by $\zeta_2 = Z_2/R_0$. These attenuation factors determine the way in which the total shell energy of the nucleus increases between its saddle and scission configurations. Thus b = 0 means that the total shell energy

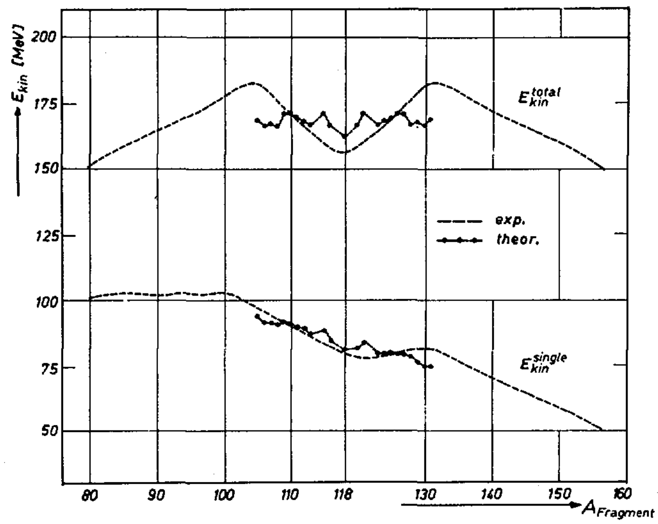

FIG. 2. Theoretical (solid lines) and experimental [7] (dashed lines) distributions of the mean total (upper curve) and mean individual (lower curve) kinetic energies of the fragments at infinity for the thermal neutron-induced fission of ^{235}U. The attenuation constant is b = 1.

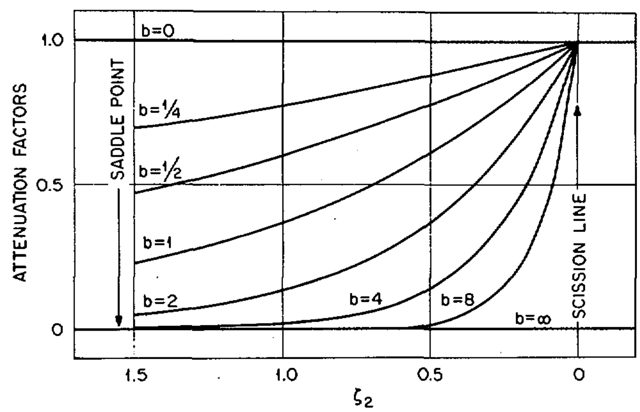

FIG. 3. Attenuation factors of the total shell energy from saddle to scission for various b-values. Here, $\zeta_2 = Z_2/R_0$ is the dimensionless construction co-ordinate.

consists of the full sum of the Myers and Swiatecki shell energies of the clusters or fragments, while b = ∞ means that there is no shell energy at all. In Fig. 4, the most probable values of the asymmetry coordinate $|\xi_1| = |Z_1|/R_0$ and the most probable heavy masses A_H are shown for various sets of initial values of the normal coordinates and velocities (η_F, η_A, η_V, $\dot{\eta}_F$, $\dot{\eta}_A$, $\dot{\eta}_V$), plotted versus the attenuation constant b. For example, Section (4) shows the results for initial values of 0.1 of the fission and asymmetry coordinates and for an initial velocity of 0.1 in the asymmetry direction. The lowest section, (7), gives the average over all other six sets. From the figure it can be seen that the value of the resulting most

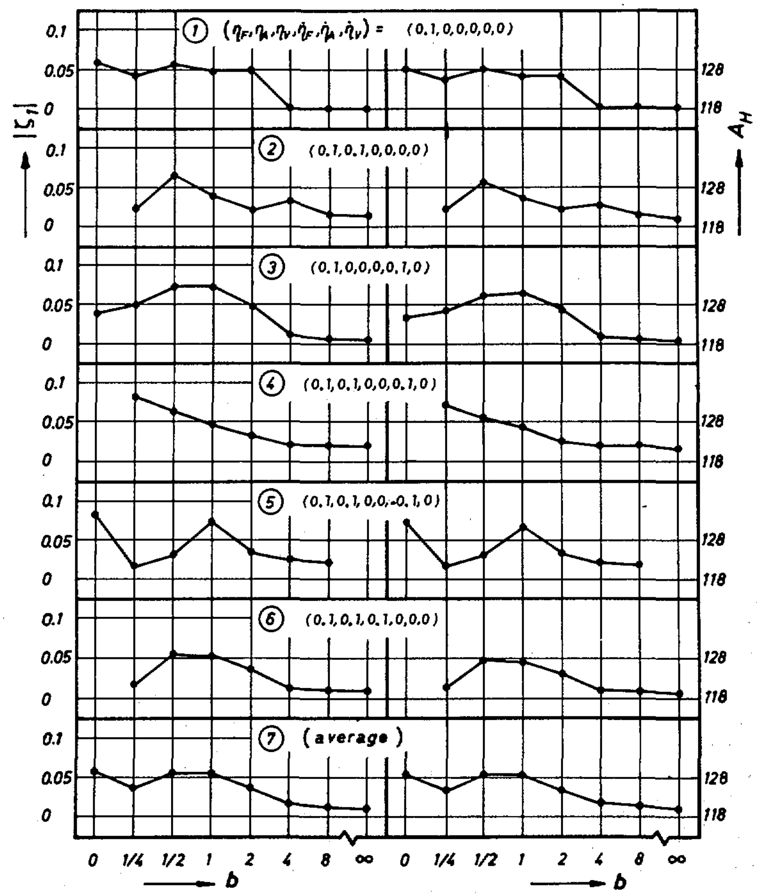

FIG. 4. The most probable asymmetry co-ordinates $|\zeta_1| = |Z_1|/R_0$ and heavy-fragment masses A_H a short time after fission, plotted versus b. The figures in parentheses in each section of this figure indicate the initial values of the normal co-ordinates and normal velocities.

probable mass appears to be very sensitive to changes of b in the region $0 \leq b \lesssim 0.75$. These apparent fluctuations are, however, caused by poor statistics (only six events have been considered) and no strong trend can be established. On the other hand, for larger b-values, there is a systematic fall-off of the most probable mass for all sets of initial conditions, leading as expected, to the symmetric value of $A_H = 118$ for $b \to \infty$ (no shell energy). The results of Fig. 4 show that there appears no heavier most probable mass than about 132 for any b-value. Thus the influence of the doubly magic nucleus ^{132}Sn is overestimated by our treatment of the total shell energy. This is probably due to the absence of any interaction between the two clusters or fragments. The distributions of the total kinetic energies are insensitive to changes in b because of the small absolute value of the total shell energy ($\approx$ - 2 MeV at the scission point).

Finally, we would like to make a few remarks about the times involved. The time required for the system to descend from saddle point to

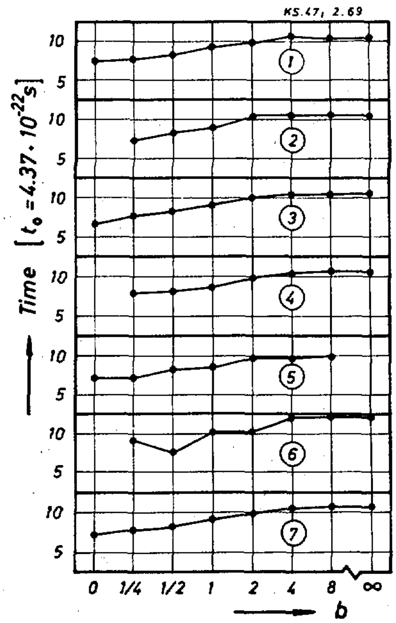

FIG. 5. The scission times in natural units of $t_0 = 4.37 \times 10^{-22}$ s, plotted versus b. The inital conditions of each section are the same as in Fig. 4.

scission decreases from $5 \cdot 10^{-21}$ to $3 \cdot 10^{-21}$ sec as b decreases from ∞ to 0, (see Fig. 5). The reason for this effect is that as the total shell energy increases with decreasing b the canal-like perturbations of the smooth liquid-drop potential become deeper. Thus the path of the nucleus becomes more and more restricted and it has less freedom to oscillate in the total potential. This results in a net decrease of transit time.

The calculations described above, carried out with the simplified total shell energy, are only the first step towards obtaining a description of the fission process of heavy elements with low excitation energies, but they show that most probable fragment mass divisions which are asymmetric can be predicted, and that experimentally known quantities can be reproduced. Hopefully, the experimentally determined most probable value of A_H of 140 for the neutron-induced fission of ^{235}U can be reproduced theoretically by making use of a more realistic shell energy.

REFERENCES

[1] NIX, J. R., SWIATECKI, W. J., Nucl. Phys. 71 (1965)1; NIX, J. R., Nucl. Phys. A130 (1969) 241.
[2] BUSINARO, U. L., GALLONE, S., Nuovo Cimento 1 (1955) 629; 1 (1955) 1277; 5 (1957) 315.
[3] DICKMANN, F., DIETRICH, K., Nucl. Phys. A129 (1969) 241.
[4] HASSE, R. W., EBERT, R., SÜSSMANN, G., Nucl. Phys. A106 (1968) 117; HASSE, R. W., Nucl. Phys. A118 (1968) 577; Phys. Lett. 27B (1968) 605; Nucl. Phys. A128 (1969) 609.
[5] GROOTE, H. v., HILF, E., Nucl. Phys. A129 (1969) 513.
[6] MYERS, W. D., SWIATECKI, W. J., Nucl. Phys. 81 (1966) 1; UCRL-11980 (1965); Ark. Phys. 36 (1967) 343.
[7] SCHMITT, H. W., NEILER, J. H., WALTER, F. J., Phys. Rev. 141 (1966) 1146.

DISCUSSION

E. R. H. HILF: Having presented Dr. Hasse's paper, I wish now to make some observations of my own. The main discrepancies between the experimental results and those of the dynamical model in the version presented are: (1) The heavy fragment mass distribution does not peak at the experimentally observed $A \approx 140$ but at $A \approx 128$-118, depending on the value of the attenuation factor. I do not think that this discrepancy is due to the neglected nuclear interaction of the two clusters, but to the fact that the magic numbers seem to be shape-dependent, as is known from Strutinsky's work; (2) The experimental hump at symmetric fission of the total kinetic energy is not reproduced by the model. This results, in my view, from neglecting the polarization of the two fragments by the interacting nuclear and Coulomb forces. With regard to the latter, S. Trepulka has shown that this can be a considerable effect, ranging up to several MeV.

The decrease of fission time with increase in the shell correction term is a purely mechanical effect in that the shell term digs a valley into the potential surface, so that the nucleus gains additional kinetic energy whenever it passes through the "magic" valley. The turning points are more pronounced also because of the "anti-magic" ridges of the shell correction term used.

H. Ch. PAULI: With reference to Dr. Hasse's paper, I should like to point out that the shell energy does not disappear at larger deformation, contrary to what Myers and Swiatecki (Ref. [6] of the paper) assume.

E. R. H. HILF: The Hasse shell energy correction term does not contradict that of Myers and Swiatecki but is just the simplest adaptation of the latter for the high deformations between saddle and scission. For the saddle shape it is approximately zero and, in the case of two infinitely separated fragments assumed to be spherical, it is the same as the sum of the Myers and Swiatecki shell terms of the two fragments. Thus, for the border cases the two shell-correction terms are the same. The Myers and Swiatecki term itself is not applicable to, and was not meant to be a prediction for, higher non-ellipsoidal deformations. A reasonable shell correction term for highly deformed and constricted shapes has not been proposed so far. The calculation presented is worthwhile, since it shows in what way the dynamic model links a shell correction ansatz to the fragment properties (mass asymmetry, kinetic energies). So this method may serve as a test for any proposed shell-correction term. The results of the dynamical calculations suggest that there should be a constricted "magic" shape between the saddle and scission points containing 140-144 nucleons on the heavy side of the neck-in line.

H. Ch. PAULI: What is the connection between Hasse's work and that of Vandenbosch?

R. VANDENBOSCH: First of all, my work, which was done quite some time ago, did not consider any dynamics. In the notation of Hasse's work, b was taken to be a function of fragment mass. We can now do much better, as we now know that b is really an oscillatory function of fragment deformation as well as a function of mass.

H. Ch. PAULI: Lastly, what mass parameters did Dr. Hasse use? They should carry also some wiggles due to the nuclear shell structure.

E. R. H. HILF: The mass parameter is essentially a tensor, the elements of which are shape-dependent. All this information has been given by Hasse et al. in Ref. [4], working on the assumption of irrotational, frictionless, incompressible, hydrodynamical flow.

I agree with you that there should be wiggles due to the shell structure in the mass tensor too, but at the moment no ansatzes for this shell effect are known for the highly deformed and constricted shapes necessary for describing the fission process.

S. S. KAPOOR: Were the constants of the Myers-Swiatecki mass formula re-determined after the curvature correction had been incorporated into the surface energy?

E. R. H. HILF: Yes, of course. In fitting the ground-state masses, we take the curvature term as a correction to the surface term, since only near-spherical shapes are considered. So, taking a curvature tension into account, the surface tension is re-determined in such a way that the sum of both terms gives the same ground-state fit as with the surface term alone. A detailed consideration of the different actions of the curvature tension and surface tension is given in von Groote's paper (Ref. [5] of the paper). Thus, it is not possible to fit the ground-state masses and threshold energies simultaneously without taking account of the curvature tension, which affects not only the binding energy of highly deformed nuclei but also the saddle-point shape.

MASS AND CHARGE DISTRIBUTIONS IN FISSION

V.S. RAMAMURTHY, R. RAMANNA
Bhabha Atomic Research Centre, Trombay,
Bombay, India

Abstract

MASS AND CHARGE DISTRIBUTIONS IN FISSION. During the last stages of the fission process, the fissioning nucleus can be very well approximated by two nuclei in close proximity, and the Hamiltonian of the system at this stage can be written as the sum of the Hamiltonians of two independent nuclei and a time-dependent interaction term. The wave function of the fissioning nucleus at any instant can be expanded in terms of base states, each representing a given mass configuration of the nascent fragments. The non-diagonal elements of the energy matrix in this representation give the probability that the fissioning nucleus goes from one base state to another. When the nascent fragments are sufficiently apart as to give a vanishingly small interaction term, changes in the mass configuration are not possible. This quantum-mechanical description of the division process is analogous to a classical stochastic process where the state space corresponding to the transition probabilities is given in terms of the non-diagonal elements of the energy matrix and the statistical weights associated with the transitions. In the present model, the authors have simplified the description by replacing the time dependence with an average time-independent transition probability matrix. The final distribution of mass and charge is evaluated as the steady-state solution of the above stochastic process.

The probability of transition from one configuration to an adjacent configuration was calculated from the transmission probability of the last nucleon through the potential barrier separating the nascent fragments. The deformation of the nascent fragments for a given mass configuration was determined by the condition of potential energy minimization. The excitation energy of the nascent fragments is small and, on the average, assumed to be equally divided between all the nucleons.

It is shown that the asymmetric mass distribution in the low-energy fission of various heavy nuclei and the distribution of nuclear charge for fragments of given mass are well reproduced by using two adjustable parameters. The physical implications of these parameters are discussed.

1. INTRODUCTION

Studies of liquid-drop model of fission [1] have shown that the model in its present form is inadequate for a complete understanding of the fission process, especially the asymmetric distribution of fragment mass in the fission of heavy nuclei at low excitation energies. This inadequacy arises mainly as a result of neglecting the internal structure of the nucleus [2]. Attempts have been made [3] to include explicitly the internal structure of the nucleus in the description by a study of the single-particle levels in a deformed shell-model potential. The method acquires enormous mathematical complexity, once the fissioning nucleus crosses the saddle point, when it goes through a series of more complicated deformations (in contrast to the simple ellipsoidal deformations one distinguishes between the compound nucleus stage and the saddle point) and dynamical effects start playing an important role.

The statistical model of fission [4] exploits the very fact that the process is complex and asserts that the process is sufficiently quasi-static as to lead to statistical equilibrium among the various scission modes of the fissioning nucleus. In spite of the remarkable conceptual simplicity and a quantitative method of including shell effects into the formalism with essentially no free parameters, the model has not been investigated further, since the results are very sensitive to the input data, some of which are to be extrapolated out of the range of observation, and are thus subject to great arbitrariness.

In the present work it is shown that considerable simplification can occur in our understanding of the division process of the fissioning nucleus if one recognizes the fact that during the last stages of the process the fissioning nucleus can be very well approximated by two nearly independent nuclei in close proximity. In the semi-classical limit when one can separate the relative motion of the nascent fragments and the nucleon rearrangement among the fragments, the process can be treated as a stochastic process [5]. It is also shown that with certain simplifying assumptions regarding the interaction between the nascent fragments the observed distributions of fragment mass and charge in fission of a wide range of nuclei as well as their dependence on the excitation energy of the fissioning nucleus can be explained quite satisfactorily.

2. DESCRIPTION OF THE PRESENT MODEL

Near the initial compound nucleus stage and till the nucleus reaches the saddle point in the case of heavy nuclei, the Hamiltonian of the system has the simple form of that of a deformed nucleus. As the nucleus passes over the saddle point and starts descending the energy barrier towards the scission point, the process becomes more complicated. However, near the scission point, where the fissioning nucleus tends to divide into two fragment nuclei, certain simplifications take place. The Hamiltonian of the system can then be written as the sum of the Hamiltonians of two independent nuclei and an interaction term. The interaction term, in general, consists of a nuclear part plus the coulomb interaction between the nascent fragments. After the scission point, as the fragment nuclei start flying apart under the action of their mutual Coulomb repulsion,the nuclear part of the interaction term vanishes and ultimately the total Hamiltonian of the system is just equal to the sum of the Hamiltonians of two independent nuclei moving relatively to each other. A time description of the process can therefore be given as follows. In the beginning of the process, the nuclear potential as seen by a nucleon is that of a deformed nucleus. The shape of the potential then goes through a series of complicated shapes and during the last stages of the process an energy barrier develops separating two regions or clusters (the development of a neck in the language of the liquid drop model). However, as the barrier grows, continuous rearrangement of nucleons can take place between the two regions. Ultimately, when the fragments pass the scission point, the barrier is large enough to suppress all nucleon exchanges and as a result, the mass and charge of the nascent fragments can no longer change. If one makes the semi-classical approximation that the relative motion of the clusters is sufficiently slow compared to the characteristic time for a nucleon transfer, the probability for the transfer of a nucleon from one of the clusters to the other at any instant depends only on the configuration of the nucleus at that instant and is independent of the previous history of the fissioning nucleus. The process can therefore be treated as a stochastic one. Since the configuration of the nucleus is itself changing in time, the process is also to be treated as time-dependent.

We now make the assumption that the division process is quasi-static. That is, at each instant, as the deformation of the fissioning nucleus changes, a rearrangement of the nucleons inside the nucleus also takes place to leave the nucleus in its equilibrium state. This will imply that such simple thermodynamic criteria as the uniformity of temperature over the entire volume of the nucleus will apply. As the system approaches the scission point, it becomes more and more difficult to transfer mass from one nascent fragment to the other and the mass ratio approaches a constant value. The assumption of statistical equilibrium at all stages also implies that not only the fragments are in thermodynamic equilibrium within themselves, but also they attain mutual equilibrium among themselves with respect to nucleon and energy transfers. The observed distribution of fragment mass and charge should therefore correspond to the equilibrium distribution near the scission point. For a calculation of the final distribution of fragment mass and charge, we introduce the following simplifications:

(1) At any instant the condition of minimum potential energy is assumed to hold with respect to the shape of the nucleus. That is, near the scission point, for a given relative separation of the nascent fragments and given numbers of protons and neutrons on either side, the deformations of the fragment pairs adjust themselves to satisfy the condition of minimum potential energy. One can, therefore, define the configuration of the fissioning nucleus near the scission point by specifying the number of nucleons (protons and neutrons) on either side, the respective deformations of the fragments being uniquely defined.

(2) Since the nascent fragment pairs are in thermodynamic equilibrium till the scission point is reached, they should have the same temperature. The absolute value of the temperature depends on the available excitation energy for each configuration of the nucleus. With the above simplifications, the observed distributions of fragment mass and charge will be given by the steady-state probability distributions of the corresponding quantities with respect to nucleon transfers near the scission point.

3. EVALUATION OF THE STEADY-STATE PROBABILITY DISTRIBUTIONS

Let us assume, for the sake of illustration, that the nucleus consists of only one type of particles, the nucleons. Let us also neglect Coulomb effects. Then the configuration of the fissioning nucleus at any instant near the scission point can be defined by specifying the number of nucleons on either side. Let $\chi\ (M_H,\ M_L)$ be the configuration at instant t, M_H and M_L being the number of nucleons on the heavy and on the light side, respectively.

Let w_m be the probability that the fissioning nucleus has a configuration $\chi\ (m,\ M_0\ -\ m)$ where M_0 is the mass of the nucleus and m is the number of nucleons on the heavy side. Let $P_{m,n}$ be the probability that a configuration χ (m, M_0 - m) goes over into the configuration χ (n, M_0 - n) in a small interval of time. Then one has

$$w_n (t = t_0 + \Delta t) = \Sigma_m w_m (t = t_0) P_{m,n} \tag{1}$$

When steady state has been reached, we have

$$w (t = t_0 + \Delta t) = w (t = t_0) \tag{2}$$

Hence

$$w_n = \Sigma_m w_m P_{m,n} \tag{3}$$

If the unit of time Δt is sufficiently small, one can neglect multi-nucleon transfers, so that

$$P_{m,n} = 0 \text{ for } m \neq n, n \pm 1 \tag{4a}$$

$P_{m,m+1} = P_{L\to H}$ (m) .... probability of a nucleon transfer from the light to the heavy side in configuration m.

$P_{m,m-1} = P_{H\to L}$ (m) .... probability of a nucleon transfer from the heavy to the light side in configuration m.

In the case of symmetry one has also

$$\begin{aligned} w_{m_S-1} &= w_{m_S+1} \\ P_{m_S, m_S-1} &= P_{m_S, m_S+1} \end{aligned} \tag{4b}$$

Equation (3), together with the restrictions (4a) and (4b), yields

$$\frac{w_{m+1}}{w_m} = \frac{P_{m,m+1}}{P_{m+1,m}} \tag{5}$$

Thus, the ratio of the yields of fragments of mass m+1 and m is simply related to the nucleon transfer probability in the direction m $\to$ m+1 and the probability for inverse transfer.

An extension of the above arguments for the case when the nucleus consists of two types of particles (protons and neutrons) is simple and straightforward. A generalization of Eq.(2) in two dimensions gives

$$w_{t=t_0+\Delta t} (N, Z) = \sum_{N'} \sum_{Z'} w_{t=t_0} (N', Z') P_{N'Z', NZ} \tag{6}$$

The steady state solution of w is given by

$$w (N, Z) = \sum_{N'} \sum_{Z'} w (N' Z') P_{N'Z', NZ} \tag{7}$$

The probabilities w and P are also subject to the constraints

$$
\begin{aligned}
&\sum_N \sum_Z w\,(N,Z) && = && 1 \\
&\sum_N \sum_Z P_{N'Z',\,NZ} && = && 1 \qquad\qquad (8)\\
&P_{N'Z',\,NZ} && = 0 && \begin{matrix} N' \neq N,\ N \pm 1 \\ Z' \neq Z,\ Z \pm 1 \end{matrix}
\end{aligned}
$$

We have to solve Eq.(9) numerically to obtain the probability distribution w, provided the transition probabilities are known.

4. NUMERICAL EVALUATION OF THE NUCLEON TRANSFER PROBABILITIES AND THE RESULTS

Since the nucleons are Fermi particles, for zero excitation energy of the fragments the nucleons occupy an energy band up to a certain maximum energy, the Fermi energy. Let E_H and E_L be the Fermi energies for the heavy and the light fragments, respectively. If E_H is greater than E_L, it is seen that the direction of spontaneous transfer of nucleons is from the heavy to the light side. When the nascent fragments have some excitation energies, a tendency for a preferential transfer of nucleons in one direction persists, but to a lesser extent because of the more random population of the nucleon energy levels. An estimate of the relative probability of nucleon transfers in a given direction can be made by using the expressions

$$
\begin{aligned}
P_{L\to H} &\sim \int f_L(E)\, g_L(E)\, T_{L\to H}(E)\, g_H(E)\, [1 - f_H(E)]\, dE \\
P_{H\to L} &\sim \int f_H(E)\, g_H(E)\, T_{H\to L}(E)\, g_H(E)\, [1 - f_L(E)]\, dE
\end{aligned}
\qquad (9)
$$

$g_L(E)$ and $g_H(E)$ are the single-particle energy level densities in the light and heavy fragment, respectively. $f_L(E)$ and $f_H(E)$ are the Fermi-Dirac distribution functions, namely the probability that a quantum state with energy E is occupied in the light and heavy fragment, respectively. The net particle current from the light to the heavy fragment at an energy level E is equal to the number of particles in the light fragment $g_L(E)$ $f_L(E)$ times the number of available unoccupied states in the heavy fragment $g_H(E)\,[1 - f_H(E)]$ times the probability for a particle transfer from the light to an identical energy level in the heavy fragment. The total particle current for the nucleon transfer probability P is obtained by integrating over all nucleon levels.

The probability of nucleon transfer from one fragment to an identical energy level on the other may be assumed to be equal and independent of energy, i.e.

$$T_{L\to H} = T_{H\to L} = \text{constant}$$

For a numerical evaluation of the nucleon transfer probabilities from Eq.(10) one has to calculate g(E), the density of the single-particle energy levels in a nucleus, and f(E), the Fermi-Dirac distribution function.

The density of single particle levels g(E) depends on the nuclear model and is shell-dependent. If one regards the nucleus as an assembly of non-interacting Fermions confined to a given volume g(E) will be a simple function of E. If, however, one has taken account of nuclear shell effects, g(E) should be suitably modified to include the bunching of nucleon levels. In the present calculations, we make use of the Fermi gas model of a nucleus, in conjunction with a semi-empirical mass formula given by Myers and Swiatecki [6] to estimate the relative disposition of the nucleon energy levels in the fragment pairs.

Let us consider a nucleus of mass A containing N neutrons and Z protons. With respect to removal of particles, a nucleon with separation energy E_S can be assumed to have an energy $-E_S$ in the potential of the daughter nucleus. The separation energy of the last nucleon can be calculated using the semi-empirical nuclear mass formula. If the distribution of kinetic energies of the nucleons in the nucleus can be assumed to be that of an assembly of Fermions moving in a volume equal to that of the daughter nucleus, corrected suitably to include the bunching of levels, the depth of the potential well V is given by

$$V = V_0 + \Delta = -E_S - T_N$$

where V_0 is the depth of the average nuclear potential well, Δ is the rearrangement energy associated with the rearrangement of the particles in the daughter nucleus on the removal of the nucleon, and T_N is the kinetic energy of the last nucleon. From the calculated last nucleon separation energy and the kinetic energy, one can calculate V. The relative position of the other nucleon levels in the nucleus, can be calculated using this value of V assuming that the rearrangement energy Δ is the same for all particles. This assumption is valid because for low excitation energies only a few particles on the top of the Fermi sea take part in the transfers.

Two further corrections are also necessary in the above calculations. (1) In the case of protons, all proton levels are raised by an amount kZ' where Z' is the charge of the complementary fragment. An estimate of k can be made from the average kinetic energy of fission fragments. A value of k = 0.042 was used in the present calculations. Also because of the high Coulomb field in the region between the nascent fragment pairs, the transmission coefficient for proton could be less than that for neutrons. (2) Secondly, it is known that shell nuclei remain nearly spherical in the scission configuration and non-shell nuclei have a larger deformation. As a result of the deformation for non-shell nuclei, shell effects are assumed to have been washed out and also as a result of the deformation, there is an increase in the energy of particles in these nuclei. In the absence of an exact calculation of the deformation of these nuclei, it was assumed that the energies are increased by a constant C. C is treated as a parameter in the calculations. The Fermi-Dirac distribution function f(E) is given by

$$f(E) = \frac{1}{1 + e^{(E-\mu)/T}}$$

where μ is the chemical potential and T is the temperature of the fragment. μ is to be determined from the condition that the integral of f(E) g(E) over all energies should give the total number of particles. The assumption of statistical equilibrium between the fragment pairs implies equal temperature ture of the fragment pairs. We make the further assumption that one can represent the situation by an average temperature T for all fragment pairs. The transfer probabilities $P_{L\rightarrow H}$ and $P_{H\rightarrow L}$ were further weighted with factors $M_L^{\frac{1}{3}}$ and $M_H^{\frac{1}{3}}$, respectively, where M_L and M_H are the masses of the light and heavy fragments, in order to ensure a symmetric mass distribution in the absence of single-particle effects at high temperatures. Figures 1, 2 and 3 show some of the calculated distributions for some typical values of the parameters C and T.

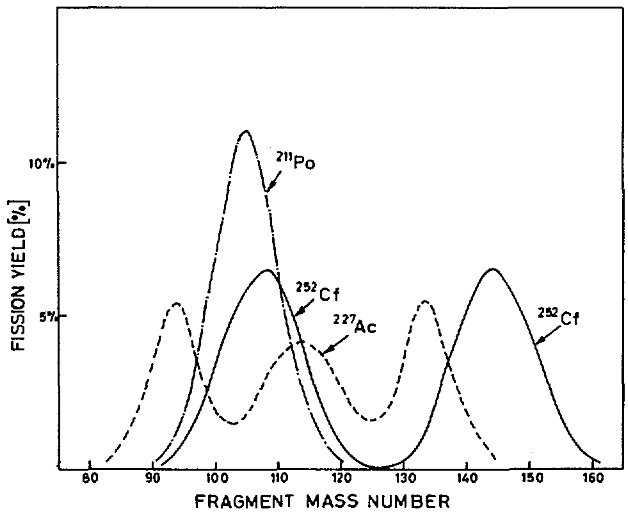

FIG.1. Calculated fragment mass yield curves for different fissioning nuclei.

———	^{252}Cf	Fission for C = 0.5	T = 1.0
-------	^{227}Ac	fission for C = 0.5	T = 3.0
-·-·-·-	^{211}Po	fission for C = 0.5	T = 3.0

5. DISCUSSION

It is seen that in spite of the drastic simplifications we have introduced in the assumed structure of single-particle levels in a nucleus as a function of the proton and neutron numbers and also its dependence on the deformation of the nucleus, most of the experimentally observed systematics in the distributions of fragment mass and charge in the fission of medium and heavy nuclei are well brought out by the present model. The pronounced asymmetry in the mass distribution of the case of low-energy fission of heavy nuclei arises as a result of the bunching of single-particle levels in the nucleus corresponding to different shell numbers. At higher excitation energies the mass asymmetry arising as

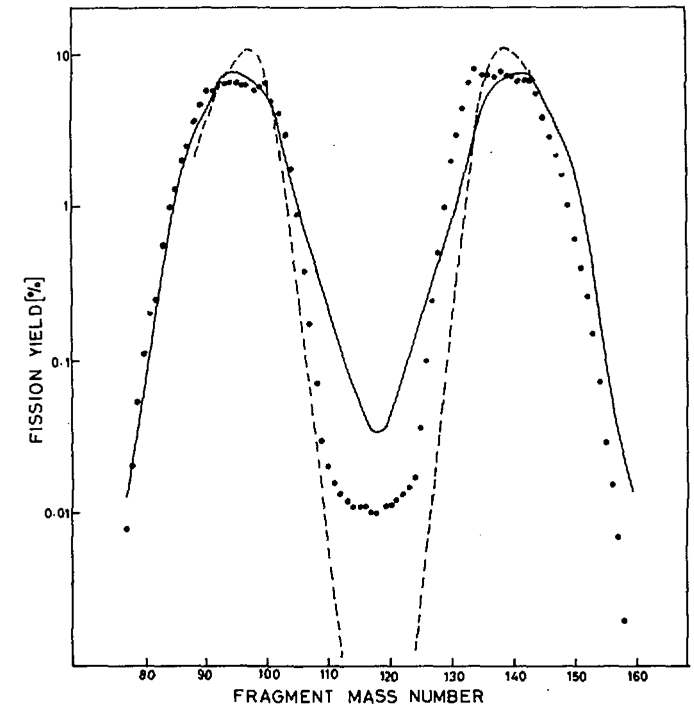

FIG.2. Calculated fragment mass yields in ^{236}U fission for two values of the parameter T.

C = 0.05 T = 1.0

C = 0.05 T = 2.0

Experimental yields in thermal fission of ^{235}U [8]

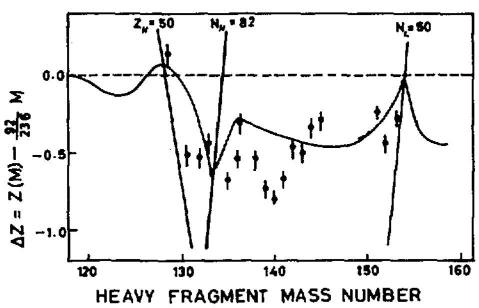

FIG.3. Experimental and calculated mean primary charge Z(M) in the fission of ^{236}U.

Calculated C = 0.5 T = 1.0

Experimental [9]

a result of the bunched single-particle levels is washed out as a result of the more random population of the levels in the pair fragments. These conclusions are in very good agreement with the qualitative speculations made by Nix [1] regarding the role of single-particle effects in fission dynamics.

Regarding the physical significance of the two parameters used in the calculations it has to be pointed out that no attempt was made to optimize them to give the best fit, because of the limited practical utility of such a procedure. The present calculations are only intended to bring out the essential validity of the model proposed. A more useful program will include the determination of the shape of the nascent fragment pairs near the scission point by a potential energy minimization calculation, similar to the work of Dickmann and Dietrich [7]. Such a calculation will also provide the relative disposition of the single-particle energy levels in the fragment pairs, and the present model can then be used to calculate the fragment mass and charge distributions.

The values T = 1 to 3 used in the present calculations are higher than the values expected on the basis of fragment excitation energies. For T ~ 0.5, the present calculations predict a very high asymmetry. This discrepancy can arise as a result of our simplifying assumption that all nuclei near the shell region retain their full shell strength near the scission point. It is, however, known that even these nuclei have some deformation near the scission point and hence are expected to have a reduced shell strength. This assumption will also account for the arbitrary normalization which we have made to ensure a symmetric mass distribution for high temperatures. The present calculations, however, demonstarte that if we start from the assumption of statistical equilibrium near the scission point, it is possible to understand the fission process satisfactorily. The present model differs from the traditional statistical model of Fong in that we include the dynamical effects and employ a different method of evaluating the equilibrium distribution without having to use many arbitrary parameters.

ACKNOWLEDGEMENT

Our thanks are due to Dr. S.S. Kapoor for many helpful discussions during all phases of the work.

REFERENCES

[1] NIX, J.R., Nucl. Physics A130 (1969) 241.
[2] HASSE, R.W., Nucl. Physics A128 (1969) 609.
[3] STRUTINSKY, V.M., Nucl. Physics A95 (1967) 420.
[4] FONG, P., Phys. Rev. 102 (1956) 434.
[5] RAMANNA, R., Phys. Lett. 10 (1964) 321;
RAMANNA, R., SUBRAMANIAN, R., RAJU, N. AIYER, Nucl. Physics 67 (1965) 529.
RAMANNA, R., RAMAMURTHY, V.S., Physics Lett. 21 (1966) 437.
[6] MYERS, W.D., SWIATECKI, W.J., Nucl. Physics 81 (1966) 1.
[7] DICKMANN, F., DIETRICH, K., Nucl. Physics A129 (1969) 241.
[8] FARRAR, H., TOMLINSON, R.H., Nucl. Physics 34 (1962) 367.
[9] WAHL, A.C., FERGUSON, R.L., NETHAWAY, D.R., TROUTNER, D.E., WOLFSBERT, K., Phys. Rev. 126 (1962) 1112.

DISCUSSION

P. ARMBRUSTER: Did you calculate the width of the charge distribution? This quantity depends to a considerable extent on the level density and temperature used, and would be a good additional test for the agreement of your calculations with the experimental results.

V.S. RAMAMURTHY: The present calculations give a width of about 1.2 charge units for the charge distribution for a given mass. In view of the approximations in our numerical calculations, no further detailed study of the distribution width was made.

J.J. GRIFFIN: One might have expected A = 132 to be predicted as the most probable fragment mass, when shell effects are incorporated in the manner you describe. Can you say what feature of the calculation leads to the prediction that the most probable fragment mass is sometimes greater than A = 132?

V.S. RAMAMURTHY: The most probable fragment mass will indeed be $A \approx 132$ if the temperature of the fragment pairs is assumed to be very small or zero. When the temperature of the fragment pairs is not very small, the peaking near $A \approx 132$ is less exact and the reduction in the nuclear separation energy in the light fragment due to the latter's deformation tends to shift the peak towards higher masses.

THEORY OF MASS YIELDS, KINETIC ENERGIES, AND FRAGMENT EXCITATION ENERGIES AS FUNCTIONS OF THE COMPOUND EXCITATION ENERGY

W. NÖRENBERG
Institut für Theoretische Physik,
Universität Heidelberg,
Federal Republic of Germany

Abstract

THEORY OF MASS YIELDS, KINETIC ENERGIES, AND FRAGMENT EXCITATION ENERGIES AS FUNCTIONS OF THE COMPOUND EXCITATION ENERGY. A first step towards a unified theory of fission is proposed in a simple model which allows the mass yield, the kinetic energies, and the fragment excitation energies to be described as functions of the compound excitation energy. The main assumptions of this model are: (1) a full statistical equilibrium of all degrees of freedom at the saddle point, and (2) strong coupling between collective degrees of freedom and weak coupling to non-collective degrees of freedom on the way from saddle to scission. The dependence of the various features of fission on the compound excitation energy comes in through the number of quasi-particle (qp) excitations at the saddle point and the collective temperature which characterizes the assumed statistical equilibrium of the collective degrees of freedom at the scission point.

In particular the so-called molecular model of fission is used. In this model the compound nucleus is described by two interacting fragments. The centre-to-centre distance of the fragments is assumed to be large enough to treat the compound nucleus as a "molecule" bound by the outer nucleons. From the above assumptions for the motion from the saddle to the scission point the eigenenergies of the mass-asymmetry motion are a linear function of the number of (qp)-excitations at the saddle point. From a simple Boltzmann distribution one obtains the energy dependence of the ratio of symmetric-to-asymmetric mass yield. This ratio increases with increasing compound excitation energy. The mean kinetic energies of the fragments are determined by the Coulomb energy at the scission point. The scission-point distance depends on the deformability of the fragments which, in turn, is a function of the number of quasi-particle excitations. The difference of the mean kinetic energy at two different compound excitation energies turns out to be approximately zero for symmetric fission and linear in the difference of the number of (qp)-excitations for asymmetric fission. For increasing compound excitation energies the mean kinetic energies of the fragments in asymmetric fission decreases. The loss in kinetic energy mainly appears as excitation energy of the heavier fragment which is nearly magic.

The dependence of the mean number of (qp)-excitations on the compound excitation is explicitly given in a simple statistical model of level densities. Some experimental data are analysed according to the theory and found to be in rather good agreement with the theory.

1. INTRODUCTION

Several experiments [1-8] (for a review see Ref. [9]) deal with the dependence of fission properties on the excitation energy of the compound nucleus. The main results of these experiments are:

(a) The ratio of symmetric-to-asymmetric mass yield increases with increasing excitation energy.

(b) The mean kinetic energy of the fragments decreases with increasing excitation energy for mass splits with one fragment near magic ^{132}Sn.

(c) The energy which is lost as kinetic energy appears mainly as excitation energy of the near magic fragment.

These effects have been most frequently discussed in terms of two modes of fission, the liquid-drop mode for the symmetric component and the asymmetric mode which is dominated by the shell structure of the fragments. It is desirable to develop a theory which can explain the experiments in a more unified way including the possibility of a two-component mechanism. In this paper, a first step towards a unified theory of fission is proposed and tested by the experimental results on the dependence of mass yield, kinetic energies, and fragment excitation energies on the compound excitation energy.

The most frequently used models of fission are the adiabatic and the statistical models (for a review see Wilets [10]). The adiabatic model (the liquid-drop model is a semi-phenomenological approach to this model) is characterized by the assumption that the single-particle motion follows the collective motion adiabatically. This assumption is valid if the collective motion is slow compared to the single-particle motion. From liquid-drop model calculations (see Ref.[11]) one obtains 10^{-21} to 10^{-20} s for the time which is needed by the compound system to get from the saddle to the scission point. A rather opposite assumption is made by Fong [12] in the statistical model. Fong postulates strong mixing of all (collective and non-collective) degrees of freedom. It seems to be likely that the fission process is somewhere in between the two opposite assumptions. Therefore, to increase our understanding of the fission mechanism, we have to weaken the assumptions in both models. In the adiabatic model we have to take non-collective degrees of freedom into account (that means at least viscosity in the liquid-drop model), and in the statistical model we have to study the consequences of an incomplete statistical equilibrium. The adiabatic model seems to be more general and, therefore, more suited as a basis for the understanding of fission than the statistical model.

The purpose of this paper is to show how the introduction of non-collective degrees of freedom in a simple "almost adiabatic" model leads to a description of the experiments mentioned above. The experimental facts turn out to be mainly related to the number of quasi-particle (qp) excitations at the saddle point. In section 2 a simple model is introduced where collective and non-collective degrees of freedom are incorporated. Then, from plausible assumptions the mass yield, the mean kinetic energies, and the fragment excitation energies as functions of the mean number of (qp)-excitations at the saddle point are derived in sections 3, 4, and 5, respectively. In section 6 the dependence of the mean number of (qp)-excitations at the saddle point on the compound excitation energy is discussed in some detail to obtain the ratio of symmetric-to-asymmetric mass yield, the mean kinetic energies, and the fragment excitation energies as functions of the compound excitation energy. In section 7 the theory is compared with experiments.

2. THE MODEL

Before discussing the fission process at higher excitation energies, let us first consider the low-energy fission when the compound nucleus has practically no excitation energy at the saddle point. If we are concerned with the case of a two-hump barrier [13] the second barrier maximum should be called the saddle point in connection with the following discussion. At the saddle point the excitation energy of the compound nucleus is converted into deformation energy. In the calculation of mean primary charges and moments of inertia, the molecular model of fission [14, 15] has been considered most suited for a discussion of the fission process in the region between the saddle and the scission point. In this model, the compound nucleus is pictured as consisting of two interacting deformed fragments separated by the centre-to-centre distance σ. The energy $V(\sigma)$ of the ground state is assumed to depend on the fragment distance σ as given in Fig. 1. The scission barrier which has been suggested by Schmitt [16] is indicated in molecular model calculations [16] for ^{240}Pu: At some distance between the saddle and the scission point, the absolute value of the derivative $\partial V_n/\partial\sigma$ of the attractive nuclear interaction between the fragments becomes larger than the absolute value of the derivative $\partial V_e/\partial\sigma$ of the repulsive Coulomb interaction since the nuclear interaction is strong and short-range. The assumption of the scission barrier is, of course, hypothetical. But in any case the potential energy $V(\sigma)$ should at least be flattened in that region. With the optical potential employed by Auerbach and Porter [18] for the heavy-ion scattering $^{197}Au\,(^{16}O,\,^{16}O)\,^{197}Au$, a valley does develop inside the barrier. Calculations by Brueckner et al. [19] and Imanishi [19] as well as experimental evidence of quasi-molecular states in the elastic scattering [20] of ^{12}C on ^{12}C lends plausibility to the picture of a scission valley as in the schematic diagram of Fig. 1.

The ordered fission motion from the saddle to the scission point is expected to be strongly damped by the coupling to other collective degrees of freedom. Additional damping of collective excitations is due to the coupling to non-collective degrees of freedom. Wilets (see Ref. [10], section 5) has considered this damping in detail and concluded that this damping is strong enough to give support to the statistical model of fission. But he did not

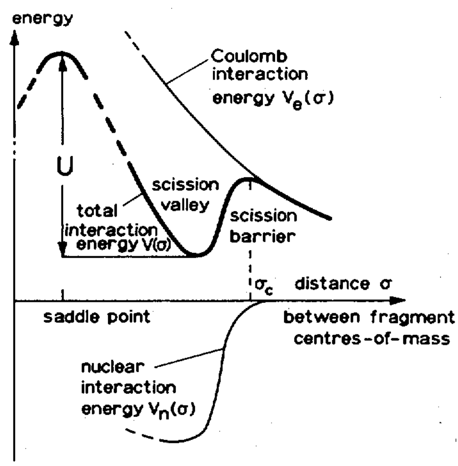

FIG. 1. Schematic diagram of the potential energy $V(\sigma)$ of the compound nucleus as a function of the distance σ between the fragment centres-of-mass.

consider the effect of the pairing gap for non-collective excitations. Because of this energy gap and since the coupling of collective states is generally stronger by one or two orders of magnitude compared to the coupling of non-collective states, it is expected [21] that a full statistical equilibrium at scission is established only between collective degrees of freedom, in contrast to the statistical model introduced by Fong [12] who assumes a statistical equilibrium between all states. If the picture of a scission valley is correct, the statistical equilibrium of collective degrees of freedom is most probably established in the scission valley. This equilibrium should not be seriously altered during the rapid passage of the scission barrier. Collective states with energies greater than the energy gap of approximately 2 MeV are more strongly coupled to non-collective states than low-lying collective states. Because of this damping, the collective temperature which characterizes the quasi-statistical equilibrium of the collective degrees of freedom is expected to be less than 2 MeV and approximately the same for all heavy fissioning nuclei.

Experiments on the angular distribution of fission fragments [22] have shown that the component of total angular momentum along the symmetry axis (K) selected at the saddle point is approximately conserved during the fission process from saddle to scission. This was first pointed out by A. Bohr [23]. The coupling of different degrees of freedom past the saddle point is therefore restricted to states with equal quantum numbers K. Note that the Coriolis coupling of states with different values of K is rather weak because of the large moment of inertia of the compound nucleus (see Ref. [15]).

Up to this point the discussion of the fission process has been restricted to low energies at the saddle point. At higher excitation energies E^* (measured from the fission threshold) a mean number $\bar{\nu}(E^*)$ of non-collective (qp)-excitations will be present at the saddle point. Since it takes the compound nucleus a long time ($\approx 10^{-17}$ s, see Ref. [24]) from the initial excitation to reach the saddle point, the number $\bar{\nu}(E^*)$ will be determined on statistical grounds (see section 6). On the way from the saddle to the scission point an additional number $\bar{\nu}_x$ of non-collective (qp)-excitations is generated by the coupling between collective and non-collective degrees of freedom. This number $\bar{\nu}_x$ should be approximately independent of the compound excitation energy E^*. Now at scission the total mean number of (qp)-excitations is

$$\bar{\mu}(E^*) = \bar{\nu}(E^*) + \bar{\nu}_x \tag{1}$$

These (qp)-excitations are distributed on both fragments, fragment 1 gets a fraction p_1 and fragment 2 a fraction $p_2 = 1 - p_1$. p_1 and p_2 are expected to be approximately independent of the compound excitation energy E^*.

In concluding this section let us repeat the assumptions and statements of the model:

(a) A mean number $\bar{\nu}(E^*)$ of (qp)-excitations at the saddle point.
(b) Statistical equilibrium between collective degrees of freedom at the scission point.
(c) Additional number $\bar{\nu}_x$ (independent of E^*) of (qp)-excitations on the way from the saddle to the scission point.

(d) Distribution of total number $\bar{\mu}(E^*)$ on both fragments with fractions p_1, p_2 (independent of E^*).

3. RATIO OF SYMMETRIC-TO-ASYMMETRIC MASS YIELD

One of the collective degrees of freedom in fission is the mass-asymmetry motion. It was shown in molecular model calculations [14] that the mixing of proton states belonging to different fragments is on the average much smaller at scission than that of neutron states. Therefore the fragment charge Z_F, with F = 1 or 2, is a rather good quantum number of the mass asymmetry motion. To make the following more transparent the eigenenergies of the collective degrees of freedom are approximately written in the form

$$E_m(\bar{\mu}, Z_F) \approx \varepsilon_m(\bar{\mu}) + V(\bar{\mu}, Z_F) \tag{2}$$

Here $$V(\bar{\mu}, Z_F) \approx \tilde{V}(p_1\bar{\mu}, Z_1) + \tilde{V}(p_2\bar{\mu}, Z_2)$$

denotes the eigenenergies of the mass asymmetry motion which in turn is approximately equated to the sum of fragment energies $\tilde{V}$. The remaining eigenenergies of collective motions are represented by $\epsilon_m(\bar{\mu})$. Because of the assumed statistical equilibrium of the collective degrees of freedom, the probability $P(\bar{\mu}, Z_F)$ of finding the charge split Z_F at the scission valley is given by the Boltzmann factor

$$P(\bar{\mu}, Z_F) = \frac{\exp[-\beta_{coll} V(\bar{\mu}, Z_F)]}{\sum_{Z_F} \exp[-\beta_{coll} V(\bar{\mu}, Z_F)]} \tag{3}$$

where $\beta_{coll}^{-1} \equiv kT_{coll}$ and k is the Boltzmann constant. This probability is expected to be not seriously altered on the rapid passage of the scission barrier.

At this point it is interesting to note how the model explains the rapid change from main symmetric fission to main asymmetric fission when going from light to heavy fissioning nuclei across ^{226}Ra. We assume $V(\bar{\mu}, Z_F)$ to have two minima as a function of the fragment charge Z_F, one for the symmetric charge split Z_F^{sym} and the other for the asymmetric charge split Z_F^{as} with one fragment near magic number Z = 50. Then from Eq.(3) the ratio of symmetric-to-asymmetric mass yield is

$$\xi(\bar{\mu}) = \frac{P(\bar{\mu}, Z_F^{sym})}{P(\bar{\mu}, Z_F^{as})} = \exp[-\beta_{coll}\{V(\bar{\mu}, Z_F^{sym}) - V(\bar{\mu}, Z_F^{as})\}] \tag{4}$$

Since β_{coll} is of the order of 1 MeV, the ratio ξ is a sensitive function of the relative position of the two minima. Only if the valleys are equal within 1 MeV, symmetric and asymmetric mass yield have similar probabilities. Therefore, a rapid change from symmetric to asymmetric fission is expected from Eq.(4) at a definite nucleus which has been determined as ^{226}Ra.

Let us now study the dependence of the ratio as a function of the number of (qp)-excitations. The potential energy $V(\bar{\mu}, Z_F)$ can be expanded in the vicinity of a value $\bar{\mu}_0 \equiv \bar{\mu}(E_0^*)$ at the excitation energy E_0^*. Up to first-order terms we get

$$V(\bar{\mu}, Z_F) = V(\bar{\mu}_0, Z_F) + (\bar{\nu} - \bar{\nu}_0)\, \bar{E}_{qp}(\bar{\mu}_0, Z_F) \tag{5}$$

where $\bar{\nu}_0 \equiv \bar{\nu}(E_0^*)$. Since $\bar{\nu}_x$ is independent of E^* the difference of (qp)-numbers at the saddle point $\bar{\nu} - \bar{\nu}_0$ is equal to $\bar{\mu} - \bar{\mu}_0$. $\bar{E}_{qp}(\bar{\mu}_0, Z_F)$ denotes the mean (qp)-energy which is given by

$$\left(\frac{\partial V}{\partial \bar{\mu}}\right)_{\bar{\mu}_0} \equiv \bar{E}_{qp}(\bar{\mu}_0, Z_F) = P_1 \bar{E}_{qp}(\bar{\mu}_0, Z_1) + P_2 \bar{E}_{qp}(\bar{\mu}_0, Z_2) \tag{6}$$

We want to restrict our discussion to the energy dependence of the mass-yield ratio defined in Eq.(4). Therefore it is sufficient to consider the ratio of ξ-values for different excitation energies or different mean numbers of (qp)-excitations

$$\frac{\xi(\bar{\mu})}{\xi(\bar{\mu}_0)} = \exp\left[(\bar{\nu} - \bar{\nu}_0)\beta_{coll}\left\{\bar{E}_{qp}(\bar{\mu}_0, Z_F^{as}) - \bar{E}_{qp}(\bar{\mu}_0, Z_F^{sym})\right\}\right] \tag{7}$$

Only the factor $\bar{\nu} - \bar{\nu}_0$ depends strongly on the compound excitation energy E^*. The rest

$$\varkappa = \beta_{coll}\left\{\bar{E}_{qp}(\bar{\mu}_0, Z_F^{as}) - \bar{E}_{qp}(\bar{\mu}_0, Z_F^{sym})\right\} \tag{7a}$$

should be approximately independent of E^*. Since $\bar{E}_{qp}(Z_F^{as}) > \bar{E}_{qp}(Z_F^{sym})$, from Eq.(7) it follows that the symmetric fission yield increases, and the asymmetric fission yield decreases with increasing excitation energies. It can be shown that the crude approximation (2) is not necessary for a derivation of Eq.(7). In the general case we only have to write, instead of Eq.(5),

$$E_m(\bar{\mu}, Z_F) \approx E_m(\bar{\mu}_0, Z_F) + (\bar{\nu} - \bar{\nu}_0)\, \bar{E}_{qp}(\bar{\mu}_0, Z_F)$$

In a similar way the energy dependence of the fragment kinetic energies can be discussed.

4. MEAN KINETIC ENERGIES OF THE FRAGMENTS

The mean kinetic energies of the fragments are determined by the mean scission point distance σ_{sp} which is expected to lie close to the top of the scission barrier (see Fig. 1). The main part of this energy is the Coulomb energy of the monopole-monopole interaction

$$E_{kin}(Z_F) = \frac{Z_1 Z_2 e^2}{\sigma_{sp}(Z_F)} \tag{8}$$

Because of the assumed statistical equilibrium at the scission valley approximately no translation energy of the fission mode is expected at the scission point.

The scission point distance strongly depends on the deformability of the fragments which in turn depends on the number of (qp)-excitations. Similar to $V(\bar{\mu}, Z_F)$ in section 3 the scission point distance $\sigma_{sp}(\bar{\mu}, Z_F)$ can be expanded in the vicinity of $\bar{\mu}_0$. Up to first-order terms one gets

$$\sigma_{sp}(\bar{\mu}, Z_F) = \sigma_{sp}(\bar{\mu}_0, Z_F)\left[1 + (\bar{\nu} - \bar{\nu}_0)\,\eta(\bar{\mu}_0, Z_F)\right] \tag{9}$$

and with Eq. (8)

$$E_{kin}(\bar{\mu}, Z_F) = E_{kin}(\bar{\mu}_0, Z_F)\left[1 - (\bar{\nu} - \bar{\nu}_0)\,\eta(\bar{\mu}_0, Z_F)\right] \tag{10}$$

It is rather unclear how the deformability varies with the number of (qp)-excitations for non-magic fragments. In any case it is reasonable to expect this dependence to be rather weak. On the other hand the deformability of fragments close to magic ^{132}Sn should strongly increase with increasing number of (qp)-excitations. Therefore, η should be significant and positive for asymmetric fission and approximately independent of the fissioning nucleus. The value of η should only depend on characteristic parameters of the magic fragment.

In the remaining part of this section the parameter $\eta(\bar{\mu}_0, Z_F)$ is calculated in a simple model. Taking the surfaces of the two fragments of the form

$$R(\bar{\mu}, Z_i; \Omega) = R_0(Z_i)\left[1 + \sum_k \alpha_k(\bar{\mu}, Z_i)\, P_k(\cos\vartheta)\right]$$

we get for the scission point distance

$$\sigma_{sp}(\bar{\mu}, Z_F) = \sum_{i=1}^{2} R_0(Z_i)\,\gamma(\bar{\mu}, Z_i)$$

with

$$\gamma(\bar{\mu}, Z_i) = \sum_k (-)^{k(3-i)}\,\alpha_k(\bar{\mu}, Z_i)$$

With these definitions the difference between the scission point distances for two different numbers of (qp)-excitations is

$$\sigma_{sp}(\bar{\mu}, Z_F) - \sigma_{sp}(\bar{\mu}_0, Z_F) = \sum_{i=1}^{2} R_0(Z_i)\left[\gamma(\bar{\mu}, Z_i) - \gamma(\bar{\mu}_0, Z_i)\right] \tag{11}$$

Thus we have to calculate the equilibrium deformation as a function of the number of (qp)-excitations. The potential energy $\tilde{V}_i$ is now expanded up to second-order terms for each fragment ($\tilde{V}_i$ is defined in Eq. (2)):

$$\tilde{V}(p\bar{\mu}, \gamma; Z) = \tilde{V}(p\bar{\mu}_0, \gamma; Z) + \left(\frac{\partial \tilde{V}}{\partial \bar{\mu}}\right)_{\bar{\mu}_0, \gamma_0}(\bar{\mu} - \bar{\mu}_0) + \left(\frac{\partial \tilde{V}}{\partial \gamma}\right)_{\bar{\mu}_0, \gamma_0}(\gamma - \gamma_0)$$

$$+ \frac{1}{2}\left(\frac{\partial^2 \tilde{V}}{\partial \bar{\mu}^2}\right)_{\bar{\mu}_0, \gamma_0}(\bar{\mu} - \bar{\mu}_0)^2 + \left(\frac{\partial^2 \tilde{V}}{\partial \bar{\mu}\partial \gamma}\right)_{\bar{\mu}_0, \gamma_0}(\bar{\mu} - \bar{\mu}_0)(\gamma - \gamma_0) + \frac{1}{2}\left(\frac{\partial^2 \tilde{V}}{\partial \gamma^2}\right)_{\bar{\mu}_0, \gamma_0}(\gamma - \gamma_0)^2$$

where $\gamma \equiv \gamma(p\mu)$ and $\gamma_0 \equiv \gamma(p\mu_0)$. Since γ_0 is the equilibrium deformation for μ_0(qp)-excitations we have $(\partial\tilde{V}/\partial\gamma)_{\bar{\mu}_0\gamma_0} = 0$. According to Eq. (6), with

$$\left(\frac{\partial^2 \tilde{V}}{\partial \bar{\mu}\partial \gamma}\right) \approx -\left(\frac{\partial \tilde{V}}{\partial \bar{\mu}}\right)_{\bar{\mu}_0} \beta(\gamma_0, Z) \tag{12}$$

and neglecting the quadratic term (BCS approximation) in $\bar{\mu} - \bar{\mu}_0$ we find

$$\tilde{V}(p\bar{\mu}, \gamma; Z) - \tilde{V}(p\bar{\mu}_0, \gamma_0; Z) = \frac{1}{2}\left(\frac{\partial^2 \tilde{V}}{\partial \gamma^2}\right)_{\bar{\mu}_0, \gamma_0}(\gamma - \gamma_0)^2 \tag{13}$$

$$+ p(\bar{\nu} - \bar{\nu}_0)\,\overline{E_{qp}}(\bar{\mu}_0, Z)\left[1 - (\gamma - \gamma_0)\beta(\gamma_0, Z)\right]$$

For $\gamma = \gamma_0$, Eq. (13) reduces to the form of Eq. (5). The first term on the right-hand side is a quadratic approximation to the energy dependence on deformation. The second term on the right-hand side includes the coupling of the equilibrium deformations to the number of (qp)-excitations. The constant β is obviously positive for magic fragments ($\gamma_0 \approx 0$, if $\bar{\mu}_0$ not too large). It is obscure how β changes for non-magic fragments. Since we deal with equilibrium deformations we have approximately

$$\frac{\partial \tilde{V}(p_1\bar{\mu}, \gamma(1); Z_1)}{\partial \gamma(1)} = \frac{\partial \tilde{V}(p_2\bar{\mu}, \gamma(2); Z_2)}{\partial \gamma(2)} = 0$$

Evaluating these equations the difference between the scission point distance, Eq.(11), becomes

$$\sigma_{sp}(\bar{\mu}, Z_F) - \sigma(\bar{\mu}_0, Z_F) = (\bar{\nu} - \bar{\nu}_0) \sum_{i=1}^{2} \frac{p_i \, \beta(\gamma_0, Z_i) \, \overline{E_{qp}}(\bar{\mu}_0, Z_i)}{(\partial^2 \tilde{V}_i / \partial \gamma^2(i))_{\bar{\mu}_0, \gamma_0}}$$

and, according to Eq.(9),

$$\eta(\bar{\mu}_0, Z_F) = \frac{1}{\sigma_{sp}(\bar{\mu}_0, Z_F)} \sum_{i=1}^{2} \frac{p_i \, \beta(\gamma_0, Z_i) \, \overline{E_{qp}}(\bar{\mu}_0, Z_i)}{(\partial^2 \tilde{V}_i / \partial \gamma^2(i))_{\bar{\mu}_0, \gamma_0}} \qquad (14)$$

For symmetric fission there are two equal but small contributions from deformed fragments

$$\eta(\bar{\mu}_0, Z_F^{sym}) = 2\eta_d \approx 0 \qquad (15)$$

For asymmetric fission there is only one contribution from a deformed fragment. The main contribution comes from the near-magic fragment:

$$\eta(\bar{\mu}_0, Z_F^{as}) = \eta_d' + \eta_m \approx \eta_m \qquad (16)$$

Thus we expect approximately

$$\frac{E_{kin}(\bar{\mu}_0, Z_F) - E_{kin}(\bar{\mu}, Z_F)}{E_{kin}(\bar{\mu}_0, Z_F)} = \begin{cases} 0 & \text{for sym. fission} \\ \eta_m(\bar{\nu} - \bar{\nu}_0) & \text{for asym. fission} \end{cases} \qquad (17)$$

where η_m is determined by parameters of the magic fragment alone, according to Eqs (14) and (16).

5. FRAGMENT-EXCITATION ENERGIES

As we have discussed in section 4 we expect a considerable decrease of mean kinetic energy with increasing number of (qp)-excitations for asymmetric fission with one fragment near magic ^{132}Sn. This effect is completely attributed to the increasing deformability of the magic fragment. This, in turn, implies that the energy which is lost as kinetic energy should mainly appear as excitation energy of the magic fragment. This excitation energy is measured by the mean number of neutrons $\bar{n}$ emitted by the magic fragment:

$$E_{kin}(\bar{\mu}_0, Z_F^{as}) - E_{kin}(\bar{\mu}, Z_F^{as}) \approx B_n\left[\bar{n}(E^*) - \bar{n}(E_0^*)\right] - p\,(E^* - E_0^*) \tag{18}$$

where B_n is the neutron binding energy, and p is the part of extra compound excitation energy carried by the magic fragment.

6. MEAN NUMBER OF QUASI-PARTICLE EXCITATIONS AT THE SADDLE POINT

The probability of finding ν (qp)-excitations at a given excitation energy E is proportional to the level density $\rho_\nu(E)$ of states with ν quasi-particles. Here E is measured from the ground state of the even-even nucleus. For calculating the level density $\rho_\nu(E)$ the following assumptions are made:

(a) The level density of (1pq)-states (neutrons and protons together) is approximated by

$$\rho_1(E) = \begin{cases} 0 & \text{for } E < \Delta \\ \rho = \text{const} & \text{for } E > \Delta \end{cases} \tag{19}$$

where Δ is the pairing gap (equal for both neutrons and protons).

(b) The Pauli principle for quasi-particles is neglected.

(c) Spin is neglected.

From these assumptions the level density of (2qp)-states is

$$\rho_2(E) = \int dE' \int dE''\, \rho_1(E')\, \rho_1(E'')\, \delta(E - E' - E'') \tag{20}$$

$$= \begin{cases} 0 & \text{for } E < 2\Delta \\ \rho^2\,(E - 2\Delta) & \text{for } E > 2\Delta \end{cases}$$

and the level density of (ν qp)-states is

$$\rho_\nu(E) = \begin{cases} 0 & \text{for } E < \nu\Delta \\ \frac{1}{(\nu-1)!}\, \rho^\nu\, (E - \nu\Delta)^{\nu-1} & \text{for } E > \nu\Delta \end{cases} \tag{21}$$

In Fig. 2 this density is plotted as a function of ν for two different values of E/Δ. The energy dependence of ρ_ν is similar to the spin-independent density function given by Ericson [25] in a more general theory. Since Ericson deals with level densities of states with definite numbers of broken pairs, a detailed comparison with the densities ρ_ν is impossible.

The mean number of (qp)-excitations is defined by

$$\bar{\nu}(E) = \frac{\sum_\nu \nu \rho_\nu(E)}{\sum_\nu \rho_\nu(E)} \tag{22}$$

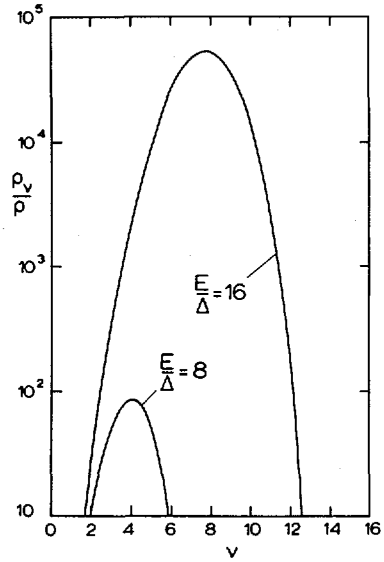

FIG. 2. The level densities $\rho_\nu(E)$ as functions of the number ν of (qp)-excitations for $E = 8\Delta$ and 16Δ according to Eq. (21) with $\rho\Delta = 2$.

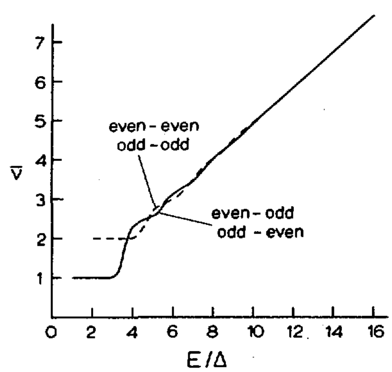

FIG. 3. The mean number $\bar{\nu}$ of (qp)-excitations as a function of the compound excitation energy E measured from the ground state of the even-even nucleus, according to Eq. (22) with $\rho\Delta = 2$.

The sum runs over all even values of ν for even-even and odd-odd nuclei and over all odd values of ν for the even-odd and odd-even nuclei. Figure 3 shows the mean number of (qp)-excitations as a function of E, calculated from Eq.(22). The curves have a significant structure for $E < 4\Delta$ because of the energy gap for (qp)-excitations. By rounding the sharp edges of the level density $\rho_1(E)$, Eq.(19), we get a more realistic model of the level densities. With this correction the structure in the mean number of (qp)-excitations as a function of E is weakened to a certain degree as indicated in Fig.4. Here the difference $\Delta\bar{\nu} \equiv \bar{\nu}(E^*) - \bar{\nu}(E^* = 0)$ is plotted for even-even, odd-odd, odd-even, and even-odd nuclei. E^* is the excitation energy measured from the particular ground states. According to Eqs (7) and (17) we see that the expressions

$$\frac{1}{\varkappa} \ln \frac{\xi(\bar{\mu})}{\xi(\bar{\mu}_0)} \quad \text{and} \quad \frac{1}{\eta_m} \frac{E_{kin}(E^*=0) - E_{kin}(E^*)}{E_{kin}(E^*=0)}$$

should vary as $\Delta\bar{\nu}(E^*)$ plotted in Fig.4.

It is not quite clear if it is possible to observe the structure shown in Fig.4 for excitation energies $E^* \approx 2\Delta$. Collective states which lie in the gap $E^* < 2\Delta$ can alter the dependence of $\Delta\bar{\nu}$ on E^* significantly. But probably an effect of this structure should be observed when experimental results on adjacent even-even, odd-even, even-odd, and odd-odd fissioning nuclei are compared. It has, of course, to be mentioned that these effects may be hidden to some extent by channel effects (for a review see Refs [9,26]) which have been observed by several authors [27].

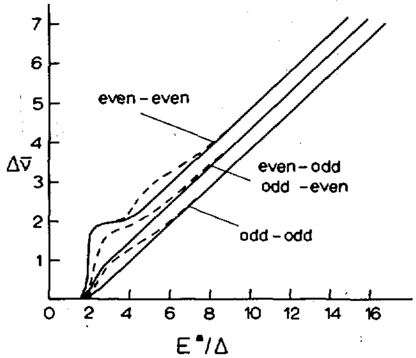

FIG.4. The difference $\Delta\bar{\nu} \equiv \bar{\nu}(E^*) - \bar{\nu}(E^* = 0)$ as a function of the compound excitation energy E^* measured from the particular ground states for even-even, odd-even, even-odd, and odd-odd nuclei ($\rho\Delta = 2$). The dashed curves indicate the effect of taking into account an increase of ρ_1 in the region $\Delta < E < 2\Delta$ which is a more realistic case.

7. COMPARISON WITH EXPERIMENTS

In the fission of ^{238}U (Ref.[7]), and ^{235}U (Ref.[8]) by neutron capture there is some indication of a step-like behaviour of the mass yield ratio as indicated in Fig.4 for $E^* \approx 2\Delta$. But these effects may also be due to different fission channels. The theory is compared with experiments only

TABLE I. PARAMETERS κ AND η_m EXTRACTED FROM EXPERIMENTS*

Fission reaction	Ref.	$E^* \approx E_p$ (MeV)	κ	η_m	Notes
$^{226}Ra(p,f)$	[2]	9-13	0.32	0.014	
	[5]	11-15	0.52	-	
$^{232}Th(p,f)$	[28]	9-12.5	0.52	-	
$^{233}U(p,f)$	[1]	7-12	0.40	≈ 0.010	-
	[3]	8.5-13		0.006	from neutron emission
$^{235}U(p,f)$	[1]	7-12	0.42	≈ 0.010	
$^{238}U(p,f)$	[1]	8-12	0.54	≈ 0.010	
$^{238}U(p,f)$	[7]	6-16	0.49	-	corrected for second- and third-chance fission
$^{239}Pu(p,f)$	[28]	8-12.5	0.45	≈ 0.008	

* Note: E_p is the incident proton energy.

in a relatively small region of E^* well above 2Δ in order to avoid further complications. From Eqs (7) and (10) including the approximations (15) and (16), the parameters κ and η_m are calculated from experimental data. The mean number of (qp)-excitations are taken from Fig.4 with Δ = 1 MeV. The values are compiled in Table I. The parameters are approximately equal within the experimental errors for different experiments. The collective temperature can be determined from a mean value for $\kappa \approx 0.45$ according to the definition (7a). Taking the difference of the mean (qp)-energy for asymmetric and symmetric mass split of the order of 1 MeV, the collective temperature kT_{coll} is approximately 2 MeV. The value of the parameter η_m is seen to be also approximately independent of the fissioning nucleus as is expected from theory. The rather large value of η_m for $^{226}Ra(p,f)$ may be attributed to a contribution from the symmetric component as discussed by Konecny and Schmitt [29].

In conclusion, it must be emphasized that the available experimental data do not allow the theory to be tested in more detail. From this point of view it is, therefore, desirable to study more extensively the various properties of fission as functions of the compound excitation energy.

ACKNOWLEDGEMENTS

The author wishes to thank Drs M. Böhning, E. Konecny, H.W. Schmitt and Professors K. Dietrich, H.J. Mang, J.O. Rasmussen and W. Wild for valuable discussions.

REFERENCES

[1] FERGUSON, R.L., BURNETT, S.C., PLEASONTON, F., PLASIL, F., SCHMITT, H.W., ORNL-Report 4230 (1968) 79 (unpublished).
[2] KONECNY, E., NÖRENBERG, W., SCHMITT, H.W. (to be published).
[3] BURNETT, S.C., FERGUSON, R.L., PLASIL, F., SCHMITT, H.W., ORNL-Report 4230 (1968) 83 (unpublished).
[4] CROALL, I.F., CUNINGHAME, J.G., Nucl. Phys. A125 (1969) 402.
[5] BOWLES, B.J., BECKET, N., Phys. Rev. 147 (1966) 852.
[6] POWERS, J.A., WOGMAN, N.A., COBBLE, J.W., Phys. Rev. 152 (1966) 1096; BRITT, H.C., WHETSTONE, S.L., Jr., Nucl. Phys. 133 (1964) B 603.
[7] BORISOVA, N.I., DUBROVINA, S.M., NOVGORODTSEVA, V.I., PCHELIN, V.A., SHIGIN, V.A., SHUBKO, V.A., Soviet J. nucl. Phys. 6 (1968) 331.
[8] VOROBEVA, V.G., DYACHENKO, P.P., KUZMINOV, B.D., TARASKO, M. Z., Soviet J. nucl. Phys. 4 (1967) 234.
[9] HYDE, E.K., "The nuclear properties of the heavy elements", 3, Fission phenomena, Prentice-Hall New Jersey (1964); OBUKHOV, A.I., PERFILOV, N.A., Soviet Phys. Usp. 10 (1968) 559.
[10] WILETS, L., Theories of Nuclear fission, Clarendon-Press, Oxford (1964).
[11] NIX, J.R., "Further studies in the liquid-drop theory of nuclear fission", UCRL - 17958 (1968); HASSE, R.W., Nucl. Phys. A128 (1969) 609.
[12] FONG, R., Phys. Rev. 135 (1964) B 1339.
[13] STRUTINSKY, V.M., Nucl. Phys. A95 (1967) 420; WEIGMANN, H., Z. Physik 214 (1968) 7; LYNN, J.E., AERE - R 5891 (1968).
[14] NÖRENBERG, W., Thesis, Technische Hochschule München, 1966, unpublished; Physics Letters 19 (1965) 589; Z. Physik 197 (1966) 246.
[15] RÖSCH, N., Z. Physik 215 (1968) 368.
[16] SCHMITT, H.W., Diskussionstagung über Neutronenphysik an Forschungsreaktoren, Jülich (1967), unpublished; Ark. Fys. 36 (1966) 633.
[17] NÖRENBERG, W., (to be published).
[18] AUERBACH, E.H., PORTER, C.E., in Reactions between Complex Nuclei (Proc. 3rd Conf.) U.C. Press, Berkeley (1963) 19.
[19] BRUECKNER, K.A., BUCHLER, J.R., KELLY, M.M., Nucl. Phys. 173 (1968) 944; IMANISHI, B., Physics Lett. 27B (1968) 267; Nucl. Phys. A125 (1969) 33.
[20] BROMLEY, D.A., KUEHNER, J.A., ALMQVIST, E., Phys. Rev. Lett. 4 (1960) 365; ALMQVIST, E., BROMLEY, D.A., KUEHNER, J.A., Phys. Rev. Lett. 4 (1960) 515.
[21] NÖRENBERG, W., Diskussionstagung über Neutronenphysik an Forschungsreaktoren, Jülich (1967), (unpublished); RASMUSSEN, J.O., NÖRENBERG, W., MANG, H.J., (to be published).
[22] ALBERTSON, E., FORKMANN, B., Nucl. Phys. 70 (1965) 209; WILKINS, B.D., UNIK, J.P., HUIZENGA, J.R., Physics Lett. 12 (1964) 243; RABOTNOV, N.S., SMIRENKIN, G.N., SOLDATOV, A.S., YSACHEY, L.N., KAPITZA, S.P., TSIPENIUK, Yu.M., Physics Lett. 26B (1968) 218; SOLDATOV, A.S., SMIRENKIN, G.N., KAPITZA, S.P., TSIPENIUK, Yu.M., Physics Lett. 14 (1965) 217.
[23] BOHR, A., Int. Conf. peaceful Uses atom. Energy (Proc. Conf. Geneva, 1955) 2, UN, New York (1956) 151.
[24] GIBSON, W.M., NIELSEN, K.O., these Proceedings.
[25] ERICSON, T., Nucl. Phys. 6 (1958) 62.
[26] FRASER, J.S., MILTON, J.C.D., Ann. Rev. nucl. Science 16 (1966) 379.
[27] BLYUMKINA, Yu.A., BONDARENKO, I.I., KUZNETSOV, V.F., NESTEROV, Y.G., OKOLOVITCH, V.N., SMIRENKIN, G.N., USACHEV, L.N., Nucl. Phys. 52 (1964) 648; BORUKHOVICH, G.Z., KAMINKER, D.M., PETROV, G.A., Soviet J. nucl. Phys. 3 (1966) 346; SERGACHEV, A.I., VOROBEVA, V.G., KUZMINOV, B.D., MIKHAILOV, V.B., TARASKO, M.Z., Soviet J. nucl. Phys. 7 (1968) 475; BOLSHOV, V.I., KUZNETSOV, V.F., SMIRENKIN, G.N., ERMAGAMBETOV, S.B., OKOLOVICH, V.N., Soviet J. nucl. Phys. 6 (1968) 844; SENCHENKO, V.I., SERGACHEV, A.S., MIKHAILOV, V.B., VOROBEVA, V.G., TARASKO, M.Z., KUZMINOV, B.D., Soviet J. nucl. Phys. 6 (1968) 516.
[28] FERGUSON, R.L., BURNETT, S.C., PLASIL, F., PLEASONTON, F., SCHMITT, H.W., these proceedings, Abstract SM-122/129).
[29] KONECNY, E., SCHMITT, H.W., Phys. Rev. 172 (1968) 1213.

DISCUSSION

W. JOHN: In his oral presentation Dr. Nörenberg mentioned the need for more measurements of kinetic energy distributions. I would like to call attention to some new information from four-parameter measurements made at Livermore on the gamma-rays from the spontaneous fission of ^{252}Cf (John, Nasolowski and Guy, unpublished). By sorting the data on a given gamma-ray, we can obtain the kinetic energy distribution from events where one fragment is a given isotope. I would like to know how this kind of detailed information can be used for testing theories, and what additional kind of data of this type might be desirable.

W. NÖRENBERG: I did not mention in my talk how the distribution of kinetic energies might be explained in the proposed model. Instead of taking only the mean value of the quasi-particles at the scission stage, one has to use a distribution of quasi-particle excitations. Therefore, in addition to the collective part of the width of the kinetic energy distribution, there is another part which is generated by the distribution of quasi-particle excitations. Thus the data on the distribution of kinetic energies can be used for testing the theory, but only at a later stage of development. I want to emphasize in particular the importance of knowing the dependence (if any) on compound excitation energy.

A MODEL FOR FRAGMENT MASS-VERSUS-ENERGY CORRELATIONS IN FISSION

H.W. SCHMITT
Oak Ridge National Laboratory,
Oak Ridge, Tenn., United States of America

Abstract

A MODEL FOR FRAGMENT MASS-VERSUS-ENERGY CORRELATIONS IN FISSION. A detailed investigation of the two-spheroid model of the scission configuration in fission, including the study of both the classical and quantum-mechanical properties of the system, is given. The most probable total fragment kinetic energy as a function of mass division is calculated from minimization of the total potential energy of the system. The root mean square width of the kinetic energy distribution is calculated from the quantum mechanical properties of the system.

The local effective stiffness τ as a function of fragment mass m required for these calculations was obtained solely from correlated fragment kinetic energy measurements for thermal-neutron fission of ^{239}Pu, ^{241}Pu, and ^{235}U, together with the minimum potential energy hypothesis. Strong shell effects in the function $\tau(m)$ were found to occur in the region of $m \cong 132$, where $Z \cong 50$, $N \cong 82$; however, no shell effects seem to occur in the region of $m \cong 83$, where $N \cong 50$. We may interpret this result to indicate that for N = 50 proton-deficient nuclei, the ground-state well in the nuclear potential is relatively shallow, so that when these nuclei occur in fission they occur with distorted shapes outside the ground-state well, where the effective stiffness is reduced. Effective stiffnesses obtained for fragments of mass $82 \leq m \lesssim 112$ are within ~ 20% of the liquid-drop-model value.

The stiffness parameters $\tau(m)$ are used together with minimization of the potential energy to calculate $\bar{E}_K(m)$, the average total fragment kinetic energy as a function of mass. In all cases examined to date, the calculated and experimental energies agree to within about 3%.

The root-mean-square width $\sigma_{EK}(m)$ of the total kinetic energy distribution as a function of fragment mass is determined from quantum-mechanical properties of the system. Normal modes of the system are derived, and a harmonic approximation to the potential is used. Calculated and measured widths agree within about 20% for a wide range of fissioning nuclei. Discussions of the sensitivity of these results to the stiffness parameters, to the nuclear vibrational mass parameter, and to nuclear temperature are included.

I. INTRODUCTION

The various models of nuclear fission may be broadly classified, as suggested by Wilets [1], according to the value of the adiabaticity parameter assumed. If this parameter, defined as the ratio of the characteristic frequency of collective motion to that of particle motion in the nucleus, is small, then an adiabatic model applies; for higher values the statistical model is more appropriate.

Among adiabatic models, the liquid drop model has been most thoroughly investigated. The well-known successes of these studies include the early description of some general features of fission [2], later description of the systematics of normal spontaneous fission lifetimes [3], and more recently the description of mass, kinetic energy, and excitation energy distributions and correlations in medium-excitation fission of nuclei lighter than radium [4,5].

In these last-mentioned studies it was shown that for values of the fissility parameter x, defined as the ratio of the Coulomb energy to twice the surface energy of a spherical compound nucleus, smaller than about 0.7, the saddle point and scission point are quite close together. For higher values of x, corresponding to nuclei heavier than radium, the scission point is farther removed from the saddle point. Wilets [1] gives reasonable arguments which indicate that the assumption of adiabaticity should break down in the descent from saddle to scission; however, the question as to where this breakdown occurs, relative to the formation of the fragments and the eventual determination of their masses and energies, remains open.

If the assumption of adiabaticity breaks down only very late in the fission process, i.e., just at or just before the moment of rupture but after the individual fragments have taken shape, then a relatively simple model results. Even so, detailed dynamical calculations on the basis of such a model are difficult and would involve serious extrapolations of known nuclear properties as functions of deformation, particularly for the large nuclear deformations occurring in fission.

However, if one is willing to assume further that the velocity of the system in the phase space of shape (position) and momentum coordinates is small just prior to scission, i.e., that the scission configuration only (and not the history of the process prior to scission) determines the subsequent properties of the system, than a "static" model of the scission configuration may be constructed and some observable quantities calculated.

Indications that such a model deserves serious study are present in several types of fission data, from which it appears that properties of the fragments influence experimental observables more so than properties of the fissioning system. Examples of such indications are shown in Fig. 1, where the pre-neutron-emission mass distribution is plotted for a number of low-excitation fission cases, and in Fig. 2, where the average total pre-neutron-emission fragment kinetic energy is plotted vs. heavy fragment mass for the same low-excitation fission cases. Salient features of these figures are: the almost precise congruence of the heavy-fragment peaks (except for ^{252}Cf) in the mass distributions, and the occurrence of a peak at about 132 amu (where Z = 50, N = 32) in all of the average total kinetic energy curves.

Various calculations based on static models, with particular attention to low-excitation fission, have been carried out by Vandenbosch [6], Terrell [7], Ferguson and Read [8], Norenberg [9] and by the present author in an earlier paper [10]. Similar considerations were used by Bruner and Paul [11]. Such calculations, of course, depend on unknown properties of deformed nuclei - in this case the fragments, and these authors, as well as Fong [12] in connection with his statistical model calculations, have used various methods to estimate the deformability or stiffness parameters required. All have exhibited partial success in describing the systematics of fragment kinetic or excitation energies.

It is the purpose of the present work to investigate more completely a simple static model of the scission configuration and to determine to what extent such a model is useful in predicting relationships between the various measureable quantities in fission. The scission shape will be approximated by two tangent spheroids, and we shall investigate in detail both the classical and quantum mechanical properties of the system. The motion of the system will be restricted initially to the subspace of tangent spheroids, and the actual separation of the fragments will be assumed to occur at random in time with respect to the motion.

In the subspace of tangent spheroids, the potential energy and kinetic energy of the system in the vicinity of equilibrium may be approximated by quadratic functions of the coordinates and their derivatives, respectively. Thus, the system takes on the character of a multi-dimensional harmonic oscillator and might appropriately be called by the name "scission-point oscillator."

The system is unstable in the fission direction (corresponding to separation of the tips of the spheroids), and the attractive oscillator

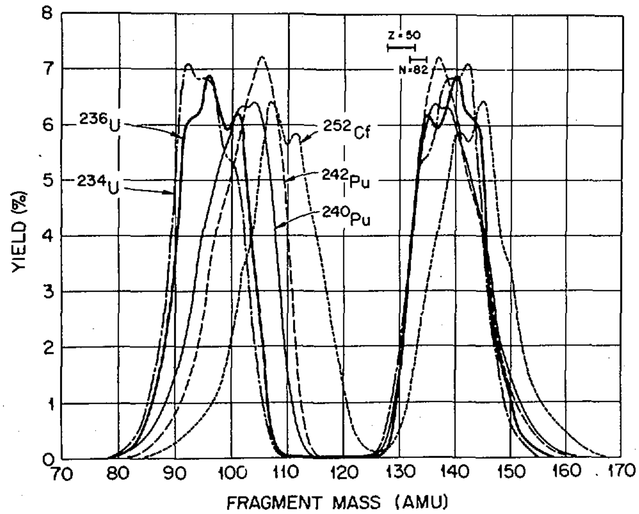

FIG. 1. Compilation of fission-fragment mass distributions. These are pre-neutron-emission distributions obtained from the data of Refs [17, 18, 20]. Labels are compound nuclei.

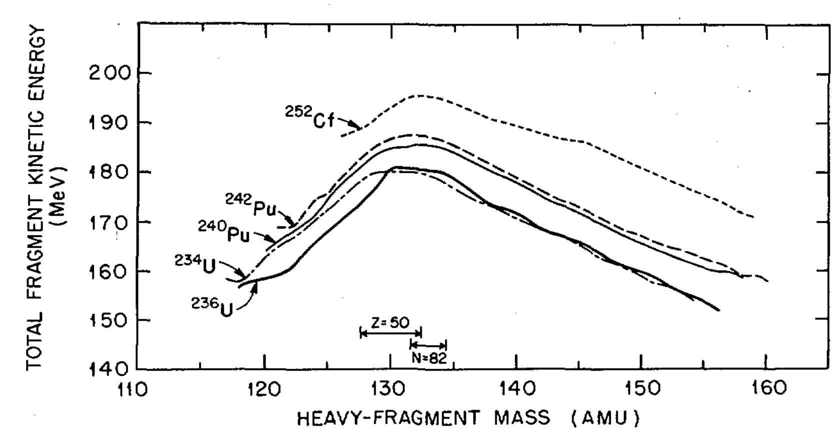

FIG. 2. Compilation of average total fragment kinetic energies versus heavy-fragment mass. These are pre-neutron-emission energies and are obtained from Refs [17, 18, 20].

potential exists only in coordinates normal to the fission coordinate. Therefore, although the "motion" of the system in the oscillator potential will be discussed, we should perhaps think of the elements of this motion as descriptive of the configurations through which the system may pass on its way to complete separation of the fragments.[1]

[1]There is some possibility that a molecular potential of some sort is operative as the separation of the fragments takes place. If this were the case, we might expect either an extended transition region at the top of the barrier or, in those cases where the scission point lies appreciably below the barrier top, a leveling out or even a shallow minimum on the side of the potential energy curve for the system in its decomposition coordinate. Either of these occurrences would give rise to a more nearly static scission configuration.

We shall derive the normal coordinates and eigenstates of the system. The properties of these states, together with simple considerations of reaction energetics, will be seen to determine the general features of the mass-vs-energy correlations observed in asymmetric fission. (All masses and energies discussed in this paper are pre-neutron-emission quantities.)

II. THE MODEL

As indicated by Nix and Swiatecki [4] and by Vandenbosch [6], the two-spheroid approximation for the scission configuration is not chosen for its close approach to realistic shapes. It is chosen because it provides an unambiguous, well-defined framework within which all relevant quantities and distributions may be calculated. One might hope that the results would indicate the degree of usefulness of more refined calculations.

The present investigation, although based on the same model as that of earlier studies mentioned above, differs significantly in its approach. In the studies of both Terrell [7] and Vandenbosch [6] the effective stiffness parameters needed to describe the potential energy were determined largely from fragment excitation energies deduced from measured neutron-emission data. In the present paper, we shall obtain these parameters solely from measured fragment kinetic energies; the fragment shapes and stiffness parameters resulting from this procedure differ in their behavior, as will be seen, from those of Vandenbosch and Terrell, particularly in the light fragment mass region.

A. Potential Energy

Consider now a static, co-linear two-spheroid configuration. The shapes of the spheroids are specified by p_1 and p_2, respectively the major-axis/minor-axis ratios of the two spheroids, and ℓ denotes the separation of centers of the spheroids. (The effects of angular momentum will be neglected, and only axially symmetric shapes will be considered for the present.) The total potential energy of the system may be written:

$$V = V_1(p_1) + V_2(p_2) + V_C(p_1,p_2) \tag{1}$$

and the conditions of minimum potential energy are given by

$$\frac{\partial V}{\partial p_1} = \frac{\partial V_1}{\partial p_1} + \frac{\partial V_C}{\partial p_1} = 0 \tag{2}$$

$$\frac{\partial V}{\partial p_2} = \frac{\partial V_2}{\partial p_2} + \frac{\partial V_C}{\partial p_2} = 0 \tag{3}$$

with

$$p_1 = \frac{c_1}{b_1} \quad , \quad p_2 = \frac{c_2}{b_2} \quad , \quad \ell = c_1 + c_2 \tag{4}$$

The semi-major axes are denoted by c_1 and c_2, the semi-minor axes by b_1 and b_2. In Equations (1-3) the variables are the shape parameters p_1 and p_2; these equations contain, in addition, two effective stiffness parameters τ_1 and τ_2 for the fragments.

The nuclear potential energy as a function of deformation has been the subject of much study recently [13], [14], and in fact the two-spheroid potential has recently been studied in the Strutinski formulation by

Dickmann and Dietrich [15]. Because this entire subject is currently under development, however, it appears worthwhile to obtain the shape of the potential energy of a fragment semi-empirically in the very limited range of deformations occurring in fission. Note from Equations (1-3) that we require only the shape of the potential vs. deformation curve; we need not consider its absolute value at all. Because the range of deformations for any given fragment nucleus occurring in fission is small (as will be seen), almost any function may be used to describe this small portion of the curve, e.g., a quadratic function, or any other function containing the shape p_i and a deformability or stiffness parameter τ_i (i = 1 or 2, corresponding to fragment 1 or 2).

In view of the notion [14] that the average behavior of nuclei, particularly at large deformations, is likely to be describable in terms of the liquid drop model, we shall use the liquid drop form for the potential, i.e.,

$$V_i = S_i \tau_i + V_{Ci} \tag{5}$$

where S_i is the surface area of a spheroid, τ_i is then an effective surface tension, and V_{Ci} is the Coulomb potential energy of the spheroid. For any mass for which the liquid drop model closely describes the nuclear potential in the limited region of deformation occurring, our value of τ will be close to the liquid drop value; where it does not, deviations from the liquid drop value will be expected and may be analyzed, perhaps in terms of shell effects or other effects.

Expressions for S_i and V_{Ci} are given in earlier publications [16,10]. These expressions contain the radius $R_i = r_o A_i^{1/3}$ of a sphere of the same volume; in this work r_o = 1.2 fermis is used as the radius constant.

The mutual Coulomb repulsion of tangent spheroids of charge Z_1e and Z_2e are given by Cohen and Swiatecki [16]:

$$V_C = (Z_1 Z_2 e^2/\ell)F \tag{6}$$

where F is a shape factor also given in the papers referenced above.

Given the parameters τ_1 for fragment Z_1, A_1 and τ_2 for fragment Z_2, A_2, Equations (2) and (3) may be solved simultaneously for the fragment shapes p_{1O} and p_{2O} corresponding to the condition of minimum potential energy. Equilibrium values for the other shape variables may then also be obtained from the appropriate geometric relations, and the value of V_{CO}, the Coulomb repulsion potential energy at equilibrium, may be calculated from Equation (6). The value of V_{CO} thus determined may be compared directly with the experimentally observed value of the most probable total fragment kinetic energy for a given fragment pair, since we assume that the velocity of the system is small just prior to scission.

B. Determination of the τ's

A bootstrap method for determination of the τ's from measured fragment total kinetic energies was described in an earlier paper [10]. In the interim, further investigations have been made to study the uniqueness of the solution reported.

Since it is our purpose to study asymmetric fission, several arbitrary values of τ for the fragment Z = 50, A = 132 were used to begin the bootstrap procedure, thereby developing corresponding sets of τ's for asymmetric mass divisions, as shown in Figure 3. Measured total fragment kinetic energies for thermal-neutron fission of ^{235}U [17], ^{239}Pu, and ^{241}Pu [18] were used in the calculation; values of τ are not included for masses in the region of symmetry where the mass yield is low, and where tails of the resolution functions of near-by high-yield, more asymmetric mass

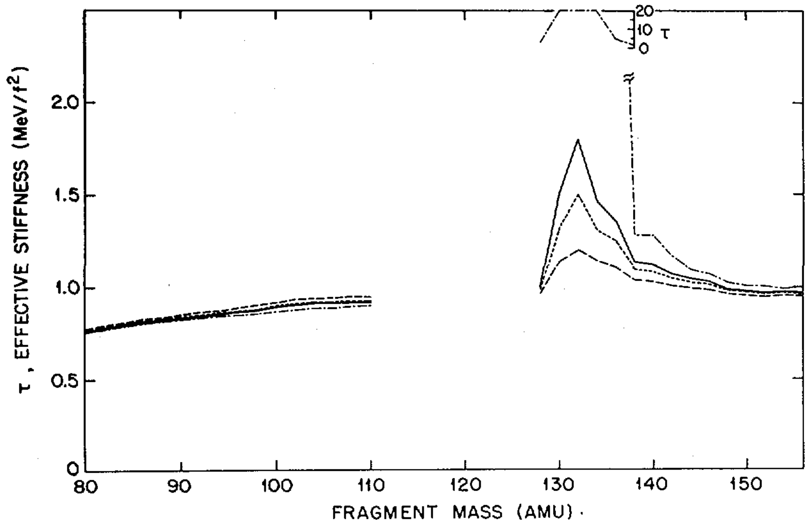

FIG. 3. Effective stiffness τ versus fragment mass. These values are intended to describe the nuclear potential in only a small region of deformations occurring at scission. The curves were obtained from a bootstrap calculation such as that described in Ref. [10]; each curve corresponds to a particular value of τ (A_H = 132 amu) chosen to initiate the calculation.

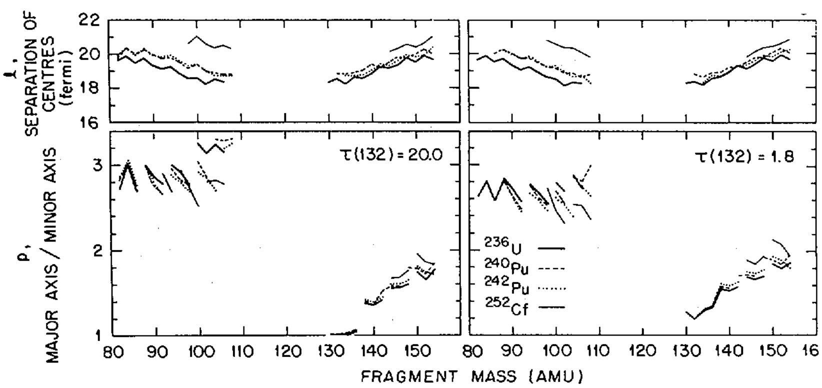

FIG. 4. Separation of fragment centres and major axis/minor axis for fragments formed in thermal-neutron fission.

divisions may affect the energies unduly. Even when the bootstrap procedure is begun at symmetry, however, the high τ values and near spherical shapes which occur in the heavy-fragment group early in the bootstrap calculations limit the region of possible gross errors in τ to that from symmetry up to about A_H = 128 amu and from symmetry down to the corresponding light-fragment masses.

In Figure 3 we see that the τ values throughout the light fragment group are very nearly the same for all four beginning values. In the heavy group, the values themselves are somewhat different from one curve to another, but the trend is similar in all four cases.

The curves for which $\tau(132) = 20.0$ and $\tau(132) = 1.8$ MeV/fermi^2 were used to obtain the equilibrium fragment shapes and the corresponding separations of centers for the four low-excitation cases shown in Figure 4. Essentially no differences in ℓ are observed. The p's for the "stiffer" heavy fragments (left-hand graph, lower section) are slightly smaller than those for the "softer" heavy fragments (right-hand graph); the light-fragment shapes show compensating behavior, being slightly higher in the left-hand graph than in the right-hand graph.

We may conclude, then, that the τ values are not completely unambiguous, but the choice of one value determines the entire curve to be used in a calculation. No choice of qualitatively different trends is available, and we shall carry out the calculations with the curve for which $\tau(A_H = 132 \text{ amu}) = 1.8$ MeV/f^2. Further discussion on this general subject is contained in Section III.

C. Classical Considerations

To study the motion of the system in the neighborhood of its equilibrium configuration, let us consider a fragment pair specified by Z_1, A_1 and Z_2, A_2. Let us define two coordinates:

$$x_1 = c_1 - c_{10} \qquad x_2 = c_2 - c_{20} \tag{7}$$

where these represent deviations from equilibrium.

We may expand the total potential energy of Equation (1) about c_{10}, c_{20}; terms involving the first derivatives vanish, therefore

$$V = \frac{1}{2}\sum_{i,j} (\partial^2 V/\partial c_i \partial c_j)_0 \, x_i x_j = \frac{1}{2}\sum_{i,j} k_{ij}\, x_i x_j \tag{8}$$

The k_{ij} are obtained by numerically differentiating Equation (1), making use of Equation (5), and are the elements of the potential energy matrix $\underset{\sim}{V}$.

The kinetic energy of the system of tangent spheroids may be written exactly:

$$\begin{aligned} T &= \frac{1}{2} m_1' \dot{c}_1^2 + \frac{1}{2} m_2' \dot{c}_2^2 + \frac{1}{2}\mu \dot{\ell}^2 \\ &= \frac{1}{2}(\mu + m_1')\, \dot{x}_1^2 + \frac{1}{2}(\mu + m_2')\, \dot{x}_2^2 + \mu \dot{x}_1 \dot{x}_2 = \frac{1}{2}\sum_{i,j} m_{ij}\, \dot{x}_i \dot{x}_j \end{aligned} \tag{9}$$

where m_1' and m_2' are the vibrational effective masses for fragments 1 and 2, $\mu = A_1A_2/(A_1 + A_2)$ is the reduced mass, and the m_{ij} are elements of the kinetic energy matrix $\underset{\sim}{T}$.

The equations of motion then are the usual coupled-oscillator equations. The eigenfrequencies ω_1 and ω_2 are obtained from the secular equation, and in the solution the ratios of the amplitudes of terms containing each eigenfrequency are respectively

$$\begin{aligned} \rho_1 &= a_{21}/a_{11} = \left[k_{11} - (\mu + m_1')\omega_1^2\right]/(\mu\omega_1^2 - k_{12}) \\ \rho_2 &= a_{22}/a_{12} = \left[k_{11} - (\mu + m_1')\omega_2^2\right]/(\mu\omega_2^2 - k_{12}) \end{aligned} \tag{10}$$

The a_{kj} may be formed into a matrix A which then diagonalizes both $\underset{\sim}{T}$ and $\underset{\sim}{V}$. The diagonalized potential energy matrix contains ω_1^2 and ω_2^2 as its elements. Normalization requires that the diagonalized kinetic energy matrix be $\tilde{\underset{\sim}{A}}\,\underset{\sim}{T}\,\underset{\sim}{A} = \underset{\sim}{1}$, from which we obtain expressions for the amplitudes in terms of ρ_1, ρ_2, μ, m_1' and m_2'.

If y_1 and y_2 are the normal coordinates of the system, the potential and kinetic energies are given by

$$V = \frac{1}{2}\,\omega_1^2 y_1^2 + \frac{1}{2}\,\omega_2^2 y_2^2\,, \qquad T = \frac{1}{2}\,\dot{y}_1^2 + \frac{1}{2}\,\dot{y}_2^2 \tag{11}$$

with y_1 and y_2, whose dimensions are $(\text{mass})^{\frac{1}{2}}$ (length), given by:

$$\begin{aligned} y_1 &= (x_2 - \rho_2 x_1)/[a_{11}(\rho_1 - \rho_2)] \\ y_2 &= (x_2 - \rho_1 x_1)[a_{12}(\rho_2 - \rho_1)] \end{aligned} \tag{12}$$

The lower-frequency mode corresponds to Nix's [4] stretching oscillation, the higher-frequency mode to his distortion-asymmetry mode.

D. Quantum Mechnaics and Statistical Mechanics

In the quantum mechanical problem the normal coordinates may be treated independently, with later transformation and combination of results to obtain observable quantities. The y_j probability distribution for the zero point motion is then gaussian, with the variance $\sigma^2_{y_j o} = \hbar/2\omega_j$. In momentum representation the probability distribution for the zero-point motion is also gaussian, with the variance $\sigma^2_{p_j o} = (\omega_j \hbar/2)$.

If it is assumed that the system is in statistical equilibrium at temperature θ, the normalized probability distribution may be written as an infinite sum which, for harmonic oscillator wave functions, may be obtained in closed form. The probability distribution in y_j is gaussian; the variance is

$$\sigma^2_{y_j} = (\hbar/2\omega_j)\coth(\hbar\omega_j/2\theta), \tag{13}$$

which approaches the classical limit θ/ω_j^2 for $\theta \gg \hbar\omega_j$ and approaches the zero-point limit $\hbar/2\omega_j$ for $\theta \ll \hbar\omega_j$. Similarly, the momentum distribution is gaussian; the variance is

$$\sigma^2_{p_j} = \frac{1}{2}\,\hbar\omega_j \coth(\hbar\omega_j/2\theta) \tag{14}$$

which approaches the classical limit θ for $\theta \gg \hbar\omega_j$ and approaches the zero-point limit $\hbar\omega_j/2$ for $\theta \ll \hbar\omega_j$.

Within the framework of the model the final total fragment kinetic energy E_{Kj} (at infinite separation) for the normal mode j in the two-spheroid system is given by

$$E_{Kj} = V_{Cj} + \frac{1}{2}\,\mu\dot{\ell}_j^2 \tag{15}$$

where $\dot{\ell}_j$ is the instantaneous relative velocity of separation of fragment centers in the subspace of tangent spheroids, and V_{Cj} is the Coulomb repulsion potential energy. The variance of the distribution of total kinetic energies is then

$$\sigma^2_{E_K j} = \sigma^2(V_{Cj}) + (\mu\sigma^2(\dot{\ell}_j))^2 \tag{16}$$

The variance $\sigma^2(V_{Cj})$ is obtained numerically from $\sigma^2(\ell_j)$, which in turn is obtained from a projection of the distributions in y_j onto the ℓ-direction. We find

$$\sigma^2(\ell_j) = \hbar\left[2\omega_j m_{j(\text{eff})} \tanh(\hbar\omega_j/2\theta)\right]^{-1} \tag{17}$$

where $m_{j(eff)} = \mu + (m_1' + m_2' \rho_j^2)/(\rho_j + 1)^2$. Similarly

$$\sigma^2(\dot{\ell}_j) = \hbar\omega_j \coth(\hbar\omega_j/2\theta)/2m_{j(eff)} \tag{18}$$

The total variance of the distribution of E_K is taken to be the sum of the variances for the two normal modes

$$\sigma^2_{E_K} = \sum_{j=1,2} \sigma^2_{E_K j} \tag{19}$$

and we may compare the values thus calculated with experimental values.

E. Temperature and Vibrational Mass Parameters

A systematic study of the sensitivity of the calculation of σ_{EK} to the temperature and vibrational mass parameters was carried out. Examples of the results are shown in Figure 5. Various multiples of the liquid-drop vibrational mass were assumed for each mass division, and values of σ_{EK} were calculated in each case for a number of temperatures. The upper section of Figure 5 indicates that the resulting σ_{EK} values are essentially independent of the vibrational effective mass for a given temperature. The lower section of the figure shows the sensitivity of σ_{EK} to temperature. It was found that the temperature which should be considered as an effective *collective temperature, is proportional to the characteristic energy* ($\hbar\omega_2$) of the normal mode of higher frequency, and the proportionality constant appears to be linear in A, the mass of the compound nucleus. The equation, based on ^{235}U, ^{239}Pu, and ^{241}Pu thermal-neutron data, is

$$\theta = 0.069(A - 218)\,\hbar\omega_2 \tag{20}$$

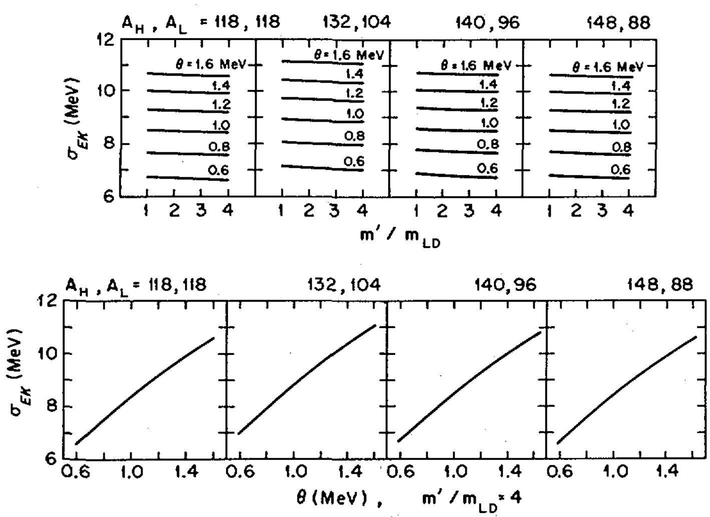

FIG. 5. Root-mean-square width σ_{EK} of the total fragment kinetic energy distribution as a function of vibrational effective mass (expressed as a multiple of the liquid-drop vibrational effective mass) for several θ values (upper section), and as a function of θ for $m'/m_{LD} = 4$. See text.

where θ and $\hbar\omega_2$ are in MeV, and A is in amu. This relation is intended to apply only to low-excitation fission; indeed it is relevant only for $A > 218$, where low-excitation fission occurs. A term containing the compound-nucleus excitation energy should be added when medium- or high-excitation fission is considered.

III. RESULTS AND DISCUSSION

The average total fragment kinetic energy is obtained as a function of mass from minimization of the potential energy as described in Section IIA. Since the τ values are obtained from combinations of fragment masses which occur in the thermal-neutron fission of ^{235}U [17], ^{239}Pu, and ^{241}Pu [18], it is expected that the calculated $\bar{E}_K$ values should agree reasonably well with the data for these cases. The comparison is shown in the left-hand section of Figure 6. In the calculations to date, we have used only the energetically preferred charge ratio Z_H/Z_L corresponding to each mass division A_H/A_L, i.e., the charge distribution has not been taken into account. The effect on the observed systematics should be small, however. The comparison of calculated and observed σ_{EK} values is shown in the right-hand section of Figure 6.

Recent measurements of fragment kinetic energies for a number of other low-excitation fission reactions have been carried out by Bennett and Stein [19]. Their average kinetic energies are plotted together with the calculated energies as functions of heavy fragment mass in Figure 7.

Results for other cases are shown in Figure 8. Calculations for ^{252}Cf are limited to the heavy-fragment masses above 144 amu, for the reason that the τ-values are given only up to 108 amu in the light-fragment region. For ^{233}U thermal-neutron fission, the average total

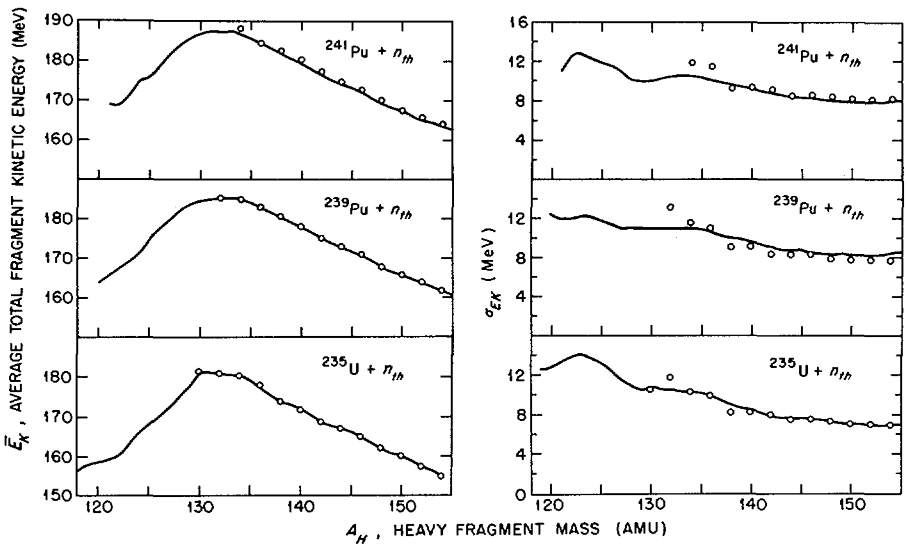

FIG. 6. Measured and calculated values of $\bar{E}_K$, the average total fragment kinetic energy versus heavy-fragment mass (left-hand portion), and measured and calculated values of σ_{EK}, the rms width of the total fragment kinetic energy distribution as a function of heavy-fragment mass (right-hand portion), for thermal-neutron fission of ^{235}U, ^{239}Pu, and ^{241}Pu. Smooth curves were drawn through the data (Refs [17, 18]); the calculated values are shown as points.

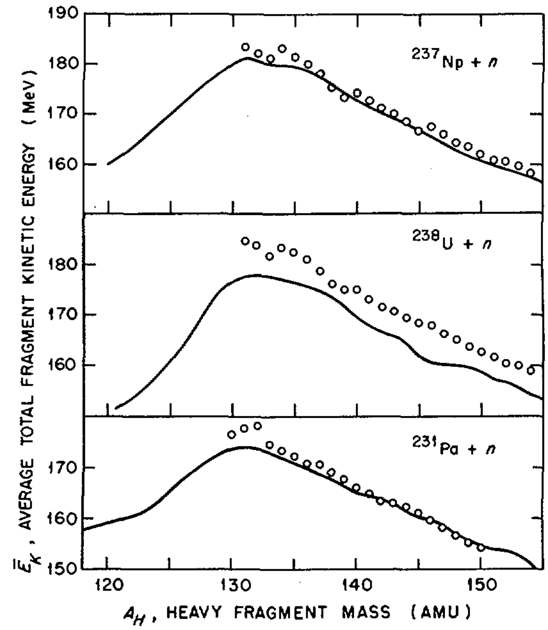

FIG. 7. Measured and calculated values of $\bar{E}_K$, the average total fragment kinetic energy, versus heavy-fragment mass, for fast-neutron fission of ^{231}Pa, ^{238}U, and ^{237}Np. Smooth curves have been drawn through the data (Ref. [19]); calculated values are shown as points.

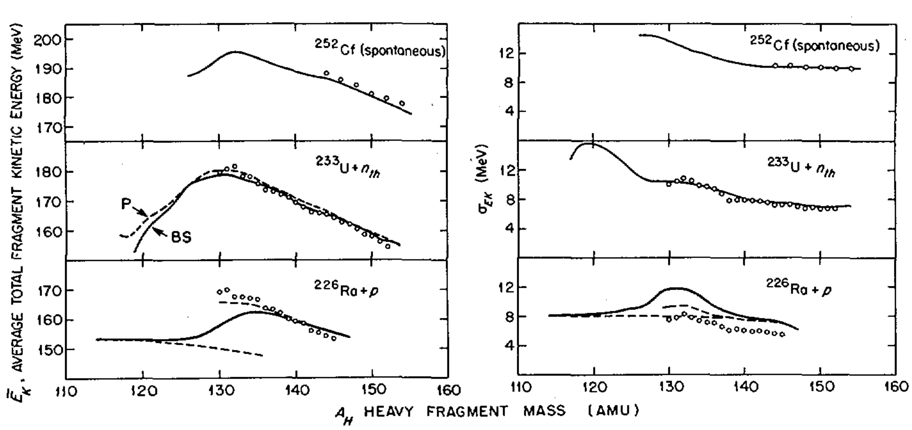

FIG. 8. Measured and calculated values of $\bar{E}_K$, the average total fragment kinetic energy versus heavy-fragment mass (left-hand portion), and measured and calculated values of σ_{EK}, the rms width of the total fragment kinetic energy distribution as a function of heavy-fragment mass (right-hand portion), for ^{226}Ra(p, f), ^{233}U(n_{th}, f), and ^{252}Cf (spontaneous). In the case of radium, the asymmetric and symmetric components of the data (Ref. 21) functions are dashed. In the case of ^{233}U(n_{th}, f), data of both Ref. [19] (BS) and Ref. [20] (P) are shown. The data for ^{252}Cf are those of Ref. [17]. Calculated values are shown as points.

kinetic energies of both Bennett and Stein [19] and Pleasonton [20] are shown; the σ_{EK} data are those of Pleasonton. The $^{226}Ra(p,f)$ data were obtained by Konečny and Schmitt [21], and were decomposed into asymmetric and symmetric components, as indicated in the figure. In the case of $\bar{E}_K(A_H)$ the comparison of the asymmetric values with the calculated values indicates reasonable agreement. The calculated values of σ_{EK}, although showing the same trend vs. A_H as the asymmetric component of the measured values, are somewhat lower - as expected on the basis that no contribution to the temperature was included for increased compound-nucleus excitation energy at 13-MeV proton bombarding energy.

Thus it appears that a relatively simple picture is constructed, which provides a relationship between the variance (or rms width) of the total fragment kinetic energy distribution and the average total fragment kinetic energy. (No distinction is made in these discussions between the most probable and average values of the total kinetic energy for a mass pair.) The average total kinetic energy, equal to the coulomb repulsion potential energy, is obtained directly from the minimization of the total potential energy, depending in the present formulation only on the local effective stiffnesses of the fragments. In this work the local effective stiffnesses are obtained semi-empirically and are used only to describe the shape of the nuclear potential in small regions about the deformations occurring at scission. The effect of the N = 50 closed shell, expected to occur at fragment masses 82 - 84 amu, is seen to be absent in $\tau(A)$ (Fig. 3). This may be a result of the weaker shell-correction term occurring in the mass formula [14] for these nuclei,that is, they may occur in fission with deformations outside the range of the shell correction term. Such a possibility would still be consistent with the low number of neutrons observed to be emitted in this mass range [22], provided only that the shell-correction term has a sufficiently small amplitude.

Calculations of a realistic nuclear potential energy as a function of deformation, based on the Strutinski [13] formulation, have recently been carried out for fragment nuclei and applied to the static two-spheroid model by Dickmann and Dietrich [15], with apparent success with regard to fragment kinetic and excitation energies.

ACKNOWLEDGMENTS

The author is pleased to acknowledge helpful discussions with T. A. Welton, K. Dickmann, K. Dietrich, and J. R. Nix. This work was begun during a one-year visit in the institute of Professor K. Beckurts at the Kernforschungszentrum Karlsruhe, whose hospitality and helpful support the author is pleased to acknowledge.

REFERENCES

[1] WILETS, L., "Theories of nuclear fission", Clarendon Press, Oxford (1964).

[2] BOHR, N., WHEELER, J. A., Phys. Rev. 56 (1939) 426.

[3] SWIATECKI, W. J., Phys. Rev. 100 (1955) 937; 101 (1956) 97.

[4] NIX, J. R., SWIATECKI, W. J., Nuclear Physics 71 (1965) 1.

[5] PLASIL, F., BURNETT, D. S., BRITT, H. C., THOMPSON, S. G., Phys. Rev. 142 (1966) 696.

[6] VANDENBOSCH, R., Nucl. Physics 46 (1963) 129-140.

[7] TERRELL, J., Int. Symposium on the Physics and Chemistry of Fission (Proc. Symposium, Salzburg, 1965) II, IAEA, Vienna (1965) 3.

[8] FERGUSON, J. M., READ, P. A., Phys. Rev. 139 (1965) B56.
[9] NORENBERG, W., Z. fur Physik 197 (1966) 246.
[10] SCHMITT, H. W., Arkiv for Fysik 36 (1967) 633.
[11] BRUNER, W., PAUL, H., Ann. der Physik 8 (1961) 146.
[12] FONG, P., Phys. Rev. 11 (1963) 375.
[13] STRUTINSKI, V. M., Int. Symp. on Nuclear Physics (Proc. Symp., Dubna, U.S.S.R. 1968); Nucl. Physics A95 (1967) 420.
[14] MYERS, W. D., SWIATECKI, W. J., Arkiv. for Fysik 36 (1967) 343.
[15] DICKMANN, K., DIETRICH, K., Nucl. Physics, in press.
[16] COHEN, S., SWIATECKI, Ann. of Physics 19 (1962) 67.
[17] SCHMITT, H. W., NEILER, J. H., WALTER, F. J., Phys. Rev. 141 (1966) 1146.
[18] NEILER, J. H., WALTER, F. J., SCHMITT, H. W., Phys. Rev. 149 (1966) 894.
[19] BENNETT, M. J., STEIN, W. E., Phys. Rev. 156 (1967) 1277.
[20] PLEASONTON, F., Phys. Rev. 174 (1968) 1500.
[21] KONECNY, E., SCHMITT, H. W., Phys. Rev. 172 (1968) 1213.
[22] See e.g., TERRELL, J., Phys. Rev. 127 (1962) 880.

DISCUSSION

J. R. NIX: I have two objections concerning your calculations. First, since a scission point is not a position of equilibrium, it cannot be determined by simply minimizing the potential energy - it is necessary to calculate the dynamical descent from the saddle point to scission. That your results are at all reasonable stems from your restriction to spheroidal shapes for the fragments. The position of the minimum potential energy of two touching drops is two spherical fragments at infinity separated by an infinitesimal neck, and your fragments would approach this configuration if more freedom were permitted.

Second, since the deviations from normalcy of the stiffnesses of nuclei arise from single-particle effects, it seems unreasonable for you to correlate stiffnesses in terms of effective surface tensions.

H. W. SCHMITT: If the motion from saddle to scission is highly damped, or is viscous, the velocity of the system in phase space may be small enough to justify the static assumption as a first approximation. This does not imply an equilibrium configuration at scission, although even that cannot be excluded, as we have seen in Nörenberg's paper (SM-122/30). Inclusion of more degrees of freedom for the fragment shapes would, in fact, not change the results qualitatively, simply because the τ values are determined from the condition that $V_C = \bar{E}_K$ along with potential energy minimization in coordinates normal to the fission direction.

As regards your second point, we have indicated in the paper that we are concerned with the shape of the potential energy curve in only a small region of fragment deformations, and any simple function may be used to represent this curve over a small range. We have chosen the form of Eq. (5) for its simplicity and in order to see whether the fragments may have liquid-drop properties when they are formed at scission. A proper description of the deformation energy for all deformations, such as that of Dietrich and Dickmann, is certainly to be preferred, but the present results may indicate qualitatively what may be expected from the theory.

U. MOSEL: I have performed preliminary calculations for the scission point, which was assumed to consist of two touching spheres, in order to get a feeling for the magnitude of the different parts of the total energy at this point. This calculation was carried out in the framework of the Thomas-Fermi theory and its application to ion-ion interaction problems, which was developed by A. Bruckner et al., in Anneaux de Collisions à Electrons et Positons (Symp. Int. Saclay, 1960) Presses Universitaires de France, Paris (1966) and W. Scheid and W. Greiner [Ann. Phys. 48 (1968)] at Frankfurt-am-Main last year. This calculation for two touching Pd nuclei has shown that there is still a nuclear interaction between the fragments at the scission point of about 20-30 MeV. Even if this quantity is lowered by taking into account the deformation of the fragments, it is still expected to have the same order of magnitude as the deformation energies V_D in Dr. Schmitt's model. Therefore, this effect should be considered in further studies, since it leads to a decrease of the total interaction energy at scission and hence also of the total kinetic energy. Furthermore, this effect will simultaneously change the deformation energies also.

H. W. SCHMITT: A very important point in this connection is that such an effect would help to retard the motion of the system through the scission point, and thereby provide a more sound theoretical basis for the relative success of "molecular model" calculations such as those reported here.

TERNARY FISSION

(Session B)

Chairman: M. Neve de Mevergnies

TERNARY FISSION
A Review

N. FEATHER
Department of Natural Philosophy,
University of Edinburgh, Scotland,
United Kingdom

Abstract

TERNARY FISSION. Experimental results in the field of light-particle-accompanied fission (including fission accompanied by 'scission neutrons') - and in relation to fission into three fragments of comparable mass - are reviewed over the last four years. These results are set against the backgound of previously ascertained fact, and certain empirical regularities are noted.

1. GLOSSARY AND DEFINITIONS

Normally, fission is a 'binary' process: only two particles, the 'primary fission fragments', are formed when the fissioning nucleus divides. These primary fragments effectively attain their full energy of motion within a time interval of 10^{-18} s, having separated by some 2×10^{-11} m. Less frequently, more than two particles appear within 10^{-18} s of the instant of scission. If precisely three particles appear within this time interval, the fission event may be classified as a 'ternary' event. If precisely four particles should appear, we might speak of 'quaternary fission', and similarly for higher multiplicities.

This review is concerned only with ternary fission - and is based upon the definition indicated above. Clearly, this is a definition which it is impossible to realize 'operationally', but at least it is conceptually precise. It will be noted that it includes the whole spectrum of three-particle events, from the extreme mode in which a 'scission neutron' accompanies two primary fragments which otherwise share the whole mass of the fissioning nucleus, to the other extreme in which three primary fragments of not very dissimilar mass are involved. By far the most intensively studied mode of ternary fission is that in which an alpha particle accompanies two heavier fragments. Many writers have used the term 'alpha-particle-accompanied fission' to describe this mode. Possibly there is some justification for distinguishing 'light-particle-accompanied (ternary) fission' (in which the lightest of the three particles has $Z < 10$) from 'true ternary fission' (in which $Z \geqslant 10$ for the lightest of the three primary fragments produced). Both these types of fission are reported on in this review.

Our knowledge of light-particle-accompanied fission modes, other than the alpha-particle-accompanied mode, has been gained almost entirely since the Salzburg symposium of 1965. This period has seen a considerable revival of interest in the phenomenon of ternary fission, made possible by the development of more powerful methods of experimentation, in particular with respect to multi-parameter data-recording. From the theoretical side, it has frequently been said that a study of light-particle-accompanied fission affords a unique opportunity of acquiring an insight into the properties of nuclear matter in a non-equilibrium configuration.

In a sense this is a truism, once it is accepted that the light particle is emitted from the region of maximum deformation of the emitting nucleus (from the 'neck' region of the fissioning nucleus at the instant of scission, or, immediately thereafter, from the collapsing 'protuberance' with which one or other of the primary fragments is 'born'). This much may be agreed, but the fact is that the significant break-through to a dynamical understanding of the process has yet to be achieved.

For the purpose of this review, it will be profitable to deal first with the experimental results concerning alpha-particle-accompanied fission, then with the corresponding results for the other light-particle-accompanied modes. Afterwards, the challenge which these results present to the theorist will be briefly explored; finally, the present position with respect to 'true' ternary fission will be summarized.

2. ALPHA-PARTICLE-ACCOMPANIED FISSION

Four years ago the basic facts regarding alpha-particle-accompanied fission were already securely established - at least in relation to spontaneous fission, and neutron-induced fission at relatively low (< 10 MeV) energies of excitation. Admittedly, these facts related almost entirely to the fission of even-even nuclei, but the pattern was so nearly constant over the whole range, from $Z = 92$ to $Z = 98$, that it was natural to assume that this mode of ternary fission would be found to occur with similar characteristics in all cases in which the initial excitation of the fissioning nucleus was low. Briefly, it was known that the fractional yield of the alpha-particle mode did not vary by as much as one order of magnitude (say from 1.5×10^{-3} to 4×10^{-3}) over all the cases investigated, that the kinetic energy spectrum of the alpha particles was very closely the same in each case (a Gaussian spectrum with a most probable energy of about 16 MeV), and that the angular distribution of the particles was strongly peaked, presumably with azimuthal symmetry around the fission axis, in a direction roughly at right angles to that axis. In one case (that of $^{236}_{92}U^*$, formed by thermal-neutron capture in $^{235}_{92}U$) it had been convincingly established that the distribution in mass of the residual fragments of the alpha-particle-accompanied mode was hardly distinguishable from that of the primary fragments of binary fission of the same nucleus (once the overall deficit of 4 units of mass had been allowed for); also, on average, the total kinetic energy of the three charged particles in this ternary mode was the same, to within a few MeV, as the total kinetic energy of the primary fragments of the binary fission of this nucleus. In relation to all these findings there was no essential disagreement between the results of workers in various laboratories - except, perhaps, in the matter of the possibility of a non-trivial variation of alpha-particle yield with energy of initial excitation of the fissioning nucleus.

In this section we survey the results of the more recent work on the various aspects of alpha-particle-accompanied fission mentioned above - and we shall take them in turn. We shall deal first with the question of the fractional yield, as it varies with A and Z and with the energy of initial excitation of the compound nucleus concerned.

Fractional yield. Experiments have been performed by various methods, and with different degrees of statistical accuracy, by Atneosen et al. [1], Thomas and Whetstone [2], Loveland et al. [3], Nagy et al. [4] and Adamov et al. [5], the results of which are now almost entirely concordant. The systems studied have been ^{232}Th + n, ^{232}Th + p, ^{232}Th + α, ^{235}U + n, ^{235}U + α, ^{238}U + n, ^{238}U + p, ^{238}U + α and ^{237}Np + d, the initial excitation of the fissioning nucleus varying from some 6 MeV to nearly 40 MeV. Broadly, the conclusion of Loveland et al. that the fractional yield 'has the nearly constant value 2.1×10^{-3} for all of the species ... for initial compound nucleus excitation energies above about 6 MeV' may be taken as representative. For spontaneous fission, the fractional yield of the alpha-particle-accompanied mode appears to be generally greater than this, and to vary somewhat from species to species. For ^{252}Cf, the species most frequently used for calibration purposes in other experiments, Thomas and Whetstone [2] have given a 'best' value of $(3.27 \pm 0.10) \times 10^{-3}$.

As indicated by Loveland et al., the near-constancy of the alpha-particle yield over a wide range of energies of initial excitation, correlates directly with the near-constancy of the mean total kinetic energy of the fragments of binary fission over the same range of excitation of the fissioning nucleus. This latter constancy is simply interpreted on the hypothesis that the scission configuration (or the compound nucleus deformation at scission) is very nearly the same at all excitations (the 'internal' excitation varying, whilst the energy of deformation remains much the same). According to this train of association of ideas, alpha-particle emission, in the fission process, is a function of the total deformation of the fissioning nucleus at the instant of scission.

Energy spectrum and angular distribution of the alpha particles. It will be advantageous, at this point, to survey recent investigations on the kinetic energy spectrum, and on the angular distribution of the alpha particles, under one head rather than two. The most significant work in this field, certainly, has been that in which energy-angle correlations have been sought. Obviously, any experiment on alpha-particle-accompanied fission is conditioned, at the design stage, by considerations of angular distributions - and almost any such experiments, nowadays, necessarily yields some information regarding the energy spectrum. Here we shall be concerned only with those experiments in which the collection of new information on these matters was a primary aim.

The most difficult part of the energy spectrum to investigate is the low-energy region - if only because the fission fragments and the natural alpha particles from the target material effectively blanket the first few MeV of this region[1]. Most workers, in fact, have been content to disregard the first 10 MeV of the spectrum, both on this account and in order to avoid other spurious effects. Recently, however, Chwaszczewska et al. [6] have paid particular attention to the energy range 6 - 17.5 MeV of the fission alpha-particle spectrum of ^{236}U* (^{235}U + thermal neutrons), and combining their results with those of Dakowski et al. [7] obtained in the same laboratory, they have shown that the whole of the accessible spectrum (6 MeV $\leq T_\alpha \leq$ 27 MeV)[2] can be represented satisfactorily by a single Gaussian of full width at half-maximum of 10 ± 1 MeV.

[1] This blanketing effect would be reduced by several orders of magnitude if an electromagnetically separated target of ^{241}Pu could be used with slow-neutron irradiation.

[2] In this review we use the symbol T for kinetic energy throughout, reserving E for energy of excitation.

Recent energy-angle correlation experiments have been carried out by Fraenkel [8], Raisbeck and Thomas [9] and Nadkarni [10], the first two investigations using ^{252}Cf, the third employing slow-neutron-irradiated ^{235}U, as fission source. Of the three, the most detailed was that of Fraenkel. All three investigations agree in showing that the average energy of the alpha particles increases as the observed emission direction with respect to the fission axis becomes more distant from the most probable direction (roughly 82° inclined to the light-fragment direction). According to Fraenkel, this increase is itself considerably more rapid as the alpha-particle direction moves towards the direction of the heavy-fragment motion than it is when the change in alpha-particle direction is in the reverse sense. Again, all three investigations agree that the angular dispersion of alpha-particle directions is greater, the greater the energy of the alpha particles. Fraenkel's results appear to show conclusively that the essence of this last-mentioned change is a gradual 'flattening' of the originally peaked distribution characteristic of alpha-particle energies less than 20 MeV, so that ultimately, for 25 MeV $\leq T_\alpha \leq$ 30 MeV, the angular distribution function has a minimum at an angle of about 90°. Nadkarni has advanced less direct evidence for the same conclusion.

Having carried out a triple-coincidence experiment, Fraenkel [8] was able to pursue his analysis one stage farther, investigating the way in which the general conclusions outlined above require to be modified when the data are divided into groups corresponding to different values of R, the mass-ratio of the residual fragments. He discovered that even in respect of the alpha-particle energy range $T_\alpha <$ 20 MeV, when the overall angular distribution shows little variation with T_α, there are significant variations with R. For $T_\alpha <$ 15 MeV, in particular, the angular distribution broadens very considerably as R decreases below 1.1 (these values, of course, represent the relatively rare near-symmetrical modes) - and that the overall breadth of the angular distribution for $T_\alpha >$ 20 MeV is occasioned largely through the abnormally broad distributions which are characteristic of the near-symmetrical and the widely asymmetrical modes.

Trajectory computations. The investigations of Fraenkel [8] and Raisbeck and Thomas [9] were carried out specifically to provide experimental data for use in trajectory computations. The aim of such a computation is to arrive at a (distributed) set of 'initial' dynamical parameters (by a method of iteration) out of which the 'final' distributions in energy, and the angular relationships of the three particles, in light-particle-accompanied fission emerge naturally as in accord with experiment. The first preliminary essay towards this aim was made by Tsien [11] in 1948 in relation to the alpha-particle-accompanied mode (and was the basis of the subsequently accepted view that the alpha particle is released in the space between the primary fragments at about the instant of scission). Halpern [12] in 1963, and Geilikman and Klebnikov [13] in 1965 elaborated these calculations, and more recently more ambitious computer programs have been run by Boneh et al. [14] and Błocki and Krogulski [15], also by Raisbeck and Thomas [9] in relation to their own experiments. Essentially, the computations of Boneh et al. were devised so as to employ to the full the detailed information concerning energy-angle correlations obtained by Fraenkel for the alpha-particle mode; the computations of Raisbeck and

Thomas, on the other hand, were primarily concerned with matching the energy spectra of the alpha particles and the other light particles accompanying the fission of ^{252}Cf, using a coherent set of initial parameters. Similarly, Błocki and Krogulski were more directly concerned with the energy spectra than with the angular distributions of the various light charged particles accompanying the fission of $^{236}U^*$. Here, then, we are immediately interested in the computations of Boneh et al. rather than in the others (though we shall have occasion to refer to these later). In all three computations, it hardly needs to be said, non-relativistic classical mechanics and classical electrostatics provided the necessary theoretical basis, a point-charge model being used. Of necessity, conservation of angular momentum was observed, but no consideration of effects involving changes of intrinsic angular momentum of the interacting particles was possible within the scope of the model.

According to the model of Boneh et al. [14], the alpha particle 'materializes' at the scission point, as the neck breaks, with an initial kinetic energy belonging to a Maxwellian distribution, and an initial direction which is isotropically distributed. The actual point of scission is symmetrically distributed about the point of minimum electrostatic potential between the fragments, with a maximum probability (per unit distance) at this point, and half this probability at points some 5×10^{-15} m on each side of this point. The mean energy of the Maxwellian distribution is assumed to vary inversely as the square of the electrostatic potential at the actual point of scission. It is concluded that the 'best' account of the experimental facts concerning energy-angular correlations is obtained if the distance between the centres of the fragments at scission is 26×10^{-15} m and the most probable mean value of the initial kinetic energy of the alpha particle is 3.0 MeV. On this basis the mean value of the total kinetic energy of the separating fragments is some 35 MeV at the instant of scission. Admittedly, using these initial parameters, not all aspects of the experimental results are faithfully reproduced, and, in particular, the overall spectrum of kinetic energies is significantly narrower than the spectrum deduced from experiment.

Raisbeck and Thomas [9] obtained a good fit with the experimental kinetic energy spectrum of the fission alpha particles of ^{252}Cf in terms of a model in which the alpha particle 'materialises' at a point on the line of centres between the fragments at a time t after binary scission has occurred. At the instant of scission the fragments are assumed to have zero velocity, and, when the alpha particle appears, it does so with an initial kinetic energy belonging to a Gaussian distribution, and an initial direction which is isotropically distributed. (In the computation, attention is paid to the conservation of mass and momentum in this process of alpha-particle 'materialization'). As in the model of Boneh et al., it is assumed that the most probable point of appearance of the alpha particle is at the electrostatic potential minimum point between the fragments. Around this point, Raisbeck and Thomas assume a Gaussian distribution of appearance probability. They obtained their 'best' fit with the overall energy spectrum in terms of the following parameters: $t = 0.4\times10^{-21}$ s (unique value); standard deviation of position of appearance point, 1.5×10^{-15} m; mean initial kinetic energy of alpha particle, 2.0 MeV. On this basis the mean separation of fragment centres at scission is 20.5×10^{-15} m, and, at the instant of alpha particle 'materialization', 21.5×10^{-15} m. At that time the mean value of the total kinetic energy of the large fragments is some 7.5 MeV.

For many reasons, the detailed investigation of the alpha-particle-accompanied mode is more difficult when fission is produced by charged-particle bombardment of a target than it is, either when thermal neutrons are used, or when spontaneous fission is in question. Nevertheless, Atneosen et al. [1] succeeded in determining the energy spectrum of the fission alpha particles of $^{239}Np^*$ (22.4 MeV excitation, induced by 17.5 MeV protons on ^{238}U) - and Thomas and Whetstone [2] successfully studied the angular distribution of these alpha particles in relation to the fission axis, using protons of 11, 15, 17 and 21 MeV for the target bombardment. In each case comparison was made with the corresponding feature of the alpha-particle-accompanied mode of ^{252}Cf spontaneous fission. Within the limited accuracy of the first experiment, the energy spectra of the fission alpha particles appeared to be identical for $^{239}Np^*$ and ^{252}Cf; with greater confidence, the results of the second experiment showed that for $^{239}Np^*$ the angular distribution of these particles was essentially the same at all energies of proton bombardment, and that it differed only from the angular distribution of the fission alpha particles of ^{252}Cf by being characterized by a somewhat greater Gaussian breadth (standard deviation $14.7 \pm 0.4°$, as against $12.0 \pm 0.4°$). In the light of the trajectory calculations of Boneh et al. that we have just considered, these results provide additional confirmation for the view that any initial excitation of the fissioning nucleus is largely irrelevant at the instant of scission: the critical scission configuration is essentially independent of the degree of internal excitation of the nucleus concerned.

Mass and kinetic energy distributions of the fragments. As already mentioned, before 1965, the distribution in mass of the primary fragments of alpha-particle-accompanied fission had been investigated only in the case of $^{236}U^*$. Since such an investigation almost necessarily involves use of a triple-coincidence arrangement in which the energies of the 'coincident' (post-neutron-emission) fragments are separately determined, we may usefully consider the more recent work on the total kinetic energy release along with that on the fragment mass distribution in the alpha-particle-accompanied mode.

In the ultimate analysis, each of these investigations is beset with the same difficulty. In binary fission, on the assumption that the prompt neutrons are emitted isotropically from the fully accelerated fragments, the ratio of the measured kinetic energies of the post-neutron-emission fragments, for a unique mode of mass division, has a most probable value $(A_H/A_L)^2\ (A_L - \nu_L)/(A_H - \nu_H)$, whereas the ratio of the measured velocities of these fragments has a most probable value (A_H/A_L). Here A_H, A_L are the mass numbers of the primary (pre-neutron-emission) heavy and light fragments, respectively, and ν_H and ν_L are the numbers of prompt neutrons emitted by these fragments. For a given value of the most probable energy ratio, the standard deviation of this ratio is greater as ν_H and/or ν_L is greater. Again, if T'_H and T'_L are the most probable values of the kinetic energies of the two post-neutron-emission fragments, for a given mode of mass division, the most probable kinetic energies of the pre-neutron-emission (primary) fragments are $T_H = T'_H A_H/(A_H - \nu_H)$ and $T_L = T'_L\ A_L/(A_L - \nu_L)$, respectively. Demonstrably, if we wish to determine the distribution characteristic of the total kinetic energy $(T_L + T_H)$ for each mass-division mode (A_L, A_H) - and we do - we cannot do this in terms of energy measurements alone.

So far our statements refer only to binary fission; in that case the technical difficulties involved in time-of-flight (velocity) measurements on the fission fragments have long since been successfully overcome. However, no one, as yet, has been sufficiently optimistic to apply this technique in the triple-coincidence experiments which are necessary if similarly detailed information is to be obtained in relation to ternary fission. Considerations of intensity are almost prohibitive. In light-particle-accompanied ternary fission, there is, in addition, the complication introduced by the recoil of the light particle, but that is the least of the experimenter's worries.

Having regard to the difficulties that we have just exposed, Fraenkel [8] has expressed the view that it is premature to make any precise statement concerning the distribution of fragment mass in alpha-particle-accompanied fission. From his own experiments with ^{252}Cf it is clear that the distribution characteristic of the kinetic energy ratio T'_L/T'_H is very nearly the same for the alpha-particle-accompanied mode as it is for the binary fission of this nucleus. Fraenkel is prepared to leave the matter there, for the present. He does not consider it possible, at this time, to derive the mass distribution of the residual fragments of the alpha-particle-accompanied mode with sufficient precision for a comparison with the corresponding mass distribution of the primary fragments of binary fission to be profitable according to the method of Schmitt and Feather [16] (see, also Feather [17]). In spite of this salutary caution, we may still assert, on the evidence of Fraenkel's results, that the fragment mass distribution for the alpha-particle-accompanied fission of ^{252}Cf is very little different (when the loss of 4 units of mass has been allowed for) from the corresponding distribution for the binary fission of this nucleus. Very recently, Fraenkel's experiment on the energy spectrum of the paired fragments of alpha-particle-accompanied fission has been repeated by Nardi et al. [18] with full confirmation of his findings.

In relation to any formal discussion of the 'differential energetics' of *alpha-particle-accompanied and binary fission (see below), as already* implied, we are interested in comparing, for corresponding modes of mass division, the mean values of the total kinetic energies associated with the product particles in the two 'final state configurations' some 10^{-18} s after the respective instants of scission. Although it was already evident, by 1965, that these two quantities 'are the same, to within a few MeV', for $^{236}U^*$ fission, the difficulties that we have here exposed make full precision in this matter as yet unattainable. Extending our previous notation, we may say that it is possible to determine the values of $(T'_L + T'_H)_b$ and $(T'_L + T'_H + T_\alpha)_t$ by direct experiment; what we wish to know is the difference $(T_L + T_H + T_\alpha)_t - (T_L + T_H)_b$.

Since the Salzburg symposium, values of $(T'_L + T'_H + T_\alpha)_t - (T'_L + T'_H)_b$, averaged over all modes of mass division, have been reported by Schröder [19] and Nadkarni [20] for $^{236}U^*$ (6.4 MeV) fission, and by Fraenkel [8] and Nardi et al. [18] for the spontaneous fission of ^{252}Cf. These values, slightly adjusted to common values of T_α, are 2.8 ± 1.0, 2 ± 2, 4.6 ± 0.3 and 5.7 ± 0.5 MeV, respectively. Nadkarni has also reported, though with diminished statistical accuracy, a value for $^{236}U^*$

(9.4 MeV) fission indistinguishable from the quoted value for $^{236}U^*$ (6.4 MeV) fission. For the purpose of record, we shall adopt 2.5 ± 1.0 MeV and 5.0 ± 0.5 MeV as 'accepted' values of this kinetic energy difference for the fission of ^{236}U and ^{252}Cf, respectively.

Fraenkel has shown that T_α, the mean kinetic energy of the alpha particles in ^{252}Cf fission is strikingly independent of the mass-ratio $R\,(= A_H/A_L)$. Similarly, Nardi et al. have demonstrated that $(T_L' + T_H')_b - (T_L' + T_H')_t$ is effectively R-independent for the alpha-particle mode in this case. So far, no other case of alpha-particle-accompanied fission has been investigated to this degree of detail. Tentatively accepting it as representative, however, we shall assume that in general the mean difference of the overall kinetic energy of the product particles, as between alpha-particle-accompanied and binary fission, is independent of the mode of mass division, when corresponding modes are in question.

We may estimate a crude first-order approximation to the correction that has to be applied to the measured difference $(T_L' + T_H' + T_\alpha)_t - (T_L' + T_H')_b$ by considering the most probable mode of mass division (when the mass-ratio is R_0) and assuming that the prompt neutrons are emitted equally from the two fragments. Then if $\bar{\nu}_b$ and $\bar{\nu}_t$ are the mean numbers of prompt neutrons emitted (from the two fragments) in binary and alpha-particle-accompanied fission, respectively, this correction is approximately

$$+\frac{\bar{\nu}_b - \bar{\nu}_t}{2A}\left(R_0 + \frac{1}{R_0}\right)\frac{(T_L' + T_H')_b + (T_L' + T_H')_t}{2}$$

A being the mass number of the fissioning nucleus. Taking $\bar{\nu}_b - \bar{\nu}_t = 0.6$ (see below), $A = 252$, $R_0 = 1.3$, we obtain, for the spontaneous fission of ^{252}Cf, an estimated correction of $+0.44$ MeV. Although more extreme assumptions might lead to slightly larger estimates, it is evident that in this case (in which the experimental evidence is most precise) the correction is still hardly significant having regard to present experimental uncertainties.

Prompt neutrons and gamma rays. A direct estimate of the degree of excitation of the residual fragments in alpha-particle-accompanied fission can be made if the yield of prompt neutrons and gamma rays, in this mode, is determined by experiment. Before 1965, only one report had appeared of such an investigation. Apalin et al. [21] had compared the prompt neutron yields in the binary and alpha-particle-accompanied ternary fission of $^{236}U^*$ (6.4 MeV). Using a neutron detector with a solid-angular acceptance of almost 4π, and adopting the value $\bar{\nu}_b = 2.45$, they obtained values of 1.77 ± 0.09 and 1.79 ± 0.13 for $\bar{\nu}_t$ when alpha particles of energy greater than 9 MeV and greater than 22 MeV, respectively, were recorded in coincidence. Later, Nefedov and his co-workers [22 - 24] confirmed and extended these results, showing that whether the neutrons were recorded in directions about the fission axis, or about an axis perpendicular to this, $\bar{\nu}_b / \bar{\nu}_t = 1.38 \pm 0.08$. Furthermore, it appeared that the energy spectra of the neutrons were almost identical in the two modes. Adamov et al. [25], about the same time, reported somewhat different results in relation to the spontaneous fission of ^{254}Cm. Again using large solid angles for acceptance of fission fragments and neutrons, these workers obtained $\bar{\nu}_t = 1.6 \pm 0.2$ on the basis of $\bar{\nu}_b = 2.82$ (a much larger fractional decrease in overall yield than for $^{236}U^*$), and they provided convincing evidence for a negative correlation of $\bar{\nu}_t$ with alpha particle energy: $(\partial\bar{\nu}_t/\partial T_\alpha) = -0.08$ per MeV over the range 15 MeV $\leq T_\alpha \leq$ 25 MeV. In relation to the prompt gamma rays they found no such correlation, and the overall yield appeared to be scarcely significantly different in the two modes $(\bar{\eta}_t/\bar{\eta}_b = 0.88 \pm 0.09)$.

Important information concerning the prompt neutrons associated with the alpha-particle-accompanied fission of ^{252}Cf has more recently been reported by Nardi and Fraenkel [26]. Using neutron detectors aligned along the fission axis, these workers obtained an overall value of 3.11 ± 0.06 for $\bar{\nu}_t$, assuming $\bar{\nu}_b = 3.71$. They were able to analyse their results so as to give both the variation of neutron yield with fragment mass number and its variation with total kinetic energy of the fragments. In the latter respect, they found a negative correlation between $\bar{\nu}$ and $(T_L' + T_H')$ which was insignificantly different for binary and alpha-particle-accompanied fission, and, in the former, they showed that the fractional decrease in yield, as between the binary and ternary modes, is effectively constant over all mass numbers. This second result almost certainly disposes of an earlier suggestion (Feather [17]) that the alpha particles are emitted predominantly, or exclusively, from the heavy fragments.

Very recently the work of Nardi and Fraenkel has been extended by Piekarz et al. [27]. For ^{252}Cf spontaneous fission, $\bar{\nu}_t$ is reported as 3.10 ± 0.08, the angular distribution of these neutrons is stated to be 'quite similar' to that of the neutrons of binary fission, the distribution of yield between light and heavy fragments is 'similar' in the two cases, and it is found that the yield decreases as the kinetic energy of the coincident alpha particle increases – on the average by 0.04 ± 0.01 per MeV.

Characteristic X-rays. Characteristic X-rays are emitted among the prompt radiations of fission as a result of the internal conversion of prompt gamma rays. Since the X-rays are characteristic of the charge number of the nucleus of the emitting atom, their quantum energies are determined by the Z values of the primary fragments, prompt neutron emission being of no consequence. On the other hand, the intensities of the X-rays are not directly representative of the primary-fragment yields (reckoned according to Z values), being significantly dependent on the nature and scale of the spectrum of low-lying excited states of the post-neutron-emission fragments, from which most of the prompt gamma rays originate, and on the variation of internal conversion coefficients and Auger coefficients with Z. Over a small range of A and Z the spectrum of low-lying excited states may be of very different character for different nuclei. In spite of these considerations, a close comparison of the characteristic X-rays emitted 'promptly' in binary and ternary fission must provide information of considerable interest. The first detailed comparison of this character was reported by Kapoor et al. [28] in relation to the spontaneous fission of ^{252}Cf. Somewhat earlier, Rochette et al. [29] had carried out a very similar comparison, using the same material, but had not published an account of their work.

In broad outline, these two groups obtained essentially concordant results. The doubly-peaked energy spectrum of the X-rays proved to be very little different for the binary and ternary modes. The peaks were less broad in the ternary mode, but the ratio of the peak heights was closely the same in each, the decrease in breadth being occasioned by a loss of intensity of the higher-Z X-rays of each peak. Naively interpreted, it was as if alpha-particle emission resulted in loss of charge predominantly by the heavier light fragments and the heavier heavy fragments. In respect of absolute yield, Kapoor et al. deduced values of 0.568 ± 0.006 quanta per binary fission and 0.66 ± 0.03 quanta per alpha-particle-accompanied fission. If this difference is substantiated, it will pose an interesting problem in detailed interpretation. A possible approach lies in the consideration that the nucleon-parity types of the residual (ternary) fragments may be differently distributed as compared with those appropriate to the primary fragments of the binary mode (see below). On this basis there could conceivably be a greater preponderance of even-Z nuclei amongst the post-neutron-emission fragments of the ternary mode than amongst the corresponding fragments of the binary mode.

A short account of a comparison of the characteristic X-rays emitted 'in coincidence' with the fragments of binary and alpha-particle-accompanied fission of $^{236}U^*$ (6.4 MeV) has very recently been given by Solovev and Eysmont [44]. Results entirely analogous to those for ^{252}Cf fission were obtained, but the statistical accuracy was no better than to fix the ratio of ternary to binary X-ray yield as 0.9 ± 0.2.

3. OTHER LIGHT-PARTICLE ACCOMPANIED MODES 'SCISSION NEUTRONS'

The term 'scission neutrons' has latterly been applied to the residue of prompt neutrons which appear, under detailed analysis, to have an angular distribution which is isotropic in the laboratory space, after the majority of the prompt neutrons of binary fission have been accounted for in terms of velocity distributions characteristic of the light and heavy fragments from which they are emitted, the centre-of-mass motion of the fully accelerated fragments having been allowed for. Even today, the most convincing evidence for the existence of these 'central' neutrons comes from the pre-1965 investigation of Bowman et al. [30] with ^{252}Cf. The basic conclusion of these investigators, that it is impossible to account for all the prompt neutrons of fission in terms of post-scission emission from fully accelerated fragments was shortly afterwards supported, in relation to $^{236}U^*$ (6.4 MeV) fission, by Kapoor et al. [31] and by Skarsvag and Bergheim [32]. It appeared that some 10 – 15% of all prompt neutrons belong to this central group, and that the average energy of these neutrons is somewhat greater than that of the prompt neutrons generally. To refer to them as 'scission neutrons', obviously implies that they are emitted at or about the instant of scission – and, if this view is taken, then, of necessity, the process of neutron-accompanied ternary fission is in question. It is for that reason that we deal with the matter here. Essentially, there is no difference between this particular light-particle-accompanied ternary mode, and any other such mode of fission, except that the light particle, in this case, is an uncharged particle, and that the fractional yield is of the order of 0.35 of all fissions, if the conclusions drawn from the experimental results are accepted.

In 1965 Sargent et al. [33] published the results of a detailed, but less than comprehensive, survey of the prompt neutrons from the photofission of ^{232}Th. These investigators looked for the effect of a central component, but were unable to demonstrate its existence with any measure of confidence (0.07 ± 0.09 of all prompt neutrons). On the other hand, in the same year, at the Salzburg symposium, Milton and Fraser [34], reporting on an unfinished experiment on the thermal-neutron induced fission of ^{235}U and ^{239}Pu, concluded that in each case it was impossible adequately to represent the experimental results simply 'by assuming that all the neutrons arise from the moving fragments'. 'Some neutrons more nearly isotropic in the laboratory system are needed'. In a later account of the same work (which has yet to be published in detail) Milton [35] was more specific: 'There is thus no doubt that fragment emission alone cannot account for the fission neutron distribution. Good agreement can be obtained by assuming a central component, but the details of this component are obscured by our lack of understanding of its origin and by experimental difficulties...'. However, the results reported for ^{240}Pu* fission were of sufficient statistical accuracy for analysis in four intervals of fragment mass ratio and three intervals of total fragment kinetic energy. This analysis showed that 'in all cases an acceptable fit could be obtained only if a central component was assumed'. Overall, it appeared that the proportion of central neutrons was significantly greater for ^{240}Pu* fission than for ^{236}U* fission.

In 1966 Blinov et al. [36] reported a detailed comparison of the energy spectra of the prompt neutrons from the thermal-neutron induced fission of ^{233}U and ^{235}U, and of the intensities of these neutrons, at three angles to the fission axis. Thick targets had to be employed, involving the necessity of very fine adjustments in discrimination, but these workers satisfied themselves that the energy spectra were indistinguishable at all three angles, and that the angular distributions were essentially the same (from their figure, the ratio of the intensities at 90° and 0° to the fission axis was $2.5 \pm 2\%$ greater for ^{234}U* fission than for ^{236}U* fission). They concluded that if scission neutrons are in fact emitted in the one case, then they occur with essentially the same fractional yield in the other.

The most recent publication to deal with the problem of the scission neutrons is that of Cheifetz and Fraenkel [37]. Primarily concerned with a possible central component in the prompt neutrons arising from the fission of ^{238}U induced by 12 MeV protons, these investigators calibrated their time-of-flight arrangement using a source of ^{252}Cf. Incidentally, in the course of this calibration, they obtained a value of 0.25 ± 0.20 neutrons per fission for the central component from this source. For ^{239}Np* (17 MeV) they found a central component of 0.62 ± 0.25 neutrons per fission. Earlier work having led to the expectation that there would be some 0.34 ± 0.10 central neutrons per fission associated with second-stage fission (p, nf), it is possible to see in these results a marginally significant indication of a small component of scission neutrons also.

In summary, it has to be concluded that the problem of the reality of the scission neutrons still poses a serious challenge to the experimenter. There would be added confidence, perhaps, if under the same experimental conditions the distribution of prompt neutrons from one mode of fission were to be found not to need the central component for its full description, whilst the distribution relative to another mode required such a component. Possibly a more extended comparison than has hitherto been achieved of the distributions relative to alpha-particle-accompanied fission and binary fission of the same nucleus might provide such a situation. Pik-Pichak [38] was probably the first to express the opinion that 'there appears to be little likelihood that non-evaporation neutrons will be emitted in ternary fission along with the alpha particle'.

Light charged particles other than alpha particles. The first indication that light charged particles other than alpha particles might be emitted in the fission process was provided by the discovery of tritium in neutron-irradiated uranium by Albenesius [39] in 1959. Using a source of ^{252}Cf, Watson [40] was the first to identify the tritons as particles, and to obtain a rough energy spectrum, employing a $\Delta T, T$ double detector to distinguish these long-range particles from the alpha particles. By 1965, it was generally accepted that triton-accompanied ternary fission is a regular mode, having a fractional yield somewhat less than 10% of that of the alpha-particle mode.

In confirming the results of Watson with ^{252}Cf, and using essentially the same method, but with greater statistical accuracy, Whetstone and Thomas [41], in 1965, established the presence of protons in smaller yield (deuterons were not observed) and of ^{6}He particles with a yield of about 1.5 per hundred alpha particles. They reported indications of ^{8}He particles, and of particles of charge numbers 3 and 4, though with less confidence. Further investigations of the light charged particles from $^{236}U^*$ (6.4 MeV) were carried out by Marshall and Scobie [42], Chwaszczewska

TABLE I. MEASURED RELATIVE YIELDS OF LONG-RANGE PARTICLES IN ^{252}Cf SPONTANEOUS FISSION (FROM COSPER et al. [45])

Particle	^{1}H	^{2}H	^{3}H
Measured relative yield	1.10 ± 0.15	0.63 ± 0.03	6.42 ± 0.20
Kinetic energy interval (MeV)	7.3 - 18.8	5.3 ± 21.5	6.5 - 24.3
Particle	^{3}He	^{4}He	^{6}He
Measured relative yield	$< 7.5 \times 10^{-3}$	100	1.95 ± 0.15
Kinetic energy interval (MeV)	14.2 - 21.3	8.3 - 37.7	10.0 - 33.3
Particle	^{8}He	Li isotopes	Be isotopes
Measured relative yield	$6.2 \pm 0.8 \times 10^{-2}$	0.126 ± 0.015	0.156 ± 0.016
Kinetic energy interval (MeV)	9.3 - 27.7	15.2 - 37.3	23.0 - 49.1

et al. [43] and Dakowski et al. [7]. The Warsaw groups, in particular, obtained evidence for the emission of all the particles reported by Whetstone and Thomas with ^{252}Cf, and were the first to identify the weak deuteron component with any certainty. Dakowski et al. investigated the kinetic energy spectra of protons, deuterons, tritons, alpha particles and ^{6}He particles, showing that the spectra were of Gaussian shape, with the peak energies very little different for the $Z = 1$ particles, though markedly less for the ^{6}He particles than for the alpha particles. For the tritons and alpha particles they quoted peak energies of 8.6 ± 0.3 MeV and 15.7 ± 0.3 MeV, respectively.

In February 1967 groups at Los Alamos and Berkeley reported their more detailed findings with ^{252}Cf. Essentially, their results are in full agreement, though the Berkeley workers, Cosper et al. [45], used equipment of greater discrimination (an array of four detectors, ΔT_1, ΔT_2, T_1 and T_2) and were able to claim higher statistical accuracy than the others (Whetstone and Thomas [46]). For sake of the record, we reproduce here the central part of the summary table of Cosper et al., indicating the measured relative yields of particles of the various types and the kinetic energy intervals to which these 'uncorrected' yields apply. We have omitted from this table the relative yields of the individual lithium and beryllium isotopes: these were studied only over the uppermost intervals of kinetic energy (> 25 MeV and >40 MeV, in the two cases, respectively). Only in the case of the lithium isotopes was the information obtained in this way sufficient to indicate individual yields with some confidence. It appears that the yield of ^{7}Li is, in fact, at least five times as great as that of ^{6}Li, ^{8}Li or ^{9}Li, though all these isotopic particles were separately identified.

Very recently, the Warsaw group (Błocki et al. [47]) has published the results of yield determinations for the total lithium and beryllium isotopes in $^{236}U^*$ (6.4 MeV) fission. Recording only those particles having kinetic energies greater than 11.5 MeV and 17.1 MeV, in these two groups, they quote relative yields of 0.088 ± 0.002 (Li) and 0.185 ± 0.002 (Be) per hundred alpha particles.

A first detailed determination of relative yields of the light charged particles from $^{240}Pu^*$ (6.4 MeV) fission has just been reported by Krogulski et al. [48]. Only the $Z = 1$ and $Z = 2$ particles were identified, but the measured yields were almost identical with those quoted in Table I. A similarly recent report by Cambiaghi et al. [49] refers to $^{234}U^*$ (6.7 MeV). These workers find fewer tritons and deuterons, and fewer ^{6}He particles, relative to the alpha particles, than would correspond to the entries in Table I - and they are the first to claim a significant yield of ^{3}He particles. It will be interesting to see whether these results for $^{234}U^*$ fission are substantiated.

All the investigations so far mentioned refer to the emission of light charged particles in thermal-neutron-induced or spontaneous fission. Adamov et al. [5] have compared the relative yields of protons (after correction for background effects), tritons (together with unresolved deuterons) and alpha particles in the fission of ^{235}U induced by thermal and 14 MeV neutrons, respectively. The relative yields appear to be indistinguishable at these two energies, within the uncertainty of the experiment, and the overall ratio of ternary to binary modes appears to be the same to within 5%, or thereabouts.

The relative yields (occurrence probabilities) of the various light-particle-accompanied modes will eventually be crucial for any dynamical theory of the fission process; currently, however, the simple energetics of the process is of more immediate interest. It has already been stated that the trajectory calculations of Raisbeck and Thomas [9] and Blocki and Krogulski [15] were concerned primarily with matching the kinetic energy spectra of the alpha particles and the other light particles involved. In this connection the experiments of Raisbeck and Thomas provide certain essential data. These workers were the first to observe any of the light charged particles, other than the alpha particles, in coincidence with the fission fragments. They were thus able to investigate the angular distributions of these particles relative to the fission axis as well as the kinetic energy spectra (concerning which abundant information was already available). Their demonstration that all the various particles with the possible exception of the protons, 'are strongly peaked at 90° with respect to the major fragments', was the first objective verification of the generally held belief that all 'are probably released by a common mechanism'. This had been the obvious hypothesis ever since it had been shown that the kinetic energy spectrum of the tritons was almost the same as that of the alpha particles, once the energy scale had been reduced by a factor 0.5 (Watson [40]).

We have already listed the set of initial parameters which Raisbeck and Thomas found adequate, in their trajectory calculations, to describe the observed energy spectrum of the alpha particles: these workers found that the same set of initial parameters, with the same value of the mean energy of particle release, was equally satisfactory as a basis for the description of the energy spectrum of the tritons which they directly determined. For the other particles they had to rely on the energy spectra obtained by other workers (specifically Cosper et al. [45]). In those cases the agreement between the calculated and the observed spectral shapes was not so precise, but the general decrease in the peak energy with increase in mass number of the $Z = 2$ particles was faithfully reproduced. Overall, the belief in a common mechanism of release for all light charged particles was greatly strengthened by these investigations. Błocki and Krogulski [15] compared the results of their trajectory calculations with the experimental energy spectra of the Warsaw groups [43, 44] and reached conclusions very similar to those of Raisbeck and Thomas. In each set of calculations difficulty was found in satisfactorily matching the angular distributions and the energy spectra of the various particles simultaneously. This difficulty is probably to be ascribed to the extreme simplification of the models used.

Apart from trajectory questions, the other aspect of the energetics of the less probable modes of light-particle-accompanied fission that has recently come within the scope of experiment is that of light-particle/fragment kinetic energy correlation. Nardi et al. [18] have extended this type of investigation from the alpha particles to the tritons and protons in the case of ^{252}Cf spontaneous fission. In a four-parameter correlation experiment, these workers obtained for each recorded event, a light-particle-type signature, the kinetic energy of the particle, and the kinetic energies of the two residual fragments in coincidence with it. On this basis they were able to conclude that the distribution in mass of the residual fragments of triton-accompanied fission is almost identical with that of the alpha-particle-accompanied mode, and the overall distribution of total fragment kinetic energy almost the same in all three modes (proton-, triton-, and alpha-particle-accompanied modes). In greater detail, they showed that the variation of mean total fragment kinetic energy with fragment mass ratio, R, follows the same general trend in all three modes. Only in two aspects did the proton-accompanied mode appear somewhat anomalous. The distribution in mass of the residual fragments was more markedly different from that of the primary fragments of binary fission than in the other cases (possibly indicating a preponderance of proton-accompanied events with near-symmetrical mass division), and the inverse correlation between the kinetic energy of the light particle and the total kinetic energy of the residual fragments (characteristic, equally, of the triton- and alpha-particle-accompanied modes) was not in evidence. These are matters on which further research will clearly be profitable.

In summary, it is now well established that fission involving light-charged-particle emission occurs in many modes: particles having charge numbers 1 to 4 ($Z = 5$ and $Z = 6$ particles have been tentatively reported [9]), and mass numbers 1 to 10, have been definitely identified. With some slight reservation in respect of protons, it appears that the release process is of the same character for all these particles.

4. CHALLENGE TO THE THEORIST

In a contribution to the Salzburg symposium, Halpern [50] posed the essential problem which the theorist has to encompass if he is to provide a dynamical description of the phenomenon of light-particle-accompanied fission. 'Generally', he wrote, 'the [energy stored in the collective degrees of freedom associated with the distortion of the fissioning nucleus] is handed on to the distortions of the individual [binary] fragments, but on rare occasions it is made available to a third particle'. The problem for the theorist is to provide a formal description of this process of 'handing on' of energy. An important 'boundary condition' is the extreme shortness of the time scale - of the order of 10^{-21} s. Broadly speaking, no real progress towards a solution to the problem has been made in the last four years. Halpern himself concluded 'that the release of the [light particle] is a sudden rather than an adiabatic process'. The matter has effectively rested there, ever since.

In relation to this theoretical problem, it is obviously important to know how much energy is available, and how much has to be concentrated on the emitted particle in the act of separation. In respect of the alpha-particle-accompanied fission of $^{236}U^*$ (6.4 MeV), information in respect of the first point is provided by the detailed investigation of Schmitt et al. [51]. These workers determined the total kinetic energy distribution for the fragments of binary fission of this nucleus as a function of the fragment mass-ratio R. Over the range of values of R significant for the alpha-particle-accompanied mode, they found the root-mean-square width of this distribution to vary monotonically (R increasing) from $\pm$ 10.5 MeV to $\pm$ 7 MeV. On the basis of energy conservation, these values give the corresponding spread of the energies of initial deformation-excitation of the binary fragment pairs. Making use of information concerning the variation of prompt neutron yield with R, and checking their conclusions against Q-values calculated from tabulated masses, Schmitt et al. also deduced the mean values of the total fragment deformation-excitation energies in their dependence on R. The picture that finally emerges is that the total initial deformation-excitation energy of the paired fragments in this case varies from 29±10.5 MeV for the mode of mass division (107/129), through a minimum of 22±10 MeV for the mode (102/134) to a greatest value 30.5±7 MeV for the more asymmetrical mode (85/151).

Concerning the amount of energy that has to be concentrated on the emitted particle in the act of separation, the estimate generally adopted is that of Halpern [50]. Halpern's estimate is based on a much simplified model of the separation process, and in the published account, at least, he has given numerical values only in relation to equal division of mass and charge between the fragments. Effectively, Halpern starts with these binary fragments 'at rest at infinity', then he considers the different amounts of work that have to be done (a) to bring the fragments reversibly to the scission-separation D, (b) first to separate the light particle from one of them and then bring the three resultants of the ternary mode reversibly into a linear configuration in which the (ternary) fragments are at separation D and the light particle is mid-way between them. The amount by which the work in (b) exceeds that in (a), is taken by Halpern to provide a measure of the energy that has to be concentrated on the light particle, at or shortly after the instant of scission, in the ternary mode. In estimating the electrostatic potential energy component of this energy total, Halpern used the point-charge (or spherical nucleus) approximation. If the binary fragments are of charge number Z, and the light particle is an alpha particle, Halpern's treatment leads to the result

$$E_R = B_\alpha + \frac{6Z-8}{Z^2} V_0$$

where B_α is the energy required to separate the alpha particle from one of the fragments in (b) and V_0 is the mutual electrostatic potential energy of the binary fragments at separation D - or, to a sufficient approximation, to

$$E_R = B_\alpha + \frac{3}{2} V_\alpha \tag{1}$$

V_α being the mutual potential energy of the alpha particle and the binary fragment from which it separated, at separation D/2. Taking 5 MeV as a representative value for B_α, and adopting 2.0×10^{-14} m for D, Halpern obtained 24 MeV for E_R, the energy which has to be concentrated on the alpha particle to effect its release (with zero kinetic energy) in the space between the fragments in the ternary mode.

Although it is clear that Halpern's result must be correct as to order of magnitude, it is open to doubt whether it can be more reliable than this. This doubt focuses on the approximations inherent in the model. It must be admitted, on the weight of all the evidence, that the light-particle-accompanied mode 'develops out' of the binary mode at a late stage in the process. It is highly unrealistic, therefore, to employ a model which describes the process of light-particle separation as the abstraction of charge (or nucleons) from a spherically-symmetrical binary fragment: it must be the case that the constituents of the alpha particle (for example) are already present in the neck of the fissioning nucleus at the stage when the 'decision' between binary or ternary fission is effected. This criticism has already been expressed by Fraenkel [8], and the present reviewer has recently explored the matter from this point of view (Feather [52]). The basic assumption is that at two succeeding instants, the one immediately before, the other immediately after, the light particle 'becomes identifiable (in thought) in the space between the fragments', the distribution of charge in the system is essentially the same. The pertinent question is: by how much must the energy of deformation-excitation of the fragments be suddenly reduced (in the interval between these two instants) if the light particle is to be set free exoergically? In general, different numerical answers are obtained, depending upon the fragment mass-ratio R, and upon the way in which the constituent nucleons of the emitted particle are assumed to be drawn from the two 'nascent' binary fragments. If these fragments are denoted by (A_L, Z_L), (A_H, Z_H), and if the light particle is an alpha particle, there are nine ways in which the four nucleons can be assembled from the fragments (Feather [53]). The nucleons drawn from the nascent light fragment may be 0, 1n, 1p, 2n, 2p, 1n1p, 2n1p, 1n2p or 2n2p, the remaining nucleons being drawn from the heavy fragment. In this case, if we label these various modes of alpha-particle assembly using subscript r (r = 1, 2, ..., 9), and if ΔE_r is the amount by which the deformation-excitation energy must be reduced if an alpha particle is to be released in the r th mode, we obtain

$$\Delta E_r \geqq B_r(L) + B_r(H) - B(\alpha) + V_r(L_r) + V_r(H_r) - V_r(\alpha) \qquad (2)$$

Here $B_r(L)$ denotes the total energy which has to be supplied to separate, one by one, from the nucleus (A_L, Z_L) in its ground state, the various nucleons contributed by this nascent light fragment to the alpha particle in mode r, similarly for $B_r(H)$, and $B(\alpha)$ denotes the total energy necessary to separate the alpha particle into its four constituent nucleons. $V_r(L_r)$ denotes the energy which has to be expended (against purely electrostatic forces), to bring, from infinity, into suitable conjunction with the residual ternary light fragment L_r, the nucleons which, in mode r, separate from the nascent binary fragment L - similarly for $V_r(H_r)$. In this connection, 'suitable conjunction' implies that, the residual ternary fragment having the initial deformation of the ternary mode, the separated nucleons are brought up to it in such a way as to reconstitute the configuration of the nascent binary fragment with initial deformation appropriate to the developing binary mode. $V_r(\alpha)$ is the corresponding work performed (against purely electrostatic forces) in assembling the alpha particle out of the two groups of nucleons of mode r ($V_r(\alpha)$ is different from zero only when one proton is contributed by each of the nascent binary fragments). It will be noted that inequality (2) has precisely the same form as Halpern's equation (1), the right-hand member involving the sum of contributions of particle binding energy and electrostatic potential energy, respectively. However, the individual contributions are not the same.

In Table II numerical values are given, calculated on the basis of inequality (2), using the same value of D as Halpern used, setting $V_r(\alpha) = 0.9$ MeV for those modes in which this quantity is not identically zero, and taking values of the relevant binding energies from the compilation of Zeldes et al. [54]. The entries in the table relate to four reference modes of binary fission of ^{236}U, chosen as near-most-probable modes, and as representing the four possibilities in respect of nucleon-parity type for the paired fragments. For an (e, e) fissioning nucleus, such as we are here concerned with, the two complementary fragments of binary fission must always be of the same nucleon-parity type (Feather [53]).

Two conclusions emerge directly from the data presented in Table II. In the first place, the values of the minimum 'expense in energy' of alpha-particle separation are consistently less, by a considerable margin than the value estimated by Halpern. Secondly, even for this compact sample of 'corresponding' binary modes of mass and charge division, the minimum energy expense varies almost by a factor of two, depending on the nucleon-parity type of the binary mode, and on the mode of assembly of the four nucleons of the alpha particle from the nascent binary fragments. Only when all four nucleons are taken from the same fragment (modes 1 and 9), or two neutrons from one fragment and two protons from the other (modes 4 and 5), is the energy expense relatively insensitive to the nucleon-parity type of the binary fragments concerned. Taking these four alpha-particle assembly modes together, the least expense is incurred when a pre-formed alpha particle separates entire from the heavy fragment in an (e, e) binary mode. Amongst the other modes, however, there are several for which the energy expense is considerably less than this. Pre-eminent is the case in which ($r = 6$) one proton and one neutron are contributed by each of a pair of complementary binary fragments of type (o, o); next in order of 'profitability' are those in which ($r = 3$) a single proton is contributed by an odd-Z light fragment and one proton and two neutrons by the complementary heavy fragment. For the modes of mass and charge division represented in Table II, these three least unprofitable modes of alpha-particle release are characterized by values of minimum energy expenditure of 11.5, 12.8 and 13.4 MeV, respectively.

TABLE II. CALCULATED MINIMUM VALUES (IN MeV) OF THE REDUCTION IN DEFORMATION-EXCITATION ENERGY OF THE FRAGMENTS NECESSARY TO PERMIT SEPARATION OF AN ALPHA PARTICLE IN THE FISSION OF ^{236}U. VARIOUS MODES OF ASSEMBLY OF THE ALPHA PARTICLE SPECIFIED BY r (SEE TEXT). NASCENT BINARY LIGHT FRAGMENT (A_L, Z_L); NUCLEON-PARITY TYPE OF NASCENT BINARY FRAGMENTS GIVEN IN TERMS OF NEUTRON AND PROTON NUMBERS (N, Z).

r / (A_L, Z_L)	1	2	3	4	5	6	7	8	9	(N, Z)
(93, 37)	16.8	19.8	12.8	19.7	17.4	15.4	14.2	18.8	17.2	(e, o)
(94, 37)	16.2	15.4	13.4	18.5	18.3	11.5	14.1	16.1	17.5	(o, o)
(95, 38)	16.2	15.8	17.1	20.0	16.3	16.3	19.4	14.4	17.1	(o, e)
(96, 38)	15.7	19.3	17.7	19.0	17.4	20.2	19.5	19.5	17.6	(e, e)

From a detailed examination of the experimental evidence, it has been estimated (Feather [55]) that the mean initial deformation-excitation energy of the residual fragments of the alpha-particle-accompanied fission of $^{236}U^*$ (6.4 MeV) is less than the corresponding quantity for the fragments of binary fission of that nucleus by 6.5 ± 2 MeV. This difference, on any view, is considerably smaller than the mean amount of nascent binary fragment deformation-excitation energy which has to be expended in alpha-particle release. To fix a value for this latter quantity on the basis of inequality (2), it would be necessary to extend Table II to cover the whole range of binary fragment mass and charge, and to know, in much greater detail than we do, the relative weights to assign to the division-modes of the different nucleon-parity types. In the absence of such knowledge, we can only guess what the 'correct' value should be. Accepting 15 MeV as such a guess, and allowing an additional 2 MeV for the mean energy of alpha-particle release, we conclude that the alpha-particle-accompanied ternary mode develops out of the binary mode, in this case, only when the total deformation-excitation energy of the nascent binary fragments is, on average, some 10 MeV greater than the mean value for binary modes generally. These developing binary modes, being modes of unusually large deformation, are, by the same token, modes involving greater-than-normal fragment separation at scission, and less-than-normal fragment kinetic energy. In accordance with the numerical values that we have already adopted, we may conclude that the separation at scission, for those binary modes which develop into ternary modes through alpha-particle release, is some 1.3×10^{-15} m greater than the average separation for all binary modes, in this case. It may be noted that, if Halpern's estimate of E_R (Eq. (1)) were used in this argument, we should have to conclude that 20 MeV greater-than-normal nascent binary fragment deformation characterizes those fission events which exhibit the ternary mode. This is too large a value to be plausible, having regard to the findings of Schmitt et al. [51] which we have already discussed.

This section is entitled 'Challenge to the theorist'. The essence of that challenge is to provide a formal description, within the framework of accepted theory, of the process of binary scission, and from that description to educe the naturally inherent features which anticipate the possibility of the sudden collapse of deformation leading to light-particle release. If such a description can be achieved it may, perhaps, provide a clear answer to the question whether deformation collapse of this sudden type is more likely at the instant of scission, abstracting energy from the over-stretched neck of the fissioning nucleus, or slightly later, in the tip of a more-than-usually prominent protuberance on a newly formed fragment. Alternatively, the successful theoretical account of the process may well indicate that this particular distinction is devoid of all meaning. It is not for a non-theorist to hazard a guess in this respect.

5. 'TRUE' TERNARY FISSION

Basically, there are only three experimental methods available for the study of the phenomenon of 'true' ternary fission: the nuclear emulsion method, the method of triple coincidence between individual particle detectors, and the method of radiochemical analysis. Effectively exploited, the last-mentioned method can give unambiguous, negative, answers to certain specific questions ('does the radioactive species X occur as a fission product with yield greater than y per cent?'). On the other hand, it is much more difficult to extract unambiguously positive conclusions from observations made by either of the other techniques. The ternary yield being small in any case, the difficulty lies in distinguishing the genuine from the spurious event, the particle ranges being short.

The nuclear emulsion method provided the earliest indications of the possible occurrence of ternary fission leading to three fragments of not very disparate mass, but it is now largely superseded by the other methods listed. Benisz and his colleagues [56], however, have continued to employ this method, and have recently reported ternary-to-binary ratios between 5×10^{-4} (for $^{239}U^*$ (19 MeV) fission) and 3×10^{-3} (for $^{233}Th^*$ (8 MeV) fission) - having in each case rejected some 85% of all observed three-pronged tracks as spurious. It must be stated that there is no confirmation of any sort for an overall yield of ternary fission events of this order of magnitude.

By far the most sustained investigation of true ternary fission has been that initiated by Muga some eight years ago, of which a progress report [57] was given to the Salzburg symposium in 1965. Using three semiconductor detectors arranged, in coincidence, with their axes symmetrically disposed in a plane, so as to converge on the fission source, Muga and his colleagues have reported [58, 59] positive results, and a ternary yield of the order of 10^{-6} per binary fission, with ^{252}Cf, $^{242}Pu^*$, $^{240}Pu^*$, $^{236}U^*$ and $^{234}U^*$. Much importance is attached to the empirical result that the crude pulse-height spectra of the triple coincidences is significantly different for $^{236}U^*$ and $^{234}U^*$, and again for $^{242}Pu^*$ and $^{240}Pu^*$ fission. (In each case, the excited compound nucleus is that formed by thermal-neutron capture.) Moreover, the spectral differences are of the same nature for these two isotope pairs. The argument is that if the coincident events were spurious (arising from binary fragment scattering), then there should be no appreciable difference between the triple-coincidence energy spectra for two fission sources of which the physical dimensions and chemical composition were precisely the same (only the isotopic compositions being different). At face value, this argument appears convincing - though it has to be admitted that the authors' view, that the differences in question, which are correlated with a difference of two neutrons in the constitution of the fissioning nuclei, exhibit 'the dominant effect of underlying shell structure in forming the product fragments', seems much less securely based.

Not content to rely on the internal evidence just mentioned, Muga et al. [58] made an independent experimental (and theoretical) investigation of the scattering of fission fragments incident normally on a UF_4 target. Their arrangement reproduced that of their primary experiment as nearly as possible, and they were able to show, in relation to the symmetrical (120° - 120° - 120°) disposition of detectors, that scattering effects were insignificant. This was not the case for a less symmetrical (130° - 100° - 130°) disposition (for which their theoretical estimates, also, predicted significant scattering). As a result of these various checks, this group of workers is led to claim positive evidence for true ternary fission recorded by detectors in the 120° - 120° - 120° configuration, but no such unambiguous evidence when the configuration is slightly changed to 130° - 100° - 130°. On the basis of their theoretical estimates, Muga et al. recognize that the detector configuration 140° - 80° - 140° should be significantly 'safer', in relation to scattering effects, than the fully symmetrical configuration which they have traditionally employed. It would seem that further work with this 'safe' configuration would be desirable. In the only comparison for which figures are published, ternary yields appear to be smaller, by a factor between 3 and 7, when this particular configuration is used, than they are with the fully symmetrical (equiangular) configuration of particle detectors.

In summary, Muga et al. claim to have evidence for true ternary fission, with a yield of about 10^{-6} per binary fission, with several nuclei at low excitation (< 7 MeV), the phenomenon being sharply restricted as to relative spatial orientation, and probably sharply defined in relation to the identity of the lightest fragment (mass number somewhere in the range 28 to 38, or, alternatively, in the range 50 to 60).

The last-mentioned restriction does not arise directly out of the experimental results of the coincidence experiments (in which mass-number resolution is of the order of several units); it is essentially imposed by consideration of the work of the radiochemists. There would be a glaring inconsistency between the two sets of experimental findings if it were not accepted: over the whole range of mass numbers from 28 to 60, the radiochemists have consistently failed to identify radioactive products of low-energy fission in appropriate yield – whenever they have been able adequately to test for their presence. An appearance of consistency between the radiochemical and the instrumental findings would be impossible to maintain if the hypothesis of certain sharply defined light-fragment mass numbers (preferably those of stable species) were not invoked. Representative of the more recent radiochemical work on low-energy fission is that of Stoenner and Hillman [60]. For $^{236}U^*$, these investigators report apparent yields as follows: ^{42}A $(1.1 \pm 1.7) \times 10^{-13}$, ^{41}A $(2.8 \pm 0.2) \times 10^{-11}$, ^{39}A $(3.10 \pm 0.02) \times 10^{-9}$, ^{37}A $(8 \pm 2) \times 10^{-10}$, ^{56}Co $(4 \pm 4) \times 10^{-10}$ per binary fission – and they are not entirely convinced that even these low figures do not represent residual impurity effects.

One positive result from radiochemical studies derives from the work of Iyer and Cobble [61] – but it does not refer positively to low-energy fission. Under conditions of extreme stringency in respect of chemical purity, these workers have collected radioactive fission products of low mass number (and have failed to identify products in the complementary range of high mass number), by the method of recoil, when ^{238}U is bombarded by helium ions of energy up to 120 MeV. In the case of individual products (^{24}Na, ^{28}Mg and ^{38}S) they have investigated the variation of yield with the energy of the bombarding particle. For ^{28}Mg (the most thoroughly investigated product) the yield decreases steadily by a factor of 10^4 as the bombarding energy is decreased from 120 MeV to 24 MeV – by which stage it is no more than 10^{-7} in comparison with that of ^{89}Sr, a high-yield binary fission product which was similarly studied as a reference standard. Putting together this new evidence with that from earlier studies, by the same group, of the binary-fragment mass-yield curve obtained under bombardment with helium ions of 39 MeV, it appears that the smallest yield in the low mass-number range is for $A \approx 47$, or thereabouts. For $A < 47$ the yield increases again as A decreases (unmatched by a similar increase with increasing A for $A > 195$). This general result, and other detailed observations, lead the authors to conclude that true ternary fission (with a light fragment having $A < 47$) begins to be appreciable when the excitation energy of the fissioning nucleus ($^{242}Pu^*$) exceeds 19 MeV. If it occurs at smaller excitations than this, then they have no evidence of it in terms of the low-A products which they investigated. There we must leave the question of true ternary fission at low excitations for the present - with many pertinent questions still unanswered.

It is almost outside the scope of this review to refer to experiments at higher energies and relating to heavier compound nuclei, but it may be mentioned that Fleisher et al. [62], in an exploratory study of the fission of ^{232}Th induced by bombardment with 400-MeV argon ions, have reported a ternary yield as high as 1/30 of the binary yield - and by more conventional methods, Karamyan et al. [63], using neon and argon ions having energies up to 8 MeV per nucleon, have obtained positive results with targets of ^{209}Bi (^{40}A ions, 310 MeV) and ^{238}U (^{22}Ne ions, 183 MeV; ^{40}A ions, 270 and 310 MeV), and negative results with ^{197}Au (^{22}Ne ions, 185 MeV). Their detection limit was something better than 10^{-5} per binary fission, and the largest positive effect observed ($^{238}U + ^{40}A$, 310 MeV) represented a ternary-to-binary ratio of $(1.3 \pm 0.3) \times 10^{-3}$. In considering these results, Muzychka et al. [64] have concluded that they are more likely to be evidence for a two-stage process of tripartition (a highly excited heavy fragment undergoing second-stage binary fission), rather than for 'true' (instantaneous) ternary fission.

REFERENCES

[1] ATNEOSEN, R.A., THOMAS, T.D., GARVEY, G.T., Phys. Rev. 139 (1965) B307.

[2] THOMAS, T.D., WHETSTONE, S.L., Phys. Rev. 144 (1966) 1060.

[3] LOVELAND, W.D., FAIRHALL, A.W., HALPERN, I., Phys. Rev. 163 (1967) 1315.

[4] NAGY, L., NAGY, T., VINNAY, I., Yadern. Fiz. 8 (1968) 443.

[5] ADAMOV, V.M., KOVALENKO, S.S., PETRZHAK, K.A., TYUTYUGIN, I.I., Yadern. Fiz. 6 (1967) 930; (translation: Soviet J. nucl. Phys. 6 (1968) 677).

[6] CHWASZCZEWSKA, J., DAKOWSKI, M., KROGULSKI, T., PIASECKI, E., SOWIŃSKI, M., STEGNER, A., TYS, J., Acta phys. pol. 35 (1969) 187.

[7] DAKOWSKI, M., CHWASZCZEWSKA, J., KROGULSKI, T., PIASECKI, E., SOWIŃSKI, M., Phys. Lett. 25B (1967) 213.

[8] FRAENKEL, Z., Phys. Rev. 156 (1967) 1283.

[9] RAISBECK, G.M., THOMAS, T.D., Phys. Rev. 172 (1968) 1272.

[10] NADKARNI, D.M., Preprint, privately circulated.

[11] TSIEN SAN-TSIANG, J. Phys. Radium 9 (1948) 6.

[12] HALPERN, I., CERN Rep. (1963), unpublished.

[13] GEILIKMAN, B.T., KLEBNIKOV, G.I., Atom. énerg. 18 (1965) 218.

[14] BONEH, Y., FRAENKEL, Z., NEBENZAHL, I., Phys. Rev. 156 (1967) 1305.

[15] BŁOCKI, J., KROGULSKI, T., Nucl. Phys. A122 (1968) 417.

[16] SCHMITT, H.W., FEATHER, N., Phys. Rev. 134 (1964) B 565.

[17] FEATHER, N., Proc. R. Soc. Edin. 66A (1964) 192.

[18] NARDI, E., GAZIT, Y., KATCOFF, S., Phys. Rev. (to be published).

[19] SCHRÖDER, I.G., thesis, Columbia Univ. (1965), unpublished; Nucl. Sci. Abstr. 20 (1966) 30513.

[20] NADKARNI, D.M., Nucl. Phys. A112 (1968) 241.

[21] APALIN, V.F., DOBRYNIN, Yu.P., ZAKHAROVA, V.P., KUTIKOV, I.E., MIKAELYAN, L.A., Atomn. Énerg. 7 (1959) 375; (translation: J. nucl. Energy 13A (1960) 86).

[22] NEFEDOV, V.N., KROSHKIN, N.I., KHARIN, V.P., MEL'NIKOV, A.K., Atomn. Énerg. 20 (1966) 342.

[23] NEFEDOV, V.N., IVANOV, O.I., KHARIN, V.P., TISHIN, A.S., Yadern. Fiz. 3 (1966) 465; (translation: Soviet J. nucl. Phys. 3 (1966) 337).

[24] IVANOV, O.I., KROSHKIN, N.I., NEFEDOV, V.N., KHARIN, V.P., Yadern. Fiz. 5 (1967) 737; (translation: Soviet J. nucl. Phys. 5 (1967) 523).

[25] ADAMOV, V.M., DRAPCHINSKII, L.V., KOVALENKO, S.S., PETRZHAK, K.A., TYUTYUGIN, I.I., Yadern. Fiz. 5 (1967) 923; (translation: Soviet J. Nucl. Phys. 5 (1967) 655).

[26] NARDI, E., FRAENKEL, Z., Phys. Rev. Lett. 20 (1968) 1248.

[27] PIEKARZ, H., BŁOCKI, J., KROGULSKI, T., PIASECKI, E., private communication.

[28] KAPOOR, S.S., RAMAMURTHY, V.S., RAMA RAO, P.N., Phys. Rev. 166 (1968) 1190.

[29] ROCHETTE, R., FRASER, J.S., SPECHT, H.J., MILTON, J.C.D., private communication.

[30] BOWMAN, H.R., THOMPSON, S.G., MILTON, J.C.D., SWIATECKI, W.J., Phys. Rev. 126 (1962) 2120.
BOWMAN, H.R., MILTON, J.C.D., THOMPSON, S.G., SWIATECKI, W.J., Phys. Rev. 129 (1963) 2133.

[31] KAPOOR, S.S., RAMANNA, R., RAMA RAO, P.N., Phys. Rev. 131 (1963) 283.

[32] SKARSVAG, K., BERGHEIM, K., Nucl. Phys. 45 (1963) 72.

[33] SARGENT, C.P., BERTOZZI, W., DEMOS, P.T., MATTHEWS, J.L., TURCHINETZ, W., Phys. Rev. 137 (1965) B89.

[34] MILTON, J.C.D., FRASER, J.S., in Physics and Chemistry of Fission (Proc. Symp. Salzburg, 1965) 2, IAEA (Vienna, 1965) 39.

[35] MILTON, J.C.D., Mechanics of Fission (Symp. Pittsburgh, 1966) unpublished.

[36] BLINOV, M.V., KAZARINOV, N.M., PROTOPOPOV, A.N., Yadern. Fiz. 4 (1966) 1179; (translation: Soviet J. nucl. Phys. 4 (1967) 848).

[37] CHEIFETZ, E., FRAENKEL, Z., Phys. Rev. Lett. 21 (1968) 36.

[38] PIK-PICHAK, G.A., Yadern. Fiz. 4 (1966) 1147; (translation: Soviet J. nucl. Phys. 4 (1967) 826).

[39] ALBENESIUS, E.L., Phys. Rev. Lett. 3 (1959) 274.

[40] WATSON, J.C., Phys. Rev. 121 (1961) 230.

[41] WHETSTONE, S.L., THOMAS, T.D., Phys. Rev. Lett. 15 (1965) 298.

[42] MARSHALL, M., SCOBIE, J., Phys. Lett. 23 (1966) 583.

[43] CHWASZCZEWSKA, J., DAKOWSKI, M., KROGULSKI, T., PIASECKI, E., PRZYBORSKI, W., SOWINSKI, M., Phys. Lett. 24B (1967) 87.

[44] SOLOVEV, S.M., EYSMONT, M.P., Izvestiya Akad. Nauk SSSR (Fiz.) 33 (1969) 159.

[45] COSPER, S.W., CERNY, J., GATTI, R.C., Phys. Rev. 154 (1967) 1193.

[46] WHETSTONE, S.L., THOMAS, T.D., Phys. Rev. 154 (1967) 1174.

[47] BŁOCKI, J., CHWASZCZEWSKA, J., DAKOWSKI, M., KROGULSKI, T., PIASECKI, E., SOWINSKI, M., STEGNER, A., TYS, J., Nucl. Phys. A127 (1969) 495.

[48] KROGULSKI, T., CHWASZCZEWSKA, J., DAKOWSKI, M., PIASECKI, E., SOWINSKI, M., TYS, J., nucl. Phys. A128 (1969) 219.

[49] CAMBIAGHI, M., FOSSATI, F., PINELLI, T., Nuovo Cim. 59B (1969) 236.

[50] HALPERN, I., in Physics and Chemistry of Fission (Proc. Symp. Salzburg, 1965) 2, IAEA (Vienna, 1965) 369.

[51] SCHMITT, H.W., NEILER, J.H., WALTER, F.J., Phys. Rev. 141 (1966) 1146.

[52] FEATHER, N., submitted for publication, Proc. R. Soc. Edin.

[53] FEATHER, N., Phys. Rev. 170 (1968) 1127.

[54] ZELDES, N., GRILL, A., SIMIEVIC, A., Mat.-fys. Skr. Dan. vid. Selsk., 3 5 (1967) 1.

[55] FEATHER, N., Phys. Rev. 170 (1968) 1118.

[56] BENISZ, J., PANEK, T., Acta phys. pol. 32 (1967) 485.
BENISZ, J., Acta phys. pol. 35 (1969) 67.
BENISZ, J., JASIELSKA, A., PANEK, T., URBAŃSKI, E., private communication.

[57] MUGA, M.L., in Physics and Chemistry of Fission (Proc. Symp. Salzburg, 1965) 2, IAEA, Vienna, 1965) 409.

[58] MUGA, M.L., RICE, C.R., SEDLACEK, W.A., Phys. Rev. Lett. 18 (1967) 404; Phys. Rev. 161 (1967) 1266.

[59] MUGA, M.L., RICE, C.R., Univ. Florida, Rep. ORO-2843-13 (1968).

[60] STOENNER, R.W., HILLMAN, M., Phys. Rev. 142 (1966) 716.

[61] IYER, R.H., COBBLE, J.W., Phys. Rev. Lett. 17 (1966) 541; Phys. Rev. 172 (1968) 1186.

[62] FLEISHER, R.L., PRICE, P.B., WALKER, R.M., HUBBARD, E.L., Phys. Rev. 143 (1966) 943.

[63] KARAMYAN, S.A., KUZNETSOV, I.V., OGANESKYAN, Yu.Ts., PENIOUZHKEVICH, Yu.E., Yadern. Fiz. 5 (1967) 959; (translation: Soviet J. nucl. Phys. 5 (1967) 684).

[64] MUZYCHKA, Yu.A., OGANESYAN, Yu.Ts., PUSTYLNIK, B.I., FLEROV, G.N., Yadern. Fiz. 6 (1967) 306; (translation: Soviet J. nucl. Phys. 6 (1968) 222).

DISCUSSION

R. VANDENBOSCH: Could you explain to me why, for the configuration in the right-hand sketch of Fig. A, the energy is lower when the alpha particle is close to one fragment than for a similar configuration with the alpha particle midway between the two fragments?

FIG. A. Fragment configurations.

N. FEATHER: I do not make that assertion. On the other hand, I do assert that Halpern's model, which postulates a large change in Coulomb energy at the instant of alpha-particle appearance, is an unrealistic one. I prefer to go to the other extreme and postulate that the change of Coulomb energy is zero (the constituents of the alpha particle 'are there already').

R. VANDENBOSCH: I believe your estimates of B_α are based on mass equations. Is that correct?

N. FEATHER: Yes.

R. VANDENBOSCH: I think that if you perform a consistent analysis of the energies you will find that you must use a scheme more like Halpern's. The mass equation from which B_α is calculated accounts for the change in Coulomb energy for removing an alpha particle from an isolated fragment to an infinite separation from the residual nucleus.

N. FEATHER: The B_α deduced from the mass equation certainly involves an electrostatic potential energy component, but I am prepared to argue that this component appears a second time when the problem of alpha particle release is treated according to the model now proposed. A full treatment has been accepted for publication in the Proceedings of the Royal Society, Edinburgh.

C. SYROS: As is known from heavy ion reactions, alpha-clusters and even heavier clusters are formed on the surface of nuclei. The separation of an alpha particle from a fission fragment does not therefore appear surprising. If, however, ternary fission is a sequential process, some angular correlation should exist between two of the three fission fragments. Have you any experimental evidence to show such a correlation?

N. FEATHER: The angular distribution of alpha-particles with respect to the fission axis is satisfactorily explained by the trajectory calculations, independently of any assumption about the precise mode of appearance of the alpha particle. All that is assumed (in the calculations made to date) is that the 'appearance point' lies between the fragments and not far from the fission axis.

TERNARY FISSION OF $^{240}Pu^{*}$ AND $^{242}Pu^{*\dagger}$

M.L. MUGA
Chemistry Department and Physics Department,
The University of Florida, Gainesville, Fla.
and
Nuclear Engineering Department
Brookhaven National Laboratory, Upton, N.Y.
and
C.R. RICE
Chemistry Department,
The University of Florida, Gainesville, Fla.
United States of America

Abstract

TERNARY FISSION OF $^{240}Pu^{*}$ AND $^{242}Pu^{*}$. Using the facilities of the Brookhaven Graphite Research Reactor (BGRR) continuation of ternary fission investigations has been made by extending previous experiments to cover the fissioning systems $^{240}Pu^{*}$ and $^{242}Pu^{*}$. The experiment involves fission fragment detection and energy analysis by three solid-state detectors positioned 120° apart in a plane about a fission source. The output pulse from each detector is digitally analysed and recorded event by event whenever a parallel triple coincidence circuit is satisfied. Earlier data, indicating clear distinctions in the ternary fission of these two nuclei, have been confirmed with much greater statistical confidence. The frequency of occurrence is approximately one per 10^6 binary-fission events, the total-kinetic-energy release is slightly less than that for binary fission, about 150 MeV and 165 MeV for the systems $^{240}Pu^{*}$ and $^{242}Pu^{*}$, respectively. In general, we find that the characteristics of this fissioning pair ($^{240}Pu^{*}$ and $^{242}Pu^{*}$) are in many respects remarkably similar to the features observed for the comparable fissioning pair, $^{234}U^{*}$ and $^{236}U^{*}$. The differences between members in each pair closely parallel each other; this is especially true when the individual fragment-kinetic-energy spectra and the fragment mass distributions are compared. The distinction between the individual fragment-kinetic-energy spectra clearly rules out the possibility of Coulomb scattering, accidental, or spurious events as probable causes of the triple-coincidence data. Evidence of light-mass fragment production in or near the range 30 - 40 amu and 50 - 60 amu is also observed. The fission type ratio (I/II) defined in previous work has been evaluated as 0.6 ± 0.1 for $^{240}Pu^{*}$ and 2.7 ± 0.8 for $^{242}Pu^{*}$ further emphasizing the distinction between the two fissioning systems and reconfirming, in our interpretation, the extensive role which underlying shell-structure effects exhibit with respect to the tripartite mode of fission.

1. INTRODUCTION

In a previous publication [1] on the fission of heavy nuclei into three large fragments, clear distinctions in the ternary fission features of the systems $^{240}Pu^{*}$ and $^{242}Pu^{*}$ were reported. The total numbers of events were few, however; accordingly, we have continued the investigation, using the facilities of the Brookhaven Graphite Research Reactor (BGRR) in order to confirm the reported trends with much greater statistical confidence.

---

* Denotes excited compound nucleus system.

† Work supported by the US Atomic Energy Commission through contract AT(40-1)-2843 Report ORO-2843-14.

TABLE I. PERCENT COMPOSITION OF DIFFERENT PLUTONIUM SAMPLES USED AS FISSION SOURCES IN THIS WORK

Isotope mass	^{239}Pu	^{241}Pu	^{241}Pu
238	-	0.001	-
239	99.18	0.552	1.25
240	0.81	0.134	5.12
241	0.01	99.25	92.67
242	<0.01	0.061	0.96
244	-	0.001	-

2. THE EXPERIMENTAL METHOD

The experimental method, previously described [2, 3] consists of three solid-state detectors positioned 120° apart in a plane about the plutonium fission source. The solid-state silicon detectors, of the surface barrier type and 5 mm × 5 mm in active area, were placed at a radial distance of 1.5 cm from the source. The physical properties of the sources were essentially identical and consisted of a plutonium tetrafluoride deposit on 20 $\mu g/cm^2$ VYNS film support; areal densities varied around 100 $\mu g/cm^2$; isotopic composition of the plutonium, obtained from the Oak Ridge National Laboratory, is shown in Table I. Calibration against the binary-fission fragment spectrum was made for each foil before and after each experiment. The output pulse from each detector was digitally converted and recorded event-by-event on punched paper tape whenever a parallel triple-coincidence circuit (20 ns resolution) was satisfied. Energy calibration was achieved by comparing the binary-fission fragment spectrum with that from time-of-flight data [4] in order to locate the energy position of the average light and heavy masses. A mass-dependent calibration [3, 5] was then applied to obtain individual fragment energies.

3. RESULTS AND DISCUSSIONS

The fissioning systems reported on in this paper are:

$$^{239}Pu + n_{th} \rightarrow (^{240}Pu^*) \rightarrow TF \tag{1}$$

and

$$^{241}Pu + n_{th} \rightarrow (^{242}Pu^*) \rightarrow TF \tag{2}$$

where TF stands for ternary fission.

The frequency of occurrence of ternary fission was 4 ± 1 and 3 ± 1 ternary fissions per 10^6 binary fissions, respectively, for the systems

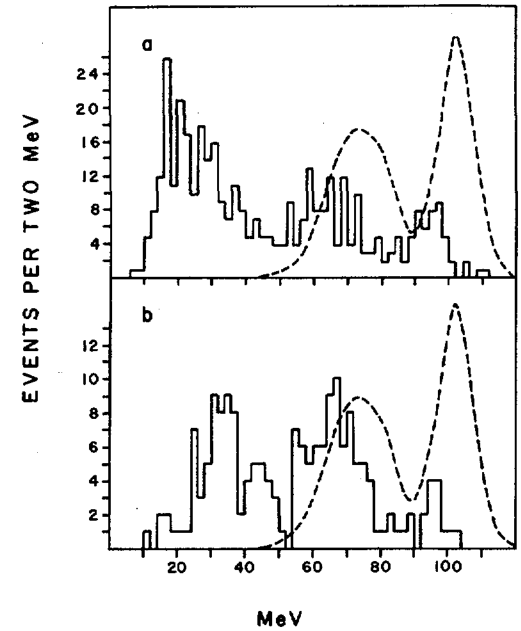

FIG.1. Single fragment kinetic-energy spectrum of triple events for the system. a) $^{239}Pu + n_{th} \rightarrow TF$, and b) $^{241}Pu + n_{th} \rightarrow TF$. The dashed line represents the individual binary-fission fragment spectrum (arbitrary scale).

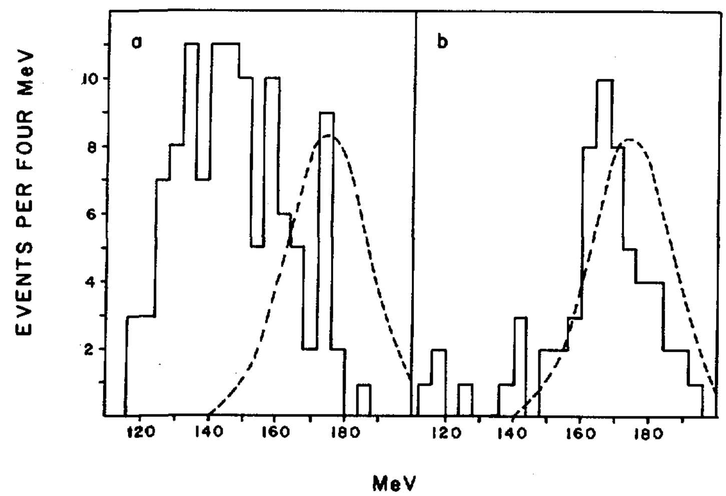

FIG.2. Total fragment kinetic-energy spectrum of triple events for the system. a) $^{239}Pu + n_{th} \rightarrow TF$, and b) $^{241}Pu + n_{th} \rightarrow TF$. The dashed line represents the total kinetic-energy release in binary fission.

$^{240}Pu^*$ and $^{242}Pu^*$. These values are comparable (but significantly lower) to the figures of 15 ± 2 and 7 ± 2 per 10^6 binary fissions reported [3] for the systems $^{234}U^*$ and $^{236}U^*$. Because of the fixed experimental arrangement, the rate of angular dependence was not studied; hence, these values represent lower limits for the ratio TF/BF (BF represents binary fission).

The energy distributions of the individual fragments are shown in Fig. 1. A distinct difference is evident for these two spectra. Specifically, the ratio of the number of fragments in the 60-70-MeV range to the number having energies in the 90 - 100 MeV interval is different; also, the relative number of lower-energy fragments (10 - 30 MeV) is much greater for the $^{240}Pu^*$ fissioning system. Overall, these differences closely parallel similar variations in the fragment kinetic energy spectra observed for the two comparable fissioning systems, $^{234}U^*$ and $^{236}U^*$ [1, 3]. This distinction between the individual fragment kinetic energy spectra clearly rules out the possibility of Coulomb scattering as a probable mechanism for the following reason. Coulomb scattering, as applied to fission fragments colliding with heavy nuclei, depends predominantly on two factors: a) mass, energy and charge of scattered fission fragment, and b) mass, energy and charge of the recoil nucleus, mainly $^{239,241}Pu$. Since for both fissioning systems ($^{240}Pu^*$ and $^{242}Pu^*$) these two factors are essentially identical, Coulomb scattering should result in virtually identical energy spectra. Hence, the clear differences in the two individual fragment-kinetic-energy spectra (Figure 1) precludes the possibility that the observed events originate from a scattering process. Also excluded is the possibility that the triple events arise from instrument malfunctions or other spurious causes.

On the other hand, we interpret the marked difference in these two spectra (Fig. 1) as being associated with the two-neutron difference in fissioning systems ($^{240}Pu^*$ vs $^{242}Pu^*$) and as indicative of the extensive role which underlying shell structure effects exhibit with respect to the ternary fission mode of decay.

The total fragment-kinetic-energy release is somewhat less than for binary fission as evidenced in Fig. 2. Again we find a similarity in comparing the two plutonium systems with the two uranium isotopes previously studied (Table II).

TABLE II. TOTAL-KINETIC-ENERGY RELEASE

Fissioning system	E_{total} (MeV)	
	Ternary fission	Binary fission
$^{242}Pu^*$	165 ± 3	174
$^{240}Pu^*$	149 ± 9	174
$^{236}U^*$	155 ± 5	168
$^{234}U^*$	144 ± 4	167

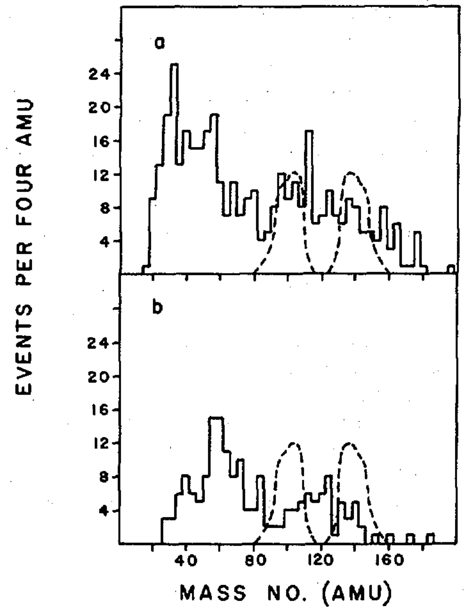

FIG.3. Mass distribution of individual fragments from a) $^{239}Pu + n_{th} \rightarrow TF$, and b) $^{241}Pu + n_{th} \rightarrow TF$. The dashed line represents the approximate mass yield (arbitrary scale) from binary fission.

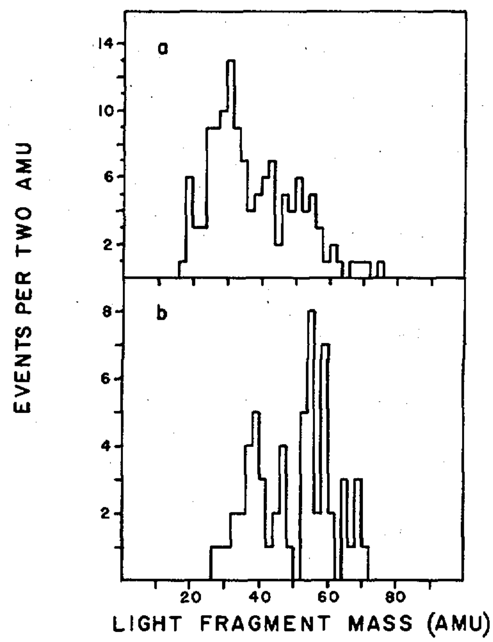

FIG.4. Light-mass-fragment yield in ternary fission of a) $^{240}Pu^*$, and b) $^{242}Pu^*$.

For each pair, the lower mass member ($^{240}Pu^*$, $^{234}U^*$) releases much less total kinetic energy relative to the higher mass member ($^{242}Pu^*$, $^{236}U^*$) and also relative to binary fission. The lower total kinetic-energy release for the ternary fission mode indicates that a larger amount of energy is tied up at an intermediate stage (scission configuration in the fission process) as distortion energy and subsequently becomes available as excess excitation energy within the newly formed fragments. Excessive neutron evaporation and gamma emission should be experienced by, at least, one of these three fragments, possibly resulting in stable (non-radioactive) fragment products.

The mass distributions computed from these experimental data are shown in Fig. 3. The significant aspect here is the observation of low-mass fragments outside the binary-fission fragment mass range. The distinctive features of each fissioning system are shown in more striking form in Fig. 4 which shows the mass spectra of the lightest mass fragment only. Again, as in earlier work on uranium fission [1, 2], the presence of two low-mass peaks is suggested; a lower one in the 30-40-amu region and a higher one in the 50-60 amu range; the spectra for the two fissioning systems ($^{240}Pu^*$ and $^{242}Pu^*$) are, nevertheless, quite distinct. Furthermore, these mass peaks may be considerably narrower than shown here, the observed width accounted for by the uncertainty (± 10°) in the angular resolution of each detector which in turn is reflected into a mass uncertainty.

Following the procedure of earlier reports, we distinguish events as to type I or II based on the mass value of the lightest fragment. Using the mass 39-40 cut to separate the two types (type I corresponds to the higher range, and type II to the lower range), the ratio of type I to type II (I/II) is taken as a measure of the effect of underlying shell structure in influencing the trivision (division into three parts). This ratio is listed in Table III along with results from other fissioning systems. The difference in the ratio (I/II) is quite distinct within each of the two pairs (Pu and U) of fissioning nuclei and the lower mass member (within each pair) has the lower value for the ratio (I/II).

It should be pointed out that the graphical data reported herein are composites from multiple series of identical experiments for which, typically, 5 - 25 triple events were recorded per experiment. In all

TABLE III. RATIO OF TYPE-I TO TYPE-II EVENTS AS FUNCTION OF FISSIONING SYSTEM

Fissioning system	$\frac{\text{Type I}}{\text{Type II}}$	Fission parameter Z^2/A	Neutron excess N-Z
^{252}Cf	15 ± 4	39.11	56
$^{242}Pu^*$	2.7 ± 0.8	36.66	54
$^{240}Pu^*$	0.6 ± 0.1	36.97	52
$^{236}U^*$	0.9 ± 0.1	36.02	52
$^{234}U^*$	0.3 ± 0.1	36.33	50

cases, for a given set of experimental conditions, the results from individual runs were consistent and reproducible within statistical limits.

These experiments were all performed with a symmetrical arrangement of the three detectors about the fission source, i.e. at 120° apart. Hence, all data presented and conclusions drawn pertain to tripartite division in which the three fragments are mutually repelled at approximately 120° from each other.

In summary, we find that the triple coincidence data from the experiments on $^{240}Pu^*$ and $^{242}Pu^*$ are similar in some respects (total kinetic-energy release, frequency of occurence) to that from the comparable pair, $^{234}U^*$ and $^{236}U^*$. On the other hand, we note the difference (individual fragment kinetic energy, mass ratio I/II) between members in the plutonium pair closely parallel similar differences between the uranium fissioning pair of isotopes. More importantly, these experimentally reproducible differences are inconsistent with an interpretation based on a Coulomb scattering mechanism, instrumental malfunctions or other spurious causes. Finally, the apparent effect of a two-neutron difference (in the fissioning pair of isotopes, $^{240}Pu^*$ and $^{242}Pu^*$) in producing distinctly different tripartite mass and energy distributions is advanced as evidence of the dominant role of underlying shell structure in the ternary-fission process.

ACKNOWLEDGEMENTS

Part of the data presented herein was collected at the Brookhaven National Laboratory using the facilities of the BGRR. The hospitality of Dr. M. Hillman of the Nuclear Engineering Department is much appreciated.

REFERENCES

[1] MUGA, M.L., RICE, C.R., SEDLACEK, W.A., Phys. Rev. Lett. 18 (1967) 404.
[2] MUGA, M.L., in Physics and Chemistry of Fission (Proc. Symp. Salzburg, 1965) 2, IAEA, Vienna (1965) 409.
[3] MUGA, M.L., RICE, C.R., SEDLACEK, W.A., Phys. Rev. 161 (1967) 1266.
[4] MILTON, J.C.D., FRASER, J.S., Can. J. Phys. 40 (1962) 1626.
[5] SCHMITT, H.W., GIBSON, W.M., NEILER, J.H., WALTER, F.J., THOMAS, T.D., in Physics and Chemistry of Fission (Proc. Symp. Salzburg, 1965) 1, IAEA, Vienna (1965) 531.

DISCUSSION

N. FEATHER: Is it a fact that the counter configuration 140-80-140 is 'safer' in respect of spurious (scattering) events than the 120-120-120 configuration used in the experiments? Very few results using the 140-80-140 arrangement have been reported. Do you believe that true ternary fission is predominantly symmetric in laboratory space, even though the mass spectrum is so broad?

M.L. MUGA: Yes, the 140-80-140 is slightly better as far as scattering with heavy nuclei (U, Pu, Cf) is concerned, but not when lighter nuclei (e.g. Cl, Ni) might be the culprits.

We have collected data from U-236* ternary fission at several angular configurations, but have concentrated on the 120-120-120 arrangement since our first objective is to establish firmly the existence of this phenomenon and not to elucidate its character. However, we do not believe the mass spectrum in the low-mass region is so broad; indeed, we have clear experimental evidence for more narrow peaks as the angular resolution of the detectors is improved. And in fact some very, very preliminary data from a time-of-flight mass spectrometer experiment suggest the possibility of unique mass formation.

R. ARMBRUSTER: Do the data which you obtained rule out the possibility of a two-step fission mechanism as a description of ternary fission? One of the fission fragments of binary fission could be formed as a shape isomer which has (compared to ground-state fission) a highly increased fission yield. The half-life of this isomeric state has to be shorter $\sim 10^{-10}$ s (0.1 cm of flight path) in order to be taken as ternary fission.

M.L. MUGA: No, not directly, since the detectors still "see" all fragments as coming essentially from the same origin. I would think such a mechanism as you suggest to be unlikely because it would require the subsequent second fission of a medium-mass nucleus, which we know to have rather high fission barriers. It would have to be already very highly deformed.

CORRELATED EMISSION OF LIGHT NUCLEI AND NEUTRONS IN ^{235}U AND ^{252}Cf FISSION

J. BŁOCKI, J. CHWASZCZEWSKA, M. DAKOWSKI,
T. KROGULSKI, E. PIASECKI, H. PIEKARZ, J. TYS
Institute of Nuclear Research,
Świerk, Warsaw, Poland

Abstract

CORRELATED EMISSION OF LIGHT NUCLEI AND NEUTRONS IN ^{235}U AND ^{252}Cf FISSION. The yields of protons and tritons in relation to the α-particle yield were measured in coincidence with the prompt fission neutrons from spontaneous fission of ^{252}Cf and thermal neutron fission of ^{235}U. A conclusion on the relation between the average number of prompt neutrons and the type of charged particles involved was made by making assumptions on the angular and energy distributions of the neutrons.

High excitation of fission fragments is a well-established fact. But it is not yet clear whether there is any difference between the excitation energies of fragments in binary and in various kinds of ternary fission (with emission of various types of charged particles). The excitation energy of fission fragments is released mainly in the neutron evaporation process. The average number of prompt neutrons emitted $\tilde{\nu}$ is therefore regarded as a measure of fragment excitation. More precisely, this energy is determined by the product $\tilde{\nu}\,\partial E^*/\partial\tilde{\nu}$ rather than merely by $\tilde{\nu}$. The excitation energy of the fragments in binary and ternary fissions was compared in Refs [1, 2] by determining the values of $\partial E^*/\partial\tilde{\nu}$ and $\tilde{\nu}$ independently. As a next step, it is interesting to compare various types of tripartition. In this paper, a comparison of $\tilde{\nu}$ has been carried out for tripartition in which nuclei with $Z = 1$ or $Z = 2$ are emitted.

The average number of neutrons emitted in proton, triton and alpha tripartitions may be compared by measuring the neutron yield in proton and triton tripartitions related to the neutron yield in alpha tripartition. This relative neutron yield can be defined from the ratio of proton or triton yields to that of α-particles if it is measured with and without coincidence with the neutrons. Such an experiment was performed for the ^{252}Cf spontaneous fission and the thermal neutron fission of ^{235}U.

A diagram of the experimental arrangement is presented in Fig. 1. A 2 mg/cm^2 U_3O_8 target (enriched in ^{235}U to 95%) 16 mm in diameter was irradiated with a neutron beam of 6×10^8 n/cm^2 s flux. In the case of ^{252}Cf measurements a source with $\sim 10^7$ decays/min and 7 mm in diameter was used. The telescope counter consisted of a 50 μm ΔE transmission detector and of an E detector with the sensitive region of 1.5 mm. The particles could be identified by registering the signals from both of these detectors in a two-parameter 40×40 channel analyser. The telescope was protected from the fragments by an aluminium foil 4 mg/cm^2 and 6.5 mg/cm^2 thick in the case of ^{235}U and ^{252}Cf, respectively.

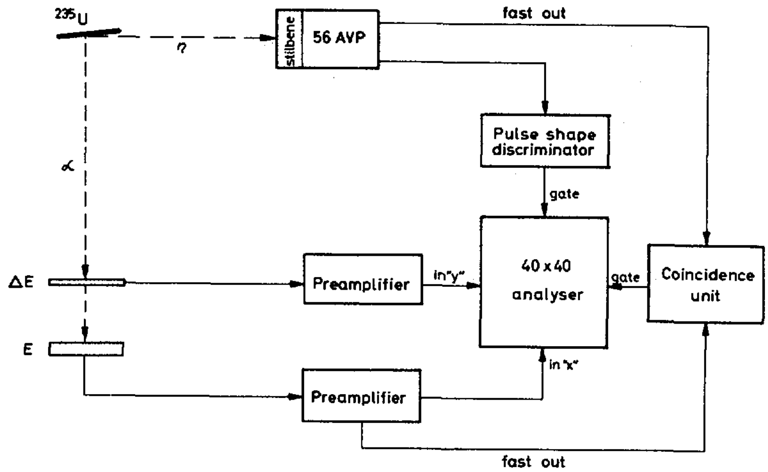

FIG. 1. Diagram of experimental arrangement.

TABLE I. RELATIVE PARTICLE YIELDS

	Particle	E_{min} [a] (MeV)	Relative yields [b]			
			without coincidence	with coincidence		without coincidence / with coincidence (corrected)
				non corrected	corrected	
^{252}Cf	tritons	6	9.3 ± 0.3	8.2 ± 0.6	8.3 ± 0.6	1.12 ± 0.09
^{235}U*	protons	8	0.96 ± 0.02	0.77 ± 0.10	0.86 ± 0.10	1.11 ± 0.13
	tritons	5	8.0 ± 0.05	7.3 ± 0.3	7.4 ± 0.3	1.08 ± 0.04
particles		13 [c] / 15 [d]	100	100	100	1

[a] Only the parts of spectra higher than E_{min} are taken into account.
[b] The errors given are statistical ones.
[c] For ^{252}Cf measurements.
[d] For ^{235}U measurements.

The neutron counter consisted of a stilbene crystal 30×5 mm/40×40 mm in ^{252}Cf measurements, coupled with a 56-AVP photomultiplier. To reduce the intensity of low-energy gamma rays the crystal was shielded by a 15-mm lead sheet. The separation of gamma rays from neutrons was effected with a pulse-shape discriminator. The admixture of gamma-ray pulses to the neutron pulses was estimated to be less than 5%. The neutron registration threshold was set at about 0.5 MeV. The highest efficiency of the neutron counter corresponded to about 0.7 MeV neutron energy.

The axes of the neutron counter and the telescope counter were perpendicular to one another. Besides, in the case of ^{252}Cf, spontaneous tripartition measurements were performed, in which the telescope and the neutron counter had a common axis, which entails the registration of the events of neutrons and charged particle emission in opposite directions.

A typical fast-slow coincidence system was used. The fast coincidence ($2\tau = 30$ ns) between the signals from the photomultiplier and the E detector opens one gate of the analyser. The neutron signal from the pulse-shape discriminator opens the second gate. The random coincidences did not exceed 5% of the true ones.

In the measurements of ^{236}U tripartition the time of the runs in which charged particles were registered with and without coincidence with fission neutrons was 140 and 21 hours, and the average rates were 1.8/min and 560/min, respectively. Accordingly, in the case of ^{252}Cf the measurements lasted 120 and 8 hours and the rates were 0.7/min and 215/min.

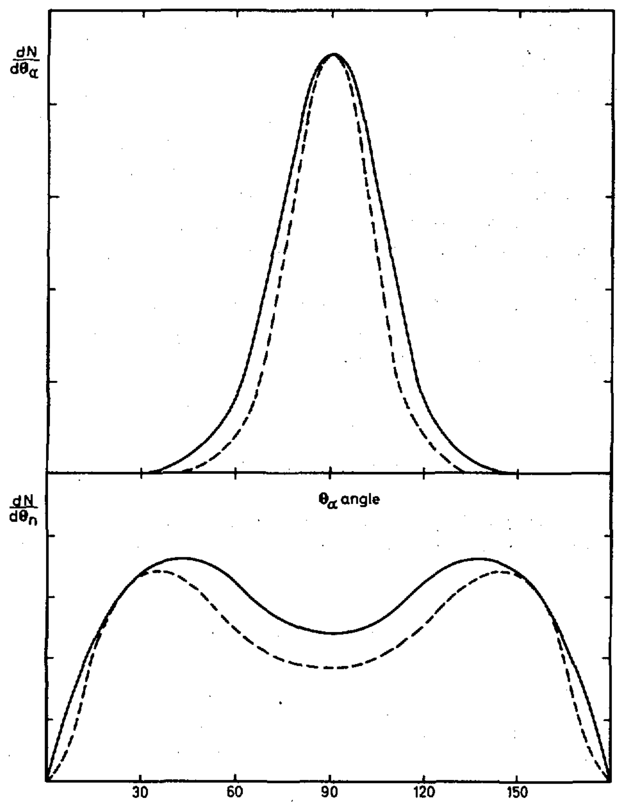

FIG.2. Angular distributions of α-particles (upper curves) and neutrons (lower curves). The dashed lines represent the registered parts of the distributions.

The relative yields of tritons (with an admixture of non-distinguished deuterons) and protons with respect to the emission of 100 α-particles were calculated for coincident and non-coincident measurements. The results are presented in the fourth and fifth columns of Table I. In the sixth column the results of coincidence measurements with corrections providing for the difference between the angular distributions (with respect to the fragments) of α-particles, tritons and protons [3] are presented. The results of the measurements performed with collinear counters, which are not included in this table, are quite consistent with the remaining ones within the error limits.

The finite sizes of the target and both detectors were taken into account, and the angular distribution of prompt neutrons was assumed to be independent of the type of light charged particle. In Fig. 2 the parts of angular distributions of the neutrons and α-particles registered when the axes of the detectors were perpendicular are shown. However, the efficiency of our neutron counter depended on the energy of neutrons. Hence, when interpreting the results of our experiment it should be assumed that the energy distribution of prompt neutrons does not depend significantly on the type of particles considered, or that the differences between the distributions for various types of tripartition are not larger than those for the binary fission and α-tripartition of ^{236}U (see Ref. [4]).

It was calculated that the probability of two neutrons being simultaneously registered is as small as 2% - 4% of the probability of a single neutron being registered. Having this in mind, we can conclude, on the basis of the results listed in Table I, that the amount of prompt neutrons accompanying the proton and triton tripartition of ^{236}U and ^{252}Cf is smaller by about 10% than that in the α-tripartition. This difference lies within the limits of a single and two standard deviations for the protons and tritons, respectively.

The present results seem to indicate that if the values of $\partial E^*/\partial\bar{\nu}$ are the same for the types of tripartition investigated the amounts of excitation energy released by prompt neutrons do not differ very much (not more than 10%).

ACKNOWLEDGEMENTS

The authors are greatly indebted to Drs Z. Sujkowski and J. Żylicz for their continuous encouragement during the execution of this work.

REFERENCES

[1] NARDI, E., FRAENKEL, Z., Phys. Rev. Lett. 20 (1968) 1248.
[2] PIEKARZ, H., BŁOCKI, J., KROGULSKI, T., PIASECKI, E., (to be published).
[3] RAISBECK, G.M., THOMAS, T.D., Phys. Rev. 172 (1968) 1272.
[4] IVANOV, O.I., KROSHKIN, N.T., NEFEDOV, W.N., CHARIN, W.P., Yad. Fiz. 5 (1967) 737.

PROPRIETES DES PARTICULES ALPHA DE TRIPARTITION DE L'URANIUM-235 PAR LES NEUTRONS THERMIQUES

C. CARLES, M. ASGHAR, T.P. DOAN, R. CHASTEL
Laboratoire de physique nucléaire,
Faculté des sciences de Bordeaux
et
C. SIGNARBIEUX
Centre d'études nucléaires de Saclay,
France

Abstract — Résumé

PROPERTIES OF THE ALPHA PARTICLES EMITTED DURING THE TRIPARTITION OF URANIUM-235 BY THERMAL NEUTRONS. Using the charged nuclear emulsions method, the authors studied the emission of alpha particles during the tripartition of ^{235}U by thermal neutrons. About 3000 events were analysed.

The main aim of the experiment was to obtain a very high precision (± 2°) in the measurement of the angle between the alpha particle and the light fission fragment. However, the accurate measurement of the range of the two fragments (± 1 μm) enables the authors to find the ratio of the fragment masses with an accuracy of about 10%. It was, thereby, possible to study the variation of a certain number of parameters as a function of this ratio.

We obtained the following main results: 1. The most probable value of the energy of the alpha particle seems to be independent of the ratio between the fission fragment masses. 2. The most probable value of the angle between the alpha particle and the light fission fragment grows with the ratio of the fission fragment masses. This curve shows discontinuities corresponding to fragments having a magic number of nucleons. 3. The most probable value of the kinetic energy of the alpha particle varies very strongly with the final emission angle of this particle with respect to the light fragment and shows a minimum in the neighbourhood of the most probable value (~83°). 4. The angular distribution of the alpha particles with respect to the light particle increases with the kinetic energy of these particles.

These results are compared with existing data on other fissile nuclei and an attempt is made to interpret them phenomenologically.

PROPRIETES DES PARTICULES ALPHA DE TRIPARTITION DE L'URANIUM-235 PAR LES NEUTRONS THERMIQUES. Les auteurs ont étudié l'émission de particules alpha de tripartition de l'uranium-235 par les neutrons thermiques, par la technique des émulsions nucléaires chargées. Environ 3000 événements ont été analysés. Le but principal de l'expérience était d'obtenir une très bonne précision (± 2°) dans la mesure de l'angle entre la particule alpha et le fragment léger de fission. Cependant, la mesure précise du parcours des deux fragments (± 1 μm) permet d'obtenir une précision d'environ 10% sur le rapport des masses des fragments, ce qui donne la possibilité d'étudier la variation d'un certain nombre de paramètres en fonction de ce rapport.

Les principaux résultats obtenus sont les suivants: 1. La valeur de l'énergie la plus probable de la particule alpha semble indépendante du rapport des masses des fragments de fission. 2. La valeur la plus probable de l'angle entre la particule alpha et le fragment léger de fission croît avec le rapport des masses des fragments de fission. Cette courbe présente des discontinuités correspondant aux fragments possédant un nombre magique de nucléons. 3. La valeur de l'énergie cinétique la plus probable de la particule alpha varie très fortement avec l'angle d'émission final de cette particule par rapport au fragment léger et présente un minimum aux alentours de la valeur la plus probable (~ 83°). 4. La distribution angulaire des particules alpha par rapport au fragment léger s'élargit lorsque l'énergie cinétique de ces particules augmente.

Ces résultats sont comparés avec les données existant sur les autres noyaux fissiles et les auteurs essaient de donner une interprétation phénoménologique de ces résultats.

1. INTRODUCTION

L'étude de la tripartition dans laquelle une particule légère (une particule α dans à peu près 95% des cas) est émise à partir du col joignant les deux fragments de fission peut donner des informations complémentaires et plus précises que l'étude des neutrons de fission sur la forme et le comportement dynamique des fragments de fission et du col.

La présente étude porte sur la mesure de la variation de l'énergie cinétique finale la plus probable de la particule légère en fonction de l'angle final entre cette particule et le fragment léger, $\theta_{\alpha\ell}$, et en fonction du rapport des masses des gros fragments R. Nous avons également mesuré la variation de l'angle $\theta_{\alpha\ell}$ en fonction du rapport R des masses des gros fragments.

Alors que les mesures effectuées à l'aide de détecteurs à semi-conducteurs donnent une meilleure précision sur les énergies cinétiques des fragments, la technique des émulsions nucléaires chargées permet d'effectuer des mesures plus précises de distributions angulaires. En effet, dans ce cas, les angles sont mesurés avec une grande précision. De plus, il est possible de tenir compte du recul imposé aux gros fragments par la particule légère, ce qui est très difficile avec les semi-conducteurs. En outre, les résultats concernant la mesure des énergies des particules légères sont également bien précis, car aucun écran n'est interposé sur le parcours de celles-ci, contrairement à ce qui a lieu lorsqu'on utilise les détecteurs à semi-conducteurs.

2. DISPOSITIF EXPERIMENTAL

Des plaques photographiques dont l'émulsion était chargée avec de l'uranium enrichi à 93% en ^{235}U servaient à la fois de cible et de détecteur. Ces plaques étaient imprégnées durant 45 minutes dans une solution tamponnée de nitrate d'uranyle. De cette manière nous avons introduit environ $2,5 \times 10^{18}$ noyaux d'uranium par cm^3 d'émulsion, répartis d'une manière homogène. Nous avons ainsi un détecteur 4π ayant une efficacité de 100% pour le phénomène que nous nous proposons d'étudier.

Ces plaques étaient irradiées dans un faisceau de neutrons thermiques fournis par la pile EL3 du CEN de Saclay. Le flux était de l'ordre de 10^7 $n/s \times cm^2$. Etant donné ces caractéristiques une irradiation de 3 minutes procurait un nombre suffisant d'événements.

Le bruit de fond était dû principalement aux particules alpha de la radioactivité naturelle de l'uranium-234 qui entre pour 0,7% dans la composition de l'uranium utilisé et qui a une activité très importante. Pour diminuer l'importance de ce bruit de fond, nous avons dû réduire le plus possible la durée de toutes les opérations effectuées pendant que l'émulsion est sensible. Les conditions dans lesquelles nous avons opéré nous ont permis d'obtenir un bruit de fond tout à fait acceptable.

3. MESURES EFFECTUEES

La recherche des événements et leur mesure sont effectuées à l'aide du microscope. Nous avons mesuré 3000 événements environ.

On utilise, pour rechercher les événements, un grossissement de 500 fois, et pour effectuer les mesures, un grossissement de 1000 fois. Ces mesures sont les suivantes:
- longueur de la projection horizontale de chaque trace,
- longueur de la projection verticale de chaque trace,
- angle entre chacune des projections horizontales.

Un certain nombre de tests sont effectués [1] pour éliminer les événements parasites.

4. PRECISION DES RESULTATS

Nous devons distinguer la précision des mesures de la précision des résultats, puisque nous effectuons des mesures dans un plan et nous les transformons en résultats dans l'espace en tenant compte du coefficient de contraction de l'émulsion à la suite de son traitement.

Les mesures sont effectuées avec les précisions suivantes:
- 0,5 microns sur les projections horizontales,
- 0,5 microns sur les projections verticales,
- 1 degré sur les angles.

Il en résulte les précisions suivantes sur les résultats bruts:
- 0,7 microns sur les longueurs des parcours,
- entre 1 et 2 degrés sur les angles.

De ce fait la résolution en énergie des particules alpha se trouve être de l'ordre de 300 keV, et celle des fragments de fission de 7 MeV (ce qui entraîne une erreur d'environ 10% sur la valeur du rapport des masses R des gros fragments de tripartition).

Il est important de noter que notre méthode de mesure nous permet de tenir compte de façon exacte du recul imposé par la particule alpha aux gros fragments de tripartition, alors qu'on ne peut effectuer qu'une correction moyenne lorsqu'on utilise des semi-conducteurs. En effet, si on néglige ce recul, on obtient la relation suivante:

$$M_1E_1 = M_2E_2 \tag{1}$$

où M_i et E_i sont respectivement la masse et l'énergie du fragment i.

Si on tient compte de l'impulsion de la particule alpha, la relation (1) devient:

$$M_1E_1 = c^2M_2E_2$$

avec

$$c = \frac{\sin(\beta+\gamma)}{\sin\beta}$$

où les angles β et γ sont ceux indiqués sur la figure 1.

L'erreur sur la mesure des angles étant très faible, l'angle $\theta_{\alpha\ell}$ entre la particule alpha et le fragment léger de fission est, en principe, bien mesuré. Toutefois, lorsque le rapport des masses R des gros fragments de tripartition est voisin de l'unité, l'imprécision sur la connaissance de $\theta_{\alpha\ell}$ devient très grande. En effet, l'erreur sur la mesure des parcours peut faire que l'on inverse le rapport des masses et que l'on attribue une masse supérieure au fragment léger et inférieure au fragment lourd. Dans ce cas, au lieu de mesurer l'angle $\theta_{\alpha\ell}$, on mesure un angle qui est proche de son supplément.

Nous appellerons ces cas-là des cas douteux et nous avons recherché la proportion de tels cas pour divers domaines de valeurs de R. Nous estimons qu'un cas est douteux lorsque la différence des parcours mesurés est inférieure ou égale à l'erreur commise sur la mesure de cette différence. Nous obtenons alors les résultats suivants:

$1 \leq R < 1,1$	77% de cas douteux
$1,1 \leq R < 1,2$	23% de cas douteux
$1,2 \leq R < 1,3$	5% de cas douteux
$R \geq 1,3$	moins de 1% de cas douteux.

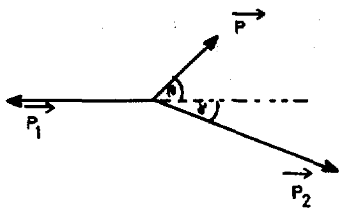

FIG. 1. Composition des impulsions en tripartition.

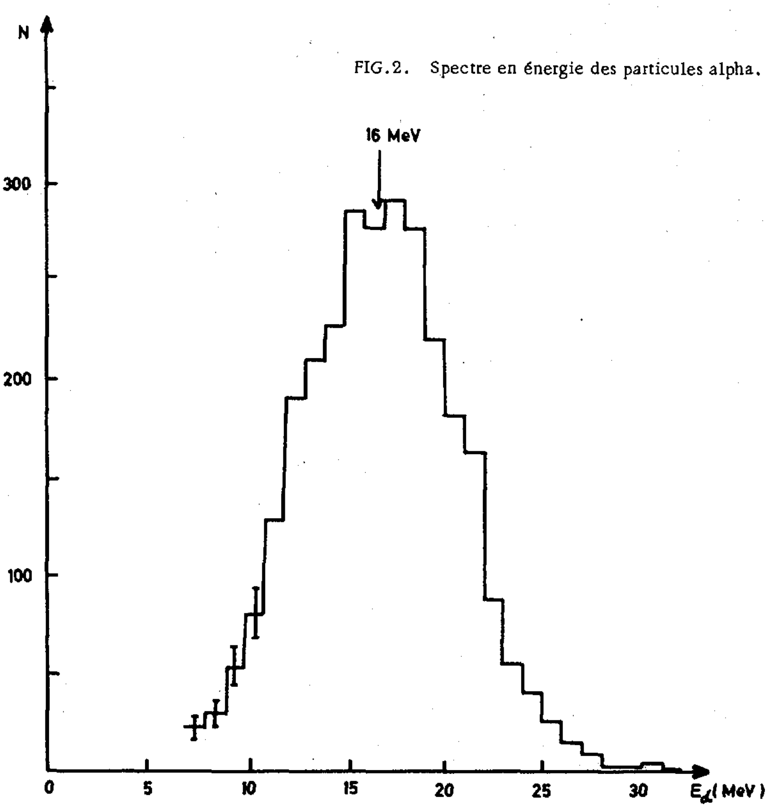

FIG. 2. Spectre en énergie des particules alpha.

Nous pouvons donc penser que les résultats des mesures de $\theta_{\alpha\ell}$ que nous obtenons pour $1 \leq R < 1,1$ ne sont pas significatifs; lorsque $1,1 \leq R < 1,2$ nous pouvons penser que le spectre est légèrement élargi, mais la valeur du maximum est exacte; pour tous les autres cas, les spectres sont corrects.

5. RESULTATS

Le spectre des particules alpha que nous obtenons est porté sur la figure 2, il possède un maximum assez large situé aux environs de 16 MeV et la valeur maximale est située vers 32 MeV. Ces résultats sont en accord avec ceux déjà obtenus par divers auteurs [2-7], mais nous devons remarquer que nous n'avons pas eu besoin d'effectuer de correction d'écran, contrairement à la plupart des auteurs cités ci-dessus, et que nous avons mesuré un nombre relativement important d'événements, ce dont découle la précision de nos résultats.

Sur la figure 3, nous pouvons voir la distribution de l'angle $\theta_{\alpha\ell}$ entre la particule alpha et le fragment léger de fission; nous avons discuté plus haut la précision de cette distribution. La valeur la plus probable se trouve à 83° et la largeur à mi-hauteur est de 29°; cette largeur relativement faible est due à notre bonne résolution angulaire associée à une assez bonne statistique.

Sur la figure 4, nous avons porté la valeur la plus probable de l'énergie de la particule alpha en fonction du rapport R des masses des gros fragments de tripartition. Nous pouvons constater que cette énergie ne varie pratiquement pas dans les limites de précision des mesures d'énergie des particules alpha. Notons que nous avons trouvé un résultat similaire au cours d'une étude réalisée à l'aide de détecteurs à semi-conducteurs dans laquelle la précision sur la valeur du rapport de masse était supérieure, mais celle sur l'énergie de la particule alpha était moins bonne [1].

Sur la figure 5 est tracée la variation de l'énergie la plus probable de la particule alpha en fonction de l'angle $\theta_{\alpha\ell}$. Nous voyons que cette courbe possède un minimum d'une valeur un peu inférieure à 16 MeV aux alentours de l'angle le plus probable et qu'elle accuse une légère dissymétrie par rapport à cet angle.

Nous avons porté sur ce même diagramme deux points mesurés par Schneeberger [8] à des angles égaux à 20° et 60°. Ces résultats s'accordent bien avec les nôtres. Nous pouvons néanmoins noter que la variation que nous trouvons est plus rapide que celle trouvée par Fraenkel [2] dans le cas de la fission spontanée du ^{252}Cf, dont les résultats sont portés sur le même graphique.

Si nous traçons la distribution de l'angle $\theta_{\alpha\ell}$ pour différents domaines de valeurs du rapport R des masses des gros fragments de tripartition, nous obtenons des histogrammes ayant tous à peu près la même largeur, lorsque R est supérieur à 1,1. Nous avons vu plus haut que les résultats n'étaient pas significatifs lorsque $1 \leq R < 1,1$.

Sur la figure 6, nous avons porté la valeur la plus probable de l'angle $\theta_{\alpha\ell}$ en fonction du rapport des masses des gros fragments de tripartition. Nous obtenons une courbe dont la pente est plus faible pour des valeurs de R comprises entre 1,3 et 1,8 qu'aux deux extrémités.

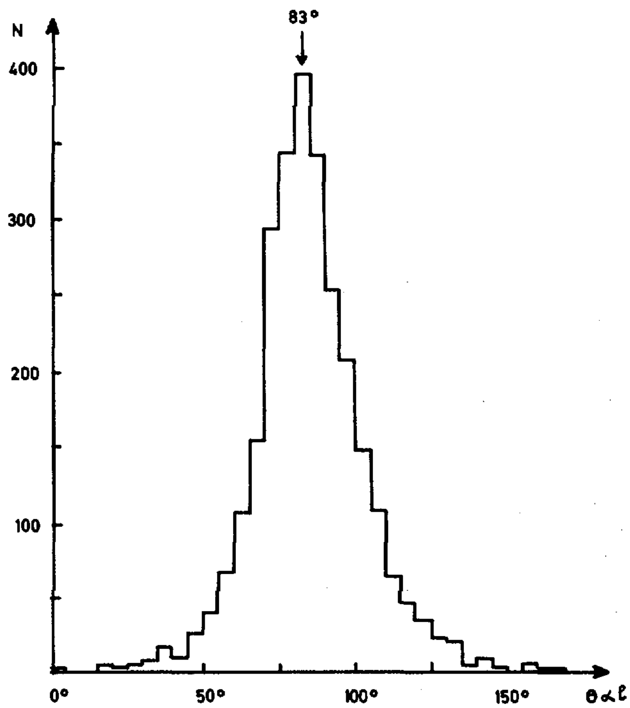

FIG.3. Distribution angulaire des particules alpha par rapport au fragment léger.

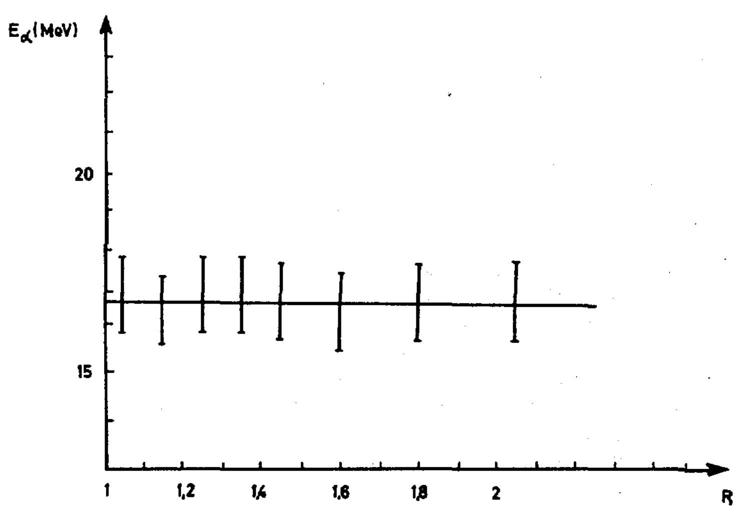

FIG.4. Variation de l'énergie la plus probable des particules alpha en fonction du rapport des masses des gros fragments de tripartition.

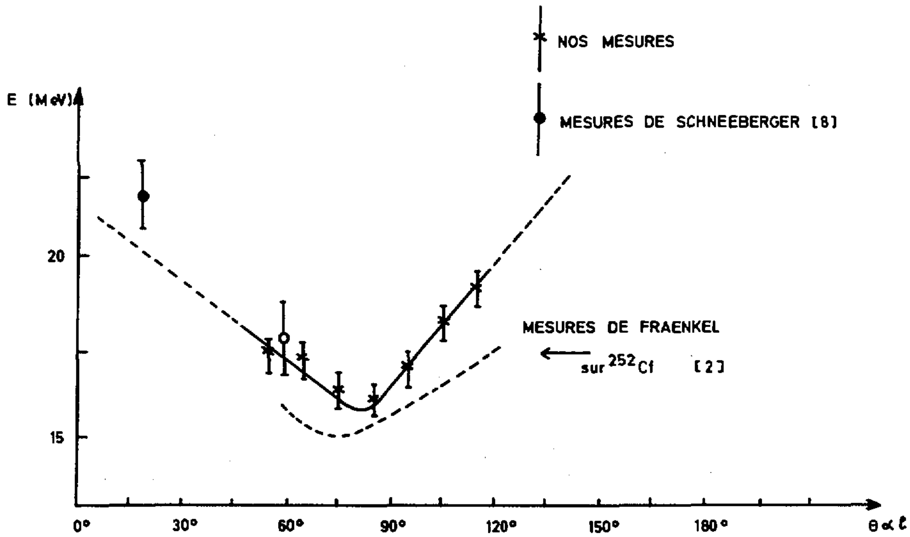

FIG. 5. Variation de l'énergie la plus probable des particules alpha en fonction de l'angle $\theta_{\alpha\ell}$.

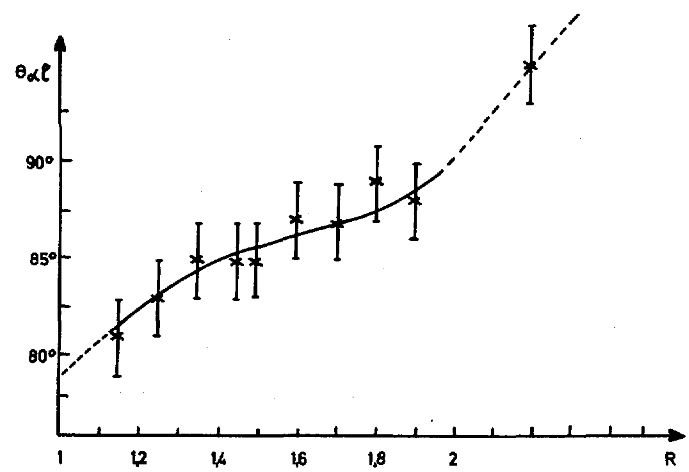

FIG. 6. Variation de l'angle $\theta_{\alpha\ell}$ le plus probable en fonction du rapport des masses des gros fragments.

En nous référant aux calculs de Milton [9] donnant la charge la plus probable d'un fragment de fission de masse donnée, nous constatons que lorsque R = 1,3, l'un des fragments est le $^{132}_{50}$Sm, qui est un noyau «doublement magique»; lorsque R = 1,8, l'un des fragments est le $^{84}_{34}$Se, qui possède un nombre magique de neutrons.

La figure 7 montre la distribution de l'angle $\theta_{\alpha\ell}$ pour divers domaines de l'énergie cinétique de la particule alpha. Nous constatons que les trois premiers spectres ont des formes assez semblables bien que la largeur semble augmenter légèrement lorsque l'énergie cinétique de la particule

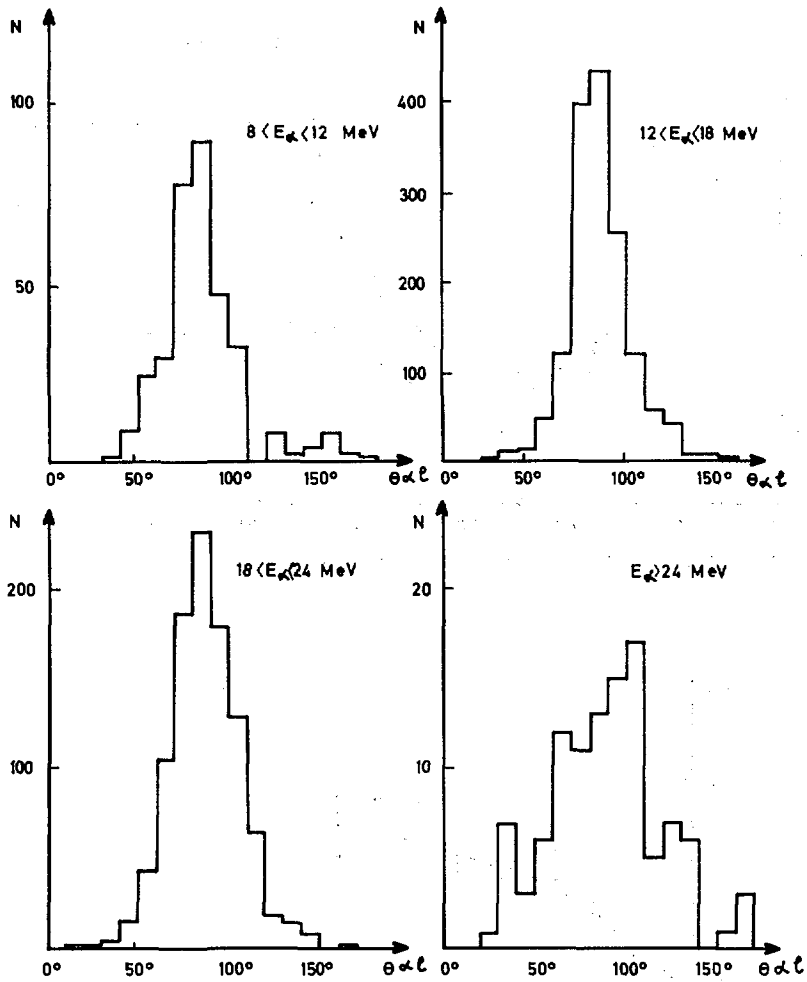

FIG.7. Distribution de l'angle $\theta_{\alpha\ell}$ pour divers domaines de l'énergie cinétique de la particule alpha.

alpha augmente. Lorsque cette énergie est très grande ($E_\alpha > 24$ MeV), la distribution de $\theta_{\alpha\ell}$ devient très large. Ces résultats sont en accord avec ceux déjà obtenus par Perfilov et al. [10] sur le ^{235}U et par Fraenkel [2] sur le ^{252}Cf.

6. DISCUSSION

Nous allons essayer de donner une explication des différentes distributions que nous avons montrées au paragraphe précédent.

Etudions tout d'abord la distribution de l'énergie de la particule alpha en fonction du rapport des masses des gros fragments (fig. 4).

Les calculs effectués par divers auteurs [11-16] montrent que l'énergie finale de la particule alpha dépend principalement des deux paramètres suivants: énergie initiale de la particule alpha et énergie potentielle de cette particule due à l'influence coulombienne des deux gros fragments sur celle-ci. Dans l'hypothèse du modèle de l'haltère dissymétrique de Whetstone [17] et Vladimirski [18], les dimensions du col joignant les deux gros fragments ne dépendent pas du point de rupture du col. Si la particule alpha se trouve à l'intérieur du col, Halpern [13] a montré que l'énergie cinétique initiale de la particule alpha est donnée par la relation suivante:

$$E_\alpha^0 \simeq \frac{3}{2}\frac{\hbar^2}{M_\alpha}\left(\frac{\pi}{L}\right)^2$$

avec

$$L^3 = \frac{4\pi}{3} r_0^3 A_N$$

A_N représente le nombre de nucléons dans le col qui est supposé être constant dans le modèle cité ci-dessus. Donc, l'énergie E_α^0 ne dépend pas du rapport des masses des gros fragments R.

D'autre part, Doan et al. [12, 19] ont montré que l'énergie potentielle varie très peu en fonction du rapport R.

Il en résulte que l'énergie finale de la particule alpha doit varier très peu en fonction de R puisque les deux principaux paramètres qui déterminent cette énergie sont eux-mêmes presque constants en fonction de R.

Examinons maintenant la variation de l'énergie la plus probable de la particule alpha en fonction de l'angle $\theta_{\alpha\ell}$ que fait cette particule avec le fragment léger (fig. 5).

Lorsque la particule alpha passe près d'un des fragments ($\theta_{\alpha\ell}$ petit ou grand) elle doit vaincre une répulsion coulombienne importante. Par conséquent, dans ce cas, son énergie initiale doit être élevée et supérieure à la valeur la plus probable de la distribution de l'énergie cinétique initiale. Or, Halpern [13] montre que la valeur de l'énergie cinétique finale des particules alpha augmente quand l'énergie cinétique initiale croît. Il en résulte que, dans les régions où $\theta_{\alpha\ell}$ a des valeurs voisines de 0° ou de 180°, l'énergie finale des particules alpha doit être assez élevée.

De plus, la répulsion coulombienne que doit vaincre la particule alpha est plus élevée si sa trajectoire passe près du fragment lourd que si elle passe près du fragment léger. Donc son énergie initiale doit aussi être plus élevée dans ce cas. Ceci explique que l'énergie cinétique de la particule alpha croît plus rapidement du côté des grandes valeurs de $\theta_{\alpha\ell}$.

Remarquons que ce même raisonnement permet de comprendre que lorsque l'énergie de la particule alpha est grande, la distribution de l'angle $\theta_{\alpha\ell}$ est large (fig. 7). En effet, une énergie finale grande provient d'une énergie initiale grande. Or, si son énergie initiale est grande, la particule alpha a la possibilité de passer près de l'un des fragments (l'effet de focalisation à 90° est moins important).

La pente de la courbe de variation de l'angle $\theta_{\alpha\ell}$ en fonction de R change pour des valeurs de R correspondant au cas où l'un des fragments possède un nombre magique de nucléons (fig. 6).

Le fait que la pente soit plus faible pour $1,3 < R < 1,8$ résulte du fait que, dans ce domaine des valeurs de R, la distance entre les gros fragments diminue en même temps que le point d'émission se rapproche du fragment léger: ces deux effets sur $\theta_{\alpha\ell}$ tendent à se compenser. En effet, l'angle $\theta_{\alpha\ell}$ dépend, d'une part, de la position initiale de la particule alpha par rapport au fragment léger, et, d'autre part, de la distance entre les deux fragments.

La figure 8 permet de comprendre ce phénomème. Bien que la distance entre la particule alpha et le centre du fragment léger soit la même dans les deux cas, l'angle $\theta_{\alpha\ell}$ est plus grand dans le premier que dans le second à cause de la variation de l'importance de la répulsion coulombienne due au fragment lourd.

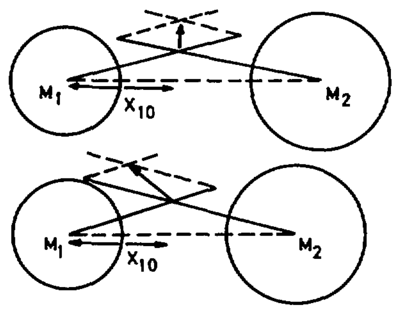

FIG. 8. Influence de la distance entre les fragments sur l'angle $\theta_{\alpha\ell}$.

Le changement de pente se produit quand la variation de la distance entre les fragments devient très rapide par rapport à la distance entre la particule alpha et le fragment léger. Or, la variation rapide de distance entre les fragments se produit dans les régions où l'un des fragments est sphérique, donc dans les régions où R est proche soit de 1, 3 soit de 1, 8 (intervention des nombres magiques).

7. CONCLUSION

Nous avons pu expliquer d'une manière cohérente les résultats obtenus au cours de ce travail moyennant les hypothèses suivantes:

- La forme du noyau fissionnant, au moment de la scission, est correctement décrite par le modèle de l'haltère de Whetstone [17] et Vladimirski [18] si l'on tient compte de l'influence des couches fermées sur la forme des fragments.
- La particule alpha est émise à partir du point de rupture du col à un instant très proche de la scission.
- L'énergie cinétique initiale de la particule alpha, au moment de son émission, possède une distribution autour d'une valeur la plus probable.

Toutefois, le problème important du mécanisme d'émission de la particule légère reste posé. En effet, aussi bien le processus adiabatique de Geilikman et al. [16] que le processus de «sudden approximation» de Halpern [13] permettent d'expliquer les résultats que nous avons obtenus.

REMERCIEMENTS

Les auteurs tiennent à exprimer leurs très vifs remerciements à Monsieur M. Ribrag, du CEN de Saclay, pour l'aide précieuse qu'il leur a apportée au cours de ce travail.

REFERENCES

[1] CARLES, C., Thèse, Bordeaux (1969).
[2] FRAENKEL, Z., Phys. Rev. 156 (1967) 1283.
[3] TITTERTON, E.W., Nature 168 (1951) 590.
[4] PERFILOV, N.A., Soviet Phys. JETP 37 (1960) 1157.
[5] DAKOWSKI, M., CHWASZCZEWSKA, J., KROGULSKI, T., PIASECKI, E., SOWINSKI, M., Phys. Letters 25B (1967) 213.
[6] FULMER, C.B., COHEN, B.L., Phys. Rev. 108 (1957) 370.
[7] NOBLES, A.J., Phys. Rev. 126 (1962) 1508.
[8] SCHNEEBERGER, M., Thèse, Vienne (1968).
[9] MILTON, J.C.D., Rapport UCRL (1962) 9883.
[10] PERFILOV, N.A., SOLOV'EVA, Z.L., Soviet Phys. JETP 10 (1960) 825.
[11] KATASE, A., J. phys. Soc. Japan 25 (1968) 933.
[12] DOAN, T.P., Thèse, Bordeaux (1969).
[13] HALPERN, I., Rapport CERN 68-12 (1963).
[14] BONEH, Y., FRAENKEL, Z., NEBENZAHL, I., Phys. Rev. 156 (1967) 1305.
[15] RAISBECK, G.M., THOMAS, T.D., Phys. Rev. 172 (1968) 1272.
[16] GEILIKMAN, B.T., KHLEBNIKOV, G.I., C.r. Congrès Int. Phys. Nucl. Paris, 1964, Centre national de la recherche scientifique, Paris (1964) 1129.
[17] WHETSTONE, S.L., Jr., Phys. Rev. 114 (1959) 581.
[18] VLADIMIRSKI, V.V., Soviet Phys. JETP 5 (1957) 673.
[19] DOAN, T.P., CARLES, C., CHASTEL, R., C.r. hebd. Séanc. Acad. Sci. Paris 264 (1967) 900.

DISCUSSION

G. BEN-DAVID: *Speaking as an old emulsion physicist I fear that* I can discern some discrepancies between the results of this paper and a similar experiment carried out at the Soreq reactor using solid-state detectors. We have analysed some 10^5 long-range alpha events in thermal fission of ^{236}U. The most serious discrepancy seems to be in the most probable angle of alpha emission. Our work shows (see Fig. A of this Discussion) emission of alpha particles towards the light fragment with increasing mass ratio, in contrast to the results reported in this paper by the Bordeaux group using emulsions.

The source of the discrepancy ought to be resolved before final conclusions can be drawn from trajectory calculations. Using calculations similar to those carried out by Boneh et al., we find that the angular and energy distributions of our experiment are best fitted by the following initial scission parameters:

Fission-fragment separation	23 F
Alpha-particle energy	2 MeV
Fission-fragment energy	25.5 MeV

This last result is in excellent qualitative agreement with the liquid-drop calculations carried out by J.R. Nix for ^{236}U. Would you care to comment?

M. ASGHAR: Perhaps I may reply to Dr. Ben-David's observations. His results on $\theta_\alpha^\ell(R)$, where R is the fragment mass ratio, disagree seriously with ours. Let me point out, however, that with the use of semi-conductor detectors it is quite difficult to measure with high precision the angular distribution of the ternary-fission alpha particles; this is due to the fact that here the angular resolution is very much worse than what can be obtained with emulsions. Moreover, in the case of emulsions, one can take exact account of the alpha-particle recoil effect, which is not so with semi-conductor data.

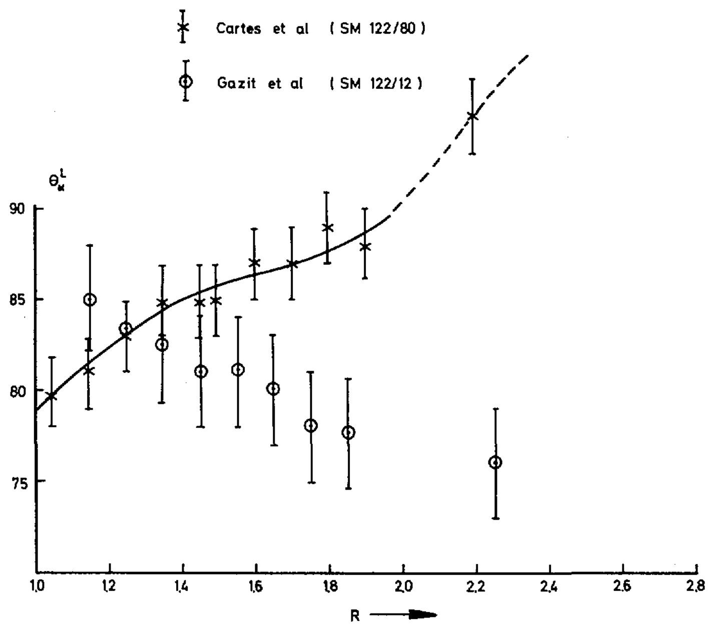

FIG. A. Emission of alpha particles towards the light fragment.

Figure B shows the alpha particle emission probability, $P_\alpha(M)$, based on our measurement on the ^{235}U target nucleus with the use of thermal neutrons. This measurement covers the complete mass range. The curve of $P_\alpha(M)$ shown here has a shape which is strikingly similar to the well-known neutron data. This similarity shows that the factors that play an important role in the emission of neutrons, $\nu(M)$, are also important for the emission of the alpha particle.

We know that the Whetstone dumb-bell model very adequately explains the form of the $\nu(M)$ data and should, therefore, explain $P_\alpha(M)$ too. The same model gives a consistent explanation of our data on $\theta_\alpha^\ell(M)$.

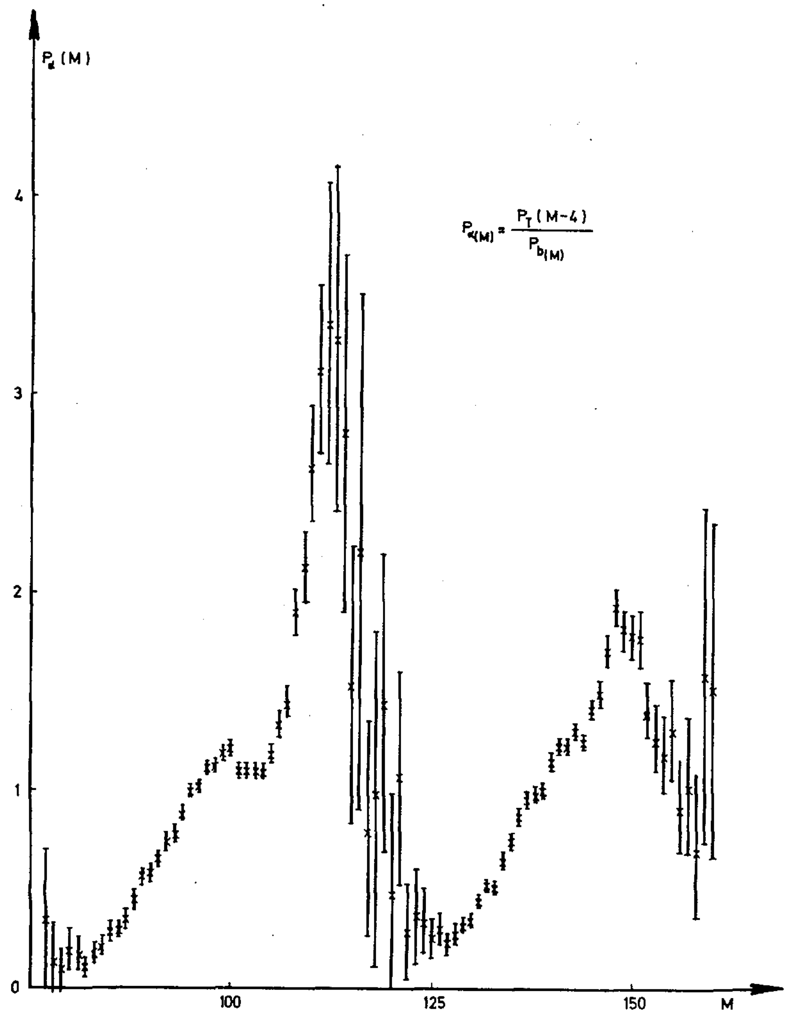

FIG. B. Alpha-particle emission probability $P_\alpha(M)$ versus mass M.

N. FEATHER: Is it possible that the process of rejection of spurious events (2000 out of 5000) has left in the 'accepted' class some events of large R (or R $\approx$ 1) which are not genuine? The equal error bars on the figure showing the most probable alpha particle energy as a function of R suggest that roughly the same number of events was measured in each range of R. Was this in fact the case?

C. CARLES: As explained in the paper, these events were rejected after completion of various tests that were carried out on these measured events. When R $\approx$ 1, there is a difficulty in deciding which of the two fragments is the light one; this arises because the ranges of the two fragments in this region are almost identical. However, there is not difficulty in comparison when R is large.

The error bars on the most probable kinetic energy of the alpha particle as a function of R are not statistical errors, but depend on the precision with which the fragment range curves are known and the accuracy of the microscope measurements. We found that this amounted to about 0.5 MeV for the most probable masses and we took the same value for all R.

S.S. KAPOOR: May I comment that the validity of the dumb-bell model in predicting the angular distribution of alpha-particles for various mass ratios necessarily assumes that these particles are emitted prior to the actual breaking of the neck, i.e. before the neck collapses and the fragments acquire equilibrium configuration. The basis of application of the dumb-bell model is therefore quite different from that underlying all those models of ternary fission in which the alpha-particle is assumed to be emitted as a result of sudden collapse of the neck.

C. CARLES: In invoking the dumb-bell model to order to explain the behaviour of $\theta_\alpha^\ell(R)$, one does not need to assume the emission of the alpha particle before the breaking of the neck; one could identify the point of emission of the alpha particles with the point of scission (break).

J. GRIFFIN: Would it be convenient to list the values of the parameters for a scission configuration which would give your results and to compare them with those which Dr. Ben-David said would describe his data?

C. CARLES: We have not carried out calculations concerning the scission configuration. However, using the trajectory calculation results of Kataze (J. Phys. Soc. Japan 25 (1968) 933) in conjunction with our experimental data on $\theta_\alpha^\ell(R)$ we obtain a value of about 3 MeV as the alpha-particle initial kinetic energy; this value is consistent with the results obtained by Boneh (Fraenkel and Nebenzahl, (Phys. Rev. 156 (1967) 1305) and Raisbeck and Thomas (Phys. Rev. 172 (1968) 1272).

STATISTICAL THEORY OF NUCLEAR FISSION: α-PARTICLE EMISSION

P. FONG
Physics Department, Emory University,
Atlanta, Ga.
United States of America

Abstract

STATISTICAL THEORY OF NUCLEAR FISSION: α-PARTICLE EMISSION. Experimental information on angular correlation of the long-range α-particle emitted in ternary fission with the main fission fragments has recently become available. The results may be compared with theoretical predictions and, as it turned out, provide a very sensitive test of the theory of the fission mechanism. The moving apart of the two fragments and the α-particle under the action of the Coulomb forces between them is a classical three-body problem; it can be solved numerically by a high-speed computer if the initial conditions, i.e. the initial positions and velocities of the three particles at the scission point, are given. The initial conditions are so numerous and the dependence of the angular correlation on these conditions is so sensitive that it is impossible to reconstruct the initial conditions from the final experimental results. The statistical theory of nuclear fission dealing with the mechanism of fission leads to a complete specification of the initial conditions of the present problem and the computer calculation of the angular correlation based on them may be compared with the experimental results in a critical test of the theory. The calculated results are in good agreement with the experiments. In asymmetric fission in which the heavy fragment involves the 82-neutron shell, the α-particle is emitted veering towards the light fragment as expected from shell-effect considerations of nuclear deformability. On the other hand, in far asymmetric fission in which the light fragment involves the 50-neutron shell, the simple shell-effect argument predicts the α-particle veering towards the heavy fragment initially, but detailed dynamical calculation shows that this initial movement leads the α-particle into a region of retarding field and the α-particle is eventually pushed back and emitted veering towards the light fragment as experimentally observed. This reversal occurs only when the inital kinetic energy of the α-particle takes a value as small as that predicted by statistical theory (about 0.5 MeV). All dynamical theories are likely to lead to a higher value of this energy and it is, therefore, more difficult to account for the angular correlation observed.

Introduction

Fraenkel and Thompson [1] published in 1964 early results of angular correlation of the long-range α-particle emitted in spontaneous fission of Cf^{252} with the main fission fragments. The interesting feature is that in the most probable asymmetric fission modes in which the heavy fragment completes the 82-neutron shell (mass ratio R $\sim$ 1.1), the α-particle is emitted veering towards the light fragment, whereas in the far asymmetric fission modes in which the light fragment completes the 50-neutron shell (R $\sim$ 2.0), the α-particle is emitted veering towards the heavy fragment. They correlated this variation of angular correlation with the prompt neutron distribution and offered the following explanation: The fission fragments that have completed the 82- or 50-neutron shell are very stiff to deform and therefore assume nearly spherical shapes with the consequences that the number of prompt neutrons emitted by them is very small and the Coulomb force exerted by them on the α-particle, presumably located at the scission point between the two nascent fission fragments, is larger than that of the other fission fragment (which has nucleon configurations between two closed shells and thus is easily deformed and assumes a highly elongated configuration) so that the α-particle is emitted veering away from the closed shell fragments as observed.

However, Fraenkel [2] has later corrected the earlier results by incorporating a recoil correction. The corrected results show that the α-particle is emitted always veering towards the light fragment, making an angle θ_L with it of about 80° with a variation of ±2° as the mass ratio of splitting R increases from 1 (symmetric fission) to 2 (far asymmetric fission). How, then, can we reconcile the result of α-particle angular correlation with that of prompt neutron emission in the far asymmetric fission region involving the 50-neutron shell? The results of Fraenkel [2] have been analyzed extensively by computer calculation by Boneh, Fraenkel and Nebenzahl [3] in many other respects but this important point has not been dealt with adequately.

The present author [4] has previously performed a statistical-theory calculation on the distributions of fission products, taking the empirical dependence of the nuclear stiff constant on the closed shell effect into consideration. The theory predicts the most probable deformation shapes for various mass ratios of splitting. Indeed, the deformation parameters for the closed-shell fragments calculated are small and those of the complementary fragments are large as expected on the above qualitative discussion. On this basis one can calculate the prompt neutron distribution $\nu(A)$ and explain its saw-tooth shaped distribution curve. Moreover, one can calculate the kinetic energy distribution of the fission fragments and explain the drastic dip of the kinetic energy distribution curve at symmetric fission.

It is obvious that the results of the most probable deformation shapes may also be used to calculate the α-particle angular distribution. Indeed all necessary information for such a calculation is contained in previously published papers [4,5] and no adjustable parameters need to be introduced. We are interested in knowing how the theoretical predictions of the statistical theory agree with experimental results and how the apparent discrepancy between the α-particle angular correlation and the prompt neutron distribution is to be resolved.

The Classical Three Body Problem

The angular correlation of the α-particle with the main fragments is determined by the dynamics of the motion of the three bodies, the two fragments and the α-particle, under the action of the Coulomb force among them. The three bodies can be reasonably approximated by three charged mass points and thus the problem is reduced to the well-known classical three body problem which has no exact solution.

Nevertheless, with the help of high speed computers, the dynamical problem may be integrated numerically. Once a set of initial conditions is specified we are in a position to predict the complete future history of the three particles. As the Coulomb force is a central force it is reasonable to approximate the problem as a two-dimensional problem. Each particle is thus specified by two rectangular coordinates (x,y) and two equations of motion may be set up according to Newton's second law with two Coulomb forces acting on it by the two other particles. The dynamical problem is thus formulated by a set of six simultaneous second-order differential equations. The six equations are interlocked because the forces entering into the equations of motion are dependent on the six position coordinates of the three particles themselves.

Once the initial conditions of position and velocity of the three particles at t_0 are given we can calculate the positions and velocities of the three after an infinitesimal time increment Δt by assuming the acceleration to be uniform in the infinitesimal time interval. The information at time $t_o + \Delta t$ may now be used as initial condition to calculate the position and velocity of the three particles at time $t + 2\Delta t$, and so on, ad infinitum. In practice we choose $\Delta t = 10^{-23}$ sec and repeat the calculation 200 times within which period the crucial dynamical changes would have taken place so that the remaining calculation will not change the main feature of the results obtained. Accordingly at the end of the 200 iterations the time interval Δt is changed to 10^{-22} sec and the calculation is repeated for another 100 times, at the end of which Δt is changed to 10^{-21} sec and the calculation is repeated another 100 times, and so on, until a total of 1000 iterations have been carried out corresponding to a total time of integration of 10^{-13} sec. The directions of the velocity vectors of the three particles at that time determine the angular correlation of the α-particle with the main fragments. The magnitudes of the velocities determine the kinetic energy distribution of the fission fragments and the α-particle together with their correlation. These may be compared with experimental results.

The Initial Condition According to Statistical Theory

The whole dynamical calculation is based on a knowledge of the initial condition of position and velocity at time t_o. We take the initial time t_o to be the scission point, i.e., the moment the two fragments and the α-particle separate from one another. Previous studies have established that the α-particle is emitted during the breaking up of the fissioning nucleus (not a post-fission effect). The scission point represents the time at which the three-body problem begins.

The scission point also represents the time at which the fission process ends. The initial condition of the three body problem is thus the final condition of the fission problem which should be predictable from a systematic theory of the fission process. The statistical theory [5] of the fission process is in a position to give a complete specification of the final condition of the fission process. In fact the essence of the statistical theory is that the fission product distributions of mass, charge, kinetic energy, prompt neutrons and so on are determined by and thus derivable from the final condition of the fission process rather than the initial condition. This prediction on the final condition can now be used as the initial condition of the three body problem. Verification of the three body calculation by the α-particle experimental results may be taken as an independent experiment proof of the statistical theory of the fission process.

The initial position of the three particles are taken to be along the same straight line (taken as the x-axis) with the α-particle in the middle (taken as the origin of the coordinate system). The α-particle is assumed to be a sphere of radius $1.2 \times 10^{-13} \times \sqrt[3]{4}$ cm (1.904×10^{-13}cm). Though the sphere acts as a point charge concentrated at the center, the extension does affect the initial position of the two main fragments for they are now not in contact with each other as in binary fission but are separated by an additional distance of 3.808×10^{-13}cm. The two main fragments are assumed to have the same deformation shapes as in binary fission. The statistical theory calculated deformation parameters of binary fission fragments [4] are taken over and assumed here. From the deformation shape the charge center of the deformed nucleus may be calculated [5]. The initial position of the three mass points are thus determined.

The initial velocities of the three particles are determined as follows: According to the statistical theory [5] the two fragments in binary fission are expected to have a total kinetic energy at the scission point of about 0.5 MeV. The same is assumed for the two main fragments in ternary fission. The velocities corresponding to such an energy are so small, as previous computer calculation [6] shows, that they can be safely neglected in the three body problem calculation. Thus we take the initial velocities of the two main fragments to be zero. The statistical theory also leads to the conclusion that the α-particle is expected to have a most probable kinetic energy at the scission point of about 0.5 MeV. Previous computer calculation [6] shows that this energy of the α-particle not only cannot be neglected but also plays a crucial role in determining the outcome of the three-body problem. This energy determines the magnitude of the initial velocity of the α-particle (4.91×10^8 cm/sec). The direction of the initial velocity is assumed to be in the y-direction, perpendicular to the line joining the three particles initially. The reason is that, if the α-particle has a sizable initial velocity component in the x-direction, it will soon move into one of the main fragments, as previous computer calculation shows, and the α-particle will not be emitted. Thus the initial position and velocity of the three particles are specified.

The computer integration of the three-body problem in ternary fission has been carried out by a number of authors. The present work is a continuation of that of Ertel [6], who first used statistical theory determined initial conditions, with the following differences: 1. Extended α-particles is assumed here whereas point α-particle was assumed in the earlier work. This change affects the calculated total kinetic energy. 2. The small effect of the forces the α-particle exerts on the two main fragments was neglected in the earlier work but is now included here for completeness. The present result thus will show to what degree this recoil effect changes the kinetic energy of the fission fragments; this information will be useful in making the "recoil correction" in the experimental determination of the masses of the main fragments such as applied by Fraenkel [2].

Results of Calculation

The calculated results of angular correlation are shown in Fig. 1 in which the angle θ the α-particle makes with the fission fragments (light and heavy) is plotted as a function of the mass number A of the fragment in the continuous curve. The experimental results of θ_L [2] are plotted in horizontal bars, (θ_H for heavy fragment obtained by reflection). The agreement is satisfactory. The calculated α-particle kinetic energy as a function of mass ratio R, shown in Fig. 2, agrees well with that of experiment. The detailed results of kinetic energy distribution and correlation of the three particles will be reported later.

Discussion

The agreement between the calculated and experimental angular correlation of the α-particle lends support to the predicted scission configuration by the statistical theory. Still, we want to know why in the far asymmetric fission region the closing of the 50-neutron shell in the light fragment, while making the number of prompt neutrons emitted from the light fragment small, does not cause the α-particle to be emitted veering towards the heavy fragment as discussed by Fraenkel and Thompson [1].

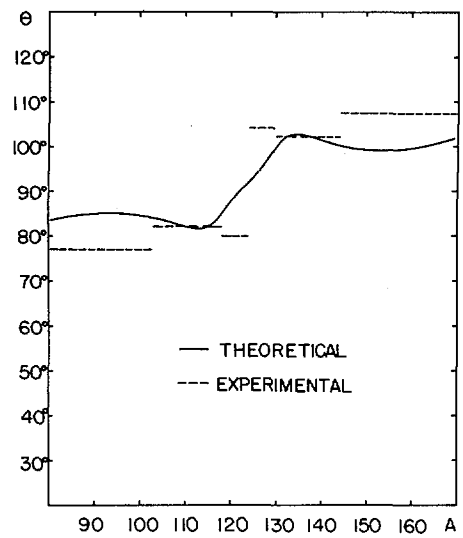

FIG. 1. Angular correlation of α-particle with fission fragments.

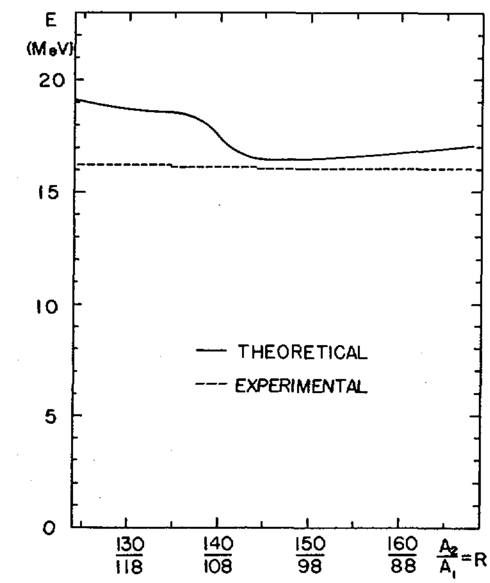

FIG. 2. α-particle kinetic energy E versus mass ratio R.

A close examination of the detailed dynamical history of the α-particle reveals that in this case the α-particle was actually veering towards the heavy fragment in the beginning as expected from the shell consideration. However, as it moves closer to the heavy fragment the Coulomb force from the heavy fragment increases and that from the light fragment decreases so that eventually the former dominates over the latter and consequently the α-particle experiences a deceleration in the x-direction away from the heavy fragment. The deceleration is strong enough to reverse the sign of the x-component velocity and therefore the

α-particle is eventually emitted veering towards the light fragment as experimentally observed.

The reversal of the sign of the x-component velocity of the α-particle will be called a reflection of the α-particle. The detailed dynamical history obtained by computer calculation for fission modes in the peak-yield asymmetric fission region, where the heavy fragment completes the 82-neutron shell, shows that there is no such reflection. Thus the α-particle emission correlates with the prompt neutron emission as previously expected. In the far asymmetric fission region reflection takes place once and no second reflection follows thus giving rise to the apparent discrepancy.

The occurrance of the reflection and the number of reflections depend largely on the initial velocity of the α-particle which determines how fast the α-particle escapes the accelerating field of the two main fragments - a very fast escape does not allow time for a reflection to develop. Computer calculation [6] shows that if we assume the initial kinetic energy of the α-particle at the scission point $E_{\alpha o}$ to be 2 MeV or more there would be no reflections for all fission modes of any mass ratio of splitting (very fast escape realized). The α-particle in the far-asymmetric fission modes would be emitted veering towards the heavy fragment, contracting experimental results. If $E_{\alpha o}$ were less than 0.5 MeV, a reflection might take place in a fission mode in the peak-yield region, again contradicting experimental results. Each reflection changes the direction of the α-particle from veering towards one fragment to towards the other and the onset of the reflection differs from one mass ratio to another so that it is nearly impossible to adjust the value of $E_{\alpha o}$ as a parameter to fit the experimental data. Therefore the verification of the angular correlation curve becomes a very sensitive test to the value of $E_{\alpha o}$. The value of 0.5 MeV for $E_{\alpha o}$ according to the statistical theory represents the energy of the α-particle on the "noise level" and so is not likely to be reducible any further. Any dynamical theory involving a specific dynamical mechanism for the fission process is likely to endow to the α-particle an extra amount of kinetic energy above the energy of the noise level at the scission point. Otherwise the theory is likely to be indistinguishable from the statistical theory. Yet an increase of $E_{\alpha o}$ from 0.5 MeV (to the neighborhood of merely 2 MeV, for example) is likely to lead into disagreement with experimental results of α-particle angular correlation unless we change the initial condition on the position drastically. In that case there is little hope of being able to explain the prompt neutron and kinetic energy distributions at the same time. Thus the very sensitive test of the value of $E_{\alpha o}$ by the α-particle angular correlation strongly supports the statistical theory. Any reasonably complete theory of fission should yield a prediction on $E_{\alpha o}$ and thus should be tested by the experimental information of α-particle angular correlation.

Boneh, Fraenkel and Nebenzahl [3] tried to reconstruct the initial condition at the scission point by making use of the experimental information of α-particle distributions. This turns out to be a tremendously difficult task because there are so many parameters involved in the initial conditions and the number of combinations of possible parameters is so large that it is impossible to try out all sets by performing a three body calculation for each of them (to find a needle in a hay stack). As a result they determined the value of $E_{\alpha o}$ to be 3 MeV by other considerations which they admitted are open to question. Their computer calculation program is hinged on this choice. As discussed before when $E_{\alpha o}$ is set at 3 MeV there are no reflections at all. Thus they were exploring an area beyond the "storm center" of the three body problem and missed many interesting features of the dynamic system. They calculated several distributions but left out the most sensitive part, the angular correlation. Even the set of initial parameters representing best fit turns out to be in a position difficult to reconcile with the experimental results of prompt neutron distribution. Moreover their calculation makes use of a Δt that increases in length as iteration goes on. This procedure, while safe for $E_{\alpha o} = 3$ MeV, is dangerous when a reflection is involved - when the x-coordinate returns to the initial value zero by reflection, the time increment in iteration Δt should be taken as small as the Δt at the initial time t_o, which they took to be 10^{-23} sec, but in their procedure it takes a value somewhat longer; this may introduce significant computational errors which may be compounded through iterations. In the present calculation the "storm center" is covered by the first 200 iterations with a uniform Δt of 10^{-23} sec for all 200 iterations.

REFERENCES

[1] Z. Fraenkel and S. G. Thompson, Phys. Rev. Letters 13, 438 (1964).
[2] Z. Fraenkel, Phys. Rev. 156, 1283 (1967).
[3] Y. Boneh, Z. Fraenkel and I. Nebenzahl, Phys. Rev. 156, 1305 (1967).
[4] Peter Fong, Phys. Rev. Letters, 11, 375 (1963).
[5] Peter Fong, Phys. Rev. 102, 434 (1956).
[6] J. P. Ertel, M.S. Thesis, Emory University (1968), published in Peter Fong, Statistical Theory of Nuclear Fission, Gordon and Breach, New York (1969). P. 191.

DISCUSSION

E. NARDI: I would like to comment on the model used in your calculations, in which you assume very low initial kinetic energies and a very "short" neck. It seems that the two most prominent features of alpha-accompanied fission are the wide distributions of both angular distribution and energy spectrum of the alpha particles. The trajectory calculations by Boneh et al. and Raisbeck and Thomas show that the width of the angular distribution cannot be obtained using low initial kinetic energies like the ones you propose, especially if the neck is a very short one.

Another comment on your model in which no reference to trajectory calculations is made is the following: If you insert a triton instead of an alpha particle between the fragments and calculate the total energy of the system using point charge approximation, you get in your model about 10 MeV more potential energy for alpha fission than for t-fission. The experimentally determined total energy of the three particles would therefore be 10 MeV higher in alpha fission. We have measured this difference and obtained 7.4 ± 0.45 MeV. According to your model this would give a distance of 28.5 F at scission between both fragments.

How do you deal with these two problems in your model?

P. FONG: In my approach, the distribution width is to be determined by the distribution of the deformation slopes of the fission fragment determined by the statistical theory. The nature of the three-body problem is that no one can predict the outcome until the computer finishes the calculation. This is a painfully learned experience! The conclusion that $E_{\alpha 0}$ must be large is premature.

According to my model the scission distance D will certainly not be 28.5 F. This would make the energy difference in the two cases several times larger than both values quoted. I see no reason why my calculation on t-fission cannot be in agreement with measured values.

E. NARDI: May I also make a few observations on the so-called "opposite behaviour" in the variation of the most probable angle of emission of the alpha particle as a function of R, the mass ratio? Analysing Fraenkel's experimental data, Boneh et al. found that the scission point actually moves in the direction of the light fragment as the mass ratio increases. This is in qualitative agreement with the behaviour of the deformation energy of the fragments as derived from measurements of the average number of neutrons as a function of fragment mass. We can use these deformation energies together with the radii of the fragments at scission (obtained from the data of Boneh et al.) to derive "stiffness coefficients" of the fission fragments. It has been found (and will be published in a forthcoming paper) that these coefficients do not essentially vary with mass. I do not think that this is unreasonable, since it seems that shell effects should be washed out at the very large deformations obtained for the fragments in calculations of the type done by Boneh et al. To summarize, I do not therefore feel that the behaviour of the most probable angle as a function of R obtained by Fraenkel is unreasonable.

P. FONG: The conclusion that the stiffness constant does not change with mass number at large deformation should be tested by experimental evidence before being used as the basis to prove a point. I have never said that Fraenkel's most probable angle as a function of mass ratio is unreasonable. On the contrary, I have taken it as an established experimental fact, and emphasized the point that this fact is very difficult for any dynamical theory of fission to explain and, therefore, favours the statistical theory.

J.R. NIX: There are two questions I should like to ask. First, how have you determined the initial distance between the centres of charge of the fragments? Second, what would happen if you tried to "improve" your calculations by including more terms in the expansion of the fragments' radius vectors?

If you did try to do this, you would surely find that the centres of charge of the fragments would separate to infinity. As discussed earlier, this is associated with the impossibility of determining a scission configuration by minimizing the potential energy. There is therefore an underlying arbitrariness in your initial conditions.

P. FONG: We established the initial distance between the centres of charge of the fragments by determining the most probable deformation shapes of the fragment from first principles and experimental nuclear data (without adjustment of the parameters). The shape determines the charge centre.

As far as the second question is concerned, we are interested in realistic deformation parameters which would explain all related experimental results. When more terms of expansion are used, the agreement in kinetic energy distribution becomes worse; this means that the liquid-drop model is not realistic and should not be used as the basis for investigating other related problems such as alpha-particle distribution.

Regarding your last comment, this is a difficulty of the liquid-drop model, not of the fissioning nucleus.

H.W. SCHMITT: The effect of the finite sizes and non-spherical shapes of the fragments could perturb the results of such trajectory calculations appreciably. Have any estimates been made of this effect? Also, how does the time of interaction of the three particles, i.e. the time of separation to "large" distances, compare with the estimated vibration periods of the fragments?

P. FONG: The effect of the extended alpha particle is to lower the total kinetic energy to a value comparable to the experimental level. The trajectories are sensitively dependent on the deformation shapes of the fragments. The important point here is that the set of deformation shapes previously determined to explain kinetic energy and prompt neutron distributions is one that also explains ternary fission well. Any change of the shapes will lead to disagreement in all three experiments. As to the point-particle approximation, the validity has been discussed by previous authors in this field.

The estimated vibration period is of the order of 10^{-20} s. In trajectory calculations the angular distribution no longer changes after 10^{-21} s. Thus, the "interaction" is over long before 1/10 of the vibration period has elapsed.

TRAJECTORY CALCULATIONS IN LIGHT-PARTICLE FISSION

E. NARDI
Israel Atomic Energy Commission,
Soreq Research Center and
Weizmann Institute of Science, Rehovot
and
Y. BONEH
Nuclear Research Center, Negev
and
Z. FRAENKEL
Weizmann Institute of Science, Rehovot, Israel

Abstract

TRAJECTORY CALCULATIONS IN LIGHT-PARTICLE FISSION. Trajectory calculations based on a three-point-charge model were carried out for fission accompanied by ^1H, ^2H, ^3H, ^4He, ^6He, ^8He emission. The calculations were carried out with the intent of obtaining for each of these modes of fission the initial conditions which best fit the experimental results. The results indicate that both the initial distances between the fission fragments at scission and the initial kinetic energies of the particles tend to decrease as the mass of the light particle increases. In addition it was found that the experimental results could be better fitted by assuming that the particles are emitted off the axis connecting both fission fragments rather than on this axis.

1. INTRODUCTION

The emission of light nuclei in the fission process has recently been the subject of several experimental investigations [1-5]. These studies were mainly concerned with the emission probability and with the kinetic energy spectrum of the various light nuclei emitted in the fission of ^{252}Cf and $^{235}U^*$.

Of the light nuclei emitted in fission only alpha-particle-accompanied fission (LRA fission) has been extensively studied [6-8]. A most important feature of LRA fission is the great similarity in the characteristics of the fission fragments and of the neutrons evaporated from the fragments in this mode of fission and binary fission [7, 8]. On the basis of this similarity, it was postulated that the characteristics of the binary and LRA scission configurations be essentially the same [7, 8]. Alpha-particle emission in fission can, therefore, serve as a powerful tool in the investigation of the scission process. Trajectory calculations of the LRA fission process have been carried out by Geilikman and Khlebnikov [9], Halpern [10], Boneh, Fraenkel and Nebenzahl [11], and, more recently, by Katase [12]. By comparing the results of these calculations with the experimental data, these authors were able to obtain the initial conditions at scission. The more important conclusions of the calculations of Halpern [10] and of Boneh et al. [11] were that at scission the fission fragments are already moving with an appreciable part of their final kinetic energy.

It is reasonable to assume that, just as in the case of LRA fission, the scission characteristics of fission accompanied by other light particles do not differ essentially from those of binary fission. It is, therefore, of great interest to attempt to calculate the initial conditions at scission for light-particle-accompanied fission, on the basis of the available experimental information. Such a program has recently been carried out by Raisbeck and Thomas [4] for the spontaneous fission of ^{252}Cf and Błocki and Krogulski for ^{236}U [13]. Raisbeck and Thomas observed that the experimental data cannot be fitted satisfactorily by using the same initial conditions for the various particles. It is the purpose of our calculations to obtain for each of the particles the initial conditions which fit best the experimental data, and to see if any trends could be observed in the initial conditions.

In section 2 of this paper we discuss the model used in the calculations, and in section 3 the calculations are described. The results are presented in section 4 and discussed in section 5.

2. THE MODEL

Detailed trajectory calculations have been carried out by Boneh, Fraenkel and Nebenzahl [11] (to be referred to in the following as BFN) for the long-range-alpha (LRA) fission of ^{252}Cf. These calculations were based on the experimental properties of the alpha particles and fission fragments as determined by Fraenkel [7] for the LRA fission of ^{252}Cf.

Following essentially the method of BFN, we shall attempt here to obtain the initial conditions at the scission point for ^{252}Cf fission accompanied by ^{1}H, ^{2}H, ^{3}H, ^{6}He and ^{8}He. The experimental data for these processes presently available are the following: the kinetic-energy spectra of these particles [1, 2, 4], the kinetic energies and mass distribution of the fission fragments for ^{1}H and ^{3}H fission [5], the widths of the angular distribution of the particles in ^{1}H ^{2}H ^{3}H and ^{6}He-accompanied fission [4]. The shapes of the energy spectra of the Li and Be isotopes are not clear at this stage since the results of Cosper et al. [1] and of Raisbeck and Thomas [4] are in substantial disagreement. The trajectory calculations were therefore not carried out for Li and Be.

The trajectory calculations of BFN were based on a three-point-charge model. For sake of simplicity, the momenta of three particles were assumed to lie in one plane, i.e., the calculations were two-dimensional. The trajectory calculations gave the final values of the kinetic energies and the final directions of the alpha particles. These results were compared with the experimental values and the initial conditions were varied until agreement with experiment was achieved. In this manner, the initial conditions at scission were obtained. Obviously, this method can be used for other charged particles emitted in fission. The only two parameters to be changed are the charge and the mass of the emitted particles.

The initial dynamical variables used in the calculations of this paper are listed as follows (Figure as in BFN):

1. E_{P0}, the initial kinetic energy of the light particle.
2. E_{F0}, the sum of the initial kinetic energies of both fission fragments.

3. D, the distance between the fission fragments (which are represented by point charges).
4. θ, the angle of emission of the light particle relative to direction of the light fission fragment.
5. x, the distance of the point of emission of the light particle from the heavy fragment along the fission axis (x-axis).
6. Y, the initial distance of the point of emission of the light particle from the fission axis.

The distribution of the initial kinetic energy of the emitted light particle was assumed to be of Maxwellian form, i.e.

$$N(E_{P0}) = E_{P0} \exp(-E_{P0}/T) \tag{1}$$

The average initial kinetic energy of the fission fragments $\overline{E}_{F0}$ used in the calculations was given by

$$\overline{E}_{F0} = \overline{E}_T - V_0 - \overline{E}_{P0} \tag{2}$$

where $\overline{E}_T$ is the average total final kinetic energy of the three particles, V_0 is the total potential energy at scission which depends among other things on the quantity D, and $\overline{E}_{P0}$ is the average initial kinetic energy of the light particle (see Eq. 1). $\overline{E}_T$ was assumed to be equal to the average value of the final kinetic energy of the fission fragments, $\overline{E}_F$, plus the average final energy of the light particle $\overline{E}_P$. The latter values are known for the light particles. However, $\overline{E}_F$ was measured for LRA [5, 7] and for triton- and proton-accompanied fission only [5]. In deuteron-accompanied fission we assumed that the experimental value of $\overline{E}_F$ is equal to that value in triton-accompanied fission while for ^6He and ^8He-accompanied fission this value was assumed to be equal to that of LRA fission. The value of D, was held fixed in the calculation while $\overline{E}_{F0}$ was assumed to have a Gaussian distribution. The standard deviation of E_{F0}, $\sigma(E_{F0})$ was determined on the basis of the experimental results for ^1H, ^3H and LRA fission while for the other light particles for which the fragment kinetic energy distribution has not been measured, the magnitude of this value was assumed on the basis of the results for ^1H, ^3H and α-particles (see section 4).

The angular distribution of the emitted light particle was assumed to be isotropic. However, because of the presence of the fission fragments, θ is confined to the region $30° < \theta < 150°$. In BFN, on the other hand, it was assumed that the particles are emitted only at 90° with respect to the direction of the light fission fragment.

The distribution of the point of emission of the light particles along the fission axis $N(x_p)$ was derived on the basis of the distribution $N(x_\alpha)$ found by BFN for LRA fission. The values of x_α and x_p denote, respectively, the distance of the point of emission of the alpha particle and light particle from the centre of the heavy fission fragment. The distribution of $N(x_p)$ assumed here was based on the assumption that fission accompanied by light particles does not differ substantially from LRA fission. It was pointed out by Raisbeck and Thomas [4] that the N(x) distribution has a relatively weak effect on the final energy distribution of the light particles.

In BFN it was postulated that the alpha-particles are emitted from the "neck" of the scissioning nucleus. It was assumed that the "neck"

TABLE Ia. INITIAL CONDITIONS GIVING SATISFACTORY AGREEMENT WITH EXPERIMENTAL DATA, Y = 0

Particle	$\bar{E}_{P0}$ (MeV)	D $\times 10^{-13}$ (cm)	$\bar{E}_{F0}$ (MeV)	$\sigma(E_{F0})$ (MeV)
^{1}H	1.6	34.0	71	9.3
^{2}H	2.4	26.0	40	
^{3}H	2.0	24.0	29	8.5
^{4}He	3.0	24.0	28	8.2
^{6}He	1.2	22.0	15	
^{8}He	1.0	21.0	7	

TABLE Ib. INITIAL CONDITIONS GIVING SATISFACTORY AGREEMENT WITH EXPERIMENTAL DATA, Y = 3

Particle	$\bar{E}_{P0}$ (MeV)	D $\times 10^{-13}$ (cm)	$\bar{E}_{F0}$ (MeV)	$\sigma(E_{F0})$ (MeV)
^{1}H	2.0	38.0	83	9.4
^{2}H	3.0	29.0	60	
^{3}H	2.4	26.0	46	8.7
^{4}He	3.8	26.5	40	8.8
^{6}He	1.8	25.0	34	
^{8}He	1.8	25.0	34	

extends from the point which is at a distance of 6F from the centre of the heavy fragment to the point at 6F from the centre of the light fragment. It will be seen in Table I that the values of D_p, the initial distance between the fission fragments at scission for light particle fission, are not necessarily equal to the D_α of LRA fission. The N(x) distribution of BFN was therefore adjusted to that of light-particle fission by assuming that $N(x_p) = N(x_\alpha)$ for the value of x_α which satisfies

$$\frac{x_p - 6}{x_\alpha - 6} = \frac{D_p - 12}{D_\alpha - 12} \tag{3}$$

The distance Y of the point of emission of the light particle from the axis connecting the fission fragments was kept constant. At the first glance, it might seem that initial conditions with $Y \neq 0$ evolve from starting conditions in which Y = 0. However, it should be stressed that the initial configuration is by definition that configuration for which the initial kinetic energy distributions of the three particles are uncorrelated with each other. Since the "Maxwellian" shape of the initial particle kinetic energy spectrum is not conserved as the three particles separate, the initial conditions at $Y \neq 0$ do not evolve from a starting configuration in which $Y = 0$.

Summarizing, we can say that the initial variables that were obtained by comparing the calculations with the experimental results are $\overline{E}_{P0}$, D and $\sigma(E_{F0})$.

3. THE CALCULATION

The trajectories of the two fission fragments and the light particle were calculated using the BFN trajectory computer program. The initial conditions in our calculations were picked up by means of a Monte-Carlo method which used the distributions discussed above as weighting functions. Each set of initial conditions gave rise to final values of the three particles, and upon repeating the process a distribution of the final values was obtained. With the exception of protons, the experimentally determined energy spectra of the light nuclei with which we compared our calculations were not correlated with the direction of the fission fragments. Hence, a weighting factor of $\sin\theta$ was given to each event in which the light nucleus was emitted at an angle θ with respect to the final direction of motion of the light fission fragment. Each final distribution was obtained from approximately 3000 trajectory calculations. The calculations were performed on the "Golem" computer of the Weizmann Institute and each trajectory calculation took about 1/5 of a second.

4. RESULTS

We carried out the calculations in order to obtain the initial conditions fitting best the experimental data for each particle. For ^{2}H, ^{3}H, ^{4}He, ^{6}He and ^{8}He-accompanied fission the calculated results were compared with the experimental data of Cosper et al. [1], which have the best statistical accuracy. The spectral shapes of these particles are well approximated by Gaussian distributions. In proton-accompanied fission the data of Raisbeck and Thomas [4] were used. The background in the measured proton spectrum is probably lower in the results of Raisbeck and Thomas [4] than in the results of Cosper et al. [1].

The final spectrum of the light particles depends on D, the initial distance between the fragments, and on $\overline{E}_{P0}$ the initial average kinetic energy of the particle. For a given value of D, an increase in the value of $\overline{E}_{P0}$ will result in a larger value of the width of the particle kinetic energy spectrum and, to a lesser extent, in an increase of the most probable final kinetic energy of the particle. Similarly, lowering the value of D and keeping the value of $\overline{E}_{P0}$ constant results mainly in a higher value of the most probable particle energy and, to a lesser extent, the particle energy spectrum is broadened. The value of $\sigma(E_F)$, the standard deviation of the final total kinetic energy spectrum of the fission fragments is, to a first approximation, determined by $\sigma(E_{F0})$, the standard deviation of the initial fragment kinetic-energy distribution. The values of $\sigma(E_F)$ were obtained experimentally for LRA [5, 7] triton-and-proton-accompanied fission [5]. For ^{6}He and ^{8}He $\sigma(E_{F0})/\overline{E}_{F0}$ was assumed equal to the value

TABLE II. COMPARISON BETWEEN CALCULATED AND MEASURED ENERGY SPECTRA OF LIGHT PARTICLES AND PROPERTIES OF PREDICTED ANGULAR DISTRIBUTION

Particle	Most probable energy (MeV)			HWHM of kinetic energy distribution (MeV)			Most probable angle (degrees)		FWHM of angular distribution (degrees)	
	Calculated		Measured [1]	Calculated		Measured [1]	Calculated		Calculated	
	Y = 0	Y = 3		Y = 0	Y = 3		Y = 0	Y = 3	Y = 0	Y = 3
^1H	6.5	6.5	~6.5 [4]	2.7	2.5	~2.5 [4]	80	85	35	39
^2H	8.0	8.4	8.0 ± 0.5	3.1	3.6	3.6 ± 0.5	82.5	83.0	32	40.0
^3H	8.2	8.2	8.0 ± 0.3	3.3	3.1	3.1 ± 0.3	80	83.0	25	35
^4He	16.0	16.2	16.0 ± 0.2	5.4	4.9	5.1 ± 0.2	81	82.0	25	33.0
^6He	11.8	12.2	12.0 ± 0.5	4.5	4.2	4.0 ± 0.5	80	81.0	15	28.0
^8He	10.0	10.4	10.2 ± 1.0	4.9	4.4	4.0 ± 1.0	80	79.0	15	28.0

in LRA fission while for ^{2}H this ratio was assumed equal to that obtained in ^{3}H-accompanied fission.

Table Ia shows the initial conditions for the various light particles which give the best fit to the experimental particle kinetic-energy spectra. These calculations were carried out for the condition $Y = 0$, i.e. the particles were emitted from points along the axis connecting the fission fragments. In Table II the experimental and calculated most probable energies and widths of the different light-particle spectra are compared. The predicted properties of the angular distribution are also given in Table II.

The agreement between the calculated and experimental energy spectra is satisfactory. We note, however, that the calculated widths of the ^{4}He, ^{6}He and ^{8}He kinetic-energy spectra tend to be somewhat wider than the experimental results; such a behaviour was also observed by Raisbeck and Thomas [4]. The value of D in Table I for LRA fission is lower than that obtained by BFN. This follows from the fact that in the present calculations the particles were emitted in all directions and not only at 90° with respect to the direction of the fission fragments as in BFN. As a result the final kinetic energy of the particle is lower than for the same event in the BFN calculations, and the value of D must be decreased in order to obtain the correct experimental result. Because of the lower value of D and also of $\overline{E}_{P0}$ the calculated angular distribution in LRA fission is also narrower here than that obtained by BFN.

Table Ia shows that the calculated values of D and $\overline{E}_{P0}$ for ^{6}He-accompanied fission are substantially lower than these values in LRA fission. As a result the calculated angular distribution of ^{6}He is much narrower than that of LRA fission. On the other hand, the experimental results of Raisbeck and Thomas [4] indicate that both these angular distributions are of equal width. We find that, although the particle energy spectra are in satisfactory agreement with the calculations, the angular distributions of ^{6}He do not agree with the experimental results.

On the basis of the results presented above it can be concluded that for ^{4}He, ^{6}He and ^{8}He the values of $\overline{E}_{P0}$ (which affect the width of the final particle kinetic-energy spectrum) tend to be somewhat too large. However, if we lowered $\overline{E}_{P0}$ in order to obtain a narrower distribution, the peak value of the particle spectrum would also decrease to give a value which is too low. The situation can be improved by choosing $Y \neq 0$. In the latter case $\overline{E}_{P0}$ can be lowered to give a narrower final kinetic-energy distribution while the value of the peak of the spectrum would not be lowered, since for $Y \neq 0$ a larger fraction of the initial particle potential energy is transformed into final particle-kinetic energy than for $Y = 0$. It was found that there is essentially no difference in the agreement that can be obtained when Y is in the range of 2 to 5 f, however, the values of D and $\overline{E}_{P0}$ are different for the different values of Y. The calculations described here were carried out for $Y = 3F$.

The initial conditions obtained for $Y = 3$ are listed in Table Ib and in Table II the experimental and calculated results for the different light nuclei are compared. It is seen that good agreement could be obtained within the framework of the present model. As an example the calculated and measured kinetic-energy distributions of the tritons are plotted in Fig.1. The predicted angular distributions of the particles which are given in Table Ib are observed to be wider here than those obtained for the calculations with Y = 0. For LRA fission the calculated width is equal to that of BFN. The angular distribution of ^{6}He is somewhat narrower than that of ^{4}He, however, the agreement is much better than for Y = 0.

The calculations for both Y = 0 and Y = 3 show that the width of the angular distribution decreases as the mass of the particle increases. This trend has been confirmed by the results of Raisbeck and Thomas [4] for ^{1}H, ^{2}H, ^{3}H, and ^{4}He.

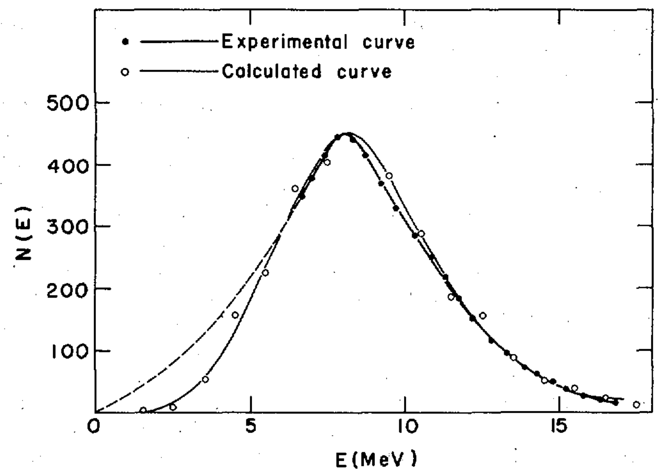

FIG. 1. Experimental and calculated kinetic-energy spectrum of tritons.

5. CONCLUSIONS

The results given in Table I for both Y = 0 and Y = 3 show that the value of D tends to decrease as the mass of the light particle increases. This trend may indicate a less deformed scission configuration (small D) for fission accompanied by the emission of heavier particles. Hence, they may be expected to emit a smaller amount of neutrons. This conclusion is supported by the fact that fewer neutrons are emitted in LRA fission than in binary fission [8]. But, above all, this trend would indicate that the scission configuration in binary fission is even more elongated than in LRA fission. The D values listed in Table I for the protons, however, seem extremely high.

The results of Table I also indicate that for ^{8}He, ^{6}He, ^{3}H and ^{2}H the values of $\overline{E}_{P0}$ tend to decrease as the mass of the light particle increases. This trend is not followed by the protons. This result together with the relatively high value of D obtained for protons may indicate that a different mechanism may be responsible for proton emission. It should be pointed out, however, that the value of $\overline{E}_{P0}$ for alpha particles is larger than that of ^{3}H and ^{2}H, a fact which is not in agreement with the above-mentioned trend.

We note that calculations based on a model in which light particle emission results from the fast potential change in the neck region of the fissioning nucleus [14] predict that the average initial kinetic energy of the light particle decreases as the particle mass increases, in qualitative agreement with the trend found here.

It would seem that the most drastic assumption in our model is the approximation of the two fission fragments and the light particle by three-point-charges. However, the assumption is not expected to affect the essential features of our results [10]. Another assumption made here is that the initial energy distribution of the light particles is of "Maxwellian" shape. A different initial kinetic energy distribution may result in somewhat different values of D and $\bar{E}_{P0}$ but the main features of our results will again remain unchanged.

REFERENCES

[1] COSPER, S.W., CERNY, J., GATTI, R.C., Phys. Rev. 154 (1967) 1193.

[2] WHETSTONE, S.L., Jr., THOMAS, T.D., Phys. Rev. 154 (1967) 1174.

[3] DAKOWSKI, M., CHWASZCZEWSKA, J., KROGULSKI, T., PIASECKI, E., SOWIŃSKI, M., Phys. Lett. 25B (1967) 213.

[4] RAISBECK, G.M., THOMAS, T.D., Phys. Rev. 172 (1968) 1272.

[5] NARDI, E., GAZIT, Y., KATCOFF, S., Phys. Rev. (to be published).

[6] SCHMITT, H.W., NEILER, J.H., WALTER, F.J., CHETHAM-STRODE, A., Phys. Rev. 9 (1962) 427.

[7] FRAENKEL, Z., Phys. Rev. 156 (1967) 1238.

[8] NARDI, E., FRAENKEL, Z., Phys. Rev. Lett. 20 (1968) 1248.

[9] GEILIKMAN, B.T., KHLEBNIKOV, G.I., Atomn. Energ. 18 (1963) 218. English translation: Soviet J. atom. Energy 18 (1965) 274.

[10] HALPERN, I., in Physics and Chemistry of Fission (Proc. Symp. Salzburg, 1965) 2, IAEA, Vienna (1965) 369; CERN Report No. CERN-6812 (1963) (unpublished).

[11] BONEH, Y., FRAENKEL, Z., NEBENZAHL, I., Phys. Rev. 156 (1967) 1305.

[12] KATASE, A., J. phys. Soc. Japan 25 (1968) 933.

[13] BŁOCKI, J., KROGULSKI, T., Nucl. Phys. A 122 (1968) 417.

[14] BONEH, Y., FRAENKEL, Z., NARDI, E. (to be published).

DISCUSSION

K. DIETRICH: The parameters D of your best fits correspond to a stage quite a bit later than the point of rupture. Did you extrapolate backward so as to obtain the kinetic energies of the fragments and of the light particle at an earlier stage corresponding to the still connected fragments?

E. NARDI: If we extrapolated our distributions backward for the case of Y = 3 to Y ≈ 0, we would obtain an initial kinetic-energy distribution of the particles different from the initial "Maxwellian" distribution. Hence we would not be within the framework of the model we assume. Now, we might indeed construct initial conditions using this new distribution and thus have a reduced value of D. However, as can be seen in Table I, of the paper, the values of D for Y = 3 are relatively high and this, when extrapolated back to Y = 0, would still probably be large. Thus, the initial kinetic energy of the fission fragments would likewise still be large.

L. WILETS: When Y is not equal to zero, so that the alpha particle is off axis, did you assume planar motion? And if so, what is the effect of the ϕ-motion?

E. NARDI: For Y off the axis we assume planar motion. The validity of this assumption is discussed by Boneh et al. These authors compare their two-dimensional results to the three-dimensional calculations of Halpern and conclude that the two-dimensional restriction does not substantially affect the results.

H.W. SCHMITT: It would seem reasonable to include a distribution in Y_0, the initial distance of the alpha-particle from the fragment-fragment axis, in your calculations. The basis for this is just the occurrence of the bending mode of oscillation in fission. Could you please comment?

E. NARDI: I agree that one should assume a distribution in the value of Y; this would also follow on the basis of the uncertainty principle. We would, however, have to add an additional parameter (the width of distribution) and we would therefore have to seek three parameters which give the best fit with the data of each particle. Now, if we introduce an additional parameter, I think I would prefer to have it in the initial kinetic energy of the particles, which is specified by only one parameter. But to summarize, I do not think that a distribution in Y would affect the basic features of the results, and we essentially are only stressing them.

M. ASGHAR: It has just been shown by Professor Fong (paper SM-122/108) that starting with 0.5 MeV as the initial alpha-particle kinetic energy, one gets the right value of its most probable final kinetic energy as a function of the fragment mass ratio. Now, your trajectory calculations come out with a value of 3 MeV. How does that happen? Is it because Fong does not consider the alpha particle as a point charge, but gives an extension to it?

Incidentally, we can demonstrate that our curve in the final angle θ_α with respect to the light fragment as a function of the fragment mass ratio shown a little while ago is consistent with the value of 3 MeV for the alpha-particle kinetic energy.

E. NARDI: The discrepancy between our data and those of Fong results from the fact that we are fitting the angular and energy distributions, which seem to be the main characteristics of light particle emission, while he has not done this. Moreover, we have no trouble with θ_α as a function of fragment mass (see my comments on paper SM-122/108).

P. FONG: There exist many sets of initial parameters that fit the experimental results of alpha-particle distribution. My set happens to have $E_{\alpha 0} = 3$ MeV. The set used by Boneh, Fraenkel and Nebenzahl started with $E_{\alpha 0} = 3$ MeV and the others were then determined to fit the experiment. But there is one difference between the two sets. There is greater difficulty in making their set agree with the prompt neutron data. No a priori and a posteriori reasons supporting $E_{\alpha 0} \cong 3$ MeV have been definitely established. The wide angular distribution width is to be determined by the distribution of the deformation shapes of the two main fragments which can be reduced to a combination of the distribution of the alpha-particle position for a fixed D and a distribution of D itself; the former has been taken into consideration by the earlier authors but the latter has not. Thus, the angular distribution does not require a large value of $E_{\alpha 0}$ in the neighbourhood of 3 MeV. Therefore, taking all experimental results including the prompt neutron data into consideration, $E_{\alpha 0} = 0.5$ MeV is preferred.

SHELL STRUCTURE EFFECTS IN FISSIONING NUCLEI

(Session C)

Chairman: L. Wilets

SHELL-STRUCTURE EFFECTS IN THE FISSIONING NUCLEUS
A Review

V.M. STRUTINSKY *, H.C. PAULI †
The Niels Bohr Institute,
University of Copenhagen, Denmark

Abstract

SHELL-STRUCTURE EFFECTS IN THE FISSIONING NUCLEUS. A survey of the present state of fission theory is presented, with special emphasis on developments in the past few years. An attempt is made to bring out the more important problems to be settled by future experiments and theory.

1. *INTRODUCTION*

After some new and exciting discoveries made in the last few years, the problem of the intrinsic structure effect in nuclear fission is widely discussed at the present time. Some of these effects were already considered at the previous Symposium on the fission process.

Among these, two are most characteristic in demonstrating that some of the essential qualitative features cannot be explained by any classical-model-type theory, such as the liquid-drop model (LDM). They are

(1) The channel structure of the passage over the fission barrier which was described by A. Bohr [1] as due to the specific structure of the intrinsic nucleonic states in the colder deformed nucleus near the fission barrier (see Fig.1). At lower energies, the channel effects were observed in the fission cross-sections of many nuclei as a step-like increase in the fission probability with increasing energy and in the angular distributions of the fission fragments, which exhibit drastic changes when new channels open.

(2) Another important discovery is related to the distribution of neutrons emitted from fission fragments. Examples of such a distribution are shown in Ref. [2]. The strange saw-tooth distribution was explained as due to the fact that the intrinsic structure of the two fragments having comparable masses may still be rather different. The minimal value of ν was obtained for fragments with $A \approx 130$, which was immediately related to the presence of a doubly magic shell $Z = 50$, $N = 82$. Such a fragment is "born" with an almost spherical shape. However, the complementary fragment with a relatively close mass is strongly distorted and therefore has a larger excitation energy and emits more neutrons.

Other deviations from the predictions of the classical model were not so drastic but no less important. For example, it was observed that the measured fission barriers in heavy nuclei do not decrease as fast as the LDM predicts. In fact, they remain rather constant, equal to 5-7 MeV.

---

* On leave from the I.V. Kurchatov Institute for Atomic Energy, Moscow, USSR.
† On leave from the University of Basel, Switzerland.

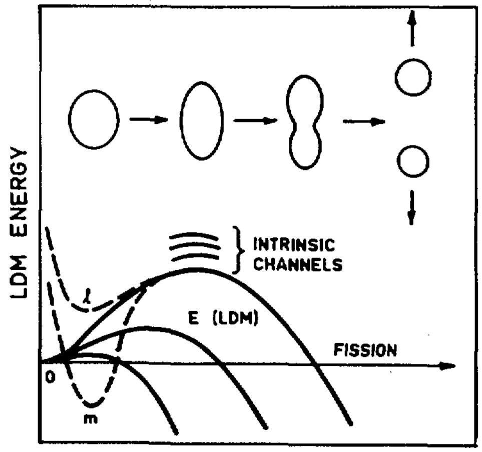

FIG.1. Traditional representation of the nuclear deformation energy in fission. Dotted lines ℓ and m correspond to two different corrections suggested for the deformed nuclei.

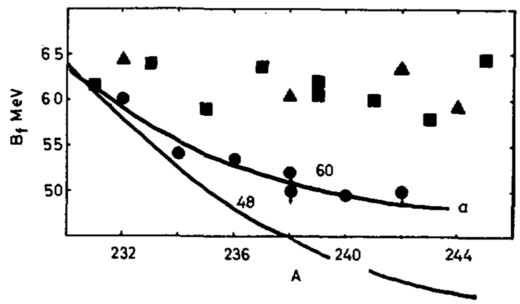

FIG.2. Fission barriers obtained from the measured fission cross-sections [3]. The two lines correspond to the LDM fit with $(Z^2/A)_{crit}$ = 48 and 60.

Some of the measured fission barriers are shown in Fig.2. In this region of nuclei, the traditional LDM theory predicts a sharp decrease of the fission barriers as given approximately by the cubic law

$$E_f = \text{const.}\ (1 - x)^3$$

where

$$x = (Z^2/A)/(Z^2/A)_{crit}$$

As is seen there, the observed dependence of E_f on A can be explained only with a very high value of the parameter $(Z^2/A)_{crit}$ equal to 55-60, which does not agree with the fit of the LDM to the nuclear masses. (Sometimes, the directly measured values for the barrier heights are presented together with values extracted from the spontaneous fission lifetimes. This feature is not so clearly seen in that case.)

This deviation from the LDM is very important because of its obvious relationship with the problem of stability of the very heavy elements. It shows that the LDM cannot be adequate in describing the stability of the very heavy nuclei.

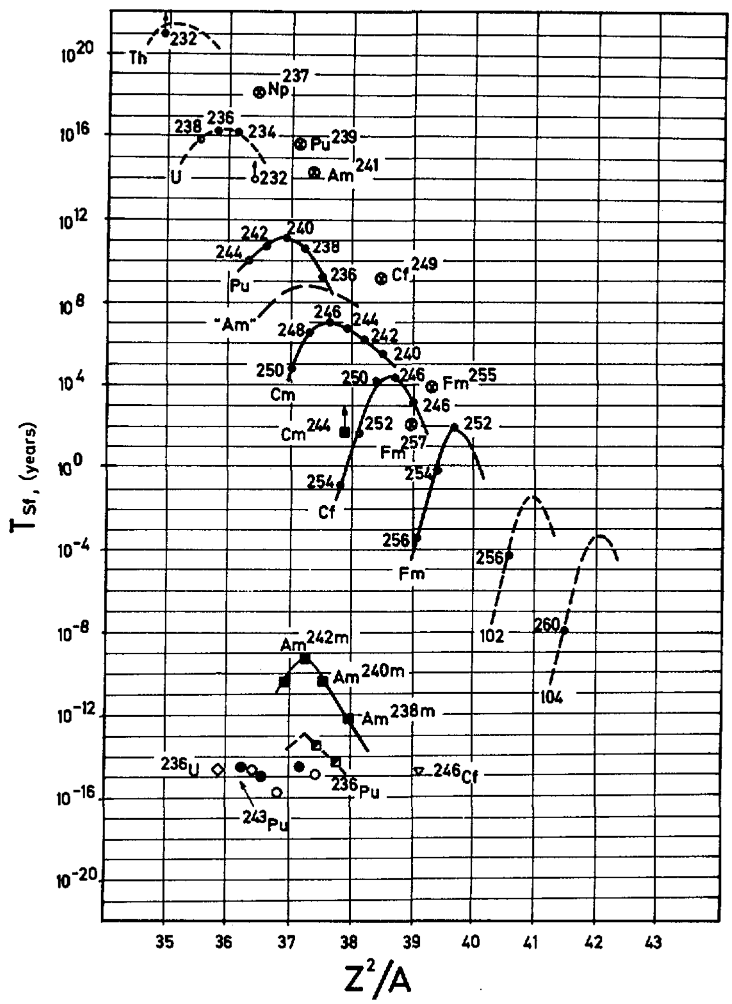

FIG.3. Spontaneous fission lifetimes. Recently measured lifetimes for the spontaneous fission isomers are also shown (from Ref.[15]).

Recently, new discoveries have been made, which are in direct conflict not only with the common understanding of the process, but seem to contradict also more general ideas in nuclear physics.

In 1960-63, in the Heavy-Ion Laboratory in Dubna, in the course of careful studies of all kinds of activities which might be related to new heavy elements, a spontaneous fission activity was observed with a period of 14 ms. This activity was found to belong to ^{242}Am whose ground

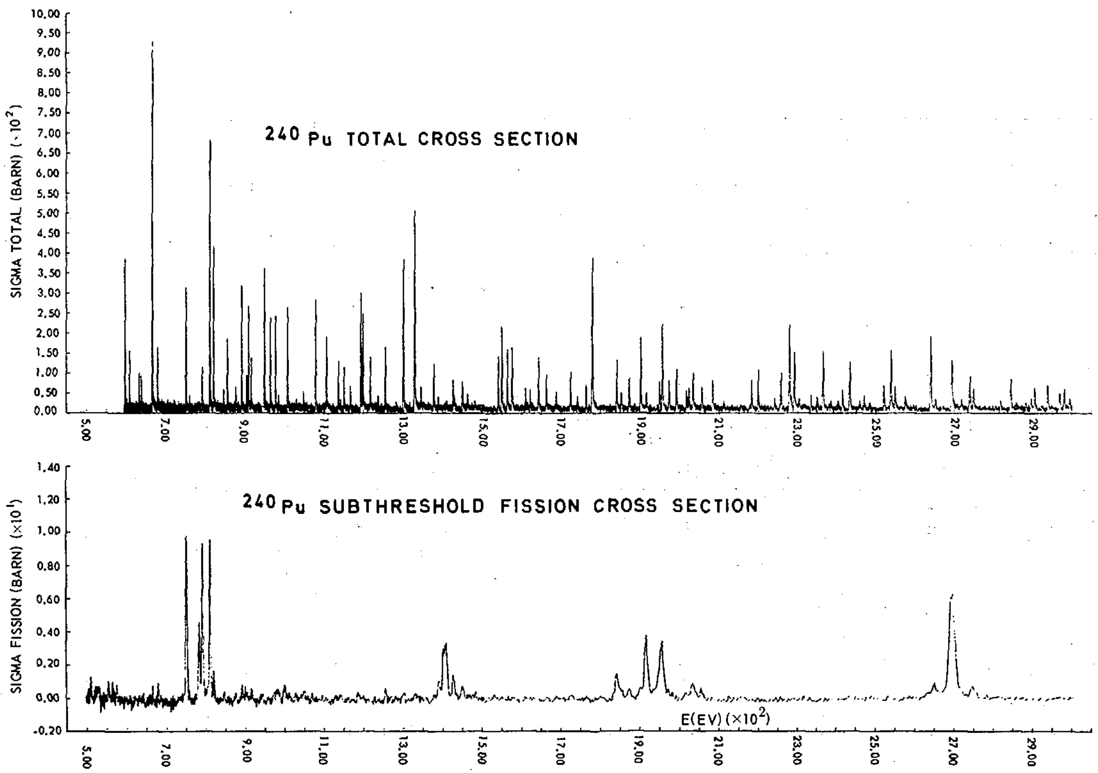

FIG.4. The fission cross-section of ^{240}Pu is compared with the total cross-section to demonstrate grouping of the fission resonances.

state has a spontaneous fission lifetime of the order of 10^{10} years. It seemed impossible to understand how an excited state with a spontaneous fission lifetime 10^{19} times shorter than the ground-state spontaneous fission lifetime resists α-deexcitation for 14 ms [4]. In addition, it soon became clear that the isomeric state does not have a large spin. Since then, many new spontaneous fission isomers have been found (see, e.g. Ref.[5]). Some of them are shown in Fig.3.

Another strange phenomenon was observed in fission induced by resonance neutrons in ^{237}Np [6] and in ^{240}Pu [7] (see Fig.4). The fission widths (among the resonances of the compound nucleus) were found to be abnormally large for some approximately equally spaced groups of resonances and extremely small between them, instead of being randomly distributed, as expected. This phenomenon, which is known as an intermediate structure effect, was also found in other nuclei. These important new features are discussed in many papers submitted to this Symposium.

We shall turn now our attention to some of the shortcomings of the traditional theory and some more recent developments of it. Qualitatively, deviations from the classical theory were in one way or the other always attributed to the so-called single-particle effects, or to a shell structure in the finite-size nuclei, but opinions differed as to what exactly those effects should be. Attempts to extend the existing microscopic theories to large deformations which are important for fission have failed, since they could not reproduce even qualitatively the fission barriers.

Phenomenological corrections to the LDM were scarcely of great help either. Anyway, in this way one could never obtain more than was built in before. This was especially clearly demonstrated when attempts were made to account for such a well-established feature as non-sphericity of certain heavy nuclei in their ground state. One can find some papers in which less stability is predicted for deformed nuclei, while in others more stability was claimed, as is shown by the dotted lines in Fig.1. There was much better agreement in the predictions for larger deformations. It was simply assumed that all these effects should disappear there and pure LDM should be applied as is shown in Fig.1.

The need for a unified theory which could give balanced roles to the LDM and the shell model was quite evident.

2. THE LIQUID-DROP MODEL AND THE SHELL CORRECTIONS

Before outlining one way of doing this, we must clarify some basic definitions related both to the LDM and to the shell model. Concerning the LDM, we can regard it simply as a phenomenological classical description of the average static properties of nuclear matter based on the assumption of low compressibility and the existence of a relatively thin surface. In it, a few parameters are introduced in a relatively simple way and their values are determined from the best fit to the nuclear masses, essentially. This model gives a reasonable phenomenological description of the average properties of the fission process and nuclear masses but ignores fluctuation effects due to shells.

From this definition it also follows that the LDM is characterized by smooth terms.

With only a few free parameters introduced in the model, all having a simple physical meaning and a reasonable magnitude, the liquid drop model was quite successful, as can be seen, for example, from Fig.5, where the LDM is compared with empirical masses of nuclei. Still, some significant deviations can be seen there, which are mainly attributed to the shell structure.

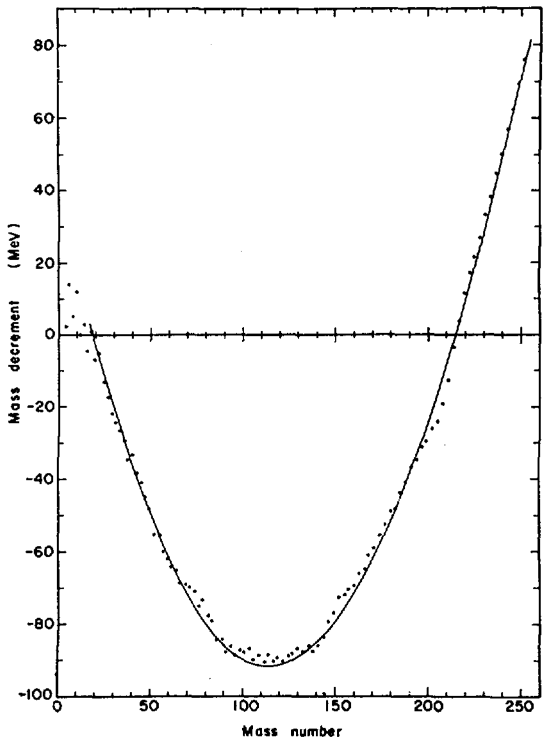

FIG.5. Measured masses of the nuclei are compared with the best fit of the LDM (from Ref. [8]).

The shells are usually thought of as related to the degeneracy of the single-particle states, mainly due to sphericity of the nuclear shape. However, this is not true. Instead, the shell may be regarded more generally as a large-scale non-uniformity in the distribution of the single-particle states. Grouping of this kind may always be expected in the finite-size nuclei.

This "soft" definition of shells is very important, because from it it immediately follows that

1. Shells are characteristic not only of the spherically symmetric case, but may be expected for any type of the average field and shape of the nucleus. In fact, several shells may be expected in the same

nucleus at different deformations. The presence of shells is a rather common phenomenon. Conversely, the absence of shells must be considered to be an exception.

2. The relation to the LDM also follows from this definition. Indeed, the LDM may be understood as a phenomenological average related to smoothed distributions of the nucleons. One can analyse the non-uniformities which appear in single-particle models and relate them to some appropriately chosen average, which may be thought of as represented by the LDM. One can evaluate the related energy difference and obtain the required shell correction to the LDM average.

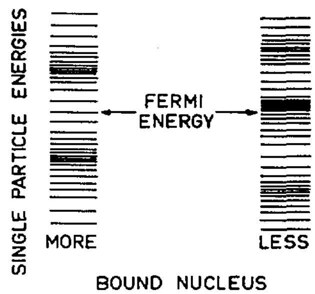

FIG.6. Effect of the local level density on the binding energy of the nucleus.

The shell correction to the energy is closely connected to the fluctuations of the density of the single-particle states near the Fermi energy. The nucleus is more bound when there is a shell (i.e. a thinning-out) near the Fermi energy because the nucleons occupy the lower states in this case. Conversely, an increased density leads to a reduced binding, as is illustrated in Fig.6.

Calculations show that the energy fluctuations related to these density fluctuations are of the order of 5-10 MeV, which is all-decisive for the stability of nuclei and the fission problem. This leads us to the important conclusion that the presence of shells at different deformations in deformed nuclei as well as in spherical nuclei is most important for the stability of particular nuclear shapes. It may be said that the ground-state equilibrium deformations of nuclei, spherical and not, are those for which a shell near the Fermi energy is present.

When a nucleus is deformed, as in fission, it should be noted that a thinning-out of the single-particle levels alternates with a compression, and this leads to a modulation of the smooth LDM deformation energy of the nucleus.

The reason for this is easily understood by considering a schematic distribution of single-particle states, as shown in Fig.7.

Depending both on the number of nucleons and the shape of the nucleus, the shells in real heavy nuclei form a rather regular structure resembling that shown in Fig.7. It is characterized by two "periods", equal, respectively, to $A^{2/3}$ and $A^{-1/3}$, and this feature is quite independent of the specific properties of the average nuclear field.

As it seems now, the so-called magic properties of nuclei should be characterized not only by the magic numbers of nucleons but also by some specific deformations. In this way, there are spherical magic nuclei with Z = 50, 82, 114-120 and N = 50, 82, 126, 184; magic nuclei with shells at the deformation 0.2-0.3 (Z, N = 60-64, 100, N = 150-152). There are essential shells also at larger deformations, such as the proton shells Z = 86-88 for an ellipsoidal-shape nucleus with the ratio of the two axes d $\approx$ 1.8, Z $\approx$ 110 at d $\approx$ 2.0, Z = 116-118 at d $\approx$ 1.45. The neutron shells at large deformations can also be found for N = 116-118 at d = 1.5-2.0, N = 146-148 at d = 2.0-2.4, N = 170-174 at d = 1.5.

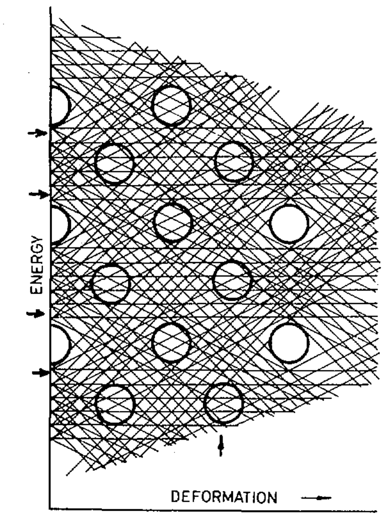

FIG. 7. Qualitative picture of the distribution of single-particle states in the deformed nucleus. The low density regions (shells) are shown by circles. Arrows show the places where transitions between sphericity and non-sphericity occur (from Ref. [10]).

These "magic numbers" are obtained in calculations with a realistic deformed Saxon-Woods potential well. Close results are obtained with other reasonable models for the potential. It should be remembered that the "shells" are, in fact, relatively broad regions centred at these magic numbers of nucleons and deformations. The shells at the deformation d = 1.2-1.3 are responsible for the ground-state deformations of all nuclei in the rare-earth and actinide regions.

The possible presence of shells in more strongly deformed heavy nuclei may have far-reaching consequences for fission; this will be discussed below.

The qualitative arguments find strong support from actual calculations of the nuclear deformations and the shell corrections to the ground-state masses of nuclei.

The location of shells in the potential well is a function of both the single-particle energy (E) and the deformation (β). It is convenient to introduce a quantity

$$\delta g(E,\beta) = g_{shell}\ (E,\beta) - \tilde{g}(E,\beta), \tag{1}$$

where g_{shell} is a local density of the single-particle states, which is obtained by averaging over an energy interval of the order of 1-2 MeV, and $\tilde{g}$ is the uniform (smeared) background density distribution. The quantity (1) describes deviations of the level density from its average value at the same energy. In the shell regions, $\delta g < 0$.

In a reasonable approximation, the shell corrections for the LDM deformation energy of the nucleus may be related to the level-density fluctuation by the following expression:

$$\delta M\ (N,\beta) = \int_{-\infty}^{\lambda} (E - \lambda)\, \delta g\, (E,\beta)\, dE \qquad (2)$$

where λ is the Fermi energy.

Alternatively, the shell correction can be defined as a difference between the total sum of the single-particle energies and a sum of "uniform" single-particle energies, which is defined by the smoothed distribution $\tilde{g}$

$$\delta M = 2 \sum_{(E_j < \lambda)} E_j\ (\beta) - 2 \int_{-\infty}^{\lambda} E\tilde{g}(E)dE \qquad (3)$$

This shell correction is closely related to the deviation of the real spatial distribution of the nucleons $\rho(r)$ from a Saxon-Woods type average $\tilde{\rho}(r)$, such as assumed in the classical phenomenological models. It can be shown [10] that Eqs (2) and (3) are correct with an accuracy up to $(\delta\rho)$, where

$$\delta\rho = \rho(\vec{r}) - \tilde{\rho}(\vec{r}) \qquad (4)$$

Thus, it is a reasonable approximation even in strongly distorted nuclei.

The total mass of the nucleons is represented as

$$M = \tilde{M} + \delta M + P \qquad (5)$$

where $\tilde{M}$ is the LDM part. In Eq.(5), the pairing energy P is added and the sum of the proton and neutron terms is taken. (More detailed definitions and equations may be found elsewhere [10].) Considered as a function of the deformation, this gives us the potential energy of the deformed nucleus, which is important for fission. The equilibrium deformations are found by minimizing Eq.(5) with respect to parameters which describe the shape of the nucleus and the average field.

With the method of energy-shell correction, the single-particle energy correction part δM and the pairing energy P are evaluated for any given single-particle model, and it was shown that the results, even the quantitative ones, are rather insensitive to the details of the single-particle model and are generally in agreement with the experiment (see, e.g. Ref. [10]). Different single-particle models, when used with the shell correction method, give quite similar results: in the deformation energy, for example, the difference usually does not exceed one or two MeV. This is due to the fact that with this method one extracts only essential gross-structure effects in the distribution of the single-particle energies and they appear as a common feature of all the independent-particle models.

The stability of the results obtained with the shell correction method, together with the possibility of a transparent physical interpretation, seem to be an essential advantage of this approach, important for the reliability of the theoretical predictions for larger deformations and new regions of nuclei.

Detailed calculations of the shell corrections to the nuclear masses were done in Ref. [10] and, more recently, by Seeger and Perisho [11], and with an improved Nilsson model by Nilsson et al. [12]. It was observed by these authors that even a rather fine detail in the empirical mass systematics could be reproduced.

However, one finds also that a noticeable, though not very large, systematic discrepancy remains. Further improvements of the theory are necessary, in which zero-point vibration energies and a better treatment of the residual interactions, especially in spherical nuclei, are included in addition to the refinements of the average field.

Qualitatively, the calculations prove that the effects of the shells in the energy is essentially determined by the local density of the single-particle states near the Fermi energy, averaged over an energy interval of the order of 1-3 MeV. The most essential part comes from the single-particle energy term (3). Other factors including the pairing are relatively less important, because for them much larger energy intervals and therefore much more smoothed distributions are involved.

Examples of the calculated energy shell corrections are shown in Fig.8. When they are compared with the contour maps of the level-density fluctuation δg near the Fermi energy, a remarkable resemblance appears demonstrating the simple correlation of these two quantities mentioned above.

Minima in the contour map in Fig.8 correspond to shell regions. It is seen that for a given number of nucleons there are usually a number of minima in the deformation energy, which may give rise to different quasi-equilibrium shapes of the nucleus.

3. THE FISSION BARRIERS

The shell effects are important for the fission barriers. In the so-called deformed nuclei, the first shell appears at smaller deformations (β = 0.2-0.3). This shell gives rise to an increased stability for these nuclei in their deformed ground state; in particular, it enhances their stability against fission. Thus, in plutonium or californium, the fission barriers are increased by approximately 3 MeV due to the presence of the neutron shell $N \approx 150$ in the ground state, as illustrated in Fig.9. This would correspond to the curve m in Fig.1 (compare with Ref. [13]). It makes about one half of the measured fission barriers in these nuclei. (In the doubly magic spherical ^{208}Pb, the shells also provide about one half of the observed 25 MeV barrier [8].) This is, however, not the only effect produced by the shells in the fission barriers. Because of the compression of the single-particle states at a somewhat larger deformation, the deformation energy there is <u>increased</u> by a few MeV above the LDM average which, together with the ground-state correction, makes a 5 to 7 MeV barrier, preventing the nucleus from fission.

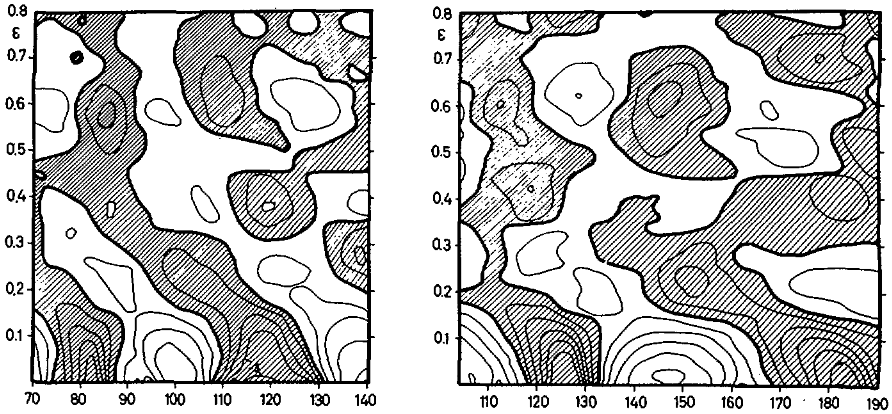

FIG. 8. Contour diagrams of the proton (left) and neutron energy shell corrections plotted as functions of the nucleon numbers and the ellipsoidal deformation parameter ϵ. The ratio of axis is $d = (1 + \frac{1}{3}\epsilon)/(1 - \frac{2}{3}\epsilon)$. A Saxon-Woods model was used in these calculations for Z = 92, A = 235, recommended for the region of the actinide nuclei. The increment between contour lines is 1 MeV. Regions of negative shell corrections ("the shells") where $\delta u + \delta p < 0$ are shaded. (From Ref.[9]).

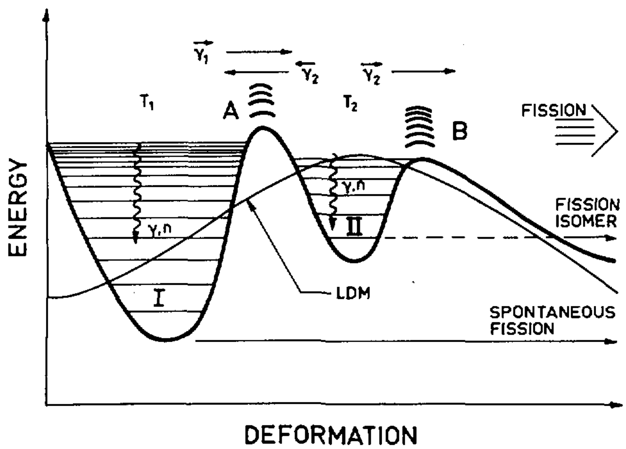

FIG. 9. Two-humped barrier in the deformation energy of a heavy nucleus. Transitions between the two families of stationary states are indicated.

As a result, the fission barriers in this region of nuclei are somewhat larger than predicted by the LDM and are less sensitive to the parameters of the LDM. This seems to be in at least qualitative agreement with the experimental evidence, as shown in Fig.2. It should be mentioned that, at the present time, there is a tendency to revise the existing experimental data on the value of E_f in many nuclei. Earlier identifications of the fission barriers have often been made on the basis of the presence of some anomaly in the fission cross-section, presumably related to the lowest A. Bohr channel at the saddle point. Because of the possible presence of the vibration-type resonance structure related to the second well state, this interpretation is called in question now, in particular in the case of the (d,pf)-reaction [14]. The true fission barriers should then be somewhat larger than in Fig.2 and still less sensitive to the value of the $(Z^2/A)_{crit}$, which would only increase the discrepancy.

In the theory, the fission barriers are determined by the relative heights of the extrema of the deformation energy. Of the two barriers usually present in the heavy nuclei, the higher one should be taken as the fission barrier although, at lower excitations, anomalies should be present near the energy corresponding to the top of the lower barrier. It is expected that the second barrier (B in Fig.9) is higher in lighter nuclei as a result of the increased LDM deformation energy, and the second minimum should be relatively shallow in the nuclei near ^{230}Th. However, in practical calculations, it was found that both the Nilsson model and the common Saxon-Woods model, fitted to reproducing the position of a few single-particle states near the ground-state Fermi energy, have the feature of relatively too strong effects at large deformations near the second minimum and maximum of the deformation energy. This results usually in too high second barriers, which seems to contradict the available information about the relative heights of the barriers A and B, the position of the vibration resonances, etc. More work must be done before any of these models can be used with sufficient confidence.

4. THE INTERMEDIATE STATE IN FISSION

A second shell minimum of the deformation energy in the heavy nuclei appears at a deformation which is approximately twice that of the ground state. This is easily understood from the qualitative model in Fig.7 and seen in the contour map of Fig.8. In the medium weight nuclei, the second shell is also present, but this does not necessarily lead to the appearance of a minimum in the total deformation energy, because there the effective surface energy increases very steeply with deformation.

The situation is different in heavy nuclei. There, the surface tension forces are largely compensated by the Coulomb repulsion and the second shell produces a significant minimum in the deformation energy. In some cases, the nucleus can be captured in the second well and stay there for a relatively long time. This will influence the fission process in several important ways[1]. The situation is illustrated qualitatively in Fig.9. Here, the heavy line represents the deformation energy with the shell corrections included, and the thin line corresponds to the LDM.

If the two wells are deep enough, we have two distinct equilibrium states in the same nucleus at different deformations. At higher excitations, some aspects of fission may be described in simple terms of transitions between the stationary states of the two wells and within each of them.

Typical transitions are shown in Fig.9. There, T_1 and T_2 are the temperatures in either of the two wells which characterize the density of intrinsic states at a given total excitation energy. In addition to usual

[1] A more detailed discussion can be found in Ref.[15].

γ-transition and neutron emission which presumably take place within each well, non-radiative transitions between the wells are also possible.

The dynamics of these transitions is described by a system of simple kinetic equations

$$\frac{dn_1}{d\tau} = -\gamma_1^{tot}\ n_1 + \overleftarrow{\gamma}_2\, n_2$$

$$\frac{dn_2}{d\tau} = \overrightarrow{\gamma}_1\, n_1 - \gamma_2^{tot}\ n_2 \qquad (4)$$

where $n_1(\tau)$ and $n_2\,(\tau)$ are the populations of the two wells which depend on the time τ. The probability of various kinds of decay of the compound nucleus may be found from these equations.

The initial conditions depend on the specific type of reaction in which the compound nucleus is produced. For example, for the neutron capture case,

$$n_1\ (\tau=0) = 1$$

$$n_2\ (\tau=0) = 0$$

Another condition is used when the compound nucleus is formed in the course of the de-excitations of a highly excited nucleus.

Some transitions in the second well lead to the occupation of the lowest states there. In this case, the nucleus stays in the second well for a very long time, because the probability of escape is greatly reduced by the presence of the potential barrier separating the two wells. A large mass, of the same order of magnitude as the total mass of the nucleus, is involved here. Therefore, the probability of γ-transitions to the ground state is reduced to about the same order of magnitude as the probability of fission from the second well. Thus, the existence of the fission isomers is explained.

The γ-transition for the second well to the ground state in the first well should be extremely small if the width γ_2^{tot} is small compared to the spacing D_I of the levels in the first well. In this case

$$\Gamma_\gamma^{(g.st.)} \approx \gamma_{s\cdot p}\, P_A \qquad \text{(small dissipation)} \qquad (5)$$

where $\gamma_{s\cdot p}$ is the usual average value for the γ-width and P_A is the penetration factor for the first barrier. In the case of a strong overlap $D_I < \gamma_2^{tot}$ the ground-state γ-width is much larger

$$\Gamma_\gamma^{(g.st.)} \approx \hbar\omega\ P_A \qquad \text{(strong dissipation)} \qquad (6)$$

where ω is of the order of the oscillation frequency in the second well.

The theory outlined above predicts that the second well is most pronounced in the deformed nuclei with N = 144 - 148, Z = 86 - 90 and there it is two or three MeV higher than the ground-state well. This prediction agrees with the experimental data. Indeed, the observed isomers lie close to this region [5]. The energy of the isomeric state was first determined from the excitation functions of the fission isomers produced in charged-particle reactions and later by other methods. They all give values which agree with such an interpretation.

5. INTERMEDIATE STATE RESONANCES

The presence of the intermediate stationary states in fissioning nuclei strongly modifies the probability of fission. At lower excitations, the intrinsic excitation energy in the second well may be relatively low, of the order of one or two MeV. (This is so because, in some nuclei, the second well is 3-4 MeV above the first and this amount of energy is subtracted from the total excitation energy.) Here, almost pure collective vibrational states may exist. Considered as a function of the energy in the fission degree of freedom (ϵ), the penetration function for a two-humped barrier shown in Fig.9 has resonance maxima whenever this energy coincides with the state in the second well, see Fig.11. Exact numerical solutions are described by Nix [16], by Bang and Wong [17], and in Ref. [14]. A simple approximate solution of the problem was obtained recently by Gai et al. [18] who discuss also some applications to the analysis of the fission resonance distribution, including compound-type resonances.

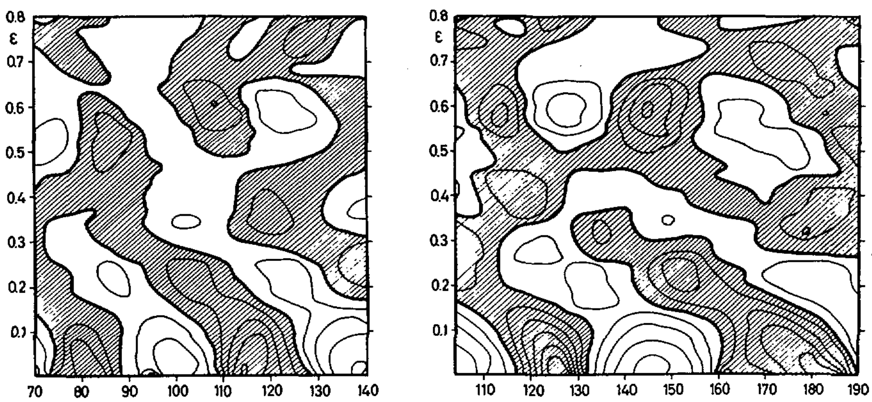

FIG.10. The same as in Fig.8, evaluated for the region of the super-heavy elements around Z = 114, N = 184. In these calculations, the surface thickness of the potential was constant (from Ref. [9]).

The first experimental case where a vibration resonance was identified was the fission of ^{230}Th by 0.3-2 MeV neutrons [19], see Fig.12. Since then, more cases have been studied, in particular in the (d,pf) reaction, where states of even compound nuclei may be excited below the neutron binding energy and the maxima cannot be confused with those which may arise because of the competition with the (n,n')-reaction. Examples of the fission probability function obtained recently in the (d,pf) reaction are presented and discussed in detail in Ref. [14]. Note that, in the previous, less accurate measurements, the maxima at lower excitation energies were understood as plateaux related to A. Bohr's channels at the saddle. It is important that, in the traditional model, it is not possible to explain why the fission probability should drop when the excitation energy of the nucleus increases. Therefore, one is dealing here with a feature of principal importance.

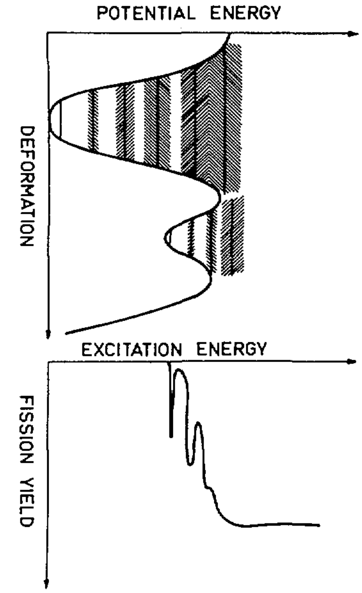

FIG. 11. Qualitative representation of the penetration function for the case of a double-humped barrier with a vibration state in the second well (from Refs [14, 15]).

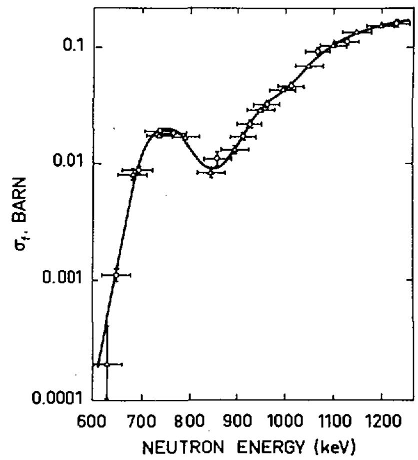

FIG. 12. A case of a possible vibration resonance in the fission cross-section of ^{230}Th.

Another strong confirmation of the presence of a stationary intermediate state in fission comes from an unusual distribution of fission resonances, such as shown in Fig.4. This unexpected behaviour of the fission width is now well understood. According to E. Lynn, fission takes place only when the energy of the compound nucleus state coincides with one of the states in the second well. The intrinsic excitation in the second well is by a few MeV less than that in the first well. Therefore, the compound level spacing is increased 100-1000 times and the widely spaced groups observed in ^{240}Pu and other nuclei are interpreted as corresponding to these states. The observed width of these groups is the same as the internal width γ_2^{tot} of the second-well states, which includes the widths of the non-radiative transition $\overleftrightarrow{\gamma}_2$.

The distance D_2 between the groups of fission resonances varies from one nucleus to another, depending on the relative height of the second well. Thus, this important quantity could be estimated directly from the ratio of D_2 to the average distance D_1 between the states in the first well and, obtained in this way, it agrees with the estimates available from spontaneous fission isomers data. At excitations close to the top of the barrier, the groups overlap as a result of increasing γ_2^{tot} and less distinct structure is observed. Here, more sophisticated statistical methods should be used to prove the presence of intermediate structure.

This compound-nucleus type of resonance structure should be strongly dependent on the depth of the second potential well. In lighter nuclei, such as thorium, where the second well is shallower, this structure should turn into vibration resonances similar to those considered above. In some transitional cases, this vibration resonance structure would appear as a broad envelope over many intrinsic states in the second well, in just the same way as optical model single-particle resonances do in the case of scattering of neutrons by complex nuclei. It seems interesting to investigate this problem more thoroughly.

6. ANOMALIES IN THE ANGULAR ANISOTROPY

Important changes in A. Bohr's model for the channel effect in fission anisotropy will result from the fact that the nucleus stays long enough in the second well to "forget" the specific properties of the channel states, which it had when passing over the first barrier A in Fig.9. In particular, this is true for the value of the projection of the total spin on the nuclear axes, which is important for the angular anisotropy of fission. (For this, the lifetime of the second-well state must be rather long because only the weak Coriolis forces can change this quantity.)

In such a case, the observed channel structure should correspond to the second barrier B. If this barrier is higher than the first (A), the familiar picture of channel structure in near-barrier fission should nevertheless be valid. In this case, it is the second barrier that corresponds to the effective energy threshold. However, if the barrier B happens to be one or two MeV lower than the first, no pronounced structure in the angular distribution is observed, because many channels with

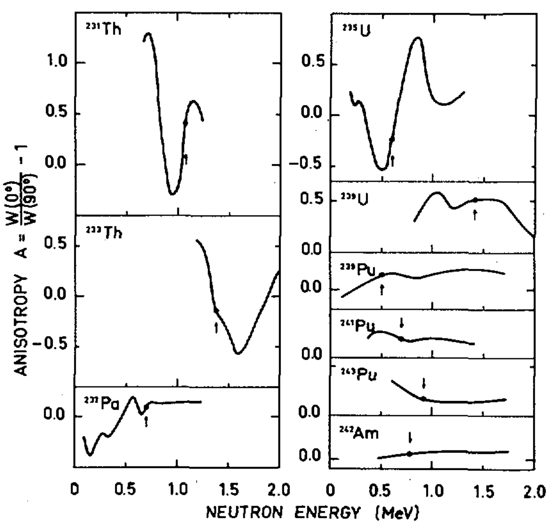

FIG.13. Anisotropies of the fission-fragment angular distributions for fission induced by MeV neutrons. The "structure" in the anisotropy disappears in heavier nuclei (from Ref. [15]).

different spin-projection quantum numbers are available in contrast to the traditional picture. This may be expected for some heavy nuclei and the experiments show that it is really true. No channel structure in the angular distribution is observed in some under-the-barrier fissions, which normally is characteristic of a few MeV excitation. This is illustrated in Fig.13, where some of the observed fission fragment anisotropies are shown as a function of the excitation energy at the saddle. It is clearly seen that a large anisotropy in near-threshold fission is definitely not a general feature. This is a significant deviation from the traditional picture. A more detailed discussion and references can be found in Refs [15, 20].

The ideas about a double-humped barrier seem to be rather helpful also in treating many other more ordinary data. Information about the relative heights of barriers A and B, the depth of the potential well, etc. has recently been obtained from neutron and photofission experiments performed in Obninsk, Dubna and Moscow and in Bucharest. These studies shed new light on this interesting problem.

7. STABILITY OF THE SUPER-HEAVY ELEMENTS

There is another problem which is widely discussed at present and is closely related to fission and the shell structure. This is the problem of stability of the super-heavy elements. It seems certain now that the stable nuclei may exist beyond the limit $Z^2/A = 45$ or 48 provided by the liquid-drop model. If even such familiar nuclei as uranium or plutonium are stable, much owing to the presence of shells, then it is less unexpected that some still heavier nuclei may exist which should be stable only due to the shells.

In Fig.10, two contour maps of the proton and neutron shell corrections to the deformation energy are presented. They were evaluated in Ref. [9] for the region of the super-heavy nuclei with a commonly used Saxon-Woods potential well for the IPM, with the skin thickness kept constant along the nuclear surface. The magnitude of the shell part of the barrier in these nuclei as well as the extent of the region where the long-lived nuclei may occur are clearly seen (somewhat different results are predicted for modified Saxon-Woods potentials [24].)

Though the shell stability cannot completely prevent the disruptive effect of the Coulomb repulsion, it can move the upper limit of stability to higher values of Z and A. Some years ago, W. Swiatecki has predicted an island of stability around the heaviest doubly-magic nucleus. The most likely candidates at present are nuclei with $Z = 114 - 120$ and $N = 184$. (These numbers characterize the centres of the corresponding shell regions.) The Nilsson model did not seem to be reliable for extrapolation to the new regions of nuclei; the first calculations of the fission barriers in these super-heavy nuclei were done with an approximate model of the Saxon-Woods type [21, 22]. These calculations have shown that, despite the effect of a very strong Coulomb field in these nuclei, the fission barriers may be as high as 5 - 10 MeV. Similar numbers were obtained later in the shell-correction calculations with an improved Nilsson model, see, e.g. Refs [10, 22, 23] and with the deformed well Saxon-Woods potential [9, 27]. Some other models were considered in Ref. [24]. Some of these nuclei should be close to the β-stability line and are relatively stable to α-decay [24, 25]. In Ref. [23] some estimates for the spontaneous fission lifetimes of such super-heavy nuclei are presented. It was found there that the partial fission lifetimes may be even as long as millions of years. These estimates of the lifetimes should probably not be taken too literally, but if these are true, then such nuclides which are at the moment only hypothetical may become very important in the future. This problem attracts, of course, great interest, and numerous exciting studies are under way.

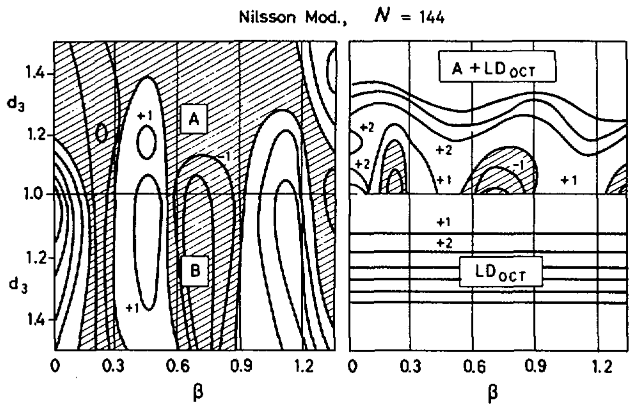

FIG. 14. Dependence of the shell effects in the deformation energy on the octupole deformation parameter d_3 equal to the ratio of the left and right semiaxes $d_3 = 1$, corresponds to pure ellipsoidal deformations. The diagram A is for the r^2Y_3 and B is for the r^3Y_3 octupole term. In the upper left diagram, the octupole LDM term normalized to ellipsoidal shape energy is added to the shell correction A. Evaluated for the N = 144 with the Nilsson model.

8. THEORIES FOR THE DEFORMATION ENERGY

In the last two or three years, many calculations of the nuclear deformation energies were performed. In many cases the shell-correction method was used, which seems to be the most reliable at present. In these calculations, different single-particle models were used and new types of deformation were considered in addition to the ellipsoidal ones. This was done mainly in order to check the stability of the second potential well against these deformations and to obtain better estimates of the fission barriers. For the Nilsson model, detailed consideration of the P_4 -type of deformations can be found in Ref. [23]. In Ref. [25], the stability of the second well against the non-axial γ-deformation was demonstrated.

The stability against asymmetric octupole type deformation for the case of the Nilsson model was recently considered by one of the authors (H.C.P.). One example of the results is shown in Fig.14. Two different radial dependencies in the octupole term, as r^2 and r^3, are compared there. It is seen that the minima are more stable against the octupole deformation when the shell correction is added to the LDM, while near the maxima the stiffness is less than in the LDM. This effect could be of interest for the problem of the asymmetry in nuclear fission. However, since there is such an appreciable difference between these two equally reasonable assumptions about the radial dependence of the field, no definite conclusions can be drawn until the problem is investigated more thoroughly.

This example illustrates a basic ambiguity and limitation of the Nilsson model. Originally introduced as a convenient and very successful compromise with the technical problem of solving the Schrödinger equation for a deformed field, this model is only vaguely related to even the most generally known properties of nuclear matter. Such phenomena as the existence of a relatively thin surface, the finite nucleon binding energies, etc. are not present in this model. This makes difficult, if not impossible, any definite extrapolation of this model to larger distortions, more complicated shapes or the unknown regions of nuclei.

The ambiguity should be less in the case of the Saxon-Woods type model, although the general picture of the shell distribution and the magnitude of the shell effects in the deformation energy is not expected to be very different.

Some time ago, effective methods of solving the Saxon-Woods problem for strongly deformed nuclei were developed. (One of them [27] was used in the evaluation of the single-particle levels which correspond to the shell correction map in Fig.8). This method was found very suitable for calculations of the shell effects in the strongly deformed nuclei. It was recently generalized in such a manner that it became possible to obtain a solution for any given shape of the nucleus including those with a pronounced neck and without the reflection symmetry for any reasonable type of the average field [28]. From this, the energy shell corrections are obtained for any given shape of the nucleus that might appear in the process of fission.

The analysis of the results has not been completed yet. In the calculations, a realistic Saxon-Woods type of the nuclei average field was usually assumed with the skin thickness constant along the surface. Shapes were chosen such as to make it possible to describe the formation of the neck, in addition to another degree of freedom corresponding to the elongation deformation. (Without the "neck" formation, the LDM energy would steeply increase for larger deformations.) The neck degree of freedom can be important in view of possible dynamic instabilities in this direction at large deformations. In the future, it is intended to take into account more degrees of freedom, including those which describe the asymmetry.

It was found that, for moderate deformations, all essential features of the shells are very much the same as obtained earlier with the other models. However, for the agreement with the existing information about the heights of the barrier, energy differences between the two wells, position of the vibration resonances in lighter nuclei, etc., additional refinements of the model are required. This work is under way now.

Examples of the calculated deformation energies are shown in Fig.15, which represents contour maps of the deformation energies analogous to Figs 8 and 10 but evaluated for a sequence of shapes along the so-called LDM valley. (Some of these shapes are shown there.)

At very large deformations, quite definite and strong shell effects are observed which in some cases produce noticeable instability against neck formation. The connection of these shells with the shells in the fragments is not clear as yet. A final decision can be made only if some asymmetry of deformation is included.

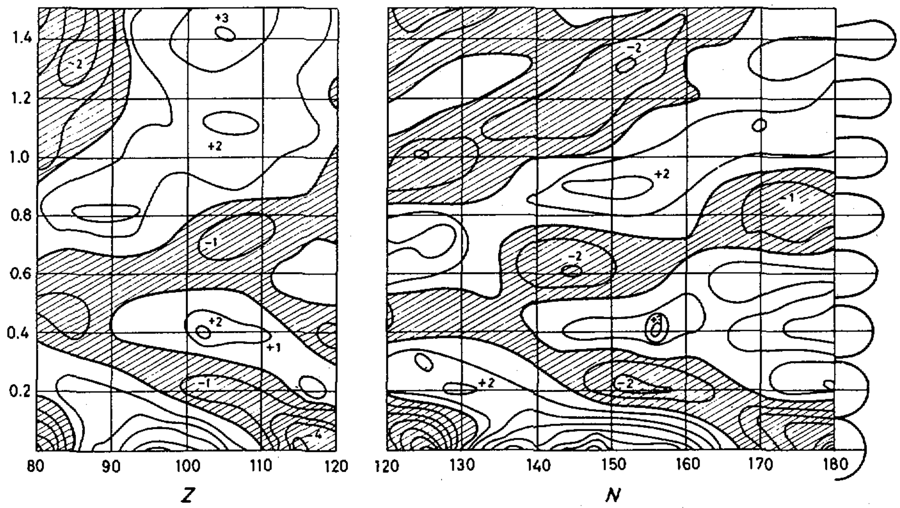

FIG. 15. The shell corrections to the deformation energy of the nucleus evaluated for a sequence of shapes approximately corresponding to the valley of the liquid-drop model. The contour lines are drawn with increments equal to 1 MeV. The shell regions ($\delta u + \delta p < 0$) are shaded. (From Ref.[30]).

9. THE DYNAMICS OF FISSION

The deformation energy alone does not determine the "trajectory" of the fissioning nucleus in the space of the degrees of freedom defining the state of the nucleus. Therefore, it gives no answer to the problem of distribution of the fragments (unless a stationary state exists just at the scission, as is the case in the pure LDM for the values of the parameter $x = 0.6 - 0.65$ or as it may also be due to the presence of a shell there). However, the dynamics of the non-stationary state of the nuclear matter is one of the very few problems almost completely untouched by the hectic development of nuclear theories.

In the case of mechanic (or quantum-mechanic) motion, the trajectory is determined by the competition between the forces defined as the derivatives of the deformation energy function and the related inertia parameters that characterize the response of the system to these forces. In the case of a strong friction, the latter are replaced by corresponding friction coefficients, and the equations of motion are completely different. Not much is known at present about the character of the collective motion in fission, and this important problem requires special attention.

The theory commonly used at present for the higher excitations (above the fission barrier) generally assumes strong dissipation. It is assumed that the fission kinetic energy is of the order of the nuclear temperature and is therefore much less than the total excitation energy.

This still does not help in finding the trajectory but some simple quantities can be found, such as the total fission probability or the partial populations of specific channels of the barrier that are of importance for the statistical theory of the fission fragment angular anisotropy. (In principle, the viscosity is essential even there but, as was found by Kramers in 1940 [29], there is a large region of the viscosity values where the simple Bohr-Wheeler formula can be used.) This kind of problems can be solved with simple static models which give only the extrema of the deformation energy.

At lower excitations and, in particular, in the theory of spontaneous fission, a purely mechanical type of motion is assumed. The trajectory problem is sometimes resolved simply by identifying the trajectory with the so-called steepest descent line, assuming some kind of slow motion. However, this model conflicts with the original assumption about the mechanic type of motion. In addition, in some qualitative discussions, equal inertia parameters are implicitly assumed for different degrees of freedom, for which there is no reason whatsoever. The steepest-descent method can be generalized to non-equal masses and to non-orthogonal co-ordinates, but the important intrinsic inconsistency remains since the "slow motion" can only be due to strong dissipation of the collective motion and, in this case, the relative dissipation coefficients rather than the inertia parameters are relevant, and there is no idea of how to evaluate the barrier penetrability if this is the case.

The collective degrees of freedom describing the shape of the nucleus are not immediately related to transfer of any definite pieces of the nuclear matter. Therefore, the related inertia parameters are defined only with the corresponding degrees of freedom and should normally be considered as co-ordinate-dependent. With reasonably defined deformation parameters, this should lead to a smooth dependence of the mass parameters on the deformations.

Although a separate discussion of these quantities has not much meaning, some recent calculations [20] have demonstrated that there is a quite definite shell structure effect also in the inertia parameters: they have the same oscillating behaviour as the deformation energy, reflecting essentially the level density fluctuations near the Fermi energy. In spite of the increased pairing, the quadrupole-type deformation mass parameter is approximately twice larger near the top of the shell barrier than at the minima of the deformation energy. For the spontaneous fission, the trajectory problem is of exceptional importance. In the case of the co-ordinate-dependent mass parameter, the lowest-action trajectory may even pass by the saddle point if more penetrability is gained there, where the mass parameter is lower.

This situation is not very likely to occur, but there is one interesting aspect of the problem, which may be important for the penetrability of the potential barriers at larger deformations such as the barrier B in Fig.9. Instead of further elongation, fission may take place simply by cutting the neck in the relatively elongated nucleus[2]. In the static model,

[2] In the LDM for some fixed large values of the distance ρ between the centres of the two halves of the nucleus not exceeding a certain critical value, there are two branches of the equilibrium shapes, one corresponding to continous shapes and another to separated fragments of proper shapes, and for some large values of $\rho < \rho_{crit}$, the latter have from 10 to 15 MeV lower energy. For $\rho > \rho_{crit}$, only the second type of equilibrium shapes exists. Thus, ρ_{crit} was considered as an LDM scission point [31].

this is prevented by some local stability or a potential barrier which separates the continuous shape from two oblate fragments with approximately the same distance between the centres of mass. However, this barrier may prove to be rather penetrable if the related effective mass parameter is small, as this is to be expected for a "neck" degree of freedom.

The presence of a shell in a strongly deformed nucleus with a pronounced neck, its stability or instability against different kinds of deformations can strongly affect the final stages of the fission process. There seems to be good qualitative reason for such a "third" shell in view of the presence of shells in the fragments just after the separation.

The presence of a shell in a strongly deformed nucleus with a pronounced neck, its stability or instability against different kinds of deformations can strongly affect the final stages of the fission process. There seems to be good qualitative reason for such a "third" shell in view of the presence of shells in the fragments just after the separation. A shell should develop already in the continuous nucleus before scission, and turn later into the fragment shells. In some cases, such a shell could stabilize the nucleus against further elongation (the "third well"). Fission would take place preferentially by decreasing the thickness of the neck with a relatively small distance between the centres of the two halves. This should be the case of instability against formation of shells in spherical-shape magic fragments. In other cases, the shells would enhance stronger deformations of fragments before scission. This is closely related to the touching-fragment shell model, suggested some years ago by Vandenbosch [32] (see also Ref. [33]), which was supposed to explain some "strange" data, such as the saw-tooth curve for ν and the kinetic energy distribution.

At large deformations, new types of motion arise, such as formation of the neck, its position along the main deformation axis, etc. Stability of the equilibrium shapes against all these should be investigated.

The essential multi-dimensionality of the fission process at large deformations imposes very hard conditions on the quality of the theoretical and numerical methods used to solve the problem. Technical difficulties increase too fast with the increasing number of degrees of freedom, and it is one of the most urgent problems how it is possible in the most direct way to describe important types of deformation with the smallest possible number of parameters. The Hollywood people have encountered the same problems some years ago when they decided that only three measures were sufficient to describe the shape of the body. The nucleus is probably a more complicated system. However, one may hope to manage with at least no larger number of parameters when a better qualitative understanding of the process is reached.

The new explorations in fission will certainly require more extensive theoretical studies. It is a great challenge to try to reach a still better understanding of the intrinsic structure effects in the fission process as well as in the nuclear masses. The fission process is a very good testing ground for many nuclear theories - a very hard but very useful one.

REFERENCES

[1] BOHR, A., Int. Conf. peaceful Uses atom. Energy (Proc. Conf. Geneva, 1955) 2, UN, New York (1955) 151.
[2] APALIN, V.F., GRIZYUK, Yu.N., KRUTIKOV, I.E., LEBEDEV, V.I., MIKAELYAN, L.A., in Physics and Chemistry in Fission (Proc. Symp. Salzburg, 1965) IAEA, Vienna (1965) 587.
[3] IGNATYUK, A.V., SMIRENKIN, G.N., Phys. Lett. 29B (1969) 159.
[4] POLIKANOV, S.M., DRUIN, V.A., KARNAUKHOV, V.A., MIKHEEV, V.L., PLEVE, A.A., SKOBELEV, N.K., SUBBOTIN, V.G., TERAKOPYAN, G.M., FOMICHEV, G.M., Soviet Phys. JETP 15 (1962) 1016;
PERELYGIN, V.P., ALMAZOVA, S.P., GVOZDEV, B.A., CHUBURKOV, Yu.T., Soviet Phys. JETP 15 (1962) 1022.
[5] LARK, N., PEDERSEN, J., SLETTEN, G., BJØRNHOLM, S., submitted to Nuclear Physics (1969).
[6] PAYA, D., BLONS, J., FUBINI, A., MICHAUDON, A., in Nuclear Structure (Proc. Int. Symp. Dubna, 1968), IAEA, Vienna (1968) 483 (short contribution).
[7] MIGNECO, E., THEOBALD, J.P., Nucl. Physics A112 (1968) 603.
[8] MYERS, W., SWIATECKI, W., Nucl. Physics 81 (1966) 1.
[9] PASHKEVICH, V.V., private communication (1968); JINR Report P4-4383 (Dubna, 1969).
[10] STRUTINSKY, V., Nucl. Physics A112 (1968) 1 and other references therein.
[11] SEEGER, P.A., PERISHO, R.C., Los Alamos Report LA 3751 USA (1967).
[12] NILSSON, S.G., THOMPSON, S.G., TSANG, G.F., Physics Lett. 28B (1969) 458.
[13] SWIATECKI, W., Phys. Rev. 104 (1956) 993.
[14] PEDERSEN, A., KUZMINOV, B.D., Physics Lett. 29B (1969) 176;
BACK, B.B., BONDORF, J.P., OTROSHENKO, G.A., PEDERSEN, J., RASMUSSEN, B., these Proceedings.
[15] STRUTINSKY, V., BJØRNHOLM, S., to be published in Nucl. Physics (1969); same as Ref. [6], p.431.
[16] NIX, R., Abstract in these Proceedings.
[17] BANG, J., WONG, C.Y., Abstract in these Proceedings.
[18] GAI, E.V., IGNATYUK, A.V., RABOTNOV, N., SMIRENKIN, G.N., Thesis, 19th Symposium on the Nuclear Structure and Spectroscopy, Erevan 2 (Leningrad, 1969) 79; submitted to Yad.Fiz. USSR 1 (1969); paper in these Proceedings.
[19] VOROTNIKOV, P. et al., Soviet nucl. Phys. 5 (1967) 210,
LYNN, E., in The theory of neutron resonance reactions, (Symp. Oxford, 1968) and in Nuclear Data for Reactors, IAEA, Vienna (1967).
[21] STRUTINSKY, V., MUZICHKA, Yu.A., in Heavy Ions (Proc. Int. Conf. Dubna, 1966) 2 (1966) 51.
[22] MUZICHKA, Yu.A., PASHKEVICH, V.V., STRUTINSKY, V.M., JINR Report PI-3733 (Dubna, 1968); Yad. Fiz. USSR (1969).
[23] NILSSON, S.G., TSANG, C.F., SOBICZEWSKI, A., SZYMANSKI, Z., WYCECH, S., GUSTAFSON, C., LAMM, I.-L., MÖLLER, P., On the Nuclear Structure and Stability of Heavy and Superheavy Elements, LRL Report (January, 1969).
[24] MUZICHKA, Yu.A., JINR Reports P7-4133, E7-4141, Dubna (1968); Phys. Lett. 28B (1969) 539.
[25] MUZICHKA, Yu.A., JINR Report P7-4435, Dubna (1969).
[26] PASHKEVICH, V.V., JINR Report E4-4384, Dubna (1969).
[27] PASHKEVICH, V.V., STRUTINSKY, V.M., Yad. Fiz. USSR 9 (1969) 56.
[28] DAMGAARD, J., PAULI, H.-C., PASHKEVICH, V.V., STRUTINSKY, V.M., submitted to Nucl. Physics (1969).
[29] KRAMERS, H.A., Physica VII (1940) 284.
[30] DAMGAARD, J., PAULI, H.-C., STRUTINSKY, V.M., WONG, C.Y., JENSEN, A., BRACK, M., these Proceedings.
[31] STRUTINSKY, V.M., LYASHTCHENKO, N.Ya., POPOV, N.A., Nucl. Physics 46 (1963) 639.
[32] VANDENBOSCH, R., Nucl. Physics 46 (1963) 129.
[33] IGNATYUK, A.V., Yad. Fiz. USSR 7 (1968) 1043.

DISCUSSION

J.J. GRIFFIN: Could you comment in greater detail on the difference between the calculations "A" and "B" of octupole effects in the Nilsson model, and on the reasons why you abandoned the Nilsson model in favour of the Woods-Saxon potential?

V.M. STRUTINSKY: In the Nilsson model two different radial dependences were used in the octupole term. As I have mentioned, the difference illustrates essentially the ambiguity of the definition of more complicated shapes in the Nilsson model. The ambiguity with the other parameter is even worse and cannot be resolved by fitting single-particle states near the ground states in certain nuclei. It is therefore better to use more "physical" models in this type of calculation.

Another reason is that a model which can satisfactorily explain the ground state deformations and give reasonable shell corrections should not be regarded as absolutely reliable in the case of extrapolations. These features are largely independent of the details of the single-particle model; on the other hand, different independent-particle models, all giving the same quality fit near the ground state, lead to somewhat different quantitative results at larger deformations or higher nucleon numbers. Results obtained with different models should, at any rate, be compared before any precise conclusions are drawn.

K. DIETRICH: In your presentation you indicated that there was a third minimum besides the ones corresponding to the ground state and to the usual isomeric state of the nucleus. This third minimum would correspond to a highly deformed shape beyond the saddle point with the two fragments already preformed. Would you agree that this shape, if it exists, could be approximately described by two touching fragments? If this is so, it may explain the relative success of very simple scission-point models — a question that aroused some discussion.

V.M. STRUTINSKY: The "third" shells can be somehow related to the fragment's shells although no exact correspondence is expected. We do believe that these shells can strongly influence the fission process at larger deformations, i.e. at the later stages. They may also stabilize some specific scission shapes against further elongation. However, these problems require further investigation.

E.R. HILF: I have three remarks relating to your talk, which we enjoyed so much. First, if I understand you correctly, your total energy E consists of two parts, the liquid-drop (LD) part, which you take from an experimental fit, and a shell correction term E_{shell}, which you extract from a shell model by summing up the single-particle levels and subtracting their Strutinsky average. The LD part you used does not however contain the whole smooth trend of E with regard to terms proportional to $A^{1/3}$, as is done, for example, in the droplet model of W.D. Myers. Theoretically, the LD part can be calculated directly from the shell model using the leptodermous approximation $A^{1/3} \gg 1$, as has been shown, for example, by S. Knaak et al. in Phys. Lett. 23 (1966) for surface tension. As long as you are interested in the shell fluctuations and not in quantitatively determining the (experimental) data where the smooth part also enters, e.g. threshold energies, this difference does not affect your results. But with regard to quantitative results, one would trust a shell correction term extracted from a shell-model potential only if the LD part is determined from the same model and gives the right results. According to our experience this is possible only for potentials which have any of the usual non-local parts — well known from scattering theory — and not for the local one which you used.

Second, I admit that the method of calculating the shell-correction term which you introduced has had great stimulating effects on both experimentalists and theoreticians especially with regard to double-hump barriers. But I have no confidence in the plot of potential energy versus deformation which you presented, for example in Fig. 9 of your paper, since the summing up of the single-particle energies only works in the case of equilibrium shapes. Furthermore, this ought to be done in a self-consistent way. Even if, in subtracting the experimentally determined LD term, one takes into account the main part of the "self-consistency correction", the difference between self-consistency and non-self-consistency enters into your shell correction term $E - E_{LD}$ with the same relative strength. Thus, calculating in a self-consistent way may lead to a shell correction term which differs considerably and quantitatively. I would consider that approach to be more reliable.

Third, you predicted a third minimum near the scission point for some nuclei and extend your model to non-equilibrium states of the nucleus (say, between saddle and scission). But this does not seem to me to be closely related to the physics of nuclei, for two reasons: (a) In the non-equilibrium states the nucleus has some excitation energy, it is "heated up". But then one cannot use the single-particle levels of a "cold" nucleus of the same shape, since the levels themselves, individually, are temperature-independent and this leads to a considerable change of the level density, too; (b) Summing up the single-particle energies as an approximation for the total energy breaks down as the nucleus gains excitation energy, since the interaction terms increase rapidly.

V.M. STRUTINSKY: I would like to reply to the three remarks made by Mr. Hilf. First, modifications of the liquid-drop part do not affect the shell correction. The liquid-drop model appears in the calculations after re-normalization has been performed and the shell correction evaluated. The "uniform energy" does not contain anything that cannot be thought to be contained in the liquid-drop model.

Second, the usual objections to the Mottelson-Nilsson summation procedure cannot be directly used against the shell-correction method, which is based on different arguments. The method may require some refinements and improvements. We would appreciate any specific arguments.

Third, the average-field approximation for the intrinsic excitations near the Fermi energy, on which the calculation is based, is hardly destroyed by the excitation; unless the average single-particle excitation, or the temperature, becomes comparable to the Fermi energy, i.e. extremely high. There is hardly any danger on this score.

L. WILETS (Chairman): I would like to make some comments that pertain to all attempts to utilize single-particle energy levels and eigenfunctions to obtain the total energy of the nucleus as a function of deformation. These comments will be relevant to the papers presented earlier in the Symposium, to Prof. Strutinsky's work and to papers we will hear later.

We use the term "model" to denote (1) an analogue system of well-defined mechanics or (2) an empirical parameterization of a system whose mechanics, even if defined, are not solvable. (The term is used for other purposes as well.) It is in the latter sense that we speak of an 'independent-particle model'. It is essential, however, to have a concept of the meaning of the model in order to obtain new information (e.g. total energy vs. deformation) from empirical input (e.g. equilibrium-level structure, nuclear saturation, liquid-drop model, etc.). W. Bassichis and

I have studied this question (Phys. Rev. Lett. and abstract SM-122/112). The single-particle models, we suggest, are to be interpreted as (modified) Hartree-Fock solutions of the many-body problem. Away from equilibrium, this involves the introduction of a constraint, i.e. a Lagrange potential which deforms the nucleus. This Lagrange potential contributes to the energy eigenvalues and helps to determine the wave functions, but must not be included in the total energy. We find that errors due to ignoring this can be large and not smooth in deformation. The Strutinsky results, for example, are probably qualitatively correct, but there are important quantitative questions which remain. It may be possible to reinterpret the results in terms of a redefinition of nuclear deformation (matter vs. potential, which are not self-consistent except at equilibrium).

These comments were intended as a warning signal concerning the interpretation and quantitative meaning of such calculations.

V.M. STRUTINSKY: I believe that the shell correction method is a reasonable approximation, especially as a kind of Hartree-Fock-type approximation, that it approximately satisfies the self-consistency condition and, moreover, that it does not contradict the results obtained with the Lagrange multiplier method.

The energy of the nucleus can always be split into two parts, one of which is characterized by smooth quantities. Now, for this part no detailed microscopic theory should really be necessary; a phenomenological liquid-drop model type of approximation would suffice. L.D. Landau used to say that it was so much easier to measure surface tension that one should not waste one's time trying to "evaluate" it.

The energy, related to the difference between the realistic distribution in a small-size quantum system like the nucleus and the model smooth distribution, is, up to the second-order terms, the difference between the relevant single-particle energies. I have tried to explain this in my papers on the shell-correction method [see, for example, Nucl. Phys. 112A (1968) 1, in particular sections 8 and 11]. In calculations with the shell model, it is assumed that the shell-model average field is consistent with such smooth distribution. As I understand it, this is the basic assumption and meaning of the practical shell model.

There are some points which must be understood before any comparison is made with other models. In particular, in the shell correction method the deformations are defined taking into account the uniform part of the distributions, the shape of the spatial smoothed density distribution, its volume, etc. In the Lagrange multiplier method, deformation is usually defined as the total quadrupole moment of the real distribution, which is a different quantity and corresponds to another subsidiary condition. For the above-mentioned parameters used in the shell correction method as adiabatic external degrees of freedom, the approximate consistency is almost trivial. To require exact consistency for them would, in fact, mean solving the complete Schrödinger equation with real forces, which is hardly a very enticing prospect.

R.H. DAVIS: Would you please comment on the importance that attaches to studies of collisions between fragments, i.e. heavy ion collisions? Several aspects of such collisions appear relevant. First, the entrance channel dynamical parameters can be varied. Second, for a given "compound system" the asymmetry (mass ratio of the collision partners) can be chosen.

V.M. STRUTINSKY: The usual reversibility arguments cannot be directly applied to the fission process, in which the cross-section is averaged over so many intrinsic states, whereas in fusion other combinations of states may be important. This is reflected in the classical picture of fission in which the fragments are assumed to be of prolate shape, while in fusion the shapes of the ions are oblate.

However, there is no doubt that the heavy-ion collisions can give valuable information on the deformability of the nuclei and some other dynamic features of the nuclear matter.

H.W. SCHMITT: Have any estimates been made of the lifetime of vibrational states in the second minimum for gamma decay to the ground state of the second minimum? Is there an estimate of the relative yield of such a process in regard to prompt fission from such vibrational levels?

V.M. STRUTINSKY: Such a probability should always contain a penetration factor for the barrier A. Qualitatively, this reduces it, at least, to the same order of magnitude as the probability of fission from the second well. More serious estimates would require a deeper understanding of the nature of such states.

SINGLE-PARTICLE CALCULATIONS FOR DEFORMED POTENTIALS APPROPRIATE TO FISSION*

M. BOLSTERLI, E.O. FISET, J.R. NIX
University of California,
Los Alamos Scientific Laboratory,
Los Alamos, New Mexico,
United States of America

Abstract

SINGLE-PARTICLE CALCULATIONS FOR DEFORMED POTENTIALS APPROPRIATE TO FISSION. We consider the calculation of single-particle energies and wave functions in potentials whose shapes are appropriate to nuclear fission. Each potential contains three terms: (1) a spin-independent axially symmetric part V_1, obtained by folding a Yukawa interaction with a uniform sharp-surface distribution that simulates the nuclear density distribution, (2) a Coulomb potential determined in an analogous way by integrating the Coulomb interaction over the corresponding sharp-surface charge distribution, and (3) an invariant spin-orbit term $\vec{\sigma} \cdot \vec{\nabla} V_1 \times \vec{p}$. For a spherical nucleus, V_1 is similar to a Woods-Saxon potential. As the nucleus deforms, V_1 deforms in a corresponding way, with a surface thickness that remains approximately constant for small deformations. At larger dumbbell-like deformations, the potential is somewhat deeper in the ends of the dumbbell, which is surrounded on all sides by nucleons, than in the neck region.

Apart from its geometrical shape, the potential for neutrons contains four parameters: a depth, a radius, an analog of the surface thickness, and the spin-orbit interaction strength. These are determined by fitting the neutron single-particle and single-hole levels in ^{208}Pb. The sharp-surface nuclear shape is considered to be axially symmetric and is specified in terms of smoothly joined portions of three quadratic surfaces of revolution (e.g. two spheroids connected by a hyperboloidal neck). The two-dimensional coupled Schrödinger equations are solved by a finite-difference method that is an improved version of the procedure described by Dickmann.

We present here our preliminary results for the neutron levels near the Fermi surface in ^{234}U for shapes ranging from a sphere to an elongated symmetric dumbbell beyond the saddle point. The calculated levels at the saddle point are compared with the transition states deduced from ^{235}U fission cross-sections and fission-fragment angular distributions. The preliminary comparison indicates approximate agreement between the calculated and experimental transition states, but there are calculated states of high angular momentum near the Fermi surface that are not excited in the low-energy neutron-induced fission of this nucleus.

INTRODUCTION

Many diverse fission phenomena are believed to be associated with single-particle effects in the vicinity of the fission saddle point and beyond. Familiar examples include the most probable asymmetric mass division, the sawtooth neutron-emission curve, and the increased fission-fragment kinetic energy for asymmetric mass divisions. Also, the fission cross sections and fission-fragment angular distributions of odd compound nuclei are connected with the single-particle states at the saddle point, the so-called transition states. Of more recent interest are spontaneously fissioning isomers and the intermediate structure in fission cross sections, which have been attributed to a secondary minimum in the potential energy of deformation; this minimum is thought to be due to shell structure in the single-particle levels. An accurate description of phenomena such as these re-

* This work was performed under the auspices of the US Atomic Energy Commission.

quires an accurate calculation of the single-particle states for very deformed shapes near and beyond the saddle point.

The importance of such calculations has already been recognized, and several attempts have been made to calculate single-particle states at large deformations. However, these studies generally have taken methods appropriate to small deformations and applied them at large deformations. Such procedures seem unsatisfactory to us for three reasons: (1) the parametrizations used to describe the geometrical shape of the potential are inappropriate to large deformations, (2) the single-particle potentials themselves have unphysical features, and (3) the mathematical procedures used for calculating the energies and wave functions lead to inaccuracies at large deformations.

In this work we have developed techniques more suited to large deformations. The parametrization used is particularly adapted to very deformed shapes, the potential has desirable properties at large deformations, and the method of solution is essentially as accurate at large deformations as for a sphere. However, it should be stressed that these objectives are achieved at the expense of an increase in computation time and some loss of numerical accuracy for shapes close to a sphere.

Of the many possible applications we will discuss here only our preliminary results for the neutron levels near the Fermi surface in ^{234}U for shapes ranging from a sphere to an elongated symmetric dumbbell beyond the saddle point. We are concentrating on these levels because of the wide experimental interest in the transition states deduced from ^{235}U fission cross sections and fission-fragment angular distributions. The calculated levels at the saddle point will be compared with the various sets of experimental states.

SINGLE-PARTICLE POTENTIAL

General features

The basic problem in defining the single-particle potential is that of generating a potential related to a given shape. If the procedure is to be useful for deformations near and beyond the fission saddle point, it must be capable of handling shapes of the sort shown in the lower left-hand side of Fig. 1, and also shapes that are not reflection-symmetric. Fortunately, for most fission phenomena it is sufficient to consider only shapes with axial symmetry.

For spherical nuclei the Woods-Saxon and harmonic-oscillator potentials are frequently used. However, there are obvious difficulties in generalizing these potentials to more complicated dumbbell-like shapes, such as those in Fig. 1. For these shapes we expect the potential to be somewhat deeper in the ends of the dumbbell, which is surrounded on all sides by nucleons, than in the neck region. This is illustrated in the lower right-hand portion of Fig. 1. It does not seem possible to generalize a Woods-Saxon or harmonic-oscillator potential so as to reproduce this behavior without also producing unphysical cusps in some of the equipotentials.

Recently GREENLEES, PYLE and TANG [1] proposed a somewhat different parametrization of the potential, which, with some modification, is also appropriate to deformed shapes. In their method the spin-independent single-

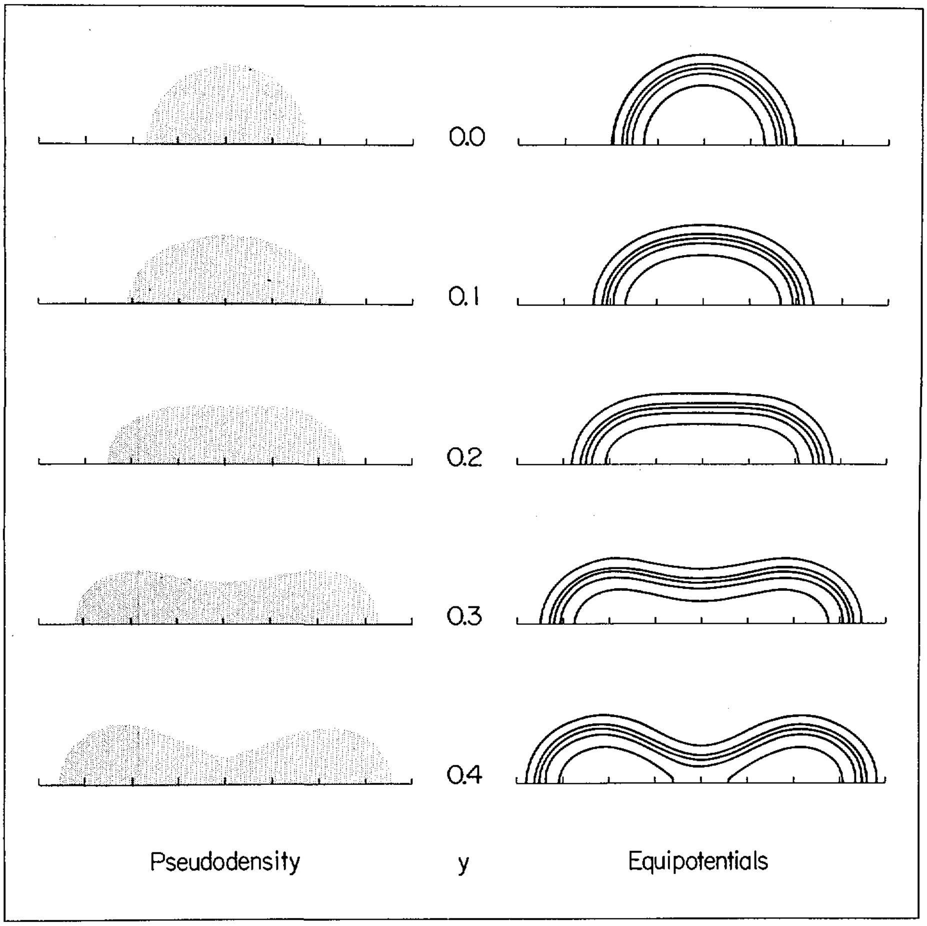

FIG. 1. The uniform sharp-surface pseudodensity distribution that characterizes the shape, and the resulting equipotentials of the folded Yukawa spin-independent nuclear potential V_1, for various values of the deformation co-ordinate y. The equipotential contours refer to the energies $-0.1\ V_0$, $-0.3\ V_0$, $-0.5\ V_0$, $-0.7\ V_0$, and $-0.9\ V_0$, where V_0 is the well-depth parameter [see Eqs (4), (5), and (8)]. The volume of the pseudodensity is appropriate to the nucleus ^{234}U; each division on the scales represents 5 fm.

particle potential V_1 is obtained by folding an effective two-nucleon interaction f with the nuclear density ρ, i.e.

$$V_1(\vec{r}) = \int f(\vec{r} - \vec{r}\,')\ \rho(\vec{r}\,')\ d^3\vec{r}\,' \tag{1}$$

In Ref. 1 it is shown that this procedure produces a potential that is adequate for fitting proton-nucleus scattering.

The folding procedure of Eq. (1) can be modified so as to allow a simple parametrization of the single-particle potential for both spherical and deformed shapes. We have chosen to replace $\rho(\vec{r})$ by a uniform sharp-surface "pseudodensity" that is characterized solely by the shape assumed; i. e., $\rho(\vec{r})$ is taken to be the average number density A/V if $\vec{r}$ is inside the specified surface and zero if it is outside. The volume V of the shape is assumed to remain constant as the shape is changed. For both physical reasons and simplicity we have taken the function f representing the "pseudo nucleon-nucleon interaction" to be a Yukawa potential with adjustable strength and range. Figure 2 shows a comparison between a potential parametrized in this way and a Woods-Saxon potential for the spherical nucleus ^{208}Pb. The advantages of using this folding procedure to parametrize V_1 are simplicity, good behavior around the nuclear surface, and adaptability to very deformed shapes.

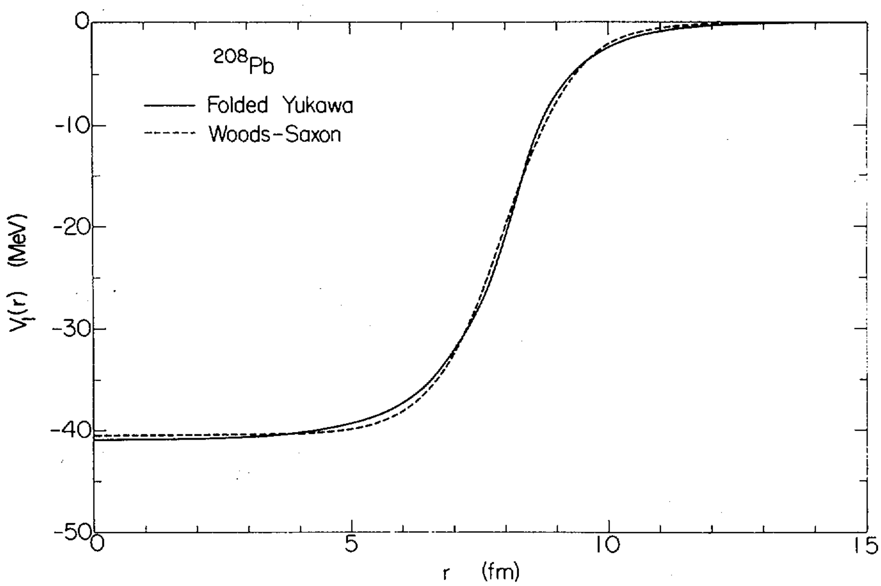

FIG. 2. A comparison of the folded Yukawa spin-independent nuclear potential and the Woods-Saxon potential [2] for the spherical nucleus ^{208}Pb.

Besides the spin-independent part of the potential, there is an additional potential arising from the interaction between the nucleon spin and orbital angular momentum. The simplest form for the spin-orbit interaction that has the right symmetry properties for deformed nuclei is $\vec{\sigma} \cdot \vec{\nabla} V' \times \vec{p}$, where V' is any local spin-independent scalar function. In spherical nuclei this reduces to the familiar $\vec{l} \cdot \vec{s}$ spin-orbit coupling. For V' we have used the spin-independent potential V_1 described above.

Finally, for protons, there is the Coulomb interaction; this is parametrized in a similar way to the spin-independent nuclear potential by folding the electrostatic potential with the charge pseudodensity, which is Z/V inside the surface of the shape and zero outside.

Detailed formulation

To be more specific, the complete potential felt by a nucleon is given by

$$V = V_1 + V_{so} + V_C \tag{2}$$

The spin-independent part is

$$V_1(\vec{r}) = - C \frac{A}{V} \int_V \frac{e^{-|\vec{r} - \vec{r}'|/a}}{|\vec{r} - \vec{r}'|/a} d^3\vec{r}' \tag{3}$$

where C and a are respectively the strength and range of the Yukawa interaction; the integration is over the volume of the shape. As the shape is deformed, the magnitude of this volume is kept fixed, so that V is equal to $4\pi R_0^3/3 = 4\pi A r_0^3/3$, where the radius R_0 of the spherical shape is taken to be $R_0 = r_0 A^{\frac{1}{3}}$. It is convenient to normalize the pseudointeraction and rewrite Eq. (3) as

$$V_1(\vec{r}) = - \frac{V_0}{4\pi a^3} \int_V \frac{e^{-|\vec{r} - \vec{r}'|/a}}{|\vec{r} - \vec{r}'|/a} d^3\vec{r}' \tag{4}$$

where the well-depth parameter is given by

$$V_0 = 3C \, (a/r_0)^3 \tag{5}$$

The potential V_1 thus contains the three parameters V_0, r_0, and a, apart from the geometrical coordinates describing the shape of the pseudodensity.

The spin-orbit term is

$$V_{so}(\vec{r}) = - \lambda(\hbar/2mc)^2 \, \vec{\sigma} \cdot \vec{\nabla} V_1 \times \vec{p}/\hbar \tag{6}$$

and thus contains the additional parameter λ characterizing the spin-orbit interaction strength. Finally, the Coulomb potential for protons is

$$V_C(\vec{r}) = e^2 \frac{Z}{V} \int_V \frac{d^3\vec{r}'}{|\vec{r} - \vec{r}'|} \tag{7}$$

and contains no additional parameters.

In practice we have used Gauss' divergence theorem to transform the above volume integrals into surface integrals, and have evaluated the resulting two-dimensional integrals numerically by use of Gaussian quadrature rules.

Parameter determination

Our calculations so far have concentrated on neutron single-particle levels. For neutrons the single-particle potential contains four parameters: V_0, r_0, a, and λ. These have been determined from the experimental neutron single-particle and single-hole levels of the spherical nucleus ^{208}Pb. To facilitate a comparison between our results and those obtained by ROST [2] with a Woods-Saxon potential, the experimental data used by ROST [2] were also used to determine our parameters, even though there is some evidence [3]

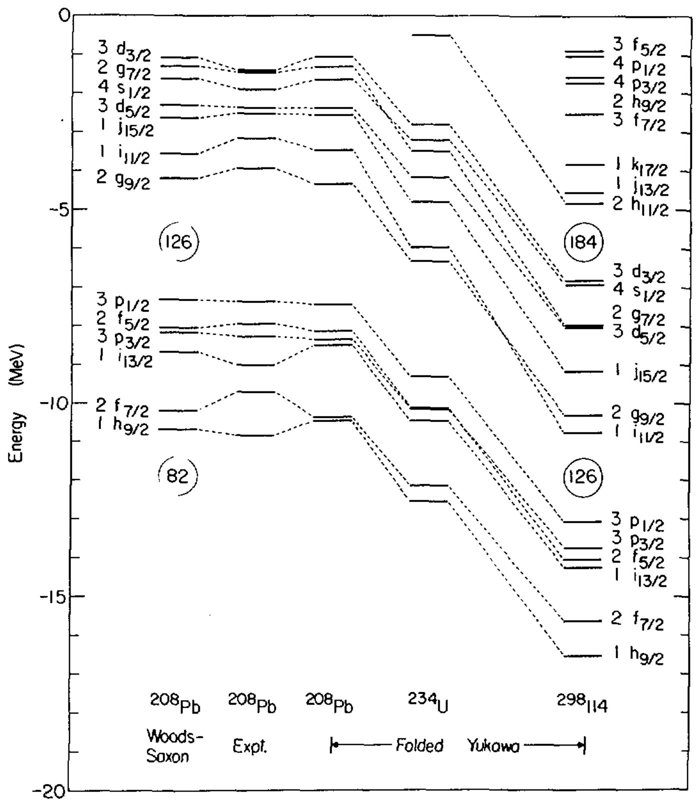

FIG. 3. Calculated neutron single-particle and single-hole levels for various spherical potentials, and experimental neutron levels for ^{208}Pb.

that the $1j_{15/2}$ single-particle level should be at a somewhat higher energy. The values of the 4 parameters, which were adjusted to minimize the rms deviation between the calculated and experimental energies, are

$$
\begin{aligned}
V_0 &= 41.1 \text{ MeV} \quad , \quad & r_0 &= 1.374 \text{ fm} \\
a &= 1.01 \text{ fm} \quad , \quad & \lambda &= 37.2
\end{aligned}
\tag{8}
$$

Shown in Fig. 3 is a comparison between the experimental levels for ^{208}Pb and those computed with the best Woods-Saxon[1] and folded Yukawa potentials, which are seen to produce very similar results. However, the Woods-Saxon potential reproduces the lower-lying single-hole states somewhat better than the folded Yukawa potential, and consequently the rms deviation between the calculated and experimental levels is slightly smaller for the Woods-Saxon potential (0.26 MeV) than for the folded Yukawa potential (0.31 MeV).

---

[1] Of the several sets of parameters listed in Ref. 2, the relevant set for the present comparison is there denoted by the label N O T.

The two potentials used in calculating these single-particle levels are the ones shown earlier in Fig. 2. Note the close similarity between the potentials, which intersect at four places in the nuclear surface. As regards finer details, the folded Yukawa potential is slightly deeper in the nuclear interior and begins to rise somewhat more quickly than the Woods-Saxon potential.

The folded Yukawa potential obtained for ^{208}Pb has been extrapolated to ^{234}U and ^{298}114 (only A and hence R_0 changes), and the single-neutron levels for these extrapolated potentials are also shown in Fig. 3. Since U is deformed in its ground state, the former results are of interest only for comparison with the calculations of the next section. However, the results for ^{298}114 are important because of the possibility of producing super-heavy nuclei in this region. As would be expected from the close similarity between this study and that of ROST [2], our results for the neutron levels in ^{298}114 are very similar to his. They both show a substantial gap at $N = 184$ and essentially no gap at $N = 196$; some computations with modified harmonic-oscillator potentials have shown gaps at both 184 and 196.

Shape coordinates

A nucleus undergoing fission changes its shape from an initial spherical or slightly deformed ground state, through very deformed saddle and scission shapes, to separated fragments at infinity. A method for describing such a wide variety of shapes in terms of a small number of deformation coordinates is discussed in Ref. 4, where a shape is represented as the surface formed by smoothly joined portions of three quadratic surfaces of revolution (e. g. two spheroids connected by a hyperboloidal neck). This parametrization contains a total of six degrees of freedom, of which three represent reflection-symmetric deformations and three reflection-asymmetric deformations (one of these is an over-all shift of the center of mass and may therefore be disregarded).

To display graphically the behavior of the single-particle energies as a nucleus deforms from a spherical shape to its saddle-point shape and somewhat beyond, it is convenient to use the deformation coordinate y introduced by HILL and WHEELER [5]. This coordinate is defined in terms of the saddle-point shapes for an idealized uniformly charged liquid drop; specifically, the saddle-point shape corresponding to a given value of the fissility parameter x [4,5] represents a deformation of

$$y = 1 - x \tag{9}$$

Thus, as y ranges from 0 to 1 the sequence of shapes ranges from a single sphere through symmetric dumbbell-like shapes to two tangent spheres. To first order, y is related to the coordinates that describe spheroidal and Legendre-polynomial P_2 distortions by

$$y = \frac{2}{7}\,\epsilon = \frac{2}{7}\,\delta = \frac{3}{7}\,\alpha_2 = \frac{3}{7}\left(\frac{5}{4\pi}\right)^{\frac{1}{2}}\beta \approx 0.270\,\beta \tag{10}$$

The shapes shown on the left-hand side of Fig. 1 illustrate these deformations for values of y ranging from 0.0 to 0.4; the corresponding folded Yukawa spin-independent nuclear potentials are shown on the right-hand side. It should be stressed that in general a fissioning nucleus does <u>not</u>

undergo the exact deformations described by the single coordinate y. Nevertheless, since the sequence of shapes described by y includes both the ground state and the saddle point (for an idealized drop), the use of this coordinate provides a convenient means of interpolating between the two shapes that are of primary interest.

RESULTS FOR DEFORMED SHAPES

Method of calculation

For axially symmetric shapes the Schrödinger equation with the potential (2) can be reduced to two coupled partial differential equations in two variables. Since for large deformations expansion in a limited set of basis functions can introduce substantial truncation errors (see for example Ref. 6), we have instead solved the equations by use of a finite-difference method, which is in some respects similar to the procedure outlined by DICKMANN [7]. To permit the grid points to be distributed advantageously, we have used prolate spheroidal coordinates with eccentricity appropriate to the particular shape rather than cylindrical coordinates. Also, to ensure in a simple way that the matrix to be diagonalized is symmetric, we have derived the finite-difference equations by use of the variational principle.

The results presented here were calculated with a two-dimensional grid containing 20 intervals in one dimension and 40 in the other. The coupling between the equations doubles the number of points to be considered, but because the grid points on the boundaries can be eliminated, the resulting finite-difference matrix is of dimension 1482×1482. By properly ordering the grid points, we are led to a matrix with a relatively small band width (79 for these results). This allows the energies and wave functions to be found in an efficient way by use of inverse iteration, with the linear system of equations solved by a direct rather than by an iterative method. Once the potential has been computed, about 20 seconds of CDC-6600 computing time are required to determine each level. The energies near the Fermi surface calculated in this way are accurate to within about 0.1 MeV for nodeless states and to within about 0.5 MeV for states with many nodes. (States with angular nodes are computed more accurately than states with a comparable number of radial nodes.) Our results are therefore less accurate at small deformations than those computed by expanding the wave function in a set of basis functions, but are substantially more accurate at large deformations.

Single-neutron levels for ^{234}U

For ^{234}U, Fig. 4 shows our preliminary results for the single-neutron energies near the Fermi surface as a function of the deformation coordinate y defined at the end of the previous section. The levels are labelled by the projection K (or Ω) of the total angular momentum on the nuclear symmetry axis and the parity of the single-particle state. We will discuss these results in connection with neutron single-particle states in ^{235}U, although they refer equally well to single-hole states in ^{233}U.

At the ground-state equilibrium deformation for ^{235}U, which corresponds to $y = 0.053$, the calculated level of the last neutron is $\frac{5}{2}^-$. The three next higher levels are $\frac{1}{2}^+$, $\frac{7}{2}^+$, and $\frac{7}{2}^-$, and the two next lower levels are $\frac{5}{2}^+$ and $\frac{3}{2}^-$. The experimentally observed ground-state level in ^{235}U is $\frac{7}{2}^-$, and the four next higher single-particle levels (lowest members of rotational bands) are $\frac{1}{2}^+$, $\frac{5}{2}^+$, $\frac{5}{2}^+$, and $\frac{3}{2}^+$. Such a partial coincidence of

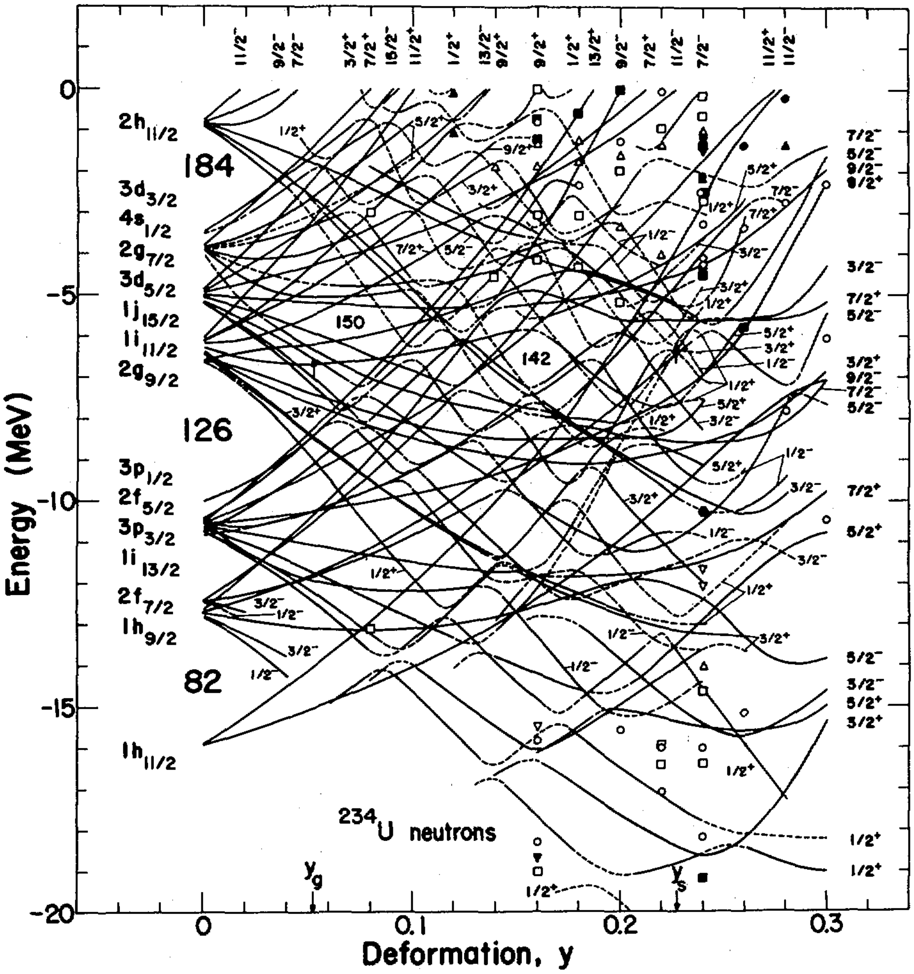

FIG. 4. Preliminary single-neutron energies near the Fermi surface for ^{234}U as a function of the deformation co-ordinate y. The levels are labelled by the projection K (or Ω) of the total angular momentum on the nuclear symmetry axis and the parity of the single-particle state. Shown at the left are the quantum numbers for the spherical levels; the splitting of the actually degenerate spherical levels provides a measure of the accuracy of the calculations. The four arrows indicate for ^{235}U the locations of the ground-state and saddle-point deformations and the corresponding levels of the last neutron. A dashed line is used in a region where the exact position of the level is uncertain, e.g. when two levels of identical quantum numbers nearly cross. A step length of 0.02 in y has been used; however, away from the Fermi surface and at deformations close to y = 0.3 not all energies have been found yet. Calculated energies not connected by lines are indicated by points (notation: solid, positive parity; open, negative parity; circle, $\frac{1}{2}$; square, $\frac{3}{2}$; upward-pointing triangle, $\frac{5}{2}$; downward-pointing triangle, $\frac{7}{2}$; and hexagon, $\frac{9}{2}$).

the calculated and experimental quantum numbers can be regarded as fairly good agreement, since the parameters of the single-particle potential have been extrapolated from the single spherical nucleus ^{208}Pb. A detailed comparison of the calculated and experimental single-neutron energies will not be made, since it would require considering the shifts due to core-polarization effects and residual interactions.

At the larger deformation $y \approx 0.16$, a gap of about 1.4 MeV appears in the single-particle spectrum at neutron number $N = 142$. As emphasized by Strutinsky [8], for nuclei containing close to 142 neutrons such a gap would be expected to lead to a lowering of the potential energy at this deformation and consequently to a fission barrier containing two peaks separated by a secondary minimum. Some previous calculations with generalized harmonic-oscillator and Woods-Saxon potentials for spheroidal and P_2 deformations have indicated the presence of such a secondary gap instead at $N = 146$ or 148.

Comparison with ^{235}U transition states

Our primary interest here is in comparing calculated and experimental single-particle states at the much larger saddle-point deformation. This deformation, which has been estimated on the basis of the liquid-drop model, with the values of Ref. 9 used for the constants of the semi-empirical nuclear mass formula, corresponds to $y = 0.227$. Here the calculated level corresponding to the last neutron is $\frac{1}{2}^+$, the three next higher levels are $\frac{1}{2}^-$, $\frac{3}{2}^+$, and $\frac{3}{2}^-$, and the two next lower levels are $\frac{3}{2}^+$ and $\frac{7}{2}^+$. At this deformation the levels near the Fermi surface are changing rapidly and their level density is fairly high, corresponding to an average spacing of about 150 keV. However, slightly below the Fermi surface, there is a gap in the single-particle spectrum of about 1 MeV.

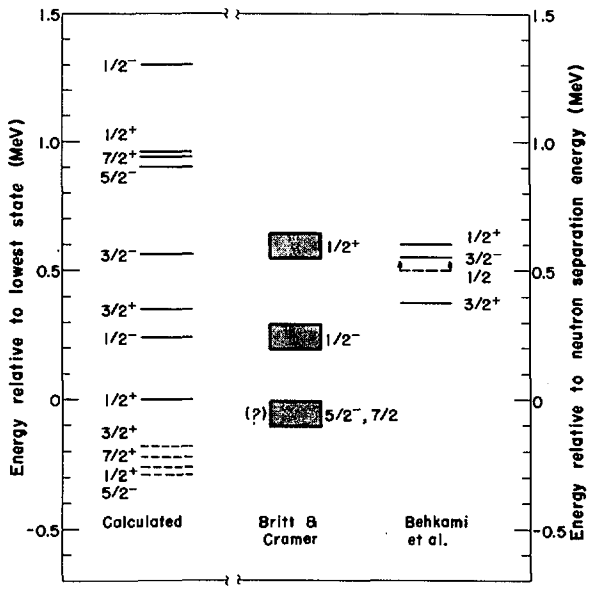

FIG. 5. A preliminary comparison of the calculated single-neutron states at the liquid-drop-model saddle-point deformation with the experimental transition states of Britt and Cramer [10] and Behkami et al. [11]. The question mark inside parentheses indicates that this state may not be present experimentally.

These levels are shown in greater detail in Fig. 5, where we have also included for comparison two sets of experimental transition states deduced from ^{235}U fission cross sections and fission-fragment angular distributions [10,11]. An arbitrary over-all shift of the calculated levels relative to the experimental ones is possible, since the former are plotted relative to the energy of the lowest state and the latter relative to the neutron separation energy.

The results of BRITT and CRAMER [10] are preliminary estimates based on data from fission induced by (d,p) and (t,p) reactions. There is some indication in this work of a $\frac{5}{2}^-$ or $\frac{7}{2}^-$ level at an energy below that of the lowest state deduced from studies of neutron-induced fission by BEHKAMI et al. [11]; because of its large angular momentum and low excitation, this level would not be expected to be excited by low-energy neutrons. However, the angular distribution data is poor at very low energies, and the cross-section peak on which this assignment is based might not be due to a transition state at all but rather to a resonance associated with a secondary minimum in the fission barrier. The two next higher transition states deduced by Britt and Cramer are $\frac{1}{2}^-$ and $\frac{1}{2}^+$, and the average level spacing is about 300 keV.

As shown in the figure, the levels deduced by BEHKAMI et al. [11] are $\frac{3}{2}^+$, $\frac{1}{2}$, $\frac{3}{2}^-$, and $\frac{1}{2}^+$, and they have an average spacing of about 75 keV. Since the analysis that gave these levels assumed a fission barrier with a single peak rather than one with two peaks, there is some uncertainty associated with these levels. In particular, it was necessary to assume a considerably thinner barrier for the $\frac{1}{2}^+$ level than for the others so that this level could dominate at low energies even though it lies higher than the others.

An earlier analysis of neutron-induced fission experiments by LAMPHERE [12] gave low-lying transition states with assignments $\frac{1}{2}^+$, $\frac{3}{2}^-$, and $\frac{1}{2}^-$ and separated by the order of a few hundred keV. The energies of the individual states were not obtained so they are not included in Fig. 5.

Our summary of the present experimental situation is that the exact order and position of the transition states are unknown, but that the states $\frac{1}{2}^+$, $\frac{1}{2}^-$, $\frac{3}{2}^+$, and $\frac{3}{2}^-$ are located within an energy region of roughly 500 keV, and that in addition there is possibly a state of high angular momentum lying below these. (Any states of high angular momentum lying at higher excitation energies would probably be missed experimentally.)

In comparing the experimental states with our preliminary calculations, it should again be stressed that the calculated transition states depend rather sensitively upon the exact location of the saddle point. Because of single-particle effects, it is expected that there are in fact two saddle points, with the position of the second one shifted somewhat from the liquid-drop-model result that we have used. With this reservation in mind, we see from Fig. 5 that the four lowest calculated transition states are the ones generally observed experimentally (but not necessarily in the same order), and that their average spacing agrees roughly with the experimental spacings. In addition, the low-lying $\frac{5}{2}^-$ or $\frac{7}{2}^-$ state possibly observed by Britt and Cramer could be either the calculated $\frac{7}{2}^+$ state or $\frac{5}{2}^-$ state lying slightly below the Fermi surface at $y = 0.227$, since these states both move above the Fermi surface at a deformation just beyond the liquid-drop-model saddle point.

SUMMARY AND CONCLUSION

To summarize, we have discussed our techniques for calculating single-particle energies and wave functions at the large deformations of interest in fission. These techniques include (1) using a shape parametrization that is particularly suitable for large deformations, (2) generating the potential by folding an effective two-nucleon interaction with a uniform sharp-surface pseudodensity, and (3) employing a finite-difference method of solution whose accuracy does not deteriorate at large deformations.

We have illustrated our procedure by calculating the single-neutron energies near the Fermi surface for ^{234}U for shapes ranging from a sphere to a symmetric dumbbell beyond the saddle point. The calculated energies at the saddle point were compared with transition states deduced from ^{235}U fission cross sections and fission-fragment angular distributions. The preliminary comparison indicates that the calculated and presently available experimental states are qualitatively similar, but there are calculated states of high angular momentum near the Fermi surface that are not excited in the low-energy neutron-induced fission of this nucleus. We hope that our calculations will encourage future experiments designed to determine single-particle transition states, and that they will also prove useful as a guide in their analysis.

In conclusion, we would like to comment that most discussions of the fission phenomena mentioned in the introduction have been qualitative, and that a more adequate treatment requires calculating the potential energy as a function of deformation. The techniques developed here should be useful for this purpose at large deformations near and beyond the saddle point.

ACKNOWLEDGEMENTS

We would like to thank B. L. Buzbee for writing the computer program we have used for finding the eigenvalues and eigenvectors of a band matrix, and H. C. Britt, P. Concus, J. D. Cramer, G. H. Golub, E. Rost, W. J. Swiatecki, and R. L. Tarp for their contributions to this work.

REFERENCES

[1] GREENLEES, G. W., PYLE, G. J., TANG, Y. C., Phys. Rev. 171 (1968) 1115.

[2] ROST, E., Univ. of Colorado Rep. COO-535-570 (no date); Phys. Letters 26B (1968) 184.

[3] IGO, G. J., BARNES, P. D., FLYNN, E. R., ARMSTRONG, D. D., Phys. Rev. 177 (1969) 1831.

[4] NIX, J. R., Lawrence Radiation Laboratory Rep. UCRL-17958 (1968); Nucl. Phys., to be published (1969).

[5] HILL, D. L., WHEELER, J. A., Phys. Rev. 89 (1953) 1102.

[6] HOUVIEZ, J., Saclay Rep. CEA-R-3645 (1968).

[7] DICKMANN, F., Z. Phys. 203 (1967) 141.

[8] STRUTINSKY, V. M., Nucl. Phys. A95 (1967) 420; Nucl. Phys. A122 (1968) 1.

[9] MYERS, W. D., SWIATECKI, W. J., Ark. Fys. 36 (1967) 343.

[10] BRITT, H. C., CRAMER, J. D., "Direct-reaction fission of odd-A uranium and plutonium isotopes", abstract, these Proceedings; private communication.

[11] BEHKAMI, A. N., ROBERTS, J. H., LOVELAND, W., HUIZENGA, J. R., Phys. Rev. 171 (1968) 1267.

[12] LAMPHERE, R. W., Physics and Chemistry of Fission (Proc. Symp. Salzburg, 1965) I, IAEA, Vienna (1965) 63; Nucl. Phys. 38 (1962) 561.

DISCUSSION

U. MOSEL: You claim in your paper that your model gives without fail not only qualitative but also quantitative results. However, since the work of Green many years ago we know that it is quite essential to include non-local parts in the single-particle potentials; only in this manner can you get the correct total energy of a nucleus by summing up the single-particle energies, which is necessary also in the Strutinsky method. This shows the large influence of such terms, and indeed a calculation of this type has already been done by Meldner (see abstract SM-122/47). He has even used self-consistency, which is also very important in the light of the work of Bassichis and Wilets referred to in abstract SM-122/112. Therefore, I think that the Strutinsky method for calculation of shell corrections, which consists in the unsatisfactory mixing of two different models, will become unnecessary in the near future when one is able to derive all these effects from a non-local and self-consistent "single-particle" potential. These improvements should be included in a quantitative calculation.

J.R. NIX: To reproduce the observed nuclear binding energies, it is indeed necessary to use a non-local, or alternatively momentum-dependent, potential. We plan to proceed with our work along two independent lines: (1) self-consistent Hartree (not Hartree-Fock) calculations with an effective interaction similar to the one used here but also including a momentum dependence; and (2) local static calculations with the Strutinsky shell correction method used for obtaining the total energy. When the shell correction method is used, only the levels near the Fermi surface make a substantial contribution, and for these levels it is not crucial to use a momentum-dependent potential.

The non-local calculations of Meldner have been performed only for spherical shapes because they entail solving an integral-differential equation, which is an order of magnitude more difficult than our calculations; it is not practical, at present, to generalize Meldner's calculations to very deformed shapes.

P. von BRENTANO: I would like to comment on the potential radius $r_0 \sim 1.35$ fm you used for comparison with the single-particle states around ^{208}Pb, and for extrapolation to the super-heavy elements. I think this radius is too large. From a study of the dependence of the spectroscopic factors measured in the ^{208}Pb(d, p) Coulomb stripping experiment on the potential radius r_0, W.R. Hering and M. Dost [Phys. Lett. 19 (1965)] determine a radius $r_0 \sim 1.24 \pm 0.02$ fm. A similar radius is also obtained from a fit to the Coulomb displacement energies by F.G. Perey and J.P. Schiffer [Phys. Rev. Lett. 17 (1966)] and also by A.G. Blair et al. [Phys. Lett. 20 (1966)]. Thus, it seems dangerous to determine a radius from a fit of the energy levels alone.

J.R. NIX: First, it should be stressed that our radius parameter refers to the radius of the pseudo-density rather than to the radius of the potential. The corresponding radius of our potential is slightly smaller, but not so small as that determined from the studies you mention. There does appear to be a significant discrepancy between the value of the radius parameter determined from energy levels and the value determined from other data. For the present we have determined our parameters from the energy levels of a single nucleus, but we plan in the future to consider other nuclei throughout the periodic table and also other properties of these nuclei.

U. MOSEL: If a calculation is performed with a view to obtaining very accurate results, one should look also for shell effects in the Coulomb energy. This point has been completely neglected in all fission calculations till now, which have used only classical Coulomb energies or Coulomb potentials. These shell effects in the Coulomb energy can be investigated by treating this term directly as a two-body operator from the beginning instead of first folding this operator with a pseudo-density and then going on with the Coulomb single-particle potential so obtained. Have you already considered the shell effects in the Coulomb energy, which might have an appreciable influence on your results?

J.R. NIX: Yes, shell effects in the Coulomb energy may indeed be important, and we plan to make a study of them. But for the present we have concentrated on neutron states because the experimental single-particle transition states are for neutrons.

L. WILETS (Chairman): What would you think of turning your calculations "around" in the sense of utilizing them, as a function of y, in order to determine which deformation (y) yields the correct barrier level structure (the barrier is, of course, an equilibrium configuration)? This might be a useful way to determine the location of the barrier.

J.R. NIX: At present the experimental transition states are not sufficiently well determined to permit this to be done. But when more accurate experimental transition states become available, they could indeed be used to determine both the location of the barrier peak and the values of the parameters of the potential.

FISSION BARRIERS AND SADDLE-POINT SHAPES

H.J. KRAPPE, U. WILLE
Hahn-Meitner-Institut für Kernforschung Berlin,
Sektor Kernphysik,
Berlin

Abstract

FISSION BARRIERS AND SADDLE-POINT SHAPES. The energy of rare-earth and heavy fissile nuclei is calculated as a function of quadrupole, octupole, and hexadecapole deformations. The liquid-drop model is used with shell corrections according to a method proposed by Strutinsky. The liquid-drop part of the deformation energy is treated exactly by numerical integration. In the shell-model part we used potentials of the Saxon-Woods type as well as harmonic oscillator potentials. Though the latter can more easily be treated numerically, certain ambiguities arise from the various parameters entering in their definition. These are investigated by comparison with the results obtained with use of the Saxon-Woods potential.

The symmetry energy and charge radius parameters in the liquid-drop part of the binding energy were taken from Seeger's work. The geometrical parameters defining the single-particle potential and the spin-orbit coupling strength were fitted to the energy-level sequence near the Fermi surface or to nucleon scattering data analysed within the optical model. The pairing strength is chosen to reproduce the region of deformed nuclei correctly and to give the over-all trend of odd-even mass differences.

The ground-state deformations, fission-barrier heights and locations, and the excitation energy of shape isomers are calculated for various nuclei of the rare-earth and actinide region.

1. INTRODUCTION

Recently there has been considerable progress in calculating the dependence of nuclear binding energies on deformation by adding a shell-correction term to the usual liquid-drop expression for the binding energy [1, 2]. Extensive studies by Nilsson and his collaborators [3, 4] have shown that this procedure yields the same results as the Bès-Szymański calculations [5] for small deviations from the spherical shape, but is superior to the latter for large deformations. In fact, the existence of shape isomers was first successfully explained by employing Strutinsky's shell-correction method [1, 3]. In this paper we extend these investigations of the deformation energy by including an octupole in addition to the quadrupole and hexadecapole degrees of freedom. We further discuss the influence of the geometrical parameters of the single-particle potentials on the deformation energy.

2. CHOICE OF SINGLE-PARTICLE POTENTIALS

The shell-correction to the binding energy has mostly been calculated with Nilsson's harmonic oscillator in stretched co-ordinates (Appendix A of Ref. [6]):

$$H = \tfrac{1}{2}\hbar\omega_0\ (\epsilon, \epsilon_\mu)\left\{-\Delta_\rho + \rho^2 - \tfrac{2}{3}\epsilon P_2 \rho^2 + 2\sum_{v=1,3,4} \epsilon_\nu P_\nu \rho^2 + \frac{\epsilon}{3}\left(2\frac{\partial^2}{\partial\xi^2} - \frac{\partial^2}{\partial\xi^2} - \frac{\partial^2}{\partial\eta^2}\right)\right\}$$

$$- \kappa(N)\hbar\mathring{\omega}_0 \left\{2\vec{\ell}_\rho\cdot\vec{s} + \mu(N)\ (\ell_\rho^2 - \tfrac{1}{2}N(N+3))\right\} \tag{1}$$

with

$$\xi = x\left\{\frac{m\,\omega_0(\epsilon)}{\hbar}\left(1 + \frac{\epsilon}{3}\right)\right\}^{\frac{1}{2}} \tag{2a}$$

$$\eta = y\left\{\frac{m\,\omega_0(\epsilon)}{\hbar}\left(1 + \frac{\epsilon}{3}\right)\right\}^{\frac{1}{2}} \tag{2b}$$

$$\zeta = z\left\{\frac{m\,\omega_0(\epsilon)}{\hbar}\left(1 + \frac{2}{3}\epsilon\right)\right\}^{\frac{1}{2}} \tag{2c}$$

$$\rho^2 = \xi^2 + \eta^2 + \zeta^2 \tag{2d}$$

For the calculation of deformation energies the choice of the energy scale factor $\hbar\omega_0(\epsilon, \epsilon_\mu)$ is very important. Conventionally one requires the conservation of equipotential volume to simulate the incompressibility of nuclear matter. This yields

$$\left(\frac{\omega_0(\epsilon)}{\mathring{\omega}_0}\right)^3 = \left(1 + \frac{\epsilon}{3}\right)^{-1}\left(1 - \frac{2}{3}\epsilon\right)^{-\frac{1}{2}}\frac{1}{2}\int_{-1}^{1}\left\{1 - \frac{2}{3}\epsilon P_2(x) + 2\sum_{v=1,3,4}\epsilon_\nu P_\nu(x)\right\}^{-3/2} dx \tag{3}$$

Here $\hbar\mathring{\omega}_0$ is fitted to the mean square radius of protons and neutrons, respectively. Depending on which method is used, the values for $\hbar\mathring{\omega}_0 A^{\frac{1}{3}}$ vary from 32.74 MeV [7] (for protons) and 42.95 MeV [7] (for neutrons) to 53 MeV [1].

To check the usefulness of relation (2) and fix an appropriate value for $\hbar\mathring{\omega}_0$, we compare the single-particle spectra and the shell corrections generated by the Hamiltonian (1) and by a Woods-Saxon potential. The latter possesses a less anbiguous energy scale. It is defined by

$$V(r,\vartheta) = -V_0\ f(r,\vartheta) - \frac{\kappa V_0}{\hbar}\ (\vec{\sigma}\times\vec{p})\vec{\nabla}f \tag{4}$$

$$f(r,\vartheta) = \left\{1 + \exp\left(\frac{r - R(\vartheta)}{a}\right)\right\}^{-1} \tag{5}$$

$$R(\vartheta) = r_0 A^{\frac{1}{3}}\left(1 + \sum_{\nu=0} \alpha_\nu P_\nu(\cos\vartheta)\right) \tag{6}$$

For the parameters V_0, r_0, α, and κ we use the values given by Faessler and Sheline [9]. These authors require the correct level sequence, correct binding energy for the last nucleon and consistency with an extrapolation of the optical-model parameters to negative energies. As the parameters seem to be rather weakly dependent on the atomic number we also use them for the lighter actinides. In this paper we follow the practice of Ref.[9] to simulate the Coulomb potential by smaller values for V_0 and a instead of explicitly adding the Coulomb potential to the right-hand side of Eq.(4). Furthermore, we do not take into account the deformation dependence in the spin-orbit coupling term.

Figure 1 shows the neutron single-particle levels near the Fermi energy of ^{235}U calculated with the spherical Nilsson Hamiltonian (1) and the spherical Woods-Saxon potential (4). For $\kappa(N)$ and $\mu(N)$ we have used an interpolation formula given by Seeger and Perisho [7]

$$\kappa = \kappa_0 \{ \tfrac{1}{2}(N+1)(N+2)\}^{-\frac{1}{3}} ; \qquad \mu(N) = \mu_0 = \text{const.} \tag{7}$$

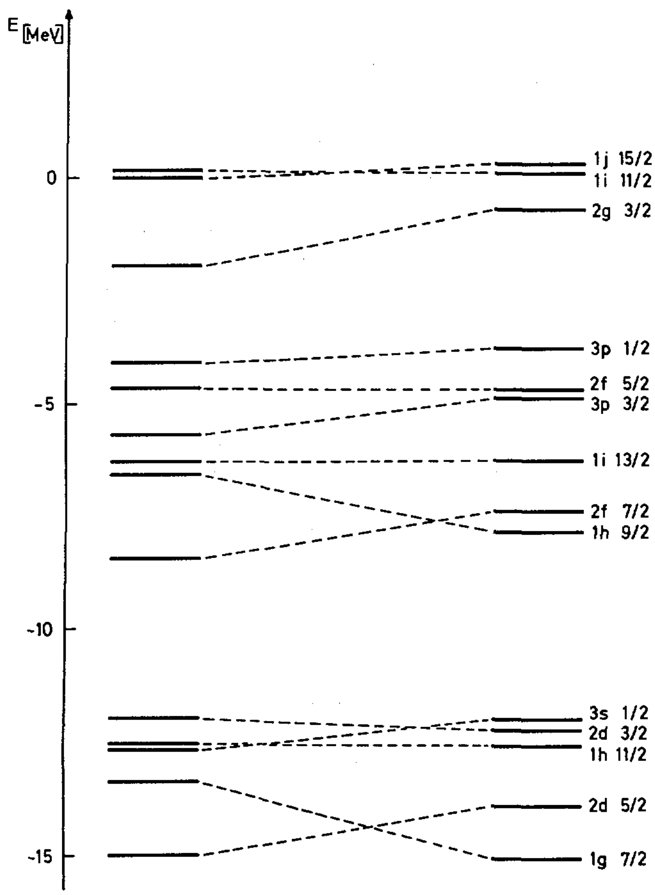

FIG.1. Single-neutron level scheme in a spherical Nilsson potential (left) and a spherical Woods-Saxon potential (right). ^{235}U parameters are used in the Woods-Saxon potential; in the Nilsson potential $\hbar\mathring{\omega}_0 = 41\ A^{-1/3}$ MeV.

The parameters κ_0 and μ_0 are adjusted to give the correct level sequence near the Fermi surface of heavy nuclei. We fix the energy scale for the oscillator potential by the requirement that it should reproduce the average level density of the Woods-Saxon potential in the neighbourhood of the Fermi energy. The values $\hbar\mathring{\omega}_0 A^{1/3} = 44$ MeV for the neutrons and 38 MeV for the protons used in Ref. [8] are consistent with this requirement.

To find the set of deformation parameters a_1, a_2, a_3 ... (Eq. (6)) corresponding to a given set of Nilsson's parameters ϵ_1, ϵ_2, ϵ_3... one should equate the mass multipole moments of an A-particle state calculated in an oscillator potential to those calculated with a Woods-Saxon potential. Instead, we simply expand an equipotential line of the harmonic oscillator in the form (6). It is expected that this yields nearly the same results because the mass density is known to follow closely the equipotential lines, [4]. In actual calculations one has to keep in mind that the expansion of a spheroidal shape according to expression (6) is rather slowly convergent.

The effect of the spin-orbit coupling term for large deformations depends crucially on the way it is extrapolated from the ground state to larger deformations. As this term has a purely phenomenological character, the only thing one knows in advance is that in the limiting case of the scission configuration the deformation dependence should yield two spin-orbit terms roughly of the usual spherical type with respect to the centres of the two fragments. This requirement is met by the Thomas term in expression (4), but not by the spin-orbit coupling in the Nilsson potential (1). In our calculations we have not included the deformation dependence in the Thomas term. Therefore, we cannot check whether Nilsson's spin-orbit term still gives reliable results for deformations corresponding to the second saddle-point of actinides with double-humped fission barriers.

Another parameter whose deformation dependence is not known is the strength of the pairing force. As Nilsson [3] has shown, calculated barrier heights depend strongly on the assumptions made about the deformation dependence of this parameter. Unfortunately, theoretical derivations of this quantity are not reliable. Therefore it must be kept as a phenomenological parameter. Its value should be fitted to the observed barrier heights.

3. SHELL CORRECTION CALCULATIONS

The shell correction to the binding energy is defined by [1, 7]:

$$E_{\mathrm{corr}} = (E_{\mathrm{BCS}} - U)_{\mathrm{protons}} + (E_{\mathrm{BCS}} - U)_{\mathrm{neutrons}} \tag{8}$$

$$E_{\mathrm{BCS}} = \begin{cases} 2\sum\limits_{k=1}^{n} \left(E_k - \dfrac{G}{2}\vartheta_k^2\right) - \dfrac{\Delta^2}{G} & \text{for an even number of nucleons} \quad (9a) \\[2ex] E_\ell + 2\sum\limits_{\substack{k=1 \\ k\neq\ell}}^{n} \left(E_k - \dfrac{G}{2}v_k^2\right) - \dfrac{\Delta^2}{G} & \text{for an odd nucleon in level } \ell \quad (9b) \end{cases}$$

$$U = \int_{-\infty}^{\lambda} g(\epsilon)\,\epsilon\, d\epsilon \tag{10}$$

$$g(\epsilon) = \frac{1}{\gamma\sqrt{\pi}} \sum_k \left(\frac{3}{2} - X_k(\epsilon)^2\right) e^{-X_k(\epsilon)^2} \tag{11}$$

$$(\gamma = 0.7\ \hbar\mathring{\omega}_0)$$

$$X_k(\epsilon) = \frac{\epsilon - E_k}{\gamma} \tag{12}$$

Here E_k are the single-particle levels of the shell model, G is the pairing strength parameter, v_k^2 the occupation probability of level k, 2Δ is the energy gap, and λ is determined from the equation

$$n = 2\int_{-\infty}^{\lambda} g(\epsilon)\, d\epsilon \tag{13}$$

where n is the number of protons or neutrons.

Figures 2 and 3 show the neutron contribution to the shell correction of the binding energy of ^{236}U calculated with the Nilsson potential (1) and the Woods-Saxon potential (4). We have used the following set of neutron parameters:

$\hbar\mathring{\omega}_0 = 44\ A^{-\frac{1}{3}}$ MeV	$V_0 = 46.33$ MeV
$\kappa_0 = 0.21$	$\kappa = 0.423\ fm^2$
$\mu_0 = 0.308$	$r_0 = 1.25$ fm
$G = 14.0\ A^{-1}$ MeV	$a = 0.64$ fm

For the protons the corresponding set is

$\hbar\mathring{\omega}_0 = 38\ A^{-\frac{1}{3}}$ MeV	$V_0 = 35.24$ MeV
$\kappa_0 = 0.18$	$\kappa = 0.556\ fm^2$
$\mu_0 = 0.62$	$r_0 = 1.25$ fm
$G = 19.6\ A^{-1}$ MeV	$a = 0.52$ fm

In the BCS calculation we include all levels below the Fermi energy and the same number above. The values of κ_0 and μ_0 are taken from Ref.[7], the values of G from Ref.[3], and the Woods-Saxon parameters from Ref.[9]. Figure 4 gives the shapes of equipotential lines for the ϵ and ϵ_3 values used in Figs 2 and 3.

In Fig. 5 the total shell correction of ^{236}U (minimized with respect to ϵ_3 and ϵ_4) is displayed as a function of ϵ. Figure 6 gives the cut $\epsilon_3 = 0$,

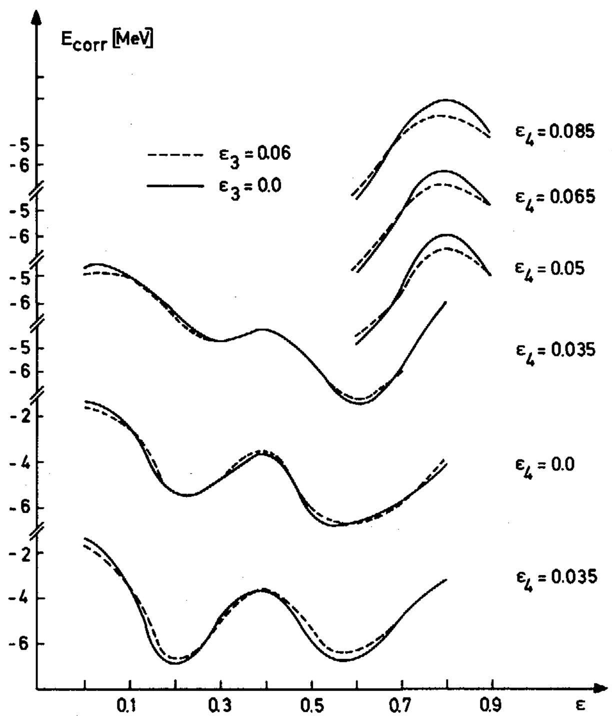

FIG.2. Neutron contribution to the shell correction for ^{236}U as a function of ϵ for several values of ϵ_3 and ϵ_4 (Nilsson potential).

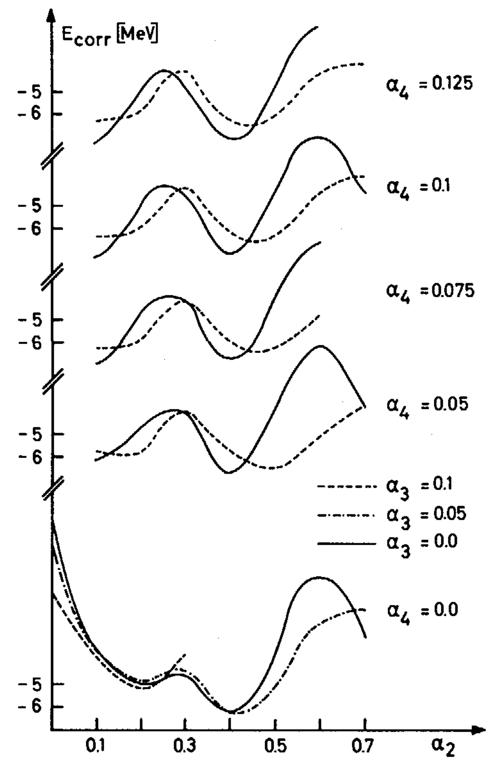

FIG.3. Neutron contribution to the shell correction for ^{236}U as a function of α_2 for several values of α_3 and α_4 (Woods-Saxon potential).

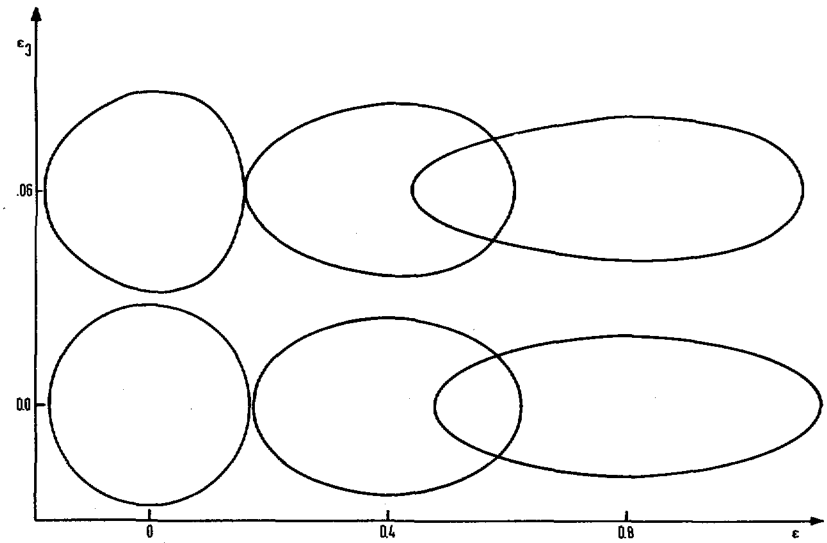

FIG.4. Nuclear shapes for $0 \le \epsilon \le 0.8$, $0 \le \epsilon_3 \le 0.06$, $\epsilon_4 = 0$.

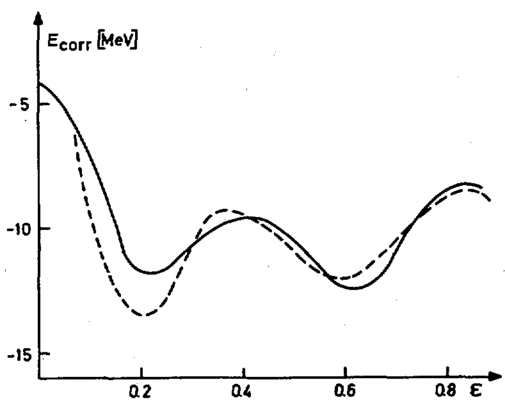

FIG.5. Total shell correction for ^{236}U (minimized with respect to ϵ_3 and ϵ_4 for each ϵ) as a function of ϵ. The solid line is calculated with the Nilsson potential, the dotted line with the Woods-Saxon potential.

$\epsilon_4 = 0$ through the surface of the shell correction of ^{170}Yb. The qualitative agreement between the curves corresponding to the Nilsson and the Woods-Saxon potential conceals the fact that the extrema are not always found at corresponding ϵ_3 and ϵ_4 values though the dependence on the most important deformation parameter ϵ or α_2 is essentially the same for both potential types.

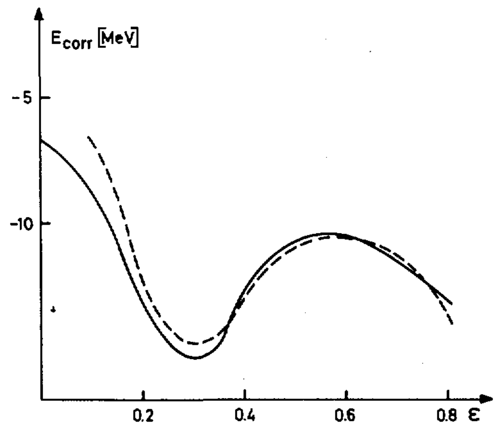

FIG. 6. Total shell correction for ^{170}Yb as a function of ϵ ($\epsilon_3 = 0$, $\epsilon_4 = 0$). The solid line corresponds to the Nilsson potential, the dotted line to the Woods-Saxon potential (with the α_ν converted into the ϵ_ν).

4. DEFORMATION ENERGIES AND FISSION BARRIERS

The liquid-drop part of the deformation energy contains the surface term

$$E_s = \left\{ -\tilde{\gamma} + \tilde{\eta} \left(\frac{N-Z}{A} \right)^2 \right\} A^{2/3} (g-1) \tag{14}$$

and the Coulomb term

$$E_c = 0.864 \frac{Z^2}{R_0 A^{\frac{1}{3}}} (1-f) \tag{15}$$

The shape-dependent quantity g is the ratio of the surface of the deformed drop to the surface of the sphere with the same volume; correspondingly, f is defined as the ratio of the Coulomb energy of a homogeneously charged deformed drop to the Coulomb energy of the undeformed drop. Tables I and II give some values of f and g in terms of the deformation parameters ϵ, ϵ_3, ϵ_4, which have been evaluated by numerical integration.

The parameters $\tilde{\gamma}$, $\tilde{\eta}$, and R_0 were taken from the work of Seeger and Perisho [7]:

$\tilde{\gamma} = 20.067$ MeV $\quad\quad \tilde{\eta} = 47.883$ MeV $\quad\quad R_0 = 1.193$ fm

Another set of parameters which is often used is the one given by Myers and Swiatecki [2]:

$\tilde{\gamma} = 17.94$ MeV $\quad\quad \tilde{\eta} = 31.99$ MeV $\quad\quad R_0 = 1.225$ fm

In Fig. 7 we show the total deformation energy of ^{236}U (minimized with respect to ϵ_3 and ϵ_4) as a function of ϵ for both parameters sets.

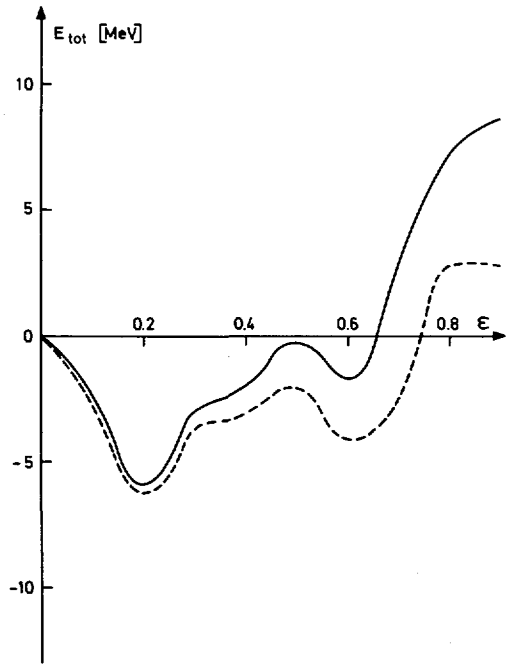

FIG.7. Total deformation energy of ^{235}U (minimized with respect to α_3 and α_4 for each α_2) as function of ϵ. The solid line is calculated with the liquid drop parameters of Seeger and Perisho, the dotted line with the parameters of Myers and Swiatecki.

Only for large deformations the two curves differ considerably. Therefore, also properties of strongly deformed nuclei should be used for the determination of the liquid-drop parameters, and not only ground state binding energies.

In Table III the positions and heights of minima and saddle points of the deformation energy surface are listed for several rare-earth and actinide nuclei. We have used the Hamiltonian (1) and Seeger and Perisho's liquid-drop parameters. The results should be compared with similar calculations in Ref.[3] where the parameters of Myers and Swiatecki are used. The fission barriers given in this paper came out about 6 MeV higher than in our calculations. As one should expect that the energy surface does not vary discontinuously if one goes from an even-even nucleus to its odd-even neighbour. Generally, the minima and maxima of the energy surface with respect to ϵ or α_2 are rather steep. Therefore, their ϵ values are well defined and do not depend on the type of potential used. As can be seen from Fig. 5 the shell correction depends very little on ϵ_3. Only for very large ϵ the inclusion of octupole deformation reduces the shell correction. But as the liquid drop part of the deformation energy favours symmetrical shapes all stationary points of the energy surfaces we have investigated do not correspond to pearshaped deformations[1]. For the

[1] During the completion of this manuscript we learned about a similar investigation by Nilsson et al. [10] who obtained similar results.

TABLE I. THE SHAPE-DEPENDENT FACTOR g-1

ϵ_4	ϵ_3	$\epsilon = 0.0$	0.1	0.2	0.3	0.4	0.5	0.6	0.7	0.8	0.9
-0.034	0.0	0.0012	0.0033	0.00964	0.0207	0.0370	0.0593	0.0888	0.1270	0.1764	
	0.03	0.0019	0.0040	0.01042	0.0215	0.0379	0.0604	0.0901	0.1286	0.1785	
	0.06	0.0039	0.0062	0.12774	0.0241	0.0408	0.0636	0.0940	0.1335		
0.0	0.0	0.0	0.0018	0.0074	0.0171	0.0315	0.0510	0.0767	0.1098	0.1523	
	0.03	0.0006	0.0025	0.0081	0.0179	0.0323	0.0520	0.0768	0.1111	0.1539	
	0.06	0.0026	0.0046	0.0103	0.0203	0.0349	0.0648	0.0801	0.1151	0.1589	
0.034	0.0	0.0011	0.0028	0.0078	0.0165	0.0293	0.0466	0.0692	0.0983	0.1353	
	0.03	0.0017	0.0034	0.0085	0.0173	0.0301	0.0474	0.0702	0.0994	0.1367	
	0.06	0.0035	0.0054	0.0106	0.0195	0.0324	0.0500	0.0731	0.1028		
0.050	0.0							0.0670	0.0943	0.1290	0.1733
	0.06							0.0707	0.0985	0.1341	0.1795
0.068	0.0							0.0657	0.0915	0.1241	0.1657
	0.06							0.0692	0.0954	0.1288	0.1713
0.085	0.0							0.0654	0.0897	0.1205	0.1595
	0.06							0.0687	0.0934	0.1248	0.1647

TABLE II. THE SHAPE-DEPENDENT FACTOR 1-f

ϵ_4	ϵ_3	0.0	0.1	0.2	0.3	0.4	0.5	0.6	0.7	0.8	0.9
-0.034	0.0	0.0002	0.0012	0.0044	0.0100	0.0185	0.0304	0.0462	0.0669	0.0937	
	0.3	0.0004	0.0015	0.0047	0.0104	0.0189	0.0308	0.0468	0.0677	0.0948	
	0.06	0.0010	0.0022	0.0054	0.0113	0.0200	0.0322	0.0486	0.0701		
0.0	0.0	0.0	0.0009	0.0038	0.0090	0.0167	0.0275	0.0418	0.0604	0.0841	
	0.03	0.0002	0.0011	0.0041	0.0093	0.0171	0.0279	0.0423	0.0610	0.0849	
	0.06	0.0007	0.0018	0.0048	0.0101	0.0180	0.0290	0.0437	0.0628	0.0842	
0.034	0.0	0.0002	0.0011	0.0038	0.0086	0.0158	0.0258	0.0389	0.0559	0.0774	
	0.03	0.0004	0.0013	0.0040	0.0089	0.0161	0.0261	0.0393	0.0564	0.0780	
	0.06	0.0009	0.0019	0.0047	0.0096	0.0170	0.0271	0.0405	0.0578		
0.05	0.0							0.0380	0.0542	0.0749	0.1009
	0.06							0.0394	0.0560	0.0771	0.1038
0.068	0.0							0.0372	0.0529	0.0728	0.0977
	0.06							0.0386	0.0546	0.0748	0.1003
0.085	0.0							0.0368	0.0520	0.0711	0.0951
	0.06							0.0381	0.0535	0.0729	0.0974

TABLE III. POSITION OF STATIONARY POINTS ON THE ENERGY SURFACE

Nucleus	Ground state		First barrier	Isomeric state			Second barrier		
	ϵ	ϵ_4	Height above ground state (MeV)	ϵ	ϵ_4	Height above ground state (MeV)	ϵ	ϵ_4	Height above ground state (MeV)
^{154}Sm	0.2	-0.035							
^{170}Yb	0.25	0.0							
^{186}Os	0.2	0.05							
^{230}Th	0.2	-0.035	2.0	flat region			1.0	0.1	
^{232}Th	0.2	-0.035	2.5	flat region			1.0	0.1	
^{235}U	0.2	-0.04	5.0	0.6	0.06	4	0.9	0.1	14
^{236}U	0.2	-0.04	4.5	0.6	0.06	3.5	0.9	0.1	15
^{239}Pu	0.2	-0.035	5.5	0.6	0.065	4	0.95	0.1	13
^{246}Cm	0.2	-0.015	7.0	0.55	0.075	5	0.9	0.1	12.5
^{247}Cm	0.2	-0.015	7.0	0.55	0.075	5.5	0.9	0.1	12.5
^{257}Md	0.2	-0.015	7.5	0.65	0.085	5	0.9	0.1	9

Woods-Saxon potential the dependence of the shell correction on the octupole deformation is more pronounced. Therefore an instability against asymmetric deformations occurs for very large α_2. No systematic investigation of the stability of saddle-point shapes against pearshaped deformations has been performed with the Woods-Saxon potential for a larger number of nuclei. Therefore no definite results can be reported.

The hexadecapole dependence of the shell correction with the Nilsson potential is only pronounced near the ground state. For large ϵ the ϵ_4-dependence of the deformation energy is mainly due to the liquid-drop energy.

This work is being continued with the Woods-Saxon potential and larger and more complicated deformations. Especially, the inclusion of non-axially symmetric deformations might possibly lower the fission barriers given in Table III.

ACKNOWLEDGEMENTS

The authors are indebted to Dr. F. Dickmann for his kind permission to use his computer code for the solution of the BCS equations and to Miss A. Eickhoff, F. Sichelschmidt, and K. Möhring for their help with the numerical calculations.

APPENDIX

In the following we give some details of the evaluation of single-particle spectra and of the quantities f and g in the expressions for the liquid-drop energies.

The single-particle Hamiltonians with deformed oscillator and Woods-Saxon potentials were diagonalized in the spherical harmonic oscillator representation. All oscillator states of the first 13 main shells were taken into account. The inclusion of the 14th shell was found to have little influence on the single-particle levels near the Fermi surface of heavy nuclei for the range of deformation parameters investigated.

The central part of the Woods-Saxon potential was expanded in Legendre polynomials.

$$f(r, \vartheta) = \sum_{\mu=0}^{\mu_{max}} g_\mu(r) P_\mu(\cos\vartheta) \tag{17}$$

In all calculations the choice $\mu_{max} = 6$ turned out to be sufficient. For reasons of computational simplicity the Thomas term in Eq. (3) was replaced by $\kappa V_0 r^{-1} (\vec{l} \cdot \vec{\sigma}) df/dr$. The parameters α_0 and α_1 were determined from the requirement that the equipotential volume and the centre of mass must be independent of deformation. To lowest order in α_2, α_3, and α_4 one obtains

$$\alpha_0 = -\sum_{\lambda=1}^{4} \frac{\alpha_\lambda^2}{2\lambda+1} \tag{18}$$

$$\alpha_1 = -\alpha_3 \frac{\frac{54}{35}\alpha_2 + \frac{24}{21}\alpha_4}{1 + \frac{12}{15}\alpha_2} \tag{19}$$

In a similar way one finds for the Nilsson potential

$$\epsilon_1 = \epsilon_3 \frac{\frac{8}{7}\epsilon_4 - \frac{18}{35}\epsilon}{1 + \frac{17}{15}\epsilon} \tag{20}$$

The quantity f contains a one-dimensional integral, which is evaluated by 40 point Gauss-Legendre quadrature. The two radial integrals contained in g can be calculated analytically. The remaining three-dimensional angular integral is evaluated by a $40 \times 40 \times 40$ Gauss-Legendre quadrature after removing the singularities of the integrand by subtraction of the corresponding integral for the sphere.

REFERENCES

[1] STRUTINSKY, V.M., Yad. Fiz. 3 (1966) 614; Ark. Fys. 36 (1967) 629; Nucl. Phys. A95 (1967) 420; Nucl. Phys. A122 (1968);
MUZICHKA, Y.A., PASHKEVICH, V.V., STRUTINSKY, V.M., preprint P7-3733 Dubna (1968).

[2] MYERS, W.D., SWIATECKI, W.J., Nucl. Phys. 81 (1966) 1; Ark. Fys. 36 (1967) 343.

[3] NILSSON, S.G., NIX, J.R., SOBICZEWSKI, A., SZYMAŃSKI, Z., WYCECH, S., GUSTAFSON, C., MÖLLER, P., Nucl. Phys. A115 (1968) 545;
NILSSON, S.G., Varenna Lectures, Course 40 (1968); preprint UCRL - 18355 Berkeley (1968).

[4] NILSSON, B., Nucl. Phys. A129 (1969) 445.

[5] BES, D., SZYMANSKI, Z., Nucl. Phys. 28 (1961) 42.
SZYMAŃSKI, Z., Nucl. Phys. 28 (1961) 63.

[6] NILSSON, S.G., Mat Fys. Medd. Dan. Vid. Selsk. 29 16 (1955).

[7] SEEGER, P.A., PERISHO, R.C., in Atomic Masses (Proc. 3rd Int. Conf. Winnipeg, 1967) 85.

[8] DICKMANN, F., DIETRICH, K., Nucl. Phys. A129 (1969) 241.

[9] FAESSLER, A., SHELINE, R., Phys. Rev. 148 (1966) 1003.

[10] NILSSON, S.G., TSANG, C.H., SOBICZEWSKI, A., SZYMAŃSKI, Z., WYCECH, S., GUSTAFSON, C., LAMM, I.L., MÖLLER, P., NILSSON, B., preprint Berkeley (1969).

DISCUSSION

E.R.H. HILF: The parameters of the "liquid-drop" part of the nuclear binding energy, say surface tension σ and the curvature tension γ, can be determined in two ways:

(1) In using experimental data for a fit, one has to seek processes where these tensions really come into play, i.e. where the surface and curvature of the nucleus are changed substantially, as during the fission process. So from the experimental threshold energies one gets $\sigma = 17.8$ MeV and $\gamma = 6.8$ MeV [H. von Groote and E. R. H. Hilf, Nucl. Phys. 129 (1969)]. A fit neglecting the curvature tension always leads to discrepancies;

(2) Since the liquid-drop model is nothing other than the shell model using the leptodermous assumption $A^{1/3} \gg 1$, one can determine σ and γ theoretically from the shell model. Using the realistic, velocity-dependent, self-consistent shell model potential, we arrived at $\sigma = 17.8$ MeV [S. Knaak, G. Süssmann, E.R.H. Hilf and H. Büttner, Phys. Lett. 23 (1966)].

H. J. KRAPPE: I prefer to take the liquid-drop energy parameters as phenomenological constants, which should be fitted to experimental barrier heights and excitation energies of the fission isomers. Single-particle models seem to be less suitable for calculating surface properties because correlations, especially α-correlations, must be expected to play an essential role in the dynamics of the nuclear surface.

U. MOSEL: Would you agree that the violation of parity conservation due to the dipole and the octupole terms in your Hamiltonian (1) could lead to some spurious structure in your total energy?

H. J. KRAPPE: The uncertainty regarding the deformation energy due to spurious states comes not only from parity violation but also from the lack of spherical symmetry. It is of the order of the corresponding collective excitation energies, which are some 10 keV. Therefore, the uncertainties attaching to the shell-model parameters are expected to have a larger effect on the deformation energy than the spurious states.

MASS AND INERTIA PARAMETERS FOR NUCLEAR FISSION

J. DAMGAARD, H.C. PAULI,* V.M. STRUTINSKY,†
C.Y. WONG,** M. BRACK,* A. STENHOLM-JENSEN
The Niels Bohr Institute,
University of Copenhagen, Denmark

Abstract

MASS AND INERTIA PARAMETERS FOR NUCLEAR FISSION. The effective mass parameter and the moments of inertia for a deformed nucleus are evaluated using the cranking-model formalism. Special attention is paid to the dependence of these quantities on the intrinsic structure, which may arise due to shells in deformed nuclei. It is found that these inertial parameters are very much influenced by the shells present. The effective-mass parameter, which appears in an important way in the theory of spontaneous fission, fluctuates in the same manner as the shell-energy corrections. Its values at the fission barrier are up to two or three times larger than those at the equilibrium minima. This correlation comes about because for the effective mass the change in the local density of single-particle states is very important, much more so than the change in the pairing correlation. The moments of inertia which enter in the theory of angular anisotropy of fission fragments, also fluctuate as a function of the deformation. At low temperatures, the fluctuation is large and shows a distinct but more complicated correlation with the shells. At high temperatures, the moments of inertia fluctuate with a smaller amplitude about the rigid-body value in correlation with the energy-shell corrections. For the first and second barriers, the rigid-body values are essentially reached at a nuclear temperature of 0.8 to 1.0 MeV.

1. INTRODUCTION

Large-scale collective motion associated with the fission process puts it a special position among other nuclear phenomena. The shape of the nucleus changes very appreciably and to describe the related flow of the nuclear matter, one should know the dynamics of this non-stationary process.

To study the dynamics of such a process, its multi-dimensionality is very important. Consequently, the trajectory can be found only if all $\frac{1}{2}n(n+1)$ mass parameters are known for the n degrees of freedom introduced in the definition of the shape of the nucleus. It is not simple to solve the relevant dynamic equations even for the very unrealistic case of the incompressible classical liquid-drop nucleus with an irrotational flow. In real nuclei, it is even more complicated because the effective mass parameters will be greatly influenced by the intrinsic structure, particularly by the shells present in the deformed nucleus.

At lowest excitations, especially in the case of spontaneous fission, an adiabatic motion is assumed. This allows one to use a simple cranking model theory [1] for the mass parameters related to generalized deformation co-ordinates. Some results of the numerical calculations of these quantities are described here. Special emphasis is laid on providing simple physical interpretations in order to pave a way for the complete theory of

---

* On leave from the University of Basel, Switzerland.
† On leave from the I. V. Kurchatov Institute for Atomic Energy, Moscow, USSR.
** On leave from Oak Ridge National Laboratory, USA.

the process in the future and to give a more solid basis for extrapolations to large and fancy distortions of the nucleus in fission or to unknown regions of nuclei. To illustrate these points, some calculations were performed for a simple case of the large ellipsoidal distortion of the Nilsson potential, a case considered recently also by Sobiczewski et al. [2]. Calculations with the Saxon-Woods type potential have been performed also but will not be presented here.

There is another closely related problem which is also relevant to other aspects of the fission process. This is the problem of the effect of intrinsic structure on the moments of inertia of a nucleus, which appear, for example, in the theory of angular distribution of the fission fragments. To study the dependence of the moment of inertia on deformation and excitation of a nucleus, we have performed calculations, also with the cranking-model formula, by using a Nilsson potential with ellipsoidal deformation. Calculations performed with the Saxon-Woods type potential, for a more general deformation of the nuclear surface, are in progress.

More detailed results will be published elsewhere. Qualitative discussion of the subject matter can also be found in Ref. [3].

2. EFFECTIVE MASS PARAMETER

In the adiabatic description of the collective behaviour of a nucleus, the nucleons are assumed to move in a uniform average non-spherical field. Vibrations and rotational motion are then described in terms of changes in this average field. We start with a Hamiltonian which may include effects of residual interaction, such as the pairing interaction. Next, the potential in which the particles move is set in motion. One obtains the increase in the energy of the system in the second-order terms in the time derivatives of the collective co-ordinates q_i:

$$K = \frac{1}{2} \sum_{i,j=1}^{n} B_{ij} \dot{q}_i \dot{q}_j \tag{1}$$

which is identified with the kinetic energy of the collective motion. The formula for the effective mass parameters is [1]

$$B_{ij} = 2\hbar^2 \sum_m \frac{\langle 0|\partial/\partial q_i|m\rangle\langle m|\partial/\partial q_j|0\rangle}{E_m - E_0} \tag{2}$$

where $|0\rangle$ is the ground state and $|m\rangle$ is an excited state of the system.

In Eq. (2), no specific assumptions are made concerning the wave functions $|m\rangle$ of the system, provided that their dependence on the collective variables q_i is known.

The collective degrees of freedom q_i are usually introduced by means of the Lagrange multiplier method [4]. Thus, the nucleons are put into an external field which restricts the intrinsic motion in such a way that the collective variables are kept constant and have given values.

However, in practical applications when the shell model is used, one has already such a field; this is the average field of the model which is assumed to be the same for all single-particle states near the Fermi energy. Therefore, the parameters which appear in the definition of the average field, especially those which describe its shape, can be considered as collective adiabatic variables. The response of the system to slow changes of the shape can be determined directly from the cranking-model formula (2), where the wave functions are adiabatic solutions for the fixed deformed shell-model field.

In practical applications of the cranking-model formula, one usually assumes that the excited states of the even-even system are combinations of two-quasiparticle excitations $|\mu\nu\rangle$ with the energy $E_\mu + E_\nu$, where $E_\mu = \sqrt{(\epsilon_\mu - \lambda)^2 + \Delta^2}$. Here, ϵ_μ is the single-particle energy, λ and Δ are the Fermi energy and the pairing gap of the system. With this assumption, we obtain the matrix elements for the operator $\partial/\partial q_i$ as [5]

$$\left\langle \mu\nu \left| \frac{\partial}{\partial q_i} \right| 0 \right\rangle = - \frac{U_\mu V_\nu + U_\nu V_\mu}{E_\mu + E_\nu} \left(\frac{\partial H}{\partial q_i}\right)_{\mu\nu} \qquad \text{for } \mu \neq \nu \tag{3}$$

where $(\partial H/\partial q_i)_{\mu\nu}$ is the matrix element of $\partial H/\partial q_i$ between single-particle states $|\mu\rangle$ and $|\nu\rangle$. In the case when $E_\mu = E_\nu$ (or when one quasi-particle is the time reversed state of the other), one has non-vanishing matrix elements of $\partial/\partial q_i$ due to the variation of the occupation amplitudes U and V with respect to deformation. The result is [5]

$$\left\langle \nu\nu \left| \frac{\partial}{\partial q_i} \right| 0 \right\rangle = \frac{1}{2E_\nu^2} \left[- \Delta \left(\frac{\partial H}{\partial q_i}\right)_{\nu\nu} + \Delta \frac{\partial \lambda}{\partial q_i} + (\epsilon_\nu - \lambda) \frac{\partial \Delta}{\partial q_i} \right] \tag{4}$$

where

$$\frac{\partial \lambda}{\partial q_i} = \frac{-(ac_i + bd_i)}{a^2 + b^2}; \qquad \frac{\partial \Delta}{\partial q_i} = \frac{ad_i - bc_i}{a^2 + b^2}$$

$$a = \Delta \sum_\nu \frac{1}{E_\nu^3}, \qquad b = \sum_\nu \frac{\epsilon_\nu - \lambda}{E_\nu^3}$$

$$c_i = -\Delta \sum_\nu \frac{(\partial H/\partial q_i)_{\nu\nu}}{E_\nu^3} \qquad d_i = \sum_\nu \frac{(\partial H/\partial q_i)_{\nu\nu}(\epsilon_\nu - \lambda)}{E_\nu^3}$$

Therefore, the effective mass is given by

$$\begin{aligned} B_{ij} = 2\hbar^2 \Bigg\{ & \sum_{\mu\nu} \frac{(\partial H/\partial q_i)_{\mu\nu} (\partial H/\partial q_j)_{\nu\mu}}{(E_\mu + E_\nu)^3} (U_\mu V_\nu + U_\nu V_\mu)^2 \\ & + \frac{1}{8} \sum_\nu \frac{1}{E_\nu^5} \Bigg[\Delta^2 \frac{\partial \lambda}{\partial q_i} \frac{\partial \lambda}{\partial q_j} + (\epsilon_\nu - \lambda)^2 \frac{\partial \Delta}{\partial q_i} \frac{\partial \Delta}{\partial q_j} \\ & + \Delta(\epsilon_\nu - \lambda) \left(\frac{\partial \lambda}{\partial q_i} \frac{\partial \Delta}{\partial q_j} + \frac{\partial \lambda}{\partial q_j} \frac{\partial \Delta}{\partial q_i} \right) - \Delta^2 \left\{ \left(\frac{\partial H}{\partial q_i}\right)_{\nu\nu} \frac{\partial \lambda}{\partial q_j} + \left(\frac{\partial H}{\partial q_j}\right)_{\nu\nu} \frac{\partial \lambda}{\partial q_i} \right\} \\ & - \Delta(\epsilon_\nu - \lambda) \left\{ \left(\frac{\partial H}{\partial q_i}\right)_{\nu\nu} \frac{\partial \Delta}{\partial q_j} + \left(\frac{\partial H}{\partial q_j}\right)_{\nu\nu} \frac{\partial \Delta}{\partial q_i} \right\} \Bigg] \Bigg\} \end{aligned} \tag{5}$$

which, for the sake of convenience, can be written as

$$B_{ij} = \sum_{\mu\nu} (M_{ij})_{\mu\nu}$$

The effective mass formula (5) can be generalized to the case where the excitation of a nucleus can be described in terms of a nuclear temperature T. The resulting formula is

$$B_{ij}(T) = \frac{1}{2} \sum_{\mu\nu} (M_{ij})_{\mu\nu} \left(\tanh \frac{E_\mu}{2T} + \tanh \frac{E_\nu}{2T} \right)$$
$$+ \sum_{\mu \neq \nu} (U_\mu U_\nu - V_\nu V_\mu)^2 \frac{(\partial H/\partial q_i)_{\mu\nu} (\partial H/\partial q_j)_{\nu\mu}}{(E_\mu - E_\nu)^3} \left(\tanh \frac{E_\mu}{2T} - \tanh \frac{E_\nu}{2T} \right) \quad (6)$$

where the occupation amplitudes U and V, and E depend on the temperature indirectly through the dependence of Δ and λ on T.

It is easy to see that, for the pure independent-particle motion, the values of the mass parameters obtained with the formulas (2) or (5) should be abnormally small. Indeed, the mass parameters are directly related to the derivatives of the wave functions with respect to the deformation parameters. In the pure independent-particle model (IPM), these are known to be very small. (An exceptional case occurs when two proper levels cross.) This is different when there are residual interactions the most important of which is the pair correlation. With the pair correlations, the composition of the nuclear wave functions changes more strongly with the deformation. In this cause, the predominant contribution to the effective mass comes from the diagonal matrix elements within an energy interval of 2Δ near the Fermi energy. This corresponds to a relatively small energy denominator in Eq.(5), of the order of 2Δ, instead of a value of $2\hbar\omega$ for the pure IPM, and leads to increased values of the mass parameters, in comparison with the very low values of the IPM. This is so, however, only because it is the IPM value which is too low, and as soon as some pairing correlations are present, the dependence of the mass parameters on the strength of the residual interaction is much more moderate. In fact, the mass parameters decrease with further increase of the pair correlation strength.

The pairing effect disappears when a certain critical temperature is reached. In this case, it is inappropriate to apply formula (6) because residual interactions other than pairing become important. The treatment of these residual interactions is beyond the scope of the present study. We shall therefore limit our attention to the cases with a significant pairing gap, in the hope that the other residual interactions are less important.

A simple approximate expression is known for the mass parameter, when the pairing gap is sufficiently large ($\Delta \gg G$, where G is the pairing matrix element). The latter condition ensures that the terms with $\partial\Delta/\partial q$ and $\partial\lambda/\partial q$ in Eq.(5) are small so that the main contribution comes from the first sum. There, the most important are the diagonal matrix elements arising from single-particle states in an energy interval of 2Δ at the Fermi sea. Let g_{eff} be some effective local density of single-particle states near the Fermi sea and $\overline{|\partial H/\partial q|^2}$ the average of the square of the matrix elements for these states. Since the factor involving the occupation numbers U and V is of the order of unity and the energy denominator is of the order of 2Δ, we have

$$B \sim \frac{\hbar^2}{2} \overline{\left|\frac{\partial H}{\partial q}\right|^2} \frac{g_{eff}}{\Delta^2} + \delta \tag{7}$$

where the second term, which is approximately constant and very small compared to the first term, denotes all other contributions.

In some cases in the deformed region, there is a significant shell in the single-particle spectrum so that the pairing gap is very small. We have then essentially the case of the IPM. If now proper levels cross each other at the Fermi sea, the terms in Eq.(5) involving $\partial\lambda/\partial q$ and $\partial\Delta/\partial q$ become much larger than the first sum since the wave function changes drastically with deformation. No simple expression such as Eq.(7) is obtained as the mass parameter becomes singular. In that case, it is inappropriate to apply expressions (6) and (7) because residual interactions other than pairing become important. The treatment of these residual interactions is beyond the scope of the present study. We shall therefore limit our attention to the cases when a significant pairing gap is present ($\Delta > 0.3$ MeV, say) in the hope that the other residual interactions are less important.

The pairing effect disappears when a certain critical temperature is reached. The method cannot be applied to temperatures higher than the critical temperature for reasons mentioned above. In this work, we shall consider mass parameters at zero temperature only.

The correspondence between this equation and the numerical calculations is illustrated in Figs 1-3. There, the mass parameters are shown evaluated for the case of ellipsoidal distortion of the Nilsson potential well. As the deformation coordinate ρ, we have taken one half of the distance between the centres of mass of the two halves of the nucleus, divided by the value of the undeformed radius[1]. The specific choice of the deformation parameter is not very essential[2]. For another deformation parameter x, the relevant mass coefficient is related to B in the following way:

$$B_x = B_\rho \left(\frac{d\rho}{dx}\right)^2 \tag{8}$$

Figure 1 shows the dependence of the calculated mass parameter B_ρ on the parameter $\tilde{\Delta}$ which characterizes the strength of the pairing correlation ($\tilde{\Delta}$ is the energy gap parameter for a uniform distribution

---

[1] A convenient unit of reference for the effective mass is the reduced mass for two equal fragments at large distance, which is equal to

$$B_\rho = 0.0240\ r_0^2 A^{5/3} (\hbar^2/\text{MeV})$$

[2] The use of the ϵ-parameter of the Nilsson model is rather inconvenient. With the ϵ-parameter defined in a finite interval $\epsilon \leq 1.5$, one obtains [2] a spurious divergence of B_ϵ at larger values of ϵ, which makes it difficult to see any finer structure.

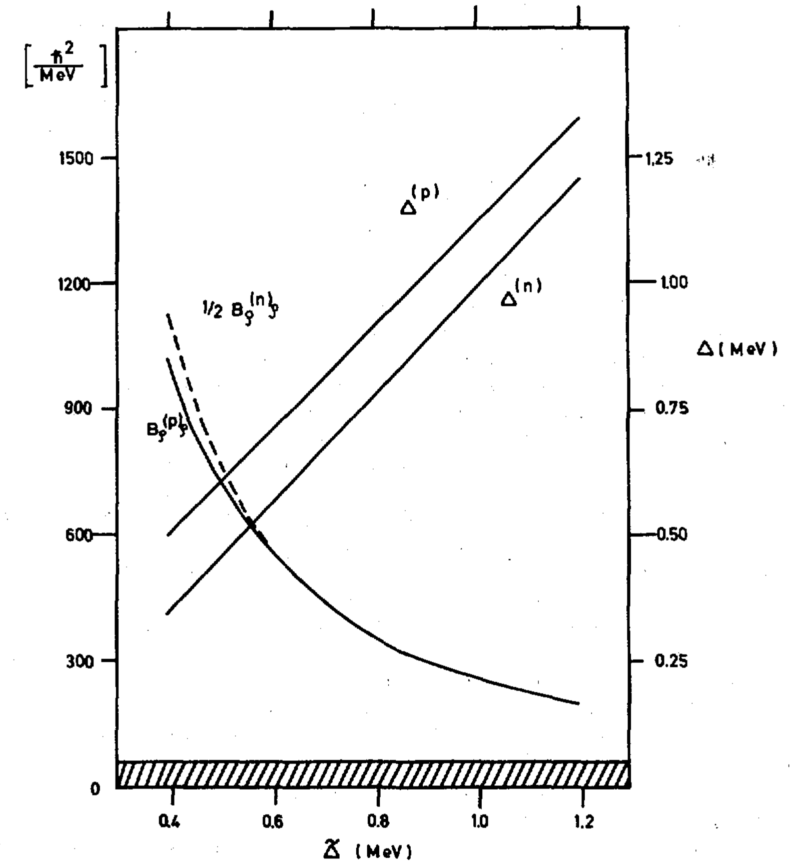

FIG. 1. Mass parameter B_ρ multiplied by ρ shown as a function of Δ. The calculation was performed for N = 146 and Z = 94 at a deformation of $\rho = 0.45$ corresponding to $\epsilon = 0.28$. The gap parameters $\Delta^{(n)}$ and $\Delta^{(p)}$ are also shown here. It can be seen that after subtracting a value represented by the shaded region, the quantity B_ρ^ρ behaves like $\tilde{\Delta}^{-2}$.

of the single-particle states). For larger values of Δ, they are in clear agreement with Eq. (7). This seems, however, to contradict the results shown in Fig.2 where the same quantities together with the shell corrections to the nuclear binding energy ($\delta U + \delta P$) are presented as functions of the deformation. Very significant fluctuations are clearly seen, the larger values of B_ρ^ρ coinciding approximately with the larger values of the Δ parameter, evaluated for the same deformations. This apparent contradiction is resolved if the fact is taken into account that the effective energy region in Eq. (5) is very small — of the order of 2Δ — and the level density for such an energy interval g_{eff} shows very strong oscillations due to shell structure (see, e.g. Ref. [6]). This is a more important effect than the changes of Δ. The importance of the shell structure is further evidenced by the correlations between the fluctuations of the effective-mass parameters and their corresponding shell-energy corrections which are known to be roughly proportional to the fluctuations of the local level density near the Fermi energy [6].

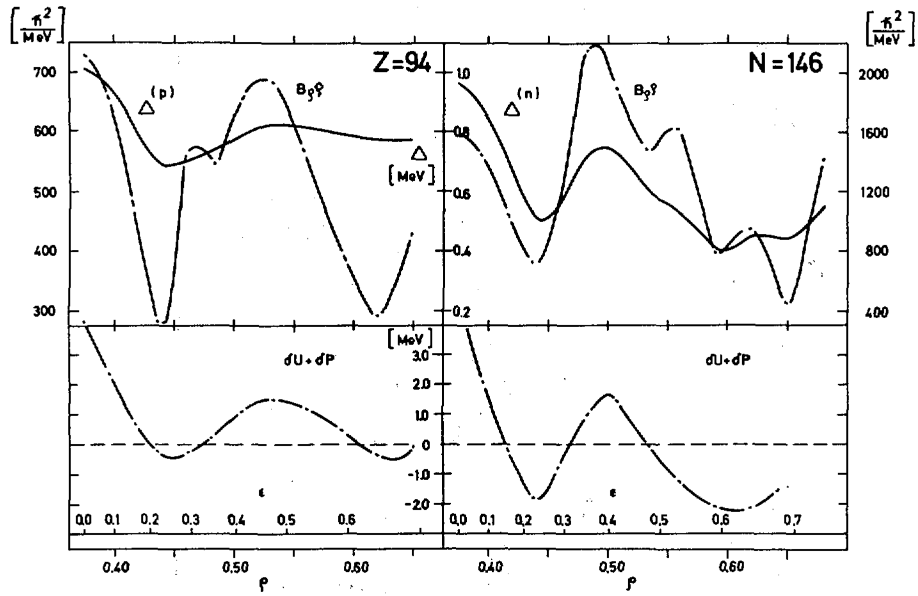

FIG. 2. In the upper diagrams the quantities B_ρ^ρ and Δ for Z = 94 and N = 146 are shown as functions of the parameters ρ and ϵ. The corresponding shell corrections are shown below.

Even though the energy gap Δ has a strong exponential dependence on the density of single-particle states, the charge in Δ is a less important factor here. This can be understood because, in the BCS pairing theory, and energy interval much larger than 2Δ is essential. Therefore, the effective level density which appears in the BCS equation should be identified with a much more smoothed density function rather than the local density g_{eff} which appears in Eq.(7) and also in the energy shell corrections.

In Fig. 3, some results obtained by Sobiczewski et al. are also shown, These data were re-evaluated by means of Eq.(8) from B_ϵ values presented in Ref.[2]. While the average value, which is equal to about 15 units of the reduced mass, seems to agree with our results for $\tilde{\Delta}$ = 0.6 MeV (which gives the correct value for Δ at the ground-state deformation), some essential discrepancy is evident[3]. This should change appreciably the estimates of same spontaneous fission lifetimes given in Ref.[2].

[3] The equation used in Ref.[2] for evaluating the effective mass can be written schematically as follows

$$B_\epsilon \approx (2\hbar^2 \Sigma_3)\left(\frac{dQ/d\epsilon}{2\Sigma_1}\right)^2 \quad (9)$$

It can be shown that up to the first order in ϵ the second factor in Eq.(9) should be equal to the square of the constant κ which characterizes the strength of the coupled deformed field. (This is true also when the corrections due to pairing are taken into account.) Therefore, Eq.(9) is, up to a smooth function of the deformation, identical to our Eq.(5). In Ref. [2], however, the ratio in the second factor was determined numerically. The result may be erroneous owing to some inaccuracy in evaluating the poorly converging term Σ_1.

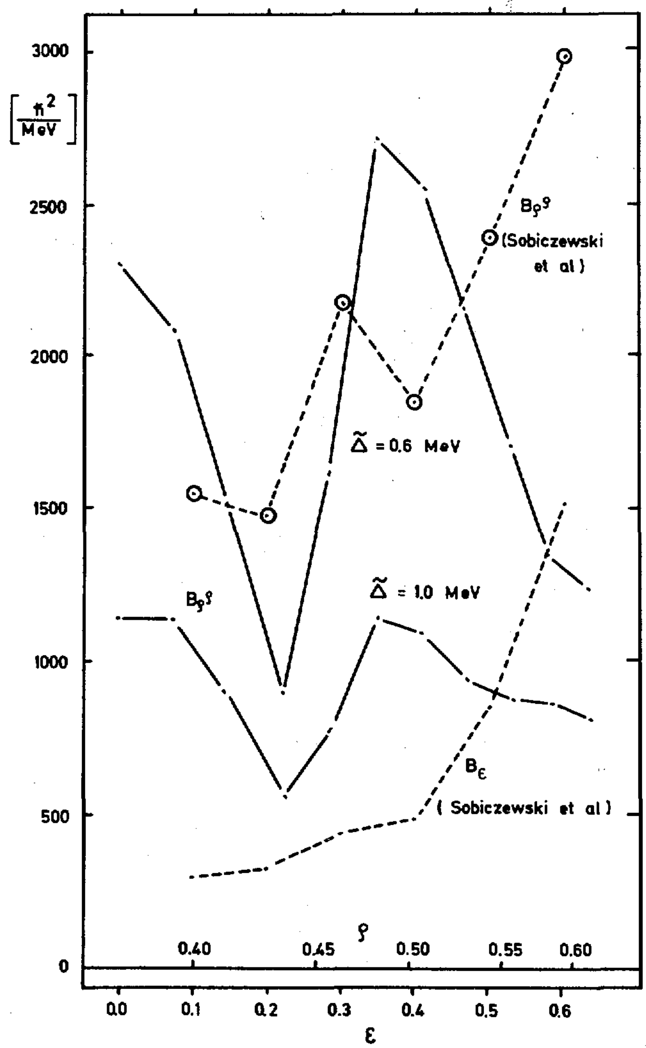

FIG. 3. The solid curves are the calculated values of B_ρ^ρ for ^{240}Pu for the cases when $\tilde{\Delta}$ is equal to 0.6 and 1.0 MeV. The lower dotted curve is the quantity B_ϵ obtained by Sobiczewski et al. It is a rapidly increasing function of ϵ. This quantity B_ϵ can be converted to B_ρ^ρ as shown in the upper dotted curve and should be compared with our results.

The results shown in Figs 2 and 3 lead us to the important conclusion that the effective mass parameters are abnormally large near the top of the shell maxima in the deformation energy where the local level density is large. They decrease when one moves away from this point and the lowest value is obtained near the stationary shape minima of the deformation energy, corresponding to the ground-state deformation or the second minimum. The increased inertia of the nuclear matter in the region of the potential barriers is very important for estimates of the penetrability, especially in the superheavy elements.

For more definite estimates of the penetration factor, the problem of the trajectory must be considered, which requires the knowledge of the mass parameters related to other degrees of freedom. In addition, other single-particle models must also be considered, as the Nilsson model is too ambiguous to be used without reservation for the extrapolations to large deformations and new regions of nuclei.

To approach the solution of these problems, an attempt was made to develop fast numerical methods for solving the IPM with a rather generally defined average field and the shape of the nuclear surface [7], and, at the same time, to evaluate the mass parameters related to the generalized deformation co-ordinates q_i which might appear in the definition of the nuclear shape. In these calculations, the surface of the nucleus was defined by the equation

$$\Pi_{q_1 \ldots q_n}(u, v) = 0 \tag{10}$$

where u and v are the two cylindrical co-ordinates. The operators $\delta H/\delta q_i$ which appear in Eq.(5) are also computed in a rather general manner. The calculations with the Saxon-Woods model are now in progress and will be published elsewhere.

3. MOMENTS OF INERTIA

The anisotropy of the angular distribution of the fission fragments at higher excitations is determined by the value of the so-called effective moment of inertia [8]

$$\mathscr{I}_{eff} = \left(\frac{1}{\mathscr{I}_{\parallel}} - \frac{1}{\mathscr{I}_{\perp}}\right)^{-1} \tag{11}$$

where $\mathscr{I}_{\parallel}$ and $\mathscr{I}_{\perp}$ are two moments of inertia for rotation about the symmetry axis (or the fission axis) and the axis perpendicular to the symmetry axis, respectively. For $\mathscr{I}_{\parallel}$ and $\mathscr{I}_{\perp}$, the rigid-body values are usually assumed, and $\mathscr{I}_{eff}$ is then rather strongly dependent on the shape of the nucleus at the top of the fission barrier [8]. It becomes infinite when the saddle shape is spherical. This should be the case of a nucleus which is very unstable against fission. For such a nucleus, isotropic angular distribution is predicted and recently some attempts were made to determine the limits of stability of nuclei by measuring the angular anisotropy of highly excited nuclei produced in nuclear reactions with α-particles and heavy ions [10-12].

Experimental studies of $\mathscr{I}_{eff}$ are very important in view of the fact that they are probably the most direct way of investigating the shape of the nucleus at the barrier. However, this quantity may be also affected by the shell structure, which may be misinterpreted as due to a different shape of the nucleus.

For the inertia parameters, the following equation holds (which is analogous to Eq. (6))

$$\mathscr{I}_i = \sum_{\mu\nu} \left\{ \frac{(U_\mu V_\nu - U_\nu V_\mu)^2}{2(E_\mu + E_\nu)} \left(\tanh \frac{E_\mu}{2T} + \tanh \frac{E_\nu}{2T} \right) + \frac{(U_\mu V_\nu + V_\mu V_\nu)^2}{2(E_\mu - E_\nu)} \left(\tanh \frac{E_\mu}{2T} - \tanh \frac{E_\nu}{2T} \right) \right\} |\langle \mu | M_i | \nu \rangle|^2 \qquad (12)$$

where the operator M_i is

$$M_\perp = j_x$$

for $\mathscr{I}_\perp$ and (13)

$$M_\parallel = j_z$$

for $\mathscr{I}_\parallel$. Here $\hat{j}$ is the single-particle angular momentum operator. From Eqs (12) and (13) one obtains a known expression for $\mathscr{I}_\parallel$

$$\mathscr{I}_\parallel = \frac{1}{4T} \sum_\nu \frac{K_\nu^2}{\cosh^2(E_\nu/T)} \qquad (14)$$

where $K_\nu = \langle \nu | j_z | \nu \rangle$.

The moment of inertia $\mathscr{I}_\parallel$ can also be expressed in the following way

$$\mathscr{I}_\parallel = \overline{K^2}\, g_T^{\mathrm{eff}} \qquad (15)$$

where

$$g_T^{\mathrm{eff}} = (1/4T) \sum_\nu \{1/\cosh^2(E_\nu/2T)\} \qquad (16)$$

and

$$\overline{K^2} = \left(\sum_\nu K_\nu^2/\cosh^2(E_\nu/2T) \right) \Big/ \sum_\nu \{1/\cosh^2(E_\nu/2T)\} \qquad (17)$$

In the case of $\Delta = 0$, the quasi-particle energies E_ν in Eqs (14) (17) are replaced by the single-particle energies $\epsilon_\nu - \lambda$.

In Fig. 4, some results of numerical calculations are presented which demonstrate the role of the shell structure and pairing for the specific case of N = 144 with the Nilsson potential. The quantities introduced above are plotted against the deformation of the Nilsson potential well for different values of the temperature T. (In applications to real processes, the temperature would, of course, also change with deformation.) Fluctuations with respect to deformation are apparent. However, the correlation between the fluctuations and the shell structure is not simple.

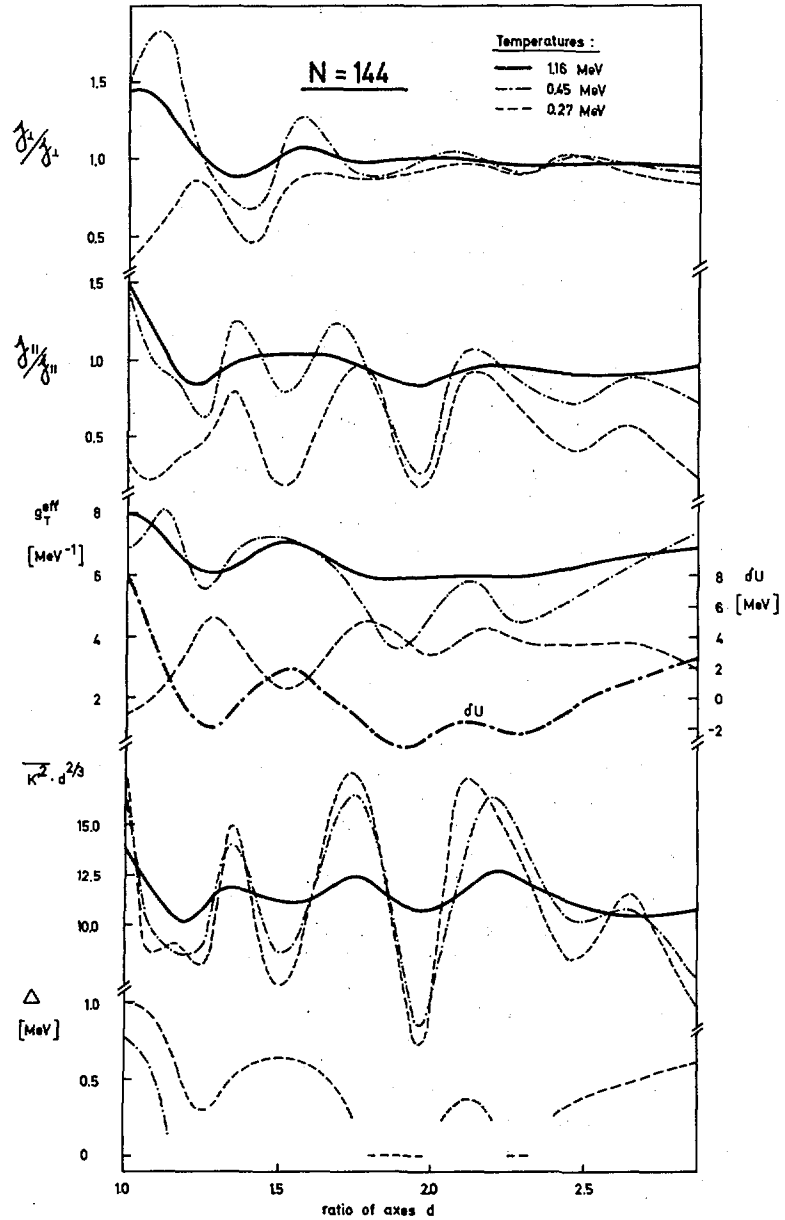

FIG.4. Moments of inertia and related quantities for N = 144 at three different temperatures are shown as functions of the deformation d which is defined as the ratio of the axes in the ellipsoidal Nilsson potential. The moments of inertia $\mathcal{J}_\perp$ and $\mathcal{J}_\parallel$ are expressed in units of the corresponding values $\tilde{\mathcal{J}}_\perp$ and $\tilde{\mathcal{J}}_\parallel$ for a rigid body with the same shape. The quantities g_T^{eff} and $\overline{K^2}$ are defined by Eqs (16) and (17), respectively. The gap Δ is calculated by taking $\tilde{\Delta}$ equal to 0.6 MeV. For T = 0.45 MeV, the gap Δ vanishes when the deformation is larger than 1.2 and is not shown in the figure. For the value of $\hbar\omega_0$ we used 55 $A^{-1/3}$ MeV which is obtained by setting the average of r^2 near the Fermi level equal to 3 $R_0^2/5$.

The gap parameter Δ is known to increase when the local density of the single-particle states near the Fermi energy increases. This can lead to a reversed effect in the quasi-particle density (16) which is exponentially decreasing with increasing Δ. Therefore, it is expected that at higher excitations, maxima and minima of $\mathscr{I}_{\parallel}$ should approximately correspond to those of the single-particle level density, while at low excitations maxima of $\mathscr{I}_{\parallel}$ correspond to minima of $g_{s.p.}$ (i.e. to maxima of the quasi-particle level density), and vice versa. While this is approximately valid for high excitations, the actual correlation at low excitations is more complicated because there is also a shell effect in the averaged value of K^2. Indeed, for low temperatures, only few states contribute to the averaging of K^2. It is known that the energies of the single-particle states with higher K values go up with deformation while those with lower K values go down. Therefore, the average value of K^2 oscillates about as frequently as that of the energy shell correction but with a different phase, see Fig. 4. The value of K^2 should have the WKB values in the middle of a shell but higher and lower values at other deformations depending on the number of nucleons N. The result for our case of N = 144 at low temperature is that for small deformations $\mathscr{I}_{\parallel}$ fluctuates in nearly the opposite phase as the energy shell correction.

For $\mathscr{I}_{\perp}$, and at low temperatures, it is known that an increase in Δ leads to a decrease in $\mathscr{I}_{\perp}$ [4]. However, this is not the only effect due to shell structure as the matrix elements of j_x are also affected. The situation is simpler at high temperatures as contributions to $\mathscr{I}_{\perp}$ come from matrix elements between states in a large energy interval. Therefore, as is the case with $\mathscr{I}_{\parallel}$, the quantity $\mathscr{I}_{\perp}$ is also correlated with the density of the single-particle states at the Fermi energy.

In any case, the shell structure influences rather strongly the moments of inertia. The fluctuation nevertheless decreases with increasing temperature. One of the problems is therefore to find the critical temperature T_s^* when the shell fluctuations become small. This is important to know for the analysis of the fission anisotropy at low excitations above the fission barrier. In these considerations, the dependence of Δ on the temperature should be taken into account in the usual way.

In Fig. 5, the quantities $\mathscr{I}_{eff}$, $\mathscr{I}_{\parallel}$ and $\mathscr{I}_{\perp}$ are shown as a function of the temperature T, evaluated for the most interesting shapes of the nucleus ^{236}U, namely the ground-state deformation, the second minimum and the two barriers. It can be seen that for the first and the second barriers, the rigid-body values of the moments of inertia are essentially reached at a nuclear temperature of $T_s^* \simeq 0.8 - 1.0$ MeV. This value is close to that for the critical temperature at which the shell-structure effects in the level density disappear as was found earlier [13]. It is also higher than the critical temperature T_c^*, at which the pair correlation effects disappear ($T_c^* \simeq 0.4 = 0.5$ MeV).

The evaluated moments of inertia are applied to the analysis of the angular anisotropy data in the neutron induced fission at lower excitations. The angular distribution of the fragments is described, in this case, approximately by [8]

$$1 + \frac{5E_n}{8T\mathscr{I}_{eff}} \cos^2\theta$$

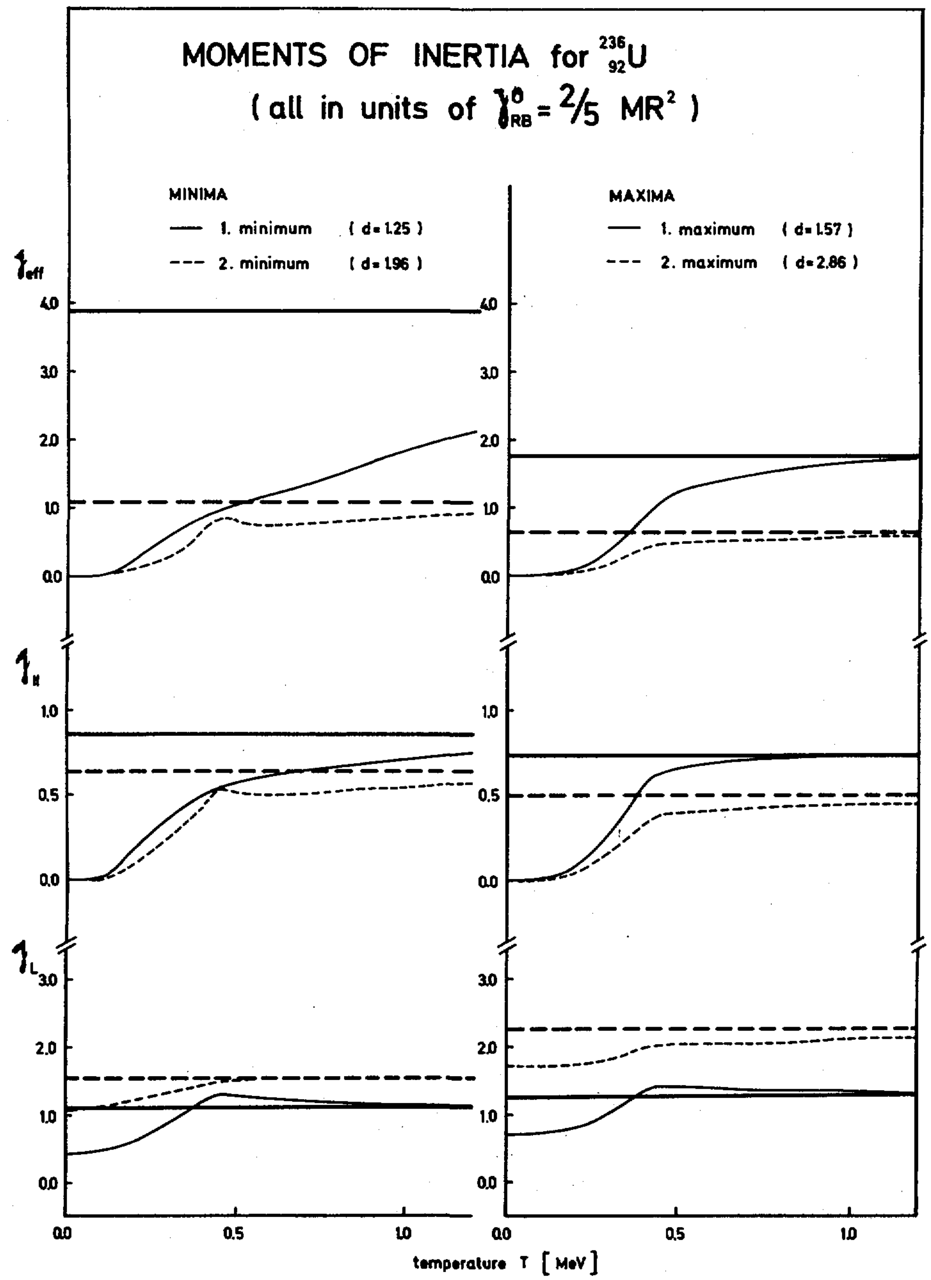

FIG. 5. The moments of inertia $\mathcal{J}_{eff}$, $\mathcal{J}_{\perp}$ and $\mathcal{J}_{\parallel}$ for ^{236}U are shown as a function of the nuclear temperature for the deformations at the ground state (d = 1.25), the second minimum (d = 1.86), the first barrier (d = 1.5) and the second barrier (d = 2.86). All the moments of inertia are expressed in units of the rigid-body value for a sphere, $\mathcal{J}_{RB}$. The thick horizontal lines, in all cases, represent the corresponding moments for a rigid rotator of the same shape. These values are reached at high temperatures.

For the specific case of the reaction $^{235}U(n, f)$ with 3 MeV neutrons, the value of the temperature is found to be equal to 0.28 MeV if the barrier shape was assumed to be the same as that for the first barrier and T = 0.33 MeV for the second barrier (with the rigid-body values these would be equal to completely unreasonable values of 0.05 MeV and 0.14 MeV, respectively).

ACKNOWLEDGEMENTS

The authors would like to thank Professors A. Bohr and B. Mottelson for illuminating discussions. They are also indebted to Dr. K. Kumar for valuable discussions and help.

REFERENCES

[1] INGLIS, D., Phys. Rev. 96 (1954) 1059.
[2] SOBICZEWSKI, A. et al., Nucl. Physics A131 (1967) 67; NILSSON, S.G. et al., Nucl. Physics A131 (1969) 1.
[3] STRUTINSKY, V.M., PAULI, H.C., these Proceedings.
[4] BOHR, A., MOTTELSON, B., Nuclear Structure, 3, to be published by W.A. Benjamin, Inc. (New York).
[5] BES, D.R., Mat. Fys. Medd. Dan. Vid. Selsk. 33 2 (1961).
[6] STRUTINSKY, V.M., Nucl. Physics A112 (1968) 1.
[7] DAMGAARD, J., PAULI, H.C., PASHKEVICH, V.V., STRUTINSKY, V.M., (to be published in Nucl. Physics).
[8] HALPERN, I., STRUTINSKY, V.M., Int. Conf. peaceful Uses atom. Energy, (Proc. Conf. 1955) Geneva 15 (1958) 408.
[9] STRUTINSKY, V.M., LJASHENKO, N.Y., POPOV, N.A., Nucl. Physics 46 (1963) 639.
[10] BATE, G.L., CHAUDRY, R., HUIZENGA, J.R., Phys. Review 131 (1963) 722.
[11] MUZYCKA, Yu.A., OGANESSIAN, Y.T., PUSTYLNIK, B.I., FLEROV, G.N., Yad. Fiz. 6 (1968) 306.
[12] OGANESSIAN, Yu.Ts., JINR E7-3942 preprint (1968).
[13] PAVLINCHUK, V.A., *private communication* (1967).

DISCUSSION

L. WILETS (Chairman): Have you been able to follow the deformation to sufficiently large values so that you could see the mass parameter asymptoting to the separated fragment value, namely the reduced mass?

H.C. PAULI: We have not got so far yet in our calculations. The fact that the quantity $B_\rho \rho$ remains on the average a constant seems, however, to indicate such behaviour. One should also remember that the data presented hold good for spheroidal shapes only. For large deformations one should use other shapes. This work is under way.

P. von BRENTANO: Could you comment on the impact of your considerations on the calculation of the life-times of fission isomers?

H.C. PAULI: The life-times of the fission isomers should be affected as well as the spontaneous fission life-time. Increased mass, as compared to the average, at the barriers will also increase the life-time.

A. SOBICZEWSKI: You mentioned the discrepancy between the values of the mass parameter B obtained in your calculations and in ours (cited in your paper as Ref. [2]). You suggest that it may come from cutting off the levels from the $N \geq 10$ shells. I agree that the poorly convergent term Σ_1, which enters into B in our approach and is not needed in your calculation, may be lowered by this cut-off but I do not think this effect could account for the whole of the discrepancy obtained. This concerns especially the low deformations for which the levels cut off lie very far from the Fermi level.

H.C. PAULI: I agree in so far as the agreement, on the average, is much better at smaller than at larger deformations.

E.R.H. HILF: Did I understand correctly that you wanted to study a nucleus of finite temperature but actually studied a cold nucleus, applying Fermi statistics of some finite temperature? So you started with the single-particle energy level density for T = 0 and filled in the nucleons, using a Fermi distribution of finite temperature. If so, you missed one of the two effects that compete with each other, being of the same order of magnitude, and come into play in a shell-model calculation for finite temperature, i.e. the temperature dependence of the level density itself. This is due to the fact that heating the nucleus (a little bit, otherwise the summation of single-particle energies becomes increasingly useless because of the interaction energies) leads to wave functions of higher energy and orbital momentum, which have a different radial distribution too, and this in due course leads to a higher concentration of high-energy nuclei at the surface. In a self-consistent calculation this would lead to a change of the potential and to a rise of the level density. In your non-self-consistent calculation you can take care of this effect approximately by some single ansatz, say a first-step calculation, since the wave functions are available to you.

H.C. PAULI: We use the energy levels of the cold system but do not expect the structure to be completely destroyed by a temperature of 1 MeV.

NIVEAUX D'ENERGIE DANS UN PUITS DE POTENTIEL DEFORME A BORDS ABRUPTS

M. GAUDIN, A.M. SAJOT
CEA, Centre d'études nucléaires de Saclay,
France

Abstract — Résumé

ENERGY LEVELS IN A DEFORMED POTENTIAL WELL WITH STEEP EDGES. This paper attempts an exact numerical determination of the energy levels of a particle in a potential well with steep edges by the determinantal method, which was already described by Hill and Wheeler in 1953. This method is applied to a very schematic nuclear model in which the mean potential is local, independent of spin and charge, and constant or infinitely deep inside a surface limiting a fixed volume. In practice one is limited to axial and reflection symmetry and a two-parameter surface family (α_2, α_4) although it is very well possible to introduce an asymmetry (α_3).

The preliminary results enable us, as far as the infinite well is concerned, to: a) obtain the position of the first levels up to four exact digits in the region $0 < \alpha_2 < 0.40$, $0 < \alpha_4 < 0.15$; b) determine the total energy of a system of independent nucleons in its ground state, by the direct method of "summation over the levels"; to compare this energy with the expression given by the classical asymptotic formula for a fermion gas (Hill and Wheeler) and to obtain — as difference — a "shell correction" (Strutinsky) referring to this schematic model; c) calculate the relative proportion of the occupied even and odd levels (reflection parity) as a function of the deformation (in connection with the ideas of Kelson and Griffin on the asymmetric fission);

As to the finite potential well, the results enable us to: d) obtain, with lower accuracy (of the order of 1%), the variation of the ensemble of levels with a deformation parameter α_2 in the region $0 < \alpha_2 < 0.45$.

NIVEAUX D'ENERGIE DANS UN PUITS DE POTENTIEL DEFORME A BORDS ABRUPTS. On présente un essai de détermination numérique précise des niveaux d'énergie d'une particule dans un puits de potentiel déformé à bords abrupts, selon la méthode déterminantale décrite par Hill et Wheeler en 1953. Cette méthode s'applique à un modèle de noyau extrêmement schématique où le potentiel moyen est local, indépendant de spin et de charge, constant ou infiniment profond à l'intérieur d'une surface limitant un volume donné. Pratiquement on s'est restreint à la symétrie axiale et de réflexion, et à une famille de surfaces à deux paramètres (α_2, α_4), bien qu'il soit très possible d'introduire une asymétrie (α_3).

Les résultats préliminaires obtenus permettent, en ce qui concerne le puits infini, a) de sortir la position des premiers niveaux avec quatre chiffres significatifs exacts dans le domaine $0 < \alpha_2 < 0,40$, $0 < \alpha_4 < 0,15$; b) de déterminer l'énergie totale d'un système de nucléons indépendants dans son état fondamental, par la méthode directe de la «somme sur les niveaux», de comparer cette énergie à l'expression donnée par la formule asymptotique classique pour un gaz de fermions (Hill et Wheeler) et d'en déduire par différence une «correction de couche» (Strutinsky) relative à ce modèle schématique; c) de calculer la proportion relative des niveaux occupés pairs ou impairs (parité par réflexion) en fonction de la déformation (référence aux idées de Kelson et Griffin sur la fission asymétrique);

En ce qui concerne le puits de potentiel fini, les résultats permettent d) de sortir avec une précision moindre (de l'ordre de 1%) la variation d'ensemble des niveaux avec le paramètre de déformation α_2 dans le domaine $0 < \alpha_2 < 0,45$.

1. INTRODUCTION

Les tentatives actuelles en théorie de la fission pour dépasser les modèles classiques insuffisants font intervenir les effets quantiques qui se manifestent dans l'existence des niveaux discrets du noyau et dans les variations de la densité de niveau traduisant les effets de couche.

Dans le sillage des études récentes, notamment celles de Strutinsky [1] basées sur le modèle réaliste de Nilsson, nous avons voulu considérer les mêmes effets [2, 3], mais dans un modèle de noyau très idéalisé qui permette certains calculs et soit libre de paramètres phénoménologiques. Nous avons donc repris le modèle de la boîte sphéroïdale ou plus exactement du puits de potentiel déformé à bords abrupts, de profondeur finie ou infinie. Il s'agit d'un modèle de noyau ultraschématique déjà considéré par Hill et Wheeler [4] et par Moszkowski [5] en particulier. On y admet les hypothèses simplificatrices de saturation extrême du modèle de la goutte liquide (surface abrupte, incompressibilité) mais dans le cadre du modèle unifié où chaque nucléon se meut indépendamment dans le potentiel moyen de profondeur constante limitée par la surface nucléaire [6]. Enfin il n'est pas question de charge, ni de spin, bien qu'il soit possible dans une étape ultérieure de modifier la profondeur moyenne du puits pour les niveaux de proton et d'introduire un terme de spin-orbite à la surface nucléaire.

2. LE MODELE

Dans un volume $V = (4/3)\pi R^3$ sont enclos N fermions de même espèce. La surface limite (S) est supposée à symétrie axiale et la courbe (C) qui la définit a pour équation polaire

$$r = F(\cos\theta) = \frac{1}{\lambda}\{1 + \alpha_2 P_2(\cos\theta) + \alpha_3 P_3(\cos\theta) + \alpha_4 P_4(\cos\theta)\} \tag{1}$$

On s'est restreint pratiquement à une famille à trois paramètres de déformation α_2, α_3, α_4, mais la fonction F peut être quelconque pourvu qu'elle soit assez régulière. La quantité $\lambda(\alpha_2\alpha_3\alpha_4)$ s'obtient en écrivant la condition de conservation du volume. Pour des raisons dimensionnelles on peut se ramener à un volume V équivalent à la sphère de rayon unité. Dans ces conditions, la fonction d'onde d'une particule de masse m enclose dans V vérifie les équations

$$\Delta\psi + k^2\psi = 0 \quad \text{dans } V \tag{2}$$

$$\psi = 0 \quad \text{sur } (S) \tag{3}$$

qui déterminent les niveaux d'énergie discrets dans le volume V de rayon équivalent R

$$E = \frac{\hbar^2}{2mR^2}\epsilon \qquad \epsilon = k^2 \tag{4}$$

Une fonction d'onde de moment angulaire axial M donné peut être développée sur la base complète des ondes sphériques

$$\psi^{(M)} = e^{iM\phi} \sum_{\ell=M}^{\infty} a_\ell j_\ell(kr) P_\ell^M(\cos\theta) \tag{5}$$

L'intérêt de cette base du point de vue numérique est que les fonctions de Bessel et de Legendre sont faciles à calculer par des récurrences à trois termes. Pratiquement le développement précédent est tronqué à un certain ordre L_1, à déterminer selon la rapidité de convergence de la série qui dépend elle-même des valeurs des paramètres k, M, etc., et finalement de la forme de la surface (S). La condition aux limites (3) qui achève de déterminer ψ se traduit par l'identité en x ($x = \cos\theta$)

$$\phi(x) \equiv \sum_{L=1}^{L_1} A_L j_{L+M-1}(kF(x)) P^M_{L+M-1}(x) \equiv 0 \tag{6}$$

La fonction angulaire $\phi(x)$ définie sur $[-1, +1]$ dépend de L_1 coefficients indéterminés A_L: elle ne peut donc être nulle identiquement, mais en général seulement en L_1 points x_i qu'il faut choisir de sorte que $\phi(x)$ soit le plus voisin possible de zéro. Le théorème [7] sur lequel est basé la méthode d'intégration numérique de Gauss-Jacobi donne la réponse. En choisissant la subdivision [8] x_i formée des L_1 zéros du polynôme $P_{L_1}(x)$, les égalités $\phi(x_i) = 0$, $i \in [1, L_1]$ entraînent que les coefficients du développement de $\phi(x)$ sur les $P_\ell(x)$ sont nuls jusqu'à l'ordre L_1 inclus. Le choix convenable de L_1 points sur la courbe méridienne permet donc de supprimer les oscillations angulaires jusqu'à l'ordre L_1. Ce choix fait, l'équation aux valeurs propres en k s'écrit évidemment

$$\Delta_{L_1}(k) \equiv \det \left| j_{L+M-1}(kF_i) P^M_{L+M-1}(x_i) \right|_{L,i} = 0 \tag{7}$$

On est donc ramené au calcul d'un déterminant d'ordre L_1: c'est une fonction de la variable k dont on détermine les zéros par interpolation linéaire itérée.

La méthode se généralise aisément au puits de potentiel fini à bords abrupts dont la profondeut V_0 n'intervient que par le paramètre

$$x = \left(\frac{2mV_0R^2}{\hbar^2}\right)^{1/2} \tag{8}$$

On est encore amené à chercher les zéros d'une fonction de k ($0 < k < x$) qui se présente comme un déterminant d'ordre $2L_1$

$$\tilde{\Delta}_{2L_1}(k) = \left| \begin{array}{c|c} j_{L+M-1}(kF_i) P^M_{L+M-1}(x_i) & h_{L+M-1}(qF_i) P^M_{L+M-1}(x_i) \\ \hline kj'_{L+M-1}(kF_i) P^M_{L+M-1}(x_i) & qh'_{L+M-1}(qF_i) P^M_{L+M-1}(x_i) \end{array} \right| \tag{9}$$

avec $q = \sqrt{x^2 - k^2}$. Les fonctions h sont les fonctions de Hankel sphériques, $h_0(x) = e^{-z}/z$, etc.

TABLEAU I. PUITS INFINI SPHERIQUE: NIVEAUX D'ENERGIE ET NOMBRES MAGIQUES

k	$\epsilon = k^2$	Nombres quantiques	N	A = 4N	$\frac{\hbar^2}{2mR^2}$
3,1416	09,8696	1s	1	4	4,900
4,4934	20,1907	1p	4	16	1,940
5,7634	33,2175	1d	9	36	1,125
6,2832	39,4784	2s	10	40	1,050
6,9879	48,8311	1f	17	68	0,737
7,7252	59,6795	2p	20	80	0,662
8,1825	66,9543	1g	29	116	0,516
9,0950	82,7192	2d	34	136	0,464
9,3558	87,5312	1h	45	180	0,385
9,4248	88,8264	3s	46	184	
10,4171	108,516	2f	53	212	0,346
10,5128	110,520	1i	66	264	0,299
10,9041	118,900	3p	69	276	
11,6570	135,886	1j			
11,7049	137,005	2g			

3. CALCUL NUMERIQUE

Il a été effectué sur CDC 6600. La méthode décrite ci-dessus a été contrôlée par une série de tests numériques, portant sur la rapidité de convergence d'une série telle que la série (6), sur la précision de calcul des fonctions d'entrée, d'un déterminant d'ordre élevé, etc. Ceci définit un domaine de variation de l'ensemble des paramètres en dehors duquel la précision tombe.

Comme point de repère, nous avons les niveaux du puits infini sphérique et leurs nombres quantiques rassemblés dans le tableau I, d'après Feenberg [9]. Pour atteindre un remplissage de A = 260 (ce qui donne N = A/4 = 65) il suffit de se limiter à l'intervalle en k compris entre 3 et 11. Comme nous devons nous limiter à des formes nucléaires dont le rapport grand axe/petit axe soit inférieur à 2, l'argument kr des

TABLEAU II. PUITS INFINI, TEST DE LA SPHERE EXCENTREE
Niveaux d'énergie M = 0, L_1 = 15 (subdivision à 15 nœuds)

c \ n	1s	1p	1d	2s	1f	2p
0	3,14159265					
0,2	3,14159265	4,493409	5,763459	6,283185	6,987932	7,725252
0,4	3,14159265	4,493409	5,763459	6,283185	6,987932	7,725252
0,5	3,14159265	4,493409	5,763459	6,283185	6,987932	7,725252
0,6	3,14159265	4,493409	5,763459	6,283185	6,987932	7,725252
0,7	3,14159265	4,493409	5,763459	6,283185	6,987932	7,725252
0,8	3,14159261	4,493409	5,763459	6,283185	6,987933	7,725252
0,9	3,60	4,487448	5,778834	6,282926	6,963789	7,726094
c \ n	**1g**	**2d**	**1h**	**3s**	**2f**	**1i**
0						
0,2	8,182561	9,095011	9,355812	9,424778	10,417118	10,512835
0,4	8,182561	9,095011	9,355812	9,424778	10,417118	10,512802
0,5	8,182561	9,095011	9,355803	9,424778	10,417118	10,512323
0,6	8,182560	9,095011	9,355689	9,424778	10,417119	10,508871
0,7	8,182547	9,095011	9,354856	9,424778	?	?
0,8	8,182449	9,095010	9,351011	9,424778	?	?
0,9	8,206308	9,093959	9,320629	9,42485	?	?

c = excentricité; n = nombre quantique du niveau.

fonctions de Bessel varie en gros dans le domaine de 1, 5 à 20. Dans un tel domaine on a huit chiffres exacts pour les fonctions de Bessel jusqu'à l'ordre $\ell = 20$. Cet ordre maximal du moment angulaire admis fixe L_1, donc la dimension des déterminants.

Les éléments de la méthode une fois éprouvés, il restait à appliquer celle-ci à un cas dont les résultats fussent connus a priori ou d'autre façon. On a choisi le «test de la sphère excentrée». La courbe méridienne (c_0) d'équation

$$r = F_0(x) = cx + \sqrt{1 - c^2(1 - x^2)} \qquad 0 < c < 1 \tag{10}$$

$$x = \cos\theta$$

est un cercle de rayon 1 et de centre $(\theta = 0,\ r = c)$. La surface (S_0) est donc une sphère excentrée par rapport au centre de développement des ondes sphériques, et l'on doit retrouver les niveaux du puits infini sphérique. Les tableaux II et III rassemblent des résultats pour une subdivision de quinze nœuds, «l'excentricité» c variant de 0, 2 à 0, 9. Dans un domaine suffisant on peut compter sur 4 ou 5 chiffres exacts pour la plupart des niveaux. Les tableaux ne donnent que $M = 0$ et $M = 4$ et 5, mais les valeurs intermédiaires sont aussi bonnes et la dégénérescence en M est vérifiée à la même précision. Pour des niveaux d'ordre trop élevé $k \gtrsim 10, 5$, celle-ci baisse entre 10^{-3} et 10^{-2}. Le fait important dans ce test est la chute de précision assez brusque au-delà de $c = 0, 7$. Ceci vient uniquement de l'insuffisance des moments orbitaux admis dans la fonction d'onde (dans ce cas $\ell \leq L_1 = 15$). En conséquence, pratiquement, on se limitera à des formes de surface dont on puisse définir une «excentricité» qui soit inférieure à 0, 7 environ. Ce qui nous donne un rapport d'axes en gros inférieur à 2. Cette inférence n'est pas parfaitement convaincante, cette notion d'excentricité étant qualitative pour une courbe quelconque. L'idéal serait évidemment d'avoir comme élément de comparaison les niveaux de la boîte ellipsoïdale, que l'on pourrait obtenir en calculant les zéros des fonctions sphéroïdales d'après les tables de Stratton [10], ou par résolution numérique de l'équation différentielle à une variable qui définit ces fonctions.

4. RESULTATS: VARIATION DES NIVEAUX AVEC LA DEFORMATION

En ce qui concerne le puits infini, les niveaux de particule ont donc été calculés dans le domaine positif des formes allongées ou cylindroïdes

$$0 < \alpha_2 < 0,45 \qquad 0 < \alpha_4 < 0,15$$

$$k^2 < 160 \qquad 0 \leq M \leq 7$$

domaine essentiellement limité par la précision. On ne peut donc pas encore atteindre les formes d'équilibre instable d'une goutte chargée au seuil de fission: Cohen et Swiatecki [11] donnent par exemple $\alpha_2 = 0, 72$

TABLEAU III. PUITS INFINI, TEST DE LA SPHERE EXCENTREE

Niveaux d'énergie M = 4 et 5 (subdivision à 15 nœuds)

c \ n	1g	1h	1i	1j
0				
0,2	8,182561	9,355812	10,512835	11,657032
0,4	8,182561	9,355812	10,512835	11,657032
0,5	8,182561	9,355812	10,512835	11,657027
0,6	8,182561	9,355812	10,512834	11,656962
0,7	8,182561	9,355812	10,512824	11,656765
0,8	8,182561	9,355813	10,512765	11,659413
0,9				

c \ n		1h	1i	1j
0				
0,2		9,355812	10,512835	11,657032
0,4		9,355812	10,512835	11,657032
0,5		9,355812	10,512835	11,657032
0,6		9,355812	10,512835	11,657027
0,7		9,355812	10,512835	11,656942
0,8		9,355812	10,512831	11,656252
0,9				

c = excentricité; n = nombre quantique du niveau.

et $\alpha_4 = 0,20$ pour un paramètre de fissionnabilité $\xi = 0,74$, ce qui correspond à un rapport

$$\frac{\text{grand axe}}{\text{petit axe}} = \frac{1,71}{0,64} > 2,6$$

Une élongation pure $\alpha_2 = 0,50$ correspondrait à peu près à $\xi = 0,80$.

Sur la figure 1 est représentée la variation séparée des niveaux pairs et impairs (parité par réflexion) en fonction de α_2 pour $\alpha_4 = 0$. On y ob-

TABLEAU IV. PUITS FINI: TEST DE LA SPHERE EXCENTREE

$x = 9,814$, $L_1 = 17$, $\epsilon = k^2$

M \ n, c	c	1s	1p	1d	2s	1f	2p	1g	2d
	0	8,10677	16,54413	27,14111	32,12089	39,76771	48,20356	54,31818	66,17264
0	0,4	8,1067	16,5441	27,1412	32,1209	39,7688	48,2035	54,3322	66,1727
	0,6	8,12	16,37	27,20	32,13	39,48	48,18	55,79	66,21
	0								
1	0,4		16,5441	27,1411		39,7678	48,2035	54,3122	66,1726
	0,6		16,53	27,01		39,20	48,20	54,55	66,16
	0								
2	0,4			27,1411		39,7673		54,3177	66,1726
	0,6			27,14		39,41		52,09	
	0								
3	0,4					39,7678		54,3200	
	0,6					39,85		54,62	64,57
	0								
4	0,4							54,3180	
	0,6							54,52	

L =19, c=0,5

M \ n	1s	1p	1d	2s	1f	2p	1g	2g
0	8,10678	16,54416	27,142	32,12088	39,781	48,20355	54,42	66,1728
1		16,5442			39,769			

c = excentricité; nombre quantique du niveau; M = moment angulaire axial. $x = (2mV_0R^2/\hbar^2)^{1/2} = 9,814$ (subdivision à 17 et 19 nœuds)

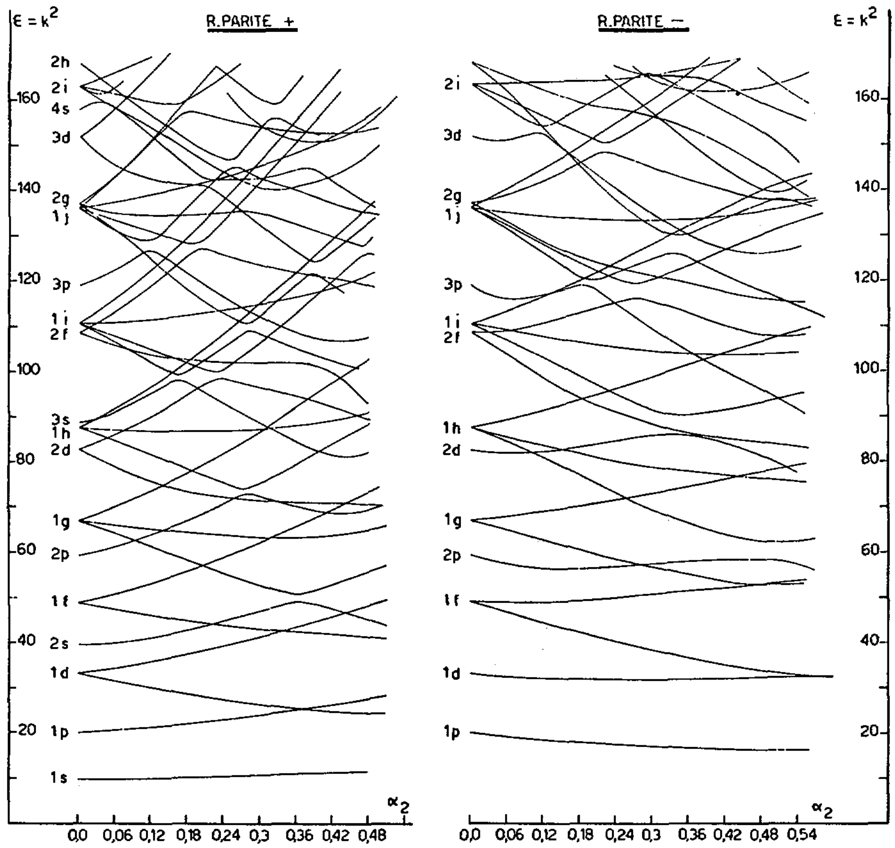

FIG. 1. Niveaux d'énergie dans le puits de potentiel infini en fonction de α_2 ($\alpha_4 = 0$, parités séparées).

serve le comportement bien connu des niveaux de même nombre quantique qui ne se croisent pas, mais s'échangent. La distance d'approche peut être assez faible et donne aussi une idée de la précision; par exemple pour $\alpha_4 = 0,10$, $\alpha_2 = 0,36$, M = 0, on a observé le doublet bien séparé $\epsilon = 116,3$ et $\epsilon = 117,3$. Hors du domaine ci-dessus défini ($\alpha_2 > 0,50$) ou pour des niveaux d'ordre trop élevé, on observe leur disparition par paires quand la déformation grandit. Ce phénomène est dû uniquement à la limitation du moment orbital maximal admis L_1. Strictement la fonction d'onde est forcée de s'annuler en des points choisis de (S), le problème aux limites n'est donc pas hermitique et les énergies peuvent devenir complexes. Lorsque le nombre de surfaces nodales de la fonction d'onde est trop grand, la particule ne voit plus une paroi qui l'enferme, mais une grille au travers de laquelle elle peut fuir dès que la longueur d'onde devient de l'ordre des dimensions de la maille.

En ce qui concerne le puits de potentiel de profondeur finie, les résultats sont moins précis. Le test de la sphère excentrée permet d'atteindre c = 0,5 avec trois chiffres exacts et au-delà jusqu'à 0,7 deux chiffres seulement (tableau IV). Les figures 2 et 3 représentent les niveaux

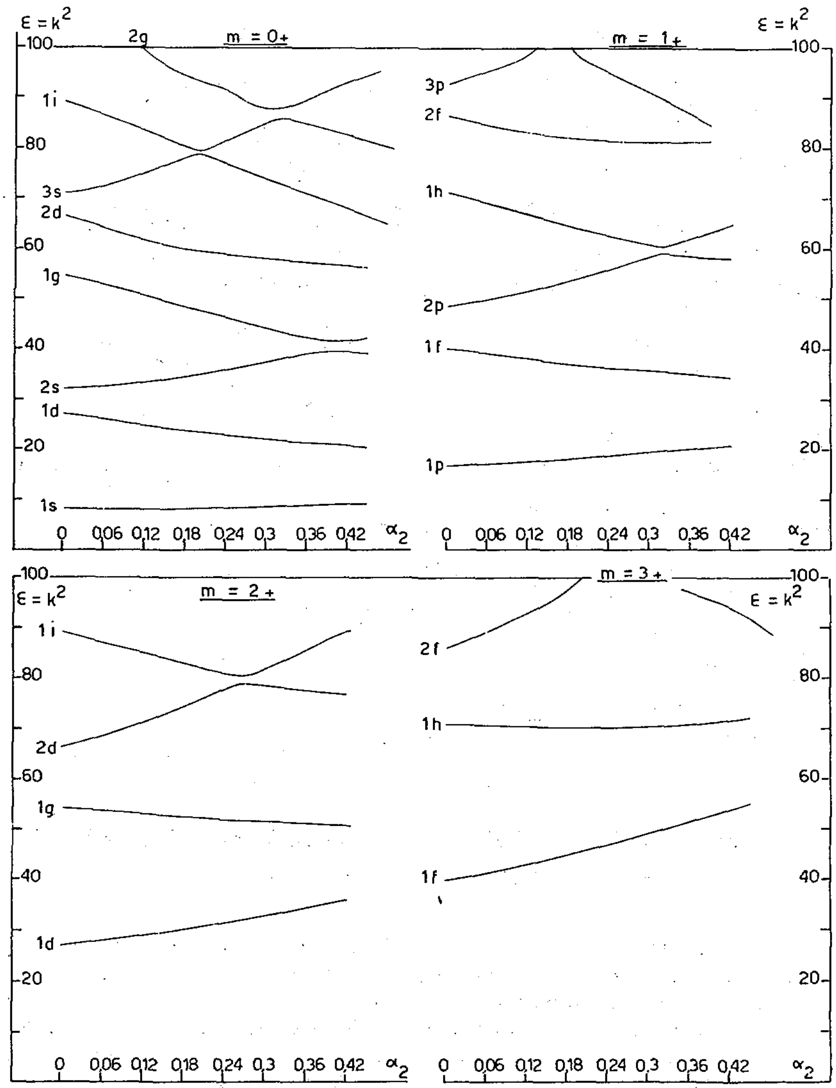

FIG. 2. Niveaux d'énergie dans le puits de potentiel fini à bords abrupts en fonction de la déformation α_2. Parité positive. x = 10.

de chaque parité en fonction de la seule déformation α_2 jusqu'à 0,50. On a choisi x = 10 (états liés jusqu'au 3p inclus environ). Qualitativement l'allure de la variation avec α_2 est semblable à celle du puits infini, sauf au voisinage immédiat de l'énergie zéro (ou du continu) où il faudrait améliorer la précision. Ce sont justement ces niveaux importants voisins du niveau de Fermi qui sont les plus intéressants à suivre avec la déformation, car leur comportement ne saurait être décrit par aucun modèle à paroi infini (modèle de la boîte ou oscillateur harmonique).

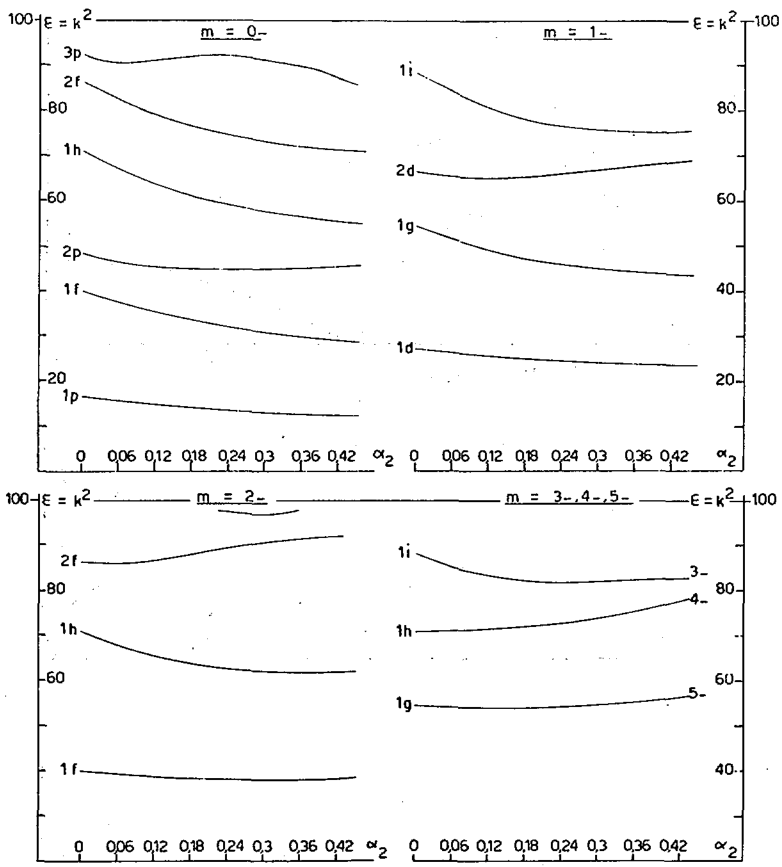

FIG. 3. Niveaux d'énergie dans le puits de potentiel fini à bords abrupts en fonction de la déformation α_2. Parité négative. $x = 10$.

5. LA CORRECTION DE COUCHE DANS LE MODELE DE LA BOITE

La précision obtenue dans le cas du puits infini (10^{-4}) permet de calculer l'énergie de l'état fondamental d'un système de N(N< 70) nucléons de même espèce, en effectuant directement la «somme sur les niveaux»

$$\epsilon_T = \sum_{i=1}^{N} k_i^2 \qquad \left(E_T = \frac{\hbar^2}{2mR^2}\,\epsilon_T\right) \tag{11}$$

puisque l'énergie est ici purement cinétique.

La figure 4 illustre la croissance assez rapide de cette quantité avec la déformation dans un cas typique. Cette croissance n'a rien de comparable avec celle que donnerait un modèle réaliste où les énergies coulombiennes et superficielles se composent dans leur variation. Ce

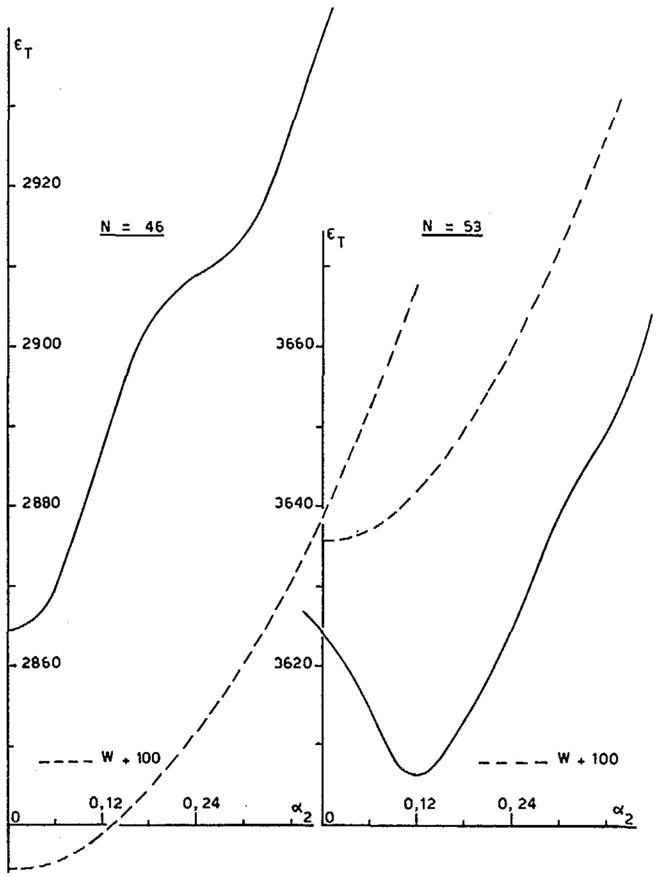

FIG. 4a. Croissance comparée de l'énergie totale ϵ_T et de l'approximation classique ϵ_{CL}. N = 46 et 53.

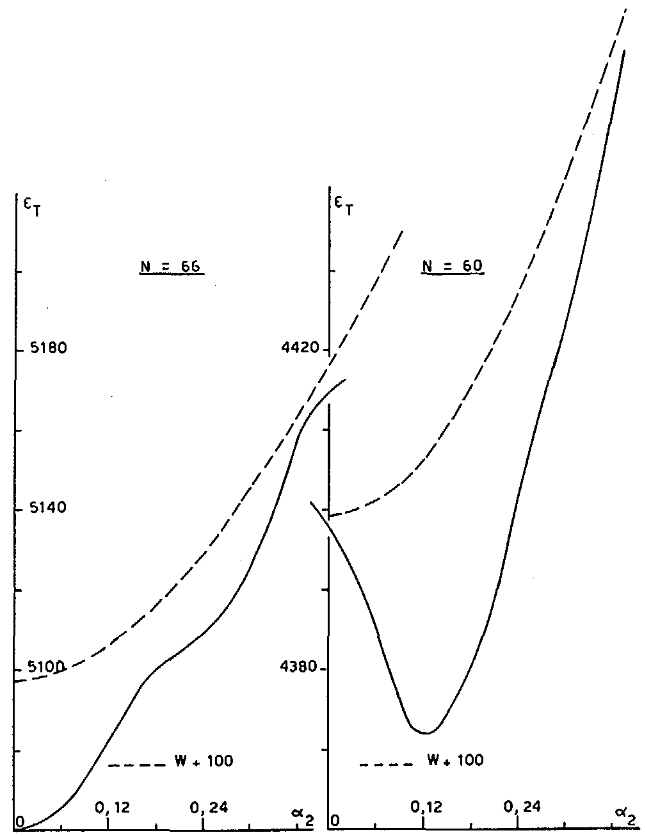

FIG. 4b. Croissance comparée de l'énergie totale ϵ_T et de l'approximation classique ϵ_{CL}. N = 66 et 60.

qui nous intéresse dans ce modèle schématique, c'est la différence entre l'énergie totale ϵ_T et l'expression ϵ_{CL} de l'énergie du système «classique» correspondant (classique signifie seulement: N grand) de façon à mettre en évidence un «effet de couche». On a pris pour ϵ_{CL} la formule asymptotique de Hill et Wheeler ([4], Appendice, fig.11), qui est un développement en puissances descendantes de la quantité

$$k_F = \left(\frac{9\pi}{2} N\right)^{1/3}$$

On obtient

$$\epsilon_{CL} = \frac{2}{15\pi} k_F^5 + \frac{1}{8} S k_F^4 + \left(\frac{3\pi}{32} S^2 - \frac{1}{3\pi} L\right) k_F^3 + 0(k_F^2) \tag{12}$$

La dépendance dans la déformation provient des quantités S et L:

$$S = \frac{\text{surface nucléaire}}{4\pi} \qquad (S = 1, \text{ pour la sphère})$$

$$L = \frac{\text{courbure moyenne}}{2\pi} \qquad (L = 2, \text{ pour la sphère})$$

Une telle formule mériterait d'être complétée jusqu'au terme constant. La figure montre en effet qu'avec ses trois termes ϵ_{CL} approche à 1,5% près la quantité ϵ_T et a la même croissance que ϵ_T avec la déformation.

La différence

$$\delta(N, \alpha) = \epsilon_T(N, \alpha) - \epsilon_{CL}(N, \alpha)$$

TABLEAU V. VALEURS DE α_2 AUX MINIMUMS DE δ EN FONCTION DE N ET DE α_4

N \ α_4	$\alpha_4 = 0$			$\alpha_4 = 0,05$		$\alpha_4 = 0,10$		$\alpha_4 = 0,15$	
45	0,33		>0,50	0,	0,33	0,	0,36	0,28	
46	0,	0,30	>0,50	0,	0,36	0,	0,34	0,	0,33
50	0,10		0,33	0,12	0,44	0,12	0,40	0,12	
54	0,15		0,42	0,16	0,39	0,15	0,39	0,15	
57	0,18		0,48	0,16	0,48	0,20	0,36	0,20	
60	0,15		0,36	0,15	0,27	0,26		0,06	0,26
63				0,27		0,04	0,27	0,04	0,30
66	0,	0,27	>0,50	0,26	>0,50	0,	0,26	0,	0,33
69	0,	0,27	>0,50	0,27	>0,50	0,	0,27	0,	0,35

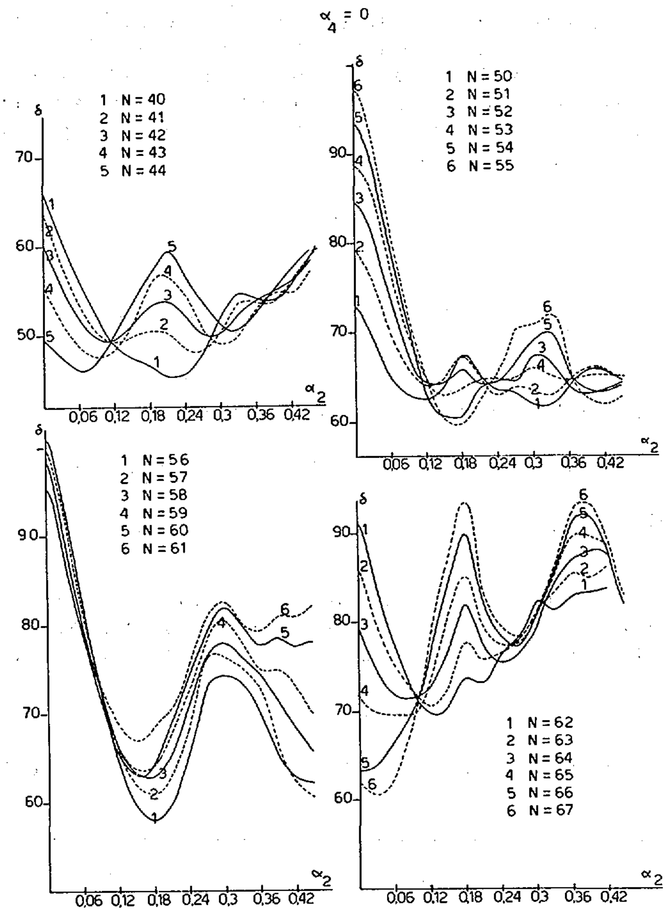

FIG. 5. Correction de couche $\delta = \epsilon_T - \epsilon_{CL}$ en fonction de α_2 et de N ($\alpha_4 = 0$).

a une amplitude de variation beaucoup plus faible (~0,5%) et constitue la correction de couche dans ce modèle. L'oscillation résiduelle δ représentée aux figures 5 et 6 a le comportement typique décrit par Strutinsky [1]. Les maximums et minimums correspondent bien aux régions de haute et basse densité de niveaux à une particule, à l'énergie de Fermi. L'amplitude de l'oscillation varie avec le remplissage N. Dans ce modèle, elle n'est atténuée par aucun effet d'interaction résiduelle ni aucune compensation dues à la présence de plusieurs types de particules. Pour avoir un ordre de grandeur, prenons par exemple N = 57; la différence entre le second maximum et le second minimum est de 15 unités, ce qui donne $15 \times \hbar^2/2mR^2 \sim 15 \times 0,32 = 4,8$ MeV pour un seul type de particule et de spin.

Le tableau V rassemble les valeurs des élongations α_2 calculées aux minimums (pour $\alpha_4 = 0$) entre N = 45 et 69.

Dans le domaine exploré $0 < \alpha_2 < 0,45$, on atteint assez rarement la remontée au-delà du second minimum, sauf lorsque le premier minimum

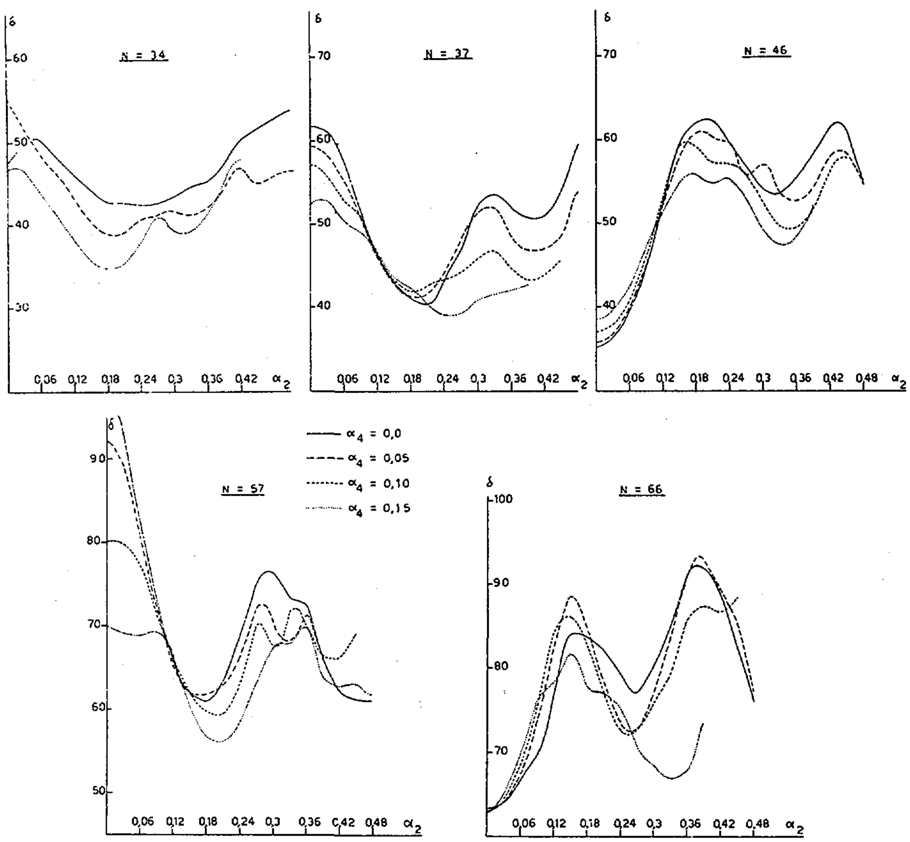

FIG. 6. Correction de couche $\delta = \epsilon_T - \epsilon_{CL}$. Continuité en α_4 pour quelques valeurs de N.

correspond à l'état sphérique. De toute façon, pour discuter des états métastables ou isomériques, il faudrait au moins reconstituer une surface d'énergie totale à partir de cette correction de couche, ce que nous n'avons pas cherché à faire étant donné le caractère incomplet et trop schématique du modèle.

Les familles des courbes δ présentées aux figures 5 et 6 montrent une continuité certaine en N et en α_4, malgré des fluctuations locales dues aux croisements aléatoires des niveaux et aux erreurs cumulées.

Notons pour finir un sous-produit de ce calcul, concernant la variation du rapport

$$R = \frac{N_+}{N_-} = \frac{\text{nombre de niveaux pairs occupés}}{\text{nombre de niveaux impairs occupés}}$$

en fonction de α_2. Ce rapport a été considéré par Kelson [12] et Griffin [13] dans leurs travaux sur la fission asymétrique. Dans une hypothèse d'évolution rapide du noyau depuis le point seuil jusqu'à la

TABLEAU VI. RAPPORT DU NOMBRE DES NIVEAUX OCCUPES PAIRS AU NOMBRE DES IMPAIRS

$R = N_+/N_-$, $(N_+ + N_- = N)$, $\alpha_4 = 0$

N \ α_2	0,06	0,12	0,18	0,24	0,30	0,36	0,42	0,48
	13/7 1,86	12/8 1,50	12/8 1,50	11/9 1,22	11/9 1,22	11/9 1,22	11/9 1,22	10/10 1,00
34	20/14 1,43	21/13 1,62	21/13 1,62	20/14 1,43	19/15 1,27	20/14 1,43	18/16 1,13	18/16 1,13
45	27/18 1,50	27/18 1,50	26/19 1,37	24/21 1,14	26/19 1,37	26/19 1,37	26/19 1,37	26/19 1,37
46	28/18 1,55	28/18 1,55	26/20 1,30	25/21 1,19	26/20 1,30	26/20 1,30	27/19 1,42	26/20 1,30
54	33/21 1,58	33/21 1,58	33/21 1,58	31/23 1,48	31/23 1,48	30/24 1,25	30/24 1,25	30/24 1,25
57	33/24 1,38	33/24 1,38	34/23 1,48	34/23 1,48	33/24 1,38	31/26 1,19	31/26 1,19	32/25 1,28
66	38/28 1,36	38/28 1,36	37/29 1,28	38/28 1,36	38/28 1,36	38/28 1,36	38/28 1,36	36/30 1,20
69	41/28 1,46	40/29 1,38	38/31 1,22	38/31 1,22	39/30 1,30	40/29 1,38	39/30 1,30	38/31 1,22

scission, le rapport R serait une borne supérieure du rapport d'asymétrie. Le tableau VI montre la variation de ce rapport avec N et α_2. Ses fluctuations avec α_2 dépendent de N (par exemple pour N = 66, R est presque constant et égal à 1,36). Il a tendance à décroître avec l'élongation, mais pas aussi régulièrement que l'indique l'évaluation asymptotique de R faite par Griffin à l'aide de la formule de Wheeler.

En conclusion, on peut penser que la méthode de Wheeler utilisée ici puisse contribuer à résoudre le problème de l'extrapolation des niveaux de particule [6] au domaine des grandes déformations, pour diverses formes de surface nucléaire, spécialement pour les niveaux les moins liés. La comparaison précise de la variation des niveaux ici obtenue avec celle que donnent les autres méthodes plus rapides ou plus raffinées (perturbations, diagonalisation de la matrice d'énergie [14, 15]) n'a pas été entreprise.

REMERCIEMENTS

Nous remercions MM. R.Joly, C.Signarbieux, Ph.Quentin, H.Nifenecker et D.Paya qui nous ont intéressés aux problèmes de la fission et auprès desquels une partie du travail a été effectuée, ainsi que M.Matuszek pour son aide dans l'exécution des figures.

REFERENCES

[1] STRUTINSKY, V.M., Nuclear Physics A95 (1967) 420; A122 (1968) 1-33.
[2] GUSTAFSON, G., LAMM, I.L., NILSSON, B., NILSSON, S.G., Nuclear Structure (11th Summer Meeting of Nuclear Physicists, Hercegnovi) I (1966) 279.
[3] MYERS, W.D., SWIATECKI, W.J., Nuclear Masses and Deformation, UCRL 11980.
[4] HILL, D.L., WHEELER, J.A., Phys. Rev. 89 (1953) 1102.
[5] MOSZKOWSKI, S.A., Handb. Phys. 39 (1957) 501.
[6] SZYMANSKI, Z., «Equilibrium deformations of the ground and excited states in nuclei», Nuclear Structure (C.r. Coll. Doubna, 1968), AIEA, Vienne (1968) 414 (références).
[7] SZEGÖ, G., Orthogonal Polynomials (1939), Théorème 3.4.1, p.47.
[8] KRONROD, A.S., Nodes and Weights of Quadrature Formulas, New York (1965).
[9] FEENBERG, E., Shell Theory of the Nucleus, Princeton University Press (1955).
[10] STRATTON, J.A., Spheroidal Wave Functions, MIT, John Wiley, New York.
[11] COHEN, S., SWIATECKI, W.J., Ann. Phys. 22 (1963) 406.
[12] KELSON, I., Phys. Rev. Lett. 20 (1968) 867.
[13] GRIFFIN, J.J., Reflection Symmetry and Fission Mass Ratios, Technical Report No.810 (avril 1968) Maryland, U.S.A.
[14] MOSZKOWSKI, S.A., Particle states in spheroidal nuclei, Phys. Rev. 99 (1955) 803.
[15] LEMMER, R.H., Single particle motion in a deformed non local potential well, Phys. Rev. 117 (1960) 1551; Phys. Rev. 119 (1960) 1043.

INTERMEDIATE STRUCTURE IN FISSION

(Session D)

Chairman: J. Ryabov

STRUCTURE PHENOMENA IN NEAR-BARRIER FISSION REACTIONS
A review

J. E. LYNN
UKAEA Research Group
Atomic Energy Research Establishment
Harwell, United Kingdom

Abstract

STRUCTURE PHENOMENA IN NEAR-BARRIER FISSION REACTIONS. The double-humped Strutinsky potential governing the behaviour of actinide nuclei in quadrupole deformation is now known to explain a wealth of data in low-energy fission. In this paper the results of various particle-induced reactions leading to fission in the near-barrier energy range are reviewed and interpreted. First, a general formal theory which allows for the discussion of structure effects within the framework of the channel theory of fission is summarized. This is applied to the treatment of the case when the second minimum in the potential energy curve is shallow, and structure in the fission yield as a function of energy can be ascribed to an undamped vibrational level in this shallow well. The neutron-induced fission cross-section of ^{230}Th seems to provide a clear example of this phenomenon. The opposite case is that in which the second minimum is quite deep and the highest vibrational states in this well are rather strongly damped into much more complicated states (class-II states) of a compound nucleus type. The class-II states are coupled to the denser fine structure resonances (class-I states) and the coupling strength relative to the fine structure spacing and class-II fission width governs a number of different phenomena. The most obvious case, when the coupling is very weak and the class-II state is narrow, gives cross-sections that can be treated consistently by simple perturbation theory. The narrow intermediate structure in the slow neutron-induced fission cross-sections of ^{240}Pu, ^{242}Pu and ^{237}Np almost certainly provide good examples of this. When the class-I-class-II coupling is large compared with the fine structure spacing the intermediate structure has basically a Lorentzian dependence. On the other hand, if the class-II fission width is large quasi-Lorentzian groups appear; these are virtually indistinguishable (in the cross-section) from the former case. Examples of the two cases are provided by the slow neutron cross-sections of ^{234}U and ^{241}Am. Intermediate cases are also discussed. Weak and moderate damping of the vibrational states of the second minimum into the class-II compound states is also a possibility that can occur. Examples of this seem to be illustrated by the ^{241}Am(n, f) and ^{239}Pu(d, pf) reactions. Finally all the data are surveyed in terms of the information they give us concerning the double-humped fission barrier. There seems to be a clear trend from a shallow second minimum in the region of ^{231}Th to maximum development around ^{241}Pu.

1. INTRODUCTION

Since the last conference on fission, at Salzburg four years ago, a variety of new data on low-energy fission and more careful reinterpretation of old data have forced on our attention the fact that our ideas, on the mixing of the fission mode into the general compound nucleus states, and on the nature of the fission barrier, have been too simple. Within the same period Strutinsky's calculations [1] of the deformation energy of even nuclei have provided a firm foundation for interpreting the new near-barrier fission phenomena.

The theory of deformation energy is treated elsewhere in this Conference. It is sufficient to state here that, according to Strutinsky's theory, shell effects modulate the well-known liquid drop potential energy curve governing the prolate (near-quadrupole) deformation of nuclei in the fission mode (i.e. through the saddle-point in the potential energy surface).

The shell effects provide negative correction terms to the total ground state energy at a given deformation when the single-particle state density, e.g. as calculated in the Nilsson [2] model, at the Fermi energy is low for that deformation, and they provide zero or positive corrections when that density is high. The detailed calculations show that in the general region of the actinide nuclei, the ground state energy has a primary minimum for moderate prolate deformations agreeing with the observed quadrupole moment (this has long been known since the work of Mottelson and Nilsson [3]) and a secondary shallower minimum at larger prolate deformations corresponding more nearly to the saddle point of the liquid drop potential energy surface. This secondary minimum should tend to disappear towards the higher end of the actinide group of nuclei.

This theory provides an immediate explanation of the existence of the spontaneously fissioning isomers [4,5,6], these being essentially the zero-point motion for vibrations in the second minimum. It also provides the key to understanding the structure phenomena in fission-reactions. The study of such fission reactions can be used to give quantitative details of the structure of nuclei at extended deformation. Confirmation of detailed theoretical studies of highly deformed nuclei in the actinide region will of course stimulate such study over the whole range of nuclei from the very light ones up to and including the extrapolation into the region of the super-heavy nuclei. Thus, the investigation of these near-barrier fission phenomena has a value transcending the immediate study of fission.

2. BETA-VIBRATIONAL MODES IN THE COMPOUND NUCLEUS

2.1 Hamiltonian of a vibrating nucleus

We assume that the dependence of the ground state total energy on deformation as calculated in Strutinsky's theory [1] gives us the potential energy of deformation of the nucleus. In particular, we are interested in this potential energy as a function of prolate extension (for which we use the parameter β) of the nucleus through the saddle point(s), minima and valleys in the potential energy surface towards the scission point as shown schematically in Fig. 1. In its early stages this prolate extension is essentially quadrupole deformation. The Hamiltonian of the nucleus is expanded to give explicitly a term H_β for the potential and kinetic energies associated with this prolate extension; thus

$$H = H_\beta + \sum_i H_i + \sum_{i<j} H'_{ij} + \sum_i H''_{i\beta} \tag{1}$$

All the other degrees of freedom of the nucleus, whether they be other collective parameters associated with the shape of the nucleus or its rotation, or single particle excitations of nucleus in the overall nuclear field, are included in the term $\sum_i H_i + \sum_{i<j} H'_{ij}$. The interaction between the β-degree of freedom and the other degrees of freedom is described by the term $\sum_i H''_{i\beta}$ (which we shall henceforth write simply as H''). This implies that the former term $(\sum_i H_i + \sum_{i<j} H'_{ij})$ describes the Hamiltonian of the other degrees of freedom for a fixed prolate deformation β_0 ; the variation of this contribution to the Hamiltonian with changing β is included in the term H''.

The eigenfunctions and eigenvalues of H_β are denoted by Φ_ν, $\mathcal{E}_\nu$, those of $\sum_i H_i + \sum_{i<j} H'_{ij}$ by χ_μ, ϵ_μ . The eigenfunctions χ_λ

(with eigenvalues E_λ) of the full Hamiltonian may be written as an expansion in the products $\Phi_\nu \chi_\mu$:

$$X_\lambda = \sum_{\nu\mu} C^\lambda_{\nu\mu} \Phi_\nu \chi_\mu \qquad (2)$$

Strictly speaking, the eigenvalues $\mathcal{E}_\nu$ and E_λ are continuous, but since we are studying nuclear reactions in which sharp resonance phenomena are conspicuous it is most useful to treat these eigenvalues as if they were discrete. They can in fact be made formally discrete by imposition of suitable boundary conditions in the open decay channels of the system, as in R-matrix theory [17]. In applications of the theory we shall employ these.

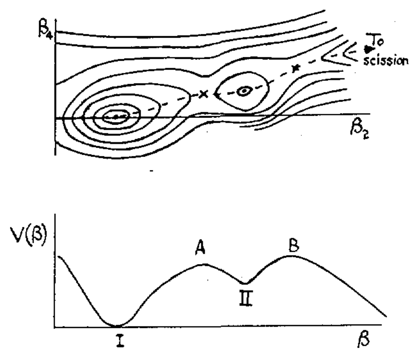

FIG. 1. Above: energy contours for two collective co-ordinates (schematic). Crosses show saddle points, dots minima. Dashed line is preferred route to fission and defines prolate deformation parameter, β. Below: section along dashed line showing double-humped fission barrier.

2.2 Classification of vibrations in a double well

We are most interested in phenomena governed by a Strutinsky "double-humped" prolate deformation potential of the type shown in Fig. 1 with a primary minimum (I), an intermediate barrier (A), a secondary minimum (II) and an outer barrier (B). We impose boundary constraints at the deformation corresponding to the outer barrier. For an eigenvalue $\mathcal{E}_\nu$ lower than the intermediate barrier the wave-function Φ_ν can be given a shape classification, depending on whether the greater amplitude resides in the primary well (type I) or the secondary well (type II). For the particular potential with numerical parameters shown in Fig. 2a the relative amplitude C of the minor part of the wave-function compared with the major part is shown in Fig. 2b. For a parabolic intermediate barrier of the kind shown the energy dependence of such relative amplitudes is given approximately by

$$C^2 \approx K \exp\left[-2\pi\left(V_A - \mathcal{E}_\nu\right)/\hbar\omega_A\right] \Big/ \left(\mathcal{E}_{\nu_I} - \mathcal{E}_{\nu_{II}}\right)^2 \qquad (3)$$

where V_A is the potential energy of the intermediate barrier and ω_A is the circular frequency associated with the inverted parabolic barrier, while $\mathcal{E}_{\nu_I}$ and $\mathcal{E}_{\nu_{II}}$ are the nearest vibrational levels of opposite class, one of which is, of course, the energy level $\mathcal{E}_\nu$ under consideration.

The constant K depends to some extent on the detailed characteristics of the primary and secondary wells. For the potential shown in Fig. 2a it is 0.006.

When the eigenvalue $\mathcal{E}_\nu$ is greater than the intermediate barrier the amplitudes of the wave-function within the two minima will be comparable. In this case we arbitrarily assign the vibrational state to class II.

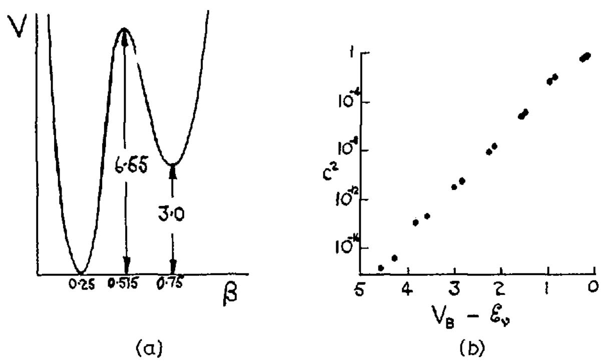

FIG. 2.a) Numerical details of potential used for calculation of vibrational wave function attenuation shown in b). Phonon energy, $\hbar\omega_I$ = 0.8 MeV, tunnelling parameter $\hbar\omega_A$ = 0.8 MeV.

2.3 Shape classification of compound states

2.3.1 Definition

Compound states that have the same shape classification as the vibrational states can be defined. Class I compound states are expanded in terms of vibrations purely of the class I type;

$$X_{\lambda_I}^{I} = \sum_{\nu_I \mu} C_{\nu_I \mu}^{\lambda_I} \Phi_{\nu_I} \chi_\mu \tag{4}$$

and class II compound states are, correspondingly,

$$X_{\lambda_{II}}^{II} = \sum_{\nu_{II} \mu} C_{\nu_{II} \mu}^{\lambda_{II}} \Phi_{\nu_{II}} \chi_\mu \tag{5}$$

Physically, of course, these definitions correspond to compound nucleus motion with shape close to that of the normal ground state nucleus in the former case, and with the more extended prolate shape of the spontaneously fissioning isomer in the second case. It is also implicit in these definitions that there is a certain amount of leakage through the intermediate barrier into the opposite well.

2.3.2 The coupling parameters

To obtain the final, proper set of compound nucleus states X_λ these two sets have to be coupled, and it can be shown that this coupling is governed by matrix elements of the form

$$H''_{\lambda_I \lambda_{II}} = \sum_{\nu_I \mu', \nu_{II} \mu''} C^{\lambda_I}_{\nu_I \mu'} \langle \nu_I \mu' | H'' | \nu_{II} \mu'' \rangle C^{\lambda_{II}}_{\nu_{II} \mu''} \quad (6)$$

It is clear that the magnitude of the coupling is small in at least two cases, provided that H'' is reasonably well-behaved in its dependence on β. The first case is that in which the eigenvalue E_λ of the state X_λ is well below the intermediate barrier. In this case the class II vibration wave-functions admixed into X_λ are very small in the region of β where the class I wave-functions are significant, and hence the terms $\langle \nu_I \mu' | H'' | \nu_{II} \mu'' \rangle$ in the expansion of $H''_{\lambda_I \lambda_{II}}$ must all be small.

The second case is one in which the class II compound states are rather complex usually because their energies are considerably higher than the "ground" state of their class (the spontaneously fissioning isomer). Most of the components $\Phi_{\nu_{II}} \chi_\mu$ of such a state will be of the type $\Phi_0^{II} \chi_\mu$, Φ_0^{II} being the "zero-point" class II vibrational wave-function and χ_μ a rather highly-excited state, approximately of independent-particle nature, many of which can be formed at a moderate excitation energy. Very few will be of the type $\Phi_{\nu_{II}(max)} \chi_0$ in which χ_0 is a very low-lying intrinsic state and $\Phi_{\nu_{II}(max)}$ is the highest class II vibrational state allowed at the excitation energy of $E_{\lambda_{II}}$. Consequently, $H''_{\lambda_I \lambda_{II}}$ will be small simply because the coefficients $C^{\lambda_{II}}_{\nu_{II}(max)\,0}$ are small for the few terms of the expansion in which $\langle \nu_I \mu' | H'' | \nu_{II} \mu'' \rangle$ may be appreciable. This can be the situation when the compound nucleus states have energies E_λ even somewhat above the intermediate barrier, as in the (n,f) reactions of the commoner fissile nuclei.

3. PROPERTIES OF CLASS-I AND CLASS-II COMPOUND STATES

3.1 Level density

The density of highly excited states of the compound nucleus is usually computed on the assumption that such states are a random superposition of independent-particle states at the same excitation energy, and this gives a level density behaviour essentially of the form

$$\rho(U) \approx C \exp\left[\sqrt{(aU)}\right] \quad (7)$$

where U is the excitation energy, and a is a parameter proportional to the density of single-particle states at the Fermi energy. The depression of the ground state of even nuclei by pairing correlations is taken into account roughly by reducing the excitation energy used in eqn. (7) by an amount equal to the energy gap. In odd-mass nuclei a partial correction of the same kind is required; the reduction in effective excitation energy in this case is $\Delta/2$.

The application of this procedure to calculation of the density of states defined in eqns. (4) and (5) is justified by the following assumptions. Firstly, the density of intrinsic states χ_μ is assumed to be that of independent-particle states. Secondly, the contribution to the density from components other than those coupled to the zero-point vibration Φ_0 is assumed negligible. If the density is computed at energy E then the effective excitation energy for independent particle state formation is $E - \mathcal{E}_0^{I}$ for class-I states and $E - \mathcal{E}_0^{II}$ for class-II states i.e. class-I states are expected to be much denser than class-II states.

More precisely, the level-density behaviour of the two classes is

$$\overline{D}_I^{-1} \equiv \rho_I(E) \approx C \exp\left[\sqrt{a_I\left(E - \delta^{I}_{Z,A}\right)}\right] \tag{8}$$

$$\overline{D}_{II}^{-1} \equiv \rho_{II}(E) \approx C \exp\left[\sqrt{a_{II}\left(E - \mathcal{E}_0^{II} - \delta^{II}_{Z,A}\right)}\right] \tag{9}$$

all energies being measured with respect to the (class-I) ground state. In these formulae the parameters a_I, a_{II} are proportional to the Fermi energy single particle densities at the deformations of the primary and secondary minima. Similarly $\delta^{I}_{Z,A}$ and $\delta^{II}_{Z,A}$ are related to the energy gaps Δ_I, Δ_{II} at these deformations, being Δ for even nuclei, $\Delta/2$ for odd-mass nuclei and zero for odd nuclei.

Calculations by Strutinsky [1] suggest that the single-particle level densities, and hence a_I, a_{II} are rather similar at the primary and secondary deformations. The relative magnitude of the energy gaps is a more difficult problem. Kennedy et al [7] suggest that the pairing force constant G depends strongly on the nuclear surface-area/volume ratio and it follows that the energy gap will be similarly affected by this quantity. Experimental information on this point is needed.

3.2 Neutron widths and excitation by particle reactions

The reduced neutron width amplitude of a state is proportional to the amplitude in the state wave-function of the configuration representing the ground state of the residual nucleus coupled to a single particle state of the neutron. Assuming that the ground state of the residual nucleus can be represented accurately by the product of the lowest class I vibrational wave-function, Φ_0^{I}, coupled to some intrinsic wave-function $\chi_\mu^{(-)}$ with three fewer (particle) degrees of freedom than the intrinsic states χ_μ, we see that while the class I compound states will generally have non-zero neutron widths, the class II state neutron widths are zero, and hence cannot be excited by simple low energy neutron bombardment in the absence of coupling to the class I states. The same applies to other simple particle reactions.

However, class II states will be excitable by higher-energy two-state particle reactions, such as (p,p'), (d,2n), proceeding through highly excited compound nucleus states that will normally include class-II vibrations in their residual nucleus configurations. Reactions such as (d,p) that are normally stripping reactions should excite class-II states through the compound nucleus process but not through the conventional stripping process; the latter leads to final states based on a single particle neutron coupled to the ground state of the target, i.e. class I states.

3.3 Fission widths

In order to discuss fission widths, the "intrinsic" component, $\sum_i H_i + \sum_{i<j} H_{ij}'$, of the Hamiltonian in eqn. (1) is defined at a fixed deformation β_0 close to the saddle point of the outer barrier. Thus the eigenstates χ_μ of the intrinsic Hamiltonian can be identified with the fission channels of A. Bohr [9]. In discussing fission widths at relatively low energy we need only consider the lowest one or few of these channels. For just one channel, in which the intrinsic state is labelled χ_0, the fission width amplitude $\Gamma_{\lambda(f)}^{1/2}$ is proportional to $\sum_\nu C_{\nu 0}^{\lambda} \Phi_\nu(\beta_0)$ i.e. to the amplitudes of the admixed vibrational states at the outer barrier. The principal contribution to this sum comes from the highest appreciably admixed vibrational state. We immediately see two reasons why the fission widths of class-II compound states are much larger than those of class-I compound states; firstly, the amplitudes $\Phi_{\nu_{II}}(\beta_0)$ are much greater (by the reciprocal of the factor C in eqn. (3)) than those of nearby class-I vibrations, and secondly the coefficients of admixture $C_{\nu 0}^{\lambda_{II}}$ are much greater than the $C_{\nu 0}^{\lambda_I}$ because the class-I states are much denser and more complex. Roughly speaking then the relative magnitudes are given by

$$\frac{\Gamma_{\lambda_I(f)}}{\Gamma_{\lambda_{II}(f)}} \approx c^2 \left(\frac{C_{\nu_I 0}^{\lambda_I}}{C_{\nu_{II} 0}^{\lambda_{II}}} \right)^2 \approx \frac{c^2 \bar{D}_I}{\bar{D}_{II}} \tag{10}$$

3.4 Radiative properties

3.4.1 Regular transitions

The primary spectrum of class I-class I transitions from states at an excitation of several MeV will be just the one that is well-known from neutron radiative capture studies, namely, a number of well separated and comparatively intense lines at high energies becoming rather weaker but much denser at lower energies. The class II-class II spectrum wil' have a similar behaviour but the widely spaced lines and cut-off will occur at a much lower energy. The strength of such transitions relative to the high energy class-I transitions will be roughly

$$\frac{\Gamma_{(\gamma;\lambda_{II}\to\lambda_{II}')}}{\Gamma_{(\gamma;\lambda_I\to\lambda_I')}} \approx \left(\frac{E_{\lambda_{II}} - E_{\lambda_{II}'}}{E_{\lambda_I} - E_{\lambda_I'}} \right)^3 \frac{\bar{D}_{II}(E_{\lambda_{II}})}{\bar{D}_I(E_{\lambda_I})} \tag{11}$$

for dipole transitions. Normally the quantities in eqn. (11) are such that we expect the class-II radiative widths of maximum energy to be at least as great as their class-I counterparts.

3.4.2 Total radiation widths

Statistical theory for total radiative widths gives the following expression

$$\Gamma_{\lambda(\gamma T)} \approx \sum_{\ell} (2\ell+1)\bar{D}(E_\lambda)\int_0^{E_\lambda} d\varepsilon_\gamma\, \varepsilon_\gamma^{2\ell+1} f_\ell(\varepsilon_\gamma)\rho(E_\lambda-\varepsilon_\gamma) \tag{12}$$

where ℓ is the multipolarity of the radiation and $f_\ell(\varepsilon_\gamma)$ is the spectral form of the intrinsic matrix elements. If a simple temperature form is used for the level density,

$$\rho(U) \propto e^{U/T} \tag{13}$$

this reduces to

$$\Gamma_{\lambda(\gamma T)} \propto 6T^4 - e^{-E_\lambda/T}\left\{TE_\lambda^3 + 3T^2E_\lambda^2 + 6T^3E_\lambda + 6T^4\right\} \tag{14}$$

under the common assumption that $f(\varepsilon_\gamma)$ is independent of ε_γ. The temperature is related to the excitation energy and single particle density parameter of the independent-particle level density law, eqn. (7), by $T = 2U^{1/2}/a^{1/2}$. For excitation energies that are not too low we find

$$\frac{\Gamma_{\lambda_I(\gamma T)}}{\Gamma_{\lambda_{II}(\gamma T)}} \approx \left(\frac{E - \delta_{Z,A}^{I}}{E - \mathcal{E}_0^{II} - \delta_{Z,A}^{II}} \cdot \frac{a_{II}^{1/2}}{a_I^{1/2}}\right)^2 \tag{15}$$

implying that the class-II radiation width is expected normally to be a few times smaller than the class-I width. The assumption that $f(\varepsilon_\gamma) \propto \varepsilon_\gamma^2$ leads to the replacement of the square by the cube power in eqn. (14). The ratio implied by eqn. (15) could however be an overestimate. The residual pairing forces of nucleons can cause the nucleus to be in its "superconducting" phase at relatively low excitation energies; in this the temperature is expected to be almost independent of excitation energy and probably considerably higher, for the class-II levels, than the value given by the independent particle model [10].

3.4.3 Cross-transitions

Cross-transitions from class-II states to class-I states or vice versa still have to be considered. The electromagnetic perturbation operator in the Hamiltonian may be split into a collective part and a single particle operator

$$\mathcal{H} = \mathcal{H}_{\text{coll}} + \mathcal{H}_{\text{sp}} \tag{16}$$

Single particle components in the transitions between class-I and class-II states are not allowed because of the orthogonality of the vibrational states. Collective components between class-I and class-II vibrational states can contribute to such transitions however. For example, there is the possibility of electric monopole transitions, leading to the emission of converted electrons: the contribution to the matrix element is

$$\sum_{\nu_I \nu_{II} \mu} C^{\lambda_{II}}_{\nu_{II}\mu} C^{\lambda_I}_{\nu_I\mu} \langle \Phi_{\nu_{II}} \chi_\mu | \mathcal{H}_{coll} | \Phi_{\nu_I} \chi_\mu \rangle$$

$$= \sum_{\nu_I \nu_{II}} \langle \Phi_{\nu_{II}} | \mathcal{H}^E_0 | \Phi_{\nu_I} \rangle \sum_\mu C^{\lambda_I}_{\nu_I\mu} C^{\lambda_{II}}_{\nu_{II}\mu} \tag{17}$$

The expression for the transition probability for $\Phi_\nu \longrightarrow \Phi_{\nu'}$ is usually written [11]

$$T_{\nu \to \nu'}(E0) = \Omega \rho^2 \tag{18}$$

The atomic factor Ω has been calculated by Church and Weneser [11], while the nuclear factor ρ^2 has been estimated by Davidson [12] for β -band to ground state transitions. For the actinide nuclei the results of these papers give lifetimes of the order of 10^{-12}s, or widths $\Gamma_{(E0,\nu \to \nu')}$ of the order of 0.5 meV. This implies that the width for the cross-decay of a class-II state, say, by electric monopole transitions will be

$$\Gamma_{\lambda_{II}(E0 \to \Sigma \lambda_I)} \approx c^2 \frac{\bar{D}_{II}}{\hbar\omega_{II}} \cdot \Gamma_{(E0,\nu_I \to \nu_I')} \tag{19}$$

Obviously such widths are negligible compared with those for regular transitions within the class.

Electric quadrupole transitions between the members of the rotational bands of such vibrational states are perhaps an order of magnitude faster; this is deduced from the paper of Davidson [12] which relates the strength of such transitions to E0 strengths. As above, we have

$$\Gamma_{\lambda_{II}(E2 \to \Sigma \lambda_I)} \approx c^2 \frac{D_{II}}{\hbar\omega_{II}} \cdot \Gamma_{(E2,\nu_I \to \nu_I')} \tag{20}$$

4. RESONANCE PHENOMENA IN DIFFERENT COUPLING CONDITIONS

4.1 Narrow class-II states; very weak coupling

When both the class-I and class-II compound states can be regarded as discrete (widths much less than all level spacings) and the coupling matrix elements are also very small we have a simple situation that can be treated by first-order perturbation theory. The wave-functions of the final states near a particular class-II level, λ_{II}, are [13]

$$X_{\lambda'} \approx X^{I}_{\lambda_I} + \frac{H''_{\lambda_I \lambda_{II}} X^{II}_{\lambda_{II}}}{E_{\lambda_I} - E_{\lambda_{II}}} \tag{21}$$

$$X_{\lambda''} \approx X^{II}_{\lambda_{II}} + \sum_{\lambda_I} \frac{H''_{\lambda_I \lambda_{II}} X^{I}_{\lambda_I}}{E_{\lambda_{II}} - E_{\lambda_I}} \tag{22}$$

These imply that in a neutron-induced fission cross-section, for example, the resonances fall into groups each of which contains one resonance with comparatively large fission width. This is the nearly pure class-II state. It will generally have a neutron width rather smaller than the average. The neighbouring resonances (nearly pure class-I states) have much smaller fission-widths rapidly attenuating with increasing distance from the class-II level. This attenuation is not expected to be monotonic, however. The coupling matrix elements are usually assumed to have a Gaussian distribution with zero mean. Thus, the fission widths of these (class-I) resonances will have a Porter-Thomas distribution about their expected values, $\langle \Gamma_{\lambda(f)} \rangle = \langle H''^{2}_{\lambda_I \lambda_{II}} \rangle_{\lambda_I} \Gamma_{\lambda_{II}(f)} / (E_{\lambda_I} - E_{\lambda_{II}})^2$

where $\langle \; \rangle_{\lambda_I}$ indicates the average over all λ_I for a single λ_{II}.

A good example of this phenomenon is provided by the slow neutron cross-section of ^{242}Pu. In this, two close fission resonances occur near 800 eV. By analysis of his fission cross-section data together with transmission data of Pattenden, James [14] has found the parameters of these resonances to be:

$$E_1 = 767 \text{ eV}, \quad \Gamma_{1(n)} = 89 \text{ meV}, \quad \Gamma_{1(f)} = 22 \text{ meV}$$

$$E_2 = 799 \text{ eV}, \quad \Gamma_{2(n)} = 465 \text{ meV}, \quad \Gamma_{2(f)} = 2{\cdot}5 \text{ meV}$$

There seems to be a clear correlation among the partial widths of the kind suggested by eqns. (21), (22), indicating the 767 eV resonance to be 85% class-II and the 799 eV resonance only 15% class-II.

The now-famous cross-sections of ^{240}Pu [15] and ^{237}Np [16][1] also seem to fall into this category [13].

4.2 Narrow class-II states; moderately weak coupling

The above case, together with that of rather stronger coupling, can be treated more exactly, provided that we need consider only the coupling

[1] There is now some evidence for the existence of a background fission cross-section of width 10 eV underlying the sharp resonances in this case. This would put the Np example in the broad class-II level situation (see Section 4. 3)

of a single class-II state with its class-I neighbours. The exact treatment [17] gives for the eigenvalues E_λ of the final states

$$\sum_{\lambda_I} \frac{H''^2_{\lambda_I \lambda_{II}}}{E_{\lambda_I} - E_\lambda} = E_{\lambda_{II}} - E_\lambda \tag{23}$$

and the admixture of the class-II state into the final states is given by

$$\left(C^\lambda_{\lambda_{II}}\right)^2 = 1 \Bigg/ \left[\sum_{\lambda_I} \frac{H''^2_{\lambda_I \lambda_{II}}}{(E_{\lambda_I} - E_\lambda)^2} + 1 \right] \tag{24}$$

These equations become more transparent for a model of uniformly spaced class-I levels with equal values of $H'^2_{\lambda_I \lambda_{II}}$. We then find

$$\frac{\pi H''^2}{D_I} \cot\text{an} \left[\frac{\pi (E_\lambda - E_{\lambda_I})}{D_I} \right] = E_{\lambda_{II}} - E_\lambda \tag{25}$$

for the eigenvalues, and

$$\left(C^\lambda_{\lambda_{II}}\right)^2 = \frac{H'^2}{(E_{\lambda_{II}} - E_\lambda)^2 + \pi^2 H''^4/D_I^2 + H''^2} \tag{26}$$

for the mixing coefficients. Thus we have a Lorentzian form of half-width $W = \sqrt{(\pi^2 H''^4/D_I^2 + H''^2)}$ for the fission widths of the resonances around a class-II state, i.e.

$$\Gamma_{\lambda(f)} = \frac{H''^2 \, \Gamma_{\lambda_{II}(f)}}{(E_{\lambda_{II}} - E_\lambda)^2 + W^2} \tag{27}$$

We surmise this Lorentzian form to hold for the more general case of non-uniform matrix elements and spacings, with the proviso that eqn. (27) now expresses an expected value of the fission width for the resonance at E_λ and in practice there will be fluctuations about this expectation value. This surmise is borne out by numerical experiments in which the class-I level spacing distribution is of the Wigner type and the coupling strengths $H''^2_{\lambda_I \lambda_{II}}$ are given a Porter-Thomas distribution. It is found, in these calculations, that the expectation value of W is

$$\overline{W} = 0{\cdot}83 \sqrt{\left(\pi^2 \overline{H''^2}^2 / \overline{D}_I^2 + \overline{H''^2}\right)} \tag{28}$$

the numerical constant having been determined with about 3% accuracy.

An example of moderately weak coupling is provided by the neutron cross-section of ^{234}U. The neutron and fission widths of most resonances have been determined up to about 800 eV neutron energy [18]. A Lorentzian energy dependence has been fitted to the fission widths, yielding a half-width value W = 26 eV. The fluctuations of the fission width data about this curve are indeed consistent with a Porter-Thomas distribution (Fig. 3).

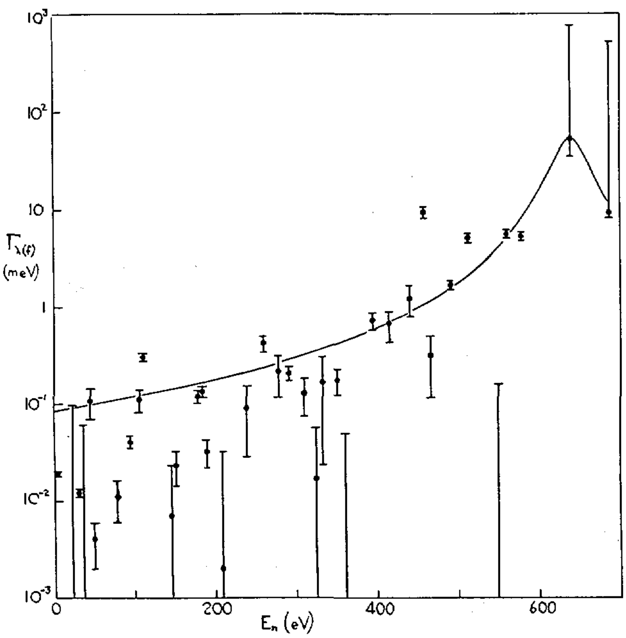

FIG. 3. Fission widths of resonances in reaction $^{234}U(n, f)$. The full curve is a Lorentz function fitted to these.

4.3 "Broad" class-II states; weak coupling

If the class-II state has a fission width that is large compared to the class-I level spacing it becomes more difficult to determine resonance properties. For moderately weak or very weak coupling the properties of the final discrete R-matrix states are still given by eqns. (24) or (21), (22) respectively, but these states are not reflected directly by the cross-section. Very strong interference, or "quasi-resonance" effects [19] appear in the cross-section, so we really need to determine the parameters of the poles of the collision matrix (or S-matrix) in the complex energy plane to obtain the correct resonance properties. These poles can be found directly from the final R-matrix states by the use of numerical techniques. For the weak coupling condition, however, perturbation theory can be used. In essence, the class-II state is first coupled to the continuum, and this continuum wave-function of class-II type is coupled to the class-I wave-function expanded in terms of class-I R-matrix states. The resulting wave-function of the system with incoming unit flux in a particle entrance channel is, in first order, just that corresponding to the class-I R-matrix states with modified wave-functions

$$X'_{\lambda_I} = X^{I}_{\lambda_I} - \frac{H''_{\lambda_I\lambda_{II}} X^{II}_{\lambda_{II}}}{E_{\lambda_{II}} - E_{\lambda_I} - \frac{1}{2} i\Gamma_{\lambda_{II}(f)}} \qquad (29)$$

This implies that the particle-induced fission cross-section has resonances close to the energies of the class-I states with fission widths

$$\Gamma_{\lambda(f)} \approx \frac{H''^{2}_{\lambda_I\lambda_{II}} \; \Gamma_{\lambda_{II}(f)}}{(E_{\lambda_{II}} - E_{\lambda_I})^2 + \frac{1}{4}\Gamma^2_{\lambda_{II}(f)}} \tag{30}$$

In addition to the narrow resonance poles, however, it can also be shown that there is a pole far off the real energy axis (the distant pole); this corresponds to the class-II state. The associated fission width is essentially that of the class-II state, while its partial neutron width is given by

$$\Gamma^{1/2}_{(n)} \approx \sum_{\lambda_I} \frac{\Gamma^{1/2}_{\lambda_I(n)} \; H''_{\lambda_I\lambda_{II}}}{E_{\lambda_I} - E_{\lambda_{II}} + \frac{1}{2}i\Gamma_{\lambda_{II}}} \tag{31}$$

As pointed out by Weigmann [20] this is no stronger, and may be much weaker, than the neutron widths of the narrow resonances. Hence the weak, broad resonance term provided by this pole may be quite indistinguishable in the cross-section.

4.4 Recognition of broad class-II levels

4.4.1 Cross-section behaviour

The Lorentzian form of the narrow resonance fission widths in eqn. (30) is identical with that of eqn. (27), apart from the fact that the half-width W of the latter is not half the class-II fission width, but, rather, half the class-II "coupling width" into the primary minimum, "$\Gamma_{\lambda_{II}(c)}$" ($\approx 1.7\pi \overline{H''^{2}_{\lambda_I\lambda_{II}}} / \bar{D}_I$, for coupling that is not too weak). The question of the physical resolution of this ambiguity is important.

In principle the two cases are distinguished by the existence of the distant pole in the broad level limit. Although the actual background cross-section provided by this pole is very weak, there is some possibility that its interference with the narrow resonances may be detectable. Numerical examples show that such interference is not strong. For example, resonance parameters and coupling matrix elements of class-I levels have been drawn at random and coupled with a class-II level (at the origin) with the parameters $\Gamma_{\lambda_{II}(f)} = 20$, "$\Gamma_{\lambda_{II}(c)}$" $= 4.3$, $\bar{D}_I = 1$.

Parameters of some of the class-I levels and of the final R-matrix levels are shown in Table I. Part of the cross-section calculated with these R-matrix parameters (circles and crosses) is shown in Fig. 4. These points have been fitted (smooth curves) with R-matrix expressions using levels based only on the observable resonances. It is apparent that this

TABLE I. CLASS-II STATE AT ZERO: $\Gamma_{\lambda_{II}(f)}$ = 20, "$\Gamma_{\lambda_{II}(c)}$" = 4.3. SOME PARAMETERS.

Class I			Coupled			Poles		Cross-section fit		
E_{λ_I}	$\Gamma_{\lambda_I(n)}$	$H^{\prime\prime 2}_{\lambda_I\lambda_{II}}$	E_λ	$\Gamma_{\lambda(n)}$	$\Gamma_{\lambda(f)}$	$E_m^{(H)}$	$\Gamma_m^{(H)}$	E'_λ	$\Gamma'_{\lambda(n)}$	$\Gamma'_{\lambda(f)}$
-0.932	0.0070	0.387	-1.011	0.0089	0.299	-0.947	0.091	-0.947	0.0077	0.0665
-0.037	0.0147	0.032	-0.056	0.0156	0.222	-0.038	0.041	-0.037	0.0182	0.0050
			0.256	0.(3)3	2.813	0.792	15.154			
0.928	0.0022	1.89				0.903	0.414	0.928	0.0024	0.390
1.072	0.0051	0.0056	1.072	0.0048	0.(3)57	1.072	0.025	1.072	0.0048	0.009
			1.934	0.0046	2.574					
2.246	0.0070	0.274				2.250	0.082	2.25	0.0070	0.053
			2.369	0.(3)2	0.605					
2.585	0.0248	0.577				2.577	0.164	2.58	0.0259	0.125
			3.141	0.0353	4.503					
3.465	0.0051	0.015	3.478	0.0016	0.255	3.465	0.028	3.47	0.0049	0.0036
4.632	0.0158	0.066	4.649	0.0130	0.084	4.635	0.047	4.64	0.0128	0.0125

fitted set (pseudo-parameters), although reproducing the circles and crosses extremely well, looks very different from the true parameters. On the other hand, they are very similar to the class-I parameters, and their fission widths are given closely by eqn. (30).

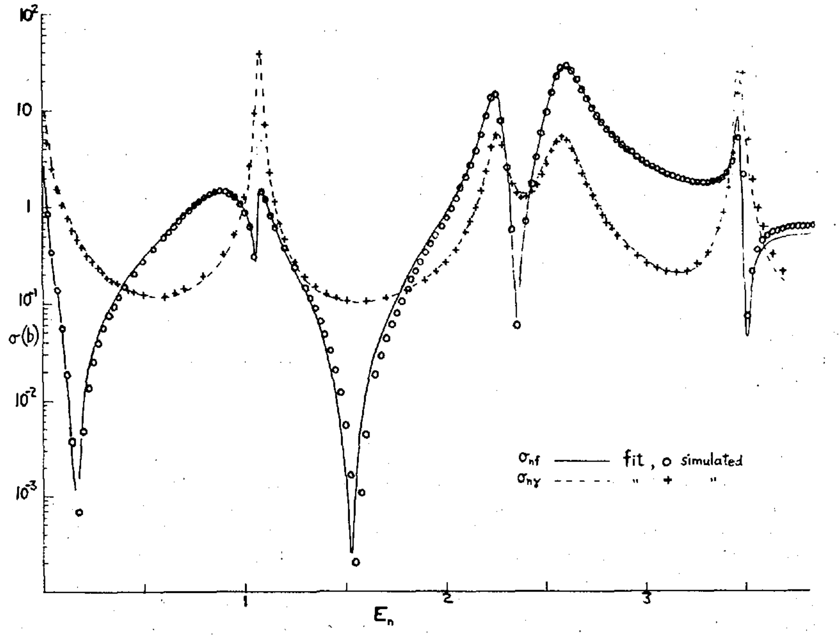

FIG. 4. Simulated cross-sections and fits for very weak coupling to broad class-II compound state. Some parameters are given in Table I.

4.4.2 Radiative properties

The radiative widths for deexcitation to the class-II "ground" state, the spontaneously fissioning isomer, may be calculated from eqn. (26) or (29). We obtain

$$\Gamma_\lambda(\gamma \to s.f.i) \approx \frac{H''^2\, \Gamma_{\lambda_{II}}(\gamma T)}{(E_{\lambda_{II}} - E_\lambda)^2 + W^2} \qquad (32)$$

where $W = \frac{1}{2}\,"\Gamma_{\lambda_{II}}(c)"$ for a narrow class-II level and $W = \frac{1}{2}\Gamma_{\lambda_{II}}(f)$ for a broad class-II level. Since $\Gamma_{\lambda_{II}}(\gamma T)$ can be estimated reasonably closely (see Sec. 3.4.2) the observation of $\Gamma_\lambda(\gamma \to s.f.i)$ provides a useful tool for distinguishing between the two cases.

One example of this has been reported. The ^{241}Am (n,f) cross-section [21] shows a distinct maximum, which we assume to be a class-II group, around 400 eV with a width of about 300 eV. The individual resonances are not resolvable in this bump, but they can be observed at very low neutron energies, [22], where they are found to have a spacing of 0.56 eV (1.1 eV per spin state), a mean fission width of 0.2 meV and a radiation width of 40 meV. In this same very low energy region it has been found that the neutron capture cross-section leading to the isomer is only 3×10^{-7} of the cross-section leading to the ground state [23] i.e. $\bar{\Gamma}_{\lambda(\gamma \to s.f.i)} / \Gamma_{\lambda_I(\gamma T)} \approx 3 \times 10^{-7}$. From eqns. (32) and (15) we deduce that $H''^2_{\lambda_I \lambda_{II}}$ is about 0.3 eV^2, and therefore "$\Gamma_{\lambda_{II}(c)}$" is only 2 eV. Hence the width of the class-II Lorentz group must be the class-II fission width.

Direct observation of the capture γ-ray spectrum may also distinguish between the two situations. As explained in Section 3.4.1 the class-II spectrum will be identifiable by widely spaced transitions at low gamma-ray energies.

4.4.3 Higher energy structure

Often structure is found in reactions leading to the fissioning compound nucleus at a much higher energy than that of the Lorentzian group under discussion. This structure may reveal that the outer barrier to fission is high, hence class-II fission widths have to be comparatively low.

An example of this is the ^{234}U (n,f) cross-section, the low energy resonance structure of which has already been mentioned (Section 4.2). Structure is apparent in the fast neutron-induced fission cross-section at 300 keV and even higher at 840 keV [24]. In addition, the angular distribution of the fission products emitted at these high energies both in the (n,f) and (d,pf) reactions shows marked structure. As pointed out by Strutinsky and Bjørnholm [25] this renders a low outer barrier unlikely; at "threshold" (the higher barrier) the low, outer barrier would yield a large number of open saddle-point fission channels with different spin projections on the cylindrical symmetry axis, thus washing out the angular anisotropy. On these grounds we expect $\Gamma_{\lambda_{II}(f)}$ to be small at energies close to the neutron threshold; the width of the 600 eV group, therefore, is probably the "coupling width" as we assumed in Section 4.2.

<u>4.5 Broad class-II states; moderate coupling</u>

When the class-II "coupling width" becomes of the same order of magnitude as the class-II fission width, the Lorentzian formula for the resonance fission widths breaks down. For small "coupling width" it can be shown that the width associated with the distant pole is $\Gamma_{\lambda_{II}(f)}$ - "$\Gamma_{\lambda_{II}(c)}$". As the "coupling width" increases this pole approaches the Lorentzian family of poles and eventually mingles with them. A numerical example of the distribution of resonance fission widths in a typical case of moderate coupling is shown in Fig. 5, in which uniform distributions of spacings and coupling widths have been assumed. A Lorentzian curve is shown for comparison. Formal treatments of two-channel reactions showing the same phenomenon have been given by Lejeune and Mahaux [26].

Some of the wider resonant states in such distributions may still be too broad to be observable as individual peaks in the cross-section but now the possibility exists that they can be identified by careful analysis. A simulated example, with parameters drawn by Monte Carlo procedures, is given in Fig. 6, circles and crosses indicating the cross-section generated by the true R-matrix parameters. Here, the class-II fission

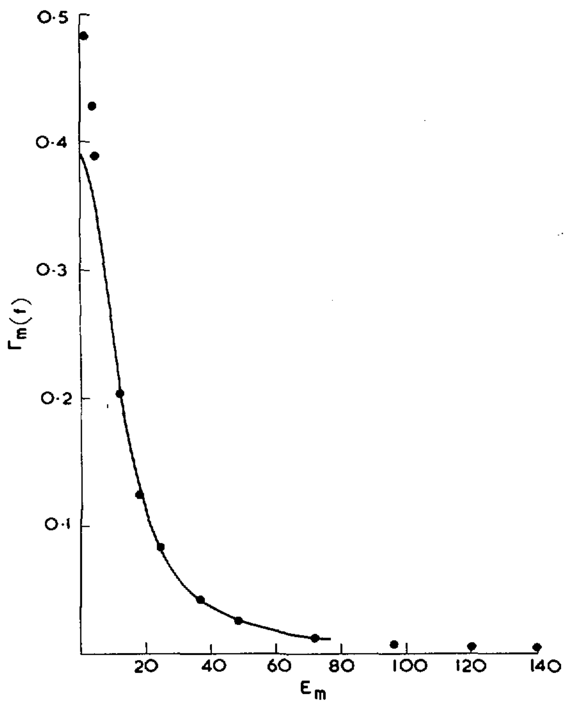

FIG. 5. Resonance fission widths when class-II fission and coupling widths are comparable: $\Gamma_{\lambda_{II}(f)} = 25$, $\Gamma_{\lambda_{II}(c)} = 13.1$, $\bar{D}_I = 1.2$.

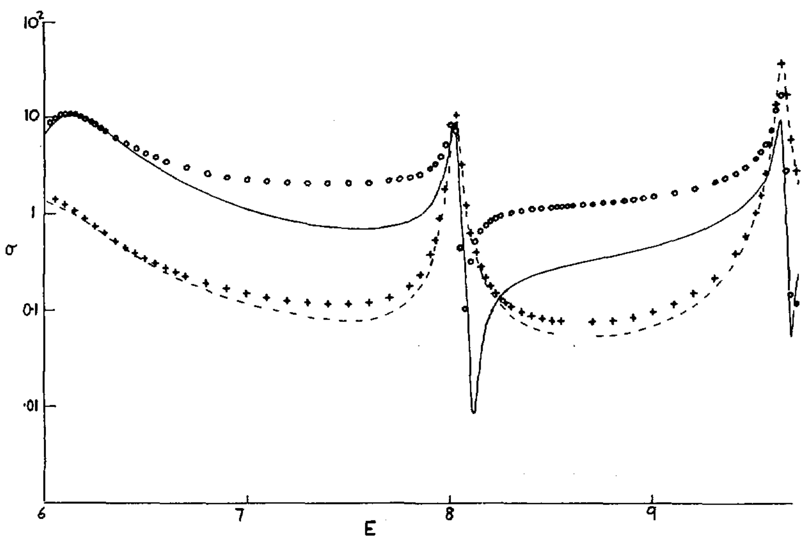

FIG. 6. Simulated cross-sections and attempted fit, when coupling is comparable to class-II fission. A broad background term underlies this region.

width is 20 times the mean resonance spacing, and the coupling width is 17 of these units. These R-matrix levels give rise to strong quasi-resonance behaviour. The best attempt at R-matrix fitting using parameters suggested by the observable peaks is shown by the smooth curves. The large discrepancy between these and the points is attributable to a broad pole in the vicinity. Where such poles do not occur the R-matrix fits are good, as shown in Fig. 7.

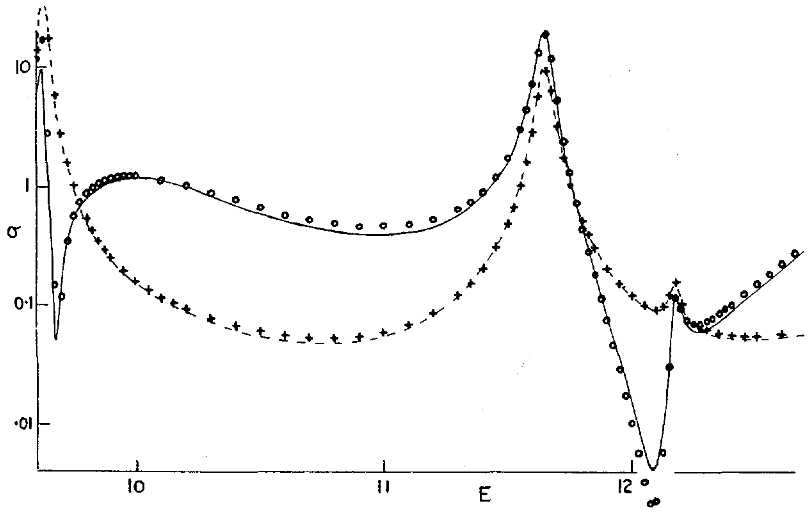

FIG. 7. As Fig. 6, but this is a neighbouring energy region where there is no background resonance indicated by the S-matrix analysis.

5. STRUCTURE PHENOMENA RELATED TO VIBRATIONAL MODE DAMPING

5.1 Spontaneously fissioning isomers

The spontaneously fissioning isomers are believed to be almost pure class-II states; specifically they are the class-II ground states of their respective nuclei, being the zero-point class-II vibration coupled to the lowest intrinsic state at the secondary deformation. The partial lifetime against decay by fission is governed by the parameters of the outer barrier (see eqn. 39). The competing process, electromagnetic decay towards the normal ground state, is given partially by eqns. (19) and (20) for cross-transitions, but there is also a contribution from the small admixture with nearly class-I states. This admixture is calculated by first-order perturbation theory; the isomer wave-functions are

$$X_{is} \approx \Phi_0^{II}\chi_0 + \sum_{\lambda_I} \frac{\langle \Phi_0^{II}\chi_0 | H'' | X_{\lambda_I}^{I} \rangle X_{\lambda_I}^{I}}{E_{\lambda_I} - E_0^{II}} \tag{33}$$

where $E_0^{II} = \mathcal{E}_0^{II} + \epsilon_0$

The second term gives a contribution to the radiation width of

$$\Gamma'_{is(\gamma)} \approx \sum_{\lambda_I} \frac{\langle \Phi_0^{II}\chi_0 | H'' | X_{\lambda_I}^{I} \rangle^2}{(E_{\lambda_I} - E_0^{II})^2} \cdot \Gamma_{\lambda_I(\gamma T)} \tag{34}$$

The matrix element in eqn. (34) may be expressed thus

$$\langle \Phi_0^{II} \chi_0 | H'' | X_{\lambda_I}^{I} \rangle^2 \approx c^2 \langle \Phi_{\nu_I} \chi_0 | H'' | X_{\lambda_I}^{I} \rangle^2 \tag{35}$$

where Φ_{ν_I} is the class-I vibration nearest in energy to $\mathcal{E}_0^{II}$. The last matrix element can in turn be expressed as the Lorentzian half-width $W_{\nu_I 0}$ for mixing of the mode $\Phi_{\nu_I} \chi_0$ into the class-I states; thus,

$$\langle \Phi_0^{II} \chi_0 | H'' | X_{\lambda_I}^{I} \rangle^2 \approx c^2 \frac{W_{\nu_I 0} \bar{D}_I}{\pi} \tag{36}$$

We can now estimate the sum in eqn. (34) and obtain

$$\Gamma'_{is(\gamma)} \approx c^2 \frac{\pi}{2} \cdot \frac{W_{\nu_I 0}}{D_I} \cdot \Gamma_{\lambda_I(\gamma T)} \tag{37}$$

We see that radiation due to the class-I impurity in the isomer exceeds the zero-order width (eqn. 20) by a factor

$$\frac{\Gamma'_{is(\gamma)}}{\Gamma_{\lambda_{II}(E2\to\Sigma\lambda_I)}} \approx \frac{W_{\nu_I 0}}{\bar{D}_I} \cdot \frac{\Gamma_{\lambda_I(\gamma T)}}{\Gamma_{(E2;\, \nu_I \to \nu_I')}} \tag{38}$$

which will usually be two or three orders of magnitude. The width can be estimated for the potential of figure 2a and an odd nucleus. The factor C^2 is only 2.5×10^{-13} (fig. 2b); at an excitation energy of 3 MeV the class-I spacing will be 200 eV (Lang and Le Conteur's level density formula [39]), the radiation width will be about 12 meV (eqn. (15) combined with neutron resonance data), and we assume $W_{\nu_I 0}$ to be 50 keV. We find $\Gamma'_{is(\gamma)} \approx 10^{-13}$ eV or the partial half-life $\tau_{is(\gamma)} \approx 1\, ms$. This is not too inconsistent with the observed isomer half-lives, which range around 0.1 to 10 m in the odd americium isotopes.

5.2 Pure vibrational levels

The spontaneously fissioning isomers are probably the purest examples of class-II vibrational states that are essentially unmixed with other class-II states. Other examples are probably to be found among the first and second excited class-II vibrational states, especially in the even and odd-mass nuclei in which the existence of the energy gap gives rise to a very low density of more complex class-II states that could cause damping.

From a simple statistical point of view, such vibrational states can be viewed as one-dimensional states bounded by a potential barrier in both directions, the dense states of the primary minimum now being regarded as a continuum. The standard estimates for the fission width $\Gamma_{II(f)}$ for penetrating the outer barrier and the coupling width $\Gamma_{II(c)}$ for passing the intermediate barrier are

$$\Gamma_{II(f)} = \frac{\bar{D}_{II}}{2\pi} \Big/ \left\{ 1 + \exp\left[2\pi (V_B - E_{II}) / \hbar\omega_B \right] \right\} \tag{39}$$

$$\Gamma_{II(c)} = \frac{\bar{D}_{II}}{2\pi} \Big/ \left\{ 1 + \exp\left[2\pi (V_A - E_{II}) / \hbar\omega_A \right] \right\} \tag{40}$$

where $\bar{D}_{II}$ is here the vibrational state spacing $\hbar\omega_{II}$. We may now evaluate the mean fission width of a fine structure resonance close to the vibrational level. Using Blatt & Weisskopf's argument [27] for the period of classical recycling of a system with quantum levels with spacing D_λ we have

$$\frac{\Gamma_{\lambda(f)}}{D_\lambda} = \frac{T_V}{2\pi} \tag{41}$$

where T_V represents the probability of exciting the vibrational level followed by de-excitation through fission:

$$T_V = \frac{\Gamma_{II(c)}\, \Gamma_{II(f)}}{(E_\lambda - E_{II})^2 + \frac{1}{4}(\Gamma_{II(c)} + \Gamma_{II(f)})^2} \tag{42}$$

Alternatively, T_V can be computed as the transmission coefficient of a free wave through a double-humped barrier. This has been done for combinations of quadratic barrier and secondary well-shape in references [28] and [29].

In the formalism of the present paper the vibrational state has the simple wave-function

$$X_{\lambda_{II}}^{II} = \Phi_{\nu_m}^{II} \chi_0 \tag{43}$$

χ_0 being an "intrinsic" state that is low-lying at the outer barrier; the notation ν_m indicates that the vibrational level is the highest energetically available. Such a state has a fission width $\Gamma_{\lambda_{II}(f)}$ that is the product of the squared amplitude of the vibrational wave-function at the outer barrier with a factor for penetration through the remainder of the barrier. Coupling with the class-I states gives the vibrational state a "coupling width" also: this is

$$\text{“}\Gamma_{\lambda_{II}(c)}\text{”} \approx 1{\cdot}7\pi\, \overline{H''^{\,2}_{\lambda_I \lambda_{II}}} \,/\, \bar{D}_I \tag{44}$$

which, on using the eqns. analogous to (35), (36), becomes

$$"\Gamma_{\lambda_{II}(c)}" \approx 2c^2 W_{\nu_I 0} \tag{45}$$

At least one well-founded example of a vibrational state, apart from the isomers, is known. Its properties have been determined from the ^{230}Th (n,f) reaction in which it is observed as a narrow sub-barrier peak at about 700 keV neutron energy. Recent high-resolution measurements by Earwaker and James [32] have shown that the overall width of this peak is about 30 keV and the maximum cross-section is 130 mb. Their measurements also show that any underlying sub-structure must have a spacing very much less than 2 keV, the best resolution used. This indicates that it is most unlikely that there is any fluctuating structure (such as class-II compound state structure) wider than the resonance fine-structure. These are the grounds for interpreting the peak as an essentially pure vibrational state.

The coupled intrinsic state χ_0 (the fission channel) is known to have spin projection K = $\frac{1}{2}$ from fission product angular distribution measurements [41]. Its parity is unknown. In analyzing the cross-section data we must consider the rotational band structure built on the vibrational level. Thus, if χ_0 has even parity, neutron s-waves excite compound nucleus states of spin $\frac{1}{2}$, which fission through the K = $\frac{1}{2}$, I = $\frac{1}{2}$ vibrational level, while neutron d-waves excite compound states of spin $^3/_2$ and $^5/_2$, fissioning through the I = $^3/_2$ and $^5/_2$ rotational members of the band. Higher neutron l-waves are negligible at this energy. Fig. 8 shows the cross-section data of James and Earwaker together with possible fits. The smooth curve, which gives the best fit, is based on the assumptions that the moment of inertia of the rotational band is four times greater than value for the ground state rotational band in ^{231}Th while the decoupling parameter a = - 0.5. The half-width of the Lorentzian profile of fission widths of the fine-structure resonances (eqn. 27) is only 7 keV. This last figure can hardly be varied; it is given rather critically by the leading slope of the cross-section peak. The moment of inertia and decoupling parameters can be varied, but not within wide limits; the conclusion remains that, if the intrinsic state has even parity, the moment of inertia is much greater than the normal value associated with the primary minimum. The broken curve assumes odd parity for the intrinsic state χ_0, and a separation of the I = $\frac{1}{2}$ and I = $^3/_2$ members of the band of 17 keV; because the decoupling parameter cannot also be fixed this tells us little about the moment of inertia.

As usual, it is completely ambiguous whether the Lorentzian width 2W is the vibrational state fission width or the "coupling width" connecting to class-I states. Whichever it is, the analyses described above give 1.9 keV for the other width.

Other possible class-II vibrational states have been revealed by (d,pf) measurements. For example, sharp sub-barrier peaks have been observed [30] in the fission probability ($P_f = \sigma(d,pf)/\sigma(d,p)$) of ^{234}U, (4.4 & 5.0 MeV), ^{236}U (4.8 MeV) (see Fig. 9). Such measurements with high resolution below the neutron threshold are of great potential value for the exploration of the spectroscopy of the secondary minimum. Gamma-ray emission is the only process competing with fission, so measurements can, in principle, be made far below the barrier.

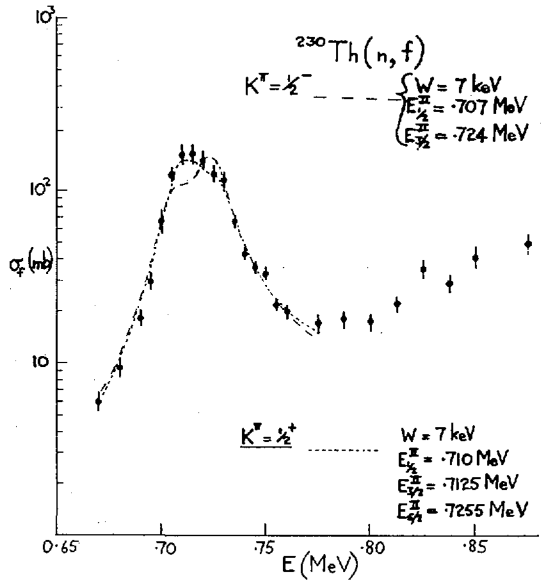

FIG. 8. The ^{230}Th(n, f) cross-section. Fitting assumes pure class-II vibrational state. Absolute scale (σ) is preliminary.

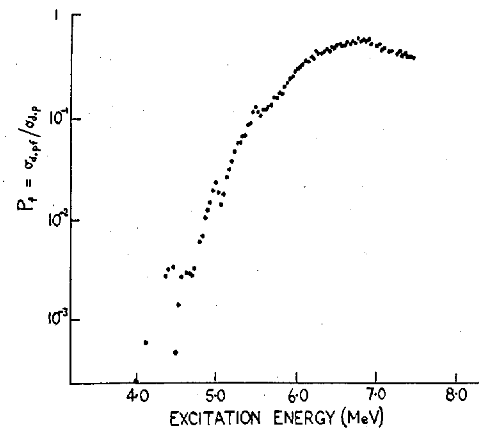

FIG. 9. The ^{233}U(d, pf) reaction indicating class-II vibrational states.

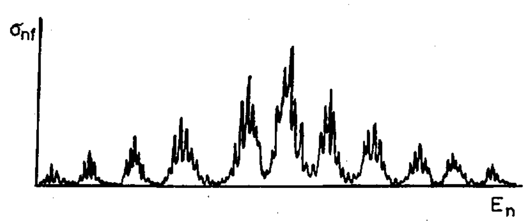

FIG. 10. Schematic diagram of neutron induced fission cross-section across a weakly-damped class-II vibrational state.

5.3 Damped vibrational states

Other gross structure in fission reactions seems to be attributable, not to pure vibrational states, but to class-II vibrations already damped to some extent by mixing with other states of the class-II type as in eqn. (5). This mixing however is not so severe as to spread the fission mode rather uniformly over class-II compound states in a wide energy interval. The general appearance of the fission cross-section will be that of groups of fine-structure resonances, the average fission strength of each group increasing as the energy is increased through the vibrational state and then decreasing beyond this level (Fig. 10).

Strong evidence for a damped vibrational state is found in the ^{242}Am (n,f) reaction. Fine structure resonances with mean spacing of 0.56 eV and a mean fission width of 0.2 meV have been observed at very low energies [22]. At higher neutron energies (up to a few keV) there is rather distinct evidence for class-II structure with a spacing of about 0.5 keV, while the overall behaviour of the cross-section up to about 50 keV [21] reveals strong peaking of the mean fission width, the peak being centred at about 15 keV and having a half-width of about 7 keV [17]. There is no strong evidence for rotational band splitting. It has already been shown (Section 4.4.2) that the lowest class-II group seems to be an example of very weak coupling of the class-I states to a broad class-II level. From this fact it can be deduced [31] that the gross behaviour of the mean fission width (over the first few tens of keV) is due to the variation of the coupling strength in a qualitatively Lorentzian fashion. This behaviour of the coupling matrix element reflects the behaviour of the coefficient $C^{\lambda_{II}}_{\nu_m 0}$ in its expansion, eqn. (6), in the double-humped potential picture. The very low value, 14 keV, of the damping width of the vibrational state into the class-II states is rather surprising. At this excitation energy of the compound nucleus the ratio of the class-II level spacing (500 eV) to the class-I spacing indicates that the effective excitation energy in the second minimum of the odd ^{242}Am nucleus is about 2.4 MeV.[2]

The fission width of the vibrational state $\Phi^{II}_{\nu_m} \chi_0$ is inferred to be about 30 keV. That this natural width is not reflected in the width of the Lorentz peak for $\overline{\Gamma}_f$ is apparently a result of the coupling strength, as well as the class-II fission widths, being of Lorentz form. Numerical calculations of the resonance pole behaviour bear this out. For Fig. 11 it was assumed that the discrete vibrational level with fission width 11 keV was mixed into the class-II compound states with a damping width of 10 keV. The coupling strengths of the class-II levels to the class-I levels, as well as the class-II level fission widths, was assumed proportional to this mixing with a value 1700 eV^2 at the centre of the vibrational level. After coupling to the fission continuum three families of poles were found as shown in the diagram. Only the lowest, dense family corresponds to fine structure resonance peaks. The fission strength behaviour averaged over individual class-II groups shows a peaking behaviour with a width of just over 10 keV (close to the vibrational damping width). Essentially the same behaviour for the fission strength is found when the damping width of the vibrational level is halved so that the fission width exceeds it; the fine structure resonance strength is peaked with the damping width.

---

[2] This discussion may have to be amended in the light of a recent measurement by Migneco et al. (SM 122/140, abstract in these Proceedings) of $^{241}Am(n,f)$. They do not confirm the structure seen in Ref. [21]; apart from fine-structure resonances, their cross-section up to 3keV seems very featureless.

Damped vibrational behaviour is also indicated by the reaction ^{234}U (n,f). In this the fine structure resonances and narrow intermediate structure found at low neutron energies (section 4.2) seem to be associated with the wing of a damped vibrational level. The relevant level may be the one that is revealed by the structure at 300 keV neutron energy; this is known, from the angular distribution of the fission products, to be associated with a $K = \frac{1}{2}$ fission channel. With the assumption of an outer barrier at 600 keV (neutron energy) and a tunnelling parameter $\hbar\omega_B \approx 0{\cdot}8\,\mathrm{MeV}$, the class-II fission width, $\sim 0{\cdot}3$ eV, deduced from the data below 1 keV can be explained by a vibrational level damping width of about 30 keV. Recent high resolution measurements by Earwaker and James [42] confirm that the width of the 300 keV structure is of this order of magnitude (perhaps nearer 80 keV; the difference can be explained as Porter-Thomas fluctuation). The magnitude of the cross-section at 300 keV is consistent with this hypothesis.

High resolution (d,pf) reactions exploring the compound nucleus far below the neutron threshold have revealed damped vibrational phenomena in ^{240}Pu among other nuclei [33]. The fission probability P_f, defined as $P_f = \sigma(d,pf)/\sigma(d,p)$ shows a gross peak at 5 MeV compound nucleus excitation energy about 170 keV wide. There has been some debate as to whether this is a true peak in the fission probability or a residual

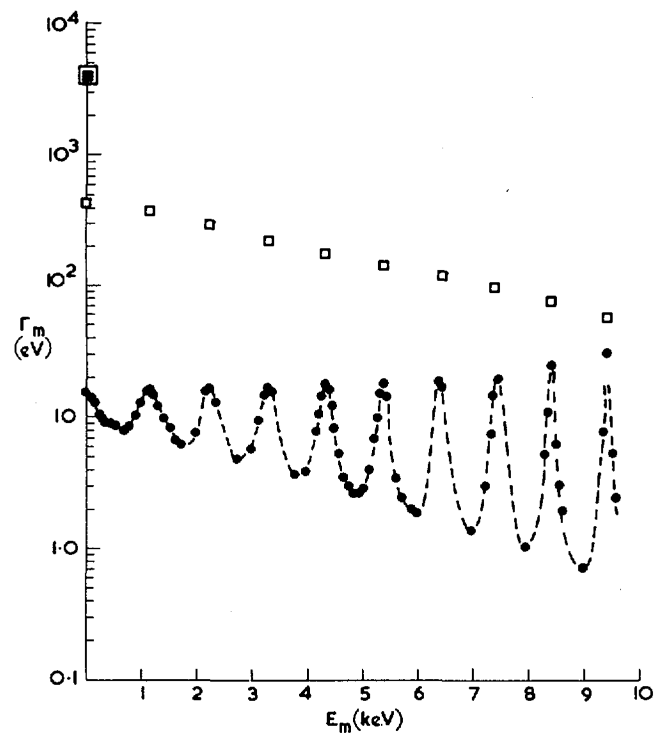

FIG. 11. S-matrix poles of the weakly damped vibrational mode. There is one far-distant pole corresponding approximately to the vibrational state, a family of moderately-distant poles corresponding to the class-II compound states, and a dense family of near poles, giving the narrow resonances, that is approximate to the class-I compound states.

effect from structure in particular angular momentum states of the (d,p) reaction. Recent ^{240}Pu (p,p'f) measurements [34] suggest that the fission probability has a plateau rather than a peak in this energy region. The matter is still inconclusive but its resolution may have something to do with the fact that the (p,p') reaction is expected to excite class-II states as well as class-I states, whereas the (d,p) reaction should strongly favour class-I states (see Section 3.2). When competition with γ-ray emission is taken into account, the fission yield from the class-II excitation could be found to saturate over a wide energy region even though the fission widths themselves show peaking.

Sub-structure in the gross peak has been revealed by the 15 keV resolution (d,pf) measurements [33]. These indicate that the spacing of the underlying class-II structure is itself of the order of 50 keV. This is not inconsistent with the difference in potential energy between the primary and secondary minima (2.4 MeV) that is deduced from narrow intermediate structure observed in the compound nucleus resonances of the ^{239}Pu (n,f) reaction [35, 36].[3]

5.4 Strongly damped modes

When the class-II vibrational mode is strongly damped into the class-II compound states, gross structure in the fission cross-sections will be washed out although narrow intermediate structure may exist even in dramatic form. By strong damping we mean that the damping width of the vibrational mode is of the order of the vibrational spacing.

The assumption of strong damping somewhat simplifies the estimation of the coupling strength between class-I and class-II compound states. The coefficients $(C^{\lambda_I}_{\nu_I\mu})^2$ and $(C^{\lambda_{II}}_{\nu_{II}\mu})^2$ become, on average, roughly $\bar{D}_I/\hbar\omega_I$ and $\bar{D}_{II}/\hbar\omega_{II}$. Following the treatment given in [17] we find that the average class-II state "coupling widths" should be

$$\text{“}\Gamma_{\lambda_{II}(c)}\text{”} \approx \frac{2\pi\,\overline{H''^{2}_{\lambda_I\lambda_{II}}}}{\bar{D}_I} \approx 4c^2\bar{D}_{II} \tag{46}$$

provided that ω_I and ω_{II} have similar values, ω. If we substitute in eqn. (46) the expected value of the separation $|\mathcal{E}_{\nu_I} - \mathcal{E}_{\nu_{II}}|$ namely $\frac{1}{4}\hbar\omega = 0.2$ MeV and the value of the constant K determined for the potential of Fig. 2 we find

$$\text{“}\Gamma_{\lambda_{II}(c)}\text{”} \approx 0{\cdot}15\,\bar{D}_{II}\exp\left[-2\pi\left(V_A - E_{\lambda_{II}}\right)/\hbar\omega_A\right] \tag{47}$$

which is essentially the formula found by statistical methods [25].

There is as yet no evidence for gross structure in the fast neutron induced fission cross-sections of a number of nuclei, for example, ^{237}Np, ^{238}Pu, ^{242}Pu, and it may be supposed that the class-II vibrational

[3] Some of the sub-structure has been interpreted as rotational structure by Back et al. (these Proceedings) yielding a moment of inertia of about twice that of the ground-state band.

states are rather strongly damped at the excitations involved. Certainly the class-II compound state spacings as revealed in the neutron resonance work are rather small, indicating a deep secondary minimum, and this is consistent with rather strong damping.

From eqn. (47) and the neutron resonance data on narrow intermediate structure we can make rough deductions about the height of the intermediate barrier. In the case of the ^{242}Pu (n,f) and ^{237}Np (n,f) reactions it is believed that the class-II states have been identified as sharp resonances (see Section 4.1) and the deduced coupling strengths can be used immediately in eqn. (47).

The analysis of the ^{238}Pu (n,f) reaction is not so clear. The cross-section as measured by Silbert [37] is shown in Fig. 12; the full curve is an attempted fit (my own) with Lorentzian behaviour of the resonance

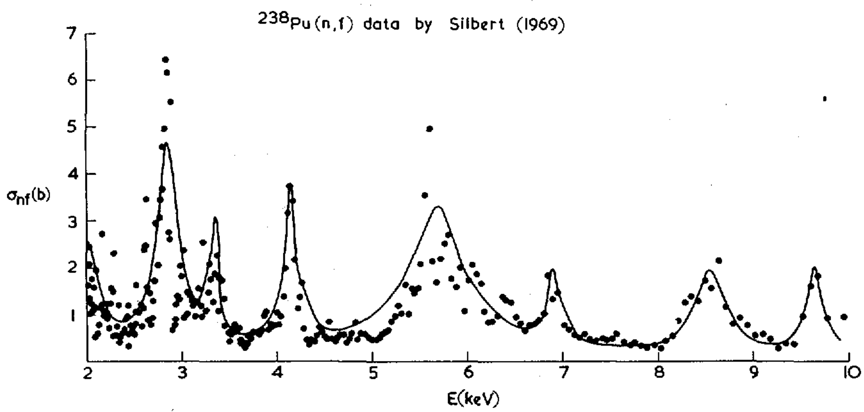

FIG. 12. The ^{238}Pu(n, f) cross-section. Data by Silbert [39]. Curve is a crude Lorentzian fit with parameters given in Table II.

TABLE II. VERY CRUDE ANALYSIS OF ^{238}Pu (n, f) CROSS-SECTION

$E_{\lambda_{II}}$(eV)	Lesser $\Gamma_{\lambda_{II}}$(f) or (c)	Higher $\Gamma_{\lambda_{II}}$(c) or (f)	Remarks
290	$\gg$ 0.25	$\ll$ 170	$\Gamma_{\lambda_{II}}(f)\,\Gamma_{\lambda_{II}}(c) \approx 400$
720	1	100	
2000	2.5	200	
2850	15	85	
3300	2	100	
4150	10	60	
5700	50	250	perhaps 3 groups
6900	5	100	
8550	15	250	
9650	10	90	

fission widths using the parameters of Table II. We are obviously dealing with a case in which the secondary minimum is deep and the barriers are close to the neutron separation energy. The apparent lack of correlation between the class-II fission and "coupling" widths is interesting. It suggests the availability of different and/or more than one saddle-point channel for the two barriers; this is consistent with the strong-damping hypothesis.

It is to be noted however that in the cross-section of the ^{240}Pu (n,f) reaction up to a few hundred keV neutron energy [38] there are some signs of gross structure with widths of the order of 50 keV or more. This suggests that even in this group of nuclei with deep secondary minima vibrational damping may still be incomplete.

6 DEDUCTIONS ABOUT THE FISSION BARRIER

Data of the kind discussed in Sections 3 to 5 yield much information about the new, complex picture that we have of the fission barrier. All this information is summarised in Table III.

Spontaneous fission isomer half-lives yield an estimate of the quantity $(V_B - \mathcal{E}_0^{II})/\hbar\omega_B$, if it is assumed that the outer barrier is of inverted harmonic oscillator form. Barrier heights are also obtained from the reaction induced fission data. If the properties (fission width and coupling width) of the class-II vibrational state can be obtained, then barrier heights, as ratios of the tunnelling parameters, $\hbar\omega_A$ and $\hbar\omega_B$, can be deduced from eqns. (39) and (40). Otherwise it is assumed that the condition of strong damping of the vibrational state holds and eqn. (47), and its equivalent for the class-II fission width, may be used to deduce the barriers. In all estimates of fission barriers given in the table, it was assumed that $\hbar\omega_A = \hbar\omega_B = 0.8$ MeV. Direct data for the greater of the two barriers are also obtained from the induced-fission yield curves. Uncertainties in all these estimates of barriers probably amount to two or three hundred keV.

The difference in primary and secondary potential minima (or, more exactly, the difference between the energies of the ground state and spontaneously fissioning isomer) has sometimes been measured directly from the excitation curve for formation of the isomer [6, 43]. In other cases it has been deduced from the observed ratio of class-II to class-I level spacings in the slow neutron induced fission data. For this last purpose it has been assumed that the single particle level density parameters, in eqns. (8), (9), a_I and a_{II}, and also the energy gap quantities Δ_I, Δ_{II}, are equal. In the calculations of ground state energy by Nilsson et al [8], the pairing force was assumed proportional to surface area. If the same assumption were employed here the secondary minimum would be lowered by up to 0.5 MeV for odd-mass nuclei and nearly one MeV for even nuclei.

The general trend that emerges from Table III is one of a weak, secondary minimum in the thorium nuclei, becoming considerably deeper in the lighter uranium nuclei without the barriers changing appreciably. In the neptunium, plutonium series of nuclei the secondary minimum seems to reach its greatest development, and there seems to be a definite persistence for the outer barrier to be higher than the inner one (although some workers would argue on the basis of fission product angular distribution data that the opposite is true; see e.g. [44]). In the americium nuclei the secondary minimum seems to be shallower again and there also

TABLE III. SUMMARY OF EXPERIMENTAL OBSERVATIONS ON THE STRUTINSKY FISSION BARRIER

The inferred barrier properties are very crude with errors that will usually be of the order of a few hundred keV. Channel effects are not mentioned explicitly, although these can be inferred in some cases from the remarks or the spin assignment against $\bar{D}_I$.

Compound Nucleus	Observation	Isomer ½-life (μs)	Class-II vibrational state $E_{\nu_{II}^0}$ (MeV)	$\Gamma_{\nu_{II}^0(D)}$ (keV)	$\Gamma_{\nu_{II}^0(f)}$ (keV)	$\Gamma_{\nu_{II}^0(c)}$ (keV)	$\bar{D}_I$ (eV)	$\bar{D}_{II}$ (eV)	"$\Gamma_{\lambda_{II}(c)}$" (eV)	$\Gamma_{\lambda_{II}(f)}$ (eV)	Barrier properties (in MeV) E_0^{II}	V_A	V_B	Greater of V_A, V_B	Remarks
^{231}Th	(n, f)[32]		5.74	0	12	1.9					$\gtrsim$4.3	6.0	6.2	$\gtrsim$ 6.1	(a),(b) (c),(f)
^{233}Th	(n, f)		6.7	Total	width $\approx$	150								$\gtrsim$ 6.8	(b)
^{232}Pa	(n, f)[47]		5.99	Total	width $\lesssim$	50								$\gtrsim$ 6.7	(b)
^{233}U	(n, f)[48]						5($J^\pi=\frac{1}{2}^+$)			~50(?)				< 5.9	(d),(c)
^{234}U	(d, pf)[30] isomer [46]	 0.035	4.4 5.0										E_0^{II} + 3.7 6.0	$\gtrsim$ 5.4	(e) (f) (f)
^{235}U	isomer [46] (n, f) [18] (n, f) [42]	0.024	5.55	≈80	≈10	≈50	12($J^\pi=\frac{1}{2}^+$)	7 × 10^3	50	0.3	2.7	5.6	5.9	$\gtrsim$ 5.9	(f) (c),(b)
^{236}U	isomer [46] (n, f) [49] (d, pf) [30]	0.067	4.8				0.5($J^\pi=3^-4^-$)	$\gtrsim$ 260†			> 2.6		> 6.5	$\gtrsim$ 5.3	(f) (e)
^{238}Np	(n, f) [16]	0.034					0.67($J^\pi=2^+3^+$)	54	3.3	0.4	2.2	5.4 *	6.2 *	$\gtrsim$ 6.1	(b),(f)
^{239}Pu	isomer [43]	0.034									4.1			8	(f)
^{239}Pu	(n, f) [37]						13($J^\pi=\frac{1}{2}^+$)	10^3	≈120	≈10	2.1	5.6	5.9		(a),(f) (d)

* Values reversed if existence of broad weak resonance terms can be confirmed (see papers Dabbs et al., Paya et al., these Proceedings)

† Based on correlogram analysis which is very difficult (see James and Patrick, Perez et al., these Proceedings).

TABLE III.(cont.)

Compound Nucleus	Observation	Isomer $\frac{1}{2}$-life (μs)	Class-II vibrational state				$\bar{D}_I$ (eV)	$\bar{D}_{II}$ (eV)	"$\Gamma_{\lambda II(c)}$" (eV)	$\Gamma_{\lambda II(f)}$ (eV)	Barrier properties (in MeV)				Remarks
			$E_{\nu_{II}^0}$(MeV)	$\Gamma_{\nu_{II}^0(D)}$(keV)	$\Gamma_{\nu_{II}^0(c)}$(keV)	$\Gamma_{\nu_{II}^0(c)}$(keV)					E_0^{II}	V_A	V_B	Greater of V_A, V_B	
^{240}Pu													6.0		(f)
	isomer [43]	0.009						460†			2.4†				
								≈ 50 × 10³			2.3*			$\gtrsim$ 4.9	(g), (e)
	(n, f) [35]						3 (J^π=1+)						5.8		(f)
	(d, pf) [33]		5.0	≈ 170			160(J^π=0+)	700	50	0.1	1.9	5.6	6.4		(c), (f)
														$\gtrsim$ 6.2	(b)
^{241}Pu	isomer [43]	0.03													
	(n, f) [15]						14(J^π=$\frac{1}{2}$+)								
	(n, f) [38]		5.57	≈ 100											
^{242}Pu	isomer [43]	0.05											5.9		(f)
	(d, pf) [30]		4.8					$\lesssim$ 28 × 10³	$\lesssim$ 20	0.025	$\lesssim$3.3	~5.8	$\lesssim$6.6	$\gtrsim$ 5.9	(b)
^{243}Pu	isomer [43]	0.06													
	(n, f) [14]						14(J^π=$\frac{1}{2}$+)				3.4		8.1		(f)
^{238}Am	isomer [51]	60									2.9		6.9		(f)
^{239}Am	isomer [43]	0.16									3.2		8.4		(f)
^{240}Am	isomer [6]	900									2.5		6.7		(f)
^{241}Am	isomer [43]	1.5									2.9		8.4		(f)
														$\gtrsim$ 6.4	(b)
^{242}Am	isomer [23]	14 × 10³						500	2	300	3.1	6.4	5.6		(f)
	(n, f) [21]						0.56(J^π=2⁻, 3⁻)		(at E_n=400 eV)						
	(n, γ→is)[23]		5.495	15	30	0.05									

* Back et al. also give 2.3 MeV for E_0^{II}, 6.0 MeV for V_A, 5.8 MeV for V_B.

† Correlogram analysis very difficult (James and Patrick, Perez et al.) but D_{II} ≈ 400 eV confirmed by $\bar{\alpha}$-measurements (Schomberg, Sowerby).

Remarks:

(a) Ambiguity between fission and coupling widths, hence V_A, V_B may be interchanged.

(b) Last column is rough estimate from (n, f) reaction.

(c) K = $\frac{1}{2}$ intrinsic state.

(d) Strong fission observed in slow neutron resonances.

(e) Last column from analysis of Ref. [50] (0⁺ channel).

(f) Assumed that $\hbar\omega_B \approx 0.8$ MeV for barrier heights.

(g) $\bar{D}_I$ extrapolated from slow neutron resonances (excitation 6.4 MeV) to 5 MeV.

appears to be a reversal of the barrier heights. Other peculiarities occur here e.g. the tunnelling parameter $\hbar\omega_B$ seems to be much smaller than the 0.8 MeV that seems acceptable for other nuclei, and ground state spontaneous fission is anomalous with respect to the isomer [45]. One gains the impression that there is a definite discontinuity in the characteristics of the potential energy surface in the plutonium-americium region.

REFERENCES

1 STRUTINSKY, V. M., Nucl. Phys. A95 (1967) 420 and A122 (1968) 1.

2 NILSSON, S. G., Mat. Fys. Medd. Dan. Vid. Selsk. 29 (1955) No. 16.

3 MOTTELSON, B. R., NILSSON, S. G., Mat. Fys. Skr. Dan. Vid. Selsk. 1 (1959) No. 8.

4 FLEROV, G. N., POLIKANOV, S. M., GAVRILOV, K. A., MIKHEEV, V. L., PERELYGIN, V. P., PLEVE, A. A., JETP 45 (1963) 1396.

5 POLIKANOV, S. M., Uspeki Fiz. Nauk 94 (1968) 43.

6 BJØRNHOLM, S., BORGGREEN, J., WESTGAARD, L., KARNAUCHOV, V. A., Nucl. Phys. A95 (1967) 513.

7 KENNEDY, R. C., WILETS, L., HENLEY, E. M., Phys. Rev. 12 (1964) 513.

8 NILSSON, S. G., Rep. UCRL-18355 (1968).

9 BOHR, A., Int. Conf. Peaceful Uses atom. Energy (Proc. Conf. Geneva, 1955) 2, UN, New York (1956).

10 KAMMURI, T., Prog. Theor. Phys. 31 (1964) 595.

11 CHURCH, E., WENESER, J., Phys. Rev. 103 (1956) 1035.

12 DAVIDSON, J. P., Nucl. Phys. 86 (1966) 561.

13 LYNN, J. E., "Theory of Neutron Resonance Reactions", p.463 Clarendon Press, Oxford, 1968.

14 JAMES, G. D., Nucl. Phys. A123 (1969) 24.

15 MIGNECO, E., THEOBALD, J. P., Nucl. Phys. A112 (1968) 603.

16 FUBINI, A., BLONS, J., MICHAUDON, A., PAYA, D., Phys. Rev. Lett. 20 (1968) 1373.

17 LYNN, J. E., UKAEA Rep. AERE-R5891(1968)

18 JAMES, G. D., SLAUGHTER, G. G., to be published.

19 LYNN, J. E., in "Nuclear Structure Study with Neutrons", (NEVEDE MEVERGNIES, VAN ASSCHE, VERVIER, Eds.), North-Holland, Amsterdam (1966).

20 WEIGMANN, H. Zeit. Phys. 214 (1968) 7.

21 SEEGER, P. A., HEMMENDINGER, A., DIVEN, B. C., Nucl. Phys. A96 (1967) 605.

22 BOWMAN, C. D., COOPS, M. S., AUCHAMPAUGH, G. F., FULTZ, S. C., Phys. Rev. 137 (1965) B326.

23 POLIKANOV, S. M., Nuclear Structure (Proc. Int. Symp., Dubna, 1968) IAEA, Vienna (1968), 449.

24 LAMPHERE, R. W., Physics and Chem. of Fission (Proc. Symp. Salzburg, 1965) 1, IAEA, Vienna (1965) 63.

25 STRUTINSKY, V. M., BJØRNHOLM, S., Nuclear Structure (Proc. Inst. Symp., Dubna, 1968), IAEA, Vienna (1968), 431.

26 LEJEUNE, A., MAHAUX, C., Nucl. Phys. A113 (1968) 272.

27 BLATT, J. M., WEISSKOPF, V. F., "Theoretical Nuclear Physics", p. Wiley, New York (1952).

28 CRAMER, J. D., NIX, J. R., Contribution to this Conference SM-122/103.

29 WONG, C. Y., BANG, J., Phys. Letts. 29B (1969) 143.

30 PEDERSEN, J., KUZMINOV, B. P., Phys. Letts. (1969).

31 LYNN, J. E., Nuclear Structure (Proc. Int. Symp., Dubna 1968), IAEA, Vienna (1968), 463.

32 EARWAKER, L., JAMES, G. D., Contribution to this Conference SM-122/61.

33 SPECHT, H. J., FRASER, J. S., MILTON, J. C. D., DAVIES, W. G., Contribution to this Conf. SM-122/128.

34 BRITT, H. C., CRAMER, J. D., BURNETT, S. C., Contribution to this Conf. SM-122/102.

35 PATRICK, B. H., JAMES, G. D., Phys. Letts. 28B (1968) 258.

36 MICHAUDON, A., Nuclear Structure (Proc. Int. Symp., Dubna, 1968), IAEA, Vienna (1968), 485.

37 SILBERT, M. G., LASL Rep. LA-4108-MS (1969).

38 BYERS, D. H., DIVEN, B. C., SILBERT, M. G., Neutron Cross Section Technology (Proc. Conf. Washington, 1966) 2, p.903, USAEC Rep. CONF-660303 (1966).

39 LANG, J. M. B., LE COUTEUR, K. J., Proc. Phys. Soc., A67 (1953) 586.

41 GOKHBERG, B. M., OSTROSCHENKO, G. A., SHIGIN, V. A., Dokl. Akad. Nauk. SSSR 128 (1959) 1157.

42 EARWAKER, L., JAMES, G. D., Private communication.

43 LARK, N., SLETTEN, G., PEDERSEN, J., BJØRNHOLM, S., to be published.

44 KAPITZA, S. P., RABOTNOV, N. S., SMIRENKIN, G. N., SOLDATOV, A. S., USACHEV, L. N., TSIPENYUK, Yu. M., JETP Letts., 9 (1969) 73.

45 NIX, J. R., WALKER, G. E., Los Alamos Rep. LA-DC-10, 114 (1968).

46 ELWYN, A., FERGUSON, A. T. G., private communication.

47 DUBROVINA, S. M., SHIGIN, V. A., Doklady Akad. Nauk. SSSR 157 (1964) 561.

48 FARRELL, J. A., Contribution to this conf. SM-122/105.

49 CAO, M. G. MIGNECO, E., THEOBALD, J. P., Phys. Letts. 27B (1968), 409.

50 BRITT, H. C., RICKEY, F. A., HALL, W. S., Phys. Rev. 175 (1968), 1525.

51 BORGGREEN, J., GANGRSKY, Y. P., SLETTEN, G., BJØRNHOLM, S., Phys. Letts. 25B (1967) 402.

DISCUSSION

L. WILETS: It appears that current experiments leave open the question of determining the location of the isomeric well. For example, in some cases at least, the second minimum could be oblate (60° in a β-γ plot). Shape isomers of this character were discussed very early by Wheeler, and the 1953 Hill-Wheeler paper [Phys. Rev. 89 (1953) 1102] also pointed out that the "minimum" might be either shallow or unstable (saddle points) in respect of gamma-motion. This has been confirmed by K. Kumar and M. Baranger [Nucl. Phys. A110 (1968) 529] in the first rare-earth region, but such calculations have not been performed for the fissile nuclei. (Note that pairing does tend to stabilize axially symmetric shapes.) It would be well if the analysis of isomeric phenomena were to keep open the possibility of oblate deformations. If, for example, we could verify experimentally that the shapes are prolate (as we usually presume), this would add credence to the Strutinsky model.

J.E. LYNN: The theory that I have outlined in this paper does not, in fact, exclude the existence of a path towards fission through an oblate minimum. The narrow intermediate structure in the (n, f) cross-sections, particularly of ^{237}Np and ^{240}Pu, does however imply the existence of only one effective path towards fission for the class-I states, this path being through the secondary minimum regardless of whether this is oblate or prolate. This is because the ratio of fission strength in the class-II groups to that between the groups is much too large to allow the existence of an alternative route for the class-I states.

Concerning the question of deciding whether the secondary minimum is prolate or oblate, we hope that measurements of the kind I have shown on ^{230}Th(n, f) will ultimately settle this.

K. DIETRICH: The coupling between the class-II and class-I states has a lot in common with the coupling of analogue states to the $T_<$-states they are embedded in. The coupling of the shape isomers to the class-I states is likely to exhibit more diversity, because the strength of the coupling depends on the detailed form of the barrier. Furthermore, I feel that the coupling between the class-I and class-II states involves a complication which is absent in the corresponding coupling of the analogue states, namely that the most adequate decomposition of the Hamiltonian into vibrational, intrinsic and coupling parts depends on whether one wishes to describe class-I, class-II or saddle-point states. An intrinsic state, which is a simple 1p-1h excitation in relation to the lowest-lying class-II state, appears to be a superposition of a great many p-h excitations if expanded in terms of basic functions which are adapted to the class-I states. As long as you are discussing the general formalism, this complication does not occur. But I fear that it will appreciably complicate the actual calculation of the coupling matrix-elements.

J.E. LYNN: This is true. The intrinsic part of the Hamiltonian in the formal theory I described has to be specified for a fixed deformation, say β_0. If one is interested in the fission widths of states and fission cross-sections, as here, then it is natural to specify β_0 as the deformation corresponding to the outer barrier. The intrinsic states then correspond to Bohr channels. As you suggest, in this case a simple state of, say, class-I type may then appear rather complicated when expanded in terms of the intrinsic states at β_0. Nevertheless, I believe that the calculation of matrix elements under the assumption that H'' is just $H_{int}(\beta) - H_{int}(\beta_0)$ may still be possible.

H.J. SPECHT: You have mentioned that the neutron widths of the class-II states are zero so that a (d,p)-reaction would not excite class-II states (at least not via its direct part), whereas a (p, p')-reaction might. I wonder whether this difference would still appear if the coupling between the class-I and class-II states were taken into account, for example at the position of a vibrational resonance.

J.E. LYNN: This is true if the question is made to refer rather to the probability of different reactions leading to fission. In the absence of coupling a direct (d, p)-reaction will lead to negligible fission, whereas a (p, p')-reaction could give appreciable fission (by excitation of class-II states). The existence of coupling, which essentially mixes the class-I and class-II states into the final states, allows the (d, p)-process to be followed by fission and also increases the yield of fission following (p, p'), because the class-I states that would be excited in the absence of coupling can now decay by fission. The actual rates for these processes will depend on the degree of coupling and the competition from radiative decay.

P. von BRENTANO: I would like to ask you about the life-times of the isomers. Looking at the observed life-times in the uranium, plutonium and, if the assignments are correct, in the curium isotopes, we find that all of them lie in the 5-1000 ns range. On the other hand, the spontaneous half-lives of these nuclei vary by a factor of 10^9. Could you explain this difference?

J.E. LYNN: A large part of the difference is certainly due to the fact that the ground states have to tunnel through the entire potential barrier, while the isomers only have to penetrate a single hump. Whether or not the existing range of isomer half-lives is reasonable after this point is taken into consideration, and the whole question of possible systematics of isomer half-lives, are probably better left for discussion when the papers on shape isomers are presented at the next session.

STATISTICAL TESTS FOR THE DETECTION OF INTERMEDIATE STRUCTURES IN THE FISSION CROSS-SECTIONS OF ^{235}U AND ^{239}Pu

P.B. PEREZ, G. de SAUSSURE
Oak Ridge National Laboratory,*
Oak Ridge, Tenn.

and

M.N. MOORE,
San Fernando Valley State College,
Northridge, Calif., United States of America

Abstract

STATISTICAL TESTS FOR THE DETECTION OF INTERMEDIATE STRUCTURES IN THE FISSION CROSS-SECTIONS OF ^{235}U AND ^{239}Pu. The existence of intermediate structures in the neutron-induced fission cross-sections of ^{235}U and ^{239}Pu was pointed out in 1957 by Egelstaff. An interpretation, recently proposed by Cao et al. and Blons et al., was based on the Strutinsky calculations of the deformation energies of the compound nucleus when shell effects are included in the liquid-drop model. The theoretical interpretation in terms of current reaction theories has been given by Weigmann and Lynn.

The purpose of this paper is to develop and evaluate various statistical tests intended for the detection and interpretation of these narrow intermediate fission structures. A fission cross-section was computed in the interval 0-5 keV using randomly generated parameters with distributions chosen to mock up the ^{235}U nucleus. The $J^{\pi} = 4^-$ state fission width was "modulated" in the manner suggested by Weigmann's work.

Auto-correlation and cumulative average tests were done on these mock-up cross-sections to determine if the correct average spacing of the shape isomer levels could be obtained by such tests. It is shown that the usual correlation tests tend to overestimate the spacing between structures. A proposed technique is based on the direct analysis of the averaged cross-section which affords a method of correcting for peaks of the intermediate structure below the detectability limit of the usual statistical tests. The techniques developed on the basis of the mock-up cross-sections were used to analyse the fission cross-sections of ^{235}U and ^{239}Pu. Average spacings of 227 and 312 eV were found for those two nuclei, respectively. These values are somewhat lower than the ones reported by Cao and Blons, which were based only on the auto-correlation analysis.

The energy of the second minimum in the fission barrier was found to be 3.1 MeV for ^{235}U and 2.9 for ^{239}Pu. Both values are in close agreement with the values of 3 MeV predicted by Strutinsky.

I. INTRODUCTION

Recently Migneco and Theobald [1] observed the presence of fission resonances groups in the subthreshold fission cross section of ^{240}Pu, which showed an average spacing roughly two orders of magnitude larger than the average level spacing in the compound nucleus. Similar findings were reported by Paya et al. [2] in the ^{237}Np nucleus. An interpretation of this subthreshold pattern has been given by several authors, Lynn [3], Weigmann [4], and Feshbach and Kerman [5]. The central feature of the theoretical model is the presence of a second minimum in the fission barrier for highly deformed nuclei. This peculiar structure was found by Strutinsky [6] after correcting the liquid drop model of the nucleus by shell effects. Provided that the second well is shallower than the compound nucleus potential minimum, the levels in the Strutinsky well will

* Operated by Union Carbide Corporation, Nuclear Division, for the US Atomic Energy Commission.

act as intermediate states leading to resonances whenever a matching occurs between levels in the two potential wells. There is ground to believe that this subthreshold structure will also appear in fissile nuclei like ^{235}U and ^{239}Pu, due to the tunneling of the fission modes through the double-humped fission barrier in those channels which are partially open. The presence of this narrow intermediate structure besides being of relevance in the understanding of the fission process itself might provide an explanation for the wide fluctuations observed in the capture to fission ratio, α, of various fissile nuclei.

The purpose of this paper is to evaluate various statistical tests for the detection of subthreshold fission lines in the presence of the epithreshold fission arising from the fully open channels. The basic approach is to mock-up the fission cross sections of both nuclei by Monte Carlo techniques. A subthreshold fission cross section component is also manufactured in a similar way and combined with a Breit-Wigner component, to mock-up fission cross sections with intermediate structures. The various statistical tests are then applied to the artificial fission cross sections, evaluated and extrapolated to the corresponding experimental cross sections.

The first section is devoted to an elementary derivation of the modified Breit-Wigner lines arising from the presence of the second Strutinsky well, and to a cursory explanation of the technique to obtain the mocked-up cross sections. The correlation test, ratio of variance to squared average test, and distribution tests are presented in subsequent sections. We introduce the following nomenclature; the fission cross section for s-wave neutrons without the intermediate structure is given as $(S_3 + S_4)$ for ^{235}U and as $(S_0 + S_1)$ for ^{239}Pu. The symbols S_4^1 and S_1^1 indicate that the spins S_4 for ^{235}U and S_1^1 for ^{239}Pu have been modulated by the Strutinsky effect.

II. THE STRUCTURE OF THE SUBTHRESHOLD FISSION MODES AND CROSS SECTION CALCULATIONS

Rigorous treatments of the structure of the subthreshold fission modes have been given by Weigmann [4] and Lynn [3]. A, perhaps less rigorous but quite transparent, derivation can be obtained by adapting the classical Breit-Wigner treatment of resonance lines to the case of two interacting potential wells. We assume a physical picture in which the neutron and radiation eigenstates interact only with the first potential well. The fission modes have sources at both potential minima, which in turn interact with each other. Calling $b_\alpha(t)$ the time dependent amplitudes of the various modes (α = n, r, f, j, and k for the neutron, radiation, fission, and bound states of the first and second wells, respectively), we have from the usual time-dependent perturbation theory:

$$\frac{d}{dt} a_\alpha(t) = -\frac{i}{\hbar} \sum_j H_{\alpha j}\, a_j(t) e^{i(\omega_\alpha - \omega_j)t} \qquad (\alpha = n,r) \tag{1}$$

$$\frac{d}{dt} a_f(t) = -\frac{i}{\hbar} \sum_j H_{fj}\, a_j(t) e^{i(\omega_f - \omega_j)t} - \frac{i}{\hbar} \sum_k H_{fk}\, a_k(t) e^{i(\omega_f - \omega_k)t} \tag{2}$$

$$\frac{d}{dt} a_j(t) = -\frac{i}{\hbar} \sum_\alpha H_{j\alpha}\, a_\alpha(t) e^{i(\omega_j - \omega_\alpha)t} - \frac{i}{\hbar} \sum_k H_{jk}\, a_k(t) e^{i(\omega_j - \omega_k)t} \tag{3}$$

$$(\alpha = n,r,f)$$

and

$$\frac{d}{dt} a_k(t) = -\frac{i}{\hbar} \sum_f H_{kf}\, a_f(t) e^{i(\omega_k - \omega_f)t} - \frac{i}{\hbar} \sum_j H_{kj}\, a_j(t) e^{i(\omega_k - \omega_j)t} \tag{4}$$

where calling H_1 the perturbation operator, one has:

$$H_{\alpha\beta} = \langle \varphi_\alpha | H_1 | \varphi_\beta \rangle \tag{5}$$

$$a_\alpha(t) = b_\alpha(t) e^{i\omega_\alpha} \tag{6}$$

and

$$\hbar\omega_\alpha = E_\alpha \tag{7}$$

Laplace transformation of the above differential equation, yields, after elimination of the neutron, radiation and fission modes:

$$\begin{aligned} &(p + \frac{1}{2\hbar} \Gamma_j)\, a_j(p) = \\ &= -\frac{i}{\hbar} \frac{H_{jn_o}}{p - i(\omega_j - \omega_{n_o})} - \sum_k \left(\frac{1}{2\hbar} \Gamma_f^{jk} + \frac{i}{\hbar} H_{jk}\right) a_k[p - i(\omega_j - \omega_k)] \end{aligned} \tag{8}$$

$$\left(p + \frac{1}{2\hbar} \Gamma_k\right) a_k(p) = -\sum_j \left(\frac{1}{2\hbar} \Gamma_f^{kj} + \frac{i}{\hbar} H_{kj}\right) a_j[p - i(\omega_k - \omega_j)] \tag{9}$$

where we have neglected the effect of neighboring levels in both wells, and used the following definitions of the various widths:

$$\frac{1}{2} \Gamma_z^{xy} = \lim_{p \to 0^+} \frac{1}{\hbar} \sum_z \frac{H_{xz} H_{zy}}{p - i(\omega_x - \omega_z)} \tag{10}$$

and

$$\begin{aligned} \Gamma_j &= \Gamma_{nj} + \Gamma_{rj} + \Gamma_{fj} \\ \Gamma_{fk} &= \lim_{p \to 0^+} \frac{1}{\hbar} \sum_f \frac{H_{kf} H_{fk}}{p - i(\omega_f - \omega_k)} \end{aligned} \tag{11}$$

Next, we neglect the widths, Γ_f^{jk} and Γ_f^{kj}, which are second order in the coupling between wells, versus H_{kj}, and obtain from Eqs. (8) and (9):

$$a_j(p) = - \frac{(i/\hbar)\left(H_{jn_o}\right)}{[p - i(\omega_j - \omega_{jn_o})]\left(p + \frac{1}{2\hbar}\tilde{\Gamma}_j\right)} \tag{12}$$

and

$$a_k(p) = - \sum_j \frac{H_{kj}\, H_{jn_o}}{\hbar^2[p - i(\omega_k - \omega_{n_o})]\left[p - i(\omega_k - \omega_j) + \frac{1}{2\hbar}\Gamma_j\right]\left[p + \frac{1}{2\hbar}\tilde{\Gamma}_k\right]} \tag{13}$$

where the following effective widths have been introduced

$$\frac{1}{2\hbar}\tilde{\Gamma}_j = \frac{1}{2\hbar}\Gamma_j + \sum_k \frac{H_{jk}\, H_{kj}}{\hbar^2\left[p - i(\omega_j - \omega_k) + \frac{1}{2\hbar}\Gamma_k\right]} \tag{14}$$

and

$$\frac{1}{2\hbar}\tilde{\Gamma}_k = \frac{1}{2\hbar}\Gamma_{fk} + \sum_j \frac{H_{kj}\, H_{jk}}{\hbar^2\left[p - i(\omega_k - \omega_j) + \frac{1}{2\hbar}\Gamma_j\right]} \tag{15}$$

Summing over all the levels in the first well and neglecting their widths results into:

$$\tilde{\Gamma}_k = \Gamma_{fk} + \Gamma_{ks} \tag{16}$$

with the spreading width Γ_{ks} defined as

$$\Gamma_{ks} = \lim_{p\to 0^+} \frac{1}{\hbar} \sum_j \frac{H_{kj}\, H_{jk}}{p - i(\omega_k - \omega_j)} \tag{17}$$

Laplace inversion of Eqs. (12) and (13) and utilization of Eq. (6) yields the following asymptotic behavior of the fission modes amplitudes, $b_f(t)$:

$$b_f(t) = \frac{i}{\hbar}\left[\frac{e^{i(\omega_f - \omega_{n_o})t} - 1}{\omega_f - \omega_{n_o}}\right]\left(\sum_j\left\{\frac{(i/\hbar)\, H_{jn_o}\, H_{fj}}{i(\omega_j - \omega_{n_o}) + \frac{1}{2\hbar}\tilde{\Gamma}_j}\right.\right.$$

$$\left.\left. + \sum_k \frac{H_{kj}\, H_{jn_o}\, H_{fk}}{\hbar^2\left[i(\omega_j - \omega_{n_o}) + \frac{1}{2\hbar}\Gamma_j\right]\left[i(\omega_k - \omega_{n_o}) + \frac{1}{2\hbar}\tilde{\Gamma}_k\right]}\right\}\right) \tag{18}$$

from which the asymptotic probability, $W_f(t)$, can be obtained by means of the relation

$$W_f(t) = \lim_{t\to\infty} \int_{-\infty}^{\infty} d\omega_f\, \rho(\omega_f)\, |b_f(t)|^2 \tag{19}$$

Utilization of the relationship between cross section and the transition rate computed from the expression, Eq. (19), yields for a given spin component:

$$\sqrt{E}\,\sigma(E) = \frac{c}{\hbar^2}\, g \sum_j \left(\frac{\Gamma_{onj}\, \Gamma_{fj}}{|W_j + \delta_j|^2} + \sum_k \frac{\Gamma_{fk}\, A_{kj}\, \Gamma_{onj}}{\hbar^2 |W_j|^2\, |W_k|^2}\right) \tag{20}$$

where Γ_{onj} and Γ_{fj} are the reduced neutron width and fission width, respectively, of the levels in the first well, and where

$$c = 6.5210^5 \text{ (barns eV}^{1/2}\text{)}$$

$$A_{kj} = H_{kj}\, H_{jk},$$

$$W_j = (1/2\hbar)\, \Gamma_j + i(\omega_j - \omega_{n_o})$$

$$W_k = (1/2\hbar)\, \Gamma_k + i(\omega_k - \omega_{n_o})$$

$$\hbar\, \omega_{n_o} = E \text{ (neutron energy)}$$

$$\delta_j = \sum_k (A_{kj}/\hbar^2\, W_k)$$

$$g = \text{statistical factor.}$$

The result, Eq. (20), shows that there are two contributions to the fission cross section. The first term within the curly bracket corresponds to a Breit-Wigner line with an effective total width equal to $\Gamma_j + \delta_j$. An additional contribution arises from the second well by virtue of the coupling between the two potential minima. Under the assumption that the spreading width, Γ_{ks}, is smaller than the probability of the second well decaying by fission, one obtains, neglecting fourth order terms in the coupling matrix elements H_{kj}, the result:

$$\sqrt{E}\ \sigma(E) = cg \sum_j \frac{\Gamma_{onj}\ \hat{\Gamma}_{fj}}{(E_j - E)^2 + \frac{1}{4}(\hat{\Gamma}_j)^2} \tag{21}$$

with

$$\hat{\Gamma}_{fj} = \Gamma_{fj} + \sum_k \frac{\Gamma_{fk}\ A_{kj}}{(E_k - E)^2 + \frac{1}{4}\ \hat{\Gamma}^2_{fk}} \tag{22}$$

and

$$\hat{\Gamma}_j = \Gamma_{nj} + \Gamma_{\gamma j} + \hat{\Gamma}_{fj} \tag{23}$$

Hence, the subthreshold fission modes are given in terms of Breit-Wigner lines with resonant fission widths.

The mocked-up cross sections for both the ^{235}U and ^{239}Pu were obtained by Monte Carlo techniques. The neutron and fission widths were sampled from Porter-Thomas distributions with the appropriate number of degrees of freedom. The radiation widths were assumed constant and the level spacing extracted from a Wigner distribution. Tables I and II show the average parameters utilized for the cross section calculations.

The computation of the subthreshold cross section starts by obtaining first the resonant fission widths, Eq. (22). The product $\Gamma_{fk}\ A_{kj}$ was assigned an average value, adjusted to preserve the average value of that spin component containing the subthreshold lines. Both Γ_{fk} and A_{kj} were assumed to follow a Porter-Thomas distribution with one degree of freedom.

Examples of this type of calculation are shown in Figs. 1 and 2. The former is a comparison of the actual fission cross section for the ^{235}U nucleus with the mocked-up cross section. Doppler broadening and resolution effects were introduced in the manufactured cross section for ^{235}U. The subthreshold fission cross section resulting from the expression, (21), is shown in Fig. 2, which exhibits a strong qualitative similarity to the subthreshold measurements of Paya et al. [2].

III. AUTOCORRELATION TESTS

Correlation techniques for statistical studies of neutron cross sections were introduced by Egelstaff in 1958 [9]. Let

$$y_i = \int_{E_i - \frac{1}{2}W}^{E_i + \frac{1}{2}W} \sqrt{E}\ \sigma(E) \tag{24}$$

TABLE I. AVERAGE LEVEL PARAMETERS FOR THE ^{235}U NUCLEUS[a]

J	g	$\langle\Gamma_{o_n}\rangle$ (meV)	$\langle\Gamma_\gamma\rangle$ (meV)	$\langle\Gamma_f\rangle$ (meV)	ν_n[b]	ν_f[b]	$\bar{D}$[c] (eV)
3	7/16	0.097	47.9	65.1	1	4	1.06
4	9/16	0.097	47.9	65.1	1	4	1.06

[a] Values taken from Schmidtt's compilation [7].

[b] ν_n and ν_f number of degrees of freedom for the neutron and fission width distributions, respectively.

[c] Average level spacing.

TABLE II. AVERAGE LEVEL PARAMETERS FOR THE ^{239}Pu NUCLEUS[a]

J	g	$\langle\Gamma_{o_n}\rangle$ (meV)	$\langle\Gamma_\gamma\rangle$ (meV)	$\langle\Gamma_f\rangle$ (meV)	ν_n	ν_f	$\bar{D}$ (eV)
0	1/4	0.939	41.6	1500	1	2	9.6
1	3/4	0.334	41.6	42.0	1	1	3.2

[a] Values taken from Schmidtt's compilation [7] and from Derrien et al. [8].

be the averaged cross section in a given interval, W, corresponding to the midpoint energy, E_i, and define similar averages for the intermediate structure, s_i, and the Breit-Wigner component w_i. Then the input process can be written in the form

$$y_i = s_i + w_i \tag{25}$$

where s_i is given analytically by Eqs. (21) and (24). For a given random variable, x_i, with a fluctuation δx_i around the average, $\langle x_i \rangle$, one defines the autocorrelation function

$$c_{r,x} = \langle \delta x_i \; \delta x_{i+r} \rangle \equiv \mathrm{Cov}\,(x_i,\, x_{i+r}) \tag{26}$$

where (rW) is the energy displacement between the samples x_i and x_{i+r}, and the brackets indicate averages over an infinite record length of data.

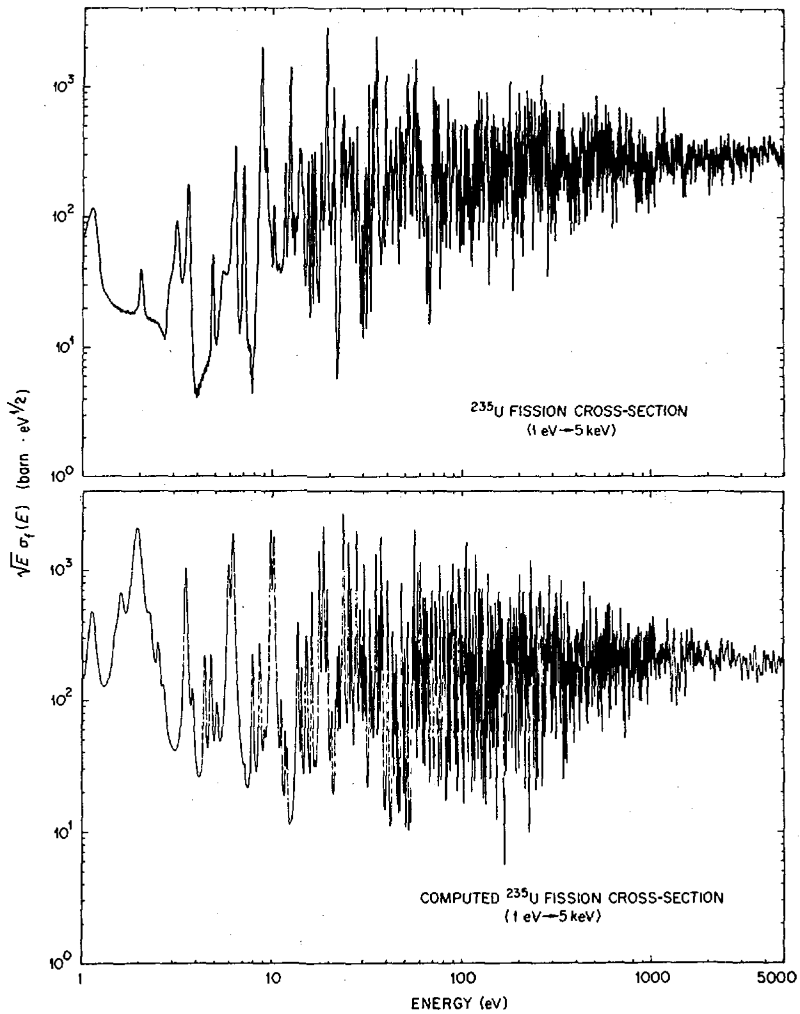

FIG. 1. (a) ^{235}U fission cross-sections; (b) mocked-up ^{235}U fission cross-section computed by Monte-Carlo techniques. Experimental data from G. de Saussure, L.W. Weston, R. Gwin, R.W. Ingle, and J.H. Todd, ORNL, and R.W. Hockenbury and R.R. Fullwood, RPI. (Proc. Nuclear Data for Reactors, 2 IAEA, Vienna (1967) 239).

Applying the definition, Eq. (26), to δy_i, one obtains

$$c_{r,y} = c_{r,s} + c_{r,w} + \mathrm{Cov}(s_i, w_{i+r}) + \mathrm{Cov}(s_{i+r}, w_i) \qquad (27)$$

Under the conditions: (1) s_i and w_i are independent random variables, (2) The Breit-Wigner component, w_i, is almost white noise, the autocorrelation function of the data will yield that of the subthreshold fission cross section. The

FIG. 2. Qualitative comparison between a mocked-up sub-threshold fission cross-section following Eq. (21) and the corresponding magnitude for ^{237}Np.

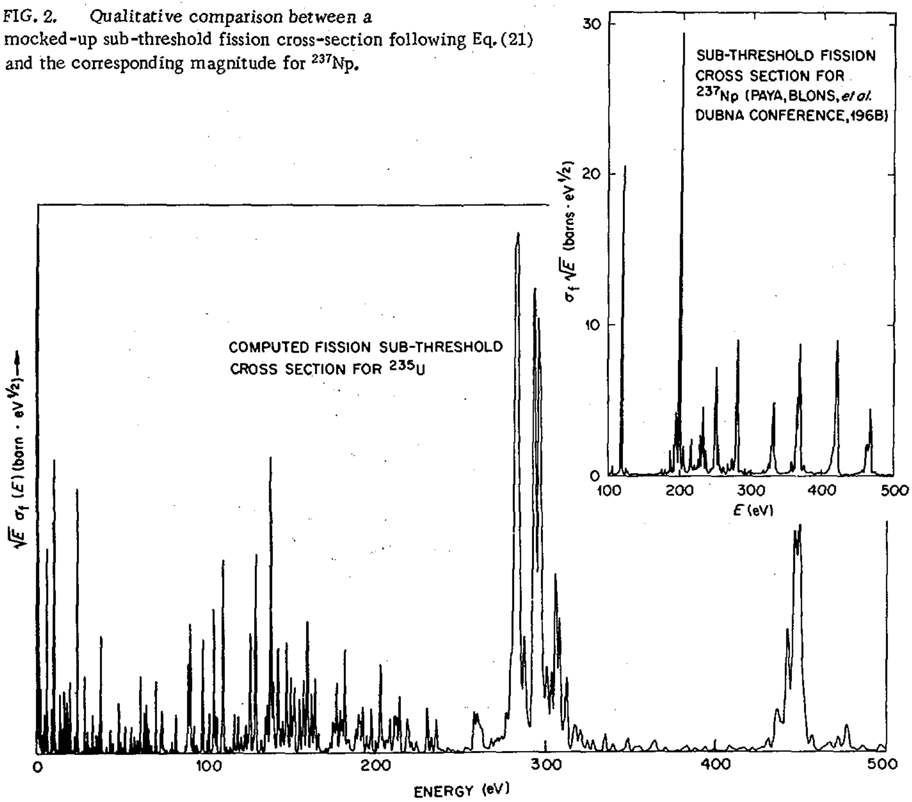

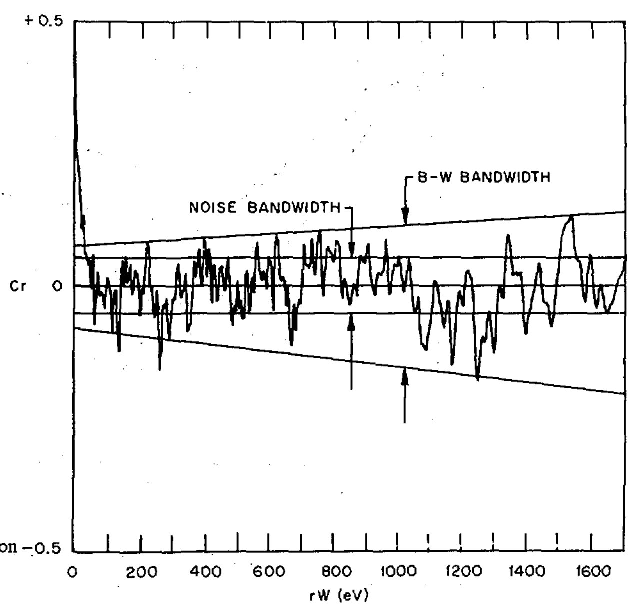

FIG. 3. Correlogram for the mocked-up ^{235}U fission cross-section without intermediate structure. Averaging interval, W = 10 eV.

first condition is satisfied assuming that the nuclear resonance parameters belonging to different spin components are effectively uncorrelated. The second condition is not applicable to the Breit-Wigner noise as shown in Fig. 3, where the normalized correlation function

$$C_r = \frac{c_r}{\{[\langle w_i^2\rangle - \langle w_i\rangle^2]\,[\langle w_{i+r}^2\rangle - \langle w_{i+r}\rangle^2]\}^{1/2}} \tag{28}$$

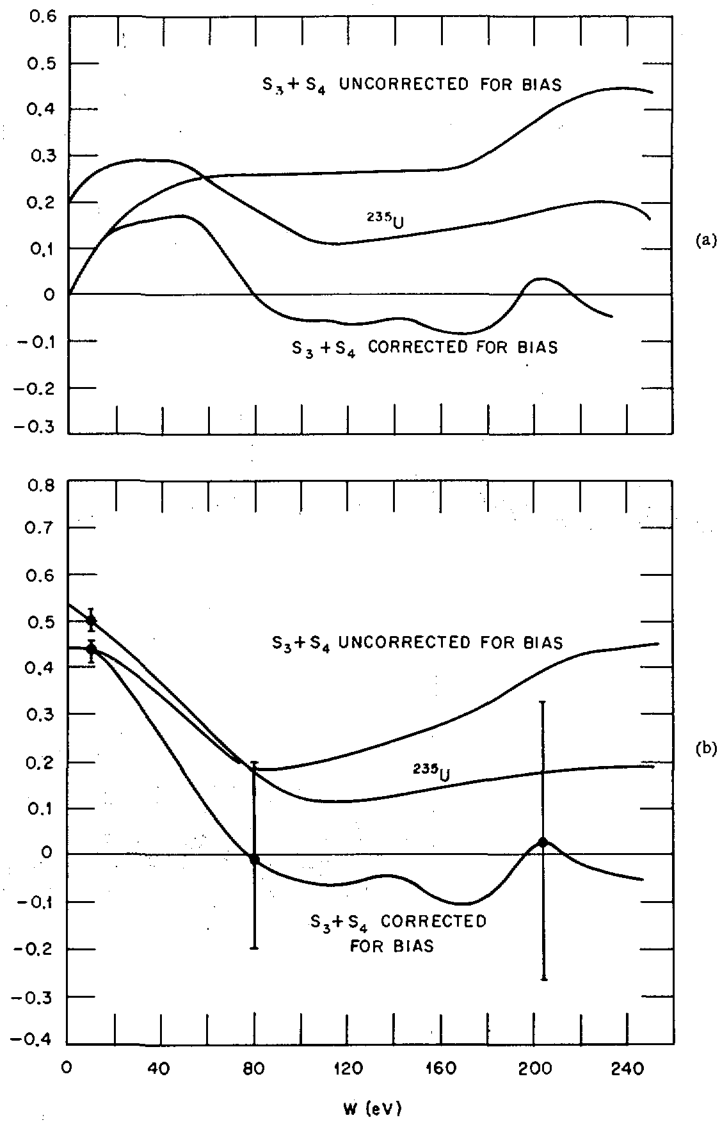

FIG. 4. (a) The first correlation coefficient C_1 versus W for a variable record length; (b) the first correlation coefficient C_1 versus W for a constant record length (0-5 keV).

for the mocked-up fission cross section of ^{235}U, without intermediate structure, exhibits a much larger bandwidth than that corresponding to the autocorrelation function of a randomized set of data. Hence, the correlation background of the Breit-Wigner noise has to be accounted for while performing correlation tests.

These tests in the field of cross section studies have been used in two different contexts. Egelstaff [10] studied the behavior of the first correlation coefficient, $C_1(W)$, as a function of the averaging interval W. For large values of W, (larger than an average correlation range), the function, $C_1(W)$, should become either zero or very small, within the statistical error limits. Results of this test for both the measured and computed ^{235}U fission cross section are shown in Fig. 4b. The first correlation coefficient first decreases as W increases and later on takes an upward trend which is due to an energy bias arising from the $\sqrt{E}$ dependence of the neutron widths entering in the total width. This effect was evaluated by computing the ratio

$$\gamma = y_i/y \text{ (at 1 eV)} = \left\langle \frac{\Gamma_{\lambda n}\ \Gamma_{\lambda f}}{\Gamma_\lambda} \right\rangle \Bigg/ \left\langle \frac{\Gamma_{\lambda n}\ \Gamma_{\lambda f}}{\Gamma_\lambda} \right\rangle_{1\text{ eV}} \tag{29}$$

with the ^{235}U parameters and distributions given in Table I. The above ratio can be fitted by the expression

$$\gamma = \frac{1}{1 + 0.00294\sqrt{E}} \tag{30}$$

which was used as a correction factor in the computation of the first correlation coefficient. The effect of this correction is also shown in Fig. 5. The first correlation coefficient oscillates about the zero correlation line beyond W = 80 eV. The correlation width at half maximum is about 40 eV and it is assumed to represent experimental resolution effects. In connection with this test, one may rémark that similar tests performed by Egelstaff [10] and Michaudon [11], used a variable record length to take account of the varying degree of experimental resolution of the data. When this is done $C_1(W)$ is first very small for low values of W, goes through a broad maximum between W = 15 eV and W = 40 eV, and then it decreases to lower values around 100 eV, Fig. 4a. This behavior led the previous authors to assign a correlation range of about 100 eV for the ^{235}U fission cross section. Nevertheless, if one continues to plot the first correlation coefficient for still larger values of the averaging width, W, one finds the upward trend due to the energy bias effect. The experimental ^{235}U fission cross section shows a less noticeable bias probably because the stablizing effect of the p-wave component. This test, when properly corrected by the γ-factor, seems to be mostly sensitive to experimental resolution effects.

Cao and Migneco [11], Patrick and James [12], and Blons, Eggerman and Michaudon [13] have utilized the structure of the correlogram as a function of the energy displacement, rW, in attempts to extract the average spacing of the intermediate structure of some fissile nuclei cross sections. The implicit idea behind this technique being, that the distance between peaks in the correlation function, represents the average level spacing in the second potential well. To analyze this attractive possibility, consider a train of unit pulses spaced according to a Wigner distributions. The corresponding autocorrelation function is the probability that a unit pulse will be found at a distance, rW, from a

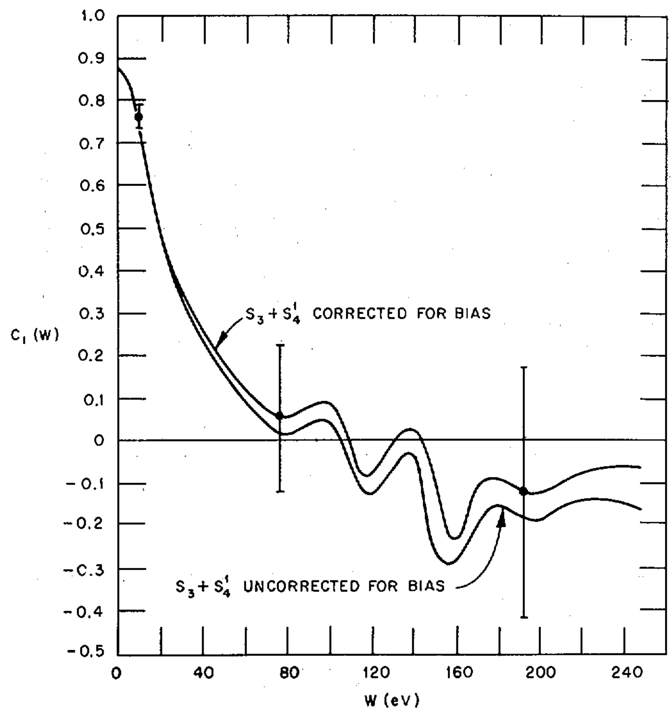

FIG. 5. The first correlation coefficient C_1 versus W for the mocked-up ^{235}U fission cross-section with intermediate structure.

given pulse, regardless of the number of pulses present between them. This function has been found by Dyson [14], who gives the following expression*

$$DC_r' = 1 - [s(y)]^2 - \frac{ds(y)}{dy} \int_y^\infty s(y')dy' \tag{31}$$

where D is the average spacing of the Wigner-distributed pulses and

$$y = \pi \; rW/D$$
$$s(y) = \frac{\sin y}{y} \tag{32}$$

*The correlograms utilized in the literature and in the present work correspond to C_r' with the asymptotic behavior subtracted, the whole expression being normalized at zero energy displacement.

The resulting correlation function is according to Eq. (31) a monotonically increasing function quickly approaching its asymptotic value $C_\infty = D^{-1}$. Another illustrative example can be drawn from the correlation of a set of unit pulses with spacings, ϵ, distributed according to the law $p(\epsilon) = D^{-1}\, x\, e^{-x}$, with $x = \epsilon/D$, showing, as the Wigner distribution, the usual level repulsion effect. It is easily seen that the autocorrelation function is given by the expressions

$$D\, C_r'(x) = 1 + P_o(x) + \int_o^x P_o(x')\, P_o(x - x')\, dx'$$

$$+ \int_o^x \int_o^{x'} P_o(x'')P_o(x' - x'')P_o(x - x')\, dx' dx'' + \ldots$$

with $P_o(x) = xe^{-x}$, yielding the result:

$$D\, C_r'(\epsilon) = 1 + \frac{1}{2}\left(1 - e^{-2\epsilon/D}\right) \qquad (33)$$

which again exhibits a monotonically increasing behavior. In fact, an "oscillatory" behavior of the correlation function in the cases discussed above will only appear for records of finite length, corresponding to given levels of truncation in the expansion of the closed expressions, Eqs. (31) and (33). In this event, the average spacing extracted from the correlation will be a function of record length. Further illustrations of the behavior of the correlograms of nonperiodic functions, as the ones just utilized in this discussion, is shown in Fig. 6a and 6b. The former was obtained numerically from a set of Wigner distributed pulses with a record length of 5 keV, with D = 106 eV. Figure 6b corresponds to the same numerical calculation for a total record length of 1 MeV (only the range from 0 to 40 keV is shown in the figure). The shorter record length example shows large end effects producing the structure of the correlogram. The long record exhibits a δ-function like behavior followed by a narrow bandwidth due to statistical fluctuations.

For an actual cross section the width distribution as well as Doppler broadening and resolution effects must be convoluted into the correlogram. Subthreshold fission cross section correlograms were mocked-up for ^{235}U and ^{239}Pu with average level spacings of 106 and 460 eV, respectively, Figs. 7b and 8c. The correlogram of the mocked-up subthreshold fission cross section for ^{235}U, $(S_3 + S_4^1)$, does not show any number of peaks spaced around the 106-eV average level spacing introduced in the calculation. The average level spacing for the significant peaks found in the first 1600 eV energy range of the correlogram shows an average spacing of 309 eV. Assuming that this corresponds to a "third harmonic" of the correlogram one obtains D = 103 eV. Unfortunately the average so obtained depends strongly on the length of the correlogram chosen for the analysis. The autocorrelation function for the ^{239}Pu mocked-up subthreshold fission cross section shows an average level spacing of 376 eV, which again is not in agreement with the value of 460 eV introduced in the manufactured cross section.

Figure 7a shows the autocorrelation function for the ORNL ^{235}U fission cross section data. There are four peaks emerging from the Breit-Wigner bandwidth. The first peak yields a spacing of 282 eV. The average of the distance between the peaks is of 364 eV. Cao and Migueco [12] obtained very similar results from their ^{235}U data.

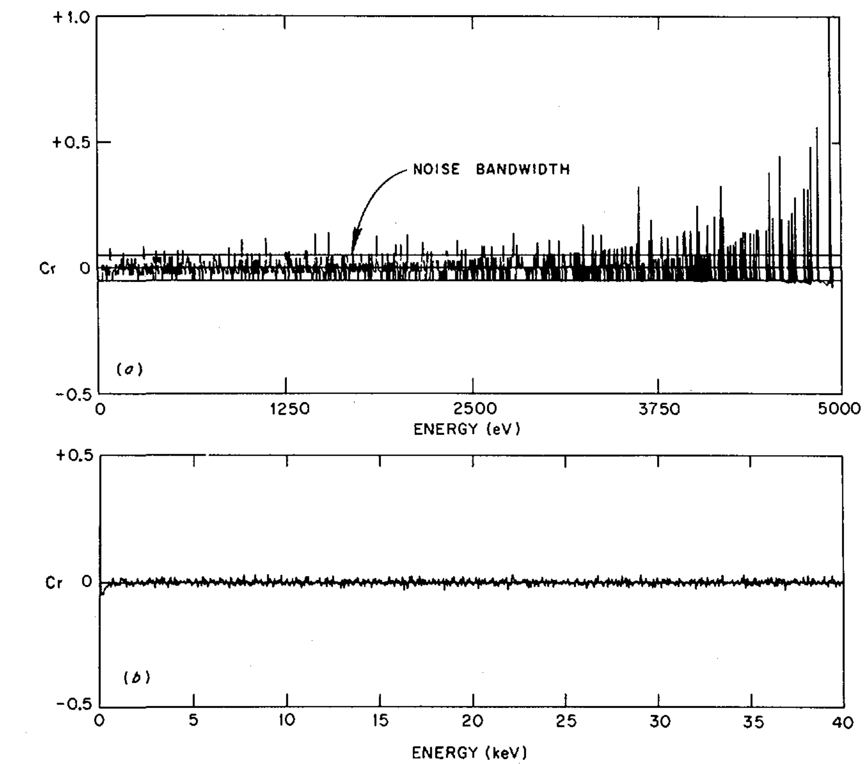

FIG. 6. The correlograms for a set of Wigner-distributed unit pulses: (a) corresponds to a record length of 5 keV as utilized for all the correlograms in this paper; (b) shows the first 40 keV of a total record length of 1 MeV.

The correlogram for ^{239}Pu shown in Fig. 8a is from the work of Patrick and James [14], and that based on Los Alamos data of Shunk, Brown, and LaBauve [15] is shown in Fig. 8b. These data as well as the correlogram found by Blons, Eggermann, and Michaudon [13] show peaks indicating an a average spacing of around 460 eV. In the light of the previous analysis the meaning of the correlogram results is then doubtful. The oscillations observed in them are due to end effects and the statistical fluctuations of the resonance parameters. In order for this technique to become a suitable tool in the identification of the subthreshold fission lines one has to find the connection between the period of the correlogram oscillations and the average spacing of those lines, taking into account both end effects and the statistical distributions of the level parameters.

IV. VARIANCE AND DISTRIBUTION TESTS

In this section we investigate the effect of narrow intermediate structures on the statistics of fission cross sections. The first statistics to be considered is the ratio of the variance to the square of the averaged cross section, that is, using the quantities defined in Eq. (24):

$$\delta(W) = W \frac{V_{ar}\,(y_i)}{\langle y_i \rangle^2} \tag{34}$$

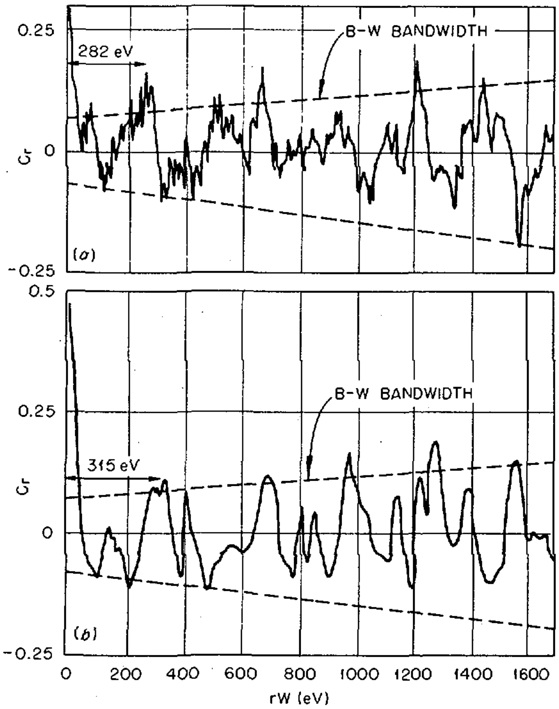

FIG. 7. (a) The correlogram for the ^{235}U fission cross-section (W = 10 eV). Experimental data from G. de Saussure, L. W. Weston, R. Gwin, R. W. Ingle, and J. H. Todd, ORNL, and R. W. Hockenbury and R. R. Fullwood, RPI. (Proc. Nuclear Data for Reactors, 2 IAEA, Vienna (1967) 233); (b) The correlogram for the mocked-up sub-threshold fission cross-section for ^{235}U (W = 10 eV). The average level spacing for the second Strutinsky minimum was taken to be 106 eV.

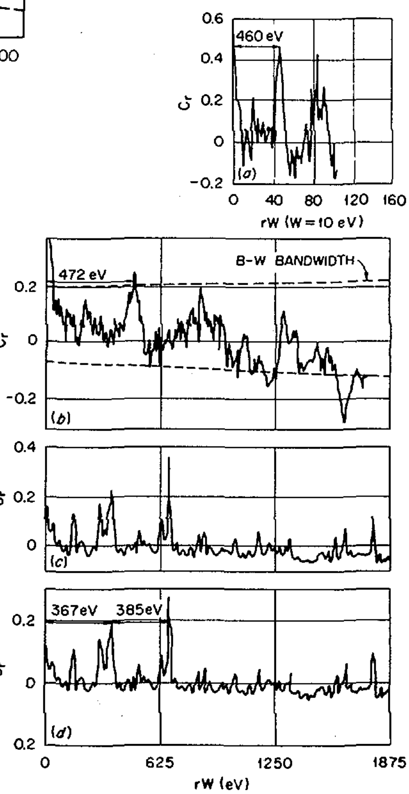

FIG. 8. (a) ^{239}Pu correlogram, Patrick and James [12], W = 10 eV; (b) ^{239}Pu correlogram, W = 10 eV, obtained from the experimental data of Shunk, Brown, and La Bauve [15]; (c) correlogram for the mocked-up ^{239}Pu fission cross-section with intermediate structure; (d) correlogram for the mocked-up sub-threshold fission cross-section with an average level spacing for the second Strutinsky minimum of 460 eV.

FIG. 9. The ratio of the variance to the squared average cross-section versus the averaging interval, W, for ^{235}U.

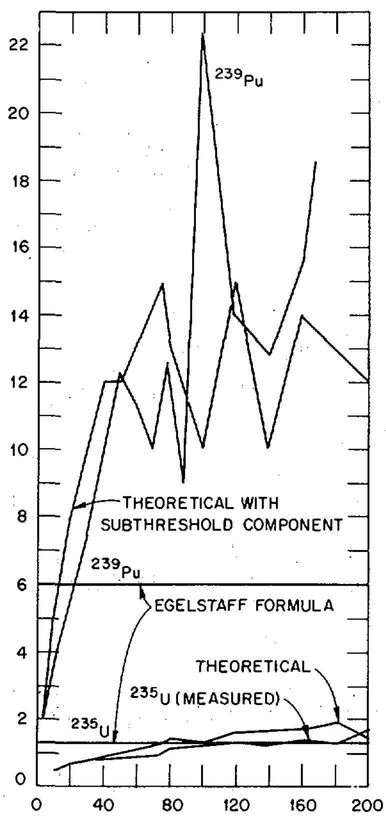

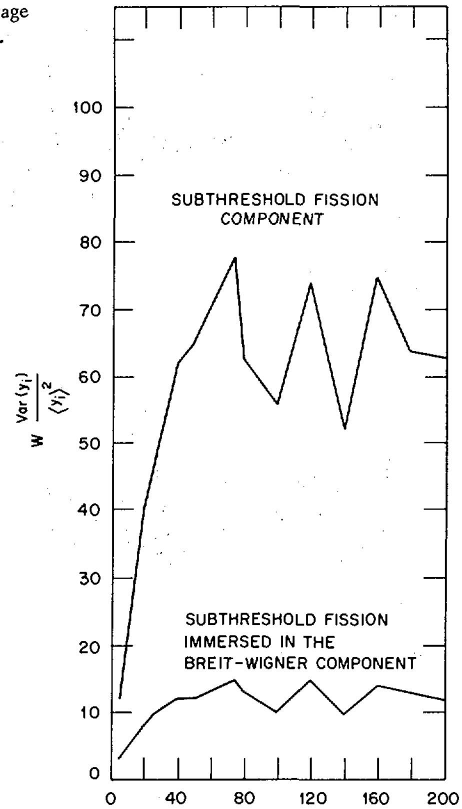

FIG. 10. The ratio of the variance to the squared average cross-section versus the averaging interval, W, for ^{239}Pu.

Egelstaff [10] under the assumption that the various resonance parameters, as well as the values y_i, are uncorrelated obtains the expression:

$$\delta(W) = \langle D\rangle \frac{g_1(F_f)_1 + g_2(F_f)_2}{(g_1 + g_2 S)^2} \tag{35}$$

where $\langle D\rangle$ is the observed average level spacing, g_1 and g_2 are the statistical weight factors for each of the spin components,

$$S = \langle\Gamma_f/\Gamma\rangle_{J_1} / \langle\Gamma_f/\Gamma\rangle_{J_2}$$

and

$$F_f = \frac{V_{ar}(\Gamma_n^o)}{\langle\Gamma_n^o\rangle^2} + \frac{V_{ar}(D)}{\langle D\rangle^2} + \frac{V_{ar}(\Gamma_f/\Gamma)}{\Gamma_f/\Gamma\rangle^2}$$

Hence, except for statistical fluctuations, the ratio of the product of the cross section variance with the interval, W, to the square of its average should be independent of the averaging interval, W. In the presence of an intermediate structure the function, $\delta(W)$, should increase smoothly until a plateau is reached for values of W close to the average spacing of the groups of resonances. The function $\delta(W)$ for the mocked-up subthreshold fission cross section of ^{235}U is shown in Fig. 9. As expected it exhibits substantial deviations from Egelstaff formula. It reaches a plateau around 60 eV followed by oscillations due to statistical fluctuations. However, when the Breit-Wigner component is added to the subthreshold component, the deviations from the uncorrelated behavior are much less apparent (Fig. 9). Both the theoretical (without the subthreshold component) and experimental fission cross sections for ^{235}U follow very accurately the behavior predicted by Egelstaff formula, Fig. 10.

The results corresponding to the experimental ^{235}Pu fission cross section are shown in Fig. 10. In contrast with the behavior of the ^{235}U data, there is a sizable deviation from the trend indicated by the function $\delta(W)$ obtained via Egelstaff equation.

The next effect to be investigated is the influence of the intermediate structure in the distribution function of the fission cross section. In Fig. 11 we show the mocked-up subthreshold fission cross section for ^{239}Pu, with an average level spacing of the second well of 460 eV, and averaged in steps of 50 eV. The lines arising from the second potential minimum have been labelled to show the fact that they do not necessarily correspond to the larger resonances. As expected, large fluctuation of the Breit-Wigner noise can occur which will complicate the detection of intermediate structures, based on the usual detectability limits technique. The distribution functions for the variable $x = y_i/\langle y\rangle$ are shown in Fig. 12a, b, and c for the measured ^{235}U, the corresponding mocked-up fission cross section and for the Breit-Wigner component added up to a subthreshold fission component (average level spacing $\langle D\rangle$ = 106 eV). The first two distributions peak very sharply around x = 1 (width at half maximum value is 0.3 $\bar{\sigma}$). In this case neither distribution function exhibits cross section values larger than 1.5 of the average value. The distribution function in the presence of the intermediate structure is much wider and shows a relatively larger tail (width at half maximum value is 0.7 $\bar{\sigma}$). An attempt has been made to fit those distributions with the Böhning distribution function [16].

$$P(x) = \frac{N_2}{\Gamma(N_2)} \sum_{n=1}^{\infty} a_n \, x^{n + N_2 - 1} \exp(-N_\infty x) \tag{36}$$

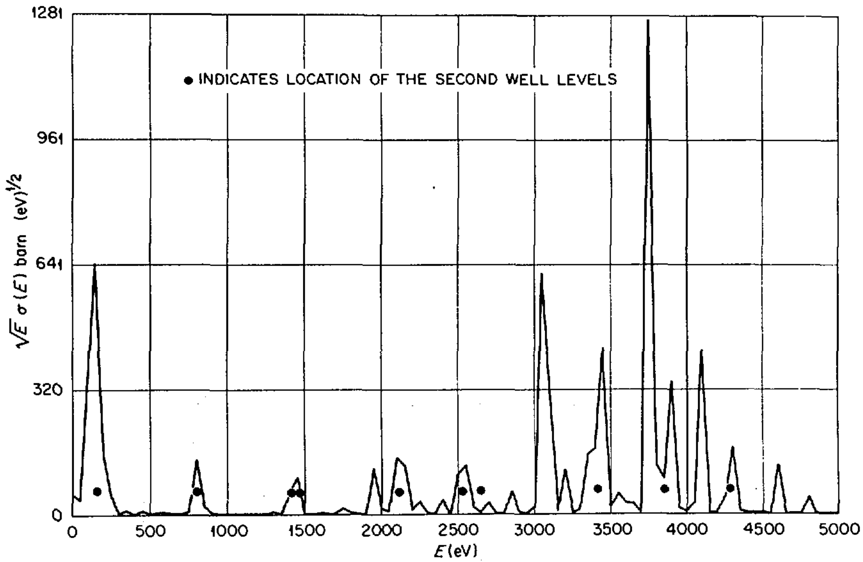

FIG. 11. The mocked-up sub-threshold fission cross-section for ^{239}Pu, averaged in intervals of W = 50 eV.

The distribution P(x) which has been derived by Böhning, from very general considerations, is essentially a χ^2-distribution of $2N_2$ degrees of freedom in the neighborhood of x = 1, having a tail of a χ^2-distribution of $2N_\infty$ degrees of freedom. The fits shown in Fig. 12 utilized the expression, (36), truncated at n = 1. The ratios N_2/N_∞, which indicate the degree of departure from χ^2-distributions, are 1.08 for both the experimental and theoretical ^{235}U and 1.1 for the fission cross section with the intermediate structure. These ratios roughly indicate that the distribution for the mocked-up ^{235}U cross section can be described by a χ^2-distribution of about 27 degrees of freedom. In contrast the presence of the intermediate structure widens the distribution, which in this case corresponds to a χ^2-distribution with a number of degrees of freedom between five and six.

A similar comparison for the ^{239}Pu data is not presently available, although preliminary results show that the distribution function for the fission cross section of this nucleus is much wider than the corresponding one for the ^{235}U data.

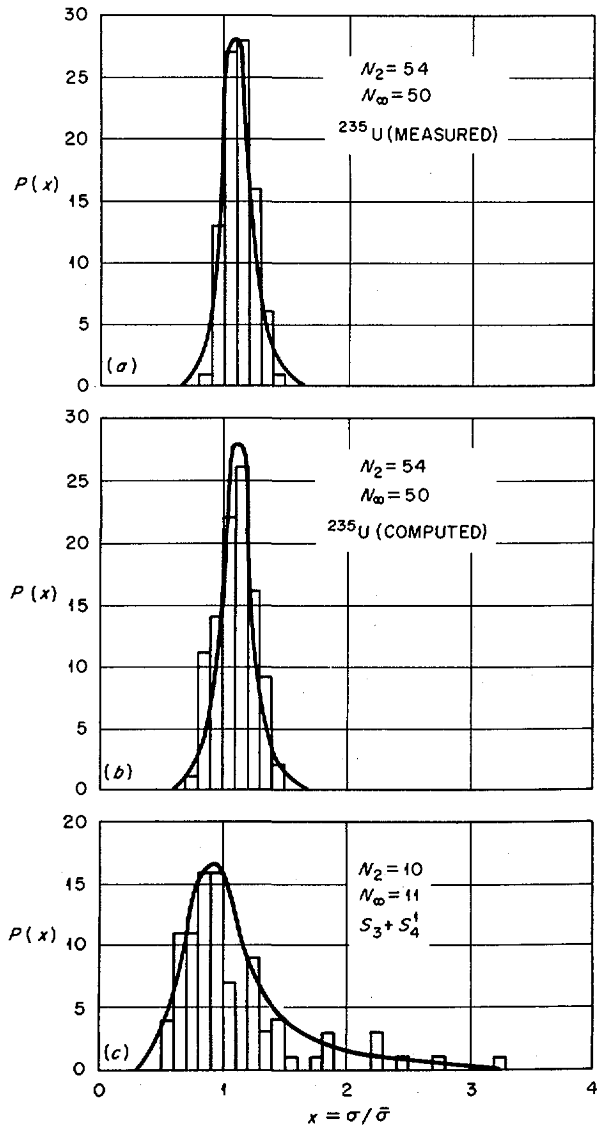

FIG. 12. (a) The distribution function for the ^{235}U data; (b) the distribution function for the mocked-up ^{235}U fission cross-section without the intermediate structure; (c) the distribution function for the mocked-up ^{235}U fission cross-section with the sub-threshold fission cross-section included.

V. CONCLUSIONS

There is an obvious analogy between the objective of this paper and the parallel communication problem of detecting a signal masked by noise. However, analogies may be misleading unless proper care is taken of whatever differences exist between the two problems. In our judgement this is the case regarding the use of correlation techniques in the analysis of narrow intermediate structures. In communication theory one deals mostly with periodic functions immersed in nearly white noise. In this case, the correlation function is periodic with the same period as the signal, while the noise correlation function approaches, within resolution and statistical effects, a δ-function behavior, Lee [17]. Neither one of the previous conditions are satisfied by the components of the cross section, as examined in Section III of this paper. End effects and width fluctuations combine to give a correlogram structure whose relation to the parameters of the subthreshold fission component is not clear as yet. Figure 7 shows that when the bandwidth of the Breit-Wigner noise correlogram is superimposed on the experimental correlogram, only a few peaks of the latter survive the test. The level of significance of those peaks should be further studied by taking into account the fluctuations of the Breit-Wigner bandwidth itself. Nevertheless, the width of the correlation function, as shown by Ericson [18], is related to the average width of the subthreshold modes and probably contains valuable information after proper consideration of resolution effects.

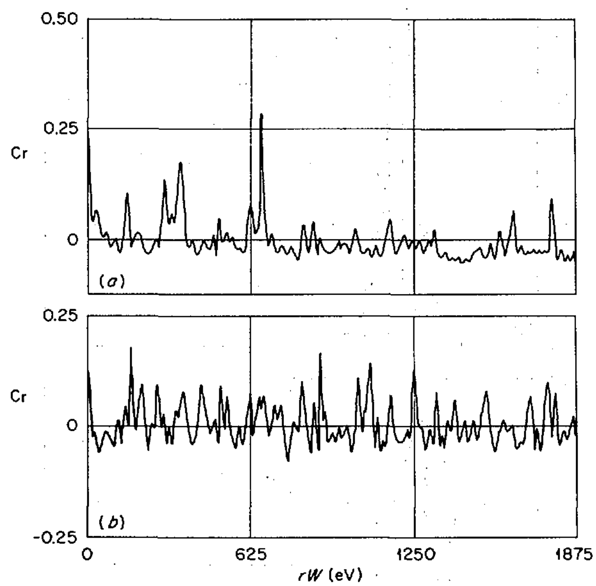

FIG. 13. (a) The correlogram for the mocked-up ^{239}Pu sub-threshold fission cross-section, W = 10 eV; (b) the correlogram for the mocked-up ^{239}Pu fission cross-section without the intermediate structure, W = 10 eV.

The correlation found by Egelstaff [9] in the ^{235}U cross section was not reproduced by the mocked-up cross section with the subthreshold fission lines. This correlation effect rather than indicating the presence of an intermediate structure is a consequence of the energy bias arising from the energy dependence of the neutron widths, as discussed in Section III of this paper. Although our theoretical model failed to reproduce the correlogram of Patrick and James [12] for ^{239}Pu and the one derived from the Los Alamos data [15], Fig. 8, the theoretical correlogram did not show any obvious relation between the average level spacing introduced in the calculations for the subthreshold component and the distance between the peaks of the correlogram. There is, however, a clear difference between the correlograms of the pure subthreshold component, $S_1^1 + S_0$, and the mocked-up ^{239}Pu without the subthreshold component, $S_0 + S_1$, as shown in Fig. 13. The latter exhibits a much less pronounced pattern than the former. This points toward the conclusion that the correlogram technique, although a useful technique to detect the existence of intermediate structures, needs more analytical development in order to extract quantitative information.

The statistical tests based on the study of the ratio of the variance to the squared averaged cross section, although strictly of a qualitative nature, show clear departures from the "uncorrelated behavior when the subthreshold fission component is present. On this basis the ^{235}U fission cross section either does not contain any intermediate structure or it is too weak to be detected by this test. In the case of the ^{239}Pu fission cross section, this test suggests the possibility of a subthreshold component.

The distribution function of the cross section also appears to be sensitive to the presence of the intermediate structure. In agreement with the previous test, the distribution function test does not indicate the presence of a subthreshold component in the ^{235}U fission cross section either. The fact that the intermediate structure widens the distribution can be used to determine the number of peaks above a given detectability limit belonging to that structure. The determination of the fraction of peaks missed is, nevertheless, complicated by the complex structure of the subthreshold modes, so that a technique has to be developed to discriminate between the "true" second well resonances and the mere fluctuations of the Breit-Wigner lines as shown in Fig. 11. It is interesting to see that both the experimental and theoretical distribution functions follow quite well the Böhning distribution. With this knowledge, it seems feasible to develop a policy-making theory to decide about the presence or absence of the intermediate structure and obtain some of its characteristic parameters. This method could then be checked by the utilization of generated cross sections via Monte Carlo techniques as the one utilized in this work.

At the present level of knowledge, in our opinion, it is only possible to make general qualitative statements regarding the presence of subthreshold fission lines in ^{235}U and ^{239}Pu nuclei. This latter nucleus seems to be, however, the strongest candidate for such an intermediate structure.

ACKNOWLEDGMENTS

The authors gratefully acknowledge the comments and suggestions of R. Coveyou, L. Dressner, C. Bowman, and P. Egelstaff.

REFERENCES

[1] MIGNECO, E., THEOBALD, J. P., Nucl. Phys. A112 (1968) 603.

[2] PAYA, D., et al. Dubna Conf., 1968, SMNF 624/68.

[3] LYNN, J. E., AERE-R5891, September 1968.

[4] WEIGMANN, H., Zeitschrift für Physik 214 (1968) 7.

[5] FESHBACH, H., KERMAN, A. K., "Comments on Nuclear and Particle Physics" Vol. II, No. 4 (1968) 125.

[6] STRUTINSKY, V M., Nucl. Phys. A95 (1967) 420.

[7] SCHMIDTT, J. J., KFK 120 (EANDC-E-35U), February 1966.

[8] DERRIEN, H., et al., Proc. Conf. Nuclear Data for Reactors, International Atomic Energy Agency, Vienna, 1967, Vol. II.

[9] EGELSTAFF, P. A., J. Nucl. Energy 7 (1958) 35: See also Michaudon, CEA-R-2552.

[10] EGELSTAFF, P. A., Proc. Phys. Soc. London 71 (1958) 71: See also Michaudon, CEA-R-2552.

[11] CAO, M. G., MIGNECO, E., Phys. Letters 27B (1968) 409.

[12] PATRICK, B. H., JAMES, G. D., Phys. Letters 28B (1968) 258.

[13] BLONS, J., EGGERMANN, C., MICHAUDON, A., C. R. Acad. Sci. Paris 267 (1968) 901.

[14] DYSON, F. J., J. Math. Phys. 3 (1962) 166: See also P. A. Moldauer Phys. Rev. 135 (1964) B642.

[15] SHUNK, E. R., BROWN, W. K., LA BAUVE, R., CONF-660303 (1966) 979.

[16] BÖHNING, M., Zeitschrift für Naturforschung 21a Heft 7 (1966) 881.

[17] LEE, Y. W., "Statistical Theory of Communication," John Wiley and Sons, Inc., New York (1961).

[18] ERICSON, T. E., "Lectures in Theoretical Physics" Vol. VIII, p. 299, University of Colorado Press, Boulder, Colorado.

DISCUSSION

J.P. THEOBALD: The autocorrelation analysis of our σ_f data of ^{235}U gives, with a high significance level, a quasi-periodical serial autocorrelation coefficient. Although in the light of Dr. Perez' paper it is difficult to relate this periodicity to parameters and spacings of the possible intermediate states, I think that this is nevertheless a strong indication that an intermediate structure exists in this cross-section, regardless of its interpretation. Our published interpretation (Ref. [1] of the paper) is merely a proposal.

R.B. PEREZ: From our studies of the correlogram for the Monte Carlo-generated fission cross-sections, we have learned that it is indeed true that when the intermediate structure is present the correlogram shows a more pronounced pattern. However, we are still far from being able to interpret it correctly. In my opinion, we stand a better chance of understanding the intermediate structure in the ^{235}U and ^{239}Pu nuclei by a direct analysis of both total and fission cross-sections.

A. MICHAUDON: I would like to say that I am completely in agreement with what Dr. Perez has just said and in this connection mention the case of the fission cross-section of ^{237}Np. This cross-section shows an extremely marked effect of intermediate structure, as is shown in paper SM-122/90. Nevertheless, the autocorrelations are rather low.

J.P. THEOBALD: Dr. Michaudon's argument that the fission cross-section of ^{237}Np has an intermediate structure but does not yield a periodical correlogram only shows that the correlation analysis is not a tool for finding any intermediate structure but when there is a periodical correlogram with high significance levels, there is also a quasi-periodical structure. Whether it is found or not by this method depends on the actual spacings of the possible intermediate levels in the finite statistical sample given by the cross-section display.

R.B. PEREZ: This is in fact the main reason justifying the development of decision-making policies that allow identification of the signal, in this case the intermediate structure, in the presence of the Breit-Wigner noise.

STRUCTURE INTERMEDIAIRE DANS LES SECTIONS EFFICACES DE FISSION DU NEPTUNIUM-237 ET DU PLUTONIUM-239

D. PAYA, J. BLONS, H. DERRIEN, A. MICHAUDON
CEA, Centre d'études nucléaires de Saclay,
France

Abstract — Résumé

INTERMEDIATE STRUCTURE IN THE FISSION CROSS-SECTIONS OF NEPTUNIUM-237 AND PLUTONIUM-239. The total (σ_T) and fission (σ_f) cross-sections of ^{237}Np and ^{239}Pu for resonance neutrons have been measured by the time-of-flight method. The cross-section σ_f of ^{237}Np consists of resonance groups of certain discrete energies whose mean spacing is about hundred times that of the resonances observed in σ_T. The analysis of the resonances forming the first "group" of 40 eV shows that the intermediate structure in σ_f of ^{237}Np is due to the coupling of the compound-nucleus states (corresponding to the resonances of σ_T) to the fission exit channels, which is strongest at certain discrete energies where the resonance groups appear. This phenomenon may be interpreted as one of the consequences of the double-humped fission barrier resulting from Strutinsky's calculations. Compound-nucleus states (termed class-II states by Lynn) may exist between the two humps; these states should be responsible for the increase of the coupling to the fission exit channels of certain energies. A careful study of σ_f of ^{237}Np also shows other small resonance groups suggesting the existence of a type of coupling which, on the average, should be weaker than the preceding one, which essentially corresponds to the large groups. One can thus be led to the assumption of two types of barrier which could correspond to the two spin states 2^+ and 3^+. A finer analysis of σ_f in the 40 eV group shows that there exists a large resonance below the narrow resonances, characteristic of the weak coupling in which the first hump of the fission barrier (between the two minima) is higher than the second one.

A study of the autocorrelations in σ_f of ^{239}Pu suggests the existence of an intermediate structure whose mean spacing might be about 450 eV. An analysis of the resonances up to 660 eV shows that the mean fission width of the 1^+ resonances decreases very rapidly at about 600 eV. Therefore an intermediate structure due to the 1^+ fission exit channel (or channels) exists. Nevertheless the probable presence of autocorrelations in σ_T and the variations of the local density function as a function of the energy do not exclude the possible existence of an intermediate structure due to the entrance channel.

STRUCTURE INTERMEDIAIRE DANS LES SECTIONS EFFICACES DE FISSION DU NEPTUNIUM-237 ET DU PLUTONIUM-239. Les sections efficaces totale (σ_T) et de fission (σ_f) de ^{237}Np et ^{239}Pu pour des neutrons de résonances ont été mesurées par la méthode du temps de vol. La section efficace σ_f de ^{237}Np est constituée de groupes de résonances à certaines énergies discrètes dont l'espacement moyen est environ cent fois celui des résonances observées dans σ_T. L'analyse des résonances qui composent le premier «groupe» à 40 eV montre que la structure intermédiaire dans σ_f de ^{237}Np est due au couplage des états du noyau composé (correspondant aux résonances de σ_T) aux voies de sortie de fission, lequel est plus intense à certaines énergies discrètes, là où apparaissent les groupes de résonances. Ce phénomène peut être interprété comme une des conséquences de la barrière de fission à deux bosses qui résulte des calculs de Strutinsky. Entre les deux bosses peuvent exister des états du noyau composé (appelés états de classe II par Lynn) qui seraient responsables de l'augmentation du couplage aux voies de sortie de fission à certaines énergies. L'examen attentif de σ_f de ^{237}Np révèle aussi d'autres petits groupes de résonances, suggérant l'existence d'un type de couplage qui, en moyenne, serait plus faible que le précédent, lequel correspond essentiellement aux grands groupes. On peut ainsi être amené à postuler l'existence de deux types de barrière, pouvant correspondre aux deux états de spin 2^+ et 3^+. Une analyse plus fine de σ_f dans le groupe à 40 eV montre l'existence d'une résonance large, au-dessous des résonances étroites, caractéristique du couplage faible dans lequel la première bosse de la barrière de fission (entre les deux minimums) est plus haute que la seconde.

L'étude des autocorrélations dans σ_f de ^{239}Pu suggère l'existence d'une structure intermédiaire dont l'espacement moyen serait de 450 eV environ. L'analyse des résonances jusqu'à 660 eV montre que la largeur moyenne de fission des résonances 1^+ décroît très rapidement vers 600 eV. Il existe donc une structure intermédiaire due à la voie (ou aux voies) de sortie de fission 1^+. Cependant, la présence probable d'autocorrélations dans σ_T et les variations de la fonction de densité locale en fonction de l'énergie n'excluent pas la possibilité d'une structure intermédiaire due à la voie d'entrée.

1. INTRODUCTION

L'accélérateur linéaire d'électrons de 45 MeV de Saclay a été utilisé comme source pulsée de neutrons pour l'étude systématique de certains aspects de la fission induite par des neutrons de résonances.

La méthode consiste à mesurer les sections efficaces totale (σ_T) et de fission (σ_f) par la technique du temps de vol, puis à les analyser pour en extraire des informations relatives au processus de fission (paramètres de résonances, corrélations, structure intermédiaire...).

Nous présentons ici brièvement les résultats relatifs à la structure intermédiaire observée dans la section efficace σ_f de deux noyaux: ^{237}Np (non fissile par neutrons lents) et ^{239}Pu (fissile par neutrons lents).

2. NEPTUNIUM-237

Lorsque l'étude de ce noyau fut entreprise, des autocorrélations (alors inexpliquées) avaient été trouvées dans les sections efficaces σ_T et σ_f de ^{235}U [1, 2]. Il fut suggéré, par le groupe du MIT [3], que la présence de ces autocorrélations pouvait être due à des états-portes dans la voie d'entrée. C'est pour rechercher un tel phénomène, dans le cas d'un noyau non fissile, et aussi pour avoir plus d'informations sur la barrière de fission, que les sections efficaces σ_T et σ_f de ^{237}Np ont été étudiées.

La section efficace σ_T est compatible avec le modèle statistique habituel. En revanche, la section efficace σ_f présente un effet très net de structure intermédiaire [4-7]. Il est visible sur la figure 1 où la courbe expérimentale $\sigma_f\sqrt{E}$ est tracée en fonction de E dans la gamme d'énergie de 10 eV à 500 eV. Au lieu d'être distribuées d'une façon régulière en fonction de l'énergie (avec un espacement moyen de 0, 5 eV), comme dans σ_T, les résonances apparaissent seulement groupées en touffes au voisinage de certaines énergies discrètes (40 eV, 120 eV, etc.). L'espacement moyen de ces groupes ou îlots de résonances (que nous appellerons simplement «groupes» dans la suite de ce travail) est de 50 eV environ, soit à peu près cent fois plus grand que celui des résonances dans σ_T. Dans le premier groupe, situé à 40 eV, les résonances sont bien séparées et peuvent être analysées. Ce n'est plus le cas pour les groupes situés au-delà de 150 eV où la résolution se détériore rapidement quand l'énergie augmente.

La figure 2 représente les histogrammes cumulés des largeurs neutroniques réduites $2g\Gamma_n^0$ (courbe A) et des largeurs de fission Γ_f (courbe B) pour les résonances situées à basse énergie. Vers 40 eV, l'histogramme B présente une grande discontinuité, contrairement à l'histogramme A dont la pente n'accuse pas de changement notable. La structure intermédiaire n'est donc pas due à des états-portes dans la voie d'entrée, mais seulement au couplage des états du noyau composé (correspondant aux résonances dans σ_T) aux voies de sortie de fission qui est plus intense à certaines énergies discrètes, là où apparaissent les groupes. De tels groupes furent observés plus tard dans la section efficace de fission au-dessous du seuil d'autres noyaux: ^{240}Pu [8], ^{234}U [9] et ^{242}Pu [10].

L'explication de ce phénomène semble devoir être trouvée dans les travaux de Strutinsky [11] qui ont montré que, pour des noyaux tels que ^{237}Np, la barrière de fission pouvait comporter deux (ou même trois)

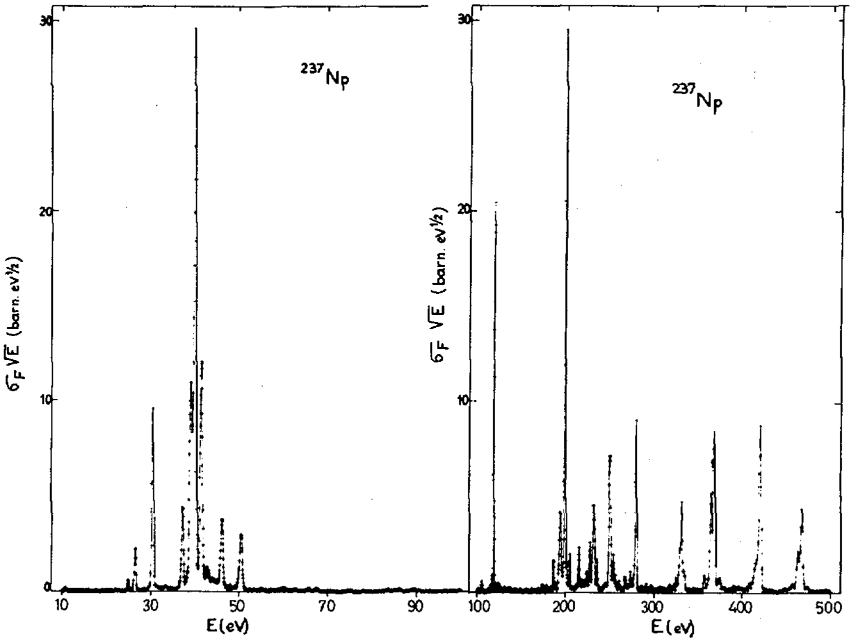

FIG.1. Section efficace de fission σ_f (multipliée par $\sqrt{E}$) de ^{237}Np tracée en fonction de l'énergie E des neutrons incidents de 10 eV à 500 eV.

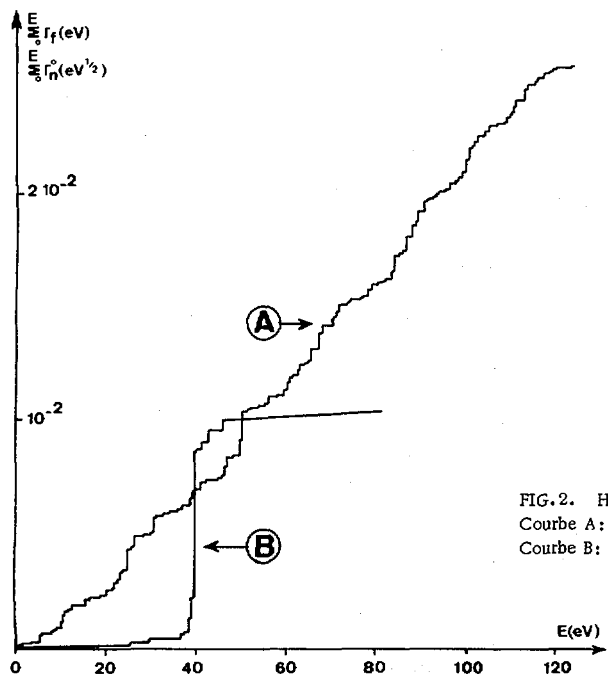

FIG.2. Histogrammes cumulés.
Courbe A: largeurs neutroniques réduites.
Courbe B: largeurs de fission.

bosses. Entre les deux bosses, donc au-dessus du deuxième minimum (pour $\beta \approx 0,5$ à $0,6$), peuvent se trouver aussi d'autres états du noyau composé (appelés états de classe II, les états de classe I se trouvant au-dessus du premier minimum [12]). En se basant sur ces travaux, Lynn [12] et Weigmann [13] ont explicitement proposé que les états de classe II pouvaient être responsables de la structure intermédiaire dans la section efficace de fission au-dessous du seuil.

Dans le cas de σ_f de ^{237}Np, les groupes tels que ceux qui sont visibles sur la figure 1 ne sont pas les seuls à exister. D'autres, de plus faible amplitude et donc plus difficiles à déceler, apparaissent néanmoins dans le tracé en fonction de E de la quantité $\sigma_f' \sqrt{E}$ définie comme suit:

$$\sigma_f' (E) \sqrt{E} = \frac{1}{\mu\sqrt{\pi}} \int_{E_1}^{E_2} \sigma_f (E') \sqrt{E'} \exp\left[-\frac{(E-E')^2}{2\mu^2}\right] dE' \qquad (1)$$

E_1 et E_2 sont les bornes de l'intervalle d'intégration centré sur E et grand par rapport à μ (ici pris égal à 4, 3 eV).

L'un de ces groupes de faible amplitude apparaît, par exemple, à 87 eV dans la figure 3.A, où la courbe $\sigma_f' \sqrt{E}$ est tracée de 15 eV à 145 eV. On peut effectivement le retrouver dans la figure 3.B où est tracée, dans la même gamme d'énergie, la courbe expérimentale $\sigma_f \sqrt{E}$.

De tels groupes de faible amplitude ont pu être mis en évidence grâce à une réduction importante du bruit de fond du détecteur [14]. Leur apparition ne paraît pas être due à des effets parasites (défaut de fonctionnement du codeur de temps de vol, diffusion des neutrons par les parois du détecteur, etc.) car le groupe à 87 eV est visible dans deux mesures effectuées dans des conditions différentes (détecteurs, longueurs de vol, etc.). A moins d'être due à des impuretés non détectées, l'existence de ces groupes de faible amplitude semble donc réelle.

La figure 4 représente la distribution intégrale des surfaces A de tous les groupes observés jusqu'à 2 keV. On constate un excès de petites valeurs de A qui rend la distribution expérimentale incompatible avec une seule loi en χ^2, et ceci d'autant plus que le nombre des petits groupes est certainement sous-estimé. Il en résulte que la structure intermédiaire dans σ_f de ^{237}Np semble composée de deux familles de groupes, d'importance comparable en nombre mais dont la contribution est très différente (le rapport des surfaces moyennes des groupes dans chaque famille est égal à environ 25). Ceci suggère que le couplage des états de classe I aux voies de sortie de fission se fait de deux façons différentes, peut-être par l'intermédiaire de deux barrières différentes pouvant correspondre aux deux états de spin. Cette hypothèse ne peut pas être vérifiée pour le moment. Il faudrait, par exemple, montrer que non seulement les résonances d'un seul groupe mais aussi que toutes celles des groupes d'une même famille (en particulier celle des groupes de grande amplitude) ont le même état de spin. Si elle était vérifiée, une telle hypothèse expliquerait pourquoi la distribution des espacements des grands groupes est compatible avec une loi de Wigner (une seule population) [5, 6].

Le rapport de l'espacement moyen des groupes (donc des états de classe II) à celui des résonances de σ_T(donc des états de classe I) permet de connaître la hauteur du deuxième minimum, si l'on suppose que le paramètre a, qui entre dans la formule de densité des niveaux sous la forme exp $2\sqrt{a}\,V$, est le même pour des déformations du noyau correspondant aux deux minimums. En choisissant a = 25 on trouve que le deuxième minimum est à 2,7 MeV au-dessus du premier.

La hauteur et la forme des bosses de la barrière sont plus difficiles à préciser. Par exemple, on ne peut pas, d'après les paramètres de résonances, distinguer si la première barrière (située entre les deux minimums) est plus haute (cas dit du couplage faible) ou plus basse (couplage fort) que la seconde. Afin d'élucider ce point, dans le cas de ^{237}Np, nous avons analysé le groupe à 40 eV suivant une méthode proposée par Mottelson [15]. Elle consiste à vérifier si la section efficace σ_f, dans le groupe considéré, peut être reproduite fidèlement à partir des résonances étroites connues qui le composent. La figure 5 montre le meilleur accord qui a été obtenu,

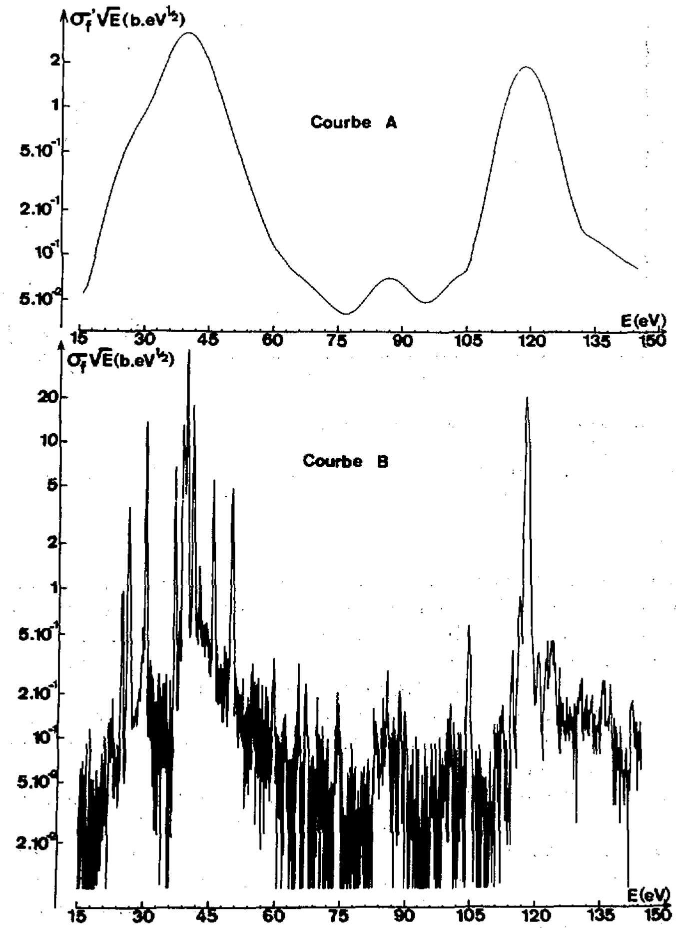

FIG.3. Section efficace de fission (multipliée par $\sqrt{E}$) de ^{237}Np tracée en fonction de l'énergie E des neutrons incidents de 15 eV à 145 eV.
Courbe A : valeurs moyennées $\sigma_f'\sqrt{E}$ (voir texte).
Courbe B : valeurs non moyennées $\sigma_f\sqrt{E}$.

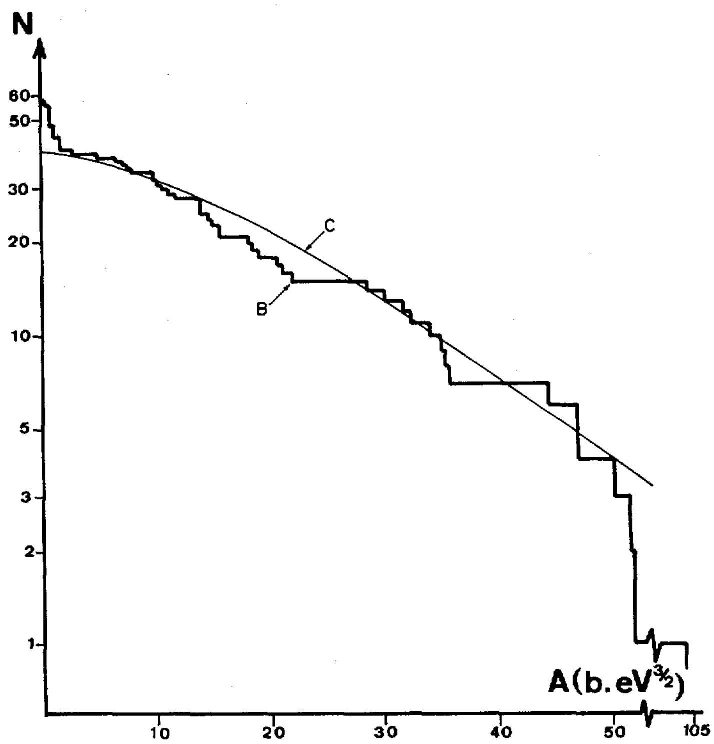

FIG.4. Distribution des aires des groupes de résonances.
B: Histogramme expérimental.
C: Loi en χ^2 ($\nu = 4$) ajustée sur les plus grandes valeurs de A. Noter la discontinuité dans l'abscisse entre 50 b·eV$^{3/2}$ et 105 b·eV$^{3/2}$.

par la méthode des moindres carrés, entre les points expérimentaux et une courbe théorique. On constate que, entre les résonances importantes du groupe, les points expérimentaux sont systématiquement au-dessus de la courbe théorique. Il ne semble pas que les résonances qui sont manquées dans σ_T puissent jouer un rôle important dans σ_f puisque leurs largeurs neutroniques sont faibles. Pour que la courbe théorique corresponde mieux aux points expérimentaux, il faut admettre l'existence d'une résonance large au-dessous des résonances étroites. Cette analyse montre que, dans le cas du noyau composé ^{238}Np, nous serions devant un couplage faible [15] et que cette résonance large serait la petite composante, en classe I, de l'état de classe II responsable du groupe à 40 eV. La forme de cette résonance large semble d'ailleurs dissymétrique, ce qui peut être expliqué par un effet d'interférence avec les résonances larges similaires des grands groupes voisins (ceci suppose que ces résonances larges et donc ces groupes eux-mêmes sont du même état de spin). L'allure de la section efficace peut suggérer aussi que le groupe et la résonance large à 40 eV sont doubles; il y aurait alors deux groupes et deux résonances larges vers 30 eV et 40 eV.

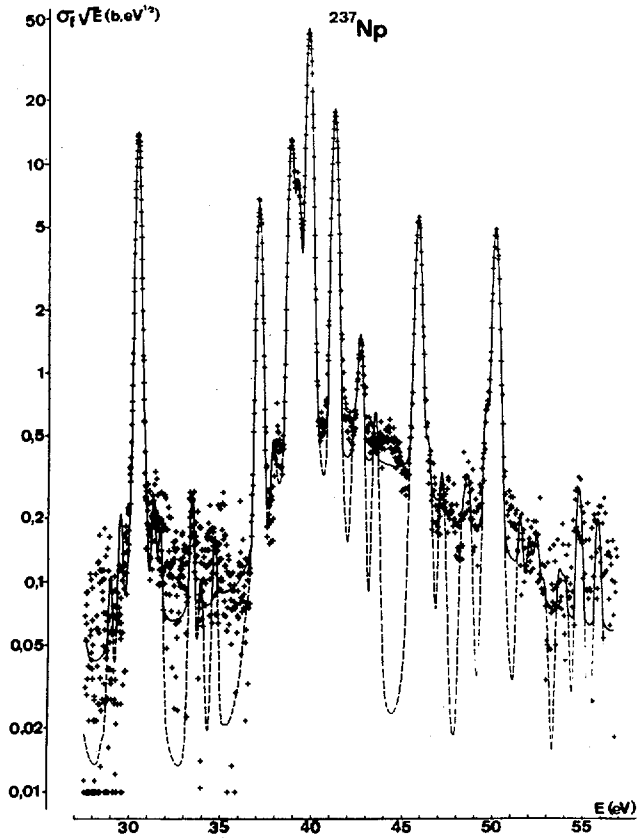

FIG.5. Ajustement des points expérimentaux par une courbe théorique dans le groupe de résonances à 40 eV.

\+ Points expérimentaux.

--- Courbe théorique (résonances étroites seulement)

___ Courbe théorique (résonances étroites et résonance large ayant Γ = 9 eV)

Les courbes théoriques ne sont pas corrigées du faible effet de l'impureté ^{239}Pu.

Dans le cas du couplage faible, on a les relations suivantes [16]:

$$\gamma_2^t \approx \frac{1}{2\pi\rho_2}\left(N_{(A)} + N_{(B)}\right) \tag{2}$$

$$\langle\Gamma_f\rangle \approx \frac{1}{2\pi\rho_1}\,\frac{N_{(A)} \times N_{(B)}}{N_{(A)} + N_{(B)}} \tag{3}$$

γ_2^t = largeur totale de l'état de classe II

ρ_1 = densité des états de classe I

ρ_2 = densité des états de classe II
$\langle\Gamma_f\rangle$ = largeur moyenne de fission des résonances étroites observées dans σ_T
$N_{(A)}$ = nombre effectif de voies de sortie pour la première barrière
$N_{(B)}$ = nombre effectif de voies de sortie pour la deuxième barrière.

Dans le cas de la fission induite dans ^{237}Np:

$$\langle\Gamma_f\rangle \approx 0,2 \text{ meV} \tag{4}$$

$$\gamma_2^t \approx 7 \text{ eV} \tag{5}$$

$$1/\rho_1 \approx 1 \text{ eV (par état de spin)} \tag{6}$$

$$1/\rho_2 \approx 50 \text{ eV (pour une famille de groupes seulement)} \tag{7}$$

On en déduit aisément:

$$N_{(A)} \approx 1,25 \times 10^{-3} \qquad N_{(B)} \approx 0,87 \tag{8}$$

La valeur de $N_{(A)}$ correspondant à la première barrière, supposée être ici la plus haute, montre que $\hbar\omega \approx 600$ keV, valeur compatible avec l'allure de σ_f au voisinage du seuil qui apparaît pour des neutrons d'une énergie de 650 keV.

Le sommet de la deuxième barrière serait, d'après la valeur de $N_{(B)}$, à une énergie inférieure de quelques centaines de keV à l'énergie de liaison du neutron dans ^{238}Np.

3. PLUTONIUM-239

La structure intermédiaire dans la section efficace de fission au-dessous du seuil peut également exister dans σ_f d'un noyau fissile si la contribution de certaines voies de sortie de fission, dont les états de transition sont au-dessus de l'énergie de liaison du neutron, est assez importante [5]. C'est le cas de ^{239}Pu pour lequel le premier état de transition 1^+ dans le noyau composé ^{240}Pu est à environ 200 keV au-dessus de l'énergie de liaison du neutron [17]. La section efficace $\sigma_{f_{1^+}}$, due à la voie (ou aux voies) 1^+, peut donc présenter un effet de structure intermédiaire contrairement à $\sigma_{f_{0^+}}$, due à la voie (ou aux voies) 0^+, puisque le premier état de transition 0^+ est à 1,6 MeV au-dessous de l'énergie de liaison du neutron. Néanmoins, dans la section efficace telle qu'elle est mesurée, toute structure intermédiaire dans $\sigma_{f_{1^+}}$ est masquée par les fluctuations de $\sigma_{f_{0^+}}$, d'autant plus que $\sigma_{f_{0^+}}$ est, en moyenne, plus importante que $\sigma_{f_{1^+}}$.

L'examen visuel de la section efficace σ_f, mesurée à 77°K et avec une résolution nominale de 1 ns/m, montre qu'elle comporte des groupes de hautes résonances émergeant d'une section efficace résiduelle assez importante [18]. Le calcul d'autocorrélation confirme, en effet, que σ_f n'est pas compatible avec un modèle statistique simple. Le coefficient d'autocorrélation r_k [1], calculé pour W = 10 eV dans la gamme 4 eV - 2004 eV, est tracé en fonction de k dans la figure 6.

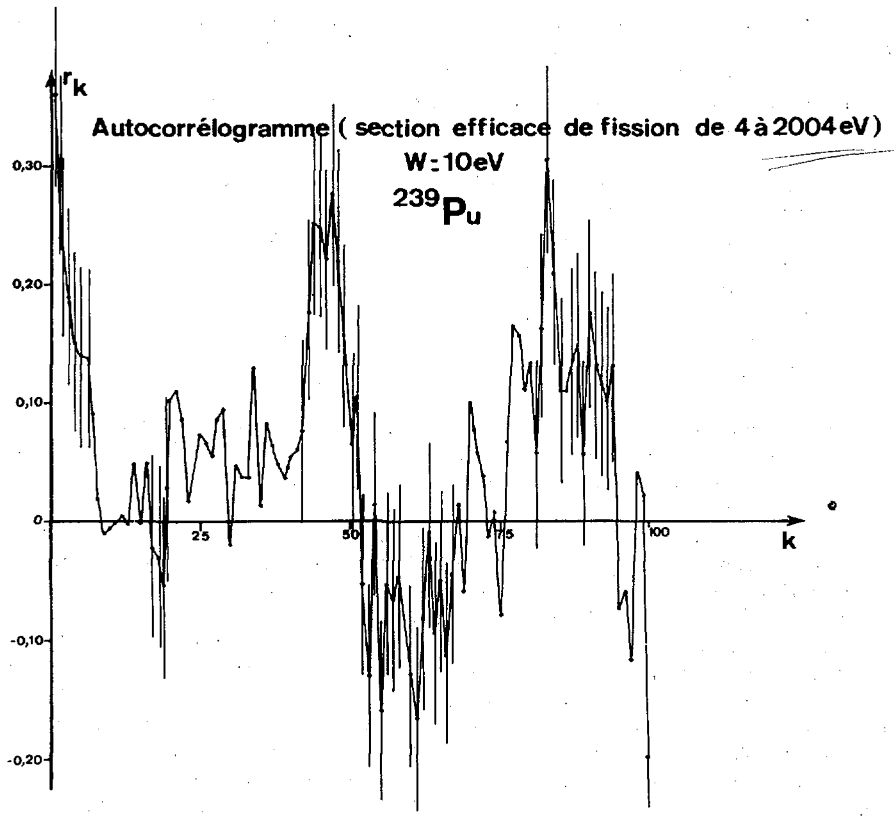

FIG. 6. Autocorrélogramme r_k tracé en fonction de k. Les lignes verticales représentent les barres d'erreur (erreur d'échantillonnage).

L'allure de l'autocorrélogramme ainsi obtenu, où r_k prend des valeurs nettement différentes de zéro et supérieures aux barres d'erreur, suggère l'existence d'une structure intermédiaire dont l'espacement moyen serait de 450 eV environ, résultat tout à fait semblable à celui obtenu indépendamment à Harwell [19].

L'origine de cette structure intermédiaire peut difficilement être déterminée par l'étude des autocorrélations dans σ_f, d'autant plus qu'elles semblent exister aussi dans σ_T. Ceci voudrait dire que la voie d'entrée joue un certain rôle dans la structure intermédiaire observée dans σ_f. Il est possible d'étudier séparément les contributions respectives de la voie d'entrée et des diverses voies de sortie de fission grâce à la qualité actuelle des mesures de σ_T et de σ_f qui permet d'obtenir les paramètres de résonances jusqu'à une énergie de 660 eV [20], donc dans une gamme d'énergie supérieure à l'espacement de la structure intermédiaire. Pour connaître la variation des propriétés statistiques des paramètres en fonction de l'énergie, nous avons fractionné la gamme de 0 à 660 eV en six intervalles de 110 eV et nous avons tracé la distribution des largeurs de fission pour chacun d'eux. Les six histogrammes ainsi obtenus ont tous la même allure et sont constitués par la superposition de deux familles correspondant très certainement aux deux états de spin [21].

La valeur moyenne de Γ_f, pour les deux états de spin 0^+ et 1^+, varie alors de la façon suivante (voir aussi [22]):

E (eV)	$\langle \Gamma_f \rangle_{0^+}$ (meV)	$\langle \Gamma_f \rangle_{1^+}$ (meV)
0-110	2100	30
110-220	1600	64
220-330	2400	36
330-440	2500	36
440-550	1800	25
550-660	1600	6

Pour l'obtention de tous ces résultats, une contribution égale à Γ_{γ_f} = 3,5 meV, correspondant au processus (n, γ_f)[23], a été retranchée des largeurs de fission obtenues par l'analyse de forme des sections efficaces.

On constate que les variations relatives de $\langle \Gamma_f \rangle_{0^+}$ sont faibles. D'ailleurs elles ne sont pas significatives car les résonances 0^+ sont trois fois moins nombreuses que les résonances 1^+ d'une part, ce qui réduit d'autant l'échantillonnage, et d'autre part sont très larges, ce qui entraîne une grande imprécision dans la détermination de Γ_f.

Les variations de $\langle \Gamma_f \rangle_{1^+}$ sont, au contraire, très importantes. Ceci est visible sur les histogrammes des figures 7 et 8 relatifs aux intervalles 110-220 eV et 550-660 eV pour lesquels $\langle \Gamma_f \rangle_{1^+}$ prend les valeurs extrêmes respectivement égales à 64 meV et 6 meV. On note la diminution spectaculaire de $\langle \Gamma_f \rangle_{1^+}$ dans l'intervalle 550-660 eV. Elle est visible à la comparaison des sections efficaces σ_T et σ_f. Vers 600 eV, les résonances étroites de σ_f sont toujours visibles mais fortement atténuées dans σ_f, alors que les résonances larges apparaissent dans ces deux sections efficaces avec des amplitudes comparables (figure 9). Ceci n'est donc pas dû à l'élargissement de la fonction de résolution, et d'autant moins que de nouvelles résonances étroites apparaissent dans σ_T et σ_f au-delà de 660 eV.

La présence d'une structure intermédiaire dans σ_f est donc confirmée par cette analyse qui, de plus, précise qu'elle provient de la voie (ou des voies) de sortie 1^+. Cependant, il n'est pas exclu qu'il existe aussi une structure intermédiaire due à la voie d'entrée car, d'une part, des autocorrélations sont trouvées dans σ_T et, d'autre part, la fonction de densité locale, calculée pour chacun des six intervalles de 110 eV définis plus haut, accuse des variations, non corrélées avec celles de $\langle \Gamma_f \rangle_{1^+}$ et moins importantes, mais supérieures aux barres d'erreur. La brusque diminution de $\langle \Gamma_f \rangle_{1^+}$ vers 600 eV explique la décroissance brutale de σ_f à cette énergie et vérifie l'hypothèse que nous avions avancée [5] selon laquelle ce fait expérimental pouvait être dû à une structure intermédiaire dans la partie de σ_f due à la voie (ou aux voies) 1^+. Cet effet s'accompagne d'une augmentation de $\alpha = \sigma_c/\sigma_f$ d'autant plus importante que toute diminution de $\langle \Gamma_f \rangle$ provoque, en moyenne, non seulement une diminution de σ_f mais aussi une augmentation de σ_c.

La modulation de $\langle \Gamma_f \rangle_{1^+}$ en fonction de l'énergie peut être interprétée comme provenant du couplage des résonances étroites (correspondant à des états de classe I) à un (ou plusieurs) état(s) de classe II et de spin 1^+ dont

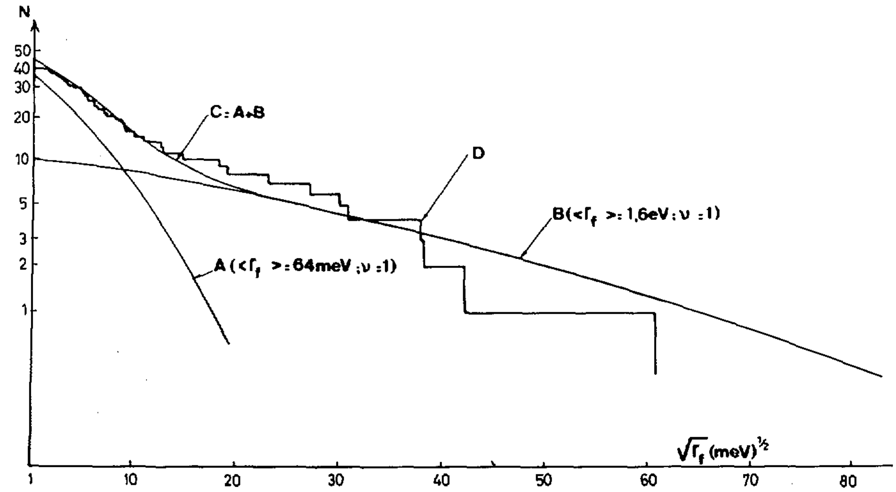

FIG.7. Distribution des largeurs de fission des résonances de ^{239}Pu situées dans la gamme d'énergie 110 eV-220 eV. N est le nombre de résonances ayant une valeur de $\sqrt{\Gamma_f}$ (meV)$^{\frac{1}{2}}$ supérieure à l'abscisse.
A. Distribution en χ^2 ; $\nu = 1$, $\langle\Gamma_f\rangle$ = 64 meV (famille des résonances étroites).
B. Distribution en χ^2 ; $\nu = 1$, $\langle\Gamma_f\rangle$ = 1, 6 eV (famille des résonances larges).
C. Distribution globale, somme des distributions A et B.
D. Histogramme expérimental.

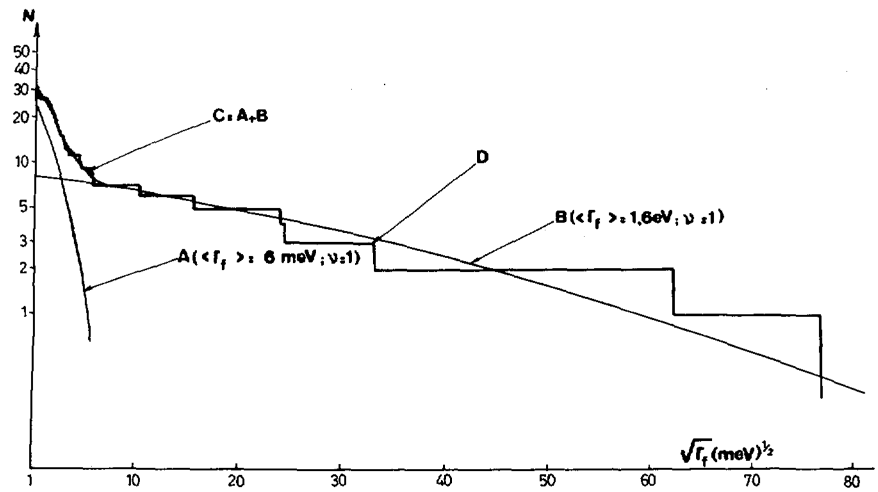

FIG.8. Distribution des largeurs de fission des résonances de ^{239}Pu situées dans la gamme d'énergie 550 eV-660 eV.
A. Distribution en χ^2 ; $\nu = 1$, $\langle\Gamma_f\rangle$ = 6 meV (famille des résonances étroites).
B. Distribution en χ^2 ; $\nu = 1$, $\langle\Gamma_f\rangle$ = 1, 6 eV (famille des résonances larges).
C. Distribution globale, somme des lois A et B.
D. Histogramme expérimental.

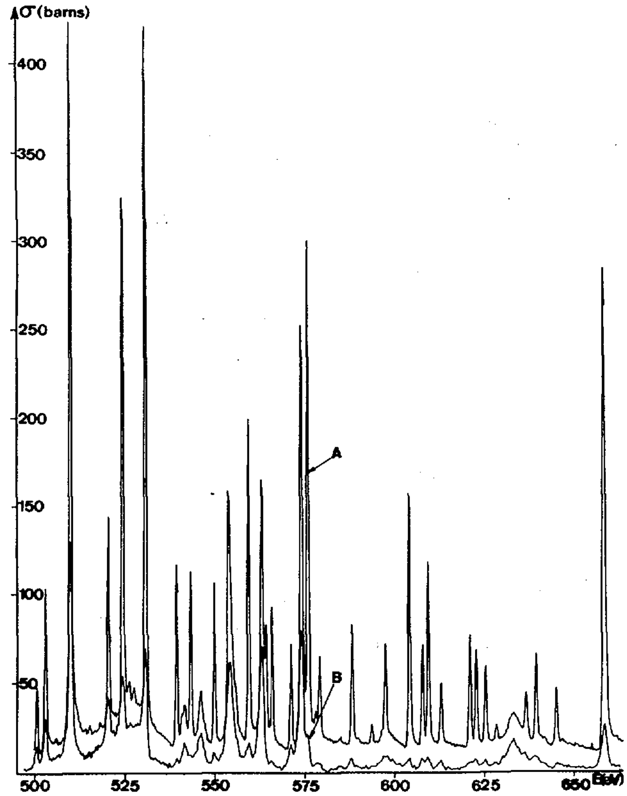

FIG. 9. Sections efficaces de ^{239}Pu de 500 eV à 660 eV.
A. Section efficace totale.
B. Section efficace de fission.

la largeur totale serait de quelques centaines d'eV. A basse énergie, le couplage est voisin de sa valeur maximale et les paramètres de fission alors obtenus ne sont pas représentatifs de l'ensemble de l'interaction ^{239}Pu (n, f). Pour ce faire, il faut étudier une gamme d'énergie nettement supérieure à l'espacement des groupes de la structure intermédiaire.

4. CONCLUSION

L'effet de structure intermédiaire qui est évident dans σ_f de ^{237}Np a pu également être clairement mis en évidence dans σ_f de ^{239}Pu. Pour ces deux noyaux, il est dû à une (ou des) voie(s) de sortie de fission.

Dans le cas de ^{237}Np l'existence de groupes de faible amplitude suggère qu'il existe en fait deux types de structure intermédiaire pouvant provenir de deux couplages différents aux voies de sortie de fission (peut-être dus à deux barrières assez différentes pour les deux états de spin 2^+ et 3^+). L'analyse du premier groupe à 40 eV montre l'existence d'une résonance très large, au-dessous de l'ensemble des résonances étroites, caractéristique du couplage faible (première barrière de fission plus haute que la deuxième).

Dans le cas de ^{239}Pu, l'analyse de plus de 250 résonances a montré l'existence d'une structure intermédiaire due à la voie (ou aux voies) de sortie de fission 1^+. Mais l'étude des autocorrélations et la variation de la fonction de densité locale en fonction de l'énergie n'excluent pas la présence d'une autre structure intermédiaire due à la voie d'entrée. Des études plus complètes sont nécessaires pour préciser ce dernier point.

REMERCIEMENTS

Nous remercions Mlle M. Sanche de l'aide précieuse qu'elle nous a apportée dans l'élaboration de ce travail.

REFERENCES

[1] EGELSTAFF, P.A., J.nucl.Energy 7 (1958) 35.
[2] MICHAUDON, A., Thèse, Paris, mai 1964; Rapport CEA n° 2552 (1964).
MICHAUDON, A., et al., Nucl.Phys. 69 (1965) 545.
[3] FESHBACH, H., KERMAN, A., Communication privée, 1964.
[4] PAYA, D., et al., ds Nuclear Data for Reactors (C.r. Conf. Paris, 1966) II, AIEA, Vienne (1967) 128 (résumé) et suppl.; J.Phys. 29 Suppl. n° 1 (1968) 159.
[5] MICHAUDON, A., Neutron Cross Sections and Technology (Proc. Conf. Washington DC, 1968) I, NBS Special Publication 299, Washington DC (1968) 427.
[6] FUBINI, A., et al., Phys.Rev.Lett. 20 (1968) 1373.
[7] MICHAUDON, A., ds Nuclear Structure (C.r.Coll.Doubna, 1968) AIEA, Vienne (1968) 483.
[8] MIGNECO, E., THEOBALD, J.P., Nucl.Phys. A112 (1968) 603.
[9] JAMES, G.D., RAE, E.R., Nucl.Phys. A118 (1968) 313.
[10] JAMES, G.D., Rapport AERE R5924, Harwell.
[11] STRUTINSKY, V.M., Nucl.Phys. A95 (1967) 20.
[12] LYNN, J.E., ds Nuclear Structure (C.r.Coll.Doubna, 1968), AIEA, Vienne (1968) 463.
[13] WEIGMANN, H., Z.Phys. 214 (1968) 7.
[14] PAYA, D., et al., Revue Phys.appl. 4 (1969) 289.
[15] MOTTELSON, B.R., Communication privée, 1968.
[16] STRUTINSKY, V.M., BJØRNHOLM, S., ds Nuclear Structure (C.r. Coll.Doubna, 1968), AIEA, Vienne (1968) 431.
[17] MICHAUDON, A., J.Phys. 29, Suppl. n° 1 (1968) 51.
[18] BLONS, J., et al., C.r. Séanc.hebd. Acad.Sci., Paris 267 (1968) 901.
[19] PATRICK, B.H., JAMES, G.D., Phys.Lett. 28 B (1968) 258.
[20] BLONS, J., et al.; DERRIEN, H., et al., à paraître.
[21] MICHAUDON, A., ds Nuclear Data for Reactors (C.r.Conf.Paris, 1966) II, AIEA, Vienne (1967) 161.
[22] DERRIEN, H., et al., ds Nuclear Data for Reactors (C.r.Conf.Paris, 1966) II, AIEA, Vienne (1967) 195.
[23] LYNN, J.E., Phys.Lett. 18 (1965) 31.

DISCUSSION

J.P. THEOBALD: The small Γ_f values of the enhanced resonances of the first resonance group in the ^{237}Np (n, f) cross-section (around 38 eV) and the assumption that the capture widths of these resonances are not extremely small suggest that the components of the (n, γ, f) process should be sought in these resonances. The gamma-decay takes place inside the second Strutinsky potential minimum leading to the shape isomer level. This isomer would then decay within a time comparable with the time spread of the resonances in the time-of-flight spectrum (some 100 ns). If this reasoning is correct, the Γ_f values should contain the components of Γ_γ.

A. MICHAUDON: I think that qualitatively you are right. However, in the particular case of ^{237}Np, as I have just shown, the effect you mention is very weak. The average value of Γ_f for the class-I resonances of the group at 40 eV is actually about 1 meV. The wide class-II resonance has a total (i.e. fission) width of about 10 eV; this must be compared with its radiative de-excitation width in the well above the second minimum, which is about 10 meV, namely a thousand times lower. The value of the $\Gamma_{\gamma f}$ width for the class-I resonances and for the process which you describe is thus also a thousand times lower than their fission width, i.e. negligible.

J.J. SCHMIDT: I would like to mention briefly the results of statistical theory calculations which I performed very recently on the quantity $\alpha = \sigma_\gamma/\sigma_f$ for ^{239}Pu for energies below about 2 keV at which s-wave processes predominate. The experimental α-values at these energies show a rather regularly fluctuating structure, which can be explained unequivocally by corresponding fluctuations in the fission widths of the 1^+ resonance component of the fission cross-section. The $\overline{\Gamma}_f^{1^+}$ values so obtained are of the same magnitude as those obtained from the resolved resonance measurements reported by Michaudon and thus support his results and conclusions regarding the intermediate structure of the 1^+ s-wave sub-threshold fission of ^{239}Pu.

E. MIGNECO: Dr. Michudon, your very interesting results on ^{237}Pu, which permit a direct observation of the intermediate structure deduced previously by autocorrelation analysis, are a proof of the usefulness of this method for qualitative detection of similar effects. The broad structure which seems to underlie the first group of resonances in ^{237}Np attains values of only about 0.03 b. Can you please tell me what background corrections you had to apply there?

A. MICHAUDON: The wide resonance which appears below the narrow resonances of the group at 40 eV has a surface which is about 8% of the sum of all the others. It emerges clearly below the residual cross-section outside the group, which is often lower than 1 mb. As I pointed out in my presentation, this measurement, which was performed in June 1967, was made with a detector specially designed to give very low background noise. In several calculations, the number of counts was actually zero.

As regards the statistical criterion which, applied to the autocorrelations, enables us to deduce the presence of intermediate structure, I can only refer you to Dr. Perez' paper (SM-122/121). In our work we observed autocorrelations not only in σ_f but also in σ_T. If we confined ourselves to these results only, we would be tempted to deduce that the intermediate structure came from the entrance channel. But microscopic analysis of resonances up to 660 eV demonstrates the existence of an intermediate structure due to the exit channel of fission, J^+. I cannot but agree with Dr. Perez that the autocorrelations should be interpreted with great caution, at least for the time being.

EFFECTIVE K QUANTUM NUMBERS IN FISSION OF ORIENTED ^{235}U*

J.W.T. DABBS
Oak Ridge National Laboratory,
Oak Ridge, Tenn., United States of America
and
C. EGGERMAN, B. CAUVIN, A. MICHAUDON, M. SANCHE
Centre d'Etudes Nucléaires, Saclay,
France

Abstract

EFFECTIVE K QUANTUM NUMBERS IN FISSION OF ORIENTED ^{235}U. The angular anisotropy of fission fragments produced in neutron-induced fission of aligned ^{235}U nuclei has been measured for neutron energies between 0.3 eV and 175 eV, using time-of-flight techniques at the pulsed 45 MeV electron linear accelerator at Saclay. The low-temperature nuclear-alignment apparatus used was a modified version of the apparatus described at the Salzburg conference, and gave an average temperature of 0.61 K for the four $UO_2Rb(NO_3)_3$ single crystal samples during a measurement period of approximately 220 h. The flight path was 5 m and the electron pulse length was 100 ns. Multilevel fits to the observed 0° and 90° fission cross-sections have been made using the Adler and Adler formalism with the aid of a program developed by G. de Saussure. The most striking result obtained in the analysis of some 16 of 100 levels or groups of levels is a strong correlation between small fission width and an effective value of $K \cong J$. All 5 resonances in the group of 16 for which results are final, for which $K \cong J$ is deduced, have exceptionally small widths. This result suggests that the small widths are associated with a large rotational energy and consequent diminution in available deformation energy, so that these 5 resonances are effectively sub-threshold resonances; such a suggestion is quite in accord with the ideas of Bohr. The preponderance of other resonances so far analysed have effective K values of 1 or 2. An analysis of all resolvable resonances is presented.

1. INTRODUCTION

As discussed at the earlier conference [1], the effective value of the K quantum number in the transition region of fission can be inferred from a study of the angular distribution of fission fragments from aligned nuclear targets. A considerable extension of the earlier work has been made by changing from the reactor-crystal monochromator neutron source to a time-of-flight system at the Saclay 45-MeV electron linear accelerator, which permitted simultaneous measurement over a range of neutron energies with fairly good neutron energy resolution.

2. RESUME OF THEORY

The basic assumption is that the angular distribution of the fission fragments is the same as the angular distribution of the nuclear symmetry axis during the relatively long period spent by the nucleus in the transition region. This assumption, and the use of symmetric-top wave functions

* Research jointly sponsored by the US Atomic Energy Commission under contract with the Union Carbide Corporation and by Centre d'Etudes Nucléaires.

$D^J_{MK}(\alpha, \beta, \gamma)$ to describe the pertinent angular distributions of the axis of symmetry of the target and compound nuclei and the populations of the various M states (known, at least approximately, from the type and amount of initial nuclear alignment) leads to an expression

$$W(\beta) = 1 + \frac{A_2}{T} P_2(\cos\beta) \tag{1}$$

for the angular anisotropy of the fission fragments. In the present case the amount of alignment is proportional to $1/T$, the absolute temperature. The coefficient A_2 has a dependence for pure K's, with no interference effects [2] given by

$$A_2 \propto [3K^2 - J(J+1)]/[J(J+1)] \tag{2}$$

where J is, of course, the total angular momentum quantum number of the compound nucleus. There are also numerical factors depending only on the target nucleus spin I and the coupling constant P, which is a measure of the nuclear quadrupole moment-crystalline electric field gradient which leads to the nuclear alignment in the $UO_2Rb(NO_3)_3$ crystal [3]. The previous work [1] clearly showed that no higher terms than $P_2(\cos\beta)$ can be present in the angular distribution. Accordingly, in the present experiments and in other measurements at very low neutron energies [4] a system of detectors at 0° and 90° to the crystal c axis were used. Table I gives the expected values of the expected ratio of counting rates at 0° and 90° angles to the crystal c axis, based on a value of $Phc/k = 0.0154$°K [3] for various pure J, K values in ^{235}U and a temperature of 0.79°K.

TABLE I. EXPECTED RATIO OF COUNTING RATES AT 0° AND 90°

K	$J=3^-$	$J=4^-$
0	1.153	Parity forbidden
±1	1.114	1.129
±2	1.00	1.060
±3	0.83	0.950
±4		0.81

3. APPARATUS AND EXPERIMENTAL ARRANGEMENTS

Cryostat. The cryostat was a modified version of the ^{3}He continuous-flow refrigerator cryostat previously reported [1]. The major changes were (1) provision for mounting four crystals and four detectors simultaneously, (2) substitution of a stainless steel expansion frit for the needle valve used previously in the ^{3}He circulation system, and (3) increase by a factor of 2 in ^{3}He circulating forepump capacity. This apparatus was flown to the Saclay laboratory.

TABLE II. OPERATING CONDITIONS

Electron beam burst length	100 nsec
Electron energy	45 MeV
Peak beam current	280 mA (typical)
Repetition rate	1000 pps
Effective average power into ^{235}U target	0.9 KW[a]
Moderator	$20 \times 20 \times \sim 3$ cm

[a]Includes effect of downtime due to dropouts, etc.

Linear Accelerator. The cryostat was mounted in a flight path (No. 2) 18° forward from the normal to a polyethylene slab moderator which was adjacent to the water-cooled natural-U metal linac target, at the shortest available distance from the moderator (5 m).

Operating conditions for the linear accelerator are given in Table II.

Beam Collimation and Shielding. A converging aluminium cone 3 m long surrounded by B_4C served as the main beam collimator. This was followed by a 2-in.-thick Pb disk with a central hole of 70 mm diameter, and final collimation (also conical), made of 20 cm of LiF-loaded epoxy and 15 cm of Pb, reduced the beam at the entrance to the cryostat to 30 mm diameter. A layer of Cd (0.5 mm) surrounded the lower end of the cryostat and was in turn surrounded by borated paraffin (10 cm). This reduced the background fission rate from external neutrons to a negligible value. The collimation was, however, inadequate for higher-energy neutrons, and a small residual fission background was deduced to have existed.

Beam Filter. A beam filter located in the final collimation section consisted of 69 mg/cm^2 of cadmium plus 131 mg/cm^2 of natural gadolinium metal plus 20 mg/cm^2 of ^{157}Gd in liquid form as gadolinium nitrate in a solution of DNO_3. This beam filter was designed to give a sudden cutoff in neutron intensity at about 0.2 eV. The gadolinium portions served to fill the broad dip in the cadmium neutron cross-section in the neighbourhood of 0.04 eV. Thus the calculated neutron intensity was reduced to at most 6% of the intensity at 0.35 - 0.4 eV for all times greater than 850 μs after the electron pulse at the neutron target distance of 5 m. The times between ~860 μs and 960 μs after the electron pulse were used to measure alpha particles which were spontaneously emitted by the ^{235}U. In this way an independent measurement of the degree of nuclear alignment actually obtained was available. The degree of alignment can be stated in terms of an "effective temperature" at the active surface of the sample crystals.

Sample Crystals. As in the earlier works [1, 4] the sample crystals were single crystals of $^{238}UO_2Rb(NO_3)_3$ with a thin coating of $^{235}UO_2Rb(NO_3)_3$ grown on the outer surface from hot HNO_3 solution [5].

The sample crystals were mounted in the collimated neutron beam from the accelerator and were attached thermally to a copper plate cooled to 0.61°K (average). The crystals were enclosed in a gastight can which served to contain a low pressure of cold ^{3}He gas for heat exchange, thus

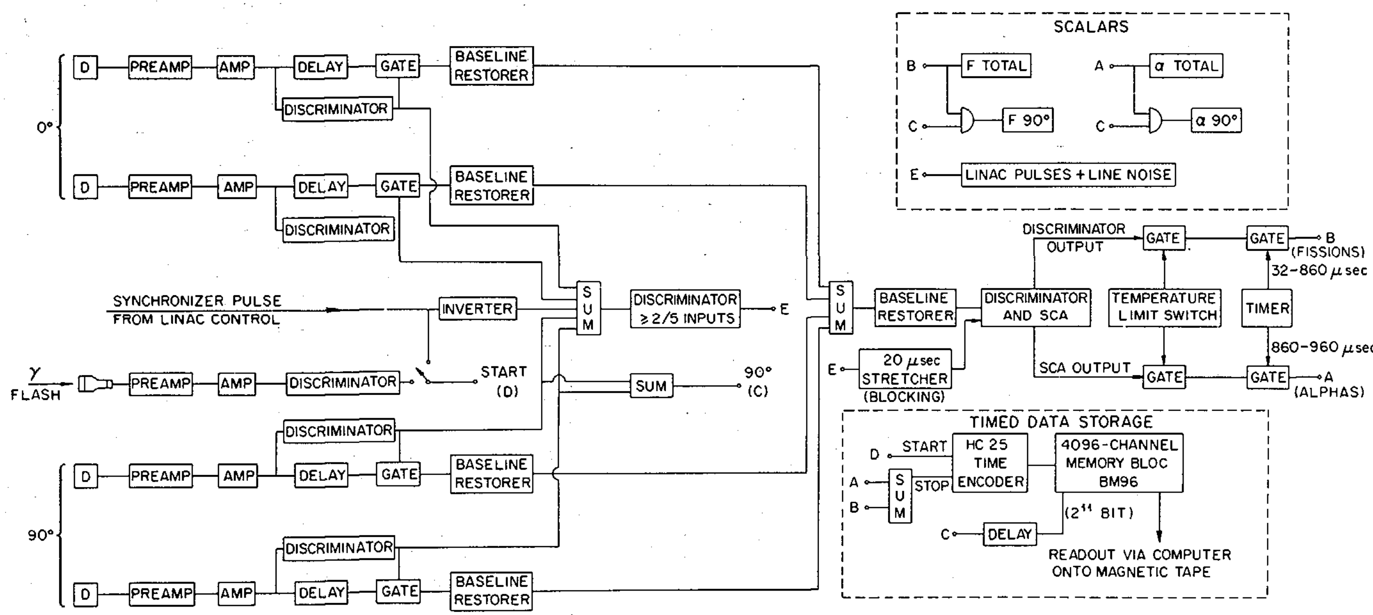

FIG. 1. Block diagram of electronic system: an example of international cooperation. Most of the equipment in the left half of the diagram was made in the US., while most of that in the right half was French.

ensuring temperature equilibrium between the crystal surfaces and the cold plate. The cold can, of fluorothene plastic, acted as its own gasket. To permit egress of the fission fragments and alpha-particles, a total of 30 cm^2 of apertures were cut in its walls and covered with 40 $\mu g/cm^2$ of VYNS film (six layers) and 50 $\mu g/cm^2$ of gold [6]. The energy loss for fission fragments was ~ 4 MeV. At 1.6°K, an additional surround of nickel (133 $\mu g/cm^2$) with an evaporated coating of gold (50 $\mu g/cm^2$) served as a radiant energy reflector and caused an additional loss of similar amount in fragment energy.

Detectors. The detectors were mounted at 90° intervals around the crystals and cryostat vertical axis and carefully aligned so that two detectors were along the c-axis direction of the crystals and two were perpendicular to the axis. These were called the 0° and 90° detectors, respectively. The neutron beam passed between detectors; since only s-wave neutron capture is involved, the beam direction was inconsequential. The detectors were masked with aluminium collimators to give each an effective area of 5.25 cm^2; each was made of 450-ohm-cm n-type silicon and designed to be operated at the low temperature (81°K) used [7].

Electronics. A block diagram of the electronic system used is shown in Fig. 1. Separated chains with preamplifier, amplifier, integral discriminator, and linear gate were used for each detector so that the signal from a given detector would be accompanied by its own noise only. Because of the intense burst of gamma-rays accompanying each linac pulse, a scattered gamma-ray pulse was produced in each detector at time t_0 of ~ 2000 MeV equivalent. A modification of the preamplifier for reduced gain and fast return to the base line [8] avoided overload and permitted (with the help of a base-line restorer) normal operation within 20 - 25 μs after the gamma flash. Line noise elimination was ensured by a "two out of five" coincidence circuit (output E in Fig. 1) which blocked the output of the combined discriminator and single-channel analyser. The synchronizer input pulse into the line noise circuit was added when it was discovered that during dropouts (and startup and shutdown of the aceelerator) gamma flash pulses could trigger one detector alone instead of four simultaneously; this led to false counts in the scalar monitoring system. The single-channel analyser was chosen for its particularly stable channel limits [9] and was modified so that the upper limit of the channel served also as an integral discriminator lower limit. Thus pulses greater than the upper level were taken as fission fragments and pulses within the channel were taken as alpha-particles. This discrimination, together with the time gating system, gave essentially complete separation of the two types of particles. The shape of the alpha spectrum was an indication of the average ^{235}U layer thickness (~ 2 mg/cm^2). The upper A24 limit was set at approximately 5 MeV; the fission spectrum was measured (at low gain) to extend to ~ 75 MeV, but the gains were set so that the main amplifiers saturated at ~ 10 MeV, since the (thick source) fission spectrum itself was quite flat and featureless.

For purposes of monitoring scalars were provided as shown in Fig. 1. Timed data was stored in a 4096 (2^{12}) channel core memory which was used as a multiscalar. The address was advanced by a time encoder [10] which permitted, by means of a diode plug-in board, the selection of a

TABLE III. TIMING PROGRAM

Period No.	Length (units of 3.2 μs)	Length (μs)	No. of channels	Width (ns)
Initial delay	8	25.6		
1	10	32	640	50
2	10	32	320	100
3	26	83.2	416	200
4	35	112	280	400
5	40	128	160	800
6	61	195.2	122	1600
7	110	352	110	3200
Total	300	960	2048	

timing program as shown in Table III. Only the last 31 channels were occupied with the alpha-particle information. A routing signal from the summed 90° discriminators (signal C, Fig. 1) served to place all 90° information in the "second half" of the BM96 core memory by setting the 2^{11} bit in the address. Thus 0° and 90° data were treated in exactly the same way except for the data storage location. Provision was made for periodic (usually daily) readout of the contents of the BM96 onto magnetic tape via the CAE 510 computer located in the linac building at Saclay. Each of these read-outs was called a "run". Subsequent manipulation of the data (e.g. summation of runs, background generation and subtraction, etc.) was carried out on the CAE 510, using the rather large programme library which had been previously developed [11].

4. RESULTS

In addition to background, calibration, and normalization runs at "high" temperature (4.2°K), a total of 17 acceptable runs were carried out at low temperatures between 0.70 and 0.48°K. The total time included in these runs was approximately 220 hr, and the average temperature was calculated (after weighting with total counts in each run) to be 0.61°K. However, it was found that the average effective temperature of the sample crystal surfaces was 0.79°K, as determined from the alpha-particle anisotropy. Unhappily, because of an accelerator shutdown at Saclay, incomplete data were obtained in the high-temperature calibration runs, and resort was made to a normalization of the data to the earlier results at low neutron energies [1, 4]. A degree of uncertainty thus exists in the absolute values of effective temperature and degree of alignment [3], but the relative results from resonance to resonance are unquestionable.

The average value of the 0°/90° fission ratio for all fission events recorded was 1.089, which, from Table I, corresponds to an average effective K quantum number of ~1.22 (J = 3) or ~1.58 (J = 4).

The most striking single result is associated with a very small resonance at 4.85 eV (see Fig. 2). In this case, the 0°/90° ratio was

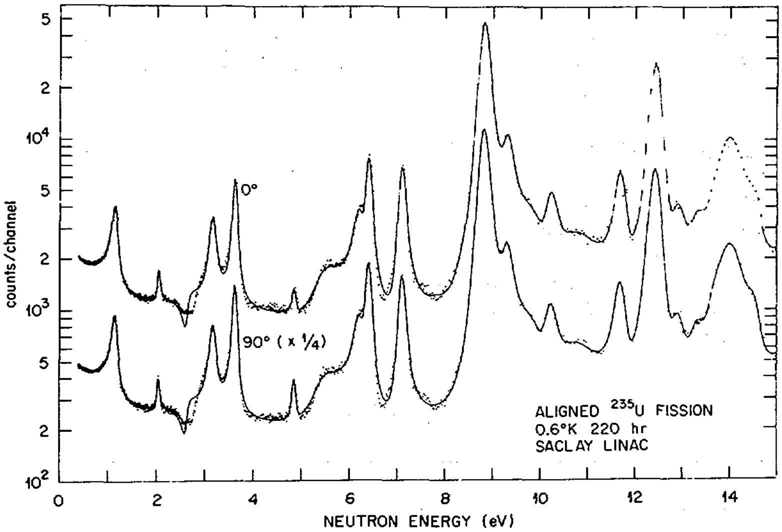

FIG.2. Example of ^{235}U cross-sections as measured at 0° and 90° to c-axis of $^{235}UO_2Rb(NO_3)_3$ crystals held at 0.61°K. The ratio of the areas for a given resonance peak is a measure of the K-quantum number in the transition region. Points are data; smooth curve is a least-squares fit to data (see text). Misfit at 2.7 eV is unimportant; a resonance in the beam filter distorts the data near this energy. The plot is scaled to 0.4 μs/channel.

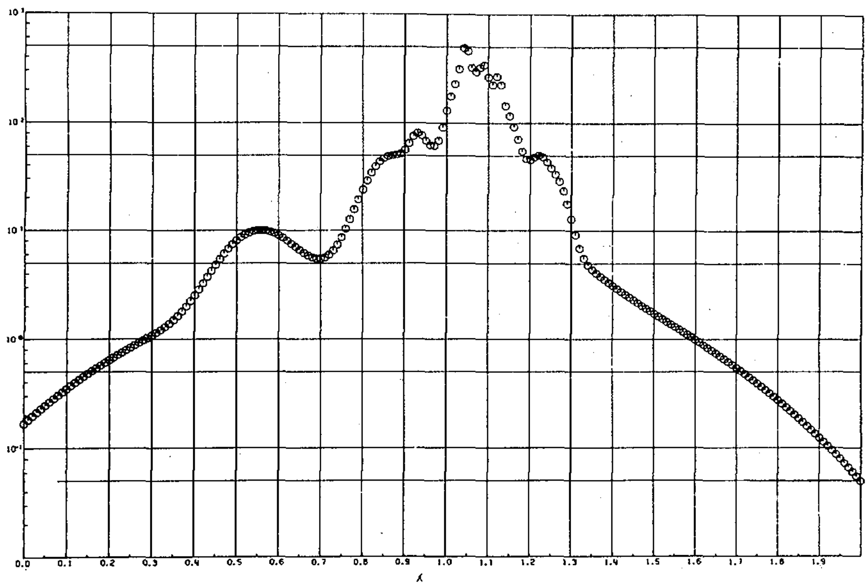

FIG.3. "Pseudo-histogram" of results of Table IV. The value of Y is given by $Y = (1/\sqrt{2\pi}) \sum_i (1/\sigma_i) \exp[-(x - 0°/90°)^2/2\sigma_i^2]$. Values of x may be compared with 0°/90° values in Table I. Semilogarithmic scale; total area = 46 units.

certainly less than 1. This effect was clearly visible in every single run as well, and corresponds to the K ~ J case in Table I. A good determination of the ratio of the 0° and 90° peak areas is rather difficult, but the qualitative result is quite obvious and reliable.

Analysis. Because of uncertainties in background subtraction, a simple determination of the ratio of peak heights or of the total integral count between energy limits is inadequate. An accurate determination of the background would have required additional data with "black resonance" filters; one such resonance in the ^{157}Gd filter appears at ~ 2.7 eV (Fig. 2). The accelerator shutdown in May and June 1968 prevented such measurements, as well as sufficient "high" temperature normalization runs, as mentioned above.

TABLE IV. RESULTS OF LEAST-SQUARES FIT ANALYSIS

G_f	E_n	0°/90°	σ	G_f	E_n	0°/90°	σ
1.73	● 4.84	0.552	0.053	22.44	24.23	1.052	0.041
20.95	49.5	0.63	0.20	138.4	25.65	1.056	0.011
11.56	10.76	0.86	0.026	193.3	39.5*	1.056	0.014
10.57	12.85	0.847	0.033	22.87	35.75	1.059	0.11
9.18	13.65	0.86	0.042	5.90	3.16	1.069	0.017
91.02	21.07	0.93	0.012	3.01	5.42	1.069	0.031
106.2	42*4	0.92	0.022	111.8	23.5*	1.082	0.012
192.8	48*3	0.97	0.017	69.42	26.44	1.081	0.018
79.98	14.0	1.006	0.009	6.69	1.14	1.088	0.005
6.68	18.98	1.009	0.17	10.07	6.23	1.089	0.015
0.83	2.03	1.029	0.027	14.11	7.08	1.091	0.014
9.95	3.61	1.030	0.010	9.19	13.30	1.091	0.041
16.61	6.39	1.022	0.011	9.60	10.16	1.11	0.026
30.59	40.5	1.04	0.10	212.6	44*5	1.11	0.014
15.93	9.29	1.04	0.017	23.95	16.09	1.121	0.023
177.2	● 8.77	1.042	0.005	41.49	18.04	1.127	0.017
103.1	●12.40	1.041	0.008	291.0	●19.3	1.124	0.004
555.9	●51*5	1.044	0.010	69.31	27.81	1.135	0.019
597.6	●35*5	1.046	0.005	13.89	11.66	1.15	0.025
120.6	46.9*	1.045	0.023	22.70	15.42	1.148	0.023
35.34	16.66	1.047	0.018	12.53	30.6	1.23	0.20
6.09	14.55	1.049	0.11	135.2	32.1	1.22	0.014
35.91	22.94	1.054	0.026	95.21	33.5	1.26	0.019

Note: Filled circles indicate prominent resonances; asterisks denote groups; the number after the asterisk is the number of levels in the group (if exceeding two).

To take account of tails from other resonances at a given energy, multilevel fits to the data are required; since the parameters of the fission resonances in ^{235}U are relatively well known [12], this task is somewhat simplified. A fitting programme which was developed by G. de Saussure and utilized to make a simultaneous fit to the capture and fission cross-sections (i.e. using common values for the energies and total width) is thus ideally suited to make a simultaneous fit to the 0° and 90° data. This programme is based on the Adler and Adler formalism [13] which represents interference terms by means of a skew function added to the symmetric part of each resonance. The formalism is ideal for the present application, since the integral over the skew function is zero.

Results of this analysis for 46 resonances (or groups) below ~ 50 eV are presented in Table IV and Fig. 3. In Table IV, the first column is the value of G_f [13] in barn-$eV^{3/2}$ as obtained by de Saussure et al. [12]. Filled circles are included to indicate the 4.84 eV resonance mentioned above and a number of prominent resonances. Note the grouping near the values of 0°/90° ~ 1.04, and the clear separation from the values for 4.84 and 19.3 eV. Asterisks denote groups; the number after the asterisk is the number of levels in the group if more than 2. Values of σ (standard deviation on 0°/90°) are equivalent to 1.5 times the statistically expected standard error in the ratio. A plot of σ vs $E^{3/2}/G_f$ was used to simplify the determination of σ from values determined in representative cases.

The distribution of the K-values, as shown in Fig. 3 seems difficult to explain in terms of the theory of Bohr [14] when the fission barrier has one single hump only. If this approximation is used, the distribution of the K-values can be determined if the spectrum of transition states at the saddle point usually obtained from the analysis of (d, pf) data is known. Still in the case of a single-hump fission barrier, the analysis carried out by Britt [15] who takes a rather low value of $\hbar\omega$ ($\hbar\omega$ = 0.35 MeV), indicates that the octupole bands are at the following energies (relative to the neutron binding energy):

$K = 0^-$	− 0.80 MeV
$K = 1^-$	− 0.35 MeV
$K = 2^-$	− 0.20 MeV

Britt already noticed that this scheme of transition states is not appropriate to an explication of data obtained with resonance neutrons (N_{eff} = 0.5 and ν = 25.3).

If the same spectrum is used to interpret our results, then we should obtain a broad distribution covering about equally the values of K from 0 to 2. On the contrary, the values of K obtained from our experiment are lumped around a value between 1 and 2. If the spectrum of transition states is modified by raising the $K = 1^-$ and 2^- bands while keeping the $K = 0^-$ at the same energy, then the experimental results should show a predominance of the contribution of K = 0 over that of K = 1 and K = 2, which is not observed. Rather, the K = 1 and K = 2 components are more important than K = 0.

Values of K greater than 2, corresponding to values of 0°/90° smaller than 1 (i.e. K ~ J) are observed only for small fission resonances, indeed so small as to be difficult to analyse.

In conclusion, the single-hump fission barrier seems inadequate to explain the experimental distribution of K values. A more detailed analysis needs to be performed not only on these results but also on resonance neutron and (d, pf) data, using our present knowledge of more sophisticated fission barriers, such as those described by Strutinsky [16]. One can then speculate about the coupling of class-I compound nucleus states observed as resonances in the ^{235}U cross-sections, to class-II states in the second well of the potential. The properties of the fission process and among them the value of K at scission may be strongly influenced by the properties of these class-II states. They can, for example, enhance a given mode of fission, such as a given value of K.

REFERENCES

[1] DABBS, J.W.T., WALTER, F.J., PARKER, G.W., in Physics and Chemistry of Fission, (Proc. Symp. Salzburg), IAEA, Vienna, (1965) 39.

[2] DIETRICH, K., (Kernforschungszentrum Karlsruhe) has pointed out the possibility of such interference effects.

[3] Unfortunately, our present knowledge of the exact value of P is rather uncertain, perhaps by ~20%. In Table I an estimate is used which is taken from observed alpha-particle anisotropies in aligned ^{233}U. For details, see Ref. [1]. This uncertainty does not, of course, affect the comparison of results from level to level in this work.

[4] DABBS, J.W.T., PARKER, G.W., NEVILLE, G.B. (unpublished).

[5] We are indebted to G.W. PARKER, Reactor Chemistry Division, Oak Ridge National Laboratory, who grew and coated the crystals.

[6] DABBS, J.W.T. (to be published).

[7] ORTEC model 7906.

[8] We are indebted to J.B. AYRES (who was responsible for the original preamplifier design, ORTEC model 109-F) for providing a rapid and satisfactory solution to this problem.

[9] Supplied by SAIP, 92 Malakoff, France; CEA type reference A24.

[10] Both the time encoder (model HC 25) and the block memory (model BM96) were made by Intertechnique, Paris. The time encoder is based on a 40-MHz crystal oscillator and is extremely flexible and well adapted to time-of-flight spectroscopy.

[11] Under the direction of Mlle. M. SANCHE.

[12] DE SAUSSURE, G. et al., Simultaneous Measurements of Neutron Fission and Capture Cross Sections for ^{235}U for Incident Neutron Energies from 0.4 eV to 3 keV, Oak Ridge National Laboratory report, ORNL-TM-1804 (November 21, 1967).

[13] ADLER, D.B., ADLER, F.T., in Breeding, Economics and Safety in Large Fast Power Reactors, (Argonne, 1963) Proc. Conf. National Laboratory report, ANL-6792, 695.

[14] BOHR, A., Int. Conf. peaceful Uses atom. Energy, (Proc. Conf. Geneva, 1955) UN, New York (1956).

[15] BRITT, H.C. et al., Phys. Rev. 175 (1968) 1525.

[16] STRUTINSKY, V.M., BJØRNHOLM, S., in Nuclear Structure (Invited Papers Int. Symp. Dubna, 1968), IAEA (Vienna, 1968) 431.

DISCUSSION

N.J. PATTENDEN: We have carried out an experiment at the Harwell electron linear accelerator similar to the one described by Dr. Michaudon, as mentioned in abstract SM-122/57. The cryostat, which was designed and made in Holland, is shown in Fig. A. It incorporates a ^{3}He-^{4}He dilution refrigerator, which can run for long periods at temperatures well below 0.1°K. Our samples consist of a mozaic of many crystals of rubidium uranyl nitrate, cut into thin slabs to improve thermal conductivity; the slabs, all similarly oriented, are attached to a copper plate. Semiconductor fission-fragment detectors are located at 0° and 90° to the crystal c-axis,

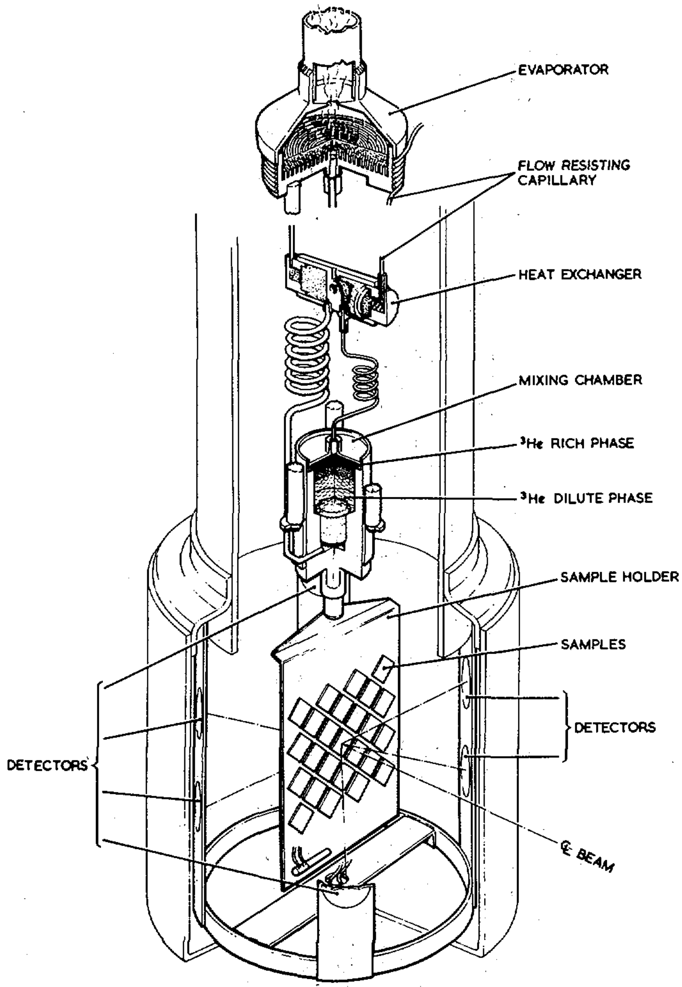

DILUTION SYSTEM INCLUDING SAMPLE AND DETECTOR ASSEMBLIES

FIG. A. Cutaway picture of the cryostat.

and are out of the neutron beam. We have used this apparatus to study the fission-fragment angular distributions from resonance fission in ^{235}U, ^{233}U and ^{237}Np. The analysis of the results is at present continuing, but I can show here some preliminary results on ^{235}U, and mention some very recent data on the first ^{237}Np runs.

Figure B shows the variation of the effect in ^{235}U with $1/T$ for an incident neutron energy range of 0.07-0.09 eV. As the temperature is reduced, the effect departs markedly from a linear dependence on $1/T$, and tends to saturation below 0.1 K. It is possible to obtain, from such data, independent information on the quadrupole coupling constant, but we have so far used the same value as in the paper under discussion to

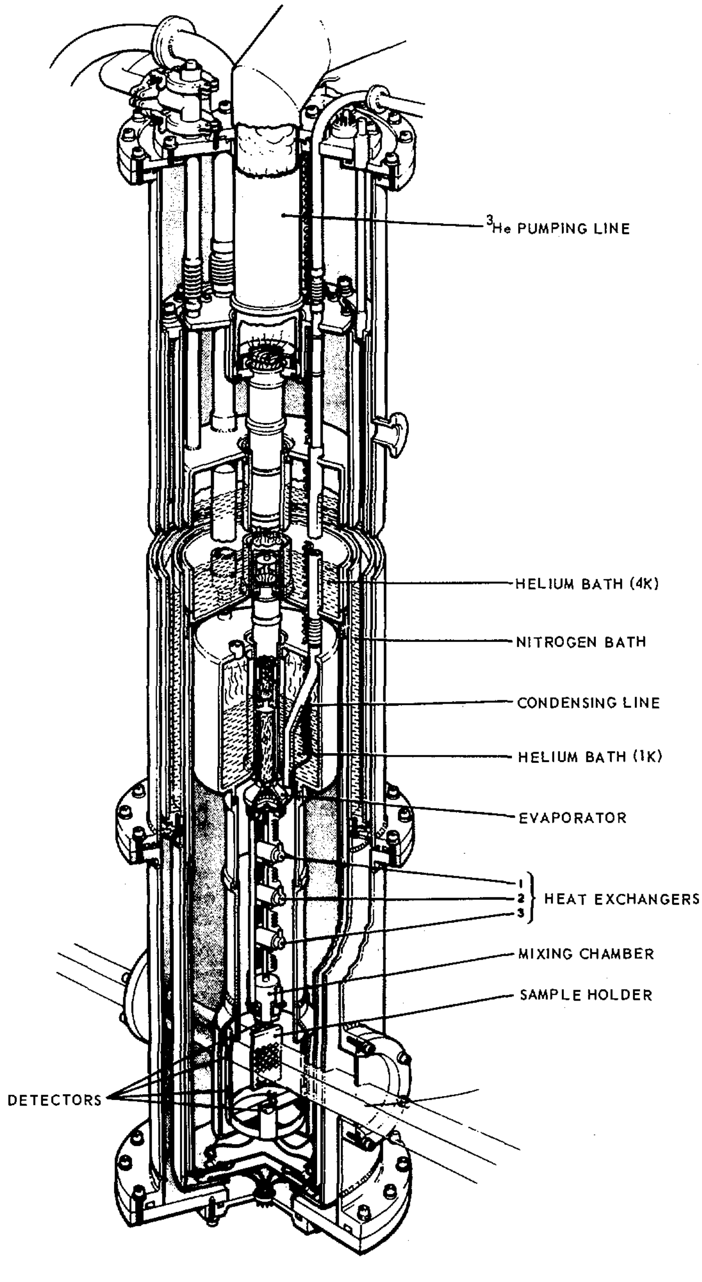

DILUTION REFRIGERATOR FOR NUCLEAR ORIENTATION EXPERIMENTS

FIG. A. (cont.)

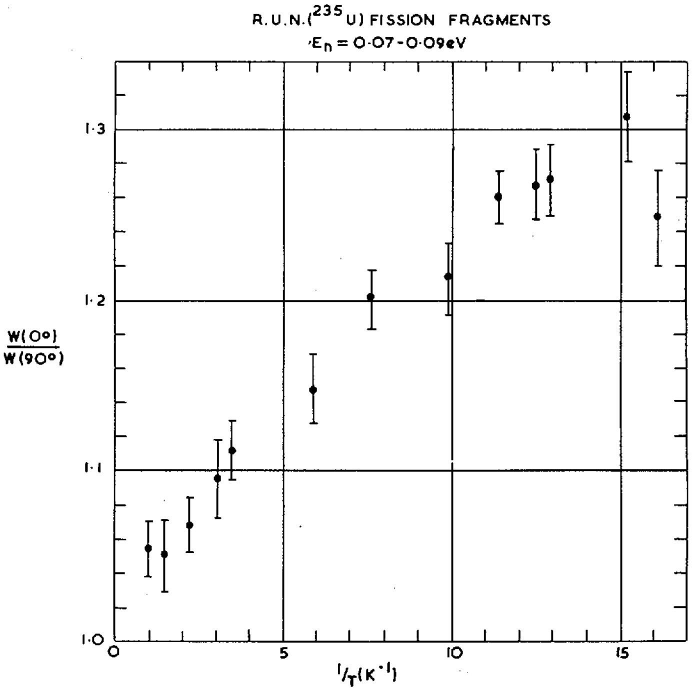

FIG.B. Variation of the effect in ^{235}U with 1/T.

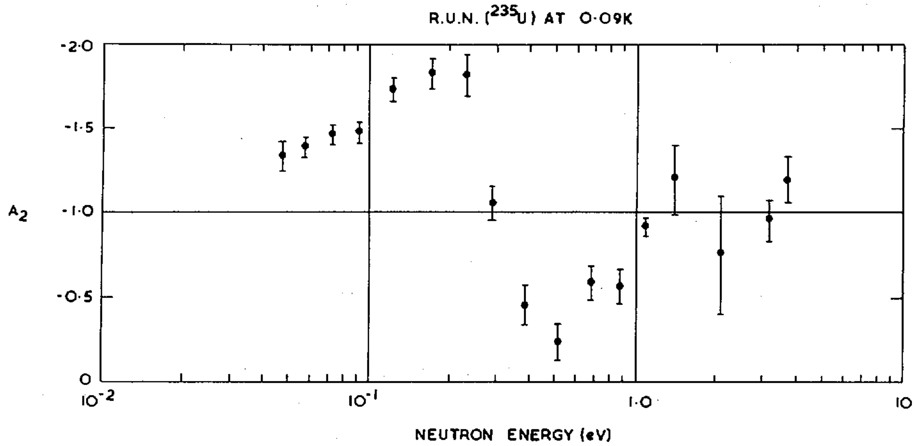

FIG.C. Variation of A_2 with neutron energy from 0.05 to 4 eV.

determine the orientation parameter f_2, mentioned in the abstract. Knowing f_2, the anisotropy factor A_2 can be obtained, and Fig. C shows its variation with neutron energy from 0.05 to 4 eV. It can be seen to vary markedly in a way which agrees qualitatively with the results reported by Dabbs et al. at the 1965-Symposium (Ref. [1] of the paper).

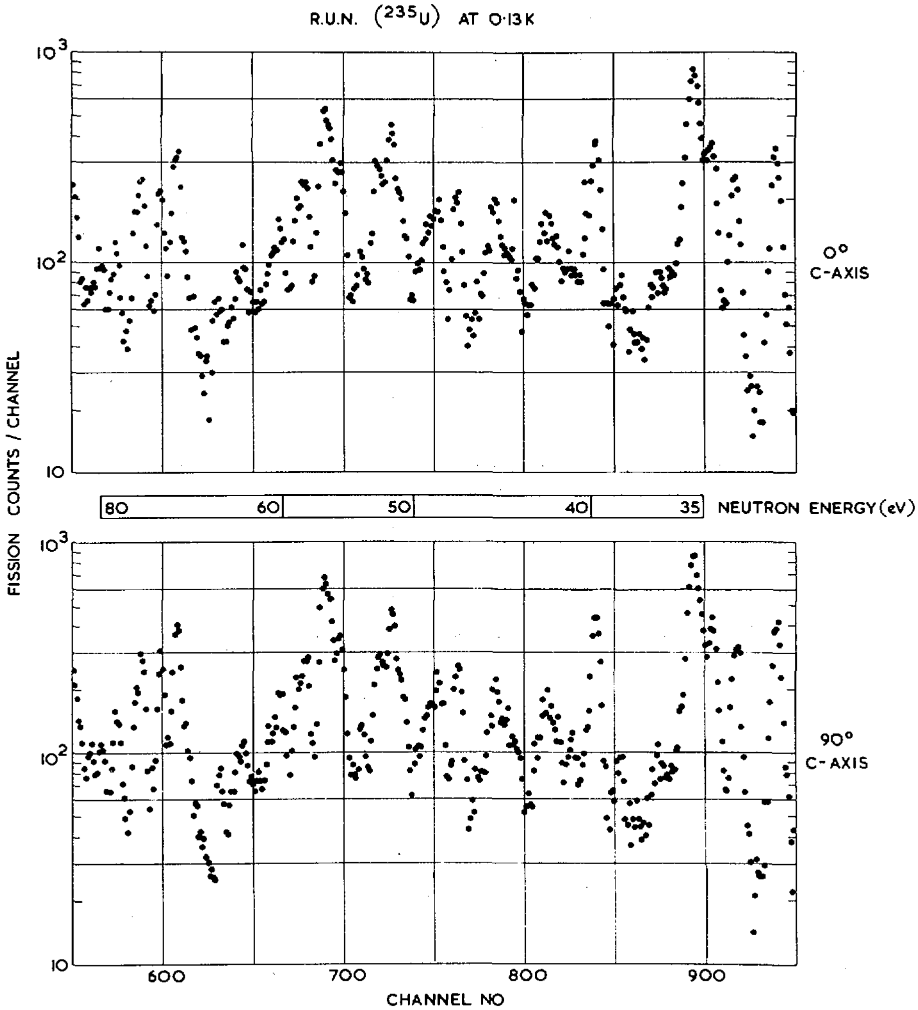

FIG.D. Example of the ^{235}U experimental data from 35 to 80 eV.

Figure D shows an example of the experimental time-of-flight spectra in the neutron energy region from 35 to 80 eV. Values for A_2 have been obtained for the larger resonances below 60 eV, and Fig. E shows a histogram giving their frequency distribution. For our purposes, A_2 depends on J^π and K, and Fig. E also shows the calculated $A_2(J^\pi, K)$ values. Thus, our preliminary results indicate that K values of other than 1 and 2 must occur only rarely. The general conclusion to be drawn from our results agrees with that of the paper under discussion but we do not observe resonances with $K \simeq J$. In particular, there is disagreement between the two experiments on the 4.85 eV resonance, for which we have no explanation, as yet.

TABLE A. ^{237}Np RESONANCE FISSION ANISOTROPY (preliminary results at T = 0.12K)

E_R (eV)	W(0°)/W(90°)	Statistical error	$\sigma_0\Gamma_F$ (b.eV) (Saclay[a])
30.6	0.77	0.13	0.52 ± 0.05
37.4	0.72	0.16	0.22 ± 0.03
39.3	0.81	0.10	(0.41 ± 0.46)[b]
40.1	0.75	0.06	1.74 ± 0.2
41.8	0.83	0.12	0.683 ± 0.085
43.3	0.98	0.39	0.045 ± 0.007
46.2	0.87	0.23	0.21 ± 0.03
50.8	0.44	0.19	0.196 ± 0.026
120.0[c]	0.95	0.18	
201.0[c]	0.86	0.11	
252.5[c]	0.92	0.22	
372[c]	0.99	0.28	
424[c]	0.77	0.18	
871[c]	0.68	0.12	

[a] PAYA, D. et al., Supplement to Proc. Nucl. Data for Reactors Conf. Paris (1966), (IAEA INDC/156 (1967)).

[b] Resolved into two resonances.

[c] Probably resonance groups.

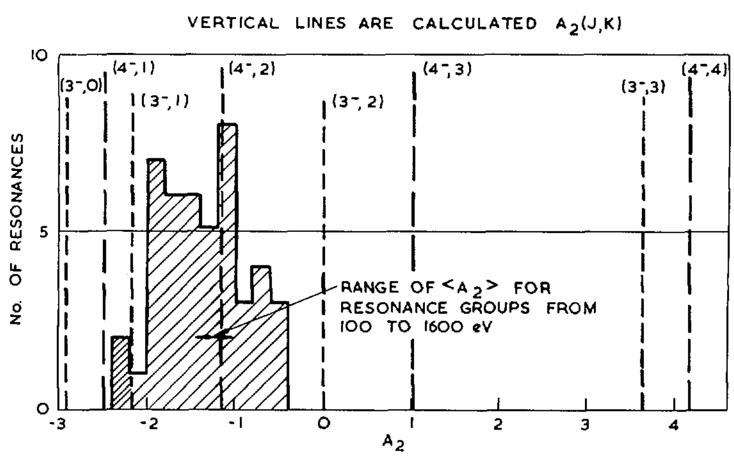

FIG. E. ^{235}U resonance A_2 distribution.

Table A gives some preliminary experimental data on ^{237}Np. Because of the small fission cross-section, the statistical errors are large. These results indicate that there are no large variations in the effect from resonance to resonance in the group at about 40 eV, nor are there large variations from one resonance group to another. This may be considered to support the suggestion by Dr. Michaudon in his paper on ^{237}Np (SM-122/90) that these groups are all in the same spin state.

Yu.V. RYABOV (Chairman): Dr. Michaudon, do the results of the paper under discussion agree with the earlier data of Dabbs et al. in the overlapping energy range?

A. MICHAUDON: The results presented here cover the energy range from 0.2 eV to about 50 eV. The lower limit of 0.2 eV was chosen after a special study of the filter in order to take account of Dabbs' earlier work near the resonance at 0.3 eV. Considering the difference in experimental resolution, the two works are in good agreement in this energy range. It is for this reason, moreover, that the new results were normalized over the earlier ones which, from this point of view, are of superior quality.

ДВУГОРБЫЙ БАРЬЕР В КВАЗИКЛАССИЧЕСКОМ ПРИБЛИЖЕНИИ

Е.В.ГАЙ, А.В.ИГНАТЮК, Н.С.РАБОТНОВ, Г.Н.СМИРЕНКИН
Физико-энергетический институт, Обнинск,
Союз Советских Социалистических Республик

Abstract — Аннотация

DOUBLE-HUMPED BARRIER IN THE QUASI-CLASSICAL APPROXIMATION. The energy dependence of the penetrability of a double-humped potential barrier with a valley between the peaks is determined in the quasi-classical approximation. It is shown that the penetrability of the barrier fluctuates sharply, reaching maximum values at energies coinciding with the positions of the quasi-stationary levels in the valley. The results are used in analysing experimental data on neutron fission.

ДВУГОРБЫЙ БАРЬЕР В КВАЗИКЛАССИЧЕСКОМ ПРИБЛИЖЕНИИ. В квазиклассическом приближении определена энергетическая зависимость проницаемости двугорбого потенциального барьера с ямой между максимумами. Показано, что проницаемость испытывает резкие колебания, достигая максимальных значений при энергиях, совпадающих с положениями квазистационарных уровней в яме. Результаты применяются для анализа экспериментальных данных по делению ядер нейтронами.

В последнее время появились экспериментальные данные [1–3] и теоретические соображения [4,5] , указывающие на то, что потенциальный барьер, препятствующий делению тяжелых ядер, может иметь два максимума, и при достаточной глубине ямы между ними сам процесс деления может быть двухступенчатым. Модель двугорбого барьера открывает новые интересные возможности для интерпретации экспериментальных данных. В работе [5] указывалось, что некоторые важные черты новой физической картины можно понять на простейшей схематической модели одномерного симметричного двойного барьера [6] . В данной работе рассматривается более общая одномерная задача о двойном барьере произвольной формы, и полученные результаты используются при обсуждении некоторых экспериментальных данных по делению ядер.

1. Рассмотрим движение частицы с массой μ в потенциальном поле, имеющем вид барьера с двумя максимумами A и B, разделенными ямой C. Для определенности будем полагать, что левый максимум выше правого. Основные обозначения введены на схематическом рис.1. В квазиклассическом приближении специального рассмотрения требует лишь случай, когда $E_C < E < E_B$ и, следовательно, имеются четыре точки поворота. Введем следующие обозначения:

$$\kappa(x) = \hbar^{-1}\sqrt{2\mu[E - V(x)]}; \qquad \varphi(E) = \int_{a_2}^{a_3} \kappa(x)\,dx;$$

$$P_A = \exp\left\{-2\int_{a_1}^{a_2} |\kappa(x)|\,dx\right\}; \quad P_B = \exp\left\{-2\int_{a_3}^{a_4} |\kappa(x)|\,dx\right\} \tag{1}$$

P_A и P_B – вычисленные в квазиклассическом приближении проницаемости барьеров А и В, взятых по отдельности. Просто оценить проницаемость двойного барьера позволяет следующее рассуждение: вероятность пройти через первый барьер есть P_A, после этого частица попадает в яму, где у нее имеется выбор– либо вернуться обратно, либо проникнуть через следующий барьер В. Относительная вероятность последнего события есть, очевидно, $P_B / (P_A + P_B)$, и полная проницаемость равна $P_A P_B / (P_A + P_B)$. Покажем, что это выражение справедливо лишь для средней проницаемости, детальная энергетическая зависимость сложнее.

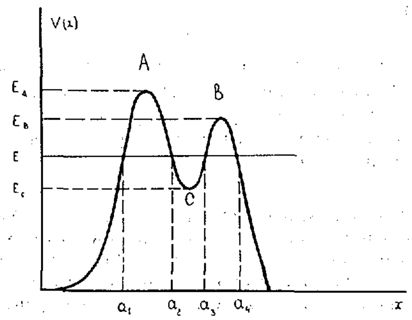

Рис.1. Схематическое изображение двугорбого барьера: V(x) – потенциальная энергия деформации, x – параметр деформации.

Для волновой функции в области $x > a_4$ имеем:

$$\psi = \frac{c}{\sqrt{\kappa}} \exp\left\{ i \int_{a_4}^{x} \kappa dx' \right\}$$

Продолжая это решение в область $x < a_1$, имеем:

$$\psi = \frac{c}{\sqrt{\kappa}} \left\{ A(E) \exp\left(i \int_{x}^{a_1} \kappa dx' \right) + B(E) \exp\left(-i \int_{x}^{a_1} \kappa dx' \right) \right\}.$$

и коэффициенты

$$A(E) = \frac{i}{8} \frac{P_A P_B - 16}{\sqrt{P_A P_B}} \cos\varphi + \frac{1}{2} \frac{P_B - P_A}{\sqrt{P_A P_B}} \sin\varphi$$

$$B(E) = \frac{1}{8} \frac{P_A P_B + 16}{\sqrt{P_A P_B}} \cos\varphi - \frac{i}{2} \frac{P_A + P_B}{\sqrt{P_A P_B}} \sin\varphi$$

Для коэффициента проницаемости получим:

$$P(E) = |B(E)|^{-2} = 64 P_A P_B \left\{ (P_A P_B + 16)^2 \cos^2\varphi + 16 (P_A + P_B)^2 \sin^2\varphi \right\}^{-1}$$
$$\approx \frac{P_A P_B}{4} \left\{ \left(\frac{P_A + P_B}{4} \right)^2 \sin^2\varphi + \cos^2\varphi \right\}^{-1} \quad (2)$$

Квазистационарные уровни в яме между горбами можно определить из условия отсутствия приходящей из $-\infty$ волны; т.е. $B(E^\circ) = 0$ или

$$\mathrm{ctg}\,\varphi\,(E^\circ) = 4i\,\frac{P_A + P_B}{16 + P_A P_B} \simeq \frac{i}{4}\,(P_A + P_B) \tag{3}$$

Решение этого уравнения позволяет определить энергии уровней и их ширину

$$\varphi\,(E_n^0) = \pi\,(n + 1/2) \tag{4}$$

$$\Gamma = \frac{Д_2}{4\pi}\,(P_A + P_B) \equiv (\Gamma_A + \Gamma_B)\;/\;2 \tag{5}$$

Здесь $Д_2 = \pi\,(d\varphi/dE)^{-1}$ – расстояние между уровнями в яме С (частота колебаний).

Проницаемость P(E) испытывает резкие колебания при изменении энергии, достигая максимальных значений при $E = E_n^0$ и минимальных – между квазистационарными уровнями

$$\begin{aligned} P_{max} &= P(E_n^0) = 4\,P_A P_B\,/\,(P_A + P_B)^2 \\ P_{min} &= P_A P_B\,/4 \end{aligned} \tag{6}$$

Вблизи квазистационарных состояний проницаемость имеет лоренцовскую зависимость от энергии (рис.2).

$$P(E_n^0 + \Delta E) = \frac{\Gamma_A \Gamma_B}{(\Gamma_A + \Gamma_B)^2/4 + (\Delta E)^2} \tag{7}$$

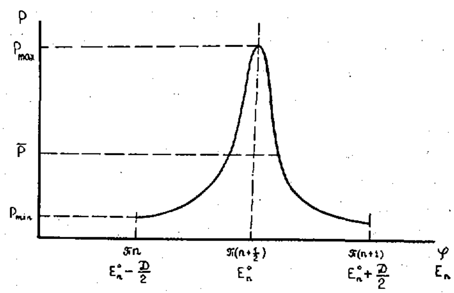

Рис.2. Схематическое изображение энергетической зависимости в окрестности квазистационарного состояния.

Усредняя (2) по интервалу между уровнями, получим:

$$\bar{P}(E) = Д_2^{-1}\int_{E_n^0}^{E_{n+1}^0} P(E)dE \simeq \frac{1}{\pi}\int_{-\pi/2}^{\pi/2} P\,(\varphi)\,d\varphi = \frac{P_A P_B}{P_A + P_B} \tag{8}$$

что подтверждает полученную выше оценку. Для симметричного двойного барьера $P_A = P_B$ получаем известный [6] результат $P_{max} = 1$, $P_{min} = P_A^2/4$. Так как проницаемость экспоненциально зависит от высоты барьера, то при сколько-нибудь существенной разнице высот имеем для несимметричного барьера $P_A \ll P_B$. В этом важном частном случае (9)

$$P_{max} = 4P_A/P_B\,; \quad P_{min} = P_A P_B/4\,; \quad \bar{P} = P_A \tag{9}$$

Как видно, средняя проницаемость такая же, как если бы "работал" только один, более высокий, из горбов. Этот вывод совпадает с результатом, который получен в работе [5] на основании статистических соображений. Проницаемость меньшего барьера определяет "коэффициент усиления" этой средней проницаемости при $E = E_n^0$ и ее ослабление вдали от резонансов. Отметим тождественное соотношение, вытекающее из (7-8): $\bar{P} = \sqrt{P_{max} \cdot P_{min}}$.

2. Полученные результаты кажется возможным использовать для анализа резонансных структур, наблюдаемых в сечении деления. Если быть последовательным в отношении рассмотренной модели, то квазистационарные состояния в яме С (рис.1) следует связать с вибрационными состояниями делящегося ядра. Такие состояния, вероятно, ответственны за широкие резонансы в сечении деления вблизи порога [7,8]. Однако использование рассмотренной выше модели для анализа наблюдаемых резонансов осложняется тем, что кроме ширины Γ (5), связанной с проницаемостью барьера, в полную ширину вибрационных состояний реальных ядер дают вклад процессы диссипации энергии вибрационного движения в нуклонные степени свободы $\Gamma_{tot} = \Gamma + \Gamma_d$. Можно ожидать, что $\Gamma_d \ll \Gamma$ только при условии $\Gamma \simeq \frac{\hbar\omega}{4\pi}(P_A + P_B) \simeq 0{,}1 P_A \lesssim Д$, где Д – расстояние между многонуклонными состояниями возбужденного составного ядра во второй яме. Реализация этого условия существенно зависит от детальной структуры кривой потенциальной энергии: глубины второй ямы и высоты барьеров. Эти вопросы были рассмотрены в работе [5]. Для большинства наблюдаемых вблизи порога резонансов вклад Γ_d, вероятно, велик, поэтому анализ таких экспериментальных данных выходит за рамки рассмотренной выше простой модели. Феноменологически диссипацию вибрационных состояний можно учесть путем введения комплексного потенциала, как это было предложено Линном [8].

3. Кроме гросс-структур с ширинами $\sim 0{,}1$ Мэв, в сечении деления нейтронами наблюдаются структуры с ширинами порядка десятков и сотен электронвольт [1 ÷ 3], которые, вероятно, связаны с многочастичными состояниями ядра во второй яме. Их анализ в рамках R – матричной теории был проведен Линном [9] и Вайгманном [10]; полученные ими выражения для делительных ширин формально совпадают с результатами квазиклассического приближения (6,7). Представляется интересным распространить результаты данной модели на всю совокупность состояний во второй яме. При этом, конечно, необходимо помнить об ограниченной применимости предлагаемой модели, так как состояния во второй яме несомненно имеют более сложную природу, чем одномерное движение; рассматриваемая простая модель отражает только наиболее существенную часть полной картины.

Принятые предположения позволяют записать делительную ширину в виде $\Gamma_f = \frac{Д_1}{2\pi} P(E)$, где $Д_1$ – среднее расстояние между уровнями составного ядра в первой яме. Тогда колебания проницаемости будут отражаться на энергетической зависимости делительной ширины. Это означает, что, если энергия возбуждения, соответствующая поглощению ядром нейтронов, попадает в интервал $E_C \lesssim E < E_B$, то при делении нейтронами должны наблюдаться некоторые особенности:

а) Делительные ширины нейтронных резонансов модулируются колебаниями проницаемости, то есть группы уровней, энергия которых находится в пределах ширины состояний во второй яме, имеют аномально большую делительную ширину. Этот факт хорошо известен экспериментально для ядер ^{237}Np [1], ^{240}Pu [2], ^{234}U, ^{242}Pu [3] и уже неоднократно отмечался как указание на сложную структуру барьера деления. Наиболее подробные данные имеются для ^{240}Pu и ^{237}Np.

б) Делительные ширины и плотности уровней сильных и слабых делительных резонансов находятся между собой в таком соотношении, что делительная ширина, усредненная по всем резонансам, является средним геометрическим значением ширин, полученных усреднением по группам "сильных" и "слабых" уровней отдельно.

Ядро ^{240}Pu достаточно подробно изучено для проверки этого утверждения. Согласно результатам работы [2], $\Gamma_{f\,max} = 130$ мэв, $\Gamma_{f\,min} = 0{,}007$ мэв [11], $\overline{\Gamma}_f = 3{,}5$ мэв, $\sqrt{\Gamma_{f\,max}\Gamma_{f\,min}} = 1$ мэв, что находится в качественном согласии с отмеченным соотношением (максимальная и минимальная ширины отличаются в 20 тыс. раз). Оценим P_A и P_B для этого ядра. С помощью (9) и с учетом, что $Д_1 = 16$ эв, получаем $P_A = \overline{P} = 2\pi\overline{\Gamma}_f / Д_1 = 1{,}5\cdot10^{-3}$; $P_B = (4\overline{P}/P_{max})^{1/2} = 10^{-1}$. Параметр кривизны вершины барьера, который в рассматриваемой интерпретации относится к барьеру A, согласно измерениям сечения деления на быстрых нейтронах, равен $\hbar\omega_A = 650$ кэв, а высота барьера $E_A - B_n = 0{,}7$ Мэв. Предположив для простоты, что $\hbar\omega_A = \hbar\omega_B$, можно оценить высоту барьеров A и B; $E_A = 6{,}2$ Мэв, $E_B = 5{,}7$ Мэв. Авторы [2] оценивают по отношению плотностей уровней в первой и второй ямах высоту второй ямы над минимумом, соответствующим основному состоянию. Эта величина $E_C = 2{,}1$ Мэв. По совокупности этих результатов можно восстановить структуру двойного барьера составного ядра ^{241}Pu.

в) У пороговых элементов, плохо делящихся резонансными нейтронами, значение делительной ширины часто известно лишь для первого резонанса. Этот резонанс с большей вероятностью будет принадлежать к более многочисленной категории "слабых" (их в $Д_2/\Gamma_2$ больше, чем "сильных"). Поэтому его делительная ширина в подавляющем большинстве случаев будет иметь значение значительно меньшее, чем экстраполированные в эту область значения средних ширин, которые получены при измерениях на быстрых нейтронах усреднением по всем уровням. В тех редких случаях, когда эпитепловый резонанс является "сильным", будет

ТАБЛИЦА 1. СРАВНЕНИЕ ДЕЛИТЕЛЬНЫХ ШИРИН, НАБЛЮДАЕМЫХ В РЕЗОНАНСНОЙ ОБЛАСТИ $\Gamma_{рез.}$ И ПОЛУЧЕННЫХ ЭКСТРАПОЛЯЦИЕЙ $\overline{\Gamma}_{быстр.}$ (см. текст и примечание)

Ядро-мишень	$\Gamma_{рез.}$ мэв	$\overline{\Gamma}_{быстр.}$ [a] мэв	$\hbar\omega_A/2\pi$ кэв	$\Gamma_{рез.}/\overline{\Gamma}_{быстр.}$
^{232}Th	$2\cdot10^{-4}$	10^{-7}	60	$2\cdot10^{3}$
^{231}Pa	$6\cdot10^{-3}$	0,1	70	$6\cdot10^{-2}$
^{234}U	$2\cdot10^{-2}$	1	80	$2\cdot10^{-2}$
^{237}Np	$1{,}5\cdot10^{-3}$	$5\cdot10^{-2}$	90	$3\cdot10^{-2}$
^{238}Pu	1	50	100	$2\cdot10^{-2}$
^{240}Pu	$6\cdot10^{-3}$	3	100	$2\cdot10^{-3}$
^{242}Pu	$2\cdot10^{-2}$	2	100	10^{-2}
^{241}Am	0,2	0,2	100	1

[a] Оценка $\overline{\Gamma}_{быстр.}$ путем экстраполяции из области экспоненциального спада Γ_f ($E_n \sim 0{,}5$ Мэв) к $E_n = 0$ производилась с использованием значений $\hbar\omega_A/2\pi$ [13], приведенных в 4-ой колонке.

наблюдаться резкое обратное неравенство. Этим объясняется видимое противоречие, неоднократно отмечавшееся при анализе экспериментальных данных по делению нейтронами [12] и иллюстрируемое таблицей 1. Для ^{240}Pu и ^{237}Np известны значения $\overline{\Gamma}_{медл.}$, усредненные по "сильным" и "слабым" резонансам и равные, соответственно, 3,5 мэв [2] и $7\cdot10^{-2}$мэв [1]. Они хорошо согласуются с оценками $\overline{\Gamma}_{быстр.}$. Таким образом, в средних ширинах никакого противоречия нет.

4. Можно получить и явный вид статистического распределения делительных ширин нейтронами резонансов в случае двугорбого барьера. Согласно изложенному выше, кривые проницаемости являются примерно огибающими делительных резонансов. Тогда формула (2) непосредственно преобразуется в распределение делительных ширин относительно среднего значения

$$\varphi(x)\,dx = \frac{dx}{\pi x}(x - x_{min})^{-1/2}(x_{max} - x)^{-1/2} \tag{10}$$

где

$$x = \frac{\Gamma_f}{\overline{\Gamma}_f}\ ; \quad x_{max} = \frac{\Gamma_{f\,max}}{\overline{\Gamma}_f} = \left(\frac{\Gamma_{f\,max}}{\Gamma_{f\,min}}\right)^{1/2}; \quad x_{min} = \frac{\Gamma_{f\,min}}{\overline{\Gamma}_f}$$

В действительности, конечно, кривая проницаемости является огибающей средних значений делительных ширин по небольшим интервалам, содержащим несколько уровней, и на каждом таком участке ширины флуктуируют относительно этих локальных средних значений $\widetilde{\Gamma}_f$. Для получения более реалистического полного распределения необходимо поэтому свернуть (10) с распределением, которое описывало бы локальные флуктуации.

Предположим, что локальные флуктуации описываются распределением Портера-Томаса (ρ^2 – распределением) с числом степеней свободы ν, которое имеет вид:

$$f_\nu(z) = \frac{z^{\frac{\nu}{2}-1}\,e^{-z}}{\Gamma(\nu/2)} \tag{11}$$

где $z \equiv \frac{\nu}{2}\frac{\Gamma_f}{\widetilde{\Gamma}_f}$, а $\Gamma(\nu/2)$ – гамма-функция. Пусть $\varphi(x)dx = \varphi(\widetilde{\Gamma}_f/\langle\Gamma\rangle)d(\widetilde{\Gamma}_f/\langle\Gamma\rangle)$, тогда получается следующее распределение для величины $\nu/2\cdot\Gamma_f/\langle\Gamma_f\rangle \equiv y$

$$\Psi_\nu(y)\,dy = \int_{x_{min}}^{x_{max}} \varphi(x) f_\nu(y/x)\,d(y/x)\,dx$$

$$= e^{-yx_{min}}\ y^{\frac{\nu}{2}-1}\,\frac{(x_{max} - x_{min})^{\frac{1}{2}}}{\pi\Gamma(\nu/2)} \tag{12}$$

$$\int_0^1 \left(z + \frac{x_{min}}{x_{max} - x_{min}}\right)^{\frac{\nu}{2}} e^{-yz(x_{max}-x_{min})}\cdot z^{-\frac{1}{2}}(1-z)^{-\frac{1}{2}}\,dz$$

Для важного частного случая $\nu = 2$ (экспоненциальное распределение) интеграл берется и

$$\Psi_\nu(y)dy = \left\{ x_{min} e^{-y\frac{x_{max}-x_{min}}{2}} \quad I_0\left(y\frac{x_{max}-x_{min}}{2}\right) \right.$$
$$\left. + \frac{x_{max}-x_{min}}{2} e^{-yx_{max}} \quad F\left(1/2,\ 2,\ y(x_{max}-x_{min})\right)\right\} dy \tag{13}$$

где I_0 – функция Бесселя мнимого аргумента, а F– вырожденная гипергеометрическая функция. Результаты удобнее представить в том виде, в котором обычно производится сравнение с экспериментом, а именно, в форме интегральных распределений, показывающих, какая доля резонансов имеет ширину больше заданной. Для распределений (10) и (13) получаем соответственно:

$$f(\Gamma_f' \geq \Gamma_f) = \frac{1}{2} + \frac{1}{\pi} \arcsin\left\{\frac{\langle \Gamma_f \rangle}{\Gamma_f} \frac{2}{x_{max}-x_{min}} - \frac{x_{max}+x_{min}}{x_{max}-x_{min}}\right\} \tag{14}$$

$$\Psi_2(\Gamma_f' \geq \Gamma_f) = \exp\left(-\frac{\Gamma_f}{\langle \Gamma_f \rangle} \frac{x_{max}+x_{min}}{2}\right) I_0\left(\frac{\Gamma_f}{\langle \Gamma_f \rangle} \frac{x_{max}-x_{min}}{2}\right) \tag{15}$$

Экспериментальное распределение ширин для случая с группировкой построено в работе [1] для ^{237}Np. Результаты сравниваются с выражениями (14 – 15) на рис.3. Согласие вполне удовлетворительное.

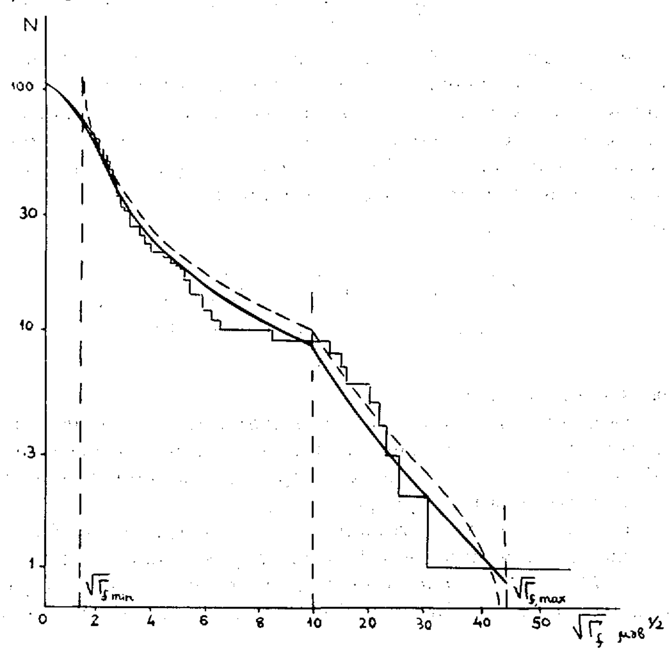

Рис.3. Сравнение экспериментального и расчетных распределений делительных ширин для реакции ^{237}Np (n, f). Гистограмма – эксперимент (работа [1], линия В на рис.1), сплошная кривая рассчитана по формуле (15), пунктирная – (14) в предположении $\Gamma_{f\,min} = 2{,}3 \cdot 10^{-3}$мэв, $\Gamma_{f\,max} = 2$ мэв, $\langle \Gamma_f \rangle = 6{,}8 \cdot 10^{-2}$мэв согласно [1]. Справа и слева от пунктирной линии $\Gamma_f^{1/2} = 10$ μэв$^{1/2}$, разный масштаб по оси абсцисс.

Одно свойство распределений типа (10) следует отметить особо. Они имеют очень большую дисперсию. Непосредственное вычисление дает:

$$\sigma^2_{\Gamma_f} = \frac{\langle \tilde{\Gamma}_f^2 \rangle}{\langle \tilde{\Gamma}_f \rangle^2} - 1 = \frac{x_{max} + x_{min}}{2} - 1 \qquad (16)$$

В случае ^{240}Pu эта величина равна, например, ~ 15. Напомним, что одноканальное распределение Портера-Томаса – максимально "широкое" из тех, которые используются для описания статистических распределений ширин ядерных уровней, имеет дисперсию $\sigma^2_{\Gamma_f} = 2$. Поэтому различные функции ширин, усредняемых по флуктуациям и используемым при расчете сечений, могут сильнее отличаться от средних значений, чем в случае распределений Портера-Томаса. Так, для функции $S = \left\langle \frac{\Gamma_f}{\Gamma_f + \Gamma_c} \right\rangle \Big/ \frac{\langle \Gamma_f \rangle}{\langle \Gamma_f \rangle + \Gamma_c}$ в случае распределения (10) получается:

$$S = (1 + \alpha)(\alpha + x_{max})^{-1/2} \cdot (\alpha + x_{min})^{-1/2} \qquad (17)$$

где $\alpha = \Gamma_c / \langle \Gamma_f \rangle$, а Γ_c – полная ширина процессов распада, конкурирующих с делением. Для $x_{max} = x_{min}^{-1} \simeq 30$, которые примерно соответствуют ^{240}Pu и ^{237}Np, вид этой функции показан на рис.4, где для сравнения приведена аналогичная функция для одноканального распределения Портера-Томаса

$$S = (1 + \alpha)\left\{1 - \sqrt{\frac{\pi}{2}\alpha}\; e^{\alpha/2}\left[1 - \Phi\left(\sqrt{\frac{\alpha}{2}}\right)\right]\right\} \qquad (18)$$

где Φ – интеграл ошибок. Разница весьма существенна, и ее следует учитывать при расчете сечения деления в околопороговой области.

5. Полученные в рамках данной модели результаты можно использовать для описания энергетической зависимости сечения деления σ_f ^{240}Pu нейтронами в районе порога. Имеющаяся экспериментальная информация [14,15] изображена на рис.5. Там же приведены кривые, рассчитанные по формуле

$$\sigma_f = \frac{\pi \lambda\!\!\!^{-2}}{2} \sum_{I,K,\pi} (2I+1)\, T_l^I \frac{\Gamma_f^{IK\pi}}{\sum\limits_{K' \le I} \Gamma_f^{IK'\pi} + \Gamma_n^{I\pi} + \Gamma_\gamma} \cdot S_{IK\pi} \qquad (19)$$

в следующих предположениях:

а) В яме C ядро живет достаточно долго по сравнению с характерным периодом миграции K – проекции момента I на ось симметрии, благодаря чему "забываются" состояния на барьере A, и распределение K определяется спектром каналов на барьере B.

б) Спектр доступных состояний при $E \approx E_A$ настолько богат, что в делении реализуются все значения K и π, допускаемые величиной угловых моментов $I \le 7/2$, $l \le 3$. Основанием является соответствие угловых распределений осколков $^{240}Pu(n,f)$ вблизи порога статистическому распределению.

в) Расчет $\Gamma_f^{IK\pi} = \frac{\bar{Д}_1^{\,I}}{2\pi} N_{IK\pi} P_A$ производится по формуле

$$P_A(E_n) = \left\{1 + \exp\left(2\pi \frac{E_A - B_n - E_n}{\hbar\omega_A}\right)\right\}^{-1} \qquad (20)$$

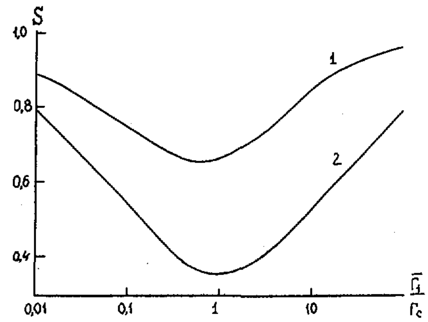

Рис.4. Поведение функции S : 1 – одноканальное распределение Портера-Томаса (18), 2 – распределение (17).

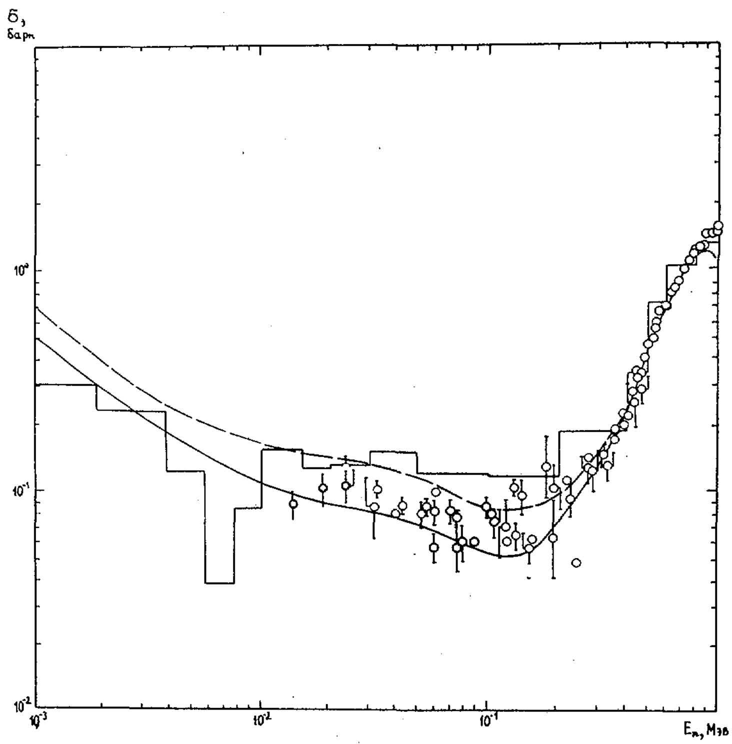

Рис.5. Энергетическая зависимость сечения деления ^{240}Pu нейтронами: ○ – экспериментальные данные [14] ; гистограмма [15] ; сплошная кривая – расчет с учетом флуктуаций Γ_f ; пунктирная – без учета флуктуаций, $S_{IK\pi} = 1$.

в предположении $N_{IK\pi} = 1$ и $\Gamma_{f(0)}^{IK\pi}$ = мэв [2] для всех I, K, π. В принятом предположении об однородности распределения угловая анизотропия отсутствует. Поскольку последняя мала, мы полагаем, что, благодаря исключению ее из рассмотрения, достигается значительное упрощение расчетов без существенной потери в точности описания $\sigma_f(E_n)$.

г) Значения $S_{IK\pi}$ определялись по формуле (17) при $E_n < E_B - B_n$ и – (18) при $E_n > E_B - B_n$.

д) Использовались параметры оптической модели [14] и значения $\Gamma_\gamma = 26$ мэв, $\bar{Д}_1 = 16$ эв [2] .

Результаты расчетов для подобранных $E_A - B_n = 0{,}75$ Мэв и $\hbar\omega_A/2\pi = 0{,}115$ Мэв удовлетворительно согласуются с экспериментальными данными во всем рассмотренном диапазоне экспоненциального изменения P_A вплоть до 0,8 – 0,9 Мэв. При более высоких энергиях расчетная кривая загибается вниз, указывая на необходимость включения большего числа каналов $N_{IK\pi}$. Согласие расчетной кривой с экспериментом ниже 30 кэв, где в сечении образования составного ядра преобладает s – волна, является еще одним свидетельством того, что подавление вероятности деления s – нейтронами [12] является кажущимся эффектом, и в среднем отсутствует.

Физические предпосылки, положенные в основу рассмотренной модели двугорбого барьера, являются, конечно, весьма грубыми, но можно надеяться, что простота модели заслуживает внимания, а полученные результаты указывают на возможность ее использования для анализа широкого круга экспериментальных данных.

Авторы выражают благодарность В.М.Струтинскому за обсуждения, стимулировавшие данную работу, и В.С. Ставинскому – за ценные замечания.

ЛИТЕРАТУРА

[1] FUBINI, A., BLONS, J., MICHAUDON, A., PAYA, D., Rhys. Rev. Let. 20 (1968) 1373.
[2] MIGNECO, E., THEOBALD, G., Nucl. Phys. A112 (1968) 603.
[3] JAMES, C.D., RAE, E.R., Nucl. Phys. A958 (1968) 313.
[4] СТРУТИНСКИЙ, В.М., Nucl. Phys. A95 (1968) 420.
[5] STRUTINSKY, V.M., BJØRNHOLM, S., Nucl. Structure Dubna symp. 1968, IAEA (1968) 431.
[6] ГОЛЬДМАН, И.И., КРИВЧЕНКОВ, В.Д., Сб.задач по квантовой механике, Гостехиздат, 1957, стр.13;
БОМ, Д., Квантовая теория, Изд. "Наука", 1965, стр.334.
[7] ВОРОТНИКОВ, П.Е., ДУБРОВИНА, С.М., ОТРОЩЕНКО, Г.А., ШИГИН, В.А., ЯФ 5 (1967) 295;
ВОРОТНИКОВ, П.Е., ЯФ 5 (1967) 583.
[8] LYNN, J.E., Nuclear Data for Reactors, Vienna 2 1967, p.89.
[9] LYNN, J.E., Nucl. Structure Dubna symp. 1968, IAEA (1968) 463.
[10] WEIGMANN, H., Z. für Physik 214 (1968) 7.
[11] Neutron Cross Sections, BNL – 325, suppl. 2 111 1965.
[12] РАБОТНОВ, Н.С., СМИРЕНКИН, Г.Н., Препринт ОИЯИ – 1845, 1964, стр.112:
RAE, E.R., Phys. and Chem. Fission, Vienna 1 1965, p.187;
ВОРОТНИКОВ, П.Е., ЯФ 5 (1967) 1021.
[13] ЕРМАГАМБЕТОВ, С.Б., КУЗНЕЦОВ, В.Ф., СМИРЕНКИН, Г.Н., ЯФ (1967) 257.
[14] ЕРМАГАМБЕТОВ, С.Б., КОЛЕСОВ, В.Е., НЕСТЕРОВ, В.Г., СМИРЕНКИН, Г.Н., ТИШИН, А.С., ЯФ 8 (1968) 704.
[15] BYERS, D.H., DIVEN, B.C., SILBERT, M.G., LA – 3586, 1966.

DISCUSSION

J.R. NIX: Your results for the penetrability through a two-peaked barrier on the basis of the quasi-classical or WKB approximation are very useful for describing the resonances at energies below the tops of the barriers. However, at energies at and above the barrier tops your WKB results would be expected to differ substantially from the exact results. Since most experimental data are for such energies, I think it is preferable to use an exact method for computing the penetrability. As indicated in abstracts SM-122/103 and 119, such methods have been described by, among others, Cramer and Nix and Wong and Bang.

C.Y. WONG: Yes, Bang and I have obtained the exact solution for the penetrability through a double barrier by parameterizing the potential as two or three parabolas joined with each other. Such a solution is better than the classical one, since the latter is inaccurate in the region near the top of the barriers.

I do not think that the authors' method of obtaining the penetrability can be applied to the analysis of the fine structure resonances observed in ^{237}Np(n, f). At a realistic potential, each quasi-bound state in the second well is separated by an energy of the order of about 500 keV. Owing to damping, each of these quasi-bound states spreads its strength over many levels. In the case of ^{237}Np, these levels are the fine structure resonances whose separation is of the order of 100 eV, and cannot be treated as quasi-bound states obtained in the calculation of the penetrability, as the authors have done.

E.R.H. HILF: I would like to point out that in the fission process the barrier is not one-dimensional but actually a saddle-point in, let us say, the three dimensions of fission (barrier), vibration and asymmetry (oscillators). So in calculating penetrabilities one has to solve the three-dimensional problem, especially since the strengths of the two oscillators seem to change a good deal during the fission when passing from the saddle-point area towards the scission point. The first attempt in this direction was made by R. Weidelt of Würzburg in 1968.

INTERMEDIATE STRUCTURE IN FISSION AND ISOMERIC FISSION

(Session E)

Chairman: S. Bjørnholm

ANALYSIS OF RESONANCES OBSERVED IN (d, pf)-REACTIONS

B.B. BACK, J.P. BONDORF, G.A. OTROSHENKO,
J. PEDERSEN, B. RASMUSSEN
The Niels Bohr Institute,
University of Copenhagen, Denmark

Abstract

ANALYSIS OF RESONANCES OBSERVED IN (d, pf) REACTIONS. Fission cross-sections in the (d, pf)-reaction on $^{233,235}U$ and $^{239,241}Pu$ have been measured with 37 keV resolution. A model is proposed for describing the observed pronounced resonance structure in the excitation function. The cross-section is assumed to be $\sigma_{d,pf} = \Sigma\sigma_{d,p}\Gamma_f/(\Gamma_f + \Gamma_\gamma)$. For the analysis of data, $\sigma_{d,p}$ is calculated in the DWB-approximation using the Nilsson-model single-particle states. The fission penetrability is calculated by numerical integration for a double-humped fission barrier. Thus, we assume that the observed resonances in the (d, pf)-reaction can be interpreted as quasi-bound states in the second minimum of the fission barrier.

1. INTRODUCTION

Evidence for a second minimum in the fission barrier [1] follows from the observation of 1) fission isomers [2], 2) narrow sub-barrier fission resonances of compound type observed in (n, f) experiments [3], and 3) broad resonances of vibrational type in, for example, (n, f) [4] and (d, pf) experiments [5].

The presence of intermediate quasi-bound states in this second minimum will certainly influence the fission probability. Figure 1 shows a two-humped fission barrier with its vibrational states corresponding to the two wells. At the fission-barrier energy we can assume that the vibrational states are completely damped into the closely spaced compound levels while the vibrational states in the second well may be much less damped because of lower effective excitation energy. At energies corresponding to an excitation energy of these vibrational states, one can expect to see an enhanced fission probability.

In the light of this new picture, we have reinvestigated the (d, pf)-process experimentally and made an attempt to interpret the observed structure by using a double-humped fission barrier model.

2. EXPERIMENT

2.1. Procedure

The experiments were performed with 13-MeV deuteron beams, and the outgoing protons were detected at 140° in a 2-mm Li-drifted silicon detector. The over-all resolution was ~37 keV. The fission fragments were detected in a surface barrier detector which was placed perpendicular to the beam axis and subtended an angle of about 90°. Fast signals from the two detectors were sent to a time-to-height converter. Both real and random coincidence spectra were registered, the difference between them giving a coincidence proton spectrum corrected for accidental contributions.

The targets were made by vacuum evaporation of the oxides on carbon backings. The target thickness ranged from 50 to 150 $\mu g/cm^2$.

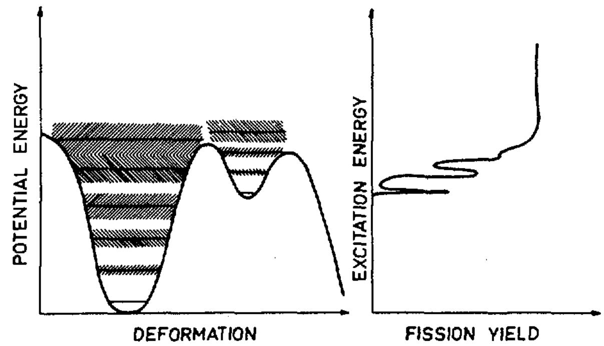

FIG.1. A model of the vibrational states in the two-well model. The heavy lines represent vibrational states. Damping is indicated with hatched lines. To the right, the corresponding fission yield as a function of excitation energy is shown quantitatively.

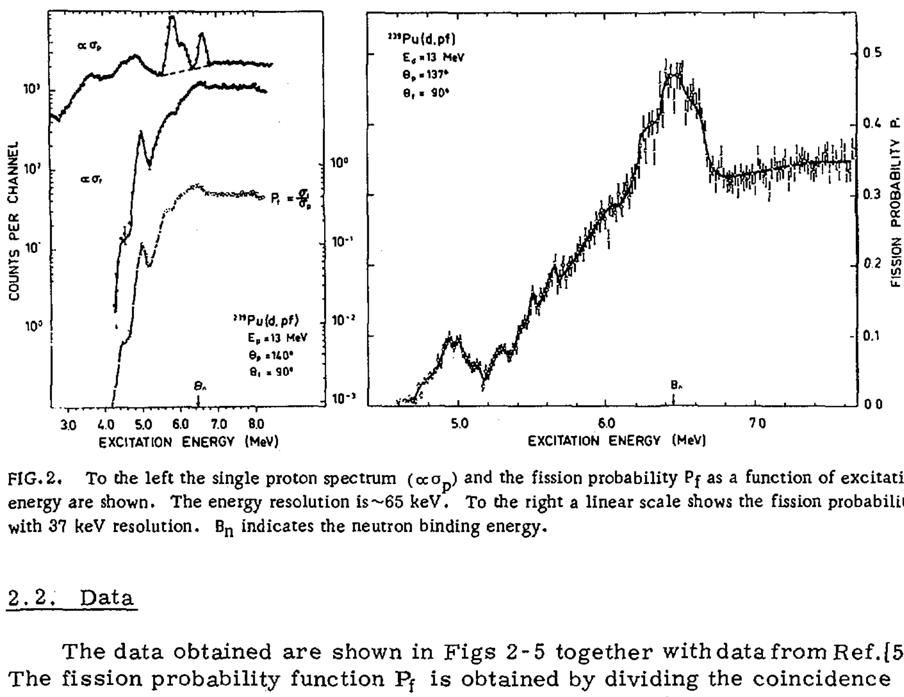

FIG.2. To the left the single proton spectrum ($\alpha\sigma_p$) and the fission probability P_f as a function of excitation energy are shown. The energy resolution is ~65 keV. To the right a linear scale shows the fission probability with 37 keV resolution. B_n indicates the neutron binding energy.

2.2. Data

The data obtained are shown in Figs 2-5 together with data from Ref.[5]. The fission probability function P_f is obtained by dividing the coincidence proton spectrum by the single-proton spectrum. In this calculation, the coincidence spectrum is normalized to 100% fission detection efficiency assuming an isotropic angular distribution of the fission fragments (the error introduced hereby is considered to be small, ≤10%). On the left-

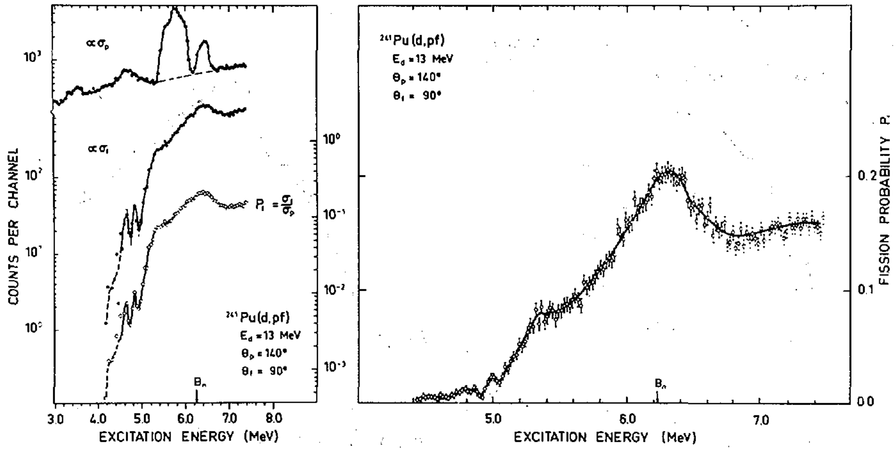

FIG.3. To the left the single proton spectrum ($\propto\sigma_p$) and the fission probability P_f as a function of excitation energy are shown. The energy resolution is ~65 keV. To the right a linear scale shows the fission probability with 37 keV resolution. B_n indicates the neutron binding energy.

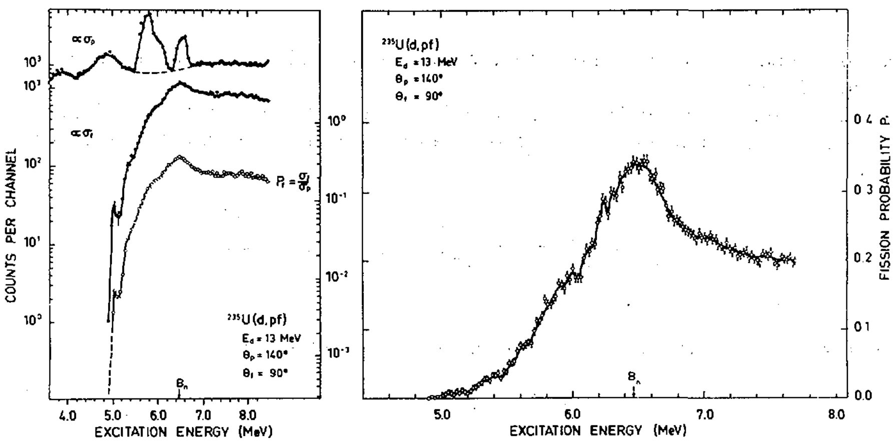

FIG.4. To the left the single proton spectrum ($\propto\sigma_p$) and the fission probability P_f as a function of excitation energy are shown. The energy resolution is ~65 keV. To the right a linear scale shows the fission probability with 37 keV resolution. B_n indicates the neutron binding energy.

hand side of the figures we see the data from Ref. [5] where the protons are detected by means of a particle identifier system (65 keV resolution) and on the right-hand side we have the fission probability functions from the present measurements (~37 keV resolution).

3. THEORY

3.1. Reaction mechanism and formalism

In the analysis we assume that the (d, pf)-process proceeds in two independent steps: 1) population of isolated nuclear levels λ by the (d, p)-

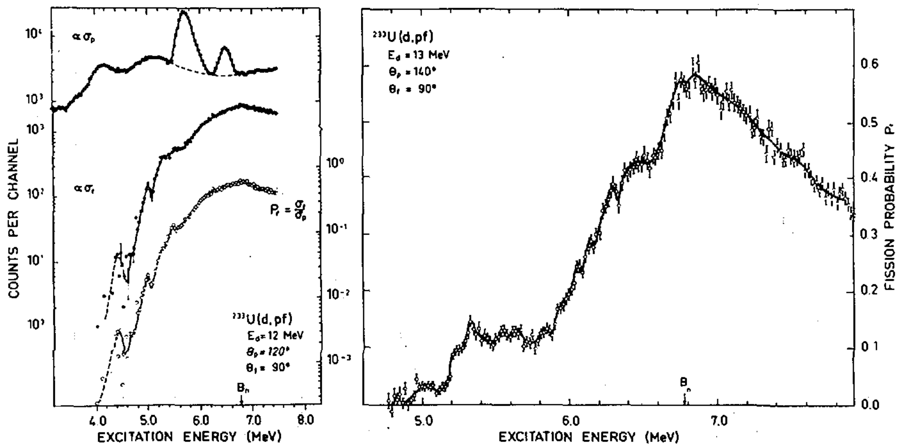

FIG. 5. To the left the single proton spectrum ($\propto\sigma_p$) and the fission probability P_f as a function of excitation energy are shown. The energy resolution is ~65 keV. To the right a linear scale shows the fission probability with 37 keV resolution. B_n indicates the neutron binding energy.

process, and 2) decay of these levels by fission and gamma rays via the compound motion.

The cross-section for the unpolarized incident beam integrated over the fission fragment angle can be written for one level λ in the fissioning nucleus

$$d\sigma_{d,pf}^{\lambda I\pi}(\theta_p) = d\sigma_{d,p}(\lambda, I, \pi, \theta_p)\,\frac{\Gamma_f^{\lambda I\pi}}{\Gamma^{\lambda I\pi}} \tag{1}$$

where the fission width is the sum of channel partial widths

$$\Gamma_f^{\lambda I\pi} = \sum_K \Gamma_f^{\lambda I\pi K} \tag{2}$$

and the total width is

$$\Gamma^{\lambda I\pi} = \Gamma_f^{\lambda I\pi} + \Gamma_\gamma^{\lambda I\pi} \tag{3}$$

Averaging over an energy interval including many class-I levels λ around the excitation energy E in the fissioning nucleus we obtain

$$\langle d\sigma_{d,pf}(E,\theta_p)\rangle$$

$$= \sum_{I\pi} \langle d\sigma_{d,p}(I,\pi,E,\theta_p)\rangle \left\langle \frac{\sum_K \Gamma_f^{\lambda I\pi K}}{\sum_K \Gamma_f^{\lambda I\pi K} + \Gamma_\gamma^{\lambda I\pi}} \right\rangle \tag{4}$$

The branching ratio of Eq.(1) varies strongly from one compound resonance to another. It is expected that the fission width $\Gamma_f^{\lambda I\pi K}$ has a Porter-Thomas distribution whereas $\Gamma_\gamma^{\lambda I\pi}$ does not fluctuate because it is composed of many partial widths. Making these assumptions, and defining the parameter r by

$$r = r(I,\pi,E) = \left(\frac{\langle\Gamma_\gamma^{\lambda I\pi}\rangle}{2\langle\Gamma_f^{\lambda I\pi K}\rangle}\right)^{\frac{1}{2}} \tag{5}$$

one obtains the average branching ratio

$$\left\langle\frac{\Gamma_f^{\lambda I\pi K}}{\Gamma_f^{\lambda I\pi K}+\Gamma_\gamma^{\lambda I\pi}}\right\rangle = 1-\sqrt{\pi}\, r\, \exp(r^2)\,[1-\mathrm{erf}(r)]^{1} \tag{6}$$

which in general is smaller (up to 30%) than

$$\frac{\langle\Gamma_f^{\lambda I\pi K}\rangle}{\langle\Gamma_f^{\lambda I\pi K}\rangle+\langle\Gamma_\gamma^{\lambda I\pi}\rangle} \tag{7}$$

particularly in the interval r = 0.1 to 10. Here it is assumed that only one K-value contributes in Eq.(6). When there are N independent fission channels contributing for a given $I\pi$, the distribution of Γ_f is approximately a χ^2 distribution of N^{th} order, and the average branching ratio becomes closer to expression (7).

3.2. Formation

The differential cross-section for stripping a neutron into states of given $I\pi$ through a given Nilsson orbital in a non-spherical even-Z odd-N target nucleus with initial state I_0, $K_0 = \Omega_0$ can be written

$$d\sigma_{d,p}(I,\pi,E,\theta_p) = \sum_{K,j,\ell} g^2 \langle I_o j K_o \Delta K | IK\rangle^2 \times C_{j\ell}^2(\Omega)\phi_\ell(\theta_p) \tag{8}$$

where

$$C_{j\ell}(\Omega) = \sum_\Lambda a_{\ell\Lambda} \langle \ell \tfrac{1}{2} \Lambda \Omega-\Lambda | j\Omega\rangle \tag{9}$$

Here $K = |\Omega_0 \pm \Omega|$ refers to the final state and Ω to the capturing orbital. The energy E has discrete values. The quantum numbers j and ℓ are the total and the orbital angular momentum of the transferred neutron, respectively, and g^2 is a factor equal to 2 when two neutrons in identical

[1] The error function $\mathrm{erf}(r) = \frac{2}{\sqrt{\pi}} \int_0^r e^{-x^2} dx$.

TABLE I. CALCULATED VALUES FOR THE QUANTITY $\{d\sigma_{d,p}(I, \pi, E, \theta_p)\}_{av.} / \{\sum_{I\pi} d\sigma_{d,p}(I, \pi, E, \theta_p)\}_{av.}$ at $\theta_p = 140°$

Nucleus	0^+	1^+	2^+	3^+	4^+	5^+	6^+	7^+	8^+
^{234}U	0.00	0.04	0.11	0.10	0.14	0.17	0.05	0.07	0.01
^{236}U	0.00	0.00	0.01	0.02	0.03	0.04	0.04	0.03	0.01
^{240}Pu	0.02	0.10	0.19	0.27	0.14	0.06	0.01	0.00	0.00
^{242}Pu	0.01	0.03	0.14	0.20	0.16	0.16	0.05	0.04	0.01
Nucleus	0^-	1^-	2^-	3^-	4^-	5^-	6^-	7^-	8^-
^{234}U	0.00	0.01	0.03	0.06	0.07	0.06	0.04	0.02	0.01
^{236}U	0.00	0.03	0.07	0.15	0.19	0.13	0.13	0.04	0.05
^{240}Pu	0.00	0.01	0.02	0.06	0.06	0.03	0.02	0.00	0.00
^{242}Pu	0.00	0.01	0.02	0.03	0.04	0.05	0.04	0.02	0.00

orbits combine to K = 0, and equal to one otherwise. The $a_{\ell\Lambda}$ are the Nilsson wave-function coefficients and $\phi_\ell(\theta)$ has been evaluated by means of a DWB-approximation in the present case (the optical parameters are taken from Ref. [6]).

The cross-section calculated in this way shows that the strength of the different Nilsson states expected within a region of about 3 MeV around the fission threshold (~ 5.5 MeV) is concentrated on the following four orbitals, all with positive parity: [602↑], [611↑], [611↓] and [613↓]. The negative-parity states present in the same region have formation cross-sections that are smaller by a factor of four. Consequently, the (d, p)-reaction on $^{233}U(5/2^+)$, $^{239}Pu(1/2^+)$ and $^{241}Pu(5/2^+)$ will predominantly excite positive-parity states and predominantly negative-parity states for $^{235}U(7/2^-)$ [17].

Table I shows the calculated values for the quantity $\{d\sigma_{d,p}(I, \pi, E, \theta_p)\}_{av.}$ / $\{\sum_{I\pi} d\sigma_{d,p}(I, \pi, E, \theta_p)\}_{av.}$ at $\theta_p = 140°$ where the averaging is over an energy interval from 4.0 to 7.0 MeV. In the following calculations it is assumed that the average cross-section $\{d\sigma_{d,p}(I, \pi, E, \theta_p)\}_{av.}$ determines the average population $\langle d\sigma_{d,p}(I, \pi, E, \theta_p)\rangle$ of Eq. (4). Deviations from this are discussed later, in comparison with experimental data.

3.3. Decay

At excitation energies below the neutron binding energy, only fission and gamma-ray de-excitation are allowed. The gamma width $\Gamma_\gamma^{\lambda I\pi}$ has been measured for a number of heavy elements at the neutron binding energy and seems to be independent of excitation energy (for the region of interest here), angular momentum and parity [7]. In these calculations we have assumed $\langle\Gamma_\gamma^{\lambda I\pi}\rangle = \Gamma_\gamma = 30$ meV.

The average fission width $\langle\Gamma_f^{\lambda I\pi K}\rangle$ is obtained from the formula of Bohr and Wheeler [8]

$$\langle \Gamma_f^{\lambda I\pi K} \rangle = \frac{D(I, \pi, E)}{2\pi} T(I, \pi, K, E) \tag{10}$$

where T(I, π, K, E) is the penetration function for the fission barrier and D(I, π, E) is a statistical level spacing calculated in a conventional way (Gilbert and Cameron [9])

$$\frac{1}{D(I, \pi, E)} = \frac{\sqrt{\pi}}{12} \frac{\exp[2(aE^*)^{\frac{1}{2}}]}{a^{1/4}\, E^{*5/4}} \frac{(2I+1)\exp[-(I+\frac{1}{2})^2/2s^2]}{2(2\pi)^{\frac{1}{2}}\, s^3} \tag{11}$$

where $E^* = E - P(N) - P(Z)$. P(N) and P(Z) are pairing-energy corrections (0.6 MeV each), s is the spin cut-off factor (= 5.0). The level-density parameter a is for each nucleus determined by using formula (11) to reproduce the level spacings found in neutron-resonance experiments. The a-values vary from 24 to 25.

For I, π = 0^+ at ~ 5.5 MeV excitation energy one finds that

$$\langle\Gamma_\gamma^{\lambda I\pi}\rangle \times 2\pi/D(0+) \sim 2\times 10^{-3}$$

which means that the average branching of Eq. (6) is equal to 0.5 for $T \simeq 2 \times 10^{-3}$. Thus a small opening of the fission channel can lead to saturation in the fission probability. This will put the fission-barrier heights 0.5 - 1.0 MeV higher than was assumed previously. Because of the spin dependence in the level-distance formula (11), the fission probability will be enhanced most strongly for both low and high spin values compared with intermediate spins.

3.4. Penetrability

In Eq. (10) the penetration factor $T(I, \pi, K, E)$ for transmission through the barrier is connected with the compound-nucleus width and spacing in the statistical model [10]. We assume that $T(I, \pi, K, E)$ can be determined in a one-dimensional model for which there exists a fission barrier characteristic of each set of quantum numbers $I\pi K$. We use the hypothesis that the simplest deformation mode (stretching of the nucleus) with K = 0 dominates the penetration for the lower values of E for an even nucleus, and it is assumed that the potential corresponding to this fission channel has two humps [1].

In analogy to usual compound reaction theory, T is calculated by considering the inverse process of elastic scattering of fission waves in channel $I\pi K$. Thus, the transmission coefficient is

$$T = 1 - |\eta|^2 \tag{12}$$

where η is the scattering amplitude for elastic scattering in channel $I\pi K$. In the exterior region, the fission waves are approximated by

$$\psi_{ext} = e^{-ik'\beta} - \eta e^{ik'\beta} \tag{13}$$

The fission potential has a shape which is indicated in Fig. 6. It is assumed constant beyond a certain value β_{max} of the deformation co-ordinate β. This determines k' in Eq. (13). The shape of the potential $V(\beta)$ is, in accordance with usual practice, composed of smoothly joined parabolas, the parametrizations of which are given in Fig. 6.

For small values of the deformation co-ordinate, we expect complete absorption of the wave which could be accounted for by an imaginary potential. Since complete damping can also be described by the ingoing-wave boundary-condition method [11] we have used this method so that the wave function for deformation $\beta \leq \beta_{min}$ is only an ingoing one:

$$\psi_{int} = A \cdot e^{-ik\beta} \tag{14}$$

As a first approximation, we have assumed a real potential in the second well. In a more refined analysis one could also include absorption in the second well which gives rise to damping of the fission resonant states. It is worth noticing that for a real potential, probability conservation gives

$$T = \frac{k}{k'} |A|^2 \tag{15}$$

The Schrödinger equation for the fission wave function is now

$$\left(-\frac{\hbar^2}{2B}\frac{d^2}{d\beta^2} + V(\beta) - E\right)\psi(\beta) = 0 \tag{16}$$

which is solved by numerical integration with the given potential and matched to Eqs (13) and (14). The mass parameter B is assumed constant throughout the potential, but the numerical integration method makes it, in principle, easy to calculate a wave function with a varying mass parameter. A varying B also requires a modification of Eq.(16).

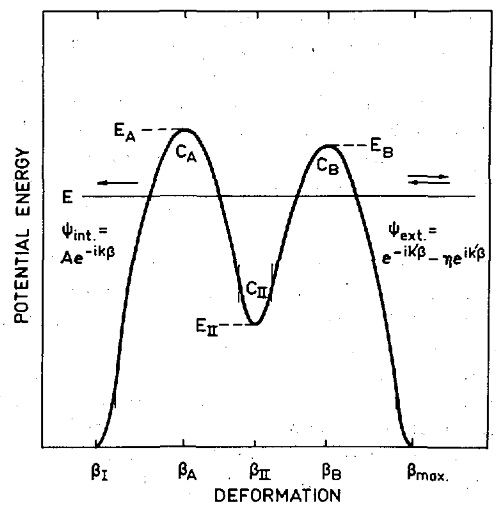

FIG. 6. The potential consists of smoothly joined parabolas of the form $1/2C\,(\beta-\beta_{extremum})^2$. In the formalism, the wave numbers k and k' can be different, but in the calculations we have put them equal since the value of k' affects the transmission coefficient very little.

The transmission coefficient exhibits resonances at the positions of quasi-bound states in the second potential well. T goes to unity for values of E much above the barrier and also, in the case of a symmetric potential, at the top of a resonance.

We assume that T depends on the compound spin I through a shift Δ_I in the potential relative to E where the shift is the saddle-point rotational energy

$$\Delta_I = \frac{\hbar^2}{2\mathcal{I}} I(I+1) \tag{17}$$

and $\mathcal{I}$ is the moment of inertia. In this way we get

$$T(I,\pi,K,E) = T(K,\pi,K,E-\Delta_I) \tag{18}$$

which has been used in the calculation. Equation (18) causes a given resonance to be split into several humps, each with a characteristic spin. This assumption of a constant shift of the whole potential is oversimplifying the calculations somewhat since presumably the moment of inertia is deformation-dependent.

4. COMPARISON BETWEEN THEORY AND EXPERIMENT

The fission probability, P_f, for ^{239}Pu (Fig. 2) shows a resonance-like structure at 5 MeV and beyond this energy rises up to 6.45 MeV, where the neutron channel opens. The proton spectrum also has a somewhat broader maximum around 5 MeV which could possibly contribute to the increase in the fission probability. The spin and parity distribution is, nevertheless, assumed constant and equal to the calculated average value. The error introduced in P_f by this assumption is estimated to be less than 10%.

In the averaging procedure for the $d\sigma_{d,p}$, a total of 37 Nilsson orbitals ranging from [631↓] to [602↓] at deformation $\epsilon = 0.25$ [12] has been used. Averaging over 4.0 - 7.0 MeV yields a distribution ratio of about 4 between even and odd parity states. Using an energy interval from 4-10 MeV, the ratio decreases to 3. A more realistic calculation using a Saxon-Wood potential is in progress.

Our basic assumption is that the lowest fission-channel band has K = 0 and even parity. It includes channels of spin and parity 0^+, 2^+, 4^+, 6^+. The prominent resonance at 5.0 MeV has an anisotropy characteristic for K = 0 and is attributed to this fission band [13]. From Table I it is seen that this channel band will have a maximum value P_f of ~0.3. Thus, only little room is left for opening up more fission bands below the neutron binding energy. The small resonance around 5.3 MeV is assumed to be a resonance with K = 0 and negative parity. (γ, f) experiments show an anisotropy at this energy characteristic for a 1^- state [14]. Thus we ascribe spins and parity 1^-, 3^-, 5^- to this band.

TABLE II. POTENTIAL PARAMETERS

$K\pi$	E_A (MeV)	E_B (MeV)	E_{II} (MeV)	$\hbar\omega_A$ (MeV)	$\hbar\omega_B$ (MeV)	$\hbar\omega_{II}$ (MeV)	$\frac{\hbar^2}{2I}$ (keV)
0^+	6.00	5.80	2.30	1.30	1.30	2.00	4
0^-	6.35	6.15	2.65	1.30	1.30	2.00	4
2^+	6.45	6.25	2.75	1.30	1.30	2.15	4

The mass parameter $B = 100\ \mathrm{MeV}^{-1}\,\hbar^2$.

The relative populations of the channel bands used in the calculations in Fig.7 are:

0^+	2^+	3^+	4^+	5^+	1^-	3^-	5^-
0.02	0.17	0.25	0.12	0.05	0.02	0.08	0.05

The next band is assumed to have K = 2 and even parity (states 2^+, 3^+, 4^+, 5^+, ...).

The barriers for $K\pi = 0^-$ and 2^+ are assumed to have the same shape as that of the 0^+ channel band. With these assumptions we have made a calculation, the result of which is shown in Fig. 7. The potential parameters are given in Table II.

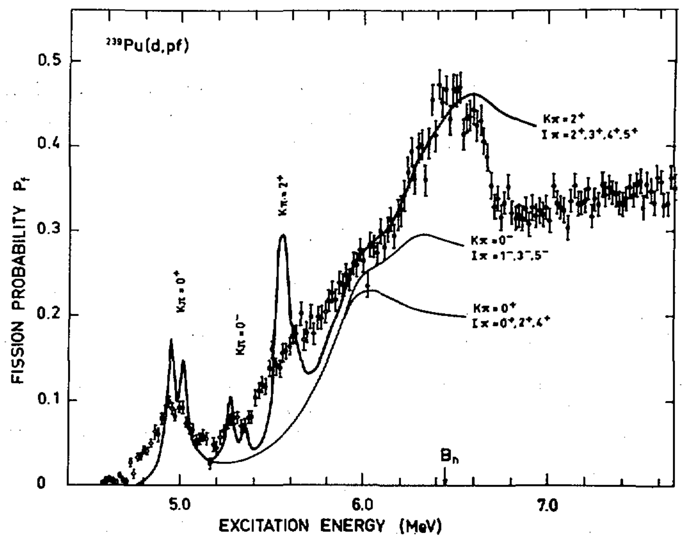

FIG. 7. The experimental points are the fission probability $P_f^{(exp)} = d\sigma(d, pf)/d\sigma(d, p)$. The theoretical curve is obtained from Eq. (4) and is

$$P_f^{(th)} = \sum_{I\pi} \frac{\{d\sigma_{d,p}(I, \pi, E, \theta_p)\}_{av.}}{\{\sum_{I\pi} d\sigma_{d,p}(I, \pi, E, \theta_p)\}_{av.}} \times \left\langle \frac{\sum_k \Gamma_f^{\lambda I\pi K}}{\sum_K \Gamma_f^{\lambda I\pi K} + \Gamma_\gamma^{\lambda I\pi}} \right\rangle$$

The theoretical curve consists of three contributions. The lowest curve is for $K\pi = 0^+$, the next one after adding the contribution from $K\pi = 0^-$, and the last one after adding the $K\pi = 2^+$ contribution.

The calculation has shown that the two barriers must be of the same height (within 1 MeV) in order to produce a resonance of such prominent size as seen in ^{240}Pu (see also Ref. [15]).

It is seen that the calculated peaks, although broadened by rotational structure, are appreciably narrower than the experimental ones. This suggests, that damping should be included in the second well, e.g. by incorporation of an imaginary potential. Considerable damping is required in the K = 2 band in order to eliminate the calculated resonance at 5.6 MeV. Calculations of this type are under preparation.

The best fit gives rather large values of $\hbar\omega$ for the inverted parabola barriers (1.3 MeV) while the "level spacing" $\hbar\omega$ in the second well is around 2 MeV. However, recent mass-parameter investigations [16] seem to indicate a non-constant mass parameter. This feature, too, will be included in future calculations and may alter the $\hbar\omega$'s rather drastically from the conventional values.

The interpretation given in this section is subject to considerable uncertainty, particularly with respect to height and curvature of the lowest barrier. However, the present comparison with experiment has shown that the previous estimates of $\hbar\omega$ should be revised because the penetrability function in the double-hump interpretation includes enhancement due to resonances in the second well.

ACKNOWLEDGEMENTS

We gratefully acknowledge helpful discussions with J. Bang, S. Bjørnholm and B. Mottelson. We are indebted to G. Sletten for preparing the targets and to N.J.S. Hansen for help with the electronics.

REFERENCES

[1] STRUTINSKY, V.M., Nucl.Phys. A95 (1967) 420; STRUTINSKY, V.M., Nucl.Phys. A122 (1968) 1; NILSSON, S.G., UCRL 18355 (1968).
[2] FLEROV, G.N., POLIKANOV, S.M., C.r. du Congres International de Physique Nucléaires 1, Paris (1964) 407.
[3] MIGNECO, E., THEOBALD, J.P., Nucl.Phys. A112 (1968) 603; FUBINI, A., BLONS, J., MICHAUDON, A., PAYA, D., Phys.Rev.Lett. 20 (1968) 1373.
[4] HOLMBERG, M., STRÖMBERG, L.G., WALLIN, L., Nucl.Phys. A127 (1969) 149; LYNN, E., these Proceedings.
[5] PEDERSEN, J., KUZMINOV, B.D., Phys.Lett. 29B (1969) 176.
[6] BIØRNHOLM, S., DUBOIS, J., ELBEK, B., Nucl.Phys. A117 (1968) 241.
[7] LYNN, E., The Theory of Neutron Resonance Reactions, Clarendon Press, Oxford (1968) 316.
[8] BOHR, N., WHEELER, J.A., Phys.Rev. 56 (1939) 246.
[9] GILBERT, A., CAMERON, A.G.W., Can.J.Phys. 43 (1965) 1446.
[10] HAUSER, W., FESHBACH, H., Phys.Rev. 87 (1952) 366.
[11] ODA, N., HARADA, K., Progr.theor.Phys. 15 (1956) 545; RAWITSCHER, G.H., Phys.Rev. 135B (1964) 605.
[12] NILSSON, S.G., Mat.fys.Medd.Dan.vid.Selsk. 29 (1955) 16.
[13] BRITT, H.C., RICKEY, F.A., Jr., HALL, W.S., Phys.Rev. 175 (1968) 1525; SPECHT, H.J., FRASER, J.S., MILTON, J.C.D., private communication.
[14] KAPITZA, S.P., RABOTNOV, N.S., SMIRENKIN, G.N., SOLDATOV, A.S., USACHEV, L.N., TSIPENYUK, Yu.M., JETP Lett. 9 (1969) 73.
[15] IGNATYUK, A.V., RABOTNOV, N.S., SMIRENKIN, G.N., Phys.Lett. 29B (1969) 209.
[16] PAULI, H.C., WONG, C.Y., STRUTINSKY, V.M., private communication.
[17] SPECHT, H.J., FRASER, J.S., MILTON, J.C.D., Phys.Rev.Lett. 17 (1966) 1187.

A HIGH-RESOLUTION STUDY OF THE ^{239}Pu (d, pf)-REACTION

H.J. SPECHT*, J.S. FRASER, J.C.D.MILTON, W.G. DAVIES
Chalk River Nuclear Laboratories,
Atomic Energy of Canada Limited,
Chalk River, Ontario, Canada

Abstract

A HIGH-RESOLUTION STUDY OF THE ^{239}Pu (d, pf)-REACTION. The (d, pf)-reaction on ^{239}Pu has been studied at a bombarding energy of 11.5 MeV using the Chalk River MP Tandem Accelerator. A Brown-Buechner magnetic spectrograph equipped with a 1 m long hyperbolically shaped wire spark chamber detected protons at an angle of 132.5° with respect to the incoming deuteron beam. The energy resolution of the system, which included separation of protons and deuterons by time-of-flight, was ~ 18 keV FWHM. The angular distribution of fission fragments was measured in coincidence with protons, using an array of 14 wire proportional counters arranged at 10° intervals, with a solid angle increasing monotonically from the classical recoil axis (taken as 0°) to a maximum at 90° without reduction of angular resolution. The overall coincidence resolving time was ~ 10 ns FWHM.

Particular attention was given to the excitation energy region from 4.3 MeV to 5.2 MeV in the residual nucleus where experiments with ~ 100 keV resolution had shown a peak in the probability ($\sigma_{d,pf}/\sigma_{dp}$) around 5.0 MeV and a weak plateau below the peak. In the present experiment, ~ 3300 events were accumulated in this region, representing ~210 hours of beam time. Preliminary analysis shows prominent structure in the fission probability consisting of at least seven lines in the peak. The "weak plateau" below the main peak also appears to contain several lines and does not consist of only one narrow line. The fission fragment angular distribution data are consistent with the interpretation that all lines in the region 4.69 to 5.16 MeV have the same angular distribution.

The width of the lines in all cases is that of the experimental resolution and their spacing is consistent with present ideas of the level density in the second well. It is unlikely that the fine structure is produced by the mechanism of the (d, p) reaction although it may serve to enhance the structure.

1. Introduction

The nucleus ^{240}Pu is one of the best investigated fissioning systems to date as far as fission induced by direct reactions is concerned; measurements on both fission probability and fragment angular correlations have been reported for the reactions ^{239}Pu(d,pf)[1-7], ^{239}Pu(t,df)[8], ^{240}Pu(α,α'f[9] and ^{240}Pu(p,p'f)[10]. Attempts to interpret the results in terms of low-lying vibrational bands[11] in the transition state spectrum have been partially successful. However, a number of remarkable deviations from the simple channel model of the fission process remained unexplained, among these a pronounced peak in the fission probability (instead of the expected plateau) at an excitation energy of 5.0 MeV, and the abnormally large values for the gamma width Γ_γ necessary [6] to obtain good fits - apparently pointing to fission of essentially sub-barrier character even above 5 MeV.

One way to resolve these difficulties is provided by the concept of the double-humped fission barrier, proposed recently by Strutinsky [12] as a result of introducing shell corrections to the smooth liquid drop potential energy surface. Experi-

* Present address: Sektion Physik, Universität München, Germany.

mental evidence supporting this model has been rapidly accumulating over the last year and is, in fact, a matter of extensive discussion at this conference. One of the consequences of the model is the occurrence of sub-barrier transmission resonances [13,14] at the position of quasi-bound (β-) vibrational states in the second well. The width of these resonances depends on the penetrabilities of the two single barriers and the amount of damping (mixing of the vibrational state into compound states) in the second well and decreases rapidly with decreasing excitation energy. As suggested by Strutinsky and Bjφrnholm [13], the above-mentioned peak in the fission probability observed in ^{239}Pu(d,pf) might, in fact, be due to a sub-barrier resonance.

We have initiated a new study of the ^{239}Pu(d,pf) reaction, with an energy resolution for the protons superior to previous investigations by about a factor of 5, using a magnetic spectrograph rather than a semiconductor detector. The motivations for this considerable increase in experimental complexity were several-fold: the hope of gaining more insight into the true nature of the peak in the fission probability, specifically with regard to its width, which was obscured before by poor resolution, - of finding the next lower "resonance," which would have completely escaped previous investigations because of its very much smaller width, - of observing fine structure corresponding to compound levels in the second well, equivalent to the grouping observed in neutron-induced sub-barrier fission [15-18], - and finally of learning something about the role of the (d,p) reaction mechanism.

2. Experimental set-up

The basic experimental arrangement is shown in Fig. 1. The (d,pf) reaction was studied using deuterons of 11.5 MeV from the Chalk River MP Tandem accelerator. Protons at an angle of 132.5° with respect to the incoming deuteron beam were analyzed in a Brown-Buechner magnetic spectrograph. A 1 m long hyperbolically shaped wire spark chamber, triggered by a parallel plate proportional counter behind the spark gap, was placed along the focal plane to measure the position of the protons. Mass identification, primarily separation of protons and deuterons, was achieved by measuring the flight time of the particles through the spectrograph between a very thin window transmission counter at the entrance and the parallel plate counter. The overall energy resolution of the system was $\sim$ 17 keV FWHM. The angular distribution of the fission fragments was measured in coincidence with protons, using an array of 14 wire proportional counters arranged at 10° intervals around the target, with the classical recoil axis taken as the symmetry axis [2,6]. The position signal from the spark chamber, the linear signals from the counters, the various time relations and the fragment array, were fed via 6 ADC's into a PDP-1 online computer and stored event-by-event on magnetic tape. Final data analysis was done off-line on a PDP-10 computer.

A few details of the detectors are worth mentioning. Fig. 2 shows a transverse cross section of the spark chamber system [19,20]. Particles enter the chamber through a mylar window, traverse the spark gap (consisting of a Ti foil and a wire mesh with 2 wires/mm) and end up in the parallel plate proportional counter (consisting of a thin aluminized mylar electrode and a rigid Al back plate, polished and suitably

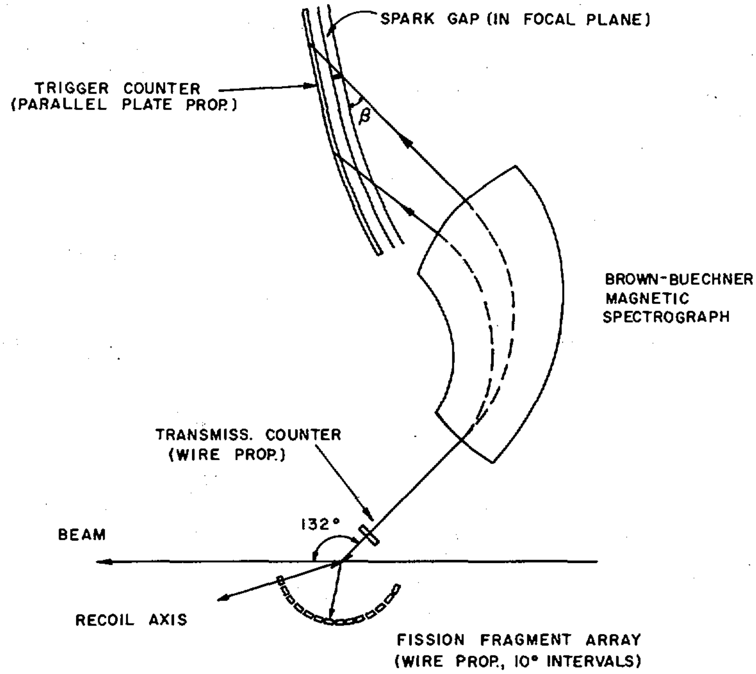

FIG. 1. A schematic drawing of the experimental set-up.

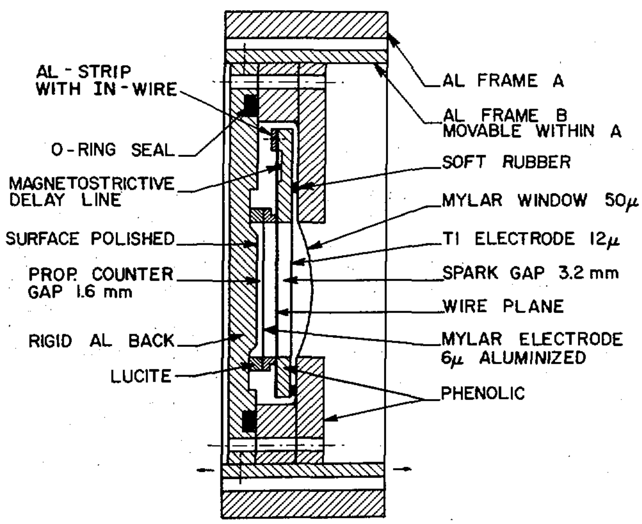

FIG. 2. Transverse cross-section of the spark-chamber system.

shaped to eliminate the danger of edge sparking). This counter has a coincidence resolving time of the order of a few ns. Magnetostrictive delay-line read-out is used to obtain the position signal from the spark gap; the spatial resolution achieved is of the order of 1/4 mm FWHM over the full length of 1 m. With a pulsed clearing field, the system can handle particle rates well beyond 1000/sec.

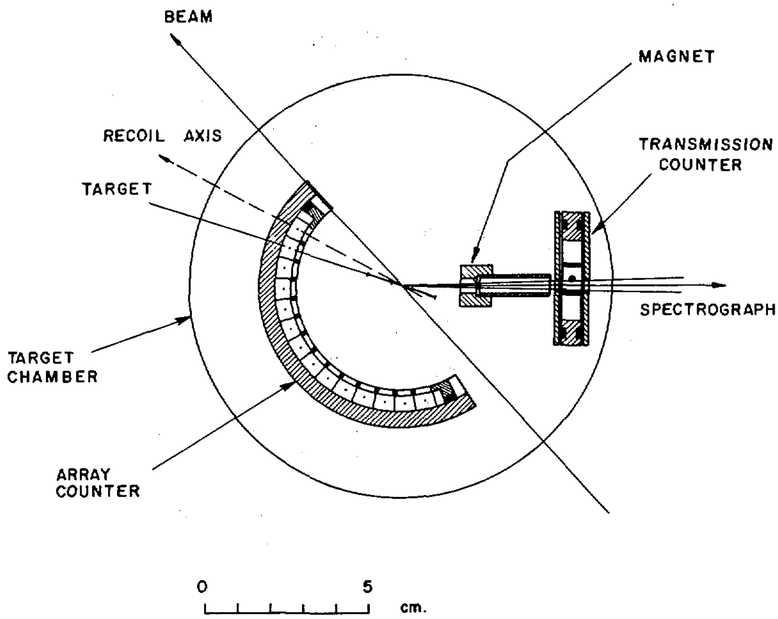

FIG. 3. Inside of target chamber showing the geometry and cross-sections of the transmission counter and the fission-fragment array counter. The magnet was necessary to reduce the number of electrons entering the transmission counter.

Fig. 3 shows a closer view into the target chamber. The transmission counter [20], necessary for the time-of-flight method, is a wire proportional counter with a very small sensitive volume ($\sim$ 1/2 cm^3) defined by field tubes at their appropriate potential. It is operated with ethyl alcohol vapour at $\sim$ 10 Torr; very thin VYNS windows (with a Au layer) are used resulting in a total thickness of the counter, including gas layer, of $\sim$ 60 $\mu g/cm^2$. The target was used in transmission for best resolution (see Fig. 3), unfortunately obscuring by self-absorption angles near the recoil axis. The counter array for the fragments [20] operates under very similar conditions ($\sim$ 5 Torr of methanol) to the transmission counter. The individual elements subtend an angle of $\sim 9.5^{o}$ in the reaction plane with a dead space of $\sim 0.5^{o}$ between them. Fragments enter through a aluminized mylar foil. The coincidence resolving time of $\sim$ 7 ns compares reasonably well with what is routinely obtained in semi-conductor detector arrays.

A photograph of the array is shown in Fig. 4. The front lid including the windows has been taken off the main body.

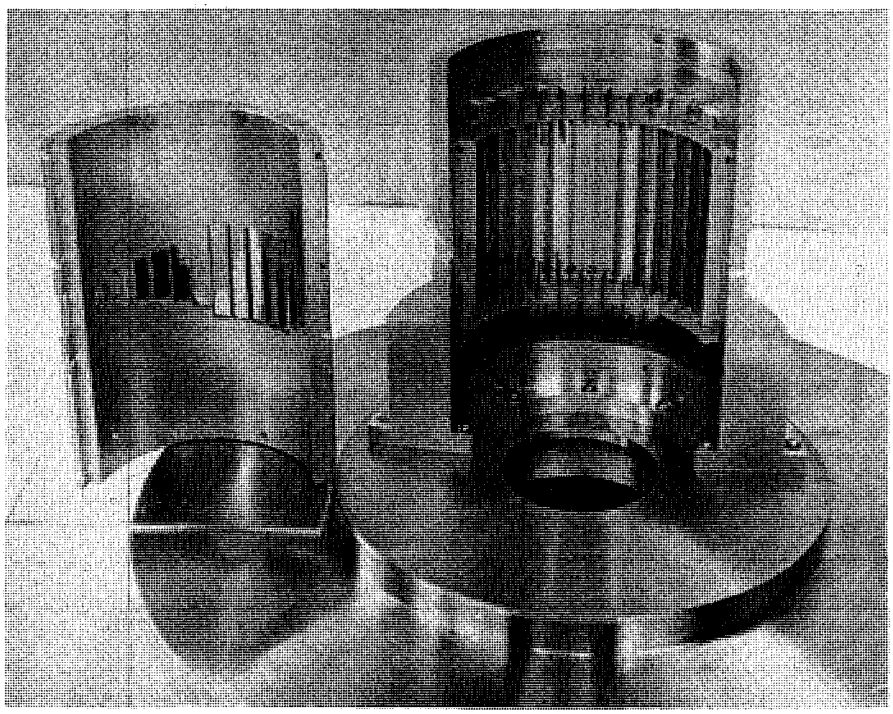

FIG. 4. Photograph of the fission fragment counter array. The front section with the windows has been taken off the main body.

The acceptance angle of the elements perpendicular to the reaction plane increases monotonically from the recoil axis (0° element) to a maximum at 90° such as to keep the angular resolution constant. The overall solid angle of the array is thereby maximized ($\sim$ 0.1 of 4π), compensating partially for the very low solid angle of the spectrograph. The main advantage of the array, and the primary reason for developing it, is its reliability and complete insensitivity to radiation damage.

3. Results and discussion

The data accumulation rate was extremely slow, in $\sim$ 210 hours of beam time only $\sim$ 3300 events were accumulated in the region of the peak around 5.0 MeV. The direct proton spectra corrected for chance coincidence events are displayed in Fig. 5, covering the excitation energy region in ^{240}Pu from 4.2 to 5.6 MeV. The energy scale was calibrated with the Q-value for the ground state transition $Q_0 = 4.230$ taken from mass tables [21]. The (d,p) spectrum (singles) is shown in the lower part of the figure, the (d,pf) spectrum (coincidences summed over all elements of the array counter) in the upper. The statistics are evidently poor, but a few significant conclusions can still be drawn.

a) The natural width of the peak in the fission probability around 5.0 MeV is of the order of 250 keV, as has been shown by

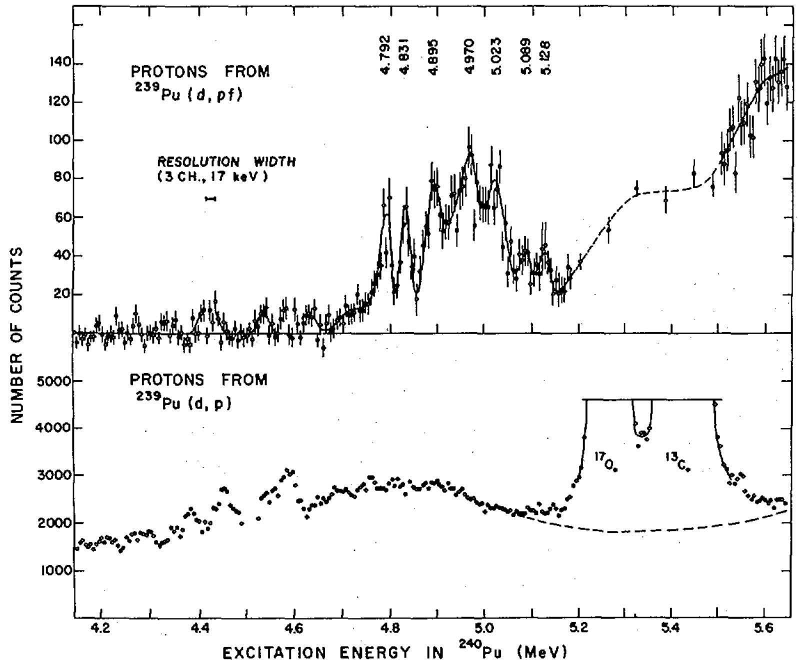

FIG. 5. Direct experimental results showing singles and coincidence proton spectra (summed over all elements of the array). Error bars give statistical standard deviations.

the latest semiconductor experiments [5,7]. There is also a rather flat peak in the singles, but much wider and displaced to lower excitation energies by ~ 150 keV; it appears to be even wider than observed previously [6].

b) Looked at with high resolution, the peak shows prominent structure consisting of a number of lines, partly poorly resolved, but two of them, those at 4.792 and 4.831 MeV, sufficiently isolated to show a width equal to the instrumental resolution. There are very likely more lines between 4.9 and 5.1 MeV than indicated by the smooth line drawn through the measured points. Within the present statistical accuracy, the singles proton spectrum does not show any fine structure at all in this region.

c) The weak "plateau" below the main peak, which was observed in the latest semiconductor experiments [5,7], also seems to consist of weak isolated lines, scattered over the whole region between 4.4 and 4.7 MeV. It evidently does not consist of a strong narrow single resonance.

The discussion of the origin of the observed line structure will follow two paths: the influence of the reaction mechanism, and the influence of a possible double-humped barrier. Even if it is assumed that only one single spin is predominantly involved in this region (as is, in fact, suggested by the analysis of the angular correlation data, see below), the average level spacing of, for example, levels of spin 2 at an excitation energy of 5 MeV is of the order of 10 or 20 eV, as estimated from a suitable level density formula [22]. This is to be compared with an observed spacing of somewhere between 10 and 40 keV for the stronger lines in the bump. It is hardly conceivable that the (d,p) stripping process alone could be responsible for the fact that only such a small fraction (10^{-3}) of all the levels available have a significant fission width. It should be pointed out in this connection that a bump in the fission probability around 5 MeV has also been recently observed in ^{239}Pu(p,p'f)[10] reaction, although weaker by about a factor of two than in ^{239}Pu(d,pf). It is quite conceivable that the (d,p) reaction enhances the phenomenon under discussion, because of the selective angular momentum distribution available [3], (see also below), but it is not thought to be primarily responsible for it.

Turning now to the role of the double-humped barrier, we note first two facts: 1) a spontaneously fissioning isomer of ^{240}Pu has recently been found with a half-life of 4 ns [23,24], and 2) a fission resonance grouping with a mean spacing of 460 eV has been observed in the ^{239}Pu(n,f) [17] reaction. Under the assumption that this spacing represents that of the 1^+ levels [18] in the second well, a depth of 3.55 MeV is deduced from a commonly used level density formula [22]. This places the second minimum 2.90 MeV above the first. Now if we extrapolate downwards from 3.55 MeV to 2.10 MeV (equivalent to an excitation energy of 5.0 MeV above the first minimum), an average level spacing of 9 keV is deduced for levels of spin 2. This estimate is surprisingly close to the observed spacing; and although the assumption of the 460 eV spacing being due to 0^+ levels would yield lower values for the extrapolated level spacings, it is by no means clear that all the levels present in this region would have a large fission width.

We conclude therefore that the observed line structure might indeed be due to compound levels in the second well, arising for the same reason as the grouping observed in neutron induced fission. The "gross-structure bump", that is the envelope of the line structure, might then be due to a transmission resonance through the barrier, its width representing the amount of damping, i.e. of mixing of the strength of the vibrational level into compound levels of the second well, rather than the penetration width. It should be noted that estimates of the penetration width [14] yield values of ~ 10 keV for a transmission resonance only 100 keV below the lowest barrier; and there are indications that the lowest barrier is significantly higher than 5 MeV [10]. The weak structure observed at excitation energies between 4.4 and 4.7 MeV might still arise from some scattered strength of the same vibrational resonance; the next lower resonance could well be unobservable with present techniques because of its excessively small width.

If indeed the observed structure is due to compound levels of the second well, the analysis of the fission fragment angular correlation should yield information about their spins. The results of the correlation have been fitted with a least squares routine to the function

$$W(\theta) = A_0 \{1 + \sum_{\lambda=2,4,6} A_\lambda P_\lambda(\cos\theta)\}$$

where A_0 and the A_λ's are adjustable parameters and the $P_\lambda(\cos\theta)$ Legendre polynomials; the angle θ is measured from the recoil axis [2,6]. The relative solid angles of the fragment array

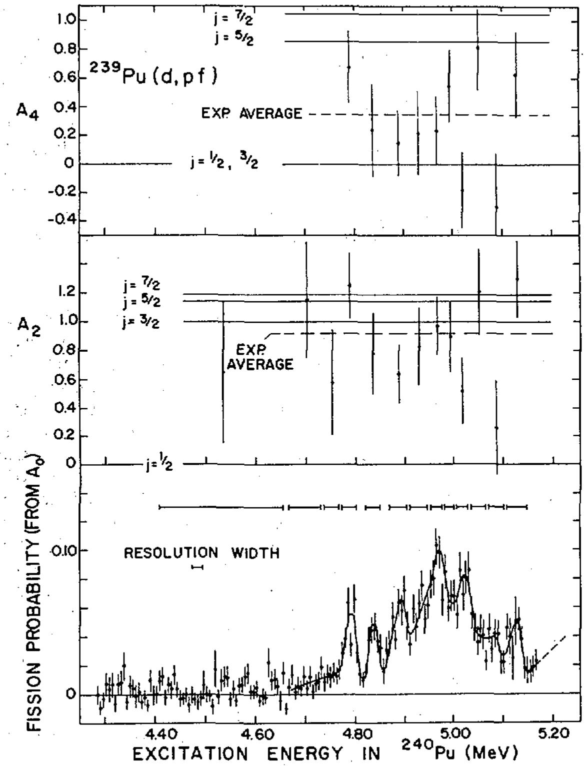

FIG. 6. Fission probability (from A_0) and angular-correlation coefficients A_2 and A_4. Solid lines give calculated coefficients for various total angular momenta j of the neutron transferred in (d, p) under the assumption K = 0. The bars show the areas of the fission probability selected for extracting A_2 and A_4. Below 4.8 MeV, A_4 was set $A_4 \equiv 0$.

were determined by fitting the observed angular distribution to the previously measured one [6] in the excitation energy region from 6.1 to 6.4 MeV, where the anisotropy coefficients are rather small. The fission probability (from A_0 and the singles proton spectrum) and the coefficients A_2 and A_4 (with $A_6 \equiv 0$) are plotted in Fig. 6 as a function of excitation energy, covering the range from 4.3 to 5.2 MeV. Because of the very poor statistics, the coefficients A_2 and A_4 are determined in selected energy intervals (indicated by horizontal bars in the lower part of the figure) corresponding either to the lines seen in the fission probability, or in some cases to the intervals between.

The coefficients A_λ can also be calculated in the usual manner [2,25]; they depend - for an individual level - on the spin I, the effective projection K of this spin on the deformation axis, and the total angular momentum j of the neutron transferred in the (d,p) reaction. Specifically, for a target nucleus with a spin $I_i = 1/2$, there are rather distinct differences in the coefficients A_λ for different combinations of these quantum numbers, suggesting that - at least in principle - the measurement of these coefficients for individual levels would yield unambiguous assignments of I_f, K and j. For the special case of K = 0 (which seems to dominate the whole region around 5 MeV, as is suggested by the large average values of A_2 and A_4 [6]), the coefficients A_λ for an initial spin I_i = 1/2 depend only on j, not on the final spin I_f and these values are drawn as thin lines in the diagram for j up to 7/2.

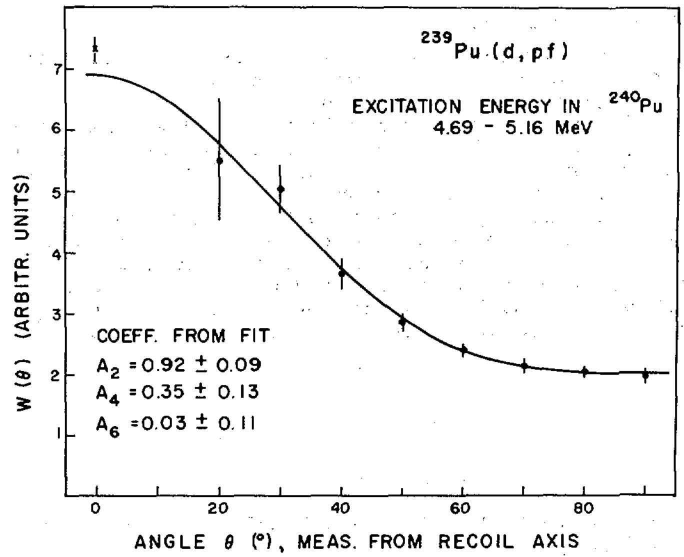

FIG. 7. Measured angular correlation and least-squares fit for the excitation energy region 4.69 - 5.16 MeV. The single point (cross) was taken from previous measurements [5, 6], but not used in the fitting procedure.

Unfortunately, the statistical errors of the measured values of A_2 and A_4 are so large that it is quite difficult to draw immediate conclusions regarding the spins involved. We will therefore first argue about the average distribution, taking the whole region from 4.69 to 5.16 MeV. The measured angular distribution and the least squares fit to it are shown in Fig. 7. The single point (cross at 0°) is taken from previous measurements [6,5], but not used in the fitting process. The measured values for A_2 and A_4 given on the figure agree quite closely with previous determinations [6], the value for A_6 is smaller (probably due to the lower beam energy), and higher terms are absent [6]. Assuming K = 0, the contributions from j = 3/2, 5/2 and 7/2 relative to that from j = 1/2 can be directly determined from A_2, A_4 and A_6; we obtain 3.3, 2.0 and 0.3 respectively. This preference for j = 3/2 and 5/2 does seem to support previous speculations [3] about the specific selectivity of the (d,p) process, but it could alternatively reflect some other selectivity perhaps in the second well. If it is further assumed that only the spin sequence 0^+, 4^+ ...[11] is involved we have to conclude that the relative contributions of spins 0, 2, 4 are 1, 5.3 and 0.3 respectively, in other words - spin 2 seems to dominate this region.

Going back then to Fig. 6 and assuming again K = 0, the first strong isolated line, at 4.792 MeV, suggests pure j = 5/2, leading to the assignment of spin 2. The next one, at 4.831 MeV, contains much more $j = 3/2$, suggesting a spin 2. It is fairly certain that neither of these have spin 0. Nothing conclusive can be said about the detailed structure higher up because it is not sufficiently well isolated. The structure at 5.089 possibly represents the only example of $j = 1/2$, leading to spin 0.

4. Summary and conclusions

It has not been possible to assign definite spins and K values to the fine structure observed in this work. However two definite conclusions can be drawn:

a) The "peak" in the fission probability at 5 MeV excitation in the ^{239}Pu(d,pf) reaction is not simple but consists of at least 7, and possibly more, fine structure peaks, each with a width equal to the experimental resolution.

b) The fission probability at energies below the 5 MeV peak is not concentrated in a single narrow resonance, but is scattered over a wide area. One somewhat less definite conclusion is

c) The fine structure is not introduced by the (d,p) stripping process, although it may be enhanced by it, and is consistent with our present knowledge of level densities a second well.

References

[1] NORTHROP, J.A., STOKES, R.H. and BOYER, K. Phys. Rev. 115 (1959) 1277.

[2] BRITT, H.C., GIBBS, W.R., GRIFFIN, J.J. and STOKES, R.H. Phys. Rev. 139 (1965) B354.

[3] SPECHT, H.J., FRASER, J.S. and MILTON, J.C.D. Phys. Rev. Lett. 17 (1966) 1187.

[4] WOLF, K.L., VANDENBOSCH, R., LOVELAND, W.D. Phys. Rev. 170 (1968) 1059.

[5] SPECHT, H.J., FRASER, J.S. and MILTON, J.C.D. Bull. Am. Phys. Soc. 13 (1968) 1407.

[6] BRITT, H.C., RICKEY, F.A., Jr. and HALL, W.S. Phys. Rev. 175 No.4 (1968) 1525.

[7] PEDERSEN, J. and KUZMINOV, B.D. Phys. Lett. 29B (1969) 176.

[8] BRITT, H.C. and CRAMER, J.D. Phys. Rev. To be published.

[9] BRITT, H.C. and PLASIL, F. Phys. Rev. 144 (1966) 1046.

[10] BRITT, H.C., BURNETT, S.C. and CRAMER, J.D. paper SM-122/102, of this conference.

[11] BOHR, A. Proc. of the I. Intern. Conf. on the peaceful Uses of Atomic Energy, Vol. 2 (1955) 15.

[12] STRUTINSKY, V.M. Nucl. Phys. A95 (1967) 420 and A122 (1968) 1.

[13] STRUTINSKY, V.M. and BJΦRNHOLM, S. Proc. Symp. on Nuclear Structure, Dubna (1968) 431.

[14] WONG, C.Y. and BANG, J. Phys. Lett. 29B (1969) 143.

[15] MIGNECO, E. and THEOBALD, J.P. Nucl. Phys. A112 (1968)603.

[16] FUBINI, A., BLONS, J., MICHAUDON, A. and PAYA, D. Phys. Rev. Lett. 20 (1968) 1373.

[17] PATRICK, B.H. and JAMES, G.D. Phys. Lett. 28B (1968) 258.

[18] LYNN, J.E. AERE-R5891, Harwell (1968); paper SM-122/204 of this conference.

[19] SPECHT, H.J., FRASER, J.S. and MILTON, J.C.D. Bull. Am. Phys. Soc. 13 (1968) 558.
[20] SPECHT, H.J., FRASER, J.S. and MILTON, J.C.D. To be published.
[21] MATTAUCH, J.H.E., THIELE, W. and WAPSTRA, A.H. Nucl. Phys. 61 (1965) 1.
[22] LANG, J.M.B. and LeCOUTEUR, K.J. Proc. Phys. Soc. A67 (1953) 586.
[23] WOLF, K.L. and VANDENBOSCH, R. Bull. Am. Phys. Soc. 13 (1968) 1407.
[24] LARK, N., SLETTEN, G., PEDERSEN, J. and BJΦRNHOLM, S. Preprint (1969).
[25] FRASER, J.S. and MILTON, J.C.D. Ann. Rev. Nucl. Sc. 16 (1966) 379.

FISSION INDUCED BY THE ^{240}Pu (p, p'f)-REACTION*

H.C. BRITT, S.C. BURNETT, J.D. CRAMER
Los Alamos Scientific Laboratory,
Los Alamos, New Mex.,
United States of America

Abstract

FISSION INDUCED BY THE ^{240}Pu (p, p'f)-REACTION. It has been suggested that the threshold peak at ~ 5-MeV excitation energy observed in the fission probability for the ^{239}Pu (d, pf) reaction may be due to a resonance in the fission penetrability through a two-peaked potential barrier. However, the interpretation of this peak is ambiguous because it appears at the same excitation energy as a gross structure resonance in the (d, p) cross-section.

An attempt has been made to resolve the question of whether the observed resonance in the ^{239}Pu (d, pf) results is due to a resonance in the fission penetrability or in the (d, p) stripping process. Fission probabilities and angular correlations for the fission of ^{240}Pu excited by the (p, p') reaction were obtained from measurements of coincident events at 7 independent fission angles. A 20-MeV proton beam was used and inelastically scattered protons were detected at 90° with an energy resolution of 150 keV (FWHM). The fragment angular correlations were fitted as a function of the excitation energy of the residual nucleus (^{240}Pu) to a series of even Legendre polynomials and the resultant fission cross-section is divided by the (p, p') cross-section to obtain a fission probability. Detailed structure observed in the fission probability is compared to the (d, pf) results. The angular correlations are less strongly peaked than previous (d, pf) results. This effect indicates that $\theta_p = 90°$ is not a sufficiently large angle for the plane wave approximation to be valid. This effect plus the poorer statistical accuracy of the (p, p'f) data combine to obscure the detailed structure in the angular correlation coefficients that has been observed in the (d, pf) experiments.

Near the threshold the fission probability from the (p, p'f) results shows a rise to a plateau at $E^* \sim 5$ MeV with a value for the fission probability of ~1/2 the peak value observed in the (d, pf) results. The results are consistent with the hypothesis that the shape of the resonance in the fission probability in the (d, pf) results is dominated by the gross structure resonance in the (d, p) process. However, the magnitude of the fission probability for the (p, p'f) reaction at $E^* \sim 5$ MeV is significantly less than would be expected for fission through fully open transition states from a K = 0$^+$ rotation band. The experimental probabilities from both (p, p'f) and (d, pf) measurements are compared with penetrability calculations for fission through a two-peaked barrier.

INTRODUCTION

Recently there has been considerable interest in the detailed shape of the fission barrier. For nuclei in the actinide region single particle calculations first proposed by Strutinski [1] have indicated that there may be a secondary minimum in the potential energy surface at a deformation greater than that observed for these nuclei in their ground state. Experimentally the existence of a secondary minimum has been confirmed by the discovery of fission isomers [2] and intermediate resonances [3] in the sub-barrier fission of even-even targets.

In their review [4] of the evidence for these secondary minima, Strutinski and Bjørnholm suggested that the threshold peak observed in the ^{239}Pu(d,pf) reaction might be an example of fission through a resonant state near the top of the secondary well. This interpretation could be consistent with results showing an angular correlation for this threshold peak which indicated fission through a K = 0$^+$ band and a rather low fission probability that is consistent

* Work performed under the auspices of the US Atomic Energy Commission.

with the relevant fission channels being not fully open. However, the threshold peak in the $^{239}Pu(d,pf)$ results occurred at an energy coincident with a strong gross structure resonance in the (d,p) reaction. For this reason it was difficult to determine whether the characteristics of the threshold fission peaks were dominated by fission through a resonant state in the secondary minimum or by the gross structure peak in the (d,p) process.

In this paper results are reported from the $^{240}(p,p'f)$ reaction. By comparison of results from the (d,pf) and (p,p'f) reactions which both produce the excited nucleus ^{240}Pu it should be possible to separate effects peculiar to the direct reaction process from those dominated by the fission process. The (p,p'f) results are compared in detail to previous (d,pf) results [5] and both sets of data are compared to calculations for an idealized model incorporating fission through a two-peaked barrier.

EXPERIMENTAL PROCEDURE

The experimental system and data reduction procedures have been discussed in detail previously [5,6] and will be only briefly reviewed here. In this experiment inelastic protons from an incident 20-MeV beam were detected at 90° and coincident proton spectra were measured for fission fragments emitted at 7 angles. The resulting angular correlations were fitted by a least squares procedure as a function of excitation energy to a function

$$W(\theta) = A_0(1 + \sum_{L=2,4,6} g_L P_L(\cos\theta))$$

The angles θ are measured relative to the kinematic recoil angle for the (p,p') reaction and the data are all transformed to the rest system for the fissioning nucleus. As in previous experiments [5,6], the relative solid angles of the fission detectors were determined by comparing singles fission rates in the detectors with a measured (p,f) angular distribution. The absolute solid angle of the fission detectors was determined to ±10% by comparing singles fission rates with those for a detector with a known solid angle. From the absolute solid angle the coefficient A_0 from the fits can be converted to a fission cross section, σ_f, and fission probability determined from $P_f = \sigma_f/\sigma_{pp'}$ where $\sigma_{pp'}$ is the cross section for exciting the residual nucleus to a particular excitation energy.

In this experiment a $^{240}PuO_2$ target of ∿250 μg/cm² deposited on a 60 μg/cm² carbon backing was used. The ^{240}Pu had an isotopic purity of 98%.

RESULTS

The fission probability, P_f, and angular correlation coefficients, g_2 and g_4, from the $^{240}Pu(p,p'f)$ results are shown in Fig. 1. If the angular correlations can be described by a plane wave calculation [7], one would expect the g_2 and g_4 coefficients to be slightly larger for the (p,p'f) reaction than for the (d,pf) results because of the absence of target spin decoupling effects. As seen in Fig. 1, the measured correlation coefficients are much lower than those observed for (d,pf) reaction. The most reasonable explanation of these results is that the plane wave approximation is not valid for inelastic protons emitted at 90°. A similar effect has been observed previously for protons emitted at 90° for the $^{239}Pu(d,pf)$ reaction [5,8]. Therefore, it appears that very little information can be obtained from the angular correlation coefficients and further discussion will center primarily on a comparison of the fission probabilities from the (d,pf) and (p,p'f) reactions.

The fission probabilities and singles proton spectra from the (p,p') and (d,p) reactions are shown in Fig. 2. For the (p,p') reaction the proton angle of 90° was chosen such that the excitation energy region, 5.0-6.5 MeV,

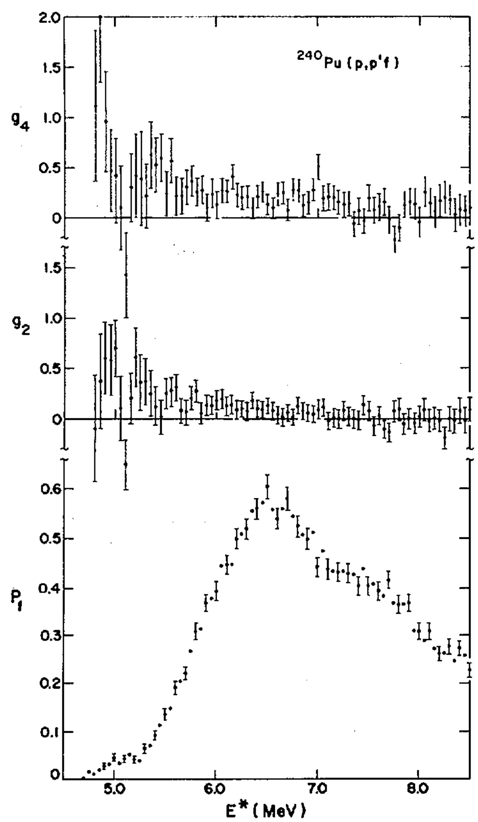

FIG. 1. Fission probabilities and angular correlation coefficients as a function of energy for the ^{240}Pu (p, p'f) reaction.

would be free from ^{12}C and ^{16}O peaks. The peak observed in the proton spectrum at E*∿7 MeV is due to excitation of the 4.43-MeV level in ^{12}C. The rise in σ_s as E* decreases below 5.5 MeV is due to a tail on the very intense ^{12}C elastic peak which occurs at E*(^{240}Pu) ∿2.5 MeV. The dashed line in Fig. 2 shows the assumed dependence for σ_s used in calculating P_f for the ^{240}Pu(p,p'f) reaction. Alternatively, if σ_s is assumed to be constant throughout the region of interest, a very similar P_f distribution is obtained. In the comparison of the ^{240}Pu(p,p'f) and ^{239}Pu(d,pf) results in Fig. 2, the fission probabilities are estimated to be accurate to ±10%. The excitation energy scales have an estimated uncertainty of ±.05 MeV.

In the threshold region (E*∿5 MeV) the ^{240}Pu(p,p'f) results show a plateau in place of the somewhat stronger peak observed in the ^{239}Pu(d,pf) results. If the prominent gross structure peak at ∿5 MeV in the (d,p) reaction is predominantly due to excitation of positive parity states then these results are consistent with the ^{239}Pu(d,pf) threshold peak being created by a modulation of the relative formation cross sections due to the gross structure peak in the (d,p) process. The fission probability observed near E* ∿ 5 MeV for the ^{240}Pu(p,p'f) reaction is much too small for fission through fully open channels of the K=0$^+$ ground state band unless it is assumed that the (p,p') reaction excites almost entirely negative parity levels. This assumption seems unlikely and the most reasonable explanation of these results is that in the region $E^* \sim 5$ MeV fission is proceeding through a sub-barrier resonance in the secondary minimum of a two-peaked fission barrier. This hypothesis will be investigated in terms of the model calculations presented below.

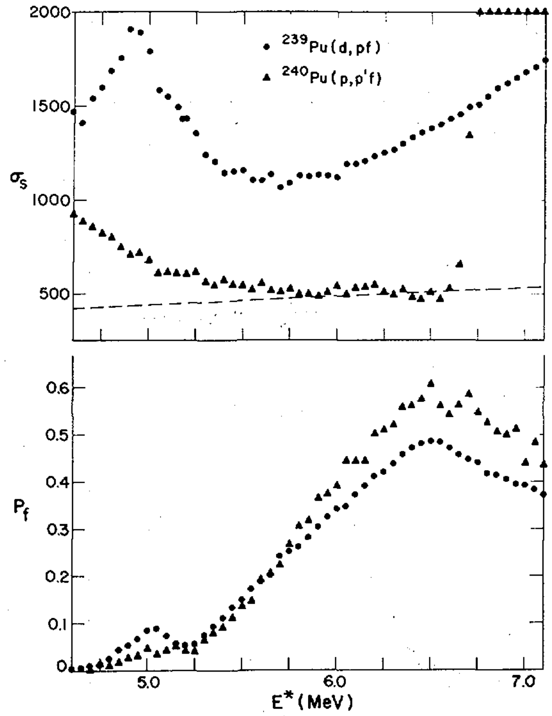

FIG. 2. Comparison of fission probability and proton singles spectra from ^{239}Pu (d, pf) and ^{240}Pu (p, p'f) reactions.

MODEL FOR DIRECT REACTION FISSION PROCESS.

The present (d,pf) and (p,p'f) results are compared with calculations based on a simplified model of the direct-reaction fission process. The present model is a direct extension of previous calculations [5] with the major difference being the addition of a two-peaked fission barrier. As in the previous case, it is assumed that the distribution of angular momenta for the states, J^{π}, excited by the direct reaction is given by

$$N(J^{\pi}) = \sigma(J^{\pi}) \times \rho(J^{\pi})$$

where $\sigma(J^{\pi})$ are the relative direct reaction cross sections obtained from DWBA calculations [9] and $\rho(J^{\pi})$ is the density of states available for excitation. It is assumed that $\rho(J^{\pi})$ can be adequately described by a statistical spin density function [10]. In the decay process the competition between fission and gamma-ray de-excitation is considered. In this calculation the average value of Γ_f is taken as

$$\langle \Gamma_f(E^*J^{\pi}) \rangle = [2\pi\rho(E^*J^{\pi})]^{-1} \nu_f(E^*J^{\pi})$$

where $\rho(E^*J^{\pi})$ is a statistical level density taken from Gilbert and Cameron [10] and $\nu_f(E^*J^{\pi})$ is the sum of the fission penetrabilities for all transition states with spin-parity of J^{π}. Within this framework the fission probabilities and angular correlation coefficients can be calculated as described in Ref. 5.

In the calculations presented below all of the level density parameters are held fixed [10] and the value used for Γ_{γ} is taken from analysis of neutron resonance data [11]. For the (p,p'f) data and the (d,pf) data at excitation energies above the (d,p) gross structure resonance, it is assumed that there are equal contributions from positive and negative parity states. For the (d,pf) results in the region of the gross structure resonance ($E^* = 4.5-5.5$ MeV) it is assumed that the (d,p) cross section contains two components: (1) a background cross section extrapolated from the higher energy region which is assumed to contain equal positive and negative parity contributions and (2) the remaining cross section in the gross structure resonance which is assumed to be 3/4 positive parity and 1/4 negative parity excitations. These assumed ratios of positive to negative parity excitations were held fixed during attempts to fit the experimental data.

The fission penetrabilities used in these calculations were obtained from exact calculations of the penetrability through a two-peaked fission barrier described by three smoothly joined parabolic sections. This barrier is described by six independent parameters: E_1 and $\hbar\omega_1$, the height and curvature of the first peak; E_2 and $\hbar\omega_2$, the minimum and curvature for the intermediate well; and E_3 and $\hbar\omega_3$, the height and curvature of the second peak. The details of these penetrability calculations are described in Ref. 6. A similar penetrability calculation has been recently reported [12].

ANALYSIS AND DISCUSSION

Using the model described in the previous section an attempt has been made to simultaneously reproduce the features of the fission probability and angular correlation coefficients from the ^{239}Pu(d,pf) results and the fission probability from the ^{240}Pu(p,p'f) results. In the model calculations the only parameters which were allowed to vary were the 6 fission barrier parameters and the positions of the transition states. The set of barrier parameters was somewhat restricted by requiring that an acceptable barrier yield approximately the correct spontaneous fission half-life ($\tau \sim 10^{11}$ years) [13] and have an isomer which decays by fission with approximately the correct half-life ($\tau \sim 5 \times 10^{-9}$ sec) [14].

A limited investigation of possible barrier shapes has yielded fits to the ^{239}Pu(d,pf) and ^{240}Pu(p,p'f) results shown in Figs. 3 and 4. The barrier shape associated with these fits and the penetrability of this barrier broadened by a resolution function with 0.12 MeV FWHM is shown in Fig. 5. The parameters and characteristics of this barrier are shown in Table I and the other parameters of the model calculation are given in Table II. The barrier parameters and the transition state spectrum are very similar to "best" fits obtained for ^{240}Pu(t,pf) and ^{242}Pu(t,pf) results [6].

At present a systematic survey of the sensitivity of the calculations to variations in various parameters has not been completed and it has not been determined to what extent the present parameter set is unique. However, within the framework of the present model certain qualitative conclusions can be made about (1) the acceptable range of the barrier parameters and (2) some obvious limitations of the present model.

If the values of $\hbar\omega_2$ and $\hbar\omega_3$ for the barrier were held fixed, it then appeared from the limited investigation of parameter sets that the other four parameters for the barrier shape were relatively well determined. In this case E_3 is most sensitive to the apparent fission threshold; E_1, to the absolute magnitude of the observed fission probabilities; $\hbar\omega_1$, to the spontaneous fission half-life and E_2, to the isomer half-life and the resonance structure observed in the fission probability. In addition the range of acceptable values for $\hbar\omega_3$ is limited to the approximate range $0.4 \leq \hbar\omega_3 \leq 0.6$. At $\hbar\omega_3 \sim$

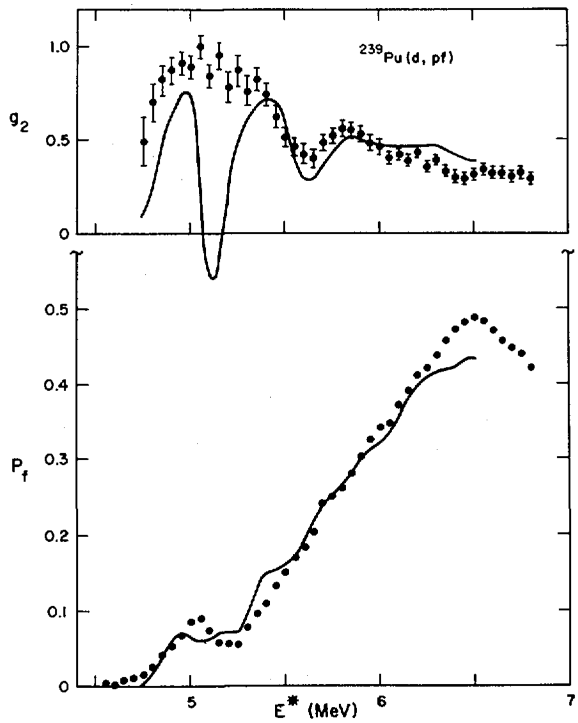

FIG. 3. Comparison of experimental fission probability and angular correlation coefficient, g_2, with model calculations described in the text for the ^{239}Pu (d, pf) reaction.

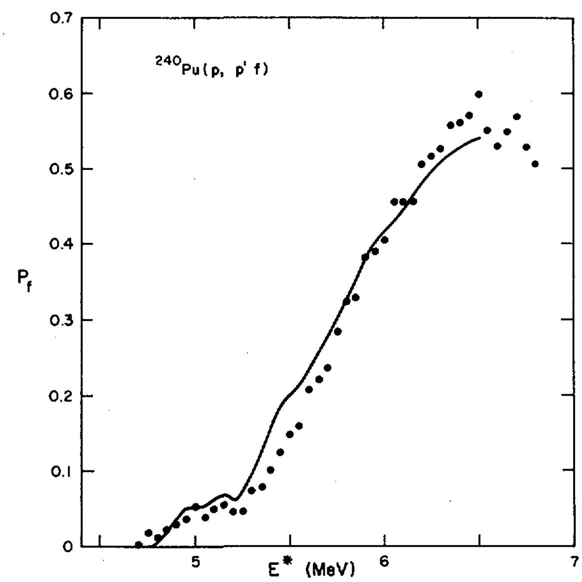

FIG. 4. Comparison of the experimental fission probability with model calculations described in the text for the ^{240}Pu (p, p'f) reaction.

TABLE I. PARAMETERS AND CHARACTERISTICS OF THE FISSION BARRIER USED IN THE MODEL CALCULATIONS AND ILLUSTRATED IN FIG. 5.

i	Energies, E_i (MeV)	Curvatures, $\hbar\omega_i$ (MeV)
1	5.95	1.30
2	2.10	2.00
3	5.25	0.48

Resonance Energies (MeV)	FWHM (keV)	Max. Penetrability
2.92	0.16×10^{-3}	0.44×10^{-6}
4.13	0.10	0.011
4.91	1.86	0.910
5.42	233.00	0.130

Spontaneous fission half-life = 7×10^{12} years.
Fission isomer half-life = 12 ns.

TABLE II. TRANSITION STATE SPECTRUM AND STATISTICAL PARAMETERS USED IN MODEL CALCULATIONS. TRANSITION STATE ENERGIES $\Delta E(K^{\pi})$ ARE RELATIVE TO LOWEST K = 0^+ STATE FOR THE LOWEST STATE IN EACH VIBRATIONAL BAND.

Level density parameters, a^a	=	27.41 MeV^{-1}
Spin cutoff parameters, s^a	=	6.45
Gamma-ray width, $\Gamma_\gamma{}^b$	=	0.040 eV
Rotational constant, E_R	=	0.005 MeV
$E(0^+)$	=	0.00 MeV
$E(2^+)$	=	0.20 MeV
$E(0^-)$	=	0.45 MeV
$E(1^-)$	=	0.75 MeV
$E(2^-)$	=	1.05 MeV

[a] Values taken from Gilbert, A., Cameron, A.G.W., Can. J. Phys. 43 (1965) 1446.
[b] Value taken from Hennies, H.H., Atomics International Report No. NAA-SR-11980 (1967), unpublished.

0.4 the first peak becomes sharp enough so that the calculations predict that the isomer should decay predominantly by γ-ray emission and at $\hbar\omega_3 \sim$ 0.6 one approaches the condition where the two barriers are of equal width. In fitting results from the (t,pf) reaction [6] it appeared that $\hbar\omega_3$ values in the range 0.5-0.6 tended to give structure in the angular correlation coefficients that is much less pronounced than observed experimentally. Therefore, acceptable $\hbar\omega_3$ values may be more restricted than indicated above.

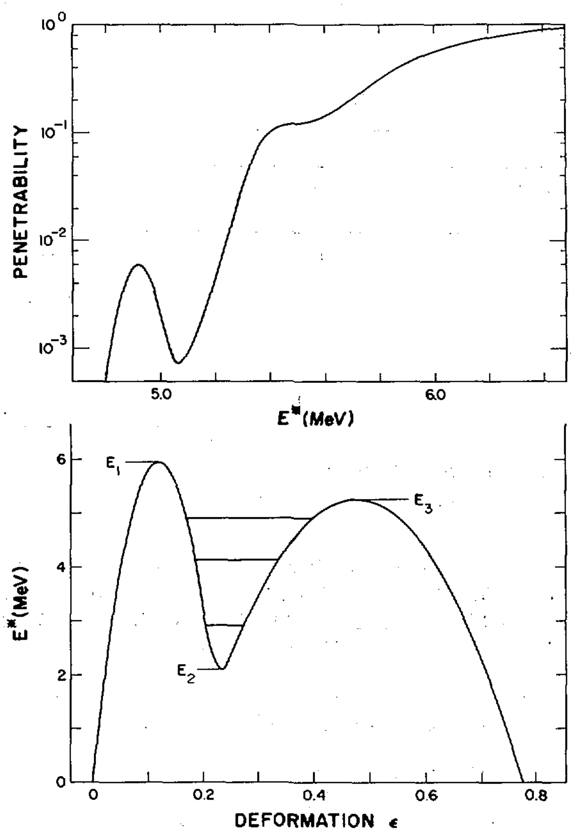

FIG. 5. Shape of the fission barrier used in the model calculations and the calculated fission penetrability of this barrier as a function of energy. The calculated penetrability has been broadened by an experimental resolution function with width 0.12 MeV (FWHM).

The present model is a significant improvement over previous calculations [5] with a simple parabolic barrier in the sense that experimental results can be semi-quantitatively reproduced with a reasonable description of the formation and decay processes for the fissioning nucleus (i.e., realistic level density functions, values for Γ_γ, etc.). The reason for the success of the present model can be seen by examining the penetrability function shown in Fig. 5. An important feature is the rapid rise in penetrabilities between 5.1 and 5.4 MeV to a value of $\sim$0.12 followed by a relatively slow increase after that point. This allows for sharp structure in the fission probability distribution with plateaus that correspond to fission widths considerably less that a fully open channel. This effect is also consistent with many of the neutron resonance results where an analysis of fission width fluctuations indicates several channels contributing while an analysis of the average fission width indicates a relatively small total penetrability for the fission barrier.

The major discrepancy between the calculations and the experimental results is in the g_2 angular correlation coefficient for the $^{239}Pu(d,pf)$ reaction. The calculations show a strong dip in g_2 at $E^* \sim 5.1$ MeV which is not present in the experimental results. A similar discrepancy is observed between experiment and calculation for the $^{242}Pu(t,pf)$ reaction [6]. In the present case the dip results from fission in the $K = 2^+$ band through the $E^* = 4.91$ MeV resonance in the fission probability†. The fundamental reason for the discrepancy between the calculation and the experimental results is not clear but a much better fit to the experimental data would result if there were no sub-barrier fission through the 4.91 MeV resonance when the nucleus was excited to states in the $K = 2^+$ band. Since these effects occur at energies below the top of both peaks in the fission barrier it may be that there is a significant probability for K to change in the intermediate well in which case the present model would not adequently describe the experimental results.

An additional difference between the calculations and the experimental results is that the resonance structure from the calculations is much sharper than the structure observed experimentally. This effect is also apparent in attempts to analyze (t,pf) results [6].

In addition to approximately reproducing the resonance observed at ~ 5 MeV, the model calculations give a weak resonance at ~ 4.15 MeV with a peak value $P_f \sim 3 \times 10^{-4}$. This resonance qualitatively corresponds to the resonance observed [15,16] in the $^{239}Pu(d,pf)$ reaction at 4.5 MeV with $P_f \sim 8 \times 10^{-3}$. If the calculated resonance at 4.15 MeV were arbitrarily moved to 4.5 MeV it would yield a fission probability in approximate agreement with the experimental results. It may be that with a different parameter set the top two resonance levels can be moved closer together and give a better representation of the (d,pf) experimental results.

It should be remembered that the exact shape of the calculated P_f distribution near 5 MeV for the (t,pf) results is also sensitive to the assumptions made about the character of the gross structure resonance in the (d,p) process (see section entitled Model for Direct Reaction Fission Process). Furthermore, if it is not assumed that the gross structure peak in the (d,p) reaction is predominantly positive parity, then the calculations would yield a fission probability much too small in the $E^* \sim 5$ MeV region.

The transition state spectrum and the statistical parameters used in the model calculation are given in Table II. The statistical parameters are all taken from other sources and held fixed. The fits to the experimental results determine the positions of $K = 2^+$ and $K = 0^-$ bands to an accuracy of $\pm.05$ MeV and the positions of higher bands are less well determined. Near the neutron binding energy the fits to the fission probability distributions would be somewhat better if one or two more transition states were added but the data and the model are not good enough to determine which states would be most appropriate. In this transition state spectrum, the relative excitation energies

---

†The dip is created by resonance fission for the $K = 2^+$ band occurring at an energy relative to the $K = 0^+$ band ($\Delta E^*_{2^+} = .20$ MeV) where the penetrabilities for members of the $K = 0^+$ band are very small (see Fig. 5); the addition of a $K = 0^-$ band ($\Delta E^*_{0^-} = .45$ MeV) then causes g_2 to rise again. The dip near $E^* = 5.6$ MeV is caused by super-barrier fission through the $K = 2^+$ band followed by the $K = 0^-$ band. Calculations were performed with various relative positions for the $K = 2^+$ and $K = 0^-$ bands in an attempt to eliminate the dip at 5.1 MeV. It was found that any combination which eliminated the dip gave a much poorer qualitative fit to the g_2 results in the super-barrier region ($E^* \sim 5.5$-6.5 MeV).

for the various bands above the K = 0^+ band (ΔE_K^*) are approximately 0.3 MeV less than deduced previously [5] when no provisions were made for a two-peaked barrier.

SUMMARY

A comparison of the experimental results for the ^{239}Pu(d,pf) and ^{240}Pu(p,p'f) reactions indicates that fission in the region of $E^* \sim 5$ MeV is proceeding through a sub-barrier resonance. For the ^{239}Pu(d,pf) reaction the analysis shows that the sub-barrier fission is modulated by a predominantly positive parity gross structure peak in the (d,p) process. Model calculations utilizing penetrabilities through a two-peaked fission barrier confirm this conclusion and give a reasonable description of both sets of experimental results. Discrepancies between the data and calculations may indicate that the assumption that K remains fixed during the entire barrier penetration process may not be adequate in some cases.

REFERENCES

[1] Strutinski, V.M., Nucl. Phys. A95 (1967) 420.

[2] Flerov, G.N., Pleve, A.A., Polikanov, S.M., Tretyakova, S.P., Martalogu, N., Poenaru, D., Sezoni, M., Vilcov, I., and Vilcov, N., Nucl. Phys. A97 (1967) 444; Flerov, G.N., Pleve, A.A., Polikanov, S.M., Tretyakova, S.P., Boca, I., Sezoni, M., Vilcov, I., Vilcov, N., ibid. A102 (1967) 443; Bjørnholm, S., Borggreen, J., Gangrsky, Y.P., Sletten, G., and Bjørnholm, S., Phys. Letters 25B (1967) 402.

[3] Fubini, A., Blons, J., Michaudon, A., and Paya, D., Phys. Rev. Letters 20 (1968) 1373; Migneco, E., and Theobold, J.P., Nucl. Phys. A112 (1968) 603.

[4] Strutinski, V.M., and Bjørnholm, S., in Int. Symp. Nucl. Struc. (Proc. Conf. Dubna, 1968).

[5] Britt, H.C., Rickey, R.A., Jr., and Hall, W.S., Phys. Rev. 175 (1968) 1525.

[6] Cramer, J.D., Thesis, University of New Mexico (1969); Los Alamos Scientific Laboratory Report No. LA-4198, unpublished.

[7] Britt, H.C., Gibbs, W.R., Griffin, J.J., and Stokes, R.H., Phys. Rev. 139 (1965) B354.

[8] Wolf, K.L., Vandenbosch, R., and Loveland, W.D., Phys. Rev. 170 (1968) 1059.

[9] We are indebted to R.M. Drisko and R.H. Bassel, Oak Ridge National Laboratory, for supplying us with a copy of the code JULIE.

[10] Gilbert, A., and Cameron, A.G.W., Can. J. Phys. 43 (1965) 1446.

[11] Hennies, H.H., Atomics International Report No. NAA-SR-11980.

[12] Wong, C.Y., and Bang, J., Phys. Letters 29B (1969) 143.

[13] Viola, V.E., Jr., and Wilkins, B.D., Nucl. Phys. 82 (1966) 65.

[14] Wolf, K.L., and Vandenbosch, R., Bull. Am. Phys. Soc. 13 (1968) 1407.

[15] Specht, H.J., Fraser, J.S., and Milton, J.C.D., Bull. Am. Phys. Soc. 13 (1968) 1407.

[16] Pedersen, J., and Kuzminov, B.D., Preprint (1969).

DISCUSSION

Discussion on papers SM-122/74, SM-122/128 and SM-122/102

C.Y. WONG: I would like to make a general observation. In all the model analyses, it is clear that the populations of different spin-states are very important. In a way these populations are reflected in the fits for the (d,p) and (p,p') excitation functions. We have seen fits to the fission probability P_f. However, fits to the (d,p) and (p,p') reactions are not mentioned. Would Dr. Britt like to make a comment?

H.C. BRITT: We have attempted fits to the observed gross structure from the (d,p) reaction. The model employed single-particle calculations using a Saxon-Woods potential with parameters that fit the observed single-particle states in Pb. We were only partially successful in fitting the (d,p) cross-section for ^{239}Pu and we believe that the single-particle calculations were not giving a very good description of the negative parity states from the N = 7 shell. Most of these states are coming from spherical lèvels that would be at quite high excitation energies in Pb, and have not been observed in experiments.

C.Y. WONG: All these points lead to the conclusion that the (d,p) and (p,p') reactions need further study at high excitation energies for deformed nuclei.

H.C. BRITT: I agree.

H.J. SPECHT: I would like to ask both Dr. Pedersen and Dr. Britt to what extent the fits which they have described would improve if allowance were made for damping, for example redistribution of K in the second well.

H.C. BRITT: Our fit to the fission probability would improve if damping were included in order to smooth out some of the sharp structure. It is not clear whether a mixing of K in the second well is needed to improve the fits.

J.J. GRIFFIN: Dr. Pedersen, could you compare your double-humped barrier with that used by Britt in his calculations?

J. PEDERSEN: We get the biggest difference for E_3 and $\hbar\omega_3$. The theoretical curve is mostly sensitive to the penetrability of the second barrier and not to absolute height as long as it is lower than the first barrier. Our values for E_3 and $\hbar\omega_3$ may not give the right half-life for the isomer, but this half-life depends on the total area of the second barrier, whereas in the (d,pf) experiment we measure the $\hbar\omega$ only at the very top of the barrier.

J.J GRIFFIN: Dr. Specht, could you comment in more detail on the question of how many fine-structure lines might actually be hidden under the eight or so peaks seen in the damped vibrational resonance?

H.J. SPECHT: If the width of the hidden weaker lines were equal to that of the two main resolved lines, then there should be quite a few more lines (perhaps two or three times more) than indicated by the smooth line drawn through the measured points. Of course, one cannot exclude the possibilities of an underlying continuum or of lines with a width larger than that of the instrumental resolution. Only an experiment with an even better resolution would give a clear answer to this question.

J.P. BONDORF: I want to comment on the damping and penetration problem. In the optical model of fission used in paper SM-122/74 the damping of the fission resonances into Class II states can be taken into account by an imaginary potential in the second well. This broadens the resonances and some flux is absorbed from the fission channel. When this flux comes back into the fission channels, K (the Bohr channel) may be either preserved or mixed. The angular distributions resulting from these two possibilities are, in general, very different. If a varying mass parameter, which varies as the Strutinsky potential (see paper SM-122/62), is used in the calculation of the transmission coefficient, we get narrower calculated peaks than those of a constant mass parameter. This supports the argument that damping is observed in the experimental data of ^{239}Pu (d, pf). Lastly, the numerical integration method for calculating the transmission coefficient is quite adequate for the inclusion of both absorption and varying mass parameter.

L.G. MORETTO: Dr. Britt, to which of the two fission-barrier humps does your K quantum number assignment refer? If it refers to the first, would you not expect mixing to take place in the secondary well? As for your considerations on the pairing gap, I do not understand why you think that there should be a reduction in 2A by comparison with the previously accepted value.

H.C. BRITT: We assume that the internal degrees of freedom are decoupled from motion in the fission degree of freedom. Therefore, our model does not allow for mixing of K. I believe that our previous estimate of the pairing gap was too large because our estimate of the fission barrier was too low. We now believe that the peak in the fission probability is a sub-barrier resonance.

P. von BRENTANO: The different results obtained in the three experiments discussed are confusing. In the (d, pf) experiments we see a strong enhanced hump and fine structure, whereas both these seem to be absent in the (p, p'f) experiment. Dr. Britt, can you account for this? Could you give the experimental resolutions in the three cases?

H.C. BRITT: The experimental resolution (~ 120 keV) in the (p, p'f) and our (d, pf) measurements is not sufficient to allow us to observe fine structure of the type presented in the previous two papers.

J.P. WURM: Dr. Specht, what is the experimental evidence for or against the existence of isomeric states with half-lives longer than, say, 5 ns? In this connection, would you comment on the possibility that the structure observed at lower excitation energy - 4.4 to 4.7 MeV - is due to states which are rather close to the bottom of the second well and could be identified using delayed coincidences?

H.J. SPECHT: I personally do not know of an isomeric state in ^{240}Pu with a half-life different from the 4-5 ns reported independently by several groups. Since the coincidence resolving time of our system was approximately 10 ns (FWHM) any isomeric state with a half-life less than that should be included in the spectrum. Any structure due to isomeric states with half-lives longer than a few nanoseconds could, in principle, be identified by delayed coincidence techniques; however, the problem of chance coincidence counts might be quite prohibitive because of the very small yields.

A.J. ELWYN: At Harwell, Ferguson and I have found a second activity to be associated with ^{240}Pu, along with the known ~ 5 ns period, with a half-life of 29 ns but with an intensity of only 0.1, that of the shorter-lived activity. I will talk about this in a little more detail in connection with papers SM-122/110 and 59.

G. SLETTEN: We bombarded ^{239}Pu by 13.0 MeV deuterons and found indications of a fission isomer having a half-life of about 5 μs. This could, of course, be a double isomer in one of the americium isotopes, but the possibility of the isomer being ^{240}Pu formed through a (d,p) reaction cannot yet be ruled out.

R.H. DAVIS: I have a question for Dr. Britt and possibly for Dr. Pedersen. To what extent does the magnitude of the peak in your penetrability curve depend on the ratio of the barrier penetrabilities taken separately?

H.C. BRITT: The magnitude and position of the peak in the penetrability curve is very sensitive to many of the parameters of the barrier. In particular, small changes in the well depths can make very large changes in the resonant penetrabilities.

R.H. DAVIS: I think that you will find an enhancement in the transmission through both barriers when two conditions hold good. First, as you have said, where the transmission is via a state in the outer well. Second, and this is of importance to the question of fixing the double barrier parameters, this transmission is enhanced when the penetrabilities for the two barriers are equal.

S. BJØRNHOLM (Chairman): In concluding the discussion of these three papers, I would like to emphasize two points. First, we have had a long discussion based on detailed experimental evidence of the damping, or coupling, of the third, fourth or fifth vibrational state in the second well to the underlying intrinsic states. Such a discussion was never possible before with the higher phonon states of the first well; so we see here how fission studies are contributing to the study of the more general problems of nuclear structure and spectroscopy. Second, we have also seen that there are too many parameters to allow a unique choice on the basis of the data. I think that intensified study of the photofission will be especially valuable here; at least, you know that only the spins 1^- and 2^+ contribute in that case.

CORRELATION ANALYSES OF THE TOTAL AND FISSION CROSS-SECTIONS OF ^{239}Pu

G.D. JAMES, B.H. PATRICK
UKAEA Research Group,
AERE Harwell,
United Kingdom

Abstract

CORRELATION ANALYSES OF THE TOTAL AND FISSION CROSS-SECTIONS OF ^{239}Pu. A correlation analysis, of the type suggested by Egelstaff, of high-resolution ^{239}Pu total-cross-section data indicates a modulation of the cross-section with a spacing of about 460 eV. The regions of high-correlation coefficients are not so highly significant as those discovered for the fission cross-section but they cannot be explained by a modulation of the fission widths and suggest a modification of the neutron widths. It is found that the three regions of high fission cross-section below 600 eV are also regions of high total cross-section and that these explain the correlations found in the total cross-section. Analysis of the data between 716 eV and 5683 eV indicates a pronounced modulation of the fission cross-section but no modulation of the total cross-section. The fission cross-section modulations are analysed on the assumption of a Lorentzian dependence and the parameters of this dependence are given.

1. INTRODUCTION

In an earlier publication [1] it was shown that a correlation analysis, of the type suggested by Egelstaff [2], on the results of a high-resolution measurement [3] of the fission cross-section of ^{239}Pu showed highly significant correlations. These were interpreted as modulations of the fission cross-section due to fission occurring through levels, with a spacing of 460 ± 80 eV, built on the second minimum in the fission potential as predicted by Strutinsky [4]. In this paper we present the results of similar correlation analyses of the total cross-section of ^{239}Pu which were undertaken to ensure that the modulations discovered in the fission cross-section are absent in the total cross-section and that they are indeed due to modulations of the fission widths and not due to modulations of the neutron widths. It will be shown that at 50 eV, 250 eV and 516 eV both the fission and total cross-sections show regions of high cross-section which are thus due to large values of the neutron widths. Analysis of the data between 716 eV and 5680 eV indicates a pronounced modulation of the fission cross-section but no modulation of the total cross-sections. It is found that by expressing the mean fission cross-section in this energy range as the sum of ten resonances each having a Lorentzian energy dependence, the correlogram is transformed to the type expected for an unmodulated cross-section. In the energy range 716 eV to 2750 eV the total cross-section has an unexpected feature in that the average value of $(\sigma_T - 10.3)\sqrt{E}$, where σ_T is the total cross-section and E is the neutron energy, increases from 375 b$\sqrt{\text{eV}}$ to 484 b$\sqrt{\text{eV}}$ instead of being energy-independent.

As well as increasing our knowledge of the second minimum in the fission potential barrier, the modulations of the ^{239}Pu cross-sections which we describe may have important consequences for nuclear reactor calculations, notably for the calculation of the Doppler coefficient of fast plutonium reactors, in that the resonance parameters obtained from the resolved resonance region which extends to a few hundred electron volts may well be atypical of the average resonance parameters in the keV region.

2. METHOD OF CORRELATION ANALYSIS

Both the fission and total cross-section data available for analysis extend from 50 eV to 30 keV [3]. The sequence

$$a_j(W) = \int_{(j-1)W}^{jW} \left[\frac{\sigma(E)\sqrt{E}}{\langle\sigma(E)\sqrt{E}\rangle} - 1\right] dE \tag{1}$$

is calculated for values of the energy interval W ranging from 1 eV to 3 keV. Here σ is either the fission cross-section σ_f or $(\sigma_T - 10.3)$, the total cross-section reduced by the potential scattering cross-section so as to obtain a quantity which has on average a $1/\sqrt{E}$ dependence. For a given W, the maximum energy limit (i.e. the highest value of $j = j_{max}$) is determined by terminating the calculation either when the width W contained fewer than three data points or when an energy of 30 keV is reached. For values of $W \leq 100$ eV this upper limit is reduced to 5 keV so that for this range of W the data analysed are due almost entirely to S-wave interactions. The number of $a_j(W)$ values ranged from 399 for W = 1 eV to 9 for W = 3 keV. For most of the analyses the quantity $\langle\sigma(E)\sqrt{E}\rangle$ is obtained by averaging over the energy range from the lowest neutron energy used to $j_{max}W$. At a later stage the supposed energy dependence of the average cross-section is imposed on this quantity to transform the correlograms to the type expected for cross-sections that have energy independent values of $\langle\sigma(E)\sqrt{E}\rangle$. The serial correlation coefficient $r_k(W)$ is determined from the relation

$$r_k(W) = \frac{\mathrm{cor}\,[a_j(W);\ a_{j+k}(W)]}{[\mathrm{var}\ a_j(W).\ \mathrm{var}\ a_{j+k}(W)]^{\frac{1}{2}}} \tag{2}$$

The maximum value of k for each W is $\frac{1}{2} j_{max}$. Errors in the serial correlation coefficients, σ_k, are obtained by transforming to the quantity $Z = \frac{1}{2} \ln (1+r)/(1-r)$ which for uncorrelated data is normally distributed with a variance given by var $Z = 1/(j_{max} - 3)$ (see Ref. [5]). Neutron cross-section data, even when they are not modulated, are not completely random and it is estimated by numerical experiment that for data similar to the fission cross-section of ^{239}Pu the variance of Z is given by var $Z \approx 2.25/(j_{max} - 3)$.

3. COMPARISON OF TOTAL AND FISSION CORRELATION COEFFICIENTS

In Fig. 1 we present a comparison of the correlation coefficients for the fission and total cross-section data. In Fig. 1a all values of $r_k(W)$ for the fission cross-section which are above the 2% significance level are shown by a circle on a log W-log k plane. Such high values of $r_k(W)$ have less than 0.1% chance of being derived from a random set and approximately less than 2% chance of being derived from data similar to the fission cross-section of ^{239}Pu in the absence of modulations. A similar plot for the total cross-section data is shown in Fig.1b. Straight lines in the diagrams at 45° to the axes indicate hyperbolae with kW = constant. Figure 1c shows the fission cross-section correlogram for W = 10 eV and also a line corresponding to the 2% significance level. The total cross-section correlogram is shown in Fig.1d. The most interesting feature of these data are the highly significant values of $r_k(W)$ obtained when kW = 460 eV for the fission cross-section and 475 eV for the total cross-section. It should also be noted that the number of highly significant values of $r_k(W)$ is greater for the fission cross-section data than for the total cross-section and also that the maximum values obtained for $r_k(W)$ are much higher for the fission cross-section data in Fig.1c than for the total cross-section data (Fig.1d). The reason for these differences becomes clear on examination of Fig.2 which shows $\sigma_f\sqrt{E}$ and $(\sigma_T - 10.3)\sqrt{E}$ averaged, for each data point, over $33\frac{1}{3}$ eV intervals. It is seen that below 600 eV there are three regions of high cross-section both in the total and in the fission cross-section. Above this energy modulations of the fission cross-section at a spacing of about 460 eV persist whereas the total cross-section shows no modulation at this spacing but does show an unexpected increase of $(\sigma_T - 10.3)\sqrt{E}$ over the energy range 716 eV to 2750 eV. These features are shown more clearly in Figs 3(a) and (b) which also illustrate by the solid lines an energy variation of the mean cross-sections which are given by Eq.(3) for the fission cross-section and Eq.(4) for the total cross-section

$$\langle \sigma_f \sqrt{E} \rangle = 70.0 + \sum_{q=1}^{10} \frac{K_q}{(E-E_q)^2 + \frac{1}{4} G_q^2} \tag{3}$$

$$\left.\begin{aligned} \langle (\sigma_T - 10.3)\sqrt{E} \rangle &= 0.05572\,E + 329.05, \quad \text{for} \quad 716\ \text{eV} < E < 2750\ \text{eV} \\ \langle (\sigma_T - 10.3)\sqrt{E} \rangle &= 0.00126\,E + 496.04, \quad \text{for} \quad 2750\ \text{eV} < E < 5716\ \text{eV} \end{aligned}\right\} \tag{4}$$

The parameters used to calculate the cross-section in Fig.3(a) are given in Table I. The parameters given in Eq.(4) were obtained by a least-squares fit to the total cross-section data. In Fig.4 we show the correlograms obtained for the data of Fig.3 using a simplified form of Eq.(1) given by Eq.(5)

$$a_j(33\tfrac{1}{3}) = \frac{\overline{(\sigma(E)\sqrt{E})_j}}{\langle \sigma(E)\sqrt{E} \rangle_j} - 1 \tag{5}$$

Here $\overline{(\sigma(E)\sqrt{E})_j}$ are the average values over $33\frac{1}{3}$ eV illustrated by each point in Fig.3 and $\langle \sigma(E)\sqrt{E} \rangle_j$ is the energy-independent average value of the data for the correlograms of Figs 4(a) and 4(b) and is given by Eq.(3) for the correlogram of Fig.4(c) and Eq.(4) for the correlogram of Fig.4(d). In each diagram in Fig.(4) the ordinates give the serial correlation coef-

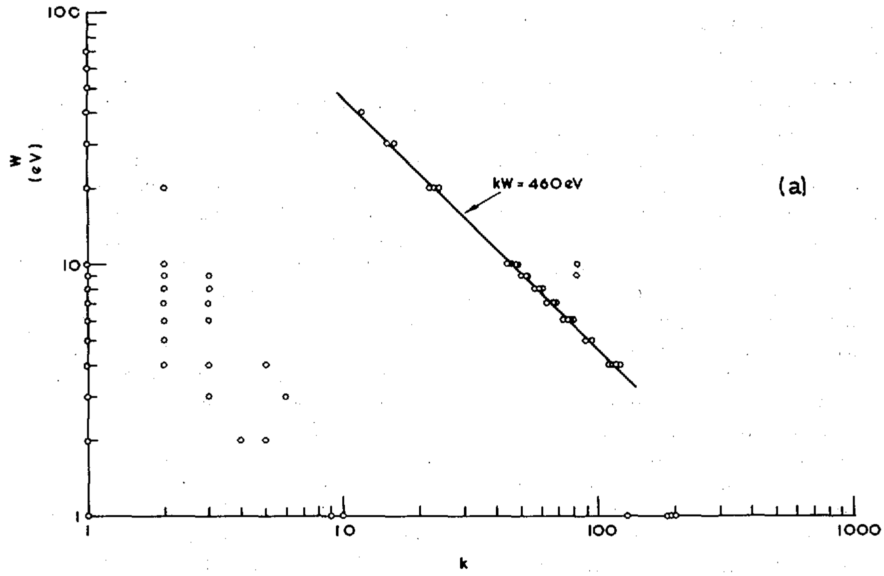

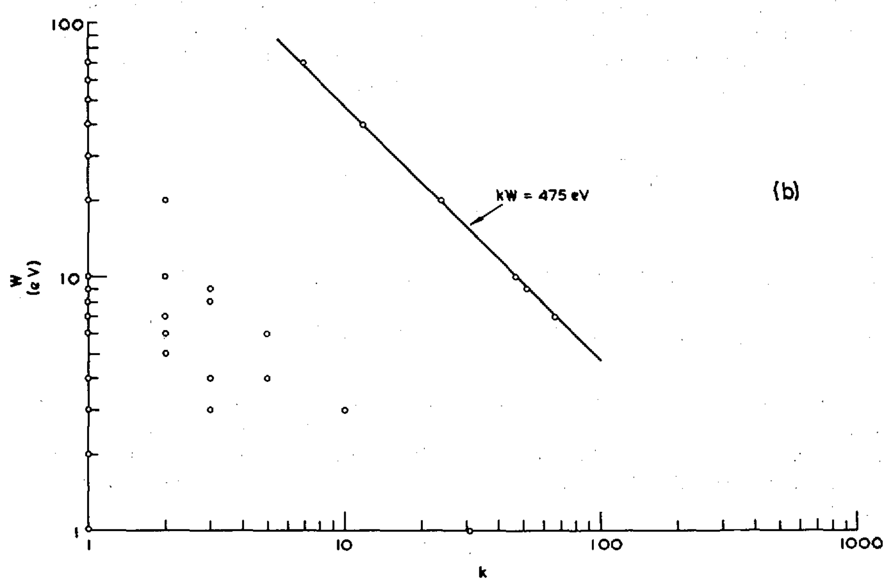

FIG. 1. Representation of the correlation coefficients for the fission-cross-section data ((a) and (c)) and total-cross-section data((b) and (d)). In (a) and (b) all values of $r_k(W)$ above the 2% significance level are represented by a circle. The solid lines at 45° to the axes indicate kW = constant. Sections (c) and (d) are correlograms showing $r_k(W)$ for W = 10 eV against log k.

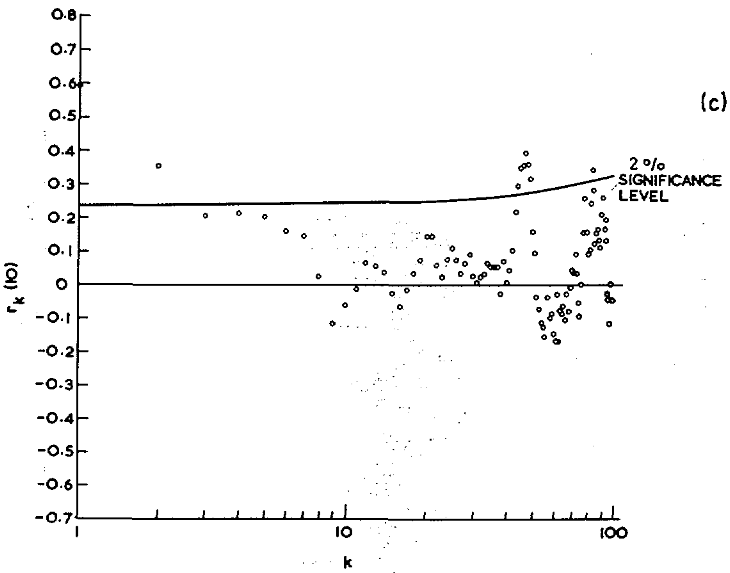

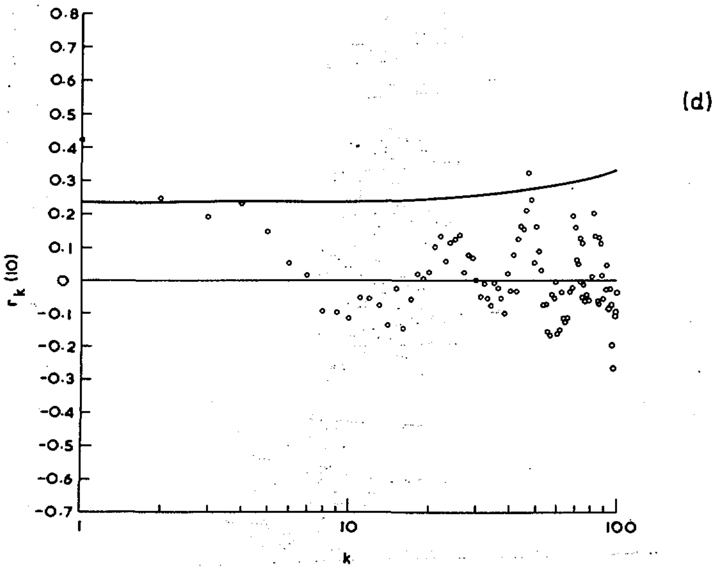

ficient in units of its standard deviation. (The standard deviation used here is that for a random set of data with r = 0.)

The correlogram for the fission cross-section data (Fig.4(a)) shows features which are typical for modulated data. The values of r_k is large and positive for k = 1 and decreases to a minimum at k = 7. At the first minimum value of r_k the product kW = 231 gives roughly the width of the modulation peaks. For further increases in k the values of $r_k(W)$ become

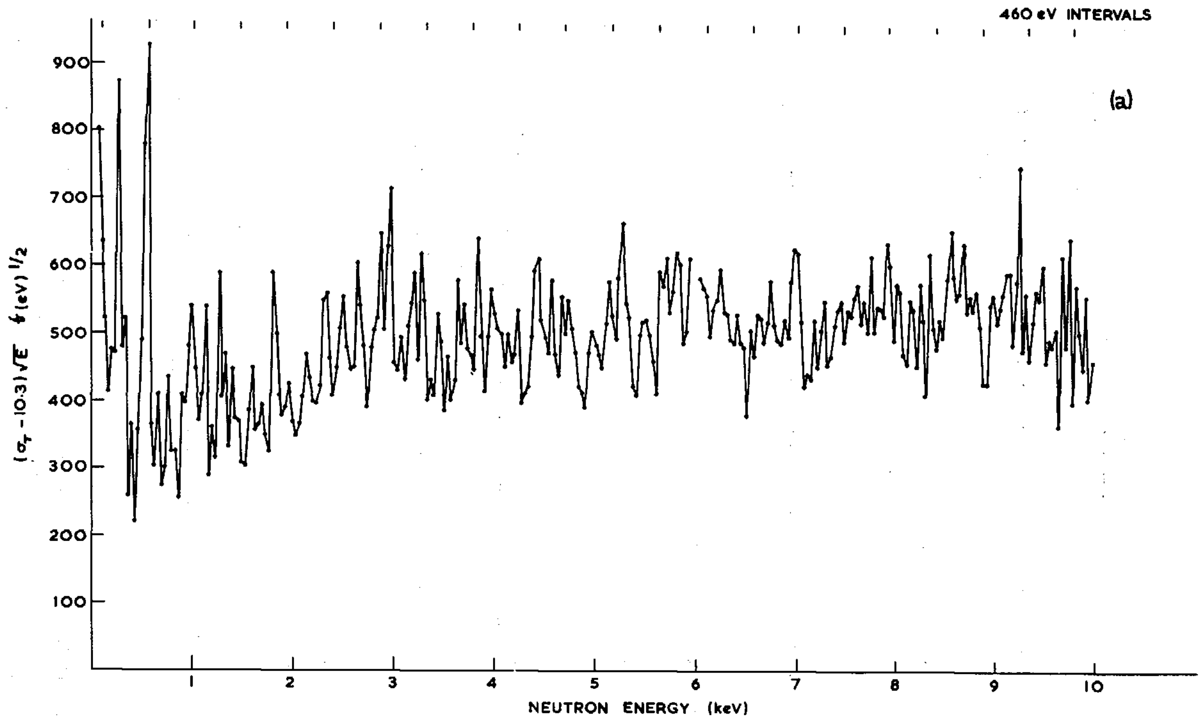
460 eV INTERVALS
(a)
$(\sigma_T - 10.3)\sqrt{E}\ \Phi\,(eV)^{1/2}$
900
800
700
600
500
400
300
200
100
1
2
3
4
5
6
7
8
9
10
NEUTRON ENERGY (keV)

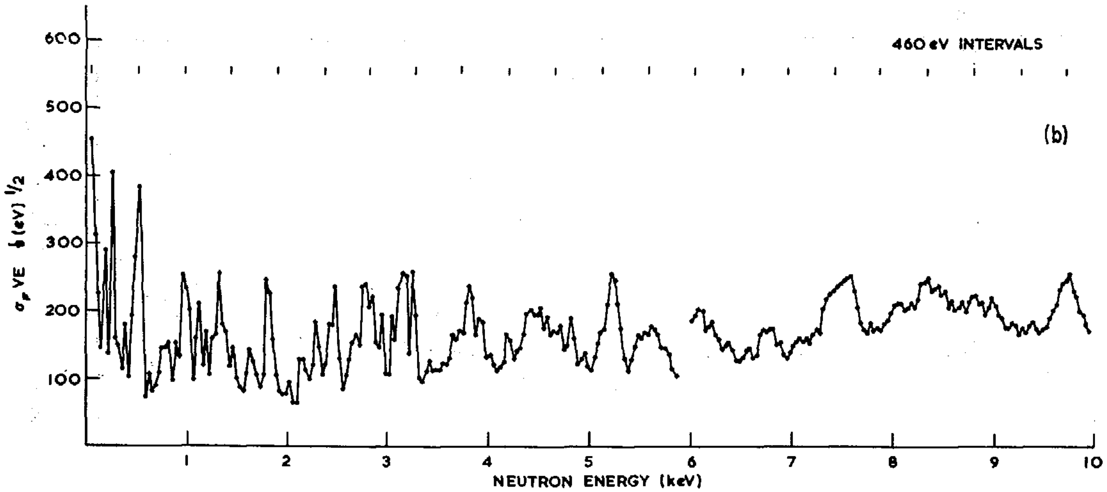

FIG.2. (a) Values of $(\sigma_T - 10.3)\sqrt{E}$ averaged over $33\frac{1}{3}$ eV as a function of neutron energy from 50 eV to 10 keV.
(b) Values of $\sigma_f\sqrt{E}$ averaged over $33\frac{1}{3}$ eV as a function of neutron energy from 50 eV to 10 keV.

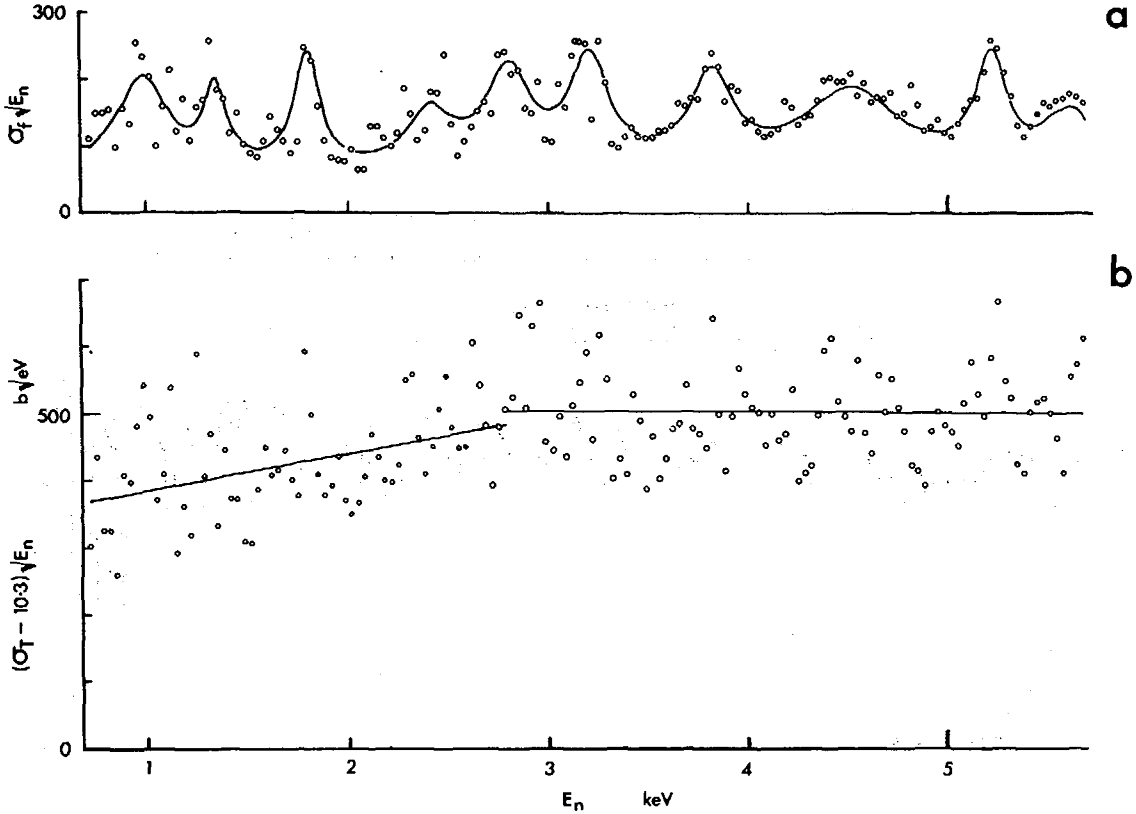

FIG. 3. (a) Average values of $\sigma_f\sqrt{E_n}$ over $33\frac{1}{3}$ eV from 716 eV to 5683 eV. The solid line shows the curve given by Eq.(3) and the parameters of Table I.
(b) Average values of $(\sigma_T - 10.3)\sqrt{E_n}$ over $33\frac{1}{3}$ eV from 716 eV to 5683 eV. The solid lines are given by Eq.(4).

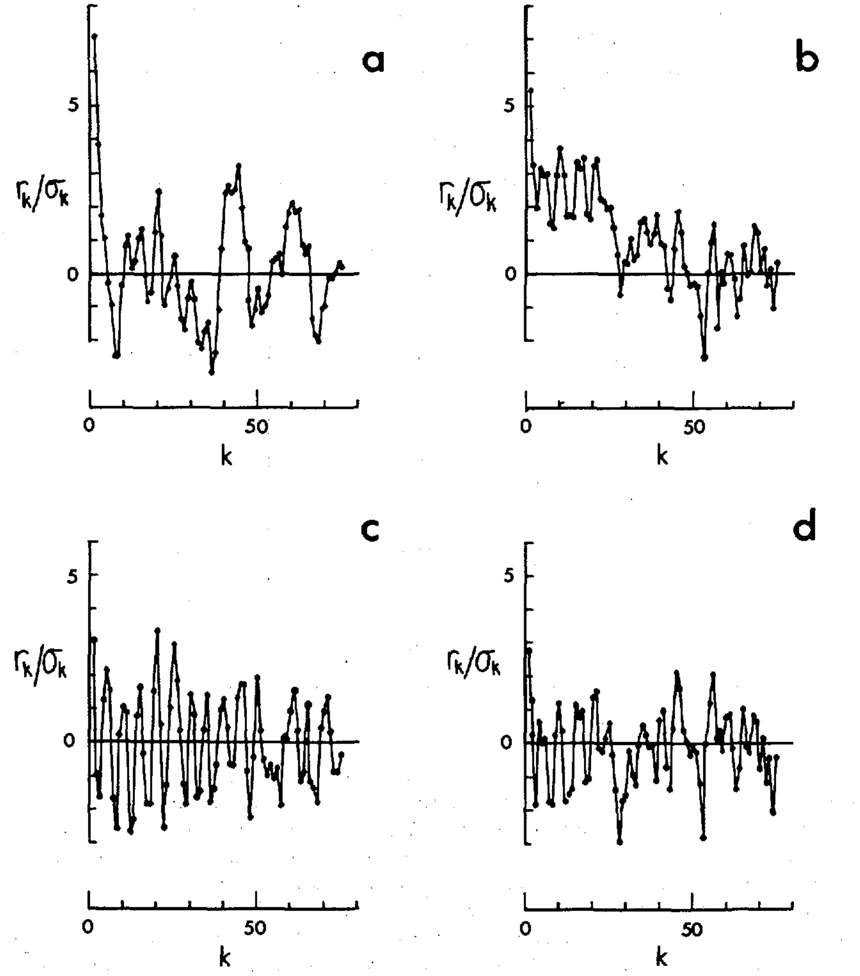

FIG.4. Correlograms for the fission-cross-section data of Fig.3a ((a) and (c)) and for the total-cross-section data of Fig.3b ((b) and (d)). In (a) and (b) the values of $\langle\sigma\sqrt{E}\rangle$ in Eq.(5) were energy independent. In (c) and (d) the values of $\langle\sigma\sqrt{E}\rangle$ in Eq.(5) have the energy dependence described by Eqs (3) and (4).

significantly positive at values of kW which roughly correspond to the 1st, 2nd and higher order spacings of the modulation peaks. As shown in Fig.4(c) these features disappear when the structure of Fig.3(a) is compensated by introducing the modulated mean of Eq.(3) into Eq.(5). The only notable feature of the total cross-section correlogram, Fig.4(b), is that $r_k(W)$ remains positive up to $k = 42$. This behaviour is removed by compensating by using Eqs (4) for the energy dependence of the mean total cross-section. The correlograms of Figs 4(c) and (d) are typical of those for unmodulated energy independent mean values of $\sigma\sqrt{E}$. For each of these curves the number of data points outside $r/\sigma = \sqrt{2.25}$ is about 30% as expected and there are no regions of k where r/σ are persistently positive or negative.

TABLE I. PARAMETERS OF AVERAGE FISSION CROSS-SECTION CURVE

E_q (eV)	K_q (10^4 b.eV$^{5/2}$)	G_q (eV)
982.4	372	317
1348.7	53	133
1800.0	101	150
2416.6	154	266
2800.0	264	266
3200.0	227	233
3816.6	248	266
4516.6	1140	600
5216.6	164	200
5616.6	217	316

4. CONCLUSION

Examination of the fission and total cross-sections of ^{239}Pu in the energy range 50 eV to 5683 eV shows that below 600 eV both cross-sections have similar energy-dependent modulations which must be attributed mainly to modulations of the neutron widths. Between 716 eV and 5683 eV the average fission cross-section shows pronounced modulation which is adequately described by Eq.(3) and the parameters of Table I. Over this energy range the total cross-section does not show a periodic modulation but has an unexpected feature in that the average of $\langle(\sigma_T - 10.3)\sqrt{E}\rangle$ is not constant with energy between 716 eV and 2150 eV. As suggested previously [1] the modulations of the fission cross-section probably arise from the presence of levels in the second fission potential barrier minimum and indicate an upper limit to the spacing of these levels given by $D_{II} \sim 515$ eV. Both Lynn [6] and Weigmann [7] have shown that under certain conditions of coupling between states in the first and second fission potential barrier minima the average fission widths will have a Lorentzian energy dependence, and this prediction has recently been confirmed by James and Slaughter [8] by an analysis of the first narrow intermediate structure resonance in ^{234}U. The next step in the analysis of the ^{239}Pu fission cross-section should therefore be based on a Lorentzian energy dependence of the average (spin J = 1) fission widths. These results would enable a correction for missed levels to be applied to the value of D_{II}. The strong fluctuations of the cross-section due to the fine compound nuclear resonances will make it difficult to evolve objective criteria for determining the parameters of the intermediate structure modulations.

ACKNOWLEDGEMENTS

The authors are grateful to Dr. B. Rose, Dr. E.R. Rae and Mr. J.E. Lynn for their helpful comments on this work.

REFERENCES

[1] PATRICK, B.H., JAMES, G.D., Physics Lett. 28B (1968) 258.
[2] EGELSTAFF, P.A., J. nucl. Energy 7 (1958) 35.
[3] PATRICK, B.H., SCHOMBERG, M.G., SOWERBY, M.G., JOLLY, J.E., Proc. IAEA Conf. on Nuclear Data for Reactors, Paris (1966) 2, IAEA, Vienna (1967) 117.
[4] STRUTINSKY, W.M., Nucl. Phys. A95 (1967) 420.
[5] KENDALL, M. G., STUART, A., The Advanced Theory of Statistics, Griffin, London (1963) 390.
[6] LYNN, J.E., UKAEA Report AERE R 5891.
[7] WEIGMANN, H., Z. Phys. 114 (1968) 7.
[8] JAMES, G.D., SLAUGHTER, G.G., UKAEA Report AERE R 6039 and Nucl. Phys., to be published.

DISCUSSION

R. BLOCK: I note that your level spacings vary only from about 400 eV to 200 eV. Have you looked at the level-spacing distribution of the subthreshold-fission groups?

G.D. JAMES: No, because I felt that with only 10 levels it is hard to draw conclusions about the distribution of their spacing.

R. BLOCK: We have just completed some measurements of neutron capture and fission of ^{240}Pu at the Rensselaer Polytechnic Institute linear accelerator and we observe about 15 groups of subthreshold fission below ~ 30 keV. In plotting up our level-spacing distribution, it is hard to say whether we came closer to agreeing or disagreeing with a Wigner distribution. I saw the Geel linear accelerator data last week and they claim, perhaps, a few more levels than we do. This would improve the fit to a Wigner distribution. In any case, we do observe a factor of 3 to 4 in the variation of level spacings of the subthreshold groups.

J.J. SCHMIDT: To which J^{π} value do you attribute the fluctuations, say the Class-II states, seen in your analysis?

G.D. JAMES: We would attribute these levels to the $J^{\pi} = 1^{+}$ state because slow neutron resonances in this state in ^{239}Pu are known to be subthreshold.

CHANNEL ANALYSIS OF NEUTRON-INDUCED FISSION OF ^{236}U *

J.R. HUIZENGA, A.N. BEHKAMI †
University of Rochester, Rochester, New York
and
J.H. ROBERTS
Northwestern University, Evanston, Illinois

Abstract

CHANNEL ANALYSIS OF NEUTRON-INDUCED FISSION OF ^{236}U. Fission-fragment angular distributions were measured for the fission of ^{236}U induced with mono-energetic neutrons of energies 400, 500, 600, 700, 800, 900 and 1100 keV. The fission fragments are detected with approximately 2π geometry with a polycarbonate resin detector. At the lower energies the experimental angular distributions are peaked in the direction of the neutron beam. However, by the time the neutron energy has reached 700 keV the angular distribution has a peak at an angle which is intermediate between the parallel and perpendicular directions to the beam. Statistical model calculations of the fission cross-sections and angular distributions are performed as a function of neutron energy. These calculations are of the Hauser-Feshbach type and include all the open decay channels for fission, neutron and gamma ray emission. The calculation includes also the level-width fluctuation correction. The number and type (K, π) of transition-state fission channels and their energy parameters are varied in the calculation to give the best agreement with the experimental cross-section and angular distribution data. Assignments of quantum numbers to transition states in the deformed ^{237}U nucleus and the relative heights of the postulated two-humped fission barrier for this nucleus will be discussed.

1. Introduction

One of the most useful concepts in discussing nuclear fission phenomena is that of the transition nucleus. In 1955, A. Bohr[1] suggested that low-energy fission may be understood in terms of one or a few levels in the transition nucleus. Although the level spacing in the compound nucleus at an excitation energy of about 6 MeV is of the order of one eV or less, most of this excitation energy goes into deformation energy during the passage from the initially excited nucleus to the more deformed transition nucleus.

Information on the properties of the transition levels in odd A nuclei is obtained from studies of fragment angular distributions from neutron-induced fission of even-even target nuclei. Each one of the transition levels can be described in terms of the quantum numbers, J, K, M, π, where J represents the total angular momentum, π is the parity of the level, K is the projection of J on the nuclear-symmetry axis, and M is the projection of J on some space-fixed axis (neutron beam axis for our case). The relationship between these quantum numbers is illustrated in Fig. 1.

If one assumes that the fission fragments separate along the nuclear symmetry axis and that K is a good quantum number

---

* This work was supported by the United States Atomic Energy Commission.

† Present address: Pahlavi University, Shiraz, Iran.

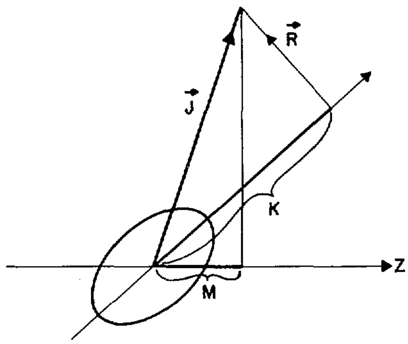

FIG. 1. Angular momentum coupling scheme for a deformed nucleus. The vector J defines the total angular momentum. The quantity M is the component of the total angular momentum on the space-fixed Z axis. We define this direction as the beam direction. The quantity K is the component of the total angular momentum along the nuclear symmetry axis. The collective rotational angular momentum, R, is perpendicular to the nuclear symmetry axis; thus, K is entirely a property of the intrinsic motion.

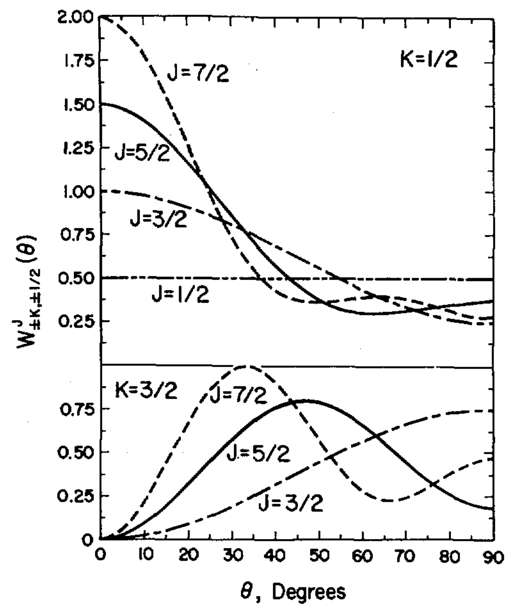

FIG. 2. Theoretical fission-fragment angular distributions for neutron fission of even-even targets calculated with Eq. (1). The axis of quantization is along the beam direction and both values of M, + 1/2 and - 1/2, are included in the results. The top part of the figure is for fission through states in a band with K = 1/2 and J values of 1/2, 3/2, 5/2 and 7/2. Each curve is normalized such that

$$\int_0^{\pi} W^J_{\pm\frac{1}{2},\pm K}(\theta)\sin\theta d\theta = 1$$

The bottom part of the figure is for fission through states in a band with K = 3/2 and J values of 3/2, 5/2 and 7/2. Again each curve is normalized in the above way.

in the passage of a nucleus from its transition state to the configuration of separated fragments, the directional dependence of the fission fragments resulting from a transition state with quantum numbers J, K, and M is uniquely determined. For neutron-induced fission of an even-even target nucleus with zero spin, $I_o = 0$, the fission fragment angular distribution is given by,

$$W^J_{\pm\frac{1}{2},\pm K}(\theta) = \frac{2J+1}{4}\left\{|d^J_{+\frac{1}{2},K}(\theta)|^2 + |d^J_{-\frac{1}{2},K}(\theta)|^2\right\} \tag{1}$$

where the $d^J_{M,K}(\theta)$ function is defined by the following relation[2,3]

$$d^J_{M,K}(\theta) = \{(J+M)!(J-M)!(J+K)!(J-K)!\}^{1/2}$$

$$\times \sum_X \frac{(-1)^X(\sin\theta/2)^{K-M+2X}(\cos\theta/2)^{2J-K+M-2X}}{(J-K-X)!(J+M-X)!(X+K-M)!X!} \tag{2}$$

where the sum is over X=0, 1, 2, 3... and contains all terms in which no negative value appears in the denominator of the sum for any one of the quantities in parenthesis. This equation is symmetric in M and K and may be written also in a form in which M and K are interchanged. Since the target spin is zero and the neutron spin is 1/2, only two values of M are allowed, $M = \pm 1/2$. Eq. (1) has been simplified already by the symmetry relations,

$$|d^J_{\frac{1}{2},K}(\theta)|^2 = |d^J_{-\frac{1}{2},-K}(\theta)|^2 \text{ and } |d^J_{-\frac{1}{2},K}(\theta)|^2 = |d^J_{\frac{1}{2},-K}(\theta)|^2$$

and, in addition, is normalized so that $\int_0^\pi W^J_{\pm\frac{1}{2},\pm K}(\theta)\sin\theta d\theta = 1$. Some typical $W^J_{M,K}(\theta)$ functions are plotted in Fig. 2 and serve to illustrate the "signatures" of various transition states.

In this paper we wish to report the results of measurements of the fission-fragment angular distributions at several energies for the $^{236}U(n,f)$ reaction. Information on the K quantum number, parity, energy, and characteristic energy $\hbar\omega$ of the transition states of ^{237}U near the fission barrier is obtained by examining the energy variation of the fission cross section and fragment angular distributions for the $^{236}U(n,f)$ reaction. Some of the details of the Hauser-Feshbach[4] type of calculation used to extract the above parameters is described in Section 3. This method of analysis, whereby both the fission cross section and fragment angular distributions are fitted, has been used previously.[5,6,7]

Even though the fission barrier is thought to be double-humped for many actinide nuclei,[8-11] we assume a smooth parabolic barrier for the transition states of ^{237}U in the calculations described in Section 3. No isomers have been found for ^{237}U and it may be reasonable to assume that the second barrier is higher than the first barrier for this nucleus.

TABLE I. ^{236}U (n, f) FISSION-FRAGMENT ANGULAR DISTRIBUTIONS

	Mean Angle, θ					
E_n (keV)	5.0°	12.5°	17.5°	22.5°	27.5°	32.5°
400	451 ± 69	362 ± 55	340 ± 45	329 ± 40	371 ± 38	331 ± 32
500	1739 ± 135	1801 ± 116	1987 ± 110	2033 ± 101	1948 ± 89	1924 ± 81
600	1220 ± 113	1214 ± 101	1317 ± 89	1306 ± 79	1249 ± 71	1186 ± 62
700	2511 ± 162	2592 ± 209	3105 ± 194	2983 ± 169	2919 ± 152	3127 ± 139
800	1514 ± 126	1409 ± 110	1653 ± 100	1708 ± 115	1748 ± 83	1654 ± 71
900	7190 ± 306	6877 ± 479	8189 ± 465	9137 ± 434	10316 ± 410	9756 ± 346
1100	7546 ± 300	5983 ± 428	7088 ± 406	6808 ± 372	6294 ± 315	5756 ± 263

E_n (keV)	37.5°	42.5°	47.5°	52.5°	58.7°
400	314 ± 46	349 ± 44	330 ± 41	278 ± 37	264 ± 28
500	1977 ± 116	1960 ± 105	1956 ± 101	2070 ± 100	1840 ± 77
600	1176 ± 89	1211 ± 82	1180 ± 77	1193 ± 75	1142 ± 70
700	3184 ± 148	3148 ± 133	3257 ± 130	3448 ± 129	3157 ± 101
800	1753 ± 109	1930 ± 104	2073 ± 103	2107 ± 100	1837 ± 76
900	10282 ± 264	11694 ± 256	11572 ± 238	10967 ± 220	11544 ± 185
1100	5596 ± 264	5682 ± 262	5211 ± 228	4966 ± 217	5352 ± 177

E_n (keV)	66.2°	72.5°	77.5°	82.5°	87.5°
400	335 ± 34	325 ± 40	303 ± 38	293 ± 37	277 ± 36
500	2137 ± 121	2105 ± 145	1845 ± 134	1882 ± 134	1902 ± 132
600	1110 ± 85	1190 ± 109	1102 ± 103	1102 ± 102	1029 ± 99
700	3397 ± 154	3210 ± 184	3017 ± 171	2936 ± 167	2840 ± 158
800	1906 ± 79	1907 ± 97	1786 ± 92	1769 ± 91	1765 ± 90
900	13077 ± 405	12612 ± 471	12303 ± 447	12278 ± 461	12322 ± 469
1100	5806 ± 195	5746 ± 226	5253 ± 210	5130 ± 216	5015 ± 216

2. Experimental Results

Monoenergetic neutrons produced by the $^7Li(p,n)^7Be$ reaction, impinged on an isotopically enriched ^{236}U target of 0.5 mg/cm^2 thickness. The isotopic content of the target was ^{234}U(0.0015%), ^{235}U(0.192%), ^{236}U(99.76%) and ^{238}U (0.043%). The high enrichment of the ^{236}U is very essential in this experiment since its fission cross section(12) is very small at the lower neutron energies and the ^{235}U impurity contributes a sizable fraction of the events at these energies. The neutron energy spread was 20 keV. The protons were accelerated with the 3-MeV Van de Graaff of the Reactor Physics Division of the Argonne National Laboratory.

The fission fragments from the $^{236}U(n,f)$ reaction were detected at all angles between 0° and 90° for each energy with a polycarbonate resin detector described previously(6). Both the ^{236}U target and the resin detector were enclosed in a thin-walled, evacuated aluminum scattering chamber. After

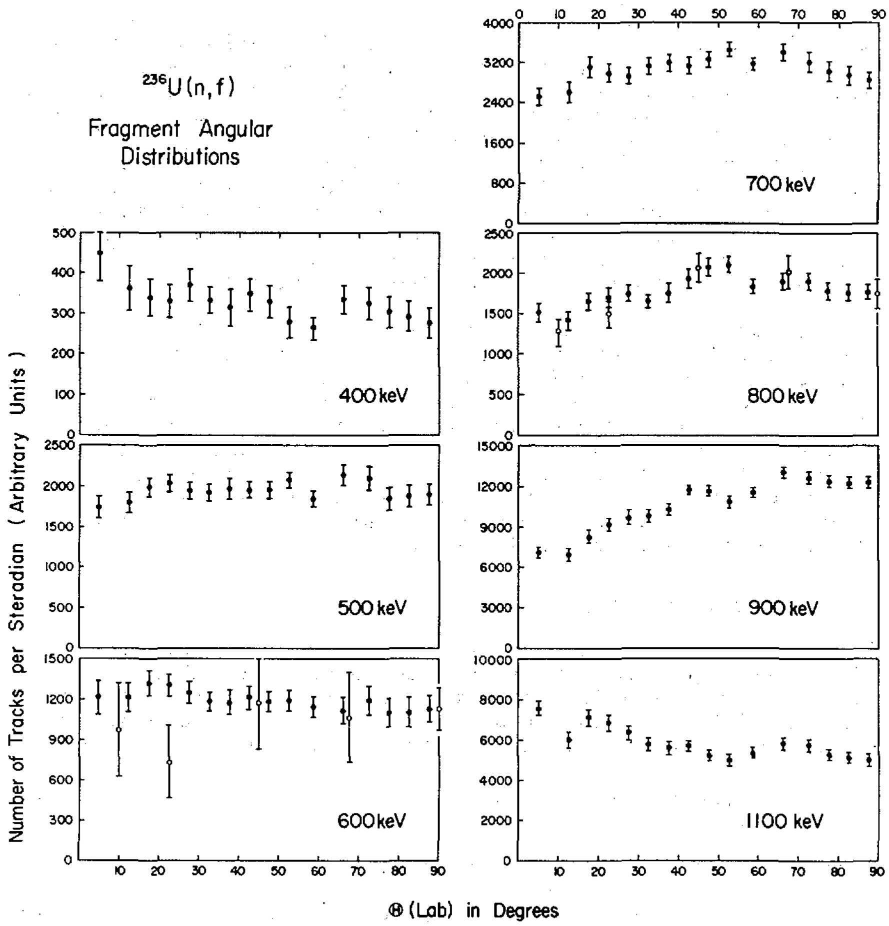

FIG. 3. Fission-fragment angular distributions for the ^{236}U (n, f) reaction at several incident neutron energies. The neutron-energy resolution is approximately 20 keV. Solid points are present measurements and open circles are measurements of Simmons and Henkel [13] normalized to our ordinate scale.

irradiation, the detector material was chemically etched (6N NaOH for 2 days at room temperature), and the resulting fragment "tracks" were viewed with optical microscopes.

The fission-fragment angular distributions for the ^{236}U(n,f) reaction as a function of neutron energy are shown in Table I and Fig. 3. The raw data were corrected for the experimental angular resolution of 9° due to (a) the size of the proton beam spot on the ^7Li target (b) the size of the ^{236}U target, and (c) the summing over finite scanning area. The data were not corrected for fission induced by neutrons scattered from the chamber walls and components because the calculated magnitude of the effect is small. The relative number of fissions at each neutron energy produced by neutrons from the $^7Li(p,n)^7{}^*Be$ reaction which leaves ^7Be in its first excited state is negligible also.

No correction was made to the data for fission due to the $^{235}U(n,f)$ reaction. Although the $^{234}U/^{235}U$ ratio of our target is greater than 500, the contribution of fission events due to ^{235}U may be as much as 50% at our lowest neutron energy of 400 keV. This is due to the fact that the fission cross section of ^{236}U at this energy is very small and known only qualitatively. However, since the fission fragment angular distribution for neutron-induced fission of ^{235}U at the lowest energies is not very different from our observed angular distributions, no qualitative difference in these angular distributions would result if a correction for ^{235}U were made. For $E_n \geq 600$ keV, the fission contribution due to ^{235}U is negligibly small.

The data of Simmons and Henkel[13] for $E_n = 600 \pm 100$ keV and $E_n = 850 \pm 100$ keV are included as circles in Fig. 3. Their data for $E_n = 850 \pm 100$ keV is plotted on the figure along with our 800 keV data. Their energy resolution is rather large and overlaps our energy. Within the assigned experimental errors the two sets of data for each of the two energies are in reasonable agreement. The 600 keV data of Simmons and Henkel[13] has large experimental errors and, in addition, some uncertainty exists at this energy since no isotopic analysis of their target was reported.

3. Theory and Calculational Procedure

The deduction of the transition state parameters including the K quantum number, parity, energy and characteristic energy $\hbar\omega$ is made from detailed fitting of the energy variation of the fission fragment cross section and angular distribution. The total fission cross section is given by,

$$\sigma_f(E) = \sum_{J,\pi,K} \sigma_f(J,\pi,K,E) \qquad (3)$$

and the angular distribution of fragments by,

$$W(\theta,E) = \sum_{J,\pi,K} \sigma_f(J,\pi,K,E)\; W^J_{\pm\frac{1}{2},\pm K}(\theta) \qquad (4)$$

where $W^J_{\pm\frac{1}{2},\pm K}(\theta)$ is defined by Eq. 1. The quantum number M does not appear in the summations of Eqs. 3 and 4 because for neutron fission of an even-even target with zero spin only two values of M are possible, $\pm 1/2$. These two M values are equally probable and both are included in $\sigma_f(J,\pi,K,E)$ and $W^J_{\pm\frac{1}{2},\pm K}(\theta)$.

The neutron fission cross section of a zero spin target for a particular channel (J,π,K) may be written in terms of the various transmission coefficients in the following form,

$$\sigma_f(J,\pi,K,E) = \frac{1}{2}\pi\lambdabar^2(2J+1)\left\{T^{\ell-\frac{1}{2}}_{\lambda n}(J,\pi,\ell,E_n) + T^{\ell+\frac{1}{2}}_{\lambda n}(J,\pi,\ell,E_n)\right\} R \qquad (5)$$

where
$$R = \frac{2T_{\lambda f}(J,\pi,K,E)\quad S_{\alpha\alpha'}}{\sum_i 2T_{\lambda f}(J,\pi,K,E) + \sum_{I'}\sum_j T_{\lambda n}(J,\pi,\ell,E'_n) + T_{\lambda\gamma}(J,\pi,E)}$$

and i represents a sum over all transition states with parity π and $K \leq J$, I' is the sum over all states in the target nucleus which are reached by neutron emission and j is a sum over allowed values of $\ell \pm 1/2$ for each I'. For the case of neutron fission under discussion where the target spin I_o is zero, the compound state J of particular parity can be reached by only one of the two transmission coefficients in brackets.

The fission cross section given by Eq. 5 is derived by averaging many integrated Breit-Wigner cross sections of single resonances λ over a given energy interval. Experimentally, this energy interval corresponds to the energy resolution of the neutron beam and is very large compared to the average spacing between levels. The factor $S_{\alpha\alpha'}$ is a level width fluctuation correction factor given by,

$$S_{\alpha\alpha'} = \frac{\left\langle \dfrac{\Gamma^{(\alpha)}_{\lambda J\ell} \quad \Gamma^{(\alpha')}_{\lambda J\ell}}{\Gamma_{\lambda J}} \right\rangle}{\dfrac{\left\langle \Gamma^{(\alpha)}_{\lambda J\ell} \right\rangle \left\langle \Gamma^{(\alpha')}_{\lambda J\ell} \right\rangle}{\left\langle \Gamma_{\lambda J} \right\rangle}} \tag{6}$$

where $\Gamma^{(\alpha)}_{\lambda J\ell}$ is the partial width for entrance channel α, $\Gamma^{(\alpha')}_{\lambda J\ell}$ is the partial width for exit channel α', and $\Gamma_{\lambda J}$ is the total width of the resonance λ. In the calculation of $\sigma_f(J,K,\pi,E)$ we assume each of the neutron and fission partial widths has a χ^2 distribution with a single degree of freedom (for $\nu=1$, $S_{\alpha\alpha'}$ varies from 1 to 1/2 for $\alpha \neq \alpha'$ and from 1 to 3 for $\alpha=\alpha'$).

The various transmission coefficients in Eq. 5 are related to their respective average widths by

$$\left\langle \Gamma_{\lambda f} \; (J,\pi,K,E) \right\rangle = \frac{\left\langle D(J,\pi,E) \right\rangle}{2\pi} \, T_{\lambda f}(J,\pi,K,E) \tag{7}$$

$$\left\langle \Gamma_{\lambda n} \; (J,\pi,\ell,E) \right\rangle = \frac{\left\langle D(J,\pi,E) \right\rangle}{2\pi} \, T_{\lambda n}(J,\pi,\ell,E) \tag{8}$$

$$\left\langle \Gamma_{\lambda \gamma} \; (E) \right\rangle = \frac{\left\langle D(J,\pi,E) \right\rangle}{2\pi} \, T_{\lambda \gamma}(J,\pi,E) \tag{9}$$

where $\langle D(J,\pi,E)\rangle$ is the average spacing of levels in the compound nucleus with angular momentum J, parity π and excitation energy E. Note should be taken of the factor of 2 preceding $T_{\lambda f}$ (J,π,K,E) in the definition of R. This factor of 2 must be included (to account for double degeneracy) for all K states except K=0.

In the present calculations, the values of T_f (J,π,K,E) were computed from the equation [14,15]

$$T_f \; (J,\pi,K,E) = \frac{1}{1 + \exp\left\{2\pi\left[B_f(J,\pi,K) - E\right]/\hbar\omega(J,\pi,K)\right\}} \tag{10}$$

where B_f (J,π,K) is the fission barrier of state (J,π,K), E is the compound nucleus excitation energy, and $\hbar\omega$ (J,π,K) is a characteristic energy which defines the curvature of the barrier. The fission barrier heights of the rotational members of a particular K band in the transition nucleus are calculated with the expression,

$$B_f(J,\pi,K) = B_o(\pi,K) + \frac{\hbar^2}{2\mathcal{J}_\perp} \{J(J+1)-\alpha(-1)^{J+1/2}(J+1/2)\delta_{K,1/2}\} \quad (11)$$

where $B_o(\pi,K)$ is a constant for a particular (π,K) rotational band, $\mathcal{J}_\perp$, is an effective moment of inertia, α is the decoupling constant for K=1/2 bands and $\delta_{K,1/2}$ is the Kronecker delta. In most calculations, we assume $\hbar^2/2\mathcal{J}_\perp$ equal to 5 keV and $\alpha = 1$. The effect of the variation of these parameters on the partial fission width is small.

The neutron transmission coefficients were calculated with the optical model potential of Perey-Buck(16). The available levels(17) of the residual nucleus ^{236}U which were used in the calculation are given in Table II.

The gamma emission (radiation) channels are treated assuming dipole γ-ray emission and a statistical model of the nuclear level density. The quantity $\langle \Gamma_{\lambda\gamma}(E)\rangle$ is the average partial width for γ-ray decay of a compound state λ with total angular momentum J, parity π, and excitation energy E and $\langle D(J,\pi,E)\rangle$ is the average spacing of levels with total angular momentum J, parity π and excitation energy E.

TABLE II. LOW-LYING LEVELS IN ^{236}U

Energy (MeV)	Total angular momentum	Parity
0.000	0	+
0.045	2	+
0.149	4	+
0.312	6	+
(0.528) [a]	8	+
(0.688) [a]	1	-
(0.758) [a]	3	-
(0.795) [a]	10	+
(0.884) [a]	5	-
(0.908) [a]	0	+
0.953	2	+

[a] Assignment based on systematics.

The energy dependence of the average radiation width for dipole γ-ray emission may be calculated from the relation,

$$\langle\Gamma_{\lambda\gamma}(E)\rangle = C_1 \int_0^E \frac{\{\rho(J-1,E-\varepsilon)+\rho(J,E-\varepsilon)+\rho(J+1,E-\varepsilon)\}\varepsilon^3 d\varepsilon}{\rho(J,E)} \quad (12)$$

where E is the initial excitation energy and ε is the gamma ray energy. The spin and energy dependent level density is,

$$\rho(J,E) = C_2\ (2J+1)\ (E-\Delta)^{-2}\exp\{2a^{1/2}(E-\Delta)^{1/2}-(J+1/2)^2/2\sigma^2\} \quad (13)$$

The angular momentum dependence of the level densities in the numerator and denominator of Eq. 12 cancels approximately to give a radiation width which is independent of angular momentum, namely,

$$\langle\Gamma_{\lambda\gamma}(E)\rangle = C_1 \int_0^E \left[\frac{(E-\Delta-\varepsilon)^{-2}\exp\{2a^{1/2}(E-\Delta-\varepsilon)^{1/2}}{(E-\Delta)^{-2}\exp\{2a^{1/2}(E-\Delta)^{1/2}}\right] \varepsilon^3 d\varepsilon \quad (14)$$

If the energy factor preceding the exponential in the numerator is neglected, the right-hand side of Eq. 14 may be integrated to give,

$$\langle\Gamma_{\lambda\gamma}(E)\rangle = C_3\ X(E,a) = C_3\ \{x^4-10x^3+45x^2-105x+105\} \quad (15)$$

where $x = 2a^{1/2}\ (E-\Delta)^{1/2}$. In Eq. 12 to 15, C_1, C_2, C_3, Δ and a are constants. The constant a is the level density parameter defined by $a = \pi^2 g_o/6$, where g_o is the average number of single particle states per MeV, and Δ is an energy correction which accounts for the different nuclear types.

With the results of Eqs. 12 to 15, the spin and energy dependence of $T_{\lambda\gamma}(J,\pi,E)$ may be written in the following useful form,

$$T_{\lambda\gamma}(J,\pi,E) = \frac{2\pi\langle\Gamma_{\lambda\gamma}(E')\rangle}{\langle D(J',\pi,E')\rangle}\ \frac{X(E,a)}{X(E',a)}\ \frac{\rho(J,E)}{\rho(J',E)} \quad (16)$$

where $\langle\Gamma_{\lambda\gamma}(E')\rangle / \langle D(J',\pi,E')\rangle$ is the average radiation width divided by the average level spacing for levels of spin J' at excitation energy E'. From resonance neutron capture in even-even nuclei one obtains values [19] of $\langle\Gamma_{\lambda\gamma}(E')\rangle$ and $D(\frac{1}{2},+,E')$, where E' is the neutron binding energy. Experimental values of $T_{\lambda\gamma}(\frac{1}{2},+,E')$ calculted from the above quantities are plotted as points in Fig. 4. The solid line in Fig. 4 is calculated with Eq. 16 for $a=30\ \mathrm{MeV}^{-1}$ and $\Delta = 0.55$ MeV and a value of $T_{\lambda\gamma}(\frac{1}{2},+,5.3) = 0.019$. The energy dependence of $T_{\lambda\gamma}(J,\pi,E)$ is rather insensitive to X(E,a) and the neglect of the pre-exponential energy factor in the level density in the derivation of X(E,a) gives a negligible error. Values of $T_{\lambda\gamma}(J,\pi,E)$ may be calculated from the spin dependence of the level density (assume σ=6). The cross section for the radiation channels is relatively small and, hence, the results of the overall calculation are rather insensitive to the parameters assumed for the gamma-ray channels.

The actual calculations are done in the following manner. One or more states of particular K and π are chosen (the rotational members of the chosen K bands are always included). In addition, a range of values of $B_0(\pi,K)$ and $\hbar\omega(J,\pi,K)$ are chosen with appropriately chosen increments in each quantity. The computer program calculates in succession the

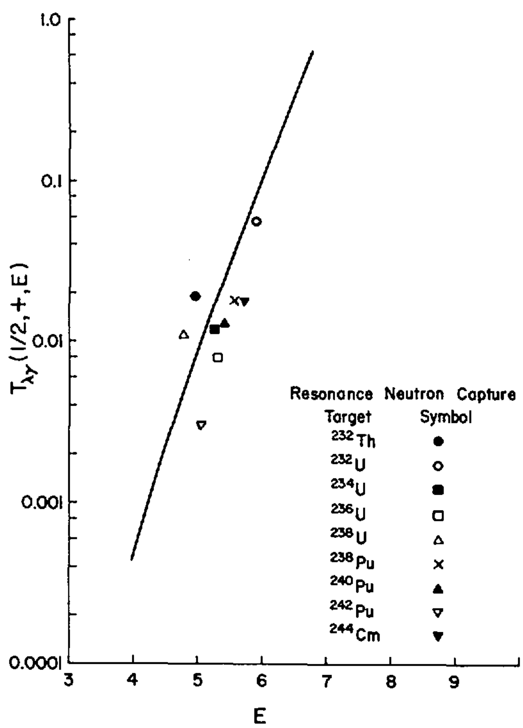

FIG. 4. Dependence of $T_{\lambda\gamma}(\frac{1}{2}, +, E)$ on the excitation energy E for an odd A heavy nucleus. The normalization is performed with the experimental values of $2\pi \langle \Gamma_{\lambda\gamma}(B_n)\rangle$ divided by $\langle D(\frac{1}{2}, +, B_n)\rangle$ for resonance capture on several nuclei listed on the figure. The data for resonance capture on ^{232}Th and ^{238}U are given greater weight since these isotopes have been studied more thoroughly. The solid line is calculated with Eq. (16) for a = 30 MeV^{-1} and Δ = 0.55 MeV.

theoretical values of $\sigma_f(E)$ and $W(\theta,E)$ for each combination of $B_0(\pi,K)$ and $\hbar\omega(J,\pi,K)$ and compares these values as a function of energy with the appropriate experimental values. Such a search can involve hundreds of calculations when two or more channels are included. As a guide in the quantitative evaluation of the agreement between the theoretical and experimental fission cross sections and angular distributions, we used a χ^2 criterion. Hence, for a chosen set of (K,π) states the values of $B_0(\pi,K)$ and $\hbar\omega(J,\pi,K)$ which give the best agreement with experiments are determined. Then another set of (K,π) states are chosen and the calculations repeated.

4. Results of the Calculations

The first set of calculations was performed for three neutron energies, 600, 700 and 800 keV, with five different combinations of two transition states. Each transition state is characterized by its values of (K,π), $B_o'(\pi,K)$ and $\hbar\omega$. The quantity $B_o'(\pi,K)$ is defined by the relation, $B_o'(\pi,K) = B_o(\pi,K)-B_n$, where B_n is the neutron binding energy and equal to 5.30 MeV. Each transition state is composed of a set of rotational levels and the fission barrier of each of these levels is calculated with Eq. 11. As mentioned previously, the neutron transmission coefficients are calculated with the optical model potential of Perey-Buck.(16) A value of 0.005 was used in the calculation for $T_{\lambda\gamma}(1/2,+,5.3)$ since this value reproduced the experimental values(19) of the (n,γ) cross section.

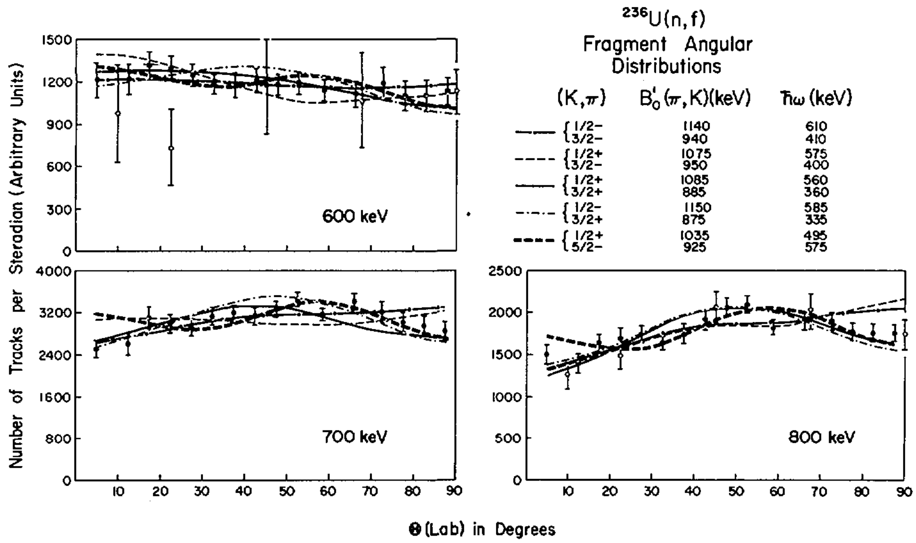

FIG. 5. Comparison of the experimental and theoretical fission-fragment angular distributions for neutron energies of 600, 700 and 800 keV with five different sets of transition states, $1/2^-$ and $3/2^-$; $1/2^+$ and $3/2^-$; $1/2^+$ and $3/2^+$; $1/2^-$ and $3/2^+$; $1/2^+$ and $5/2^-$. Each of these sets of transition states gives and excellent agreement between the experimental and theoretical fission cross-sections.

The comparison of the experimental and theoretical fission fragment angular distributions are shown in Fig. 5 for five sets of transition states, $1/2^-$, $3/2^-$; $1/2^+$,$3/2^-$; $1/2^+$,$3/2^+$; $1/2^-$,$3/2^+$; and $1/2^+$,$5/2^-$. The values of the energies of $B_o'(\pi,K)$ and $\hbar\omega(\pi,K)$ for each combination of transition states which give the best fit to the experimental fission cross sections and angular distributions are tabulated in Fig. 5. It is assumed that $\hbar\omega(\pi,K)$ is independent of J for a particular rotational band. With the energy parameters listed in Fig. 5, all five combinations of transition states give an excellent fit to the experimental fission cross sections

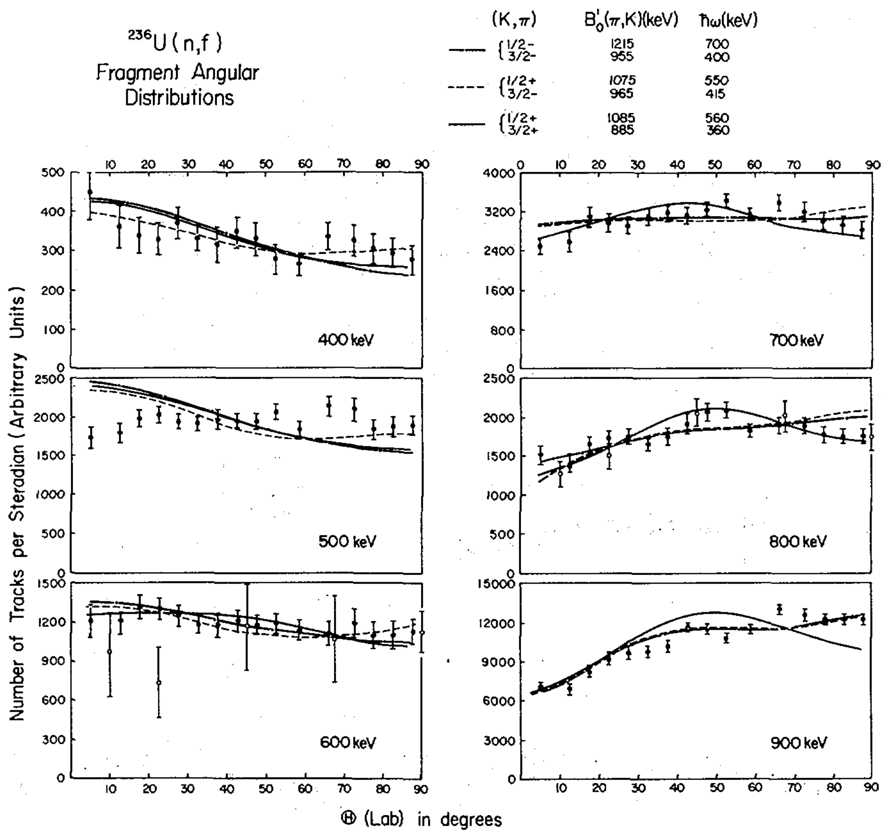

FIG. 6. Comparison of the experimental and theoretical fission-fragment angular distributions for neutron energies of 400, 500, 600, 700, 800 and 900 keV with three different sets of transition states, $1/2^-$ and $3/2^-$; $1/2^+$ and $3/2^-$; $1/2^+$ and $3/2^+$.

at 600, 700 and 800 keV neutron energies. Although the set of transition states $1/2^+$ and $3/2^+$ give the best agreement between the experimental and theoretical angular distributions for these three neutron energies, several of the other sets of transition states cannot be ruled out on the basis of the comparison shown in Fig. 5.

In Fig. 6, the experimental and theoretical angular distributions for six neutron energies are compared for three combinations of two transition states. The values of $B_0'(\pi,K)$ and $\hbar\omega$ for each combination of transition states are listed on the figure. The theoretical and experimental fission cross sections are compared in Fig. 7. With two transition states, one is able to account for the energy dependence of the neutron induced fission cross section of ^{236}U up to neutron energies of 900 keV. Although the theoretical cross section for the pair of transition states $1/2^+$ and $3/2^+$ is slightly low at 900 keV, this may be due to the fact that the transition parameters for this pair of states was taken from the previous fits of the three energies 600, 700 and 800 keV and a new search of the best parameters for the additional energies was not made. From the theoretical angular distributions plotted in Fig. 6, it can be seen that the $3/2^+$ transition state gives stronger peaking at intermediate angles than the $3/2^-$ state. Although the 800 keV experimental angular distribution data fit better with a pair of transition states which include a $3/2^+$ state, examination of the fits shown in Fig. 6 for all the neutron energies suggests that no unique parity assignments can be made from the present data.

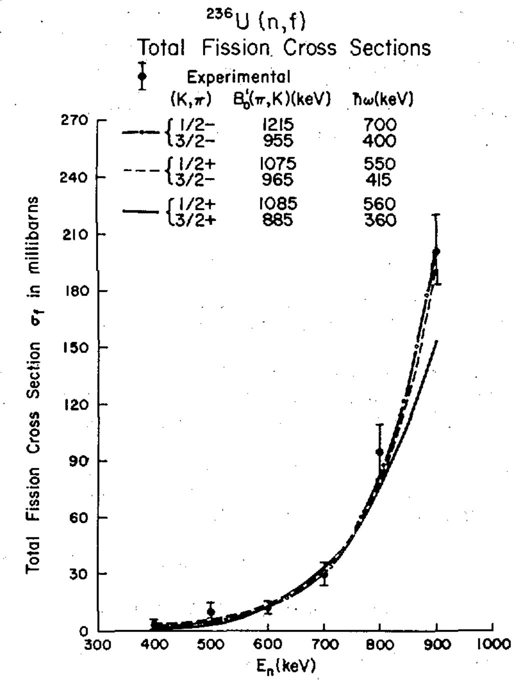

FIG. 7. Comparison of the experimental and theoretical fission-fragment cross-sections for neutron energies of 400, 500, 600, 700, 800, and 900 keV with three different sets of transition states, $1/2^-$ and $3/2^-$; $1/2^+$ and $3/2^-$; $1/2^+$ and $3/2^+$.

We conclude that the experimental fission cross sections and angular distributions for the $^{236}U(n,f)$ reaction are reasonably well explained up to neutron energies of 900 keV with two transition states, one with K=1/2 and one with K≥3/2. From our present data we are not able to make a unique (π,K) assignment for the states. The combinations of (π,K) values for the K≥3/2 state are limited to $3/2^-$, $3/2^+$ and $5/2^-$. The fission barrier energies for the two states are $B_0'(\pi,K=1/2) = 1150 \pm 100$ keV and $B_0'(\pi,K\geq 3/2) = 925 \pm 50$ keV. In order to obtain the corresponding values of $B_0(\pi,K)$ defined in Eq. 11, one must add the value of the neutron binding energy which is equal to 5.30 MeV. If the data are to be fitted with two states, the value of $\hbar\omega$ for the 1/2 state needs to be considerably larger than for the $K \geq 3/2$ state. Although somewhat superior fits may be obtained by adding one or more additional transition states, we have adopted the working philosophy that a minimum number of states be used in the fitting. The experimental angular distribution peaks at forward angles again for the 1100 keV data and this result may be theoretically reproduced by adding one or more K=1/2 states.

The present results indicate that the energy dependence of the fission cross section and angular distribution is due to a single barrier. In the present two-humped barrier picture, this is interpreted to mean that the second barrier is the higher one. If the first barrier were the higher one controlling the energy dependent cross section, one might expect that the angular distributions would exhibit statistical character and not show the definite intermediate angle peaking observed at some energies.

REFERENCES

[1] BOHR, A. Int. Conf. peaceful Uses atom. Energy (Proc. Conf. Geneva, 1955) 2 UN, Geneva (1955), 151.

[2] WIGNER, E.P., (translated by GRIFFIN, J.J.), "Group Theory and its application to quantum mechanics of atomic spectra," Academic Press, New York (1959).

[3] WHEELER, J.A., "Fast Neutron Physics, Part II," (MARION,J.B. and FOWLER, J.L., Eds.), Interscience Publishers, New York (1963) 2051.

[4] HAUSER, W., FESHBACH, H., Phys. Rev. 87 (1952) 366.

[5] VANDENBOSCH, R., Nucl. Phys. A101 (1967) 460.

[6] BEHKAMI, A.N., ROBERTS, J.H., LOVELAND, W., HUIZENGA J.R., Phys. Rev. 171 (1968) 1267.

[7] BEHKAMI, A.N., HUIZENGA, J.R., ROBERTS, J.H., Nucl. Phys. A118 (1968) 65.

[8] STRUTINSKY, V.M., Nucl. Phys. A95 (1967) 420.

[9] MIGNECO, E., THEOBALD, J.P., Neutron Cross Sections and Technology (GOLDMAN, D.T., Ed.), NBS Special Publication 299, Vol. 1 (1968) 527.

[10] MICHAUDON, A., Neutron Cross Sections and Technology (GOLDMAN, D.T., Ed.), NBS Special Publication 299, Vol. 1 (1968) 427.

[11] LARK, N. Proceedings of the International Symposium on Nuclear Structure, Dubna, USSR, July (1968).

[12] LAMPHERE, R.W., "Physics and Chemistry of Fission" IAEA, Vienna, (1965), V1 63.

[13] SIMMONS, J.E., HENKEL, R.L., Phys. Rev. 120 (1960) 198.

[14] HILL, D.L., WHEELER, J.A., Phys. Rev. 89 (1953) 1102.

[15] LANDAU, L.D., LIFSHITZ (translated by SYKES, J.B., BELL, J.S.) "Quantum Mechanics," Pergamon Press, London (1965) 2nd Edition, p. 176.

[16] AUERBACH, E., PEREY, F., Brookhaven National Laboratory Report No. BNL-765 (T-286), (1962) unpublished.

[17] LEDERER, C.M., HOLLANDER, J.M., PERLMAN,I., "Table of Isotopes" (Sixth Edition) John Wiley and Sons, Inc. New York (1968).

[18] MOLDAUER, P.A., ENGELBRECHT, C.A., DUFFY, G.J., Argonne National Laboratory Report No. ANL-6978, (1964) unpublished.

[19] HUGHES, D.J., SCHWARTZ, R.B., "Neutron Cross Sections" Brookhaven National Laboratory Report BNL-325 (1958) and Second Edition (1965).

DISCUSSION

H.C. BRITT: I would like to comment that in the general case a conclusion as to the relative heights of the two barriers based on a correlation or lack of a correlation between structure in the fission cross-section and angular correlation coefficients is risky. In the case of the barriers used for calculating the distributions we presented, the first barrier was about 0.7 MeV higher than the second, but from the calculation we still see correlated structure in the fission cross-section and angular correlation coefficients. The sharp structure is produced by the low, broad second barrier, and the high, sharp first barrier simply modulates the cross-section. Thus, I would caution against drawing conclusions from the qualitative aspects of the data. The actual situations may be very complicated.

J.R. HUIZENGA: I agree completely with this comment. If the second barrier is lower than the first and no mechanism exists for mixing the K-states, then the original K-values will be conversed through the whole fission process. Hence, the observation of structure is in no way a strong argument for the second barrier being higher. I should like to emphasize the reverse situation as well. The experimental observation of forward peaking and smooth fission-fragment angular distributions is by no means a strong argument for the second barrier being lower than the first barrier.

J.R. NIX: You say that you have used a one-peaked barrier rather than a two-peaked barrier in order not to introduce additional parameters. But you have other additional parameters in the form of a different barrier curvature for each transition state. Is it not possible that the substantially different value of $\hbar\omega$ that you obtain for the individual transition states is a spurious result arising from the use of a one-peaked rather than a two-peaked barrier?

J.R. HUIZENGA: This may be the case. The additional parameters introduced with two-humped barriers may well enable us to make fits with a common value of $\hbar\omega$ and I agree that this should be tried. However, this discussion points out that the whole procedure of extracting information on transition states is somewhat arbitrary at present when such choices must be made without other information.

R. VANDENBOSCH: I agree with Nix that some of the fluctuations in the $\hbar\omega$ values obtained in previous analyses may be attributed to the structure associated with a double barrier. But I would also say that there are good theoretical reasons to believe that the $\hbar\omega$ values for different channels in odd-A nuclei need not be identical.

I would also like to ask a question of Dr. Strutinsky or Dr. Bjørnholm. They have suggested that the disappearance of structure in anisotropy for the heavier odd-A and odd-odd nuclei is evidence for the right-hand barrier becoming lower than the left-hand barrier. This implies strong K-mixing beyond the first barrier. On the other hand, the structure in anisotropy in Britt's ^{240}Pu results suggests less mixing. Do you think there are theoretical reasons for K-mixing to depend strongly on the even-odd character of the nucleus?

V.M. STRUTINSKY: There is a tendency now to relate some of what used to be regarded as barrier channel structure in the (d, pf) reactions to the sub-barrier resonances. This may partly explain the difference. Generally, stronger mixing is to be expected in the odd-A and odd-odd nuclei, where more states may contribute. However, we still do not know much about the non-adiabaticity effects which produce non-purity of the K-values. This is one of the interesting problems that need investigation.

J.R. HUIZENGA: I would like to ask Dr. Strutinsky or anyone else from the USSR if measurements of the full angular distribution of neutron-induced fission of the plutonium isotopes have been made in the USSR. Or have only the 0°/90° ratios been measured?

V.M. STRUTINSKY: The anisotropy data I quoted in paper SM-122/203 were extracted from the detailed angular distribution data, in particular those that were obtained recently in Obninsk (USSR). Their results are discussed in detail in paper SM-122/134.

N. VÎLCOV: I want to make a short comment on whether it is possible to distinguish which of the two peaks of the two-humped barrier is higher. There is another way, namely analysis of the excitation function shape in the (n, γ) reactions. As was shown in the case of the ^{241}Am (n, γ) ^{242mf}Am reaction, studied by our group in Bucharest, the excitation function can be peaked only if the first barrier is higher than the second. I think this can be a more general way of obtaining valuable information on the relative heights of the two barriers.

УГЛОВАЯ АНИЗОТРОПИЯ И СТРУКТУРА БАРЬЕРА ДЕЛЕНИЯ

Х.Д.АНДРОСЕНКО, С.Б.ЕРМАГАМБЕТОВ, А.В. ИГНАТЮК,
Н.С.РАБОТНОВ, Г.Н.СМИРЕНКИН, А.С.СОЛДАТОВ,
Л.Н.УСАЧЕВ, Д.Л.ШПАК
Физико-энергетический институт, Обнинск,
Союз Советских Социалистических Республик

С.П.КАПИЦА, Ю.М.ЦИПЕНЮК
Институт физических проблем, Москва,
Союз Советских Социалистических Республик

И.КОВАЧ
Центральный институт физических исследований, Будапешт,
Венгерская Народная Республика

Abstract — Аннотация

ANGULAR ANISOTROPY AND THE STRUCTURE OF THE FISSION BARRIER. The authors report on measurements of the angular distributions of fragments produced in the neutron-induced fission of ^{232}Th, ^{238}U, ^{237}Np, ^{238}Pu, ^{240}Pu, ^{242}Pu and ^{241}Am target nuclei and photon-induced fission of ^{232}Th, ^{238}U, ^{238}Pu, ^{240}Pu and ^{242}Pu target nuclei. The (n, f) reaction was investigated using electrostatic generators of the Institute of Physics and Power Engineering, while the photofission reaction was studied with the help of the 12-MeV mictrotron at the Institute of Physical Problems. Particular attention is paid to excitation energies near the threshold. The experimental data do not fit the traditional picture of fission probability, but can be satisfactorily explained in terms of double-humped barrier concepts. In discussing the results of the measurements, the authors touch on the quasi-stationary states of the nucleus in the second valley, the structure of barriers, even-odd differences in fission probability, and the question of the penetration probability at certain energies in the case of highly deformed nuclei.

УГЛОВАЯ АНИЗОТРОПИЯ И СТРУКТУРА БАРЬЕРА ДЕЛЕНИЯ. Сообщаются результаты измерений угловых распределений осколков деления нейтронами ядер – мишеней ^{232}Th, ^{238}U, ^{237}Np, ^{238}Pu, ^{240}Pu, ^{242}Pu, ^{241}Am и фотонами – ^{232}Th, ^{238}U, ^{238}Pu, ^{240}Pu, ^{242}Pu. Исследования реакции (n, f) производились на электростатических генераторах ФЭИ, фотоделения – на микротроне ИФП АН СССР на 12 Мэв. Главное внимание уделено изучению околопороговой области энергий возбуждения. Полученные экспериментальные данные не укладываются в рамки традиционного описания вероятности деления, но получают удовлетворительное объяснение с помощью представлений о двугорбом барьере. В связи с обсуждением результатов выполненных измерений затронуты вопросы о квазистационарных состояниях ядра во второй яме, о структуре барьеров, о четно – нечетных различиях вероятности делений и энергетической щели ядра при больших деформациях.

Угловая анизотропия разлета осколков деления является следствием преимущественной ориентации углового момента ядра $\vec{I}$ относительно пучка бомбардирующих частиц и неоднородности распределения проекций момента K на ось симметрии (направление разделения). Реализующийся спектр f(K) зависит от энергии возбуждения в переходном состоянии $E^* = E - E_f$ и способа возбуждения, определяющего доступный набор угловых моментов. Специальный интерес представляет область малых E^*, когда ядро – холодное и в делении участвует небольшое число переходных квантовых состояний – каналов деления [1,2]. С дискретностью спектра нижайших каналов деления связывается появление сложной структуры в энергетической зависимости угловых распределений осколков $W(\upsilon)$ вблизи порога, наблюдаемого в сечении σ_f .

Исследования околопорогового деления ядер обнаружили ряд качественных эффектов, свидетельствующих о плодотворности идей модели каналов деления. Наиболее важными представляются результаты изучения четно — четных делящихся ядер, применительно к которым данная модель, использующая для спектра каналов деления аналогию со спектрами возбужденных равновесных состояний, ведет к конкретным следствиям. Ожидаемая квантовая структура барьера наблюдалась при изучении фотоделения [3] и реакций типа (d,pf) [4,5] .

Однако более подробные эксперименты и детальный количественный анализ энергетической зависимости угловой анизотропии [6 — 10] выявили неполноту традиционного описания деления ядер вблизи порога [1,2] . Объяснение ряда свойств и явлений, не укладывающихся в рамки общепринятой концепции Н.Бора — Уилера — О.Бора, в том числе и угловой анизотропии, стало возможным благодаря пересмотру представлений о форме барьера деления. В 1967 году Струтинским [11] были осуществлены расчеты потенциальной энергии деформации ядра с учетом оболочечных эффектов, показавшие значительные отступления формы барьера деления от параболической, которая мотивировалась моделью жидкой капли. Согласно [11] , реальный барьер деления в обычно используемом одномерном представлении имеет форму кривой с двумя максимумами. Физические идеи, связанные с новыми представлениями о форме барьера и квазистационарными состояниями в яме между максимумами [12, 13] , дали начало так называемой модели двугорбого барьера деления.

Данная работа посвящена исследованию актуальных вопросов, связанных с угловой анизотропией и структурой барьера деления. Экспериментальная часть работы включает в себя некоторые результаты измерений, выполненных в последние годы с моноэнергетическими нейтронами на электростатических генераторах ФЭИ и с фотонами тормозного излучения на микротроне ИФП АН СССР.

Большинство представленных данных получено с помощью трековой методики.

Здесь мы не ставим перед собой задачу детального описания экспериментов и их результатов. Это будет сделано позднее. Цель данного сообщения — продемонстрировать недостаточность традиционного описания угловой анизотропии деления и обсудить возможность его уточнения на основе модели двугорбого барьера.

I. ЭКСПЕРИМЕНТАЛЬНЫЕ РЕЗУЛЬТАТЫ И СЛЕДСТВИЯ

А. Деление $^{232}Th(n,f)$ вблизи порога

Результаты измерений сечения деления σ_f [14] и угловых распределений осколков $W(\upsilon)$ представлены на рис. 1 и 2. Кривые на рис. 2 — $W(\upsilon) = \sum_{n=0}^{3} a_{2n} P_{2n}(\cos \upsilon)$, где $P_{2n}(\cos \upsilon)$ — полиномы Лежандра, рассчитаны с помощью метода наименьших квадратов. Данные об угловой анизотропии $\frac{W(0^\circ)}{W(90^\circ)}$ изображены на вставке к рис. 1, где они сравниваются

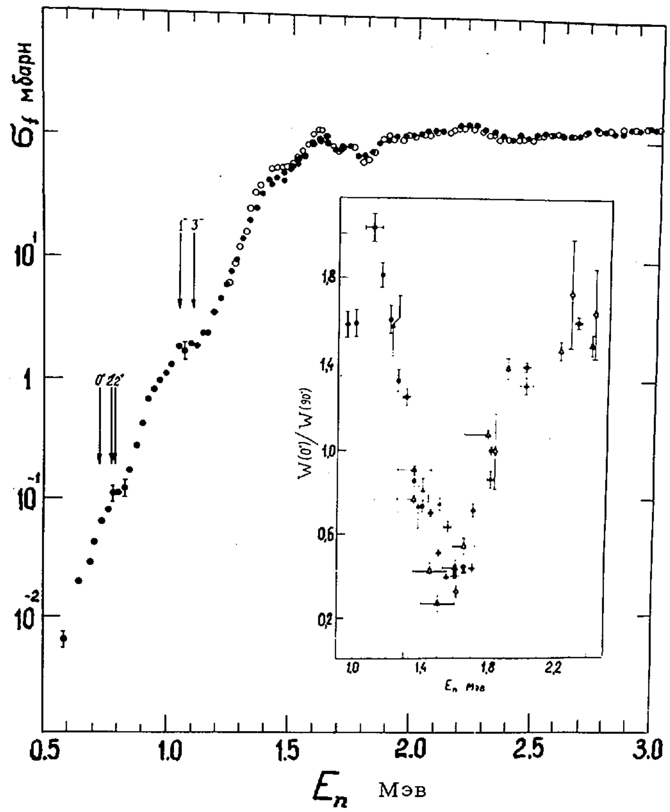

Рис. 1. Зависимость сечения деления ^{232}Th от энергии нейтронов E_n: — • — [14], ○ — данные Атласа нейтронных сечений. На вставке — угловая анизотропия: • — данная работа, △ — [8], △,◇ — [15].

с результатами других измерений [8,15,16]. Угловые распределения, измеренные разными авторами [15,16], согласуются между собой хуже, чем данные об угловой анизотропии.

Задачей данного эксперимента было получение подробной информации о σ_f и $\frac{d\sigma_f(\upsilon)}{d\Omega} \sim W(\upsilon)$ для каналового анализа. Идентификация преобладающих каналов деления K^{π} и восстановление энергетической зависимости проницаемости барьеров $P_{K^{\pi}}(E_n)$ производились, как обычно, путем эмпирического подбора таких квантовых характеристик, которые бы обеспечивали согласие расчета

$$\frac{d\sigma_f(\upsilon,E_n)}{d\Omega} \approx \frac{\lambda\!\!\!^{-2}(E_n)}{4}\sum_{I,K,\pi}(2I+1)\,T_l^I(E_n)\,\frac{P_{K\pi}(E_n)\,\gamma_{IK}}{\sum\limits_{l',j',m} T_{l'}^{j'}(E_n - E_m)}\,W_{IK}(\upsilon) \qquad (1)$$

с экспериментом. В выражении (1) мы пренебрегли в знаменателе делительной Γ_f и радиационной Γ_γ ширинами по сравнению с нейтронной шири-

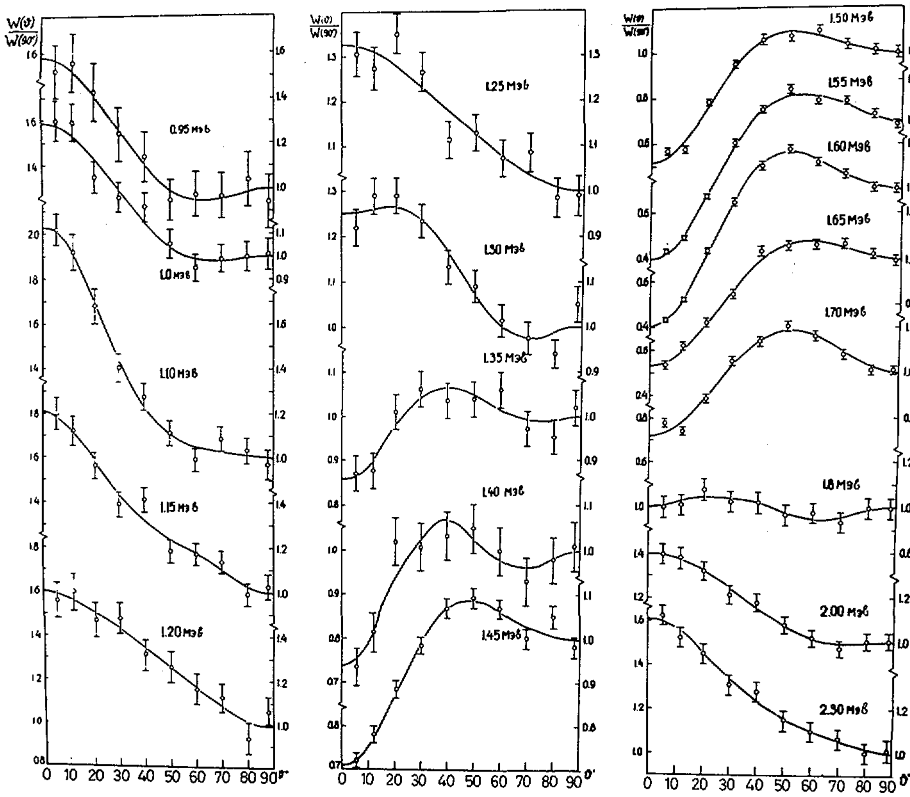

Рис. 2. Угловые распределения осколков деления ^{232}Th нейтронами.

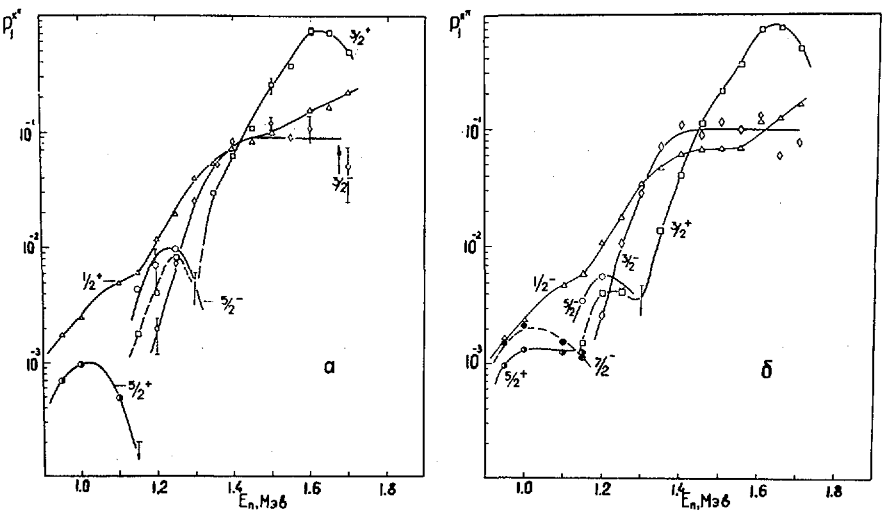

Рис. 3. Зависимость проницаемости барьера деления ^{232}Th (n,f) от энергии нейтронов E_n для различных квантовых состояний ядра K^{π}: (a) – в предположении, что четность каналов K = 1/2 положительна, (b) – отрицательна (см. текст).

ной $\Gamma_n \sim \sum_{l;j;m} T_{l'}^{j'}(E_n - E_m)$; λ – длина волны нейтрона; T_l^j – оптические коэффициенты проницаемости нейтронов [17] ; $\pi = (-1)^l$; индекс m – нумерует уровни ядра – мишени; γ_{IK} – учитывает зависимость проницаемости барьера деления от полного углового момента I в соответствии с обычно принимаемым предположением, что различия $P_{K\pi}$ для разных I сводятся к вычитанию энергии вращения $E_{rot} = \frac{\hbar^2}{2\mathcal{J}}\left[I(I+1) - K(K+1)\right]$ из энергии, концентрирующейся в делительных степенях свободы (в расчетах принималось $\frac{\hbar^2}{2\mathcal{J}} = 4$ кэв).

Классическая схема каналового анализа [2] состоит в отыскании высоты барьера $E_f^{K\pi}$ и параметра кривизны $\hbar\omega_{K\pi}$, связанных с $P_{K\pi}(E_n)$ известным соотношением Хилла – Уилера для параболического барьера:

$$P_{K\pi}(E_n) = \left[1 + \exp\left(2\pi\,\frac{E_f^{K\pi} - E_n - B_n}{\hbar\omega_{K\pi}}\right)\right] \qquad (2)$$

где B_n – энергия связи нейтрона.

Такие расчеты были осуществлены для реакций ^{232}Th (n,f) [16] и ^{234}U (n,f) [18] , однако они не дают детального описания хода $\sigma_f(E_n)$, так как выражение (2) монотонно зависит от E_n и игнорирует резонансные явления, отмеченные в [6,7] . В данной работе анализ производился способом, предложенным Воротниковым [6] , в котором никаких ограничений на энергетическую зависимость $P_{K\pi}(E_n)$ не накладывается.

Отметим наиболее важные результаты анализа:

а) При всех E_n удается добиться согласия расчета $W(\upsilon)$ с опытом в пределах коридора экспериментальных ошибок, используя лишь две – три комбинации доминирующих состояний K^π . Основной качественной чертой реализующегося спектра K^π является резкое изменение в узком интервале энергий $E_n \sim 0{,}1 - 0{,}2$ Мэв роли отдельных состояний (вступление и исчезновение), что свидетельствует о нерегулярном "резонансном" поведении $P_{K\pi}(E_n)$, не согласующемся с (2).

б) Идентификации даже преобладающих каналов деления свойственна неоднозначность. Не удается определить четность состояний $K = 1/2$, вносящих значительный вклад при всех изученных энергиях; трудно различить состояния $K^\pi = 3/2^+$ и $5/2^-$, $5/2^+$ и $7/2^-$, соответственно. По этой причине на рис.3 приводятся два варианта результатов анализа для $K^\pi = 1/2^+$ (а) и $1/2^-$ (б), а на каждом из этих рисунков в отдельных областях E_n – по две возможности $P_{K\pi}$, дающих примерно одинаковое согласие с опытом (пунктирная и сплошная кривые). Источником ошибок может явиться также неопределенность параметра $\hbar^2/2\mathcal{J}$. Однако, к отсутствию детальной информации об уровнях ядра – мишени выше 1,2 Мэв идентификация K^π (но не абсолютная величина $P_{K\pi}$) нечувствительна.

в) Благоприятным обстоятельством является тот факт, что к неопределенности идентификации квантовых характеристик каналов некритичен главный результат анализа: наличие резонансов $P_{K\pi}(E_n)$ с шириной порядка 0,1 Мэв. Нерегулярности $\sigma_f(E_n)$ в районе 1,1 и 1,6 Мэв связаны с резонансами $P_{\frac{1}{2}\pi}$ и $P_{\frac{3}{2}\pi}$,соответственно; привлекавшееся прежде традиционное объяснение конкуренцией нейтронной ширины [2] в этих случаях неприемлемо. Величина $P_{\frac{1}{2}\pi}(0)$, полученная путем экспоненциальной экстраполяции к $E_n = 0$, сильно расходится с проницаемостью, оцененной по сечению деления ^{232}Th тепловыми нейтронами [19] . Последняя более чем в тысячу раз превосходит экстраполированное значение [14]. Этот факт показывает, что нерегулярное изменение проницаемости барьера сохраняется в глубоко подбарьерной области возбуждений. Наиболее яркая картина резонансных эффектов P(E) наблюдалась в работе [20].

Б. Деление ^{238}U, ^{237}Np, ^{238}Pu, ^{240}Pu, ^{242}Pu, ^{241}Am нейтронами

Измерение угловых распределений осколков деления ^{238}U, ^{240}Pu, ^{242}Pu выполнены преимущественно в околопороговой области энергий нейтронов, для ^{237}Np, ^{238}Pu, ^{241}Am – вплоть до порога (n,nf) – реакции. Коэффициент угловой анизотропии $A = \frac{W(0°)}{W(90°)} - 1$ для пяти ядер-мишеней изображен на рис.4. Для трех из них ^{238}Pu (≈ 85%), ^{240}Pu (≈ 93%) и ^{242}Pu (≈ 95%) точность измерений в подпороговой области лимитировалась изотопными примесями.

Общим свойством исследованных ядер является практически полное отсутствие каналовых эффектов в угловом распределении осколков. Полученные для изотопов Np, Pu, Am угловые распределения при всех энергиях, в том числе и под порогом, хорошо описываются простым выражением:

$$\frac{W(\upsilon)}{W(90°)} = 1 + A\,\mathrm{Cos}^2\upsilon \qquad (3)$$

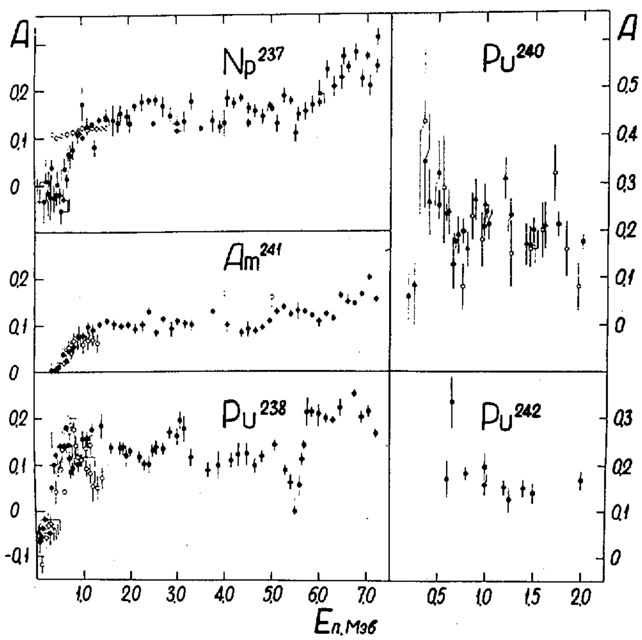

Рис. 4. Зависимость коэффициента угловой анизотропии деления от энергии нейтронов для ядер-мишеней ^{237}Np: ○ – [21], ■ – [22]; ^{241}Am: ○ – [23]; ^{238}Pu: ○ – [24]; ^{240}Pu: □ – [25], ▲ – [8], ■ – [26]; ^{242}Pu: ■ – [26]. Для всех ядер: ● – данные настоящей работы.

Соответствие анизотропной части $W(\upsilon)$ квадратичной зависимости от $\cos\upsilon$ при достаточных возбуждениях обычно рассматривается как признак статистического распределения K [27] :

$$f(\kappa) \sim \exp\left(-\frac{K^2}{2K_0^2}\right) \tag{4}$$

Для описания $W(\upsilon)$ в этом случае широко используется соотношение статистической теории

$$W(\upsilon) \sim \sin^{-3}\upsilon \int_0^{p\sin^2\upsilon} x^{1/2}e^{-x}I_0(x)\,dx = \sin^{-3}\upsilon\ \varphi(p\sin^2\upsilon) \tag{5}$$

при малом $p = \frac{\langle I^2 \rangle}{2K_o^2}$, т.е. малой анизотропии, переходящее в (3). У обсуждаемых ядер $A \le 0{,}2$.

Тем не менее, соответствие экспериментальных данных о $W(\upsilon)$ соотношению (3) в реакции (n, f) без дополнительного анализа нельзя рассматривать как достаточный признак распределения (4). Дело в том, что зависимость (3) выполняется при любом спектре каналов для малых энергий $E_n \le 0{,}5$ Мэв, когда в сечении образования составного ядра доминируют волны с $l \le 1$. Лишь вклад более высоких угловых моментов приводит к отступлениям от (3).

Убедимся на примере ^{238}Pu(n,f), что экспериментальные угловые распределения осколков нельзя объяснить, привлекая малое число состояний K^π . Эта реакция еще интересна и тем, что для нее в работе [24] был выполнен каналовый анализ, приведший к противоположному выводу. Согласно [24] , деление ^{238}Pu нейтронами имеет порог при $E_n \approx 0{,}8 - 1{,}0$ Мэв и происходит вплоть до 1,5 Мэв преимущественно через два типа состояний $K^\pi = 1/2^-$ и $3/2^-$. На рис.5, полученные нами экспериментальные распределения сравниваются с расчетом, произведенным по использованной выше схеме при анализе реакции ^{232}Th(n,f). Иные простые комбинации K^π дают еще большее расхождение с опытом.

Яркая демонстрация участия в делении тяжелых ядер вблизи порога большого числа состояний была получена при изучении реакции ^{238}U(n,f) [9] . Коэффициент угловой анизотропии согласуется с данными Лэмфира [8] и достигает 0,6. В этом случае приближение (3) не является удовлетворительным, и для проверки гипотезы (4) необходимо пользоваться выражением (5). Наиболее интересная часть экспериментальных данных изображена на рис.6 в компактном представлении, использующем, согласно (5), тот факт, что

$$\frac{W(0^\circ)}{W(\upsilon)} = \frac{2}{3}\,\frac{(p\sin^2\upsilon)^{3/2}}{\varphi(p\sin^2\upsilon)} \tag{6}$$

зависит от единственного параметра $x = p\sin^2\upsilon$. Правая часть (6), как показано на рис.6 , при $p \le 1$ с хорошей точностью линейно зависит от x. Таким образом, деление ^{238}U(n,f) под порогом на 0,5 – 0,7 Мэв происходит так, как если бы в нем принимало участие значительное число каналов.

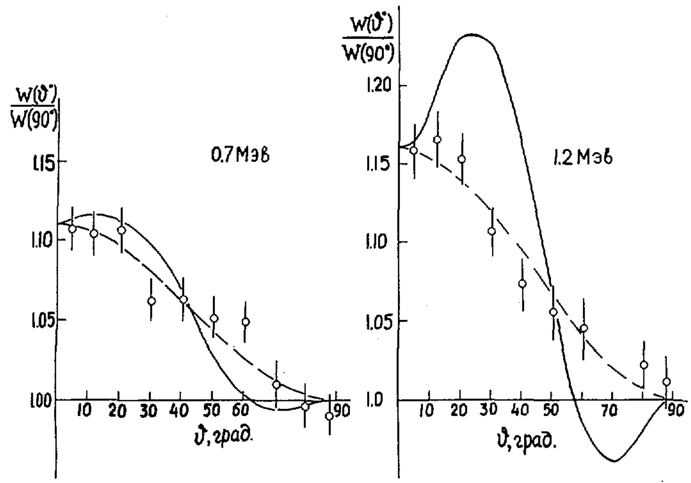

Рис. 5. Угловые распределения осколков при делении ^{238}Pu нейтронами: ○ – [9], кривые – расчет (см. текст).

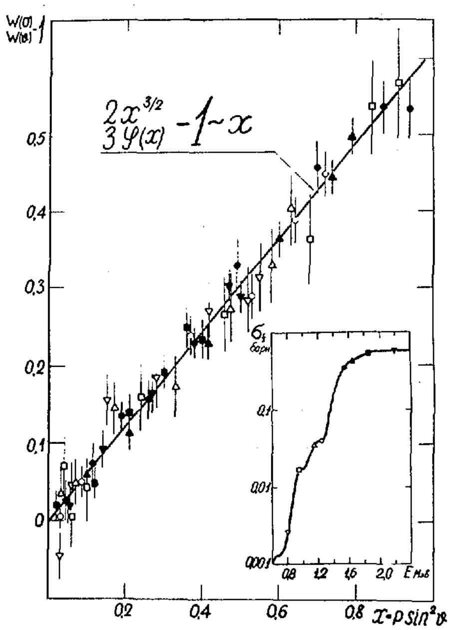

Рис. 6. Сопоставление экспериментальных данных о W(υ) ^{238}U с выражением (5) статистической теории угловых распределений осколков деления (см. текст).
На вставке – энергетическая зависимость сечения деления $\sigma_f(E_n)$ ^{238}U нейтронами.
Обозначения : ▽ – 0,8 Мэв, □ – 0,95 Мэв; △ – 1,15 Мэв, ○ – 1,25 Мэв, ● – 1,55 Мэв, ▲ – 1,65 Мэв, ■ – 1,85 Мэв, ▼ – 2,2 Мэв.

Резкое изменение характера и зависимости от энергии углового распределения осколков при увеличении числа нуклонов на несколько единиц в области, где свойства равновесных ядер изменяются мало, удивительно. Никаких ограничений по A и Z на реализацию каналовых эффектов для ядер с одинаковой четностью числа нуклонов модель О.Бора не накладывает.

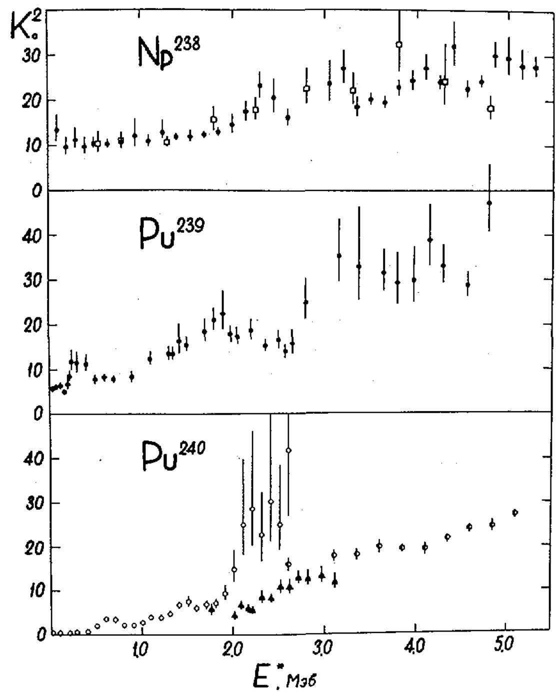

Рис. 7. Зависимость параметра K_0^2 от энергии возбуждения E^* для делящихся ядер ^{238}Np, ^{239}Pu, ^{240}Pu.
На нижнем рисунке: o – [5] , ● – [28] , ▲ – [29] .

Интерес представляет также немонотонный характер энергетической зависимости угловой анизотропии при значительных возбуждениях, где справедливость статистического описания не вызывает сомнения. Определенная из данных об угловой анизотропии (на рис.4) энергетическая зависимость K_0^2 (E^*) для составных ядер – нечетно – нечетного ^{238}Np и нечетного ^{239}Pu – сравнивается на рис.7 с аналогичной зависимостью для четно – четного ядра ^{240}Pu, делящегося в реакциях ^{239}Pu(d,pf) [4,5] и ^{239}Pu (n,f) [28,29] . Энергия возбуждения в первых двух случаях вычислена как разность $E_n - E_{nf}$, где E_{nf} – энергия нейтронов, при которой наблюдается порог в сечении деления.

Наличие ступенчатой структуры в ходе K_0^2 (E^*) ^{240}Pu в работе [4] и ряде последующих работ [5,29] было истолковано как следствие энергетической щели 2Δ в спектре внутренних возбуждений. Основываясь на оценке скачка K_0^2 ,

$$\delta K_0^2 = 2\langle K_p^2\rangle = \frac{N(N+1)}{3} \approx 20 \qquad (7)$$

связанного с разрывом пары нуклонов, авторы [4] для переходного состояния получили величину $\Delta f \approx 1{,}3$ Мэв, почти вдвое превосходящую равновесное значение $\Delta_o \approx 0{,}7$ Мэв. В (7)$\langle K_p^2 \rangle$, равное значению K_o^2 для одной неспаренной частицы, оценено как среднее по всем одночастичным уровням последней незаполненной оболочки с полным квантовым числом $N = 7$-8. Анализ энергетической зависимости K_o^2 (E^*) в более широкой области возбуждений до 30 Мэв привел Гриффина [28] к заключению, что критическая энергия фазового перехода E^*_{kp} из сверхтекучего состояния в ферми – газовое составляет примерно 19 Мэв, что также соответствует аномально высокому значению $\Delta_f \approx 1{,}2$ Мэв.

В дальнейшем интерпретация скачкообразной зависимости $K_o^2(E^*)$ при низких возбуждениях и надежность определения Δ_f, E^*_{kp} и $\langle K_p^2 \rangle$ были подвергнуты сомнению [30,31]. Пересмотр анализа [28] привел в работе [31] к существенно более низким значениям $E^*_{kp} = 9{,}5 \pm 3$ Мэв и $\Delta_f = 0{,}77 \pm 0{,}15$ Мэв, близким к равновесным. K_o^2, как следует из рис.7, при $E^* \to 0$ (^{238}Np и ^{239}Pu) стремится к значениям, соответствующим $\langle K_p^2 \rangle \approx 5$, а не ≈ 10, как по оценке (7), см. также [29]. Из рис.7 видно, что уменьшение $\langle K_p^2 \rangle$ вдвое при значительном разбросе данных о K_o^2 для ^{242}Pu ведет к большой неопределенности установления величины Δ_f. Наконец, из-за наличия ступенчатой структуры K_o^2 (E^*) у ^{238}Np и ^{239}Pu, спектр переходных состояний которых не имеет энергетической щели, неочевидной становится сама возможность определения Δ_f по величине скачка δK_o^2 (7).

Отказ от предположения об аномальной величине энергетической щели делает необходимым переосмысливание физической природы четно – нечетных различий для барьеров деления. Во многих работах, в особенности, посвященных систематизации экспериментальных данных о периодах спонтанного деления и высоте барьеров, различия четных и нечетных

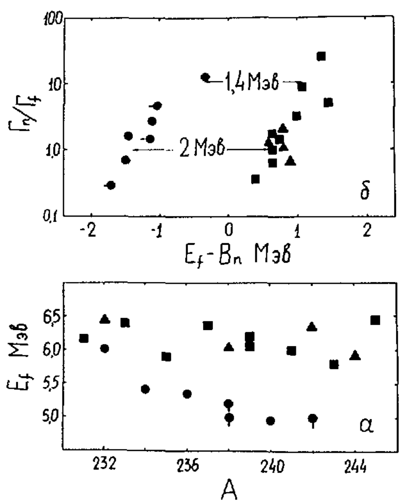

Рис. 8. а) Пороги вынужденного деления четно-четных – ●, нечетных – ■ и нечетно-нечетных – ▲ ядер;

б) Отношение средних нейтронной и делительной ширин Γ_n / Γ_f в зависимости от разности $E_f - B_n$. Обозначения те же, что и для а).

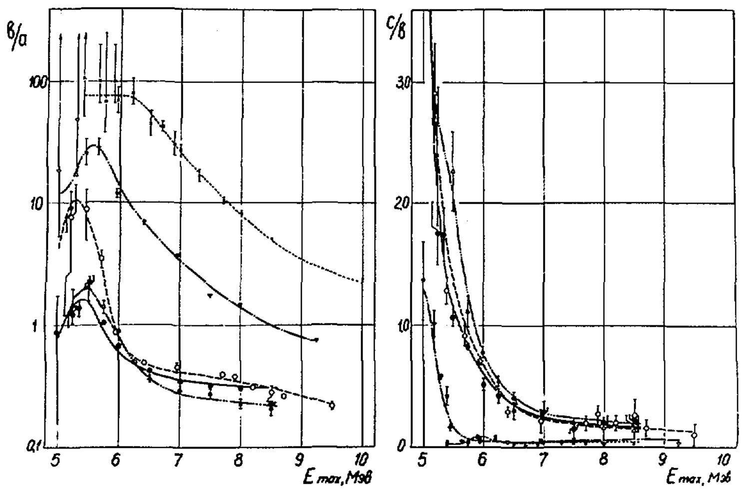

Рис. 9. Отношения коэффициентов b/a и c/b в зависимости от E_{max}(x – для ^{232}Th; ∇ – для ^{238}U; Δ – для ^{238}Pu; ○ – для ^{240}Pu; • – для ^{242}Pu).

ядер связываются с разностью энергетических поверхностей в переходном и равновесном состояниях, т.е. $\Delta_f - \Delta_o$. Примеры таких систематик [33] представлены на рис.8. В них использованы значения E_f, как обычно, определенные для четно – четных делящихся ядер из каналового анализа угловой анизотропии деления в (d,pf) и (γ,f) – реакциях [5,10] (см.ниже таблицу 1), для нечетных и нечетно – нечетных – из порога, наблюдаемого в сечениях деления нейтронами. Расстояние между двумя ветвями зависимости Γ_n/Γ_f от $E_f - B_n$ из статистических соображений может быть оценено как $\Delta_f + \Delta_o$. Оно, согласно рис.8б, составляет примерно 2 Мэв. Как эта величина, так и расщепление E_f на рис.8а соответствуют предположению о значительной разности $\Delta_f - \Delta_o$, составляющей в среднем 0,5 – 0,7 Мэв. Однако, это широко распространенное объяснение четно – нечетных различий E_f противоречиво, поскольку в рамках предположения о значительной разнице Δ_f и Δ_o должно было бы наблюдаться расщепление данных рис.8а и 8б у нечетных и нечетно – нечетных ядер на величину $\Delta_f - \Delta_o$, а оно отсутствует (см. подробнее [32]).

Таким образом, вопрос о природе четно – нечетных различий барьеров деления не может быть решен с помощью гипотезы о возрастании энергетической щели с деформацией ядра, но остается также открытым, если принять $\Delta_f \approx \Delta_o$.

B. Фотоделение четно – четных ядер ^{232}Th, ^{238}U, ^{238}Pu, ^{240}Pu, ^{242}Pu

Измерения производились на внутренней вольфрамовой мишени сильноточного микротрона в интервале граничных энергий тормозного спектра γ – квантов E_{max}= 5 – 8 Мэв. При возбуждении фотонами этих энергий четно – четные ядра образуются лишь в состояниях I^π 1^- и 2^+ в результате дипольного и квадрупольного поглощения, соответственно. Полное угловое распределение осколков, поэтому, в самом общем случае имеет вид:

$$W(\upsilon) = a + b \sin^2\upsilon + c \sin^2 2\upsilon \qquad (8)$$

Если, согласно гипотезе О.Бора [1], пороги деления для состояний $I^{\pi};K$ удовлетворяют соотношениям $E_f(1^-,1) > E_f(1^-,0) > E_f(2^+,0)$, то качественно энергетическая зависимость угловых распределений осколков должна сводиться к следующему: отношения

$$b/a = \frac{P(1^-,0) - P(1^-,1)}{P(1^-,1)} \quad \text{и} \quad c/b \approx \frac{3}{4}\frac{\sigma_\gamma^{2+}P(2^+,0)}{\sigma_\gamma^{1-}P(1^-,0)} \qquad (9)$$

растут с уменьшением энергии возбуждения. Это соответствует наблюдаемой картине (рис.9). При высоких энергиях оба отношения малы, поскольку $P(1^-,0) - P(1^-,1) \ll P(1^-,1)$ и $\sigma_\gamma^{2+}/\sigma_\gamma^{1-} \ll 1$, но в подбарьерной области b/a достигает значения 100 (^{232}Th, E_{max}= 5,4 Мэв), а $c/b \gtrsim 3$ (^{240}Pu, E_{max}= 5 Мэв).

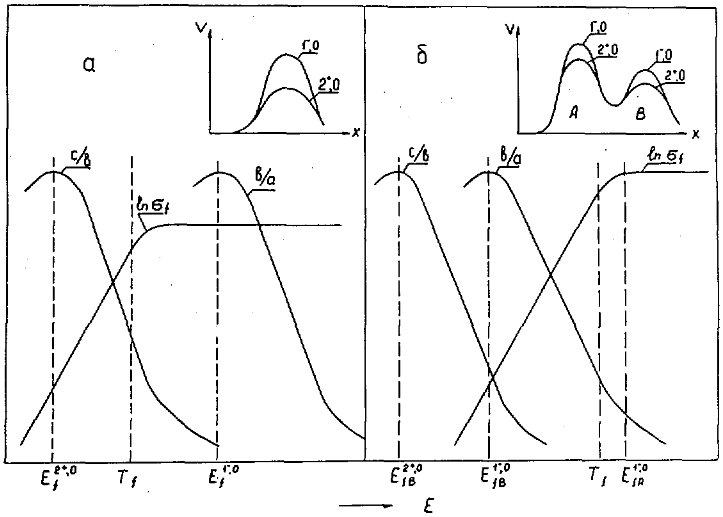

Рис.10. Схематическое изображение зависимостей анизотропии и сечения фотоделения для случаев одногорбного (а) и двугорбого (б) барьеров.

Однако попытка количественного объяснения наталкивается на серьезную трудность. Отношение проницаемостей двух барьеров, имеющих разную высоту и кривизну вершины, вообще говоря, немонотонно зависит от энергии и имеет максимум при энергии, совпадающей с вершиной нижнего из барьеров. Полное сечение фотоделения вблизи порога $\sigma_f \approx \sigma_\gamma^{1-}\frac{P(1^-,0)}{P(1^-,0) + P_c}$, где ниже энергии связи нейтрона $P_c = \frac{2\pi\Gamma_\gamma}{Д} \ll 1$, должно сравниваться с сечением фотопоглащения σ_γ и выходить на плато при $P(1^-,1) \ll P(1^-,0) \approx P_c \ll 1$, т.е. при энергии наблюдаемого порога T_f, которая несколько ниже $E_f(1^-,0)$ [33]. Эта ситуация схематически показана на рис.10а.

На рис.11 вверху изображены непосредственные экспериментальные результаты в виде зависимости выходов осколков Y_i ($\Sigma Y_i = Y$), соответствующих различным компонентам в угловом распределении (8), от граничной энергии тормозного спектра. По этим кривым было произведено восстановление энергетических зависимостей парциальных состав-

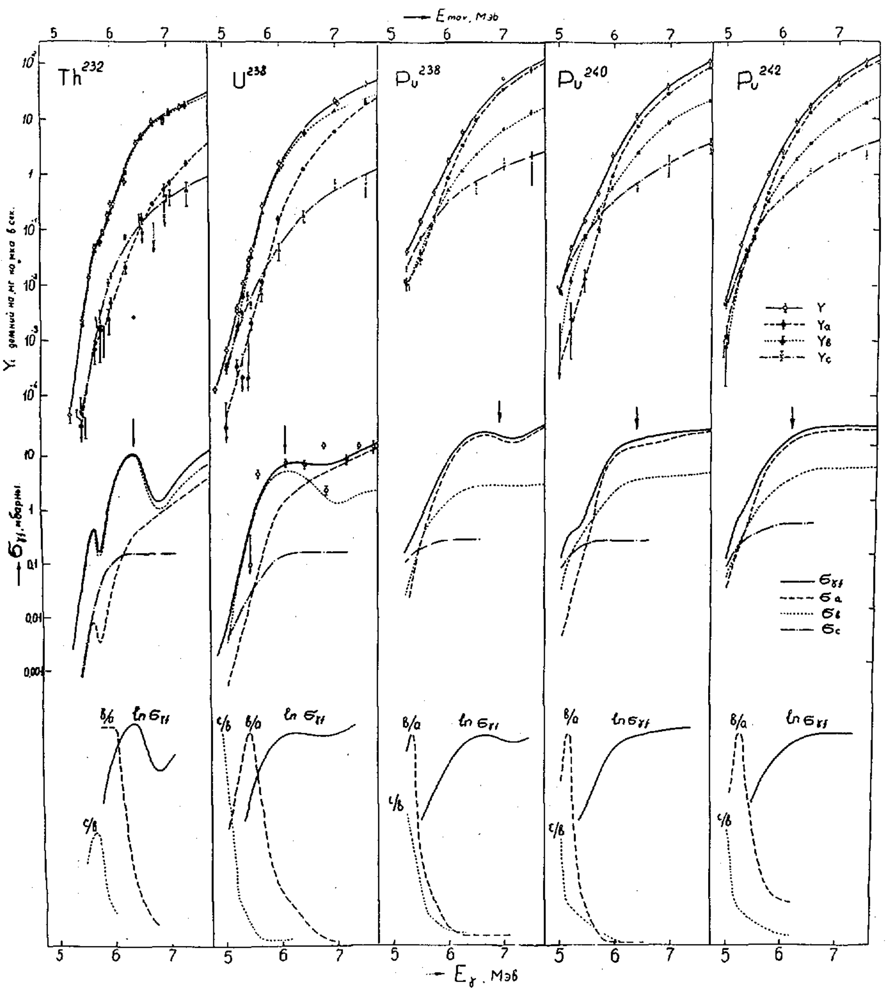

Рис.11. Энергетические зависимости выхода $Y(E_{max})$, сечения деления $\sigma_f(E_\gamma)$ и их угловых компонент $Y_i(E_{max})$, $\sigma_{fi}(E_\gamma)$ в реакции (γ, f).
E_{max} – граничная энергия тормозного спектра,
E_γ – энергия монохроматических фотонов.
Вверху $Y(E_{max})$ и $Y_i(E_{max})$, посередине – $\sigma_f(E_\gamma)$ и $\sigma_{fi}(E_\gamma)$, внизу отношения – c/b, b/a и $\ln \sigma_f$ как функции в произвольных единицах. Вертикальные стрелки показывают положение энергии связи нейтрона B_n.

ляющих сечений фотоделения $\sigma_{fi}(\Sigma \sigma_{fi} = \sigma_f)$ в пересчете на монохроматические γ – кванты (рис.11 посередине). На рис.11 внизу приведены соответствующие энергетические зависимости b/a, c/b и σ_f.

Парадоксальным, с точки зрения только что изложенных простых представлений, является следующий факт: значение энергии, при которой анизотропия – отношение b/a – достигает максимального значения, лежит у изотопов плутония почти на 1 Мэв ниже наблюдаемого порога T_f, в то время как согласно общепринятому описанию эта точка должна быть выше T_f (рис. 10а). Количественно расхождение является очень резким: там, где b/a принимает максимальное значение, сечение фотоделения должно примерно совпадать со своим значением в плато и $\sigma_\gamma^{1^-}$, а фактически оно в сто раз меньше. Пока рассматривались только данные о выходах Y_i, b/a и c/b в зависимости от E_{max}. Этот факт проявлялся не так резко, но тем не менее отмечался нами ранее как труднообъяснимый в рамках традиционных представлений, и мы высказывали два предположения [3,34], в соответствии с которыми наблюдаемый в угловой анизотропии порог $E_f^{1^-} \sim T_f$, а не больше T_f. Однако после дифференцирования $Y_i(E_{max})$ выяснилось, что этот порог меньше T_f, причем разница выходит за пределы любых неопределенностей.

II. ИНТЕРПРЕТАЦИЯ

Перечислим наиболее существенные результаты обсуждения представленных экспериментальных данных.

1. В энергетической зависимости проницаемости барьера наблюдаются отступления от экспоненциального монотонного хода в виде резонансов. Положения резонансов $P_{K\pi}$, соответствующие разным квантовым характеристикам K^π, не совпадают.

2. С увеличением числа нуклонов в узкой области масс делящихся ядер каналовые эффекты вблизи наблюдаемого в сечении порога исчезают, смещаясь в подпороговую область энергий.

3. Выдвинут ряд аргументов против гипотезы о значительной разнице в энергетической щели в переходном и равновесном состояниях. Однако отказ от этого предположения не устраняет трудности объяснения четно — нечетных различий в барьерах деления.

Круг явлений, не укладывающихся в традиционную картину деления, значительно шире и выходит за рамки вопросов, связанных с угловой анизотропией разлета осколков (спонтанноделящиеся изомеры, группировка резонансов сечения деления медленными нейтронами). Для их объяснения весьма плодотворной оказалась модель двугорбого барьера деления [12,13]. Согласно [12], переходное состояние во второй яме (между максимумами А и В) подобно обычному компаунд — состоянию ядра равновесной формы. Если вероятность диссипации энергии коллективного движения в нуклонные степени свободы велика, то ядро, прежде чем разделиться, будет дважды претерпевать эволюцию перехода внутренней энергии в энергию деформации. В этом смысле реакция деления может рассматриваться как двухступенчатый процесс. Это качественно новая особенность и является источником обсуждаемых эффектов.

Наличие квазистационарных уровней во второй яме приводит к тому, что проницаемость барьера, в отличие от монотонной функции (2), в окрестности уровней изменяется резонансным образом [12,35]. Кроме резонансов с шириной ~ 0,1 Мэв, типа тех, которые реализуются при делении ^{232}Th быстрыми нейтронами, в сечении деления медленными нейтронами наблюдается группировка сильных и слабых резонансов — структура с шириной резонансов огибающей порядка 0,01 — 0,1 кэв и расстоянием между резонансами порядка 0,1 — 10 кэв. Согласно [12], первые связываются с вибрационными состояниями, вторые — с состояниями внутреннего возбуждения.

Первоначально резонансы первого типа пытались относить к состояниям в первой яме [7,36] , однако, соображения о диссипации колебательной энергии во внутренние степени свободы эту возможность поставили под сомнение [12,13] . Для обсуждения данного вопроса, по-видимому, весьма существенна принадлежность резонансов проницаемости к определенной комбинации K^{π} (см.рис.3). Если вибрационные состояния связывать с первой ямой, то для объяснения этого факта придется привлечь слишком сильное предположение о сохранении K в продолжение всей эволюции делящегося ядра.

Положения резонансов с разными K^{π} не обнаруживают регулярной структуры, расстояние между ними во многих случаях (рис.3) значительно меньше ожидаемого для вибрационных состояний ($\sim \hbar\omega \approx 0,5 - 1$ Мэв). Этот факт, по-видимому, свидетельствует о том, что резонансы $P_{K\pi}$ для разных комбинаций K^{π} следует относить к вибрационным состояниям в разных ямах. Иначе говоря, он свидетельствует о наличии расщепления кривых потенциальной энергии деформации в зависимости от квантовых характеристик, в соответствии с основной идеей модели О.Бора. Квазистационарные состояния во второй яме, благодаря резонансному изменению $P_{K\pi}(E)$, играют значительную роль в развитии каналовых эффектов при делении ядер.

Исчезновение каналовых эффектов в угловой анизотропии деления вблизи порога, наблюдаемого в сечении, при увеличении числа нуклонов в делящемся ядре, согласно [12] , связано с изменением структуры двугорбого барьера: уменьшением максимума B и углублением ямы между максимумами. Допустим, следуя [12] , что яма на барьере достаточно глубока и ядро в ней живет достаточно долго по сравнению с характерным периодом миграции величины K. В этом предположении ядро "забывает" о квантовых состояниях, в которых оно находилось при прохождении первого барьера A, и дальнейшее развитие процесса деления будет определяться спектром состояний на барьере B.

Очевидно, что в случае $E_{fB} \gtrsim E_{fA}$ будет осуществляться традиционная ситуация : разнообразие форм $W(\upsilon)$ и значительный масштаб изменения угловой анизотропии вблизи наблюдаемого порога деления. В противо-

ТАБЛИЦА 1. ПАРАМЕТРЫ БАРЬЕРА ДЕЛЕНИЯ ПО ДАННЫМ РЕАКЦИИ (γ,f)

Ядро	$E_{fB}^{2^+,0}$	$E_{fB}^{1^-,0}$	$T_f(\lesssim E_f^{1^-,0})$	δ_{AB}
	Мэв	Мэв	Мэв	Мэв
^{232}Th	5,7	6,0	6,0	0[a]
^{238}U	5,0	5,4	5,8	0,4
^{238}Pu	5,2	5,4	6,1	0,7
^{240}Pu	5,0	5,1	6,0	0,9
^{242}Pu	5,0	5,2	6,1	0,9

[a] Значения характеристик, приведенные в таблице, следует рассматривать как оценки, имеющие точность $\sim$0,2 Мэв.

положном случае $E_{fB} < E_{fA}$ может возникнуть принципиально новая картина, так как наблюдаемый в сечении порог определяется высотой большего из барьеров, т.е. E_{fA}, а реализующийся спектр каналов деления—энергией возбуждения в критической точке B. При достаточной разнице $\delta_{AB} = E_{fA} - E_{fB} > 0$ каналовые эффекты в угловых распределениях осколков будут проявляться в существенно подбарьерной области энергий. При этом около порога плотность каналов деления может быть уже значительной, так что на опыте будет реализовываться распределение K, близкое к статистическому.

Экспериментальная картина изменений $W(\upsilon)$ и $A(E)$ в рассмотренных в данной работе случаях удовлетворительно согласуется с этим описанием. Полученные из анализа экспериментальных данных по фотоделению (рис.10б и 11) значения порогов приведены в табл.1. Нижняя оценка $\delta_{AB} \approx T_f - E_{fB}^{1,0}$ увеличивается от тория к плутонию, в соответствии с предсказаниями работы [12]. Мы полагаем, что положение максимумов b/a не связано с квазистационарными состояниями $(I^\pi, K) = (1^-, 0)$, поскольку σ_b в окрестности порога $E_{fB}^{1,0}$ ведет себя плавно, экспоненциально спадая с уменьшением энергии фотонов. Поскольку в большинстве случаев c/b монотонно растет с уменьшением энергии, для порога $E_{fB}^{2,0}$ в таблице приведены верхние граничные значения.

Значения δ_{AB} в табл.1 согласуются с оценками, полученными из анализа группировки резонансов сечения деления ^{237}Np и ^{240}Pu медленными нейтронами [35]. Отметим, что обсуждаемое явление — смещение каналовых эффектов в угловой анизотропии в подбарьерную по сечению деления область энергий, по-видимому, наблюдается также в исследованиях реакций типа (d,pf). Экспериментальные данные [4,5] показывают, что максимум угловой анизотропии, за который ответственны состояния $K = 0$, находится в области $E < B_n$, где делимость ядер $\sigma_f/\sigma_c \approx \Gamma_f/\Gamma_\gamma \ll 1$. Для объяснения этого парадокса авторы [5] допускают, по нашему мнению, слишком сильное предположение, что радиационная ширина Γ_γ примерно на порядок превосходит значения, наблюдаемые при $E \approx B_n$ в (n,γ) — реакциях.

В рамках изложенных представлений модели двугорбого барьера деления можно также понять природу четно — нечетных различий E_f, представленных на рис.8. Поскольку данные о высоте барьеров деления, определенные из энергетических зависимостей угловой анизотропии (четно — четные ядра) и сечения деления (нечетные и нечетно — нечетные ядра) относятся к различным барьерам B и A, соответственно, при анализе четно — нечетных различий E_f необходимо учитывать разность δ_{AB}. Расщепление E_f на рис.8а именно и соответствует этой величине, уменьшающейся, как и в табл.1, в сторону более легких делящихся ядер. Расстояние между ветвями семейства $\Gamma_n/\Gamma_f = f(E_f - B_n)$ для тяжелых ядер ($\Gamma_n/\Gamma_f < 1$) включает в себя $\delta_{AB} = 2$ Мэв $- (\Delta_f + \Delta_o) \approx 0{,}6$ Мэв при $\Delta_f \approx \Delta_o \approx 0{,}7$ Мэв. Для легких ядер ($\Gamma_n/\Gamma_f \gg 1$), как показано на рис.8б, это расстояние уменьшается до $\Delta_f + \Delta_0 \approx 2\Delta_0 \approx 1{,}4$ Мэв, согласуясь с $\delta_{AB} \approx 0$.

Отметим, в заключение, еще одно обстоятельство, касающееся описания вероятности деления в целом. Свойства угловых распределений осколков показывают, что, кроме каналовых эффектов, связанных с квазистационарными состояниями во второй яме, при делении реализуются каналовые эффекты в старом смысле, т.е. обусловленные расщеплением состояний на барьере B. При этом отсчет числа каналов, определяющих вероятность деления следует вести от барьера B, а не от дна второй ямы, как можно было бы ожидать, исходя из роли квазистационарных состояний. Данное предположение подтверждает величина K_0^2 при энергиях, близких к порогу: K_0^2 для четно – четных ядер по мере приближения к барьеру В стремится к нулю, а для нечетных – к одночастичному значению (рис.7). Пример расчета сечения деления ^{240}Pu быстрыми нейтронами в этом предположении, позволяющем получить удовлетворительное описание экспериментальных данных в околопороговой области энергий, приведен в работе [35] .

Авторы выражают глубокую благодарность П.Л.Капице, А.И.Лейпунскому, В.М.Струтинскому за интерес к исследованиям и М.К.Голубевой и Н.Е.Федоровой – за большой труд по просмотру стеклянных детекторов, широко использовавшихся в измерениях.

ЛИТЕРАТУРА

[1] BOHR, A., Int. Conf. Peaceful Uses Atomic Energy, (Proc. Conf. Geneva, 1955) 2 UN, New York (1955) 151.

[2] WHEELER, J.A., "Fast Neutron Physics", Part II (J.B.Marion, J.L.Fowler, Eds), Intersci. Publ., New York II (1963) 2051.

[3] РАБОТНОВ, Н.С., СМИРЕНКИН, Г.Н., СОЛДАТОВ, А.С., УСАЧЕВ, Л.Н., КАПИЦА, С.П., ЦИПЕНЮК, Ю.М., Physics and Chemistry of Fission (Proc. Symp. Salzburg 1965) IAEA, Vienna 1 (1965) 135.

[4] BRITT, H.C., GIBBS, W.R., GRIFFIN, J.J., STONES, R.H., Phys. Rev. Lett. II (1963) 343; Phys. Rev. 139 B354 (1965).

[5] BRITT, H.C., RICKEY, F.A., HALL, W.S., Rep. LA - DC - 9562 (1968).

[6] ВОРОТНИКОВ, П.Е., ДУБРОВИНА, С.М., ОТРОЩЕНКО, Г.Н., ШИГИН, В.А., Ядерная физика 5 (1967) 295;
ВОРОТНИКОВ, П.Е., Ядерная физика 7 (1968) 1228.

[7] LYNN, J.E., Nuclear Data for Reactors (Proc. Symp. Paris) IAEA, Vienna 2 (1967) 89.

[8] LAMPHERE, R.W., Physics and Chemistry of Fission (Proc. Symp. Salzburg 1965) IAEA, Vienna 1 (1965) 63.

[9] АНДРОСЕНКО, Х.Д., СМИРЕНКИН, Г.Н., Письма ЖЭТФ 8 (1968) 181;
ШПАК, Д.Л., СМИРЕНКИН, Г.Н., Письма ЖЭТФ 8 (1968) 545; 9 (1969) 196.

[10] КАПИЦА, С.П., РАБОТНОВ, Н.С., СМИРЕНКИН, Г.Н., СОЛДАТОВ, А.С., УСАЧЕВ, Л.Н., ЦИПЕНЮК, Ю.М., Письма ЖЭТФ 9 (1969) 128.

[11] STRUTINSKY, V.M., Nucl. Phys. A95 (1968) 420.

[12] STRUTINSKY, V.M., BJØRNHOLM, S., Nucl. Structure Dubna Symp. 1968, IAEA (1968) 431.

[13] LYNN, J.E., Nucl. Structure Dubna Symp. 1968, IAEA (1968) 463.

[14] ЕРМАГАМБЕТОВ, С.Б., КУЗНЕЦОВ, В.Ф., СМИРЕНКИН, Г.Н., Ядерная физика 5 (1967) 257.

[15] HENKEL, R.L., BROLLEY, J.E., Phys. Rev. 103 (1956) 1292;
LO NIGRO, S., MILONE, C., Nucl. Phys. A96 (1967) 617.

[16] BEHKAMI, A.N., ROBERTS, J.H., LOWELAND, W., HUIZENGA, J.R., Nucl. Phys. A118 (1968) 65 .

[17] ЕРМАГАМБЕТОВ, С.Б., КОЛЕСОВ, В.Е., НЕСТЕРОВ, В.Г., СМИРЕНКИН, Г.Н., ТИШИН, А.С., Ядерная физика 8 (1968) 704.

[18] BEHKAMI, A.N., ROBERTS, J.H., LOWELAND, W., HUIZENGA, J.R., Phys. Rev. 171 (1968) 1267.

[19] КОРНЕЕВ, Е.И., СКОБКИН, В.С., ФЛЕРОВ, Г.Н., ЖЭТФ 37 (1959) 41.

[20] PEDERSEN, J., KUZMINOV, B.D., Phys. Lett. 29B (1969) 176.

[21] ГОХБЕРГ, Б.М., ОТРОЩЕНКО, Г.А., ШИГИН, В.А., ДАН 128 (1959) 1157.

[22] SIMMONS, J.E., HENKEL, R.L., Phys. Rev. 120 (1960) 198.

[23] ВОРОТНИКОВ, П.Е., ДУБРОВИНА, С.М., ОТРОЩЕНКО, Г.А., ШИГИН, В.А., ДАН 169 (1966) 314.

[24] ВОРОТНИКОВ, П.Е., ДУБРОВИНА, С.М., ОТРОЩЕНКО, Г.А., ШИГИН, В.А., Ядерная физика 3 (1966) 479.

[25] НЕСТЕРОВ, В.Г., СМИРЕНКИН, Г.Н., БОНДАРЕНКО, И.И., Атомная энергия 10 (1961) 620.

[26] SIMMONS, J.E., PERKINS, R.B., HENKEL, R.L., Phys. Rev. 137 (1965) B809.
[27] СТРУТИНСКИЙ, В.М., Атомная энергия 2 (1957) 508.
[28] GRIFFIN, J.J., Phys. Rev. 132 (1963) 2204.
[29] HUIZENGA, J.R., BEHKAMI, A.N., MEADOWS, J.W., KLEMA, E.D., Phys. Rev. 174 (1968) 1539.
[30] СТРУТИНСКИЙ, В.М., ПАВЛИНЧУК, В.А., Physics and Chemistry of Fission (Proc. Symp. Salzburg 1965) IAEA, Vienna 1 (1965) 127.
[31] СМИРЕНКИН, Г.Н., НЕСТЕРОВ, В.Г., ТИШИН, А.С., Ядерная физика 6 (1967) 921.
[32] IGNATYUK, A.V., SMIRENKIN, G.N., Phys. Lett. 29B (1969) 159.
[33] УСАЧЕВ, Л.Н., РАБОТНОВ, Н.С., ПАВЛИНЧУК, В.А., Атомная энергия 17 (1964) 479.
[34] RABOTNOV, N.S., SMIRENKIN, G.N., SOLDATOV, A.S., USACHEV, L.N., KAPITZA, S.P., ZIPENYUK, JU.M., Phys. Lett. 26B (1968) 218.
[35] ГАЙ, Е.В., ИГНАТЮК, А.В., РАБОТНОВ, Н.С., СМИРЕНКИН, Г.Н., Доклад на 2-ой Симпозиум по физике и химии деления, SM – 122/132, Вена, 1969.
[36] ГЕЙЛИКМАН, Б.Т., Ядерная физика 9 (1969) 535.

DISCUSSION

J. PEDERSEN: I want to hear your comment on the ^{240}Pu (γ, f) experiment. I cannot understand how you get a sharp peak in the b/a ratio using a channel picture. Could not this peak be due, instead, to a 1^- resonance state?

I. KOVÁCS: I think that this possibility cannot be ruled out; however, it is difficult to solve this problem without further investigation. In our paper it is mentioned that the quantitative explanation of the experimental data is rather complicated.

J.R. HUIZENGA: I wish to suggest an alternative explanation for the decrease in the value of b/a with decreasing photon energy. This comment is made in a spirit of speculation. If the second or outer barrier is higher than the inner barrier, one may at very low energies have delayed fission due to an isomer competing with prompt fission. In this case, one would expect b/a to decrease at very low energies owing to the fact that the original angular momentum alignment is lost for isomer fission. Hence, an isotropic contribution is introduced and b/a decreases.

P. von BRENTANO: Let us consider the photofission of even nuclei. The new idea about the double barrier introduced here implies that after transition through the first barrier with a given K-quantum-number you can have a change of K-value before you go over to the second barrier, and therefore you lose the anisotropy associated with the first lowest channel. Now, these are exactly the same nuclei we have discussed this morning in connection with papers SM-122/74, 128 and 102. We think there is strong evidence here of vibration at intermediate states, and the transition through the second well is quite fast. Therefore it seems to me that there is a contradiction in the interpretation offered here in terms of channels. There is a confusion as regards, on the one hand, vibration energy and, on the other hand, change in the K-quantum-number in the passage through the second well in the photofission experiment. I do not think that both can be true. Either we have resonances and K is preserved, unless the damping is excessively strong, or we have channels, strong damping, in which case we can lose the anisotropy.

Depending on the photon energy, we can gain the anisotropy and lose it again. That looks like resonance coming in and disappearing again.

J.R. HUIZENGA: In answer to Brentano, I wish to point out that his comments are applicable to fission induced with relatively high-energy charged particles. For very low photon energies the ratio of isomeric to prompt fission may be much larger.

SPONTANEOUS FISSION ISOMERS WITH VERY SHORT HALF-LIVES*

R. VANDENBOSCH, K.L. WOLF
University of Washington, Seattle, Wash.,
United States of America

Abstract

SPONTANEOUS FISSION ISOMERS WITH VERY SHORT HALF-LIVES. A technique has been developed to investigate spontaneously fissioning isomeric states with half-lives in the nanosecond region. Decay of the isomers is observed in the time intervals between cyclotron beam bursts, which are 2 ns in duration and separated by 88 ns intervals. The time distribution of the delayed events is obtained by using a time-to-pulse height converter to measure the time between the arrival of a beam burst and the detection of a fission fragment by a solid-state counter. A number of spontaneous fission isomers of plutonium isotopes have been discovered in helium ion bombardment of uranium isotopes. Isotopic assignments are based on excitation functions for the isomeric states. Spontaneous fission isomers which have been identified are ^{237}Pu ($t_{1/2}$ = 120 ns), ^{239}Pu ($t_{1/2}$ ≥ 400 ns), and ^{240}Pu ($t_{1/2}$ = 4.4 ns). Upper limits for the half-lives of ^{236}Pu and ^{238}Pu have also been obtained. The half-life results are discussed in relationship to the systematics of ground-state spontaneous-fission half-lives, with emphasis on odd-even effects. Isomer ratios have also been meausred, and from these ratios approximate isomeric excitation energies are deduced.

INTRODUCTION

Some years ago Polikanov and collaborators [1] discovered a short-lived spontaneous fission activity whose half-life was much too short to be attributed to spontaneous fission from a nuclear ground state and was therefore assigned to the decay of an isomeric state. Interest in spontaneous fission isomers has increased considerably with the determination of the excitation energy of such an isomer and the realization that the spin of the isomeric state was considerably lower than the value required to account for the gamma decay retardation by a spin-forbiddenness effect. These developments led to increased interest in the idea that spontaneous fission isomers were actually shape isomers, corresponding to a second minimum in the potential energy along the fission degree of shape deformation. Calculations by Strutinsky [2] indeed predicted that such a secondary minimum in the deformation energy should be expected over a considerable mass region in the heavy elements. At the time this study was initiated the only known spontaneously fissioning isomers were, with one exception, odd-odd americium nuclei. It was felt that if shape isomerism were responsible for fission isomers, it should occur in all types of nuclei.

Since a search [3] had already been made in the half-life region of 10 μs to one hour, we decided to investigate shorter lifetimes. If the odd-even variation in spontaneous fission half-lives of nuclei in their ground states was also present in isomeric half-lives, half-lives between a microsecond and a nanosecond would be quite likely. An independent study in this time range has been pursued by Lark and collaborators [4] using a technique based on fission-in-flight of recoiling reaction products.

* Research supported in part by the US Atomic Energy Commission.

EXPERIMENTAL METHOD

The method employed in this study is a direct electronic measurement of the time between the arrival of a burst of particles at the target and the time of fission decay of the isomeric state. The University of Washington 60-inch cyclotron has been used in most of the experiments reported here. This cyclotron produces beam bursts of less than 2 ns width at 88 ns intervals, with no observable beam between beam bursts. An electrically-driven beam chopper [5] was used in some of the measurements to deflect away two out of each three beam bursts and hence increase the time between beam bursts to 264 ns. The energy of the helium ion beam of the cyclotron is varied by the use of degrader foils in front of the target. One experiment was also performed using the University of Washington FN tandem Van de Graaff. The helium ion beam was chopped and bunched [6] to obtain 6 ns wide beam bursts at 420 ns intervals.

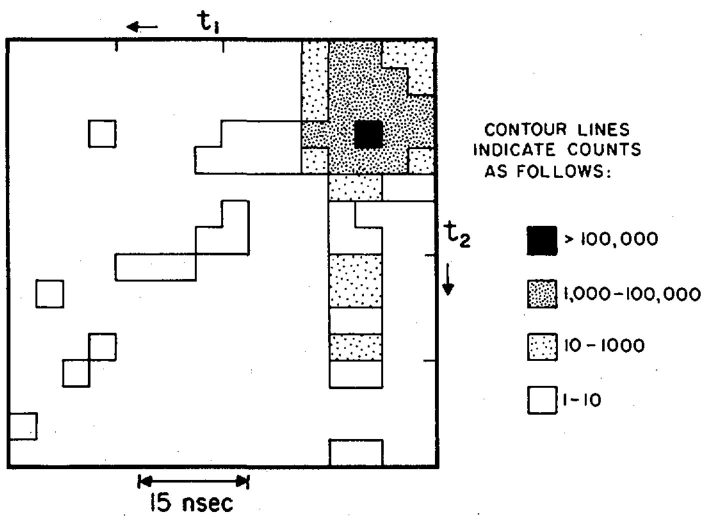

FIG. 1. Example of a two-dimensional time spectrum. The prompt peak is in the upper right-hand corner, and the events along the diagonal correspond to delayed fission.

The time distribution of fission events is determined by using a fast signal from a semiconductor fission detector and a signal from the cyclotron or buncher oscillator to start and stop, respectively, a time-to-amplitude converter. The time resolution of the prompt fission peak is typically 2.5 ns full width at half-maximum, which is comparable to the beam-burst duration. The difficulty is that the ratio of delayed to prompt fission is usually of the order of 10^{-5}, so what is of interest in order to distinguish true delayed fission events from prompt events is the width of the prompt peak at about 10^{-6} of its maximum intensity. The delayed side of the prompt peak exhibits a tail which does not drop off at 10^{-6} of the maximum of the prompt peak until 15 to 20 ns have elapsed. This tailing is presumably due to pile-up effects in the detector and fast electronics. It is possible to eliminate most of this effect by using two independent time-measuring systems with the two fission detectors at 180° with respect to each other so as to detect complementary fragments. The probability that the rare pile-up effects will occur simultaneously in both detectors is very small. The signals from the two time-to-amplitude converters are presented to a 1024 channel two-dimensional analyser whose gate is only opened when the two time-to-amplitude converter signals are in coincidence and when the energy deposited in the detectors corresponds to that expected from fission fragments. A two-dimensional time spectrum is illustrated in Fig. 1. The prompt peak occurs at the upper right-hand corner. Those events where one detector system gave spurious time information lie along the edges of the time spectrum where they cannot be confused with true delayed events which lie on a diagonal line extending down from the prompt peak. The absence of coincident events with tailing in both detectors is demonstrated by the cleanness of the region between the diagonal and the edges of the time spectrum.

RESULTS

The results of various reactions studied will be discussed as they relate to the various plutonium isomers characterized or searched for in this work.

^{240}Pu

This isomer was produced when ^{238}U was bombarded by 23 to 28 MeV helium ions. The decay curve for this isomer is shown in Fig. 2. The half-life of 4.4 ± 0.8 ns was extracted from the decay data using the average lifetime method of Peierls [7]. The assignment of this activity as an isomer of ^{240}Pu is primarily based on the excitation function displayed in Fig. 3. An $(\alpha, 2n)$ is the only reaction one expects to exhibit a maximum at a helium ion energy of 25 MeV. Further support for this assignment is obtained from the absence of this activity in deuteron bombardment of ^{238}U and ^{237}Np. The isomer ratio σ_m / σ_g is $(8.6 \pm 2.4) \times 10^{-4}$, based on the excitation function for the ground state reported by Wing et al. [8]. It has been assumed here and for the remainder of the isomer ratios reported in this work that the only mode of decay of the isomer is spontaneous fission. If other decay modes compete the isomer ratio will increase.

^{239}Pu

Helium ions with an energy higher than 28 MeV produce a much longer-lived isomer which is identified from the excitation function shown in Fig. 4 as being due to the $^{238}U(\alpha, 3n)^{239}Pu$ reaction. Attempts to measure the half-life have met with only limited success because the half-life is long compared to the interval between cyclotron beam bursts, even when the interval between beam bursts is increased to 264 ns by use of the beam chopper. At present a lower limit of 400 ns has been set for the half-life. As long as the half-life is longer than the time between beam bursts it is possible to obtain an isomer ratio, and a value of approximately 5×10^{-4} is obtained assuming a cross-section for the ground state of 65 mb [8].

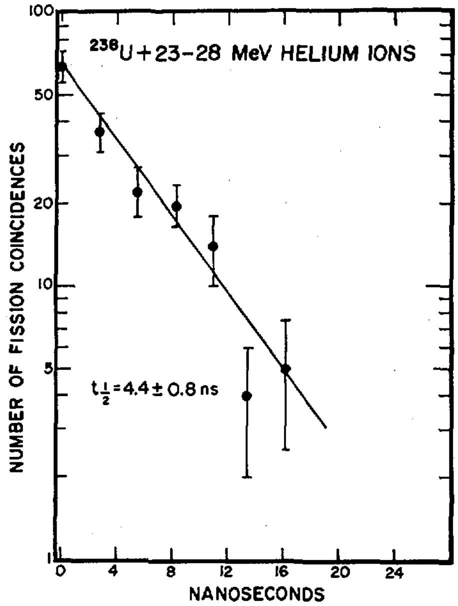

FIG. 2. Decay curve for ^{240m}Pu.

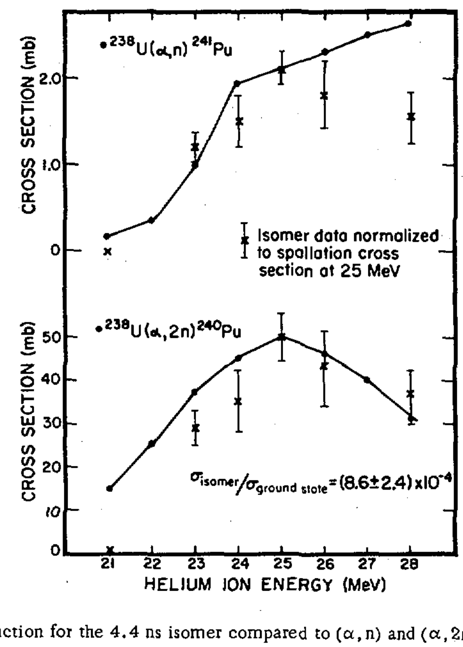

FIG. 3. Excitation function for the 4.4 ns isomer compared to (α, n) and $(\alpha, 2n)$ excitation functions of *Wing et al.*, *identifying* the isomer is being produced by the $^{238}U(\alpha, 2n)^{240}Pu$ reaction.

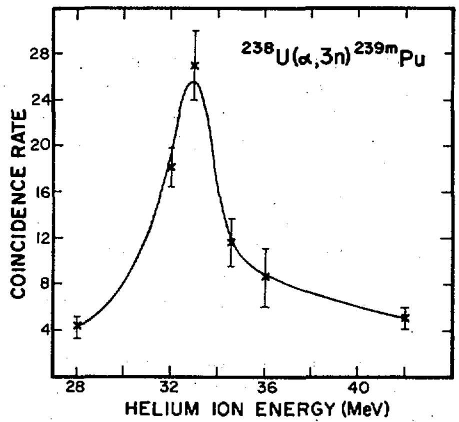

FIG.4. Excitation function for the $^{238}U(\alpha, 3n)^{239m}Pu$ reaction.

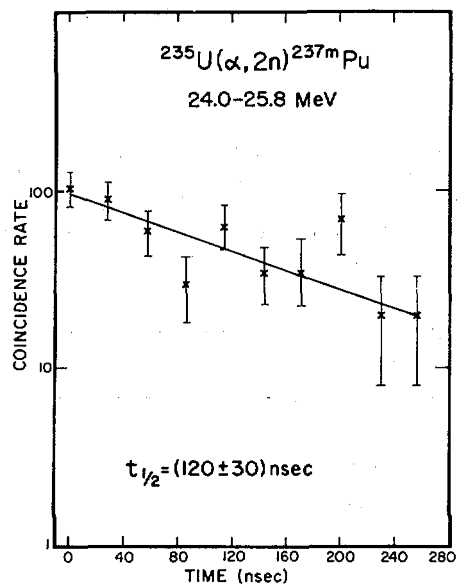

FIG.5. Decay curve for ^{237m}Pu.

^{238}Pu

Attempts to produce this isomer by the $^{238}U(\alpha, 4n)$ and $^{236}U(\alpha, 2n)$ reactions were unsuccessful. If one assumes that the isomer ratio is 5×10^{-4} or greater, an upper limit of 2 ns can be placed on the half-life of ^{238m}Pu.

^{237}Pu

There have been some difficulties and confusion in the characterization of this isomer. Delayed fission observed between cyclotron beam bursts of 34 MeV helium ions on ^{236}U gave a half-life of less than 50 ns. Use of the beam chopper on the cyclotron to produce bursts at 264 ns intervals, however, revealed that the decay curve was complex, with a longer-lived component also present. To further characterize the longer-lived ^{237}Pu isomer, the $^{235}U(\alpha, 2n)$ reaction was employed using the longer time intervals between beam bursts achievable with the tandem Van de Graaff beam chopper. The decay curve is shown in Fig. 5. The half-life is found to be 120 ± 30 ns and the isomer ratio is $(4.1 \pm 1.0) \times 10^{-4}$, based on a ground-state cross-section of 15 mb [9].

We are therefore left in the unpleasant situation of having isomers with two periods, both of which, as excitation functions or cross bombardments indicate, should be attributed to the same isotope. Our tentative explanation of this anomaly is that, indeed, there are two fissioning isomers in ^{237}Pu, differing in spin and having different half-lives. The shorter-lived isomer is presumed to have a high spin and not to be produced in significant yield by 25-MeV alphas or 13-MeV deuterons. 34-MeV alphas bring in a maximum angular momentum which is a factor of two higher and the higher-spin, shorter-half life isomer is then produced in significant yield.

^{236}Pu

Attempts to produce ^{236m}Pu by the $^{236}U(\alpha, 4n)$ and the $^{234}U(\alpha, 2n)$ reactions were unsuccessful. If the isomer ratio is 5×10^{-4}, an upper limit of 4 ns can be set on the half-life of ^{236m}Pu. It should be mentioned, however, that a 34 ns isomer was observed in the proton bombardment of ^{237}Np by Lark et al. [4] and attributed to ^{236m}Pu.

TABLE I. PROPERTIES AND METHOD OF PRODUCTION OF SPONTANEOUS FISSION ISOMERS

Isomer	Reaction	Half-life (ns)	Isomer ratio
^{240}Pu	$^{238}U(\alpha, 2n)$	4.4 ± 0.8	$(8.6 \pm 2.4) \times 10^{-4}$
^{239}Pu	$^{238}U(\alpha, 3n)$	≥ 400	$(5^{+1}_{-1.5}) \times 10^{-4}$
^{238}Pu	$^{238}U(\alpha, 4n)$	< 2	
	$^{236}U(\alpha, 2n)$		
^{237}Pu	$^{236}U(\alpha, 3n)$	(Complex decay)	
	$^{235}U(\alpha, 2n)$	120 ± 30	$(4.1 \pm 1.0) \times 10^{-4}$
^{236}Pu	$^{236}U(\alpha, 4n)$	< 4	
	$^{234}U(\alpha, 2n)$		

A summary of the results is presented in Table I. We wish, in particular, to call attention to the isomer ratios, all of which are within a factor of two of each other. We have assumed in all cases that spontaneous fission is the only decay mode of the isomers.

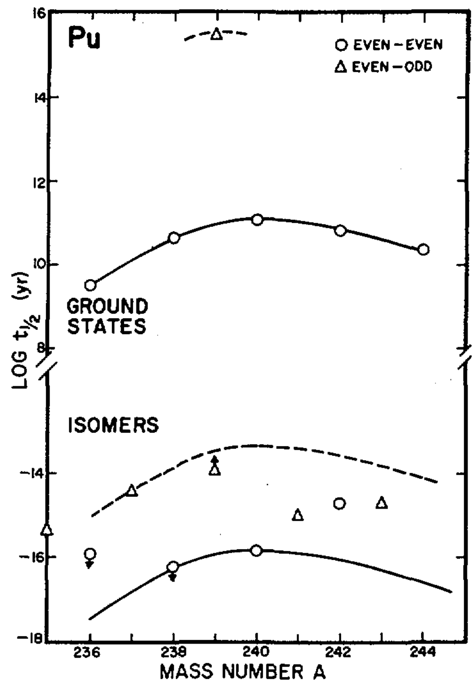

FIG. 6. The logarithm of the spontaneous fission half-life is plotted as a function of mass number for the plutonium isotopes. The solid and dashed curves for the isomeric-state half-lives have the same A dependence as exhibited by the even-even ground states, and have been normalized to ^{240m}Pu and ^{237m}Pu, respectively. The half-lives for ^{241m}Pu, ^{242m}Pu, and ^{243m}Pu have been taken from the work of Lark et al. [4].

DISCUSSION

Figure 6 shows the spontaneous fission half-lives for both the ground state and isomeric states of the plutonium isotopes. Our results are shown by the open symbols, and those of Lark et al. by the closed symbols. Note, first of all, that the isomeric-state half-lives are some 10^{28} times shorter than the ground-state half-lives.

The full curve at the bottom for the even-even isomers has the same variation with mass number exhibited by the ground-state half-lives and has been normalized at A = 240. Our results indicate that the even-even isomeric states are consistent with this trend. The results of Lark et al. for ^{236}Pu and ^{242}Pu are, however, longer than expected. The isomer ratio reported by Lark et al. for ^{236}Pu is a factor of 20 lower than that exhibited by neighbouring isotopes. A possible interpretation of this result is that the isomeric state they observed is a two-quasi-particle state with an unusually long half-life and an unusually low yield. This is supported by the measured excitation energy of the isomer, which is more than 1 MeV higher than for the neighbouring heavier isomers. Less is known about the ^{242}Pu isomer, and further work is necessary to conclusively determine its relationship to the systematics.

The retardation of the even-odd spontaneous fission rates that we observe appears to be of the order of a factor of 100. A similar but larger effect is known for ground-state spontaneous-fission half-lives and has been attributed to a "specialization energy" associated with the non-zero angular momentum of an odd-mass-number nucleus. Since the total angular momentum of the nucleus must remain constant with deformation, a nucleus with an unpaired nucleon must stay in a Nilsson level of a certain spin as the nucleus deforms until another level of the same spin is crossed. Then the odd nucleon can readjust its orbit if it is energetically advantageous. Similar effects can operate in odd-odd nuclei, or for the two quasi-particle state proposed above. For an even-even nucleus the spin of the lowest nucleonic state at any deformation is zero since all nucleons are paired. The paired nucleons can always exploit level crossings to stay in the nucleonic state of lowest energy and still conserve angular momentum. Nuclei with unpaired nucleons will therefore tend to have a higher fission barrier and consequently longer life-times than even-even nuclei. The effective mass is also probably different with unpaired nucleons.

Our results for the half-life and isomer ratio of the even-even nucleus ^{240}Pu may shed some light on the origin of the half-life anomaly in ^{242m}Am. It has been known for some time that it is impossible to construct a one-dimensional two-humped fission barrier for ^{242}Am which is consistent with the known ground-state barrier height, isomeric-state excitation energy, and ground state and isomeric state spontaneous fission half-lives. Calculations performed here and elsewhere [10] using the half-life and excitation energy of the isomer and the barrier height of the ground state predict a ground-state half-life which is a factor of approximately 10^{13} too long. Alternatively, the anomaly may be characterized as a discrepancy between the observed excitation energy of the isomer, 2.9 ± 0.4 MeV, and the excitation energy required to account for the two half-lives, which is less than 1.5 MeV.

It has been suggested by a number of people that this may be evidence for the necessity of considering another dimension in the potential-energy surface, such as non-axially symmetric or reflection asymmetric (P_3) deformations. In this view there would be a path in the two-dimensional surface from the equilibrium ground state deformation to the point of emergence from the fission barrier which would have a higher penetrability than the product of the penetrabilities for the paths connecting the ground state and the isomeric state, and the isomeric state to the point of emergence from the fission barrier. If another dimension in the deformation is responsible for the ^{242m}Am discrepancy, one might expect it to be a general phenomenon and be operative in even-even ^{240}Pu also. A test of this hypothesis can be made for this case, as the ground- and isomeric-state spontaneous fission half-lives are known as well as the fission barrier for the ground state (5.15 MeV). Using the formalism of Nix and Walker [10], one concludes that the excitation energy of the isomer must be less than 2.8 MeV to be consistent with a one-dimensional potential energy surface.

Although there has been no direct measurement of the excitation energy of the isomer, it is possible to deduce a value from the spacing of intermediate structure in neutron-induced fission of ^{239}Pu. The value we deduce from the intermediate structure [11] is 2.3 MeV. (This differs from the value deduced by Patrick and James [11], perhaps because of a difference in the level-density parameter used and the treatment of pairing-energy corrections. Our value is based on a level-density parameter obtained by matching the observed compound nuclear level density at the neutron binding energy, and assuming a pairing correction of 1.2 MeV at both the ground-state and isomeric-state deformations.) This value of

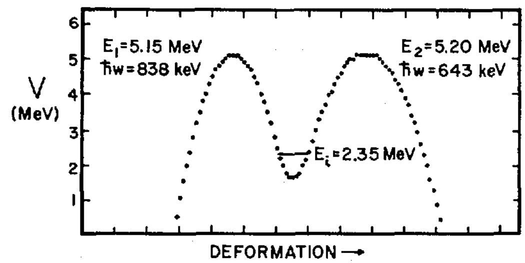

	EXP.	CALC.
$t_{1/2}$(isomer)	4.4×10^{-9} sec	4.4×10^{-9} sec
$t_{1/2}$(g.s.)	1.3×10^{11} yr	1.3×10^{11} yr
Isomer ratio	8.6×10^{-4}	8×10^{-4}
Intermediate structure (D_{II})	460 eV	460 eV
Gross structure:		
E_{R1}	4.95 MeV	4.95 MeV
E_{R2}	4.4	4.34

FIG.7. Comparison of experimental values with those calculated for the one-dimensional barrier illustrated.

the isomer excitation energy is consistent with a one-dimensional interpretation of the relationship between the half-lives, barrier height and isomer excitation energy, although this comparison of course does not exclude the role of other dimensions. It does suggest that another effect is probably responsible for the large discrepancy in the case of ^{242}Am. A possible explanation is that the specialization energies of the gound and isomeric states are different in ^{242}Am. These states are not expected to have the same spin, and therefore their potential-energy surfaces may be quite different. In the caseoof ^{240}Pu, the spin of both the isomeric and ground states is expected to be zero.

I would like to pursue this ^{240}Pu case a bit further and see to what extent all of the available data for this nucleus can be made consistent with a single one-dimensional potential. The result is shown in Fig.7. The potential is shown in the upper part of the figure, and the calculated quantities are compared with the experimental values in the lower part of the figure. The calculation of the penetration through a double-humped barrier has been performed using the method of Wong and Bang [12]. The isomeric state half-life is dependent on the height and curvature of the right-hand barrier. The ground state half-life is dependent on all the barrier parameters. The isomer ratio depends on the height of the lowest barrier and the depth of the second minimum. The intermediate-structure spacing is also dependent on the depth of the second minimum. The gross structure is dependent on all of the barrier parameters in this parametrization. It can be seen that a satisfactory account of all the observed quantities can be obtained. I should like to emphasize, however, that this comparison only demonstrates consistency with this potential, and not the uniqueness of this potential.

ACKNOWLEDGEMENTS

We would like to acknowledge the assistance of Mr. Ronald Aley in performing the calculations with the double barrier, and to thank S. Bjørnholm and J.R. Nix for helpful correspondence and discussions.

REFERENCES

[1] POLIKANOV, J.M., DRUIN, V.A., KARNAUKHOV, V.A., MEKHEEV, V.L., PLEVE, A.A., SKOBELEV, N.K., SUBBOTIN, V.G., TER-AKOPYAN, G.M., FOMICHEV, A.A.V.A., J. éxp. theor. Phys. 42 (1962) 1464 [translation: Soviet Phys. JETP 15 (1962) 1016].

[2] STRUTINSKY, V.M., Nucl. Phys. A95 (1967) 420.

[3] BRENNER, D.S., WESTGAARD, L., BJØRNHOLM, S., Nucl. Phys. 89 (1966) 267.

[4] LARK, N., Bull. Am. phys. Soc. 14 (1969) 102; LARK, N., SLETTEN, G., PEDERSEN, J., BJØRNHOLM, S., to be published.

[5] FAUSKA, H., KARNS, R.E., DRAKE, D.M., Nucl. Instrum. Meth., to be published.

[6] FAUSKA, H., WARD, N.G., LILLEY, J., WILLIAMSON, C.F., Nucl. Instrum. Meth. 63 (1968) 93.

[7] PEIERLS, R., Proc. R. Soc. (London) A149 (1935) 467.

[8] WING, J., RAMLER, W.J., HARKNESS, A.L., HUIZENGA, J.R., Phys. Rev. 114 (1959) 163.

[9] VANDENBOSCH, R., THOMAS, T.D., VANDENBOSCH, J.E., GLASS, R.A., SEABORG, G.T., Phys. Rev. 111 (1958) 1358.

[10] NIX, J.R., WALKER, G.E., Bull. Am. phys. Soc. 13 (1968) 1408.

[11] PATRICK, B.H., JAMES, G.D., Physics Lett. 28B (1968) 258.

[12] WONG, C.Y., BANG, J., Physics Lett. 29B (1969) 143.

CHARGED-PARTICLE STUDIES OF ISOMERIC FISSION

V. METAG, R. REPNOW, P. VON BRENTANO, J.D. FOX *
Max-Planck-Institut fur Kernphysik, Heidelberg
Federal Republic of Germany

Abstract

CHARGED-PARTICLE STUDIES OF ISOMERIC FISSION. Delayed fission events due to isomeric fission have been produced using ^{3}He and ^{4}He beams from the Max-Planck-Institut MP Tandem Van de Graaff accelerator. The isomeric nuclei which recoil from the target and subsequently fission in flight are detected by a square cone array of plastic foil detectors mounted along the beam direction. From the distribution of fission tracks along the plates, half-lives are calculated on the assumption that the recoil has its full momentum. In the following, we list the bombarded targets, the most probable reactions, the assumed final nucleus in which isomerism occurs, the bombarding energies, and the deduced half-lives: ^{233}U (^{4}He, 2n) ^{235}Pu, 26.1 MeV, 20 ns; ^{235}U(^{4}He, 2n) ^{237}Pu, 26.1 MeV, 50 ns; ^{236}U (^{4}He, 2n)^{238}Pu, 26.1 MeV, about 500 ns; ^{238}U (^{4}He, 2n) ^{240}Pu, 26.1 MeV, 7 ns; ^{237}Np (^{3}He, pn)^{238}Pu, 26.1 and 30 MeV, about 500 ns; ^{237}Np (^{3}He, p2n) ^{237}Pu, 26.1 and 30 MeV, 40 ns; ^{237}Np(^{4}He, 2n)^{239}Am, 26.1 MeV, 110 ns; ^{239}Pu (^{3}He, p2n)^{239}Am, 30 MeV, 110 ns; ^{239}Pu (^{4}He, 2n)^{241}Cm, 26.1 MeV, 20 ns; ^{242}Pu + ^{3}He, 30 MeV, half-life of the order of 1 μs; ^{241}Am + ^{3}He leading to Cm or Bk, 30 MeV, 45 ns. As only few cross bombardments have been made and the assignment of the reaction mode is often not unique, many of our isotopic assignments are somewhat tentative.

INTRODUCTION

Fission isomerism has been observed in the uranium region [1–3]. We have studied the isomeric fission with ^{3}He and ^{4}He induced reactions. Previously isomers have been studied by (p,xn), (d,p), and heavy ion spallation reactions. [1–3] The study of isomers with ^{4}He and ^{3}He beams has some advantages over the lighter bombarding particles. The recoiling isomers have a higher velocity and this will reduce multiple scattering in the target and one can in principle obtain rather accurate measurements of the life-time of the isomers. The lowest bombarding energy of the helium ions which can be used for the production of isomers is, however, twice as high as for the single charged particles. Therefore also the excitation energy of the compound nucleus is much higher for the experiments with helium ions than for the experiments with protons and deuterons. The high excitation energy of the compound nucleus allows many possible decay channels as (xn)- and (xnyp)-channels with various integer numbers x and y are open. This makes the assignment of isomeric fission to a particular nuclide considerably more difficult than in the case where fewer reactions are possible.

EXPERIMENTAL PROCEDURE

A: EXPERIMENTAL SET UP AND SCANNING TECHNIQUE

The basic technique used for lifetime measurements was the recoil-distance method, using 10 μm Makrofol plastic foils as detectors for the fission fragments from the recoiling isomers. The beams of ^{3}He and ^{4}He were obtained from the Max-Planck-Institut Model MP Tandem Van de Graaff accelerator with energies of 26.1 and 30.0 MeV. Beam currents obtained varied between 1 and 3 μA. The targets were prepared by electroplating of approximately 100 μg/cm^2 of the oxide of the isotope onto a nickel backing of 1mg/cm^2 by the radiochemical group at Kernforschungszentrum, Karlsruhe. Two experimental arrangements were used. The arrangements shown in Figure 1 in which four Makrofol

* On leave of absence from Florida State University Tallahasee

detectors are placed in a square cone array around the beam axis was used for the cross section and life-time measurements, while a stopper foil arrangement shown in Fig. 2 was used for an angular distribution measurement of the recoil isomeric products and for checking the existence of isomers with half-lives longer than 500 nsec. Following the bombardments, the detector foils were etched in 6N NaOH at 70°C for 15 minutes, washed, dried, and then scanned with a high voltage probe[4] in order to enlarge and blacken the holes made in Makrofol by fission fragment tracks.

A modification to this scanning technique has been used which allows rapid processing of the Makrofol foils and makes the use of even larger foils quite feasible. After the Makrofol detector foils are etched and dried in the usual way, they are placed on a grounded copper plate. The detector foil is then covered by a second plastic foil, which is aluminized on the side touching the Makrofol. The aluminum surface is then brought into contact with a high voltage probe and the voltage

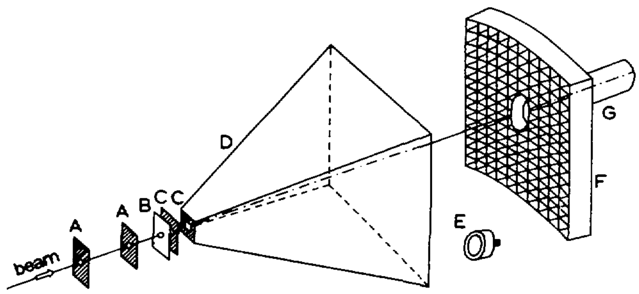

FIG. 1. Recoil arrangement used for measuring half-lives of isomers. The parts indicated are : A) Beam collimators; B) target, C) fission isomer collimators, D) detector cone, E) monitor counter, F) "black-body" isomer trap, G) Faraday cup.

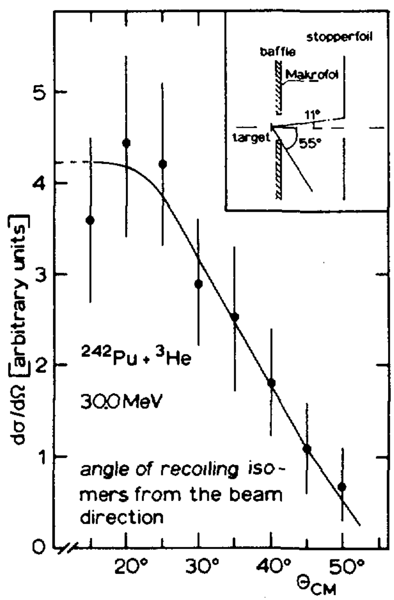

FIG. 2. Angular distribution of recoiling isomers of the reactions ^{242}Pu + ^{3}He, which in this case leads probably predominantly to the 14 ms ^{242}Am isomer. A schematic drawing of the stopper foil arrangement used in this measurement is also shown in the figure; the method of measurement is discussed in the text.

raised until sparking occurs at the etched holes. The sparking not only darkens the holes in the Makrofol but burns off the aluminum coating. This terminates the sparking in the vicinity of each hole and prevents short circuiting. The aluminum foil can as well be scanned in the manner used for the Makrofol itself.

B: BACKGROUND EFFECTS

Makrofol foils etched and scanned show a few holes in places, where they were not hit by fission fragments The background rate varies; it is about 0.05 tracks/cm^2 for 10 μm Makrofol. As we use trapezoidal shaped foils mounted in a square cone the background becomes noticeable only at distances bigger than about 15cm from the target. Background from the foils is therefore mainly a problem for isomers with long half-lives for which the decay extends nearly over the whole length of the foils; it is less important for the detection of very short-lived isomers although the deduced half-life depends on the background subtraction. The background rate is very much reduced for 15 μm Makrofol, but the detector efficiency is down by a factor 2 as the angle of acceptance is only about $\pm$ 40° with the vertical to the foil surface whereas it is $\pm$ 60° for 10 μm Makrofol. Other foils as Hostaphan can be used for the detection of fission fragments too. It is our experience that 10 μm Hostaphan foil has less background than a Makrofol of the same thickness.

C: ANGULAR DISTRIBUTION OF THE RECOILING ISOMERS

An important consideration in the determination of the cross sections and lifetime for the isomers is the angular distribution of the isomers leaving the target foil. The calculations of the cross sections take the angular distribution into account since the angular acceptance of the cone arrangement is just $\pm$ 20° on either side of the beam axis. The assumption that the recoiling isomer moves with the full recoil energy given by the nuclear reaction is justified only if the angular distribution of the isomers does not indicate that appreciable scattering has occured in the target. Thus, an angular distribution strongly peaked in the forward direction for isomers produced in a compound nucleus type reaction with the evaporation of slow neutrons would indicate that the multiple scattering of the isomeric recoils was not appreciable. A broad angular distribution would indicate the possibility of large energy losses in the target. The angular distribution of the recoiling isomers can, in the stopper foil technique, be reflected in the radial distribution of tracks in the detector foil. The experimental set-up for the measurements of angular distributions is shown in the insert of Figure 2. Isomeric recoils moving at angles between about 11° and 55° to the beam axis are stopped in the stopper foil and fragments from their fission are detected in the detector foil mounted on the baffle. The angular distribution measured from the isomers resulting from ^{242}Pu + ^{3}He is shown in Figure 2. The isomer in this case is probably the 14 ms isomer of ^{242}Am [1,3] formed via the (^{3}He, 2np) reaction. As can be seen from the figure, the strong peaking of the angular distribution in the forward direction implies that the energy losses in the target are small if these losses are mainly of the nuclear scattering type.

RESULTS

The results of our work are summarized in Table I. We have indicated in the table the target, bombarding particle, incident energy, the probable reaction responsible for each isomer, the half-life, and the cross section calculated from our data. The decay curves from which the half-lives and cross sections were calculated are shown in figures 3–7. Discussions for specific cases are given below.

For each but one of the cases considered here, it is assumed that the isomeric recoil ion leaves the target with the full momentum imparted by the incoming helium ion. The exception is the ^{235}U(d,p) ^{236}U reaction which we discuss below. The evaporation of neutrons and charged particles leading to the isomeric state is considered not to appreciably alter the recoil velocity and, because of the small acceptance angle of the cone arrangement, it is assumed that no appreciable energy loss has occured during the passage of the recoil isomer through the target material. Some of the reactions which have not been discussed in a previous paper [5] will be discussed in some detail in the following:

TABLE I. SUMMARY OF RESULTS. THE STATISTICAL ERRORS IN HALF-LIFE DETERMINATION ARE ESTIMATED TO BE ± 30%

Target	Bombarding Particle	Bombarding energy (MeV)	Assumed reaction	Half-life (nsec)	Cross-section (μb)
^{233}U	^{4}He	26,1	$(^{4}He,2n)^{235}Pu$	20	0,18
^{235}U	^{4}He	26,1	$(^{4}He,2n)^{237}Pu$	60	0,45
^{236}U	^{4}He	26,1	$(^{4}He,2n)^{238}Pu$	~ 500	0,3
			$(^{4}He,n)^{239}Pu$	30	0,06
^{238}U	^{4}He	26,1	$(^{4}He,2n)^{240}Pu$	7	0,05
^{237}Np	^{4}He	26,1	$(^{4}He,2n)^{239}Am$	110	0,65
^{237}Np	^{3}He	26,1	$(^{3}He,2np)^{237}Pu$	40	0,15
			$(^{3}He,np)^{238}Pu$	~ 500	0,4
			$(^{3}He,p)^{239}Pu$		
		30,0	$(^{3}He,2np)^{237}Pu$	50	0,05
			$(^{3}He,np)^{238}Pu$	~500	0,4
			$(^{3}He,p)^{239}Pu$		
^{239}Pu	^{4}He	26,1	$(^{4}He,2n)^{241}Cm$	20	0,04
^{239}Pu	^{3}He	30,0	$(^{3}He,2np)^{239}Am$	110	0,14
^{241}Am	^{3}He	30,0	Bk,Cm	45	0,06
^{242}Pu	^{4}He	26,1	$(^{4}He,n)^{245}Cm$	12	0,02
			$(^{4}He,2n)^{244}Cm$	≥500	~0,2
^{241}Am	^{4}He	26,1	$(^{4}He,n)^{244}Bk$	100	0,02
			$(^{4}He,2n)^{243}Bk$		

The absolute cross-sections quoted are very uncertain because of the unknown chemical and surface properties of the target. The correction factors to the given cross-sections could be factors 10 or even larger. The brackets indicate that the observed half-lives and cross-sections can be assigned to any isotope within the bracket.

$^{236}U + {}^{4}He$

When bombarding ^{236}U with ^{4}He particles of 26.1 MeV we see two isomers with half-lives of 30 nsec and about 500 nsec respectively (see fig. 3). The 30 nsec half-life was obtained by subtracting the contribution of the long-lived component. The isotopic assignment is rather difficult in this case. As the Copenhagen group [3] does not observe any isomer of those half-lives in Np, these two isomers are probably in Pu produced by $(^{4}He, 2n)$ and $(^{4}He,n)$ reaction; the $(^{4}He,3n)$ reaction can be excluded by energy considerations. From cross-section arguments [6] we would tend to assign the long component (0.3 μb) to ^{238}Pu because generally the $(^{4}He, 2n)$ reaction is dominant. The 30 nsec isomer (0,06 μb) should then be in ^{239}Pu. However, results obtained by VANDENBOSCH [7] indicate that the long-lived component is in ^{239}Pu. As we observe an overlap of two exponential decays in this case our cross-section values might not be very reliable: from our data we can not exclude the possibility that the assignment given above is to be reversed.

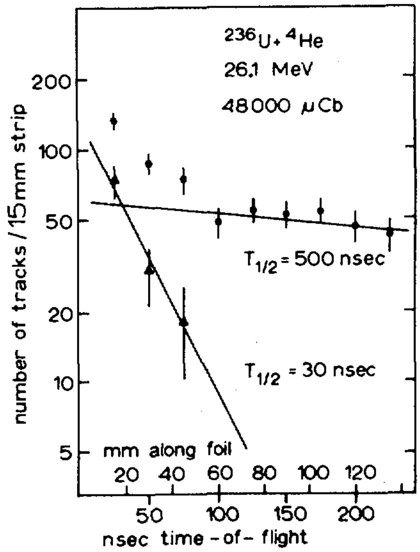

FIG. 3. Decay curve obtained from ^{4}He-bombardment of ^{236}U. The circles indicate the number of tracks observed on the foils plotted versus the distance from the target. The triangular points are found by subtracting the long component. The conversion from distance to time-of-flight is made assuming full momentum transfer.

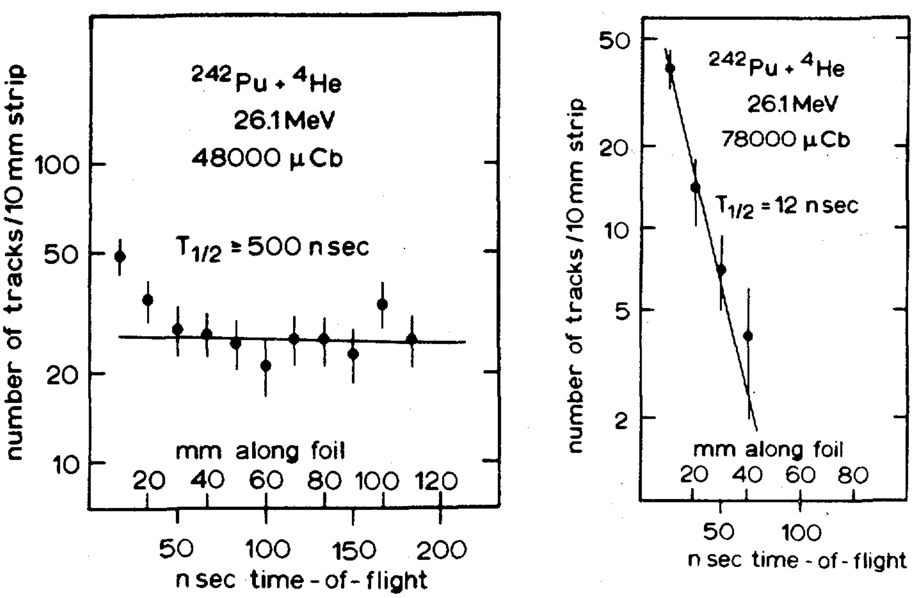

FIG. 4. a) Decay-curve for ^{4}He + ^{242}Pu;
b) the same as Fig. 4a after subtraction of long-lived component.

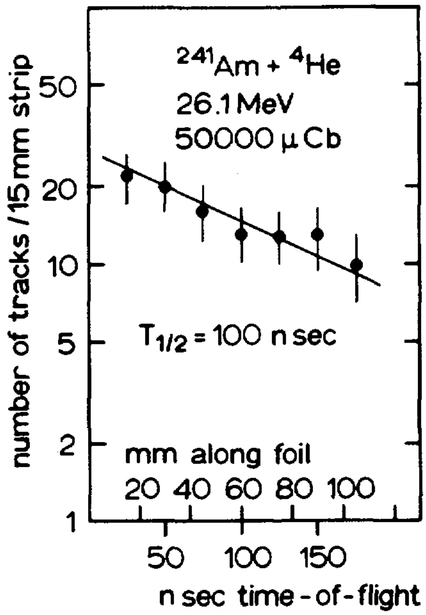

FIG. 5. Decay curves for isomers resulting from bombardment of ^{241}Am with ^{4}He particles.

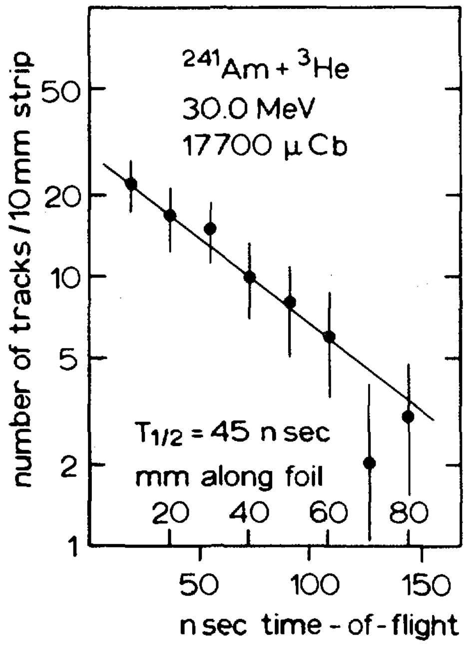

FIG. 6. Decay curves for isomers resulting from bombardment of ^{241}Am with ^{3}He particles.

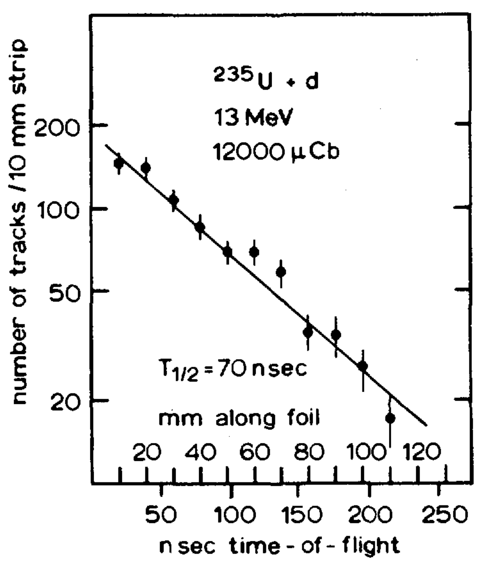

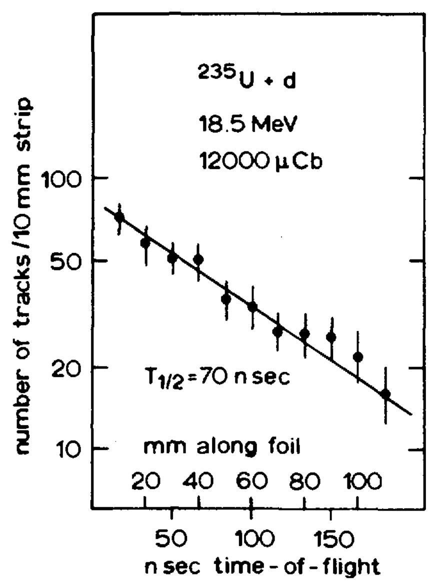

FIG. 7. Decay of the isomer resulting from ^{235}U + d at E_d = 13 MeV (a) and 18.5 MeV (b). The conversion of distance to time-of-flight is discussed in the text.

$^{242}Pu + {}^{4}He$

Bombarding ^{242}Pu with ^{4}He we find a situation similar to that in the case $^{236}U + {}^{4}He$. We observe a superposition of two decays with half-lives of 12 nsec and $\geq$ 500 nsec respectively (see figures 4a and 4b). Again from cross section arguments we tend to assign the long-lived isomer to ^{244}Cm, the short-lived one to ^{243}Cm. Other spallation reactions, e.g. (^{4}He,pn) can be excluded because they would lead to known isomers with half-lives different from those observed here.

$^{241}Am + {}^{4}He$

We observe the decay of a fission isomer with half-life of about 100 nsec following the bombardment of ^{241}Am with ^{4}He. The cross section is rather small (0.02 μb) leaving the assignment open. Perhaps we have observed an isomer in Bk (probably in $^{243,244}Bk$).

$^{241}Am + {}^{3}He$

The reaction induced by ^{3}He-particles at 30 MeV leads to an isomer decaying with a half-life of 45 nsec. At the high excitation energy of the compound nucleus obtained with incident ^{3}He ions reactions with the emission of charged particles are favoured according to spallation data [6]. It is therefore possible that we deal with a (^{3}He,p) reaction producing an isomer in ^{243}Cm to which POLIKANOV and G. SLETTEN [8] assign an isomer with a half-life of 37 nsec.

The (^{3}He,pn) reaction can be excluded as this would lead to ^{242}Cm for which the Copenhagen group does not observe any decay they could assign to this isotope. It cannot be a (^{3}He,p2n) reaction either because we have assigned to ^{241}Cm an isomer with a half-life of 20 nsec. Nevertheless the possibility that we have a (^{3}He,xn) reaction going on leading to an isomer in Bk can not be excluded.

^{235}U (d,p) ^{236}U

Bombarding ^{235}U with deuterons of 11 and 13 MeV the Copenhagen group observed an isomer in ^{236}U with a half-life of 110 nsec produced by the (d,p) reaction [3]. We measured the same isomer for deuteron energies varying from 13 to 20 MeV (see figures 7a and 7b). Assuming full momentum transfer from the incoming to the recoiling particle we would derive a half-life of 110 nsec too. However, we think that the outgoing proton with an energy of about the deuteron bombarding energy contributes appreciably to the recoil momentum. As in our arrangement only recoils within 20° with the beam direction are allowed to decay within the cone the corresponding protons have to be emitted with backward angle larger than 120° giving the recoils a higher velocity. Therefore we deduce for the isomer in ^{236}U the somewhat smaller value $T_{1/2}$ = 70 nsec.

In the discussion given in the text we have in some cases used the hypothesis that there is only one isomer in each isotope. Recent measurements by Elwyn and Ferguson presented at this conference (Abstract SM-122/54, and discussions) cast doubt on this hypothesis.

CONCLUSIONS

We should like to point out that while the cross bombardment technique with He ions can, in some cases, clarify the isotopic assignments, the situation is not entirely clear in all cases. The higher excitation energies produced by helium ions at bombarding energies above the Coulomb barrier lead to many possible final nuclei since several neutrons and perhaps even charged particles may be evaporated. Bombardments with ^{4}He are rather certain to produce (^{4}He,n) and (^{4}He,2n) reactions in the energy range from 25–30 MeV although, for isomers produced with very small cross sections, other reactions are possible. ^{3}He induced reactions proceed from a very energetic compound nucleus and the evaporation of up to three neutrons or two neutrons and a proton is very likely.

Although the techniques used here, and by other workers [3,7] are prejudiced in favour of the detection of isomers with half-lives in the 5 to 500 nsec region, we feel it is remarkable that so many of the isomers already identified have half-lives in this region. The implication of this near constancy of half-life is either that, except for those known cases of the even Americicium isotopes, the barrier regulating the fission decay of the isomers is remarkably constant over a large region of the periodic table, or that the nuclear state determining the half-life is somehow a common property of these isotopes and that the usual description of the fission decay of these isomers is incorrect.

In addition it seems also that the half-lives of the isomers are not proportional in a simple way to the half-lives of the spontaneous decay of the ground states. E.g. the half-lives of the isomers in ^{239}Pu and ^{240}Pu are 500 and 7 nsec respectively, whereas the ground states have half-lives of $5.5 \cdot 10^{15}$ y and $1.2 \cdot 10^{11}$ y. Also we find for the isomer in ^{236}U a half-life of 70 nsec and for the isomer in ^{242}Cm a half-life of 12 nsec whereas the spontaneous half-lives are $2 \cdot 10^{16}$y for ^{236}U and $1.4 \cdot 10^{7}$y for ^{244}Cm. These problems certainly warrant further theoretical studies and they may probably also be clarified by the experimental observation of more isomers which would help to establish a systematics.

ACKNOWLEDGEMENT

We wish to thank Dr. Hans Körner for his assistance in running these experiments and for valuable discussions. It is our pleasure to express our gratitude to the radio-chemistry group at Kernforschungszentrum Karlsruhe and in particular to Prof. Dr. Seelman-Eggebert for his interest in this work. We also want to thank Dr. P. Wolf, Dr. H. Münzel and Mr. Reinhard for the preparation of the very fine targets used in this work. The authors wish to acknowledge useful discussions with various members of the Copenhagen group, in particular with S. Bjørnholm, J. Pedersen and G. Sletten, and express appreciation for their communication of results prior to publication.

REFERENCES

(1) POLIKANOV,S.M., DRUIN, V.A., KARNAUKHOV, V.A., MIKHEEV, V.L., PLEVE, A.A., SKOBELEV, N.K., SUBBOTIN, V.G., TER–AKOP'YAN, G.M., FOMICHEV, V.A., J. Exptl. Theoret. Phys. (U.S.S.R.) 42 (1962) 1464, Soviet Physics JETP 15 (1962) 1016

(2) BRENNER, D.S., WESTGAARD, L., BJØRNHOLM, S., Nucl. Phys. 89 (1966) 267.

(3) LARK, N.L., SLETTEN, G., PEDERSEN, J., BJØRNHOLM, S., Nucl. Phys. 89 (1966) 267

(4) LARK, N.L., Nucl. Instr. Methods 67 (1969) 137

(5) METAG, V., REPNOW, R., VON BRENTANO, P., FOX, J.D., Z. Physik 226 (1969) 1

(6) GLASS, R.A., CARR, R.J., COBBLE, J.W., SEABORG, G.T., Phys. Rev. 104 (1956) 434. VANDENBOSCH, R., THOMAS, T.D., VANDENBOSCH, S.E., GLASS, R.A., SEABORG, G.T., Phys. Rev. 111 (1958) 1358

(7) WOLF, K.L., VANDENBOSCH, R., Bull. Am. Phys. Soc 13 (1968) 1407 and private communication.

(8) SLETTEN, G., POLIKANOV, S.M., private communication

DISCUSSION

Discussion on papers SM-122/110 and SM-122/29

A.J. ELWYN: I would like to report on some measurements of the half-lives and production cross-sections for spontaneously fissioning isomers in isotopes of U and Pu induced by fast neutrons of energy 2.2 MeV and 0.55 MeV. The measurements were performed by Dr. A.T.G. Ferguson and myself.

Neutrons in pulses of about 1 ns duration are generated by the 3-MeV-pulsed-proton beam from the IBIS Van de Graaff machine. For production of 2.2 MeV neutrons a Mo windowed tritium gas target was used and for the 0.55 MeV neutrons a Li metal target was employed. The fissile samples were deposits 1.5 mg/cm^2 thick as oxides on platinum backings. Fission fragments were detected in a Si surface barrier counter and the time distribution of the pulses was measured relative to the proton beam pulse with a time-to-amplitude converter.

With the experimental arrangement at the IBIS accelerator the intensity of any residual beam between beam bursts in the machine is found to be less than about 10^{-6} of the main beam intensity. Thus, the time distribution of the pulses in any, even weakly excited, delayed fission process could be observed quite cleanly.

Figure A shows the time distribution of the pulses following neutron bombardment of the ^{239}Pu sample (time increases to the left in this figure). The large peak near channel number 855 corresponds to the prompt fission of ^{239}Pu induced by 2.2 MeV neutrons. In an analysis of the events in the "tail" of this peak, the observed distribution is found to be consistent with the existence of two short-lived periods - a fairly intense 5 ns activity, and a weaker activity with a half-life of 28 ns. Figure B shows more clearly the analysis of the events in this tail after a small background of time-independent counts has been subtracted.

In a similar manner analysis of the distributions for the U isotopes are, except for ^{238}U, consistent with the existence of short-lived activities that have half-lives between 20 and 67 ns. For ^{238}U no activity with a half-life greater than about 2 ns was observed, and the shape of this distribution could be taken as representative of the shape of the "prompt" peak.

As a test, the time distribution of α-particles in the $^{10}B(n,\alpha)^6Li$ reaction was obtained. On the basis of an analysis of this time distribution, it is concluded that for the fissile samples no activity with half-life $\gtrsim$ 15 ns and an intensity as great as 5×10^{-5} of the intensity of the "prompt" peak should be observed, if it is assumed that the neutrons responsible for any spurious "tail" have an energy close to that of the primary neutrons. For neutrons of any lower energy this limit can be substantially reduced because of the increasing ratio of the (n,α)-to-prompt-fission cross-sections at lower energies.

The results from analysis of the time distributions for the nuclei studied are shown in Table A.

The half-lives and integrated intensities listed in columns 3 and 4 are based on, at least, two independent runs for each sample, and involve

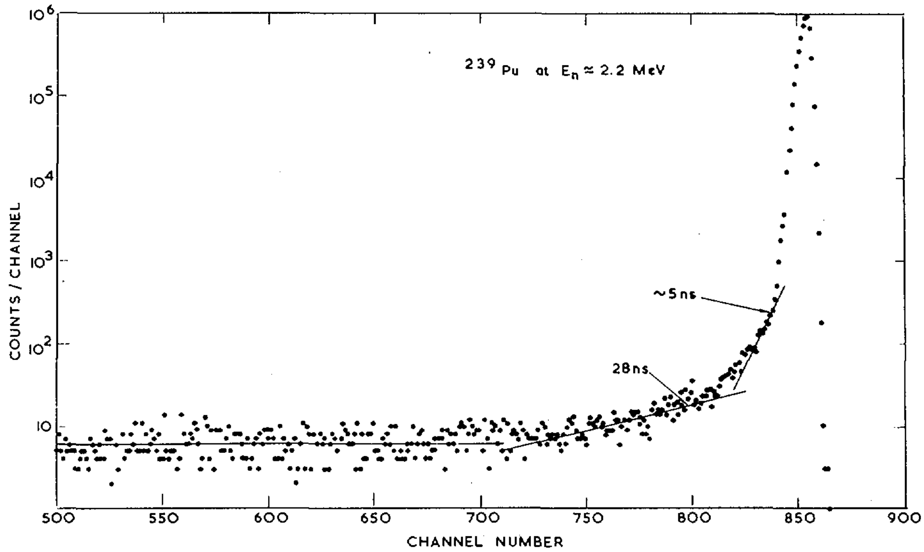

FIG.A. Time distribution of pulses following neutron bombardment of ^{239}Pu sample.

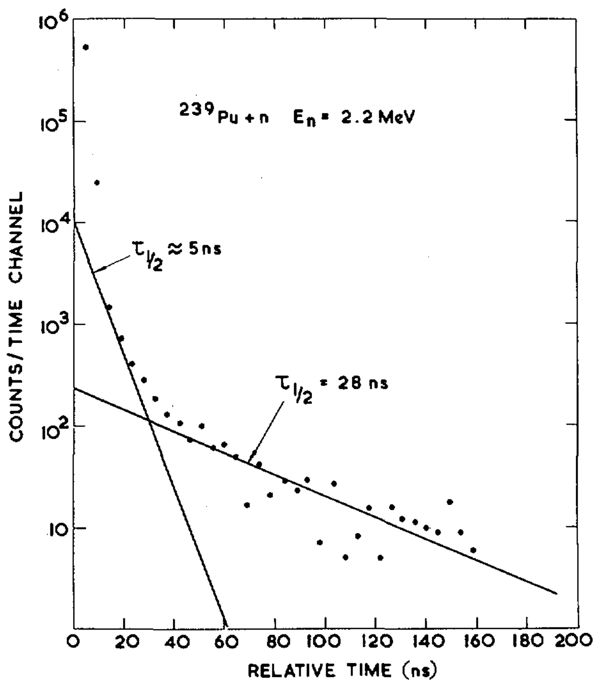

FIG.B. Analysis of events in "tail" of Fig.A.

TABLE A. RESULTS FROM ANALYSIS OF TIME DISTRIBUTIONS

Energy (MeV)	Target ($\times 10^{-9}$ sec)	$\tau_{\frac{1}{2}}$ ($\times 10^{-9}$ sec)	$\frac{\text{Delayed}}{\text{Prompt}} = R$* ($\times 10^{-4}$)	Prompt σ_{nf}** ($\times 10^{-24}$ cm)	Delayed σ_{nf}* ($\times 10^{-28}$)
2.2	^{239}Pu	29.0 ± 3.8	4.1	2.0	8.2
		4.1 - 5.2	4.3	2.0	86.0
	^{233}U	30.4 ± 4.9	4.7	2.1	9.6
	^{234}U	19.7 ± 4.9	1.2	1.5	1.8
	^{235}U	66.6 ± 8.7	3.1	1.3	4.0
	^{238}U	No lifetime observed			
0.55	^{233}U	34.9 ± 4.5	7.4	2.0	15.0

* Error about ±50%.
** Taken from BNL 325 - Ref.[5].

the detection of not less than 7.5×10^6 events in the prompt peak. For ^{233}U at 0.55 MeV, the total number of counts in the prompt peak was 3×10^6. Note that the half-life measured at 0.55 MeV is in agreement with the result at 2.2 MeV. The errors quoted on the half-lives are based on a combination of the statistical uncertainties in the analysis, and on estimates of systematic errors in the experiment.

It is reasonable to assume that the observed activities are associated with nuclei produced in the (n, γ) reaction on the targets listed in Table A. For ^{240}Pu (produced in the ^{239}Pu (n, γ) reaction), as mentioned previously, two activities are observed. The 5-ns half-life is in agreement with results reported by a number of experimental groups (N. Lark et al., in Nuclear Structure (Proc. Int. Symp. Dubna, 1968) 90; K.L. Wolf and R. Vandenbosch, Bull. Am. phys. Soc. Series 2E 13 (1968) 1407, and contribution SM-122/110 to this Conference; V. Metag et al., contribution SM-122/29 to this Conference), but the 29-ns activity with an intensity smaller by a factor of 10 than the shorter decay, has not previously been observed. In the studies of the ^{233}U, ^{234}U and ^{235}U samples, leading to the production of ^{234}U, ^{235}U and ^{236}U final nuclei, respectively, single activities were seen. The 67-ns activity associated with ^{236}U is in agreement with other results (see References above). No previous activity associated with ^{234}U and ^{235}U final nuclei have been reported.

In summary, the results shown in Table A suggest that short-lived activities are observed in the neutron-induced fission of ^{233}U, ^{234}U, ^{235}U and ^{239}Pu. The integrated intensities associated with these lifetimes are $\gtrsim 10^{-4}$ of the intensity in the prompt-fission process, and appear, therefore, to be larger than some previously reported results (see References above) based on charged-particle-induced fission. These ratios (as seen in column 4 of Table A) are furthermore considerably larger than those previously reported (G.N. Flerov et al., Nucl. Phys. A97 (1967) 444) for neutron-induced reactions leading to the production of the Am isomer states. By demonstrating the existence of more than one short-lived isomer in ^{240}Pu this work emphasizes the complexity of the situation with regard to fissioning isomers.

H.W. SCHMITT: We are currently working on experiments at Oak Ridge which, we hope, may provide a connection between the vibrational states in the second minimum and fission isomers. The idea is shown schematically in Fig.C. The double barrier is shown, and a level corresponding to a vibrational state in the second minimum is indicated. The effect of such a level, according to Bjørnholm and Strutinsky (Nuclear Structure (Proc. Symp. Dubna, 1968), IAEA, Vienna (1968) 431), is that a peak appears in the subthreshold-fission cross-section, such as that which occurs at a neutron energy E_n = 1.4 MeV in the ^{236}U (n, f) reaction cross-section (left-hand side of Fig.C).

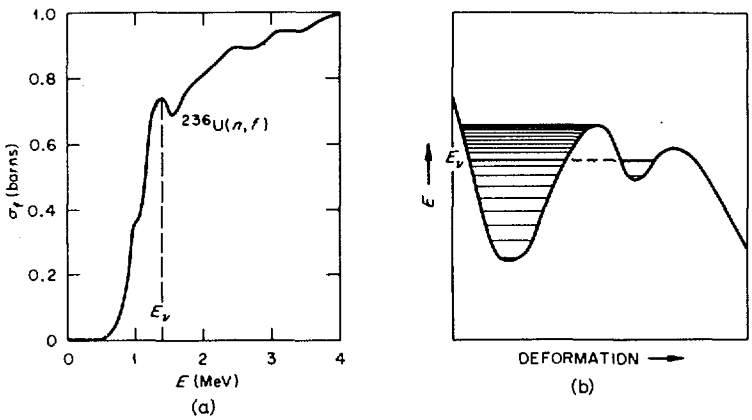

FIG.C. a) ^{236}U(n, f) reaction cross-section versus neutron energy; b) Connection between vibrational states in second minimum and fission isomers.

Let us now consider the following argument: Most of the fission events observed at E_n = 1.4 MeV will be prompt events, corresponding to direct penetration of the barrier at that energy. If, however, the system is somehow trapped in this vibrational level, perhaps with small but finite probability, then this state may occasionally decay by gamma emission to the ground state of the second minimum, i.e. in competition with prompt fission. In these rare cases, then, the fission events which are observed should be delayed, and their half-life should be equal to that of the corresponding fission isomer.

A preliminary experiment to test this idea has been carried out. A pulsed beam of monoenergetic neutrons was obtained by means of the T (p, n) reaction at the Oak Ridge 3-MV pulsed Van de Graaff accelerator. With the experimental arrangement shown in Fig.D, the distribution of times between the proton beam pulses and fission fragment pulses in the surface barrier detector was measured. The corresponding fragment pulse amplitudes were simultaneously recorded in a second parameter, and analyses which were carried out indicated the absence of pulse

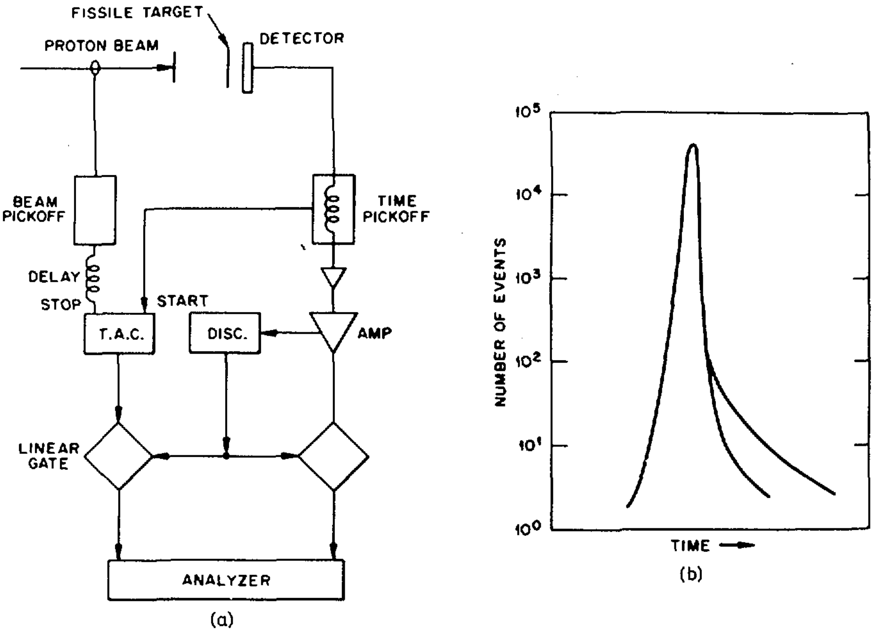

FIG.D. a) Experimental arrangement; b) number of events versus time (see text).

amplitude effects on the observed time distributions. Runs were made at E_n = 1.1, 1.4, 1.6 and 1.8 MeV.

To summarize the results, at E_n = 1.1, 1.6 and 1.8 MeV the time spectra of fission events were essentially the same, and are represented by the lower curve sketched in Fig.D. At E_n = 1.4 MeV a curve such as the upper one sketched in Fig.D and showing a small component of delayed fission events was obtained. The half-life obtained was about 3 ns and the ratio of delayed to prompt fission events was about 10^{-3}. Repeated runs at the various energies gave essentially the same results. If these results are confirmed by the experiments now being initiated, in which the beam time-profile will be independently monitored (a problem in all fission isomer experiments with pulsed beams), it would appear that isomer formation might in these cases show resonance behaviour as a function of excitation energy and that it might not be unreasonable to expect the correction proposed above between vibrational states in the second minimum and fission isomers.

G. SLETTEN: I would like to present some recent results on fission isomers obtained by Dr. Polikanov and myself in Copenhagen. We have heard in the three preceding papers on fission isomers that there might be more than one fission isomer ascribed to the same nucleus. Probably this is also the case with the americium isotopes. In Fig.E we see that the bombardment of ^{243}Am with 13.0 MeV deuterons gives two new fission isomers. We assign to ^{243}Cm the nanosecond activity detected by the fission-in-flight method and polycarbonate detectors and to ^{244}Cm the microsecond activity detected electronically with a pulsed beam technique. In Fig.F you see the half-life curve obtained. The assignment of both isomers is made on the basis of their excitation function behaviour. The above preliminary result means that, in addition to the already known 1.1-ms isomer in ^{244}Am, we probably have a second isomer with 6.5-μs half-life. This finding suggested that the same thing could be possible also for the other odd-odd americium isomers.

	$T_{1/2}$	ISOMER
^{238}Pu + p	5 nsec	^{237m}Am
^{239}Pu + d	~4 μsec	^{239m}Am?
^{240}Pu + d	~100 μsec	^{240m}Am?
^{241}Am + d	27 nsec	^{241m}Cm?
^{243}Am + d	35 nsec	^{243m}Cm
	6.5 μsec	^{244m}Am?

FIG. E. Some recent results on fission isomers.

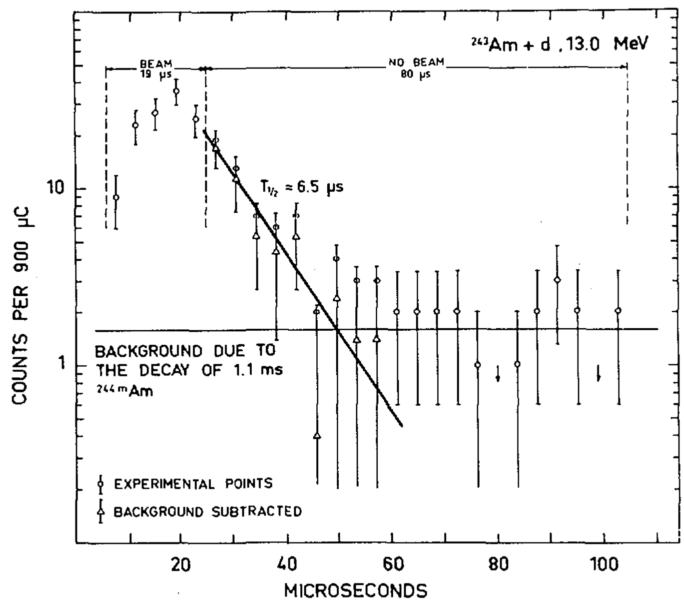

FIG. F. Half-life curve obtained with ^{243}Am + d, 13.0 MeV reaction.

In bombarding ^{240}Pu with deuterons at 13.0 MeV, we observe an isomer with about 100-μs half-life as indicated in Fig.E. We believe that the decay is due to an isomer in ^{240}Am formed through a (d, 2n) reaction since, in carrying out the (p, 2n) reaction on ^{241}Pu that leads to the same final nucleus, we observe a similar half-life. As you know, an isomer of 0.9-ms half-life in ^{240}Am has already been reported.

We think therefore that this nucleus also has two fission isomers. In Fig.E we have also indicated the possibility of an approximately 4-μs fission isomer in ^{239}Am, in which a 180-ns isomer has already been reported. The assignment of the new 4-μs isomer is however uncertain, but it implies, in any case, the existence of one more double isomer, since the most probable reaction products ^{240}Pu and ^{239}Am already have isomers assigned to them. In conclusion, one may say that the existence of more than one fission isomer in the same nucleus seems to be the rule rather than the exception.

In Fig.E we also present the observation of a 5-ns fission isomer in ^{237}Am. The assignment here is unambiguous, since the excitation function shows a threshold behaviour typical of a (p, 2n) reaction. This half-life also fits nicely into the half-life systematics which is known already to exist for the odd-odd and odd-A americium fission isomers. (Lark, N., Sletten, G., Pedersen, J. and Bjφrnholm, S. submitted to Nucl. Phys. (1969).)

We also observe a 27-ns isomer on bombarding ^{241}Am with deuterons. Proton bombardments of both ^{241}Am and ^{243}Am at energies where (p, 2n) reactions are the most probable seem to rule out the existence of nanosecond isomers in both ^{240}Cm and ^{242}Cm and the assignment of the 27 nsec activity to ^{241}Cm. Therefore, our tentative conclusion on the Cm isomers is that we have an odd-even effect in the half-lives.

As regards the results presented by Dr. Elwyn on the work done by him and Dr. Ferguson, I would like to mention that we, too, have observed the ^{236}U isomer, which we populate through the (d, p) process. On the other hand, we fail to observe either the ^{234}U or the ^{235}U isomer. For ^{234}U we have a limit which is 30 times less than the cross-section we measure for ^{236}U, while Elwyn and Ferguson get the same cross-section within a factor of two.

Lastly, I would like to say that much of the information we now have on fission isomers has not contributed significantly to the understanding of the phenomenon as such. Many new levels have been put on the isotope chart but I think that we must, in the future, focus our attention more on the precise description of the individual isomers.

J.P. THEOBALD: Since there are so many laboratories working on shape isomerism, I would like to ask if any of you knows about the existence of a shape isomer in ^{238}Np and its half-life, because there is some confusion in the literature. This is also interesting in view of the Saclay experiments on subthreshold fission.

G. SLETTEN: I would just say that we observe, on bombarding ^{238}U with neutrons, a 300 ns fission activity, which in an earlier report we assigned to ^{238}Np. However, this assignment is rather uncertain and I think today we are in no position to say that there is an isomer ^{238}Np. We are more inclined to ascribe this to ^{239}Np, but this is very uncertain.

S. BJφRNHOLM (Chairman): It must be said that with the many new isomers that have been reported the present situation is confusing. In addition to these mentioned here, F. Ruddy and J. Alexander of the University of Stoney Brook, USA, for example, report nanosecond isomers in the Po - Rn and $^{147-150}$Gd regions. This is another very important challenge to our understanding of what is going on. At present, we certainly seem to be in a growth phase rather than one of clarification.

О ВАРИАЦИИ КИНЕТИЧЕСКОЙ ЭНЕРГИИ ОСКОЛКОВ ПРИ ДЕЛЕНИИ ^{235}U НЕЙТРОНАМИ С ЭНЕРГИЕЙ 0,006 – 20 эв

С.БОЧВАРОВ, Е.ДЕРМЕНДЖИЕВ, Н.КАШУКЕЕВ
Объединенный институт ядерных исследований,
Дубна (СССР)

Abstract — Аннотация

VARIATION OF KINETIC ENERGY OF FRAGMENTS IN FISSION OF ^{235}U WITH 0.006 - 20eV NEUTRONS. Utilizing the LNF ONYaI neutron spectrometer working in the energy range between 0.006 and 20 eV, the variation in fragments' kinetic energy (E_K) was studied, applying the method of relative yields (W) measurements, in the thermal neutron region and at 11 resonances of ^{235}U. It was found that the resonances at 0.29, 2.04, 3.14, 4.84, and 7.09 eV can be sorted in a group of resonances with small values of W and E_K. The resonances at 1.14, 3.60, 6.40, 8.78, 12.4, and 19.3 eV form a group with big values of W and E_K. Comparison of W with radiochemical data on fragments' yield at thermal and resonance region of ^{235}U showed that E_K is larger at more asymmetrical fission. From the values $\overline{W}$ (I) and W(II) for the two groups of resonances, the change in the average kinetic energy of fragments $2\Delta\overline{E}_K = 0.74 \pm 0.32$ MeV was determined.

О ВАРИАЦИИ КИНЕТИЧЕСКОЙ ЭНЕРГИИ ОСКОЛКОВ ПРИ ДЕЛЕНИИ ^{235}U НЕЙТРОНАМИ С ЭНЕРГИЕЙ 0,006 – 20 эв. На нейтронном спектрометре ЛНФ ОИЯИ в диапазоне энергий нейтронов 0,006 – 20 эв методом измерения относительного выхода W осколков из двух различных по толщине мишеней исследовалась вариация кинетической энергии осколков E_K в тепловой области и в 11 резонансах ^{235}U. Найдено, что резонансы 0,29 эв, 2,04 эв, 3,14 эв, 4,84 эв и 7,09 эв можно выделить в группу резонансов с меньшим значением W и, соответственно, E_K, а резонансы 1,14 эв, 3,60 эв, 6,40 эв, 8,78 эв, 12,4 эв и 19,3 эв – в группу с большим W и E_K. Сопоставление значений W с радиохимическими данными по выходам осколков деления в тепловой области и в резонансах ^{235}U показывает, что, по-видимому, E_K больше при более асимметричном делении. Из значений W(I) и W(II) для двух групп резонансов определено изменение средней суммарной кинетической энергии осколков $2\Delta\overline{E}_K = 0{,}74 \pm 0{,}32$ Мэв.

В каналовой теории деления [1] предполагается, что при делении тяжелых ядер нейтронами ряд характеристик процесса деления может зависеть от значений спина I и проекции спина K на ось симметрии делящегося ядра в седловой точке.

Андреевым [2] и Усачевым [3] обсуждались причины, которые могли бы вызвать изменение кинетической энергии осколков E_K при делении ядер s- и p – нейтронами. Экспериментальное исследование зависимости средней кинетической энергии осколков E_K от энергии бомбардирующих нейтронов E_H для ^{233}U и ^{235}U [3] показало, что E_K отлична для s- и p – нейтронов. Зависимость E_K от определенного значения I можно было бы получить, изучая E_K в резонансной области E_H при делении тяжелых ядер s – нейтронами. Возможные изменения E_K в нейтронных резонансах ^{235}U исследовались в работе [4]. В данной работе приводятся результаты исследования вариации E_K при делении ^{235}U нейтронами в диапазоне энергий 0,006 – 20 эв. Расширение энергетического интервала в сторону малых E_H позволяет сопоставить возможные изменения E_K в резонансах с наиболее надежными данными Сэйлора [5] и Даббса [6] о спинах первых нейтронных резонансов ^{235}U, которые были получены при помощи поляризационной техники.

МЕТОДИКА ИЗМЕРЕНИЙ

Исследование зависимости $E_K(E_H)$ для ^{235}U осуществлялось путем сравнения относительных выходов осколков деления из двух мишеней разной толщины в одном и том же интервале энергий нейтронов [4]. В качестве детектора осколков использовалась двойная импульсная ионизационная камера с сетками. Одна половина камеры регистрировала осколки, вылетающие из тонкой мишени, а другая – осколки из толстой мишени. В разных сериях измерений использовались мишени разной толщины: толщина урановых слоев менялась в пределах $\bar{\rho} \approx 30 - 350$ мкг/см^2 и $1 - 4$ мг/см^2 для тонкой и толстой мишеней соответственно. Импульсы от осколков, зарегистрированных в соответствующих половинах камеры, далее усиливались, пропускались через пороговое устройство и поступали в Измерительный центр Лаборатории нейтронной физики Объединенного института ядерных исследований (ОИЯИ). Временные спектры деления для толстой и тонкой мишеней измерялись многоканальными временными анализаторами с промежуточной памятью. Обработка полученной информации проводилась на ЭВМ.

В качестве источника тепловых и резонансных нейтронов использовался импульсный реактор ИБР ОИЯИ [7] . При работе реактора ИБР совместно с микротроном [8] камера устанавливалась на расстоянии $L = 16{,}5$ м от активной зоны реактора, и разрешение нейтронного спектрометра составляло $\sim 0{,}2$ мксек/м. В реакторном режиме разрешение было ~ 3 мксек/м. Для уменьшения фона от рассеянных нейтронов камера окружалась защитой.

Более подробное описание детекторной аппаратуры и некоторые особенности использования ее для спектрометрии осколков деления в условиях работы с импульсным источником нейтронов – реактором ИБР приводятся в работе [9] .

РЕЗУЛЬТАТЫ ИЗМЕРЕНИЙ

Относительные выходы осколков определялись как отношение W числа зарегистрированных делений в соответствующих резонансах ^{235}U или интервалах E_H временных спектров деления толстой и тонкой мишеней.

Фон во временных спектрах в области первых резонансов ^{235}U определялся при помощи резонансных фильтров из Cd, Rh, Ag и Br, поставленных на пропускание. Например, при работе реактора ИБР совместно с микротроном величина фона во временных спектрах деления для толстой мишени в резонансах 8,78 эв, 4,84 эв и 0,29 эв составляла 1%, 18% и 0,6% от суммы счетов под соответствующими резонансами. В области E_H 0,08 – 0,04 эв фон был порядка 0,3% от суммы счетов делений в каждом из энергетических интервалов.

Условия измерений в данной работе выбирались такими, что наиболее существенные поправки – на мертвое время анализатора и ослабление нейтронного потока в толстой мишени – не превышали 1% для наиболее сильного резонанса 8,78 эв. Условия, в которых проводилось каждое из измерений величин W, подробно описаны в [10]. Значения W калибровались на величину W = 1,00 для резонанса 0,29 эв.

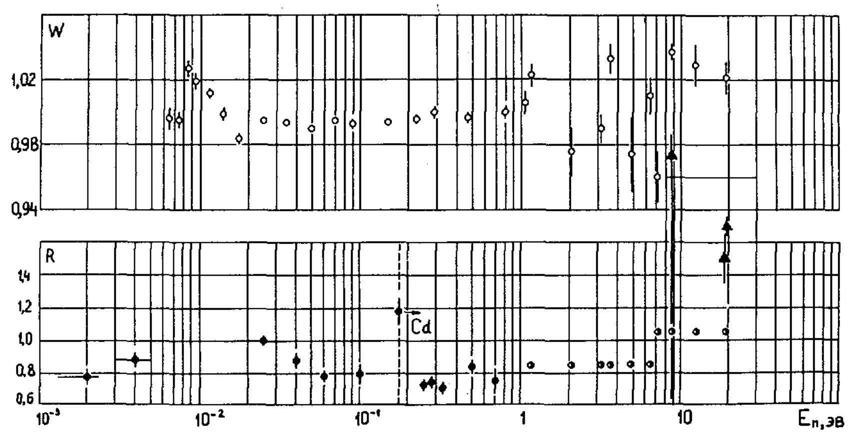

Рис.1. Зависимость $\overline{W}$ и асимметрии деления R [12] от E_H. ● – данные работы [12]; ◑ – [15]; ▲ – [16]; о – $\overline{W}$.

На рис.1 представлены значения $\overline{W}$, которые являются средними по всем измерениям. Можно отметить, что для резонансов 0,29 эв, 2,04 эв, 3,14 эв, 4,84 эв и 7,09 эв $\overline{W} \leq 1{,}00$, а для резонансов 1,14 эв, 3,60 эв, 6,40 эв, 8,78 эв, 12,4 эв и 19,3 эв $\overline{W} \geq 1{,}01$. Возможность разделения резонансов на две группы по величине W проверялась при помощи "нулевой" гипотезы о совпадении центров распределений [11] обеих групп при уровнях значимости q = 0,01 и 0,05. Проверка показала, что можно допустить существование двух групп величин W с центрами распределений W(I) и W(II). В разделах 1 и 2 таблицы 1 приводятся средневзвешенные и средние арифметические значения W(I) и W(II), а также разность W(II) – W(I), характеризующая величину эффекта разделения резонансов на две группы. Можно отметить совпадение в пределах ошибок величин W(I), W(II) и W(II) – W(I) из обоих разделов таблицы для каждого измерения и для средних по всем измерениям. Сравнение величин W(II) – W(I) для измерений 7,8 и 9, которые проводились при порогах дискриминации 20,55 и 80 Мэв в канале толстой мишени, показывает, что при повышении порога имеется тенденция к увеличению эффекта разделения резонансов на группы.

Между резонансами 0,29 эв и 1,14 эв значение $\overline{W}$ близко к 1,00, возрастая до W ~ 1,01 по мере приближения к резонансу 1,14 эв. Из рис.1 видно, что в интервале E_H 0,02 – 0,2 эв величина W имеет промежуточное по сравнению с W в резонансах значение. В области 0,008 – 0,012 эв имеется небольшой подъем в значениях $\overline{W}$, который выходит за пределы ошибок. В работе [12], примерно в том же диапазоне E_H, также отмечалась нерегулярность в значении величины R(E_H), характеризующей асимметрию деления ^{235}U.

Необходимо отметить некоторое сходство между зависимостью $\overline{W}$(E_H) на рис.1 и изменением выходов наиболее длиннопробежных тяжелых осколков при делении ^{235}U нейтронами, которое исследовалось в

ТАБЛИЦА 1. РЕЗУЛЬТАТЫ ИЗМЕРЕНИЙ

Измерение	1		2	
	W(I) W(II)	W(II) – W(I)	W(I) W(II)	W(II) – W(I)
1	0,997 ± 0,005 1,036 ± 0,005	0,039 ± 0,007	0,974 ± 0,011 1,033 ± 0,008	0,059 ± 0,014
2	0,997 ± 0,018 1,036 ± 0,007	0,039 ± 0,019	0,993 ± 0,028 1,028 ± 0,010	0,035 ± 0,030
3	0,999 ± 0,010 1,041 ± 0,014	0,042 ± 0,017	0,995 ± 0,019 1,043 ± 0,020	0,048 ± 0,028
4	0,997 ± 0,010 1,031 ± 0,014	0,034 ± 0,017	0,997 ± 0,022 1,030 ± 0,021	0,033 ± 0,031
5	0,995 ± 0,008 0,993 ± 0,008	- 0,002 ± 0,011	0,989 ± 0,025 0,989 ± 0,009	0
6	0,992 ± 0,007 1,013 ± 0,006	0,021 ± 0,009	0,971 ± 0,017 1,005 ± 0,007	0,034 ± 0,018
7	0,997 ± 0,009[a] 1,019 ± 0,010	0,022 ± 0,014	0,968 ± 0,025[a] 1,012 ± 0,013	0,044 ± 0,028
Среднее по всем измерениям	0,997 ± 0,003 1,029 ± 0,003	0,032 ± 0,004	0,980 ± 0,008 1,025 ± 0,005	0,045 ± 0,010

[a] – W(I) для измерения 7 сосчитаны без резонанса 4,84 эв.

Примечания: 1. В измерениях 1-4 пороги регистрации осколков из толстой мишени устанавливались на уровне 35 – 45 Мэв. В измерениях 5,6 и 7 пороги равнялись 20,55 и 80 Мэв соответственно.

2. В колонках 1 и 2 приводятся средневзвешенные и средние арифметические значения соответственно.

работе [13], как в тепловой области E_H, так и при E_H, равной 0,29 эв, 1,14 эв, 2,04 эв, 4,84 эв, 6,40 эв, 7,09 эв и 8,78 эв.

ОБСУЖДЕНИЕ

1. О вариации E_K

Наблюдаемые в данной работе вариации значений $\overline{W}$ в нейтронных резонансах ^{235}U и разделение резонансов на две группы по величине $\overline{W}$ можно сопоставить как со значениями I^{π}, определенными в работах [5,14], так и с условными разделениями резонансов на две группы, которые проводились авторами работ [4,6,15–19], хотя трудность такого сопоставления из-за отсутствия полной и достаточно надежной информации о спинах резонансов ^{235}U очевидна.

В таблице 2 для резонансов, которые исследовались в данной работе, приводятся величины I^{π}, условные значения спина или данные, на основе которых проводилось разделение резонансов на две группы. Полученные нами значения $\overline{W}$ для первых трех резонансов согласуются с выводами авторов [5,17] о том, что спины резонансов 0,29 эв и 2,04 эв должны отличаться от спина резонанса 1,14 эв. С результатами Даббса [6] наше распределение по значениям $\overline{W}$ для резонансов 0,29 эв, 1,14 эв и 8,78 эв также совпадает. Наиболее полно (за исключением резонанса 6,40 эв) наши результаты согласуются со спиновой идентификацией, проведенной Кирпичниковым и др. [19] на основании результатов интерференционного анализа сечений. С данными других работ [4,14–16,18,19] наши результаты согласуются частично.

На рис.1, вместе с результатами Фалера и Тромпа [12] по асимметрии деления ^{235}U, приводятся данные работы [15] и более поздние данные тех же авторов [16] для сильных резонансов 8,78 эв и 19,3 эв. Можно отметить, что для них большей величине $\overline{W}$ соответствует существенно большая по сравнению с тепловой точкой асимметрия деления R. В работе [12] обнаружено, что выход осколков симметричного деления в резонансе 0,29 эв в 1,3 раза больше, чем при делении нейтронами тепловых энергий. По значению $\overline{W}$ резонанс 0,29 эв попадает в группу резонансов с меньшими $\overline{W}$. Хотя число резонансов, для которых $\overline{W}$ сравниваются с асимметрией R, к сожалению, мало, сопоставление этих величин наводит на мысль о том, что резонансам с пониженным по сравнению с тепловой точкой выходом осколков симметричного деления соответствуют большие значения $\overline{W}$ и, соответственно, большие E_K осколков и наоборот. Канальная теория деления предсказывает, что деление составного ядра ^{236}U по каналу с $I^{\pi} = 3^-$ является более асимметричным, чем при делении по каналу с $I^{\pi} = 4^-$ [1]. На основе этого предположения и отмеченной выше связи между значениями величин $\overline{W}$ и асимметрией деления можно было бы считать вероятным, что в резонансах ^{235}U с $I^{\pi} = 3^-$ E_K в среднем больше, чем в резонансах с $I^{\pi} = 4^-$. Для выяснения вопроса о том, какая из величин больше, $E_K(3^-)$ или $E_K(4^-)$, очевидно необходимо провести исследования относительных выходов осколков W для большего числа резонансов и при более высоких E_H. С другой стороны, необходимо устранить противоречие между значениями спинов для резонансов 0,29 эв ($I^{\pi} = 3^-$) и 1,14 эв ($I^{\pi} = 4^-$), определенными Сэйлором [5] и противоположными значениями I для них, которые следуют из совокупности данных работ [6,14,19].

ТАБЛИЦА 2. ДАННЫЕ О РЕЗОНАНСАХ ^{235}U

E, эв	Данная работа		[15,16]	[5]	[14]	[6]	[17]	[19]		[18]		[4][a]	
	E_K		Выход симметричного деления	I	I	I	I	R		Γ_f (3⁻)	Γ_f (4⁻)	E_K	
	меньше	больше	$(Ag^{111}/Mo^{99})\cdot 10^{-3}$					(3⁻)	(4⁻)			меньше	больше
0,29	+		1,175	3		I_2	I_2			+			
1,14		+	"	4		I_1	I_1	+		+			
2,04	+		"	3			I_2		+		+		
3,14	+		"				I_2	+		+			
3,60		+	"				I_1	+		+			
4,84	+		"				I_2		+		+		
6,40		+	"				I_2		+		+		
7,09	+		0,95				I_2	+			+		
8,78		+	0,95(0,47± 72%)		3	I_1		+		+	+	+	
12,4		+	0,95		4				+		+		
19,3		+	0,95(0,67 ± 10%) (0,59 ± 3%)						+	+			+

a – данные взяты из таблицы 1 работы [4]

2. О количественной оценке изменения E_K в нейтронных резонансах ^{235}U

Хотя статистическая точность измерений, ограниченная условиями опыта, и является относительно невысокой, тем не менее можно пытаться количественно оценить изменение E_K от одной группы резонансов (с большим $\overline{W}$) к другой группе резонансов (с меньшим $\overline{W}$) следующим приближенным способом. Согласно работе [20], зависимость между пробегом R и энергией E осколков деления дается полуэмпирическим выражением:

$$R = \beta E^{\alpha} \tag{1}$$

где обе величины β и α зависят от вида осколка и вещества, в котором происходит торможение осколка. Для группы осколков в слое мишени, имеющих одну и ту же начальную кинетическую энергию E и пробег R, нетрудно получить выражение, которое связывает изменение относительного числа зарегистрированных осколков с относительным изменением начальной энергии осколков:

$$X_i \cong \left(\frac{dN/N}{dE/E}\right)_{Ei} \cong \frac{1 - A_i}{A_i} \cdot \frac{\alpha}{1 - (E_i/E)^{\alpha}} \tag{2}$$

В формуле (2) E_i – энергетический порог регистрации осколков, $A_i = (N/N_0)_{Ei}$ – отношение числа зарегистрированных осколков ко всем осколкам в мишени (с начальной кинетической энергией E). В работе [21], в частности, показано, что расчеты средней остаточной энергии осколков, доли осколков, вышедших из мишени, в предположении некоторого среднего пробега $\overline{R}$ и средней энергии осколков $\overline{E}$ для всех осколков, хорошо согласуются с более строгими расчетами этих же величин с учетом действительного энергетического распределения начальных энергий осколков. Поэтому далее для простоты полагалось, что $R = \overline{R} = 7{,}4$ мг/см² для UO_2 [21] и $E = \overline{E} = 84$ Мэв при делении ^{235}U тепловыми нейтронами [22]. Величины A_i, необходимые для вычисления X_i при разных E_i и ρ, определялись из данных работы [21]. Значения X_i (E_i, ρ), которые требуются для расчетов по формуле (2), представлены графически на рис.2. Переходя к конечным приращениям в (2), величину $\Delta N/N$ можно найти из соотношения:

$$\frac{\Delta N}{N} \cong \frac{W(II) - W(I)}{W(II)} \tag{3}$$

Разности W(II) – W(I) приводятся в таблице 1.

Следует отметить, что неоднородность слоя мишени может привести к тому, что в действительности доля осколков, выходящих из мишени и зарегистрированных детектором, будет отличаться от A_i для данного значения средней толщины слоя ρ. Поэтому нами определялась "эффективная" толщина $\bar{\rho}_{эфф.}$ мишени [10], которая соответствует действительной величине A_i. Для мишени, которая использовалась в измерениях 5 – 7 $\rho_{эфф.} = 1{,}8 \pm 0{,}15$ мг/см².

Изменение средней кинетической энергии осколков $\overline{\Delta E}$ или средней суммарной кинетической энергии парных осколков $2\overline{\Delta E}$ определялось по формуле (2) с использованием значений X_i (E_i) из рис.2 для $\rho = \bar{\rho}_{эфф.} = 1{,}8 \pm 0{,}15$ мг/см². Для $E_i = 20$ Мэв (измерение 5) W(I) и W(II) практически одинаковы. По разностям средневзвешенных и средних арифметических W(II) и W(I) (таблица 1) для $E_i = 55$ Мэв получаем $(2\overline{\Delta E})_{ср.взв.} = 0{,}74 \pm 0{,}32$ Мэв и $(2\overline{\Delta E})_{ср.арифм.} = 1{,}22 \pm 0{,}66$ Мэв соответственно. В ошибки этих величин входят погрешности в определении $\overline{\rho}_{эфф.}$ и ошибки разности ΔW. Сопоставим более точную из величин $(2\overline{\Delta E})_{ср.взв.} = 0{,}74 \pm 0{,}32$ Мэв с оценками энергетического интервала между уровнями 3^- (K = 0) и 4^- (K = 1) для составного ядра ^{236}U в седловой точке. В последних работах [23,24] величина этого интервала оценивается в $\sim 0{,}45$ Мэв [23], а в [24] приводятся две существенно отличающиеся по величине оценки: 0,8 Мэв и 0,3 Мэв. Наше значение несколько выше величины 0,45 Мэв, хотя и согласуется с нею в пределах ошибок, и близко к величине 0,8 Мэв из работы [24] .

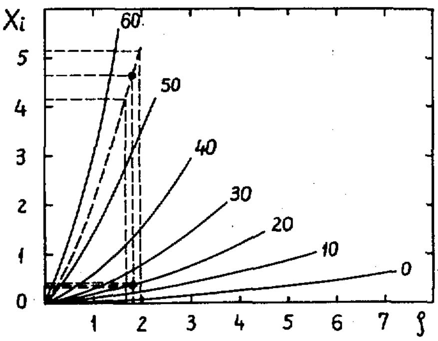

Рис.2. Кривые $X_i(E_i,\rho)$. Пороги E_i указаны в Мэв. Пунктирная кривая соответствует $E_i = 55$ Мэв. Толщина слоя ρ в мг/см^2.

Можно указать на некоторые факторы, которые могут вызвать дополнительное возрастание разности ΔW. По данным работ [15,16], выход осколков симметричного деления меняется в резонансах ^{235}U на 30–40%. Однако гораздо более существенным могло бы оказаться даже малое изменение выхода наиболее вероятных (и в среднем наиболее высокоэнергетических)осколков деления.

В заключение авторы выражают благодарность Ф.Л.Шапиро, В.И.Мостовому и Л.Б.Пикельнеру за обсуждения и полезные советы и Н.Чикову – за участие в наладке аппаратуры.

ЛИТЕРАТУРА

[1] WHELLER, J., Physica 22 (1956) 1103.
[2] АНДРЕЕВ, В.Н., "Тезисы докладов совещания по делению ядер", Ленинград, Изд. АН СССР, 1961.
[3] BLYUMKINA, J.A. et al., Nucl. Phys. 52 (1964) 648.
[4] MELKONIAN, E., MENTA, G.K., "Physics and Chemistry of Fission" (IAEA, Vienna) II 1965, p. 355.
[5] SCHERMER, R. et al., Phys. Rev. 167 (1968) 1121.
[6] DABBS, J.W.T. et al., "Physics and Chemistry of Fission" (IAEA, Vienna) I 1965, p. 39.
[7] БЛОХИН, Г.Е. и др., Атомная энергия 10 (1961) 437.
[8] АНАНЬЕВ, В.Д. и др., Препринт Р-2313, ОИЯИ (1965).
[9] АКИМОВ, Ю.К. и др., Препринт 13-4403, ОИЯИ (1969).

[10] БОЧВАРОВ, С., ДЕРМЕНДЖИЕВ, Е., КАШУКЕЕВ, Н., Препринт Р3-4110, ОИЯИ (1968).
[11] СМИРНОВ, Н.В., ДУНИН-БАРКОВСКИЙ, И.В., "Курс теории вероятностей и математической статистики", Москва, "Наука", 1965.
[12] FALER, K.T., TROMP, R.L., Phys. Rev. 131 (1963) 1746.
[13] MILLER, L.G., MOORE, M.S., Phys. Rev. 157 (1967) 1055.
[14] POORTMANS, F. et al., "Nuclear Data for Reactors" (IAEA, Vienna) II 1967, p. 215.
[15] COWAN, G.A. et al., Phys. Rev. 122 (1961) 1286.
[16] COWAN, G.A. et al., Phys. Rev. 130 (1963) 2380.
[17] КИРПИЧНИКОВ, И.В., ИГНАТЬЕВ, К.Г., СУХОРУЧКИН, С.И., Атомная энергия 16 (1964) 216.
[18] ВАН ШИ-ДИ, ВАН ЮН-ЧАН, ДЕРМЕНДЖИЕВ, Е., РЯБОВ, Ю.В., "Physics and Chemistry of Fission" (IAEA, Vienna) I 1965, p. 287.
[19] ASGHAR, M. et al., Phys. Letters 26B (1968) 664.
[20] ALEXANDER, J.M., GAZDIK, M.F., Phys. Rev. 120 (1960) 874.
[21] KAHN, S. et al., Nucl. Sci. Engineering 23 (1965) 8.
[22] MILTON, J.C.D., FRASER, J.S., Can. J. Phys. 40 (1962) 1626.
[23] BRITT, H.C., RICKEY, H.C., Bull. Amer. Phys. Soc. 13 (1968) 36.
[24] LYNN, J.E., "Nuclear Data for Reactors" (IAEA, Vienna) II 1967, p. 89.

PROMPT NEUTRONS AND GAMMA RAYS

(Session F)

Chairman: G. C. Hanna

NEUTRON MULTIPLICITY MEASUREMENTS FOR ^{233}U, ^{235}U AND ^{239}Pu RESONANCE FISSION*

S. WEINSTEIN, R. REED, R.C. BLOCK
Rensselaer Polytechnic Institute,
Troy, N.Y.,
United States of America

Abstract

NEUTRON MULTIPLICITY MEASUREMENTS FOR ^{233}U, ^{235}U AND ^{239}Pu RESONANCE FISSION. The dependence of the fission-neutron multiplicity on incident neutron energy was investigated for ^{233}U, ^{235}U and ^{239}Pu. The experiments used the Rensselaer Electron Linear Accelerator as a source of neutrons, a 70-cm diameter gadolinium-loaded scintillation tank to detect the fission neutrons, and multiplate ionization chambers to detect the fission events.

The results of measurements for 20 resolved resonances in ^{239}Pu below 100 eV show that the $\bar{\nu}$ values fall into two groups. The grouping is strongly correlated with the spins of the individual resonances with the J=0 levels corresponding to high values of neutron multiplicity and the J=1 levels corresponding to low values. The average multiplicity for the J=0 group is about 3% higher than the average for the J=1 group. The observed multiplicity grouping would lead to assignments of J=1 for the 0.298 and 23.9 eV levels, both of which were previously unassigned.

Variations in fission-neutron multiplicity were observed among the low-energy resonances of both ^{233}U (below 10 eV) and ^{235}U (below 25 eV), and spin assignments have been made for 13 resonances in ^{235}U. The results in the energy region from 0.01 to 0.3 eV show that the multiplicity is independent of energy for ^{233}U but show a statistically significant decrease for ^{235}U in going from 0.3 to 0.01 eV.

1. INTRODUCTION

Experiments over the past few years have shown that some features of the fission process vary from resonance to resonance in the common fissile nuclides. For example, Cowan and others [1] have observed variations in the fission-product mass yield, and Melkonian and Mehta [2] have shown that the kinetic energy of fission differs significantly from one resonance to another. These results can be interpreted as indicating that the mean number of neutrons emitted per fission $\bar{\nu}$ should also vary in a systematic manner among these resonances, and the experiments described here are an attempt to measure this variation. The results presented in this paper are restricted to the energy region from 0.01 eV to 100 eV for ^{239}Pu, 0.01 eV to 5.5 eV for ^{233}U, and 0.01 eV to 25 eV for ^{235}U.

2. EXPERIMENTAL TECHNIQUE

For the experiments reported here the neutrons were produced by the Rensselaer 100 MeV Electron Linear Accelerator. The detector system consisted of a multiplate fission ion chamber at the centre of a 70 cm

* Work sponsored by the US Atomic Energy Commission under Contract AT(30-3)-328.

gadolinium-loaded liquid scintillator tank which was located 25 metres from the source of neutrons (see Fig.1). Fission events were detected by the occurrence of a coincidence between the signals from the fission chamber and prompt-fission gamma-ray events from the scintillation tank. The fission neutrons were detected, after thermalization in the scintillant, by means of the gamma radiation emitted following neutron capture in the gadolinium. These events were counted by a 10 MHz scaler for 32 μs following the detection of the coincidence. The detected neutron multiplicity (up to a maximum value of 11) for each of 256 time-of-flight channels was first stored in a temporary buffer in a specially designed logic circuit and then transferred to a 256 $\times$ 12 array in the memory of a PDP-7 on-line computer.

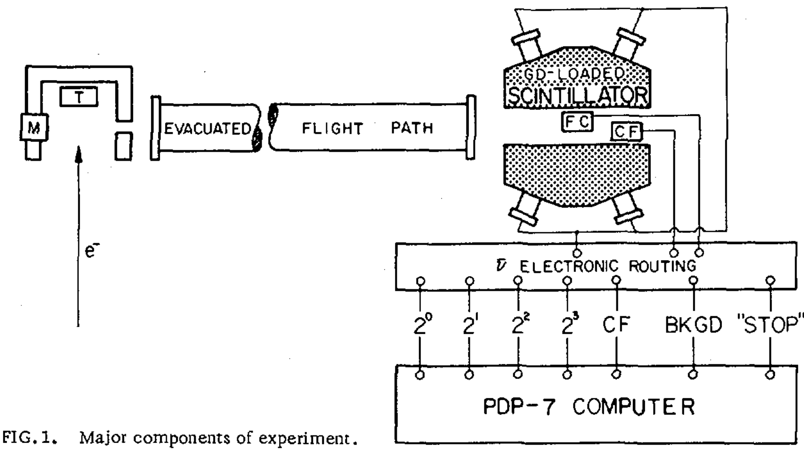

FIG.1. Major components of experiment.

There was a significant probability that a background event would have been detected during the 32-μs counting interval. It is to be expected that the background multiplicity per fission gate would be correlated with the scattering, capture, and fission cross-sections of the materials present in the fission chamber. To determine the number of background events per gate (as a function of time of flight) background sampling pulses from a free-running pulse generator were used to initiate simulated fission coincidences. The multiplicity data associated with the background sampling pulses were treated exactly as were data from fission coincidences, and were stored in an additional 256 $\times$ 12 array in the computer. To prevent accidental events due to overlap of two or more fissions (or backgrounds) no events (fission or background) were stored which occurred within 120 μs of another event.

The interpretation of the experimental data, that is the extraction of $\bar{\nu}$ values, requires the application of corrections for several effects. The principal ones are spontaneous fission, accidental coincidences, and scaler dead-time. Spontaneous fissions were detected only from the ^{239}Pu chamber and, as the rate was independent of neutron time of flight, the corrections can be applied with some confidence. However, the accidental coincidence rate was correlated with the scattering and capture cross-sections of the materials in the fission chamber. Since the accidental coincidence rate is highest at resonances where the capture-to-fission ratio α is highest, it is important that the correction be carefully applied if one is to avoid spurious correlations between α and $\bar{\nu}$. For ^{239}Pu both the spontaneous fission and accidental coincidences of the corrections amounted to 0.1 to 2% of $\bar{\nu}$. Corrections in the range of 0.3 to 2% were applied for scaler dead-time effects. The variations in this correction were primarily associated with the time-of-flight dependence of the observed background multiplicity.

Ultimately, the confidence with which these corrections can be applied, and in fact the credibility of the experimental conclusions, depends upon the reproducibility of the results under a variety of experimental conditions. For this experiment data were taken, for selected time-of-flight regions, with the neutron intensity (fission rate) varying by a factor of four, with a factor-of-twenty variation in the accidental coincidence rate, and with approximately a factor-of-four variation in the ratio of the spontaneous to induced fission rates. The $\bar{\nu}$ values inferred from all of these data agreed to within 0.5%, the precision of these sensitivity measurements.

A ^{252}Cf fission chamber was permanently mounted in the "through tube" of the scintillation tank, and ^{252}Cf spontaneous fission $\bar{\nu}$ data were taken concurrently with data from the plutonium or uranium chambers. Thus, all neutron-induced fission $\bar{\nu}$ values could be expressed relative to the ^{252}Cf $\bar{\nu}$ value, permitting data acquisition that was nearly independent of electronic gain drifts. Because of differences in location and geometry, no absolute intercalibration was made between the neutron multiplicity values for ^{252}Cf spontaneous fission and ^{233}U, ^{235}U, or ^{239}Pu neutron-induced fission. The set of $\bar{\nu}$ data for each nuclide was separately normalized to a standard prompt $\bar{\nu}$ value at thermal-neutron energy (0.0253 eV). The standard values, which were based on Westcott's [3] recent evaluation, were:

$$\bar{\nu}\ (^{233}\mathrm{U}) = 2.5007$$

$$\bar{\nu}\ (^{235}\mathrm{U}) = 2.4266$$

$$\bar{\nu}\ (^{239}\mathrm{Pu}) = 2.8698$$

3. ^{239}Pu RESULTS

The manner in which the fast memory of the PDP-7 computer was configured limited the number of time-of-flight channels to 256. Thus, to obtain adequate energy resolution, it was necessary to take the resonance fission data in three sets of overlapping runs, one from 0.01 to 13 eV, another from 6.5 to 45 eV and a third from 20 to 100 eV. Even with three fields of data the energy resolution is not good enough to permit the complete separation of close-lying levels. It was, therefore, necessary to develop criteria that would permit the selection of time-of-flight regions assignable to a single level. A rather subjective approach was used that involved selecting resonances which appeared isolated and which would be predicted to be isolated on the basis of multilevel fitting parameters [4]. Also analysed as single levels were regions containing two levels which were not resolved in the present

TABLE I. ^{239}Pu RESONANCE SPIN (J) ASSIGNMENTS

Resonance energy (eV)	Present work	DIRECT			INDIRECT		
		Sauter and Bowman [5]	King and Block [6]	Asghar [7]	Cowan et al. [1]	Melkonian and Mehta [2]	Farrell [4]
0.298	1						
7.85	1	1					
10.95	1	1					
11.9	1	1					
14.3	1	1					1
14.7	1	1		1			1
15.5	0	0			1		0
17.7	1	1		1	1		1
22.3	1	1		1	1	1	1
23.9	1						1
26.2	1			1	1	(1)	1
32.3	0	0			(0)	0	0
41.5	1	1	1	1	1	(0)	1
44.5	1	1	1	1	1	(1)	1
47.6	0	0		0	1	1	0
52.6	(0)*	1	1	1	1	1	1
62.7	0						0
75.0	1	1	1	1	1	1	1
81.0	0				0		0
90.0	0		0	1			

* Parentheses indicate uncertain assignments.

experiment but which appear to have the same compound nuclear spin, e.g. the 74.2 and 75.0 eV J=1 levels. The values for the 20 time-of-flight regions are shown in Fig.2 as a function of E_0, the resonance energy; the error bar on each point corresponds to a standard deviation determined from the counting statistics. It can be seen that there

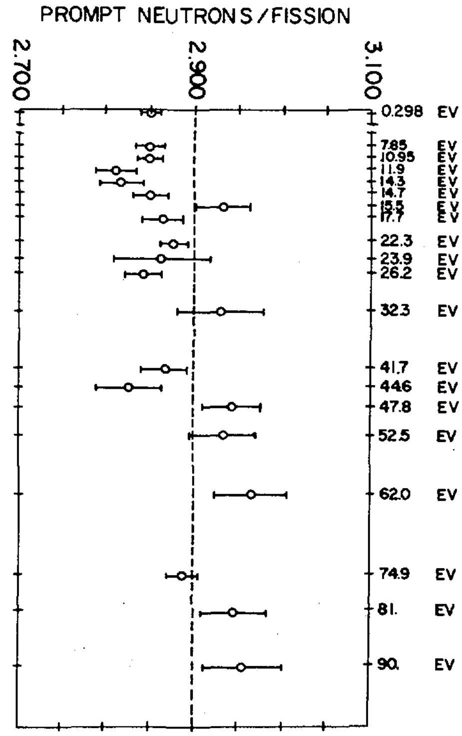

FIG.2. ^{239}Pu $\bar{\nu}$ values for 20 resonances below 100 eV.

are variations among the $\bar{\nu}$ values for these resonances, and that the values appear to fall into two distinct groups. A grouping of all of these levels with $\bar{\nu}$ values greater than 2.900 into one set (high) and all below into another set (low) has been made. Each of the sets has been tested with a weighted chi-square fit and found to be consistent with the hypothesis that the values conform to a normal distribution about a constant (mean) value. On the other hand, when the entire set of 20 levels was similarly tested, it was found that the probability was less than 0.01 that the individual values are from a normal distribution about a single mean. The results of these tests have led to the conclusion that $\bar{\nu}$ does vary from resonance to resonance for the neutron-induced fission of ^{239}Pu and that $\bar{\nu}$ for any isolated level can in all likelihood have just one of two possible values.

On the basis of a very simple model of the fission process it might be expected that a low-lying fission channel would be associated with a

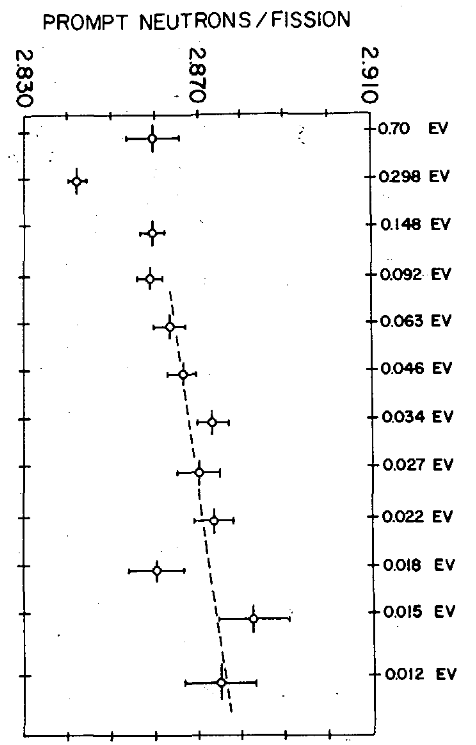

FIG.3. ^{239}Pu $\bar{\nu}$ variation for incident neutrons below 1 eV.

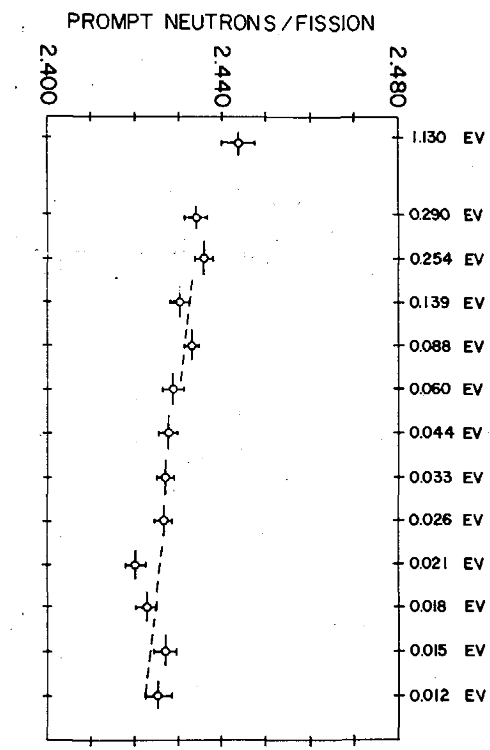

FIG.4. ^{235}U $\bar{\nu}$ variation for incident neutrons below 1 eV.

higher value of fission neutron multiplicity than a channel that lies higher at the fission saddle point. Since, for low-energy neutron-induced fission of ^{239}Pu, the 0^+ channel almost certainly lies below the 1^+, it would follow that the high group of $\bar{\nu}$ values would be attributed to the 0^+ channel and the low values to the 1^+. Spin assignments based on the $\bar{\nu}$-grouping have been made for the 20 resonances studied and are listed in Table I. Also shown in the table are direct spin assignments (statistical g-value determinations) by Sauter and Bowman [5], King and Block [6], and Ashgar [7], and indirect assignments by Cowan et al. [1] (fission yield asymmetry), Melkonian and Mehta [2] (fission fragment kinetic energy variations), and Farrell [4] (multilevel fit to the ^{239}Pu fission cross-section). The agreement among assignments based on the $\bar{\nu}$-grouping, the direct (g-value) determinations, and the multilevel fitting is excellent. A two-sided rank-mean test of the relationship between the $\bar{\nu}$-groupings and the direct determinations of J indicates that the probability that the observed correlation is a chance occurrence is about 0.0005. However, because of the statistical uncertainties associated with the values, it is not expected that the correlation would be perfect. The distribution of values about the two means has been shown to be approximately normal, and it would not be improbable to find an "overlap" between the two distributions. This is probably the case with the 52.6 eV resonance which falls into the J=0 group but is assigned to J=1 in all of the other table entries.

The average values of $\bar{\nu}$ have been computed separately for the two spin groups. It is found that $\bar{\nu}$ (J=0) is about 3% greater than $\bar{\nu}$ (J=1), corresponding to the production of about 0.09 more neutrons for fission through the 0^+ channel. Measurements of the energy dependence of $\bar{\nu}$ for ^{235}U over a range from 0.025 to 14 MeV [8] indicate that at very low neutron energies $\bar{\nu}$ increases by 0.088/MeV of excitation energy. If the same functional relationship exists for ^{239}Pu in this energy region, and if all of the excess saddle point energy is available for additional neutron emission, then the present observed $\bar{\nu}$ difference can be interpreted as indicating that the 0^+ channel lies about 1.0 MeV lower than the 1^+ channel.

In addition to the measurements at resolved resonances there were also measurements made of the $\bar{\nu}$ variations over the thermal region. The results are shown in Fig.3. It can be seen that the value of $\bar{\nu}$ for the 0.298 eV resonance is about 1% lower than the value at 0.0253 eV. The observed distribution of $\bar{\nu}$ values suggests that a "negative energy" $J=0^+$ level is making a significant contribution to the fission cross-section at very low energies. An attempt was made to synthesize the observed $\bar{\nu}$ variation from the know parameters for the 0.298 eV level and an assumed $J=0^+$ "negative energy" level, while conserving the total measured fission cross-section. The synthesized distribution deviated from the measured one, indicating that both $J=0^+$ and $J=1^+$ "negative energy" levels might be contributing.

4. ^{235}U RESULTS

Fission multiplicity data were taken for ^{235}U over the thermal energy region and in the resonance region up to 25 eV. The thermal results are plotted in Fig.4. There is an apparent variation of $\bar{\nu}$ over the thermal

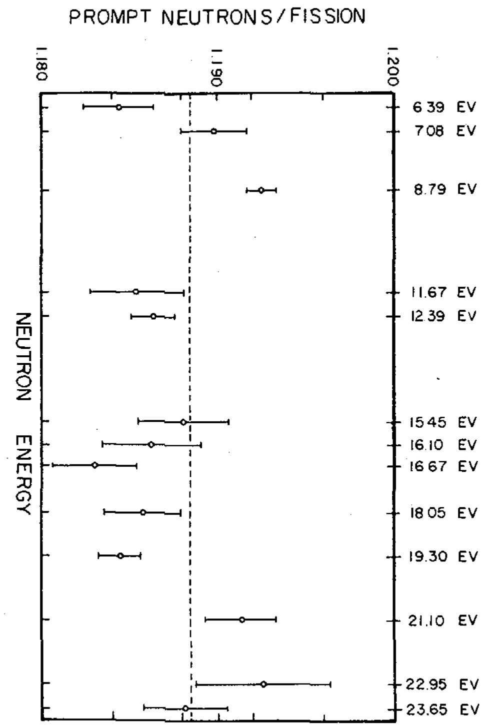

FIG.5. $^{235}U\ \bar{\nu}$ grouping for 13 resonances below 25 eV. The ordinate is arbitrarily normalized.

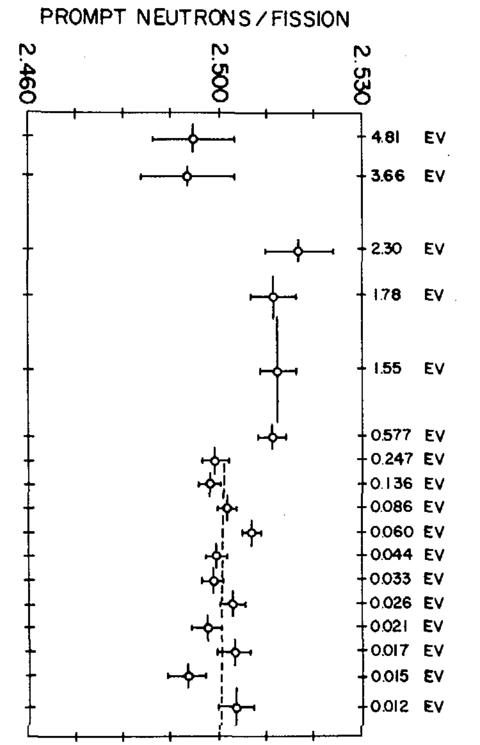

FIG.6. $^{233}U\ \bar{\nu}$ variation for incident neutrons below 5.5 eV.

TABLE II. ^{235}U RESONANCE SPIN (J) ASSIGNMENTS

Resonance energy (eV)	Present work	Ashgar et al. [9]	Weigmann et al. [10]
6.39	4	4	4
7.08	3	3	3
8.79	3	3	
11.67	4	4	
12.39	4	4	4
15.45	U*	3	3
16.10	4	(4)+	3
16.67	4	3	3
18.05	4	3	
19.30	4	4	4
21.10	3		3
22.95	3	3	3
23.65	U		4

* Unassigned
\+ Uncertain assignment.

region for this nuclide, with a multiplicity reduction of about 0.6% from the 0.3 eV resonance to 0.012 eV. Variations of this magnitude must be looked upon with suspicion because of possible systematic biases and statistical fluctuations. However, this measurement was repeated with a different set of experimental conditions and the same variation observed. From a careful consideration of possible systematic effects, a $\bar{\nu}$ variation of this magnitude cannot be attributed to any time-of-flight dependent bias. We thus conclude that the observed thermal variation is a true reflection of a change in $\bar{\nu}$.

The resonance region $\bar{\nu}$ results are plotted in Fig.5. The data for the resonance region have not been completely analysed and the results for the 13 resolved resonances shown in Fig.5 have been arbitrarily normalized. The resonance $\bar{\nu}$ values appear to fall into two groups, a high group containing the 8.79 eV level and a low group containing the 19.3 eV level. If the same method of assigning compound nuclear spins is applied to these results as was applied to the ^{239}Pu results, then the resonances with high values of $\bar{\nu}$ can be assigned to $J^{\pi}=3^-$ and the resonances with low values to $J^{\pi}=4^-$. Spin assignments for these 13 levels are shown in the Table II along with assignments by Ashgar [9] and Weigmann et al. [10] based on capture gamma ray spectra measurements. The agreement among the three sets of assignments is seen to be quite good though possibly fortuitous since the grouping might have an additional dependence on K, the rotational quantum number.

5. ^{233}U RESULTS

Data were taken for ^{233}U only for the resonances below 5 eV and for the thermal region, and the resultant $\bar{\nu}$ values are shown in Fig.6. There is an indication of a grouping of the $\bar{\nu}$ values in the resonance region, but the statistical quality is too low to permit any firm conclusions to be drawn. We have concluded however that $\bar{\nu}$ is constant (to about 0.2%) over the neutron energy range from 0.01 to 0.2 eV.

6. SUMMARY

The variation of fission multiplicity $\bar{\nu}$ has been determined up to several tens of eV for the common fissile nuclides ^{233}U, ^{235}U, and ^{239}Pu to an accuracy of a few tenths of one per cent. The measured value of $\bar{\nu}$ in isolated resonances of ^{235}U and ^{239}Pu is correlated with the compound nuclear spin, the larger $\bar{\nu}$ values corresponding to 3^- and 0^+ compound states respectively. This correlation of $\bar{\nu}$ with spin can be interpreted in terms of the channel theory of fission, with the 3^- and 0^+ states lying lower at the saddle point than the 4^- and 1^+ states. This variation of $\bar{\nu}$ from resonance to resonance has implications to reactor calculations and to the interpretation of η and α experiments which depend upon the fission multiplicity.

REFERENCES

[1] COWAN, G.A., BAYHURST, B.P., PRESTWOOD, R.J., GILMORE, J.S., KNOBELOCH, G.W., Phys. Rev. 144, (1966) 979.

[2] MELKONIAN, E., MEHTA, G.K., in Physics and Chemistry of Fission (Proc. Conf. Salzburg, 1965) 2, IAEA, Vienna (1965) 355.

[3] WESTCOTT, C.H., EKBERG, K., HANNA, G.C., PATTENDEN, N.J., SANATONI, S., Int. Conf. peaceful Uses atom. Energy (Proc. 3rd Conf. Geneva, 1964) 2, UN, New York (1965) 42.

[4] FARRELL, J.A., Phys. Rev. 165 (1968) 1371.

[5] SAUTER, G.D., BOWMAN, C.D., Phys. Rev. Lett. 15 (1965) 761.

[6] KING, T.J., BLOCK, R.C., "Neutron-scattering measurements in the resonance region", submitted for publication (1969).

[7] ASGHAR, M., Nucl. Phys. A98 (1967) 33.

[8] MATHER, D.S., FIELDHOUSE, P., MOAT, A., Phys. Rev. 133B (1964) 1403.

[9] ASHGAR, M., MICHAUDON, A., PAYA, D., Physics Lett. 26B (1964) 664.

[10] WEIGMANN, H., WINTER, J., HESKE, M., private communication.

DISCUSSION

Yu.V. RYABOV: Variations of the average number of prompt fission neutrons for ^{235}U and ^{239}Pu in the resonance neutron energy region have been investigated on the Pulsed Fast Reactor (PFR) at JINR. A 500-litre cadmium-loaded liquid scintillator was used for detecting the number of neutrons per fission event. For each resonance the value of $(\bar{\nu}\epsilon_n)$ was obtained as the ratio of the total number of neutrons recorded to the total number of fission events, taking the corresponding backgrounds into account (ξ_n is the neutron detection efficiency). The results indicated the presence of two systems of levels with $\bar{\nu}/\langle\bar{\nu}\rangle = 1.009 \pm 0.001$ ($J = 4^-$) and $\bar{\nu}/\langle\bar{\nu}\rangle = 0.989 \pm 0.002$ ($J = 3^-$) for ^{235}U, and $\bar{\nu}/\langle\bar{\nu}\rangle = 1.013 \pm 0.003$ ($J = 1^+$) and $\bar{\nu}/\langle\bar{\nu}\rangle = 0.962 \pm 0.017$ ($J = 0^+$) for ^{239}Pu.

From the currently accepted ideas about the spectrum of intermediate states at critical deformation it follows that within the energy gap a few 3^- and 4^- states belonging to different k are available for ^{235}U fission. Only two 0^+ and 1^+ states are apparently available for ^{239}Pu fission. Therefore, the observed difference in $\bar{\nu}$ is determined by the difference in the height of the effective barriers corresponding to the contributions of all the available 3^- and 4^- states for ^{235}U fission and to the 0^+ and 1^+ states only for ^{239}Pu fission. Using the known value of $d\nu/dE$, we can evaluate the difference in barrier heights for channels of various natures: $\Delta E(^{235}U) = 0.36 \pm 0.04$ MeV and $\Delta E(^{239}Pu) = 1.16 \pm 0.39$ MeV.

E. DERMENDZHIEV: I would like to draw the authors' attention to the following. Of the eight resonances of ^{239}Pu which were studied by the authors and by Ryabov et al. at Dubna, the authors of the present paper obtained opposite effects in the case of six. On the other hand, since the total fission energy is constant, the increase in the mean kinetic energy $\bar{E}_k$ of the fragments should be accompanied by a decrease in $\bar{\nu}$. For instance, in the case of the resonances in ^{235}U at 0.29 eV, 1.14 eV and 8.78 eV, which are convenient for study, we obtained data for $\bar{E}_k$ that correlated well with the Dubna results for $\bar{\nu}$ but disagreed with the results of Dr. Weinstein et al. It seems to me that the reason for disagreement between the authors' data on $\bar{\nu}$ and the Dubna results for $\bar{E}_k$ and $\bar{\nu}$ should be sought in the conditions of the experiment. I think that, as a result of relatively high thresholds of fragment registration in the chamber, the fragment spectrum above the threshold may be enriched with higher-energy light fragments in the resonances for which an increase in $\bar{E}_k$ is observed. It is known that ν increases with the asymmetry of fission. Consequently, the average number of neutrons $\tilde{\nu}$ for fragments above the threshold may be different from $\bar{\nu}$. We calculated $\tilde{\nu}$ for ^{235}U on the assumption that $\overline{\Delta E}_k = 1$ MeV. Preliminary results show that actually $\tilde{\nu}(\overline{\Delta E}_k = 1\ \mathrm{MeV}) \gtrsim \tilde{\nu}(\overline{\Delta E}_k = 0)$.

S. WEINSTEIN: It is unlikely that the fission chamber discrimination threshold could be responsible for the difference between the results obtained at the two laboratories, since our measurements have been repeated at several different threshold settings with no discernable effect on the detected $\bar{\nu}$ values. Moreover, the "conservation of fission energy" argument is incomplete, since it does not include possible fission channel variations in the relative division of the fragment excitation energy between gamma decay and prompt neutron emission.

L. WILETS: It would be helpful in visualizing Dr. Weinstein's result if he could display a histogram of the frequency of $\bar{\nu}$ versus $\bar{\nu}$.

S. WEINSTEIN: The histogram is shown in Fig. A where the area under the large peak is about four times that of the smaller one and the full width at half maximum height is the same for both.

J.R. NIX: There are at least two independent arguments one can put forward for deciding which spin group would be expected to correspond to the larger number of neutrons, and they give the opposite conclusions. The first argument is purely experimental and has been discussed by Weinstein and also by Cramer and Britt. For $^{239}Pu + n$ the mass distribution measured by G.A. Cowan et al. [Phys. Rev. 144 (1966) 979] indicates a larger number of symmetrical divisions for J = 0 states than for J = 1 states. Combining this with the second experimental result, viz. that a larger total number of neutrons are emitted for symmetrical divisions than for asymmetrical ones, we see that more neutrons should be emitted for the J = 0 group, which is in agreement with Weinstein's experimental results. On the other hand, the simplest theoretical consideration would be to assume that the fission barrier for the J = 1 state lies above the barrier for the J = 0 state by a constant amount everywhere. The J = 0 state corresponds to zero internal excitation and the J = 1 state to some internal excitation. Therefore under the simplest assumption the additional internal excitation energy in the J = 1 state would remain in the form of excitation energy and would contribute to a larger number of neutrons for this group, which is the opposite conclusion from the above.

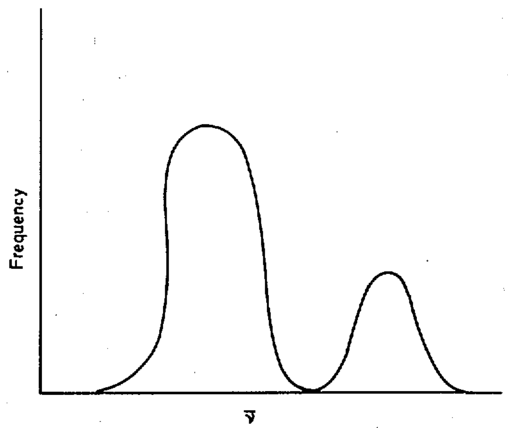

FIG. A. Frequency versus $\bar{\nu}$.

S. WEINSTEIN: It is possible that the J = 1 channel lies below the pairing gap, in which case it, too, would have no internal excitation.

Yu. V. RYABOV: I agree with the theoretical argument of Dr. Nix. Similar ideas were expressed also by Dr. V. N. Andreev (USSR).

As regards the experimental argument, we should however bear in mind that according to Cowan's data the fragment yield of a symmetric mass is greater for $J = 0^+$ (^{239}Pu) and smaller for $J = 3^-$ (^{235}U). Evidently, one cannot therefore ascribe the increase of $\langle\nu\rangle$ in the case of individual resonances solely to increased neutron emission from symmetric-mass fragments, since this effect is opposite for ^{235}U and ^{239}Pu.

J. SCOBIE: At the previous Symposium measurements were described of the ternary-to-binary fission ratio as a function of neutron energy across several resonances in ^{235}U. (Physics and Chemistry of Fission (Proc. Symp. Salzburg, 1965) 2, IAEA, Vienna (1965) 429.) As I recall, some structure was observed, and therefore I should like to ask Dr. Weinstein if he has considered the possibility that the variations he has described could be due solely to variations in the yield of the scission neutrons. It is not obvious that the yield of the latter should vary in the same way as that of the remainder of the fission neutrons across resonances. If the two groups behave differently in this respect, then it might follow that the angular distribution would vary from resonance to resonance, and this might explain the divergences between the results of Weinstein and those described by Ryabov, if the geometric arrangement of the experiments was not identical.

S. WEINSTEIN: It is my understanding that the fission neutron detection efficiency for both arrangements is relatively insensitive to the angular distribution of the emitted neutrons.

A. MICHAUDON: I should like to comment on the paper of Dr. Weinstein and the ensuing discussion. Attention has been mainly devoted to verifying whether there are correlations between the properties of the fission phenomenon (multiplicity of fission neutrons and kinetic energy of fragments) as manifest in the resonances, on the one hand, and the spin of these resonances, on the other. The discussion has accordingly related chiefly to the spin of the resonances but little to the exit channels of fission. This is quite surprising, since according to Bohr, it is the channel characteristics that influence the fission properties. These properties cannot, therefore, be tied to the spin of the resonances unless the exit channels are sufficiently different for the two spin states.

The only characteristic of the exit channel which was considered is the height of the channel barrier although it led Dr. Weinstein and Dr. Nix to opposite conclusions. In fact, even if the barrier height plays a very important role in calculating the fission probability according to the mode considered, it seems that it has little effect on the fission properties of this mode. On the other hand, accoding to Bohr's theory, the configuration of the nucleus at the threshold point is probably more important.

Let us consider, from this point of view, the case of the resonances of ^{239}Pu and ^{235}U.

1. ^{239}Pu. The resonances have spins 0^+ and 1^+. The transition states 0^+ correspond either to the ground state or to the quadrupole vibration β. These are therefore essentially symmetrical states. The same is not true of the transition state 1^+, which is considered to stem from the coupling of the two octupole vibrations $K = 0^-$ and $K = 1^-$, i.e. asymmetric states. For the two spin states, the exit channels are thus very different in nature. The same should be true of the fission properties. And this is what is found for the mass distribution of the fission products, as measured by Cowan, which shows that it is more symmetrical for 0^+ resonances than for 1^+ resonances. Besides, since the number of fission neutrons is higher in the case of symmetric fission, the multiplicity of the fission neutrons should be greater for 0^+ resonances (and not because the barrier 0^+ is lower). And this is what the Rensellaer Polytechnical Institute group has found.

2. ^{235}U. The situation is less clear than in the case of ^{239}Pu. According to the data presented by Dr. Pattenden and myself for Session D, summarized in Abstracts SM-122/57, 91 and 92, the channel $K = 0^-$ seems to be practically forbidden and the only important channels are $K = 1^-$ and $K = 2^-$. These are two octupole channels of very similar properties, both containing

the two spins 3^- and 4^-. Under these conditions, we must expect, on the one hand, that the fission properties will not vary much from resonance to resonance and, on the other, that these small variations will not necessarily be correlated with the spin of the resonances. And this is what is observed in the experimental results, in which the effects of varying the fission properties are much smaller than in the case of ^{239}Pu and the correlations with the spin of the resonances are much more dubious in nature.

ETUDE DE L'EMISSION NEUTRONIQUE DES FRAGMENTS DE FISSION DU CALIFORNIUM-252 EN FONCTION DE LEUR CHARGE

H. NIFENECKER
CEA, Centre d'études nucléaires de Saclay
et
J. FREHAUT, M. SOLEILHAC
CEA, Centre d'études nucléaires
de Bruyères-le-Châtel,
France

Abstract — Résumé

STUDY OF THE NEUTRON EMISSION OF CALIFORNIUM-252 FRAGMENTS AS A FUNCTION OF THEIR CHARGE. The charge, energy and neutron emission of californium-252 fission fragments were measured simultaneously. From these measurements the authors obtained the variations in the average number of neutrons emitted as a function of the charge and energy of the fragments. The variation in the average number ν of the neutrons emitted, studied as a function of charge, reveals the fine structures which are correlated with the fine structures of the mass distributions. These fine structures, on the other hand, do not appear to be connected with the parity of the fragment charge. The results giving the variations of $(d\nu)/(dE_T)$, of the kinetic energy of the fragments and of the widths of the different distributions as a function of Z are presented and discussed.

ETUDE DE L'EMISSION NEUTRONIQUE DES FRAGMENTS DE FISSION DU CALIFORNIUM-252 EN FONCTION DE LEUR CHARGE. Une mesure simultanée de la charge, de l'énergie et de l'émission neutronique des fragments de fission du californium-252 a été menée à bien. On a tiré de cette mesure les variations du nombre moyen de neutrons émis en fonction de la charge et de l'énergie des fragments. L'étude de la variation du nombre moyen ν de neutrons émis en fonction de la charge fait apparaître des structures fines qui sont corrélées aux structures fines des distributions en masse. Par contre ces structures fines ne paraissent pas liées à la parité de charge du fragment. Les résultats donnant les variations de $(d\nu)/(dE_T)$ de l'énergie cinétique des fragments et des largeurs des différentes distributions en fonction de Z sont présentés et discutés.

De nombreux travaux expérimentaux ont eu pour objet la mesure de l'émission neutronique prompte des fragments de fission en fonction de la masse de ces fragments. Ainsi, en ce qui concerne le ^{252}Cf, Whetstone [1] et Bowman et al. [2] ont pu mettre en évidence la fameuse courbe en «dent de scie» représentant la variation du nombre de neutrons prompts émis en fonction de la masse des fragments. Puisqu'il existe une relation entre la masse et la charge des fragments, il peut paraître superflu de mesurer leur émission neutronique en fonction de leur charge. Nous pensons toutefois que cette mesure reste intéressante pour les deux raisons principales suivantes:

- La détermination de la charge des fragments permet de mettre en évidence, sur les quantités mesurées simultanément, des effets dus à la parité du nombre de protons des fragments de fission.
- Grâce au développement des détecteurs au Si(Li), il est maintenant possible d'obtenir des résolutions expérimentales de une unité de charge,

soit environ 2,5 unités de masse. Une telle résolution est comparable aux meilleures mesures de temps de vol et présente, de plus, l'avantage d'être indépendante du nombre de neutrons émis par les fragments.

Ces considérations nous ont amenés à entreprendre l'expérience décrite ici. Nous avons pu, indépendamment de la mesure de la valeur moyenne du nombre de neutrons émis en fonction de la charge des fragments, déterminer la variance de ce nombre, la valeur moyenne de l'énergie cinétique des fragments en fonction de leur charge, la covariance de l'émission neutronique de deux fragments complémentaires et la variation du nombre de neutrons émis en fonction de l'énergie cinétique d'un fragment de charge donnée.

1. DISPOSITIF EXPERIMENTAL

Les fragments de fission étaient émis par une source de ^{252}Cf de $2 \cdot 10^5$ fissions par minute déposée sur un disque de platine. Les fragments émis à l'intérieur d'un angle solide d'environ 20° étaient détectés, et leur énergie analysée par une jonction à barrière de surface ORTEC.

Un scintillateur liquide chargé en gadolinium et réalisé par Nuclear Enterprise permettait de détecter les neutrons. Ce détecteur, ayant une forme sphérique d'un mètre de diamètre, était placé immédiatement derrière le détecteur de fragments de fission. De cette manière, les neutrons émis par le fragment détecté étaient préférentiellement comptés.

Le détecteur de rayons X était une diode Si(Li) de $200 \text{ mm}^2 \times 3$ mm montée dans un ensemble fabriqué par TMC. La résolution de l'ensemble était de 1 keV à 30 keV. Un collimateur était disposé de telle manière que seuls les rayons X émis par les fragments se dirigeant vers le détecteur ORTEC pouvaient être détectés.

Lorsqu'une coïncidence se produisait entre le détecteur de rayons X et le détecteur de fragments de fission, on procédait, d'une part à l'analyse de l'amplitude des impulsions qu'ils délivraient, d'autre part au comptage des neutrons dans deux portes de 50 μs; la première porte était ouverte immédiatement après la coïncidence, la deuxième 200 μs plus tard; cette deuxième porte permettait donc de mesurer le bruit de fond de l'expérience. Les résultats des analyses d'amplitude et des comptages étaient alors transcrits sur une bande magnétique, entraînée par une platine incrémentale, et pouvant être lue directement par les ordinateurs du centre de calcul de Saclay. Chaque événement était ainsi caractérisé par quatre quantités binaires:

- X(i) amplitude de l'impulsion délivrée par le détecteur de rayons X
- F(i) amplitude de l'impulsion délivrée par le détecteur de fragments de fission
- NU(i) nombre de neutrons détectés immédiatement après l'événement de fission
- NUB(i) nombre de neutrons comptés dans la porte de bruit de fond.

2. TRAITEMENT DES DONNEES

Les quantités NUB(i) n'étant pas corrélées avec les autres quantités, on a pu en tirer facilement le bruit de fond de l'expérience, soit 0,1757 neutrons par fission.

La valeur maximale utile de NU(i) a été trouvée égale à 4. Le nombre de canaux d'analyse des énergies de fragments de fission ayant été ramené à 64, dont 30 canaux utiles, on regroupa les données sous la forme de 5 × 30 spectres de rayons X. Après ce regroupement, la première étape du traitement fut donc d'analyser ces 150 spectres de rayons X.

2.1. Traitement des spectres fournis par le détecteur de rayons X

Nous avons traité ces spectres par une méthode de moindres carrés semblable à celle décrite par Watson et al. [3]. Les spectres étaient considérés comme des superpositions de spectres élémentaires et d'un bruit de fond. Le bruit de fond dû à des interactions Compton de haute énergie fut trouvé être compatible avec une forme parabolique. Les réponses élémentaires, correspondant chacune à la réponse du détecteur aux rayons X.K caractéristiques d'un élément chimique, furent calculées à partir des tables de Wapstra [4], de la variation de l'efficacité du détecteur en fonction de l'énergie des rayons X et de la largeur de sa fonction de résolution; la variation de cette largeur avait été déterminée à l'aide de sources étalons telles que le ^{241}Am et le ^{137}Cs.

Les tables de Wapstra ont été établies dans le cas d'un atome une fois ionisé. Toutefois Watson [5] a montré que l'ionisation élevée des fragments de fission ne conduisait pas à une modification substantielle des énergies et des intensités relatives des raies $K\alpha$ et $K\beta$.

Dans l'expérience de Watson et al. [3], les rayons X détectés étaient pratiquement tous émis par les fragments à l'arrêt. Dans le cas de notre expérience, ils sont au contraire émis par des fragments en vol. Il s'ensuit que les rayons X subissent un effet Doppler. Nous avons calculé, grâce à un programme de Monte-Carlo, les modifications apportées aux fonctions de réponse par cet effet Doppler. Pour ce faire, nous avons utilisé les valeurs des constantes de temps d'émission de rayons X données en fonction de la masse des fragments par Kapoor et al. [6]. Dans le cas de notre expérience, nous avons trouvé que l'effet Doppler se traduisait essentiellement par un élargissement de la fonction de résolution de l'ordre de 0,2 keV et par un décalage de l'énergie des raies inférieur à 0,15 keV. Nous avons vérifié que la prise en compte de cet effet ne modifiait pas substantiellement nos résultats. Aussi, étant donné l'incertitude sur la correction d'effet Doppler, nous avons préféré n'en pas tenir compte dans les résultats présentés ici.

A la suite du traitement décrit ci-dessus, nous avons donc obtenu un tableau d'intensités à trois dimensions $Y(Z, X_F, n)$, où Z est la charge du fragment, X_F l'amplitude de l'impulsion délivrée par le détecteur ORTEC, et n le nombre de neutrons détectés.

2.2. Correction de réponse des détecteurs de fragments de fission

Schmitt et al. [7] ont prescrit une méthode qui permet, à partir de l'amplitude de l'impulsion délivrée par un détecteur de fragments de fission et de la masse de celui-ci, d'obtenir la valeur de l'énergie cinétique du fragment, soit:

$$E_F = (am + b)\, X_F + cm + d$$

Les coefficients a, b, c, d sont déterminés à partir du spectre des amplitudes délivrées par le détecteur dans le cas où l'on observe une source de ^{252}Cf sans condition de coïncidence. Une mesure indépendante de l'expérience proprement dite nous a permis de déterminer ces paramètres. Par ailleurs, nous avons fait correspondre à chaque charge Z une masse moyenne des fragments donnée par les relations:

$$\overline{m} = \frac{252}{98} Z - 2 \text{ pour le fragment léger} \tag{1}$$

$$\overline{m} = \frac{252}{98} Z + 2 \text{ pour le fragment lourd} \tag{2}$$

Nous avons pu ainsi transformer le tableau $Y(Z, X_F, n)$ en un tableau $Y(Z, E_F, n)$.

L'examen du tableau bidimensionnel $\sum_n Y(Z, E_F, n)$ nous permet d'étudier la distribution des énergies cinétiques des fragments de charge donnée. En utilisant les relations (1) et (2), ces distributions peuvent être comparées à celles obtenues pour un fragment de masse donnée. La comparaison est particulièrement instructive avec les données de Schmitt et al. [8] dont nous utilisions la méthode de calibration. La figure 1 représente ainsi la variation de l'énergie cinétique moyenne des fragments en fonction de leur charge, obtenue d'une part dans ce travail, d'autre part par transformation des résultats de Schmitt et al.

On remarque que nos mesures donnent des valeurs de cette énergie cinétique systématiquement inférieures d'environ 2 à 3 MeV à celles obtenues par Schmitt et al., tout au moins pour le fragment léger. Nous ne pouvons pas fournir d'explication très satisfaisante de ce fait. Il est possible qu'il s'agisse d'une erreur d'origine expérimentale. Si cela n'était pas le cas, nous suggérons l'explication suivante:

Il existe probablement une corrélation entre les valeurs élevées du spin des fragments de fission immédiatement après la scission et la probabilité de conversion interne. Peut-être ces valeurs élevées du spin des fragments correspondent-elles à une énergie d'excitation plus importante. Nous avons l'intention d'éclaircir ce point ultérieurement.

2.3. Correction d'efficacité du détecteur de neutrons

En ce qui concerne l'émission neutronique, l'expérience peut se résumer par deux tableaux bidimensionnels. Le premier donne la valeur moyenne du nombre de neutrons détectés en fonction des valeurs de Z et E_F, le deuxième la variance de la distribution du nombre de neutrons détectés par fission en fonction des mêmes paramètres. Soit:

$$\overline{N}(Z, E_F) = \sum_n n\, Y(Z, E_F, n) \Big/ \sum_n Y(Z, E_F, n)$$

et

$$\Sigma^2(Z, E_F) = \sum_n (n - \overline{N}(Z, E))^2\, Y(Z, E_F, n) \Big/ \sum_n Y(Z, E_F, n)$$

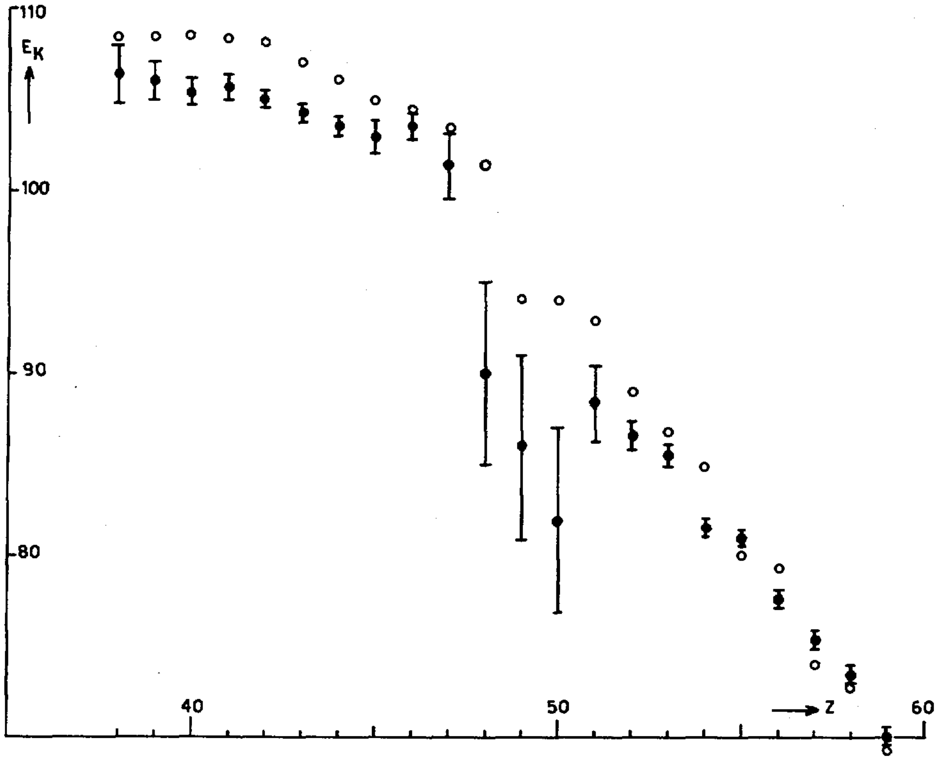

FIG.1. Variation de l'énergie cinétique E_K des fragments en fonction de leur charge Z.

● Nos résultats.

○ Valeurs obtenues par transformation des résultats de Schmitt et al. [8].

Il s'agit, à partir de ces tableaux, d'obtenir les tableaux similaires décrivant la distribution du nombre de neutrons émis par chaque fragment. La justification du traitement présenté ci-dessous se trouve dans une autre publication [9].

La première étape consiste à corriger les données pour tenir compte de la distribution des neutrons de bruit de fond B(n), de valeur moyenne $\overline{B}$ et de variance σ_B^2. Le nouveau tableau corrigé $\overline{N_C}(Z, E_F)$ est obtenu par

$$\overline{N_C}(Z, E_F) = \overline{N}(Z, E_F) - \overline{B}$$

Rappelons que

$$\overline{B} = 0,1757$$

Pour le tableau corrigé, $\Sigma_C^2(Z, E_F)$ on a de même

$$\Sigma_C^2(Z, E_F) = \Sigma^2(Z, E_F) - \sigma_B^2$$

avec

$$\sigma_B^2 = 0,1915$$

La deuxième étape consiste à prendre en compte l'efficacité de détection des neutrons. Cette efficacité est supposée dépendre du sens et de la grandeur de la vitesse du fragment émetteur. Dans la géométrie de l'expérience, elle est beaucoup plus grande pour les neutrons émis par le fragment se dirigeant vers le détecteur ORTEC. Sa valeur moyenne par fragment, pour les neutrons de fission du ^{252}Cf, a été trouvée égale à 30,4% en utilisant comme valeur de référence le nombre moyen total de neutrons prompts émis par fragment du ^{252}Cf:

$$\frac{\nu_T}{2} = 1,891$$

La variation de l'efficacité en fonction de la grandeur et du sens de la vitesse des fragments a été obtenue grâce à un calcul de Monte-Carlo simulant l'évaporation de neutrons de fission et les conditions expérimentales de détection. La proportion des neutrons détectés provenant du fragment se dirigeant vers le détecteur a été trouvée égale à environ 95%. Si on désigne par l'indice 1 le fragment se dirigeant vers le détecteur et par l'indice 2 le fragment complémentaire, on a les relations:

$$Z_2 = 98 - Z_1$$

$$M_1 = \frac{252}{98} \times Z_1 \pm 2$$

$$M_2 = 252 - M_1$$

$$E_2 = \frac{M_1}{M_2} E_1$$

$$V_1 = \sqrt{2E_1/M_1}$$

$$V_2 = \frac{M_1}{M_2} V_1$$

Le nombre moyen de neutrons détectés s'écrit alors en fonction des nombres moyens de neutrons émis par les deux fragments:

$$N_C(Z_1, E_1) = A(V_1) \times \bar{\nu}(Z_1, E_1) + B(V_2)\, \bar{\nu}(Z_2, E_2) \qquad (3)$$

où A(V) est l'efficacité de détection des neutrons émis par un fragment de vitesse V se dirigeant vers le détecteur, B(V) l'efficacité de détection des neutrons émis par un fragment se dirigeant dans le sens opposé.

Pour le cas où le fragment 2 se dirige vers le détecteur, on obtient:

$$N_C(Z_2, E_2) = A(V_2)\, \nu(Z_2, E_2) + B(V_1)\, \nu(Z_1, E_1) \qquad (4)$$

Les deux équations (3) et (4) permettent de déterminer $\bar{\nu}(Z_1, E_1)$ et $\bar{\nu}(Z_2, E_2)$, nombres moyens de neutrons émis par chacun des fragments.

Pour les variances des nombres de neutrons émis $\sigma_\nu^2(Z, E)$ et leur covariance $\mu_{/\!/}(Z, E)$ on peut montrer que [9]

$$\Sigma_C^2(Z_1, E_1) = A(V_1)^2 \sigma_\nu^2(Z_1, E_1) + 2A(V_1)B(V_2)\mu_{/\!/}(Z_1, E_1) + N_C(Z_1, E_1) - A(V_1)^2 \nu(Z_1, E_1) \quad (5)$$

et une relation similaire pour $\Sigma_C^2(Z_2, E_2)$. On voit qu'il manque une équation pour résoudre le problème. Dans un premier temps, nous avons supposé que $\mu_{/\!/} = 0$.

En ce qui concerne les variances, nous nous sommes contentés de traiter les distributions du nombre de neutrons émis par les fragments de Z donné, sans tenir compte de la valeur de leur énergie cinétique. Le raisonnement précédent reste valable si l'on affecte à chaque fragment une énergie cinétique moyenne.

3. RESULTATS ET DISCUSSION

3.1. Variation du nombre moyen de neutrons émis par les fragments en fonction de leur charge

Le traitement présenté au paragraphe précédent est complet en ce sens qu'il permet d'obtenir les quantités $\nu(Z, E_F)$.

On peut en déduire facilement la valeur de $\bar{\nu}(Z)$, valeur moyenne du nombre de neutrons émis par le fragment

$$\bar{\nu}(Z) = \left[\sum_{E_F} \bar{\nu}(Z, E_F) \times \sum_n Y(Z, E_F, n)\right] / \sum_{nE_F} Y(Z, E_F, n)$$

La figure 2 et le tableau I montrent les résultats ainsi obtenus. On a également présenté la variation du nombre total de neutrons émis par fission. La figure 2 permet de dégager deux conclusions:

- Il apparaît une structure fine dans l'émission de neutrons par le fragment lourd. On distingue en particulier deux plateaux, respectivement pour les charges (52 - 53 - 54) et (55 - 56 - 57). La figure 3, où l'on a présenté la valeur moyenne du nombre de neutrons détectés et la courbe de rendement en masse pour le fragment lourd, semble indiquer une corrélation entre les structures fines de la distribution en masse et celles mises en évidence dans l'expérience présente.
- Il est facile de démontrer [11] que l'énergie libérée par la fission est, toutes choses égales d'ailleurs, augmentée en moyenne d'environ 2 MeV si les fragments ont une charge paire. Une telle quantité équivaut à l'émission d'environ 0,3 neutron supplémentaire. Un tel effet n'apparaît pas sur la figure. Si l'on calcule la valeur moyenne de l'émission neutronique totale pour les fragments de charge paire (52 - 54 - 56 - 58) et celle des fragments de charge impaire (53 - 55 - 57), on trouve respectivement:

$$\nu_{\text{pair}} = 3,66 \pm 0,06$$
$$\nu_{\text{impair}} = 3,66 \pm 0,04$$

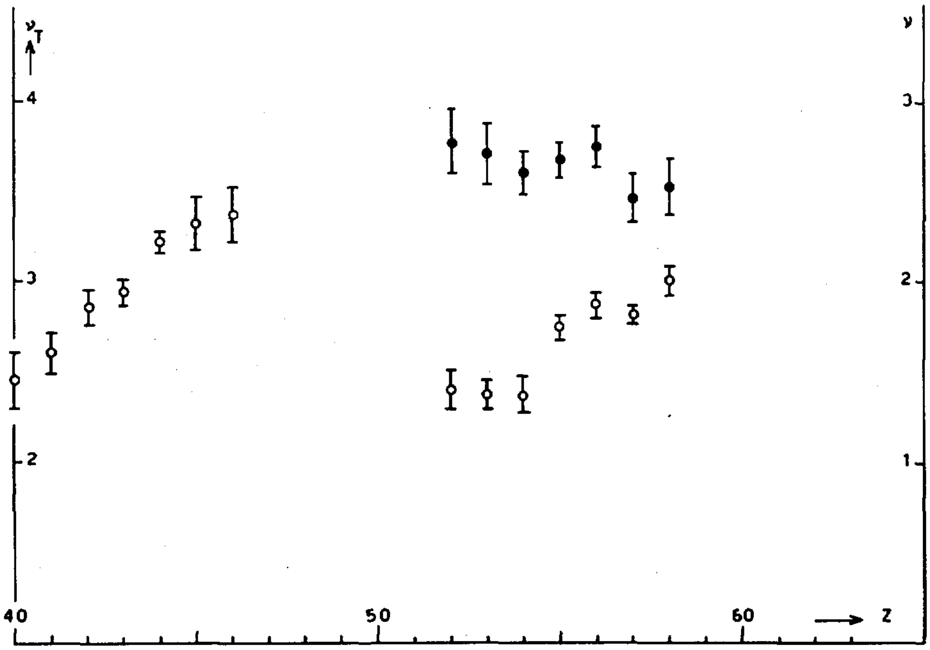

FIG. 2. Variation du nombre moyen de neutrons émis en fonction de la charge des fragments.

O Nombre de neutrons émis par fragment $\nu(Z)$.

● Nombre total de neutrons émis par les deux fragments en fonction de la charge du fragment lourd $\nu_T(Z)$.

Il semble donc que l'effet de parité soit inférieur à 0,1 neutron, soit environ 0,6 MeV.

La figure 1 montre que cet effet de parité n'apparaît pas non plus dans l'énergie cinétique des fragments. On est donc amené à supposer qu'il apparaît essentiellement sous la forme d'énergie cinétique des neutrons et surtout d'émission gamma.

3.2. Etude de la variance de la distribution du nombre des neutrons émis par les fragments

On a reporté sur le tableau I les valeurs des variances de l'émission neutronique en fonction de la charge des fragments. Ces valeurs ont été obtenues en supposant que la covariance $\mu_{//}$ était nulle. On constate une faible variation de ces quantités à l'intérieur de chacun des groupes lourd et léger. Les valeurs moyennes pondérées de ces variances valent respectivement pour le groupe lourd et le groupe léger

$$\sigma_L^2 = 1,108 \pm 0,033$$

$$\sigma_H^2 = 1,446 \pm 0,040$$

TABLEAU I. VARIATION EN FONCTION DE Z:
DU NOMBRE MOYEN $\bar{\nu}$ DE NEUTRONS EMIS PAR FRAGMENT,
DE LA VARIANCE σ_ν^2 DE CE NOMBRE,
DU NOMBRE TOTAL DE NEUTRONS EMIS PAR LES DEUX FRAGMENTS COMPLEMENTAIRES

Z	$\bar{\nu}$	$\bar{\nu}_T$	σ_ν^2
40	1,46 ± 0,146	3,53 ± 0,16	1,29 ± 0,22
41	1,61 ± 0,1	3,45 ± 0,11	1,39 ± 0,16
42	1,86 ± 0,06	3,75 ± 0,09	1,29 ± 0,10
43	1,93 ± 0,03	3,69 ± 0,05	1,00 ± 0,045
44	2,22 ± 0,05	3,60 ± 0,10	1,25 ± 0,073
45	2,33 ± 0,12	3,71 ± 0,13	1,12 ± 0,210
46	2,37 ± 0,13	3,72 ± 0,18	0,9 ± 0,193
52	1,34 ± 0,12		1,55 ± 0,30
53	1,37 ± 0,06		1,78 ± 0,12
54	1,38 ± 0,09		1,50 ± 0,20
55	1,76 ± 0,035		1,29 ± 0,07
56	1,89 ± 0,07		1,73 ± 0,11
57	1,842 ± 0,05		1,25 ± 0,09
58	2,07 ± 0,08		1,52 ± 0,13
59			1,61 ± 0,19
60			1,58 ± 0,53

Si l'on rapproche ces valeurs de la variance du nombre total de neutrons émis par fission donnée par Terrell [12] on devrait avoir:

$$\sigma_T^2 \geqq \sigma_L^2 + \sigma_H^2$$

Or

$$\sigma_T^2 = 1,55 \pm 0,04$$

On voit donc que

$$\sigma_L^2 + \sigma_H^2 > \sigma_T^2$$

Il s'ensuit qu'il doit exister une anticorrélation entre les émissions de neutrons par les fragments lourd et léger. Nous pouvons calculer la valeur minimale de cette anticorrélation en ajoutant aux équations (5) l'équation

$$\sigma_T^2 = 1,55 = \sigma_H^2 + \sigma_L^2 + 2\mu_{11}$$

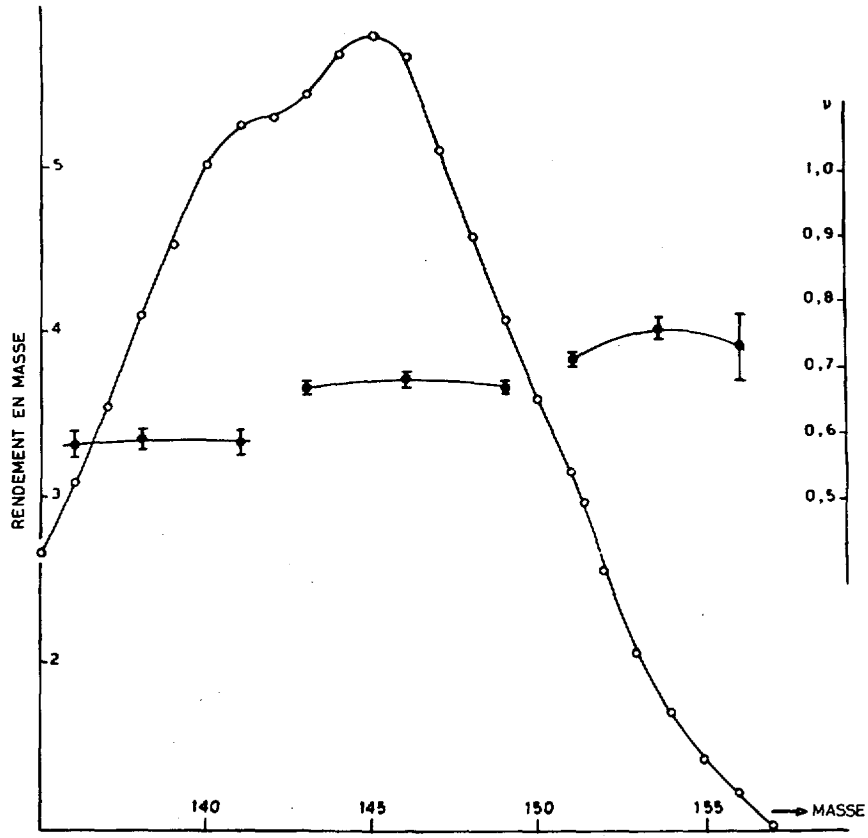

FIG.3.

○ Courbe en distribution en masse d'après Fraser et al. [10].
● Nombre moyen de neutrons détectés émis par le fragment lourd d'après nos résultats.

La correction d'efficacité du détecteur n'a pas été faite pour les données de cette figure.

On obtient alors

$$\mu_{\parallel} = -0,55 \pm 0,03$$

$$\sigma_L^2 = 1,177 \pm 0,03$$

$$\sigma_H^2 = 1,406 \pm 0,04$$

3.3. Etude de l'émission neutronique en fonction de l'énergie cinétique des fragments

La figure 4 montre la variation du nombre moyen de neutrons émis en fonction de l'énergie cinétique des fragments pour différentes charges. Ces courbes comportent toutes une zone linéaire. La valeur de cette pente

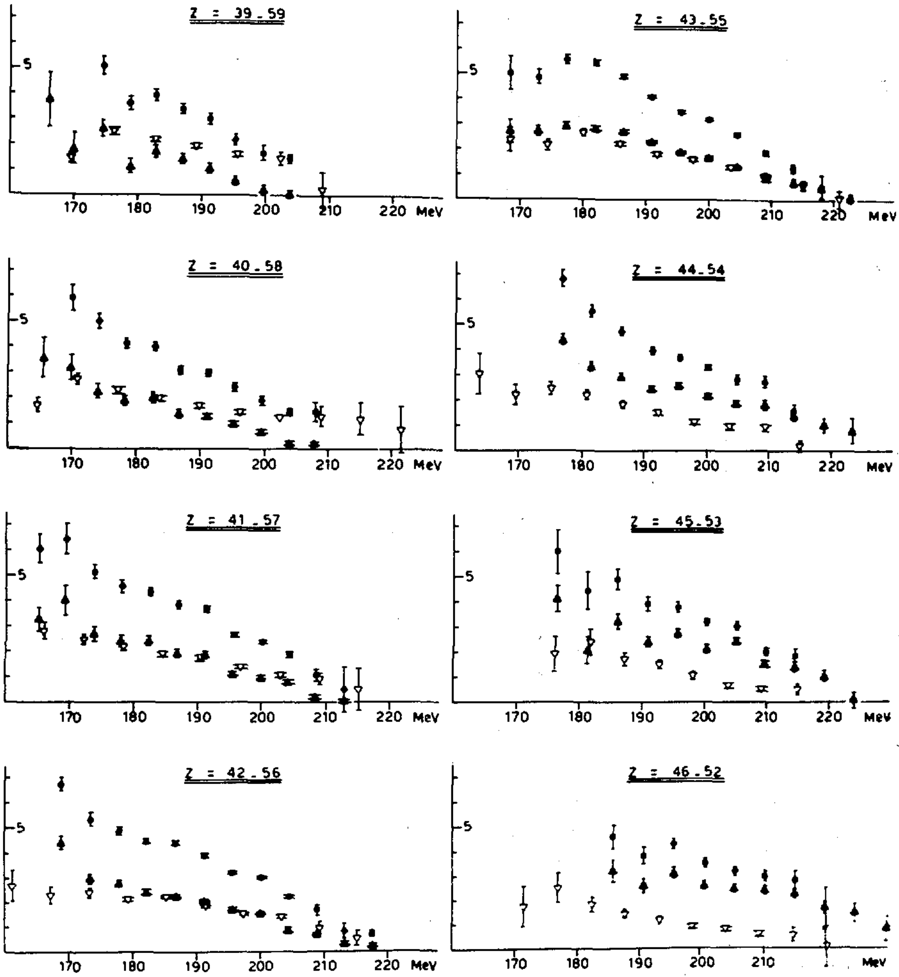

FIG.4. Variation du nombre de neutrons en fonction de l'énergie cinétique totale des fragments.

● Nombre total de neutrons émis par une paire de fragments.
▲ Nombre de neutrons émis par le fragment léger.
▽ Nombre de neutrons émis par le fragment lourd.

en fonction de la charge est reportée sur la figure 5. Il semble d'après cette figure que la valeur de la pente soit sensible à la parité de Z. Cette pente est liée à l'énergie moyenne emportée par le premier neutron émis par le fragment. D'après le modèle du noyau composé, l'effet de parité doit jouer essentiellement dans la compétition entre l'émission γ et l'émission du dernier neutron. En effet, l'émission γ sera favorisée si le dernier neutron doit emporter un grand moment angulaire; cette circonstance doit se présenter lorsque les états accessibles après émission du dernier neutron ont un spin faible, ce qui est le cas pour les fragments résiduels pair-pair. On conçoit donc que, dans la mesure où la probabilité de

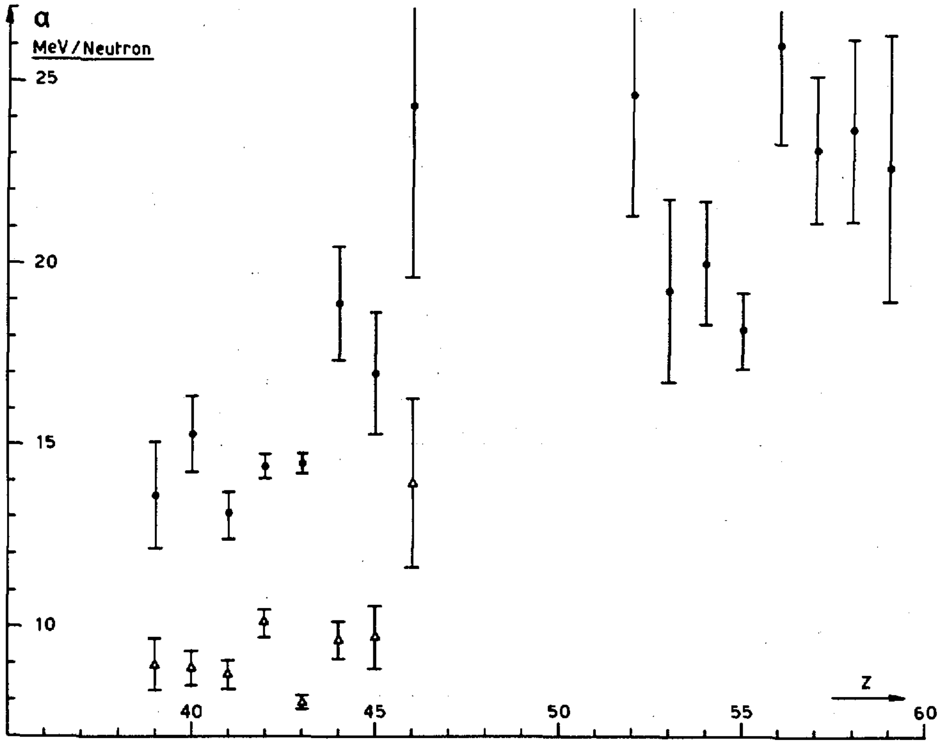

FIG.5. Energie moyenne emportée par neutron en fonction de la charge des fragments.

X Moyenne effectuée sur les deux fragments complémentaires.

● Moyenne par fragment.

n'émettre qu'un neutron n'est pas négligeable, la pente considérée ci-dessus dépende de la parité des noyaux, de même que, probablement, l'énergie émise sous forme de rayonnement γ.

4. CONCLUSION

L'étude que nous avons entreprise a permis de mettre en évidence des structures fines dans l'émission des neutrons par le fragment lourd de fission. Ces structures, qui semblent corrélées aux structures fines de la distribution en masse, pourraient servir de guide dans l'interprétation de ces dernières.

Nous avons également montré qu'il existait une anticorrélation entre les nombres de neutrons émis par les fragments complémentaires.

Enfin, si l'effet de parité de charge ne semble apparaître ni dans l'énergie cinétique, ni dans l'émission de neutrons, il semble se faire sentir dans l'énergie moyenne emportée par neutron.

REFERENCES

[1] WHETSTONE, S.L., Jr., Phys.Rev. 114 (1959) 583.

[2] BOWMAN, H.R., MILTON, J.C.D., THOMSON, S.G., SWIATECKI, N.J., Phys.Rev. 129 (1963) 2138.

[3] WATSON, R.L., BOWMAN, H.R., THOMSON, S.G., Phys.Rev. 162 (1967) 1169.

[4] WAPSTRA, A.H., NIJGH, G.J., van LIESHOUT, R., Nuclear Spectroscopy Tables, North Holland Publ. Co., Amsterdam (1959).

[5] WATSON, R.L., Thesis.

[6] KAPOOR, S.S., BOWMAN, H.R., THOMSON, S.G., Phys.Rev. 140 B (1965) 1310.

[7] SCHMITT, H.W., GIBSON, W.M., NEILER, J.H., WALTER, F.J., THOMAS, T.D., «Absolute energy calibration of solid-state detectors for fission fragments and heavy ions», Physics and Chemistry of Fission I (C.r.Coll.Salzbourg, 1965), AIEA, Vienne (1965) 531.

[8] SCHMITT, H.W., NEILER, J.H., WALTER, F.J., Phys.Rev. 141 (1966) 1146.

[9] NIFENECKER, H., AUDIAS, A., RIBRAG, M., FREHAUT, J., GAURIAU, J., Influence de la charge des fragments sur le processus d'émission des neutrons prompts de fission du ^{252}Cf, Rapport CEA, à paraître.

[10] FRASER, J.S., MILTON, J.C.D., BOWMAN, H.R., THOMSON, S.G., Can.J.Phys. 41 (1963) 2080.

[11] NIFENECKER, H., RIBRAG, M., FREHAUT, J., GAURIAU, J. Prompt neutron yields of the fission fragments of ^{252}Cf as a function of the charge of the fragments, Nucl.Phys., à paraître.

[12] TERRELL, J., «Prompt neutrons from fission», Physics and Chemistry of Fission II (C.r. Coll. Salzbourg, 1965), AIEA, Vienne (1965) 3.

DISCUSSION

W. JOHN: I have published high-resolution measurements of the yield of X-rays from fission, which show that there are large variations, of a factor of two or more, between adjacent elements. In your paper you quote a resolution of 1 keV, which is insufficient for complete separation of X-rays from the adjacent Z's. Do you feel that you have taken your resolution into account correctly in searching for an odd-even effect in the neutron emission?

H. NIFENECKER: In the first measurement we made of X-rays associated with the fission of ^{235}U we actually found wide fluctuations in the X-ray yield from charge to charge. This was reported at the March 1967 meeting of the French Physical Society. These fluctuations were found with a 1.2 keV X-ray resolution, and are in good agreement with your results.

The contribution of Z + 1 to the Z yield has been determined to be at most 10% so that this is the maximum amount by which the odd-even effect could be reduced in our data. Besides, we tried two different sets of response functions, one of which was Doppler-shifted. Both these sets gave substantially the same results.

S.S. KAPOOR: I see that your measurements on $\bar{\nu}$ versus Z do not show a pronounced saw-tooth behaviour similar to $\bar{\nu}$-versus-mass measurements. Do you have any comments on that?

H. NIFENECKER: Our measurement is, in fact, in agreement with Whetstone's results but, to some extent, at variance with those of Bowman. This could be due to the fact that we, unlike Bowman, used an extended neutron detector, as Whetstone had done. Other reasons could be the unfolding procedure used by Bowman and, possibly, underestimation of the Compton background in our experiment.

P. ARMBRUSTER: If fission fragments are formed with high primary spins, as most of the experiments have confirmed, neutron emission occurs from the high-spin state. As little angular momentum is carried off by the reactions, gamma emission starts from the high-spin states. These states are, in any case, higher in energy than the pairing gap. Such high spin levels (of the order of $10\hbar$) of even and odd nuclei do not differ appreciably. The prediction that the additional scission energy may be found as gamma energy is in agreement with our present picture of de-excitation of high-spin, highly excited nuclei.

NEUTRON EMISSION IN THE FISSION OF $^{213}At^*$

F. PLASIL, R.L. FERGUSON, H.W. SCHMITT
Oak Ridge National Laboratory,
Oak Ridge, Tenn.,
United States of America

Abstract

NEUTRON EMISSION IN THE FISSION OF ^{213}At. A thin target of ^{209}Bi was bombarded with 53.25 MeV ^{4}He ions at the Oak Ridge Isochronous Cyclotron. Two silicon surface-barrier detectors were used to measure kinetic energies of fragment pairs and to provide timing pulses for the measurement of the velocity of one of the fragments. Three pulse-heights, related to the two fragment energies and to the time-of-flight were recorded event-by-event. These correlated data were used to calculate pre-neutron and post-neutron emission masses and total kinetic energies. The average numbers of neutrons emitted from single fragments and from both fragments together were obtained as functions of fragment mass and total kinetic energy. Distributions in fragment mass and total kinetic energy, before and after neutron emission, were also obtained. The results are presented in terms of several simple distributions, such as the average number of neutrons emitted as a function of fragment mass, and also in terms of correlated distributions, such as the yield as a function of both mass and total kinetic energy.

The distributions in fragment mass and total kinetic energy peak at symmetry, in agreement with earlier results. The average total kinetic energy is 146.2 MeV before neutron emission and 141.3 MeV after neutron emission. The average number of neutrons emitted from single fragments rises monotonically from about 2.3 neutrons at fragment mass 90 to 5 neutrons at fragment mass 120. This trend is in accord with trends predicted by the liquid-drop theory of fission, but the slope of the average neutron number versus mass curve is considerably greater than predicted by theory. The average total number of neutrons emitted per fission from both fragments is 7.4 ± 0.5. The available energy for given fragment mass pairs, calculated from mass tables, is compared with the sum of the measured total kinetic energy and the two fragment excitation energies estimated from the measured neutron numbers.

I. INTRODUCTION

One of the simplest and most thoroughly investigated descriptions of the complex process of fission is provided by the liquid drop model of nuclei. Due to its basic simplicity, it was possible to obtain, from assumed initial conditions, calculated probability distributions of fragment masses, kinetic energies, excitation energies and angular momenta [1,2]. The theoretical mass distributions always peak at symmetric mass divisions, while it is a well-known experimental fact [3] that at low excitation energies mass distributions from fission of nuclei heavier than radium peak away from symmetry. In spite of this failure (which may be due to the absence of consideration of single particle effects in the liquid drop description) the model was found to account for the general features of mass and total kinetic energy distributions from the fission of nuclei lighter than radium [1,2,4]. The purpose of the study reported here is to obtain a relatively complete description of the energetics of the fission process in the region of nuclei where the liquid drop theory has been successful. This was achieved by determining simultaneously not only fragment masses and kinetic energies, but also fragment excitation energies as deduced from the numbers of neutrons emitted from fragments. Further motivation was provided by the fact that no neutron emission data were available

* Research sponsored by the US Atomic Energy Commission under contract with Union Carbide Corporation

for any nuclei lighter than radium. Neutron emission in proton-induced fission of radium was studied recently [5], and the results were discussed in terms of symmetric and asymmetric components. In the fission of ^{213}At we have previously found no indication of an asymmetric component [6], and it is therefore of interest to compare our present results with those deduced for the symmetric component of radium fission.

The neutron emission data in this work were obtained by an indirect method in which kinetic energies of fragment pairs are measured together with the velocity of one of the fragments [7]. This method is particularly well suited to studies involving relatively light nuclei where fission probabilities are small, and where background effects in direct neutron counting experiments are, therefore, expected to be large. A further advantage of this method is that it is not dependent on the assumption that neutrons are emitted from fully accelerated fragments. According to Eismont [8], when single fragment excitation energies are greater than 20 MeV, (as is true in our case), the assumption of neutron emission from fully accelerated fragments may not hold. Thus, both the direct neutron counting method [9,10], and methods which rely on differences between double time of flight and double energy experiments [11] yield results that may be in error.

The choice of the target, ^{209}Bi, the bombarding projectile, ^4He, and its energy, 53.25 MeV, were governed by the availability of target and projectile, and also by a compromise between acceptable counting rates and a minimum contribution from fission following neutron emission from the compound nucleus (second chance fission). Experimental details and a description of the data processing are given in the next section. In Section III experimental results are presented and discussed, and Section IV contains energy balance considerations and a comparison with liquid drop calculations.

II. EXPERIMENTAL ARRANGEMENT AND DATA PROCESSING

A target consisting of a vacuum-evaporated deposit of ^{209}Bi (nominal thickness: 50 $\mu g\ cm^{-2}$) on a 3 μin nickel foil was bombarded with 53.25 MeV ^4He ions from the Oak Ridge Isochronous Cyclotron. The beam level was kept at about 75 nA throughout the experiment to avoid pulse pile-up effects. The target was accurately positioned at the center of a vacuum chamber. One surface barrier semiconductor detector (detector 1) was located at the end of a flight tube which was at a 90° angle to the beam direction. Another detector (detector 2) was located in the plane defined by the beam and the flight tube. In the case of our combination of target, projectile, and bombarding energy, center of mass effects were not negligible. It was found that detector 2 had to be placed at a laboratory angle of 79° with respect to the beam direction to maintain co-linearity with detector 1 in the center-of-mass system for the most probable fission events. The active surfaces of the two detectors were at 105.93 cm and 5.40 cm, respectively, from the center of the chamber. The geometric arrangement was such that the partners of all fragments incident on detector 1 were detected by detector 2. Pulses related to the energies of the fragments were amplified with standard charge sensitive preamplifiers and linear amplifiers and corresponding channel numbers were recorded on punched paper tape with a multiparameter pulse-height analyzer. Fast timing pulses were generated by transformer coupled circuits (commercial time-pickoff units) and were used to start and stop a time-to-amplitude converter. The resulting pulses, which were proportional to the difference in time T between the arrival of the fragments at the two detectors, were also analyzed and the channel numbers recorded, in a correlated manner, together with the energy pulses. A fast coincidence circuit was used to open linear gates through which the three coincident pulses passed before reaching the analyzer. The resolution of the time system, after computer correction for amplitude dependent time shift, was about 0.45 ns.

From measured excitation functions [12] for ^4He-induced fission of ^{209}Bi, it was estimated that about 15% of the observed fissions resulted from the fission of ^{212}At rather than ^{213}At. In our data-processing procedure we used a value of 213 amu for the compound nucleus mass, A_c, but a repetition of the calculations with A_c = 212 resulted in only a small decrease in the number of emitted neutrons. This decrease was within the limits of estimated errors; therefore, we believe that our results are essentially unaffected by neutron emission prior to fission.

About 18,000 events were measured and processed on a digital computer. The calculations were based on those of reference 7 but differed in some important aspects. In particular, the large center-of-mass effect introduced serious complications.

The first step in the data analysis consisted of an event-by-event iterative calculation. The measured energy pulse heights were first converted to laboratory energies by means of mass-dependent calibration equations [13]. The laboratory energies were then corrected for target and backing thickness effects by adding to the measured energies, E_k, appropriate correction factors, ΔE_k, given by $\Delta E_k = c\, E_k^{2}$ [14], where c is a constant obtained from auxiliary experiments. The corrected laboratory energies were converted to center-of-mass energies. From the measured time difference T, the time-of-flight of fragment 1 was calculated by using the approximate time of flight of fragment 2 to the near detector. The post-neutron emission mass was then calculated by using the relationship $m_1 = (2E'_{k1}/v_1^2)$ where E'_{k1} is the actual laboratory energy of fragment 1 before target thickness correction, and v_1 is the fragment velocity calculated from its time-of-flight.

All the calculations to this point were part of the first event-by-event iteration. This was necessary because a knowledge of the masses of both fragments was required in several of the steps. Approximate values were used for the mass of fragment 2. The result of this first step was an X_1 vs. X_2 array (where X_1 and X_2 are the pulse heights associated with the kinetic energies of fragments 1 and 2) with $\bar{m}_1$ values stored at each location. Values of $\bar{m}_1$ are the averages of m_1 for given X_1 X_2 combinations.

In the second step the method of complementary points [7] was used to generate a second X_1 X_2 array with values of $\bar{m}_2$ stored in its locations. Center-of-mass conversions were also used in the calculation of this array. In the third step we obtained values of $\bar{m}_2$ for every event from the $\bar{m}_2(X_1\ X_2)$ array.

The fourth step consisted of a repetition of the iterative event-by event calculation of step 1, with the difference that at this stage we used the $\bar{m}_2$ values obtained above instead of the approximate values for m_2 used initially.

In the final step we made use of the following relationship [7]

$$m_1^* = \frac{A_c}{1 + \frac{v_1^*}{v_2^*}} \approx \frac{A_c}{1 + \sqrt{\frac{E_{k1}\ \bar{m}_2}{E_{k2}\ m_1}}} \qquad (1)$$

In this equation, as in the rest of the paper, asterisks distinguish pre-neutron emission quantities from post-neutron emission values. E_{k1} and E_{k2} are post-neutron emission fragment kinetic energies in the center of mass system. Values of E_{k1}, E_{k2}, and m_1 were all known for every event at this stage of analysis, and the calculation of m_1^* can, therefore, be made on an event-by-event basis with the following reservation: the second mass, m_2, is not known separately for each event and it is necessary to use $\bar{m}_2$ discussed above and calculated for each event in step 3. Thus the only deviation from an event-by-event procedure is due to the use of $\bar{m}_2$, which represents m_2 averaged over the small subspace defined by particular X_1 X_2 combinations. Throughout the analysis random number techniques were used, whenever appropriate, to transform distributions from one set of coordinates to another. Finally the number of neutrons emitted, ν_1, was obtained from

$$\nu_1 = m_1^* - m_1$$

and the various distributions of interest were generated.

The experiment was calibrated by means of a companion ^{252}Cf experiment performed immediately following the cyclotron bombardment. Conditions in the two experiments were kept as nearly the same as possible, and identical methods of data analysis were used in the two cases. By slight variation of the appropriate detector calibration constants, within their published uncertainties, it was possible to obtain overall averages of post-neutron emission light and heavy masses in the californium experiment which agreed to within ± 0.1% with published values [13]. Overall average measured light and heavy kinetic energies were kept within ± 0.5% of the published values. As would be expected the curve of average neutron number versus mass from this calibration experiment agreed well with direct neutron counting results [15], particularly in the light fragment region. For heavy fragments, the slope from our method is steeper than that of Bowman et al [15]. This difference is, however, understood in terms of dispersion effects [7]. It was not necessary to apply dispersion corrections to our ^{213}At data, since it was found [16] that such effects are not important when there is no deep valley present in the mass distribution.

III. RESULTS

A complete description of our results would consist of an array of total kinetic energy versus fragment mass, with a number of counts and an average number of emitted neutrons associated with each location in the array. However, the presentation and discussion of such four-parameter arrays is difficult, and we shall, therefore, concern ourselves with various doubly dimensioned arrays, simple distributions, and overall averages. Table I gives the averages and root mean square values of the pre- and post-neutron emission mass and kinetic energy distributions. The overall average number of neutrons emitted from single fragments, $\bar{\nu}_1$, and from both fragments together, $\bar{\nu}_T$, are also given in Table I. The energy and mass distribution results are consistent with earlier double energy measurements [4]. Energy balance considerations discussed in the next section indicate that our neutron emission results may be high, and, within the error limits indicated, the true average neutron emission values may be slightly lower than those given in Table I.

Figure 1 shows average number of neutrons emitted from single fragments, $\bar{\nu}_1(m_1^*)$, and from both fragments together, $\bar{\nu}_T(m_1^*)$, as functions of mass. The mass-yield curve is also shown for reference. The $\bar{\nu}_1(m_1^*)$ curve rises monotonically from light to heavy fragment masses. The characteristic "sawtooth" structure present in such curves from the fission of heavier nuclei at low excitation energies is not found in this case. However, the mass region (125 - 130 amu) associated with such dips is on the extreme high-mass wing of the mass distribution in the present experiment, and this may account for the observed absence of structure.

The slope of the $\bar{\nu}_1(m_1^*)$ curve near the peak of the mass distribution is 0.11 neutrons per amu, compared with 0.08 neutrons per amu from the

TABLE I. RESULTING DATA

	Experimental			Theoretical	
	average		rms width σ	average	rms width σ
E_K^* (MeV)	146.2	± 1.0	7.53	139.0	6.12
m_1^* (amu)	106.5[a]		10.23	106.5	7.71
v_1^* (cm/ns)	1.153	± 0.005	0.118		
$\bar{\nu}_1$	3.7	± 0.5			
$\bar{\nu}_T$	7.4	± 1.0			
dE_{x_1}/dm_1^* (MeV/amu)	0.78	± 0.03		0.17	
E_K (MeV)	141.3	± 1.0			
m_1 (amu)	103.1	± 0.5			

[a] This value is not a true measurement but results directly from the method of data processing.

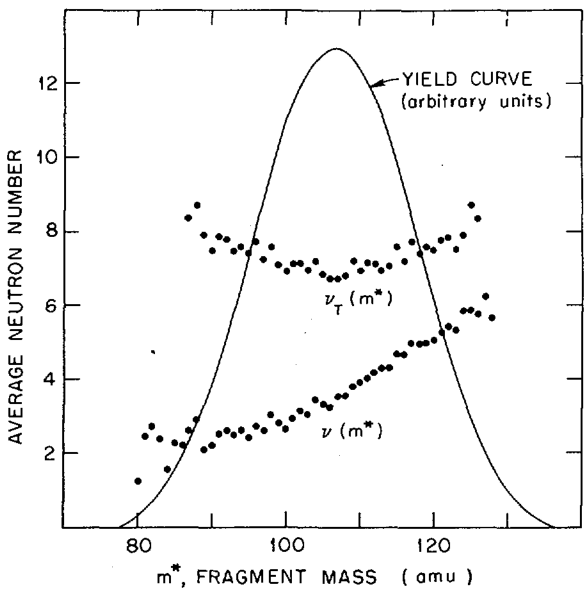

FIG. 1. Average number of neutrons emitted from single fragments, ν (m*), and from both fragments together, ν_T (m*), as a function of fragment mass. The mass-yield curve, in arbitrary units, is shown for reference.

proton-induced-fission of ^{226}Ra [5]. This may indicate a trend toward steeper slopes in the case of lighter fissioning nuclei.

The lower part of Fig. 2 shows the pre- and post-neutron emission mass distributions. Due to the steep neutron emission curve, the post-neutron emission distribution is considerably narrower (23.6 amu FWHM) than the pre-neutron emission distribution (26.0 amu FWHM). The center section

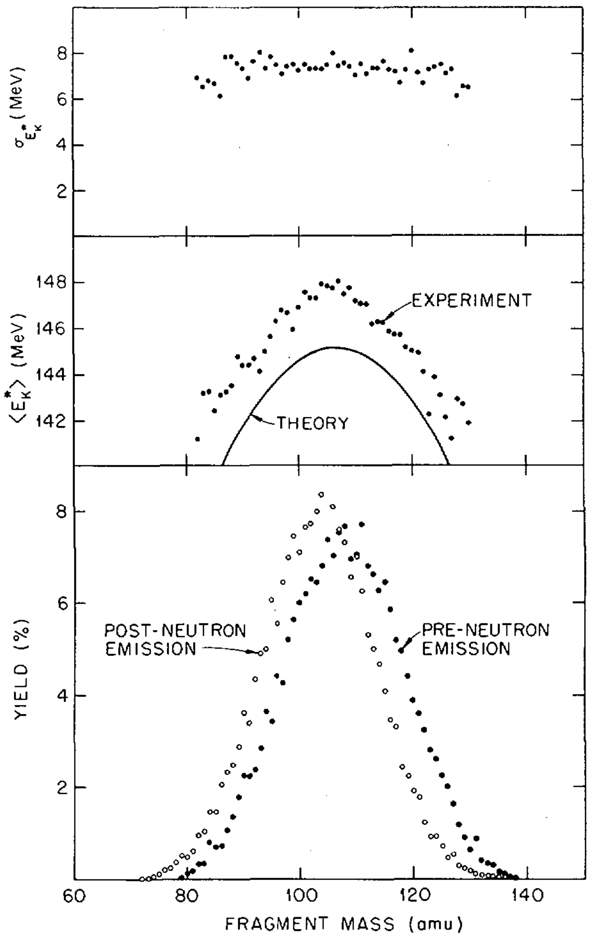

FIG. 2. Top section: root mean square widths, $\sigma_{E_K^*}(m_1^*)$ of total kinetic energy distributions as a function of mass. Centre section: experimental average total energy, $\langle E_K(m_1^*) \rangle$ as a function of mass (closed circles). The solid line gives theoretical results from Ref. [1]. Lowest section: pre- and post-neutron emission mass distributions. Total yield is normalized to 200%.

of Fig. 2 shows the average total kinetic energy, $\langle E_K^* \rangle$, as a function of mass. This curve is in good agreement with earlier results [4]. The upper section of the figure shows the root mean square widths, $\sigma_{E_K^*}(m_1^*)$, of the $E_K^*(m_1^*)$ distributions. The σ values are essentially constant over the whole range, except for a slight decrease in the wings of the mass distribution.

The contour diagrams of Fig. 3 give the most nearly complete description of our results. Due to the relatively large statistical fluctuations from one MeV-amu box to another, all contours shown in Fig. 3 were considerably smoothed by the use of compressed arrays in which events were averaged over 5 MeV by 5 amu unit areas. In the upper section of Fig. 3, the number-of-events distribution is shown. The labels on the contours refer to actual numbers of observed events in the 5 MeV by 5 amu boxes. This experimental mass-total kinetic energy distribution is similar to those of reference 4 and in good agreement with theoretical calculations.

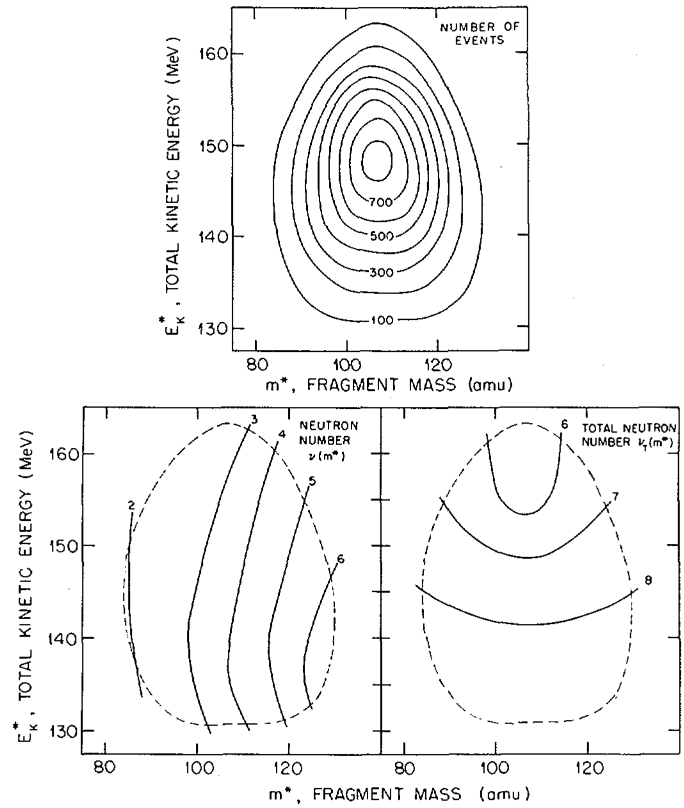

FIG. 3. Top section: contour diagram of the number of events as a function of fragment mass and total kinetic energy. The numbers on the contours refer to numbers of events per 5 MeV by 5 amu area. Lower left: contour lines of average numbers of neutrons emitted from single fragments as a function of mass and total kinetic energy. Lower right: contour lines of total number of neutrons emitted from both fragments. In both lower portions, the outermost contour from the top portion of the figure is indicated, by a dashed line, for reference.

In the lower parts of Fig. 3 the neutron emission results are shown as functions of both mass and total kinetic energy. Neutron emission results from single fragments are shown on the left and total neutron numbers (emitted from both fragments) are given on the right. In both cases the outermost contour of the yield distribution is indicated by a dashed line for reference. The diagonal orientation of the single fragment neutron number contours shown in the lower left part of Fig. 3, was anticipated on the basis of our $\bar{\nu}_1(m_1^*)$ results and simple energy considerations. Since, for a given mass division, the total energy available is a constant, increasing kinetic energies must be accompanied by decreasing fragment excitation energies and, thus, lower neutron emission. This effect, coupled with the rising values of $\bar{\nu}_1$ with increasing m_1^*, produces the observed distribution. These energy effects are also reflected in the total neutron number contours (Fig. 3, lower right), where the high kinetic energy tip of the distribution has $\bar{\nu}_T$ values of only about 6 associated with it, while in the broad low kinetic energy region, on the average, over 8 neutrons are emitted per fission event. The bending down of the $\bar{\nu}_1$ contour lines below $E_K = 140$ MeV is, however, not explained.

IV. DISCUSSION

A. Total Energy Balance

We shall now compare the total energy of both fission fragments as deduced from our measurements with the total energy, E_T, available for fission. For a specific fragment pair, E_T is given by

$$E_T = Q + E_{cm}$$

where E_{cm} is the center of mass energy of the projectile and Q is the difference in nuclear binding energy between the target and projectile on the one hand and the two fragments on the other. Values of Q can be obtained from mass tables and are a function of both the masses and the charges of fragments. For any specific charge division, a plot of Q versus fragment mass results in a parabola. Peaks of such parabolas indicate energetically favored combinations of charge and mass. The parabolas obtained from Seeger's mass formula [17] are shown in Fig. 4. Similar results have been obtained from other mass formulas [18]. The "envelope" of the parabolas of Fig. 4 provides, as a function of fragment mass, an estimate of the total

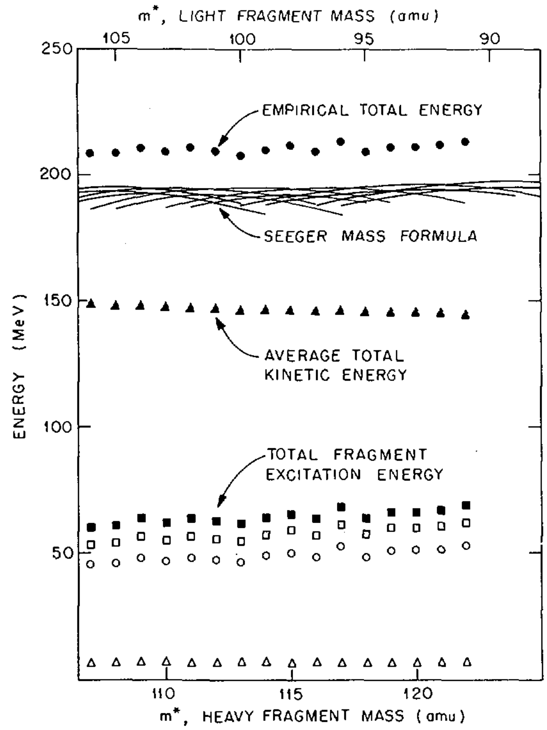

FIG. 4. The "Seeger Mass Formula" parabolas represent the total energy available for fission (see text). The open triangles represent the total energy of γ rays emitted from fragments. Open circles refer to the energy lost by the fragments due to neutron binding energies. When neutron kinetic energies are added to the binding energies, the total energy lost by neutron emission is obtained (open squares). Addition of γ and neutron energies gives the total fragment excitation energy curve (closed squares). The experimental total kinetic energy is given by closed triangles. Addition of kinetic energy and total excitation energies gives the empirical total energy (closed circles) which is to be compared with the mass parabolas. (See text for discussion).

energy available. This energy should equal the sum of the fragment kinetic and excitation energies, i.e., $E_T = E_K^* + E_X = E_K^* + E_{x1} + E_{x2}$, where E_X is the total fragment excitation energy and E_{x1} and E_{x2} are the individual fragment excitation energies. Since each evaporated neutron reduces the fragment excitation energy by the sum of the neutron binding and kinetic energies, it is possible to obtain values of E_{x1} and E_{x2} from neutron emission data and from an estimate of the effect of γ-ray emission following neutron emission. Thus the fragment excitation energy is given by

$$E_{x1} = \sum_{n=1}^{\nu} (B_{n1} + \eta_{n1}) + E_{\gamma 1}$$

where B_{n1} and η_{n1} are the binding and kinetic energies of the n'th neutron emitted from fragment 1 and $E_{\gamma 1}$ is the energy removed from fragment 1 by γ rays. The summation is carried out over all neutrons evaporated from a given fragment. A similar equation exists for E_{x2}.

We applied the above relationship to our results, and the summation was carried out over our experimental $\bar{\nu}_1(m_1^*)$ values for each value of m_1^*. The neutron binding energies for a given fragment mass were obtained from Seeger [17], using the most energetically favored charge split. Values of η were assumed to be constant and equal to 1.2 MeV, and $E_{\gamma 1}$ was taken to be one-half of the binding energy of the $(\nu + 1)$th neutron. By adding these excitation energies for complementary masses we obtained the total fragment excitation energy curve shown in Fig. 4. To these $\langle E_X(m_1^*)\rangle$ values experimental values of total kinetic energies, $\langle E_K^*(m_1^*)\rangle$, were added, and the empirical E_T curve of Fig. 4 was generated. As was discussed above, this empirical curve should coincide with the peaks of the mass-formula parabolas. It can be seen from Fig. 4 that the empirical E_T curve lies, in fact, about 12 to 13 MeV above the calculated curve. Assuming that the mass formula parabolas represent accurately the available energy, this discrepancy would indicate that our average value of the total number of emitted neutrons, $\bar{\nu}_T$, is about 1.5 neutrons too high. This is greater than the estimated error of ± 1.0 neutron and could be due to an unknown systematic error. The discrepancy, however, is rather small (6% of the total available energy) and could be due to errors in the mass tables or to our approximate treatment of the energy balance problem.

B. Comparison with Liquid Drop Theory

The liquid drop theory, with which we shall compare our results, has been developed by Nix and Swiatecki [1] and by Nix [2]. In the former work, the nuclei were parametrized in terms of two spheroids only, while in the latter work the parametrization consisted of two spheroids joined, whenever appropriate, with a hyperbolic neck. Due to the parametrization restriction of reference 1, results from the early calculation were expected to apply only to fissioning nuclei lighter than radium. The later calculations [2] are more general but have not been carried out in the same detail as those of reference 1. For example, from reference 1, we can obtain values of single fragment excitation energy as a function of mass, while the results from reference 2 yield, in the first approximation, a constant excitation energy for all masses. We have chosen to compare with the latest results [2] for the averages and rms values of overall distributions (see Table I), but in the case of comparisons of conditional distributions, $\langle E_{x1}(m_1^*)\rangle$ and $\langle E_K^*(m_1^*)\rangle$, theoretical values have been obtained from reference 1.

In the center part of Fig. 2 $\langle E_K^*(m_1^*)\rangle$ is compared with theory. It can be seen that the agreement between the shapes of the two curves is very good. Such agreement was also observed in earlier work [4]. The absolute values of the two curves are about 2 MeV apart. This discrepancy is in-

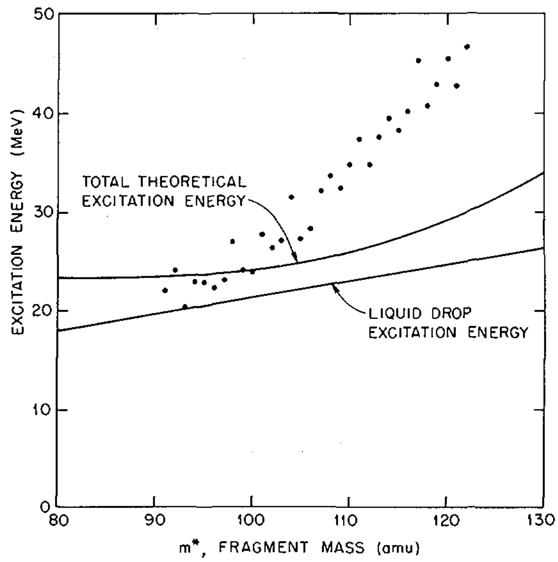

FIG. 5. Liquid drop and total theoretical excitation energies of single fragments as a function of mass (see text). Experimental results are given by closed circles.

creased to 7 MeV when the comparison is made with the recent calculations [2], as can be seen from the average E_K^* values of Table I.

The comparison of fragment excitation energies deduced from our neutron measurements with theoretical excitation energies is complicated by the fact that the liquid drop predictions are restricted to the excitation energy resulting from the deformation of the fragments (vibrational energy of references 1 and 2). The total single fragment excitation energy, E_{x1}, however, consists not only of this deformation energy, E_{d1}, but also of intrinsic internal excitation energy, E_{h1}. The total fragment excitation energy is given by

$$E_X = E_D + E_H = E_{d1} + E_{d2} + E_{h1} + E_{h2}$$

where E_D and E_H are the total excitation energies due to deformation and internal excitation respectively. In Fig. 5, the liquid drop excitation energy, $\langle E_{d1}(m_1^*) \rangle$, is shown. Values of $\langle E_{h1}(m_1^*) \rangle$ were obtained from the relationships

$$E_T = E_K^* + E_D + E_{h1} + E_{h2}$$

and

$$E_{h1}/E_{h2} = m_1^*/m_2^*$$

The first equation defines, through energy balance, the total internal excitation, E_H, while the second equation assumes that internal excitation energy divides in the same ratio as the fragment masses. For the purpose of comparing theoretical and experimental slopes of excitation energy versus mass curves, we have used values of $\langle E_T(m_1^*) \rangle$ in the above equation obtained from the Seeger [17] mass formula (see Fig. 4), while values of $\langle E_K^*(m_1^*) \rangle$ were calculated as in reference 1. The resulting $\langle E_{h1}(m_1^*) \rangle$ values were added to $\langle E_{d1}(m_1^*) \rangle$ values to give the theoretical excitation energy curve of Fig. 5. Experimental neutron numbers were converted to fragment excitation energies as described in the previous subsection IV-A and the results plotted in Fig. 5. It can be seen that the slope of the experimental curve is considerably greater than that of the theoretical curve. The values of dE_{X1}/dm_1^* near symmetric mass divisions are given in Table I. The experimental value of 0.78 MeV/amu is in considerable disagreement with the theoretical value of 0.17 MeV/amu. As an alternative to the liquid drop model calculation, we can estimate a value of dE_{X1}/dm_1^* as follows: E_X can be obtained from $E_T = E_K^* + E_X$, where E_T is again obtained from Seeger's mass formula [17], but E_K^* now is the measured total kinetic energy. If E_X is divided simply in the same ratio as the masses, we obtain a value for dE_{X1}/dm_1^* of 0.28 MeV/amu. This value is still considerably smaller than the experimental result, but is in better agreement with the experiment than the liquid drop prediction.

It is interesting to note that the experimental value of dE_{X1}/dm_1^* from the symmetric component of ^{227}Ac fission [5] is 0.49 MeV/amu, compared with a liquid drop prediction of 0.16 MeV/amu. In the ^{213}At case, the liquid drop theory prediction of 0.17 MeV/amu is similar to the theoretical value for ^{227}Ac, but the observed slope in this work, 0.78 MeV/amu, is considerably higher than that from ^{227}Ac fission. Thus, contrary to expectation, the dE_{X1}/dm_1^* results from the fission of the heavier nucleus are in better agreement with theoretical results than the results from the lighter ^{213}At.

We conclude that the liquid drop model gives a more nearly adequate description of the mass and total kinetic energy distributions, than of the excitation energy distribution. The usefulness of the model thus remains restricted to its ability to account for the gross features of observed fission distributions, but quantitative estimates based on the model have only limited success.

ACKNOWLEDGMENTS

We are pleased to acknowledge the assistance of H. J. Hargis with computer programming. Helpful discussions with S. C. Burnett, R. W. Lide, and J. R. Nix are also gratefully acknowledged.

REFERENCES

[1] NIX, J. R., SWIATECKI, W. J., Nucl. Phys. 71 (1965) 1.
[2] NIX, J. R., Nucl. Phys. A130 (1969) 241.
[3] HYDE, E. K., The Nuclear Properties of Heavy Elements Vol. III (Prentice Hall, Inc., Englewood Cliffs, N. J. 1964).
[4] PLASIL, F., BURNETT, D. S., BRITT, H. C., THOMPSON, S. G., Phys. Rev. 142 (1965) 696.
[5] KONECNY, E., SCHMITT, H. W., Phys. Rev. 172 (1968) 1213.
[6] PLASIL, F., FERGUSON, R. L., PLEASONTON, F., SCHMITT, H. W., Bull. Am. Phys. Soc. 13 (1968) 1408.
[7] SCHMITT, H. W., LIDE, R. W., PLEASONTON, F., Nucl. Inst. and Meth. 63 (1968) 237.
[8] EISMONT, V. P., Atomnaya Energiya 19 (1965) 113.
[9] HARDING, G. N., FARLEY, F. J. M., Proc. Phys. Soc. London 69A (1956) 853.
[10] CHEIFETZ, E., FRAENKEL, Z., Phys. Rev. Letters 21 (1968) 36.
[11] BRITT, H. C., WHETSTONE, S. L., Phys. Rev. 133 (1964) B603.
[12] KHODAI-JOOPARI, A., Lawrence Radiation Laboratory Report UCRL 16489 (1966).
[13] SCHMITT, H. W., KIKER, W. E., WILLIAMS, C. W., Phys. Rev. 137 (1965) B837.

[14] CUMMING, J. B., CRESPO, V. P., Phys. Rev. 161 (1967) 287.
[15] BOWMAN, H. R., MILTON, J. C. D., THOMPSON, S. G., SWIATECKI, W. J., Phys. Rev. 129 (1963) 2133.
[16] BURNETT, S. C., Oak Ridge National Laboratory Report ORNL-TM-2272 (1968).
[17] SEEGER, P. A., to be published in 3rd edition of American Institute of Physics Handbook.
[18] WING, J., FONG, P., Phys. Rev. 136 (1964) B923.

DISCUSSION

H. NIFENECKER: The authors appear to have used the calibration method of H.W. Schmitt. When this method is applied without special precautions, for example in the case of ^{235}U, the variation in the number of neutrons as a function of mass, which can be calculated from the results given by radiochemistry, is not correct. Is it not necessary to adjust the parameters given by Schmitt?

F. PLASIL: It is indeed necessary to adjust the detector constants in these experiments, because the results are very sensitive to the calibration relationships. Small variations in response characteristics are found among fission-fragment detectors. For this reason, experiments of the type described in this work are always accompanied by a ^{252}Cf experiment with the same detectors, and the calibration constants are adjusted (within the published uncertainties) so that $\nu(m)$ for ^{252}Cf agrees with the direct neutron counting experiments. The method of obtaining neutron information from radiochemical results should not be confused with the method described in this work, since the two methods differ fundamentally.

J. PÉTER: At Orsay we performed experiments on neutron emission during the fission induced by 156 MeV protons on ^{238}U and ^{209}Bi. At this bombarding energy, the mass of the fissioning nucleus was not defined, and one of the aims of the experiment was actually to measure the number of neutrons evaporated by the nucleus before fission. We measured the velocity distribution of the neutrons collected at different angles to the direction of fragments. As regards the neutrons evaporated by fragments, our results were essentially the same as those obtained by the authors in the case of bismuth, i.e. a $\nu(M)$ curve increasing smoothly with M and having a slope much greater than predicted by the liquid-drop model. In the case of uranium, the curve was modulated by the saw-tooth curve due to fissioning nuclei of low excitation energy. One question that engaged our attention was the possible neutron emission during scission. Did you consider this problem?

F. PLASIL: As regards the question of pre-fission neutrons, as I have pointed out, the bombarding energy used by us was, in our view, sufficiently low for the contribution from second-chance fission to be less than 20%. We estimated the magnitude of this effect from the measured excitation function for this reaction given in Ref. [12]. As far as the scission neutrons are concerned, these would, in our case, be indistinguishable from pre-fission neutrons. We do not, in this experiment, obtain values of either pre-fission or scission neutrons. While these may both exist, their only effect is to change the value of the compound nucleus mass used in our analysis. We have investigated the result of using the wrong compound nucleus mass, and even with 100% second-chance fission, i.e. when the compound nucleus mass was lowered by one unit, the only effect on our results was that the neutron curve was lowered by about one neutron number.

H.W. SCHMITT: In connection with Dr. Nifenecker's remarks concerning detector calibration, I would like to say that our calibration procedure, described at the 1965 Salzburg Symposium and in Ref. [13] of this paper, is based on careful measurements with ^{79}Br, ^{81}Br and ^{127}I ions. These masses bracket the light-fragment group, but use of the calibration equation over the entire range of fragment masses represents an extrapolation into the heavy-fragment region. If this extrapolation is not quite correct, the difficulty with cumulative yield calculations for ^{235}U (n_{th}, f) may be explained.

The method described by Dr. Plasil is not to be confused with the procedures used in cumulative yield calculations. They are, in fact, fundamentally different, as may be seen from detailed study of the two methods for obtaining neutron emission data.

A STUDY OF THE PROMPT GAMMA RAYS OF ^{252}Cf-FISSION

K. RUMPOLD, F. SEMTURS, P. WEINZIERL
Physics Institute, Reactor Centre Seibersdorf,
Seibersdorf, Austria

Abstract

A STUDY OF THE PROMPT GAMMA RAYS OF ^{252}Cf-FISSION. The prompt gamma-ray spectra in the range between 50 and 550 keV were measured simultaneously at angles of 90° and 180° with respect to the fragment direction. By using fission fragment energy as an additional parameter, it was possible to find well-resolved gamma lines; cases of Doppler shifts were easily observed. The amount of shift was used to deduce fragment masses. The type of Doppler spectrum was used to classify gamma life-times according to three intervals: ($t < 10^{-12}$ s, 10^{-12} s $< t < 2 \times 10^{-9}$ s, 2×10^{-9} s $< t < 10^{-7}$ s). The first limit is due to the fragment stopping time in the backing of the Cf-foil (10^{-12} s). The fragment time of flight from source to detector determined the second interval to $10^{-12} < t < 2 \times 10^{-9}$ s, while the last interval was limited by the electronic coincidence width to 10^{-7} s. About half of the gamma lines were found to lie in the second interval and could, therefore, be assigned to definite fragment masses.

1. INTRODUCTION

The fission process leads to a great number of different, highly excited fission fragments. These fragments must, therefore, emit a very complex gamma spectrum. Early measurements of this spectrum by Maienschein [1], Rau [2], using NaI-crystals, showed no prominent features because of the relatively poor energy resolution. Bowman [3] was able to resolve the spectrum to a considerable extent. In addition, he could assign the lines to definite fragment masses.

To obtain a more complete description of the de-excitation of a fission fragment, it is necessary to know also the life-time of the prompt gamma lines. Johansson [4] could show that 55-65% of all the gamma rays are emitted with a half-life of approximately 10^{-11}-10^{-10} s, 15% between 10^{-9} and 10^{-10} s and 15-25% less than 10^{-11} s, but without assigning these half-lives to definite energies.

The purpose of our measurement was to make an energy determination as well as an estimation of the life-time of the emitted gamma lines between 50-550 keV and to assign these lines as far as possible to fragment masses.

2. EXPERIMENTAL SET-UP

Figure 1 shows the experimental arrangement and the electronic block diagram. The ^{252}Cf – source was prepared by electrospraying the activity on a Pt-foil of 0.5 mil thickness. Two surface-barrier Si(Au)-detectors, arranged at right angles to each other, are used to measure the fission-fragment energies. The Ge(Li) detector measured gamma rays emitted either parallel (or antiparallel) or at right angles to the flight direction of the fragments.

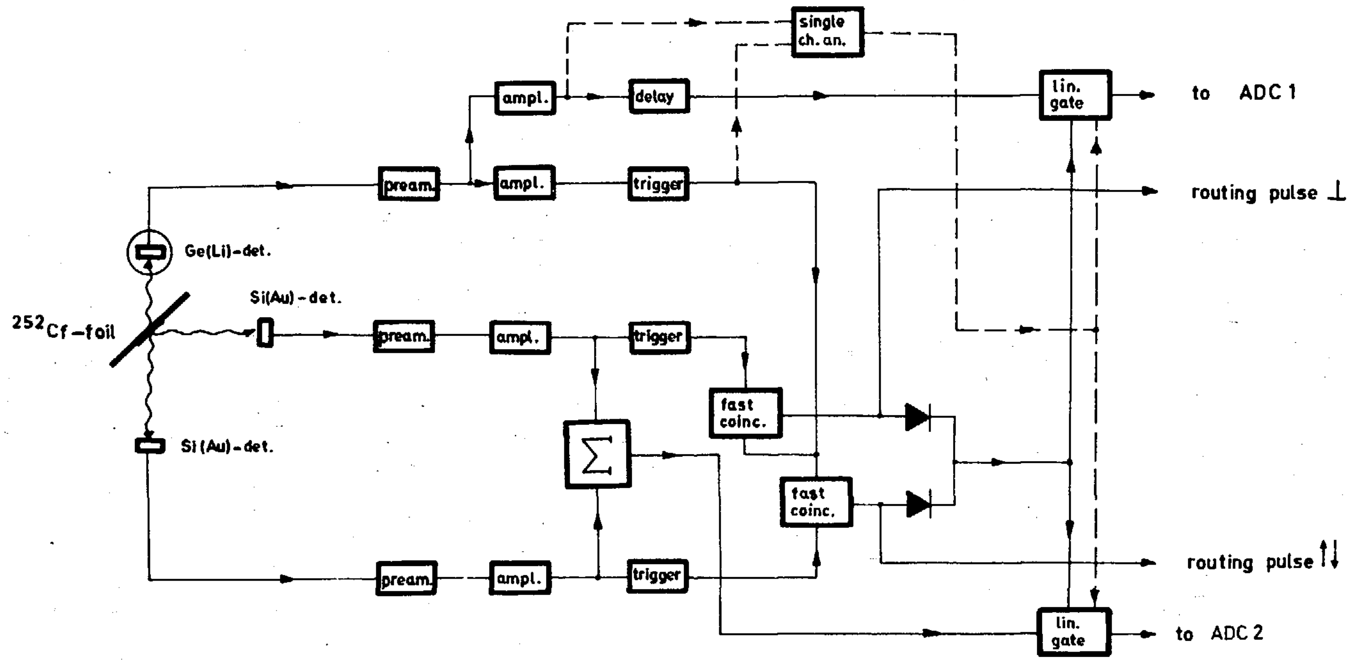

FIG.1. Experimental set-up and electronic block diagram.

In a two-parameter experiment, the gamma spectrum between 50 and 550 keV was measured as a function of fragment energy in one of the Si(Au)-detectors. Data were taken simultaneously in two geometries:

1. Emission of the prompt gamma-rays at right angles to the fragment motion .... 90°-geometry.
2. Emission of the prompt gamma-rays under 180° or 0° to the fragment motion .... 180°/0°-geometry.

The data were stored simultaneously, but separated according to these geometries in a 2-by-8-by-1024-channel matrix. Every gamma spectrum was stored in 1024 channels, and the fragment energy was subdivided into eight different groups.

The analogue part of our electronics consists of two separate fission-energy circuits, representing the two different geometries which are in fast coincidence ($2\tau = 10^{-7}$ s) with the gamma-ray spectrum. If a coincidence occurs, an event is stored in the part of the matrix which corresponds to the output of the two ADC's and to the routing pulse (which defines the geometry).

The gamma coincidence rate was about 1.3 cps for each geometry, the random rate was less than 1.5%. The energy resolution of the Ge(Li) detector was constant at 3.2 keV fwhm over the measured gamma-energy range.

3. METHOD

With our method, it is possible to relate the measured gamma lines to well-defined fragment-energy groups. In addition, lines of low intensity, which are invisible in the composite spectrum, could be found now. The measurement in two geometries now permits an estimate of the emission time of the gamma quanta [5]; in a few cases they can also be assigned to fragment masses.

When a gamma quantum of energy E_0 is emitted at an angle α with respect to the line of flight of the fission fragment, the energy E of the gamma in the laboratory system is given by the Doppler-shift formula

$$E = E_0\,(1 + v\cos\alpha/c) \qquad (1)$$

where v is the velocity of the fragment and c velocity of light. For our geometries the formula simplifies to:

$$90°\text{-geometry:}\quad E_{\perp} = E_0$$

$$180°/0°\text{-geometry:}\quad E_{\parallel} = E_0(1 \pm v/c) = E_{\perp}(1 \pm v/c)$$

Evidently, in the 90°-geometry we can measure the true gamma energy while in the 180°/0°-geometry, depending on the velocity and direction of flight of the fragments (0° or 180° relative to the gamma emission) we observe a gamma energy which is Doppler-shifted by $\pm E_0\,v/c$.

The thickness of the Pt-carrier foil of the Cf-source was such that one of the fragments was always stopped in the material.

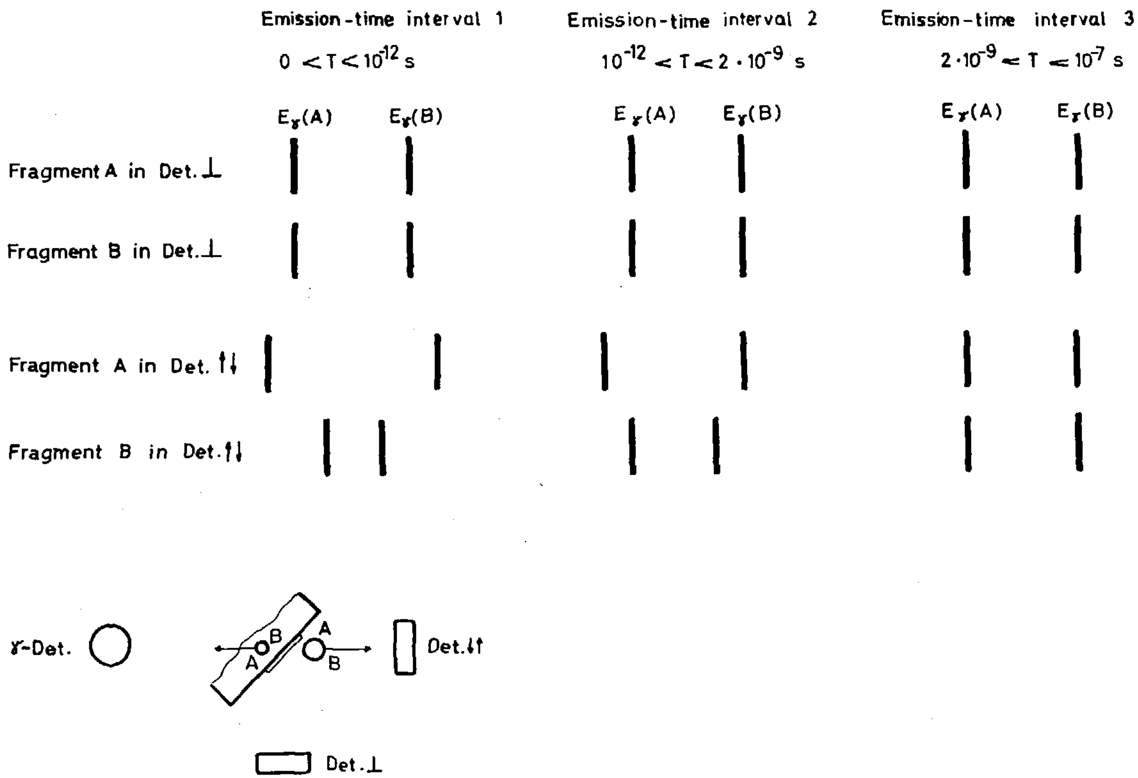

FIG.2. Doppler shift in the energy of a gamma quantum emitted from a fission fragment.

TABLE I. MEASURED GAMMA ENERGIES AND THEIR ASSIGNMENT TO FRAGMENT MASSES AND EMISSION-TIME INTERVALS

Energy (keV) ± 0.5	Mass (amu) ± 5	Time interval
248.9	132	2
244.9	143	2
220.3	148	2
216.0	149	2
207.3	-	3
202.6	-	3
198.9	-	3
196.0	132	2
194.5	-	3
191.1	-	3
189.4	151	2
187.3	161	2
186.2	-	3
181.9	-	3
176.4	115	2
171.8	-	3
154.2	133	2
141.1	125	2
139.0	97	1
128.5	102	2
119.8	-	3
111.7	152	2
105.9	-	3
101.7	-	3

This happens in about 10^{-12} s. Meanwhile the other fragment flies with a velocity v through the space until it reaches the fission detector after an average time of ≈ 2 ns, where it will also be stopped.

It can now be shown that the emission times can be classified into three intervals (Fig. 2).

Let us first assume that a fragment emits a gamma quantum in a time $T < 10^{-12}$ s (time interval 1) in the 180°/0°-geometry. If this fragment is moving toward the Pt-foil, a positive Doppler shift $+ E_\perp v/c$ is formed and if it is moving toward the fission-detector (det. ⑪) a negative shift $-E_\perp v/c$ of the gamma energy E_0 appears. If, however, the life-time of the gamma ray lies between 10^{-12} and 2×10^{-9} s (time interval 2) and if it is emitted in the 180°/0°-geometry, there is, depending on the direction of flight, either no

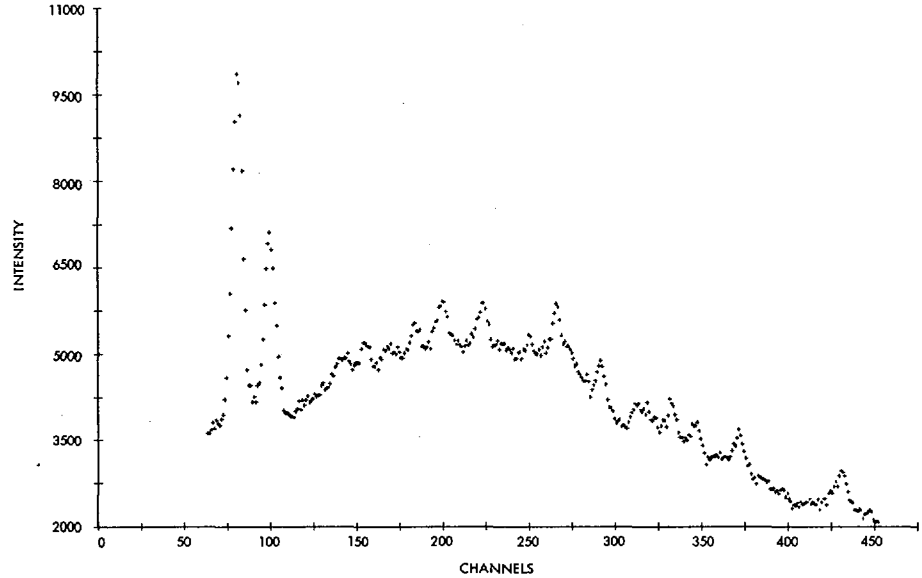

FIG.3. Gamma spectrum in 90°-geometry summed over all fragment energies.

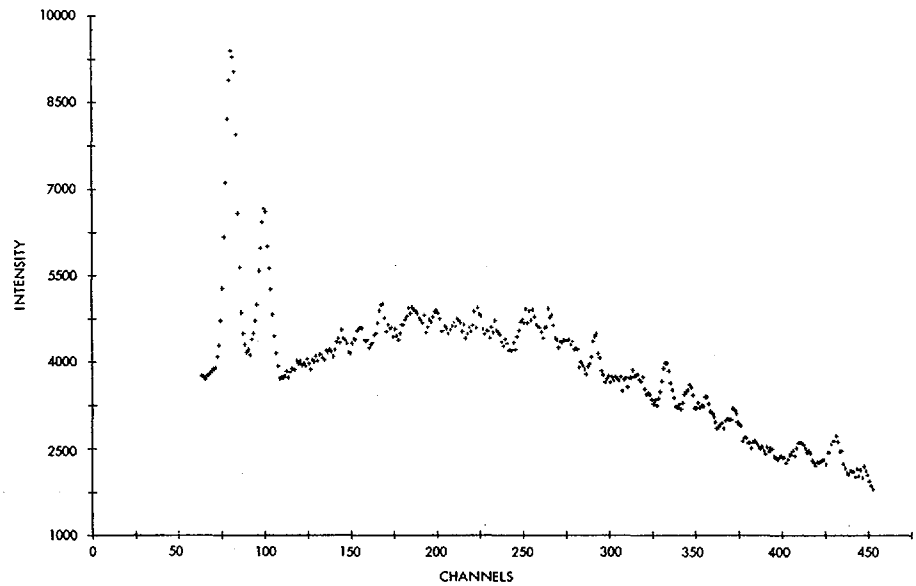

FIG.4. Gamma spectrum in 180°/0°-geometry summed over all fragment energies.

Doppler shift (because the fragment is already stopped in the Pt-foil) or a gamma line shifted by $-E_{\perp}v/c$ reaches the detector. Finally, if a quantum is emitted during the third time interval ($2 \times 10^{-9} < T < 10^{-7}$ s irrespective of whether it is moving toward the foil or toward the detector (⇕), no Doppler shift will be observed, because the emitting fragment is already at rest.

The upper limit of this range is determined by the electronic coincidence width. In the 90°-geometry, we have cos 90° = 0, and therefore none of the gamma lines are Doppler-shifted.

By comparison of the spectra of both geometries, the sign and the value of the Doppler shift of E_0 can be determined. From the type of Doppler pattern observed, the life-time can be estimated. From the value of the Doppler shift the velocity of the fragment can be calculated and from this the fragment masses which have emitted the gamma lines can be approximately determined. This mass determination can only be done for the time intervals 1 and 2 where a Doppler shift is observed.

4. RESULTS

The spectra were decomposed on an IBM-360 system by gradual peeling-off of standard spectra starting from the highest energy. This gave the results presented in Table I.

One can see that 12 of the found gamma lines are emitted in the second interval, between 10^{-12} and 2×10^{-9} s. In the first interval ($T < 10^{-12}$ s) one line could be found. The lines assigned to the 3rd interval also may be from the (n, γ)-reactions in the Ge(Li) detector, caused by fission neutrons. In intervals 1 and 2 only gamma quanta emitted from fission fragments are measured because for the neutron-capture events no Doppler shift occurs.

In Figs 3 and 4 a part of the gamma-ray spectra for the two geometries summed over all fragment energies is shown. Without any analysis program the difference between gamma-ray spectra from the two geometries can be seen.

At the beginning of each gamma spectrum there are two peaks with 66.2 keV and 75.2 keV. These are not gamma transitions of the fragment but arise from X-ray transitions (K_α and K_β) in the Pt-foil. Half of all occurring fragments are stopped in this foil and may remove electrons from the K-orbit.

ACKNOWLEDGEMENTS

The authors wish to express their gratitude to Dr. Axmann for providing the computer program, to Dr. Lanzel for preparing the Ge(Li) detector and to the SGAE for having offered the opportunity of carrying out the work for the thesis of one of the authors on which this paper is based.

REFERENCES

[1] MAIENSCHEIN, F.C. et al., 2nd Int.Conf. peaceful Uses atom.Energy (Proc.Conf.Geneva, 1958) 15 (1958) 366.

[2] RAU, F.E.W., Annls Phys. Paris 10 (1963) 252.

[3] BOWMAN, H.R. et al., in Physics and Chemistry of Fission (Proc.Symp. Salzburg,1965) 2 (1965) 125.

[4] JOHANSSON, S.A.E., Nucl.Phys. 60 (1964) 378.

[5] AXMANN, H.P., UJLAKI, E., Acta Phys.Aust. 27 (1968) 40.

DISCUSSION

P. ARMBRUSTER: The explanation of the strong K X-ray peaks you find for Pt cannot be an excitation mechanism by nearly adiabatic atomic collisions. The cross-section is much too small. A possible explanation is the photo-effect of prompt gamma rays in the backing. The K X-rays produced by this mechanism are coincident with the fission event, and the cross-sections of excitation are higher by orders of magnitude than in the case of nearly adiabatic atomic collisions.

F. SEMTURS: I do not know the cross-sections of these two processes. Of course, if the cross-section of excitation through prompt gamma rays is, as you say, really higher by orders of magnitude than the other cross-section, your explanation of the cause of the two K X-ray peaks is right.

L.V. EAST: Could the K X-rays observed by you be due to excitation in the Pt-foil from beta-decay of the fission fragments?

F. SEMTURS: Apart from the fact that the fission rate is much too small for this explanation of the observed K X-rays, it can be said that the beta-decay on fission fragments is about 10^{-7} s after the scission point. These events can only contribute to the random coincidences in our measurements.

F. HORSCH: I wonder if you have compared your results with Bowman's measurements on the fragments of the same fissioning nucleus, namely ^{252}Cf. It is somewhat surprising that none of your mass-assigned gamma-ray lines coincides with his values.

F. SEMTURS: I was also surprised that our results showed a rather poor agreement with Bowman's gamma-ray experiment on ^{252}Cf fission.

M. NEVE DE MEVERGNIES: Are you sure that all the lines you identify in your gamma-spectra are true single lines and possibly not doublets? An unresolved doublet with two components of different half-lives might give a spurious energy shift in your experiment.

F. SEMTURS: In regard to your comment, I would like to say that the value of the Doppler shift is determined only by the velocity of the fragments. It does not depend on the emission time of the gamma rays.

In reply to your question, I would say that two energy peaks from different fragments could be resolved from the computer program if these energies differed by more than 2 keV. From the velocity-mass correlation of the fragments you can see that the Doppler shift has a value of 2.5-5% and, therefore, a gamma energy of greater than 100 keV is shifted by a value greater than 2.5 keV. Thus, in these cases no unresolved doublets are possible.

PROMPT GAMMA RAYS EMITTED FROM INDIVIDUAL FRAGMENTS IN NEUTRON-INDUCED FISSION

F. HORSCH, W. MICHAELIS
Institut für angewandte Kernphysik,
Kernforschungszentrum Karlsruhe,
Federal Republic of Germany

Abstract

PROMPT GAMMA RAYS EMITTED FROM INDIVIDUAL FRAGMENTS IN NEUTRON-INDUCED FISSION. Prompt gamma rays associated with moving fission fragments of specific masses have been observed in thermal neutron-induced fission of ^{235}U. The geometrical layout of the apparatus prevents detection of photons emitted from stopped fragments and determines the effective time resolution to about 1 ns after fission. Spectra are measured by means of a high-resolution Ge(Li) detector with 3.5 % photopeak efficiency for ^{60}Co. An 8" ϕ × 9" NaI(Tl) anti-Compton shield suppresses the Compton distribution in the spectra and the recording of events produced by fast fission neutrons. The coincident fission-fragment masses are deduced from their correlated kinetic energies as measured by two Si solid-state detectors. The observed Doppler shift in gamma-ray energy allows the assignment of lines to single members of fragment pairs. Data are processed in a 256 × 256 × 2048 channel matrix. The main objective of these experiments is a study of the properties of individual neutron-rich nuclei far off the stability line.

INTRODUCTION

From a comparison of the conventional chart of the nuclides with the lines of vanishing proton and neutron separation energies as derived from semi-empirical mass formulae it is evident that the number of nuclei so far not investigated considerably exceeds the number of nuclei which have already been studied satisfactorily. Therefore, extension of the methods of nuclear spectroscopy to regions far off the stability line will certainly increase the understanding of various nuclear properties. A useful means for producing very neutron-rich nuclei which are not accessible by usual nuclear reactions is provided by the nuclear fission process. The bulk of data accumulated in the past with this process has been obtained by the application of fast chemistry or other separation techniques with subsequent investigation of the radioactive decay schemes. Since a lower limit in halflives is inherent in all these methods, it is desirable to study in an on-line experiment the prompt de-excitation mechanism of individual primary fission fragments.

Such investigations are of considerable importance also for a better understanding of the fission process itself. There is increasing evidence that in asymmetric fission the properties of the nascent fragments, rather than those of the initial compound nucleus, essentially determine the characteristics of the various distributions and correlations observed for this process.

Examining the radiation emitted from fission fragments of specific mass has become possible by the rapid development of semiconductor detector technology and associated electronics during the past few years. First studies have been performed by Bowman et al. [1] and by Watson [2] using the spontaneous fission of ^{252}Cf. It is

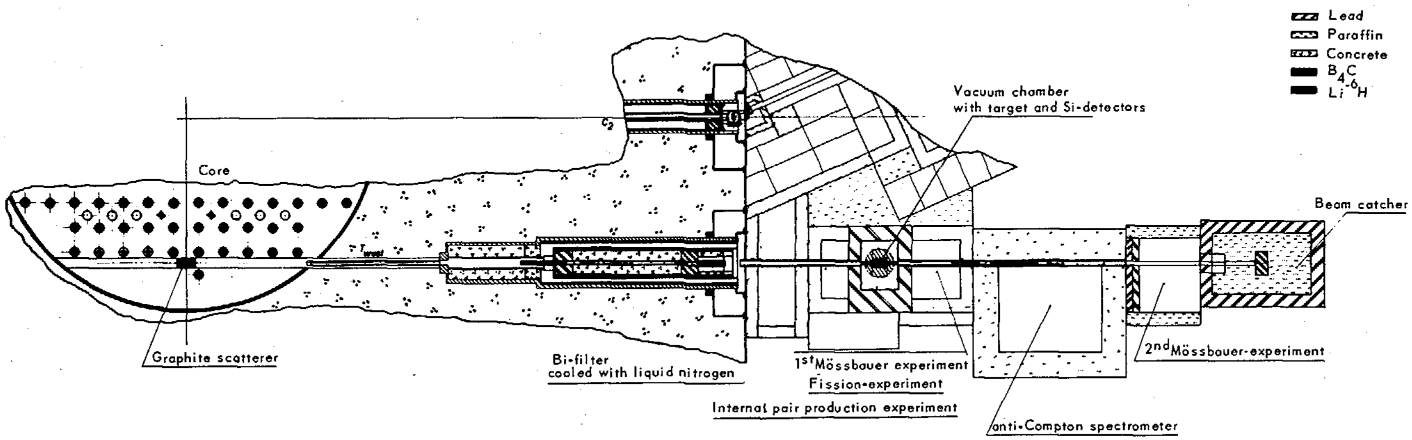

FIG. 1. Geometric arrangement at the tangential through-hole of the reactor FR 2.

desirable to extend these measurements to thermal neutron-induced fission, both in order to compare the results with those obtained from ^{252}Cf and to cover fragment mass regions where the yield in spontanious fission is low.

Various experimental difficulties are inherent in experiments of this type at a reactor. In order to insure a negligible energy loss of the fragments in the target, the source thickness is limited to about 70 $\mu g/cm^2$. Thus for the accumulation of a sufficient number of counts in a multiple parameter experiment a neutron beam of high intensity and long measuring periods are required. The beam introduces restrictions on the geometry of the experimental setup and severe background and shielding problems arise. Electronic drifts must be controlled very carefully.

The present paper describes the measurements of prompt gamma-ray spectra associated with moving fission fragments of specific masses from fission of ^{235}U by thermal neutrons. This study is a part of a more general programme for investigating with high resolution all the prompt radiations emitted in neutron-induced fission.

EXPERIMENTAL PROCEDURE

Fig. 1 shows the geometric arrangement of the installation at the Karlsruhe reactor FR 2. The instrument was located at a tangential channel which passes through the heavy water of the reflector. Collimation of the neutron beam was done in such a way that the target was irradiated only by neutrons emerging from a graphite scatterer placed in the centre of the channel. A cooled bismuth single crystal filter of 20 cm length was used to reduce the gamma radiation in the beam. The thermal flux at the target position was approximately 7×10^7 n/cm^{2}sec [3]. A 50 $\mu g/cm^2$ ^{235}U fission source[1] prepared by electrospraying [4] was placed between two 600 mm^2 Si solid-state fission detectors as displayed in Fig. 2. Gamma rays coincident with fragment pairs were measured in the energy range 100 keV to 2 000 keV by means of a 28 cm^3 coaxial Ge(Li) detector surrounded by an 8" Ø X 9" NaI(Tl) anti-Compton shield [5]. This combination improved the peak-to-Compton ratio by a factor of two to four, depending on gamma-ray energy, and reduced considerably interfering gamma lines produced by inelastic scattering of fission neutrons in the germanium counter. The geometric layout of the apparatus determines the effective time resolution to about 1 nsec after fission. The gamma-ray collimator and the rounded, i.e. doughnut-shaped, fission-fragment collimators were adjusted in such a way that photons emitted later than 1 nsec time-of-flight had to penetrate several cm of lead for triggering the triple coincidence circuit. In particular, this method prevented the detection of gamma rays emitted by stopped fragments.

In order to eliminate electronic drift during the run, the gamma detector system was digitally stabilized using an ultra-stable pulse generator [6]. For stabilization of the silicon detectors the fission spectrum itself was taken as a reference. The counters were operated in the saturation region and a constant bias was maintained throughout the experiment. The energies of fission fragments were obtained from repeatedly measured single spectra with the aid of the

---

[1] The source was supplied by CBMN, Euratom, Geel/Belgium

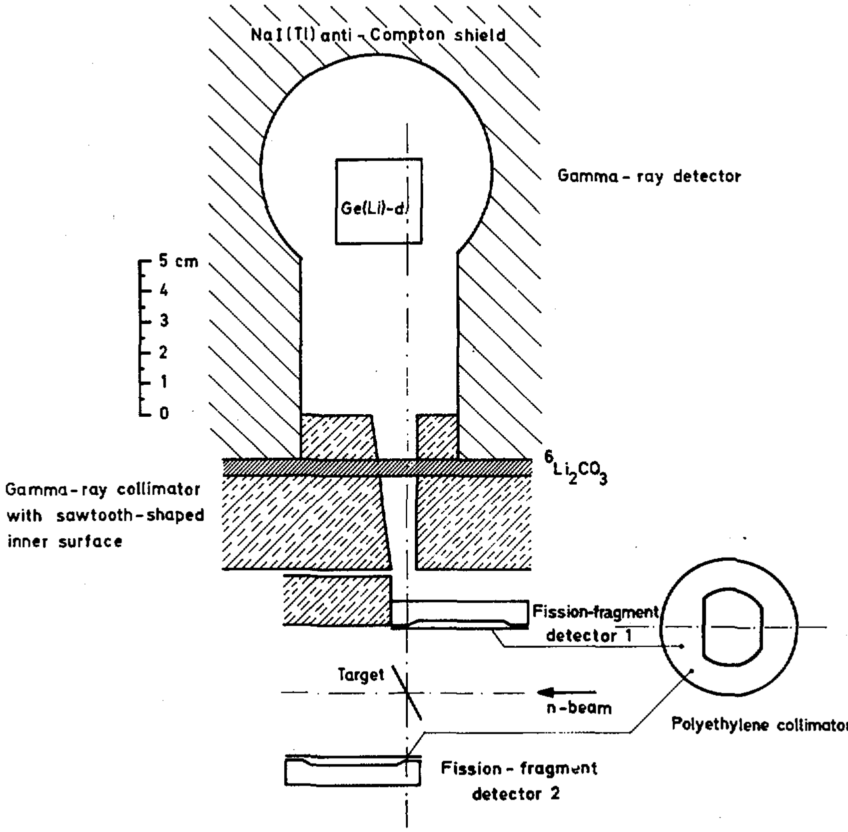

FIG. 2. Schematic view of the experimental set-up.

mass-dependent pulse-height calibration equations given in Ref. [7]. Detectors were replaced whenever the peak-to-valley ratio became smaller than 15. The fast timing was based on the leading edge principle and the electronic time resolution was 40 nsec. The measured chance coincidence rate was well below 2 % of the true coincidence rate.

The triple pulse-height data were processed in a 256 x 256 x 2048 channel matrix via the Karlsruhe Multiple Input Data Acquisition System (MIDAS). Provisional masses μ were calculated from the correlated kinetic energies using momentum and mass conservation. Data were stored on magnetic tape in the form (μ_1, E_T, X_γ). Here μ_1 denotes the mass of the fragment moving towards the Ge(Li) detector, E_T is the total kinetic energy of both fragments and X_γ represents the gamma detector pulse-height. Fragment masses before and after neutron emission were obtained by taking into account the relationships between the average number of neutrons ν and the fragment mass [8]. The variation of ν for a specific mass with the total kinetic energy of the fragments [9] introduces an additional small mass dispersion. For the individual masses considered in the following section the average number of neutrons varies by less than ± 0.5

neutrons for total kinetic energies within plus or minus one rms width of the mean [10]. This value is small compared to the average mass resolution in this experiment which is estimated to be approximately 4 amu FWHM.

RESULTS AND DISCUSSION

Sorting of the triple data according to individual final masses of the fragments revealed a pronounced structure in the corresponding gamma-ray spectra. The pattern changed clearly for different mass ratios. Examples are shown in Fig. 3, where the results are given in

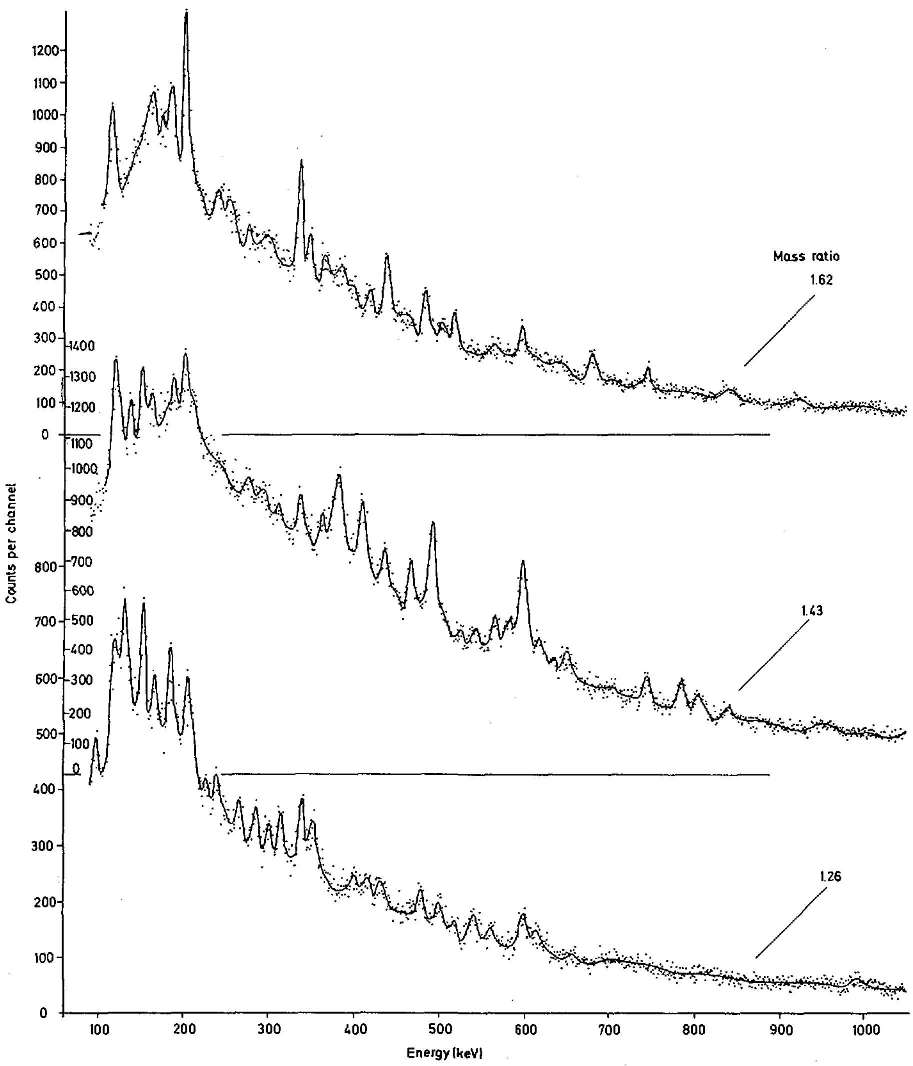

FIG. 3. Sectional display of prompt gamma-ray spectra for various values of mass ratio with the heavy fragments moving towards the gamma-ray detector. The spectra are unsmoothed.

the energy range from 100 keV to 1000 keV for the mass ratio values 1.26, 1.43, and 1.62. In all three cases the gamma counts were restricted to events in which the heavy fragments were moving towards the Ge(Li) counter.

Examples for the dependence of the gamma-ray energies on the fragment velocity and the direction of motion are given in Fig. 4. The upper spectrum in this figure represents the case where the light fragments (A = 96 ± 1) were travelling towards the gamma-ray detector, the lower spectrum holds for the light fragments moving away from the detector. The measured sign and magnitude of the Doppler shift were used for the identification of the emitting member of the fragment pair. The observed shift in energies was consistent with expected values derived from experimental fragment velocity distributions [11] and the geometry used in this experiment. Some weak unshifted lines which appear in the spectra have to be attributed to inelastic scattering of fission neutrons in the germanium

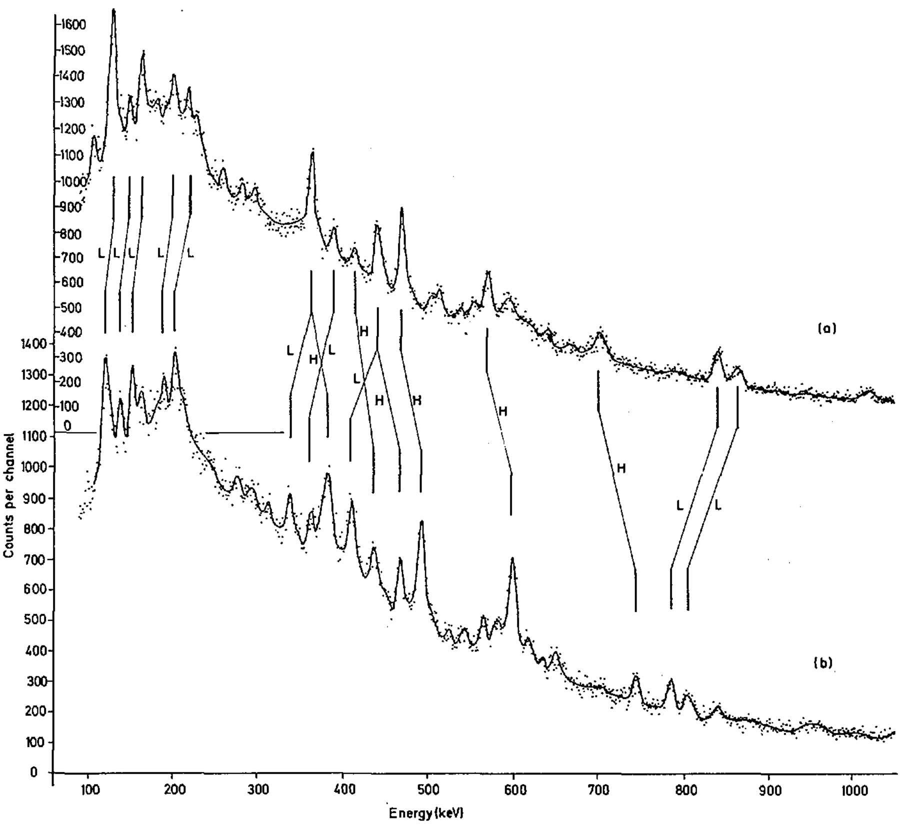

FIG. 4. Observed prompt gamma-ray spectra for the fragment mass ranges A = 95-97 and A = 136 - 138. demonstrating the dependence of gamma-ray energy on the velocity and direction of the fragment motion. The two spectra represent the cases:

(a) Light fragments moving towards the gamma-ray detector, and

(b) heavy fragments moving towards the gamma-ray detector.

The letters L and H indicate some assignments to the light and heavy fragments, respectively.

TABLE I. TENTATIVE ASSIGNMENT OF PROMPT GAMMA RAYS TO INDIVIDUAL FRAGMENTS

Neutron-induced fission of ^{235}U This work			Spontaneous fission of ^{252}Cf Refs [1] and [2]			
Fragment mass A	Most probable charge [a] Z_P	E_γ (keV)	Fragment mass A	Charge [b] Z	E_γ (keV) c	E_γ (keV) d
91 ± 1	36	706				
93 ± 1	37	144				
95 ± 2	38	249				
95 ± 1	38	813				
		834				
96 ± 2	39	376				
98 ± 1	40	193				
99 ± 1	40	123				
		157				
100 ± 1	40	98	100 ± 1	40 [e]	97	98 [f]
		210	99 ± 1	39 [e]	210	210 [f]
		351				
		495				
		622				
101 ± 1	41	325				
102 ± 1	41	174				
103 ± 2	41	518				
103 ± 1	41/42	136				
		296				
104 ± 2	41/42	(157)				
		556				
		581				
104 ± 1	42	191	105 ± 1	42 [e]	190	191 [f]
		366				
131 ± 2	51	965				
138 ± 1	53/54	585	139 ± 1	54 ± 1	586	
139 ± 1	54	283	139 ± 1			283 [g]
		372				
		482				
		723				
141 ± 2	55	475	140 ± 1	54 ± 1	479	
141 ± 1	55	357				
142 ± 1	56	429				
143 ± 2	56	492				
143 ± 1	56	115	144 ± 1	56 [e]	116	116 [f]
		198	144 ± 1	55 [e]	198	198 [f]
		330				
144 ± 1	56	507				
147 ± 1	58	294	146 ± 1			293 [g]

[a] Derived from the tables given in Ref. [12]
[b] Obtained from K-X-ray measurements.
[c] Directly measured gamma-ray energies.
[d] Calculated from conversion electron data.
[e] Atomic number assumed for calculating the gamma-ray energy listed in column 7.
[f] Calculated values with the Z assignment specified in column 5.
[g] Calculated using the most probable charge Z_P.

detector. All spectra shown in Figs 3 and 4 are unsmoothed. Only in a few cases a smoothing procedure was applied for analysis of weak lines or complex structures.

In Table I 39 gamma rays have tentatively been assigned to individual fragments. The masses were arrived at by comparing the peak intensity in adjacent mass intervals the centres of which differing in general by 2 amu. Those masses were selected where the gamma-ray lines appeared with their highest intensity. Many lines occurred distinctly only in one mass-sorted spectrum. This fact provides ample evidence for the correctness of the estimated mass dispersion and the assumed error of ± 1 amu in the mass assignment. If a gamma-ray peak which is now considered to correspond to a single gamma ray turns out to be a closely spaced doublet or a triplet, the energy listed in Table I refers only to the centroid. In some cases, a gamma line was clearly distinguished in one member of the spectrum pair whereas the Doppler shifted partner could not be located since in either possible position intense lines or complex structures occurred. Such lines were not included in the table.

The most probable charge quoted in Table I for the given fragment masses have been derived from the Tables in Ref. [12]. For comparison, data reported by Bowman et al. [1] and by Watson [2] for spontaneous fission of ^{252}Cf have also been included in Table I. Only those transitions from these measurements have been tabulated which may be identified with gamma rays observed in the present experiment. Quite good agreement is found both in photon energy and in mass assignment. The atomic numbers derived from K-X-ray measurements coincide within experimental errors with the most probable charge, and the deviation of the Z values used for calculating the transition energy from conversion electron data is also at most one unit of charge.

It is worth-while to note that in the spectra belonging to fragment masses $A > 104$ groups of gamma rays with energies between 250 and 320 keV and around 400 keV seem to come forward which might be identified with the regular structure observed by Johansson [13] in measurements of the delayed gamma radiation from fission fragments of ^{252}Cf. This structure occurred in the mass range 92 to 110 and suggested a rotational behaviour giving experimental evidence for the existence of a new region of stable deformation in this mass range. Unfortunately, the statistics in the present experiment above A=102 were still too poor to locate the gamma-ray lines with confidence.

CONCLUSIONS

The experiment described has successfully demonstrated that the various difficulties can be overcome which are inherent in reactor experiments for studying the prompt radiation emitted from individual fragments in neutron-induced fission. Though the results are still too incomplete to allow any definite theoretical conclusions, they are encouraging enough to initiate systematic studies of this type, thus extending the investigation of primary fragments to mass regions which are not covered with sufficient yield in spontaneous fission. Meanwhile a new version of the experiment with increased intensity (neutron flux $\sim 10^9$ n/cm^{2}sec) and improved system resolution has been installed at the reactor FR 2. It is reasonable to assume that such studies will reveal important information on neutron-rich nuclei far off the stability line and, via the properties of the nascent fragments, will provide a better insight into the fission process itself.

REFERENCES

[1] BOWMAN, H.R., THOMPSON, S.G., WATSON, R.L., KAPOOR, S.S., RASMUSSEN, J.O., "Symposium on the Physics and Chemistry of Fission" (International Atomic Energy Agency, Salzburg, 1965) Vol. II, 125

[2] WATSON, R.L., UCRL - 16798

[3] HORSCH, F., PIPER, I., KFK 1003 (1969)

[4] VERDINGH, V., LAUER, K.F., Nuclear Instr. and Meth. 49(1967)179

[5] HORSCH, F., MICHAELIS, W., SCHMITT, H.W., "Diskussionstagung über Neutronenphysik an Forschungsreaktoren" (Jülich 1967) 20

[6] HORSCH, F., MEYER, O., MICHAELIS, W., "International Symposium on Nuclear Electronics" (Versailles 1968) Vol. I, Paper No. 22
HORSCH, F., KFK 558 (1968)

[7] SCHMITT, H.W., GIBSON, W.M., NEILER, J.H., WALTER, F.J., THOMAS, T.D., "Symposium on the Physics and Chemistry of Fission" (International Atomic Energy Agency, Salzburg, 1965) Vol. I, 531

[8] APALIN, V.F., GRITSYUK, Yu.N., KUTIKOV, I.E., LEBEDEV, V.I., MIKAELIAN, L.A., Nucl. Phys. 71 (1965) 553

[9] MASLIN, E.E., RODGERS, A.L., CORE, W.G.F., Phys. Rev. 164 4 (1967) 1520

[10] SCHMITT, H.W., NEILER, J.H., WALTER, F.J., Phys. Rev. 141 3 (1966) 1146

[11] ANDRITSOPOULOS, G., Nucl. Phys. A 94 (1967) 537

[12] CROUCH, E.A.C., AERE-R 5488

[13] JOHANSSON, S.A.E., Nucl. Phys. 64 (1965) 147

DISCUSSION

H. NIFENECKER: Have you measured the mass and energy resolution of your fission-fragment detection, making use of the characteristic gamma rays you measured?

F. HORSCH: As you have seen in the gamma-ray spectra of Figs 3 and 4, the individual lines lie on a relatively high background. Therefore, the true intensity distribution of a specific gamma-ray line as a function of mass is affected by the background intensity distribution versus mass. Nevertheless, we have tentatively plotted such resolution curves, assuming a smooth dependence of background on energy for the specific gamma-ray line, and we found a mass resolution of about 4 mass units FWHM.

W. JOHN: I wish to report some studies of the gamma rays from isomeric transitions in primary fission fragments from ^{252}Cf. My collaborators in this work are J.J. Nesolowski and F. Guy.

In referring to "isomeric transitions", we have avoided the term "delayed", which usually means "after beta decay". Here we are concerned with prompt radiation, but with life-times more than a thousand times greater than for the bulk of the transitions, or life-times from a few nanoseconds to a few microseconds.

We have made four-parameter measurements of the isomeric gamma-rays from spontaneous fission of ^{252}Cf. Figure A is a diagram of the experiment. Fission fragments from a thin foil here are detected by Si detectors. A Ge diode detects gamma rays from fission fragments which have stopped on the left Si detector. Since the fragment is at rest, there

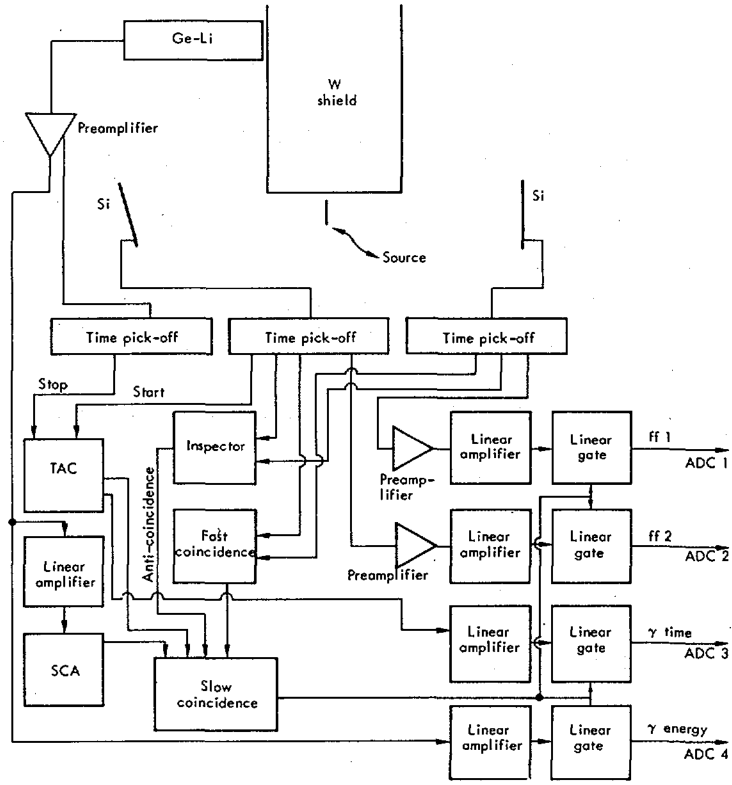

FIG. A. Diagram of experimental arrangement.

is no Doppler shift of the gamma-ray energy. A shield prevents the Ge detector from "seeing" the source and defines the fragment emitting the gamma ray. The time delay between fission and gamma emission is measured by starting a time-to-amplitude converter on the fission pulse and stopping on the gamma pulse. The four signals are digitized and recorded on magnetic tape for subsequent analysis by computer. Figure B is a plot of the relative gamma-ray yield per fragment per nanosecond versus fragment mass for three gross time intervals. All gamma-ray energies are lumped together. Note that the ordinate is per fragment, i.e. the fragment yield has been taken out. The isomeric gamma-ray yield peaks strongly in certain mass regions, roughly 92, 97, 110, 128, 134, 147 and 157. The peaks decay with time with various half-lives. For example, note how the shoulder at mass 97 for early times becomes a peak later.

In 1960 Johansson made a measurement of the prompt gammas with half-lives of the order of 10^{-11} sec using NaI. The yield versus mass had generally a saw-tooth shape. In 1964 he measured isomeric transitions with half-lives of the order of 10^{-8} s to 10^{-7} s. The yield was similar to what we have shown here. In reviewing Johansson's work, we were struck by a correlation between the early and late gamma rays, which has apparently escaped notice so far.

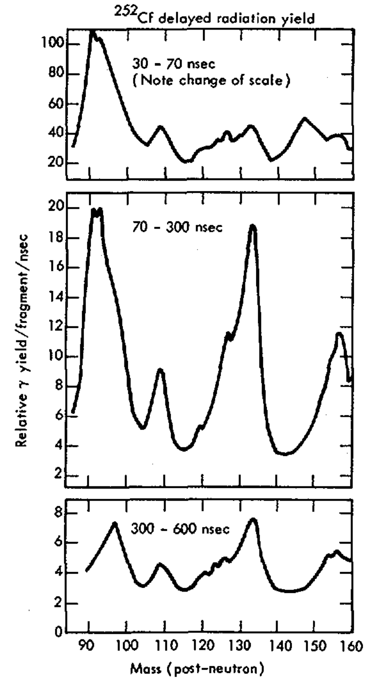

FIG.B. Yield of delayed gamma rays versus fission-fragment mass for three time intervals after fission.

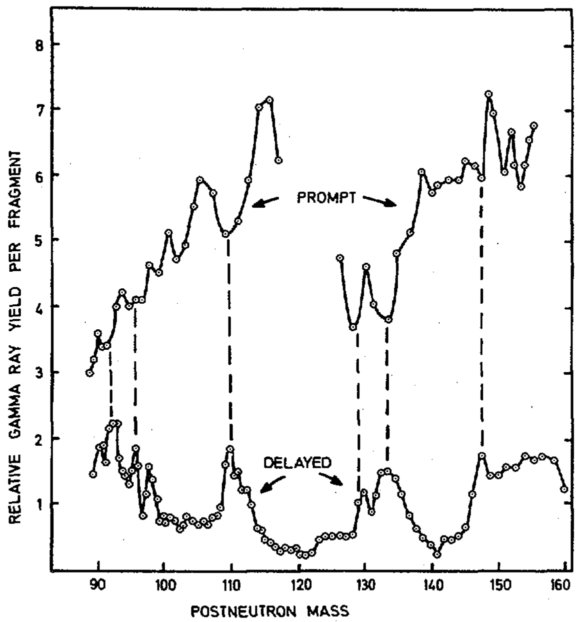

FIG.C. Relative gamma-ray yield per fragment versus fission-fragment mass, data taken from Johansson, S.A.E., Nucl. Phys. 60 (1964) 378, 64 (1965) 147. The vertical dashed lines indicate correlated structure between the prompt and delayed gamma-ray yields.

In Fig. C we have plotted Johannson's data points. He drew a line through the points. The upper curves are the early gammas, the lower the isomeric gammas. Valleys in the early yield occur at mass numbers where peaks occur in the late yield. The vertical dashed lines are drawn at the approximate masses where peaks occur in our own data. In fact, the mass scale is designated postneutron from our own work. It was necessary to shift the upper curves down by two mass units, which is probably within the accuracy of the data.

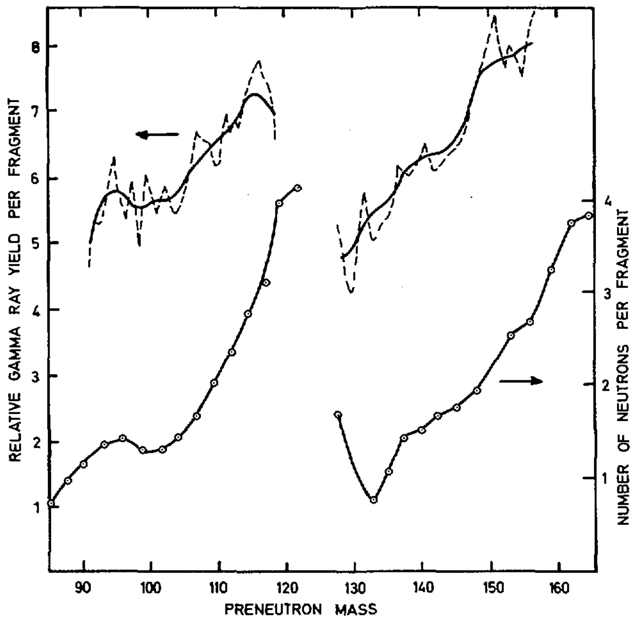

FIG.D. The upper curves are total gamma ray yields obtained by adding the prompt and delayed yields in Fig.C. The lower curves are the number of neutrons per fragment,from Bowman, et al.

This correlation suggests that the occurrence of an isomeric transition at a given mass simply subtracts from the early yield and adds to the late yield. The total yield may then be a fairly smooth function of mass. Since the data were only relative, we normalized so that the peaks at 110 and 130 approximately filled the valleys. This normalization implies that ~20% of the transitions are late. We then added the curves to produce curves of the total yield shown in Fig. D.

The upper dashed curve is the total yield; however, since no credibility can be placed on the remaining "fine" structure, we have drawn in a smooth average curve. Below we plotted the number of neutrons per fragment from Bowman et al. The similarity in the saw-tooth curves is very marked. Even the curious hump near mass 95 is apparently reproduced by the gamma curve. Here the hump is produced by the isomeric gammas.

Although we find isomeric gammas from nearly every mass, the intensity is concentrated on relatively few masses. We can use our multiparameter data for a more detailed examination. The gamma rays from the mass 130 region come predominantly from mass 134 (<u>not</u> doubly-magic 132).

FIG. E. Gamma-ray spectrum obtained by sorting the data for fragment mass 134 events for the time interval from 8 to 72 ns after fission.

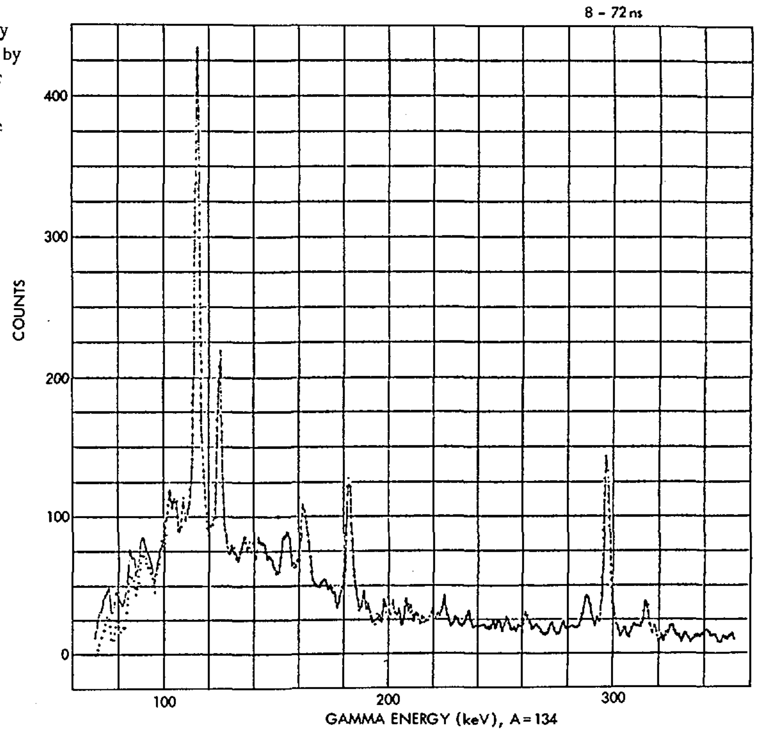

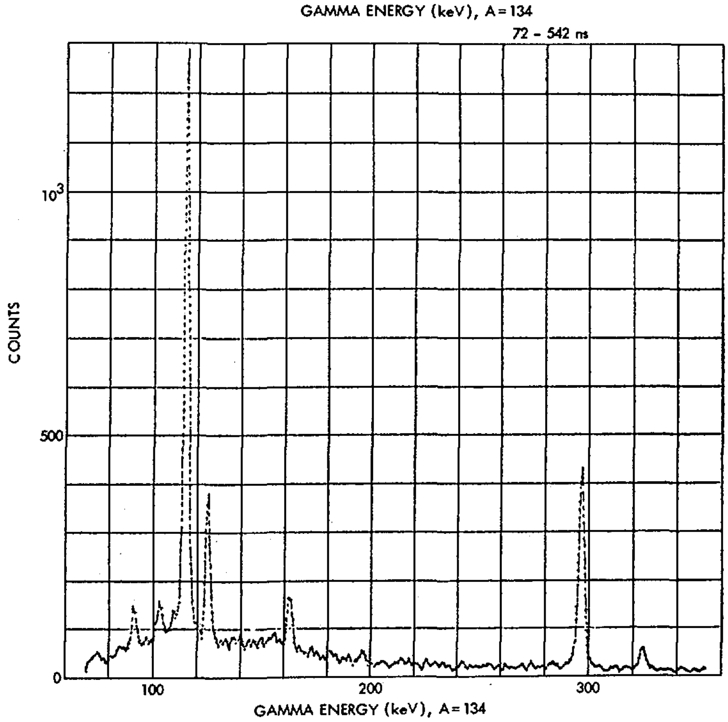

FIG. F. Gamma-ray spectrum obtained by sorting the data for fragment mass 134 events for the time interval 72-542 ns.

I will, therefore, illustrate our analysis on mass 134. Figure E is the gamma-ray spectrum from 8-72 ns from the mass 134 region. Figure F is for 72-542 ns. Note the resolution of the peaks. (The significant data extend up to ~ 1.5 MeV.) Figure G is for t = 542-1942 ns. We can now, if we wish, pick out a peak for further analysis.

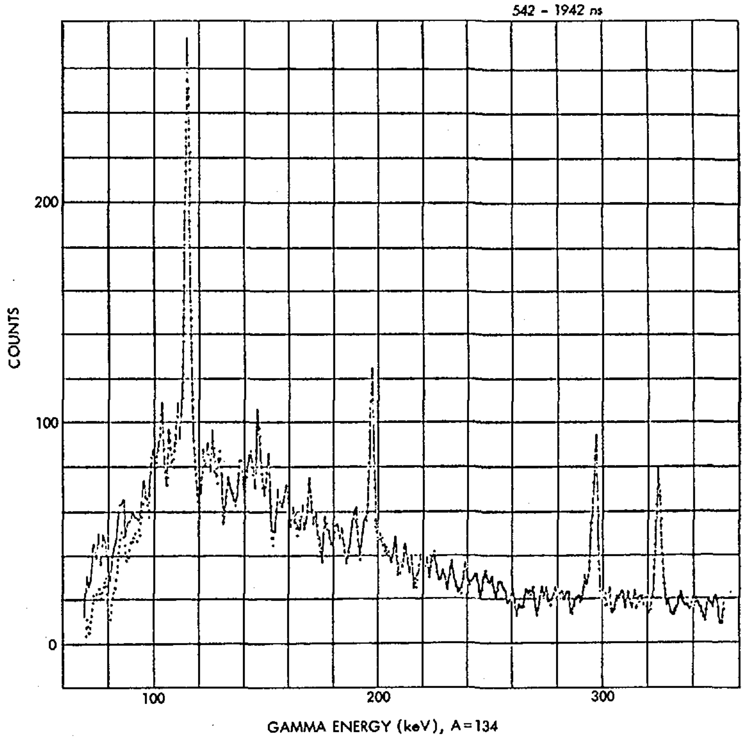

FIG. G. Gamma-ray spectrum obtained by sorting the data for fragment mass 134 events for the time interval 542-1942 ns.

Figure H represents such an analysis for a 297 keV gamma ray from mass 134. In the upper left we have counts versus gamma-ray energy to determine E_γ (296.8) and in the upper right counts versus mass showing that it peaks at 134. Below is the decay curve showing a half-life of 170 ns.

One of the strong gamma rays from mass 134 has an energy of 1280 keV. In Fig. I we plot the energy of the 2^+ to 0^+ ground-state transition energies for N = 82 nuclei. Extrapolating to Z = 52, which is believed to be the most probable charge for A = 134, we find 1.28 MeV. Therefore it appears that our gamma ray is the ground-state transition in ^{134}Te.

To date we have analysed over 100 gamma rays in this manner. Time does not permit me to elaborate; besides, the analysis is continuing. However, I would like to emphasize that we have no good explanations for the nature of these isomeric transitions.

Since the fission process populates these states in a unique manner, it may be valuable to achieve an understanding of isomerism in fission fragments.

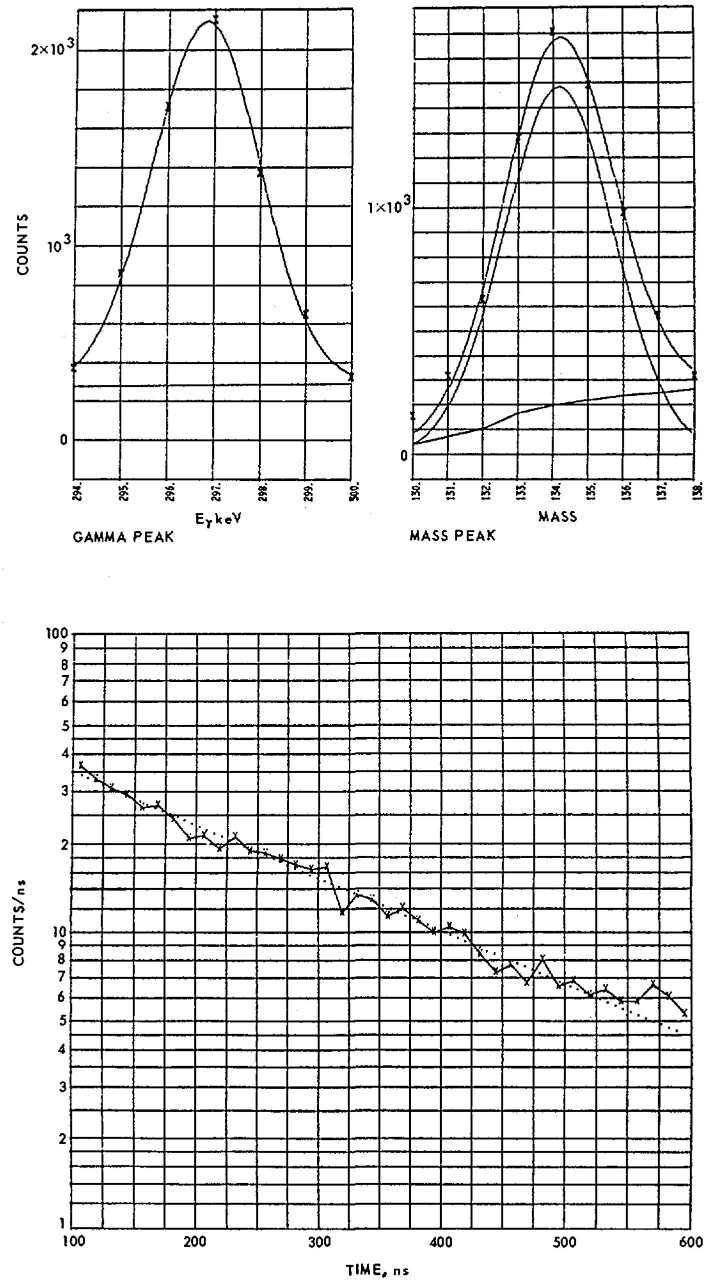

FIG. H. Detailed analysis of the data for a particular gamma-ray transition. Upper left: counts versus gamma ray energy; upper right: counts versus mass; lower half: counts versus time. The curves thus fitted to the data determine that the gamma-ray has an energy of 296.8 keV, comes from fragment mass 134, and has a half-life of 167 ns.

TABLE A. DELAYED γ RAYS FROM FISSION PRODUCTS OF THERMAL FISSION OF ^{235}U[a]

E (keV) ($\Delta E \approx \pm 1$ keV)	$t_{1/2}$ (μs)	Mass number	Relative yield
107	8.5 ± 0.5	89 ± 0,2	22
152	8.0 ± 0.5	89 ± 0.2	22
65	80	100 ± 2	17
77	30	100 ± 2	9
115	20 - 27	100 ± 2	100
125	2	100 ± 2	22
165	8 - 11	100 ± 2	43
197	8 - 9	100 ± 2	22

[a] The intensity of the 115 keV γ-transition corresponds approximately to 50% of the chain yield of mass number 100.

109	< 2	heavy group	smaller than 10
170			
190			
240			
322			
375			

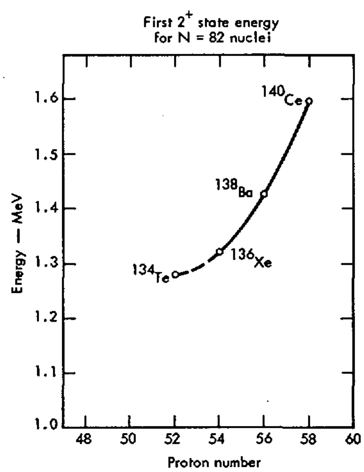

FIG.1. Plot of the energy of the first 2^+ state for N = 82 nuclei versus proton number showing that an extrapolation to Z = 52 gives 1.28 MeV, the energy of a gamma-ray observed in the present experiment from mass 134. Thus the gamma-ray is probably from ^{134}Te.

J. UNIK: In connection with Dr. John's observations, I would like to say that approximately three years ago at the Argonne National Laboratory, we performed virtually the same experiment as described by him and observed similar results, particularly in regard to the delayed gamma rays originating from primary fragments of mass 134. We further determined by examination of the characteristic K X-rays emitted from these fragments that the gamma rays assigned to mass 134 can be attributed mainly to the element tellurium (Z = 52), as he deduces.

P. ARMBRUSTER: We looked into isomeric gamma emission with our gas-filled mass separator. After a flight time of 1 μs through the separator, gamma emission in the time range (1-100) μs after fission was investigated. The following gamma-quanta were found. The mass assignment is preliminary.

K. DIETRICH: I would like to point out a possible implication of these measurements, which is probably obvious to many of you. The delayed gamma rays may originate from transitions between oblate and prolate states of the fission fragments. They could thus indicate the existence of excited states of oblate shape in medium heavy nuclei. In my view, therefore, these experiments provide extremely interesting information.

MASS DEPENDENCE OF ANISOTROPY AND YIELD OF PROMPT γ-RAYS IN ^{235}U THERMAL FISSION

P. ARMBRUSTER, F. HOSSFELD, H. LABUS, K. REICHELT
Institut für Festkörper- und Neutronenphysik,
Kernforschungsanlage Jülich,
Federal Republic of Germany

Abstract

MASS DEPENDENCE OF ANISOTROPY AND YIELD OF PROMPT γ-RAYS IN ^{235}U THERMAL FISSION. The yield of prompt γ-rays and the anisotropy of the angular correlation, γ-ray versus fission product, have been measured. A time-of-flight and energy measurement on single fragments gives the mass. γ-rays emitted in flight are observed in the time interval of 3×10^{-12}-2×10^{-10} s after fission through a slit collimator of adjustable width. Only those γ-rays emitted by the fragment the mass of which is detected in the time-of-flight energy spectrometer are recorded. γ-rays are detected in the energy range between 0.1 and 1.5 MeV by plastic scintillators for angles of emission of 30°, 90° and 150°.

1. INTRODUCTION

Information on the breaking of the nucleus in the final stages of fission may be gained by studying the properties of fission fragments. Besides the well-studied quantities as primary mass, primary charge, kinetic and excitation energy, there is a further quantity which gives only little information but which seems to be of equal interest for the breaking process: the primary angular momenta of the virgin fission fragments. The absolute size of the angular momenta determines the distribution of the excitation energy between prompt neutrons and prompt γ-quanta. An alignment of the angular momenta shows up in the angular distribution of the emitted γ-quanta.

The average values of the γ-energy, the number of γ-quanta, and the anisotropy of γ-emission have been interpreted qualitatively as an emission from nuclei with rather high values of spin ($I \sim 10\ \hbar$) aligned perpendicular to the fission axis [1, 2]. The alignment of reaction products is a general property of heavy-ion reactions and must hold true for fission fragments according to both the dynamic liquid-drop-model calculations of Nix and Swiatecki [3] and recent calculations of Rasmussen et al. within their molecular model of fission [4]. A complete alignment being assumed, the anisotropy of γ-emission may be regarded, under certain further assumptions to be discussed later, as a measure of the angular momentum [5]. On the other hand, the multiplicity of γ-emission depends on the initial spin value and excitation energy of the γ-emitting nucleus, as γ-quanta have to carry off the high angular momenta [6]. The multiplicity of γ-emission has been shown to depend strongly on the nuclear structure of the fission fragments [7, 8]. A similar dependence may be expected for the anisotropy of γ-emission.

Two methods of measuring the number of prompt γ-quanta emitted from single fragments are known. The first method applied by Johansson uses the fact that γ-emission is delayed by 10^{-12} - 10^{-10} s and fission fragments move with a velocity of 10^9 cm/s [7]. A geometrical separation on the γ-emission from the two fragments becomes partly possible by observing the γ-emission from fragments in flight through a collimator system with an aperture corresponding to the distance between the fragments, when they emit the bulk of their γ-quanta 10^{-3} - 10^{-1} cm. A second method uses the relativistic change of the solid angle between source and detector for systems emitting in flight to obtain the number of γ-quanta from single fragments [8]. This method supposes that all γ-quanta are emitted in flight. It gives the total number of all γ-quanta independent of the emission time whereas the collimator method is restricted mechanically to emission times longer than 5 ps.

The anisotropy depending on the mass ratio of a fragment pair may be measured by using a pair of solid-state detectors and an angular correlation set-up [9]. To our knowledge, there is no measurement of the anisotropy depending on the fragment mass. In the following a set-up is described, which combines an angular-correlation measurement with the collimator technique introduced by Johansson, and which may be used to measure the mass dependence of the anisotropy for γ-quanta emitted in times longer than 5 ps, the mass ratio dependence of the anisotropy for all γ-quanta, and the number of γ-quanta by both methods mentioned. The experiment has been planned to establish experimentally the close connection between the multiplicity of γ-emission and anisotropy, as both quantities are governed by the primary angular momentum of the fragment.

Two simplified models of deexcitation of a fragment have been discussed in the literature, and calculations within these models have been published [5, 10].

The high spin of the fragment may be reduced by a stretched cascade of γ-quanta. The spin change per γ-quantum emitted is then given by the multipolarity of the radiation emitted. The initial spin is given by the sum of the multipolarities of all γ-quanta emitted. The anisotropy of the γ-emission depends only on the multipolarity, and not on the value of the initial spin. Within this model, the multiplicity of γ-emission assumes a given multipolarity of the radiation, for example, mainly E2, a direct measure of the initial spin; the anisotropy, however, is independent of the initial spin, and cannot be used to provide information on the quantity of interest, the initial spin. The model gives an upper limit of the initial spin values [10].

In a second model of deexcitation, the level density of the excited nuclei to be described within the statistical model governs the deexcitation. Within this model there is no direct way to calculate the initial spin from the multiplicity, since many cascades of deexcitation depending on the nuclear structure of the fragment are open. The anisotropy of γ-emission, however, is simply connected with the initial spin. If the initial spin of a fragment is higher than the average spin of all its excited states at a certain excitation energy given by the spin-cut-off parameter of the level-density formula, but not larger than the square of this value, then a formula first derived by Strutinsky holds. The angular distribution of γ-radiation emitted in flight is given by

$$W^L(\vartheta) = 1 + k_L (I/\sigma^2)^2 \sin^2\vartheta + 2\beta \cos\vartheta \qquad (1)$$

where k_L is a factor depending on the multipolarity, $k_1 = 1/8$, $k_2 = -3/8$, I is the initial spin, σ the spin-cut-off parameter, ϑ the angle between γ-quantum and fission axis, and β the velocity in units $c = 3 \times 10^{10}$ cm/s. The second term takes only account of the relativistic change of the solid angle rather than of the relativistic change of energy.

A multipolarity of mainly L = 2 and well known values of the spin-cut-off parameter being assumed, the initial spin may be calculated from the measured anisotropy [5].

Since σ and k_L are in any case slowly varying functions of the fragment mass, a strong mass dependence of the anisotropy means, that the initial spin of the fragment depends strongly on the nuclear structure of the fragment. The stretched cascade deexcitation mechanism will not largely contribute to the deexcitation. The measurement of anisotropy may be interpreted as a means of measuring primary spins of the fragments, or, at least, as a means to decide between a statistical or stretched cascade deexcitation mechanism.

2. EXPERIMENTAL SET-UP

A ^{235}U fission product source generated in a thermal neutron beam leaving the reactor FRJ-2 vertically is surrounded by four γ-detectors and four fission product detectors arranged in circles in planes perpendicular to the neutron beam. The source is a UF_4-layer (1 mg/cm^2) on a scintillating backing. The scintillations from fission products stopped in the backing are registered by a photomultiplier seeing the source via a mirror system and generating pulses to start two time-to-pulse height converters. The time-to-pulse height converters are stopped by signals from the four fission product or four γ-detectors, i.e. the time-of-flight of fission products or of γ-quanta and prompt neutrons, respectively, is measured.

The fission product detectors are silicon surface barrier detectors with an active area of 400 mm^2. They measure the energy of the fission products and produce the abovementioned fast stop signal for the time-of-flight measurement. The flight path of the fission fragments is 20 cm. Time-of-flight and energy of a detected fission product are registered and used to determine its mass.

A mass determination by a time-of-flight and energy measurement is not restricted as severely by the target thickness as a mass determination by an energy measurement of the two complementary fission products. The flight paths provide a natural definition of the direction of flight, necessarily needed for any measurement of angular correlation. A mechanically stable source with a well-defined surface makes possible an adjustment of the source position within a few hundreds of a millimeter. The accuracy of the source positioning contributes decisively to the accuracy of the time measurement of γ-emission.

γ-emission in the directions 30°, 90° and 150° relative to the direction of flight of a fragment is observed. To achieve the highest possible degree of symmetry in the experimental arrangement, a system of eight detectors, four γ-detectors and four fission-product detectors has been chosen, each of them having geometrically the same surroundings of detectors. The γ-detectors are plastic scintillators of 5 cm thickness.

The time-of-flight difference between fast neutrons and γ-quanta from the source to the γ-detectors allows a discrimination between prompt neutrons and γ-quanta. A quantitative separation of prompt neutrons and γ-quanta has been achieved.

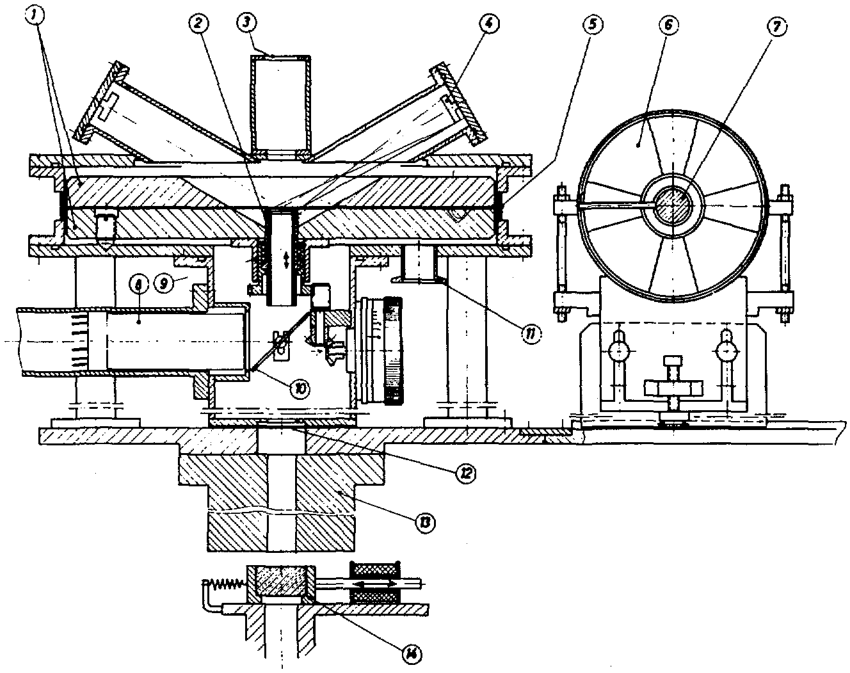

FIG. 1. Experimental set-up used to measure anisotropy and yield of prompt γ-emission. The figures refer to 1) steel collimator, 2) target holder and fine adjustment, 3) neutron beam exit window, 4) Si-surface barrier detector, 5) γ-ray exit window, 6) lead shield, 7) plastic scintillator γ-detector, 8) 56 AVP photomultiplier, 9) source adjustment, 10) mirror, 11) vacuum flange, 12) neutron beam entrance window, 13) neutron beam collimator, 14) neutron beam shutter.

The γ-detectors observe the fission source through a collimator system consisting of two parallel 3 cm thick, 40 cm diameter stell plates. The distance between the plates may be adjusted within 1 cm and 5×10^{-3} cm with an accuracy of a few hundreds of a millimeter. The source and its mechanism for adjustment are put inside a centric hole in the steel collimator. The source is moved relative to the γ-collimator in order to enable observation of either flying or stopped fragments. Source and mirror, fission-product detectors, and the collimator are mounted in a vacuum chamber, evacuated in order to prevent energy losses of fission products on their way to their detectors. The source position and the collimator width are adjusted and changed from outside the chamber without breaking the vacuum. Figure 1 shows the vacuum chamber and one of the four γ-detectors.

The electronics used to register time-of-flight and energy of the fragments, the energy of the γ-quanta, and the detector combination of the observed fission-product prompt-γ-quantum coincidence are shown in Fig. 2. The four-parameter events are recorded event by event on paper tape. An event is recorded only if one out of the four fission products and one out of the four γ-detectors have received signals within the coincidence resolution time, and if the signal registered in the γ-detector fulfils the flight-time discrimination criterion against fast neutrons. The large anisotropy of prompt neutron emission makes a quantitative discrimination against fast neutrons necessary. Figure 3 gives a time-of-flight spectrum of the counts detected in the γ-detector measured with a 50 cm flight path. A characteristic fission-product mass spectrum obtained with a 20 cm flight path may be seen from Fig. 6. The mass resolution amounts to about 10% and is by far inferior to the resolution obtained with longer flight paths or the two-detector technique. Figure 4 shows the time resolution of the collimator system. Depending on the position of the target the γ-quanta seen through the collimator are either emitted by both fragments or only by one of them. An enrichment of γ-quanta may be achieved either for quanta emitted from flying or from stopped fragments.

A combination of 16 different pairs of a γ-detector and a fission-product detector is possible. The rates of these 16 pairs are registered. Eight pairs give the intensity at 90°, four at 30° and four at 150° relative to the direction of flight of the fragment.

Measuring at angles ϑ and $\pi - \vartheta$ is advantageous in that all anisotropies from relativistic effects cancel in pairs. All these anisotropies are equal in size but different in sign for angles ϑ and $\pi - \vartheta$. Small differences in solid angle and detection efficiency of the detectors cancel as well, as each γ-detector is, relative to each fission product detector, twice a 90°-, once a 30°-, and once a 150°-detector.

Besides the abovementioned symmetry of our detector arrangement, an intensity increase by a factor of four is obtained relative to an arrangement with only one fission-fragment detector. Intensity problems are of major interest. A relative accuracy of 10% in the anisotropy coefficients which themselves are of the order of 10%, needs a counting rate of 10^4 for each subgroup the anisotropy of which is to be determined. The high mass resolution to be obtained in a double energy measurement is of no use unless the counting rates for each subgroup are, at least, 10^4. Our thick target technique with low mass resolution and γ-energy resolution gives at a collimator width of 5×10^{-2} cm, looking at both fragments, counting rates of 5/min for all detector pairs. The thermal neutron flux at the source amounts to $5 \times 10^8\ s^{-1}\,cm^{-2}$ and cannot be increased decisively for any beam of our reactor.

3. MEASUREMENTS

The coincidence rates n_{LK} of the 16 combinations of γ-detectors and fission product detectors have been measured. The coincidence rates have been corrected for the detection efficiencies and solid angles of the counters by calculating relative values of these quantities directly from the measured rates. The relative detection efficiency of a counter L is given by

$$q_L = \frac{\sum\limits_K n_{LK}}{\sum\limits_L \sum\limits_K n_{LK}} \quad \text{with} \quad \begin{array}{l} K = 1,2,3,4 \\ L = 1,2,3,4 \end{array}$$

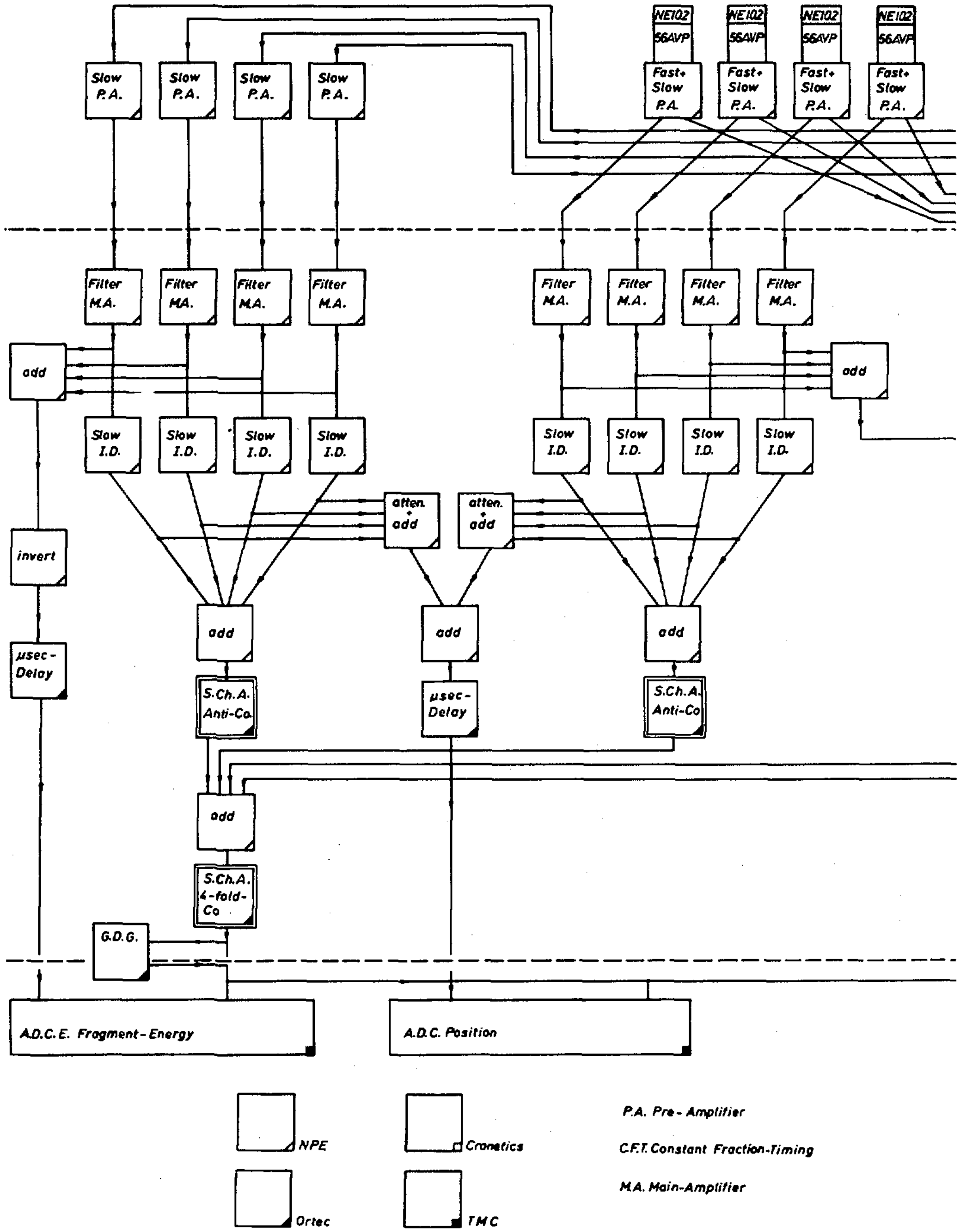
NE102
56AVP
Fast+ Slow P.A.
Slow P.A.
Filter M.A.
add
Slow I.D.
atten. + add
invert
μsec-Delay
S.Ch.A. Anti-Co
add
S.Ch.A. 4-fold-Co
G.D.G.
A.D.C.E. Fragment-Energy
A.D.C. Position
NPE
Cronetics
Ortec
TMC
P.A. Pre-Amplifier
C.F.T. Constant Fraction-Timing
M.A. Main-Amplifier

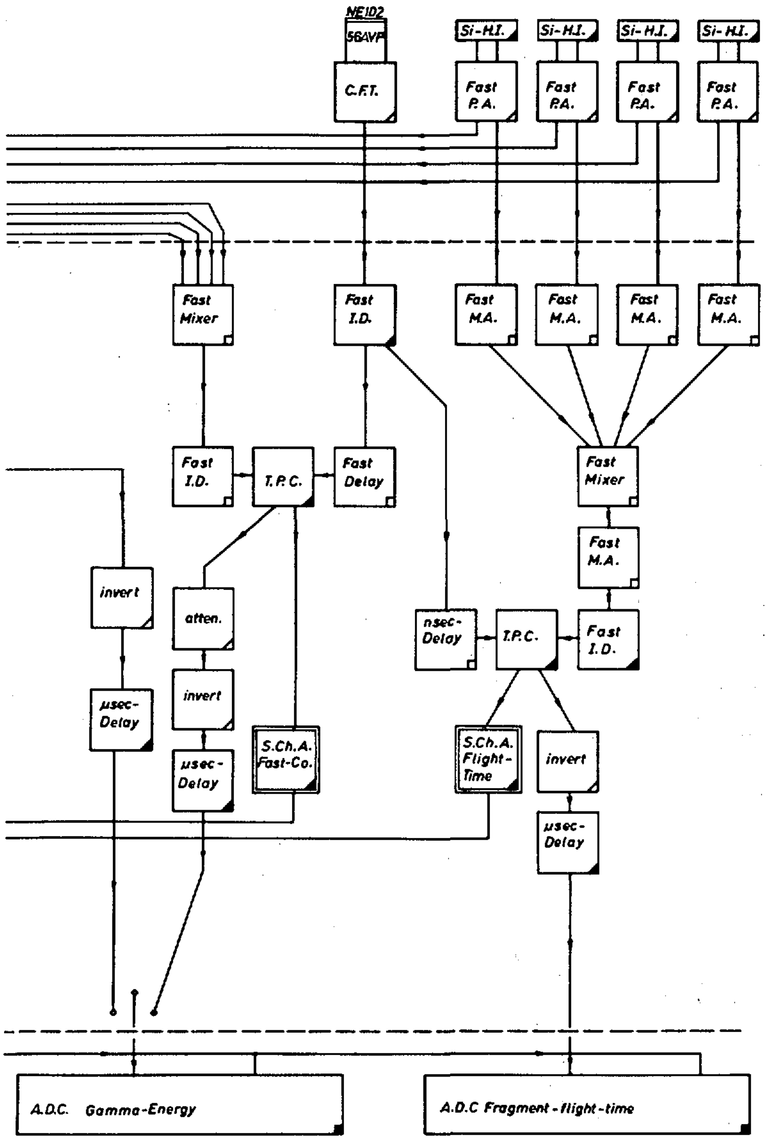

I.D.	Integral-Discriminator	A.D.C.	Analog-Digital-Converter
Si-H.I.	Silicon-Heavy-Ion-Detektor	S.Ch.A.	Single-Channel-Analyser
T.P.C.	Time-Amplitude Converter	G.D.G.	Gate-Delay-Generator

FIG. 2. Electronic equipment used to measure anisotropy and yield of prompt γ-emission.

From the rates n_{LK} the relative numbers of γ-quanta $N(\vartheta, M, E_\gamma)$ emitted from the source are calculated for the different detector combinations characterized by fixed angles between the counters:

$$N(\vartheta, M, E_\gamma) = \frac{n_{LK}(\vartheta, M, E_\gamma)}{q_L q_K}$$

$$= \frac{1}{1+\rho}\left[G_1(t)\,\rho(1+\epsilon_1\cos\vartheta+\alpha_1(t)\sin^2\vartheta)+G_2(t)(1-\epsilon_2 f_2\cos\vartheta+\alpha_2(t)\sin^2\vartheta)\right] \quad (2)$$

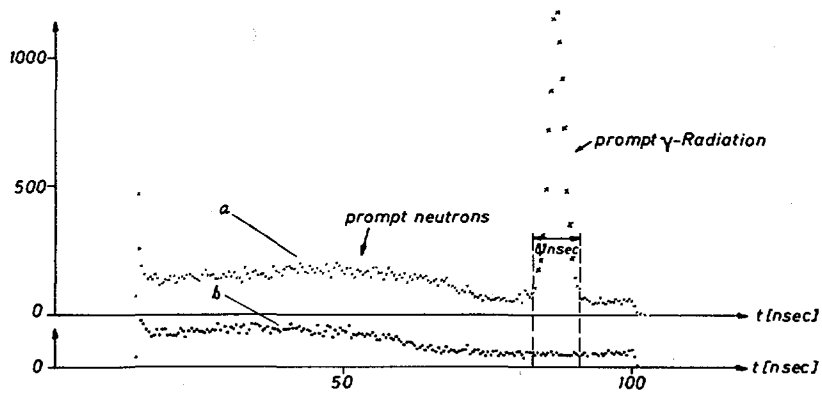

FIG. 3. Time-of-flight spectrum of events recorded in the γ-detector. The good discrimination between prompt neutrons and γ-quanta is demonstrated. Curve a: time-of-flight spectrum obtained with open γ-collimator; curve b: time-of-flight spectrum obtained with closed γ-collimator.

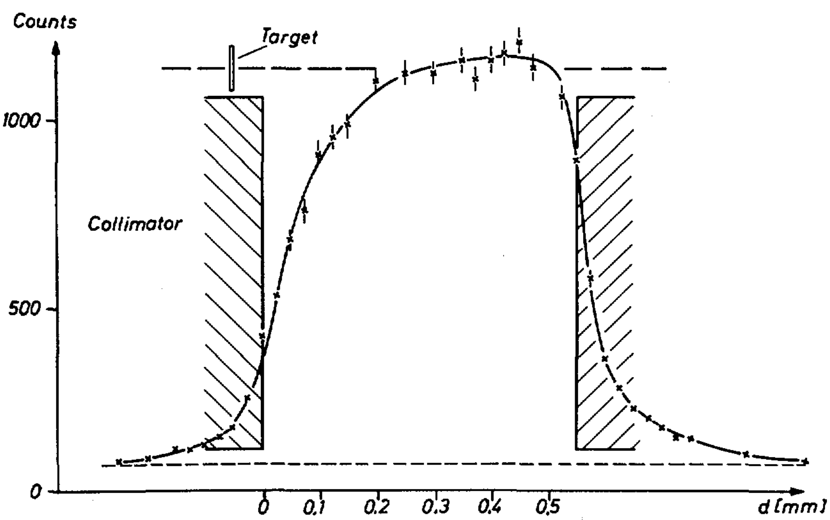

FIG. 4. Prompt γ-radiation observed through the collimator for different positions of the target. On the left-hand side, the intensity increases when the source is moved into the collimator opening since more and more γ-quanta from stopped fragments are seen by the detector. On the right-hand side, the intensity decreases as only γ-quanta from flying fragments, but not from fragments stopped in the backing are seen.

with $G_i(t)$ being number of γ-quanta emitted from a fission product at time t. The indices 1 and 2 refer to mass M and the complementary mass (A - M), respectively. ρ is the factor giving the enrichment of fragments of mass M, if a collimator is used, $\alpha_i(t)$ is the anisotropy coefficient and $\epsilon_i = (2+r)\beta_i$, the relativistic 0°/90° anisotropy, $\beta = v/c$ of the fission fragment. The factor 2 arises from the relativistic solid-angle variation. r takes account of two further relativistic effects. The number of γ-quanta surpassing an electronic threshold and the absorption efficiency change if the energy of the quanta is changed. Both quantities contribute to the relativistic anisotropy. With a threshold of 50 keV and an average spectrum of prompt γ-quanta r is equal to -0.15.

$$\overline{\beta} = \int_0^\infty e^{-\frac{t}{T}} \beta(t) \frac{dt}{T} = \frac{\beta}{1 + T/t_{ex}} = \beta f$$

gives the average values of β for fragments stopped in the backing. T is the average half-life of the prompt γ-quanta, t_{ex} a characteristic stopping time depending on the stopping power S. $t_{ex}(ps) = 1.23\ k^{-1}(mg/cm^2)\rho^{-1}A^{1/2}(ps)$ with k from $S = k\sqrt{E}$. In the plastic scintillator backing t_{ex} amounts to 1.6 ps. The stopping times vary for low- and high-atomic-number materials between 1.6 - 0.5 ps.

N(ϑ) has been measured at three angles. From these three measured rates three quantities have been derived for further evaluation:

$$\begin{aligned} N_i &\equiv \frac{1}{4}\left[N_i(\vartheta) + N_i(\pi - \vartheta) + 2N_i\left(\frac{\pi}{2}\right)\right] \\ A_i^R &\equiv \frac{N_i(\vartheta) - N_i(\pi - \vartheta)}{N_i(\vartheta) + N_i(\pi + \vartheta)} \\ A_i^N &\equiv \frac{N_i(\vartheta) + N_i(\pi - \vartheta) - 2N_i\left(\frac{\pi}{2}\right)}{N_i(\vartheta) + N_i(\pi - \vartheta) + 2N_i\left(\frac{\pi}{2}\right)} \end{aligned} \tag{3}$$

In Table I equations connecting N_i, A_i^R, and A_i^N with the quantities of interest have been compiled. The cases of no enrichment (ρ = 1 - measurement without collimator), of high enrichment ($\rho \to \infty$-view on the flying fragments and $\rho \to 0$-view on the backing), and of any enrichment are compared. The quantity γ is the ratio of the prompt γ-yields of fragments of mass M and mass (A - M).

A measurement demonstrating different degrees of enrichment is shown in Fig.5. The anisotropies given have been measured with $\vartheta = 30°$ but have been plotted as values for the generally used angles ϑ = 0°, $\pi/2$, and π. The relativistic anisotropy increases with increasing degree of enrichment.

In the following, experiments with our set-up, possible and already done, will be discussed according to a measurement of the three quantities N_i, A_i^R, and A_i^N.

TABLE I. COMPILATION OF EQUATIONS CONNECTING THE EXPERIMENTALLY DETERMINED QUANTITIES N_i, A_i^R, AND A_i^N.

enrichement factor ρ / measured quantity	$\neq 0$ $t > 10\ ps$	$\rho = 1$ $t = 0$	$\rho \to \infty$	$\rho \to 0$
N_1	$\frac{\rho G_1(t)+G_2(t)}{\rho+1}$	$\frac{G_1+G_2}{2} = \bar{G}$	$G_1(t)$	$G_2(t)$
N_2	$\frac{G_1(t)+\rho G_2(t)}{\rho+1}$	$\frac{G_1+G_2}{2} = \bar{G}$	$G_2(t)$	$G_1(t)$
A_1^R	$\frac{\gamma\varepsilon_1\rho - f_2\varepsilon_2}{\rho\gamma+1}\cos\vartheta$	$\frac{\gamma\varepsilon_1 - f\varepsilon_2}{\gamma+1}\cos\vartheta$	$\varepsilon_1\cos\vartheta$	$-f_2\varepsilon_2\cos\vartheta$
A_2^R	$\frac{\varepsilon_2\rho - f_1\gamma\varepsilon_1}{\gamma+\rho}\cos\vartheta$	$\frac{\varepsilon_2 - f\varepsilon_1\gamma}{\gamma+1}\cos\vartheta$	$\varepsilon_2\cos\vartheta$	$-f_1\varepsilon_1\cos\vartheta$
A_1^N	$-\frac{\gamma\rho\alpha_1+\alpha_2}{2(\rho\gamma+1)}\cos^2\vartheta$	$-\frac{\gamma\alpha_1+\alpha_2}{2(\gamma+1)}\cos^2\vartheta = -\bar{\alpha}\frac{\cos^2\vartheta}{2}$	$\alpha_1(t)\frac{\cos^2\vartheta}{2}$	$\alpha_2(t)\frac{\cos^2\vartheta}{2}$
A_2^N	$-\frac{\alpha_2\rho+\gamma\alpha_1}{2(\gamma+\rho)}\cos^2\vartheta$	$-\frac{\alpha_2+\gamma\alpha_1}{2(\gamma+1)}\cos^2\vartheta = -\bar{\alpha}\frac{\cos^2\vartheta}{2}$	$\alpha_2(t)\frac{\cos^2\vartheta}{2}$	$\alpha_1(t)\frac{\cos^2\vartheta}{2}$

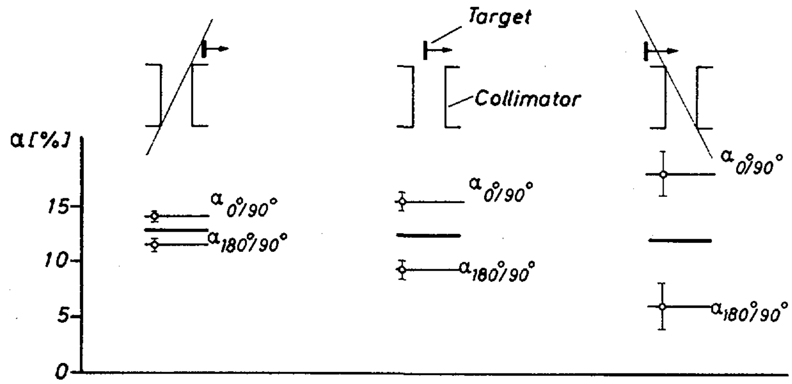

FIG. 5. Anisotropy measurement at different positions of the target demonstrating the discrimination property of the collimator system by the changing relativistic anisotropy.

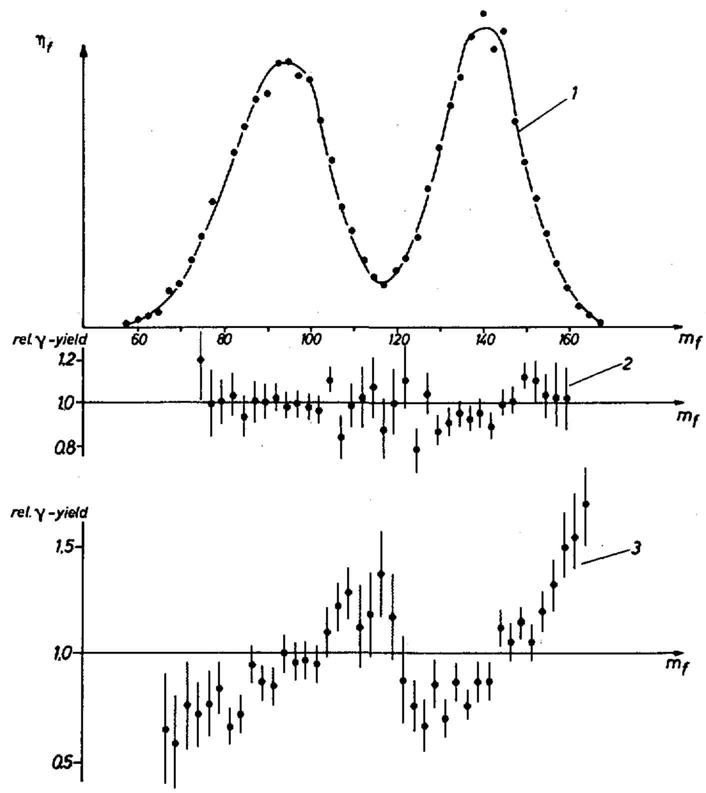

FIG. 6. The mass-yield curve obtained with our time-of-flight-energy arrangement. The relative γ-yield seen with open collimator, and the relative yield seen from a position where predominantly flying fragments are observed.

1) N_i:

From the value of N_i the γ-yields are obtained. A measurement with no collimator ($\rho = 1$) gives the average yield depending on the mass ratio and γ-energy. A measurement with collimator gives the mass dependence of the γ-yield as a function of time. With no view on the backing the clean γ-radiation from one fragment $G_i(t)$ is seen. Figure 4 shows the total counting rate for different source positions. The average emission time for the component separated by the collimator amounts to 8.5 + 1.5 p.s. The relative γ-yield for this component is plotted in Fig. 6. For comparison the relative yield for the case of no enrichment is given. This yield is the average yield from both fragments. It does not depend on the mass ratio, whereas the mass dependence of the 8.5-ps-component seems to be very strong. The agreement of our investigation of ^{235}U γ-yields with the investigation of ^{257}Cf spontaneous fission γ-yields reported by Johansson [7] is good.

2) A_i^R:

The relativistic anisotropies A_1^R and A_2^R for a pair of complementary fragments allow us to determine the enrichment factor ρ, the mass dependence of the yield ratio γ, and the mass dependence of the average emission time of all γ-quanta in fission if this time is of the order of the stopping time. The relativistic anisotropies is the case of $\rho = 1$ give the ratio of yields, and an average value of the emission time T. Our measured values averaged over the light- and heavy-fission-product group are with $\rho = 1$, $A_1^R = 3.0 + 0.5\%$ and $A_2^R = 0.3 \pm 0.5\%$. These values give $G_1/\bar{G} = 57 \pm 5\%$ and $T = 2.0 \pm 1.0$ ps. Light fragments emit a slightly higher number of γ-quanta than heavy fragments, in accordance with measurements reported earlier [11, 12]. The average emission time is much smaller than the time measured with the collimator technique. Besides the radiation observed with the collimator technique there seems to be another contribution to the prompt emission with an emission time of ~ 2 ps. Low-mass-number stopping materials with long stopping times are advantageous for the observation of this short component. The effect of emission in flight in solids has already been discussed by Skarsvag but not experimentally observed as a platinum stopper with stopping times of 0.4 ps has been used. A measurement with a high enrichment factor of flying fragments is a good means of testing the experimental set-up as the value of A_i^R approaches the known full relativistic anisotropy ϵ_i (right-hand side of Fig. 5). A high enrichment factor of fragments stopped in the backing (left-hand side of Fig. 5), which is experimentally difficult to realize, would give the average emission times as a function of mass.

3) A_i^N:

The nuclear anisotropy A_i^N has been measured with no enrichment ($\rho = 1$). The anisotropy averaged over both fragments, that is the anisotropy as a function of mass ratio, is plotted in Fig. 7. No strong mass dependence has been observed. The experimental values of A_1^N and A_2^N

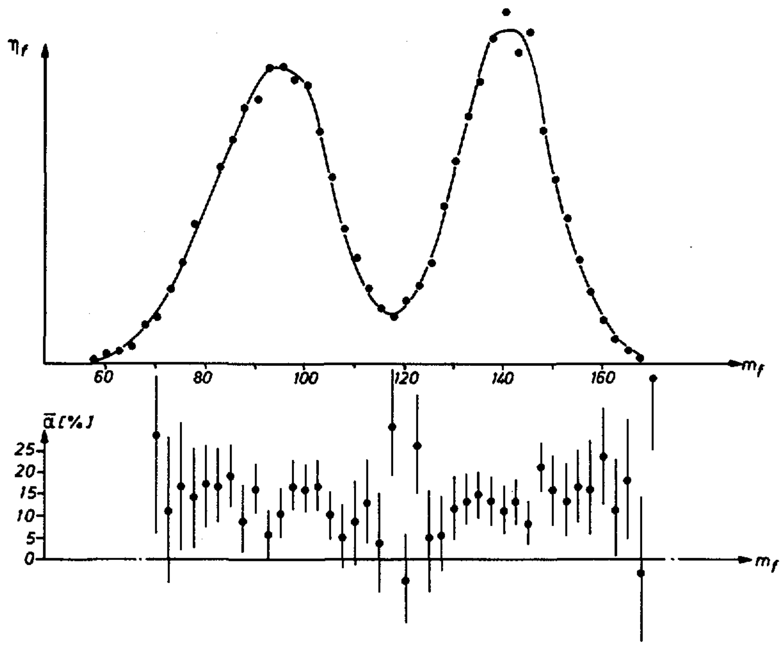

FIG. 7. Nuclear anisotropy of a fragment pair as a function of mass. The experimental values for complementary masses must be identical.

have to be identical, a criterion fulfilled within the statistics. A measurement of the time dependence of the anisotropy for single fragments is obtained with an enrichment of either flying or stopped fragments. Both measurements give the same result, but as the latter is experimentally much more difficult, the experiment is done with an enrichment of flying fragments only. Unfortunately, Fortuna has left the experimentalists shortly before the Conference and, therefore, we cannot present results on the nuclear anisotropy depending on the fragment mass as we had originally intended to do. The average value of the anisotropy of all fragments amounts to $\bar{\alpha}$ = 13.5 ± 1.1% in agreement with former experiments [13, 14].

Assuming quadrupole emission and σ = 5.0 [15] a value of I = 15 is obtained from Eq.(1). This simple evaluation has to be taken as an interpretation within a model which might not be realized in physics as simply as we think. If dipole radiation contributes considerably to the prompt γ-radiation, which is compatible with the emission times, and if a considerable amount of stretched cascade deexcitation occurs, then the observed value of the anisotropy must be interpreted as a mixture of anisotropies of L = 1 and L = 2 radiation not described within the statistical model.

REFERENCES

[1] JOHANSSON, S.A.E., KLEINHEINZ, P., SIEGBAHN, K., α-, β- and γ-Ray Spectroscopy, North Holland Publ. Comp. Amsterdam (1964).

[2] MAIER-LEIBNITZ, H., ARMBRUSTER, P., SPECHT, H.J., in Physics and Chemistry of fission (Proc. Symp. Salzburg, 1965) 2, IAEA, Vienna (1966) 1113.
[3] NIX, J.R., SWIATECKI, W.J., Nucl. Phys. 71 (1965) 1.
[4] RASMUSSEN, J.O., NÖRENBERG, W., MANG, H.J., to be published.
[5] STRUTINSKI, V.M., Soviet Phys. JETP 10 (1962) 1626.
[6] THOMAS, T.D., GROVER, J.R., Phys. Rev. 159 (1967) 980.
[7] JOHANSSON, S.A.E., Nucl. Phys. 60 (1964) 378.
[8] MAIER-LEIBNITZ, H., SCHMITT, H.W., ARMBRUSTER, P., in Physics and Chemistry of fission. (Proc. Symp. Salzburg 1965) 2, IAEA, Vienna (1966) 143.
[9] IVANOV, O.I., KUSHNIR, Yu.A., SMIRENKIN, G.N., ZhETF Pisma 6 (1967) 898.
[10] RASMUSSEN, J.O., SUGIHARA, T.T., Phys. Rev. 151 (1966) 992.
[11] KAPOOR, S.S., RAMANNA, R., Phys. Rev. 133 B (1964) 598.
[12] SKARSVAG, K., Nucl. Phys. A 96 (1967) 385.
[13] SKARSVAG, K., SINGSTAD, I., Nucl. Phys. 62 (1965) 103.
[14] HOFFMANN, M.M., Phys. Rev. 133 B (1964) 714.
[15] FACCHINI, V., SAETTA-MINICHELLA, E., Energia Nucleare 15 (1968) 4.

DISCUSSION

C. SYROS: I would first like to point out that the general remarks of Dr. Armbruster concerning the multipolarity of the gamma radiation emitted by fission fragments correspond to the theoretical result that rotational states, even with higher angular momenta, are populated more easily at the saddle point than vibrational states.

As regards the angular distributions and particularly the relativistic anistropy, I would like to ask whether there is an appreciable difference between the accuracy obtained and the effect in question. I have just seen the results obtained by Professor Fong on the fission fragment velocities, which show that in the most favourable cases - relatively small fragment masses and higher energies - the ratio V/c does not exceed 0.03. Could you please comment on the significance of the observed anisotropy of the relativistic effect?

P. ARMBRUSTER: The fragments are accelerated to this final speed in about 10^{-20} ns. Gamma-emission is too slow a process to occur in these times. All quanta are emitted later from fragments at full speed ($\frac{v}{c} \sim 4\%$).

W. NÖRENBERG: I wish to make a comment on the calculation of spin distribution of fragments in fission. Rasmussen, Mang and myself (to be published in Nucl. Phys. (1969)) have studied the bending mode in the molecular model of fission in the special case of $^{239}Pu(n_{th}, f)$. By expanding the bending mode function into spin eigenfunctions, we obtain for the fragment spin a mean value of about $7\hbar$. This calculated value is only about half the value you have obtained from experiment. Can you comment on this discrepancy?

P. ARMBRUSTER: The values of initial spins from anisotropic measurements depend on the model which is used for this evaluation. In the early stage of our knowledge of the de-excitation mechanism of fission fragments, we should not rely excessively on the absolute values of the spins we obtain. I would not definitely state that there is no agreement between spin calculation and the experiments.

H. NIFENECKER: There is some evidence that the energy carried away per neutron is greater than the 6.6 MeV value. One would expect there to be competition between neutron and gamma emissions even at very high excitation energies. For that to be possible about 10% of the gamma rays would have to be emitted in a very short time. Is this compatible with the experiments?

It would also be interesting to know if the energy carried away by gamma rays varies with the total kinetic energy of the fragments of the fission mass.

P. ARMBRUSTER: The measurements carried out recently at Oak Ridge National Laboratory by F. Pleasonton et al. may be analysed for gamma energy and gamma yields, depending on mass and kinetic energy of the fragments. These data may give an answer to your question how the energy is distributed between gamma-quanta and prompt neutrons.

R. VANDENBOSCH: With regard to the large angular momentum you have deduced, and the discrepancy with theory mentioned by Dr. Nörenberg, I should like to remark that on the basis of isomer ratios we deduced an angular momentum of about 8 $\hbar$, which is more in accordance with what one would expect.

I agree with you that there are difficulties in the statistical model calculations, but this applies to both isomer ratios and anisotropies. I believe the key element in our analysis was the use of parameters which successfully reproduce isomer ratios in reactions for which the initial angular momentum is known. I would suggest that a similar approach be applied to the anisotropy measurments.

E. HAGEBØ: I would like to stress the point that isomeric yield ratios are measured for single isolated nuclides and one should be careful in generalizing such results in order to make them valid for all fission products.

The gamma rays may also come preferentially from selected nuclei and thus may not represent all fission fragments of each mass equally well.

The latter remark should also apply to the experiment of Nifenecker et al. on neutrons, since the variations in X-ray yield along a chosen Z-value may pick only one or a few of the isotopes.

P. ARMBRUSTER: As long as the gamma-energy emitted from the fragments is of the order of a few MeV we assume that no such selection occurs.

E. HAGEBØ: I meant that the gamma-ray emission itself may select the nuclei for you.

P. FONG: When I wrote my doctoral dissertation 16 years ago, I concluded from the statistical theory that the nascent fission fragments are expected to have a probability distribution in the spin values with a most probable value of about 10. (The dissertation is now published in P. Fong, Statistical Theory of Nuclear Fission, Gordon and Breach, New York (1969); see p. 34.) The value is so large that the distinguished members of the dissertation committee were rather unhappy and asked many questions. It is gratifying to know that eventually after so many years experimental evidence supporting the prediction of high-spin values is forthcoming.

ANGULAR DISTRIBUTION OF GAMMA RAYS FROM THE FISSION OF ^{235}U INDUCED BY 14-MeV NEUTRONS

L. JÉKI, GY. KLUGE, A. LAJTAI
Central Research Institute for Physics,
Hungarian Academy of Sciences,
Hungary

Abstract

ANGULAR DISTRIBUTION OF GAMMA RAYS FROM THE FISSION OF ^{235}U INDUCED BY 14-MeV NEUTRONS. Experiments are reported which were performed to study the angular distribution of the gamma radiation following fast-neutron-induced nuclear fission. The investigations were, in particular, focussed on the influence which the angular momentum imparted to the compound nucleus by the fast neutrons has on the angular distribution of the γ-rays.

The fission of ^{235}U is induced by 14-MeV-energy neutrons from the T(d, n) α reaction. The fission fragments are detected by a gas-scintillation counter filled with a mixture of Ar and Ni gases, the γ-rays by 5 cm × 5 cm NaI(Tl) crystal with an energy threshold of 120 keV. The intensity of the γ-rays is measured at 90° and 174° to the direction of fragment motion.

The flight times of fission neutrons and γ-rays are measured with a 20-ns overlap-type time-to-pulse height converter while the background was covered simultaneously with another converter delayed with respect to the former. The signals from both converters are analysed by a multichannel analyser with divisible memory. The flight path, which is chosen to be about 70 cm, makes it possible to separate the neutron from the gamma counts. The geometry is designed to keep the direction of the outflying fission fragments nearly the same as that of the incident fast neutrons. In this way the angular momenta of the fast neutrons are normal to the flight path of the fragments.

The measured gamma intensities are extrapolated to 180° on a computer using Strutinski's formula $n(\vartheta) \sim 1 + B \sin \vartheta$. On transformation of the measured data from the laboratory system to the system of fragments the anisotropy is found to be $A = I(180°)/I(90°) = 1.33 \pm 0.05$. The main angular momentum of fission fragments is calculated from the anisotropy as 15 $\hbar$ units.

As compared with the thermal-neutron-induced fission the present results indicate an additional contribution from the angular momentum of the compound nucleus to the anisotropy of the angular distribution attributed to the effect of the angular momentum imparted to the fission fragments by non-collinear scission.

1. INTRODUCTION

The angular and energy distributions of the prompt gamma rays from the fission process are of particular interest because of the information they give about the fragment angular-momentum distribution and its role in the not yet fully understood mechanism of fission.

For thermal-neutron-induced, as well as for spontaneous nuclear fission, the angular distribution of the prompt gamma rays relative to the direction of fission fragment motion has already been analysed by several authors [1-11]. The 10-15% excess intensity of the gamma radiation in the direction of fragment motion is generally attributed to the relatively large angular momenta imparted to the fission fragments as a result of non-collinear scission. The data of the angular distribution of prompt gamma rays measured relative to the axis of fission permit the average value of the fragment angular momentum to be estimated.

The estimations based on experimental data with the use of approximate values of nuclear temperature and moment of inertia give 5-10 ħ for the average fragment angular momentum in the case of quadrupole radiation.

Investigations of the anisotropy as a function of gamma energy showed a decrease in anisotropy at higher gamma energies [3, 9, 11].

Angular-distribution measurements on gamma rays from fission induced by particles of higher than thermal energies involving larger angular momentum transfer have not been reported, as yet. The aim of the present experiments was the investigation of the changes caused in the angular distribution of the gamma radiation by the larger angular momentum imparted by fast neutrons to the compound nucleus in the direction normal to that of fragment motion. In fast-neutron fission, the average number of emitted neutrons increases as compared with slow-neutron fission because of the higher excitation energy, but the evaporation of neutrons from the fission fragments does not involve any appreciable loss of angular momentum. The estimated maximum angular momentum imparted by 14-MeV neutrons (≈ 8 ħ) is expected to lead to a considerable change in the average fragment angular momentum which should be reflected by the angular distribution of the prompt gamma rays.

2. EXPERIMENTAL ARRANGEMENT

14-MeV neutrons were produced by a T(d, n) α reaction. The angular distributions were measured with the equipment depicted schematically in Fig.1. The U-target, enriched to 96% in ^{235}U, 25 cm^2 in surface and of 2 mg/cm^2 thickness, was mounted at 6.5 cm from the tritium target. Under these conditions, the solid angle of the U-target was $\pm 20°$ for the direct neutrons. The fission fragments were detected by a gas scintillation counter. The collimator prepared from thin Al-foil, which delimited the direction of fission-fragment motion within the gas scintillation detector to an accuracy of $\pm 20°$, was mounted directly on the U-target. A mixture of 80% argon and 20% nitrogen gas, kept at a pressure of 1 atm was used in the gas scintillation counter. The gas was let into the air from the scintillation chamber. In this way, the complicated processes of gas purification could be avoided and the gas could be kept free from possible contamination. The choice of a gas scintillation counter prevented counting other than fission events, in spite of the large background contribution from fast neutrons and gamma radiation. The fission gamma rays were detected by a 5×5 cm NaI(Tl) scintillation counter mounted at 55-70 cm from the U-target, as determined by the relative position of the fission detector. This distance made it possible to separate the gamma and neutron counts with respect to flight time.

In the fast-slow coincidence system the fast pulses from the fission and gamma ray detectors were taken to three time-to-pulse height converters, each covering an interval of 30 ns, operating on the principle of overlap and delayed by 15 ns relative to one another. The background was measured by the coincidence counts between converter 1 and coverter 2 (master converter) while the coincidence counts between the master and converter 3 simultaneously measured the background and the effect pulses. Each of the measuring intervals was set to a duration of 20 ns by the pulse-height discriminators coupled to the converter outputs. The threshold energy of

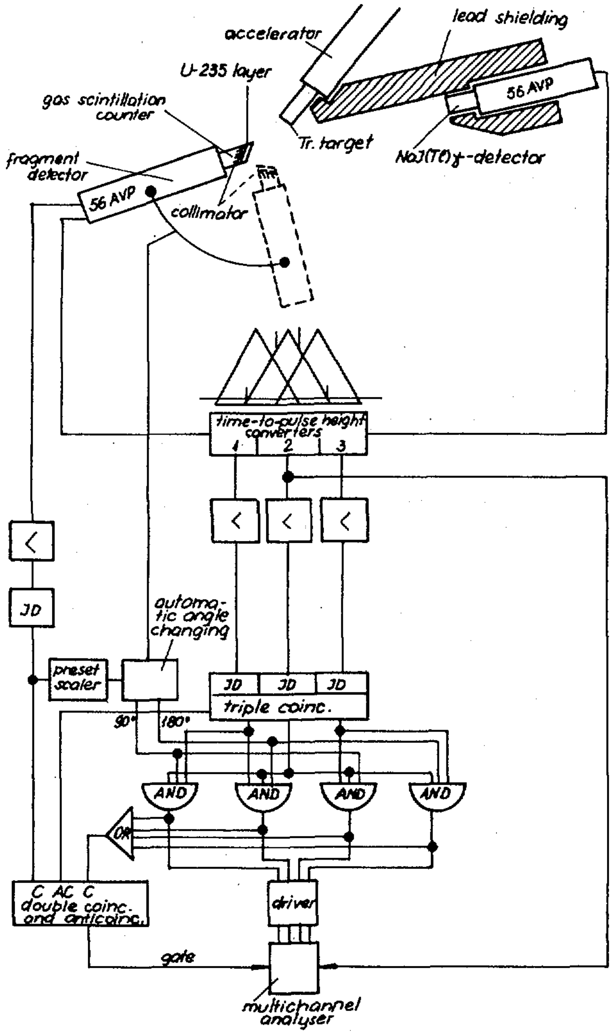

FIG.1. Schematic diagram of the experimental arrangement.

the gamma ray detector was determined by the sensitivity of the master converter and checked with the use of the 120 keV line from ^{75}Se. The output pulses from the master converter which coincided with pulses from both converters were suppressed. The 512 channel analyser was gated by a three-channel coincidence-anti-coincidence unit driven by the output pulses from the discriminator of the fission fragment detector, from the "OR" gate for coincidences and from triple coincidence events. The discriminator level of the fragment detection was set to accept only pulses generated by true fission events.

The preset scaler of this discriminator triggered the automatic change of angle after a preset number of fission counts and prevented the analyser from operating during the change of angle. The ratemeter and level recorder controlled by the output pulses from the preset scaler permitted the stability of the neutron yield, the number of angular changes and the life-times of the measurement to be observed. Since the gamma ray detector had to be kept in a fixed position because of the heavy lead shielding, the angle between the directions of fragments and gamma rays was varied by changing the position of the fission detector. The change in solid angle caused by this procedure was measured with the use of a ^{137}Cs-on-aluminium backing of the same size as that of the U-target and prepared specially for this purpose.

3. RESULTS

The intensities of the gamma rays at 90° and 174° relative to the direction of fission fragment motion were measured for a life-time of more than 900 h. Because of possible fluctuations in the neutron generator and electronic levels, the angle of detection was changed all 20 min and the results were printed and checked all 24 h. The effect and background counts were summed separately for either angle, and the angular distributions were evaluated from the "pure" counts in the two gamma peaks and corrected for the solid-angle factor.

The intensities measured at two angles were fitted by the method of least squares to the formula

$$I(\vartheta) \sim 1 + B \sin^2(\vartheta)$$

and extrapolated to 180°. The value of the anisotropy was found to be $A = I(180°)/I(90°) = 1.27 \pm 0.05$. The error of this value was estimated from the statistical error of the measured data. Upon applying the corrections for emission from flying fragments, using the method described in [10], the anisotropy in the centre-of-mass system of fragments is $A = 1.33 \pm 0.05$.

In terms of Strutinsky's theory the parameter B used in the above formula is given as

$$B = k_L \left(\frac{\hbar^2 j}{I T}\right)^2$$

where $k_L = -3/8$ in the case of quadrupole radiation, j is the average angular momentum of fragments, $I = 2/5\, m r_0^2 A^{5/3}$ is the moment of inertia of fragments (m = the nucleon mass, A = 117, the average number of nucleons per fragment and $r_0 = 1.3$ fm) and T = 0.4 MeV, the nuclear temperature of fragments upon neutron emission [3]. If we use the above expression for B, we see that the observed anisotropy requires an average fragment angular momentum of about 15 $\hbar$.

Comparison with the results obtained for thermal-neutron fission shows an increase in the anisotropy of the angular distribution of prompt gamma rays which seems to be due to an additional contribution from the angular momentum of the compound nucleus.

REFERENCES

[1] BLINOV, M.V., KAZARINOV, N.M., PROTOPOPOV, A.N., SHIRYAYEV, B.M., J.éksp.teor.Fiz. 43 (1962) 1644.
[2] DÉSI, S., GRAFF, GY., LAJTAI, A., NAGY, L., Phys.Lett. 3 (1963) 343.
[3] KAPOOR, S.S., RAMANNA, R., Phys.Rev. 133 (1964) B598.
[4] HOFFMAN, M.M., Phys.Rev. 133 (1964) B714.
[5] PETROV, G.A., J.éksp.teor.Fiz. 47 (1964) 2064.
[6] PETROV, G.A., KAMINKER, D.M., VALSKI, G.V., POPENKO, L.A., Atomn.Energ. 18 (1964) 64.
[7] SKARSVÅG, K., SINGSTAD, I., Nucl.Phys. 62 (1965) 103.
[8] GRAFF, GY., LAJTAI, A., NAGY, L., in Physics and Chemistry of Fission (Proc.Symp.Salzburg, 1965) 2, IAEA, Vienna (1965) 163.
[9] PETROV, G.A., Yad.Fiz. 1 (1965) 467.
[10] SKARSVÅG, K., Nucl.Phys. A96 (1967) 385.
[11] KLUGE, GY., LAJTAI, A., KFKI Közl. 15 (1967) 5.
[12] STRUTINSKY, V.M., J.éksp.teor.Fiz. 37 (1957) 861.

DELAYED NEUTRONS AND GAMMA RAYS

(Session G)

Chairman: P. Armbruster

DELAYED NEUTRONS IN FISSION

A Review

S. AMIEL
Soreq Nuclear Research Centre,
Yavne, Israel

Abstract

DELAYED NEUTRONS IN FISSION. A survey is given of the recent work on delayed neutron emission from fission products. The experimental, phenomenological and theoretical aspects are reviewed briefly and discussed in the light of the systematics of fission and nuclear structure.

1. INTRODUCTION

The relationship between the topic of this talk, which is "Delayed Neutron Emission", and the subject of this symposium, which is "Fission", is a genetic rather than a conceptual one. The main connection is that so far the fission process happens to be the best source for producing medium weight nuclides with a high neutron excess, where delayed neutron emission is abundant. The bearing of fission on the phenomenon of delayed neutron emission is thus mainly indirect, via the nuclidic yields and distributions,which depend of course on the mechanism of the fission process, fission systematics and the de-excitation processes of the fission fragments. However, this relation should not be pressed too far, either as an argument for motivation, or otherwise.

In this respect, I would like to touch on a point of terminology. Neutrons emitted in fission are divided into three types according to the time scale of emission. The first type includes the Scission (or Central) Neutrons. These are emitted at the instant of scission and can be regarded as really prompt neutrons. Then, $\sim 10^{-14}$ sec after scission, when the highly deformed fission fragments are far apart and fully accelerated, de-excitation by neutron emission takes place. For the sake of distinction and accuracy, these neutrons, regarded so far as 'prompt' ones, deserve to be termed 'delayed' neutrons. Many orders of magnitude after the neutron and subsequent gamma de-excitation processes are over, radioactive decay begins to take place, and it is then that we observe the 'delayed' neutrons, which should in fact be termed radioactive neutrons. The term 'delayed' neutrons is of a more phenomenological character, suitable for reactor people rather than for the physicist who aims at a definitive term. However in deference to common usage, we adopt here the usual terminology.

The state of knowledge and current work on delayed neutron emission have been reviewed and discussed several times since the treatise by Keepin (completed in 1964) [1], and the review paper presented at the previous Fission Symposium (1965) [2]; for example there is the survey "Status 1966" [3] and especially the recent comprehensive treatment of the various aspects of "Delayed Fission Neutrons" which appeared as proceedings of a panel held in April 1967 [4].

Neutron emission following the beta decay of some fission products was first observed and correctly interpreted 30 years ago. Nevertheless, the numerous investigations have till very recently yielded only an in-

TABLE I. HALFLIVES AND YIELDS OF DELAYED NEUTRON GROUPS [1, 14]

Group No. (i)	Thermal fission of ^{233}U	Thermal fission of ^{235}U	Thermal fission of ^{239}Pu	Spontaneous fission of ^{252}Cf
	$T_{\frac{1}{2}}$ (s) and relative abundance	$T_{\frac{1}{2}}$ (s) and relative abundance	$T_{\frac{1}{2}}$ (s) and relative abundance	$T_{\frac{1}{2}}$ (s) and relative abundance
1	55.00 ± 0.54 0.086 ± 0.003	55.72 ± 1.28 0.033 ± 0.203	54.28 ± 2.34 0.035 ± 0.009	0
2	20.57 ± 0.38 0.299 ± 0.004	22.72 ± 0.71 0.219 ± 0.009	23.04 ± 1.67 0.298 ± 0.035	26.8 ± 1.1 0.31 ± 0.01
3	5.00 ± 0.21 0.252 ± 0.040	6.22 ± 0.23 0.196 ± 0.022	5.60 ± 0.40 0.211 ± 0.048	6.1 ± 1.4 0.22 ± 0.02
4	2.13 ± 0.20 0.278 ± 0.020	2.30 ± 0.09 0.395 ± 0.011	2.13 ± 0.24 0.326 ± 0.033	2.0 ± 0.3 0.30 ± 0.03
5	0.615 ± 0.242 0.051 ± 0.024	0.610 ± 0.083 0.115 ± 0.009	0.618 ± 0.213 0.086 ± 0.029	0.5 ± 6.1 0.17 ± 0.05
6	0.277 ± 0.047 0.034 ± 0.014	0.230 ± 0.025 0.042 ± 0.008	0.257 ± 0.045 0.044 ± 0.016	-
Yield: ($n/10^4$ fission)	66 ± 3	158 ± 5	61 ± 3	86 ± 10

complete picture of the identity of the nuclides concerned, and their yields, and very fragmentary information on their disintegration schemes, neutron energies, etc. The difficulties lie in the very great complexity of the fission product matrix and the short half-lives of the nuclides in question, and the inaccurate data on nuclidic distributions in fission. Lack of information on the masses and structure of nuclides on the neutron excess side of the stability line handicaps any quantitative predictions and a precise treatment of this phenomenon.

The basic interest in delayed neutron emission stems from its importance in the study of nuclear structure and transitions, the shape of the nuclear energy surface, and mass and binding energy formulae in the neutron rich region, far off the nuclidic stability line. Delayed neutron emission affects to a certain extent the mass yields determined by analysis of isobaric decay products. The practical importance has to do with nuclear reactor control [5,6]. The need for accurate delayed neutron data is of crucial importance in predicting the transient behavior and stability of fast reactors, especially for the large power-breeder program and for reactors operating at very high temperatures (e.g. in nuclear propulsion) where losses by diffusion must be taken into account. Other applications are concerned with nondestructive assay of fissionable species using integral neutron counting [7] or kinetic response methods [8].

2. GROSS DECAY MEASUREMENTS; GROUPS, HALF-LIVES AND YIELDS

The number of delayed neutrons (henceforward d.n.'s) emitted per low energy fission event is in the range of 0.006 to 0.016, depending on the fission source. Regularities are observed, such as that the d.n. yield increases with the mass number of the fissionable nuclide within an isotopic series, and diminishes with increasing atomic number of the nuclides. Also, the d.n. yield depends on the energy of the fission-inducing neutrons. These regularities are consistent with the systematics of fission, and are linked with the increasing abundance of d.n. precursors as the production and relative distribution of neutron rich nuclides increases beyond the closed neutron shells.

A longstanding discrepancy, which led to all kinds of odd implications, between this regularity and the experimental yields for fission with $\sim$15 MeV neutrons has lately been resolved. It had been reported that the d.n. yields increase by a factor of 2 or more when going from thermal or fission spectrum neutrons (where yields do not vary) to 15 MeV. However the new results [9,10,11] indicate a drop in yields with energy increase, the ratios being in the range 1.60 to 1.94 at $\sim$3 and $\sim$15 MeV for different fission sources [11]. This is in accord with qualitative predictions based on fission systematics.

Analysis of the composite decay of the d.n.'s observed with different fission sources (ranging from ^{232}Th to ^{252}Cf; fission either spontaneous, or induced by thermal to 15 MeV neutrons) showed that the precursors fall into six exponential components or groups with approximate half-lives of 55 sec, 22 sec, 6 sec, 2 sec, 0.5 sec and 0.2 sec [1]. The search for longer lived groups in ^{235}U fission has lead to negative results [e.g.[12]). The first group (i=1) was found to conist of only one component - ^{87}Br - with an upper limit of 0.5% for other possible contributors [13]. Other groups are known to be composites of several precursors in each group.

Despite the striking similarity among the group half-lives in the various fission reactions, the respective values are distinctly different and group abundances vary considerably from case to case

TABLE II. EXPERIMENTAL DATA ON DELAYED NEUTRON PRECURSORS FROM FISSION

Precursor	$T_{\frac{1}{2}}$ (s)	P_n (n/100 dis.)	Cumulative fission yield (for ^{235}U); (%)	d.n. yield (n's per 10^4 ^{235}U fissions)	Comments	Reference
^{85}As			0.485	8.0		
	2.028 ± 0.012	22 ± 5		9.7 ± 8	CF $^{85,86}As$	29
	2.15 ± 0.15	11 ± 3			CF	27
^{87}As						
	1.4 ± 0.4	?			CF(d)	33
^{87}Se			1.09	0.44		
	5.8 ± 0.5	<0.8		<1.0	CF(d)	30
	5.9	0.4 ± 0.1	1.4	0.56 ± 0.14	CF	33
^{88}Se			0.65	4.16		
	2.2 ± 0.3	6.4 ± 2.5	0.8	5.1 ± 2.0	CF	33
^{87}Br			2.28	5.7		
	54.5 ± 0.9	(2.6 ± 0.5)			CF	54, (53)
		3.1 ± 0.6			CF	52
	55.4 ± 0.7				CF	13
	55.8 ± 0.5				CF	36
		2.63 ± 0.05 c			C	31
	55.4	2.2 ± 0.4		5.2	CF	32
	54.5	2.5 ± 0.4	2.4	5.9 ± 0.4	CF	33
^{88}Br			2.78	11.12		
	16.3 ± 0.8	(5.8 ± 1.6)			CF	53
		6.0 ± 1.6			CF	52
	15.9 ± 0.2	3.5 ± 0.9			CF	36
		6.0 ± 1.0 c			c	31
	15.6	4.0 ± 0.8		12.3	CF	32
		3.9 ± 0.9	2.78		CF; b	35
	16.3	4.0 ± 1.4	3.0	12.1 ± 3.3	CF	33
^{89}Br			2.42	16.94		
	4.4 ± 0.5	(12 ± 3)			CF	53
		7 ± 2			CF	52
	4.5 ± 0.8				CF	36
		5.2 ± 1.1 c			c	31
		8 ± 2		20.8	CF	32
		7.0 ± 2.8	2.7	18.8 ± 5.7	CF	33
		6.7 ± 1.4	2.42		CF; b	35
^{90}Br			1.75	21.0		
	1.6 ± 0.6	(15 ± 4)			CF	53
		23 ± 3 c			c	31
	1.6	11.5 ± 4	1.4	16.2 ± 5.2	CF; b	32, 33
^{91}Br			0.40	(5.52)		35
	~0.4				CF	33
^{92}Kr			1.68	0.07		
	1.86 ± 0.01	0.04 ± 0.0007	1.69	0.07	isn	21
^{93}Kr			0.53	1.75		
	1.19 ± 0.05	3.9 ± 0.6			CF	22
	1.29 ± 0.01	2.6 ± 0.5	0.53	1.38	isn	21

TABLE II (cont.)

Precursor	$T_{\frac{1}{2}}$ (s)	P_n (n/100 dis.)	Cumulative fission yield (for ^{235}U); (%)	d.n. yield (n's per 10^4 ^{235}U fissions)	Comments	Reference
^{94}Kr			0.08	(0.38)		
	0.2	n.d.			isx	51
^{95}Kr			0.01	(0.08)		
	<0.5	n.d.			isx	51
^{92}Rb			5.18	0.06		
	4.48 ± 0.02	0.012 ± 0.004	5.19	0.06 ± 0.02	isn	21
^{93}Rb			4.0	7.2		
	5.89 ± 0.04	1.43 ± 0.18	4.23	6.0	isn	20, 19
		2.6 ± 0.4				22
	5.86 ± 0.13	1.65 ± 0.30	4.0	6.60	isn	21
	6.2	1.8 ± 0.5	3.8	6.8	CF	33, (32)
^{94}Rb			1.9	14.2		
	2.67 ± 0.04	11.1 ± 1.1	1.9	21.1	isn	20, 19
	2.67	7.5 ± 1.9	2.3	17.2 ± 2.4	CF	33, (32)
^{95}Rb			0.66	4.7		
	0.36 ± 0.02	7.10 ± 0.93	0.46	3.3	isn	20, 19
^{96}Rb			0.17	2.15		
	0.23 ± 0.02	12.7 ± 1.5	0.06	0.8	isn	20, 19
^{97}Rb			0.02	0.4		
	0.135 ± 0.010	>20			isn	20
^{98}Y			2.9	2.3		
	~2	0.8 ± 0.4	2.4	1.8 ± 0.9	CF	33
^{134}Sb			2.19	0.18		
	11.3 ± 0.02	0.08 ± 0.02		0.28 ± 0.004	CF	29, 28
^{135}Sb			0.485	3.88		
	1.696 ± 0.021	8 ± 2		3.5 ± 0.3	CF	29
^{137}Te			0.63	(0.63)		
	3.5 ± 0.5	n.d.			CF(d)	33
^{137}I			4.11	19.7		
	24.4 ± 0.4	(3.0 ± 0.5)			CF	53
		3.0 ± 0.5			CF	52
		5.3 ± 0.6 c			c	31
	24.4	5.1 ± 1.0		22.4	CF	32
	24.4	4.8 ± 1.3	4.5	21.7 ± 3.6	CF	33
^{138}I			2.68	6.73		
	6.3	(2.2 ± 0.5)			CF	53
		1.9 ± 0.5			CF	52
		7.3 ± 0.8 c			c	31
	6.9	2.4 ± 0.8		10.3	CF	32
	6.3	2.5 ± 0.6	4.2	10.3 ± 1.6	CF	33
		3.3 ± 0.8			CF	35

TABLE II (cont.)

Precursor	$T_{\frac{1}{2}}$ (s)	P_n (n/100 dis.)	Cumulative fission yield (for ^{235}U); (%)	d.n. yield (n's per 10^4 ^{235}U fissions)	Comments	Reference
^{139}I			1.10	6.60		
	2.0 ± 0.5	(4.5 ± 1.5)			CF	53
		21 ± 3 c			c	31
	2.3	6.4 ± 1.9		13.1	CF	32
	2.0	6.0 ± 1.7	2.1	12.7 ± 3.6	CF	33
		5.7 ± 1.7			CF	35
^{140}I			0.236	2.83		
	~0.8	12 ± 8	0.8	10 ± 6	CF	32, 33
^{141}I			0.032	(0.35)		
	~0.3	n.d.			CF	33
^{141}Xe			1.14	0.06		
	1.73 ± 0.01	0.054 ± 0.009	1.14	0.06	isn	21
^{142}Xe			0.31	0.14		
	1.24 ± 0.02	0.45 ± 0.08	0.312	0.14	isn	21
^{143}Xe			0.05	(0.08)		
	<1	n.d.			isx	51
^{144}Xe			5.10^{-5}	(~0)		
	<1	n.d.			isx	51
^{145}Xe			0	(~0)		
	<1	n.d.			isx	51
^{141}Cs			4.60	0.33		
	24.9 ± 0.2	0.073 ± 0.011	4.61	0.345 ± 0.05	isn	21
^{142}Cs			3.1	0.84		
	2.5 ± 0.3	~0.1	3.48	~0.3	isn	20
	1.68 ± 0.02	0.27 ± 0.07	3.11	0.84	isn	21
^{143}Cs			1.43	1.61		
	1.69 ± 0.13	1.13 ± 0.25	1.37	1.6	isn	20
^{144}Cs			0.41	0.45		
	1.05 ± 0.14	1.10 ± 0.25	0.34	0.4	isn	20

Notes: d.n. yield in round brackets — predicted values (see Table IV); the underlined values are based on selected experimental P_n's, otherwise taken from the respective references.
Fission yields taken from Wahl's tables [44] and Z_p calculated according Ref. [48].
n.d. — detected but not determined.
isn — determined by isotopic separation and neutron counting.
isx — determined by isotopic separation and mass cross contamination.
CF — assignment by chemistry and fission systematics.
b — P_n's normalized to those of ^{87}Br (2.5) and ^{137}I (4.8), respectively.
c — calculated by considering best fit to 7 different fission reactions.
d — detection of daughter.

(see Table I). An outstanding discrepancy was until recently the case of ^{252}Cf, where only 3 groups, viz. 1–2, 4 and 5, were observed. A recent measurement however indicated [14] the presence of the expected 6-sec group (see Table I). The sixth group was not measured, due to the relatively long transit time (~0.7 sec) of the experimental set-up.

TABLE III. RATIOS AND INDEPENDENT FISSION YIELDS BY SELECTIVE RECOIL LABELLING OF HALOGEN DELAYED NEUTRON PRECURSORS (FROM ^{235}U THERMAL FISSION)

Nuclide	P_n (%)	IFY (%) (Wahl's values [44])	IFY derived from experimental ratios and accepted P_n values [a] (%)	
			labelling in CH_4 [36]	labelling in CH_3I [35]
^{87}Br	2.5	1.19	(1.19)	(1.19)
^{88}Br	4	2.14	2.32 ± 0.20	2.06 ± 0.15
^{89}Br	7	2.13	1.59 ± 0.12	2.01 ± 0.12
^{90}Br	12	1.29	-	1.10 ± 0.07
^{137}I	4.8	3.48	-	(3.48)
^{138}I	2.5	2.51	-	3.27 ± 0.2
^{139}I	6	1.08	-	1.03 ± 0.06

[a] Normalized to ^{87}Br and ^{137}I, respectively. P_n's from Tables V and VI. P_n errors were not included.

The longest lived group has not been found, due to the sharp drop in the yield of ^{87}Br in ^{252}Cf fission with the shift of the light mass peak toward the heavier range.

Since the mathematical analysis of the gross delayed neutron curves ignores growth and decay effects, which are quite important, the contributions of the shorter lived groups are increasingly underestimated and discrepancies are expected between the sums of the contributions of individual precursors and the delayed neutron group abundances - a point to which attention should be paid when compilation and comparison work is done. This is seen in Tables V and VI. The fit between the gross neutron observations (group half-lives, yields, etc.) and the sum of individual data of both identified and expected precursors is discussed in section 4.

Another observation of interest is that the variation of group yields and group ratios with energy in fission seems to show distinct and sharp changes at the threshold values for first, second and third chance fission, where the excitation energy and neutron numbers of the respective residual fissioning nuclei drop [15].

3. IDENTIFICATION OF PRECURSORS

Identification of the delayed neutron precursors from fission calls for very rapid radiochemical separation techniques, a problem which becomes very difficult as the half-lives of the species involved become shorter [16,17,18]. An added difficulty is that chemical separations yield mixtures of isotopes of the element selected, along with their respective decay products, presenting a composite, the analysis of which into individual nuclides is a major technical problem. This explains the scarcity of data on the individual nuclides.

TABLE IV. ESTIMATED AND EXPERIMENTAL NEUTRON EMISSION PROBABILITIES

d.n. precursor	Q_β^*	B_n^*	$Q_\beta - B_n$	P_n (calc.)**	P_n (exp.)***	Ratio (calc./exp.)	Cumulative fission yield in ^{235}U; (%)	d.n. yield (n/10^4 fissions of ^{235}U)	
								calculated	experimental
^{84}Ge	7.54	4.15	3.39	8.9 ± 1.1	-	-	0.093	0.83	-
^{84}As	9.99	9.06	0.93	~1.3	-	-	0.646	0.84	-
^{85}As	9.05	4.10	4.95	15.8 ± 1.8	16.5 ± 6	0.96	0.485	7.66	8.00
^{86}As	11.35	6.22	5.13	16.6 ± 1.9	-	-	0.31	5.15	-
^{87}Se	7.27	6.40	0.87	~1.1	0.4 ± 0.1	2.75	1.09	1.2	0.44
^{88}Se	6.33	4.85	1.48	2.5 ± 1.9	6.4 ± 2.5	0.39	0.65	1.62	4.16
^{87}Br	6.68	5.46	1.22	1.9 ± 1.4	2.5 ± 0.5	0.76	2.28	4.33	5.7
^{88}Br	8.98	7.15	1.83	3.5 ± 2.7	4 ± 1	0.88	2.78	9.73	11.12
^{89}Br	8.04	5.22	2.82	6.8 ± 0.8	7 ± 2	0.97	2.42	16.46	16.94
^{90}Br	10.33	6.21	4.12	12 ± 1.4	12 ± 3	1.00	1.75	21.0	21.0
^{91}Br	9.18	4.57	4.61	13.8 ± 1.6	-	-	0.40	5.52	-
^{92}Br	12.01	6.21	5.80	20.2 ± 2.3	-	-	0.07	1.4	-
^{92}Kr	5.31	5.06	0.25	< 0.5	0.04 ± 0.007	-	1.68	< 0.84	0.07
^{93}Kr	8.15	6.30	1.85	3.5 ± 2.7	3.3 ± 0.5	1.06	0.53	1.85	1.75
^{94}Kr	6.56	4.33	2.23	4.7 ± 0.5	-	-	0.08	0.38	-
^{95}Kr	9.45	6.22	3.23	8.3 ± 1.0	-	-	0.01	0.08	-
^{92}Rb	7.80	7.35	0.45	< 0.5	0.012 ± 0.004	-	5.18	< 2.09	0.06
^{93}Rb	6.62	5.14	1.48	2.5 ± 1.9	1.8 ± 0.5	1.39	4.0	10.0	7.2
^{94}Rb	9.45	7.17	2.28	4.8 ± 0.5	7.5 ± 1.9	0.64	1.9	9.1	14.2
^{95}Rb	7.87	4.64	3.23	8.3 ± 1.0	7.1 ± 0.9	1.2	0.66	5.5	4.7
^{96}Rb	10.76	6.62	4.14	12.1 ± 1.4	12.7 ± 1.5	0.96	0.17	2.05	2.15
^{97}Rb	9.03	3.92	5.11	16.6 ± 1.9	>20	0.83	0.02	0.3	> 0.4
^{97}Y	5.35	5.22	0.13	< 0.5	-	-	4.75	< 2.3	-
^{98}Y	8.24	7.55	0.69	~0.8	0.8 ± 0.4	1.00	2.9	2.3	2.3
^{99}Y	6.51	4.44	2.07	4.2 ± 0.5	-	-	0.54	· 2.27	-
							sub-total (light mass peak)	114.8	100.2

TABLE IV (cont.)

d.n. precursor	Q_β^*	B_n^*	$Q_\beta - B_n$	P_n (calc.)**	P_n (exp.)***	Ratio (calc./exp.)	Cumulative fission yield in ^{235}U; (%)	d.n. yield (n/10^4 fissions of ^{235}U)	
								calculated	experimental
^{133}Sn	7.24	7.11	0.13	< 0.5	-	-	0.42	< 0.21	-
^{134}Sn	6.07	3.43	2.64	6.1 ± 0.7	-	-	0.086	0.52	-
^{134}Sb	8.70	7.35	1.35	2.2 ± 1.7	0.08 ± 0.02	-	2.19	4.82	0.18
^{135}Sb	7.52	3.86	3.66	10 ± 1.1	8 ± 2	1.25	0.485	4.85	3.88
^{136}Sb	9.54	5.20	4.34	13 ± 1.5	-	-	0.094	1.22	-
^{136}Te	4.47	4.02	0.45	< 0.5	-	-	2.02	< 1.01	-
^{137}Te	6.48	5.63	0.85	~ 1	-	-	0.63	0.63	-
^{137}I	5.79	4.45	1.34	2.2 ± 1.7	4.8 ± 1.3	0.46	4.11	9.1	19.7
^{138}I	7.80	5.86	1.94	3.8 ± 2.9	2.5 ± 0.6	1.52	2.68	10.2	6.73
^{139}I	6.67	3.89	2.88	6.7 ± 0.8	6 ± 2	1.12	1.10	7.98	6.60
^{140}I	8.93	5.35	3.58	9.8 ± 1.1	12 ± 8	0.82	0.236	2.28	2.83
^{141}I	7.42	3.52	3.90	11.1 ± 1.3	-	-	0.032	0.35	-
^{141}Xe	5.85	5.79	0.06	< 0.5	0.054 ± 0.009	-	1.14	≪0.57	0.06
^{142}Xe	4.34	3.93	0.41	< 0.5	0.45 ± 0.08	-	0.31	< 0.15	0.14
^{143}Xe	6.65	5.59	1.06	1.5 ± 1.1	-	-	0.05	0.08	-
^{144}Xe	4.67	3.85	0.82	~ 1	-	-	0.00005	~ 0	-
^{145}Xe	7.14	5.81	1.33	2.2 ± 1.7	-	-	~ 0	~ 0	-
^{141}Cs	4.97	4.65	0.32	< 0.5	0.073 ± 0.011	-	4.60	< 2.30	0.33
^{142}Cs	7.24	6.20	1.04	1.5 ± 1.1	0.27 ± 0.1	5.56	3.1	4.64	0.84
^{143}Cs	5.73	4.09	1.64	3.0 ± 2.3	1.13 ± 0.25	2.66	1.43	4.29	1.61
^{144}Cs	8.05	6.16	1.89	3.6 ± 2.7	1.10 ± 0.3	3.27	0.41	1.48	0.45
^{145}Cs	6.07	3.83	2.24	4.7 ± 0.5	-	-	0.054	0.25	-
						sub-total (heavy mass peak)		56.33	43.3
						TOTAL		(170.8) 166.8 [a]	143.5

* Values from Garvey-Kelson mass tables [45].

** Calculated according $P_n = K(Q_\beta - B_n)^{1.54}$ (Fig. 2). Errors were taken as the average deviation of the experimental values from the calculated ones: viz. ± 12% for $Q_\beta - B_n > 2$ MeV and ± 70% for 2 > MeV $Q_\beta - B_n > 1$ MeV; if experimental P_n's of $^{142,143,144}Cs$ are taken to be systematically low by a factor of 3, the error for values below 2 MeV will decrease to ~30%.

*** For choice of values see Table II.

a corrected for ^{134}Sb.

TABLE V. COMPARISON BETWEEN GROUP (i = 1, 2, 3) YIELDS AND DETAILED PRECURSOR CONTRIBUTIONS FROM DIFFERENT FISSION REACTIONS

Group No. (i)	d.n. precursor	$T_{\frac{1}{2}}$ (s)	P_n (%)	^{233}U thermal fission		^{235}U thermal fission		^{239}Pu thermal fission		^{252}Cf spontaneous fission	
				Y_c (%)	n/10^4 fission	Y_c (%)	n/10^4 fission	Y_c (%)	n/10^4 fission	Y_c (%)	n/10^4 fission
1	^{87}Br	55	2.5	3.58	8.96	2.28	5.7	0.79	1.97	0.21	0.52
	^{133}Sn	?	(0.2)	0.09	(0.02)	0.42	(0.1)	0.13	0.03	0.02	0.004
					8.98		5.8		2.0		0.52
	Group yield:				(5.7 ± 0.3) [1]		(5.2 ± 0.5) [1]		(2.1 ± 0.6) [1]		(0) [14]
2	^{88}Br	16	4	3.03	12.14	2.78	11.1	0.85	3.41	0,174	0.70
	^{137}I	24	4.8	2.75	13.20	4.11	19.7	3.0	14.42	1.69	8.11
	^{141}Cs	25	0.073	3.66	0.27	4.60	0.3	3.16	0.23	3.2	0.23
	^{134}Sb	11	0.08	0.714	0.06	2.19	0.2	0.93	0.07	0.25	0.02
	^{134}Sn	?	(6.1)	0.095	0.58	0.09	(0.5)	0.015	0.09	0.003	0.02
					26.25		31.8		18.22		9.08
	Group yield:				(19.7 ± 0.9) [1]		(34.6 ± 1.8) [1]		(18.2 ± 2.3) [1]		(26.7 ± 3.5) [14]
3	^{87}Se	6	0.4	1.04	0.42	1.09	0.4	0.244	0.10	0.05	0.02
	^{89}Br	4.5	7	1.63	11.42	2.42	16.9	0.502	3.52	0.10	0.70
	^{92}Rb	4.5	0.012	4.52	0.05	5.18	0.06	2.25	0.03	0.498	0.01
	^{93}Rb	6	1.8	2.58	4.64	4.0	7.2	1.61	2.90	0.285	0.51
	^{138}I	6	2.5	1.31	3.27	2.68	6.7	1.34	3.36	0.788	1.97
					19.80		31.3		9.91		3.21
	Group yield:				(16.6 ± 2.7) [1]		(31.0 ± 3.6) [1]		(12.9 ± 3) [1]		(18.9 ± 3.0) [14]

Fission yields were taken from Wahl's tables (1968) [44] and Z_p calculated according to Ref. [48].
^{233}U chain yield data were taken from Ref. [47].
^{233}Pu chain yield data were taken from Ref. [46].

TABLE VI. SUMMARY OF KNOWN AND EXPECTED CONTRIBUTIONS TO DELAYED NEUTRON GROUPS 4, 5 AND 6 IN ^{235}U THERMAL FISSION

Group No. (i)	d.n. precursor	$T_{\frac{1}{2}}$ (s)	P_n (%)	Thermal fission of ^{235}U: Y_c (%)	Thermal fission of ^{235}U: n/10^4 fission
4	^{84}Ge	?	(8.9)	0.093	(0.83)
	^{84}As	?	(1.3)	0.646	(0.84)
	^{85}As	2	16.5	0.485	8.0
	^{86}As	?	(16.6)	0.31	(5.15)
	^{88}Se	2	6.4	0.65	4.16
	^{90}Br	1.6	12	1.75	21.0
	^{92}Br	?	(20.2)	0.07	(1.4)
	^{92}Kr	1.9	0.04	1.68	0.07
	^{93}Kr	1.3	3.3	0.53	1.75
	^{94}Rb	2.7	7.5	1.9	14.2
	^{98}Y	2	0.8	2.9	2.3
	^{135}Sb	1.7	8.0	0.485	3.9
	^{137}Te	?	(1.0)	0.63	(0.63)
	^{139}I	2	6.0	1.1	6.6
	^{140}I	0.8	12	0.236	2.8
	^{141}Xe	1.7	0.054	1.14	0.06
	^{142}Xe	1.2	0.45	0.31	0.14
	*^{142}Cs	2	1.5	3.1	4.6
	*^{143}Cs	1.7	3.0	1.43	4.3
	*^{144}Cs	1.0	3.6	0.41	1.5
	^{145}Cs	?	(4.7)	0.054	(0.25)
					84.48
	Group yield [1]:				(62.4 ± 2.6)
5, 6	^{91}Br	0.5	(13.8)	0.40	(5.52)
	^{94}Kr	0.2	(4.7)	0.08	(0.38)
	^{95}Kr	?	(8.3)	0.01	(0.08)
	^{95}Rb	0.4	7.1	0.66	4.70
	^{96}Rb	0.2	17.7	0.17	2.15
	^{97}Rb	0.14	>20	0.02	>0.4
	^{136}Sb		(13)	0.094	(1.22)
	^{141}I	0.3	(11.1)	0.032	(0.35)
	^{143}Xe		1.5	0.05	0.08
	^{144}Xe		1	5×10^{-5}	~0
					14.88
	Group yield [1]:				(24.8 ± 1.7)

* $^{142,143,144}Cs$ experimental values corrected; see remarks elsewhere.
The values in brackets are calculated, see Table IV.

With the recent advent of electromagnetic mass analysis methods combined in an "on-line" mode with fast radiochemical separation of fission products, the study of individually selected short-lived nuclides has become possible. A continuous "on-line" sequence of irradiation, extraction, chemical separation and isotopic separation now makes it possible to get practically non-decaying sources for interference-free measurements of a given nuclide. By collecting the nuclide on a moving conveyor, removal of the growing decay products is accomplished. On-line isotopic separation proves to be the most powerful technique for studying nuclear properties of nuclides far off stability, and a considerable amount of data (included in Table II) has already been produced with respect to delayed neutron precursors.

At Orsay, France, fission fragments from 150 MeV proton irradiated ^{238}U were allowed to recoil into hot graphite; the Rb and Cs were selectively ionized upon diffusing out, by surface ionization, and subsequently accelerated and isotopically dispersed in a mass spectrometer [19,20]. This permitted the study of d.n. precursors with half-lives as low as 135 msec(^{97}Rb).

At Ames, U.S.A., a uranium target was placed in a beam tube of a reactor and the Kr and Xe which diffused out into the ion source of the TRISTAN separator were analyzed together with their decay products [21]. Due to the relatively long transit times, $\sim$15 sec, appreciable decay occurred which limited detection to activities with half-lives longer than 1 sec. This assembly demonstrated the extreme sensitivity of delayed neutron detection, which was effective even where the neutron branching was $\sim$0.01%.

At Soreq, Israel, the SOLIS separator [22] is connected on-line with various interchangeable fission targets at the external neutron beam of a reactor. Various chemical purification steps, automated and placed on-line between the target and the separator, permit observation of a variety of elements, and when used in conjunction with controlled irradiation and pulsing of the neutron beam, this system has considerable experimental capabilities. For example, 0.19 sec ^{94}Kr is a case under study [23].

Other laboratories, e.g. Studsvik, Sweden, (the OSIRIS separator)[24], and at Grenoble, France, [25], have similar facilities for studying short-lived fission products with on-line isotopic separators.

Fast radiochemical separations have yielded the long known data on halogens, and during the last few years data on Kr, Xe, Rb, As, Se and Sb, where new delayed neutron precursors were identified and information was obtained on their respective yields and neutron branching ratios (marked as CF in Table II). The techniques employed were mainly gas sweeping based on emanation [26] and hydride formation [27,28,29,30,33]. 'Wet' chemistry, such as isotopic and ion exchange and solvent extraction, was also employed with remarkable success [9,31,32,33] yielding significant new information even for very short-lived species when use was made of a pulsed reactor and automation of operations [33].

Of special note are 'hot atom' chemistry techniques, e.g. recoil labelling by fission produced halogens in gas phase reactions [34,33, 35,36,37]. Some recoil reactions were found to proceed with atoms produced independently in fission, while the same species formed by precursor decay were discriminated against [33,34,35,36]. Combining this technique with fast gas-chromatography, correlations between relative independent fission yields and P_n values for halogens were obtained [35] (see Table III).

Table II summarizes the present knowledge of individual d.n. precursors and their abundances. A recent tabulation by del Marmol contains complementary experimental information [60].

4. DELAYED NEUTRON PRECURSOR SYSTEMATICS AND DATA EVALUATION

Delayed neutron emission is possible when β decay (of the delayed neutron precursor) leads to an energy level above the neutron binding energy of the product (the delayed neutron emitter), i.e. when $Q_\beta - B_n > 0$ *. Neutron emission will take place unless selection rules hinder such a transition, in which case de-excitation will occur by γ-ray emission. With increasing distance from stability, along the isobaric chains, Q_β values increase, neutron binding energies decrease, and neutron emission becomes more abundant.

Predictions based on theoretical and semi-empirical considerations regarding delayed neutron precursors published in the fifties [38,39,40], though of great divergence, were quite useful as guides for the experimentalists. These, as well as later attempts [41], were seriously handicapped by the lack of precise information on the nuclear energy surface and nuclear spectroscopic data on the neutron excess side of the stability line. With refinements of semi-empirical mass formulae, and especially with the prospect of experimental data from the on-line isotope separators, one may expect a radical improvement in this respect.

So far, neutron emission thresholds and probabilities P_n were inferred mainly from various parameters related to the distance from the stability line; for example, the charge displacement of the delayed neutron emitter [42] $(Z_{N-1} - Z)$ ** gave fair approximations of then unknown P_n's [38] (a recent attempt is given in Fig. 1),[43]. According to the Fermi β theory, the probability for populating levels in the neutron emitter is determined by $E^5_{\beta^-}\ \omega_{Z+1}(E^*)$ when $E_\beta < Q_\beta - B_n$. The neutron emission probability will then be $E^5_{\beta^-}\ \omega_{Z+1}(E^*)\ \frac{\Gamma_n}{\Gamma_n+\Gamma_\gamma}$, (Γ being the channel width for the corresponding de-excitation ***), Pappas et al. [41] have recently given a detailed theoretical treatment taking into account both the "energy and the angular momentum paths" , and they attempted to calculate the P_n's of ^{87}Br, ^{137}I and ^{85}As as well as the shape of the ^{87}Br spectrum,with partial success. It is clear that the accuracy of these calculations depends greatly on the spectroscopic data available, and these are practically nonexistent.

Using elementary semi-empirical and statistical considerations we can relate the neutron emission probability to the "window" width $\Delta E = Q_\beta - B_n$, to the density of available levels and to the competition between neutron and gamma ray emission. Thus $P_n = C\ (\Delta E)^k \omega_j(\Delta E)\ \frac{\Gamma_n}{\Gamma_n+\Gamma_\gamma}$.

Let us assume $\omega_j(\Delta E) = (\Delta E)^\ell$, then $P_n = C(\Delta E)^{k+\ell}\ \frac{\Gamma_n}{\Gamma_n+\Gamma_\gamma}$. If gamma competition due to spin and parity effects is ignored, an assumption which probably gains validity at higher excitation energies, then

---

* Q_β refers to the d.n. precursor, (Z,N),and B_n to the emitter, (Z+1,N-1).

** Z_{N-1} is the most stable charge corresponding to the neutron number of the delayed neutron emitter and Z is the charge of the d.n. precursor.

*** Evidence for γ de-excitation of an energy-allowed neutron emitting level is given by the observation of a 6.5 MeV γ in ^{87}Br decay; a level in ^{87}Kr at 6.5 MeV would be $\sim$1 MeV above the B_n , which is $\sim$5.5, but neutron emission from this level might be spin inhibited [49].

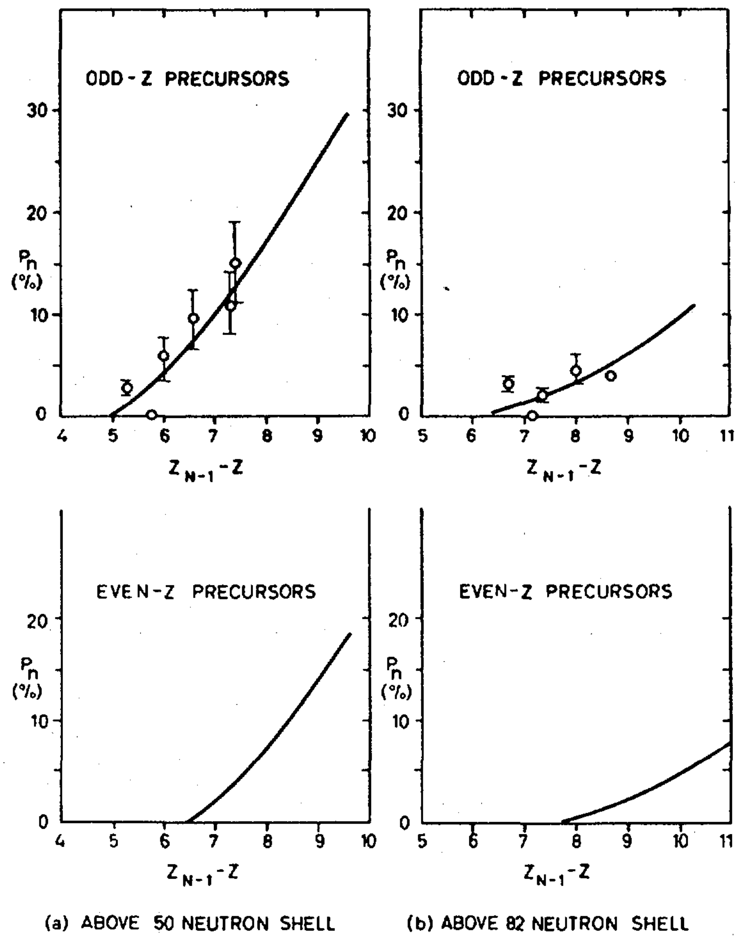

FIG. 1. Delayed neutron emission probabilities (from Ref. [43]). Z_{N-1} is the most stable nuclear charge corresponding to the neutron number (N-1) of the delayed neutron emitter; Z is the nuclear charge of the delayed neutron precursor; P_n is the delayed neutron emission probability.

for $\ell + k = m$ we have $P_n = C(\Delta E)^m$. Such a dependence should result in a linear variation of log P_n vs. log $(Q_\beta - B_n)$, m being the slope. Table IV and Fig. 2 present the results obtained (using Q_β and B_n values taken from mass tables based on experimental data [45]). No distinction is observed between the P_n's of light and heavy masses, nor between even and odd masses (contrary to what has been suggested in Ref. 38 on the basis of the P_n vs. $(Z_{N-1} - Z)$ correlations - see for example Fig. 1). The best linear fit in Fig. 2 is given by the line C , where m = 1.54. For $Q_\beta - B_n < 1$ MeV the narrow "window" reduces the number of levels, and also the selection rules due to spin and parity effects may be more pronounced so that the P_n's are expected to have lower values and be scattered below the line extrapolated from higher ΔE values. This is well demonstrated in the case of ^{134}Sb which populates a closed neutron shell configuration and may

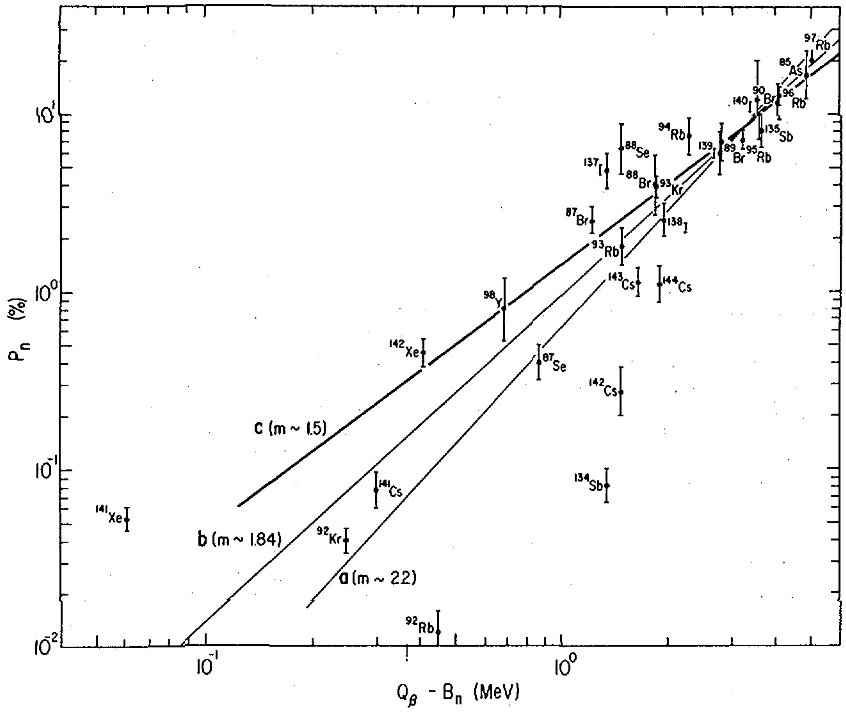

FIG. 2. Correlation of experimental neutron emission probabilities with the parameter (Q_β-B_n) using values from Ref. [45].

not be subject to a statistical treatment. $^{142,143,144}Cs$ seem to have systematically low P_n values, and from a comparison of references [21] and [20] one would suggest a correction by a factor of ~3. These considerations suggest an even smaller error in m than appears from Fig. 2. At $\Delta E < 1$ MeV, inaccuracies of the order of 100-200 keV may affect the uncertainties with respect to position and "width" of the window, and the results in this range should be taken with some reservations.

The P_n value or neutron branching ratio of a given nuclide is taken as a characteristic constant independent of the formation of the nuclide in the fission process. This assumption is legitimate as long as formation of isomers can be ruled out, as suggested by several authors [40,39,41]. This is why P_n values are often regarded as identical with the observed ratio of d.n. yield to cumulative fission yield of the precursor [41]. Since it was found recently that isomers are present just beyond closed shells in the region of interest (e.g. the 156 sec and 258 sec activities of ^{90}Rb in 150 MeV proton fission of uranium [19]) one should reconsider this assumption and its implications, in the light of possible variations of the neutron emission probability with variations of isomer ratios in different sources. A greater proportion of the isomer may lead to higher neutron branching due to a wider "window" ΔE. On the other hand, the greater the spin difference between either state and the neutron emission product, the smaller the P_n will get and vice versa. Of special interest in this respect may be the study of heavy ion induced fission where very high angular momenta may be introduced.

Another point worth mentioning is that the assumption that d.n. emission is limited to nuclides having one or more neutrons in excess of a closed shell has become outdated. More precise mass values indicate that special cases of predicted d.n. precursors may contain magic numbers of neutrons, e.g. ^{84}As, ^{133}Sn and ^{134}Sb. An experimental verification was recently given for the case of ^{134}Sb [28].

A general experimental study of the details of delayed neutron systematics in fission has recently been reported by Armbruster et al [50], who employed magnetic analysis for mass separation of fission fragments. With a separation time of ~1 μsec and a coarse resolution* it was possible to measure mass dependent yields and half-life values of d.n. activities over the entire range of fission products. Fig. 3 presents the results. The analysis of the data from ^{235}U fission indicates that (67 ± 3)% of all delayed neutrons are emitted in the light mass peak while the heavy masses are responsible for only (33 ± 3)%; maximum neutron yield appears in the 1-2 sec half-life range (i=6). A distinct amount of unknown (in 1968) activity appeared in the mass region 96-100 when compared with calculated values, and this was suggested to be $^{98,99}Y$; a small amount of unidentified neutron activity at A ~ 85 to 88 was also indicated.

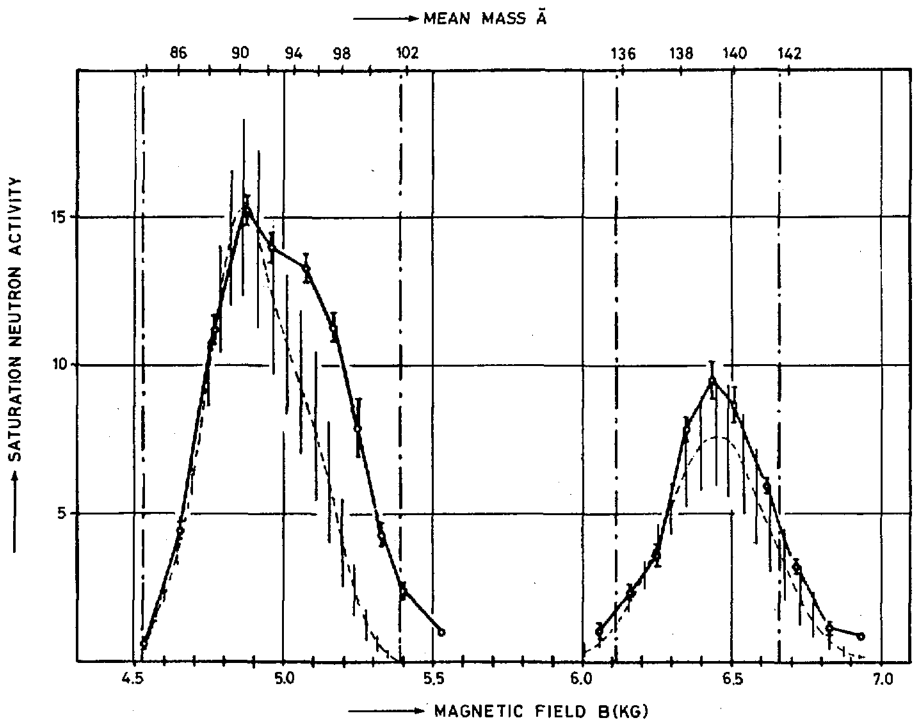

FIG. 3. Mass dependence of saturation neutron activity (determined by neutron counting of mass-separated fission fragments). From Ref. [50].

* $\left(\frac{\Delta A}{A}\right)_{FWHM}$ was ~5% to 8% for light masses and ~22% for heavy ones.

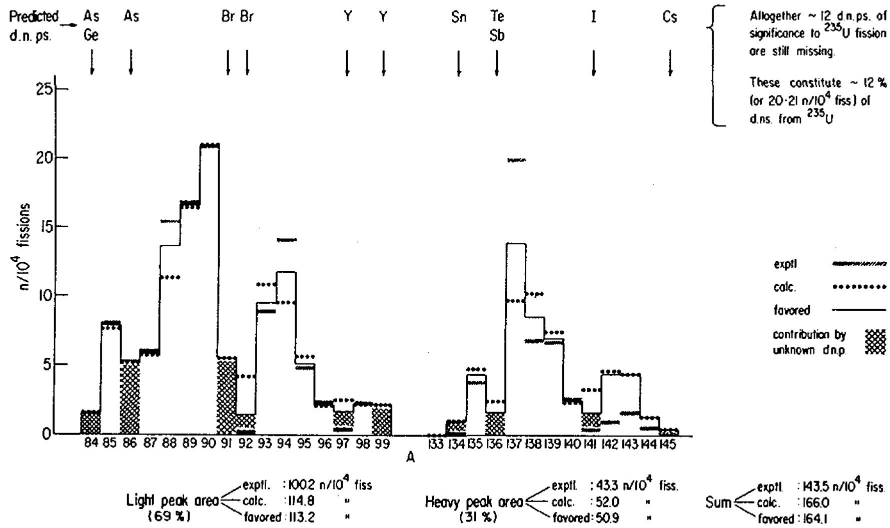

FIG. 4. Mass dependence of delayed neutron emission based on known and expected delayed neutron precursor contributions.

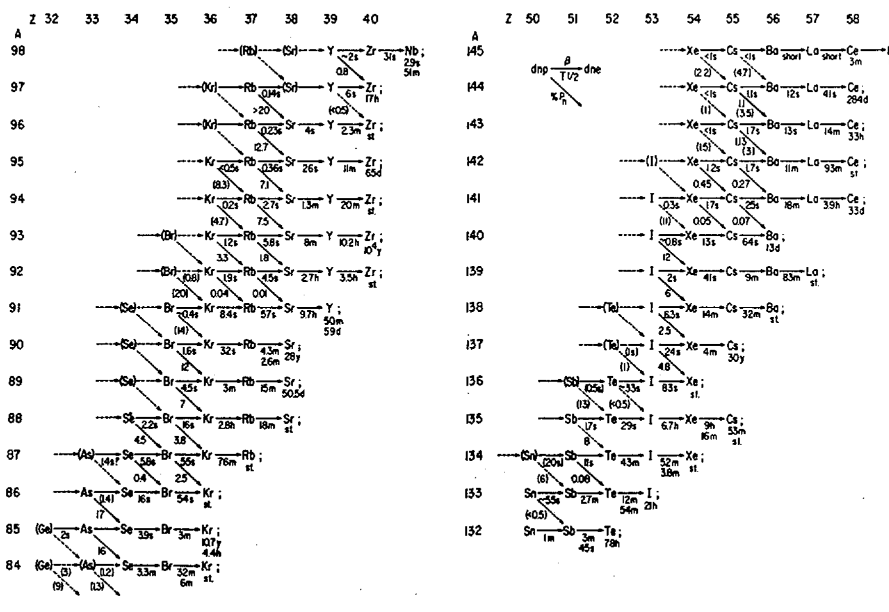

FIG. 5. β and n decay chains in the light and heavy fission product mass peaks in low-energy fission.

We have made an attempt to use carefully selected data, both experimental and calculated, for known and predicted unknown d.n. precursors, in order to obtain a complete picture of the mass dependence of d.n. emission in ^{235}U thermal fission. This is shown in Fig. 4.

At this point I would like to remark that when correlating experimental and calculated data of individual precursors, e.g. their P_n values and fission data (independent and cumulative yields etc.), the inaccuracies stemming from hypotheses like the one for charge distributions, prediction of half-lives, presence of isomers etc. must be borne in mind. Several attempts to combine d.n. data with fission systematics to obtain a consistent picture have been reported [4,2,31,33]. Tables V and VI constitute the present attempt. The figures suggest that most of the contributions to d.n. emission in fission can be accounted for by the known and the few predicted precursors.

The importance of d.n. emission in radiochemical fission yield determinations is demonstrated in Fig. 5 where both β and n decay chains of fission products are given with the respective neutron branching ratios.

5. ENERGIES OF DELAYED NEUTRONS

Our state of knowledge concerning the energies of delayed neutrons emitted from fission products is most unsatisfactory. Only spectra of poor resolution (∿10% or worse) are available, obtained from unseparated sources prepared so as to emphasize the relative contributions of the different groups in the coarse distribution patterns [55]. Such measurements, even with improved resolutions, can only provide data for reactor kinetics, but their significance in terms of nuclear properties of individual precursors is dubious.

The techniques used for neutron energy studies are ^{3}He proportional spectrometry, proton recoil spectrometry, and time-of-flight with β-n coincidence analysis. One recent attempt using a time-of-flight technique reports the presence of peaks at ∿60, ∿120 and ∿165 keV in the gross analysis of ^{235}U fission where i = 2 and 3 are emphasized [56]. However the measurements were subject to poor statistics, random coincidences and a substantial γ-ray background. Another attempt in this direction, also using the same technique, has given preliminary results which indicate about 20 discrete lines in the gross spectrum, ranging from 35 keV to 1.81 MeV [57]. However, it is clear that due to the excessive intensity of betas in unseparated fission sources, where one expects ∿10^6 or more betas per neutron count, all these techniques call for the use of separated nuclides at substantial intensities. With the advent of isotope separators placed on-line with fission sources e.g. SOLIS [58, 22] TRISTAN [59] and others, neutron spectrometry of separated precursors has now become possible.

The endpoint of individual spectra is related to the "window" (Q_β-B_n) which can serve to check the available mass values and binding energies. In addition, the shape of the spectrum, especially its low energy part, may yield information on level densities above the neutron binding energy; pronounced peaks and dips in the spectra should be related to the spins of the levels involved, etc. Thus neutron spectra may be used as a sensitive test of the assumptions made in semi-theoretical calculations of neutron emission probabilities based on the statistical model. In general, improved energy measurements of separated precursors is a prerequisite for clarifying the decay characteristics and structure of these nuclides. Such measurements must further be complemented by a study of the other de-excitation modes in the series to obtain detailed nuclear structure information. This part is still ahead of us.

In connection with neutron spectrometry, as well as with respect to the discussion of the neutron emission probabilities, it would seem that the phenomenological approach to delayed neutron emission from the fission aspect is passing away, and the search for more d.n. contributors and "missing" precursors will become of secondary importance to the study of d.n. emission from the nuclear structure aspect. The pressing need today in delayed neutron emission studies is the nuclear spectroscopic measurement of individual precursors, from which it is hoped to gain more information on the nuclear energy surface and the level structure and transitions on the neutron excess side of stability, where delayed neutron emission is quite a common phenomenon.

ACKNOWLEDGEMENT

I would like to express my very warm thanks to Mrs. Hanna Feldstein for her invaluable assistance in the calculations and preparation of the figures and tables.

REFERENCES

[1] KEEPIN, G.R., Physics of Nuclear Kinetics, Ch.4, Addison-Wesley, Reading, Mass. (1965).
[2] AMIEL, S., in Physics and Chemistry of Fission, Vol.II, p.171; IAEA, Vienna (1965).
[3] PAPPAS, A.C. and TUNAAL, T., Arkivför Fysik 36, 445 (1967).
[4] Delayed Fission Neutrons, IAEA, Vienna pp.249 (1968).
[5] KEEPIN, G.R., in ref. 4.
[6] YIFTAH, S., SAPHIER, D., in ref. 4. Also Trans. Am. Nucl. Soc. 11 (#2) 568 (1968).
[7] AMIEL, S., Anal. Chem. 34 1683 (1962).
[8] KEEPIN, G.R., in Proc. Symp. Safeguards R & D; WASH-1076, USAEC Rep. p.150 (1967).
[9] HERRMANN,G., in ref. 4.
[10] NOTEA, A., AMIEL, S., unpublished report (1967) and Ph.D. Thesis by A. Notea, Hebrew Univ., Jerusalem (1968).
[11] MASTERS, Ch., THORPE, M.M., SMITH, D.B., Trans. Am. Nucl. Soc. 11 179 (1968) and also to be published in Nucl. Sci. Engng. (Personal communication by G.R. Keepin).
[12] TOMLINSON, L., HURDUS, M.H., this symposium and personal communication.
[13] WILLIAMS,E.T.,CORYELL, C.D., Nuclear Applications 2 256 (1966)
[14] CHULICK, E.T., REEDER, P.L., EICHLER, E., BEMIS, C.E., Radiochimica Acta (to be published) and Bull. Am. Phys. Soc. 14 190 (1969).
[15] MAKSYUTENKO, B.P., RAMAZANOV, R., TARASKO, M.Z., Soviet J. Nucl. Phys. 7 (2) 189 (1968). Also MAKSYUTENKO, B.P., ibid 6 (1) 16 (1968), also MAKSYUTENKO, B.P., PYSHIN, V.K., TARASKO, M.Z., ditto 5 (3) 375 (1967) also MAKSYUTENKO, B.P., in ref. 4.
[16] AMIEL , S., in Nuclear Chemistry (YAFFE, L., Ed.) Vol. II, Ch.9, Academic Press Inc., New York, (1968).
[17] DEL MARMOL, P., in ref. 4.
[18] HERRMANN, G., Arkiv för Fysik 36 111 (1967)
[19] AMAREL, I., BERNAS, R., FOUCHER, R., JASTRZEBSKI, J., JOHNSON, A., TEILLAC, J., GAUVIN, H., Phys. Letters 24B 402 (1967)
[20] AMAREL, I., GAUVIN, H., JOHNSON, A., J. Inorg. Nucl. Chem. 31 577 (1969)
[21] TALBERT, W.L., TUCKER, A.B., DAY, G.M., Phys. Rev. 177 1805 (1969).
[22] AMIEL, S., in ref. 4.
[23] AMIEL, S., ORON, M., YELLIN, E., to be published.
[24] RUDSTAM, G., personal communication.
[25] CRANSON, J., personal communication.

[26] AMIEL, S., GILAT, J., NOTEA, A., YELLIN, E., Arkiv för Fysik 36 169 (1967).
[27] DEL MARMOL, P., NEVE DE MEVERGHIES, M., J. Inorg. Nucl. Chem. 29 273 (1967).
[28] TOMLINSON, L., HURDUS, M.H., Phys. Letters 25B 545 (1967).
[29] TOMLINSON, L., HURDUS, M.H., J. Inorg. Nucl. Chem. 30 1649 (1968).
[30] TOMLINSON, L., HURDUS, M.H., J. Inorg. Nucl. Chem. 30 1995 (1968).
[31] PATZELT, P., SCHÜSSLER, H.D., HERRMANN, G., Arkiv för Fysik 36 456 (1967).
[32] SCHÜSSLER, H.D., GRIM, W., HERRMANN, G., paper at the Deutschen Chemischen Gesellschaft, Berlin, Sept. 1967.
[33] FOLGER, H., FRANZ, H., GRIM, W., HERRMANN, G., KRATZ, K.L., KRATZ, J.V., SCHÜSSLER, H.D., paper at the German Physical Society, Freudenstadt, March 1969; personal communication, G. Herrmann.
[34] AMIEL, S., PAISS, Y., J. Am. Chem. Soc. 86 2332 (1964) and Radio-Chimica Acta 4 157 (1965).
[35] BRAUN, Ch., AMIEL, S., to be published.
[36] SILBERT, M.D., TOMLINSON, R.H., Radiochimica Acta 5 217 and 223 (1966)
[37] DEUSCHLAG, H.O., HENZEL, H.O., HERRMANN, G., Radiochimica Acta 1 172 (1963)
[38] PAPPAS, A.C., Proc. 2nd Atoms for Peace Conf., Geneva, 1958 - 15, 373 (1958) UN, N.Y.
[39] KEEPIN, G.R., J. Nucl. Energy 7 13 (1958).
[40] PAPPAS, A.C., RUDSTAM, G., Nucl. Phys. 21 353 (1960).
[41] JAHNSEN, T., PAPPAS, A.C., TUNAAL, T., in ref. 4.
[42] PAPPAS, A.C., Rep. LNS-MIT-63, AECU-2806 (1953).
[43] TOMLINSON, L., in ref. 4.
[44] WAHL, A.C., Computer Computed Fission Yield Data, personal communication (1960).
[45] KELSON, I., personal communication (1969).
[46] HYDE, E.K., The Nuclear Properties of the Heavy elements, Vol. III Ch.4, Prentice-Hall, N.Y. (1964).
[47] FERGUSON, R.L., O'KELLEY, G.D., USAEC Rep. ORNL-3305 (1962).
[48] CORYELL, C.D., KAPLAN, M., FINK, R.D., Can. J. Chem. 39 646 (1961)
[49] WILLIAMS, E.T., CORYELL, C.D., Phys. Rev. 144 945 (1966)
[50] ROECKL, E., EIDENS, J., ARMBRUSTER, P., Z. Physik 220 101 (1969); also in ref. 4.
[51] FELDSTEIN, H., EHRENBERG, B., AMIEL, S., unpublished results (1969).
[52] ARON, P.M., KOSTOCHKIN, O.I., PETIZHAK, K.A., SHPAKOV, V.I., Soviet J. At. Energy 16 447 (1965).
[53] PERLOW, G.J., STEHNEY, A.F., Phys. Rev. 113 1269 (1959)
[54] KEEPIN, G.R., WIMETT, T.F., ZEIGLER, R.K., Phys. Rev. 107 1044 (1957).
[55] BATCHELOR, R., MckHyder, H.R., J. Nucl. Energy 3, 7 (1956).
[56] PAPADOPOULOS, N.N., CHRYSOCHOIDES, N.G., ZIKIDES, C.C., Greek AEC Rep. (Final Rep. Contract 297/R2/RB July 1968).
[57] BEMIS, C.E., personal communication; also CHULICK, E.T., REEDER, P.L., EICHLER, E., BEMIS, C.E., Bull. Am. Phys. Soc. 14 190 (1969) ; and personal communication
[58] AMIEL, S., Arkiv för Fysik 36 71 (1967).
[59] TALBERT, W.L., McCONNEL, J.R., Arkiv för Fysik 36 99 (1967)
[60] DEL MARMOL, P., Nuclear Data, in press, and personal communication.

DISCUSSION

A. C. PAPPAS: You refer to odd-even effects pointed out by me 15 years ago and do not find these in your plot. You cannot expect to find odd-even effects when you plot P_n versus Q_β-B_n, as they cancel out first, an odd-odd parent (large Q_β) giving an even-even daughter (large B_n) while an even-even parent (small Q_β) gives an odd-odd daughter (small B_n). Thus this difference (Q_β-B_n) is relatively unaffected. Furthermore, your plot is a first approximation and may be expected (crudely) to represent the bell-shaped population probabilities you get from a theoretical treatment (i. e. the product of Fermi function and level density).

Did you try to plot the very light (C, N, O) delayed neutron precursors in your plot, and what about Tl?

S. AMIEL: No, I did not. I am inclined to believe that the light nuclei should be different from the medium-mass fission products; but of course it might be interesting to do as you suggest. I cannot recall a P_n value for ^{210}Tl but even here I wonder whether, in view of proximity to the lead shell, agreement will be observed.

G. HERRMANN: I would like to make two short comments and ask a question. The first comment refers to the neutron emission probabilities of ^{142}Cs and ^{143}Cs, which do not fit in your systematics (Fig. 2). Therefore, you suggest that the experimentally obtained P_n values of these isotopes are systematically low. According to your estimates (Table VI), about 40% of the alkali contribution to the 2-s group would stem from cæsium isotopes. However, the results presented in paper SM-122/22 show that the cæsium contribution is smaller by a factor of about 10, confirming the low P_n values of ^{142}Cs and ^{143}Cs.

My second comment is on the yield of the 55-s group in thermal-neutron induced fission of ^{233}U, which is smaller than what is expected according to the estimated fission yield of ^{87}Br and its P_n value. We measured the cumulative yield of ^{87}Br in this reaction and found that the low group yield results from an unexpectedly low ^{87}Br yield.

Now my question: In Table III you presented independent fission yields of iodine and bromine nuclides in the fission of ^{235}U by thermal neutrons; these were deduced from relative delayed neutron yields. If I understood you correctly, in evaluating these data you make use of the published P_n values. However, these values were derived from the same kind of experimental data by means of estimated fission yields. Hence, it seems to me that you merely get out what others have put in.

S. AMIEL: The low Cs values should not affect, to a great extent, the value of the exponent m. If we correct for the caesiums, we obtain m = 1.54; if we accept them as they are, the value is 1.84. At this point, where all P_n values have considerable experimental errors, I don't think we should place too much emphasis on the exactness of the value of m. On the other hand, I would not dare use the P_n values derived from gross delayed neutron contributions, since fission yields, chemical purity and yields etc. may introduce considerable errors. I would rather use values obtained from isotopically separated sources, as I have done in my tables. Of course, low P_n values may be understood when the statistical considerations (involving level populations etc.) which I was using fail, in cases like ^{134}Sb where level densities are very low or the difference (Q_β-B_n) is low. This information is not available as yet from experimental work.

As regards your second comment, all I can say is, let us wait for the experimental values which are at present too fragmentary to draw any conclusions.

In reply to your question, I should like to say that the independent fission yield values derived from the recoil displacement of iodine in methyl iodide are based on P_n values obtained by independent experiments. The observation that displacement takes place only with independently produced species, viz. energetic fragments, and not with halogens produced by the beta decay of the respective precursors, is consistently borne out. On the other hand, if this is the case, we can inversely derive P_n values from known fission yields and iodine or bromine ratios in displaced methyl halides. In conclusion, there is systematic agreement, which may be used to combine and check fission yields and P_n values obtained in different experiments by different authors. In view of the wide scatter of results from different sources, this is of great help.

P. DEL MARMOL: What would happen if you extrapolate your linear formula $\log P_n = m \log (Q_\beta - B_n)$ to higher $(Q_\beta - B_n)$ energies? I should think that P_n will then become higher than 100% and, in order to avoid this, I preferred to correlate P_n with $Q_\beta - B_n$ by a formula of the type $P_n = 1 - e^{-\alpha(Q_\beta - B_n)^2}$.

S. AMIEL: I am afraid that extrapolation will bring us to a region of $B_n \approx 0$ and P_n must then be $\sim 100\%$.

I do not see any basis for your formula, whereas the one I use is based on elementary considerations of delayed neutron emission. If your formula agrees with the experimental values, the two formulae may coincide.

N. PAPADOPOULOS: I just wanted to mention that we have recently improved our method (N. G. Chrysochoides et al. in Delayed Fission Neutrons (Proc. Panel Vienna, 1967) IAEA, Vienna (1968) 213) and reduced the random coincidences and the gamma background. We hope soon to obtain better results with better resolution by the time-of-flight beta-delayed neutron coincidence technique for delayed neutron-energy-spectrum measurements.

DELAYED NEUTRON PRECURSORS IN FISSION OF ^{235}U BY THERMAL NEUTRONS

H.D. SCHÜSSLER, H. AHRENS, H. FOLGER,
H. FRANZ, W. GRIMM, G. HERRMANN, J.V. KRATZ,
K.L. KRATZ
Institut für Anorganische Chemie und Kernchemie der Universität
Mainz, Federal Republic of Germany

Abstract

DELAYED NEUTRON PRECURSORS IN FISSION OF ^{235}U BY THERMAL NEUTRONS. A search for new delayed neutron precursors was performed by using thermal-neutron-induced fission of ^{235}U as the production process. Individual elements were chemically separated by rapid automatic techniques which permit counting to be started within a few seconds after irradiation, in the fastest procedure within 0.5 s. The chemical step consists of isotopic or ion exchange with preformed precipitates (Br, I, Rb, Cs, Sr), of extraction into quasi-solid reagents (Y, Zr, Nb), of volatilization as hydrides (As, Se, Sb, Te), or of recoil reactions with methane forming volatile methyl halides (Br, I). Several new precursors were found, e.g. 1.7 s ^{88}Se, 0.5 s ^{91}Br, 0.8 s ^{140}I, and 0.4 s ^{141}I.

The contributions of individual precursors to the group yields in fission of ^{235}U with thermal neutrons were measured by comparing neutron counting rates of separated and unseparated samples. In the 2-s, 6-s, 22-s, and 55-s groups, the total abundances of the identified precursors agree with the group yields.

From these abundances and estimated cumulative fission yields, neutron emission probabilities (P_n) of precursor nuclides were deduced. In addition, the P_n-value of ^{137}I was directly determined by measuring its beta and neutron emission rate.

1. INTRODUCTION

Since the first Symposium on Physics and Chemistry of Fission, our work [1] on delayed neutron precursors [2] in fission of ^{235}U by thermal neutrons has been extended because the reactor at this university became critical in 1967. This reactor can be operated in steady state at 100 kW as well as in the pulse mode producing a neutron flash with a maximum flux of 10^{15} n/cm^{2}s for about 30 ms FWHM in the latter case. Thus, we have good conditions especially for studying short-lived fission products including delayed neutron precursors.

In this work we use a rapid pneumatic tube system described in Ref. [3]. Transportation of the samples from the irradiation to the chemical separation position takes place within 0.1 to 0.2 s over a distance of 4 to 5 m. At one end of the tube system, various chemical separation units can be installed. References for the chemical techniques used are summarized in a recent review [4].

2. SEPARATIONS BY ION OR ISOTOPE EXCHANGE

Separations by exchange with preformed precipitates can be used for many elements if suitable precipitates are existing. A thin layer of the precipitate is prepared and the fission product solution is sucked

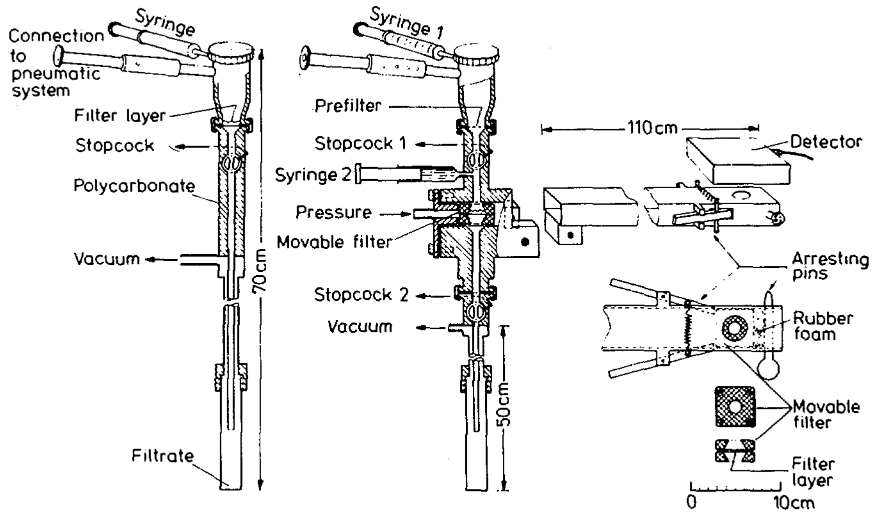

FIG.1. Set-up for rapid separations from aqueous solutions by ion or isotope exchange. In the version shown on the left-hand side, the detector is placed close to the fixed filter layer. In the version on the right-hand side, the layer can be transported to the counting position after separation.

through the filter layer within a few seconds. During this process, ions of the solution replace ions of the filter layer and are, thus, quickly and often quantitatively retained by the precipitate.

The set-up for this kind of separation is shown in Fig.1. A simple version can be seen in the left-hand part. The whole unit is connected to the pneumatic tube system. The thin filter layer (~ 10 mg/cm^2) is prepared on a membrane filter, supported by a fibrous fleece and covered by another fleece. About 2 cm^3 of the uranium solution are irradiated in a polystyrene capsule which is transported quickly into the separation unit. There it breaks by impact. The solution flows down the walls of the polycarbonate vessel and is sucked through the filter layer. A syringe injects a washing solution onto the capsule fragments and onto the filter layer. A neutron detector consisting of six ^{3}He counting tubes surrounds the filter layer. In this mode of operation, separations were performed within 1.5 s.

Sometimes shielding problems require a larger distance between filter layer and capsule fragments. Therefore, the unit shown in the right-hand part of Fig.1 works with a movable filter layer which is transported into the counting position by a second pneumatic tube system after the solution has passed the layer. The fragments remain above the prefilter. An additional syringe guarantees more effective washing. All sequent steps from the end of irradiation to the end of separation are operated automatically as described in Ref.[3]. The minimum time requirement for separation with this apparatus amounts to 3.0 s. If neutron emission probabilities, P_n , are to be measured directly a counter for beta rays is installed in addition to the neutron counter.

With this technique, iodine was separated by exchange with silver iodide, and iodine plus bromine were separated with silver chloride. These experiments led to the observation of 0.8 s ^{140}I and yielded the contributions of individual halogen precursors to the four longest groups of delayed neutron precursors. Also direct measurements of P_n -values are being carried out.

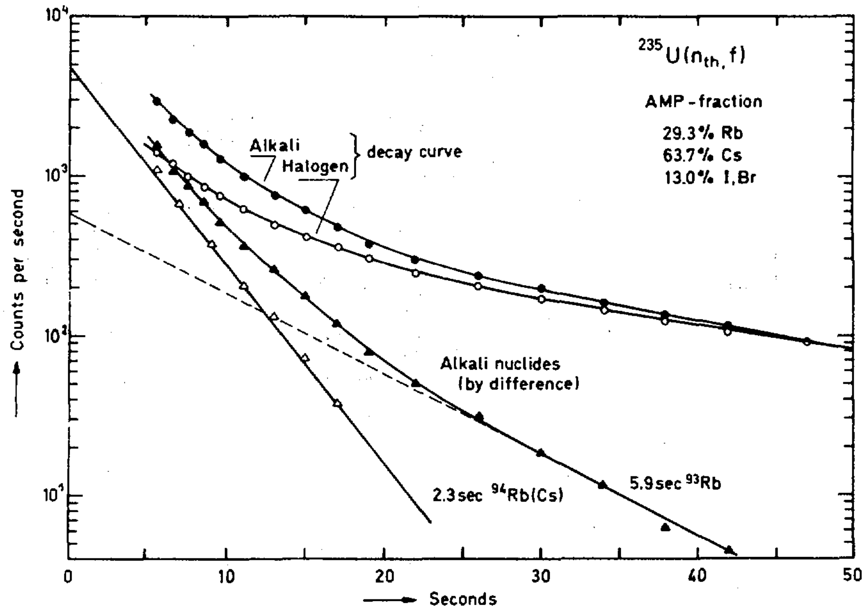

FIG.2. Neutron decay curve of the alkali fraction and its decomposition (see text).

The contributions of rubidium and caesium nuclides resulted from alkali separations with ammoniummolybdatophosphate (AMP). Figure 2 shows a decay curve and indicates the chemical yields for rubidium and caesium, as well as the contamination by halogens as deduced by the aid of long-lived tracers added to the solution before irradiation. The contamination is eliminated by subtracting a halogen decay curve, normalized in the region of the 22-s group where 97.7% of the neutron activity are due to halogens. The resulting curve is resolved into two components of 5.9 and 2.3 s half-lives attributable to 6.0 s ^{93}Rb, 2.6 s ^{94}Rb, 1.9 s ^{142}Cs, and 1.7 s ^{143}Cs [5, 6]. To measure the relative contributions of rubidium and caesium nuclides the chemical yield of rubidium relative to that of caesium was varied by a factor of three. Comparison of the observed neutron activities with the relative chemical yields of the two elements showed that 96% of the alkali fraction in the 2-s group stem from ^{94}Rb.

3. SEPARATIONS VIA RECOIL REACTIONS

A second technique (Fig.3) utilizes the formation of volatile compounds by recoil reactions and their selective adsorption as a separation step. When fission halogens are stopped in methane they are converted into methylhalides with a yield of 5 to 10%.

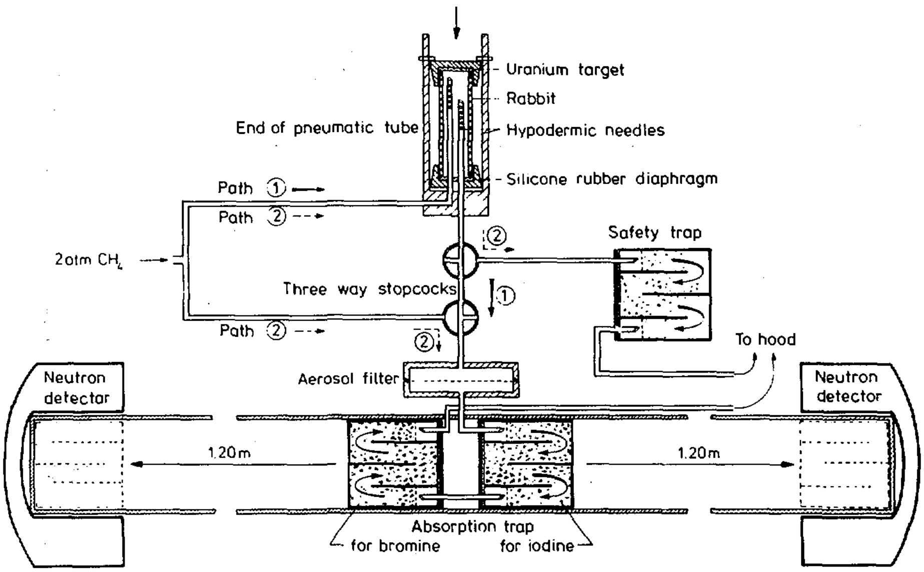

FIG.3. Set-up for rapid separations via recoil technique and following adsorption of the volatile components.

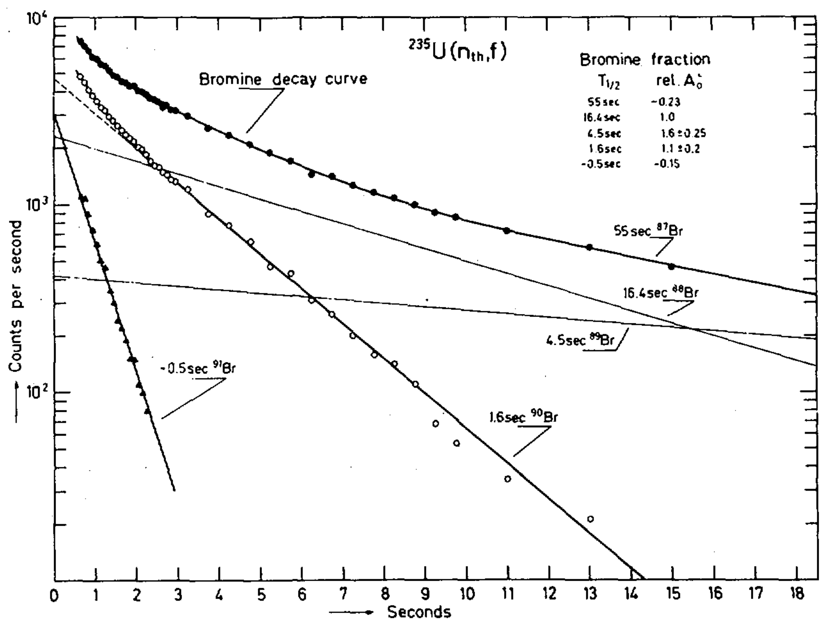

FIG.4. Neutron decay curve of the bromine fraction separated by the recoil technique.

The ^{235}U target - a thin film of UO_2 deposited on Al foil - is placed in a rabbit-containing methane. After irradiation, this rabbit is shot onto two hypodermic needles which punch through a silicone rubber diaphragm. The volatile fission products including methylhalides and aerosols are blown out of the rabbit by nitrogen or methane with a pressure of about 3 atm. The aerosols are eliminated quantitatively by a membrane filter. More than 80% of the halides and noble gases pass to the adsorption traps. In the first trap, filled with silver nitrate adsorbed on fire brick, and heated to 80°C, the methyliodide is retained. Methylbromide is adsorbed in the second trap, filled with molecular sieve. After adsorption, both traps are separated and quickly transported into the counting positions, 2.5 m away from each other, by a pneumatic tube system.

With this method separations within 0.5 s after the end of irradiation have been achieved. Nuclides with half-lives down to 0.2 s should be detectable. As an example a decay curve of the bromine fraction is shown in Fig.4. From the original curve noble gas contamination was subtracted as well as the 55-s group (^{87}Br). Further analysis showed the presence of the known bromine nuclides, ^{88}Br to ^{90}Br, and an additional component with a half-life of about 0.5 s. This component should be identical to the 0.64 s ^{91}Br detected indirectly by Patzelt et al. [7]. Analysis of the iodine fraction gave evidence for a new component with a half-life of about 0.4 s which should be assigned to 0.43 s ^{141}I observed indirectly before (Ref. [7]).

4. SEPARATIONS BY VOLATILIZATION

The separation of fission products forming hydrides has been described by various authors [4]. The apparatus used in the present work is shown in Fig.5. Irradiation of about 1 cm^3 of uranium solution in a thin glass capsule placed in a polypropylene rabbit, open at the front part, takes place in a pneumatic tube system. After irradiation the rabbit is transported to the separation apparatus. The polypropylene rabbit is stopped in front of the volatilization vessel whereas the thin glass capsule crashes inside the vessel, which contains 12 N HCl. Immediately afterwards, a surplus of zinc powder is added by turning a spoon (Fig.5). A violent burst of hydrogen occurs which sweeps the hydrides quickly into the absorption vessel containing 0.5 N NaOH. There, selenium and tellurium hydrides are absorbed whereas arsenic and antimony hydrides pass through. To separate selenium and tellurium, the absorption solution is acidified to 5 N HCl and oxidized by $KClO_3$. It is then filtered through tri-n-butylphosphate fixed on plastic grains. Tellurium is retained by this filter which is finally projected to the counting position by a second pneumatic tube system, whereas selenium is found in the filtrate. By this technique, tellurium and selenium fractions were obtained within 4 to 5 s with chemical yields of 50 and 20%, respectively, and with sufficient decontamination from other delayed neutron precursors.

As an application, the neutron decay curve of the selenium fraction is shown in Fig.6. In the late part of the curve, on the right-hand side, ^{87}Br and ^{88}Br appear as decay products of ^{87}Se and ^{88}Se. Therefore, the half-lives of ^{87}Se and ^{88}Se can be derived indirectly from the initial activities of their ^{87}Br- and ^{88}Br-daughters by varying the time between irradiation and separation. The resulting curve, plotted in Fig.6 in the upper right corner, gives 5.9 s half-life for ^{87}Se, and 1.7 s for ^{88}Se. Components of similar half-lives are also observed in the decay curve

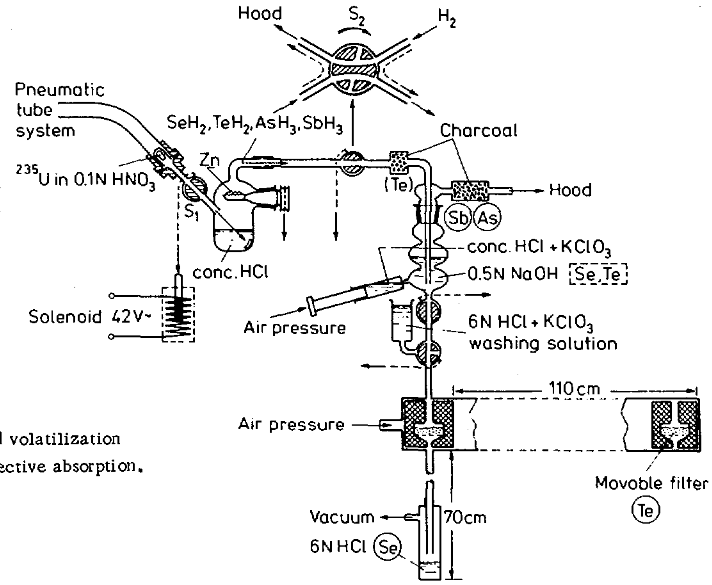

FIG.5. Set-up for rapid volatilization of hydrides and their selective absorption.

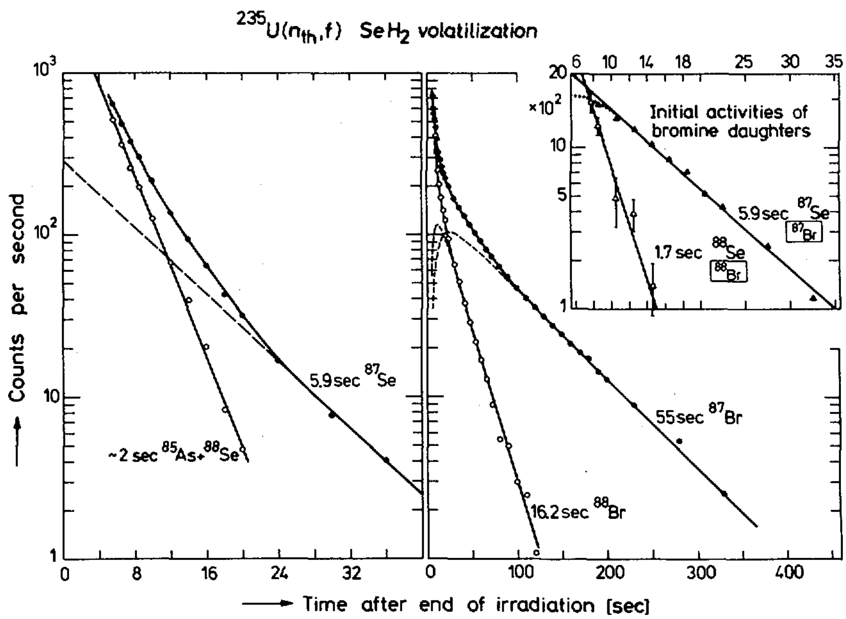

FIG.6. Neutron decay curve of the selenium fraction after volatilization of the hydrides. In the upper corner on the right-hand side, the initial activities of bromine daughters are shown, resulting from selenium separations with time delay.

of the selenium fraction as shown in the left part of Fig.6. Hence, ^{87}Se and ^{88}Se are identified as delayed neutron precursors. Some difficulties arose in the interpretation of the 2-s component because of a contamination by 2.1 s ^{85}As as a few percent of arsenic accompany selenium. The true contribution of ^{88}Se was obtained by varying the yields of selenium compared to that of arsenic, as mentioned in section 2 for the 2-s alkali activity.

Similar measurement of the tellurium fraction gave some evidence for weak delayed neutron activities with half-lives of about 20 s and 3 s which may be assigned to ^{136}Te and ^{137}Te. However, further work is required in order to confirm this conclusion.

5. HALF-LIVES AND MASS ASSIGNMENTS

In addition to neutron decay curves, gamma-ray spectra were measured with Ge(Li) detectors in some fractions obtained as outlined in the preceding sections. From these data and from the neutron decay curves, half-lives and mass assignments of several delayed neutron precursors and their ancestors were directly or indirectly obtained, as summarized in Table I.

6. DELAYED NEUTRON YIELDS

One aim of our work is to determine the contributions of individual precursors to the delayed neutron groups in fission of ^{235}U by thermal neutrons. Since halogen precursors were known to exist in the four longest groups [8] we measured - as a first step - the total contributions of bromine and iodine precursors to these groups. This was done by removing both elements from the irradiated solution by exchange with silver chloride and by counting the filtrate. The decay curves found were compared with those of unseparated samples after normalization to the same number of fissions deduced from the ^{99}Mo activities which were produced in both series of experiments. The breakthrough of the halogens into the filtrate, typically amounting to about 4%, was measured with ^{82}Br and ^{131}I tracers, and corrections were applied.

The results summarized in Table II show that both the 55-s and 22-s groups consist nearly exclusively of halogens whereas non-halogens contribute considerably to the two other groups. Hence, the 55-s group stems from ^{87}Br, and the 22-s group from ^{88}Br and ^{137}I. A possible contribution of the 35-s isomer of ^{136}I [9, 10] was checked by producing this isomer by the ^{136}Xe (n, p)^{136}I reaction, but no neutron emission was found.

The relative contributions of ^{88}Br and ^{137}I to the 22-s group were measured in two different ways. First, the late part of the neutron decay curves of unseparated samples was resolved by computer analysis into 55-s ^{87}Br, 16.3-s ^{88}Br, and 24.4-s ^{131}I. This gave the following contributions to the 22-s group:

$$36.3 \pm 2.3\% \ ^{88}\text{Br, and}$$
$$63.7 \pm 2.3\% \ ^{137}\text{I.}$$

In the second series, chemical separations were applied. ^{137}I was separated by exchange with silver iodide, and both, ^{137}I and ^{88}Br, were separated with silver chloride. By comparing these curves, which are

TABLE I. SUMMARY OF HALF-LIVES

Nuclide	Half-life (s)	Nuclide counted	Technique [a]	Half-life Literature (s)
^{83}As	13.3 ± 0.4	^{83}As	γ	14.1 ± 1.1 [i]
^{84}As	~5.6	^{84}As	γ	5.8 ± 0.5 [i]
^{84}As	6 ± 1	^{84}Se	γ	
^{85}As	~2.1	^{85}As	n	2.028 ± 0.012 [b]
^{87}As	~1	^{87}Br	n	
^{86}Se	16.7 ± 0.3	^{86}Se	γ	
^{86}Se	16.5 ± 0.5	^{86}Br	γ	
^{87}Se	5.9 ± 0.2	^{87}Se	n	5.8 ± 0.5 [b]
^{87}Se	5.9 ± 0.2	^{87}Br	n	
^{88}Se	~2	^{88}Se	n	
^{88}Se	1.7 ± 0.5	^{88}Br	n	
^{91}Br	~0.5	^{91}Br	n	0.64 ± 0.07 [g]
^{93}Rb	~5.9	^{93}Rb	n	5.6 ± 0.5 [c]
				5.1 ± 0.3 [d]
				5.89 ± 0.04 [d]
				5.86 ± 0.13 [e]
^{94}Rb	~2.3	^{94}Rb	n	2.67 ± 0.04 [f]
^{140}I	0.8 ± 0.2	^{140}I	n	0.86 ± 0.04 [g]
^{141}I	~0.4	^{141}I	n	0.43 ± 0.08 [g]
^{135}Te	16.6 ± 0.9	^{135}Te	γ	18 ± 2 [h]
^{136}Te	20.9 ± 0.5	^{136}Te	γ	33 [k]
^{137}Te	~3.5	^{137}Te	γ, n	
^{137}Te	3.5 ± 0.5	^{137}I	n	

[a] n: from neutron decay curves
γ: from gamma-ray spectra
[b] TOMLINSON and HURDUS [13]
[c] FRITZE and KENNETT [15]
[d] WAHL et al. [14]
[e] TALBERT et al. [6]
[f] AMAREL et al. [16]
[g] PATZELT et al. [7]
[h] DENSCHLAG [20]
[i] del MARMOL [21]
[k] WUNDERLICH [22]

normalized to the same number of fissions and corrected for chemical yields, the following values were found:

$$35.4 \pm 2.3\%\ ^{88}\mathrm{Br}, \text{ and}$$
$$64.6 \pm 2.2\%\ ^{137}\mathrm{I}.$$

From these values and from the absolute yield of the 22-s group, 34.6 ± 1.8 neutrons/10^4 fissions [11], the absolute neutron yields of ^{88}Br and ^{137}I were obtained. The results are given in Table III, together with the weak contributions of other precursors.

TABLE II. CONTRIBUTIONS OF NON-HALOGENS TO THE FOUR LONGEST GROUPS

Group	Contribution (%)
55-s	0.4 ± 1.0
22-s	2.3 ± 1.5
6-s	23 ± 5
2-s	44 ± 10

The absolute yields of ^{88}Br and ^{137}I are the basis for calculating the absolute yields of other precursors whose intensities were measured relative to these standard nuclides. For the halogens, the relative intensities were derived from the decay curves of bromine and iodine fractions isolated as described in sections 2 and 3. Alkali precursors were measured relative to the halogen contamination in alkali fractions, and selenium and tellurium precursors relative to their halogen daughter products. Comparison of the neutron yields of individual precursors with the group yields [11] finally gives the contributions, in per cent.

The results are shown in Table III including some data obtained by other investigators. In the 6-s group ^{93}Rb is observed to be a main constituent whereas the contribution of ^{87}Se is small. Here and in the following groups, the sum of the neutron yields found for the precursor nuclides is in reasonable agreement with the group yields obtained by Keepin et al. [11].

The 2-s group is more complex even if some minor components are omitted which contribute less than 1% to the group yield. In addition to precursors discussed in preceding sections, a weak neutron activity was found in the yttrium fraction isolated by extraction with bis (2-ethylhexyl) orthophosphoric acid; possible mass numbers are 98 or 99. A search for neutron precursors among the alkaline earths, zirconium, niobium, and molybdenum gave negative results.

Preliminary results for the two shortest periods are also given in Table III. Since some of the precursor half-lives are rather uncertain, both groups are considered together. This last part of Table III should merely indicate that the present estimates of the precursor yields are compatible with the group yields.

From the general agreement of the sum of precursor yields with the group yields it may be concluded that the main delayed neutron precursors have been identified by now. It should, however, be emphasized that, apart from experimental errors, considerable uncertainties are involved when yields of precursors having definite half-lives are compared with those of a rather complex group of nuclides characterized by an average half-life.

TABLE III. DELAYED NEUTRON YIELDS

	Half-life [sec]	Nuclide		Delayed neutron yield (n/10^4 f)
55-s group				
	54.5	^{87}Br		5.6 ± 0.3
		sum		5.6 ± 0.3
		unseparated sample:	this work	5.9 ± 0.9
			Keepin	5.2 ± 0.5 [a]
22-s group				
	16.3	^{88}Br		12.1 ± 1.5
	24.4	^{137}I		21.7 ± 2.6
	20	^{136}Te		~1.2
	24.9	^{141}Cs		0.34 ± 0.05 [b]
		sum		35.3 ± 3.0
		unseparated sample:	this work	34.6 ± 1.8 (normalized)
			Keepin	34.6 ± 1.8
6-s group				
	5.9	^{87}Se		0.34 ± 0.11
	4.4	^{89}Br		17.7 ± 4.2
	6.2	^{93}Rb		6.6 ± 1.7
	6.3	^{138}I		0.8 ± 1.9
	3.5	^{137}Te		~0.7
		sum		33.3 ± 4.9
		unseparated sample:	this work	31.5 ± 5.4
			Keepin	31.0 ± 3.6
2-s group				
	2.03	$^{85/86}$As		7.7 ± 0.8 [c]
	1.7	^{88}Se		0.32 ± 0.16
	1.6	^{90}Br		14.3 ± 3.5
	1.3	^{93}Kr		1.41 ± 0.27 [b]
	2.3	^{94}Rb		16.9 ± 3.5
	2.3	$^{(98)}$Y		1.8 ± 0.9
	1.7	^{135}Sb		3.5 ± 0.3 [d]
	2.0	^{139}I		9.9 ± 2.2
	1.94	^{142}Cs		0.65 ± 0.19 [b]
		sum		56.5 ± 5.6
		unseparated sample:	this work	60.2 ± 7.8
			Keepin	62.4 ± 2.6
0.6- and 0.2-s group				
	~0.5	^{91}Br		1.8 ± 0.7
	0.36	^{95}Rb		4.6 ± 0.7 [e]
	0.23	^{96}Rb		1.7 ± 0.3 [e]
	0.14	^{97}Rb		1.0 ± 0.5 [e]
	~0.8	$^{(99)}$Y		10 ± 10 [f]
	0.8	^{140}I		6.4 ± 3.5
	0.4	^{141}I		2.1 ± 0.7
		sum		27.6 ± 10.6
		unseparated sample:	this work	26.0 ± 2.1
			Keepin	24.8 ± 2.3

[a] KEEPIN [2]
[b] TALBERT et al. [6]
[c] Average of values from TOMLINSON [13], del MARMOL [17], and this work
[d] TOMLINSON [13]
[e] AMAREL et al. [5]
[f] ROECKL et al. [23]

7. NEUTRON EMISSION PROBABILITIES

In addition to the absolute neutron yields the neutron emission probabilities P_n are of interest. These values can be derived by dividing the neutron yields by the cumulative fission yields of the precursor.

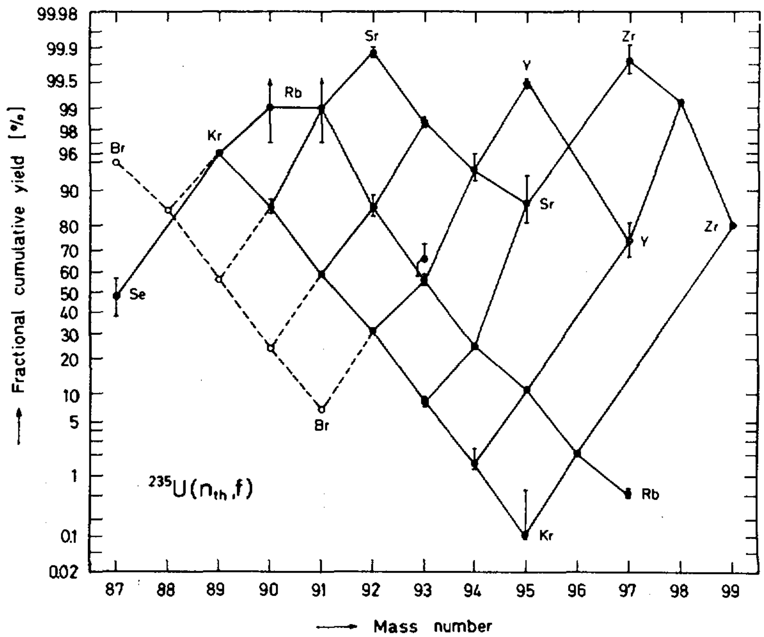

FIG. 7. Network for extrapolation of fractional cumulative mass yields (light fragments).

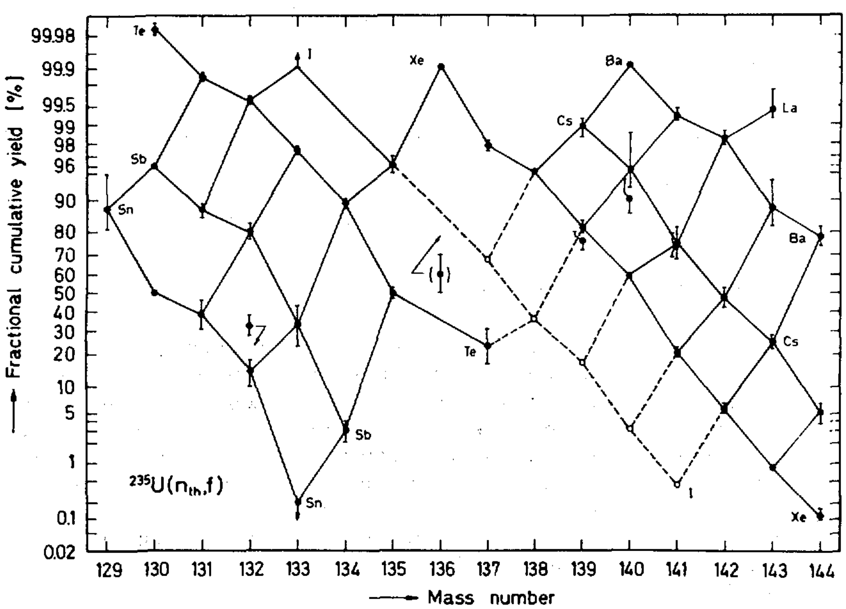

FIG. 8. Network for extrapolation of fractional cumulative mass yields (heavy fragments).

TABLE IV. NEUTRON EMISSION PROBABILITIES P_n (%)

Nuclide	Neutron yield ($n/10^4$ f)	Cumulative yield (%)	P_n (%)	P_n (%) Literature
^{87}Se	0.34 ± 0.11	1.2	0.3 ± 0.1	≤ 0.8 [a]
^{88}Se	0.32 ± 0.16	0.8	0.4 ± 0.2	
^{87}Br	5.6 ± 0.3	2.4	2.4 ± 0.1	3.1 ± 0.6 [b]
^{88}Br	12.1 ± 1.5	3.0	4.0 ± 0.5	6.0 ± 1.6 [b]
^{89}Br	17.7 ± 4.2	2.7	6.7 ± 1.6	7 ± 2 [b]
^{90}Br	14.3 ± 3.5	1.4	10.4 ± 2.5	
^{91}Br	1.8 ± 0.7	0.4	4.5 ± 1.8	
^{93}Rb	6.6 ± 1.7	2.97 [f]	2.2 ± 0.6	1.43 ± 0.18 [c]
				2.6 ± 0.4 [d]
				1.59 ± 0.29 [e]
^{94}Rb	16.9 ± 3.5	1.52 [f]	11.1 ± 2.3	11.25 ± 1.46 [c]
^{98}Y	1.8 ± 0.9	2.4	0.7 ± 0.4	
^{136}Te	~1.2	2.2	~0.5	
^{137}Te	~0.7	1.2	~0.5	
^{137}I	21.7 ± 2.6	4.2	5.2 ± 0.5	3 ± 0.5 [b]
^{137}I			4.7 ± 1.0 [g]	
^{138}I	8.0 ± 1.9	2.4	3.3 ± 0.8	2.0 ± 0.5 [b]
^{139}I	9.9 ± 2.2	1.1	9.1 ± 2.0	
^{140}I	6.4 ± 3.5	0.2	34 ± 18	
^{141}I	2.1 ± 0.7	0.02	90^{+10}_{-30}	

[a] TOMLINSON and HURDUS [13]
[b] ARON et al. [18]
[c] AMAREL et al. [5]
[d] AMIEL et al. [19]
[e] TALBERT et al. [6]
[f] CHAUMONT et al., private communication (1969) [24]
[g] Direct measurement

Most of the cumulative fission yields required are unknown, but have to be estimated from fata for adjacent nuclides. For this purpose, known or interpolated mass yields were multiplied with fractional cumulative yields extrapolated by an empirical method shown in Fig.7 for the light and in Fig.8 for the heavy fragments: when fractional cumulative yields are plotted in a probability scale versus mass number a network of nearly straight lines results for isotopes and isotones. Their cross-points serve for extrapolation of unknown yields. Another approach to estimate such yields has been applied by Wahl et al. [12] to derive P_n -values.

Our results are listed in Table IV and compared with P_n -values obtained by more or less direct measurements. With a few exceptions

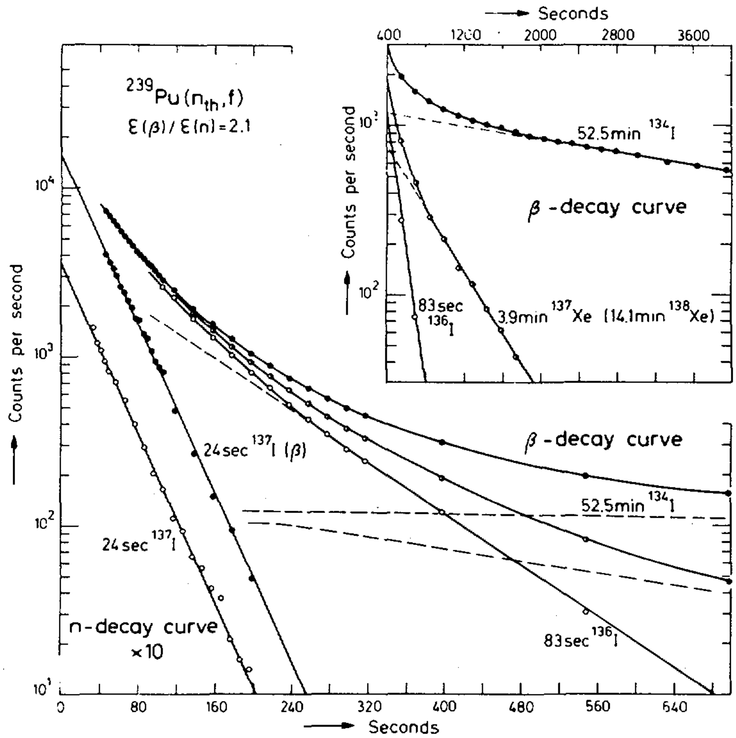

FIG.9. Neutron and beta decay curve of the iodine fraction separated by isotope exchange 20 s after the end of irradiation (direct measurement of the P_n value of ^{137}I).

the results agree within error limits. For most of the nuclides studied the P_n -values lie about 10% below the values directly measured. On the other hand, the P_n -values of ^{140}I and ^{141}I are extremely high. This may indicate that the cumulative yields decrease less steeply than was assumed in Fig.8. Since discrepancies were found between the P_n -value of ^{237}I obtained in this work and that reported in literature we have compared the beta and neutron decay rates of ^{137}I formed in fission of ^{239}Pu by thermal neutrons. The corresponding decay curves are shown in Fig.9. Preliminary analysis of these curves corroborates the P_n -value deduced indirectly.

ACKNOWLEDGEMENTS

This work has been supported by the Bundesministerium für wissenschaftliche Forschung.

REFERENCES

[1] HERRMANN, G., FIEDLER, J., BENEDICT, G., ECKHARDT, W., LUTHARDT, G., PATZELT, P., SCHÜSSLER, H.D., in Physics and Chemistry of Fission (Proc. Symp. Salzburg, 1965) 2, IAEA, Vienna (1965) 197.

[2] KEEPIN, G.R., Physics of Nuclear Kinetics, Addison-Wesley Publishing Comp., Inc., Reading (Massachusetts), Palo Alto, London (1965) 73.
[3] SCHÜSSLER, H.D., GRIMM, W., WEBER, M., THARUN, U., DENSCHLAG, H.O., HERRMANN, G., Nucl. Instrum. Methods (1969) in press.
[4] HERRMANN, G., DENSCHLAG, H.O., Ann. Rev. nucl. Sci. (1969) in press.
[5] AMAREL, I., GAUVIN, H., JOHNSON, A., J. inorg. nucl. Chem. 31 (1969) 577.
[6] TALBERT jr., W.L., TUCKER, A.B., DAY, G.M., Phys. Rev. 177 (1969) 1805.
[7] PATZELT, P., AHRENS, H., HERRMANN, G., Proc. Radioanalytical Conference, Stary Smokevec (1968) in press.
[8] PERLOW, G.J., STEHNEY, A.F., Phys. Rev. 113 (1959) 1269.
[9] LUNDAN, A., SIIVOLA, A., Annales Academiae Scientiarum Fennicae A VI (1968) 287.
[10] DENIG, R., TRAUTMANN, N., private communication (1969).
[11] KEEPIN, G.R., WIMETT, T.F., ZEIGLER, R.K., Phys. Rev. 107 (1957) 1044.
[12] WAHL, A.C., NORRIS, A.E., ROUSE, R.A., WILLIAMS, J.C., these Proceedings.
[13] TOMLINSON, L., HURDUS, M.H., J. inorg. nucl. Chem. 30 (1968) 1649, 1995.
[14] WAHL, A.C., NORRIS, A.E., FERGUSON, R.L., Phys. Rev. 146 (1966) 931.
[15] FRITZE, K., KENNETT, T.J., Can. J. Phys. 38 (1960) 1614.
[16] AMAREL, I., BERNAS, R., FOUCHER, R., JASTRZEBSKI, I., JOHNSON, A., TEILLAC, I., GAUVIN, H., Physics Lett. B24 (1967) 402.
[17] del MARMOL, P., NEVE de MEVERGNIES, M., J. inorg. nucl. Chem. 29 (1967) 273.
[18] ARON, P.M., KOSTOCHKIN, O.I., PETRZHAK, K.A., SHPAKOV, V.I., Soviet J. atom. Energy 16 (1965) 447.
[19] AMIEL, S., GILAT, J., NOTEA, A., YELLIN, E., in Delayed Fission Neutrons,(Proc. Panel Vienna, 1967) IAEA, Vienna (1968) 115.
[20] DENSCHLAG, H.O., J. inorg. nucl. Chem. (1969) in press.
[21] del MARMOL, P., J. inorg. nucl. Chem. 30 (1968) 2873.
[22] WUNDERLICH, F., Radiochim. Acta 7 (1967) 105.
[23] ROECKL, E., EIDENS, J., ARMBRUSTER, P., Z. Physik 220 (1968) 101.
[24] CHAUMONT, J., ROECKLE, E., NIR-EL, Y., KLAPISCH, R., to be published.

DISCUSSION

L. TOMLINSON: We are carrying out an investigation of delayed neutron emission from selenium isotopes similar to that reported in the paper by Schüssler. Our preliminary results are as follows:

	Half-life (s)	P_n (%)
^{87}Se	5.8	0.2 ± 0.1
^{88}Se	~ 1.4	Not yet evaluated

The results agree quite well with those given in the present paper and also those given in the abstract of del Marmol and Perricos (SM-122/69).

SEARCH FOR LONG-LIVED DELAYED NEUTRON GROUPS: PHOTOFISSION CAUSED BY FISSION-PRODUCT GAMMA-RAYS

L. TOMLINSON, M.H. HURDUS
Atomic Energy Research Establishment,
Harwell, Berks,
United Kingdom

Abstract

SEARCH FOR LONG-LIVED DELAYED NEUTRON GROUPS: PHOTOFISSION CAUSED BY FISSION-PRODUCT GAMMA-RAYS. A search has been made for long-lived delayed neutron groups with half-lives greater than 55 s in the thermal neutron fission of ^{235}U. The neutron counter used in these experiments was designed to allow one to distinguish between true delayed neutrons and neutrons produced by (γ, n) reactions on D and Be impurities. The experimental results showed the existence of apparent delayed neutron groups with half-lives greater than 55 s and of very low intensity. These were shown to be neither true delayed neutrons, nor photoneutrons from D or Be but were prompt neutrons from the photofission of ^{238}U and ^{235}U. Photofission is produced by high energy (> 4.5 MeV) gamma rays emitted from certain fission products. The intensity of the neutrons produced in this way decays with the half-lives of the fission products causing the photofission. The half-lives of the "photofission groups" were 3.1, 17 and 111 min, with absolute yields of 1×10^{-8}, 1×10^{-11} and 2×10^{-12} neutrons/fission respectively, under the best conditions. By surrounding the irradiated uranium sample with large amounts of ^{238}U, ^{235}U or ^{239}Pu, it was possible to obtain relative photofission cross-sections for these nuclides. The values obtained were: 1.0, 1.4 and 10.8 for ^{238}U, ^{235}U and ^{239}Pu respectively, in agreement with known cross-sections. It is unlikely that photofission groups with $t_{\frac{1}{2}} \geq 3.1$ min will, under any experimental or reactor conditions, be a significant fraction of the total delayed neutron yield. However, shorter-lived photofission groups ($t_{\frac{1}{2}} < 3$ min) may be important, but their yields cannot be estimated at present because of a lack of data. The most favourable case is ^{239}Pu, where the photofission cross-section is high and the delayed neutron yield is low compared to other nuclides. From the experimental results, upper limit values were calculated for the neutron branching ratios of ^{91}Rb, ^{140}Cs, ^{96}Y, and ^{133}Sb. These were: $\leq 0.7\%$, $\leq 0.1\%$, $\leq 5 \times 10^{-6}\%$ and $\leq 3 \times 10^{-6}\%$, respectively.

1. INTRODUCTION

Two previous searches have been made for long-lived delayed neutron groups with half-lives greater than 55 seconds. Kunstadter, Floyd and Borst [1] discovered long-lived delayed neutron groups during studies of the decrease in neutron flux, after shut-down of a uranium-graphite reactor. The groups had half-lives of 3, 12 and 125 min. and yields of 5.8×10^{-8}, 5.6×10^{-10} and 2.9×10^{-10} neutron per fission respectively. Later Kane, Kephart and Hammel [2], using ^{235}U foils, found that the yields of these groups were at least an order of magnitude lower than reported by Kunstadter et al [1] and doubted if they existed at all. It was suggested that the long-lived delayed neutron groups were probably photoneutrons produced by fission product gamma-rays interacting with deuterium in the small quantities of hydrogeneous material present.

Various theoretical predictions have been made of delayed neutron precursors produced in ^{235}U fission. Pappas and Rudstam [3] predict delayed neutron emission from fission products at lower mass numbers than in any other theoretical treatment. They successfully predict all the known delayed neutron precursors, and many others besides - including several precursors with half-lives greater than 55 seconds: ^{91}Rb (58 sec.), ^{140}Cs (64 sec.), ^{96}Y (2.3 mins.) and ^{133}Sb (2.7 min.). Theoretical considerations thus indicate that delayed neutron precursors with half-lives up to about 3 min. are possible, but precursors with half-lives of 12 and 125 min. are extremely unlikely.

In order to clarify the present situation, a new search has been made for long-lived delayed neutron groups in the thermal neutron fission of ^{235}U. The results are reported in the present paper. The neutron counter used in this work was designed to allow one to distinguish between true delayed neutrons and neutrons produced by (γ,n) reactions on D or Be present in the counter.

2. EXPERIMENTAL

2.1 Method of irradiation

Uranium samples were irradiated at the centre of the BEPO reactor at a thermal neutron flux of 1.40×10^{12} n cm^{-2} sec^{-1}. They were then withdrawn horizontally from the reactor along a shielded tube to a neutron counter situated 4.8 m from the reactor face. The tube used to transport the uranium samples contained several holes at the end inside the reactor. As the reactor was air-cooled and at a pressure below atompsheric, air was drawn down the tube into the reactor. This air flow, together with some helium injected through the end of the neutron counter, were sufficient to draw the uranium samples into the reactor centre. The air flow kept the surface temperature of the samples at about 190°C.

The samples were withdrawn using 0.5 mm diameter, annealed, iron wire. This was made from high purity iron (impurities: Mn 3 ppm, Si 3 ppm) to keep the level of radioactivity as low as possible. 21.4 g of uranium (isotopic composition: ^{235}U 80%, ^{238}U 19%, ^{234}U 1%) were used in the experiments. This was in the form of an alloy with aluminium containing 27% by weight of U. The alloy was contained in three stainless steel cans (1.9 cm diameter, 6.5 cm long) and formed a 3 mm thick sleeve inside each can.

2.2 Neutron counter

The neutron counter was based on a conventional system using BF_3 counters surrounded by paraffin. However, intense gamma-rays from the irradiated uranium samples cause two difficulties:

(a) Pulse pile-up of small gamma-ray pulses result in gamma-rays being counted as well as neutrons.

(b) The number of neutrons produced by $D(\gamma,n)$ reactions in the paraffin becomes significant at high gamma fluxes.

From previous experience [4], it was calculated that under the conditions of our experiment, the gamma-ray flux at the BF_3 tubes should not exceed 100-200 mR/hr if errors from the above sources were to remain small. Lead shielding was therefore introduced between the uranium samples and the paraffin moderator to reduce the gamma flux to an acceptable level. A sectional view of the final counter design is given in Fig. 1.

Fourteen high pressure BF_3 tubes (2.5 cm diameter) were connected in series with low capacitance cable and arranged symmetrically around the uranium samples. Pulses from the counters were fed via amplifiers and a discriminator to an automatic counting system. To reduce pile-up effects to a minimum the counters were operated at a gas amplification of 30 and near the edge of the plateau. To ensure that the gamma flux at the BF_3 tubes did not reach an excessive level, an ion chamber was installed (Fig. 1) to monitor this flux during an experiment.

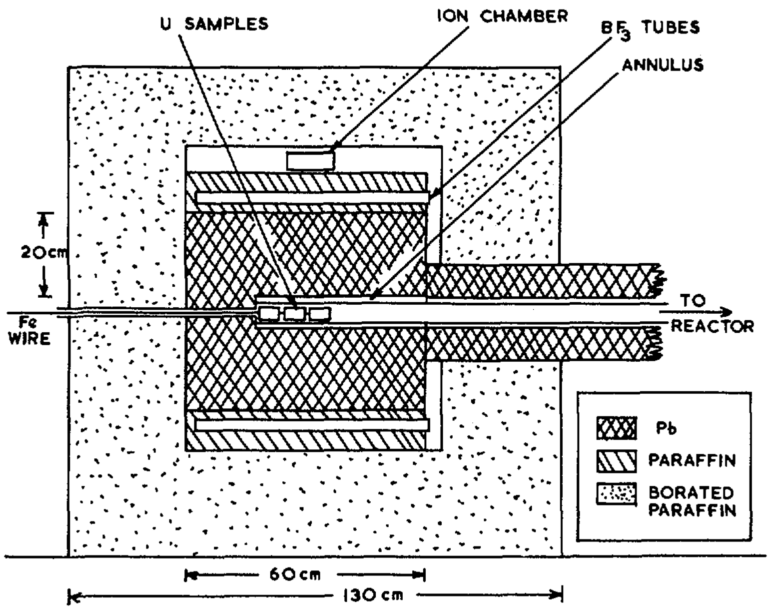

FIG. 1. Neutron counter (sectional view).

Both D and Be have sufficiently low thresholds (2.2 and 1.67 MeV respectively) that photoneutrons can be produced by interaction with fission product gamma-rays. Great care was therefore taken to exclude all hydrogeneous and beryllium-containing materials from the region of high gamma flux in the centre of the counter. All materials present in this region were analysed for Be using the (γ,n) method described by Iredale [5]. The detection limits of the method for various materials were (ppm): 0.1 mild steel, 0.6 U/Al, 0.04 Pb, 0.1 stainless steel (cans). No Be was detected in any material.

In order to detect low-intensity, long-lived delayed neutron groups, it was essential to reduce the background count rate to a low value. After surrounding the counter on all sides with cadmium sheet and 20-30 cm of borated paraffin and polythene, the background was reduced from 7,000 c/min. to an acceptable 100 c/min. Spurious pulse pick-up from the mains supply was eliminated by installing a separate mains generator.

The normal thickness of lead between the uranium samples and the paraffin moderator was 20 cm. Provision was made for increasing this to 21.3 cm by placing a lead sleeve in the counter annulus (Fig. 1). By carrying out experiments with and without the lead sleeve present, it was possible to distinguish between neutrons originating in the uranium samples and those being formed by photoneutron reactions in the moderator or pulse pile-up in the counters. Thus, the measured intensities of delayed neutron groups originating in the uranium were independent of the lead thickness, whilst those produced in the moderator or counters were reduced in intensity by at least 50% when the lead thickness was increased by 1.3 cm.

2.3 Preliminary experiments

The efficiency of the counter for Ra/Be neutrons was found to be 2.6%. The efficiency for delayed neutrons is probably higher than this because of their lower energy. However, an absolute efficiency is not required for the present work as the 55 sec. delayed neutron group can be used as a standard.

The gamma sensitivity of the counter was checked as far as possible with gamma-rays from ^{28}Al (1.78 MeV) and ^{24}Na (1.37 and 2.75 MeV). The highest strength sources which could be prepared, gave gamma fluxes at the BF_3 tubes of 20 and 40 mR/hr with ^{28}Al and ^{24}Na, respectively. In neither case did the high gamma flux cause an observable change in the background count rate.

2.4 Experimental procedure

The uranium samples were loaded into the centre of the reactor as described previously (section 2.1). After the desired irradiation time, they were withdrawn to the reactor face in a time of 10 seconds. It was possible to estimate to $\pm$ 2 seconds, the time at which the samples left the reactor core. After a cooling time of 15 minutes at the reactor face, they were finally drawn into the counter and the decay of neutron activity followed. The gamma flux was also monitored at various times.

The efficiencies of the neutron counter and ion chamber were checked at frequent intervals during the experimental programme and the background was measured separately for each run.

2.5 Photoneutrons and photofission

To study beryllium photoneutrons, 0.84 gm of beryllium in the form of a 2% Be/Cu foil was placed in the counter annulus (Fig. 1) with the lead sleeve absent. 0.5 ml of D_2O was placed in a similar position when deuterium photoneutrons were required. To study the production of photoneutrons from ^{13}C, 660 gm of graphite in the form of ten 1 cm diameter rods were placed in the counter annulus.

Studies of photofission induced by gamma rays from the uranium samples were made by removing the lead sleeve from the counter and replacing by the materials given in Table I.

3. RESULTS

3.1 Search for long-lived delayed neutron groups

A series of experiments were carried out using irradiation times of 12, 50 and 280 min; these times being chosen to emphasize the 3, 12 and 125 min. long-lived delayed neutron groups found previously [1]. Four experiments were carried out at each time, two with, and two without the lead sleeve present.

During the course of these experiments, it was found that the presence of the uranium samples in the counter, caused the background to increase by about 9 c/min. Calculations indicated that 97% of this neutron emission was due to the ^{27}Al (α,n) reaction in the U/Al alloy caused by ^{234}U α-rays and 3% was due to spontaneous fission of ^{238}U.

TABLE I. PHOTOFISSION EXPERIMENTS

Target material	Form	Weight (kg)	Distance from centre of irradiated U samples (cm)
^{238}U (natural uranium)	3 metal rods, 6.3 mm diam.	0.39	1.7
" " "	10 metal rods, 6.3 mm diam.	2.1	1.9
" " "	Metal sleeve, 4.3 mm thick	2.2	1.9
" " "	Metal sleeve, 10.5 mm thick	6.2	2.2
^{235}U (93% ^{235}U, 6% ^{238}U, 1% ^{234}U)	Metal beads	0.17	1.9
^{239}Pu (94.2% ^{239}Pu, 5.4% ^{240}Pu, 0.4% ^{241}Pu)	Oxide pellets, 10.2 mm diam.	0.29 (Pu)	1.8

The results of the experiments are shown in Fig. 2. It can be seen that long-lived delayed neutron groups were present in addition to the 55 second group. For the 12 and 50 min. irradiation times, the intensities of the long-lived groups were unchanged when the lead sleeve was used in the neutron counter - indicating that these neutrons originated in or near the uranium samples. With a 280 min. irradiation time, the later part of the decay curve appeared to be reduced in intensity, when the lead sleeve was present (Fig. 2) - indicating that some neutron counts were due to gamma-ray pulse pile-up in the BF_3 counters or to D(γ,n) reactions in the paraffin moderator. This is perhaps not surprising as the gamma flux at the BF_3 tubes, in the absence of the lead sleeve, was 100 mR/hr (at a decay time of 2000 sec.) compared to 50 mR/hr with the sleeve present.

3.2 Photoneutrons from beryllium, deuterium and carbon

In spite of the precautions taken whilst building the neutron counter, it was possible that very small amounts of beryllium or deuterium were present in sufficient amounts in the centre of the counter, to produce the observed long-lived delayed neutron groups. The photoneutron decay curves for beryllium and deuterium were therefore measured to see if they were of the same shape as the long-lived delayed neutron curve. The results (after subtracting the delayed neutron contribution) are shown in Fig. 3. For the same irradiation time, the decay curves for beryllium and deuterium photoneutrons are almost identical in shape.

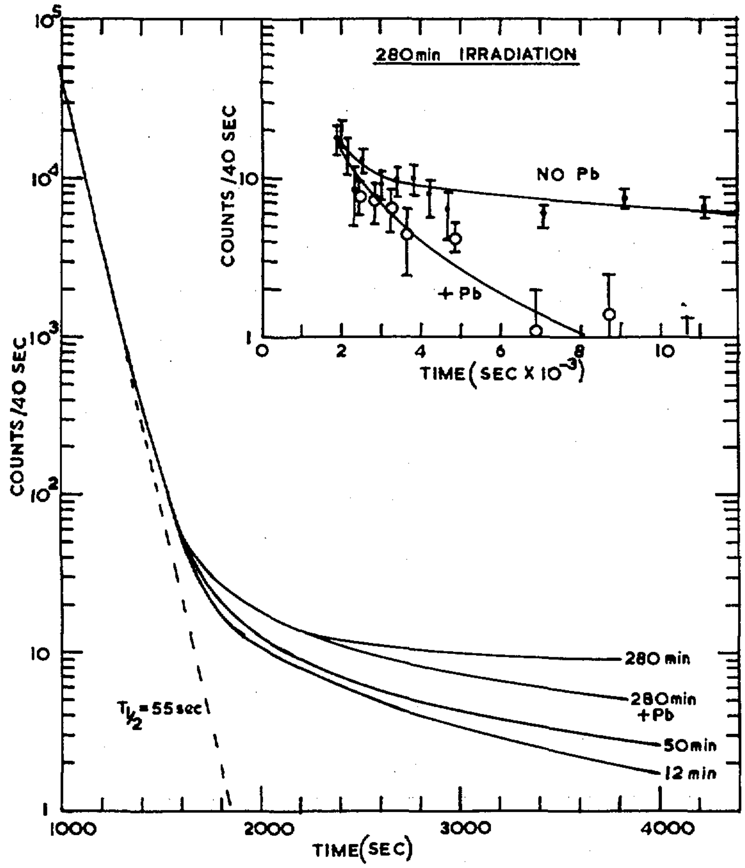

FIG. 2. Decay curves for various irradiation times. "+Pb" indicates that the lead sleeve was present. The decay curves for the 280 min irradiations are shown inset for long cooling times. These curves show the individual points - with errors - and are typical of all the curves.

In Fig. 4 the decay of the long-lived delayed neutrons (55 sec. delayed neutron group subtracted) is compared with that of beryllium photoneutrons (12 min. irradiation time). It can be seen that the two curves are of completely different shape - thus demonstrating that the long-lived delayed neutrons are not due to beryllium (or deuterium) photoneutrons. Similar comparisons at longer irradiation times revealed the same behaviour, with the long-lived delayed neutrons always decaying away more rapidly than the photoneutrons. In spite of the poor statistics it was possible to analyse the long-lived delayed neutron curve (12 min. irradiation time) into two components with half-lives ≃ 3 and 15 min. Although these half-lives were similar to those found by Kunstadter et al [1], the yields were at least 100 times lower.

At this stage of the work, it was concluded that there were 4 possible origins of the long-lived delayed neutron groups:

(a) From new delayed neutron precursors. This was ruled out by the large differences in yields found by different workers. Further-

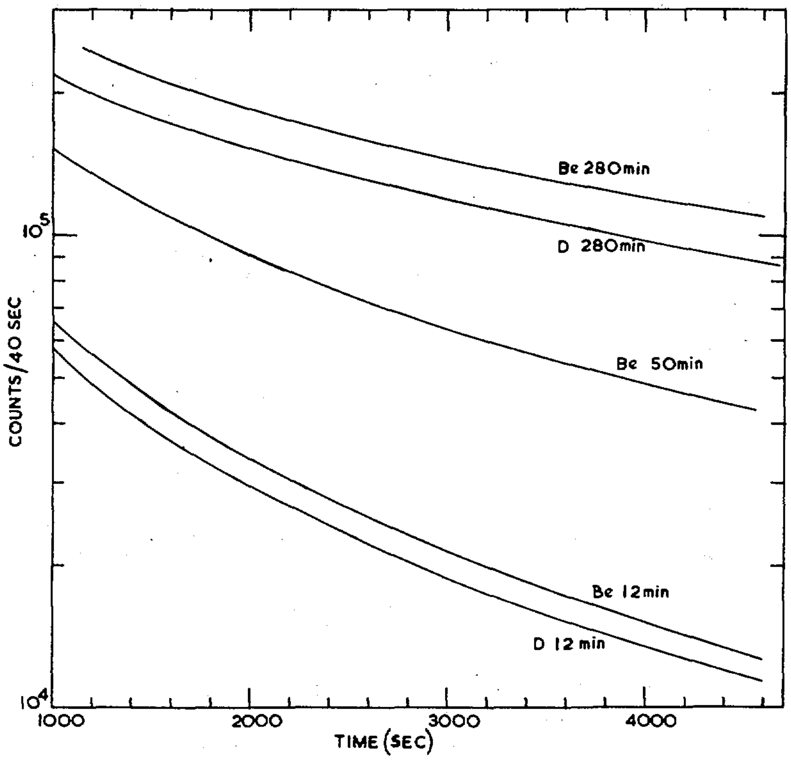

FIG. 3. Photoneutrons from beryllium and deuterium. Irradiation times shown on curves. Because of the high count rates, statistical errors are negligible.

more, from theoretical considerations (section 1), delayed neutron precursors with half-lives greater than 3 min., seem most unlikely.

(b) From the $^{13}C(\gamma,n)$ reaction. The mild steel in the vicinity of the uranium samples contained $\simeq$ 0.3 gm of ^{13}C. The threshold for this reaction is 4.9 MeV but the cross-section is very low and increases only slowly with energy [6].

(c) From ^{235}U and $^{238}U(\gamma,n)$ reactions. The thresholds for these reactions are 5.2 and 6.0 MeV, respectively [7]. The highest energy gamma-rays observed from fission products (at the appropriate time after fission) are $\simeq$ 5.3 MeV [8] and consideration of the Q_β values given in Table III indicates that the theoretical maximum is in the region of 6 MeV. It is possible therefore that some photoneutrons may be produced from ^{235}U, because of its lower threshold, but none are expected from ^{238}U.

(d) Prompt neutrons from the photofission of ^{235}U and ^{238}U. Photofission occurs at lower photon energies than photoneutron emission (Fig. 7 and references [9], [10] and [11]) and therefore seems to be the most likely source of the long-lived delayed neutron groups.

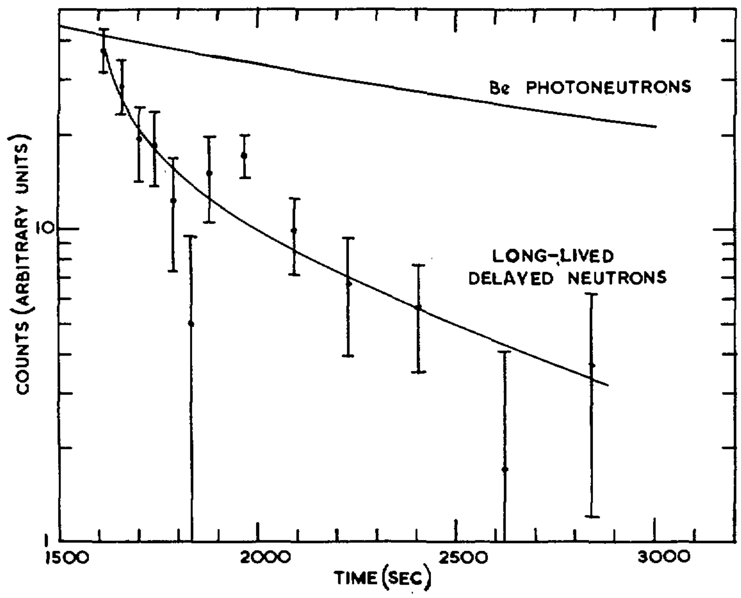

FIG. 4. Comparison of long-lived delayed neutron groups with beryllium photoneutrons (12 min irradiation time).

TABLE II. PHOTOFISSION GROUPS (ERRORS ARE ESTIMATED STANDARD DEVIATIONS)

Half-life (min.)	Absolute yields (neutrons/fission)	
	6.2 kg U sleeve present	No sleeve
3.1 $\pm$ 0.1	1.1 ($\pm$ 0.3) x 10^{-8}	5.2 ($\pm$ 2.0) x 10^{-10}
17 $\pm$ 2	9.6 ($\pm$ 4.0) x 10^{-12}	-
111 $\pm$ 11	2.0 ($\pm$ 0.3) x 10^{-12}	-

In order to test hypothesis (b), graphite was placed in the counter annulus and a 280 min. irradiation carried out. The decay curve obtained was identical to that observed in the absence of graphite - thus ruling out the $^{13}C(\gamma,n)$ reaction as the source of the long-lived delayed neutron groups. This finding agrees with previous work [1].

3.3 Photofission

In order to test hypothesis (d), various amounts of ^{238}U (Table I) were placed in the counter annulus. If the long-lived delayed neutron groups were due to photofission, then the positioning of large amounts of ^{238}U near to the irradiated uranium samples should greatly increase the yields of these groups, without affecting the 55 sec. delayed neutron group. The results (Fig. 5) show that this was exactly what happens, thus establishing the origin of the long-lived delayed neutrons.

The maximum increase in yield obtained by this method was about 20 fold. The proportion of this increase due to neutron multiplication was measured using a neutron source. The presence of the 6.2 kg uranium sleeve (Table I) increased the count rate of a Ra/Be source by 13%, whilst the 2.2 kg sleeve caused an increase of 5%. In all other cases neutron multiplication was negligible.

TABLE III. FISSION PRODUCTS ABLE TO EMIT GAMMA RAYS WITH ENERGIES ABOVE 4 MeV (HALF-LIVES ≥ 2 min.)

Fission product	Half-life (min.)	Theoretical Q_β	Observed gamma rays above 4 MeV (with absolute abundancies)	References
^{88}Rb	168 (^{88}Kr)	4.9	4.75	15
^{142}La	92	5.1		16
^{130}Sb	33, 7	5.8		16
^{94}Y	20	5.4		16
^{104}Tc	18	5.2	4.4, 4.7	16
^{100}Nb	11, 3	6.2		16
^{90}Rb	4.3, 2.6	6.1	4.1 (11%), 4.3 (13%), 4.4 (4%), 4.6 (5%), 5.1 (2%), 5.2 (4%)	17, 16
^{132}Sb	3.1	6.6		18
^{133}Sb	2.7	5.2		18
^{96}Y	2.3	6.8		16
^{148}Pr	2.0	5.1		16

In order to obtain the half-lives of the long-lived delayed neutron groups, measurements were made using long irradiation times with the 6.2 kg uranium sleeve in position. Besides enhancing the yields of these groups, the uranium sleeve also absorbs gamma rays more efficiently than the lead sleeve, so that the maximum gamma flux at the BF_3 counters was only 50 mR/hr (at 2000 sec. decay time - see section 3.1).

The decay curve for the longest irradiation time and its analysis into 3 long-lived components is shown in Fig. 6. The data from all experiments were analysed by least-squares fitting using a computer program. The average half-lives and yields obtained are shown in Table II. Instead of long-lived delayed neutron groups the more appropriate and convenient term "photofission groups" is used.

According to known data, the cross-section for ^{239}Pu photofission by fission product gamma rays should be between 4 to 10 times larger than for ^{238}U (see Fig. 7). For ^{235}U the cross-section for the same reaction should be 1.3 to 2.4 times larger than for ^{238}U - as estimated from values at higher energy [7] and a plot of fissionability versus Z^2/A [9]. 12 min. irradiation experiments were carried out with ^{239}Pu and ^{235}U in the counter

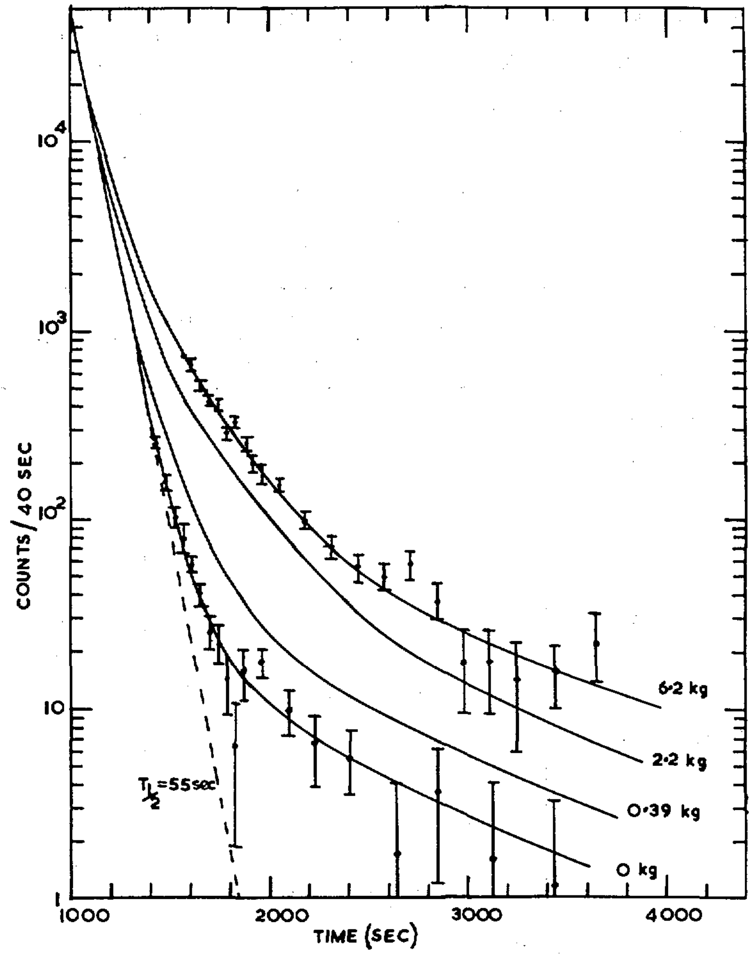

FIG. 5. Photofission effect with ^{238}U (12 min irradiation time; amounts of ^{238}U in the counter annulus are shown on each curve; experimental points are only given for 2 curves, to avoid confusion).

annulus to test these predictions. The presence of plutonium in the counter increased the background from 100 to 72,000 c/min. This required 5 identical experiments to be carried out and the results added together to obtain a reasonable accuracy. About half of the high background was due to ^{240}Pu spontaneous fission and half due to O(α,n) reactions in the oxide [12].

Using the 3.1 min. group for comparison and making allowances for mass, distance, gamma-ray absorption, and neutron multiplication, the relative photofission cross-sections for ^{238}U, ^{235}U and ^{239}Pu were found to be: 1.0, 1.40 $\pm$ 0.36, and 10.8 $\pm$ 1.5 respectively in good agreement with the predictions given above.

From a knowledge of the relative photofission cross-sections and sample geometry, it was possible to estimate the expected count rate of

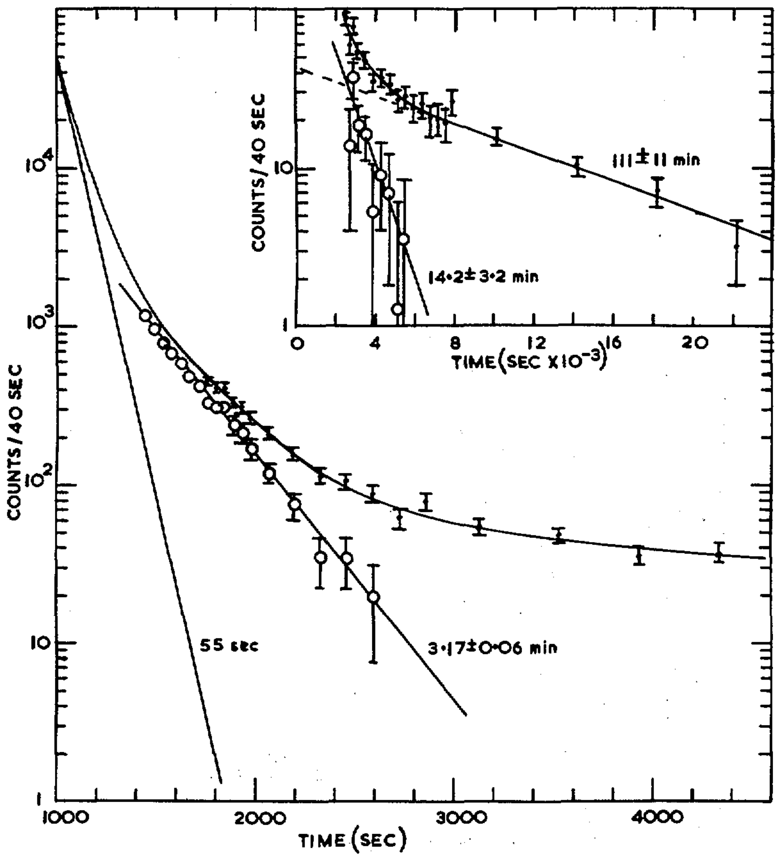

FIG. 6. Decay curve for 436 min irradiation with 6.2 kg ^{238}U in counter annulus (individual components obtained by least-squares analysis; inset is shown the curve at long cooling times).

the 3 min. group for the irradiated uranium samples alone. The estimated value was 16 ± 4 c/40 sec., which compares favourably with the observed 21.5 ± 4 c/40 sec. (at 1,700 sec.).

4. DISCUSSION

The results of this work have confirmed the existence of "delayed-neutron" groups with half lives greater than 55 seconds. The observed group half-lives of 3.1, 17 and 111 min. are in fairly good agreement with the values of 3, 12 and 125 min. found by Kunstadter et al [1]. It has been demonstrated that these "delayed neutron" groups are not due to delayed neutron precursors or to photoneutrons from beryllium or deuterium but are prompt neutrons from the photofission of ^{238}U and ^{235}U. Photofission is caused by high-energy gamma rays emitted from certain fission products.

The yields of the photofission groups observed in the present work are about 100 times less than found by Kunstadter et al [1] (e.g. 5 x 10^{-10}

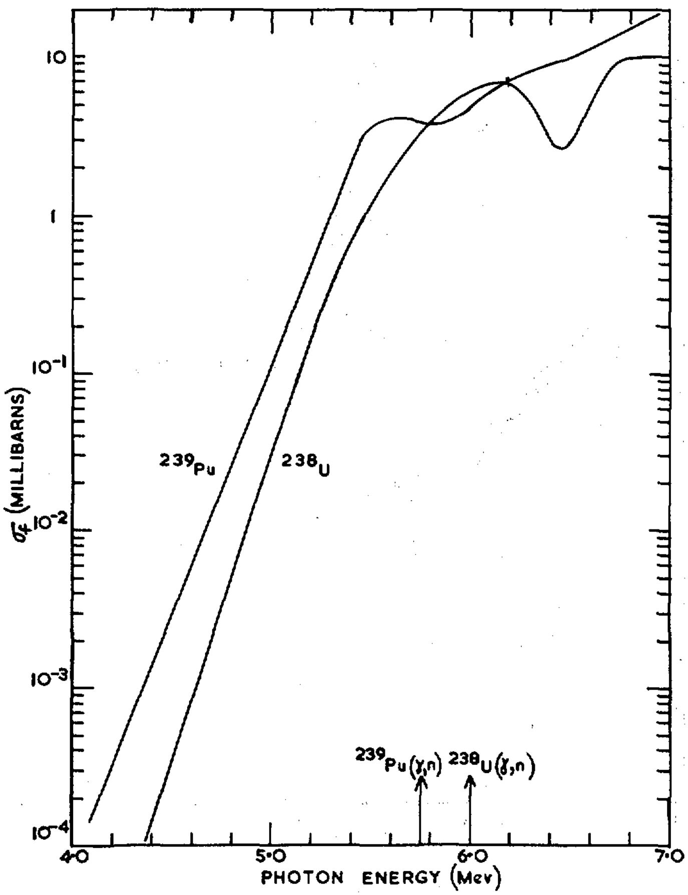

FIG. 7. Low-energy photofission cross-sections for ^{239}Pu and ^{238}U (replotted from Katz, Baerg and Brown [9]).

compared to 6 x 10^{-8} neutron/fission for the 3 min. group). However Kunstadter et al irradiated 3.5 kg of natural uranium compared to 21.4 g of 80% ^{235}U used in the present work. In the former case, about 100 times more uranium was available to undergo photofission than in the latter case and the higher yield is as expected. Kane et al [2], using ^{235}U foils obtained a low yield of photofission groups for the same reason.

Table III gives a list of fission products with half-lives greater than 2 min., which are capable of emitting gamma-rays above 4 MeV and which are probably responsible for the photofission groups. Where no experimental data were available, Q_β values were obtained from two mass equations [13, 14]; those with $Q_\beta \geq 4.9$ MeV were assumed capable of emitting gamma-rays with energies above 4 MeV. (4.9 MeV was arbitrarily chosen as the limit - so that ^{88}Rb was included).

Although few data are available on high energy gamma-rays from individual fission products, the gross gamma spectra of uranium fission products have been measured up to 6 MeV, at various times after fission

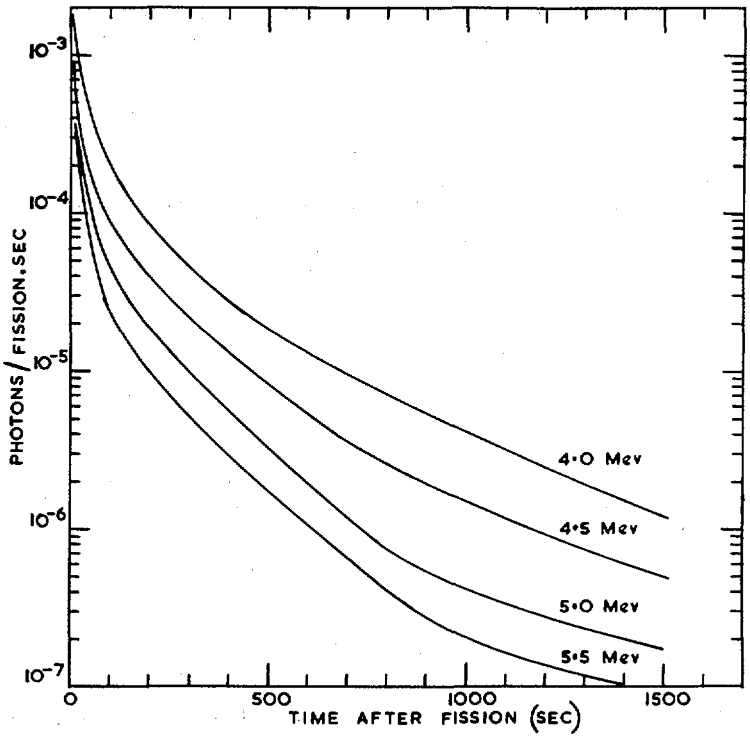

FIG. 8. Decay of gamma rays of various energies from gross fission products (replotted from Maienschein et al.[8]).

[8, 19, 20]. In Fig. 8 the data of Maienschein et al,[8] for 4.0, 4.5, 5.0 and 5.5 MeV gamma-rays are replotted as decay curves. The approximately straight region of the 5.0 and 5.5 MeV curves (between 200 and 800 sec.) has a half-life of 2-3 min. and undoubtedly represents the gamma-rays which produce the 3 min. photofission group.

In the present work, using neutron counting we have only been able to observe photofission groups with half-lives greater than 55 sec. because any shorter-lived groups would have been masked by the delayed neutrons. From a study of the gross gamma-ray decay curves (Fig. 8), it is obvious that there must be many photofission groups with half-lives less than 3 min. As the half-lives of the gamma emitters become shorter, so the average energy of the gamma rays will increase and hence the cross-section for photofission will increase (Fig. 7). Some of the highest energy gamma rays, such as those up to 6.7 MeV from ^{86}Br and ^{87}Br [21], may also be above the threshold for U and Pu(γ,n) reactions and cause some photoneutron emission.

From the data available at present, it seems unlikely that photofission groups with $t_{\frac{1}{2}} \geqslant 3.1$ min. will, under any experimental or reactor conditions, be a significant fraction of the total delayed neutron yield. However, shorter-lived photofission groups ($t_{\frac{1}{2}} < 3.1$ min.) may be important, but their yields cannot be estimated until we have more knowledge of fission product gamma-ray emission and photofission cross-sections. Photofission groups are most likely to be a significant fraction of the total delayed neutron yield in the case of ^{239}Pu - where the photofission cross-section is high and the total delayed neutron yield is low - compared to most other nuclides.

From the observed count rate of the irradiated uranium samples at a decay time of 1,700 sec., one can calculate an upper limit for the neutron branching ratio (Pn) of possible delayed neutron precursors with half-lives greater than 55 sec. After subtracting out the calculated contribution of photofission (section 3.3), the following Pn values were obtained:

^{91}Rb (58 sec.) $\leqslant 0.7\%$; ^{140}Cs (64 sec.) $\leqslant 0.1\%$; ^{96}Y (2.3 min.) $\leqslant$ $5 \times 10^{-6}\%$; ^{133}Sb (2.7 min.) $\leqslant 3 \times 10^{-6}\%$.

ACKNOWLEDGEMENTS

We are indebted to the following for assistance and encouragement during the course of this work: Mr. D. K. Cartwright, Mr. G. N. Walton, Mr. E. Mitchell and the BEPO reactor staff.

REFERENCES

[1] KUNSTADTER, J. W., FLOYD, J. J., BORST, L. B., Phys. Rev. 91 (1953) 594.

[2] KANE, W. R., KEPHART, J. F., HAMMEL, J. E., (unpublished); abstract given by KEEPIN, G. R., Progress in Nuclear Energy, Series 1, Vol. 1, Pergamon, London (1956).

[3] PAPPAS, A. C., RUDSTAM, G., Nucl. Phys. 21 (1960) 353.

[4] CARTWRIGHT, D. K., private communication.

[5] IREDALE, P., UKAEA Rep. AERE-EL/M 108 (1960).

[6] COOK, B. C., Phys. Rev. 106 (1957) 300.

[7] HUIZENGA, J. R., CLARKE, K. M., GINDLER, J. E., VANDENBOSCH, R., Nucl. Phys. 34 (1962) 439.

[8] MAIENSCHEIN, F. C., PEELLE, R. W., ZOBEL, W., LOVE, T. A., Proc. 2nd Int. Conf. on the Peaceful Uses of Atomic Energy (United Nations, Geneva, 1958) 15, 366.

[9] KATZ, L., BAERG, A. P., BROWN, F., Proc. 2nd Int. Conf. on the Peaceful Uses of Atomic Energy (United Nations, Geneva, 1958) 15, 188.

[10] GINDLER, J. E., HUIZENGA, J. R., SCHMITT, R. A., Phys. Rev. 104 (1956) 425.

[11] MANFREDINI, A., MUCHNIK, M., FIORE, L., RAMORINO, C., DE CARVALHO, H. G., LANG, J., MÜLLER, R., Nucl. Phys. 74 (1965) 377.

[12] UNRUH, C. M., Nuclear Safety 5 (1964) 378.

[13] WING, J., VARLEY, J. D., USAEC Rep. ANL-6886 (1964).

[14] HILLMAN, M., USAEC Rep. BNL 846 (T-333) (1964).

[15] BULLOCK, R. J., LARGE, N. R., UKAEA Rep. AERE-R 5646 (1968).

[16] LEDERER, C. M., HOLLANDER, J. M., PERLMAN, I., Table of Isotopes, 6th Ed., Wiley, New York (1967).

[17] AMAREL, I., BERNAS, R., FOUCHER, R., JASTRAZEBSKI, J., JOHNSON, A., TEILLAC, J., GAUVIN, H., Physics Letters 24B (1967) 402.

[18] STROM, P. O., LOVE, D. L., GREENDALE, A. E., DELUCCHI, A. A., SAM, D., BALLOU, N. E., Phys. Rev. 144 (1966) 984.

[19] BUNNEY, L. R., SAM, D., Nucl. Sci. Engng. 29 (1967) 432.

[20] FISHER, P. C., ENGLE, L. B., Phys. Rev. 134 (1964) B796.

[21] WILLIAMS, E. T., CORYELL, C. D., Phys. Rev. 144 (1966) 945.

DISCUSSION

W.L. TALBERT, Jr.: The upper limits mentioned for delayed neutron emission with precursor half-lives of the order of $T_{\frac{1}{2}} \simeq 55$ s can be lowered significantly for the cases of ^{91}Rb and ^{140}Cs. In our study of mass-separated gaseous fission products and their daughters [Phys. Rev. 177 (1969) 1805] mass 91 and 140 neutron counting rates can be used to estimate limits for P_n in the cases of ^{91}Rb and ^{140}Cs. Using for each the observation that Xe-Cs or Kr-Rb neutron yields are about equal for each mass chain, and taking 3:1 as the ratio of photoneutron to delayed neutron emission for mass 91, along with very conservative estimates for relative activities for masses 91/92 and 140/141 for our system, we find that the upper limits are:

$$^{91}\text{Rb} : P_n \lesssim 10^{-3}\%$$
$$^{140}\text{Cs} : P_n \lesssim 2 \times 10^{-5}\%.$$

S. AMIEL: Can the author indicate any mass formula which will support his search for the longer-lived precursors? I am afraid that no formula or mass tables currently in use will support such an attempt.

L. TOMLINSON: We used the predictions of delayed neutron emission given by Pappas and Rudstam [Nuclear Physics 21 (1960) 353], which indicated that there may be up to four delayed neutron precursors with half-lives greater than 55 s. Predictions based on more recent mass formulae (such as the one mentioned in your review paper) may not agree with these earlier predictions.

A.C. PAPPAS: I have one comment. Your refer to the work done by Rudstam and myself about ten years ago where we used the Cameron formula to estimate Q_β-B_n values. The nuclides you mention have, according to this formula, a very small value of $Q_\beta - B_n$ and should therefore, from energy considerations, be delayed neutron precursors. As was stressed in the paper, spin and parity restrictions are serious at these small values and the results should therefore be handled with care.

The new improved formula moves the limits further away and your results confirm the importance of spin in delayed neutron emission when $Q_\beta - B_n$ is very small.

EMISSION DE NEUTRONS RETARDES: CALCUL DES SPECTRES D'ENERGIE ET DES PROBABILITES D'EMISSION DES PRECURSEURS

H. GAUVIN*, R. de TOURREIL**
Institut de physique nucléaire,
Orsay, France

Abstract — Résumé

EMISSION OF DELAYED NEUTRONS: CALCULATION OF THE ENERGY SPECTRA AND EMISSION PROBABILITIES OF THE PRECURSORS. The calculations given in the paper are intended to explain the delayed neutron emission (energy spectra and emission probabilities P_n) which follows the β^- disintegration of the precursors produced by fission. The probability of β^- transition, the level density $\omega(E,J)$ of the emitter and the competion (β^-, γ) and (β^-, n) de-energizations are analysed for each precursor studied. All the possible channels open to the process of neutron emission on grounds of energy considerations (Q_{β^-}, B_n) are taken into account through the introduction of the spin and parity selection rules at each stage of the sequence: precursor, emitter, final nucleus.

The results of the calculations are compared with the known experimental measurements of the neutron energy spectra and probabilities P_n. The precursors ^{87}Br, ^{88}Br, ^{137}I and $^{93-97}Rb$ were selected for this examination.

This comparison shows in particular that the structure of experimental energy spectra can be well reproduced by the calculations given in the paper. Moreover, it emerges that the spectra calculated are very sensitive to the choice of the spins of the precursor and the final nucleus.

EMISSION DE NEUTRONS RETARDES: CALCUL DES SPECTRES D'ENERGIE ET DES PROBABILITES D'EMISSION DES PRECURSEURS. Les calculs présentés tendent à rendre compte de l'émission neutronique retardée (spectres d'énergie et probabilités d'émission P_n) qui suit la désintégration β^- des précurseurs produits par fission. La probabilité de transition β^-, la densité de niveau $\omega(E,J)$ de l'émetteur, la compétition des désexcitations (β^-, γ) et (β^-, n) sont, en particulier, analysées pour chaque précurseur étudié. Toutes les voies possibles ouvertes au processus d'émission de neutrons par des considérations énergétiques (Q_{β^-}, B_n) sont envisagées en introduisant les règles de sélection de spin et de parité à chaque étape de la séquence: précurseur, émetteur, noyau final.

Les résultats des calculs sont confrontés aux mesures expérimentales actuellement connues de spectres d'énergie de neutrons et de probabilités P_n. Les précurseurs ^{87}Br, ^{88}Br, ^{137}I et $^{93-97}Rb$ ont été retenus pour cet examen.

Il ressort, en particulier, de cette confrontation que la structure des spectres énergétiques expérimentaux peut être bien reproduite par les calculs présentés ici. Il apparaît, de plus, que les spectres calculés sont très sensibles au choix des spins du précurseur et du noyau final.

1. INTRODUCTION

Une interprétation semi-quantitative du processus de désexcitation suivie de l'émission de neutrons différés a conduit différents auteurs [1, 2] à estimer les tendances des probabilités d'émission de neutrons (P_n) pour des précurseurs loin de la stabilité, excédentaires en neutrons au-delà des couches fermées N = 50 et 82. L'approche semi-théorique a été par la suite précisée en considérant les effets de moment angulaire, de façon qualitative par Sugihara [3] et récemment [4] plus quantitativement par Jahnsen et al. [5].

* Laboratoire de chimie nucléaire.
** Division de physique théorique, Laboratoire associé au CNRS.

Le travail présenté ici se propose de déterminer pour des précurseurs connus les probabilités P_n d'émission de neutrons et les spectres énergétiques correspondants. S'il s'appuie sur les mêmes fondements généraux que les études précédentes, il tente de préciser l'effet de certains paramètres dans l'approche semi-théorique qui peut être actuellement menée. Nos connaissances actuelles dans les domaines de nucléides considérés, au-delà des couches fermées où apparaissent diverses anomalies, sont encore très fragmentaires. On peut penser que les calculs théoriques, tout en visant à reproduire les caractéristiques de l'émission différée de neutrons, pourraient apporter des informations sur les propriétés nucléaires des noyaux concernés dans le processus étudié.

Du point de vue expérimental, le spectre énergétique des neutrons et la probabilité totale P_n d'émission sont deux grandeurs mesurables de manière totalement indépendante. Une confrontation des résultats théoriques avec ces deux grandeurs lorsqu'elles sont simultanément connues pour un précurseur donné constitue donc le test le plus efficace de tout modèle théorique. Une telle situation ne se rencontre pas actuellement, excepté dans un cas. Si les P_n sont assez bien connus pour un ensemble de précurseurs, en ce qui concerne les spectres énergétiques on ne dispose que des mesures anciennes de Batchelor et Hyder [6] relatives aux groupes de périodes 1 à 4 dans la fission thermique de ^{235}U. Nous avons retenu pour confrontation les spectres correspondant aux groupes 1 et 2. Dans le premier cas le spectre énergétique correspondrait au ^{87}Br seul, dans le deuxième cas il résulterait pour l'essentiel de l'association ^{88}Br et ^{137}I. Les P_n ont été calculés pour ces trois précurseurs ainsi que pour $^{93\text{-}94\text{-}95\text{-}96}Rb$, isotopes pour lesquels on dispose de valeurs expérimentales récentes [7]. Pour les isotopes de Rb, les spectres énergétiques calculés sont proposés, dans l'attente des résultats expérimentaux.

2. METHODES DE CALCUL

Notation. Précurseur : Z_i, N_i, J_i, π_i
Emetteur : $Z_e = Z_i + 1$, $N_e = N_i - 1$, J_e, π_e
Noyau final : $Z_f = Z_e$, $N_f = N_e - 1$, J_f, π_f
Energie maximale de désintégration du précurseur: Q_{β^-}
Energie de liaison du neutron dans l'émetteur: B_n.

Depuis Bohr et Wheeler [8] le processus admis d'émission différée de neutrons est le suivant: le précurseur (Z_i, N_i) dans son état fondamental de spin et parité $J_i^{\pi_i}$ forme par désintégration β^- le noyau fils émetteur (Z_e, N_e) dans un état $J_e^{\pi_e}$ d'énergie d'excitation E. L'émetteur se désexcite ensuite par émission γ seule si $E < B_n$ ou par émission γ ou neutron si $E \geq B_n$. On atteint ainsi soit l'état fondamental de l'émetteur, s'il y a eu émission γ seule, soit le noyau final (Z_f, N_f) dans l'état $J_f^{\pi_f}$ d'énergie d'excitation E_f, s'il y a eu émission de neutron. Si $E_f \neq 0$, l'état fondamental du noyau final est atteint par émission γ. Nous négligeons l'éventualité de désintégrations β^- de l'état (E, $J_e^{\pi_e}$) de l'émetteur vers le nucléide ($Z_e + 1$, $N_e - 1$). On distingue donc deux étapes dans le processus de désexcitation: d'une part la formation de l'émetteur (Z_e, N_e) dans l'état $J_e^{\pi_e}$ d'énergie E, d'autre part la compétition (γ, n) dans la désexcitation de ce niveau de l'émetteur.

2.1. Formation de l'émetteur

Le schéma du processus est donné à la figure 1a. La probabilité P_β de peupler le niveau (E, $J_e^{\pi_e}$) à partir de l'état $J_i^{\pi_i}$ est donnée par le produit de la probabilité $\lambda(E_{\beta^-})$ de désintégration β^- d'énergie maximale $E_{\beta^-} = Q_{\beta^-} - E$, tenant compte des règles de sélection, et de la probabilité de trouver l'état $J_e^{\pi_e}$ avec une énergie d'excitation E, c'est-à-dire la densité de niveaux de l'émetteur $\Omega(E, J_e^{\pi_e})$.

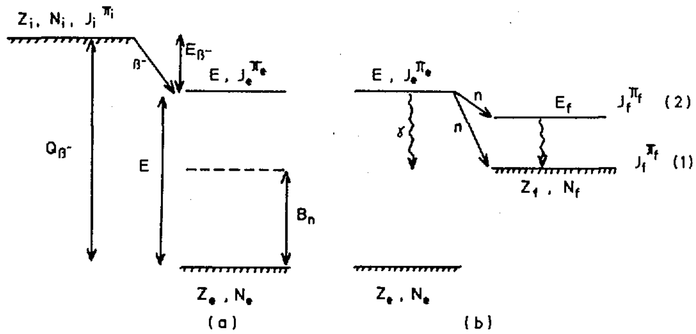

FIG.1. Schéma du processus d'émission de neutrons différés.

a) Désintégration β^-

Le premier terme $\lambda(E_{\beta^-})$, qui n'est autre que la constante de désintégration partielle, est donné par la théorie de Fermi et peut être exprimé sous la forme [9]

$$\lambda(W_0) = \int_1^{W_0} \frac{|P|^2}{\tau_0} F(Z_e, W)(W^2-1)^{\frac{1}{2}} (W_0-W)^2 W dW \tag{1}$$

où W et W_0 sont, en unités $m_e c^2$, respectivement, l'énergie totale d'un électron du spectre et l'énergie totale maximale ($E_{\beta^-} + m_e c^2$) du spectre.

Le coefficient τ_0 contient la constante de Fermi. Pour les transitions β^- permises, qui ont seules été envisagées dans le peuplement des états émetteurs de neutrons, l'élément de matrice $|P|$ est indépendant de l'énergie de transition. L'expression (1) prend alors la forme

$$\lambda(W_0) = k\, f(Z_e, W_0)$$

où

$$f(Z_e, W_0) = \int_1^{W_0} G(Z_e, W)(W_0 - W)^2\, W^2 dW$$

avec

$$G(Z_e, W) = \frac{(W^2-1)^{\frac{1}{2}}}{W} F(Z_e, W)$$

Les fonctions intégrales de Fermi $f(Z_e, W_0)$ pour les différents précurseurs sélectionnés ont été calculées à partir des Tables de Rose et al. donnant $G(Z_e, W)$ [10]. Une transformation d'unité de $\lambda(W_0)$ conduit alors à la probabilité $\lambda(E_{\beta^-})$.

Les Règles de sélection de Gamow-Teller (seules possibles ici) entraînent pour les transitions β^- permises: $\Delta J = 0, \pm 1$, sans changement de parité. Nous avons alors $J_e = \{J_i + 1, J_i, J_i - 1\}$ et $\pi_e = \pi_i$, avec pour chacune des valeurs de spin J_e un poids égal dans la transition permise.

b) Expression de la densité de niveaux

Dans le modèle du gaz de Fermi, avec l'hypothèse d'espacement équidistant des états de particules indépendantes, Ericson [11] obtient pour la densité d'états individuels de nucléons l'expression

$$\omega(E) = \frac{\pi^{\frac{1}{2}}}{12} \frac{1}{a^{1/4}\, U^{5/4}} \exp 2\sqrt{a\,U} \tag{2}$$

et pour la densité de niveaux nucléaires, dépendante du spin

$$\Omega(E, J_e) = \omega(E) \frac{2\,J_e + 1}{2(2\pi)^{\frac{1}{2}}\, \sigma^3} \exp\left[- \frac{(J_e + \frac{1}{2})^{\frac{1}{2}}}{2\,\sigma^2} \right] \tag{3}$$

Dans l'expression (2), à l'énergie E correspond une «énergie d'excitation effective» $U = E - \delta$. δ est le plus souvent assimilé à l'énergie d'appariement pour protons et pour neutrons. Pour les nucléides émetteurs, pairs en protons, qui nous intéressent ici, les variations de δ résulteraient donc de l'énergie d'appariement des neutrons. Il apparaît difficile actuellement pour ces noyaux très excédentaires de fixer l'importance de ce terme. Aussi, nous avons considéré δ comme un paramètre et nous verrons par la suite que les résultats en sont très dépendants. La courbe des valeurs du paramètre de densité de niveaux a présente une variation assez linéaire avec le nombre de masse A (en A/8 environ) mais avec des minimums très marqués au voisinage des nombres magiques en neutrons, précisément dans notre domaine d'intérêt. Les valeurs de a ont été déduites d'une récente analyse de résonances nucléaires portant sur 200 noyaux, effectuée à l'aide de l'expression (3) par Facchini et al. [12].

Compte tenu des valeurs possibles de J_e, dans une transition β^- permise, le facteur de spin dans l'expression (3) définit l'amplitude relative des différentes composantes J_e dans le spectre de neutrons et dans P_n. Dans cette expression σ(«spin cut-off») est défini théoriquement par [11]:

$$\sigma^2 = \frac{6a}{\pi^2} \langle m^2 \rangle\, T(U) \tag{4}$$

où $\langle m^2 \rangle$ est la valeur moyenne du carré de la projection du moment angulaire total pour les états de nucléons au voisinage du niveau de Fermi.

Les résultats des calculs ne dépendent pratiquement pas de $\langle m^2 \rangle$ à condition que $\langle m^2 \rangle$ soit suffisamment élevé, ce qui est le cas en prenant pour $A \sim 90$, $\langle m^2 \rangle = 5$ et pour $A \sim 140$ $\langle m^2 \rangle = 6,5$, valeurs indiquées par Facchini et al. [12]. σ^2 est souvent explicité en fonction du moment d'inertie $\mathcal{J}$ et le modèle du gaz de Fermi prédit que $\mathcal{J}$ est alors donné par $\mathcal{J}_{rigide}$. Toutefois, diverses expériences ont montré que ceci n'est vrai qu'à des énergies d'excitation assez élevées et qu'aux basses énergies $\mathcal{J} < \mathcal{J}_{rigide}$. Aussi, nous avons calculé σ^2 par son expression donnée plus haut.

Dans (4), T(U) est la température nucléaire et peut être calculé à partir de l'expression (2). L'introduction, dans les calculs, de la forme plus simple $T(U) = \sqrt{U/a}$ que nous avons utilisée ne modifie pas sensiblement les résultats par rapport à la forme, plus exacte à faible énergie d'excitation, déduite de (2). Précisons qu'à basse énergie, précisément, lorsque $U < 1$ MeV, afin d'éviter l'effet du terme $U^{5/4}$, l'expression suivante a été substituée à (2):

$$\omega(E) = \frac{\pi^{\frac{1}{2}}}{12\, a^{1/4}} \exp 2\sqrt{aU} \tag{5}$$

Pour résumer ce qui précède sur la formation de l'émetteur, la probabilité totale P_T de peupler tous les niveaux $J_e^{\pi_e}$ à partir de $J_i^{\pi_i}$ est donc donnée par

$$P_T = \int_0^{Q_{\beta^-}} P_\beta(E, J_i^{\pi_i}, J_e^{\pi_e})\, dE = \int_0^{Q_{\beta^-}} \lambda(E_{\beta^-}) \sum_{J_e} \Omega(E, J_e^{\pi_e})\, dE$$

et le poids relatif pour un niveau $J_e^{\pi_e}$ à l'énergie E est

$$P'_\beta(E, J_i^{\pi_i}, J_e^{\pi_e}) = \frac{P_\beta(E, J_i^{\pi_i}, J_e^{\pi_e})}{P_T}$$

2.2. Désexcitation de l'émetteur - Compétition γ,n

Le schéma du processus de désexcitation est présenté sur la figure 1b.

La probabilité p_n pour la désexcitation du niveau $(E, J_e^{\pi_e})$ vers un niveau $(E_f \geq 0, J_f^{\pi_f})$ par émission de neutron est donnée par

$$p_n(E_n, J_e^{\pi_e}, J_f^{\pi_f}) = \frac{\Gamma_n^{j_n}(E_n)}{\Gamma_\gamma + \sum_{J_f} \sum_{j_n} \Gamma_n^{j_n}(E_n)} \tag{6}$$

La largeur Γ_γ pour l'émission γ est dépendante du nombre de masse. Nous avons pris, d'après Stolovy et Harvey [13], pour $A \sim 90$, $\Gamma_\gamma = 0,30$ eV et pour $A \sim 140$, $\Gamma_\gamma = 0,16$ eV. Nous avons considéré Γ_γ indépendant de l'énergie E dans le domaine d'excitation exploré, ce qui est probablement une bonne approximation. $\Gamma_n^{j_n}(E_n)$ est la largeur d'émission de neutrons d'énergie $E_n = E - B_n - E_f$.

TABLEAU I. CARACTERISTIQUES DES PRECURSEURS ET DE LEUR FILIATION

Précurseur	Emetteur	Noyau final	P_n (%)[a]	Q_{β^-} (MeV)[b]	B_n (MeV)[c]	a (MeV^{-1})[d]	Γ_γ (eV)[e]	$J_i^{\pi_i}$	Etats finaux E_f $J_f^{\pi_f}$ (MeV)[f]
$^{87}_{35}Br_{52}$	$^{87}_{36}Kr_{51}$	$^{86}_{36}Kr_{50}$	3,1 ± 0,6		5,40	10,5	0,30	$3/2^-$, $5/2^-$	0 0^+
$^{88}_{35}Br_{53}$	$^{88}_{36}Kr_{52}$	$^{87}_{36}Kr_{51}$	6 ± 1,6		7	11,5	0,30	4^-, 5^-, 6^-	0 $5/2^+$ 0,55 $1/2^+$ 1,52 $3/2^+$
$^{137}_{53}I_{84}$	$^{137}_{54}Xe_{83}$	$^{136}_{54}Xe_{82}$	3,0 ± 0,5		4,40	15,7	0,16	$7/2^+$	0 0^+ 1,32 2^+
$^{93}_{37}Rb_{56}$	$^{93}_{38}Sr_{55}$	$^{92}_{38}Sr_{54}$	1,43 ± 0,18	7,55 ± 0,20		13,5	0,30	$5/2^-$	0 0^+ 0,8 2^+ 1,5 2^+
$^{94}_{37}Rb_{57}$	$^{94}_{38}Sr_{56}$	$^{93}_{38}Sr_{55}$	11,10 ± 1,10	9,70 ± 0,15		14	0,30	4^-	0 $5/2^+$ 0,25 $3/2^+$ 0,70 $7/2^+$ 0,90 $1/2^+$
$^{95}_{37}Rb_{58}$	$^{95}_{38}Sr_{57}$	$^{94}_{38}Sr_{56}$	7,10 ± 0,90	8,70 ± 0,30		15	0,30	$5/2^-$	0 0^+ 0,8 2^+ 1,5 2^+
$^{96}_{37}Rb_{59}$	$^{96}_{38}Sr_{58}$	$^{95}_{38}Sr_{57}$	12,7 ± 1,5	11,0 ± 0,25		15,5	0,30	4^-	0 $5/2^+$ 0,25 $3/2^+$ 0,70 $7/2^+$ 0,90 $1/2^+$

[a] $^{87-88}Br$ - ^{137}I, réf. [23] ; isotopes de Rb, réf. [7].

[b] Valeurs expérimentales de I. Macias Marques, R. Foucher et al. (communication privée) [18].

[c] Estimations d'après les Tables de masses [16, 17].

[d] D'après la réf. [12].

[e] D'après la réf. [13].

[f] Assignations et énergies possibles, retenues dans le présent travail.

Pour les transitions $J_e \rightarrow J_f$, le moment angulaire total des neutrons émis est donné par les règles de sélection

$$|\vec{J}_e - \vec{J}_f| \leq \vec{j}_n \leq \vec{J}_e + \vec{J}_f$$

avec $\vec{j}_n = \vec{\ell}_n \pm \frac{1}{2}$, ℓ_n ayant la parité du produit $\pi_e \times \pi_f$. Les largeurs $\Gamma_n^{j_n}$ peuvent être explicitées à l'aide des coefficients de transmission $T_{\ell_n}^{j_n}$ [14]

$$T_{\ell_n}^{j_n}(E_n) = \frac{2\pi \ \Gamma_n^{j_n}(E_n)}{D(E,\ J_e)}$$

où $D(E, J_e)$ est l'espacement moyen des niveaux J_e de même parité dans l'émetteur à l'énergie d'excitation E. $D(E, J_e)$ peut alors être donné par l'inverse de la densité de niveaux $\Omega(E, J_e)$ qui a été définie précédemment. Nous exprimons alors Γ_n sous la forme

$$\Gamma_n^{j_n}(E_n) = \frac{T_{\ell_n}^{j_n}(E_n)}{2\pi\,\Omega(E,\ J_e)}$$

Les coefficients de transmission $T_{\ell_n}^{j_n}$ ont été calculés à partir du modèle optique par Bjorklund et Fernbach [15] pour le domaine de nombre de masse A qui nous intéresse ici et pour E_n variant de 0 à 5 MeV.

Si nous posons

$$\Gamma_T(E) = \Gamma_\gamma + \sum_{J_f}\sum_{j_n} \Gamma_n^{j_n}(E_n)$$

le spectre de neutrons différés est alors donné par

$$P(E_n) = \sum_{J_e}\sum_{J_f}\sum_{j_n} P'_\beta(E,\ J_i^{\pi_i},\ J_e^{\pi_e}) \times \frac{\Gamma_n^{j_n}(E_n)}{\Gamma_T(E)}$$

et la probabilité d'émission de neutron par

$$P_n = \int_0^{Q_{\beta^-} - B_n} P(E_n)\, dE_n$$

3. RESULTATS

Les spectres de neutrons $P(E_n)$ et les probabilités P_n ont été calculés sur l'ordinateur UNIVAC 1108 de la Faculté des sciences d'Orsay. Les paramètres nécessaires pour chacune des filiations considérées sont présentés dans le tableau I. Pour $^{87-88}$Br et ^{137}I, les valeurs de B_n sont des valeurs moyennes déduites des Tables de masses de Zeldes et al. [16] et de Seeger et Perisho [17]. Pour les isotopes de Rb nous disposons de récentes mesures des énergies Q_{β^-} [18]. L'absence de valeurs B_n ou Q_{β^-} indique que nous avons examiné l'effet de $\Delta E = Q_{\beta^-} - B_n$. Le choix de ΔE comme paramètre est dicté par une double raison. D'une part il a une grande influence sur les caractéristiques que l'on se propose d'évaluer, d'autre part on peut montrer que pour un Z donné il est indépendant de l'énergie de paire et qu'il devrait être alors fonction seulement du nombre de neutrons.

Les assignations $J_i^{\pi_i}$, $J_f^{\pi_f}$ résultent de possibilités du modèle en couches et ont un caractère hypothétique, le plus souvent. A l'exception de $^{86-87}Kr$ et ^{136}Xe, les états excités finaux sont également hypothétiques et s'inspirent des schémas de nucléides voisins ayant des caractéristiques similaires en protons et neutrons.

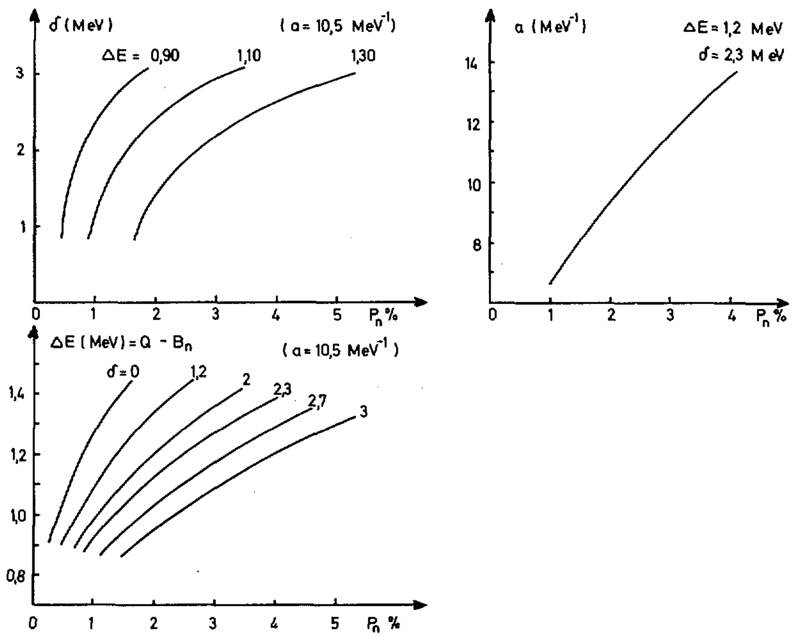

FIG.2. ^{87}Br. Variations de P_n en fonction de ΔE, δ et a.

Brome-87

La figure 2a montre, pour J_i, $\pi_i = 3/2^-$, les variations de P_n en fonction de $\Delta E = Q_{\beta^-} - B_n$ pour différentes valeurs de l'énergie δ, définie par $\delta = E - U$ (voir §2.1.b)). P_n varie rapidement avec ΔE et nous avons constaté que, tous les paramètres maintenus par ailleurs, P_n est peu sensible aux valeurs individuelles de Q_{β^-} et B_n déterminant une valeur donnée de ΔE. L'influence prévisible du paramètre d'énergie ΔE apparaît ici très nettement, puisqu'il suffit d'une variation de 250 keV environ sur ΔE pour doubler la valeur de P_n. Le paramètre de densité de niveaux a et le facteur correctif de l'énergie d'excitation δ agissent aussi fortement sur P_n, ainsi qu'il apparaît sur les figures 2b et 2c. On dispose donc d'un ensemble de paramètres ajustables dont le choix des valeurs, dans la situation actuelle, peut seulement être guidé par une nécessité de cohérence lorsqu'on examine un ensemble de précurseurs. C'est ce souci qui nous a conduit à fixer le paramètre a (tableau I) comme nous l'avons indiqué plus haut. Pour ^{87}Br, avec $\delta = 2,3$ MeV et $\Delta E = 1,2$ MeV, on obtient $P_n = 2,5\%$, en bon accord avec la valeur expérimentale. La largeur ΔE exclut donc toute désexcitation vers le premier niveau excité 2^+ du ^{86}Kr d'énergie voisine de 1,5 MeV.

La figure 3 présente le spectre de neutrons correspondant aux conditions précédentes, comparé au spectre du groupe 1 de Batchelor et Hyder. Le premier pic à $E_n < 100$ keV correspond à l'émission de neutrons de moment angulaire $\ell_n = 1$, et le second à $E_n = 420$ keV aux neutrons $\ell_n = 3$. Par la position des pics en énergie le spectre expérimental est bien reproduit. Par contre le rapport des intensités s'écarte sensiblement du rapport expérimental. Un état $J_i^{\pi_i} = 5/2^-$ du ^{87}Br qui favorise $\ell_n = 3$ aux dépens de $\ell_n = 1$ semble exclu à fortiori.

Il serait nécessaire de disposer d'un spectre expérimental du ^{87}Br obtenu plus directement et de meilleure résolution pour dégager des conclusions plus définitives. Quoiqu'il en soit il semble que les calculs rendent compte de la structure générale du spectre.

Brome-88

Une analyse en fonction de ΔE et de δ a été effectuée comme précédemment pour différentes assignations $J_i^{\pi_i}$. La figure 4a présente avec les paramètres suivants

$J_i^{\pi_i}$	ΔE (MeV)	δ(MeV)	Spectre	P_n (%)
5^-	1,92	1,90	1	6
6^-	2,25	1,90	2	5,5
6^-	1,85	3,80	3	6

les spectres de neutrons obtenus qui correspondent à P_n $(5^-) = 6\%$, P_n $(6^-) = 5,5\%$ et 6%. Dans le premier cas (5^-) la contribution vient essentiellement de $\ell_n = 1$ et 3, alors que dans le second (6^-) nous avons $\ell_n = 3$. Dans tous les cas on observe que l'émission de neutrons vers les états excités de ^{87}Kr contribue peu.

Iode-137

La situation apparaît ici beaucoup plus certaine en ce qui concerne les caractéristiques des états initial et finaux. Le non-changement de parité conduit à l'émission de neutrons $\ell_n = 2$ et 4. La figure 4b donne les spectres de neutrons avec les paramètres suivants et P_n correspondants voisins de la valeur expérimentale:

ΔE (MeV)	δ (MeV)	P_n (%)	Spectre
1,25	1,70	4	1
1,40	1,20	4	2
1,25	1,20	3	3

On constate ici une variation rapide du rapport des pics $\ell_n = 2/\ell_n = 4$. Les spectres obtenus pour les précurseurs ^{88}Br (P_n = 6%, ΔE = 1,85 MeV, δ = 3,8 MeV) et ^{137}I (P_n = 3%, ΔE = 1,25 MeV, δ = 1,20 MeV) ont été sommés avec les poids respectifs 1/3, 2/3 [19] afin de simuler le groupe 2 de 22 sec. Le spectre total est présenté sur la figure 5 ainsi que le spectre expérimental de Batchelor et Hyder. La structure d'ensemble de ce dernier est assez bien reproduite et les intensités relatives des différents pics

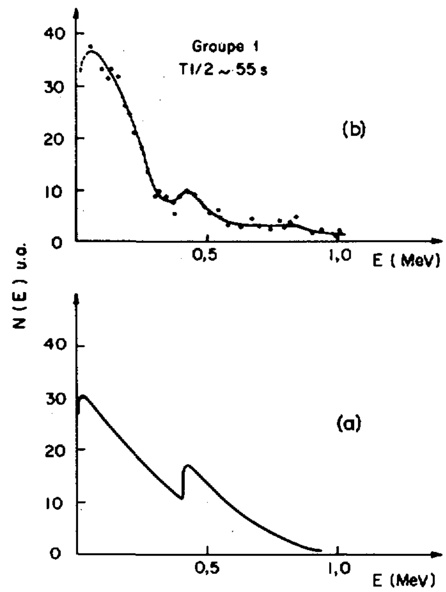

FIG. 3. Spectre énergétique calculé des neutrons différés du ^{87}Br (a) et spectre expérimental (b) du groupe 1 [6] analysé à l'aide des résultats de Keepin et al. [22].

ne sont pas en désaccord flagrant. La position en énergie des maximums est également correcte, bien que décalée vers des énergies légèrement plus élevées. Ceci peut être expliqué partiellement par la dégradation, soulignée par Batchelor et Hyder, de l'énergie des neutrons dans le spectre expérimental. Nous devons remarquer que nous sommes conduits à prendre pour ^{88}Br $J_i^{\pi_i} = 6^-$ ce qui suggère un peuplement important des niveaux d'excitation élevée de l'émetteur ^{88}Kr (0^+). Les états $J_i^{\pi_i} < 6^-$ seraient à rejeter en raison de la composante $\ell_n = 1$ qu'ils introduisent et qui alimenterait trop fortement le spectre à $E_n \sim 100$ keV en contradiction avec le spectre expérimental.

On peut souligner que dans le cas présent l'approche théorique permet de rendre compte de façon assez satisfaisante du spectre énergétique expérimental à l'aide de spectres individuels calculés en accord avec les P_n expérimentaux.

Isotopes de rubidium

Comme pour les isotopes précédents une analyse a été faite en fonction de ΔE et δ. Les $J_i^{\pi_i}$ introduits sont hypothétiques, mais possibles. Les états finaux des Sr (pair-pair) sont sans doute très probables compte tenu

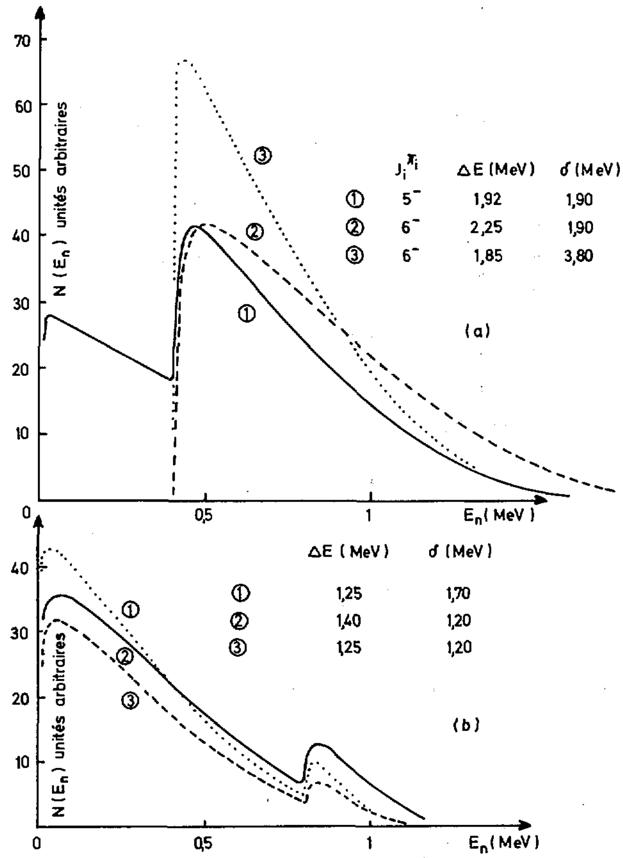

FIG.4. Spectres énergétiques calculés des neutrons différés du ^{88}Br (a) et du ^{137}I (b) pour différents cas de $J_i^{\pi_i}$, ΔE et δ.

de la systématique des noyaux voisins de mêmes caractéristiques. Par contre la séquence des états finaux introduite par les Sr (pair-impair) est assez arbitraire. Il nous a paru qu'il eut été plus arbitraire encore de ne conserver que l'état fondamental.

Les courbes $P_n = f(\Delta E)$ sont présentées sur la figure 6. Les valeurs expérimentales de P_n [7] sont obtenues, en particulier, en attribuant aux paramètres les valeurs regroupées ci-dessous:

Rb	δ (MeV)	ΔE (MeV)	P_n (%)
93	1,2	1,3	1,43
94	2	2	11,10
95	1,2	2,10	7,5
96	2	2,45	12,7

Les valeurs de δ sont voisines des énergies d'appariement de Gilbert et Cameron [20]. Les énergies ΔE pour $^{93\text{-}94}$Rb sont en bon accord avec les

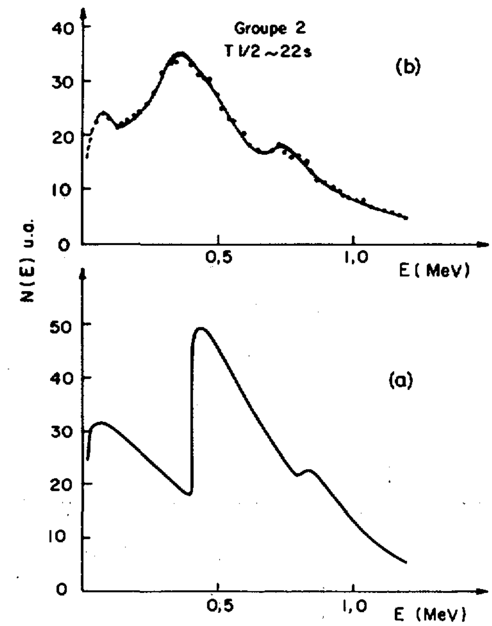

FIG. 5. Spectre énergétique calculé des neutrons différés de l'ensemble $^{88}Br + ^{137}I$ (a) et spectre expérimental (b) du groupe 2 [6] analysé à l'aide des résultats de Keepin et al. [22].

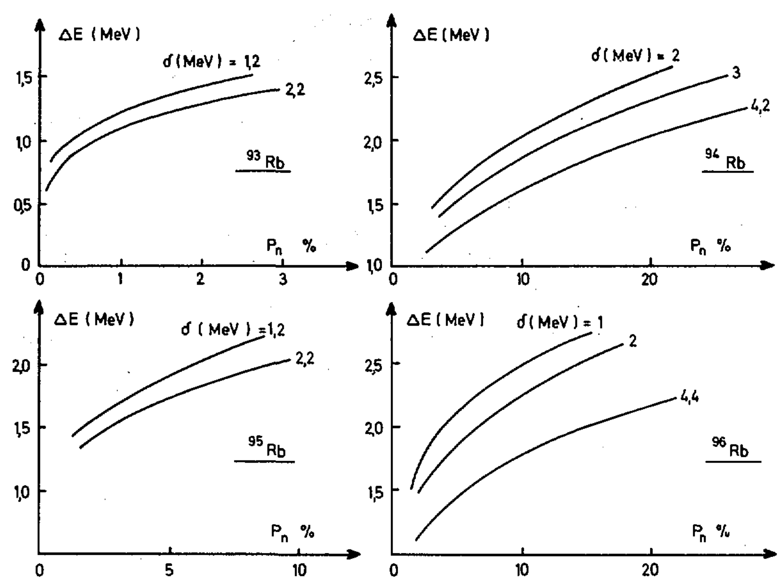

FIG. 6. $^{93-94-95-96}Rb$. Variations de P_n en fonction de ΔE.

Tables de masses [16, 17, 21]. Par contre, pour $^{95-96}Rb$ elles s'en écartent très sensiblement. Les Tables de masses conduisent à des valeurs supérieures de 50% environ. Il est clair, d'après la figure 6, que de telles valeurs de ΔE conduiraient à des valeurs prohibitives de P_n. La présente situation appelle donc une étude plus détaillée.

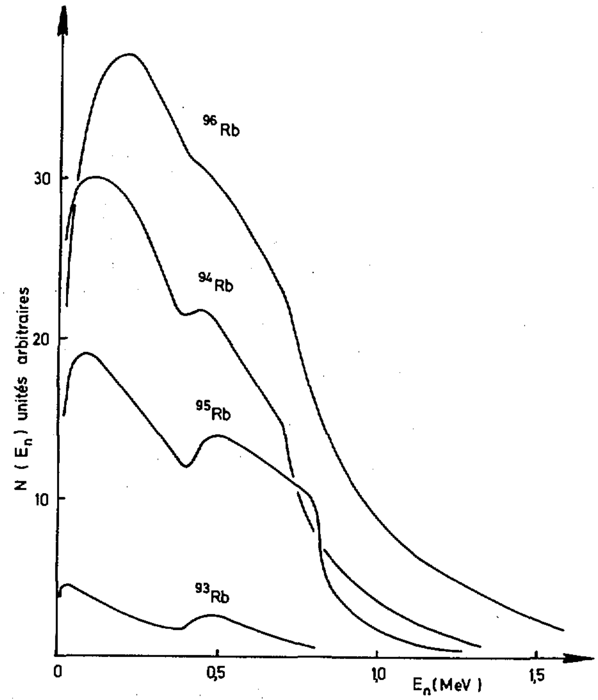

FIG.7. Spectres énergétiques calculés des neutrons différés des précurseurs $^{93-94-95-96}Rb$.

Les spectres calculés avec les conditions précisées ci-dessus sont présentés sur la figure 7. Le spectre du précurseur ^{94}Rb, qui est une composante importante du groupe 4 de 2 sec, n'est pas en contradiction avec le spectre expérimental obtenu pour ce groupe par Batchelor et Hyder [6].

On remarque que pour les précurseurs $^{94-95-96}Rb$ les spectres présentent une cassure vers 700 ou 800 keV. Ce phénomène n'apparaît que pour des valeurs $\Delta E = Q_{\beta^-} - B_n$ grandes par rapport à des énergies d'excitation assez faibles des états finaux peuplés par émission de neutrons de faible moment angulaire. Considérons par exemple le cas du ^{95}Rb où le changement de pente est le plus net dans le spectre. Nous avons envisagé la séquence

$$^{95}Rb(5/2^-) \xrightarrow{\beta^-} {}^{95}Sr^*(3/2^-, 5/2^-, 7/2^-) \xrightarrow{n} {}^{94}Sr(0^+, 2^+, 2^+)$$

Le peuplement de l'état fondamental 0^+ du ^{94}Sr s'effectue à partir des différents états $J_e^{\pi_e}$ de l'émetteur par des neutrons $\ell_n = 1$ et 3. Lorsque, dans l'échelle d'énergie des neutrons se référant à B_n, apparaît l'alimentation du premier état excité 2^+ du ^{94}Sr à 800 keV par émission de neutrons $\ell_n = 1$, la largeur totale Γ_T, donnée plus haut, prend assez brutalement des valeurs plus importantes. Il en résulte que la probabilité de désexcitation vers le fondamental, $p_n(E_n, J_e^{\pi_e}, 0^+)$ [expression (6)] diminue très sensiblement. Dans le spectre de neutrons, c'est donc la contribution partielle due aux transitions vers l'état fondamental qui doit subir cet effet. C'est bien ce que montre une analyse des calculs.

4. REMARQUES ET CONCLUSIONS

Quelques conclusions et perspectives peuvent être dégagées des résultats rapportés dans cette étude préliminaire.

D'une manière générale, il ressort que les calculs peuvent rendre compte des P_n expérimentaux avec des valeurs cohérentes et vraisemblables des paramètres qui ont été choisis, sauf dans le cas de $^{95-96}Rb$. Les spectres expérimentaux de ^{87}Br et $^{88}Br + ^{137}I$ sont dans leur structure d'ensemble assez bien reproduits. Par contre les intensités relatives des maximums ne sont encore qu'imparfaitement calculées. Il convient toutefois de souligner que la faible résolution expérimentale a tendance à niveler les spectres obtenus par Batchelor et Hyder [6], alors que dans les calculs l'effet des coefficients de transmission T_{ℓ_n} entraîne une montée assez brutale des pics. Dans ces conditions, il devient difficile d'apprécier plus en détail les calculs présentés ici, tant que nous ne disposerons pas de spectres expérimentaux plus précis.

Toutefois s'il apparaissait que les divergences observées se confirment, elles pourraient être imputées dans les calculs au terme

$$P_\beta(E, J_i^{\pi_i}, J_e^{\pi_e}) = \lambda(E_{\beta^-}) \sum_{J_e} \Omega(E, J_e)$$

Dans $\lambda(E_{\beta^-})$ une dépendance en énergie de l'élément de matrice nucléaire $|P|$ défavorisant les transitions β^- vers les niveaux les plus excités de l'émetteur aurait pour effet une atténuation des parties hautes des spectres. Une telle dépendance a été envisagée [5] et il serait sans doute intéressant que les calculs puissent en tenir compte. Par contre, on peut voir qualitativement que P_n serait diminuée. Mais les courbes $P_n = f(\Delta E)$ autorisent les ajustements de ΔE dans des limites très raisonnables.

Dans le cas du spectre donné pour le groupe 1 par Batchelor et Hyder, le désaccord observé sur la figure 3 pourrait être également expliqué par une contribution du précurseur possible, mais non encore identifié, ^{136}Te ($T_{\frac{1}{2}} = 33$ s). Les règles de sélection de Gamow-Teller, pour des transitions β^- permises, conduiraient à la séquence

$$^{136}Te\,(0^+) \longrightarrow {}^{136}I^*\,(1^+) \longrightarrow {}^{135}I\,(7/2^+) + n$$

Si $\Delta E \lesssim 500$ keV, l'émission de neutrons $\ell_n = 2$ apporterait alors une contribution dans le spectre du groupe 1 aux énergies voisines de 100 keV.

On doit remarquer que les calculs, basés sur la méthode statistique, tels qu'ils sont effectués ici conduisent à des spectres continus de neutrons. Si en réalité on est amené à observer expérimentalement des spectres de raies, les spectres calculés peuvent être vus alors comme résultant d'intégrations sur une suite d'intervalles d'énergie autour de valeurs moyennes. Il semble se dégager des calculs que, même dans ces conditions, le rapport des maximums dans le spectre de neutrons d'un émetteur peut aider, dans certains cas favorables, à fixer les spins et parités $J_i^{\pi i}$ et $J_f^{\pi f}$.

L'introduction d'états excités du noyau final ne modifie pas fondamentalement les résultats mais n'est cependant pas négligeable, surtout quand $\Delta E = Q_{\beta^-} - B_n$ devient grand. Les cas des $^{94-95-96}Rb$ en sont un exemple lorsque des conditions particulières de spin et parité se trouvent réalisées.

REMERCIEMENTS

Nous souhaitons exprimer nos remerciements à Mme I. Macias Marques et au Dr R. Foucher de nous avoir communiqué leurs résultats avant publication.

REFERENCES

[1] PAPPAS, A.C., Conf.int.util.énergie atom.fins pacif. (Actes Conf.Genève, 1958) 15, ONU, New York (1958) 373.
[2] KEEPIN, G.R., J. nucl.Energy 7 (1958) 13.
[3] SUGIHARA, T.T., Clark University, A.Prog.Rep. 6 (1962) 49.
[4] AGENCE INTERNATIONALE DE L'ENERGIE ATOMIQUE, Delayed Fission Neutrons (C.r. Groupe d'étude, Vienne, 1967), AIEA, Vienne (1968).
[5] JAHNSEN, T., PAPPAS, A.C., TUNAAL, T., in [4] 35.
[6] BATCHELOR, R., HYDER, H.R. McK., J.nucl. Energy 3 (1956) 7.
[7] AMAREL, I., GAUVIN, H., JOHNSON, A., J.inorg.nucl.Chem. 31 (1969) 577.
[8] BOHR, N., WHEELER, J.A., Phys.Rev. 56 (1939) 426.
[9] EVANS, R.D., The Atomic Nucleus, Ch.17, McGraw-Hill, New York (1955).
[10] ROSE, M.E., DISMUKE, N.M., PERRY, C.L., BELL, P.R., Beta- and Gamma-Ray Spectroscopy (SIEGBAHN, K., Ed.) North-Holland Publ.Co., ORNL Rep.1222 (1955) 875.
[11] ERICSON, T., Adv. in Physics, Phil.Mag.Suppl. 9 (1960) 425.
[12] FACCHINI, U., SAETTA-MENICHELLA, E., Energia Nucl. 15 1 (1968) 54.
[13] STOLOVY, A., HARVEY, J.A., Phys.Rev. 108 (1957) 353.
[14] BLATT, J.M., WEISSKOPF, V.F., Theoretical Nuclear Physics, Ch.VIII, John Wiley, New York (1952).
[15] AUERBACH, E.H., PEREY, F.G.J., Rep. BNL-765 (1962).
[16] ZELDES, N., GRONAU, M., LEV, A., Nucl.Phys. 63 (1965) 1, et communication privée.
[17] SEEGER, P.A., PERISHO, R.C., LA Rep. 3751 (1967).
[18] MACIAS-MARQUES, I., FOUCHER, R., Communication privée.
[19] HERRMANN, G., in [4] 157.
[20] GILBERT, A., CAMERON, A.G.W., Can. J.Phys. 43 (1965) 1446.
[21] MYERS, W.D., SWIATECKI, W.J., UCRL 11980 (1965).
[22] KEEPIN, G.R., WIMETT, T.F., ZEIGLER, R.K., Phys.Rev. 107 (1957) 1044.
[23] ARON, P.M., KOSTOCHKIN, O.I., PETRZHAK, K. A., SHPAKOV, U.J., Atomn.Energ. 16 (1964) 368.

DISCUSSION

Eiko TAKEKOSHI: I would like to inform you that some recent preliminary results are given in "An Approach to Delayed Neutron Emission with Gross Theory of Beta-decay" (unpublished note) by Kohji Takahashi and Masami Yamada of Waseda University, Japan.

A.C. PAPPAS: I wish to refer to some work done by Mrs. Tone Sverdrup in our laboratory (see abstract SM-122/51). Like Gauvin, she uses the Fermi beta-decay theory, the level density formula with pairing energy correction, and includes spin and parity considerations in all steps of the process. $\Gamma_n/(\Gamma_n + \Gamma_\gamma)$ is also taken as energy- and spin-dependent. At present the mass formula of Seeger, Zeldes and Swiatecki is used but others will also be tried. The P_n values calculated for the single light and heavy delayed neutron precursors agree within a factor of 2-4 with the experimental values, except in a couple of cases where the deviation is much larger. So far as the spectra are concerned, that of ^{87}Br has been calculated (others will be) and shows a much larger fraction of low-energy neutrons than Gauvin's results. Mrs. Sverdrup also finds - but with much lower intensity - the peak at $\sim$ 400 keV, which Gauvin obtains with about one quarter the intensity of the low-energy peak. The intensity and the shape depend strongly on the shape of the barrier (f-wave). The latter will be looked into more closely. Thus, these calculations are not, like those of Gauvin, based on parameters (level density, pairing energy etc.) obtained from the best fit between the calculated and observed P_n values and then used for calculating the spectra. A mixture of both might be the best.

H. GAUVIN: We had the opportunity of comparing our results with your, and there are indeed some divergences. It seems to me that the intensity of the second peak in the spectrum which you obtained for ^{87}Br is too low. Our methods differ particularly as regards the spin- and energy-dependence of the factor $\Gamma_n/\Gamma_n + \Gamma_\gamma$. I think we should be able to converge towards more correct results and for this purpose it would be desirable to compare the very bases of our calculations.

S. AMIEL: Since we observe, as I have mentioned in my paper (SM-122/205), a rather insensitive dependence on spin and parity considerations when calculating P_n values, I wonder whether you can verify this conclusion from your findings.

H. GAUVIN: In our work we tried basically to find out whether, using coherent and reasonable values of the selected parameters, we could obtain, for calculated P_n values in agreement with the experimental values, energy spectra which, too, would be in agreement with those available now. The preliminary results presented show clearly that spin and parity considerations have a considerable effect on both P_n and the shape of the spectra. Any calculations carried out must take account of these two characteristics of delayed neutron emission simultaneously.

SOME INVESTIGATIONS OF HIGH-ENERGY GAMMA RAYS FROM SHORT-LIVED FISSION PRODUCTS

N.R. LARGE, R.J. BULLOCK
Atomic Energy Research Establishment,
Harwell, Berks,
United Kingdom

Abstract

SOME INVESTIGATIONS OF HIGH-ENERGY GAMMA RAYS FROM SHORT-LIVED FISSION PRODUCTS. A knowledge of the high energy γ-rays emitted by fission products is of considerable value in fission studies. The use of Ge(Li) detectors makes possible accurate measurement of these γ-rays.

The γ-spectra of a number of fission products with half-lives of a few minutes to a few hours have been examined by means of a Ge(Li) detector; the fission products selected have been chosen from those likely to emit γ-rays of over 2.5 MeV. By comparison of these and other known spectra with the γ-spectrum of irradiated ^{235}U the main contributors to the high-energy portion of the fission product spectrum have been ascertained.

INTRODUCTION

A detailed knowledge of the γ-spectra of fission products is useful for shielding calculations and for the calculation of γ-heating in reactors and associated equipment such as processing plants. Information of this kind is also required in other fields, such as studies of photofission. Many measurements of the spectra of individual fission products were made with sodium iodide detectors which, however, gave rather poor resolution, and fine structure in the low energy region was often obtained by other techniques such as conversion electron spectrometry. Where gross fission products were measured it was usually possible to produce only a broad general picture, and heating and shielding calculations were either based on the condensation of these spectra into a small number of broad energy bands, or on calculations taking into account all the known spectra.

With the advent of solid state detectors it became possible to obtain well-resolved γ-spectra, and in particular to study in greater detail the high energy region of the spectra. We have investigated the γ-spectra of a number of fission products with half-lives of a few minutes to a few hours, concentrating on the 2.5-5 MeV region, and we have also determined the γ-spectra of gross fission products over this range.

EXPERIMENTAL

The methods used for the separation of individual fission products have been described elsewhere [1]. Most of these fission products were obtained from small samples of natural uranium irradiated in the DIDO reactor at a thermal flux of about 3×10^{13} n.cm.$^{-2}$sec.$^{-1}$ or from samples of 93V uranium irradiated in BEPO at a much lower flux. Rubidium-88, however, was obtained by irradiation of rubidium carbonate. For the spectra of gross fission products 1mg. samples of natural uranium encapsulated in silica were irradiated in DIDO for various times. After an appropriate cooling period the spectra were measured on a coaxial Ge (Li) detector of 50cm^3 nominal active volume, and recorded by a Northern

Scientific 2048-channel analyser (type 615). The spectra were analysed by means of a computer programme based on the GASPAN programme[2].

Calibration of the γ-spectrometer was carried out with a ^{56}Co source, and the precision of energy measurements is generally of the order of 0.5 keV. However, slight gain shifts in the electronic equipment result in errors in the absolute values of energies amounting to a few keV, and corrections for these gain shifts have not been applied to the spectra presented here.

It was found that in general satisfactory spectra of gross fission products could be obtained without removing the samples from their silica capsules, irradiation of an empty capsule indicating that the only peak in the region above 2½ MeV arose from the activation of sodium impurity. It

TABLE I. IRRADIATION, COOLING, AND COUNTING PERIODS FOR URANIUM SAMPLES

No.	Duration of Irradiation	Duration of Cooling	Duration of Counting	No. of samples combined
1	5 min.	6 min.	5 min.	11
2	15 min.	15 min.	30 min.	6
3	1 h.	1 h.	1 h.	3
4	3 h.	3 h.	3 h.	2

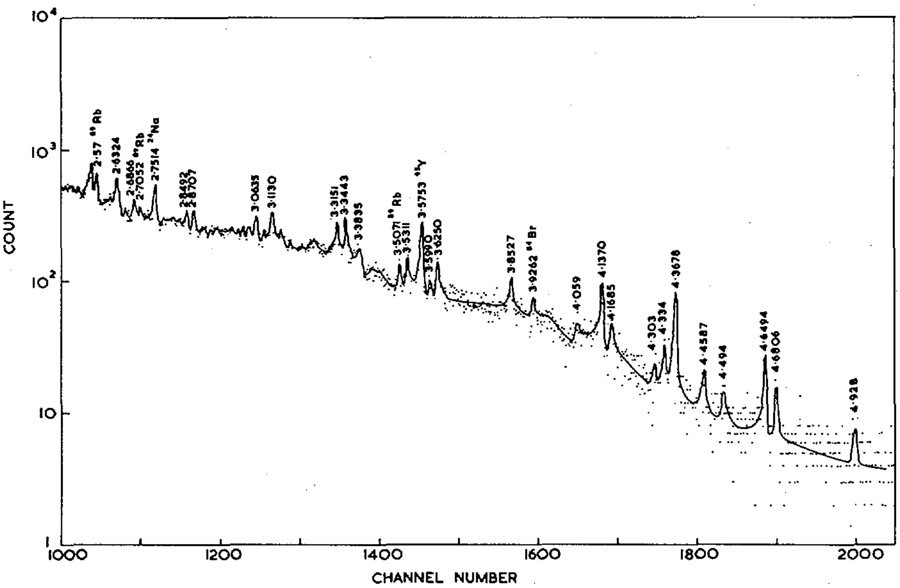

FIG. 1. The gamma spectrum of irradiated natural uranium (5 min irradiation, 6 min cooling).

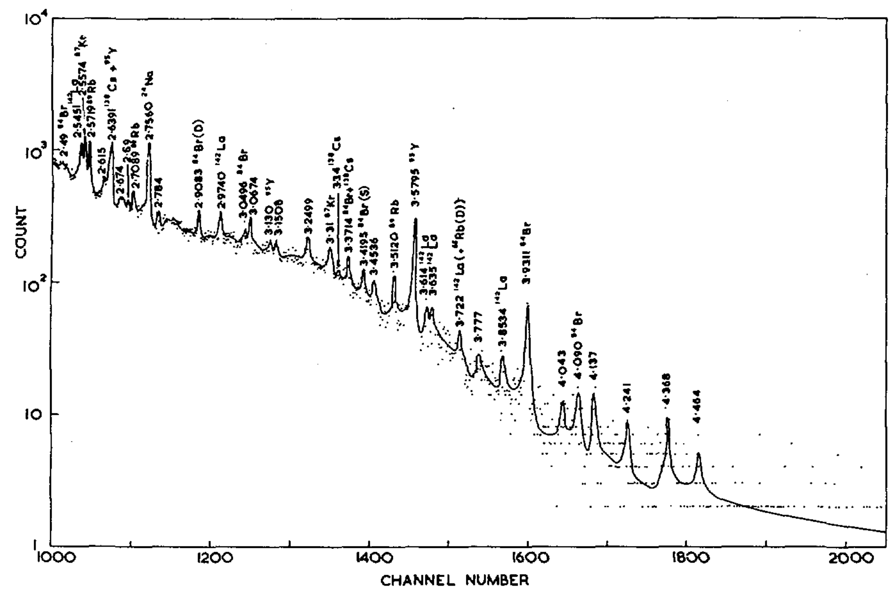

FIG. 2. The gamma spectrum of irradiated natural uranium (15 min irradiation, 15 min cooling).

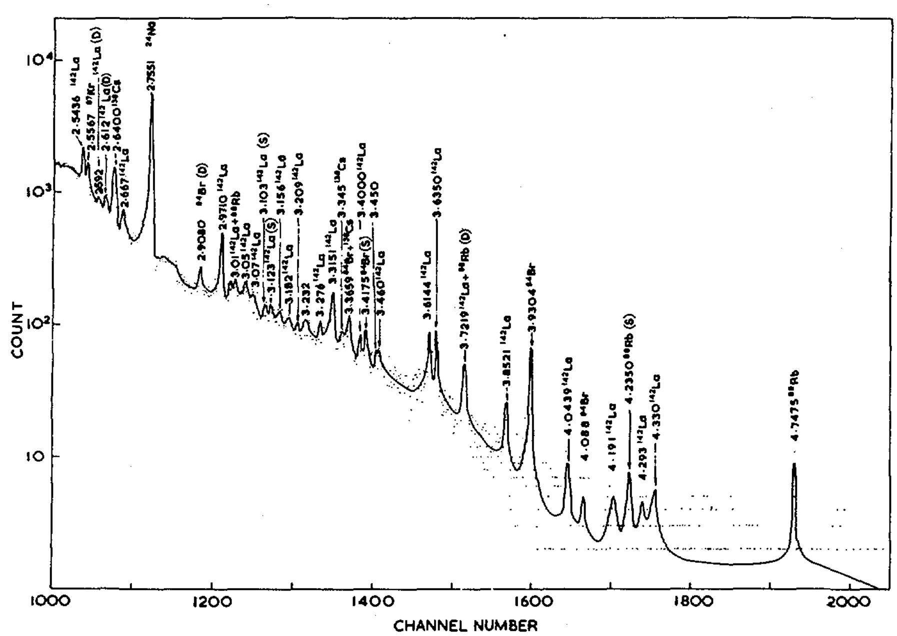

FIG. 3. The gamma spectrum of irradiated naturel uranium (1 h irradiation, 1 h cooling).

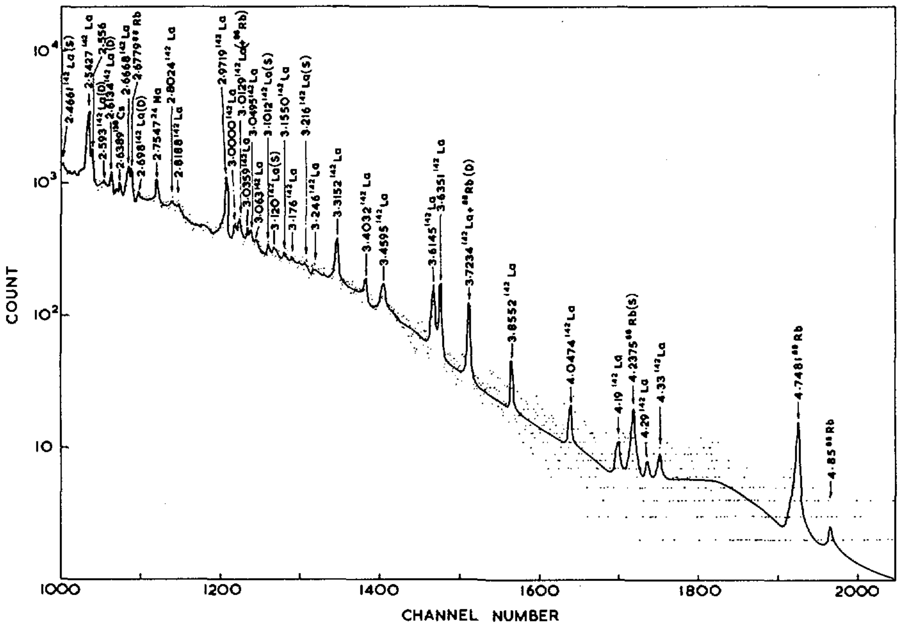

FIG. 4. The gamma spectrum of irradiated natural uranium (3 h irradiation, 3 h cooling).

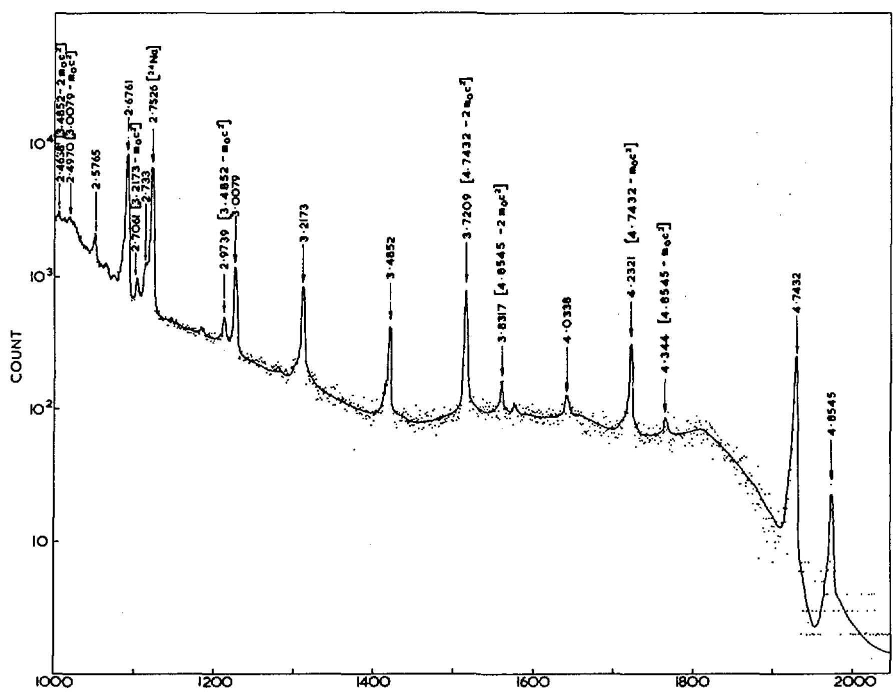

FIG. 5. The gamma spectrum of rubidium-88.

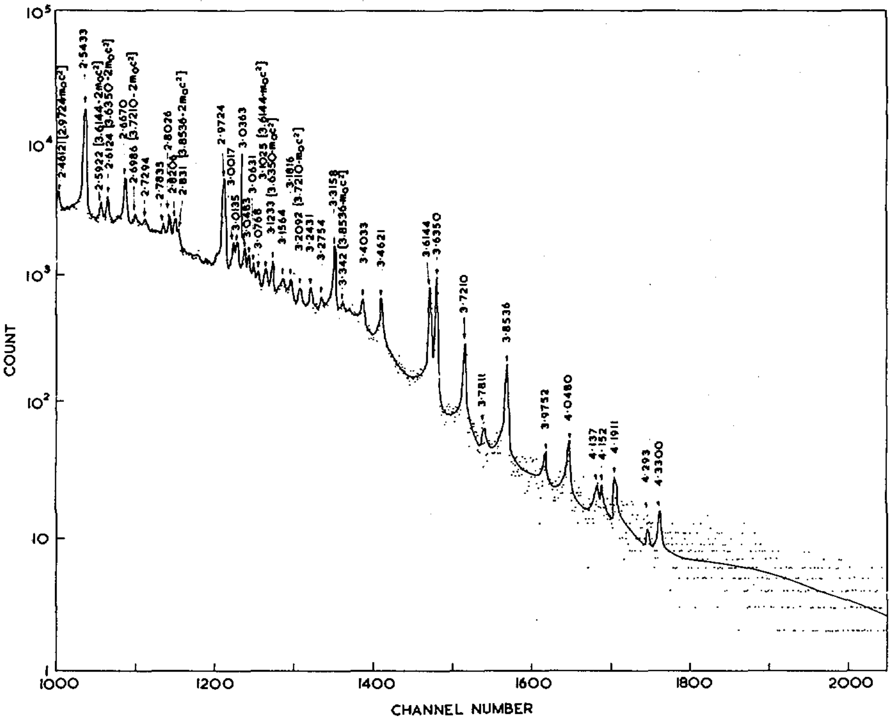

FIG. 6. The gamma spectrum of lanthanum-142.

was, however, found that in order to obtain satisfactory statistics it was necessary to combine the results of several irradiations. The irradiation, cooling, and counting periods are given in Table I.

RESULTS

The γ-spectra, in the range 2.5–5 MeV, obtained from irradiated uranium, are shown in Figs. 1 to 4. The counts are plotted on a logarithmic scale, and energies are given in MeV.

In the spectrum from the 3h. irradiation (Fig. 4) almost all the fission product gamma peaks have been identified as arising from ^{88}Rb and ^{142}La. The small peak at 2.75 MeV is due to a trace of sodium impurity, and the peak at 2.64 MeV is due to the fission product ^{138}Cs. The γ-spectra of ^{88}Rb and ^{142}La are shown in Figs. 5 and 6. ^{88}Rb has been studied by a number of workers [3,4,5,6]; our spectrum is in close agreement with that recently observed by Lycklama et al [6], and in the region of interest (2.5–5 MeV) is also in good agreement with that of Aras et al [5]. The spectrum of ^{142}La (Fig. 6) shows a number of high energy peaks not previously reported, extending to over 4 MeV.

In the spectrum from the 1h. irradiation (Fig. 3) the peaks due to ^{88}Rb and ^{142}La are still the main contributors, but there now appears a considerable contribution from ^{84}Br, whose spectrum is shown in Fig. 7. This shows several high energy peaks which do not appear in the spectrum obtained by Johnson and O'Kelley [7]. The 2.64 MeV peak due to ^{138}Cs is more prominent in the spectrum from the 1h. irradiation than in that from the 3h. irradiation, and some of the minor ^{138}Cs peaks are just observable.

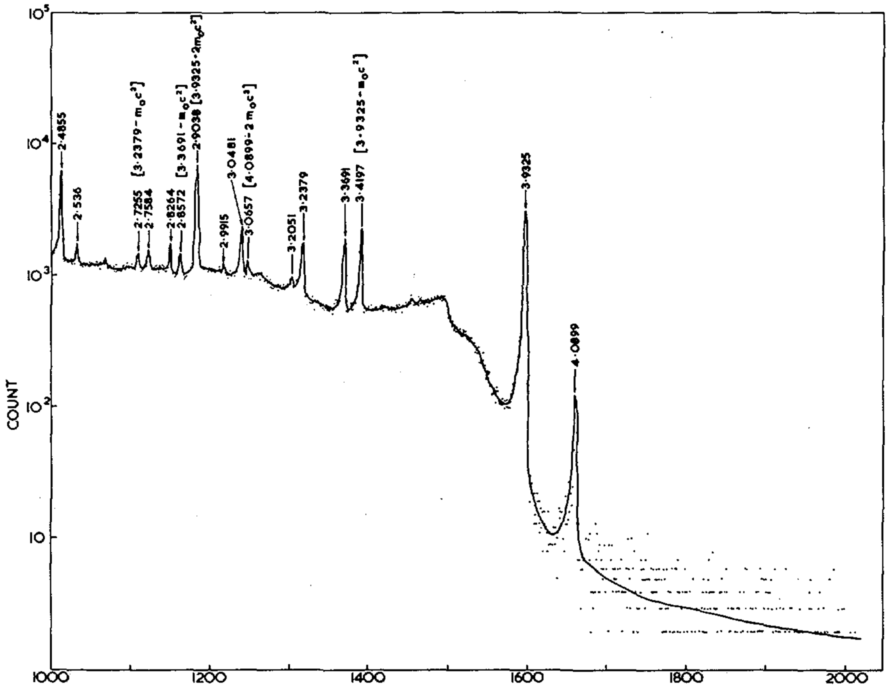

FIG. 7. The gamma spectrum of bromine-84.

The only other nuclide identifiable in the 1h. spectrum is ^{87}Kr whose 2.557 MeV peak is clearly visible. There are, however, one or two small peaks which have not been identified.

In the spectrum from the 15 min. irradiation there are quite a number of unidentified peaks, especially above 4 MeV. The identifiable contributors are ^{84}Br, ^{87}Kr, ^{89}Rb, ^{95}Y, ^{138}Cs and ^{142}La, the most prominent peaks being due to ^{84}Br and ^{95}Y. ^{88}Rb cannot be identified in this spectrum, although it probably makes a small contribution to the peak at 3.72 MeV. The high energy region of the ^{95}Y spectrum has been determined by Fiedler and Kennett [8], and the ^{87}Kr spectrum has been measured by Holm [9] and by Lycklama et al [6]. We have measured the spectrum of ^{89}Rb, and our spectrum is in good agreement with that of Kitching and Johns [10].

In the spectrum from the 5 min. irradiation very few peaks have been identified; those which have being due to ^{84}Br, ^{89}Rb, and ^{95}Y.

TABLE II. FISSION PRODUCTS WITH Q_{β}-GREATER THAN 3 MeV AND FISSION YIELD GREATER THAN 0.1%

Nuclide	Half-Life	Q_{β^-} (MeV)	Fission Yield (%)	Notes
^{83m}Se	70s.	3.6	0.56	Total yield for ^{83}Se
^{84}Br	31.8 min.	4.7	0.92	
^{86}Br	54s.	7.1	2.0	Q_{β^-}uncertain
^{87}Br	55s.	6.1	3.2	
^{87}Kr	76 min.	3.89	2.54	
^{88}Rb	17.8 min.	5.2	3.55	2.8h. precursor
^{89}Kr	3.2 min.	4.6	4.6	
^{89}Rb	15.4 min.	3.92	4.75	
^{90}Rb	2.9 min.	6.6	5.55	
^{91}Rb	1.2 min.	5.5	5.4	Q_{β}-estimated
^{92}Y	3.53h.	3.63	6.03	
^{93}Sr	8 min.	4.8	5.9	
^{94}Y	20.3 min.	5.0	6.4	
^{95}Y	10.9 min.	4.2	5.9	
^{96}Y	2.3 min.	6.9	6.0	Q_{β}-estimated
^{98}Nb	51 min.	4.6	5.9	
^{100}Nb	3 min. or 11 min.	6.1	6.4	Q_{β}-estimated
^{102}Tc	5s. or 4.5 min.	4.4	4.1	
^{104}Tc	18 min.	5.8	1.8	

DISCUSSION

There are many reported fission products with Q_{β}-values high enough for them to be capable, in principle, of emitting γ-rays of over $2\frac{1}{2}$ MeV. None of these have half-lives of more than a few days, although in a few cases they have longer-lived precursors. Table II gives a list of the more important of these potential γ-emitters, together with their half-lives, Q_{β}-values and fission yields. Half-lives and Q_{β}-values have been taken from the Table of Isotopes [11], and the fission yields are derived from Croall[12].

From the spectra of gross fission products it is clear that after 3h. irradiation and 3h. cooling the only significant high energy γ-rays arise from ^{88}Rb and ^{142}La. For irradiation and cooling periods of 1h. other nuclides, in particular ^{84}Br, become important. For shorter irradiation

TABLE II. (cont.)

Nuclide	Half-Life	Q_{β^-} (MeV)	Fission Yield (%)	Notes
^{105}Tc	8 min.	3.4	0.83	
^{106}Rh	30s.	3.54	0.38	367d precursor
^{107}Ru	4.2 min.	3.2	0.19	
^{128}Sb	11 min. or 9h.	4.3	0.50	
^{130}Sb	33 min. or 7 min.	5	2.0	Q_β-estimated
^{132}I	2.3h.	3.56	4.7	
^{134}I	52 min.	4.2	7.8	
^{136}I	83s.	7.0	6.4	
^{137}Xe	3.9 min.	4.0	6.1	
^{138}Cs	32.2 min.	4.83	7.22	17m. precursor
^{139}Cs	9.5 min.	4.0	6.42	
^{140}Cs	66s.	6.1	6.04	Q_β-estimated
^{140}La	40.22h.	3.77	6.4	12.8d precursor
^{142}La	92.5 min.	4.51	5.9	11 min. precursor
^{143}La	14.0 min.	3.3	5.7	
^{146}Pr	24.0 min.	4.2	3.05	
^{148}Pr	2 min.	4.5	1.68	
^{152}Pm	6 min.	3.5	0.26	Q_β-estimated

and cooling periods the picture is much less clear, and although some of the contributors can be identified there are many still to be identified. It is also clear from the spectra that for irradiation periods of over 15 min. there can be very little contribution from γ-rays of over 5 MeV, but for shorter periods there are obviously contributions from γ-rays of much higher energy.

REFERENCES

[1] R. J. BULLOCK and N. R. LARGE, UKAEA Rep. AERE-M 2135 (1969).

[2] V. BARNES, I.E.E.E. Trans. Nucl. Sci. NS15 3 (1968) 437.

[3] S. THULIN, Arkiv Fysik 9 (1955) 137.

[4] N. H. LAZAR, E. EICHLER and G. D. O'KELLEY, Phys. Rev. 101 (1956) 727.

[5] N. K. ARAS, E. EICHLER, G. D. O'KELLEY, and N. R. JOHNSON, Nucl. Sci. and Appl. 3 2 (1967) 58.

[6] H. LYCKLAMA, N. P. ARCHER, and T. J. KENNETT, Can. J. Phys. 47 (1969) 393.

[7] N. R. JOHNSON and G. D. O'KELLEY, Phys. Rev. 108 (1967) 82.

[8] H. J. FIEDLER and T. J. KENNETT, J. Inorg. Nucl. Chem. 28 (1966) 1129.

[9] G. HOLM, Arkiv Fysik 34 (1967) 433.

[10] J. E. KITCHING and M. W. JOHNS, Can. J. Phys. 44 (1966) 2661.

[11] C. M. LEDERER, J. M. HOLLANDER, and I. PERLMAN, Table of Isotopes 6th Edition (1967).

[12] I. F. CROALL, UKAEA Rep. AERE-R 5086 (1967).

DISCUSSION

L. V. EAST: Can you give me some numbers on the resolution you obtained with your detector in this energy range (2.5-5.0 MeV)?

N. R. LARGE: The detector had a resolution of about 5 keV for ^{60}Co and about 7 keV in the region of interest.

M. NEVE DE MEVERGNIES: Did you perform any half-life measurements on the unidentified gamma lives?

N. R. LARGE: No. The low detection efficiency for the high-energy gamma rays means that we have to accumulate results from a number of samples in order to obtain satisfactory statistics. It is therefore difficult to determine half-lives, although it would clearly be of advantage to do so.

J. EIDENS: I have a comment on Table II of the paper. At the Jülich gas-filled on-line mass separator we have determined the Q_β values of seven nuclides, and these were all above 3.0 MeV. The following Q_β values and half-lives were measured:

^{91}Kr : 5.7 MeV, 7.9 s
^{97}Y : 5.7 MeV, 1.11 s
^{99}Nb : 3.7 MeV, 14.3 s
^{99}Zr : 4.5 MeV, 2.4 s
^{100}Nb : 6.5 MeV, 6.6 s
^{101}Nb : 4.6 MeV, 7.0 s
^{101}Zr : 6.5 MeV, 3.3 s

The detailed results have been submitted to Nuclear Physics.

FUNDAMENTAL FISSION SIGNATURES AND THEIR APPLICATIONS TO NUCLEAR SAFEGUARDS*

L.V. EAST, G.R. KEEPIN
University of California,
Los Alamos Scientific Laboratory,
Los Alamos, New Mex.,
United States of America

Abstract

FUNDAMENTAL FISSION SIGNATURES AND THEIR APPLICATIONS TO NUCLEAR SAFEGUARDS.
The Los Alamos Scientific Laboratory is presently involved in a research and development program in the technology of inspection and identification of fissionable material to meet the growing need for more effective national and international controls over nuclear materials. The implementation of an effective nuclear safeguards and materials management system requires direct physical methods of detecting, identifying, and quantitatively analysing fissionable materials in various practical configurations.

Practical active interrogation methods are being developed using sources of neutrons to induce fissions in the material under investigation. In these methods, quantitative assay is based on detailed observations of the delayed and prompt neutrons and gamma rays from fission. The characteristic differences in the yields and kinetics of delayed neutrons from the various fission species provide a unique method for analysis of individual fissionable isotopes in unknown mixtures; assay methods using these signatures are described.

To investigate fully all possible signatures of individual fissionable isotopes, one must have detailed knowledge of the various emissions associated with the fission process. For this reason, a number of fundamental measurements of these emissions are being performed at Los Alamos. A review of our delayed-neutron and gamma-ray work is presented.

1. INTRODUCTION

The implementation of an effective nuclear safeguards and materials management system requires direct physical methods of detecting, identifying, and quantitatively analysing fissionable materials in various practical configurations containing both fissionable and non-fissionable materials. To be most effective and useful, such assay methods should be non-destructive, rapid, accurate, and capable of being carried out under a wide range of both laboratory and field conditions, e.g. in materials processing plants, fuel shipping facilities, and at reactor sites.

Non-destructive assay methods presently being investigated can be divided into two main categories: (1) passive assay, and (2) active interrogation. Passive assay methods involve observation of naturally occurring neutron and gamma radiations from some of the fissionable species (notably ^{239}Pu, ^{240}Pu, and ^{235}U). The naturally occurring gamma lines having sufficient intensity for passive assay applications are typically a few hundred kilovolts or less in energy and hence have limited penetrability through dense materials. For many practical

* Work performed under the auspices of the US Atomic Energy Commission.

assay problems this lack of penetrability, together with the absence of suitable passive signatures for many fissionable isotopes, often severely limits the usefulness of passive methods, and it becomes necessary to invoke active interrogation techniques which provide the higher penetrability required. From an inspection and surveillance standpoint, it is also noteworthy that active interrogation techniques are inherently more difficult to subvert or circumvent than are the simpler passive techniques.

Active interrogation involves the use of an external source of highly penetrating neutrons or photons to induce fissions in the material under investigation. Neutron sources are particularly well suited for active interrogation because of (1) high effective penetrability of fast neutrons in nuclear materials generally; (2) sharp, well-defined neutron fission thresholds which provide incisive isotopic discrimination; and, (3) readily available, inexpensive, compact neutron sources (e.g. D-T neutron generators, ^{252}Cf, etc.) of the required intensity and reliability for practical assay applications.

In active interrogation methods using either neutron or photon interrogation, quantitative assay is based on detailed observations of one or more types of emissions following fission, notably delayed and prompt neutrons and gamma rays. The delayed regime has the advantages of complete time-separation from the interrogating pulse, and permits the use of a minimum amount of counting and data reduction equipment.

The characteristic differences in yields and kinetic (time-dependent) response of the delayed neutrons from the various fission species provide a unique method for analysis of individual fission isotopes in unknown mixtures of fissionable and non-fissionable materials [1]. The experimental techniques involved in delayed-neutron assay are rapid, non-destructive, and relatively simple and inexpensive.

In addition to delayed neutrons, delayed fission gamma rays and prompt fission neutrons and gamma rays may also be used to provide very useful characteristic signatures of individual fission species. To explore fully these signatures, a number of fundamental measurements are being carried out on fission neutron and gamma-ray yields and energy characteristics.

2. FUNDAMENTAL FISSION DATA

As the first example of such fundamental measurements, we cite the recent Los Alamos studies [2] of absolute delayed-neutron yields per fission. The absolute yields of delayed neutrons from 3.1- and 14.9-MeV neutron-induced fission were measured for all of the major fission species: ^{233}U, ^{235}U, ^{238}U, ^{239}Pu, and ^{232}Th. Preliminary measurements have since been made of the delayed-neutron yields of ^{240}Pu and ^{241}Pu for 14.9-MeV neutron-induced fission [3].

The measurement involved the determination of two quantities: the number of fissions induced in the sample, and the number of delayed neutrons resulting from these fissions. A Cockcroft-Walton accelerator neutron source, modulated on and off with a duty cycle slightly less than 50% and with a period much shorter than any known delayed-neutron decay constant, was used to induce fissions in the samples. A modified long-counter neutron detector, operating in antisynchronism with the

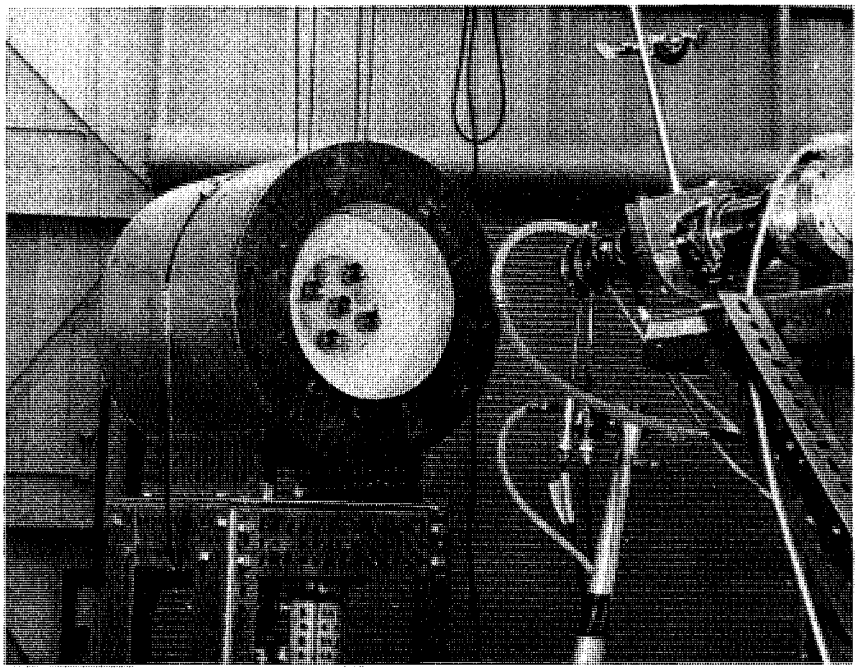

FIG.1. Experimental arrangement for absolute delayed-neutron measurements. The fission counter-sample assembly is located at the end of the accelerator target tube near the centre of the figure.

accelerator, measured the delayed-neutron output; two fission counters, sandwiching the sample, measured the number of fissions. The general experimental arrangement is pictured in Fig.1, showing the neutron detector at the left (with Cd cover removed), accelerator target tube entering from the right, and the fission-counters-plus-sample sandwich positioned at the end of the accelerator target tube. Background radiation in the long counter was measured by removing the entire fission counter-sample assembly from the neutron beam with the accelerator operating in the modulated mode.

The simple experimental arrangement shown in Fig.1 results in a minimum of scattering and thermalizing material in the immediate vicinity of the sample, as contrasted to the experimental configurations used in earlier delayed-neutron yield measurement. The technique of modulating the neutron source fully utilizes the high neutron intensities provided by compact neutron generators, allowing the use of small samples resulting in negligible self-absorption and multiplication corrections.

The results of these yield measurements are summarized in Table I, and a comparison with previous yield measurements for all but ^{240}Pu and ^{241}Pu is shown in Fig.2. For the five isotopes shown in Fig.2, the delayed-neutron yield is seen to decrease significantly in going from 3.1-MeV to 14.9-MeV fission – a result which is expected from the known behaviour of fission mass and charge distribution [4], but which is in contrast to most previous measurements at other laboratories.

TABLE I. MEASURED ABSOLUTE DELAYED-NEUTRON YIELDS (Delayed Neutrons/Fission)

Isotope	14.9-MeV fission yield	3.1-MeV fission yield	Yield Ratio $\frac{3.1\text{ MeV}}{14.9\text{ MeV}}$
^{239}Pu	0.0043 ± 0.0004	0.0069 ± 0.0007	1.60 ± 0.09
^{233}U	0.0043 ± 0.0004	0.0077 ± 0.0008	1.79 ± 0.10
^{235}U	0.0095 ± 0.0008	0.018 ± 0.002	1.89 ± 0.11
^{238}U	0.0286 ± 0.0025	0.049 ± 0.005	1.71 ± 0.10
^{232}Th	0.031 ± 0.003	0.060 ± 0.006	1.94 ± 0.11
^{240}Pu	0.0057 ± 0.0007	—	—
^{241}Pu	0.0084 ± 0.0012	—	—

Note: Indicated uncertainties are standard deviations. All yield values have been corrected to 100% isotopic purity.

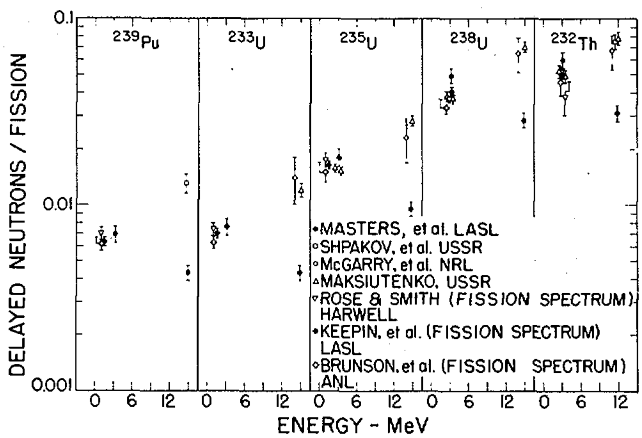

FIG. 2. Absolute delayed-neutron yield measurements versus average energy of the neutrons inducing fission.

In addition to delayed-neutron yields, the group abundances, a_i, and decay half-lives, T_i, of delayed neutrons from 14-MeV-neutron-induced fission are required in delayed-neutron assay applications based on delayed-neutron kinetics. These quantities are being measured at Los Alamos using a pulsed accelerator neutron source and a high-efficiency "slab" neutron detector [5]. Preliminary a_i, T_i data for 14.9-MeV-neutron fission of ^{235}U and ^{238}U are presented in Table II, where a comparison is made with previous measurements [6] for thermal neutron fission and fission-spectrum-induced fission (~1.5 MeV effective incident neutron energy).

TABLE II. DELAYED-NEUTRON GROUP ABUNDANCES

^{235}U			^{238}U		
Group	half-life T_i (s)	Relative abundances a_i/a	Group	half-life T_i (s)	Relative abundances a_i/a
Thermal Fissions [a]					
1	55.7 ± 1.3	0.033 ± 0.003			
2	22.7 ± 0.7	0.219 ± 0.009			
3	6.2 ± 0.2	0.196 ± 0.022			
4	2.30 ± 0.09	0.395 ± 0.011			
5	0.61 ± 0.08	0.115 ± 0.009			
6	0.23 ± 0.03	0.042 ± 0.008			
Fast Fissions ($E_n \simeq 1.5$ MeV) [a]					
1	54.5 ± 0.9	0.038 ± 0.003	1	52.4 ± 1.3	0.013 ± 0.001
2	21.8 ± 0.5	0.213 ± 0.005	2	21.6 ± 0.4	0.137 ± 0.002
3	6.0 ± 0.2	0.19 ± 0.02	3	5.0 ± 0.2	0.16 ± 0.02
4	2.23 ± 0.06	0.407 ± 0.007	4	1.93 ± 0.07	0.39 ± 0.01
5	0.50 ± 0.03	0.128 ± 0.008	5	0.49 ± 0.02	0.23 ± 0.01
6	0.18 ± 0.02	0.026 ± 0.003	6	0.17 ± 0.01	0.075 ± 0.005
14.9-MeV Fissions					
1	50.6 ± 1.9	0.063 ± 0.006	1	53.6 ± 5.1	0.023 ± 0.005
2	19.6 ± 0.7	0.188 ± 0.003	2	21.0 ± 0.8	0.148 ± 0.003
3	5.0 ± 0.4	0.234 ± 0.024	3	5.1 ± 0.5	0.162 ± 0.030
4	2.0 ± 0.1	0.357 ± 0.021	4	2.2 ± 0.2	0.369 ± 0.022
5	0.41 ± 0.09	0.118 ± 0.027	5	0.61 ± 0.07	0.183 ± 0.012
6	0.16 ± 0.07	0.04 ± 0.03	6	0.21 ± 0.02	0.115 ± 0.018

[a] From Ref. [6].

A new weighted least-squares exponential fitting code that can make a simultaneous fit to multiple data sets obtained using different irradiation and counting times has been written to obtain the a_i's and T_i's. This technique eliminates many of the problems encountered when one separately analyses pulsed irradiation data for the short periods and saturating irradiation data for the longer periods. The 14.9-MeV results shown in Table II were obtained using four different irradiation and counting times. For ^{235}U, the irradiating and counting times used were 0.1 s and 15.5 s, 2.0 s and 202 s, 30.0 s and 252.0 s, and finally 60.0 s and 302.5 s. For ^{238}U, somewhat more optimum times of 0.1 s irradiation and 15.5 s count, 2.0 s and 61 s, 10.0 s and 121 s, and 60 s irradiation and 302.5 s count were used. Background runs were also made with the samples removed from the neutron beam, and using the same irradiation and counting times.

Only the longest-and shortest-lived groups show any large changes in relative yields in going from 1.5-MeV- to 14.9-MeV-neutron-induced fission. The large increase in relative yields of these groups is actually a result of a decrease in the absolute yields of the other groups. The absolute yield of the 53-s group for ^{238}U is 0.066% at 14.9 MeV, compared to 0.054% at 1.5 MeV. This is consistent with the fact that the fission yield of the precursor for this group, ^{87}Br, does not change significantly with the energy of the fission-inducing neutrons [9]. Recent delayed-neutron measurements reported by Cox and Whiting [7] show no significant changes in the a_i's for ^{235}U for incident neutron energies between 0.25 MeV and 1.5 MeV, or for ^{238}U and ^{232}Th from fission threshold to 2.4 MeV.

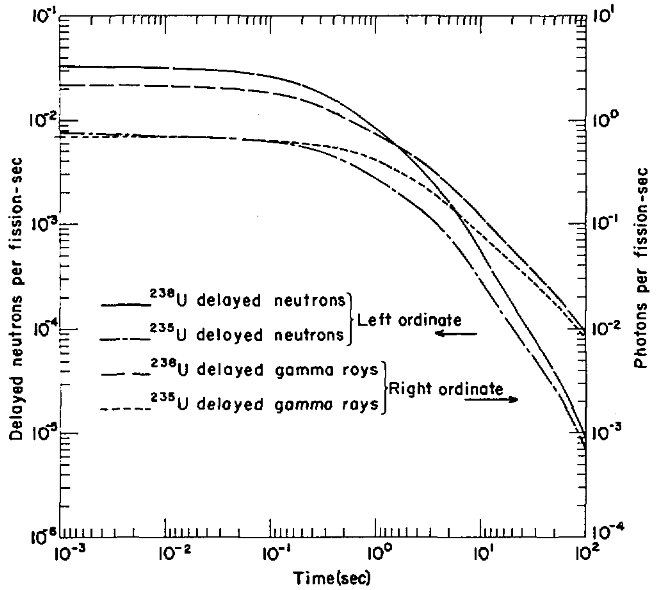

FIG.3. Gross delayed-neutron and gamma-ray activities versus time for fast-neutron-induced fission of ^{235}U and ^{238}U.

Basic delayed fission gamma-ray data may provide unique isotopic signatures or complement delayed-neutron assay methods, depending on the specific gamma-ray characteristics measured. The gross delayed gamma-ray intensity (total photons per fission-second) over the early time range from ~ 0.1 s to 100 s after fission depends on the isotope undergoing fission in much the same way as the delayed-neutron emission; i.e. longer average fission chain lengths correlate directly with larger fission yields. The similarity between delayed-neutron and delayed gamma systematics is illustrated in Fig.3, which shows gross delayed-neutron and gamma-ray activities versus time for neutron-induced fission of ^{235}U and ^{238}U. The systematics comparison indicated in Fig.3 is typical and applies rather generally to the major fission species. The delayed gamma-ray activities from ^{235}U and ^{238}U have been fitted [8] with five exponentials for times up to 2×10^3 s after fission. The resulting gross gamma-ray "periods and abundances" are given in Table III.

TABLE III. PERIODS AND ABUNDANCES FOR DELAYED GAMMA RAYS FROM NEUTRON-INDUCED FISSION OF ^{235}U AND ^{238}U

Period (j)	$T^j_{1/2}$ (s)	λ_j (s^{-1})	Abundances (Percent/Fission) b_j (^{235}U)	b_j (^{238}U)
1	2.9×10^{-1}	2.4×10^{0}	6.7×10^{0}	5.4×10^{1}
2	1.7×10^{0}	4.1×10^{-1}	1.05×10^{2}	1.76×10^{2}
3	1.3×10^{1}	5.3×10^{-2}	1.92×10^{2}	2.81×10^{2}
4	1.0×10^{2}	6.9×10^{-3}	1.73×10^{2}	2.02×10^{2}
5	9.4×10^{2}	7.4×10^{-4}	1.55×10^{2}	1.55×10^{2}

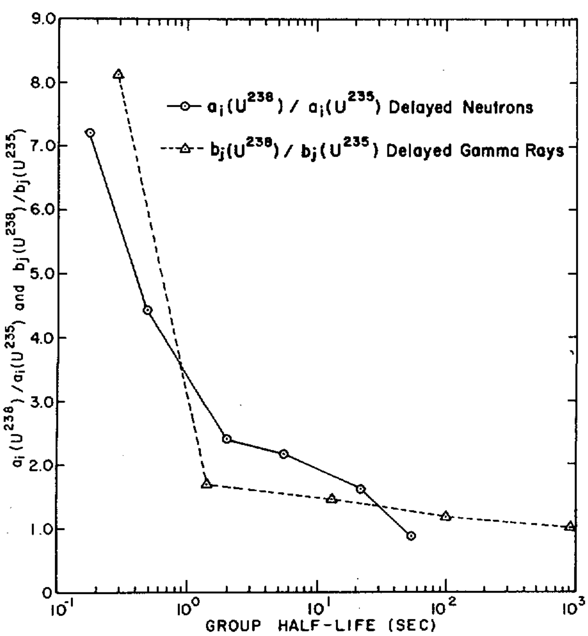

FIG.4. Ratios of delayed-neutron abundances and delayed gamma-ray abundances as functions of the appropriate group periods.

The correlation between delayed-neutron and gamma-ray yields for different fission isotopes is further illustrated in Fig.4. Here, ratios of the gamma-ray abundances (b_j) for ^{238}U and ^{235}U fission and corresponding ratios of delayed-neutron abundances (a_i) for fast fission are plotted as a function of the appropriate group periods. It is apparent that isotopic analysis based on gross delayed gamma-ray decay is both similar and complementary to the delayed-neutron kinetics method of assay.

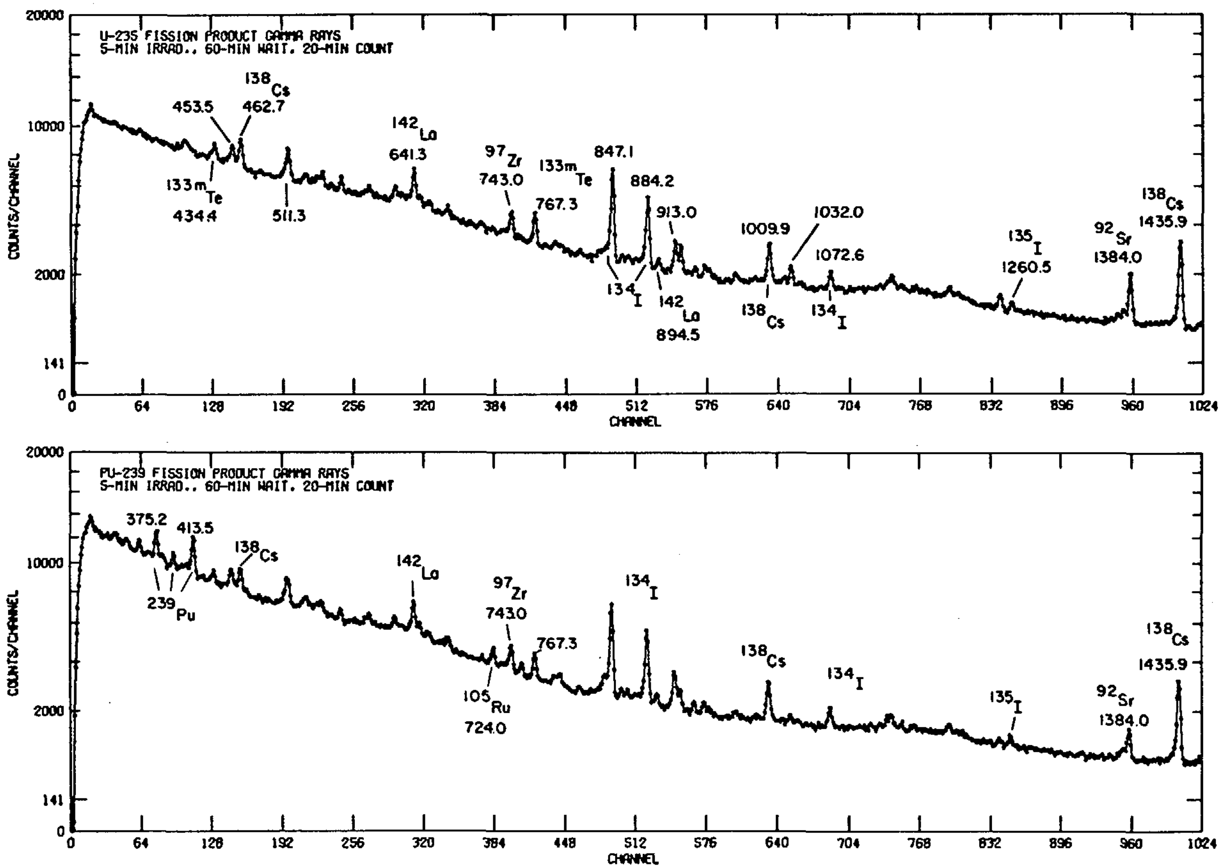

FIG. 5. Spectra of delayed gamma rays from thermal fission of ^{235}U and ^{239}Pu. Certain gamma lines are identified as to energy (in keV) and the decaying nuclide responsible.

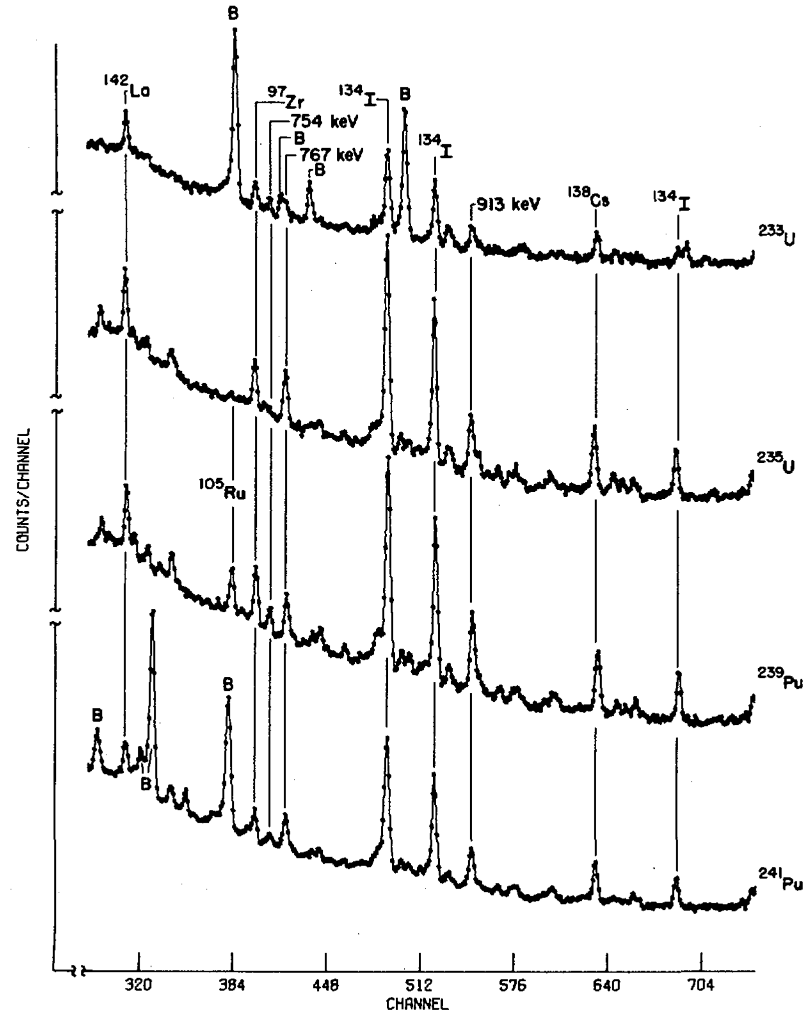

FIG. 6. A comparison of a portion of the fission product gamma-ray spectra from ^{241}Pu, ^{239}Pu, ^{235}U, and ^{233}U. The lines labeled with a "B" are background from the natural activity present in the samples.

The measurement of individual short-lived fission product gamma-ray lines can be applied to the assay of fissionable materials using techniques already developed for activation analysis. The method consists of detecting characteristic gamma rays from fission products by means of a high-resolution Ge(Li) system in the time region of a few minutes to a few hours after exposure of the sample to a neutron beam. Of particular interest for active interrogation would be any large differences in the yields of high-energy (penetrating) gamma rays from ^{235}U(n, F) and ^{239}Pu(n, F). In this case, interrogation with sub-threshold neutrons could be used to assay ^{239}Pu and ^{235}U separately, in the presence of a large quantity of ^{238}U, as occurs for example in power reactor fuels. Measurements of the spectra of delayed gamma rays emitted in the time range 10 min to 2.5 h following thermal neutron fission of ^{233}U, ^{235}U, ^{239}Pu, and ^{241}Pu have been performed.

Figure 5 shows the gamma-ray spectra observed from 8-gm samples of ^{235}U and ^{239}Pu in the energy range 300 keV to 1.45 MeV 60 min after a 5-minute thermal neutron irradiation. The samples were located $\sim$5 inches from the 20-c^3 Ge(Li) detector, which had a resolution of 3.6 keV for ^{60}Co gamma rays. A 0.25-in Pb absorber was placed between the samples and the detector to reduce the counting rate from X-rays and soft gamma rays. The most striking difference in the two spectra is the 724-keV line from ^{105}Ru which appears in the ^{239}Pu spectrum but not in ^{235}U. (The relative fission yield [9] of ^{105}Ru is a factor of 5.5 higher for ^{239}Pu than for ^{235}U.) The differences in the relative yields of ^{92}Sr and ^{138}Cs (a factor of about 1.5) can also be seen from the lines at 1384 keV and 1436 keV. A comparison of the gamma-ray spectra from ^{233}U, ^{235}U, ^{239}Pu, and ^{241}Pu obtained in the energy range of 630 keV to 1100 keV is shown in Fig.6. These spectra were obtained during a 40-min count taken 90 min after the end of a 5-min-thermal-neutron irradiation. The lines labeled "B" in the figure are from the background due to natural activity present in the samples.

In the time range of $\sim 10^{-6}$ s to 5×10^{-4} s after neutron-induced fission of ^{235}U and ^{239}Pu, nine prominent gamma rays have been observed with energies between 205 and 1330 keV [10]. These gamma rays result from the decay of four fission fragment isomers with half-lives in the range of 3.4 - 80 μs and fission yields between 0.3 and 1.3%. The yields of individual isomeric gamma rays from ^{235}U and ^{239}Pu fission differ significantly, and hence constitute a possible basis for isotopic assay; however, the corresponding data for other fissioning nuclei are not yet available.

The combined measurement of delayed-neutron and gamma-ray response to active interrogation should prove particularly useful for assay applications in which the environment of the nuclear material is unknown. Because of large differences in the attenuation characteristics of neutrons and gamma rays, such combined data can give important information about the materials surrounding, or interspersed with, the fissionable material under investigation.

3. DEVELOPMENT OF PRACTICAL NONDESTRUCTIVE ASSAY METHODS

The active interrogation methods being developed at Los Alamos utilize sources of fast neutrons to induce fissions in the material under investigation. The major emphasis to date has been on assay techniques based on total delayed-neutron yields and delayed-neutron decay as a function of time ("kinetic response" method). The use of delayed radiations has the advantage of complete separation of the interrogation signal from the measured signal. These techniques have been shown to be capable of accurate analysis of individual fissionable isotopes in unknown mixtures.

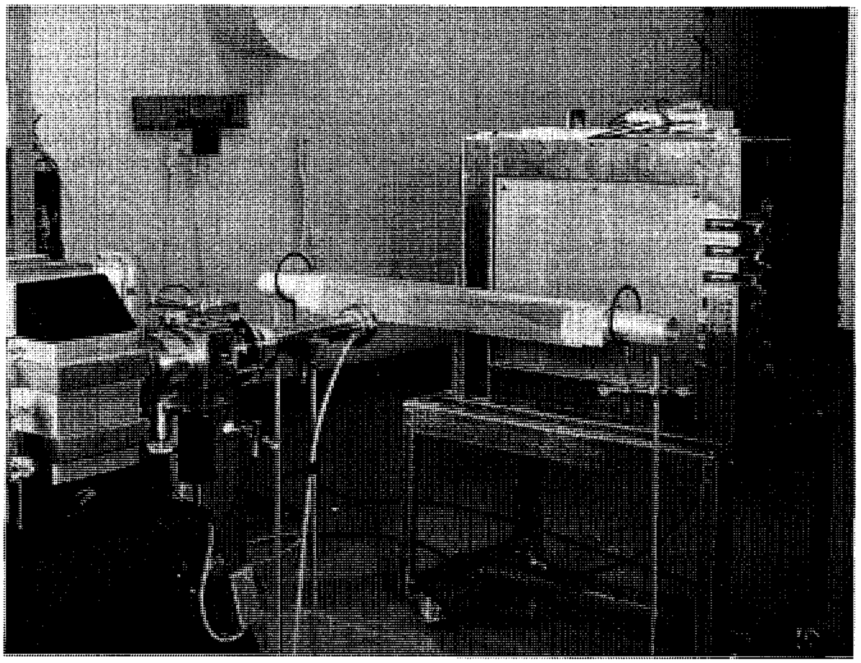

FIG. 7. Experimental arrangement for delayed-neutron assay of bare MTR-type reactor fuel elements. The neutron generator target is seen at the left, and a high-efficiency delayed-neutron detector is seen behind the fuel element.

The kinetic response method of determining relative isotopic abundance consists basically of irradiating an unknown sample with fast neutrons and observing the delayed-neutron response as a function of time. Delayed-neutron decay is characterized by six exponential decay periods, as shown in Table II, each having characteristic group abundances which are significantly different for the various fission species. The differences in abundances of the six delayed-neutron groups result in readily measurable differences in the shape of delayed-neutron decay following neutron interrogation. By counting the delayed neutrons emitted in various time intervals following neutron irradiation of a sample, these decay-shape differences result in measurable differences between the fissioning isotopes [11]. For many types of composite systems, the kinetic response method is capable of determining relative isotopic abundances to within ~ 2% accuracy.

The yield method of assay is an outgrowth of the repetitive pulsing technique employed in the absolute delayed-neutron yield measurements previously described in this paper. The unknown samples to be assayed are repetitively irradiated with short pulses (50-100 ms) alternating with delayed-neutron counting intervals of similar duration. For this mode of irradiation, the measured delayed-neutron counting rate is essentially proportional to the time-integrated delayed-neutron yield and, in turn, to the amounts of the fissionable materials present. Thus, using a suit-

TABLE IV. DELAYED-NEUTRON ASSAY OF ABSOLUTE AMOUNTS OF FISSILE MATERIAL IN MTR-TYPE FUEL ELEMENTS

14-MeV (D-T) interrogating neutrons	
Actual weighed ^{235}U content (grams)	Delayed-neutron assay determination (grams)
339.95 (fully loaded)	calibration point
320.95	320.9
302.15	303.2
283.95	283.5
265.45	266.5
247.05	249.9

Average Deviation : 0.4%

able flux monitor and/or fission monitor, the absolute amount of material present can be determined from measured delayed-neutron yield as compared to the yield from a standard of known mass. This assay technique has been applied to MTR-type fuel elements and mock-ups with an assay accuracy of better than 1% over a wide range of fuel loadings. A typical assay arrangement is shown in Fig.7. The target end of a 150-kV-neutron generator is seen at the left of the figure, and the fuel element is between the target and a high-efficiency neutron detector. Representative assay data for bare fuel elements using 14-MeV interrogating neutrons are presented in Table IV.

When the MTR fuel element is enclosed in a massive lead shield (of thickness comparable to that of spent-fuel-element shielding casks), there is little perturbing influence on the results and accuracy of fuel element assay using neutron interrogation and the delayed-neutron yield method of assay. Typical assay results for heavily shielded MTR fuel elements are accurate to ~ 1% or better [12]. The obvious implications for performing assay and burn-up determinations of spent fuel elements without removing them from their shielding casks are being actively pursued.

In both the delayed-neutron yield and kinetic response methods just described, the energy of the interrogating neutrons can also be varied to take full advantage of the greatly increased isotopic discrimination afforded by the sub-threshold and super-threshold fission characteristics of the various isotopes present in composite systems. In particular, the use of sub-threshold and super-threshold neutron interrogation provides a straightforward separation of the response of the fissile isotopes (e.g. ^{233}U, ^{235}U, ^{239}Pu) and fertile isotopes (e.g ^{238}U, ^{232}Th). This technique has been used in conjunction with the modulated accelerator delayed-neutron yield method to provide a relatively simple and accurate means of determining the isotopic composition as well as the total material present in many different types of samples [13].

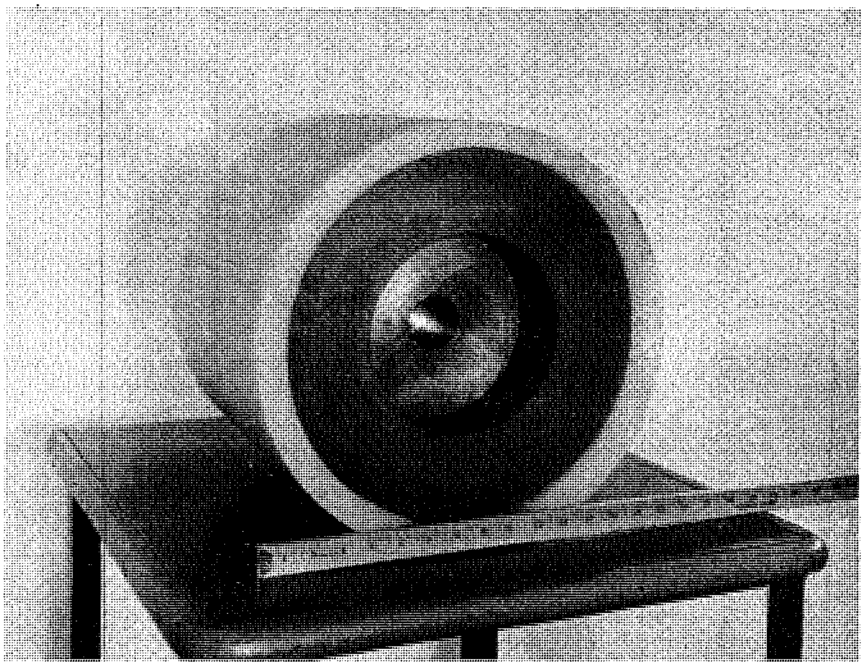

FIG. 8. Neutron moderating, or "beam tailoring", assembly consisting of tungsten, carbon, and polyethylene. The 14-MeV neutron generator target fits into the cavity in the centre of the assembly.

Different irradiating spectra are produced by surrounding the target of a 14-MeV (D-T) neutron generator with various combinations of tungsten, lead, carbon, and polyethylene which act as moderators. A typical moderator assembly is shown in Fig.8.

Figure 9 shows the delayed-neutron response for various enrichments of ^{235}U obtained using four different irradiating neutron spectra. The deviations of curves (c) and (d) from linearity are the result of absorption of the low-energy neutrons by the ^{235}U in the samples. A comparison of such measurements performed with an unknown sample and the response of standard samples of known composition gives quantitatively the fissionable materials present in the unknown sample. Table V gives a direct intercomparison between typical results using this delayed-neutron assay technique and results obtained from standard chemical and mass spectrographic techniques.

An important practical problem in special nuclear material accountability is the determination of the amount of fissile material in common fissionable scrap containers. Delayed-neutron yield and kinetics measurements offer a promising method for quantitative scrap assay. Preliminary measurements have indicated good sensitivity for detecting small (gram) quantities of fissile material in a standard 55-gallon steel barrel.

LASL's experimental program in fissionable scrap assay has been guided by computer simulation studies of delayed-neutron and gamma-

TABLE V. ASSAY OF SAFEGUARDS INVENTORY SAMPLES FROM NUCLEAR MATERIALS AND EQUIPMENT CORPORATION

	Delayed-neutron non-destructive assay (LASL)			Chemical assay (New Brunswick)	
Sample description	Total U Weight (g)	g U/g sample	% ^{235}U	g U/g sample	% ^{235}U
$UO_3 + ZrO_2$ Binary	1.44	0.750	98.6	0.7678	97.671
$UO_2 + ZrO_2$ Powder	1.40	0.766	96.4	0.7545	97.666
$UO_2 + ZrO_2$ Scrap	1.56	0.763	97.7	0.7695	97.653
$UO_2 + ZrO_2$ Scrap	1.52	0.756	96.0	0.7444	97.665
UO_2 Scrap Pellets	3.60	0.863	20.2	0.8678	20.059
UO_2 Scrap Pellets	3.60	0.884	16.0	0.8794	15.968
$UO_2 + U_3O_8$	1.67	0.840	9.91	0.8467	9.409
UO_2 Blended Oxides	1.82	0.890	4.25	0.8713	4.158
Average Deviation of LASL Results from Chemical Assay:		1.3%	1.6%		

ray response to active interrogation of small amounts of fissile material interspersed in large amounts of various scrap materials [12]. These parametric computations, summarized in Figs 10 and 11, point up the very useful general result that barrels (55-gallon size, commonly used for scrap storage) containing almost any common scrap material other than hydrogenous compounds, are effectively transparent to fast-neutron interrogation and delayed-neutron assay (see Fig.10). Assay for fissile material is thus essentially independent of composition of the matrix in which the fissile material is interspersed.

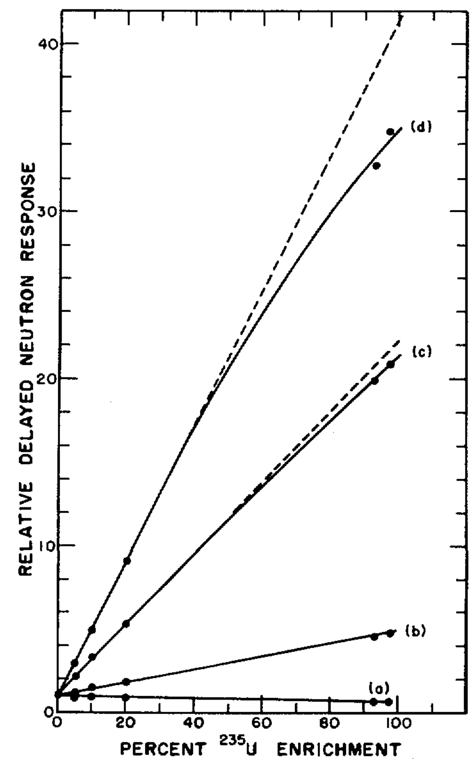

FIG. 9. Delayed-neutron response from cylindrical samples of U_3O_8 for different enrichments of ^{235}U (total mass of U held constant). Curve (a) corresponds to a 14-MeV neutron irradiation, and curves (b), (c), and (d) correspond to irradiations using moderated spectra with successively decreasing average energies.

The case of a hydrogenous matrix material is the most difficult for neutron assay applications, but even here calculations have shown that very effective fissile-material assay can be carried out by the use of a moderator-reflector together with appropriate normalization of the delayed-neutron response. Such a normalization can be obtained by a direct experimental determination of the delayed-neutron response of a small amount (nominally one gram) of each fissile species of interest as measured directly in the neutron energy spectrum of the actual system

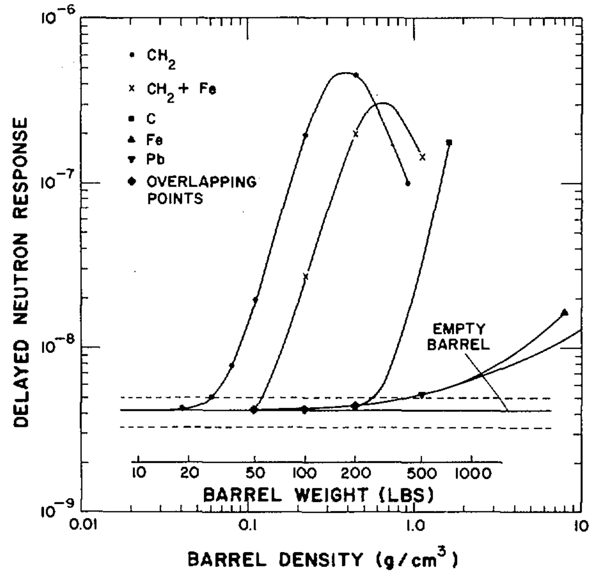

FIG. 10. Delayed-neutron response, using 14-MeV interrogating neutrons, of a simulated 55-gallon scrap barrel containing one gram of ^{235}U at 15 cm radius in representative matrix materials. The dashed lines indicate the response with no matrix materials present, ±20%.

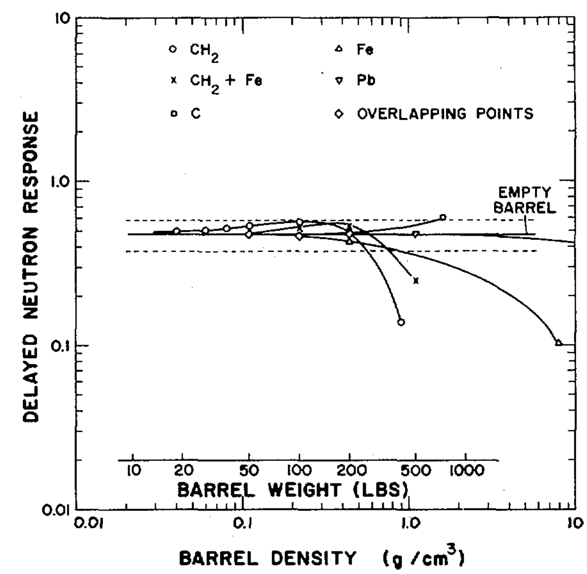

FIG. 11. Normalized delayed-neutron response (see text) of the scrap barrel of Fig. 10 surrounded by a 2.5-cm polyethylene reflector.

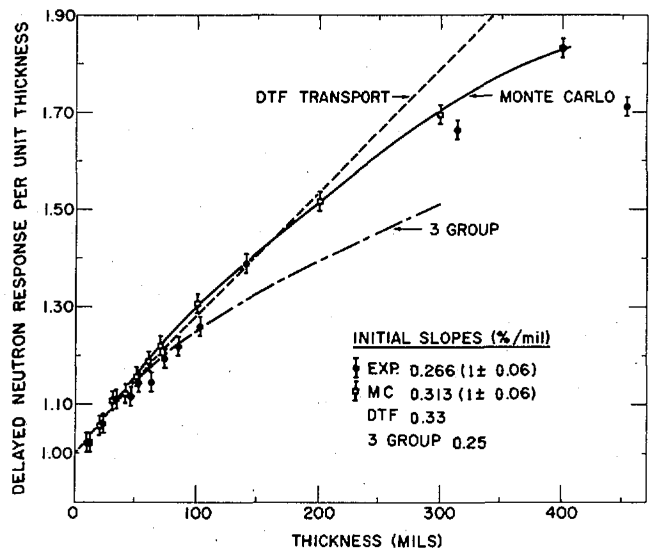

FIG.12. Calculated and measured delayed-neutron response per unit thickness for enriched U (93.6% ^{235}U, 6.4% ^{238}U).

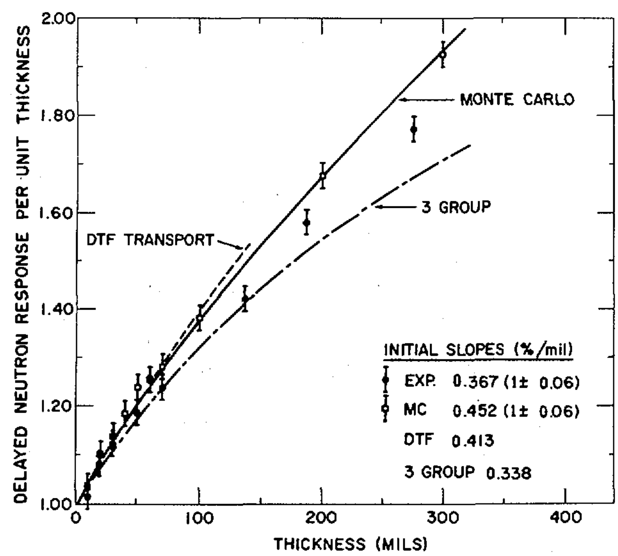

FIG.13. Calculated and measured delayed-neutron response per unit thickness for ^{239}Pu.

under interrogation. This may be accomplished by irradiating a gram of material in closest possible proximity (internally or peripherally) to the unknown sample, and then rapidly transferring the gram of material to a shielded delayed-neutron detector. This irradiation-counting sequence can be repeated as often as required to obtain the desired counting statistics for the normalization. The dramatic improvement in delayed-neutron response for bulk hydrogenous systems resulting from the use of such a normalization is clearly illustrated by comparison of Figs 10 and 11.

Another computational investigation pertinent to delayed-neutron assay in general is the study of delayed-neutron multiplication effects in small (far-subcritical) samples of fissionable material undergoing neutron interrogation [14]. Delayed-neutron multiplication increases the delayed-neutron response of a sample per unit mass and unit source, as the mass of the sample is increased. Such increased response can influence the quantitative determination of the amount of fissionable material present. The two main physical processes contributing to delayed-neutron multiplication in small samples are: (1) neutrons from fissions and nonelastic interactions induced by the interrogating source cause further fissions with the accompanying formation of delayed-neutron precursors; and (2) neutrons from delayed precursors induce fissions in the process of escaping from the sample. The fission neutrons resulting from (2) are, in effect, delayed because their ancestry includes a delayed neutron.

Three computational techniques have been used to study delayed-neutron multiplication effects: (1) a three-energy-group model with an analytic expression for neutron escape probabilities; (2) the Zero-Prompt-Lifetime Approximation in conjunction with a one-dimensional steady-state transport theory code; and (3) a three-dimensional time-dependent Monte Carlo code. The accuracy and limitations of the calculational techniques have been demonstrated by direct comparison with experimental measurements. Typical comparisons of calculated and measured delayed-neutron response for ^{235}U and ^{239}Pu are presented in Figs 12 and 13. It was concluded from this investigation that delayed-neutron multiplication effects are best calculated by Monte Carlo techniques. In all cases studied, Monte Carlo calculations were found to agree to within two standard deviations with the general shape of the measured delayed-neutron response curves.

The techniques for direct on-line non-destructive assay of fissionable materials being developed at Los Alamos are applicable not only to safeguards but to nuclear materials management and accountability problems throughout the nuclear industry. The availability of proven, on-line non-destructive assay systems, both active and passive, can be expected to have far-reaching implications, not only for worldwide safeguards and NPT inspections, but also as a means of implementing safe, efficient, and economic management of nuclear materials throughout the nuclear energy industry.

REFERENCES

[1] KEEPIN, G.R., in Safeguards Research and Development (Proc. Symp. WASH-1076, U.S. Atomic Energy Commission) (1967) 150.
[2] MASTERS, C.F., THORPE, M.M., SMITH, D.B., Nucl. Sci. Engng 36 (1969) 202.
[3] AUGUSTSON, R.H., MENLOVE, H.O., Los Alamos Scientific Laboratory, unpublished.
[4] KEEPIN, G.R., "Physics of Nuclear Kinetics", Addison-Wesley Publishing Co. (1965) 100.
[5] EAST, L.V., WALTON, R.B., to be published in Nucl. Instrum. Meth.

[6] KEEPIN, G.R., WIMETT, T.F., ZEIGLER, R.K., Phys. Rev. 107 (1957) 1044.
[7] COX, S., WHITING, E.E., DOWLING, Bull. Am. phys. Soc. 2 14 (1969) 536; Argonne National Laboratory Report ANL-7410 (1969) 27.
[8] WALTON, R.B., private communication.
[9] MEEK, M.E., RIDER, B.F., General Electric Co. (USA) Report APED-5398-A, Rev. (1968).
[10] WALTON, R.B., SUND, R.E., Phys. Rev. 178 (1969) 1894.
[11] KEEPIN, G.R., Los Alamos Scientific Laboratory Report LA-3741 (1967); AUGUSTSON, R.H., MENLOVE, H.O., HENRY, C.N., MASTERS, C.F., KEEPIN, G.R., Trans. Am. nucl. Soc. 11 (1968) 660.
[12] THORPE, M.M., HENRY, C.N., SMITH, D.B., MENLOVE, H.O., AUGUSTSON, R.H., Trans. Am. nucl. Soc. 11 (1968) 661.
[13] AUGUSTSON, R.H., MASTERS, C.F., MENLOVE, H.O., Trans. Am. nucl. Soc. 12 (1969) 94.
[14] LEE, C.E., MASTERS, C.F., TURNER, G.D., to be published.

DISCUSSION

J. MATUSZEK: In regard to your delayed neutron studies, I would like to ask you whether you are aware of patent applications by a California company for the neutron measurement technique. If so, what is your opinion on their claims, particularly in relation to the accuracy claimed for measuring ^{239}Pu in the presence of ^{235}U?

Regarding your gamma-ray spectra, have you obtained any results for fission induced with fission-spectrum or 14 MeV neutrons?

L.V. EAST: I believe I know of the company to which you refer, but I am not aware of their patent applications. They can probably indeed discriminate between ^{235}U and ^{239}Pu, but I don't know with what accuracy since, as I understand it, they base their method on the ratio of prompt to delayed neutrons emitted from fission. This ratio difference is sufficiently large for these isotopes to give good isotopic discrimination. This method does, of course, give rise to the problem of separating the neutrons inducing fission from the prompt fission neutrons. This is done, I believe, by using 100-200 keV neutrons to induce the fissions, and using a biassed detector, such as a ^{3}He counter with pulse-height discrimination, to detect prompt neutrons above this energy.

In reply to your question concerning gamma-ray spectra, we have obtained some preliminary spectra for ^{240}Pu using neutrons of about 2 MeV energy, and for ^{238}U using 14.7 MeV neutrons.

P. ARMBRUSTER: What integral fluxes did you use for activating your samples? And did you consider the use of neutron flash tubes as an active assay?

L.V. EAST: We obtain thermal neutrons by surrounding the target of a D-T neutron generator with a moderating assembly. For the delayed gamma-ray spectra shown, thermal neutron fluxes of $\sim 10^7$ - 10^8 n cm^{-2} s^{-1} were used.

We have developed a plasma-pinch device for use in such applications, but we have found that small accelerators of the Cockcroft-Walton type are much more reliable and give a quite adequate neutron yield. Please bear in mind that the short neutron pulses ($\sim 0.1\ \mu$s) obtained from plasma devices are not required for delayed neutron work; accelerator pulses of 50 to 100 μs are short enough.

J. BLACHOT: I think that the gamma transitions which you attribute to ^{133m}Te in Fig.5 are transitions of ^{134}Te.

L.V. EAST: Thank you. As was pointed out by Dr. Large (SM-122/59), it is very difficult to identify many of these gamma-lines properly owing to lack of recent information on the gamma-spectra of short-lived fission products.

J. MATUSZEK: I wish to make a brief comment concerning the problem of gamma-ray identification in fission-product gamma-spectra. An excellent compilation of gamma-ray energies has been made by Dr. Raymond Gunnink of Lawrence Radiation Laboratory, Livermore, California. It is used as a part of the computer program for analysis of Ge(Li) gamma-spectra.

J.J. SCHMIDT: Could you please comment on the discrepancy between your 15 MeV measurements of delayed neutron yields and some of the earlier measurements in that energy range, e.g. those of Maksyutenko et al. (Delayed Fission Neutrons (Proc. Panel, 1967) IAEA, Vienna, 1968?)

L.V. EAST: The feeling of the people at LASL who actually did the work in this matter is that the older measurements were performed in many cases with relatively thick samples, perhaps hundreds of grams. As our work shows, there are neutron multiplication effects that should be taken into account for such samples. Multiplication effects occur even in small samples having a thickness of a few mils. Another part of the problem is perhaps geometry. The samples were surrounded by rather massive detector arrangements with a lot of moderated material and it is not inconceivable that there are perhaps some thermal neutrons which raised the apparent yields.

G. HERRMANN: It is not quite correct to state (as is stated in the preprint) that the decrease in delayed-neutron yield which occurs when you go from 3 MeV to 15 MeV neutron fission is in direct contrast with previous measurements performed at other laboratories. I would like to draw your attention to the results obtained by Benedict and Luthardt at Mainz University reported in 1968 at the meeting of the IAEA Delayed Neutron Panel [see my contribution to this Panel, Delayed Fission Neutrons, Proc. Panel) IAEA, Vienna (1968), 147]. In this work the decrease of the yields was demonstrated by a technique different from the one which you use.

L.V. EAST: Yes, I am aware of this work. You will note that in my oral presentation I changed the wording to "most previous measurements .." from what was given in the preprint.

ENERGY, MASS AND CHARGE DISTRIBUTION

(Session H)

Chairman: A. Michaudon

MASS, ENERGY AND CHARGE DISTRIBUTION IN FISSION

A Review

A. C. PAPPAS, J. ALSTAD
Department of Chemistry, University of Oslo
Blindern, Norway
and
E. HAGEBØ
CERN, Geneva,
Switzerland

Abstract

MASS, ENERGY AND CHARGE DISTRIBUTION IN FISSION. Potentialities and limitations of modern techniques used for studies of mass and charge distribution in fission are discussed. Recent experimental developments and new findings concerning the distribution of mass, charge, and of energy — as far as the latter bear on these distributions — are reviewed and commented. This concerns results from thermal-, low-, medium- and high-energy-particle-induced fission and is limited to heavy nuclei in a brief phenomenological way.

Initial and final mass distributions as determined by pure instrumental methods are discussed, and the final distributions are compared with radiochemical results. The asymmetry and fine structure in these distributions are commented. The results from high-energy-induced fission are presented in view of the fragment shell theory and the two-fission-mode hypothesis. It is shown that asymmetric fission persists to high bombarding energies.

Recent results from range studies in high-energy-induced fission are discussed, and the importance of the observation that the scission distance increases with increasing excitation energy of the fissioning nucleus is stressed.

In connection with charge distribution and dispersion, emphasis is laid on the problem of correction of measured masses due to neutron emission which ought to be known for single fragments and not for groups of fragments as at present. The implication of this on the charge dispersion is stressed. Experimental studies of charge dispersion widths (Gaussian) in thermal-neutron-induced fission are discussed as well as shell and odd-even effects on these distributions. The equal-charge displacement hypothesis in the pre-neutron emission and closed-shell representation still gives the best fit to the experimental Z_p dependence on the initial mass.

The review includes also charge division in charged-particle-induced fission in the medium-energy range and in high-energy fission. In the latter the observation of the trend of N_p/Z_p with the fragment mass is presented and correlated with the symmetric peak of the mass distribution.

1. INTRODUCTION AND BACKGROUND

It has become clear since the last Symposium on the Physics and Chemistry of Fission at Salzburg in 1955 that many important studies of the fission process are intimately linked to salient features of mass and charge distributions. Furthermore, one of the main aims of fission theory is disclosing at which stage or stages of the process such distributions are "decided", explaining the main features of the distributions, and, finally, to make the problem tractable developing models from which these distributions can be calculated preferably without "free" parameters adjustable to facilitate agreement with observed and measured values.

A recapitulation of the main stages leading to scission might, therefore, be relevant. The deformation of the fissioning nucleus proceeds slowly in the early stages of the process during which the nucleus spends a considerable time in a transition-state configuration. At this stage, the fissile nucleus may show large deformation (saddle-point shape) and its excitation energy determines the life-time ($\approx 10^{-14}$ s for thermal-neutron capture).

Beyond the transition state the deformation proceeds slowly or rapidly, depending on nuclear properties to the scission shape. At the scission stage the nucleus divides into two (or more) deformed and excited fission fragments. The resulting distributions of mass and charge, and the charge dispersions are the initial ones (primary, pre-neutron emission).

In the post-scission stages the fragments repel each other and approach (collapse to) their equilibrium shapes. After having obtained their full kinetic energy, first neutrons are emitted ($< 4 \times 10^{-14}$ s [1]) and later γ-rays start being emitted ($< 10^{-11}$ s [2]) from the moving fragments. As a result of an internal conversion of the γ-rays electrons and K X-rays are observed. (A smaller amount of X-rays has already been emitted as a result of the disruption of the electron cloud during the act of fission.) The neutron (and γ) emission transforms the fission fragments to lower-mass primary products which are virtually stopped after a rather short time. The distribution of mass and charge and the charge dispersion are now the final ones (product, post-neutron emission).

Up to this point nothing has happened to adjust the nuclear charge of the fragments towards charges of more stable nuclides. This process takes place in the last very slow (10^{-2} s and more) stage during which the primary products undergo series of beta decays forming secondary products and end up in stable nuclei. Disregarding the slight changes due to the rare process of delayed neutron emission the ultimate mass distribution is identical with the above-mentioned final mass distribution.

During the Salzburg Symposium in 1965 three review papers [3-5] covering distribution of mass, charge and energy in fission were presented.

The authors of this paper have decided to limit their review to studies of distribution of mass and charge, and of charge dispersions, and to consider energy release mainly as far as such studies bear on the former ones.

A compilation, including an exhaustive literature list, of final mass yields[1] and mass distributions in spontaneous, thermal and 14-MeV-neutron-induced fission as measured radiochemically or mass-spectrometrically up to the end of July 1968, will be found in a paper by H. R. von Gunten to be published in Actinide Reviews [6]. The authors of the present review have been asked to write a review of the yields of primary fission products, charge distributions and dispersions in the above-mentioned processes. Therefore, a survey covering all work that has been done has not been considered necessary. We find it more adequate to discuss and comment on the different techniques used and the results obtained.

---

[1] Averaged "best" values, not weighted according to uncertainties and errors in the single values.

2. MASS DISTRIBUTION

2.1. Methods

Since the last Symposium semiconductor detectors have found extensive use in fission studies. These detectors provide good pulse-height resolution together with short response time and make possible studies of detailed correlations and, to some extent, of low-probability events.

One of the principal aims of the application of semiconductor detectors has been testing their ability to reproduce or approach the quantitative results obtained by radiochemical techniques. The general trend in mass distributions is easily obtained, but the severe weakness has been the poor resolution although the resolution is improving considerably [7].

Owing to resolution difficulties, pile-up and tailing, these instrumental methods do not reach the peak-to-valley ratio 600:1 established by radiochemical techniques for thermal-neutron-induced fission of ^{235}U. Typical values are about 100 : 1, even if about 450 : 1 has been claimed in one case [8].

The deviation is due to unsatisfactory calibration and false events in the valley region. Recently, however, a ratio of 540 : 1 has been obtained by an improved technique [9].

The kinetic-energy deficit for symmetric fission as measured by purely instrumental methods has been too large, but recent determination by Signarbieux et al. [9] gives a reasonable value and approaches the results of radiochemical range studies.

The determination of mass distributions by instrumental methods is done by correlation experiments on kinetic energies (detector pulse heights) or velocities (time of flight) of fragment pairs or on velocity and energy of single fragments. The kinetic-energy measurements are sensitive to detector calibration, which is usually done with reference to ^{252}Cf spontaneous-fission-fragment spectra. Recent reported values for energy and for time resolution (FWHM) are in the 1.0 - 3.7 MeV and in the 0.5 - 3.5 ns region [7, 10].

Since the overall feature of neutron emission is its isotropy [11] in the centre-of-mass system of the moving fragments the average velocities are essentially unchanged, and conservation of momentum gives a good relation between initial masses and velocities.

In contrast to time-of-flight measurements, kinetic-energy measurements include effects of neutron emission in a more marked way. The application of linear-momentum conservation to measured energies, therefore, results in provisional (initial) masses which differ from the real initial masses by a few mass units.

Simultaneous measurements of both velocity and kinetic energy of both fragments give information of both initial and final mass distributions.

The efficiency in the methods mentioned is found to lie in the possibility of obtaining initial and, to some extent, final mass distributions. In most cases, however, assumptions must be introduced to account for neutron emission as function of mass. (This neutron-distribution curve is only known for spontaneous and thermal fission [11-14].) Because of imperfect mass resolution[2] and low sensitivity caused by limitations in the

[2] The resolution depends on the fragment in question (light or heavy group), and reported values (FWHM) seem to be 1-5 - 3.5 amu for initial distribution and higher (up to 5 amu) for final distribution.

number of events (results are mostly plotted in linear scale) these methods cannot compete with modern radiochemical (which may include the use of isotope separation) and mass-spectrometric techniques in studies of final mass distributions. Owing to complete and unambiguous mass (and charge) resolution and the possibility of measuring fission yields over a range covering a factor of 10^8 or more, the latter approaches give the most precise and extensive determinations. It should be stressed, however, that with purely instrumental techniques it is possible to obtain the qualitative features of final mass distributions and, thereby, to avoid the time-consuming radiochemical and mass spectrometric techniques.

2.2. Initial anf final mass distributions

Spontaneous fission of ^{252}Cf is extensively used in absolute energy calibrations of semiconductor detectors [15, 16]; it might, therefore, be valuable to compare recent initial and final mass distributions for spontaneous fission of ^{252}Cf as derived from purely instrumental techniques [8, 17].

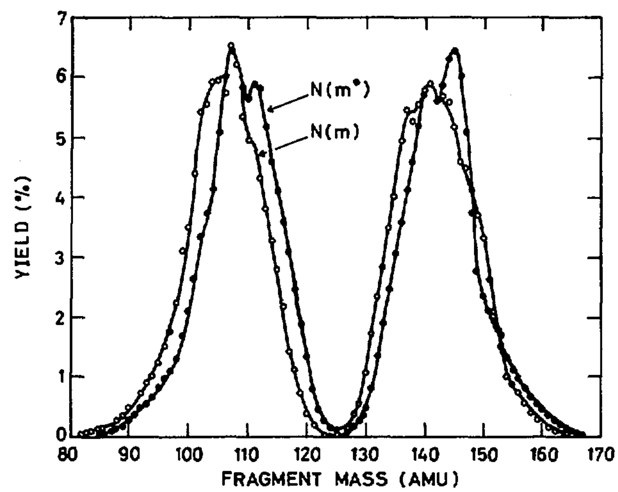

FIG. 1. Initial N(m*) and final N(m) mass distributions of spontaneous fission of ^{252}Cf both measured by purely instrumental techniques [8].

Figure 1, taken from Schmitt et al. [8], shows the resolution-corrected initial distribution N(m*) from energy-correlation studies and the resolution-corrected final distribution N(m) as obtained from energy-velocity correlation studies, also by Schmitt et al. [16]. The latter is compared with the radiochemical data [18] in Fig. 2; the general agreement is good.

Initial mass distribution curves are now available for many fission reactions: spontaneous fission [19] of ^{248}Cm, ^{250}Cf, ^{254}Cf, ^{253}Es and ^{254}Fm, for thermal-neutron-induced fission the most recent curves [8, 17, 20, 21] are for ^{233}U, ^{235}U, ^{239}Pu and ^{241}Pu, for fast-neutron-induced fission [17, 22] curves of ^{232}Th, ^{231}Pa, ^{238}U and ^{237}Np (for the latter

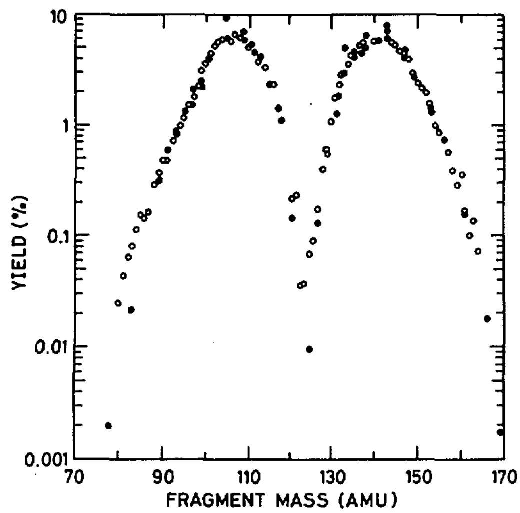

FIG. 2. Comparison of final mass distribution of spontaneous fission of ^{252}Cf determined from energy, time-of-flight correlation experiment ○ [16] with radiochemical data ● [18].

nuclides the fission barrier is slightly greater than the neutron binding energy). In addition, initial mass distributions are also becoming available for fission at higher energies.

The initial mass distribution curves for these nuclides are similar, but not identical. They are strongly asymmetric with the heavy mass peak centred around mean values of 140 to 142, while the light peak "moves" in order to account for the mass of the fissioning nucleus (Fig.3)[3]. The position of the light edge of the heavy peak is essentially constant around mass 132±1 for all these processes.

It is interesting to compare initial distributions with final radiochemical [6] ones. Some examples are shown in Figs 4 and 5 for thermal-neutron-induced fission of ^{233}U [20, 23], ^{235}U [8, 23], ^{239}Pu [21, 25] and ^{241}Pu [21, 26][4].

The final distributions have their peak centred around a mean value of about 2 mass units lower than the initial distributions. This is a slightly larger difference than the results from purely instrumental techniques seem to indicate and what one would expect from direct measurements of neutron emission distributions [12-14]. The explanation may be found in the way the "instrumental" curves are constructed.

The position of the light edge of the heavy peak does not change essentially from the initial to the final distribution in accordance with the fact that very few neutrons are emitted in this mass region [12-14].

The positions of the initial (and, consequently, also the final) distributions seem to be governed by the double-closed shell of 82 neutrons and 50 protons. Thus, asymmetric mass distribution is possible only when one fragment gets more than 82 neutrons and more than 50 protons. This is clearly demonstrated in the paper by Wahl et al. [27] in these Proceedings.

[3] Since the final distributions depend both on the initial distributions and the neutron emission, a plot like Fig.3 for final distributions will only indicate a general trend.

[4] First and second references refer to initial and final distributions, respectively.

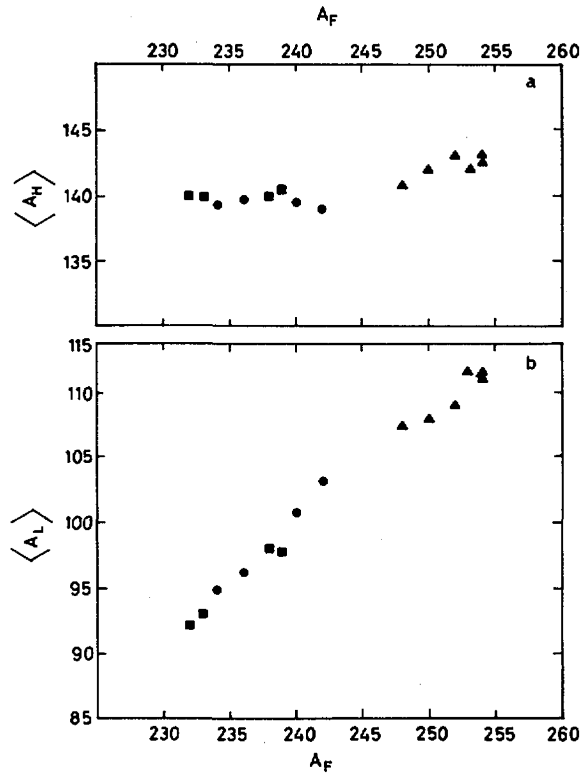

FIG. 3. Positions of (a) the heavy peak $\langle A_H \rangle$ and (b) light peak $\langle A_L \rangle$ in initial mass distribution as function of fissioning nucleus.
▲ : spontaneous fission, ● : thermal neutron fission, ■ : fast neutron fission.

Closed-shell and near-closed-shell nuclei are known to have spherical shapes and to resist deformation. As pointed out by Terrell [28] fission into a pair of fragments one of which has closed-shell configuration should be energetically most favoured (i.e. lowest total deformation and mutual Coulomb energy). A closed-shell configuration having high rigidity results therefore in high kinetic energy as also observed near the double-closed-shell mass 132. This fragment shell theory of fission has been taken up by many authors. Quite recently Dickmann and Dietrich [29] performed a theoretical study (without any parameter adjusted to fission data) based on a simple model of two osculating spheroids and the assumption that at the scission stage the sum of deformation energy and mutual Coulomb repulsion is a minimum. Their results demonstrate the importance of closed-shell effects at a late stage of fission, thus explaining the observed trend of mass distribution curves as discussed here.

2.3. Fine-structure

In the final mass distributions from spontaneous and thermal fission, fine-structure has been known for a long time as a result of radiochemical and mass-spectrometric studies. Through many years different sug-

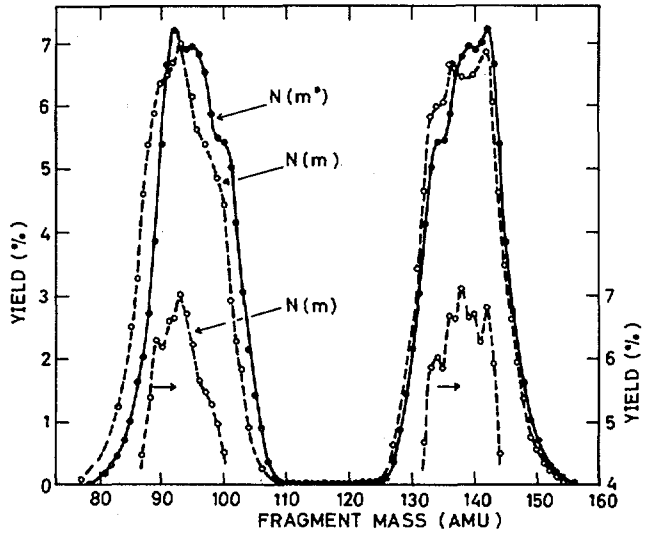

FIG. 4. Initial N(m*) and final N(m) mass distribution of ^{233}U thermal fission [20, 23]. The lower dashed curve [24] is included for comparison of fine-structure (see text).

gestions have been made to explain this fact: from artifacts to closed-shell effects and "noise" connected with ups and downs in single-particle structure.

As a result of the recent imporved techniques [7, 10, 15, 16, 30], however, a more detailed inspection of initial and of final mass distributions is made possible. This has given confidence to the existence of fine-structure in the peak regions of both distributions for spontaneous fission of ^{252}Cf, thermal neutron induced fission of ^{233}U, ^{235}U, ^{239}Pu and ^{241}Pu (see Figs 1, 4 and 5). Definite peaks or shoulders are seen in all these distributions although the relative intensities may differ.

The fine-structure in the initial distributions seems to be associated with approximately the same heavy fragment masses, around 134, 140, 146 and possibly 152, and is reflected in the light peak. The variation in neutron-emission probability with mass of the fragment is responsible for the displacement of the fine-structure and the increase or decrease in this. The net result is the fine-structure observed in the final distribution. The latter is most pronounced around mass 134.

Thomas and Vandenbosch [31] were the first to suggest a correlation between the fine-structure observed in the average total kinetic-energy distribution and the energetically preferred even-even configurations in the fragments as due to the pairing energy which depresses the (binding) energy surface for odd mass fragments below that for even-even ones. Calculations along these lines were also done by many others [8, 20, 21, 32] so that information is available for all the above-mentioned nuclides. By using empirical mass formulae [5] to calculate fission Q-values (Q is the kinetic energy plus the excitation energy of the two fragments) as a function of fragment mass, it is shown that the observed fine-structure

[5] The results are rather insensitive to the mass formula used.

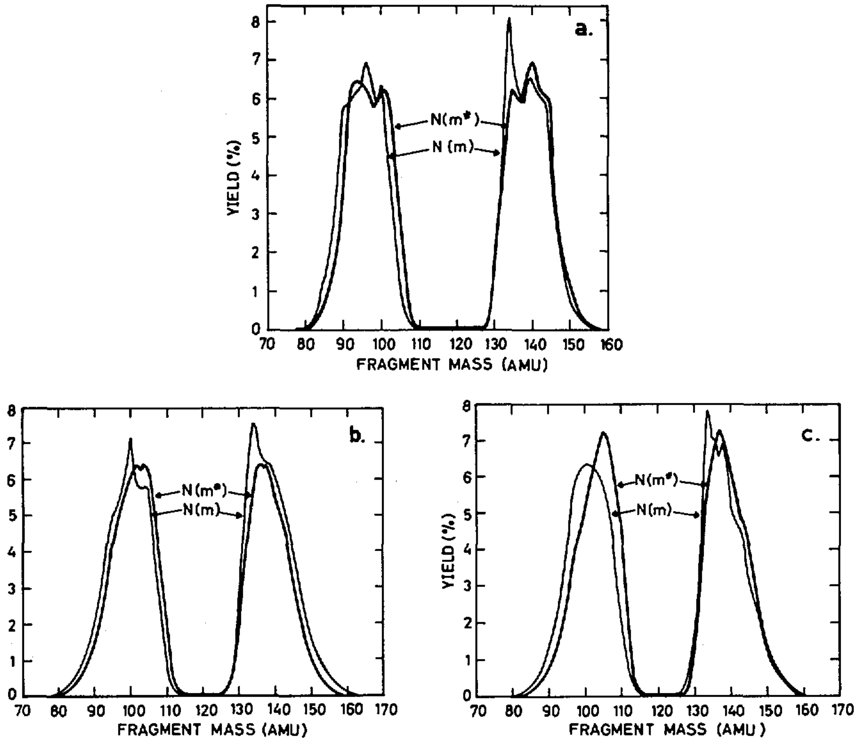

FIG. 5. Initial $N(m^*)$ and final $N(m)$ mass distributions from thermal-neutron fission of a) ^{235}U [8, 23], b) ^{239}Pu [21, 25], and c) ^{241}Pu [21, 26].

in the empirical Q-values, i. e. in the measured kinetic energies to which the energies of emitted gammas and neutrons (binding energy and kinetic energy) are added, in general, is correlated with the even-even parabolas in the calculated values. An example is shown in Fig. 6. The fine-structure observed in the initial mass distribution should similarly be correlated in location with the even-even parabolas and with maxima separated by $2A_F/Z_F$ or approximately 5 masses [31]. This is observed by Andritsopoulos [10] in a recent examination of the fine-structure in the initial and final distributions from thermal fission of ^{235}U (both measured by purely instrumental techniques) (Fig. 7). Because of neutron emission, the peaks in the final distribution are moved to slightly lower masses with respect to the peaks in the initial distribution. Thus the Thomas-Vandenbosch type of analysis seems to provide a good explanation of the origin of the fine-structure in fission.

If we look, however, at the effects expected from the empirical and calculated Q-values in the light of the observed intensity of the fine-structure peak at mass number 134 (and reflected mass) in the initial mass distributions, an additional explanation seems to be necessary. To get this explanation, one might reconsider the old idea of Wiles et al. [33] of an enhanced structural effect in the scission stage resulting in fragments with mass number ≃ 134. In this connection it should be kept in mind that ^{134}Te

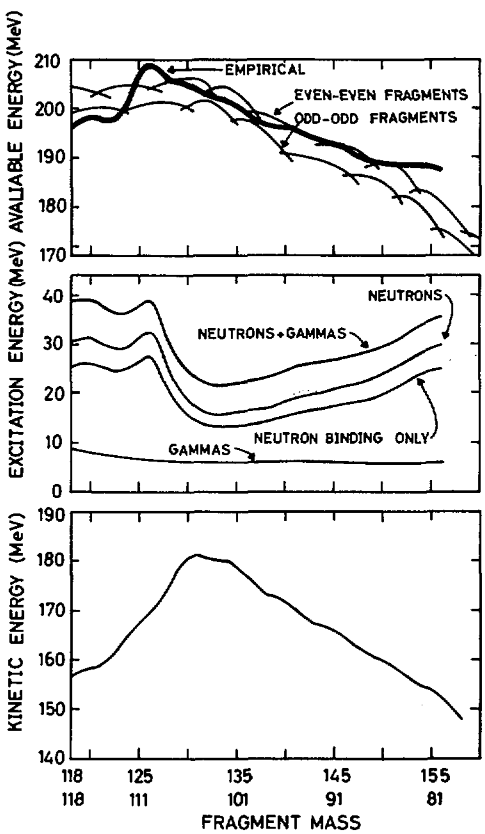

FIG. 6. Total energy balance for thermal-neutron-induced fission of ^{235}U [8] (see text).

seems to have a (radiochemical) yield too large to be mainly due to neutron evaporation [34] as is also pointed out by Wahl et al. [27] in these Proceedings.

In conclusion it should be emphasized that the Thomas-Vandenbosch type of analysis does not eliminate the possibility of shell effects in the act of fission, and that the initial fragment distributions may, in some way or other, be influenced by shells even in their final details.

2.4. Asymmetry

Kelson [35] and Griffing [36] propose that the most probable mass split is given by the ratio, at or near the saddle-point shape, of the number of nucleons in "gerade" orbits (even parity, symmetric under reflection at a plane perpendicular to the nuclear symmetry axis) to the number of nucleons in "ungerade" orbits (odd parity). Thus $\langle A_H \rangle / \langle A_L \rangle$ in the initial distribution should be a measure of this ratio. "Asymmetries" are therefore plotted in Fig. 8 to give some information on the Z_F^2/A_F dependence, and the straight line correlation does not seem too bad. The slope is, however, negative while the model in its present state predicts a positive slope.

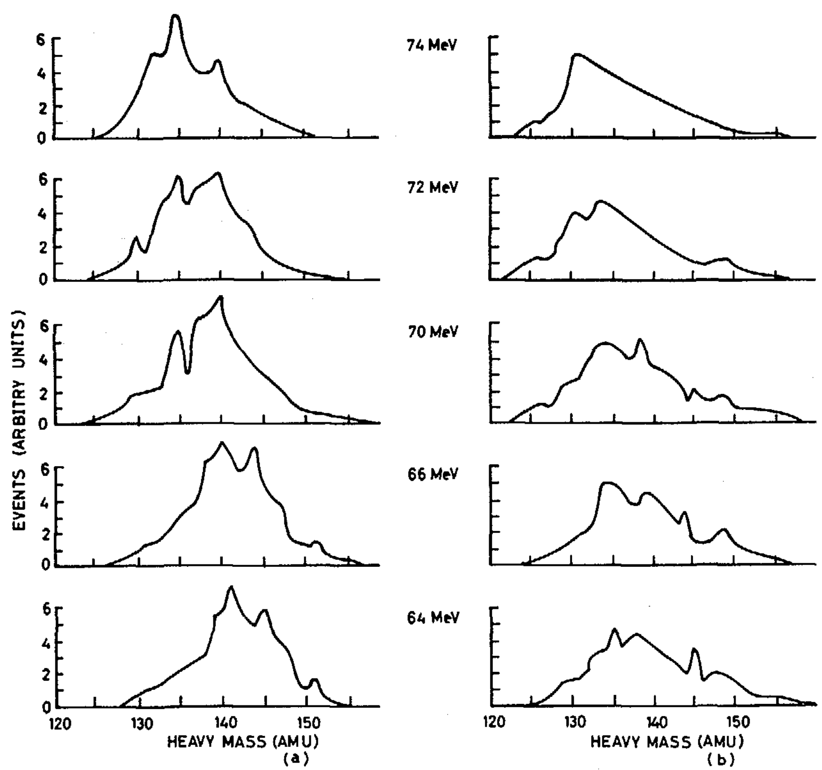

FIG. 7. Initial (a) and final (b) mass distributions for fixed kinetic energies in thermal-neutron-induced fission of ^{235}U [10].

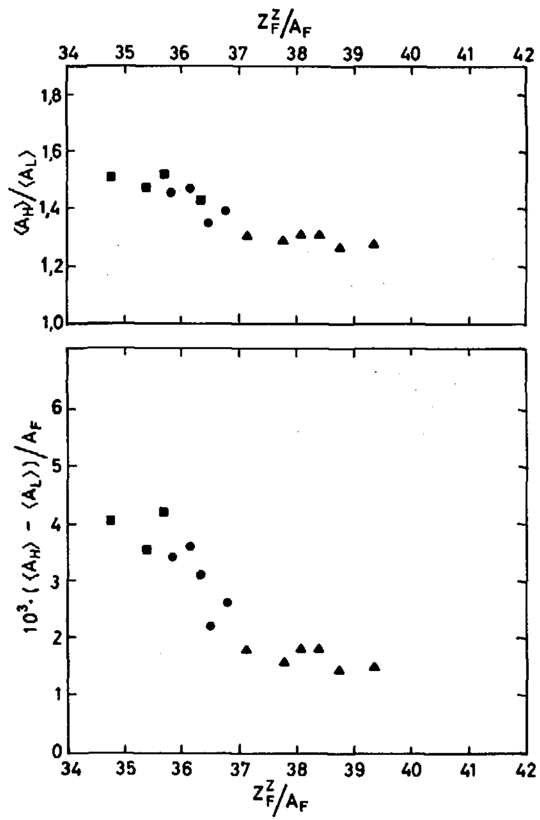

FIG. 8. Asymmetry plot (see text).

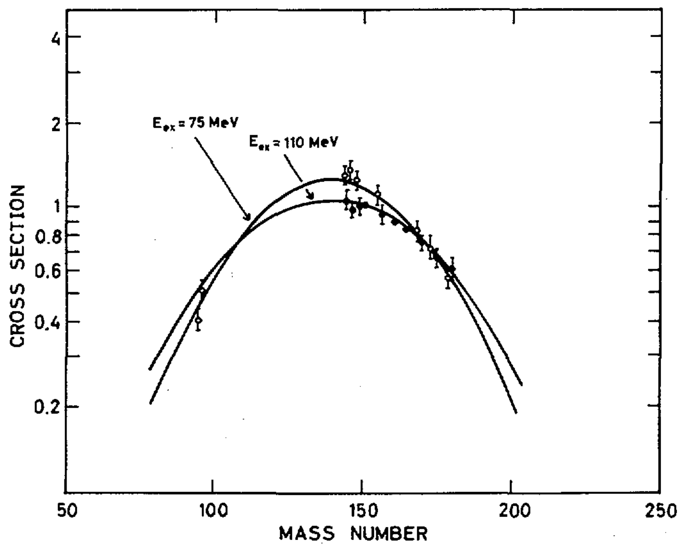

FIG. 9. Mass distribution for fission of ^{238}U bombarded with ^{40}Ar [37].

It might be of interest in this connection, even if not quite relevant, to refer to studies reported by Karamyan et al. [37] on mass distribution in ^{238}U bombarded with ^{20}Ne and ^{40}Ar of various energies (compound nuclei $^{258}102$ and $^{278}110$ with Z_F^2/A_F 40.4 and 42.1, respectively). No indication (Fig. 9) for a valley is found at the lowest excitation energies. These however, may be too high and a possible valley may have been filled. Nevertheless these curves are informative as they represent the first mass distributions from fission of nuclei with extremely high charge (102 and 110). The energy dependence of this distribution follows the usual pattern, i.e. they become wider with increasing energy.

2.5. Fission at higher energies

With mass and charge decreasing below thorium, the fission barrier increases rapidly and the probability for fission at low-excitation energies decreases strongly. The high bombarding energy necessary to cause fission in such nuclei results in symmetric mass distributions (not necessarily reflection-symmetric as assumed by many authors).

In some cases it has been possible to obtain "initial"[6] mass distributions for fission at higher bombarding energies for easily fissionable elements. Even if these distributions cannot be expected to give detailed information, they are very informative.

Thus, for a given excitation energy Petrzhak and Tutin [38] report "initial" mass distributions for increasing total kinetic energy of the fragments (i.e. with decreasing total excitation energy of the fragments) from 25 MeV photofission in ^{235}U. Figure 10 shows that with increasing total excitation energy of the fragments the relative probability for symmetric

---

[6] Quotation marks as the neutron distribution curve has to be estimated.

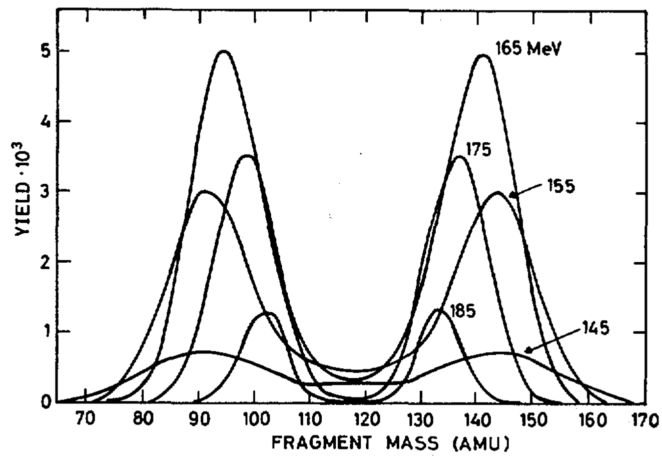

FIG. 10. "Initial" mass distribution curves for 25 MeV photofission of ^{238}U for selected total kinetic energies [38].

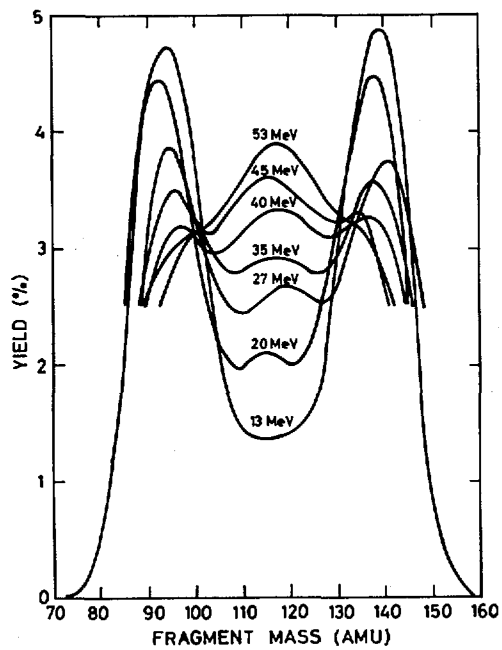

FIG. 11. "Initial" mass distribution curves for fission of ^{238}U bombarded with 13 to 53 MeV protons [39].

fission increases. This effect is heavily supported by the studies of Croall and Cuninghame [39] on fission of ^{232}Th by 13- to 53-MeV protons (Fig. 11). These authors have, in addition, studied the effect on the total "initial" mass distribution (Fig. 12). The increasing contribution from symmetric fission with increasing proton energy (excitation energy) is clear although even at 53 MeV the shoulders of the mass-distribution curve indicate asymmetric fission peaks.

That asymmetric fission is contributing substantially in fission of highly fissile nuclei when these are bombarded with high energy particles

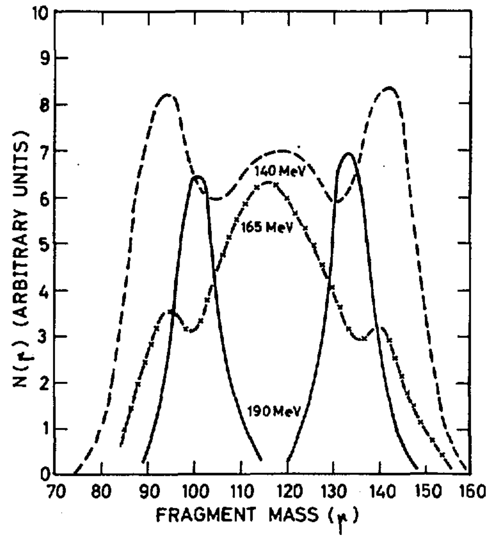

FIG. 12. Provisional mass distribution for 35 MeV proton fission of ^{232}Th for selected total kinetic energies [39].

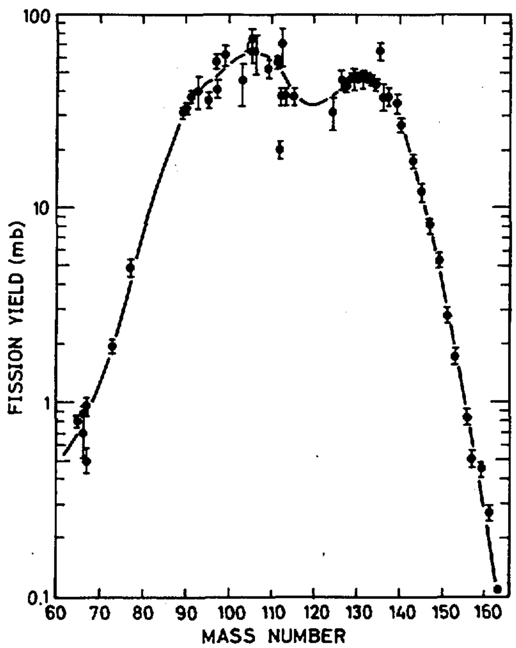

FIG. 13. Final mass distribution for fission of ^{238}U bombarded by 170 MeV protons [43].

has recently been proved both by radiochemical and purely instrumental techniques.

With increasing energy pre-fission neutron emission starts to compete with fission giving rise to first, second and later chance fission. The resulting reduction in excitation energy will favour asymmetric (or low-energy) fission in the above-mentioned nuclei. Therefore, owing to the neutron-emission competition, both the initial and final mass distributions (which are composite curves) cannot be expected to show reflection symmetry.

This was indicated by Rudstam and Pappas [40] who used low-energy fission data to estimate the symmetric-fission probability and its energy dependence assuming a fission-to-total-width independent of energy or a rapidly decreasing function of energy. Using, in addition, the two-mode fission hypothesis introduced by Turkevich and Niday [41] and first elucidated by Fairhall et al. [42] as a basis of meaningful discussion of fission at high energies, Rudstam and Pappas estimated the mass distribution in 170-MeV-proton-induced fission of ^{238}U. The general shape of the distribution (only little influenced by the two assumptions made) was neither single-peaked nor reflection-symmetric; it has recently been verified in radiochemical studies by Pappas and Hagebø [43] (Fig. 13). Using purely instrumental techniques, Galin [44] and Gauvin and Sauvage [45] were able to estimate that in bombardment of uranium with 155-MeV protons about 25% of the fission events are asymmetric. As 155-MeV protons on uranium correspond to an average deposition energy of 80 to 90 MeV [46], these results give support to the assumption that the energy is independent of the fission-to-total-width [40]. Similar results on the mass distribution are reported by Schröder et al. [46a] for 300 MeV-to-1.1 GeV photofission of ^{238}U and ^{232}Th.

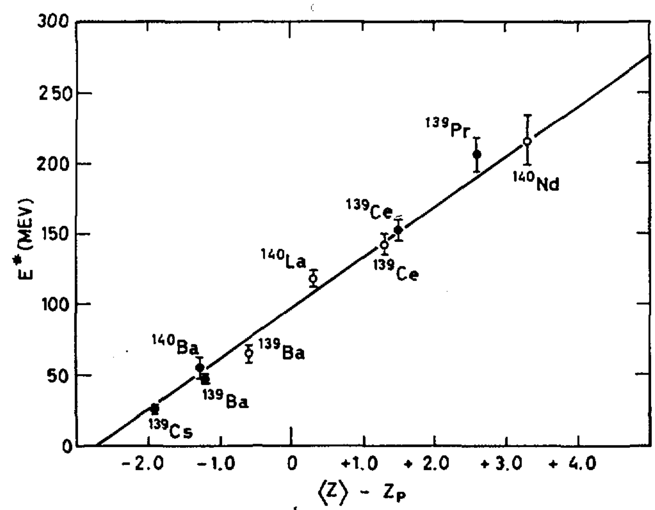

FIG. 14. Isobaric dependence of the cascade deposition energy, E^*, on the displacement of the average fission product charge, $\langle Z \rangle$, from the most probable charge Z_P for mass chains 139 and 140 from fission induced in ^{238}U by 440-MeV protons [49].

O: independent nuclides,

●: cumulative nuclides.

In going to bombarding energies in the GeV region Remsberg et al. [47] state that although there is a much broader mass spectrum of fissioning nuclei at 2.9 GeV than at lower bombarding energies, the fission mechanisms seem to be indistinguishable in the two cases. The lowest excitation energies lead to predominantly asymmetric fission with total kinetic energy averaging about 170 MeV and fragment masses centred around mass numbers 135 and 95. Higher excitation energies predominantly lead to symmetric fission centred on the average, at mass number 105 and a total kinetic energy of 155-160 MeV.

The two-mode fission hypotheses compete in some sense with the fragment shell theory of fission which has a more physical basis. As mentioned above, this theory was first suggested by Terrell and developed further by many authors [48]. The conceptual discrepancy, however, between these two is not large, the difference lying in going from a liquid drop (symmetric fission mode) to a shell configuration (asymmetric fission mode). Here the two-mode hypotheses assume the presence of these two modes in a transition region while the fragment shell theory assumes a gradual transition from one mode to the other. Thus, much more and detailed information seems to be necessary to explain mass distribution in fission.

3. KINETIC ENERGY AND RANGES OF FISSION PRODUCTS

As already pointed out, the authors do not intend to go into any details on the distributions of kinetic energy or velocities of the fission fragments. Very lately, however, some interesting results have been obtained for high-energy fission. The interest lies both in the experimental results themselves and in their interpretation. Hogan and Sugarman [49] have measured recoil properties of several members of an isobaric chain from 440-MeV-proton-induced fission, and found an increase of $\simeq$ 31 MeV per charge unit for the cascade deposition energy in the fissioning nucleus leading to their formation (Fig. 14). In the total kinetic-energy release, they find a decrease with increasing charge number along the isobaric chain. These findings explain this as being due to three different effects:

First, the loss of neutrons and, thus, of kinetic energy from the fragments is greater from the neutron-deficient ones than from the neutron-rich ones because of the higher excitation energy of the former. Second, by conservation of momentum, the heavier fragments which were highly excited, receive a smaller fraction of the kinetic energy than the lighter fragments leading to the same product mass.

The third effect is the effect of greatest interest, namely an effect of increasing deformation with increasing excitation energy of the fissioning nucleus.

These three effects are each due to about 10 per cent reduction in the total kinetic-energy release of neutron-deficient products relative to neutron-excessive products.

Crespo et al. [50] find the same 30 per cent decrease in total kinetic-energy release, but by using the Nix-Swiatecki liquid-drop model [51] in which there is no possibility for a dependence of the deformation on Z for constant A and which also implies a constant N/Z ratio for all the fragments; they claim that most of the decrease is due to the neutron evaporation after fission. In this way they get longer evaporation chains for neutron-deficient products and shorter chains for neutron-rich products than Hogan and Sugarman do.

Remsberg et al. [47] very recently completed a large study of fragment energies and velocities in fission of uranium with 2.9-GeV protons. They do not at all see the effect of decreasing velocity for increasing excitation energy of the fragments, but claim that the difference in velocity (or deformation) of neutron-rich and neutron-deficient products of the same mass is a difference between symmetric fission, having the lower velocity, and asymmetric fission. At 2.9 GeV they do not see enough asymmetric fission to notice the difference.

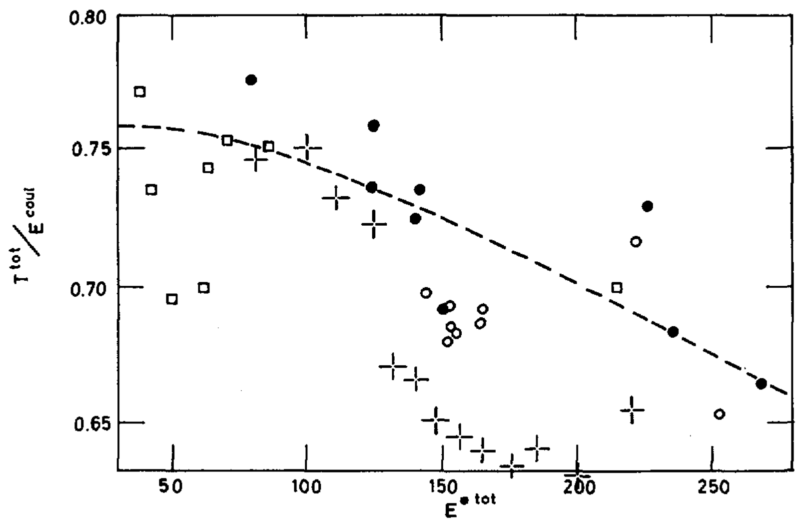

FIG. 15. Variation of the total kinetic energy of a pair of fission fragments divided by their Coulomb energy, T^{tot}/E^{coul}, with their total excitation energy, E^{*tot} [49].
●: independent nuclides [49],
□: cumulative nuclides [49],
○: (54, 55) reanalysed by the procedure given in Ref. [49],
+ : preliminary values calculated from data in Ref. [52].

From the work of Hagebø and Ravn [52], it is possible to construct a curve of the same kind as that found by Hogan and Sugarman (Fig. 15); however, the relation between T^{tot}/E^{coul} and E^{*tot} is not the same. It shows a sharper transition between the high-kinetic-energy fragments from asymmetric fission and the low-kinetic energy (more deformed) fragments in the symmetric region.

If there is a real effect of increasing deformation with the excitation energy of the fissioning nucleus, and if this deformation is determined at scission, it seems unreasonable to expect this deformation to be completely independent of the stiffness of the fragments formed. The stiffness may well be the parameter which determines the difference between the results of Hogan and Sugarman, and those of Hagebø and Ravn. Thus the latter results follow the line of Fig. 15 for the most neutron-rich products, but fall off below the 82-neutron shell where the stiffness parameter decreases and a bigger deformation is possible for the same excitation energy.

All the above considerations apply to high-energy proton-induced fission.

In fission induced by thermal neutrons, not so much is known about the deformation as a function of excitation energy. Only the symmetric fission is known to have lower kinetic energy release, and also a higher excitation energy as seen from the neutron evaporation from the individual fragment masses. In no mass region a dependence of the kinetic energy on charge or excitation energy of the fragments produced has been shown. The only indication that this effect may be general is in the measurements of recoil ranges of the shielded products ^{86}Rb and ^{136}Cs [53]. These ranges are about 10 per cent shorter than the average ranges for the mass numbers in question, and already Niday [53] suggested that this was in part due to a higher than average excitation energy and a greater deformation of the fission fragments leading to these products through neutron emission.

The fact that the scission distance increases with increasing excitation energy of the fissioning nucleus may turn out to be one of the more striking new observations in high-energy induced fission; this is the more true if a similar effect also holds for thermal-neutron-induced fission.

4. CHARGE DISTRIBUTION AND CHARGE DISPERSIONS

4.1. Charge functions and parameters

While studies of mass distribution are concerned with the division of nucleons (neutrons and protons together) in the fissioning nucleus among fragments, charge distribution studies are concerned with the division of the protons in the fissioning nucleus among the fragments. Thus it is necessary to establish the most probable charge Z_p and its dependence on fragment mass (charge distribution). As for a given mass split there are many possibilities for charge division, the charge dispersions must be known, i.e. the spread in nuclear charge for a given mass. These primary charge functions together with the mass distribution should then make it possible to derive the corresponding neutron distribution and dispersions [57].

As in mass distribution studies, it is of importance also in charge distribution studies that the parameters in question (mass and charge) are the initial ones. In contrast to neutrons, there are no protons emitted from fission fragments in spontaneous thermal- and fast-neutron-induced fission while the situation in high energy fission is not known. Initial and final charges are therefore identical and often called primary charges, to distinguish them from charges resulting from beta decay of fragments.

It is now generally accepted that the primary charge functions shall be expressed in terms of initial mass as was first applied by Pappas already in 1953 [34, 56]. The fragment masses have to be deduced from observed final masses by addition of the appropriate number of neutrons. When the variation of neutron number with fragment mass is unknown, the number of neutrons is generally taken to be proportional to the mass of the product and applied in the correction.

The average number of emitted neutrons as a function of mass is now known for spontaneous and for thermal-neutron-induced fission [12-14] and assumed to consist of a universal "saw-tooth" shaped curve with a fine-structure superimposed. By introducing a linear relationship ("saw-tooth") Wahl et al. [58] were able to arrive at a substantial improvement in the primary charge distribution. A further improvement was done by Strom et al. [59] who used the perturbed "saw-tooth" curve.

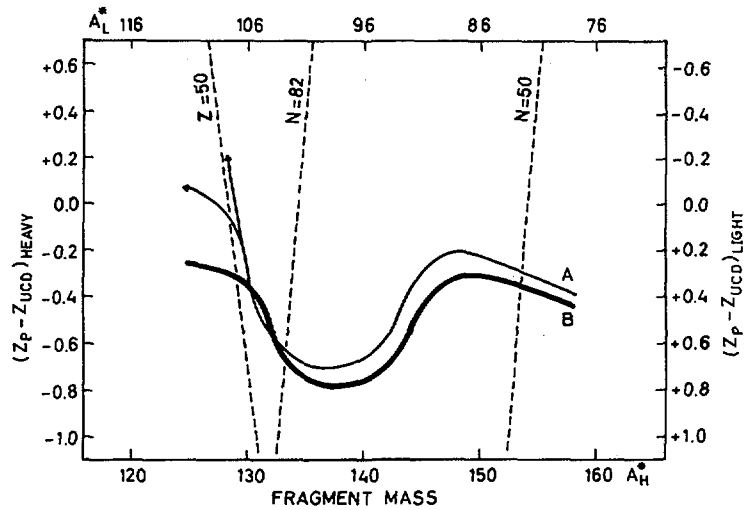

FIG. 16. The most probable primary charge Z_p for thermal-neutron-induced fission in ^{235}U as function of initial fragments mass.
A from Wahl et al. [58],
B from Strom et al. [59].

As nuclear matter does not seem to be very polarizable one might expect that the protons in the fissioning nucleus are divided among the fragments proportional with their masses. Charge distribution data are therefore plotted in relation to this ratio (unchanged charged distribution, UCD) often referred to as the Wahl plot. The results from Wahl et al. [58] and from Strom et al. [59] are shown in Fig. 16 from which also the sensitivity of the results to the neutron correction can be seen. Sistemich [60] has recently reanalysed the available neutron emission data [12-14] for consistency and on this basis replotted the radiochemically determined Z_p values (Fig. 17) in the peak regions of the mass distribution.

4.2. Methods

As stated by Nifenecker et al. [61], because of the poor mass resolution (~6 amu) in the neutron distribution curves and the selection of a given mass, possible finer variations as odd-even effects in the excitation energy of the fragments are cancelled. From the work of Thomas and Vandenbosch [31] and others, as mentioned earlier, we know that the fine-structure in the

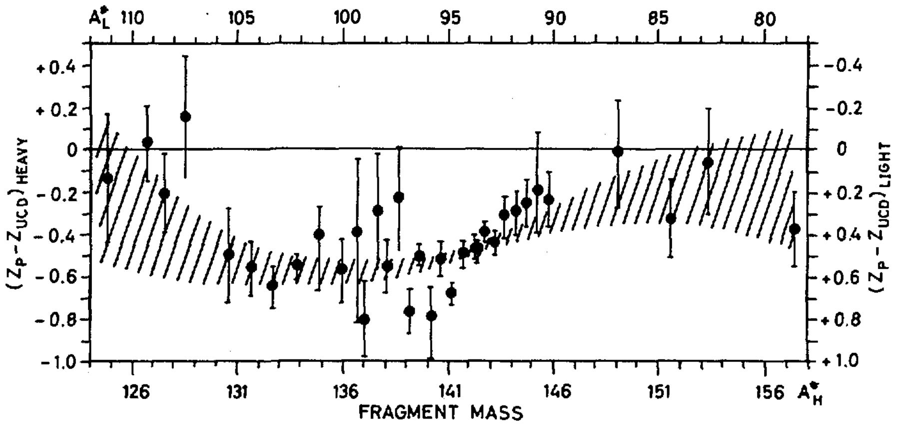

FIG. 17. Radiochemical Z_p values replotted in accordance with results of re-evaluation of neutron emission data. The cross hatching indicates the systematic trend [60].

initial mass distribution is to a large extent caused by such effects. It would therefore be advantageous to know also the neutron emission as a function of fragment charge. The first attempt was done by Nifenecker et al. [61] who measured kinetic energy, neutrons and X-rays emitted from the fission fragments of spontaneous fission of ^{252}Cf.

In all experimental techniques used at present correction for emitted neutrons cannot be avoided. The actual number, however, of neutrons emitted from a single fragment is not known because the available neutron data are all average numbers for groups of fragments. Even these data have disclosed structure in the number emitted as function of mass [12-14] thus giving hints to individual features of the nuclides.

Since charge-distribution studies should be concerned with fragments of known charge and mass, the results are much more sensitive to uncertainties in these and in neutron emission than mass-distributions are. Therefore, a crucial problem in establishing the primary charge has been and still is the corrections to be applied to the observed data in order to obtain the appropriate fragment mass and, in some techniques, also the charge. This might be the cause for some of the discrepancies between primary charge values evaluated by different approaches.

The difficulty in relating experimental values of independent radiochemical yields of products to yields of fragments is recognized by Nörenberg [62] who also points out the difference between neutron emission probability of a fragment and the average number of neutrons emitted from an average mass. He therefore proposes to study initial masses and charges by purely instrumental methods instead of radiochemical techniques.

The instrumental methods that have been developed were presented during the last Symposium and promised new ways for studying primary charges and charge dependence of kinetic energy as well as of mass.

Unfortunately, the mass resolution of a gas-filled mass separator as well as semiconductor detectors are poor for such studies and determine final masses just as the radiochemical methods do. In addition, the masses obtained are averages of a large group of single masses.

The determination of primary charge by counting beta tracks from fission products caught in nuclear emulsions [63, 64] gives results quite different from those of Sistemich [60] who make use of a 4π-plastic scintillation detector for beta counting (Fig. 18).

All data obtained along these lines have led to an apparent and as yet unexplained discrepancy to the results from radiochemical and X-rays techniques. This might [66] be due to the fact that the pure instrumental techniques to a large extent give average values [60].

K X-ray detectors for measuring fragment charges in coincidence with fission products measured with semiconductor detectors have found extensive application for primary charge determinations [65, 67, 68]. Typical energy resolution for an X-ray detector of adequate efficiency is 500 eV (FWHM). Even with the use of a bent crystal spectrometer with an accuracy of ± 2 eV in energy determination overlap of X-rays from different elements may cause disturbances.

This technique also gives results for average primary charges for groups of masses. As such the results are in fair agreement with the overall trend of the radiochemical results, i.e. $Z_p - Z_{UCD}$ is about -0.5 and $+0.5$ charge units for light and heavy masses, respectively.

The conclusion that one may draw from this discussion should be that at present the most probable primary charge for a single mass and the dispersion of the primary isobaric yield does not seem to be attainable at present by purely instrumental methods although improvements are reported in these Proceedings [70].

4.3. Primary yields

New radiochemical data for primary yields[7] have been established for many processes including spontaneous fission of ^{252}Cf, thermal-neutron-induced fission of ^{229}Th, ^{235}U and ^{245}Am, 14-MeV-neutron-induced fission of ^{232}Th and ^{238}U. Furthermore, data for a series of proton-, deuteron- and alpha-induced fission processes in nuclides such as ^{232}Th, ^{238}U, ^{237}Np and ^{239}Pu have been obtained. It is not the scope of the present review to discuss these data, but rather to try to draw some general conclusions.

4.4. Charge dispersions

The work of Wahl et al. [58] in 1962 showed that the charge dispersion for (final) fission products in 6 isobaric chains, 91, 139-143, can be represented by a Gaussian distribution. Such distributions have later been extensively used and found further support. In addition, the assumption has been made that the same charge dispersion is applicable to all mass chains.

With the neutron emission problem in mind it can of course be argued that there is no reason to believe that the final charge dispersion should always be a Gaussian even if it appears to be empirically so in the region of high mass yields. According to the statistical model proposed by Fong [71], Gaussian distribution is expected for the initial charge dispersion.

---

[7] A survey of primary yields for thermal-neutron-induced fission of ^{235}U can be found in the paper by Wahl et al. [27] in these Proceedings; see also the introduction to this review.

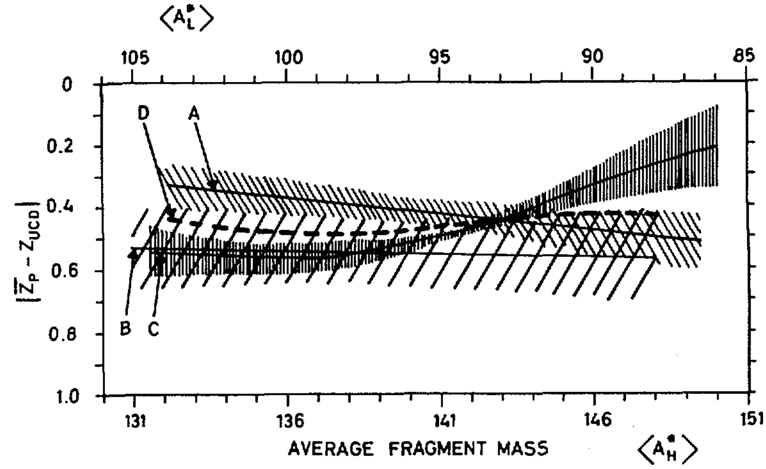

FIG. 18. Comparison between results obtained with instrumental methods and with radiochemical techniques [60].
A : Sistemich [60], B : Reisdorf and Armbruster [65],
C : Systematic trend of radiochemical results (Fig. 17),
D : Weighted average of A, B and C.

It has already been mentioned that in high-energy fission neutron emission is not equal for all members of an isobaric chain – an observation which may also hold for thermal-neutron-induced fission. The final charge dispersion should then be broader than the initial one and may very well be non-Gaussian. It has been suggested by Fong [72] that the final charge dispersion is broader than the initial one. Glendenin et al. [70] have been able, by means of high-resolution studies of K X-ray emission from ^{252}Cf fission fragments, to support this assumption for charge distributions in the regions of high mass yields.

This result agrees also with the conclusions by Gordon and Aras [74] based on calculations of neutron evaporation in fission under the assumption that the initial mass distribution and charge dispersion are smooth curves for thermal-neutron-induced fission of ^{235}U (the process the rest of this section will be devoted to). To-day, however, this assumption is not strictly valid for the initial mass distribution which is known to be perturbed as a result of pairing effects [10].

The Gaussian charge dispersion is given by

$$P(Z) = (2\pi C)^{-\frac{1}{2}} \exp[-(Z - Z_p)^2/C]$$

where C is the charge dispersion parameter. The value given to C by Wahl and his group, under the assumption (for which evidence exists) that the final charge dispersion for different mass numbers is approximately constant in width, has decreased slightly with increasing number of mass chains studied, i.e. from $C = 0.94 \pm 0.15$ [58] (six chains) to $C = 0.86 \pm 0.15$ [3] (ten chains). As a result of a new charge distribution formulation a value of $C = 0.80 \pm 0.14$ [27] will be reported by Wahl.

Two interesting problems concerning the finer details in the charge dispersion have recently aroused interest: is the charge dispersion parameter really constant and is the dispersion influenced by odd-even and shell effects?

Contributions to clarifying the first question are given by Strom et al. [75] and Delucchi et al. [76]. These authors report a decrease in the width of the charge dispersion with mass number increasing from 131 to 134. Their values of C for these chains (based on two independent and one early cumulative yield in each chain) are, respectively, 1.10 ± 0.05, 0.74 ± 0.08, 0.57 ± 0.05 and 0.55, while Denschlag [77] reports an increased width $C = 0.74 \pm 0.09$ for chain 135, compared to the lower mass chains. From the experimental point of view it is rather difficult to measure independent yields in this region.

These results can be interpreted as shell-effect perturbations and, thus, do not disapprove of the assumption that the general trend in the width of the final charge dispersion is mass independent.

Runnalis et al. [78] have analysed final charge dispersions in the mass regions 91 to 95 and 129 to 144 and conclude that these can be satisfactorily represented by a single Gaussian curve with $C = 0.80$. In some chains in which yields of consecutive elements were measured they found that the yields of odd Z isobars are below those expected from the trend given by the yields of even Z isobars. Thus, an odd-even effect is noted in the final charge dispersion. A pertinent question would then be whether this is also the case in the initial dispersion.

In studies of K X-ray yields from ^{252}Cf fission fragments Watson et al. [79] found odd-even fluctuation in X-ray yields for fragments with nuclear charge in the region 52 to 57. X-rays from odd Z products are about twice as intense as those from even Z products. Therefore, the use of X-ray measurements to determine primary fission fragment charges in this charge region may not give the true initial charge dispersion.

The Z_p function is poorly defined in the near-symmetric mass region, i.e. 107 to 127, as is seen from Figs 16-18. This is due to great experimental difficulties, including problems of isomerism, in obtaining data in this region. Up to the last Symposium only the independent yield of a member (^{121}Sn) in chain 121 was known [80]. Radiochemical yields and Z_p values have since been established for mass chains 117 (Pd) [81], 124 (Sb) [59], 126 (Sb) [58, 82] and 127 (Sb) [83]. On the basis of the "universal" charge dispersion the respective Z_p values given by the authors are 46.1, 48.5, 49.4, 49.5. As this is the region where the neutron distribution curve is poorly defined a sound estimate of the initial masses is not feasible.

Charge distribution has also been studied for spontaneous fission of ^{252}Cf both radiochemically [84] and through X-ray measurements [85]. The heaviest nuclide investigated with respect to charge division in thermal-neutron-induced fission is ^{245}Cm studied by von Gunten et al. [86]. These authors report independent yields of the shielded (from beta decay) nuclides ^{86}Rb and ^{136}Cs and estimate Z_p by using the "universal" charge dispersion [58].

4.5. Charge distribution

On the basis of evaluating Z_p values as discussed above and using the Wahl plot [58] all cases known today for spontaneous and up to 14-MeV neutron-induced fission show an average deviation from the unchanged charge distribution $Z_p - Z_{UCD}$ of +0.5 charge units and -0.5 charge units for light and heavy fragments, respectively, [87], and favour the equal-charge-displacement hypothesis of Glendenin et al. [88] in the formulation given by Pappas [56].

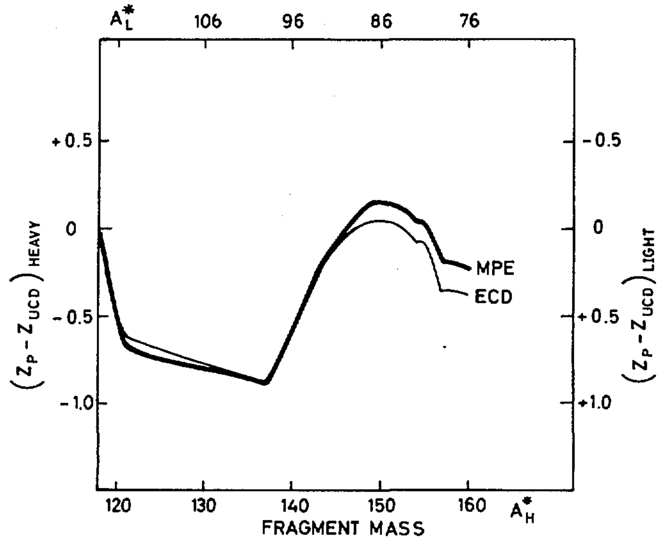

FIG. 19. Expected trends for Z_p in thermal-neutron-induced fission of ^{235}U [89] according to:
Equal charge displacement: ECD
Minimum potential energy: MPE .

The trend given by this hypothesis seems to find support in the trend expected from the fragment shell theory as shown by Pappas and Strom [89] in Fig. 19. In the fragment shell theory the specific scission point shapes are calculated by minimizing the potential energy. Using the relations due to Swiatecki as quoted by Blann [90] and normalizing to the "experimental" Z_p value for initial mass 135, a distance between the charge centres of 11.4 f is found. This is about 10 per cent lower than that of two spheres in contact. It may therefore indicate that the nucleonic configurations of the fission fragments are determined during the deformation of the nucleus from saddle point to scission.

The experimental Z_p values which are corrected for neutron emission follow the calculated trends in the peak regions while in the valley region it looks as if the experimental Z_p approached the unchanged charge distribution faster than is expected from the theory. Whether this is a result of how the data are treated or indicates a contribution from the symmetric fission mode which is known to follow the unchanged charged distribution is not clear.

4.6. Medium-energy fission

This process has been studied in a number of nuclides of which the following ones should be mentioned: ^{232}Th with deuterons [91], with protons [91, 92] and with alpha particles [93], ^{238}U with protons [94] and ^{237}Np and ^{239}Pu with alpha particles [95].

In charge distribution studies of fission at higher energies it is difficult to specify the fissioning nucleus due to the fission neutron-emission competition. Pre-fission emission of neutrons and the subsequent decrease in neutron emission from the fragments move the most probable primary charge in opposite directions [43] and according to Freid et al. [91] the differences tend to cancel.

Using their experimental data from proton and deuteron-induced-fission in ^{232}Th, Freid et al. [91] tested various neutron-distribution curves, mass formulae and postulates of charge division, but always assuming a Gaussian charge dispersion. In this way they find that a "saw-tooth" neutron distribution curve is required at these energies and that shell effects dominate. For fission of ^{232}Th with protons in the energy range 10 to 12 MeV the charge distribution is given by the equal charge displacement hypothesis but with shell-influenced values for the line of nuclear stability as proposed in Ref. [56] while 12-MeV-deuteron-induced fission on the same nuclide results in a charge distribution according to the postulate of minimum potential energy.

The same type of treatment of charge division in fission of ^{238}U with 9.5 to 11.3 MeV protons and with 11.5 MeV deuterons has been carried through by Anderson et al. [94]. In these processes the best fit is observed when the minimum-potential-energy postulate, but shell-influenced, is used. The "saw-tooth"-neutron-distribution curve seems valid.

From a consideration of the neutron-to-fission width, these authors find evidence for predominant first-chance fission in ^{238}U bombarded with protons or deuterons at these energies. In the thorium case [91], however, there are about equal contributions from first- and second-chance fission. The change from the validity of the equal-charge-displacement to the minimum-potential energy could be explained as a result of higher excitation energy in the fissioning nucleus. The estimated average excitation energies are, however, equal within a couple of MeV. Thus, for a definite choice and explanation more data are needed, first of all information on pre- and post-fission neutron emission.

The strong influence from closed shells found in these studies does not seem to hold in fission of ^{237}Np and ^{239}Pu with intermediate-energy alpha particles. In these cases Wogman et al. [95] can interpret their result better in view of the equal charge displacement hypothesis than of the unchanged charge distribution. The former must, however, not be shell-influenced. The post-fission neutron distribution from the fragments is consistent with their mass ratio.

A study of fission of ^{232}Th by protons at higher energies than discussed above, i.e. 20 to 85 MeV is made by Benjamin et al. [92]. These authors as previously done by Friedlander et al. [102] are in favour of presenting their yields in terms of N/Z of the fragment in question. In general, the conversion of the N/Z dispersion to charge dispersion requires knowledge of the charge and mass distribution.

The N/Z dispersion curves obtained show a width which is nearly constant, up to 50-MeV bombarding energy. The width increases from then on slowly reaching a value of about 50 per cent higher at 85 MeV. At the same time the maximum of the N/Z distribution approaches stability.

Attempts to correlate experimental data with the (shell-influenced) equal-charge-displacement hypothesis and the unchanged charge distribution seems to favour the latter at the higher energies. Both for uranium and thorium, however, up to about 57-MeV-proton energy, the experimental Z_p values seem to lie between these two descriptions of charge division. New data along this interesting line are presented by Yaffe et al. [103] in these Proceedings.

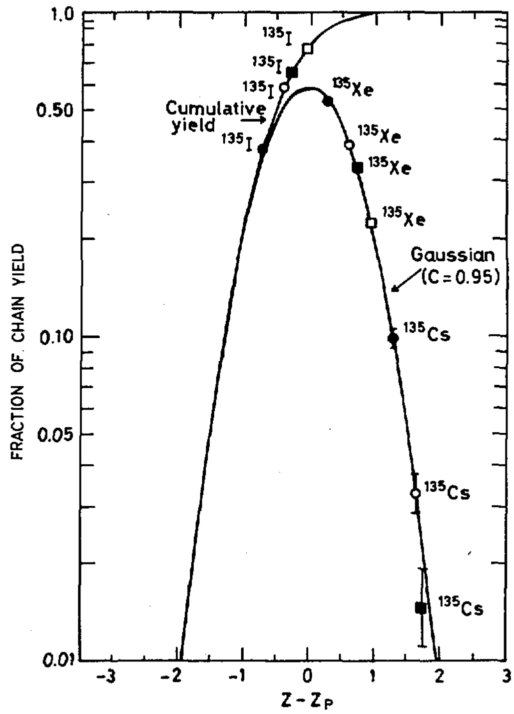

FIG. 20. Gaussian charge distribution that fits best the fractional-yield data of the mass 135 for all energies [93].

Recently a study of the charge division in ^{236}U compound nucleus excited to different energies as obtained by bombardment of ^{232}Th with alpha particles has been published. McHugh and Michel [93] have succeeded in measuring independent yields of 15 nuclides from fission of ^{236}U excited to energies 20 to 57 MeV. Figure 20 shows the fractional chain yield for three members of the mass A = 135 chain at different excitation energies. The Gaussian distribution which fits best the data from all energies has a value of $C = 0.95 \pm 0.05$ which is identical with the 1962 value of Wahl et al. [58] for thermal-neutron-induced fission of ^{235}U. Since it is the same nucleus ^{236}U that fissions an excellent proof is given for the constancy of the width of the charge dispersion over a wide range of excitation, i.e. 6.5 to 39 MeV.

The same authors compare (Fig. 21) Z_p functions for thermal-neutron-induced fission of ^{235}U and 44-MeV-alpha-induced fission of ^{232}Th with predictions of unchanged charge distribution and minimum potential energy for ^{235}U thermal fission. They use the neutron-distribution curve given by Terrel [28] in this analysis. As in so many other cases they also

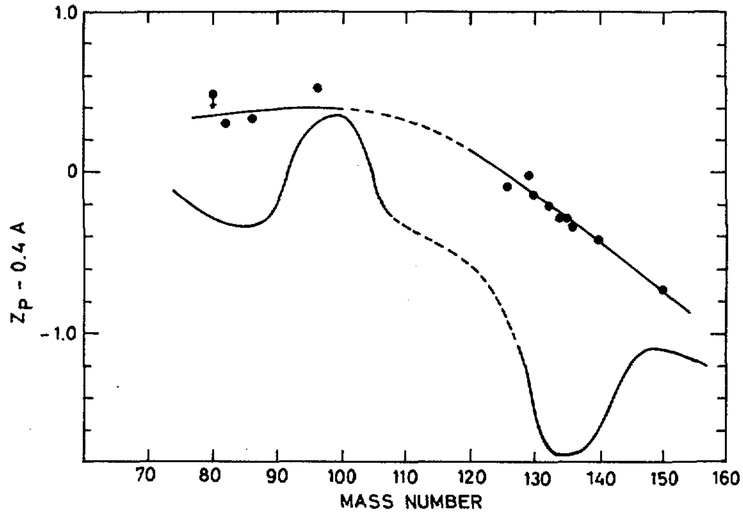

FIG. 21. Comparison of empirical Z_p trends for different excitation energies in ^{236}U [93].
——: Z_p $^{235}U + n_{th}$, $E^* = 6.5$ MeV [58],
● : $^{232}Th + \alpha \rightarrow {}^{236}U$, $E^* = 39.3$ MeV.

point out that shell-influenced treatment (mass formula) would give a better fit than non-shell treatment. Furthermore, they do not find deviations from a pure Gaussian charge dispersion in mass chains A = 135 and 136, and no fine-structure is observed in the cumulative yields of Xe isotopes. The empirical Z_p dependence on mass is, as can be seen from Fig. 21, smooth at 39-MeV excitation. These observations are taken to indicate that above 25-MeV excitation of ^{236}U there is no influence from nuclear shells.

These results, however, cannot be interpreted that asymmetric fission has vanished at this excitation as we have already seen [39, 40, 43-45, 46a, 47] that asymmetric fission persists to high bombarding energies.

4.7. High-energy induced fission

The most extensive work on charge distribution in high-energy fission has been done by members of the Oslo-Uppsala [96, 97, 43] group for fission of natural uranium with 170-MeV protons. They have determined the width of the charge dispersion curve as a function of mass number [43], as well as the position of Z_p for fission products between A = 64 and A = 142 [43].

The most striking result is shown in Fig. 22 which gives the neutron-to-proton ratio (N_p/Z_p) for the most probable fission product as a function of mass in the 170 MeV fission. The dip below the general trend of the curve is found in the same mass region as the symmetric peak in the mass distribution at energies from 440 MeV to 28 GeV have been undertaken by many authors [49, 98, 99]. A survey for fission at 440 MeV is given by Hogan and Sugarman [49], who used the curve of Pappas and Hagebø [43] recalculated for 440 MeV in order to make a complete fit to existing data from many sources. Their curve is given in Fig. 23, but does not fit too well to the recent measurements by Panontin and Porile [98] also at 450 MeV

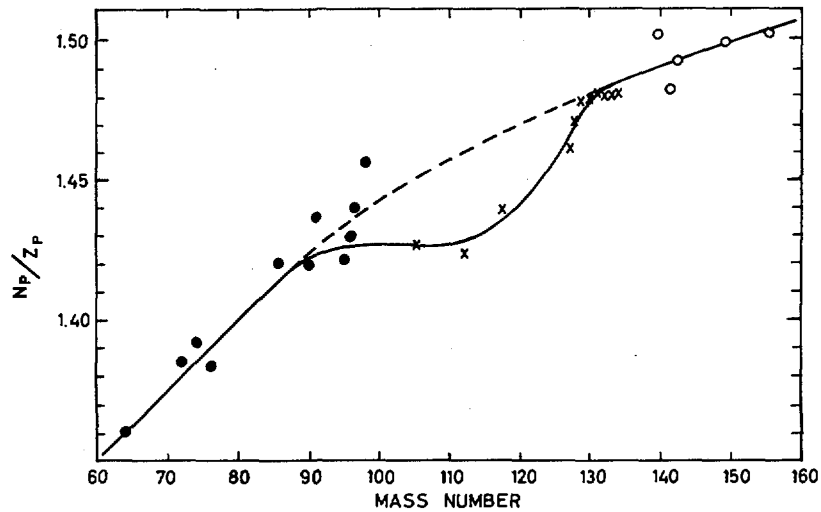

FIG. 22. The N_p/Z_p ratio for most probable products versus mass number for fission of ^{238}U with 170-MeV protons [43].

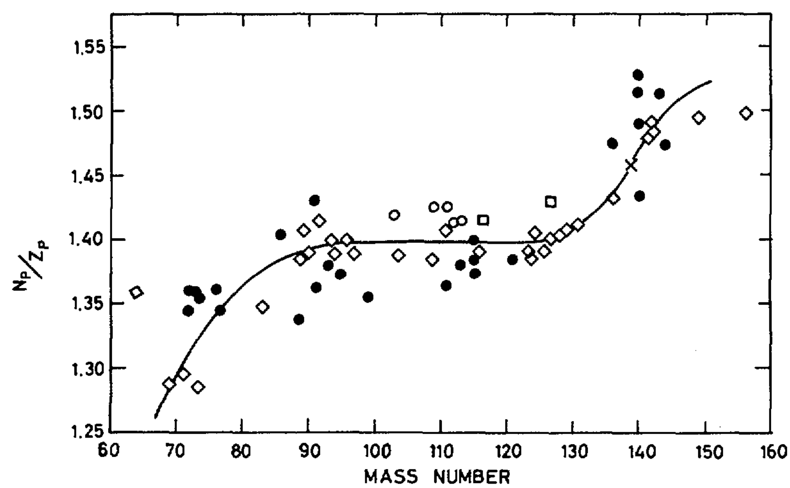

FIG. 23. Variation of the ratio of the neutron number to most probable charge, N_p/Z_p, with mass number A in high energy fission.
●: [54], ◇: [43], ○: [98], ×: [49], □: [99,100].

and by Hagebø [99,100] at 570 MeV. These studies give higher N/Z ratios for the most probable products in the symmetric region. The difference amounts to about 0.5 charge units for Z_P which is outside the experimental errors.

It is thus possible that Z_P increases more slowly with increasing proton energy than anticipated, at least in the symmetric region. In fact it is shown by several authors [99-102], but most clearly at masses 117 and 127 [99,100] that a double-humped charge dispersion curve develops

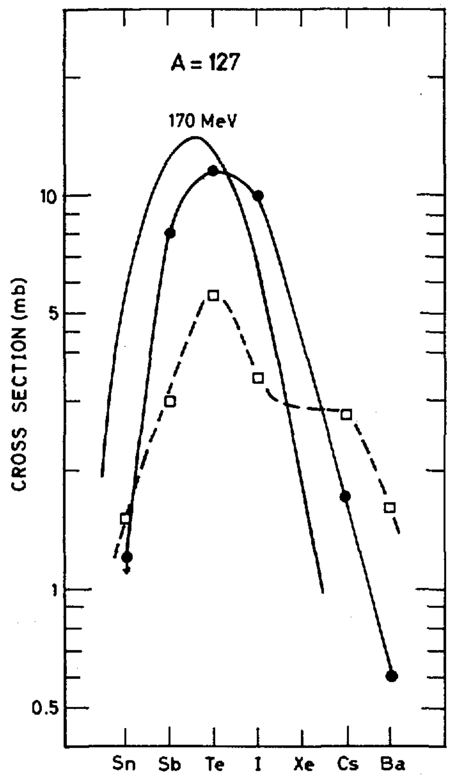

FIG. 24. Charge dispersion curves for the mass A = 127 from bombardment of ^{238}U with 170 and 570 MeV, and 18 GeV protons [99].
●: 570-590 MeV, □: 18.2-28 GeV.

above 600 MeV. The most probable primary charge for the neutron-rich hump in this curve stays constant above this energy as shown in Fig. 24.

Another important feature of the charge dispersion curves from high-energy-proton-induced fission is the width, which was thought to increase strongly with incident energy, especially after the work of Friedlander et al. [102].

In fact, by using the N_p/Z_p-curve given by Pappas and Hagebø [43], Hogan and Sugarman [49] were able to correct the Friedlander curves to be in agreement with other observations. At present we know the widths at 170 MeV and some at 440-570 MeV. At masses 103 to 117 and at 127 the width does not change significantly between 170 MeV and 570 MeV, but stays constant with FWHM 2.8 to 2.9 charge units. At mass around 140 it increases between 170 MeV and 440 MeV from ~2.2 charge units [96] to ~3.2 charge units [49].

Both the position of Z_p and the width of the charge-dispersion curve as a function of mass and proton energy prove that one cannot draw conclusions of general validity from measurement of a single mass chain only.

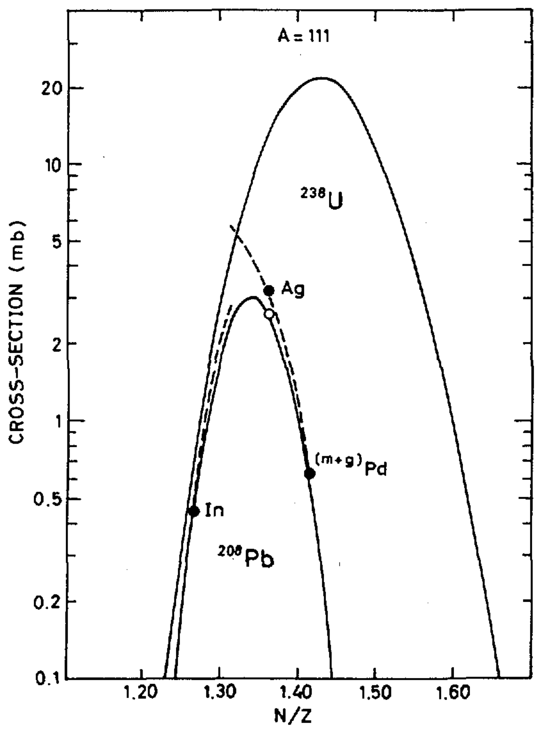

FIG. 25. N/Z dispersion of mass A = 111 products in fission of ^{208}Pb by 450 MeV protons [55].
——: calculated independent cross-sections,
----: calculated cumulative cross-sections.

Very little is known of the charge distributions from fission of other elements than uranium with high-energy protons. The only determination is due to Panontin and Porile [55] who irradiated lead with 450 MeV protons, and determined the charge dispersion curve around mass number 109 (Fig. 25). This curve is much narrower than the curve they report for uranium fission with the same energy protons [98].

Before finishing this review, the authors would like to draw the attention to the new on-line projects for studying short-lived nuclides from nuclear reactions i.e. ISOLDE, TRISTAN, OSIRIS, SOLIS and others [104]. These projects will hopefully be of great value for studying also the interesting aspects of mass and charge distributions in fission where there are still many unsolved problems left, with challenge both to experimentalists and theoreticians.

ACKNOWLEDGEMENTS

The authors are indebted to many colleagues who so kindly have made their own unpublished results or those of their groups available for this review, especially to P. Armbruster, N.A. Ballou, J.G. Cuninghame, H. Gauvin, L.E. Glendenin, H.R. von Gunten, J. Hudis, M. Lefort, J.C.D. Milton, L.P. Remsberg, K. Sistemich, E.P. Steinberg, N. Sugarman, A.C. Wahl, L. Yaffe, and many others. The never failing interest and help from Mrs. Mette Anderson, Mrs. Andrea Birch-Aune and Mrs. Lillian Sonning in preparing the manuscript for this review in an exceptionally short time, is highly appreciated.

REFERENCES

[1] FRASER, J.S., MILTON, J.C.D., Phys. Rev. 93 (1954) 818.

[2] MAIER-LEIBNITZ, H., ARMBRUSTER, P., SPECHT, H.J., in Physics and Chemistry of Fission (Proc. Symp. Salzburg 1965) 2 IAEA, Vienna (1965) 113.

[3] WAHL, A.C., in Physics and Chemistry of Fission (Proc. Symp. Salzburg 1965) 1 IAEA, Vienna (1965) 317.

[4] FRASER, J.S., in Physics and Chemistry of Fission (Proc. Symp. Salzburg 1965) 1 IAEA, Vienna (1965) 451.

[5] FRIEDLANDER, G., in Physics and Chemistry of Fission (Proc. Symp. Salzburg 1965) 2 IAEA, Vienna (1965) 265.

[6] GUNTEN, H.R. von, Actinide Reviews (1969) in press.

[7] SHIRAISHI, F., HOSOE, M., Nucl. Instrum. Meth. 66 (1968) 130.

[8] SCHMITT, H.W., NEILER, J.H., WALTER, F.J., Phys. Rev. 141 (1966) 1146.

[9] SIGNARBIEUX, C., RIBRAG, M., NIFENECKER, H., Nucl. Phys. A99 (1967) 41.

[10] ANDRITSOPOULOS, G., Nucl. Phys. A94 (1967) 537.

[11] BOWMAN, H.R., MILTON, J.C.D., THOMPSON, S.G., SWIATECKI, W.J., Phys. Rev. 129 (1963) 2133.

[12] MILTON, J.C.D., FRASER, J.S., in Physics and Chemistry of Fission (Proc. Symp. Salzburg 1965) 2, IAEA, Vienna (1965) 39.

[13] APALIN, V.F., GRITSYUK, Yu.N., KUTIKOV, I.E., LEBEDEV, V.I., MIKAELIAN, L.A., Nucl. Phys. 71 (1965) 553.

[14] MASLIN, E.E., RODGERS, A.L., CORE, W.G.F., Phys. Rev. 164 (1967) 1520.

[15] SCHMITT, H.W., GIBSON, W.M., NEILER, J.H., WALTER, F.J., THOMAS, T.D., in Physics and Chemistry of Fission (Proc. Symp. Salzburg 1965) 1 IAEA, Vienna (1965) 531.

[16] SCHMITT, H.W., KIKER, W.E., WILLIAMS, C.W., Phys. Rev. 137 (1965) B 837.

[17] BENNETT, M.J., STEIN, W.E., Phys. Rev. 156 (1967) 1277.

[18] GLENDENIN, L.E., STEINBERG, E.P., J. inorg. nucl. Chem. 1 (1955) 45; CUNINGHAME, J.G., J. inorg. nucl. Chem. 4 (1957) 1; NERVIK, W.E., Phys. Rev. 119 (1960) 1685.

[19] BRANDT, R., THOMPSON, S.T., GATTI, R.C., PHILLIPS, L., Phys. Rev. 131 (1963) 2617.

[20] PLEASONTON, F., Phys. Rev. 174 (1968) 1500.

[21] NEILER, J.H., WALTER, F.J., SCHMITT, H.W., Phys. Rev. 149 (1966) 894.

[22] SERGACHEV, A.I., VOROBEVA, V.G., KUZMINOV, B.D., MIKHAILOV, V.B., TARASKO, M.Z., Sov. J. nucl. Phys. 7 (1968) 475.

[23] KATCOFF, S., Nucleonics 18 (1960) 201.

[24] FERGUSON, R.L., O'KELLEY, G.D., American Report ORNL - 3305 (1962).

[25] FICKEL, H.R., TOMLINSON, R.H., Can. J. Phys. 37 (1959) 133 and 926.

[26] FARRAR, H., CLARKE, W.B., THODE, H.G., TOMLINSON, R.H., Can. J. Phys. 42 (1964) 2063.

[27] WAHL, A.C., NORRIS, A.E., ROUSE, R.A., WILLIAMS, J.C., Paper SM-122/116, these Proceedings.

[28] TERRELL, J., Phys. Rev. 127 (1962) 880.

[29] DICKMANN, F., DIETRICH, K., Nucl. Phys. A129 (1969) 241.

[30] SCHMITT, H.W., PLEASONTON, F., Nucl. Instrum. Methods 40 (1966) 204.

[31] THOMAS, T.D., VANDENBOSCH, R., Phys. Rev. 133 (1964) B 976.

[32] FRASER, J.S., MILTON, J.C.D., BOWMAN, H.R., THOMPSON, S.G., Can. J. Phys. 41 (1963) 2080.

[33] WILES, D.R., SMITH, B.W., HORSLEY, R., THODE, H.G., Can. J. Phys. 31 (1953) 419.

[34] PAPPAS, A.C., American report AECU-2806 (1953).

[35] KELSON, I., Phys. Rev. Lett. 20 (1968) 867.

[36] GRIFFIN, J.J., in Neutron Cross Sections and Technology (Proc. Conf. Washington, 1968) 2 975, Nat. Bur. Stand. Spec. Publ. 299 (1968).
[37] KARAMIAN, S.A., NORMURATOV, F., OGANESYAN, Yu.Ts., Preprint P7-3732, JINR, Dubna (1968).
[38] PETRZHAK, K.A., TUTIN, G.A., Sov. J. nucl. Phys. 7 (1968) 534.
[39] CROALL, I.F., CUNINGHAME, J.G., Nucl. Phys. A125 (1969) 402.
[40] RUDSTAM, G., PAPPAS, A.C., Nucl. Phys. 22 (1961) 468.
[41] TURKEVICH, A., NIDAY, J.B., Phys. Rev. 84 (1951) 52.
[42] FAIRHALL, A.W., JENSEN, R.C., NEUZIL, E.F., 2nd Int. Conf. peaceful Uses atom. Energy (Proc. Conf. Geneva 1958) 15, UN, New York (1958) 452.
[43] PAPPAS, A.C., HAGEBØ, E., J. inorg. nucl. Chem. 28 (1966) 1769.
[44] GALIN, J., Thesis, Orsay 1967, personal communication from M. Lefort (June 1969).
[45] GAUVIN, H., SAUVAGE, L., J. inorg. nucl. Chem. (1969) in press and private communication from M. Lefort (June 1969).
[46] METROPOLIS, M., BIVINS, R., STROM, M., TURKEVICH, A., MILLER, J.M., FRIEDLANDER, G., Phys. Rev. 110 (1958) 185.
[46a] SCHRÖDER, B., NYDAHL, G., FORKMAN, B., submitted to Nucl. Phys. (July 1969).
[47] REMSBERG, L.P., PLASIL, F., CUMMING, J.B., PERLMAN, M.L., Phys. Rev., in press.
[48] TERRELL, J., in Physics and Chemistry of Fission, (Proc. Symp. Salzburg 1965) 2, IAEA, Vienna (1965) 18; collection of papers presented by Geilikman, B.T., ibid. 1 121.
[49] HOGAN, J.J., SUGARMAN, N., Phys. Rev., in press.
[50] CRESPO, V.P., CUMMING, J.B., POSKANZER, A.M., Phys. Rev. 174 (1968) 1455.
[51] NIX, J.R., SWIATECKI, W.J., Nucl. Phys. 71 (1965) 1.
[52] HAGEBØ, E., RAVN, H., J. inorg. nucl. Chem., in press.
[53] NIDAY, J.B., Phys. Rev. 121 (1961) 1471.
[54] SUGARMAN, N., MÜNZEL, H., PANONTIN, J.A., WIELGOZ, K., RAMANIAH, M.V., LANGE, G., LOPEZ-MENCHERO, E., Phys. Rev. 143 (1966) 952.
[55] PANONTIN, J.A., PORILE, N.T., J. inorg. nucl. Chem. 30 (1968) 2891.
[56] PAPPAS, A.C., 1st Int. Conf. peaceful Uses atom. Energy (Proc. Conf. Geneva 1955) 7, UN, New York (1956) 19.
[57] TALAT-ERBEN, M., GÜVEN, B., Phys. Rev. 129 (1963) 1762.
[58] WAHL, A.C., FERGUSON, R.L., NETHAWAY, D.R., TROUTNER, D.E., WOLFSBERG, K., Phys. Rev. 126 (1962) 1112.
[59] STROM, P.O., GRANT, G.R., PAPPAS, A.C., Can. J. Chem. 43 (1965) 2493.
[60] SISTEMICH, K., German report Jül-574-FN (1969).
[61] NIFENECKER, H., RIBRAG, M., FREHAUT, J., GAURIAN, J., Nucl. Phys. A 131 (1969) 261.
[62] NÖRENBERG, W., Z. Physik 197 (1966) 246.
[63] ARMBRUSTER, P., HOVESTADT, D., MEISTER, H., SPECHT, H.J., Nucl. Phys. 54 (1964) 586.
[64] KONECNY, E., OPOWER, H., GUNTHER, H., GÖBEL, H., in Physics and Chemistry of Fission (Proc. Symp. Salzburg 1965) 1, IAEA, Vienna (1965) 401.
[65] REISDORF, W., ARMBRUSTER, P., Phys. Rev. Lett. 24B (1967) 501.
[66] PAPPAS, A.C., TUNAAL, T., (1964), unpublished.
[67] BOHN, E.M., WEHRING, B.W., WYMAN, M.E., Appl. Physics Lett. 12 (1968) 199.
[68] REISDORF, W., Z. Phys. 209 (1969) 77.
[69] JOHN, W., NASSEY, R., SAUNDERS, B., Physics Lett. 24B (1967) 336.
[70] GLENDENIN, L.E., GRIFFIN, H.C., REISDORF, W., UNIK, J.P., Paper SM-122/114, these Proceedings.
[71] FONG, P., Phys. Rev. 102 (1956) 434.
[72] FONG, P., quoted in Ref. [73].
[73] WING, J., FONG, P., Phys. Rev. 157 (1967) 1038.
[74] GORDON, G.E., ARAS, N.K., in Physics and Chemistry of Fission (Proc. Symp. Salzburg, 1965) 2, IAEA, Vienna (1965) 73.
[75] STROM, P.O., LOVE, D.L., GREENDALE, A.E., DELUCCHI, A.A., SAM, D., BALLOU, N.E., Phys. Rev. 144 (1966) 984.
[76] DELUCCHI, A.A., GREENDALE, A.E., STROM, P.A., Phys. Rev. 173 (1968) 1159.
[77] DENSCHLAG, H.O., J. inorg. nucl. Chem. 31 (1969) 1873.
[78] RUNNALIS, N.G., TROUTNER, D.E., FERGUSON, R.L., Phys. Rev. 179 (1969) 1188.
[79] WATSON, R.L., BOWMAN, H.R., THOMPSON, S.G., Phys. Rev. 162 (1967) 1169.
[80] WAHL, A.C., NETHAWAY, D.R., Phys. Rev. 131 (1963) 830.
[81] WEISS, H.V., ELZIE, J.L., FRESCO, J.M., Phys. Rev. 172 (1968) 1269.

[82] ARAS, N.K., GORDON, G.E., J. inorg. nucl. Chem. 28 (1966) 763.
[83] TROUTNER, D.E., WAHL, A.C., FERGUSON, R.L., Phys. Rev. B134 (1964) 1027.
[84] GUNTEN, H.R. von, GLENDENIN, L.E., FLYNN, K.F., personal communication (1969).
[85] GLENDENIN, L.E., UNIK, J.P., Phys. Rev. 140 (1965) B 1301.
[86] GUNTEN, H.R. von, FLYNN, K.F., GLENDENIN, L.E., Phys. Rev. 161 (1967) 1192.
[87] WOLFSBERG, K., Phys. Rev. 137 (1965) B 929.
[88] GLENDENIN, L.E., CORYELL, C.D., EDWARDS, R.R., Paper 52 in Radiochemical Studies: The Fission Products (CORYELL, C.D., SUGARMAN, N., Eds), Nat. Nucl. Energy Ser. 9 Div. 4, McGraw-Hill Book Co. Inc., New York (1951).
[89] PAPPAS, A.C., STROM, P.O., unpublished; STROM, P.O., Thesis, University of Oslo (1964).
[90] BLANN, M.M., USA report, UCRL-9190 (1960).
[91] FREID, S.H., ANDERSON, J.L., CHOPPIN, G.R., J. inorg. nucl. Chem. 30 (1968) 3155.
[92] BENJAMIN, P.P., MARSDEN, D.A., PORILE, N.T., YAFFE, L., Can. J. Chem. 47 (1969) 301.
[93] McHUGH, J.A., MICHEL, M.C., Phys. Rev. 172 (1968) 1160.
[94] ANDERSON, J.L., FREID, S.H., CHOPPIN, G.R., J. inorg. nucl. Chem. 30 (1968) 3167.
[95] WOGMAN, N.A., POWERS, J.A., COBBLE, J.W., Phys. Rev. 152 (1966) 3167.
[96] PAPPAS, A.C., ALSTAD, J., J. inorg. nucl. Chem. 17 (1961) 195.
[97] HAGEBØ, E., PAPPAS, A.C., AAGAARD, P., J. inorg. nucl. Chem. 26 (1964) 1639.
[98] PANONTIN, J.A., PORILE, N.T., J. inorg. nucl. Chem. 30 (1968) 2017.
[99] HAGEBØ, E., J. inorg. nucl. Chem. 29 (1967) 2515.
[100] HAGEBØ, E., J. inorg. nucl. Chem. In Press.
[101] PORILE, N.T., Phys. Rev. 148 (1966) 1235.
[102] FRIEDLANDER, G., FRIEDMAN, L., GORDON, B., YAFFE, L., Phys. Rev. 129 (1963) 1809.
[103] YAFFE, L., these Proceedings.
[104] Proc. Symposium: "Why and How Should We Investigate Nuclides Far Off the Stability Line", Lysekil (1966) Arkiv för Fysik 36 (1967).

DISCUSSION

F. PLASIL: I would like to make a comment on semantics. I am under the impression that, particularly since the Salzburg conference, the term "fission modes" implies some qualitative difference, such as different saddle points involved. There is no evidence for such a qualitative difference in most of the pertinent work, certainly not in the high-energy work mentioned by Dr. Pappas, in which I collaborated with Remsberg and others at Brookhaven National Laboratory. In general, if one obtains a distribution which appears to be a mixture of "symmetric" and "asymmetric" fission, one is always free to decompose such a distribution, and therefore I think the terms symmetric and asymmetric components should be used rather than symmetric and asymmetric modes.

NUCLEAR CHARGE DISPERSION IN THE FISSION OF HEAVY ELEMENTS BY MEDIUM-ENERGY PROTONS*

L. YAFFE
Radiochemistry Laboratory, Department of Chemistry,
McGill University, Montreal, Quebec,
Canada

Abstract

NUCLEAR CHARGE DISPERSION IN THE FISSION OF HEAVY ELEMENTS BY MEDIUM-ENERGY PROTONS. Independent yields have been determined for nuclides with masses $129 \leq A \leq 140$ produced in the fission of ^{232}Th, ^{233}U, ^{235}U, ^{238}U, and ^{239}Pu by protons of energies up to 100 MeV. Excitation functions have been compared for the nuclides produced in the different fissioning systems. The importance of the neutron-to-proton ratio, (N/Z), in the target is evident from this comparison. Neutron-deficient species occur in high yield from targets with low N/Z ratios compared with their production at the same energies from targets with high N/Z ratios. Charge dispersion curves have been obtained for all these systems. The curves broaden with increasing bombardment energy and the most probable charge, Z_p, moves towards stability. It is shown that the distance from stability, $Z_A - Z_p$, is a function of the neutron-to-proton ratio of the target. From this basis it is possible to predict the most probable charge in fission for systems yet unstudied. Calculations have been made to calculate Z_p on the basis of the unchanged-charge-distribution and equal-charge-displacement postulates. Calculations are also made from Z_p to determine the average number of neutrons emitted during fission at these energies.

INTRODUCTION

An attempt has been made to help elucidate the fission process by studying the charge dispersion of the fission products. To this end the fission of ^{232}Th, ^{233}U, ^{235}U, ^{238}U, and ^{239}Pu by protons of energies 20-85 MeV has been studied and the fission of other heavy nuclides by protons in this energy region is proceeding in our laboratory. This energy region is intrinsically very interesting because it is generally believed that a transition gradually takes place in this region from the low-energy compound nucleus type of mechanism to the direct interaction type. In this paper I report a summary of work in our laboratory in which the following, listed alphabetically and not chronologically, have been or are taking part: P. P. Benjamin, J. H. Davies, A. H. Khan, B. D. Pate, G. B. Saha, and I. Tomita.

When one considers that the nuclear charge in fission is such an important parameter, it is surprising how few data are present in the literature. At thermal energies most of the definitive work is due to Wahl and his co-workers[1-3] and deals only with ^{235}U. Wahl[4] also investigated charge distribution in fission of ^{235}U with 14-MeV neutrons. Pate, Foster, and Yaffe[5] studied the fission of ^{232}Th with protons of energies 8-87 MeV. They showed that the full-width at half-maximum of the charge distribution remained constant up to 25 MeV and then the curves widened as the bombarding energy increased.

* This work was supported by the National Research Council of Canada.

This was accompanied by a shift of the most probable charge, Z_p, towards the nuclear charge associated with stability for mass A, Z_A. The constancy of the full-width at half-maximum (FWHM) referred to above was interpreted as possibly being due to a single fissioning parent at these energies. Pate [6] attempted to analyze these data in terms of the two charge distribution postulates current at that time (and still current). These were: (a) unchanged charge distribution (UCD) [7], i. e. the fission products will have the same neutron-to-proton ratio (N/Z) as the parent fissioning nucleus and (b) equal charge displacement (ECD) [8] which postulated that the two fragments will adopt a charge distribution so that $(Z_A-Z_p)_\ell = (Z_A-Z_p)_h$ where ℓ and h refer to the light and heavy fragments respectively. Pate found that the data in ref. 4 were "not inconsistent" with the ECD postulate.

Friedlander et al [9] made a comprehensive study of the charge dispersion of various cesium isotopes formed in the fission of ^{238}U by protons of energies from 0.1 to 6.2 GeV. The shift of Z_p towards Z_A and the broadening of the charge dispersion curves were clearly evident from this work. The data were best interpreted by the UCD mechanism. These and other high-energy data are extremely well summarized by Friedlander in his Salzburg paper [10]. No further reference to energies higher than 100 MeV will be made in this paper unless it bears specifically on the work in the energy region at present under consideration. This paper will summarize and correlate results from the work described in greater detail in references 11-16.

EXPERIMENTAL

(a) Irradiations:

All irradiations were made in the circulating proton beam of the McGill 82-in. synchrocyclotron. In general, the target foils were irradiated in stacks of three to compensate for target recoils and the middle foil was used for radiochemical separation. The beam was monitored by either Al or Cu foils depending on the energy range and the monitor reactions used were $^{27}Al(p,3pn)^{24}Na$, $^{63}Cu(p,n)^{63}Zn$, and $^{65}Cu(p,pn)^{64}Cu$ in the usual way. ^{233}U was irradiated as a powder (U_3O_8) in an aluminium tube. ^{239}Pu was irradiated as the Pu-Al alloy. The beam current was of the order of 1 microampere and the irradiation time varied from 2 minutes to 15 minutes depending on the nuclides which were being investigated.

(b) Chemical separation:

Standard chemical techniques were used for the separation of the radioactive nuclides and these are given in detail in the references quoted. In the case of nuclides shielded or "semi-shielded" from formation by β^+ or β^- decay of their precursors only one chemical separation and further purification was necessary. In other cases where the half-lives of the precursors were relatively short, either one irradiation and several timed separations were made, or in some cases two separate irradiations with varying times of separation. The method is described in detail in reference 9.

(c) Activity measurements:

The activities of the nuclides were measured by end-window β^-, $4\pi\beta^-$, β^+ coincidence, NaI, and Ge(Li) counters. The decay curves were analysed by the CLSQ computer programme of Cumming(17).

(d) Treatment of data:

The counting rates were transformed to disintegration rates by correcting for counter efficiencies, branching ratios, and chemical yields. These were converted into cross sections based on the monitor cross sections used.

RESULTS AND DISCUSSION

(a) Excitation functions:

Friedlander et al(9) have shown that, in the fission of ^{238}U the higher the bombarding energy the greater is the probability of the independent production of neutron-deficient nuclides. This is shown in Figs. 1 and 2. Fig. 1, obtained by Davies and Yaffe(11), shows the excitation function for the independent formation of a typical neutron-excessive nuclide in this mass region, ^{136}Cs. It reaches a maximum at a bombarding energy of about 60 MeV. In Fig. 2, one observes the behaviour of the neutron-deficient isotopes of cesium independently formed(9). As the energy of bombardment increases, the formation of the more neutron-deficient isotopes become more probable. The same behaviour is seen with all the heavy targets studied, although

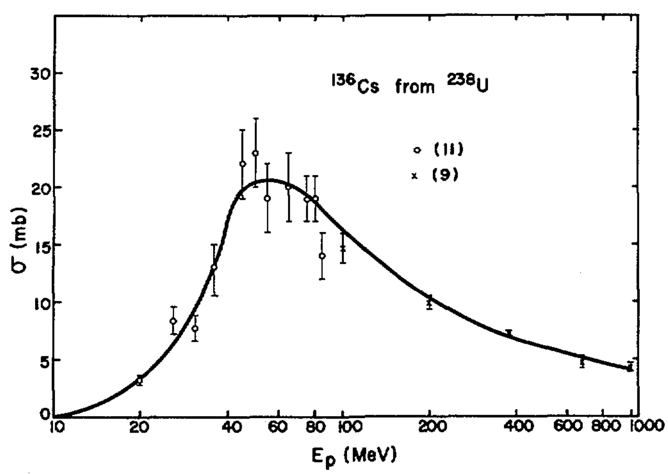

FIG. 1. Excitation function of ^{136}Cs obtained from the fission of ^{238}U.

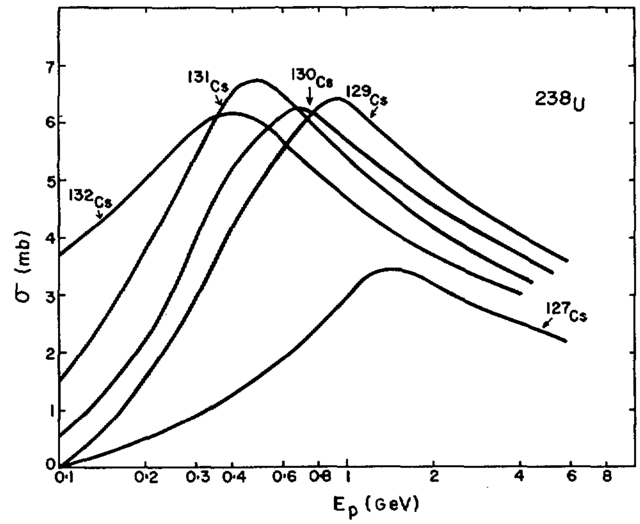

FIG.2. *Excitation functions of neutron-deficient isotopes of caesium obtained from the fission of* ^{238}U.

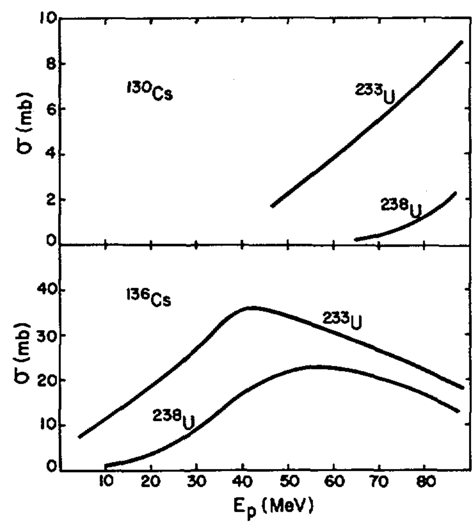

FIG.3. Excitation functions of ^{130}Cs and ^{136}Cs obtained from the fission of ^{233}U and ^{238}U.

some of these studies have not yet been taken to high enough energies to get complete excitation functions of the most neutron-deficient isotopes of cesium. However there is a distinct correlation between the neutron-to-proton ratio of the target and that of the product. In Fig. 3 are shown data for ^{136}Cs and ^{130}Cs obtained from both ^{238}U and ^{233}U targets. One can readily see that the excitation function of ^{136}Cs reaches a maximum at a lower energy when the target is ^{233}U rather than ^{238}U. Even more strikingly, the cross sections are roughly a factor of 5 higher

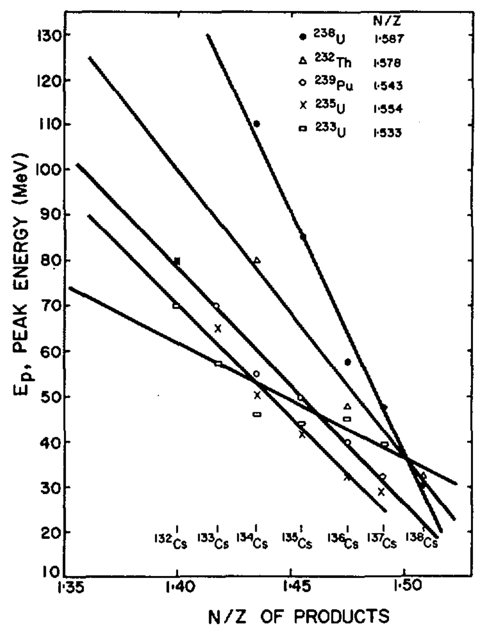

FIG.4. Energies at which the excitation functions of various Cs isotopes, obtained from the fission of ^{233}U, ^{235}U, ^{238}U, ^{232}Th, and ^{239}Pu, reach their maxima plotted against the neutron-to-proton ratio of the fission product.

in the rising portion of the excitation function for ^{233}U than for ^{238}U. The same is true for ^{130}Cs. From ^{238}U, the independent formation of ^{129}Cs was barely measureable by Friedlander et al[9] at 100 MeV, whereas from ^{233}U it has a sizeable independent formation cross section of 2.8 mb at 85 MeV[14]. These data are summarized in Fig. 4 where the energies at which the excitation functions reach their maxima are plotted against the neutron-to-proton ratio of the fission products. The trends discussed just previously can easily be seen. There is of course a fair amount of uncertainty in the determination of these peaks and thus the slopes of the lines themselves have a large uncertainty and need more data for a clearer definition. However the trends are perfectly obvious. The lines seem to converge at a value of about N/Z = 1.55. This would mean that ^{140}Cs, for example, would be formed as a fission product with very high probability at very low energies for all heavy targets, and this is indeed the case in thermal neutron and spontaneous fission of ^{235}U. This type of plot shows clearly the importance of the neutron-to-proton ratio in the target in the determination of the nature of the fission products.

(b) Charge dispersion curves:

From the cross section data one can get charge dispersion curves, if one assumes an essentially flat mass distribution in this narrow mass region. The cross sections are plotted against N/Z of the product rather than $Z-Z_A$ to avoid shell-edge discontinuities as suggested by Friedlander et al[9]. In addition, as pointed out above, the present work shows the importance of the neutron-to-proton ratio as a parameter. The right-hand portion of the curve is formed in such a manner that the sum of yields, read from the curves for the various isobars, must agree with the isobaric yield determined experimentally. This virtually defines the curve uniquely(5,9) unless one assumes some curious discontinuity. With the more neutron-deficient targets e.g. ^{233}U, ^{239}Pu, and ^{235}U as will be seen, the more neutron-excessive products fall on the right-hand portion of the curve and thus the combination of the two does define the curve exactly and lends even greater credence to this operation for the other targets.

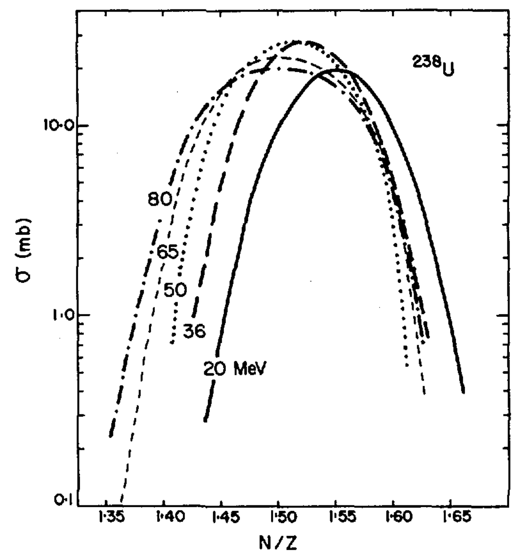

FIG.5. Charge dispersion curves from the fission of ^{238}U.

Figs. 5-9 show a series of such curves for each of ^{238}U, ^{232}Th, ^{235}U, ^{239}Pu, and ^{233}U. The behaviour is virtually the same - an increase in the full-width at half-maximum and a decrease in Z_A-Z_p, i.e. a shift towards β-stability and increased production of neutron-deficient nuclides with increase in bombardment energy. Fig. 10 shows the curves at a bombarding energy of 50 MeV for various targets and their relative displacement from Z_A.

It became apparent soon after this work commenced that the position of Z_A-Z_p depended not only on bombardment energy, but for each fission product also on the N/Z value of the target. With information available for ^{238}U, ^{232}Th, and ^{233}U the values of Z_A-Z_p were plotted as a function of bombardment energy as shown in Fig. 11. The values of Z_A-Z_p at each energy were then plotted against the N/Z value of the target as shown in Fig. 12 and predictions read from this for ^{239}Pu and ^{235}U which were then being investigated in our laboratory. The fit for ^{239}Pu, as shown

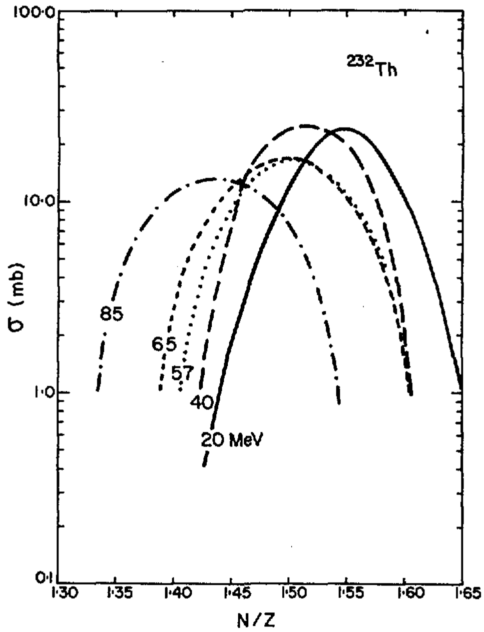

FIG.6. Charge dispersion curves from the fission of ^{232}Th.

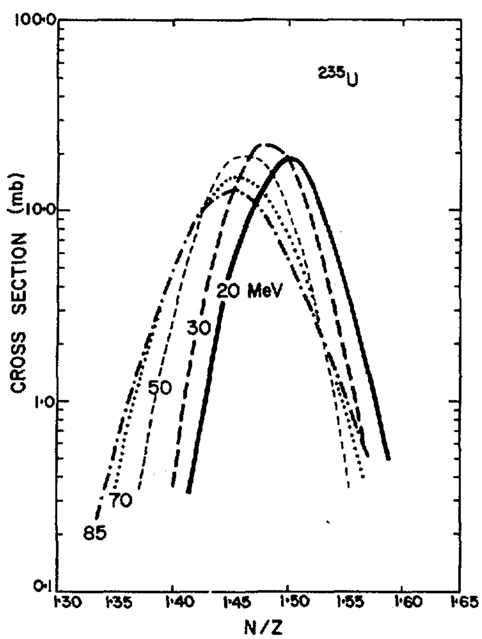

FIG.7. Charge dispersion curves from the fission of ^{235}U.

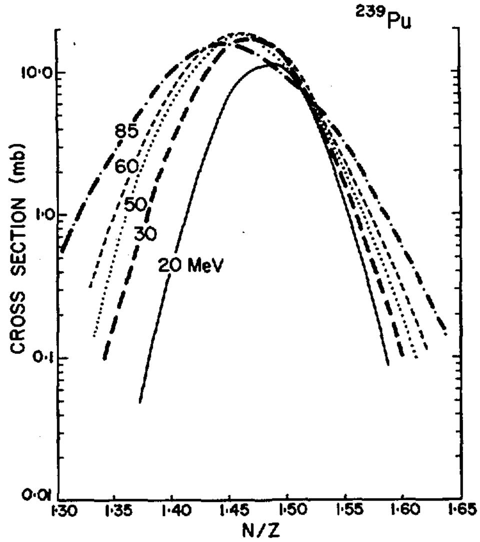

FIG. 8. Charge dispersion curves from the fission of ^{239}Pu.

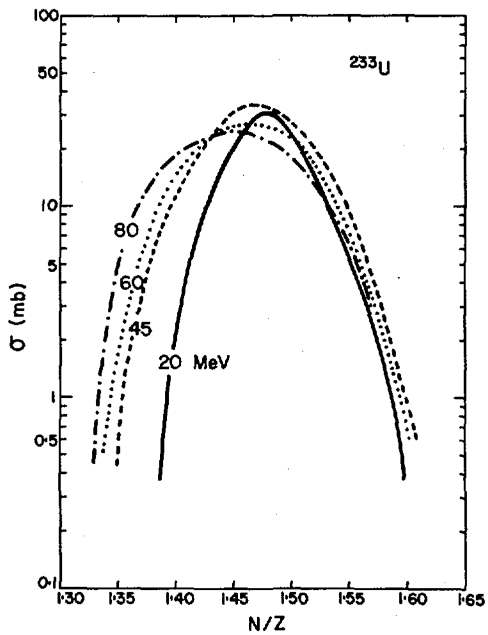

FIG. 9. Charge dispersion curves from the fission of ^{233}U.

in Fig. 13 was very good and these data were now taken to re-define more accurately the curve in Fig. 12 and thus predict the results for ^{235}U. These are shown in Fig. 14. Fig. 15 thus contains the information for all 5 targets of different N/Z and is now being used to predict Z_A-Z_p values, and thus the most probable

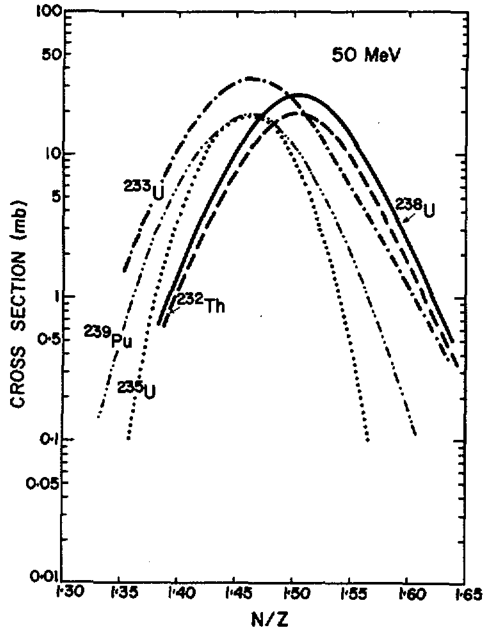

FIG.10. Charge dispersion curves at 50-MeV bombarding energy for ^{238}U, ^{232}Th, ^{235}U, ^{239}Pu, and ^{233}U.

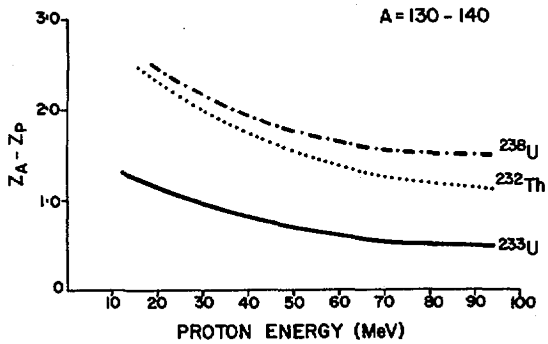

FIG.11. Displacement of most probable charge, Z_p, from stability Z_A for ^{238}U, ^{232}Th, and ^{233}U as a function of bombardment energy.

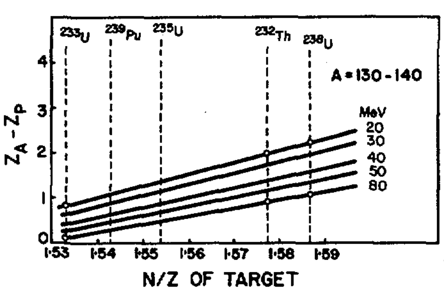

FIG.12. Displacement of most probable charge from stability as a function of the neutron-to-proton ratio of the target for various bombarding energies.

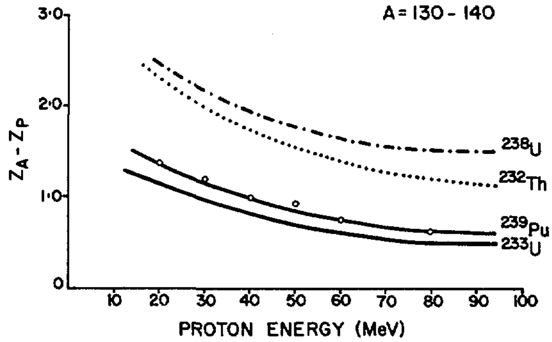

FIG.13. Displacement of most probable charge from stability as a function of bombardment energy, showing predicted and experimental values for ^{239}Pu.
——— predicted
-o——o- experimental

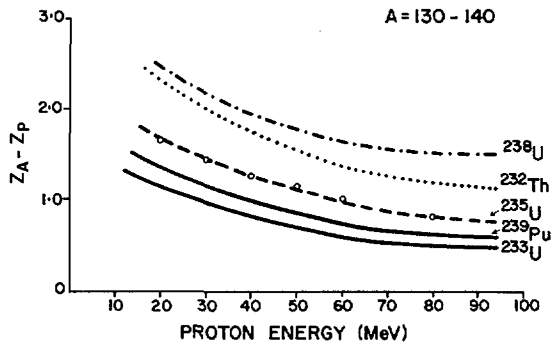

FIG.14. Displacement of most probable charge from stability as a function of bombardment energy, showing predicted and experimental values for ^{235}U.
– – – – – predicted
-o——o- experimental

charge for a variety of fissioning systems now being investigated in our laboratory. A word of caution is however in order. All of these data are for the very narrow mass range under consideration, viz. A = 129-139. It is quite conceivable that different results would be expected in another mass range and this is now being investigated, especially in the light-mass region[18].

From Fig. 15 one can see that ^{238}U at 85-MeV bombarding energy would give the same value of $Z_A - Z_p$ as ^{233}U at 20 MeV and ^{235}U at 40 MeV bombarding energies, i.e. there is a strong suggestion that the average fissioning parent (after neutron emission) is the same in each case.

(c) Z_p calculations:

It is of some interest to compare the experimental (and predicted) value of Z_p with those obtained by calculation with different postulates. We have, in all the fissioning systems studied, calculated Z_p for A = 136 by both the Equal

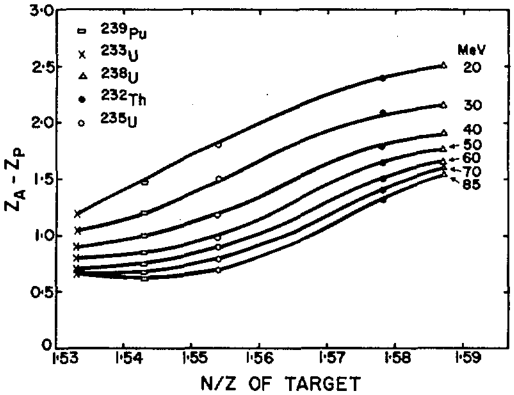

FIG.15. Displacement of most probable charge from stability as a function of the neutron-to-proton ratio of the target for a variety of bombarding energies.

Charge Displacement (ECD) and Unchanged Charge Division (UCD) hypotheses. Calculations were performed only at 30,40, and 50 MeV where one could safely assume that most of the reactions were of the compound nucleus type. The compound nucleus would be expected to undergo fission and/or neutron evaporation. The different fissioning parents were ascertained by allowing neutrons of energy B_n + 2T to evaporate, where B_n is the neutron binding energy and 2T is the kinetic energy of the neutron, T being the nuclear temperature, calculated from $U = aT^2 - 4T$[19] where U is the excitation energy of the residual nucleus and a, 10.5 MeV^{-1} [20], is the level-density parameter. A number of fragment pairs were randomly selected and the excitation energies of these fragments estimated on the simple assumption that the fragments shared the energy in proportion to their masses. Of all these fragments only those were chosen which gave rise to A = 136 after evaporation of neutrons of energy B_n + 2T. Proton emission was not considered in either the case of the fissioning parent or the fission fragment because of the neutron-excess nature of both parent and fragment and thus a low probability for such an event at these energies. Z_p values were then calculated for all of these fragments according to the ECD and UCD hypotheses. The calculated values were weighted by fission branching ratios $[\Gamma_f/(\Gamma_f + \Gamma_n)]$, obtained from Huizenga and Vandenbosch[20]. The values for ^{239}Pu and ^{235}U targets which are typical of all the systems are shown in Table I. It is evident that the values agree very well with those calculated from the UCD postulate. However, one must not lose sight of the assumptions involved in such a calculation. For example, the excitation energy was assumed to be shared between the fragments in proportion to their masses since it seemed the most likely assumption to make. If one makes the gross assumption that the heavy product received only one-half the energy determined in this way, the calculated Z_p values decrease by 0.6 charge units, but the agreement with UCD is still rather good. If one makes the inverse gross assumption that the heavy fragment receives 1.5 times this energy the calculated Z_p values

TABLE I. COMPARISON OF EXPERIMENTAL AND CALCULATED Z_p VALUE

Proton energy (MeV)	Z_p					
	^{239}Pu			^{235}U		
	ECD	UCD	Experimental	ECD	UCD	Experimental
30	54.1	55.1	55.0	53.9	54.8	54.8
40	54.3	55.3	55.3	54.2	55.0	55.0
50	54.6	55.6	55.3	54.6	55.4	55.2

increase by 1.6 charge units and agreement is good with neither mechanism - but closer to ECD. However these assumptions would seem to be so gross as to fall outside the realm of plausibility and the weight of evidence seems to point to the UCD mechanism.

(d) Total number of neutrons emitted:

McHugh and Michel[21] have shown that one can calculate the total number of neutrons, ν_T, emitted in fission from the variation of Z_p with excitation energy as follows:-

$$d\nu/dE = (dZ_p/dE)/0.38$$

where dZ_p/dE is the variation of Z_p with excitation energy. This value for the heavy fragment in this mass region is obtained for the fissioning systems from Fig. 16. However very few such data exist for the light fragment. Khan et al[18] have recently completed such a study for light-mass products in the fission of ^{235}U and ^{238}U and these are also shown in Fig. 16 as a function

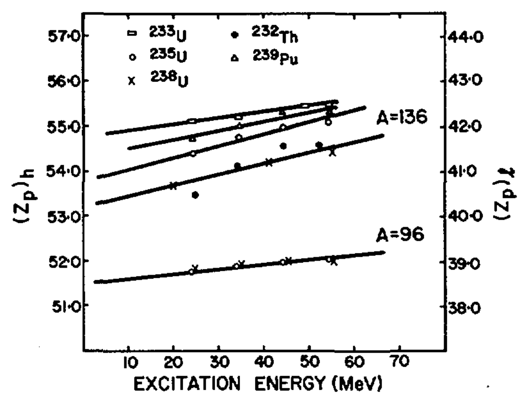

FIG.16. The most probable charge of heavy and light fragments as a function of excitation energy for various fissioning systems.

TABLE II. DATA FOR ^{235}U AND ^{238}U

Quantity	^{235}U	^{238}U
$(dZ_p/dE)_h$	0.0274 MeV^{-1}	0.0250 MeV^{-1}
$(dZ_p/dE)_\ell$	0.0111 MeV^{-1}	0.0111 MeV^{-1}
$d\nu_h/dE$	0.072 MeV^{-1}	0.066 MeV^{-1}
$d\nu_\ell/dE$	0.029 MeV^{-1}	0.029 MeV^{-1}
$d\nu_T/dE$	0.101 MeV^{-1}	0.095 MeV^{-1}

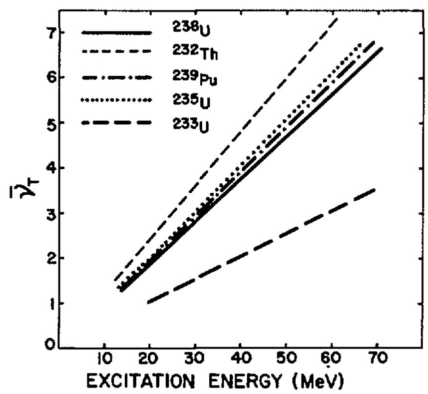

FIG.17. Total numbers of neutrons emitted from various fissioning systems as a function of excitation energy.

of excitation energy for A = 96. This enables one to obtain both $d\nu_h/dE$ and $d\nu_\ell/dE$ where h and ℓ stand for the heavy and light fragments respectively and from this $d\nu_T/dE$, since $d\nu_T/dE = d\nu_h/dE + d\nu_\ell/dE$. The data shown in Table II come from A = 136 and A = 96 for the heavy and light fragments respectively and they may well not be complementary fragments. However the assumption is made that $d\nu_h/dE$ and $d\nu_\ell/dE$ will be constant over the narrow mass regions involved. In Fig. 17 are plotted values of ν_T versus E for ^{235}U and ^{238}U. The other fissioning systems are included, the assumption being made that, like ^{235}U and ^{238}U, $\nu_h \simeq 2\nu_\ell$ for ^{233}U, ^{232}Th, and ^{239}Pu.

REFERENCES

1. A. C. Wahl, J. Inorg. Nucl. Chem. 6, 263 (1958).
2. A. C. Wahl, R. L. Ferguson, D. R. Nethaway, D. E. Troutner, and K. Wolfsberg, Phys. Rev. 126, 1112 (1962).
3. A. E. Norris and A. C. Wahl, Phys. Rev. 146, 926 (1966).

4. A. C. Wahl, Phys. Rev. 99, 730 (1955).
5. B. D. Pate, J. S. Foster, and L. Yaffe, Can. J. Chem. 36, 1691 (1958).
6. B. D. Pate, Can. J. Chem. 36, 1707 (1958).
7. R. H. Goeckerman and I. Perlman, Phys. Rev. 76, 628 (1949).
8. L. E. Glendenin, C. D. Coryell, and R. R. Edwards, Phys. Rev. 75, 337 (1949).
9. G. Friedlander, L. Friedman, B. Gordon, and L. Yaffe, Phys. Rev. 129, 1809 (1963).
10. G. Friedlander, Symposium on the Physics and Chemistry of Fission, International Atomic Energy Agency, Vienna (1965), Vol. II, p. 265.
11. J. H. Davies and L. Yaffe, Can. J. Phys. 41, 762 (1963).
12. P. P. Benjamin, D. A. Marsden, N. T. Porile, and L. Yaffe, Can. J. Chem. 47, 301 (1969).
13. S. S. Parikh, D. A. Marsden, N. T. Porile, and L. Yaffe, Can. J. Chem. 45, 1863 (1967).
14. I. Tomita and L. Yaffe, Can. J. Chem. In Press
15. G. B. Saha and L. Yaffe. To be published.
16. G. B. Saha, I. Tomita, and L. Yaffe. To be published.
17. J. B. Cumming, U. S. Atomic Energy Commission NAS-NS-3107, p. 25 (1962).
18. A. H. Khan, G. B. Saha, and L. Yaffe. To be published.
19. H. K. Vonach, R. Vandenbosch, and J. R. Huizenga, Nucl. Phys. 60, 70 (1964).
20. J. R. Huizenga and R. Vandenbosch, "Nuclear Reactions", edited by P. M. Endt and P. B. Smith, Vol. II, North-Holland Publishing Co., Amsterdam (1962).
21. J. A. McHugh and M. C. Michel, Phys. Rev. 172, 1160 (1968).

DISCUSSION

S. AMIEL: The charge dispersion curves in Figs 5, 7, 8 and 9 of this paper seem to show a broadening at lower N/Z values rather than a shift; this supports the assumption that multiple-chance fission produces a composite curve rather than that the shift is due solely to the fission reaction in question. Can you comment on that?

L. YAFFE: If you examine the figures closely, you will find that there is certainly a shift of Z_p to lower N/Z values as well as a broadening of the dispersion curves. We are at present evaluating the significance of the variations of the full-width at half maximum with energy.

S. AMIEL: My second question refers to the comparison of the behaviour of the light and heavy masses. Phenomenologically we can say that, as the heavy mass peak remains stationary for different fission reactions, it represents a relatively "harder" fragment which is very little affected by the fissioning source, whereas the lighter mass is much "softer" and strongly affected by the fission reaction. This is not corroborated in Fig.16 of the paper. Can one say that this effect is washed out by the fact that the results are a composite of multiple-chance fissions? On the other hand, in working with low-energy fission, where nuclear structure effects are still seen, we do indeed see subtle differences, e.g. in the isotopic abundances between heavy- and light-mass elements. This is seen in the Orsay Cs-Rb results, and also (though the errors are still considerable and do not permit us to say anything quantitative) in Kr-Xe distributions plotted with the use of on-line isotopic separation. Your data do not show any difference in the behaviour of light and heavy masses. Can you elaborate on this point?

L. YAFFE: Our results are certainly due to multiple-chance fission. However, I do not think that lower-energy fission can truly be called a simpler process than that which occurs at the energies I have discussed. As we have seen, there are resonance effects, etc. to be considered, which complicate the low-energy fission process.

A.C. PAPPAS: Are the mass distributions for the nuclides at these energies assumed flat (or known) in the 130-140 mass region?

L. YAFFE: We have no further information. We are obviously going to take all the data we have on charge distribution, including some on isobaric distribution. We will attempt a formulation of mass distribution curves in which we can have some confidence, but at the moment I do not have any more data.

DEPENDENCE OF FISSION-FRAGMENT TOTAL KINETIC-ENERGY AND MASS DISTRIBUTIONS ON THE EXCITATION ENERGY AND ANGULAR-MOMENTUM DISTRIBUTION OF THE FISSIONING NUCLIDE ^{210}Po

J.P. UNIK*
Argonne National Laboratory, Argonne, Ill.,
United States of America
and
J.G. CUNINGHAME, I.F. CROALL
Atomic Energy Research Establishment,
Harwell, Berks,
United Kingdom

Abstract

DEPENDENCE OF FISSION-FRAGMENT TOTAL KINETIC-ENERGY AND MASS DISTRIBUTIONS ON THE EXCITATION ENERGY AND ANGULAR-MOMENTUM DISTRIBUTION OF THE FISSIONING NUCLIDE ^{210}Po.
The fission of ^{210}Po, produced by three different nuclear reactions (^{209}Bi + p, $^{206}Pb + \alpha$ and $^{198}Pt + ^{12}C$), has been studied in detail in order to establish the dependence of various scission-point properties on the excitation energy and angular-momentum distribution of the fissioning nucleus. Excitation energies of 31, 44 and 57 MeV were chosen so as to give reasonable fission cross-sections, while avoiding a large contribution from second-chance fission. The experiments were conducted on a beam line of the Harwell Variable Energy Cyclotron.

The mean-fragment total-kinetic-energy release was found to be dependent on the ^{210}Po excitation energy and angular-momentum distribution. The variances of the total-kinetic energy and mass distributions were found to be a strongly dependent on excitation energy but not on angular momentum. The experimental results of this work were found to be in good agreement with the theoretical liquid-drop-model calculations of Nix and Swiatecki.

INTRODUCTION

Many previous experiments have demonstrated the general features of charged-particle induced fission at moderate excitation energies [1-3]. In general, the mean fragment total kinetic energies have been found to be insensitive to the excitation energy of the fissioning nucleus [4]. However, the widths of the fragment mass-yield and total kinetic energy distributions are quite dependent on the nuclear excitation energy [1]. The purpose of this study was to examine more precisely the dependence of the fragment mass and total kinetic energy distributions on the nuclear excitation energy and the initial angular momentum distribution of the fissioning nucleus.

The slightly fissionable nuclide ^{210}Po was chosen for this study in order to minimise any complications due to multichance fission (fission taking place after dissipation of a portion of the initial excitation energy by neutron emission). For the particular range of excitation

* Exchange Research Scientist at AERE, Harwell, 1968-69.

TABLE I. SUMMARY OF RESULTS FOR FISSION OF ^{210}Po*

Reaction	E_p (MeV)	E^* (MeV)	$\langle I^2 \rangle$	No. Events ($\times 10^4$)	$\langle$TKE$\rangle$ (MeV) This Experiment	$\langle$TKE$\rangle$ (MeV) Theo. [12] [13]	σ^2(TKE) (MeV^2) Exp.	σ^2(TKE) (MeV^2) Corr.	σ^2(TKE) (MeV^2) Theo. [12] [13]	σ^2(M) (amu^2) Exp.	σ^2(M) (amu^2) Corr.	σ^2(M) (amu^2) Theo. [12] [13]
^{209}Bi + p → ^{210}Po	27.0	31.8	53	0.5	142.9 ± .2	148.3 136.5	52 ± 3	46	42 39	71 ± 2	67	74 44
	39.3	44.1	75	7.9	143.7 ± .2	148.0 136.5	70 ± 3	62	59 42	112 ± 2	106	106 57
	52.7	57.6	94	2.9	145.0 ± .2	147.7 136.5	85 ± 3	74	75 46	136 ± 2	129	133 70
^{206}Pb + α → ^{210}Po	39.8	30.7	199	1.0	143.8 ± .5	148.3 136.5	59 ± 5	53	40 39	78 ± 2	74	72 43
	50.9	44.5	308	4.4	145.1 ± .3	148.0 136.5	70 ± 2	62	59 42	112 ± 3	106	107 58
	63.8	57.2	435	23.7	147.0 ± .3	147.7 136.5	81 ± 3	69	74 46	132 ± 2	124	133 70
^{198}Pt + ^{12}C → ^{210}Po	77.2	58.5	1240	0.9	151.6 ± 2	147.7 136.5	85 ± 5	73	75 46	140 ± 4	120	135 71

*Experimental errors represent the average deviations from a series of independent measurements and indicate the relative precision of these measurements. The estimated absolute errors are ± 2 MeV for $\langle$TKE$\rangle$, ± 5 MeV^2 for σ^2 (TKE) and ± 4 amu^2 for σ^2(M). The estimated absolute errors should be used when comparing the results of this work with theory or other experiments.

energies used, it can be estimated that greater than 80% of the fissions take place from the original compound nucleus [5]. Therefore both the fissioning nuclide and excitation energies are well defined in this experiment. The compound nucleus ^{210}Po was produced, using the Harwell Variable Energy Cyclotron, at well defined excitation energies and with different angular momentum distributions by three nuclear reactions:-

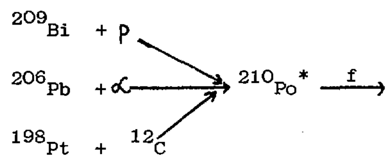

Three excitation energies were studied using the ^{209}Bi and ^{206}Pb targets; 31, 44 and 57 MeV. At this time only preliminary data are available for the ^{198}Pt target at the highest excitation energy. The energies of the various particles (E_p) used to produce these excitation energies are given in Table I. The lowest excitation energy was limited to 31 MeV due to the rapidly decreasing fission cross-sections at lower energies. The highest excitation energy was determined by the maximum proton energy (53 MeV) available from the cyclotron.

EXPERIMENTAL PROCEDURE

Two gold-surface barrier detectors placed at calculated laboratory angles corresponding to 90° and 270° in the centre-of-mass system relative to the projectile beam were used to measure the pulse-heights of the two coincident fission fragments. One detector of 100 mm^2 detection area placed 50 mm from the target defined the laboratory angle at which the fission events were measured. The second detector was also placed 50 mm from the target but was much larger, 400 mm^2, to ensure that greater than 90% of the coincident complementary fragments would be detected. A conventional fast-slow coincidence system with a resolving time of 50 ns was used to eliminate chance coincidences. The pulses from the detectors were digitised and stored in a 128 x 128 channel coincident pulse-height matrix using an associative storage technique with a PDP-8 on-line computer [6]. The gain stability of the entire electronic system and the energy resolution broadening due to high counting rates of inelastically scattered beam particles were measured directly by observing the pulse height distributions of coincident pulses from a high stability pulse generator. These pulse generator pulses were fed through the entire electronic system and recorded simultaneously with the fission data.

Targets of spectroscopically pure ^{209}Bi and ^{206}Pb (96% isotopic enrichment) were prepared by vacuum evaporation on to 90 $\mu g/cm^2$ nickel backing foils. Two sets of targets with very uniform areal densities of 30 and 120 $\mu g/cm^2$ were used. The ^{198}Pt targets were deposited directly on to 130 $\mu g/cm^2$ nickel foils by a "double ion sputtering" technique using the Harwell Isotope Separator [7]. The ^{198}Pt targets produced in this manner had an areal density equivalent to 400 $\mu g/cm^2$ of platinum. The average energy losses of the ^{210}Po fission fragments in the target materials were measured directly for each target by obtaining the average kinetic energies of the fragments, $\langle E_f \rangle$, at various angles, θ, between the target plane and the detector. This was accomplished by rotating the target over the range $\theta = 20^\circ - 60^\circ$, with the fission detector kept at a constant angle relative to the projectile beam. The average energy loss of fragments emitted at 90^{o} to the target plane is equal to

$$- d\ (\langle E_f \rangle)/d\ (\mathrm{Sin}^{-1}\theta)$$

The average fragment energy losses in the nickel backing foils were obtained from the difference of the average fragment energies for two target orientations differing by 180^{o}.

COMPUTATION

The fission-fragment energy calibrations used in this work were based on the final fragment mass-dependent energy calibration procedure described by SCHMITT et al [8], using standard ^{252}Cf fission-fragment spectra. (a) Using this energy calibration to obtain the final fragment energies after neutron emission, (b) correcting the final fragment energies for neutron emission to obtainthe initial fragment energies before neutron emission and (c) invoking conservation of linear momentum; the original fragment coincident pulse-height matrix was transformed to an initial fragment mass-initial total kinetic energy matrix. By appropriate summing over this transformed matrix the various mass and total kinetic energy correlations and their moments were obtained.

No data exist at present on the average number of neutrons emitted as a function of fragment mass for this fissioning system and therefore the assumption was made that both fragments emit an equal number of neutrons. The mean total number of neutrons emitted per fission at each excitation energy, $\langle \nu_T(E^*) \rangle$, was estimated by using Eq. 1.

$$\langle \nu_T(E^*) \rangle = (E^* + \langle E_R \rangle - \langle TKE \rangle - \langle E_\gamma \rangle)/(\langle B_n \rangle + \langle E_n \rangle) \qquad (1)$$

Here E* is the initial compound nucleus excitation energy, $\langle TKE \rangle$ the average total kinetic energy, $\langle E_R \rangle$ and $\langle B_n \rangle$ are the weighted average energy release in fission and average neutron binding energy of the fragments respectively, calculated from the work of MILTON [9], $\langle E_\gamma \rangle$is the average gamma-ray energy release in fission (6.2 MeV [10]), and $\langle E_n \rangle$ the average neutron energy [11]. The neutron values calculated were 2.4, 4.0 and 5.6 for E* = 31, 44 and 57 MeV respectively.

All data presented in the following sections (unless specifically stated otherwise) have been corrected for effects due to (a) neutron emission from the fragments, (b) energy losses of the fragments in the backing foils and target materials, (c) inherent resolution of the detectors (FWHM = 1.5 MeV), and (d) broadening of the energy resolution due to counting rate effects.

EXPERIMENTAL RESULTS

A complete summary of the moment analyses for all the data of this work, as well as other pertinent information, is given in TABLE I. The nuclear reaction, projectile energies and compound nucleus excitation energies are listed in columns 1-3 respectively. The computed mean values of the square of the compound nucleus angular momentum $\langle I^2 \rangle$ for each

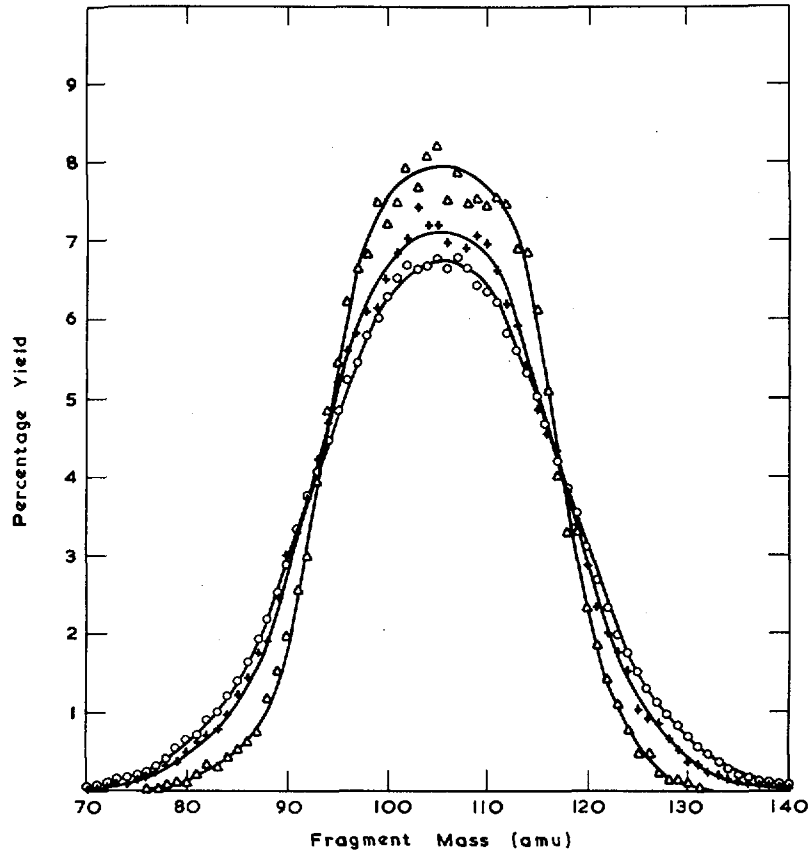

FIG. 1. Experimental fragment mass-yield distributions for fission of the compound nucleus ^{210}Po produced by bombardment of ^{206}Pb with alpha particles.

△ E_{α} = 39.8 MeV
+ E_{α} = 50.9 MeV
○ E_{α} = 63.8 MeV

reaction is given in column 4. The $\langle I^2 \rangle$ values for the proton and alpha-particle bombardments were obtained from optical-model calculations. The $\langle I^2 \rangle$ value for ^{12}C bombardment was calculated classically. The columns headed $\langle TKE \rangle$, $\sigma^2(TKE)$, and $\sigma^2(M)$ list the mean total kinetic energies, the variance of the total kinetic energy distributions and the variance of the mass-yield distributions respectively. The experimental errors given in TABLE I represent the average deviations of a series of independent measurements and indicate only the relative precision of these measurements. The absolute errors (taking into account possible inherent and systematic errors in the methods of energy calibrations, neutron corrections, etc.) are estimated to be $\pm$ 2 MeV for $\langle TKE \rangle$, $\pm$ 5 MeV^2 for $\sigma^2(TKE)$ and $\pm$ 4 amu^2 for $\sigma^2(M)$. Only one measurement was performed for the ^{12}C bombardment and hence the errors have been estimated for this case.

Also included in TABLE I is a comparison of the corrected experimental results, (Corr.), with the theoretical work, (Theo.) of NIX and

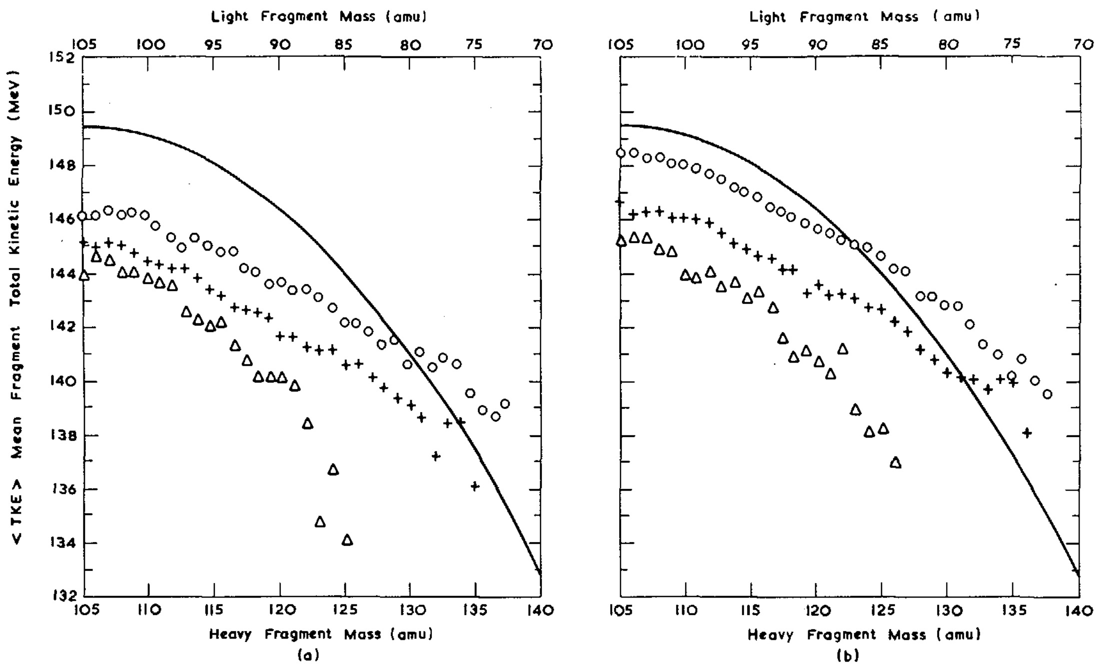

FIG. 2. Mean fission-fragment total kinetic energies as a function of fragment mass for fission of ^{210}Po at three excitation energies (E^*).

(a) $^{209}Bi + p \rightarrow {}^{210}Po^* \xrightarrow{f}$ △ $E^* = 31$ MeV

(b) $^{206}Pb + \alpha \rightarrow {}^{210}Po^* \xrightarrow{f}$ + $E^* = 44$ MeV

○ $E^* = 57$ MeV

Solid curves are from the theoretical work of Nix and Swiatecki.

SWIATECKI (non-viscous nuclei limit) [12] and of NIX [13]. Both of these theoretical studies represent advanced developments of the liquid drop model of nuclear fission applying standard static, dynamic and statistical methods without the use of adjustable parameters. The earlier work [12] was based on an approximation, applicable to the fission of nuclides lighter than radium, which described the shape of the nuclear surface in terms of two overlapping or separated spheroids. The more recent work [13] is an attempt at a more realistic parameterisation of the nuclear shape to the scission point in order to extend the calculation to fission of heavier nuclides.

Typical mass-yield distributions (uncorrected for mass resolution) obtained at three excitation energies using the ^{206}Pb + α reaction are presented in Fig. 1. All the experimental distributions in this work had excellent reflection symmetry about the symmetric mass and were therefore "folded" about this mass in order to improve the statistical accuracy of each datum point for mass dependent correlations. The dependence of $\langle TKE \rangle$ on fragment mass for the proton and alpha-particle bombardments at each excitation energy is presented in Fig. 2. Also shown in Fig. 2, as solid curves, is the theoretical prediction [12] for E* = 44 MeV. The theoretical distributions for the other E* values are virtually identical to that for E* = 44 MeV. The variances of the TKE distributions as a function of fragment mass are shown in Fig. 3, as well as the theoretical predictions [12], as solid lines. In Fig. 4 a, b and c are shown the differences, as a function of fragment mass, between the mean total kinetic energies measured in the alpha-particle bombardments and the proton bombardments at the same ^{210}Po excitation energies. Fig. 4d, e and f show the ratios of the fragment mass-yields, as a function of fragment mass, obtained in alpha-particle bombardments relative to proton bombardments at the same resultant ^{210}Po excitation energies. The data presented in Fig. 4 have not been corrected for mass resolution. Since the mass resolution in these experiments is $\sim$5 amu (FWHM), discontinuities in the presented distributions occurring over mass intervals much smaller than this should be considered only as statistical digressions.

CONCLUSIONS

The most interesting result of this study is the observation that the mean total kinetic energy, $\langle TKE \rangle$, is dependent on the excitation energy, E*, and also on the angular momentum of the fissioning nucleus. As can be seen in column 6 of TABLE I, the $\langle TKE \rangle$ values for a given E* increase with the mass of the bombarding particle and therefore with the angular momentum (or $\langle I^2 \rangle$). Also by extrapolating the $\langle TKE \rangle$ data for the ^{209}Bi + p and ^{206}Pb + α reactions to the same value of angular momentum, quite different $\langle TKE \rangle$ values are obtained at different excitation energies. This result indicates that the total kinetic energy is also dependent on excitation energy. From Fig. 4 a, b and c the differences in $\langle TKE \rangle$ between the alpha-particle and proton bombardments for a fixed excitation energy are seen to be independent of fragment mass. This indicates that the difference in $\langle TKE \rangle$ may have its origin at an earlier stage in the fission process than the scission point; more probably near the saddle point. One possible interpretation of these results may be similar in manner to an interpretation previously proposed to explain $\langle TKE \rangle$ variations near the fission threshold [14]. The initial nuclear excitation energy is distributed between collective and intrinsic excitations. Since the transition from the saddle point to the scission point is very rapid for medium weight nuclides ($\sim 2 \times 10^{-21}$ sec. [13]), there may be insufficient time for collective excitation energy, weakly coupled to the internal degrees of

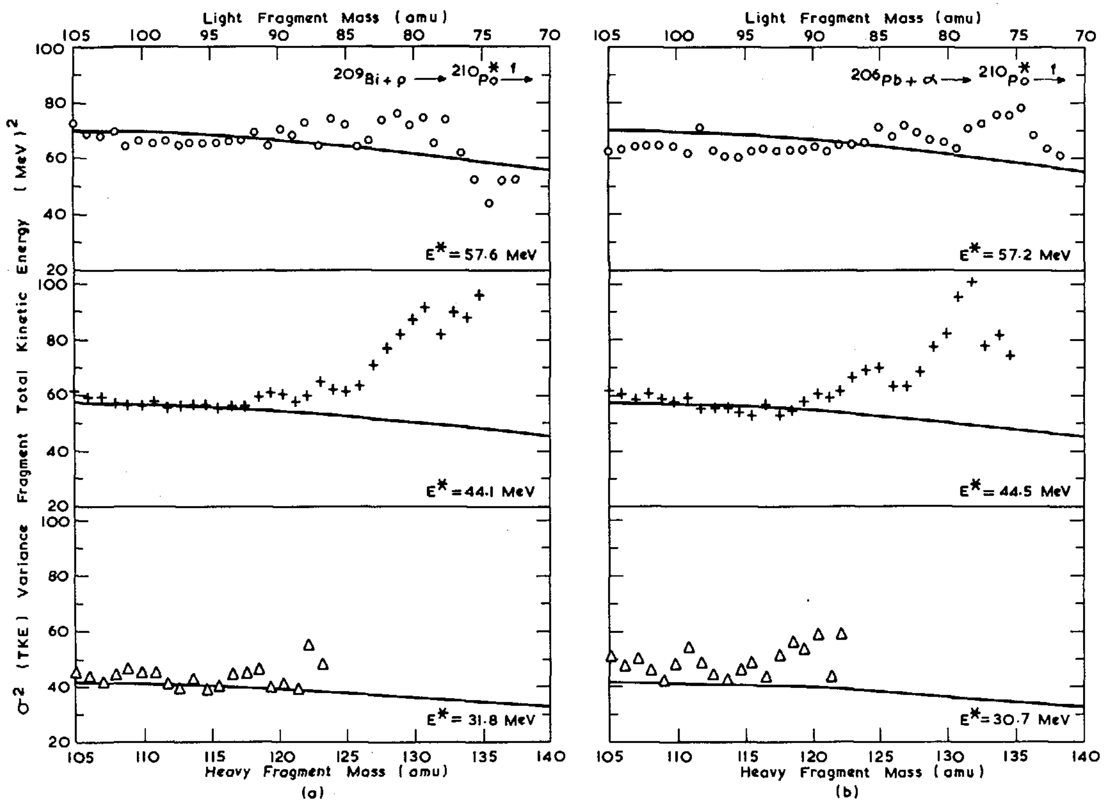

FIG. 3. Variances of fission-fragment total kinetic-energy distributions as a function of fragment mass for fission of ^{210}Po at various excitation energies (E^*).

(a) $^{209}\text{Bi} + p \rightarrow {}^{210}\text{Po}^* \xrightarrow{f}$

(b) $^{206}\text{Pb} + \alpha \rightarrow {}^{210}\text{Po}^* \xrightarrow{f}$

Solid curves are from the theoretical work of Nix and Swiatecki.

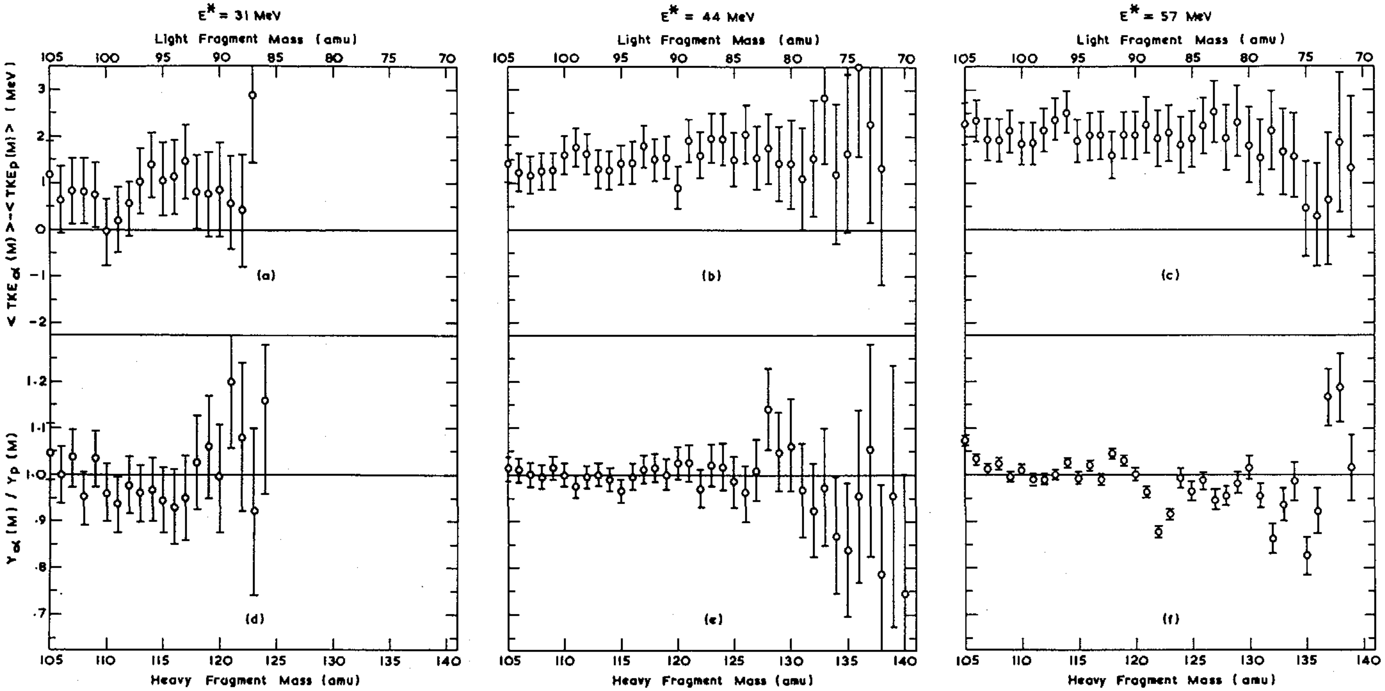

FIG. 4. Detailed comparisons of scission-point properties for fission of ^{210}Po produced by the $^{206}Pb + \alpha$ and $^{209}Bi + p$ reactions at three given excitation energies (E^*).
(a, b, c) Differences in mean-fragment total kinetic energies ($\langle TKE(M) \rangle$) as a function of fragment mass.
(d, e, f) Ratios of fission-fragment mass yields (Y(M)) as a function of fragment mass.

freedom, to be transferred to deformation energy. Therefore a portion of the energy due to collective excitations may be transferred to translational energy of the two fragments during the descent from the saddle point to the scission point. One form of collective excitation strongly dependent on angular momentum and which can be computed at this time is the rotational energy, E_R, at the saddle point given by Eq. 2

$$E_R = \frac{\hbar^2}{2\mathcal{J}_{\parallel}} K^2 + \frac{\hbar^2}{2\mathcal{J}_{\perp}} (I^2 - K^2) \tag{2}$$

Here I is the total angular momentum, K is the projection of I on the nuclear symmetry axis, $\mathcal{J}_{\parallel}$ and $\mathcal{J}_{\perp}$ are the nuclear moments of inertia about an axis parallel and perpendicular to the nuclear symmetry axis, respectively. Rearranging Eq. 2, taking average values and substituting Eq. 3, one obtains Eqs. 4 and 5

$$\langle K^2 \rangle = K_o^2 = \frac{T}{\hbar^2}\left(\frac{1}{\mathcal{J}_{\parallel}} - \frac{1}{\mathcal{J}_{\perp}}\right)^{-1} \tag{3}$$

$$\langle E_R \rangle = \frac{\hbar^2}{2\mathcal{J}_{\perp}} \langle I^2 \rangle + \frac{T}{2} = A \langle I^2 \rangle + BT \tag{4}$$

$$\langle TKE \rangle_{\text{observed}} = \langle TKE_o \rangle + \langle E_R \rangle \tag{5}$$

Here T represents the nuclear temperature at the fission saddle point and can be computed from Eq. 6:

$$E^* - E_f = \frac{M_F}{8} T^2 - T \tag{6}$$

The constant, E_f, is the effective fission threshold (E_f = 19.7 MeV for ^{210}Po, HUIZENGA et al [5]) and M_F is the mass number of the fissioning nucleus. Eq. 5 was fitted to the $\langle TKE \rangle$ values obtained in this work, with the result that every $\langle TKE \rangle$ value could be calculated to within $\pm$ 0.25 MeV of the experimental values, using A = 0.006 MeV, B = 3.42 and $\langle TKE_o \rangle$ = 140.11.

Although the explicit forms of Eqs. 4 and 5 fit the experimental data of this work quite well, the basic assumption that the observed variations in total kinetic energy are mainly due to rotational energy at the saddle point being transferred to kinetic energy of the fragments is not strongly supported by the values of A and B which were obtained. The rotational constant, A = 6 KeV, obtained from the fit of the experimental $\langle TKE \rangle$ values is near that for a spherical nucleus, 5 KeV, but is larger than the value of ~2 KeV for an elongated nucleus at the saddle point estimated from the ^{210}Po fragment angular distribution work of CHAUDHRY et al [15]. Also the constant B = 3.42 obtained by this fitting procedure is much larger than the expected value of 0.5. Obviously, further work is required definitely to establish which additional factors in the fission process may be contributing to the total kinetic energy variations observed in this study.

From the corrected values of the variances of the total kinetic energy and mass distributions given in TABLE I, the variances or widths of these distributions are seen to be quite dependent on the excitation energy. However, the variances of the total kinetic energy and mass distributions for a given excitation energy are virtually independent of the angular momentum, $\langle I^2 \rangle$, of the fissioning nucleus. This conclusion is in disagreement with the work of PLASIL et al [1] who reported that increasing angular momentum broadens these distributions. By examination of Fig. 4 d, e and f, it can be seen that there are no observable changes in the yields of specific mass fragments between the alpha-particle and proton bombardments producing ^{210}Po at the same excitation energies.

As can be seen from TABLE I and Fig. 3, the theoretical work of NIX and SWIATECKI [12] predicts the variances of the total kinetic energy and mass distributions with remarkable accuracy. The agreement between the experimental $\langle TKE \rangle$ values and those predicted theoretically is quite good when it is remembered that this theoretical work has no adjustable parameters and does not include angular momentum effects. The more generalised calculations of NIX [13] give a comprehensive insight into the various factors contributing to the total kinetic energy and mass distributions. However, the agreement between the predictions of this work and the corrected experimental values shown in TABLE I is not improved over the earlier calculations [12].

ACKNOWLEDGEMENTS

The authors gratefully acknowledge the excellent cooperation of the entire Harwell V.E.C. staff during these irradiations. We are further indebted to J. H. Freeman and T. A. Tuplin for preparing most of the targets used in the work. One of us (J.P.U.) wishes to thank the staff of the Chemistry Division of A.E.R.E. for their hospitability during the course of this work.

REFERENCES

[1] PLASIL, F., BURNETT, D. S., BRITT, H. C., and THOMPSON, S.G., Phys. Rev. 142 (1966) 696.

[2] BRITT, H. C., WEGNER, H. E., and GURSKY, J. C., Phys. Rev. 129 (1963) 2239.

[3] UNIK, J. P., and HUIZENGA, J. R., Phys. Rev. 134 (1963) B90.

[4] VIOLA, V. E., Nuclear Data 1 No. 5 (1966) 391.

[5] HUIZENGA, J. R., CHAUDHRY, R., and VANDENBOSCH, R., Phys. Rev. 126 (1962) 210.

[6] CROALL, I. F., and CUNINGHAME, J. G., Nucl. Phys. A125 (1969) 402.

[7] FREEMAN, J. H., Unpublished (1969).

[8] SCHMITT, H. W., KIKER, W. E., and WILLIAMS, C. W., Phys. Rev. 137 (1965) B837.

[9] MILTON, J. C. D., University of California Radiation Laboratory Rep. UCRL-9883-Rev. (1962).

[10] MAIER-LEIBNITZ, H., SCHMITT, H. W., and ARMBRUSTER, P., Physics and Chemistry of Fission (Proc. Conf. Salzburg 1965) 2 IAEA, Vienna (1965) 143.

[11] TERRELL, J., Phys. Rev. 127 (1962) 880.

[12] NIX, J. R., and SWIATECKI, W., Nucl. Phys. 71 (1965) 1.

[13] NIX, J. R., Nucl. Phys. A130 (1969) 241.

[14] BLYUMKINA, Y. U. A., BONDARENKO, I. I., KUZNETSOV, V. F., NESTEROV, V. G., OKOLOVITCH, V. N., SMIRENKIN, G. N., and USACHEV, L. N., Nucl. Phys. 52 (1964) 648.

[15] CHAUDHRY, R., VANDENBOSCH, R., and HUIZENGA, J. R., Phys. Rev. 126 (1962) 220.

DISCUSSION

K. M. DIETRICH: I would like to put a question to Dr. Nix. The calculated widths of the distribution of masses and kinetic energies are considerably smaller in the improved version of the liquid-drop theory than in the original version. I would have expected the opposite result, i.e. that increase in the degrees of freedom of the liquid drop would lead to an increase in the widths of distributions.

J. R. NIX: In the case of light nuclei at moderate excitation energies, the widths of the kinetic-energy and mass distributions depend primarily on the stiffness of the system at the saddle point in respect of overall elongation and mass asymmetry respectively. In determining these stiffnesses it is necessary to calculate the potential and kinetic energies in the neighbourhood of the saddle point and then perform a normal-co-ordinate transformation to obtain the appropriate normal co-ordinates. If the saddle-point shapes were the same in each of the two versions of the liquid-drop model that we have used, then the introduction of additional collective degrees of freedom would cause the calculated frequencies for elongation and mass asymmetry to decrease and hence the widths of the distributions to increase, as you would have expected. But since the saddle-point shapes are different in the two versions, this conclusion does not follow. (The theorem that the introduction of constraints increases the frequencies of the system holds only if the constraints are compatible with the equilibrium configuration.)

Since the saddle-point shapes used in the improved version (two spheroids connected by a hyperboloidal neck) are more realistic than those used in the original version (two tangent spheroids), our a priori expectation was that the improved version would yield better estimates of the stiffnesses (and hence the widths of the distributions) than the original version, but this turned out not to be the case.

F. PLASIL: I was interested by Dr. Cuninghame's comment on the possibility of an asymmetric fission component based on the widths of the kinetic-energy distributions as a function of mass. In my view, one should not draw such conclusions from data of this type but should consider the mass-yield distribution directly. Since radiochemical data indicate the existence of an asymmetric component (see T. T. Sugihara et al., Phys. Rev. 121 (1961) 1179) we have carried out an experiment, for the same compound nucleus as yours, designed to look for this component. The experiment was carried out at Oak Ridge and my collaborators were R. L. Ferguson, H. W. Schmitt and F. Pleasonton. We bombarded ^{209}Bi with 36 MeV protons and obtained more than 10^5 events. We did not find, in the mass-yield distribution, any indication of an asymmetric component. We made sure that we were not obscuring it with resolution and neutron-emission problems, and we have no explanation for the discrepancy with the radiochemical data.

J. G. CUNINGHAME: I agree entirely with you that one should look for asymmetry in the mass distributions by making mass-yield measurements directly. What I said in the paper was purely a passing comment, an attempt to account for the upturn in our kinetic-energy widths towards the wings of the mass distributions. However, we believe this upturn to be real and it probably does have to be accounted for somehow.

DISTRIBUTION OF MASS AND CHARGE IN THE FISSION OF ^{227}Th

K. F. FLYNN*
Eidgenössisches Institut für Reaktorforschung,
Würenlingen, Switzerland
H.R. VON GUNTEN
Eidgenössisches Institut für Reaktorforschung,
Würenlingen, and
Anorganisch-chemisches Institut, Universität Bern, Switzerland

Abstract

DISTRIBUTION OF MASS AND CHARGE IN THE FISSION OF ^{227}Th. The distribution of mass and charge in the thermal-neutron-induced fission of ^{227}Th has been investigated by radiochemical determination of the fission yields of 29 mass chains and one shielded nuclide (independent yield). The yields were determined relative to the known yields for ^{235}U fission and normalized to absolute values by summation to 200 per cent total fission yield. ^{227}Th is the lowest mass nuclide fissionable by thermal neutrons yet to be investigated.

The mass distribution is asymmetric; the heavy-mass group is centred at about the same position (mass 138.5) as in all previously investigated cases of low-energy fission, while the light-mass group is shifted to a lower mass number (89). The peak half width (full width at half maximum) is 11.5 mass units, and the full width at one tenth maximum is 19 mass units. All these values fall well on systematic plots for the positions of the peaks and the widths of mass distributions for various fissionable nuclides. The relative probability of asymmetric-to-symmetric fission (peak-to-valley ratio) is about 230. The fission yield data for ^{227}Th indicate a value of about 1 for $\bar{\nu}$, the average number of neutrons emitted per fission. The mass distribution shows no indication of a third peak in the region of symmetric fission.

The division of nuclear charge, as indicated by the independent yield of ^{136}Cs, is consistent with the equal-charge-displacement hypothesis characteristic of low-energy fission. A comparison of mass distributions in thermal-neutron-induced fission, reactor-neutron-induced fission and spontaneous fission for several fissioning nuclei is given.

1. INTRODUCTION

Mass and charge distributions in low-energy-fission of the heavier fissionable nuclides have been the object of numerous investigations by radiochemical, mass-spectrometric and physical methods. Accordingly, a wealth of information has been accumulated for these heavy nuclides. However, relatively little is known about the mass and charge distribution in neutron-induced fission of the lighter fissionable nuclei.

In this region mass distributions have been measured for reactor-neutron-induced fission of ^{227}Ac [1] and for thermal-neutron-induced fission of ^{229}Th [2] only. The mass distribution of ^{227}Ac shows a significant third peak in the region of symmetric fission (two equal fragments), whereas the fission of ^{229}Th is asymmetric (only two peaks). Data on the division of nuclear charge are also sparse in this mass region.

The variation in the mass of the fissioning nucleus (A_F) is manifested by a shift in the light peak of the mass-yield curve, whereas the average

* Guest scientist from Argonne National Laboratory, Argonne, Ill., United States of America.

mass of the heavy fragment is relatively independent of the mass of the fissioning nucleus.

It was found [3] that the heavy-mass peak remains fixed at mass 138.5 over a range in A_F of about 15 mass units, whereas the position of the light-mass peak follows a linear function of A_F (slope of 1) over the same range. A deviation from this pattern was noticed for the heaviest nuclides, i.e. ^{245}Cm [3], ^{249}Cf [4] and ^{252}Cf [3, 5] and possibly also for the region of the lightest nuclides (^{229}Th [2, 3]).

All these facts demonstrate that more information is needed about neutron-induced fission of the lighter fissionable nuclei. ^{227}Th can easily be milked from a ^{227}Ac source and has a half-life of 18.72 d [6]. Its thermal fission cross-section is large enough to make an investigation of mass and charge distribution possible, even though only very small amounts of this nuclide are available. The value for the fission cross-section of 1500 ± 1000 b as given in the literature [7] was found to be much too high. The value of the fission cross-section for thermal-neutron fission was determined to be approximately 250 b. This result is not final and experimental work is still in progress at our laboratory.

2. EXPERIMENTAL

2.1. Preparation of the ^{227}Th-samples

^{227}Th was extracted from a source of 10 mCi of ^{227}Ac obtained from the Radiochemical Centre, Amersham (England). A Dowex 50 × 8 (200-400 mesh) cation exchange column (1 mm inner diam., 100 mm length) was used to separate and purify ^{227}Th from Ra, Ac and daughter-products. The following procedure was used.

The solution containing ^{227}Ac, ^{227}Th and daughters was evaporated to dryness. The residue was dissolved in 1 $\underline{N}$ HNO_3 and transferred to the top of the column. Ra was eluted with 2 $\underline{N}$ HNO_3, Ac with 4 $\underline{N}$ HNO_3 and Th with 6 HNO_3 – 0.25 to 0.5 $\underline{M}$ $H_2C_2O_4$. The radioactivity of the effluent from the column was monitored continuously with a plastic scintillator to permit the collection of the ^{227}Ac-fraction (for further growth of ^{227}Th) and the fraction containing ^{227}Th. Aliquots of the resulting ^{227}Th solutions were checked for radiochemical purity with a 20-cm^3 GeLi-detector. All γ-lines present in samples prepared immediately after separation could be assigned to ^{227}Th.

During the first series of experiments the purified ^{227}Th was wrapped in aluminium foil and irradiated. After irradiation these samples were dissolved and the fission products of interest were separated radiochemically. However, difficulties occurred in the purification of the isolated fission products, due to the high α-activity of ^{227}Th and daughter-products, often leading to radiochemically contaminated samples. This contamination was reduced by orders of magnitude when fragment-recoil sources of ^{227}Th were used. These essentially weightless sources on aluminium backings were prepared by applying the technique of molecular plating [8]. Almost quantitative deposition of the ^{227}Th resulted from a solution of isopropanol containing one drop of 6 $\underline{N}$ HNO_3 and one drop of La-carrier (1 mg/cm^3) at 600 V (corresponding to a current of about 30 mA). Recoil-catcher foils of aluminium, mylar and polyethylene were used. Best results (lowest contamination by (n, γ)-activation products) were obtained with the polyethylene-catchers (approximately 9 mg/cm^2). These catchers were dissolved after irradiation in hot concentrated H_2SO_4 with the addition of a few drops of $HClO_4$.

2.2. Irradiation and chemical separations

Samples of ^{227}Th and ^{235}U (99.5%, 1 to 10 μg) were irradiated simultaneously in the Würenlingen swimming-pool reactor SAPHIR at a thermal neutron flux of approximately 2×10^{13} cm^{-2} s^{-1}. The fission yields of 30 nuclides (29 chain yields) and one shielded nuclide were determined by using radiochemical techniques. The fission yields of ^{227}Th were measured relative to the known yields for ^{235}U-fission [9]. ^{235}U-chain-yields as given in the third edition of the chart of the nuclides [6] describing a smooth mass-distribution were used in the valley region of the mass-yield curve. The specific fission products of interest were isolated from both samples using conventional radiochemical techniques (i.e. carriers were added, the samples were radiochemically purified, and thick samples were mounted for counting).

2.3. Counting-procedures

The purified samples were counted with an end-window β proportional counter and/or γ-ray spectrometer using a 3 in. $\times$ 3 in. NaI(Tl) crystal. In one of the experiments the rare-earth fraction was counted with a 20-cm^3 GeLi detector. In all cases the decay of the nuclides was followed for several half-lives. Where γ-ray spectrometry was applicable, the decay of one or more characteristic γ-photopeaks was measured. Composite decay curves were resolved graphically. A standard radioisotope was isolated from each irradiated sample for the purpose of normalizing the various runs to each other. The standards used were ^{132}Te and/or ^{141}Ce. The fission yields were calculated according to the procedure given by Ravindran et al. [2]. The activity of each sample was corrected only for chemical yield since all other corrections cancel in this comparison method. An arbitrary relative yield of the standard in ^{227}Th fission was first assumed, and the mass distribution was then normalized to a total yield of 200 per cent.

3. RESULTS AND DISCUSSION

The fission yields for the 29 mass chains (30 nuclides) determined in this work are given in Table I. The independent yield for the shielded nuclide ^{136}Cs is considered separately in Table II. The errors in the measured fission yields include one standard deviation of the experimental determinations as well as uncertainties in the values of the fission yields for ^{235}U. These uncertainties are assumed to be in the range of 5 to 10%. Calculations made under the worst assumptions showed that interference by neutron-induced fission products from ^{227}Ac or daughters of ^{227}Th present in the samples was negligible. Furthermore, significant amounts of these nuclides would have been detected by GeLi γ-ray spectrometry and decay studies of the ^{227}Th product.

TABLE I. FISSION YIELDS IN THE THERMAL-NEUTRON-INDUCED FISSION OF ^{227}Th

Fission product	Method of counting	Number of determinations	Fission yield (%)
^{77}As	β	2	1.40 upper limit
^{83}Br	β	1	1.10 ± 0.35
^{89}Sr	β	4	8.00 ± 0.43
^{90}Sr	β	2	8.72 ± 0.87
^{91}Sr	β, γ	1	6.21 ± 0.97
^{95}Zr	β, γ	7	3.40 ± 0.29
^{97}Zr	β, γ	3	2.41 ± 0.57
^{99}Mo	β, γ	2	1.44 ± 0.14
^{103}Ru	β, γ	2	0.58 ± 0.09
^{105}Ru	β, γ	2	0.28 ± 0.04
^{106}Ru	β	4	0.19 ± 0.06
^{109}Pd*	β	1	0.033 ± 0.011
^{111}Ag*	β	10	0.051 ± 0.010
^{112}Pd*	β	3	0.029 ± 0.006
^{113}Ag*	β	4	0.034 ± 0.007
^{115}Cd*	β	2	0.177 upper limit
^{121g}Sn*	β	2	0.11 ± 0.04
^{125g}Sn	β	3	0.43 ± 0.10
^{127}Sb	β	3	0.68 ± 0.16 } 0.63 ± 0.18
^{127g}Te	β, γ	2	0.53 ± 0.25
^{129m}Te	β, γ	11	1.36 ± 0.28
^{131}I	β, γ	2	2.61 ± 0.46
^{132}Te	β, γ	12	3.30 ± 0.06
^{133}I	β, γ	1	4.80 ± 1.01
^{137}Cs	β	2	6.93 ± 1.24
^{140}Ba	β, γ	2	7.71 ± 1.16
^{141}Ce	β, γ	13	7.62 ± 0.51
^{143}Ce	β, γ	7	6.97 ± 0.48
^{144}Ce	β	8	5.95 ± 0.44
^{147}Nd	γ	1	0.18 ± 0.05

* ^{235}U reference yields from Ref. [6]. All other yields for ^{235}U from Ref. [9].
Isomer ratios were assumed to be the same in ^{227}Th and ^{235}U fission.

TABLE II. INDEPENDENT FISSION YIELD OF ^{136}Cs AND EMPIRICAL Z_p VALUE

Independent fission yield for ^{235}U	$6.0 \times 10^{-3}\%$ [a]
Independent fission yield for ^{227}Th	$0.10 \pm 0.04\%$
Chain yield for ^{227}Th	7.3 %
Fraction of chain yield	$(1.4 \pm 0.5) \times 10^{-2}$
Z_p (empirical)	53.2
Estimated primary mass (A')	136.5 [b]
$Z_p - A'(Z_F/A_F)$ [c]	-0.6

[a] From Ref.[9].
[b] Neutron emission from primary fission fragment assumed to be 0.5 neutron.
[c] Z_F/A_F: charge-to-mass ratio (charge density) of the fissioning nucleus.

The observed fission yields from Table I are plotted as a function of fission product mass in Fig.1. Within the errors given, the observed data are, in general, consistent with a smooth mass-yield curve drawn through the experimental points. However, ^{77}As and ^{115}Cd are in disagreement with the distribution given. In the case of ^{77}As all samples showed composite decay curves probably due to ^{76}As (from ^{75}As, n, γ) ^{77}As, and some longer lived components. Because of the small differences in half-life of ^{76}As and ^{77}As these decay curves could not be resolved properly. Unfortunately, the activity of the samples was too small to permit measurement of γ-photopeaks. All types of recoil catcher foils (aluminium, mylar and polyethylene) give similar results. Hence, the value for ^{77}As has to be considered as an upper limit. The decay curves of ^{115}Cd were resolved into ^{115}Cd and ^{115m}Cd and proved to be radiochemically clean. Again, the high value for the fission yield may be attributed to the n, γ-reactions on ^{114}Cd present in the catcher foils. We feel that a higher mass-yield due to increased contribution by the symmetric fission mode can be excluded since ^{112}Pd and ^{113}Ag show no sign of an increase in yield. However, we plan to do more work in this region in order to clarify this point.

The observed mass distribution is asymmetric with the light- and heavy-mass groups centred at masses 89 and 138.5, respectively. The curve shows no third peak in the region of symmetric fission. The relative probability of asymmetric to symmetric fission (peak-to-valley ratio) is about 230. The peak half width (full width at half maximum) is 11.5 mass units, and the full width at one tenth maximum is 19 mass units. The measured points can be reflected through mass 113.5 (symmetric fission) indicating a value of about 1 for $\bar{\nu}$, the average number of neutrons emitted per fission. The general shape of the curve looks very similar to the mass distribution of ^{229}Th [2]. However, the trough seems to be narrower in the case of ^{227}Th.

The values found for the positions of the light and heavy mass peaks and for the width of the mass distribution for ^{227}Th fall well on systematic plots constructed for mass distributions of various fissionable nuclides.

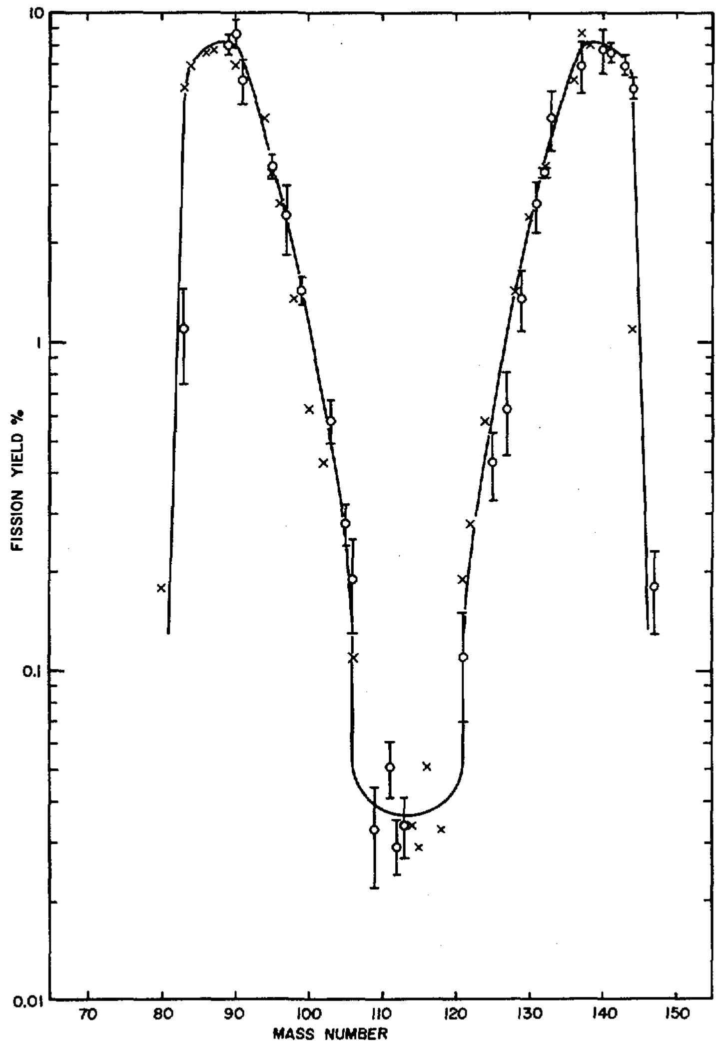

FIG.1. Mass-yield curve for thermal-neutron-induced fission of ^{227}Th. o measured points, × reflected points.

In Fig. 2 the dependency of the position of the maxima (defined as average mass-number of the fission product at half-maximum height) is shown as function of the fissioning nucleus A_F. It is seen that the position of the heavy fission fragment group A_H remains relatively fixed at mass 138.5 ± 2.5 over a range in A_F of about 18 mass units, whereas the position of the light mass peak varies linearly (slope of 1) over the same range. No deviation from this linear dependence is noticed for the lightest nuclides investigated. However, the heaviest nuclides seem to deviate from this pattern.

From Fig. 3 it is seen that the widths of mass distributions increase with increasing mass of the fissioning nucleus. If one compares the full

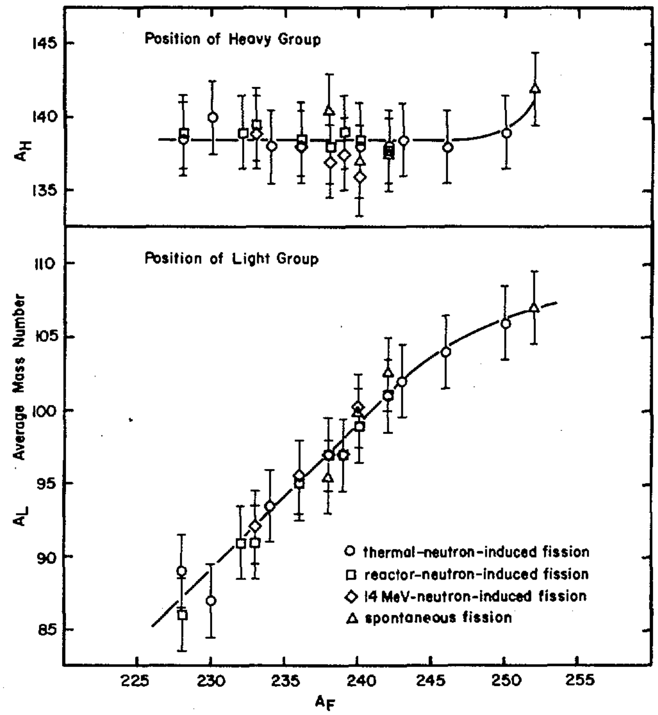

FIG. 2. Positions of light and heavy groups in the fission of various nuclides. The average mass number at half-maximum of the peaks is plotted. The data (with the exception of ^{227}Th) are taken from Ref. [13].

width at one-tenth maximum (FWTM) of the mass distribution this trend can be clearly observed. It should be noted that this effect is hardly discernible if the comparison is made on the basis of the full width at half maximum (FWHM), used to find the average mass-number for the position of the peaks. Linear functions are obtained for thermal- and reactor-neutron-induced fission and for spontaneous fission if the FWTM is plotted against the mass of the fissioning nucleus A_F. The widths are on the average about 3 mass-units wider for thermal- and reactor-neutron-induced fission than for spontaneous fission. This effect can probably be attributed to the higher excitation energies in neutron-induced fission. Higher excitation energies generally tend to broaden the mass distribution.

The observed independent fission yield for the shielded nuclide ^{136}Cs resulting from two determinations is given in Table II. The chain yield was taken from the smooth mass-yield curve of Fig. 1. The empirical value for the most probable charge Z_p was calculated from the fractional yield using the assumption of a Gaussian charge dispersion with $\sigma = 0.62 \pm 0.06$ [10]. This value for Z_p is in very good agreement with the Z_p-value found with the equal-charge-displacement hypothesis [11]. The deviation of Z_p from unchanged charge distribution (UCD) is -0.6 charge units. This value indicates a pattern of charge division which is consistent with other cases of low-energy fission [2-4, 12].

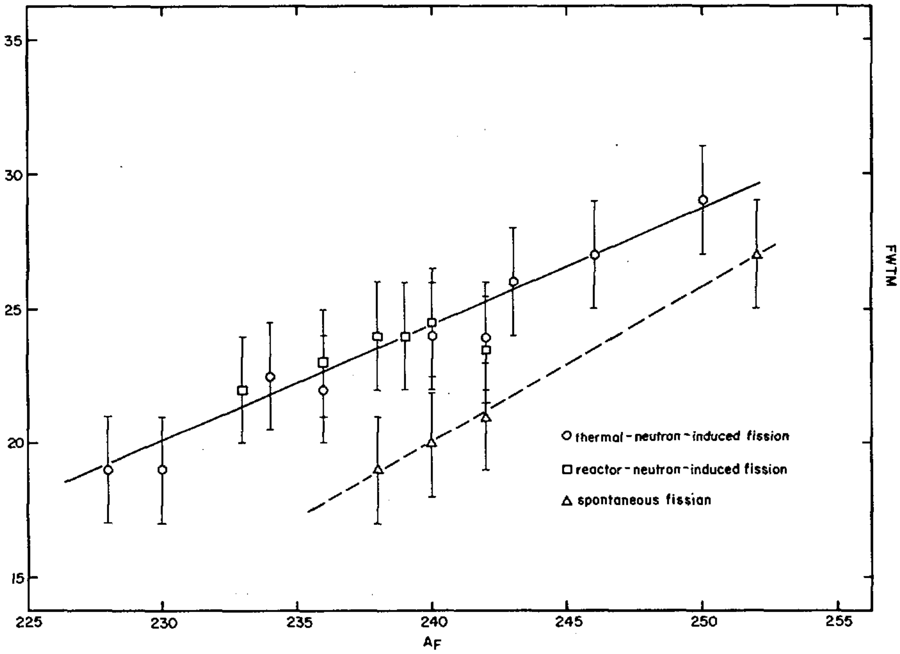

FIG.3. Widths of mass distributions (FWTM = full width at one tenth of maximum height) for various nuclides and different types of fission. The data (with the exception of ^{227}Th) are from Ref. [13].

ACKNOWLEDGEMENTS

The authors wish to thank Dr. P. Baertschi for many discussions and his interest in this work, and Dr. P. Tempus and his staff for providing space and help during the preparation of the samples. One of us (K.F.F.) expresses his thanks to EIR and ANL for making his stay in Würenlingen possible.

This work was partly supported by a Swiss National Science Foundation Grant.

REFERENCES

[1] IYER, R.S., JAIN, M.N., NAMBOODIRI, M.N., RAJAGOPALAN-RAJKISHORE, M., RAMANIAH, M.V., RAO, C.L., RAVINDRAN, N., SHARMA, H.D., Physics and Chemistry of Fission (Proc. Symp. Salzburg, 1965) 1, IAEA, Vienna (1965) 439.

[2] RAVINDRAN, N., FLYNN, K.F., GLENDENIN, L.E., J. inorg. nucl. Chem. 28 (1966) 921.

[3] VON GUNTEN, H.R., FLYNN, K.F., GLENDENIN, L.E., Phys. Rev. 161 (1967) 1192.

[4] FLYNN, K.F., VON GUNTEN, H.R., to be published.

[5] NERVIK, W.E., Phys. Rev. 119 (1960) 1685.

[6] SEELMANN-EGGEBERT, W., PFENNIG, G., MUNZEL, H., Chart of the Nuclides, 3rd Edition 1968, Bundesminister fur wissenschaftliche Forschung, Bonn.

[7] PETERSON, S., GHIORSO, A., Paper 9.19, TID-5223 (Part 2) (1952), cited in HUGHES, D.J., SCHWARTZ, R.B., BNL 325, 2nd Edition, 1958.

[8] PARKER, W., BILDSTEIN, H., GETOFF, N., Nucl. Instrum. Methods 26 (1964) 55.

[9] MEEK, M.E., RIDER, B.F., APED-5398-A (1968).
[10] WAHL, A.C., FERGUSON, R.L., NETHAWAY, D.R., TROUTNER, D.E., WOLFSBERG, K., Phys. Rev. 126 (1962) 1112.
[11] GLENDENIN, L.E., CORYELL, C.D., EDWARDS, R.R., Radiochemical Studies: The Fission Products (CORYELL, C.D., and SUGARMAN, N., Eds). McGraw-Hill, New York (1951). Nat. nucl. Energy Ser. 9, Div.4, 489.
[12] WOLFSBERG, K., Phys. Rev. 137B (1965) 929.
[13] VON GUNTEN, H.R., Actinides Reviews, in press.

DISCUSSION

W. MÜLLER: We did some experiments with ^{227}Th fission. The results are mostly in very good agreement with yours, but we had, in my view, a less time-consuming method for eliminating the thorium using an anion exchanger with Th as nitrato-complex [Radiochim. Acta 9 (1968) 181-186]. The purity of the ^{227}Th fraction was checked by gamma spectrometry as well as alpha spectrometry. We, too, had a relatively high value for ^{77}As, which was checked not only by half-life but also by gamma spectrometry. Therefore, I think the value you found for ^{77}As may be the real one and not the upper limit. We found a lower value for σ_f, of about 100 b, which is a little different from your figure. Now I would like to ask you how long you irradiated your samples. Did you make any attempts to optimize this time in order to get as many fission products as possible by avoiding too much contamination from daughter products as well as too much decay of ^{227}Th?

H.R. von GUNTEN: The irradiation time was chosen according to the half-lives of the fission products being determined, i.e. from about one hour to a few days. As for the value of ^{77}As, I still believe that it is an upper limit, since blank experiments with recoil-catcher foils showed a contamination due to ^{76}As, which may have contributed to our measurements, because the half-lives of ^{76}As and ^{77}As are very similar.

FISSION YIELDS AND RECOIL RANGES DETERMINED BY A Ge(Li) DETECTOR

S.P. DANGE, H.C. JAIN,
S.B. MANOHAR, K. SATYAPRAKASH,
M.V. RAMANIAH, A. RAMASWAMI,
K. RENGAN
Radiochemistry Division,
Bhabha Atomic Research Centre,
Trombay, Bombay, India

Abstract

FISSION YIELDS AND RECOIL RANGES DETERMINED BY A Ge(Li) DETECTOR. The excellent resolution of gamma rays by Ge(Li) detectors is used to determine ^{239}Pu fission yields and recoil ranges of fission products from ^{233}U and ^{239}Pu. A combination of a 2-cm^3 Ge(Li) detector and a low-noise, room-temperature FET pre-amplifier combination giving a FWHM of 3.6 keV for 122 keV gamma-ray was employed. Irradiation and cooling times were optimized in order to obtain best resolution for different fission products. The purity of each photopeak used was ascertained by following the decay and determining the half-life.

As part of a program on determining fission yields of several heavy-element nuclei, fission yields of ^{239}Pu were determined by this technique. Thin, electroplated targets of ^{239}Pu and ^{235}U were simultaneously irradiated with neutrons and the recoiling fission fragments were collected in superpure aluminium foils. From an analysis of the gamma-ray spectra of fission products in the catcher foils, the yields of various nuclides in the thermal-neutron-induced fission of ^{239}Pu were determined relative to that of ^{235}U. These yields were compared with available radiochemical values. Recoil ranges of fission products from ^{233}U and ^{239}Pu in aluminium were also determined gamma-spectrometrically and compared with radiochemical values. This method affords determination of fission yields with an accuracy of 2-5% and ranges with an accuracy of 1-2%.

1. INTRODUCTION

The Ge(Li) detector has revolutionized gamma-ray spectroscopy because of its excellent resolution. The new detector has found wide application in many fields as, e.g. decay scheme studies [1] and activation analysis [2], and it has virtually replaced the NaI(Tl) detector. Simultaneous developments in detector technology and low-noise electronics have substantially improved the resolution obtainable for gamma-rays. More recently, the Ge(Li) detector has been used by Gordon et al. [3], Gormon and Tomlinson [4], and Heath et al. [5] for fission studies since the data for several nuclides can be obtained simultaneously from the spectra of fission-product gamma-rays. This direct measurement avoids the time-consuming radiochemical separations and the errors associated with the various operations involved. This paper describes the results of measurements of fission yields of plutonium-239 and recoil ranges of fission fragments from uranium-233 and plutonium-239 in the thermal-neutron fission of these nuclides using the Ge(Li) detector. The results of direct measurements are compared with radiochemical and mass-spectrometric values from the present work and literature.

2. EXPERIMENTAL

2.1. Detector-analyser system

A 2 cm^3-(4 cm^2 area × 5 mm depletion depth) Ge(Li) detector supplied by Princeton Gamm Tech was used. The detector, kept at liquid-nitrogen temperature in a cryostat, was connected to an Ortec-model-118A room-temperature FET preamplifier. A Packard-model TP-6 amplifier was used together with a Packard-model-116, 400-channel pulse-height analyser. The system gave a full width at half-maximum of 3.6 keV for 122-keV gamma rays of ^{57}Co and showed a maximum drift equivalent to 2.2 keV at 660 keV during a period of 24 h. The drift was one of the handicaps in analysing the spectra.

2.2. Target preparation

Plutonium containing about 95% ^{239}Pu, enriched uranium containing about 90% ^{235}U and uranium-233 were purified chemically and used for target preparation. The targets were prepared by electroplating [6] the required amount of fissile material from isopropyl alcohol medium onto a 10-mil superpure aluminium foil electroplated first with about 50-60 $\mu g/cm^2$ of gold (which, being more electropositive than aluminium, offered a more suitable surface for electrodeposition; at the same time, the main backing was essentially aluminium with minimum scattering). The amount of fissionable material on a target varied from 10 to 50 μg depending on the length of irradiation and nuclides of interest. The actual amount deposited on a target was estimated by the difference in the amount of fissile material in the solution before and after electrodeposition [6], the amount being determined by liquid scintillation counting. The area of the fissile material was well-defined and identical on all targets, the diameter being 1 cm.

2.3. Method

The "comparison method" was used to determine the fission yields [7]. For plutonium fission yield determination, the ^{235}U and ^{239}Pu targets were covered with 1-mil superpure aluminium foils (1.5 cm dia), wrapped with another superpure aluminium foil, sealed in polyethylene and irradiated simultaneously. Both "Apsara", the swimming-pool reactor with a thermal neutron flux of $\approx 10^{12}$ n $cm^{-2}s^{-1}$ and the heavy-water-moderated reactor "CIRUS" with a thermal neutron flux of $\approx 10^{13}$ n $cm^{-2}s^{-1}$ were used for irradiations. After irradiation and sufficient cooling, the catcher foils were centred on marked aluminium plates and covered with cellophane of 6 mg/cm^2 thickness. The gamma-ray spectra of the fission products in the catcher foils from both ^{235}U and ^{239}Pu targets were followed with the Ge(Li) detector using the same geometry. Peak areas were calculated in the same way for both catcher foils. Details of the fission yield calculation were described in a previous paper [8]. The 140.7 keV photopeak area of ^{99m}Tc in equilibrium with ^{99}Mo was used as an internal standard.

For range measurements the thin-target-thin-catcher method was used. The thickness of uranium or plutonium targets used was usually about 25 $\mu g/cm^2$ and always less than 70 $\mu g/cm^2$. The target was covered with a stack of three 0.3 mil superpure aluminium foils (obtained from American

Lamotite Corporation), each foil being identical in size, but slightly larger in diameter (1.5 cm diam.) than the target (1.0 cm diam.). The assembly was wrapped in 1-mil aluminium foil. After irradiation and appropriate cooling the target assembly was opened, and the catcher foils separated. Foil 1 (closest to the target) was mounted separately while foils 2 and 3 were mounted together. The range of a fission product was calculated [9, 10] with the formula

$$R = \left[1 + \frac{(A_2 + A_3 + \cdots)}{A_1}\right](t + \tfrac{1}{2}\,CW)$$

where R is the range in mg/cm^2 of aluminium, A_1, A_2, A_3 are the activities on each foil, t is the catcher thickness (mg/cm^2), C = 1.44, and W is the target thickness (mg/cm^2).

Details of this method were described in another paper from our laboratory [11].

For radiochemical determination of ranges the foils were dissolved separately and processed as described elsewhere [11]. Neutron activation analysis of the foils used as catchers showed that they were sufficiently pure.

Depending on the activity levels, the samples were mounted in one of the three fixed geometry positions available. For each set of nuclides the spectrum was followed as a function of time, in a fixed geometry.

Several 5-minute irradiations were carried out, and the data on ^{99m}Kr, ^{139}Ba, and ^{142}La were obtained from these experiments. Data on all other nuclides were obtained from 24-h irradiations. In the preliminary investigation, the decay of the photopeaks selected for each nuclide was followed and the decay curves plotted. The time period in which the decay showed the correct half-life was determined in each case. This agreed with the expectations on the basis of known interferences in each peak (see Table I). In later irradiations, the photopeaks were followed after the selected cooling times, decay curves were plotted and activity values were taken from the graphs for calculations.

2.4. Analysis of the gamma-ray spectra

After irradiation and appropriate cooling, the gamma spectrum was obtained by starting with a convenient total counting rate not exceeding that which would give more than 30% dead time on the analyser (beyond this dead time the resolution is affected). The counting was done for a time sufficiently long to give good counting statistics, at the same time taking into account the half-life of the nuclide under consideration. The data were typed out and also plotted with the help of an X-Y plotter. The area of the photopeak was summed up and the Compton background was subtracted by visually examining the spectrum [12]. In general, for each nuclide the decay was followed to the point where the photopeak became indistinguishable from Compton contribution or where the Compton correction was so large that the error in the peak area would be very high. When the photopeak used interfered with another photopeak lying close to it and having shorter half-life, sufficient time was allowed for its decay and when the interference was from a longer-lived component, the two components were resolved

TABLE I. DATA ON NUCLIDES DETERMINED

Nuclide	$T_{\frac{1}{2}}$	Irradiation time	Energy of photopeak used (keV)	Interference nuclide, photopeak (keV)	Remarks
^{85m}Kr	4.4 h	5 min	151.2	Unknown short-lived components	Decay after six hours gave correct half-life (Fig.4A).
^{91}Sr-^{91m}Y	9.7 h	24 h	555.6	^{92}Y (560.8)	^{92}Y allowed to decay (Fig.4C).
^{95}Zr	65 d	24 h	724.1	-	Counting was done after cooling the sample for 30 days.
^{99}Mo-^{99m}Tc	66 h	From all irradiations	140.7	^{144}Ce(133.3) and ^{141}Ce(145.4)	^{144}Ce contribution is initially only of the order of 0.1%. ^{141}Ce contribution subtracted graphically (Fig.4D).
^{103}Ru	39.5 d	24 h	496.9	^{140}La (487.0)	Followed after 30 days.
^{131}I	8.05 d	24 h	364.5	^{99}Mo (366.2) and ^{97}Zr (355.6)	After 10 days cooling the photopeak was followed.
^{132}Tc-^{132}I	77.7 h	24 h	228.3	^{143}Ce(231.7)	Followed after four days. Contribution from ^{143}Ce is $<$ 1%.

TABLE I. (Cont.)

Nuclide	$T_{\frac{1}{2}}$	Irradiation time	Energy of photopeak used (keV)	Interference nuclide, photopeak (keV)	Remarks
			667.7	^{143}Ce (664.5) and ^{97}Nb (657.9)	Followed after 5 days; gives correct half-life.
^{133}I	20.3 h	24 h	529.8	^{132}I (522.7), ^{135}I (526.5) and ^{140}Ba (537.2)	Allowed ^{135}I to decay (30 h). Graphically resolved from ^{132}I(Te) and ^{140}Ba contribution (Fig.4B).
^{133}Xe	5.27 d	24 h	81.0	-	To reduce Compton background, followed after 15 days.
^{135}Xe	9.2 h	24 h	249.6	-	Photopeak becomes clear only after two days (Fig. 4C)
^{139}Ba	82.9 min	5 min	165.8	-	Followed after 1 h (Fig.4A)
^{140}Ba-^{140}La	12.80 d	24 h	162.8 328.8 815.8	- - ^{132}I (812.3)	Followed after 10 days. Followed after 10 days. Decay after 15 days gives correct half-life.
^{141}Ce	32.5 d	24 h	145.4	-	Data obtained after 30 days.
^{142}La	92.5 min	5 min	641.1	-	Counting started after 1 h. (Fig. 4A).
^{143}Ce	33 h	24 h	292.9	^{135}I (288.3)	Followed after four days (Fig. 4C).
^{144}Ce	284 d	24 h	133.6	-	-
^{147}Nd	11.06 d	24 h	91.1	-	Data obtained after 15 days.

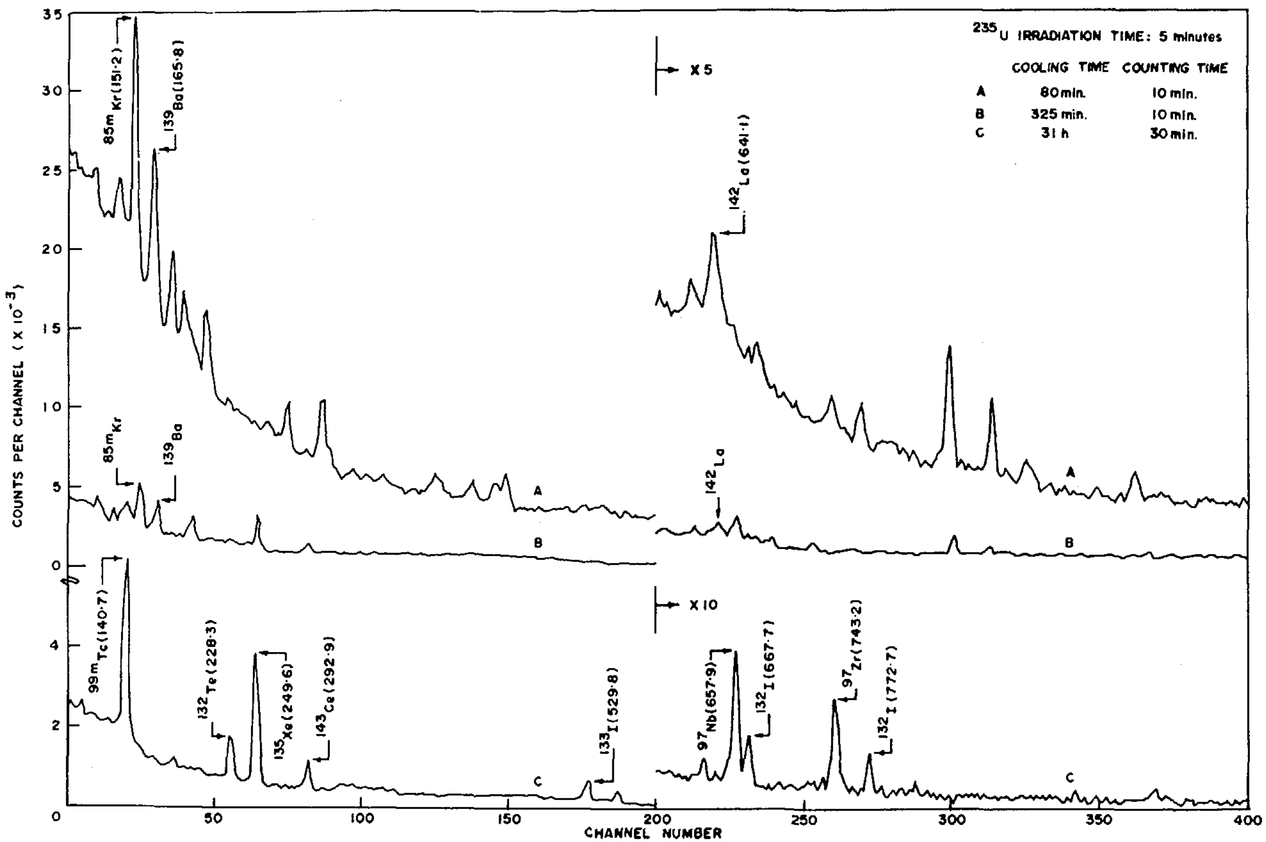

FIG.1. Fission product gamma spectra for ^{235}U.

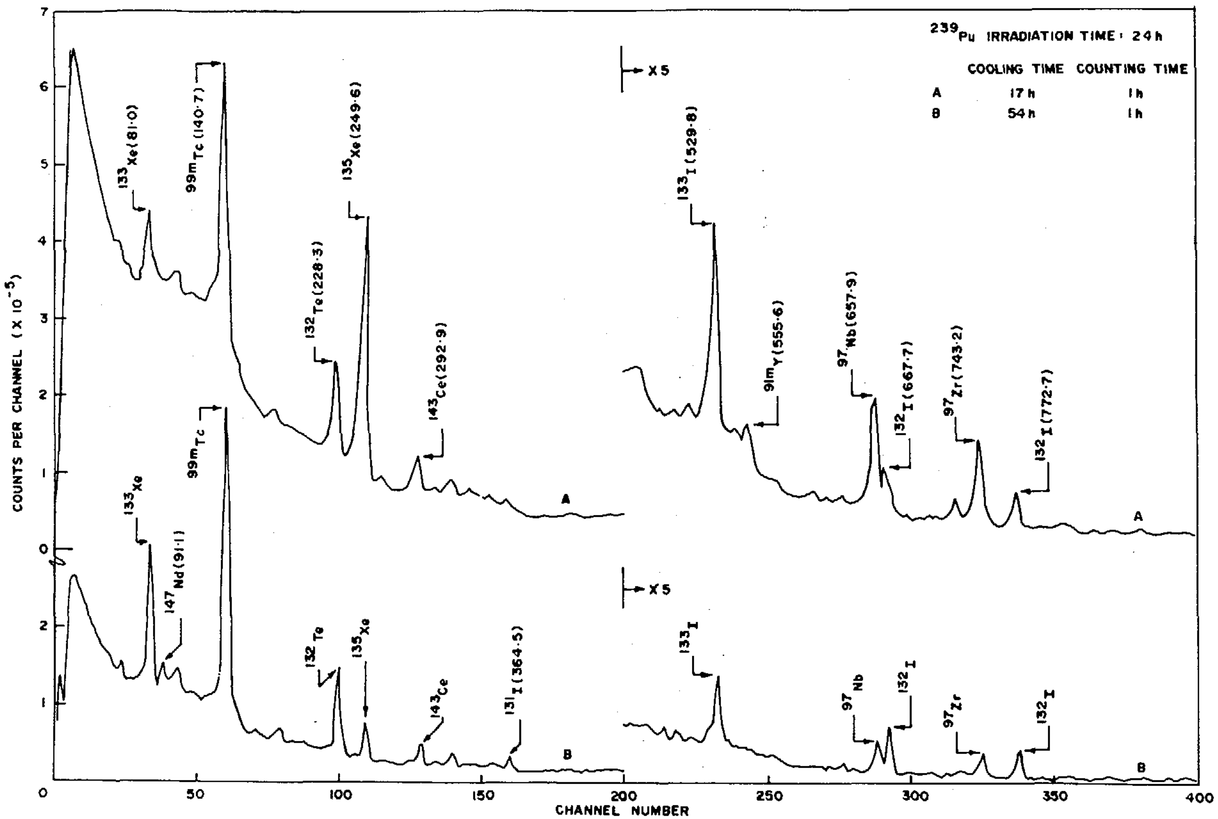

FIG.2. Fission product gamma spectra for ^{239}Pu.

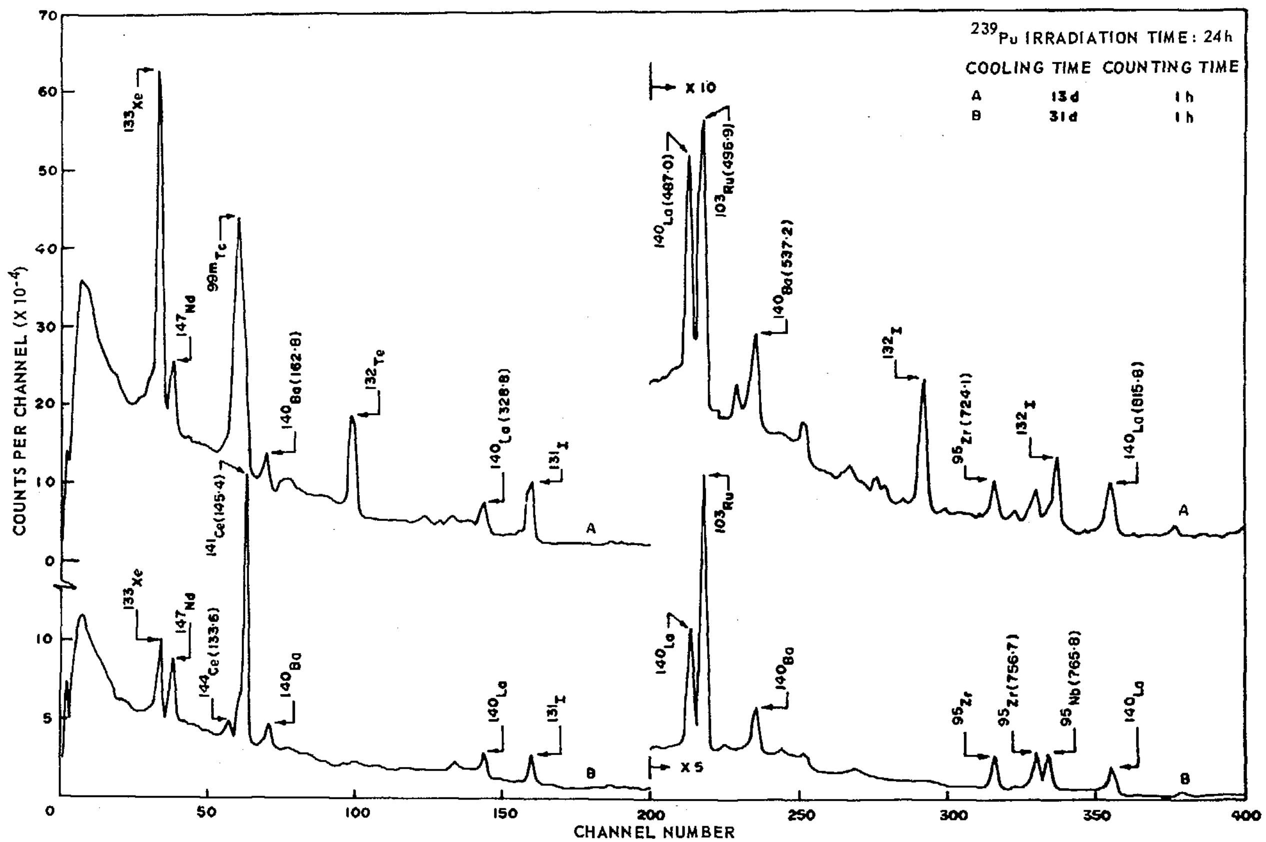

FIG. 3. Fission product gamma spectra for ^{239}Pu.

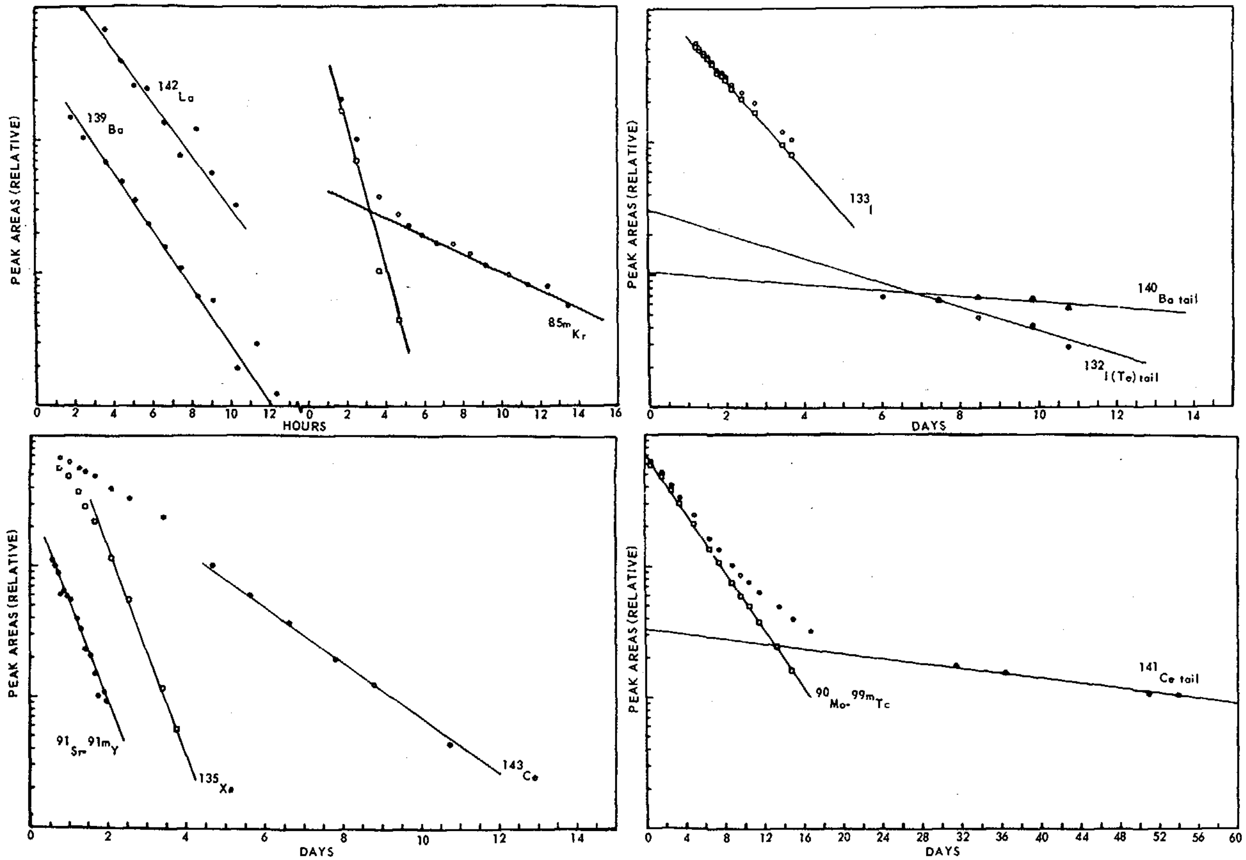

FIG.4. Typical decay curves of some nuclides.

graphically. Details of the selected photopeaks (the gamma-ray energies were taken from Heath et al. [5]) of nuclides determined together with interference, irradiation and cooling times necessary, etc. are summarized in Table I.

In the case of relatively long-lived nuclides, calculation of the areas under the photopeaks was attempted by using a computer after subtraction of the contribution from the prominent higher-energy gamma-rays. The computer method was not only expected to enable accurate subtraction of the Compton contribution from the prominent gamma-rays, but also to remove the interference from other gamma-rays originating from the same nuclide, thereby reducing interference on other peaks. The computer was programmed to peel off gamma-ray spectra of certain nuclides (stored in its memory) from the composite fission-product gamma-ray spectrum starting from the high-energy end. The procedure is briefly outlined here. Gamma-ray spectra of a number of pure nuclides were obtained, the counting being done under the same conditions used for obtaining fission-product gamma-ray spectra. These standard spectra were stored in the computer memory. From the composite spectrum the area of the highest-energy peak (815.8-keV peak of ^{140}La, in this case) was determined by the computer, and, making use of the standard ^{140}La spectrum, after proper multiplication to adjust for the peak area, the computer subtracted the contribution of ^{140}La from the composite spectrum. The subtracted spectrum was printed out. This process was repeated using gamma-ray spectra of other nuclides. In this way, the prominent gamma-rays and their Compton contributions were subtracted accurately. The small shift in some of the spectra caused by the analyser was rectified by the computer before carrying out the peeling operation.

3. RESULTS AND OBSERVATIONS

Some typical composite gamma-ray spectra of fission products with different irradiation and cooling times are given in Figs 1 to 3, and decay curves obtained from plots of photopeak area as a function of time are shown in Fig. 4 (A to D). As can be seen from these figures, the peaks selected for calculation were well-resolved, and decay curves had the right slopes indicating that there was no interference from other nuclides in the time chosen to obtain the data.

For fission-yield calculations, the activity values from corresponding portions of the decay curves were used. D and R values were obtained in the usual manner [8]. The R values in the plutonium fission were converted to fission yields by multiplying by the factor

$$\left[Y_{^{99}Mo}\,(Pu) / Y_{^{99}Mo}\,(U) \right] [Y_X(U)]$$

where $Y_{^{99}Mo}$ (Pu) and $Y_{^{99}Mo}$ (U) refer to the yields of ^{99}Mo in the thermal fission of ^{239}Pu and ^{235}U, respectively, and $Y_X(U)$ is the yield of nuclide X in the thermal fission of ^{235}U. The ^{235}U fission yield values were taken from the compilation of Meek and Rider [12a]. The determination of the

TABLE II. FISSION YIELDS OF ^{239}Pu

	Fission yield (%)				
	Ge(Li) value - present work		Literature values		
	Based on 5.61 for ^{99}Mo	Based on 6.02 for ^{99}Mo***	Marsden and Yaffe [13]	Fickel and Tomlinson [14, 15]	Others
^{85m}Kr	0.60 ± 0.02	0.64 ± 0.02(4)	-	0.535(Rb)	
^{91}Sr	1.89 ± 0.06	2.03 ± 0.06(2)	2.41	2.59 (Zr)	
^{95}Zr	4.40 ± 0.15	4.74 ± 0.16(4)	5.06	4.99	
	C 4.45	4.78			
^{99}Mo	5.61	6.02	5.61	-	6.02*
^{103}Ru	6.19 ± 0.43	6.65 ± 0.46(5)	5.79	5.63	
^{131}I	3.68 ± 0.11	3.96 ± 0.12(5)	3.80	3.77	
	C 3.64	3.91			
^{132}Te	4.62 ± 0.09	4.97 ± 0.10(10)	5.51	5.26	
	C 4.87	5.23			
^{133}I	6.23 ± 0.15	6.69 ± 0.16(4)	5.53	6.90 (Cs)	5.0**
	C 5.71	6.12			
^{133}Xe	6.44 ± 0.11	6.92 ± 0.12(3)	-	6.90 (Cs)	
^{135}Xe	6.08 ± 0.16	6.53 ± 0.17(9)		7.25 (Cs)	
	C 6.56	7.04			
^{139}Ba	5.09 ± 0.08	5.47 ± 0.09(4)	-	-	5.4**, 5.94+
^{140}Ba	4.89 ± 0.13	5.25 ± 0.14(14)	5.47	5.58 (Ce)	
	C 4.95	5.30			
^{141}Ce	4.90 ± 0.08	5.27 ± 0.09(5)	6.11	5.23	
^{142}La	4.82 ± 0.18	5.19 ± 0.19(4)	-	4.97 (Ce)	
^{143}Ce	3.71 ± 0.29	3.99 ± 0.31(9)	4.28	4.56	
	C 3.88	4.16			
^{144}Ce	3.36 ± 0.07	3.61 ± 0.07(5)	4.09	3.84	
^{147}Nd	1.78 ± 0.07	1.92 ± 0.07(5)	1.46	1.99	2.2++

C Values obtained after computer subtraction of Compton - see text. * Ref.[16], ** Ref. [17], + Ref.[18], ++ Ref.[19].
*** The number in the parenthesis is the number of determinations.

TABLE III. RANGES IN ALUMINIUM OF FISSION PRODUCTS FROM ^{239}Pu

Nuclide	Range (mg/cm^2) Ge(Li), this work*	Range (mg/cm^2), radiochemical, this work*	Range (mg/cm^2), radiochemical, Ishimori et al.[20]
^{89}Sr	-	4.11 ± 0.04 (3)	4.17 ± 0.05
^{91}Sr	4.31 ± 0.04 (4)	4.10 ± 0.05 (3)	4.16 ± 0.04
^{97}Zr	4.13 ± 0.05 (5)	4.02 ± 0.06 (4)	4.12 ± 0.10
^{97}Nb	4.12 ± 0.05 (4)	-	-
^{99}Mo	4.09 ± 0.07 (5)	4.05 ± 0.07 (3)	4.00 ± 0.05
^{103}Ru	3.87 ± 0.07 (3)	-	-
^{105}Rh	-	3.79 ± 0.08 (2)	-
^{111}Ag	-	3.70 ± 0.01 (3)	-
^{115}Cd	-	3.36 ± 0.03 (3)	-
^{121}Sn	-	3.34 ± 0.02 (4)	-
^{125}Sn	-	3.26 (1)	-
^{127}Sb	-	3.60 ± 0.03 (2)	-
^{131}I	3.43 ± 0.04 (3)		
^{132}Te	3.32 ± 0.04 (2)	3.50 ± 0.02	-
^{133}I	3.40 ± 0.02 (2)		
^{135}Xe	3.37 ± 0.02 (3)		
^{140}Ba	3.13 ± 0.05 (3)	3.05 ± 0.04 (4)	3.04 ± 0.03
^{140}La	3.09 ± 0.06 (3)		
^{143}Ce	2.95 ± 0.04 (2)	-	2.90 ± 0.06
^{144}Ce	3.08 (1)		
^{147}Nd	2.89 ± 0.02 (3)	-	-

* The number in the parenthesis is the number of determinations.

fission yield by this method involved the assumption that the genetic relationships of isobars in a decay chain are the same in the fission of ^{235}U and ^{239}Pu.

The range of a nuclide in aluminium was calculated by using the counts under the photopeak of a particular energy selected for determining the nuclide. The values for $(A_2+A_3)/A_1$ were taken from spectra of the foils recorded consecutively so that decay was negligible. When the counting time was too long, appropriate corrections for decay were made. In general, for each nuclide several counts were taken and the average values of $(A_2+A_3)/A_1$ obtained were used for the range calculations. The value of $(A_2+A_3)/A_1$ obtained at different times in different nuclides in a particular irradiation agreed within 2-3% in most cases.

The fission yields of ^{239}Pu are given in Table II. The nuclides determined in the present work were not sufficient for plotting the mass-yield

TABLE IV. RANGES IN ALUMINIUM OF FISSION PRODUCTS FROM ^{233}U

Nuclide	Range (mg/cm²) Ge(Li), this work †	Range (mg/cm²) Ge(Li), Gordon et al.[3]	Range (mg/cm²), radiochemical, this work
^{89}Sr			3.92 ± 0.05 (2)
^{91}Sr	4.16 ± 0.04 (2)	4.16 ± 0.04	4.15 (1)
^{95}Zr	4.05 ± 0.04 (3)	4.02 ± 0.03	
^{95}Nb	4.02 ± 0.04 (3)	4.04 ± 0.04	
^{97}Zr	4.08 ± 0.05 (3)	4.08 ± 0.05	
^{97}Nb	4.01 ± 0.04 (3)	4.01 ± 0.04	
^{99}Mo	4.01 ± 0.03 (4)	4.01 ± 0.03	4.01 ± 0.03 (2)
^{111}Ag			3.38 ± 0.07
^{115}Cd			3.08 ± 0.03
^{132}Te	3.28 ± 0.04 (4)	3.28 ± 0.03	
^{132}I	3.26 ± 0.04 (4)	3.26 ± 0.04	
^{133}Xe	3.07 (1)	3.24 ± 0.03	
^{135}Xe	3.21 ± 0.03	3.21 ± 0.03	
^{140}Ba	2.92 ± 0.03	3.00 ± 0.03	2.92 ± 0.01*
^{140}La	2.94 ± 0.07	3.00 ± 0.03	
^{143}Ce	2.81 (1)	2.91 ± 0.03	
^{147}Nd	2.63 (1)	2.77 ± 0.02	

† The number in the parenthesis is the number of determinations.
* From Ref. [3].

curve to obtain a normalization factor. Hence the ^{99}Mo yield in ^{239}Pu fission reported in the literature was used. Since values for the yield of ^{99}Mo in the thermal fission of ^{239}Pu reported [13, 16] differ by 7%, two sets of fission yields were calculated using two ^{99}Mo values, 5.61 and 6.02 (columns 2 and 3 of Table II). The standard deviations calculated from the experimental data are given and they do not include any systematic errors. The accuracy of the yields is, in most cases, within about 3%, exceptions being ^{103}Ru, ^{142}La, and ^{143}Ce. The fission yields calculated on the basis of 6.02 for ^{99}Mo are in general agreement with the radiochemical values of Marsden and Yaffe [13] and the mass-spectrometric values of Fickel and Tomlinson [14, 15] while the values based on 5.61 are generally lower. The fission yields of ^{85m}Kr, ^{91}Sr, ^{103}Ru and ^{143}Ce based on either ^{99}Mo value are quite different from the literature values and in the case of ^{91}Sr the difference is maximum, 20-30%. As can be seen from Fig.4, the decay curves of ^{85m}Kr, ^{91}Sr and ^{143}Ce were good in the time selected for following the decay (Table I) thereby indicating that no resolvable "contamination" existed. ^{103}Ru also decayed with correct half-life. There-

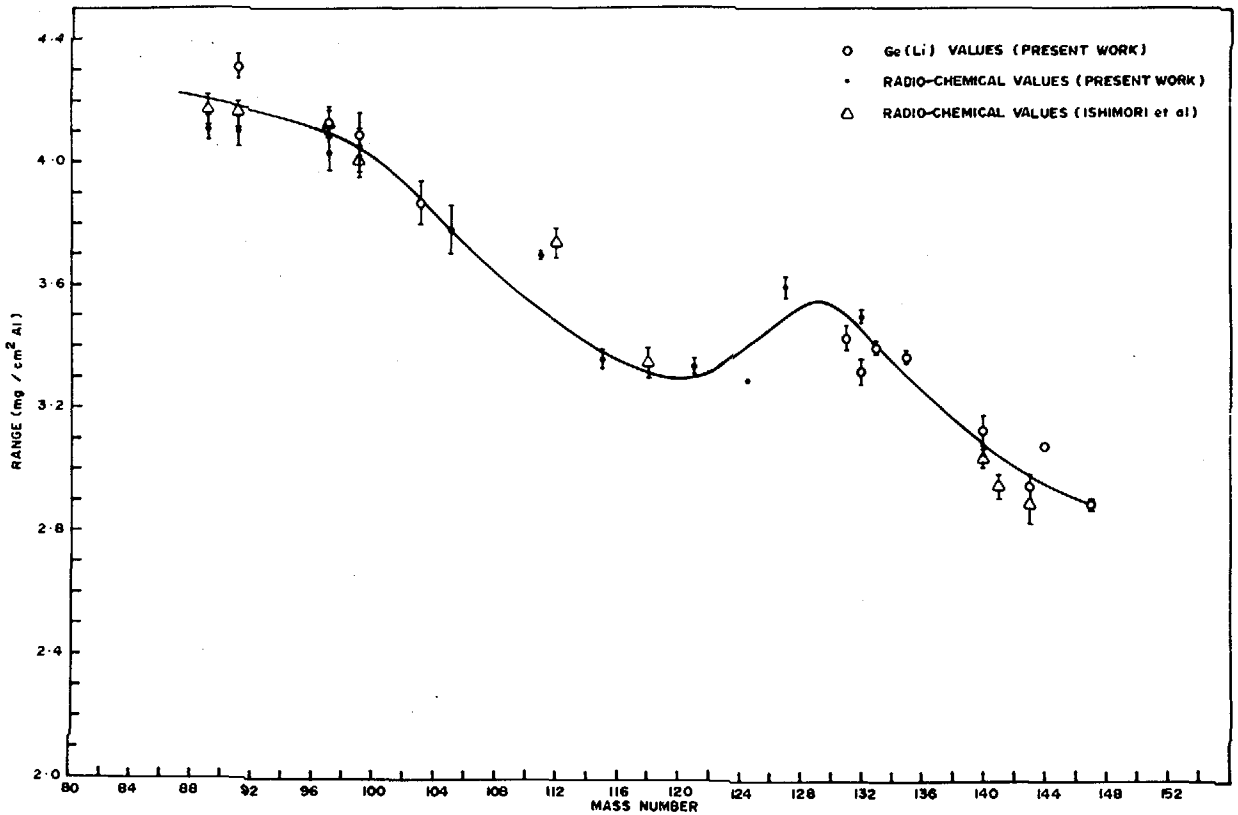

FIG. 5. Ranges in aluminium of fission products from ^{239}Pu.

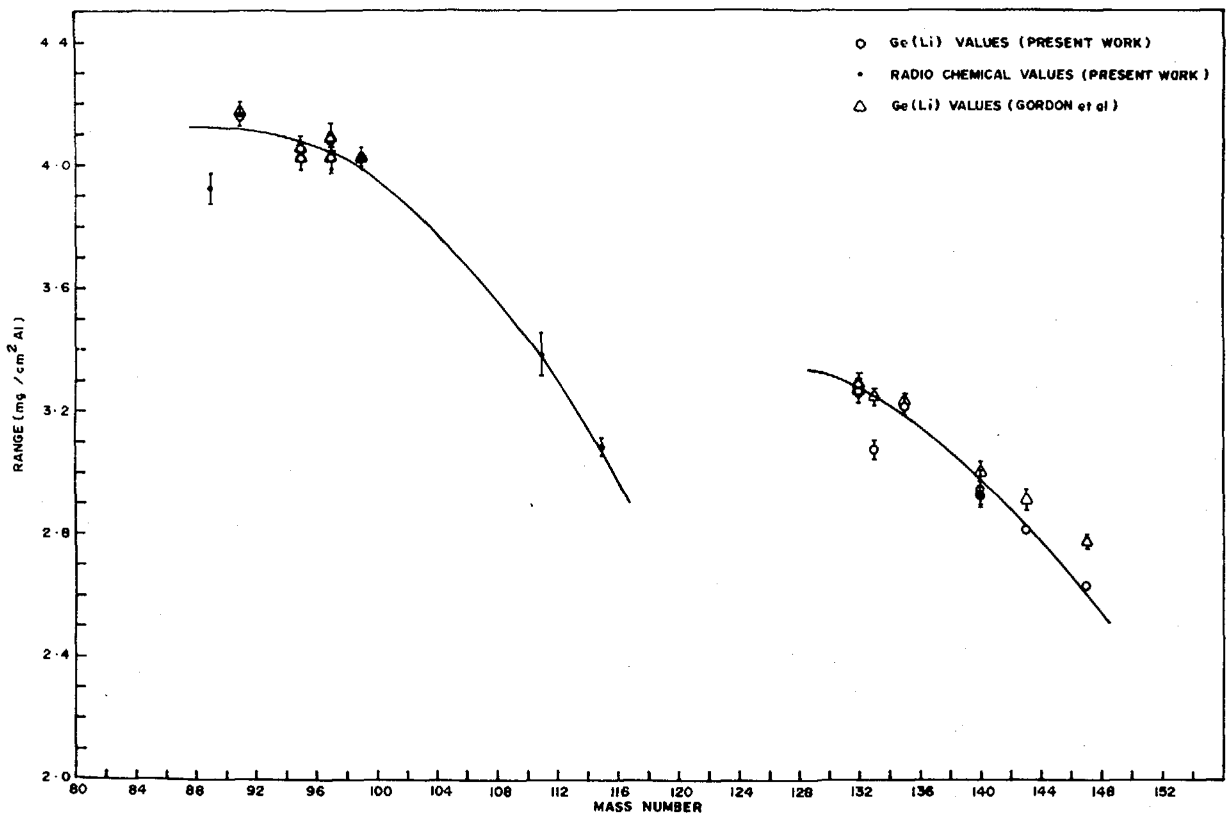

FIG.6. Ranges in aluminium of fission products from ^{233}U.

fore, further investigation is necessary before the reason for this large difference can be understood. The fission yields obtained by analysis of the gamma ray spectral data by the computer method for seven nuclides are included in Table II. It is seen that these values are within 5-6% of those obtained by the visual method of subtracting the Compton contribution. In general, these values are closer to the data in the literature. It is worth mentioning that the peeling off done with the computer in general increased the period for which the nuclides showed the correct half-life.

The ranges in aluminium of fission products from ^{239}Pu are given in Table III and plotted in Fig. 5. In the symmetric region (between ^{103}Ru and ^{131}I) no values could be determined by gamma-ray spectrometry since the yields are too low. For this reason, the ranges in this region were determined by the radiochemical method. The agreement between the radiochemical values and Ge(Li) values of this work is very good which indicates that the direct counting method is essentially good (comparison possible only in the case of five nuclides). The data of the present work agree well with the radiochemical data of Ishimori et al. [20]. The ranges in aluminium of fission products from ^{233}U are given in Table IV and plotted in Fig. 6. For comparison the values of Gordon et al. [3] obtained by the same method are included and the agreement between the two sets of data is very good except in the case of ^{133}Xe and ^{147}Nd where the difference is 4-5%.

In spite of the limitations of the experimental set-up of the Ge(Li) detector used in the present investigations, the fission yields and recoil ranges obtained compare reasonably well with the data in the literature. Further work using this technique, particularly with a better detector system and computer calculations, is considered interesting and worthwhile.

ACKNOWLEDGEMENTS

The authors are grateful to Dr. C.K. Mathews and Mr. J.K. Samuel for their help in setting up the Ge(Li) detector, to Mr. A.K. Agrawal for his help in computer calculations and to Mr. A.G.C. Nair for his help during the preparation of this paper.

REFERENCES

[1] HOLLANDER, J.M., Nucl.Instrum.Methods 43 (1966) 65.

[2] PRUSSIN, S.G., HARRIS, J.A., HOLLANDER, J.M., Anal.Chem.37 (1965) 1127.

[3] GORDON, G.E., HARVEY, J.W., NAKAHARA, H., Nucleonics 24 (1966) 62.

[4] GORMON, D.J., TOMLINSON, R.H., referred to in Can.J.Chem. 46 (1968) 2911.

[5] HEATH, R.L. et al., Rpt.IN-1218 (1968).

[6] *Procedure developed in our laboratory (to be published).*

[7] SCHMITT, R.A., SUGARMAN, N., Phys.Rev. 95 (1954) 1260.

[8] IYER, R.H., MATHEWS, C.K., RAVINDRAN, N., RENGAN, K., SINGH, D.V., RAMANIAH, M.V., SHARMA, H.D., J.inorg.nucl.Chem. 25 (1963) 465.

[9] ARAS, N.K., MENON, M.P., GORDON, G.E., Nucl.Phys. 69 (1965) 337.

[10] DOUTHETT, E.M., TEMPLETON, D.H., Phys.Rev. 94 (1954) 128.

[11] RAMANIAH, M.V., RAO, C.L., LYER, R.S., RAJKISHORE, M.S., LAUL, J.C., in Nuclear and Radiation Chemistry, (Proc.Symp. Poona) (1967) 186.

[12] COVELL, D.F., Anal.Chem. 31 (1959) 1785.

[12a] MEEK, M.E., RIDER, B.F., Rpt. APED-5398-A (1968).

[13] MARSDEN, D.A., YAFFE, L., Can.J.Chem. 43 (1965) 249.
[14] FICKEL, H.R., TOMLINSON, R.H., Can.J.Phys. 37 (1959) 916.
[15] FICKEL, H.R., TOMLINSON, R.H., Can.J.Phys. 37 (1959) 926.
[16] FORD, G.P. et al., Rpt.LA-1997 (1956).
[17] CORYELL, C.D., SUGARMAN, N., (Eds), Radiochemical Studies: Fission Products, N.N.E.S. Divn IV, McGraw Hill, New York (1951).
[18] BARTHOLOMEW, R.M., MARTIN, J.S., BAERG, A.P., Can.J.Chem. 37 (1959) 660.
[19] BUNNEY, L.R., SCADDEN, E.M., ABRIAM, J.O., BALLOU, N.E., 2nd Int.Conf.peaceful Uses atom.Energy (Proc.Conf.Geneva, 1958), 15 UN (1959) 444.
[20] ISHIMORI, J., MUNZEL, H., PFENNING, G., Radiochim.Acta 9 (1968) 187.

DISCUSSION

P. POLAK: We looked for a reasonably long-lived fission product in the symmettic region which could be measured directly in an irradiated ^{238}U sample (25 MeV protons) without any chemical treatment and found such a nuclide in ^{112}Ag (apparent half-life 21 hours), the decay scheme of which can be found in an article by E.W.A. Lingeman et al., [Nucl. Phys. A122, 557 (1968)]. In the 1600-2100 keV region there are three gamma lines which can be measured without interference from other fission products with the help of a fairly large (> 10 cm^3) Ge(Li) detector. In this way we were able to measure peak-to-valley ratios with 10-25 MeV protons.

M. RAMANIAH: With our detector we were not able to detect any specific gamma line in the symmetric region.

B. SCHRÖDER: In Lund, Dr. Forkman, Dr. Nydahl and I have made similar use of a Ge(Li) detector to investigate photofission. However, we did not use a "comparison method", since we feel that if we want to broaden the field of application of Ge(Li) detectors to situations with change dispersions different from ^{235}U, we have to use a more direct method involving branching ratios for the gamma lines, detector efficiency etc.

As to the remark of Dr. Polak, we have identified ^{112}Ag with a gamma line at 618 keV.

M.V. RAMANIAH: I agree that the comparison method has its limitations. We are planning to calibrate our detector and then determine the absolute yields.

We were not able to detect the 618 keV peak due to ^{112}Ag with our detector.

ДЕЛЕНИЕ ВОЗБУЖДЕННЫХ КОМПАУНД-ЯДЕР В РАЙОНЕ $\frac{Z^2}{A} > 37$

С.А.КАРАМЯН, Ю.Ц.ОГАНЕСЯН,
Б.И.ПУСТЫЛЬНИК, Г.Н.ФЛЕРОВ

Объединенный институт ядерных исследований,
Дубна,
Союз Советских Социалистических Республик

Abstract — Аннотация

FISSION OF COMPOUND NUCLEI IN THE REGION $\frac{Z^2}{A} > 37$. The angular mass and charge distributions of the fragments in fission of compound nuclei with Z between 85 and 110, and excitation energy between 40 and 120 MeV were studied. The compound nuclei were created by the bombardment with heavy ions. The data on anisotropy of the fission fragments were used to obtain the values of effective moments of inertia for scissioning nuclei at the saddle point and Z^2/A near to the critical value. It was shown that the effective moment of inertia is a simple function of the fission parameter (Z^2/A) and does not depend on the energy of the excited nucleus. The results are compared with the prediction of the drop model fission theory in respect to the shape of nuclei at the saddle point. The investigations of the mass and charge distribution disclose a sharp increase of charge and mass dispersion of the fragments (as a function of Z^2/A) at $\frac{Z}{A} > 37$. A strong dependence of charge dispersion on asymmetry of fission was observed. The most probable charge of the fission fragments differs substantially from those calculated on the basis of the hypothesis on charge proportionality. It agrees with the calculations based on the hypothesis of uniform charge displacement and with the condition of a minimum of potential energy in the system of the fragments. The charge dispersion of the fragment depends only weakly on the excitation energy of the scissioned nuclei, but the mass distribution broadens substantially with the rise of the excitation energy. The results obtained testify that shape of the nuclei at the moment of fission changes significantly with Z^2/A, i.e. the final division of the nucleus in two fragments occurs at different stages of the nucleus deformation. Based on the extrapolation of mass and charge distribution, a semi-quantitative analysis of possibilities to utilize the fission reaction caused by accelerated heavy ions (of ^{136}Xe type) as a tool for artificial synthesis of neutron-rich isotopes of very heavy elements (of type ^{298}114) was made. The results on number and angle distribution of neutrons from heavy-ion-induced fission are also presented. The data on $\bar{\nu}$ agree with the values obtained by studying mass and charge fragments' distribution in the same reactions. A qualitative exploration of the obtained experimental data on fission of excited nuclei with $\frac{Z^2}{A} > 37$ is given. The quantitative description of the detected phenomena requires further theoretical studies.

ДЕЛЕНИЕ ВОЗБУЖДЕННЫХ КОМПАУНД-ЯДЕР В РАЙОНЕ $\frac{Z^2}{A} > 37$. Изучены угловые, массовые и зарядовые распределения осколков деления компаунд-ядер с Z от 85 до 110 и энергией возбуждеиия от 40 до 120 Мэв, образуемые в реакциях с ускоренными тяжелыми ионами. Из данных по анизотропии осколков деления рассчитаны значения эффективных моментов инерции для седловых форм делящихся ядер с Z^2/A, близким к критическому значению. Показано, что эффективный момент инерции является однозначной функцией параметра делимости (Z^2/A) и не зависит от энергии возбуждения делящегося ядра. Результаты сравниваются с предсказаниями жидко-капельной теории деления относительно формы ядер в седловой точке. При изучении массовых и зарядовых распределений обнаружено резкое увеличение дисперсии заряда и массы осколков с ростом Z^2/A делящегося ядра при $\frac{Z^2}{A} > 37$, а также сильная зависимость дисперсии заряда от асимметрии деления. Наиболее вероятный заряд осколков деления существенно отличается от заряда,рассчитанного согласно гипотезе пропорциональности заряда массе, и хорошо согласуется с расчетами по гипотезе равного смещения заряда и из условия минимума потенциальной энергии системы разделяющихся осколков. Дисперсия заряда осколков слабо зависит от энергии возбуждения делящегося ядра, в то время как массовое распределение существенно уширяется с ростом энергии возбуждения. Полученные результаты,по-видимому, свидетельствуют, что при изменении Z^2/A делящегося ядра форма разрывных фигур существенно меняется, т.е. окончательное разделение ядра на два осколка происходит на разных стадиях процесса деформации ядра. На основе экстраполяции массовых и зарядовых распределений произведен полуколнчественный анализ возможностей использования реакции деления ядер очень тяжелымн ускоренными ионами (типа ^{136}Xe) в качестве орудия искусственного синтеза нейтронно-обогащенных изотопов сверхтяжелых элементов (типа $^{298}114$). Приведены также результаты измереннй числа и угловых распределений нейтронов деления ядер тяжелыми ионами. Данные по числу $\bar{\nu}$ согласуются с величинами, полученными при изучении массовых и зарядовых распределений осколков в тех же реакциях. Дается качественное объяснение полученных экспериментально данных по делению возбужденных ядер с $\frac{Z^2}{A} > 37$. Количественное описание обнаруженных закономерностей требует дальнейшего теоретического изучения.

С момента открытия деления ядер урана изучение механизма деления является одной из важных и интересных проблем физики атомного ядра. Теоретическое описание процесса деления возможно лишь путем построения упрощенных физических моделей этого явления. Наиболее развита в настоящее время модель жидкой капли, впервые предложенная для объяснения деления в 1939 году Н.Бором и Уиллером [1] и Френкелем [2]. Несмотря на значительные успехи жидко-капельной модели деления, последняя не в состоянии, хотя бы качественно, объяснить основные закономерности низкоэнергичного деления, что связано с чрезвычайно сильным влиянием на процесс деления особенностей микроскопической структуры ядер (оболочечных эффектов).

Возможности экспериментального изучения деления существенно расширились с появлением ускорителей заряженных частиц и развитием ускорительной техники. Бомбардировка тяжелых и средних ядер быстрыми заряженными частицами позволяет изучать деление возбужденных состояний ядер в очень широком интервале параметра делимости Z^2/A и энергии возбуждения, в то время как деление при энергиях возбуждения порядка энергии связи нейтрона в ядре испытывают лишь элементы, которые тяжелее Ra.

Экспериментально установлено, что при энергии возбуждения ядра, большей 40 Мэв, хорошо известные структурные особенности низкоэнергичного деления исчезают, деление становится в согласии с жидко-капельной моделью симметричным. Обычно это обстоятельство связывают со значительной дисперсией распределения нуклонов около границы Ферми для возбужденных состояний ядер, что, возможно, приводит к разрушению оболочечных эффектов в ядре. Можно предполагать поэтому, что изучение деления возбужденных ядер способно дать некоторые сведения о "гидродинамической стороне" процесса деления, которые нельзя извлечь из данных по низкоэнергичному делению. Естественно, что результаты, полученные для нагретого ядра, нельзя непосредственно использовать для объяснения всех закономерностей деления вблизи порога. Однако некоторые характерные черты механизма коллективной необратимой деформации ядра в процессе деления могут быть общими для деления любых ядер (например — характер движения ядра вблизи точки разрыва, распределение нуклонов между разделяющимися осколками и т.д.).

Перечисленные преимущества использования ускоренных заряженных частиц в полной мере относятся к тяжелым ионам как частицам, вызывающим деление. Для последних имеется еще и то преимущество, что ядерные реакции с тяжелыми ионами в основном идут через полное слияние ядра мишени и бомбардирующей частицы вплоть до энергий 10 Мэв/нукл. Это дает возможность изучать деление очень высоко возбужденных состояний (до $E^* = 150 - 200$ Мэв) ядер при строгой фиксации Z, A и энергии возбуждения делящейся системы. Использовать для этой цели энергичные легкие частицы (p,d) весьма затруднительно, так как в этом случае образованию компаунд-ядра предшествует быстрый процесс каскадного выбивания нуклонов, приводящий к значительной дисперсии компаунд-ядер по Z, A и энергии возбуждения.

Несмотря на это, до настоящего времени деление ядер тяжелыми ионами было изучено очень слабо, особенно в области высоких Z^2/A делящихся компаунд-ядер. Это обстоятельство объясняется, по-видимому, чрезвычайно ограниченным количеством имеющихся сейчас во всем мире ускорителей тяжелых ионов.

В данной работе дается обзор физических результатов, полученных при делении ядер тяжелыми ионами, и представлены некоторые оригинальные данные.

1. УГЛОВЫЕ РАСПРЕДЕЛЕНИЯ ОСКОЛКОВ ДЕЛЕНИЯ

При слиянии тяжелого иона с ядром мишени образуется компаунд-ядро, обладающее большим угловым моментом (до $80 \div 100\hbar$), ориентированным в плоскости, перпендикулярной направлению движения бомбардирующих частиц. Если в процессе деления вытянутая форма ядра существует в течение периода, достаточно долгого по сравнению с периодом вращения, то из соображений энергетической выгодности ось деления будет ориентироваться перпендикулярно оси вращения, что приведет к значительной анизотропии осколков деления. Если ось деления строго перпендикулярна оси вращения для всех актов деления, то угловое распределение осколков, относительно пучка бомбардирующих частиц, имеет вид $1/\sin\vartheta$ и анизотропия осколков в этом случае бесконечна. В действительности, температурные флуктуации формы делящегося ядра приводят к тому, что значение угла между осью деления и осью вращения компаунд-ядра обладает определенной дисперсией при среднем значении угла 90°, причем величина дисперсии угла существенно зависит от формы делящегося ядра, которая характеризуется эффективным моментом инерции:

$$\frac{1}{I_{эфф}} = \frac{1}{I_{\parallel}} - \frac{1}{I_{\perp}}$$

где $I_{\parallel}$ — момент инерции ядра относительно вращения вокруг оси деления; $I_{\perp}$ — момент инерции относительно вращения вокруг оси, перпендикулярной направлению деления.

Из изложенного ясно, что анизотропия осколков является конечной величиной, и что, измеряя ее, возможно определить ось делящегося ядра, если известны его температура и угловой момент.

Высказанные выше соображения лежат в основе работ О.Бора [3], а также Халперна и Струтинского [4], объясняющих угловые распределения осколков деления ядер тяжелыми ионами. В этих работах в качестве меры среднего отклонения угла между направлением деления и осью вращения от 90° выбран параметр K_0^2 — средний квадрат проекции углового момента на ось деления. K_0^2 является также мерой того, насколько сильно угловое распределение отличается от закона $1/\sin\upsilon$ и зависит от $I_{эфф}$ и температуры T делящегося ядра:

$$K_0^2 = \frac{1}{\hbar^2} I_{эфф} T$$

Согласно современным представлениям, в процессе деления ядро проходит через выделенное состояние — седловую точку, соответствующую вершине барьера. В этой точке на ядро не действуют силы; это — положение неустойчивого равновесия, поэтому в седловой точке ядро живет максимально долго по сравнению со всеми другими состояниями, проходимыми ядром в процессе деления. Отсюда является естественным приписать эффективный момент инерции делящегося ядра, определенный из угловой анизотропии осколков, той форме ядра, которую она имеет в седловой точке.

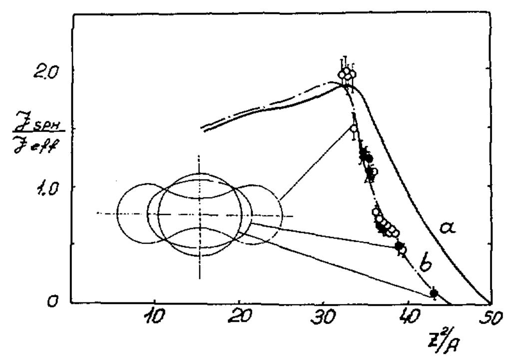

Рис.1. Зависимость $I_{сф}/I_{эфф}$ от Z^2/A делящегося ядра: точки — результаты эксперимента; кривая а — расчет по капельной модели [8]; кривая b — расчет согласно работе [9].

На рис.1 показаны значения $I_{эфф}$, полученные из экспериментально измеренных угловых распределений осколков деления ядер с различными Z^2/A. Как видно из рисунка, значение $I_{эфф}$ оказывается однозначной функцией параметра делимости Z^2/A и не зависит в пределах точности измерения от способа образования, энергии возбуждения и углового момента делящегося ядра. Этот факт находится в противоречии с результатами работы [5], но, как показано в [6], это связано лишь с тем, что авторы работы [5] неточно определяли угловой момент компаунд-ядер в реакциях с тяжелыми ионами, и эти неточности переводились в неточность определения $I_{эфф}$, который поэтому оказался сильно зависящим от энергии бомбардирующих частиц для одной и той же пары мишень — частица. Кроме того, результаты, показанные на рис.1, находятся в хорошем согласии с эффективными моментами инерции, полученными из угловых распределений осколков деления тяжелых ядер дейтонами и и α-частицами [7]. Интересно сопоставить экспериментальные данные с расчетами равновесной деформации ядер по обычной жидко-капельной модели [8]. Как видно из рис.1, качественное согласие имеется, но при больших Z^2/A обнаруживается значительное расхождение в значениях $I_{эфф}$, что указывает на меньшую деформацию ядра в седловой точке по сравнению с формой, полученной по капельной модели.

Разногласие, однако, практически устраняется, если (по-прежнему в рамках капельной модели) учесть диффузность поверхности ядра и ввести в расчет $I_{эфф}$ зависимость поверхностного натяжения от кривизны эффективной поверхности [9].

Согласие расчета с экспериментальными данными является важным обстоятельством и может свидетельствовать о том, что капельная модель является хорошим приближением при расчете потенциальной энергии и формы ядра в седловой точке. Наряду с этим, предположение о статистическом равновесии ядра на вершине барьера,по-видимому, является справедливым для всех исследованных ядер.

Крайняя точка на рис.1 при $\frac{Z^2}{A} = 43{,}5$, полученная из углового распределения ядер ^{140}La при делении ^{238}U ионами ^{40}Ar соответствует значению $\frac{I_{сф}}{I_{эфф}} = 0{,}1$. Благодаря этому, непосредственно из эксперимента можно определить достаточно точно основной параметр капельной модели $-(Z^2/A)_{крит.}$, определяющий предел стабильности ядерной материи по отношению к делению. Экстраполяция $\frac{I_{сф}}{I_{эфф}} \to 0$ (сферическая форма ядра в седловой точке) дает $\left(\frac{Z^2}{A}\right)_{крит} = 46 \pm 1$.

Отметим, что эти выводы, сделанные из экспериментально определенных значений $I_{эфф}$ для ядер с различными Z^2/A, не являются абсолютно однозначными. В принципе можно предполагать, что седловая точка не является сколько-нибудь выделенным состоянием среди всех других, проходимых ядром при делении. При этом, если полное время деформации ядра от сферической формы к разрыву больше, чем характерное время ядерного вращения, то будет возникать анизотропия осколков деления, и $I_{эфф}$, определяемый из этой анизотропии, будет относиться к некоторой средней форме ядра на пути от сферы к разделению на два осколка. В такой гипотезе при некоторых предположениях о процессе деления,по-видимому, возможно объяснить наблюдаемую на опыте зависимость $I_{эфф}$ от Z^2/A, даже не требуя того, чтобы $\left(\frac{Z^2}{A}\right)_{крит.} = 46$. Более подробное рассмотрение этой гипотезы, однако, свидетельствует, что для ее справедливости требуются гораздо более сильные и необычные предположения о процессе деления, чем те, которые были использованы в первом варианте интерпретации результатов.

В последние годы ряд авторов предсказывает существование "острова" стабильности в районе сверхтяжелых ядер. Учет оболочечной поправки в энергии деформации ядер приводит к существенной величине барьера деления у очень тяжелых ядер с $Z > 108$, которые согласно жидко-капельной модели деления обладают очень малым барьером деления и формой ядра в седловой точке, близкой к сфере. Данные же по $I_{эфф}$ показывают согласие с жидко-капельной моделью вплоть до компаунд-ядер с $Z = 110$ (реакция $^{238}U(^{40}Ar, f)$). Однако значения $I_{эфф}$ получены экспериментально для очень нейтронно-дефицитных ядер, которые согласно расчетам [10] не должны обладать никакой повышенной стабильностью; барьер деления для этих ядер с учетом оболочечных эффектов практически не отличается от жидко-капельного. Поэтому согласие экспериментальных данных с жидко-капельной теорией для нейтронно-дефицитных ядер не может говорить об отсутствии высокого барьера деления у ядер с числом нейтронов вблизи $N = 184$.

2. МАССОВЫЕ РАСПРЕДЕЛЕНИЯ ОСКОЛКОВ ДЕЛЕНИЯ ВОЗБУЖДЕННЫХ ЯДЕР

Выше было показано, что делящееся ядро достаточно долго находится в квазистационарном состоянии вблизи вершины барьера. Дальнейшее развитие процесса – движение от седловой точки к разрыву – определяет кинетические энергии, массы и заряды возникающих осколков. Если ядро на всех этапах этого движения находится в термодинамическом равновесии, то для определения основных характеристик деления достаточно рассматривать лишь конечную стадию процесса – точку разрыва. Предыстория процесса в этом случае никаким образом не будет влиять существенно в определении массы, заряда и кинетической энергии осколков, которые следует вычислить методами статистической механики, применительно к состоянию ядра в момент разрыва.

Для высоковозбужденных состояний ядра неадиабатические процессы перераспределения энергии между различными степенями свободы становятся весьма существенными. На языке жидко-капельной модели это означает, что нагретое ядро, по-видимому, обладает значительной вязкостью. Последняя способствует установлению термодинамического равновесия в системе, и предположение о наличии его на всем пути от седла до точки разрыва при делении высоковозбужденных ядер кажется обоснованным.

Поэтому представляет принципиальный интерес сравнение предсказаний статистической теории с экспериментом. Экспериментальные данные [11-13] по массовым и зарядовым распределениям осколков деления сравнительно легких ядер с Z^2/A от 30 до 35 находятся в неплохом согласии со статистической теорией. Безусловно, особый интерес представляет изучение деления очень тяжелых компаунд-ядер с параметром делимости, приближающимся к критическому значению.

Ниже будут представлены результаты опытов по измерению массовых распределений осколков деления [14] для ядер с Z^2/A от 37,5 до 43,5.

При облучении тонких мишеней ^{209}Bi и ^{238}U радиохимическим методом выделялись осколки редкоземельной группы и, в ряде случаев, тяжелые осколки от Au до Po, At [15].

В дальнейшем с помощью γ-спектрометра измерялась γ-радиоактивность осколков, и полученный спектр обрабатывался с целью идентификации изотопов и определения их вывода по известным γ-переходам, соответствующим данным ядра. Такая методика измерений оказалась достаточно надежной и давала точность в определении выхода не хуже 15%.

Для построения массовых распределений были приняты предположения о зарядовом распределении осколков, которые в дальнейшем проверялись экспериментально.

1. Для каждой массы осколка A_f выход изобаров с Z, отличными от наиболее вероятного значения $Z_p(A_f)$, описывается функцией Гаусса:

$$P_{A_f}\,(Z - Z_p(A_f)) = \frac{1}{\sqrt{\pi\sigma_z^2}}\exp\left(-\frac{(Z - Z_p(A_f))^2}{\sigma_z^2}\right)$$

2. Зависимость Z_p от A_f рассчитывалась в следующих предположениях:

а) пропорциональность заряда массе осколка;

б) равное смещение зарядов:

$$Z_p(A_{f_1}) = \frac{Z_c}{2} - \frac{Z_a(A_{f_1}) - Z_a(A_{f_2})}{2}$$

в) распределение заряда из условия минимума потенциальной энергии формирующихся осколков в момент разделения [16]. Предполагалось также, что нейтроны испаряются из осколков [17] ($\Gamma_n/\Gamma_f \ll 1$) в количестве, пропорциональном массе осколка

$$\nu_{A_f} = \frac{\nu}{A_c} A_f$$

С помощью электронно-вычислительной машины методом наименьших квадратов производился подбор параметров ν и σ_z^2 для различных зависимостей $Z_p(A_f)$, дающих наименьшее отклонение экспериментальных точек от плавной кривой, которая, как и ожидалось, удачно описывается распределением Гаусса:

$$P(A_f - A_c/2) = \frac{1}{\sqrt{\pi\sigma^2}}\exp\left(-\frac{(A_f - A_c/2)^2}{\sigma^2}\right)$$

с одним параметром σ^2.

При таком методе не отдается предпочтение той или иной гипотезе относительно зарядового распределения осколков. Последнее вытекает из наилучшего самосогласования экспериментальных точек массовой кривой.

ТАБЛИЦА 1. ЭКСПЕРИМЕНТАЛЬНЫЕ ДАННЫЕ, ПОЛУЧЕННЫЕ ПРИ ИЗМЕРЕНИИ МАССОВЫХ РАСПРЕДЕЛЕНИЙ ОСКОЛКОВ ДЕЛЕНИЯ ЯДЕР ТЯЖЕЛЫМИ ИОНАМИ

	$\frac{Z^2}{A}$	E_t^* (Мэв)	$\langle\sigma\rangle^2$	$\bar{\nu}$	σ_z^2
$^{209}Bi(^{20}Ne, f)$	37,7	100	710	10,8	0,56
$^{238}U(^{12}C, f)$	38,4	42			
$^{238}U(^{16}O, f)$	39,4	81	1280	11,2	1,7
$^{238}U(^{20}Ne, f)$	40,5	120	2280	12,6	3,3
		95	1660	11,5	2,9
		65	1130	8,9	2,7
$^{209}Bi(^{40}Ar, f)$	41,0	115	2200	9,5	2,75
$^{238}U(^{40}Ar, f)$	43,5	110	2790	13,3	3,0
		75	1980	10,6	2,9

Экспериментальные данные представлены в табл.1. Для всех реакций было найдено, что наихудшее согласие получается в предположении пропорциональности заряда массе осколка, в то время как для двух других случаев результаты практически совпадают.

Спектры масс осколков деления даны на рис.2. Используя зависимость ширины массового распределения от температуры ядра, можно получить характер изменения σ^2 от параметра Z^2/A при фиксированной энергии возбуждения. Как видно из рис.3, при $\frac{Z^2}{A} > 38$ наблюдается резкое расширение массовой кривой.

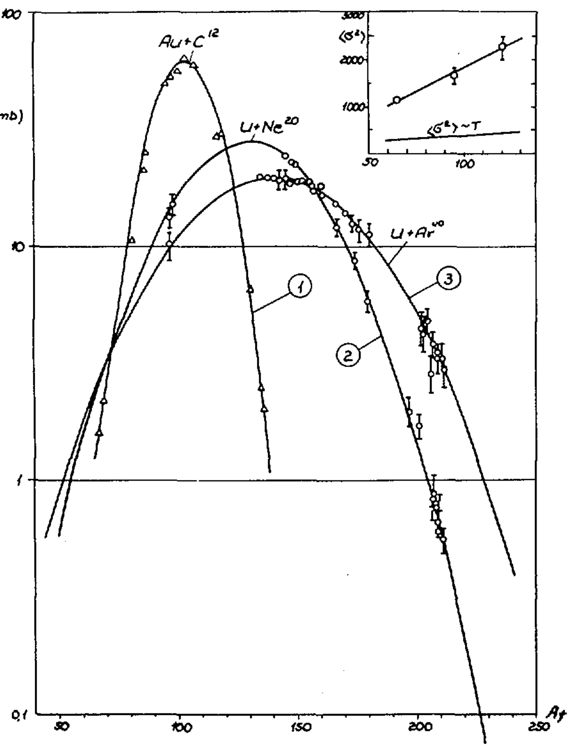

Рис.2. Спектры масс осколков деления: кривые 2 и 3 – результаты данной работы; кривая 1 – результаты работы [12].

Теперь интересно сравнить экспериментальные данные с расчетами по статистической теории. Известны несколько типов подобных расчетов; мы остановимся на методе, предложенном в работе [16], как наиболее удобном и достаточно точном.

В рамках статистической теории вероятность деления с заданным отношением масс осколков равна:

$$P(A_f) \sim \exp\left(-\frac{(A-\overline{A})^2}{\overline{A}^2\langle\Delta\delta\rangle^2}\right)$$

где

$$\overline{A} = \frac{A_c}{2}; \quad \delta = \frac{1}{2}\left(1 - \frac{2A_f}{A_c}\right); \quad \langle\Delta\delta\rangle^2 = T\left(\frac{1}{2}\ \frac{\partial^2 W}{\partial\delta^2}\right)^{-1}_{\delta=\overline{\delta}}$$

Здесь T – температура ядра,

$\frac{\partial^2 W}{\partial\delta^2}$ – вторая производная полной потенциальной энергии ядра, которая, согласно [16], может быть представлена в виде:

$$\frac{\partial^2 W}{\partial\delta^2} = \alpha_1\Delta E_s + \alpha_2\Delta E_c - \alpha_3\overline{E} - \alpha_4 E_{ds} + \alpha_5 E_{dc} - \alpha_6 A_c^{7/3}$$

где $\alpha_1, \alpha_2, \ldots, \alpha_6$ – постоянные коэффициенты,

ΔE_s, ΔE_c – разность поверхностной и кулоновской энергий для начального (сферического) ядра и двух (сферических) осколков,

E_{ds}, E_{dc} – поверхностная и кулоновская энергии деформации осколков в момент разрыва,

$\overline{E}$ – энергия кулоновского взаимодействия осколков, равная суммарной кинетической энергии; последняя весьма точно определяется из экспериментальной зависимости [18].

$$\overline{E} = (0{,}1065\ \frac{Z_c^2}{A_c^{1/3}} + 20{,}1)\ \text{Мэв}$$

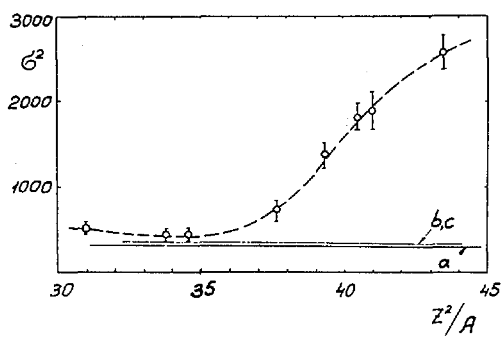

Рис.3. Зависимость дисперсии массы осколков деления от Z^2/A делящегося ядра: кривые a, b, c – расчет по статистической теории [16] с использованием различных массовых формул [19–21].

При расчете потенциальной энергии ядра использовались различные формулы масс ядер [19 – 21]. Сопоставление теоретических и экспериментальных данных на рис.3 показывает, что относительное согласие имеется лишь для области легких ядер, в то время как при $Z^2/A > 38$ наблюдается существенное различие, значительно выходящее за рамки ошибок. Отметим, что столь большое разногласие не может быть устранено никакими вариациями параметров теории в разумных пределах.

Из опытов следует также, что зависимость σ^2 от энергии возбуждения более резкая, чем это следует из теории, где $\sigma^2 \sim T$.

3. ЗАРЯДОВЫЕ РАСПРЕДЕЛЕНИЯ ОСКОЛКОВ ДЕЛЕНИЯ ВОЗБУЖДЕННЫХ ЯДЕР

Весьма важные данные для понимания механизма процесса деления могут быть получены при измерении величины дисперсии массы осколка с данным зарядом (изотопные распределения), либо дисперсии заряда для определенной массы осколка (изобарные распределения).

В статистической теории деления [16] изобарное распределение осколков описывается распределением Гаусса:

$$P_{A_f}(Z - Z_p) \sim \exp\left(-\frac{(Z - Z_p)^2}{\langle \Delta Z \rangle^2}\right)$$

где $Z_p(A_f)$ – наиболее вероятное значение заряда для изобаров с массой A_f и $\langle \Delta Z \rangle^2$ равно:

$$\langle \Delta Z \rangle^2 = \frac{A_c T}{16\beta}$$

где A_c и T – масса и температура делящегося ядра,
β – коэффициент в массовой формуле (типа формулы Вайцзеккера) при энергии симметрии ядра

$$\epsilon_{\text{сим.}} = \beta\,\frac{(A - 2Z)^2}{A}$$

Видно, что дисперсия заряда определяется лишь изменением изотопического члена энергии связи ядра при отклонении заряда осколков от наиболее вероятных значений и не зависит от изменений кулоновской энергии системы, так как $\frac{\partial^2 \epsilon_{\text{сим.}}}{\partial Z^2} \gg \frac{\partial^2 \epsilon_{\text{кул.}}}{\partial Z^2}$.

Отсюда следует, что дисперсия заряда осколка не должна зависеть от его массы, так как изменения формы разрывной фигуры и соответствующие изменения кулоновской и поверхностной энергий системы в данном случае несущественны.

Экспериментальные данные о зарядовом распределении осколков деления весьма ограниченны. Это связано с использованием в большинстве работ константы ширины зарядового распределения σ_Z^2 лишь как некоего свободного параметра для наилучшего согласования экспериментальных данных по массовому распределению. При этом значение σ_Z^2 извлекается косвенным образом в предположении, что последнее является универсальной постоянной для всех масс осколков деления в данной реакции.

Поэтому имевшиеся до настоящего времени сведения о зарядовом распределении осколков деления возбужденных ядер невозможно было систематизировать для получения зависимости дисперсии заряда от асимметрии деления, а также от энергии возбуждения и Z^2/A делящегося ядра. Ниже будут представлены результаты систематических измерений зарядовых распределений осколков, возникающих при делении возбужденных ядер с $\frac{Z^2}{A} > 38$.

ТАБЛИЦА 2. НЕКОТОРЫЕ РЕЗУЛЬТАТЫ ЭКСПЕРИМЕНТАЛЬНОГО ИЗУЧЕНИЯ ДИСПЕРСИИ ЗАРЯДА ОСКОЛКОВ РЕДКОЗЕМЕЛЬНЫХ ЭЛЕМЕНТОВ, ОБРАЗУЮЩИХСЯ ПРИ ДЕЛЕНИИ ЯДЕР ^{238}U РАЗЛИЧНЫМИ ТЯЖЕЛЫМИ ИОНАМИ

Реакция	Энергия падающего пучка E_p(Мэв)	$\frac{Z^2}{A}$	Энергия возбуждения составного ядра E (Мэв)	σ_A^2	Полное число нейтронов на деление $\bar{\nu}$	σ_A^2
$^{238}U(^{12}C, f)$	82	38,4	45	11± 1,0	8	1,6± 0,15
$^{238}U(^{20}Ne, f)$	195 166 141 116	40,3	115 90 70 50	22± 1,0 20± 1,0 18,5± 1,0 16,5± 1,5	13,5 12,5 10,5 8	3,1± 0,15 2,8± 0,15 2,6± 0,15 2,3± 0,15
$^{238}U(^{22}Ne, f)$*	173	40,0	75	18,5± 1,0	12	2,6± 0,15
$^{238}U(^{40}Ar, f)$*	270	43,5	70	20,8± 1,5	11	2,85± 0,20

Методика измерений, по существу, являлась той же самой, что и в опытах по массовым распределениям. Из продуктов деления радиохимическим способом выделялись поэлементно редкие земли, теллур, барий и золото. В качестве бомбардирующих частиц использовались ионы от ^{12}C до ^{40}Ar с различной энергией.

Подробный анализ результатов, точности измерений, возможных систематических ошибок проделан в работах [22,23]. Здесь будут представлены лишь окончательные результаты и дано их физическое обсуждение.

В табл.2 суммированы некоторые результаты этих опытов. Значения σ_A^2 и σ_Z^2 измерены для осколков редкоземельной группы от La до Gd (σ_A^2 — дисперсия по массе осколков с фиксированным Z).

На рис.4 представлена зависимость дисперсии заряда осколков σ_Z^2 от асимметрии деления A_{1f}/A_{2f} для реакций $^{238}U(^{20}Ne, f)$; $^{238}U(^{40}Ar, f)$; наблюдается существенное уменьшение дисперсии с ростом A_{1f}/A_{2f}.

Рис.5 содержит зависимость σ_Z^2 от энергии возбуждения делящегося ядра, которая оказалась более плавной функцией, чем $\sigma_Z^2 \sim T$. На рис.6 изображена зависимость σ_Z^2 от параметра делимости Z^2/A составного ядра при энергии возбуждения ~ 100 Мэв для симметричного деления $\left(\frac{A_{1f}}{A_{2f}} = 1\right)$. При $\frac{Z^2}{A} > 37$ наблюдается резкое увеличение дисперсии заряда, подобное тому, которое наблюдалось для дисперсии осколков деления по массе. На рис.4, 5 и 6 приведены также результаты расчетов по статистической теории [16] с использованием различных полуэмпирических формул для масс ядер.

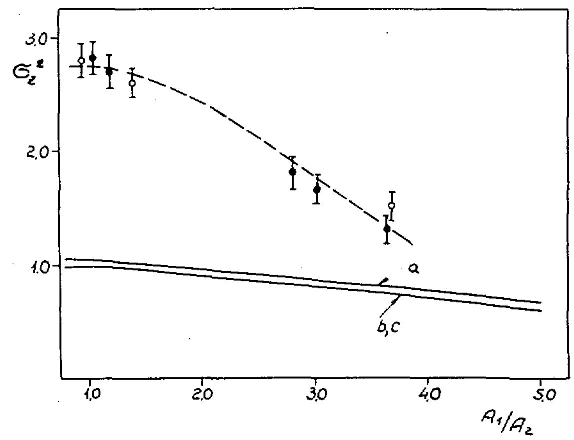

Рис.4. Зависимость дисперсии заряда осколков от асимметрии разделения ядра A_1/A_2. Экспериментальные данные получены для реакции ^{238}U (^{20}Ne, f) и ^{238}U (^{40}Ar, f).

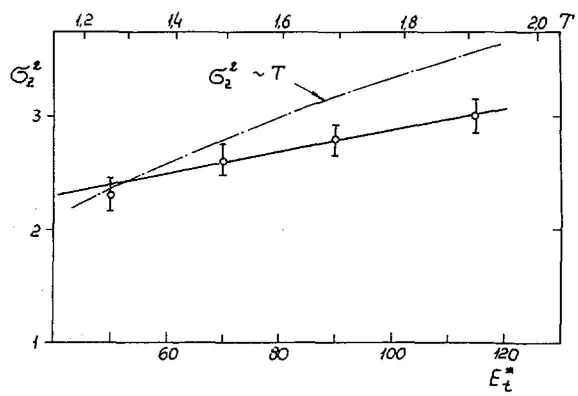

Рис.5. Зависимость дисперсии заряда осколков от энергии возбуждения делящегося ядра в реакции ^{238}U (^{20}Ne,f).

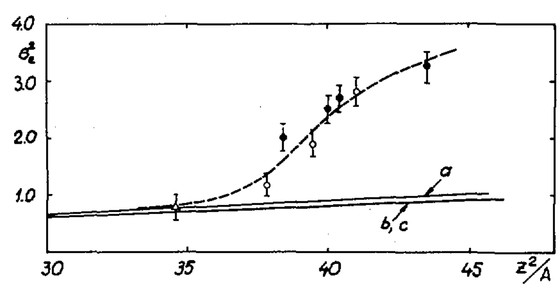

Рис. 6. Зависимость дисперсии заряда осколков от Z^2/A делящегося ядра.

4. ОБСУЖДЕНИЕ ЭКСПЕРИМЕНТАЛЬНЫХ ДАННЫХ ПО МАССОВЫМ И ЗАРЯДОВЫМ РАСПРЕДЕЛЕНИЯМ

Данные по массовым распределениям, представленные в табл.1 и на рис.2 и 3, находятся в резком противоречии с предсказаниями статистической теории, что особенно ярко проявляется в зависимости σ^2 от Z^2/A (см. рис.3), для которой статистическая теория предсказывает плавный спад с ростом Z^2/A. Следует отметить сейчас, что условия статистического равновесия в системе, необходимые для применимости статистической теории, как отмечалось в работе [24], различны для различных степеней свободы системы. Для установления статистического равновесия системы, например по отношению к асимметричным колебаниям формы, требуется, чтобы характерное время поступательной необратимой деформации ядра было значительно больше периода асимметричных колебаний: $\tau_{деф.} \gg \tau_{асим.\,кол.}$. Для установления равновесного распределения энергии во вращательных степенях свободы ядра требуется, чтобы $\tau_{деф.} \gg \tau_{вращ.}$. Подобные неравенства, вероятно, можно написать и для других степеней свободы. Отсюда следует, что при рассмотрении различных характеристик деления необходимо использовать различные критерии применимости статистической теории. Вообще, наверное, невозможно написать единый критерий применимости статистической теории для описания всех сторон процесса деления.

Неравные массы двух осколков возникают в результате асимметричных отклонений формы делящегося ядра от наиболее вероятной формы, которая в жидко-капельной модели симметрична. Поэтому для применимости статистической теории требуется выполнение условия $\tau_{деф.} \gg \tau_{асим.\,кол.}$. В ряде работ, см. например [25], дается оценка $\tau_{асим.кол.} \approx 10^{-21}$ сек. В предыдущем разделе дана оценка $\tau_{спуска} \approx (0{,}5 \div 1)\cdot 10^{-20}$ сек, в работе Никса [26] $\tau_{спуска} \approx (2 \div 3)\cdot 10^{-21}$ сек. Видно, что $\tau_{асим.\,кол.}$ не намного меньше времени спуска с вершины барьера в точке разрыва, поэтому нельзя считать обоснованной применимость статистической теории для расчета массовых распределений осколков деления сильновозбужденных тяжелых деформированных ядер.

Отметим, однако, что для небольших значений $\frac{Z^2}{A} < 36$ точка разрыва практически совпадает с седловой точкой, а в последней ядро, по-видимому, проводит время, достаточное для установления статистического равновесия по отношению к колебаниям (см. раздел 1). Поэтому в таком случае возможно проводить статистический расчет массового распределения с использованием седловых фигур и присущих им жесткостей к асимметричным вариациям формы. Для больших Z^2/A, когда время спуска сравнимо с временем асимметричных колебаний, незаконен расчет массового распределения с помощью статистической теории, примененной к точке разрыва. Незаконно также использовать равновесные характеристики ядра в седле для непосредственного определения массового распределения осколков. Необходимо решать динамическую задачу спуска с вершины барьера к точке разрыва при начальных условиях, определенных из предположения о наличии термодинамического равновесия в седловой точке.

Подобный расчет был проделан Никсом в работе [26], однако, его результаты также не согласуются с нашими данными по массовым распределениям. Последнее обстоятельство связано, вероятно, с тем, что расчет Никса, во-первых, неприменим для области $\frac{Z^2}{A} > 39-40$ из-за неточной аппроксимации седловых фигур в этой области с помощью выбранных в расчете функций. Во-вторых, жесткости фигур к асимметричным вариациям формы, рассчитанные Никсом, существенно отличаются от результатов работы Струтинского [27].

Можно высказать предположение, что в первом приближении динамический расчет массового распределения можно заменить статистическим расчетом, не применяемым ни к седлу, ни к точке разрыва, а использующим некоторые эффективные средние жесткости ядра на всем его пути от седла до разрыва. Оценки показывают, что при использовании жесткостей, рассчитанных Струтинским [27], подобный грубый расчет может дать значения σ^2 для массовых распределений, согласующиеся с экспериментом.

Перейдем к обсуждению результатов по дисперсии заряда осколков фиксированной массы. Отклонения заряда будущего осколка от наиболее вероятного равновесного значения происходят в результате температурных флуктуаций плотности заряда в объеме делящейся системы. Поэтому критерием применимости термодинамического способа к расчету дисперсии заряда осколков вероятно следует считать условие $\tau_{\text{дип. кол.}} \ll \tau_{\text{деф.}}$. Здесь $\tau_{\text{дип. кол.}}$ – период дипольных колебаний ядра, т.е. колебаний центра заряда системы относительно ее центра инерции.

Известно, что частота этих колебаний чрезвычайно высока ($\hbar\omega_g \approx 15$ Мэв), так что $\tau_{\text{дип.кол.}} < 10^{-22}$ сек. Поэтому можно быть уверенным в справедливости соотношения $\tau_{\text{дип.кол.}} \ll \tau_{\text{деф.}}$ и применимости статистических расчетов для описания дисперсии заряда осколков данной массы.

Экспериментальные данные для всех изученных нами реакций свидетельствуют о том, что зависимость наиболее вероятного заряда осколков деления, от их массы – $Z_p(A_f)$ хорошо согласуется с гипотезой равного смещения заряда (РСЗ). Это обстоятельство противоречит обычно принятым предположениям, например [28], что при высоких энергиях возбуждения делящегося ядра заряд должен распределяться пропорционально массе осколка. Последнее утверждение всегда основывалось на том, что отличие функции $Z_p(A_f)$ от $Z_p(A_f) = \frac{Z_c}{A_c} A_f$ для низкоэнергичного деления связано с застройкой оболочечной структуры осколков в процессе разделения ядра.

Гипотеза РСЗ является, с нашей точки зрения, одной из простейших формулировок гипотезы распределения заряда из условия минимума потенциальной энергии (МПЭ) системы разделяющихся осколков. Только отличия $Z_p(A_f)$ от расчетных по гипотезам РСЗ и МПЭ могут связываться с влиянием оболочек в осколках. Согласие же экспериментальных $Z_p(A_f)$ с расчетом по гипотезам РСЗ и МПЭ свидетельствует лишь о наличии термодинамического равновесия в делящейся системе по отношению к дипольным колебаниям, так что система успевает "почувствовать" имеющийся минимум потенциальной энергии в зависимости от распределения заряда между будущими осколками. Это обстоятельство не является неожиданным, оно следовало из вышеприведенных оценок времен.

Перейдем к обсуждению параметра ширин зарядового распределения σ_Z^2 в зависимости от Z^2/A, E^* и параметра асимметрии деления A_{1f}/A_{2f} [23].

Как видно из рис.6, удовлетворительное согласие экспериментальных точек с расчетами по статистической теории деления, наблюдаемое для области легких ядер $\frac{Z^2}{A}<38$, сменяется резким расхождением при больших Z^2/A. В [23] было показано, что учет всех побочных факторов эксперимента не может сколько-нибудь существенно изменить измеренные значения, чтобы улучшить это согласие. В то же время никакое изменение параметров теории в разумных пределах не может привести к согласованию теории и эксперимента.

Обратим внимание на то обстоятельство, что в статистической теории не учитывается одна из важных сторон процесса деления, которая может оказать существенное влияние на дисперсию заряда осколков. Даже при наличии термодинамического равновесия в системе для разрывной фигуры, сам разрыв шейки существенно нестационарен. Поэтому нуклоны, находящиеся в шейке, в районе плоскости разрыва будут распределяться между осколками случайным образом. Из-за случайности этого распределения возможны отклонения зарядов осколков от наиболее вероятных значений. Влияние этого эффекта на полное массовое распределение осколков пренебрежимо мало из-за очень большой дисперсии массы осколков. Однако для дисперсии заряда осколков при заданной массе оно может быть очень существенным. Если распределение заряда за счет этого процесса имеет вид распределения Гаусса, то из-за независимости процесса температурной флуктуации плотности заряда в объёме ядра и процесса случайного распределения протонов между осколками на линии разрыва суммарная дисперсия заряда будет равна:

$$\sigma_Z^2 = (\sigma_Z^2)_T + (\sigma_Z^2)_p$$

Рассмотрим вопрос о толщине шейки для разрывной фигуры. Очевидно, что, если диаметр шейки меньше или равен диаметру нуклона, о существовании такой фигуры бессмысленно говорить. В то же время линейные размеры самых тяжелых ядер всего лишь в шесть раз превышают размеры нуклона, и поэтому в жидко-капельном рассмотрении шейка диаметром, близким к размерам нуклона, является еще достаточно толстой шейкой. Если точкой разрыва считать такую форму делящейся системы, для которой кулоновские силы отталкивания двух будущих осколков равны силе поверхностного натяжения в сечении разрыва, то для ядер с большим Z из-за возрастания кулоновских сил должно увеличиваться сечение разрыва. Иными словами, более тяжелые ядра будут иметь разрывные фигуры с более толстой шейкой.

Легко показать, что, в первом приближении, при условии постоянства коэффициента поверхностного натяжения с изменением Z^2/A делящегося ядра радиус шейки разрывной фигуры будет пропорционален $Z^2/A^{2/3}$. Увеличение толщины рвущейся шейки с ростом Z должно приводить к увеличению дисперсии заряда осколков деления $(\sigma_Z^2)_p$. Зависимость радиуса шейки от заряда делящегося ядра – достаточно сильная функция, поэтому возможно, что таким образом удастся объяснить сильное уширение зарядового распределения осколков деления при $\frac{Z^2}{A} > 38$.

Из-за того, что силы кулоновского отталкивания пары осколков уменьшаются с увеличением A_{1f}/A_{2f}, должно наблюдаться уменьшение толщины рвущейся шейки и, следовательно, уменьшение дисперсии заряда с увеличением параметра асимметрии разделения. Это находится в качественном согласии с экспериментальными данными, представленными на рис.4.

Составляющая дисперсии заряда, связанная с флуктуацией нуклонов на линии разрыва, по-видимому, должна очень слабо зависеть от температуры ядра, если с изменением температуры ядра не меняется разрывная форма и толщина рвущейся шейки. Поэтому полная дисперсия заряда осколков, включающая в себя и член $(\sigma_Z^2)_T$, который возрастает за счет температурной флуктуации объемной плотности заряда, должна быть более слабой функцией температуры, чем $\sigma_Z^2 \sim T$, что и наблюдается в опыте (см. рис.5).

Возвращаясь к массовым распределениям осколков деления, отметим, что при формировании массы осколков существенную роль может играть флуктуация места разрыва шейки. Это приведет к ненулевой дисперсии массы даже при полном отсутствии асимметричных флуктуаций формы делящейся системы. Этот эффект никак не учитывается в статистической теории, хотя он может быть весьма существенным для сравнительно узких массовых распределений. Трудно, однако, предположить, что подобного рода эффекты могут объяснить столь сильное расширение массовых распределений, как это наблюдается на опыте для тяжелых ядер $\left(\frac{Z^2}{A} > 38\right)$.

Отметим, что из экспериментальных данных, кроме изложенных физических результатов, следуют два интересных обстоятельства, не затрагивающие непосредственно вопрос о механизме двойного деления возбужденных ядер.

1. Широкие массовые распределения, в реакциях $^{238}U(^{20}Ne, f)$ и $^{238}U(^{40}Ar, f)$, приводят к образованию в этих реакциях с значительным сечением тяжелых ядер-осколков с массой $A_f = 180 \div 210$. Последние, обладая значительной энергией возбуждения, могут с определенной вероятностью поделиться. Таким образом, исходное компаунд-ядро в этом случае делится в конечном итоге на три осколка сравнимой массы. Этот интересный процесс каскадного деления на три осколка изучен экспериментально и теоретически в работах [29, 30].

2. Чрезвычайно широкие массовые и зарядовые распределения осколков при делении ядер тяжелыми ионами позволяют говорить о возможности использования этих реакций в качестве орудия синтеза большого числа изотопов, далеких от области стабильности [31]. Использование еще более тяжелых бомбардирующих частиц, таких, как Kr, Xe, вероятно, позволит получать в качестве осколков деления самые тяжелые элементы периодической системы Менделеева и, возможно, даже элементы с $Z > 110$, гипотетическая стабильность которых в настоящее время активно обсуждается в литературе [21, 32 – 34].

Был проведен грубый экстраполяционный расчет сечений образования трансурановых элементов как осколков деления в реакции $^{238}U(^{136}Xe, f)$. Дисперсии заряда и массы осколков в этой реакции определялись путем экстраполяции имеющихся экспериментальных данных, полученных при делении ядер тяжелыми ионами от ^{12}C до ^{40}Ar. Наиболее вероятный заряд осколков и число нейтронов, испускаемых в акте деления, рассчитывались так же, как и в изученных реакциях. Энергия возбуждения оценивалась на основе расчетов кулоновского барьера слияния ядер ^{136}Xe

и ^{238}U с учетом деформации ядер при соударении [35] и оценок масс сверхтяжелых ядер на основе формул массы ядер [20, 23]. Сечения образования сверхтяжелых компаунд-ядер рассчитывались по способу работы [36], использовались Γ_n/Γ_f для нуклидов гипотетической новой области стабильности и трансурановых элементов, приведенные в той же работе [36].

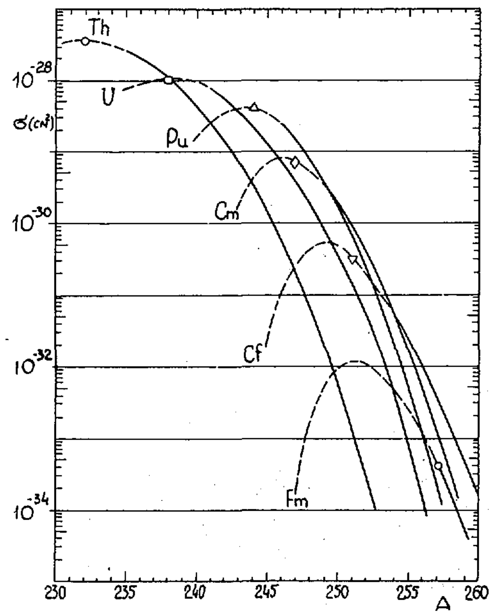

Рис.7. Рассчитанные изотопные распределения актинидов — продуктов реакции ^{238}U (^{136}Xe, f). Для каждого элемента указан наиболее стабильный изотоп.

На рис.7 показаны рассчитанные изотопные распределения актинидов — продуктов реакции $^{238}U(^{136}Xe, f)$. Видно, что очень тяжелые изотопы этих элементов (такие, как ^{250}Th, ^{254}U) могут быть получены в этой реакции с сечением $> 10^{-32}$ см^2. Резкий спад сечения для элементов с $Z > 100$ связан с возрастанием делимости Γ_f/Γ_n этих ядер. Были рассчитаны также сечения образования нейтронно-обогащенных изотопов, близких к линии β-стабильности для элементов из гипотетической новой области стабильности. Для образования изотопов $^{298}114$ и $^{294}110$ получены следующие результаты: $\sigma_{114} = 0{,}8 \cdot 10^{-29}$ см^2 и $\sigma_{110} = 0{,}7 \cdot 10^{-30}$ см^2.

Данный расчет содержал ряд предположений, недостаточно проверенных экспериментально, поэтому результаты расчета следует рассматривать как верхние границы сечений образования трансурановых элементов в реакции $^{238}U(^{136}Xe, f)$. Подробно этот расчет описан в работе [37].

5. ОБ ИЗМЕРЕНИИ СРЕДНЕГО ЧИСЛА НЕЙТРОНОВ $\bar{\nu}$ НА АКТ ДЕЛЕНИЯ ЯДЕР ТЯЖЕЛЫМИ ИОНАМИ

До настоящего времени в литературе не имелось сведений о непосредственном измерении числа нейтронов, возникающих при делении ядер тяжелыми ионами.

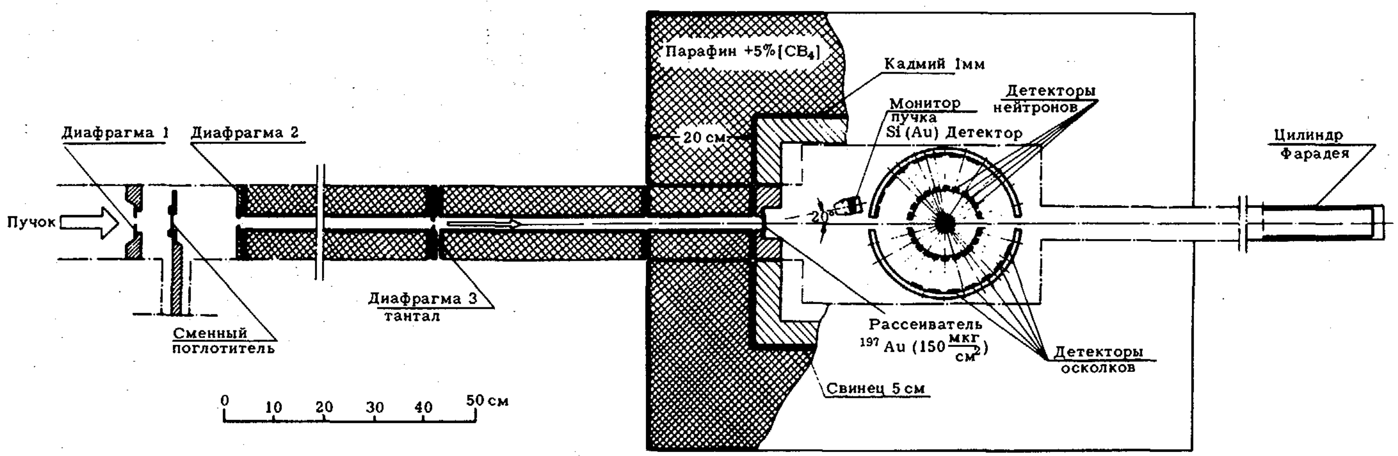

Рис.8. Схема опыта по непосредственному измерению числа $\overline{\nu}$ на акт деления ядер тяжелыми ионами.

Оценить величину $\bar{\nu}$ можно на основе результатов опытов по измерению массы и заряда изотопов – продуктов деления. Возможен также грубый расчет $\bar{\nu}$ на основе известной энергии возбуждения делящегося ядра в предположении, что последняя полностью переходит в энергию возбуждения осколков. Однако точность подобных оценок не высока, поэтому для определения числа $\bar{\nu}$ и его зависимости от энергии возбуждения и Z и A делящегося ядра безусловно необходима постановка прямых экспериментов.

Постановка наших опытов заключалась в одновременном измерении числа и углового распределения нейтронов и осколков деления, вылетающих из точки делящейся мишени при облучении ее пучком ускоренных тяжелых ионов. При этом высокие требования предъявляются из-за присутствия интенсивных фоновых потоков γ-лучей, нейтронов (быстрых и медленных) и заряженных частиц. В опытах для регистрации нейтронов применялись стекла, находившиеся в контакте с делящимся веществом-нептунием (^{237}Np). Детекторы были чувствительны к γ-лучам с энергией выше барьера деления ^{237}Np ($E_\gamma > 6$ Мэв). Однако известно, что в реакциях с тяжелыми ионами возникает быстрое γ-излучение, имеющее чрезвычайно мягкий спектр, $\bar{E}_\gamma = 500$ кэв [38], радиоактивные продукты реакций также не дают столь жестких γ-квантов ($E_\gamma > 6$ Мэв). Поэтому γ-фон можно было считать отсутствующим, детекторы экранировались от попадания заряженных частиц, возникающих на мишени. Важным преимуществом ^{237}Np является то, что он не делится тепловыми нейтронами, и поэтому детектор не чувствителен к фоновым потокам медленных нейтронов. Низкий порог деления ^{237}Np и широкое плато сечения (0,8 - 6 Мэв) обеспечивают неплохую счетную характеристику детектора. Оценки показывают, что спектр нейтронов деления возбужденных ядер должен быть настолько жестким, что влияние ненулевого порога деления ^{237}Np можно не учитывать, так как очень малая часть спектра нейтронов попадает в область нечувствительности детектора.

Схема опыта показана на рис. 8. Детекторы нейтронов помещались на малом кольце, а осколочные детекторы (стекла) – на большом. Тонкие мишени Bi и U изготавливались на Al фольге толщиной 0,7 мк. Пучок мониторировался путем регистрации полупроводниковым детектором ионов, рассеянных на специальной фольге (Au, 0,1 мк). Камера с детекторами была тщательно экранирована многослойной защитой из парафина, кадмия, свинца и железа для устранения фона быстрых нейтронов от внешних источников, которыми являются все детали циклотрона и системы транспортировки пучка, находящиеся под воздействием пучка ускоренных ионов. Коллектор тока и диафрагмы, ограничивающие размер пучка, были вынесены на значительное расстояние от детекторов и располагались вне защиты.

Каждый опыт состоял из двух облучений: одно – кратковременное, малым током для набора статистики на осколочных детекторах, второе – при высокой интенсивности пучка (1 – 3 мка), в течение 3 – 4 часов для измерения числа нейтронов, что связано с низкой эффективностью нейтронных детекторов (10^{-6}). Во время второго облучения осколочные детекторы были закрыты специальным экраном.

Из экспериментальных результатов при введении соответствующих поправок определялись в относительных единицах дифференциальные сечения образования осколков деления и нейтронов в лабораторной системе координат. Осуществлялся перевод дифференциальных сечений из лабораторной системы в систему, связанную с компаунд-ядром с помощью обычных формул:

$$\frac{d\sigma}{d\Omega_c} = \frac{1+\gamma\cos\theta_c}{(1+\gamma^2+2\gamma\cos\theta_c)^{3/2}}\frac{d\sigma}{d\Omega_l}$$

$$\sin(\theta_c - \theta_l) = \gamma\sin\theta_l$$

Средние параметры перевода γ из системы в систему для осколков и нейтронов вычислялись с использованием средних значений энергий осколков и нейтронов в системе компаунд-ядра:

$$\bar{\gamma}_f = \sqrt{\frac{E_b A_b}{\bar{E}_T A_c}}$$

$$\bar{\gamma}_n = \frac{\sqrt{E_b A_b}}{\sqrt{\bar{E}_T A_c + \sqrt{40 E_c^* A_c^3}}}$$

где E_b и $\bar{E}_T$ – кинетические энергии бомбардирующей частицы и пары осколков в сумме соответственно, $\bar{E}_c^*$ – средняя энергия возбуждения компаунд-ядра, A_b и A_c – массы бомбардирующей частицы и компаунд-ядра соответственно. При этом было сделано предположение, что спектр нейтронов в системе, связанной с осколком, есть спектр испарения по Вайскопфу с температурой, определяемой по формуле $E^* = \frac{A}{10}T^2$. Число $\bar{\nu}$ определялось по формуле:

$$\bar{\nu} = c\,\frac{I_f}{I_n}\cdot\frac{\int_0^\pi \frac{d\sigma_n}{d\Omega_n}\sin\theta_c^n\,d\theta_c^n}{\int_0^\pi \frac{d\sigma_f}{d\Omega_f}\sin\theta_c^f\,d\theta_c^f}$$

где С – константа, включающая конкретные характеристики эксперимента, такие, как величины телесных углов $\Delta\Omega_l^f$ и $\Delta\Omega_l^n$, эффективность детекторов и др. I_f и I_n – интегральные интенсивности потока бомбардирующих частиц в облучениях для измерения осколков и нейтронов соответственно. θ_c^f и θ_c^n – полярные углы в системе компаунд-ядра для нейтронов и осколков.

На рис.9 представлена зависимость $\bar{\nu}$ для всех изученных нами реакций, в зависимости от энергии возбуждения компаунд-ядер. Треугольниками обозначены данные, полученные косвенным образом в опытах по измерению массовых и зарядовых распределений осколков деления, круглые точки – результаты непосредственных измерений числа $\bar{\nu}$, произведенных описанным выше образом. Видно, что результаты того и другого типа в пределах точности эксперимента хорошо согласуются. Некоторый разброс точек может быть связан с различием $\bar{\nu}$ для делящихся ядер с разными Z и A, которое при построении графика не учитывалось.

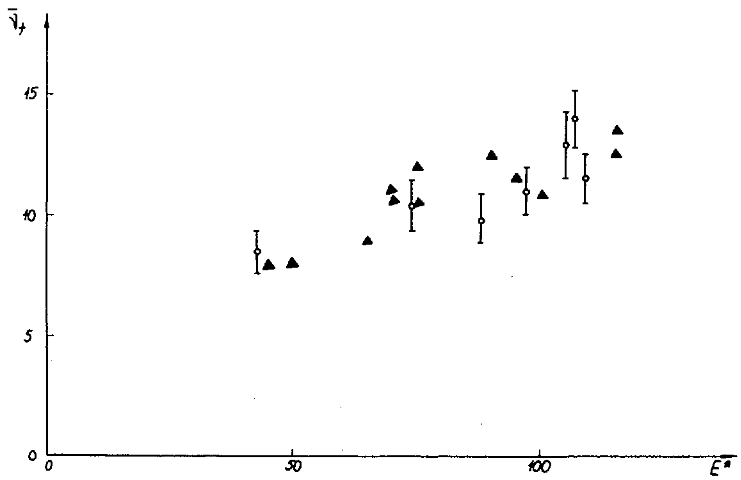

Рис.9. Значения $\bar{\nu}$, в зависимости от энергии возбуждения делящегося ядра: треугольники – результаты косвенного определения $\bar{\nu}$ при измерении массовых и зарядовых распределений осколков деления; круглые точки – данные непосредственных измерений $\bar{\nu}$.

Отсюда можно сделать вывод о справедливости предположений, принятых нами при обработке массовых и зарядовых распределений. Кроме того, экспериментальные точки наглядно демонстрируют зависимость $\bar{\nu}$ от энергии возбуждения делящегося ядра, через точки можно провести прямую линию.

Материал, представленный в данном докладе, свидетельствует о возможности получения ценной информации о механизме деления при использовании ускоренных тяжелых ионов в качестве частиц, вызывающих деление.

ЛИТЕРАТУРА

[1] BOHR, N., WHEELER, I., Phys. Rev. 56 (1939) 426.
[2] ФРЕНКЕЛЬ, Я.И., ЖЭТФ 9 641 (1939).
[3] BOHR, A., Proceed. of the Intern. Conf. on the Peaceful Uses of Atomic Energy (United Nations, New York, 1956) 2 1956, p. 151.
[4] HALPERN, I., STRUTINSKY, V., Proceed. of the Second United Nations Intern. Conf. on the Peaceful Uses of Atomic Energy (Geneva, 1958) 15 1958, p. 408.
[5] VIOLA, V.E., THOMAS, T.D., SEABORG, G.T., Phys. Rev. 129 (1963) 2710.
[6] КАРАМЯН, С.А., КУЗНЕЦОВ, И.В., МУЗЫЧКА, Ю.А., ОГАНЕСЯН, Ю.Ц., ПЕНИОНЖКЕВИЧ, Ю.Э., ПУСТЫЛЬНИК, Б.И., ЯФ 6 (1967) 494.
[7] CHAUDRY, R., VANDENBOSCH, R., HUIZENGA, I.R., Phys. Rev. 126 (1962) 220.
[8] СТРУТИНСКИЙ, В.М., ЛЕЩЕНКО, И.Я., ПОПОВ, И.А., ЖЭТФ 43 (1962) 584.
[9] СТРУТИНСКИЙ, В.М., ЯФ 1 (1965) 821.
[10] МУЗЫЧКА, Ю.А., ПАШКЕВИЧ, В.В., СТРУТИНСКИЙ, В.М., ЯФ 8 (1968) 716.
[11] ГЕРЛИТ, Ю.Б., ГУСЕВА, Л.И., МЯСОЕДОВ, Б.Ф., ТАРАНТИН, Н.И., ФИЛИППОВА, К.Ф., ФЛЕРОВ, Г.И., Сб. "Ядерные реакции при малых и средних энергиях", Москва, 1958, стр. 511.
[12] BLANN, H.M., Phys. Rev. 123 (1961) 1356.
[13] PLASIL, F., BURNETT, D.S., BRITT, H.C., THOMPSON, S.G., Phys. Rev. 142 (1966) 696.

[14] КАРАМЯН, С.А., НОРМУРАТОВ, Ф., ОГАНЕСЯН, Ю.Ц., ПЕНИОНЖКЕВИЧ, Ю.Э., ПУСТЫЛЬНИК, Б.И., ФЛЕРОВ, Г.Н., ЯФ 8 4 (1968) 690.
[15] *КУЗНЕЦОВ, И.В., МАЛЬЦЕВА, Н.С., ОГАНЕСЯН, Ю.Ц., СУХОВ, А.М.*, ЩЕГОЛЕВ, В.А., ЯФ 8 3 (1968) 448.
[16] ПИК-ПИЧАК, Г.А., СТРУТИНСКИЙ, В.М., "Физика деления атомных ядер", Госатомиздат, Москва, 1962, стр.12.
[17] SIKKELAND, T., Preprint UCRL-16348, 1965.
[18] VIOLA, V., SIKKELAND, T., Phys. Rev. 130 (1963) 2044.
[19] GREEN, A.E.S., Phys. Rev. 95 (1954) 1006.
[20] CAMERON, Q.G.W., Canad. J. of Phys. 35 (1957) 1021.
[21] MAYERS, W.D., SWIATECKI, W.J., Nucl. Phys. 81 (1966) 1.
[22] OGANESSIAN, Yu. Tz., Nuclear Structure: Dubna Symposium (1968), IAEA, Vienna, 1968, p.489.
[23] КАРАМЯН, С.А., ОГАНЕСЯН, Ю.Ц., ПЕНИОНЖКЕВИЧ, Ю.Э., ПУСТЫЛЬНИК, Б.И., Препринт ОИЯИ Р7-4024, Дубна, 1968.
[24] ГЕЙЛИКМАН, Б.Т., Proceed. of the Symposium on Physics and Chemistry of Fission, IAEA, Vienna 1 (1965) 121.
[25] ГЕЙЛИКМАН, Б.Т., АЭ 6 (1959) 298.
[26] NIX, J.R., Preprint UCRL-17958, Berkeley, 1968.
[27] СТРУТИНСКИЙ, В.М., ЖЭТФ 45 (1963) 1900.
[28] ОБУХОВ, А.И., ПЕРФИЛОВ, И.А., УФН 92 6 (1967) 21.
[29] КАРАМЯН, С.А., КУЗНЕЦОВ, И.В., ОГАНЕСЯН, Ю.Ц., ПЕНИОНЖКЕВИЧ, Ю.Э., ЯФ 5 (1967) 959.
[30] МУЗЫЧКА, Ю.А., ОГАНЕСЯН, Ю.Ц., ПУСТЫЛЬНИК, Б.И., ФЛЕРОВ, Г.Н., ЯФ 6 (1967) 306.
[31] ФЛЕРОВ, Г.Н., Препринт ОИЯИ Р7-4199, Дубна, 1968.
[32] СТРУТИНСКИЙ, В.М., МУЗЫЧКА, Ю.А., Доклад на Междунар. конф. по физике тяжелых ионов, Дубна, октябрь 1966, Труды конф., вып.2.
[33] МУЗЫЧКА, Ю.А., Препринт ОИЯИ Р7-4133, Дубна, 1968.
[34] NILSSON, S.G., NIX, J.R., SOBICZEWSKY, A., SZYMANSKI, Z., WYCECH, S., GUSTAFSON, C., MOLLER, P., Nucl. Phys. A 115 (1968) 545.
[35] MALY, J., NIX, J.R., Contribution to Intern. Conf. on Nucl. Structure (Tokyo) 224 (1967).
[36] SIKKELAND, T.S., Proc. of the Lysekil Symposium (1966) 539.
[37] КАРАМЯН, С.А., *ОГАНЕСЯН*, Ю.Ц., Препринт *ОИЯИ* Р7-4339, Дубна, 1969.
[38] ОГАНЕСЯН, Ю.Ц., ЛОБАНОВ, Ю.В., МАРКОВ, Б.Н., ФЛЕРОВ, Г.Н., Препринт ОИЯИ Р-1119, Дубна, 1962.

HIGH-RESOLUTION STUDIES OF K X-RAY EMISSION AND THE DISTRIBUTION OF MASS AND NUCLEAR CHARGE IN THE THERMAL-NEUTRON-INDUCED FISSION OF ^{233}U, ^{235}U AND ^{239}Pu *

L.E. GLENDENIN, H.C. GRIFFIN,** W. REISDORF, J.P. UNIK
Argonne National Laboratory, Argonne, Ill.,
United States of America

Abstract

HIGH-RESOLUTION STUDIES OF K X-RAY EMISSION AND THE DISTRIBUTION OF MASS AND NUCLEAR CHARGE IN THE THERMAL-NEUTRON-INDUCED FISSION OF ^{233}U, ^{235}U AND ^{239}Pu. The emission of K X-rays by fission fragments as a function of fragment mass A and nuclear charge (element) Z has been investigated in the thermal-neutron-induced fission of ^{233}U, ^{235}U and ^{239}Pu. Fission-fragment K X-ray spectra were obtained with a Si(Li) detector in coincidence with a pair of surface-barrier detectors which measured the kinetic energies of the complementary fragments for the determination of their masses. The data were recorded event-by-event in a multiparameter system. The yields of K X-rays per fission emitted by fragments in $t < 1$ ns are as follows: ^{233}U - 0.037 (light fragment group), 0.125 (heavy group); ^{235}U - 0.043, 0.120; and ^{239}Pu - 0.070, 0.134. The high resolving power of the X-ray detector (FWHM $\approx$ 800 eV) makes possible a computer analysis of the characteristic K X-ray spectra giving the relative contribution from each element. Near closed nucleon shells it is found that the average K X-ray yields for odd-Z nuclei are enhanced by a factor of two to three relative to the yields from even-Z nuclei. Away from the closed shells the yields increase rapidly with Z and A while the odd-even Z fluctuations tend to be substantially smaller. Differences in average K X-ray yields for a given Z among the three fissionable nuclei are consistent with an observed A (isotopic) dependence and a fixed yield of K X-ray emission for a given fission fragment nucleus (Z, A) in thermal-neutron-induced fission. In spite of the strong dependence of the K X-ray yields on Z and A, information on the primary charge distribution in fission in terms of average nuclear charges as a function of the fragment masses and on charge dispersion width can be obtained. The deviations of the mean primary charges of the fragments from that given by the charge densities of the fissioning nuclei lie in the range of 0.4 to 0.7 charge units for the complementary mass regions 85-110 and 130-155. The primary charge dispersion is narrower (FWHM = 1.10 ± 0.15 charge units) than the post-neutron-emission charge dispersion (FWHM = 1.56 ± 0.12) determined radiochemically. These results appear to have little dependence on total fragment kinetic energy at given mass splits.

INTRODUCTION

To the traditional radiochemical method of measuring mass and charge distributions in fission, new and more direct physical methods have been added [1]. In particular, techniques involving the simultaneous measurement of kinetic energies of complementary fission fragments and their characteristic K x rays have been demonstrated in studies of the spontaneous fission of ^{252}Cf [2,3]. Underlying assumptions are that the characteristic energy of the K x rays identifies the nuclear charge (atomic number) Z of the fragment from which it is emitted and that the masses A of the fragments can be determined from their kinetic energies through the conservation of mass and linear momentum. A considerable improvement

* Work performed under the auspices of the US Atomic Energy Commission.
** Present address: Department of Chemistry, the University of Michigan, Ann Arbor, Michigan.

over the rather poor nuclear charge resolution (several Z units) obtained in earlier studies [2,3] has been achieved in the present work by using for the x-ray detection a cooled Si(Li) diode with a charge resolution of approximately one Z unit.

In the application of x-ray spectroscopy to measurements of charge distribution in fission the method is complicated by large variations in the K x-ray emission probability K(Z,A) as a function of the composition (Z and A) of the fragments. Information on fission fragment yields can be extracted from measured K x-ray intensities only if sufficient knowledge of K(Z,A) is available. Previously observed variations include a large but relatively smooth variation with A [2,3] and a distinct odd-even dependence on Z [4]. For a time period of ~1 nsec after fission the yields of K x rays per fragment as a function of mass are the same within experimental errors for the spontaneous fission of ^{252}Cf [2,3] and the thermal-neutron-induced fission of ^{235}U [5-7]. Common factors in the K x-ray intensities have also been observed for longer times (0.1 to 1 μsec) in ^{252}Cf fission [4] and thermal neutron fission of ^{233}U [8], ^{235}U [7-9] and ^{239}Pu [8]. Therefore, there is reason to expect that K(Z,A) is very nearly the same for various fissioning nuclei and that, by studying fission of different nuclei under the same conditions, the important features of this function can be obtained.

This paper is concerned with such a comparative study of the prompt ($\leq$1 nsec after fission) K x-ray emission and its application to the problem of charge distribution in thermal neutron fission of ^{233}U, ^{235}U and ^{239}Pu.

EXPERIMENTAL PROCEDURE

Thin targets of fissionable material were exposed to a well-collimated beam of thermal neutrons (3×10^7 n cm^{-2}sec^{-1}). Complementary fission fragments were detected in coincidence with K x rays, and the corresponding pulse heights were stored event-by-event on magnetic tape. The targets (50-75 μg cm^{-2} over a circular area of 0.7 cm^2) were prepared by vacuum volatilization of UF_4 or PuF_4 onto Ni foils (90 μg cm^{-2}) supported by thin plastic frames. The isotopic compositions of the target materials were as follows (isotope, mole per cent): ^{233}U (233, 99.85); ^{235}U (234, 0.9; 235, 93.2; 236, 0.3; 238, 5.6), and ^{239}Pu (239, 91.0; 240, 8.2; 241, 0.7; 242, 0.04).

The target and detectors were situated in a vacuum chamber in the arrangement shown in Fig. 1. The fragment detectors (Si-Au surface barrier, 400 ohm-cm, operated at 70 volts) were selected for acceptable performance [10] and replaced when a fragment dose of approximately 10^8 cm^{-2} was reached [11]. The cooled Si(Li) x-ray detector (0.3 cm x 1.0 cm^2) was enclosed by a separate vacuum chamber equipped with a Be window (46 mg cm^{-2}) and a Mylar shield (4 mg cm^{-2}) to prevent contamination of the window. A time limit of ~1 nsec for x-ray detection was imposed by Cu shields which restricted the view of the x-ray detector to roughly the first cm of fragment flight. The absolute detection efficiencies

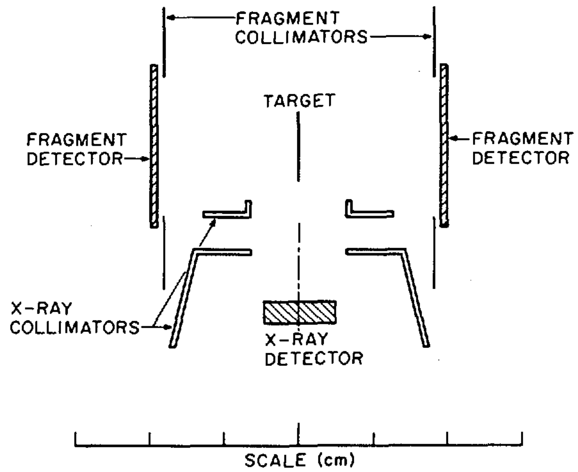

FIG. 1. Diagram of target and detector arrangement. The neutron beam intersects the target at an angle of 60° with respect to the plane of the figure and perpendicular to the axis of the X-ray detector.

for a point source at target center were determined with standardized samples of ^{65}Zn, ^{75}Se, ^{85}Sr, ^{109}Cd, ^{133}Ba, ^{139}Ce, ^{153}Gd, ^{170}Tm and ^{241}Am. The actual geometry for detection of the K x rays emitted by the flying fragments is estimated to be within 20% of the point-source geometry. The response functions for the K x-ray standards were in good agreement with published values for the energies and relative intensities of the $K\alpha_1$, $K\alpha_2$, $K\beta_1$ and $K\beta_2$ components [12] and showed that the system had excellent linearity. Resolution for the 26.3 keV γ-line of ^{241}Am was 770 eV, full width at half maximum (FWHM).

Signals from the x-ray and fragment detectors were processed and recorded as shown in Fig. 2. Pile-up rejection circuits were used to reduce distortion of fragment spectra by chance coincidences with α particles. A time-to-amplitude converter set on a time range of 0.5 μsec was used to provide information required for correction of the observed K x-ray spectra for chance events. Delay in the x-ray channel was arranged so that pulses in the first 0.15 μsec of the range represented only chance events. The remaining 0.35 μsec of the time range determined the coincidence resolving time of the entire system. The electronic system efficiency (~80%) was determined with a dual pulser which was also used for monitoring the stability in all channels. Correction for instabilities in the fission channels was made off-line in the event-by-event computer analysis; correction for instabilities in the x-ray channel was made by periodic adjustments of the baseline and amplification. For each target a total of $\sim 2.5 \times 10^5$ K x-ray events coincident with fission were collected at a rate of ~10 events per minute.

A separate measurement consisted in recording fragment-fragment coincidences for determination of the mass-yield distributions.

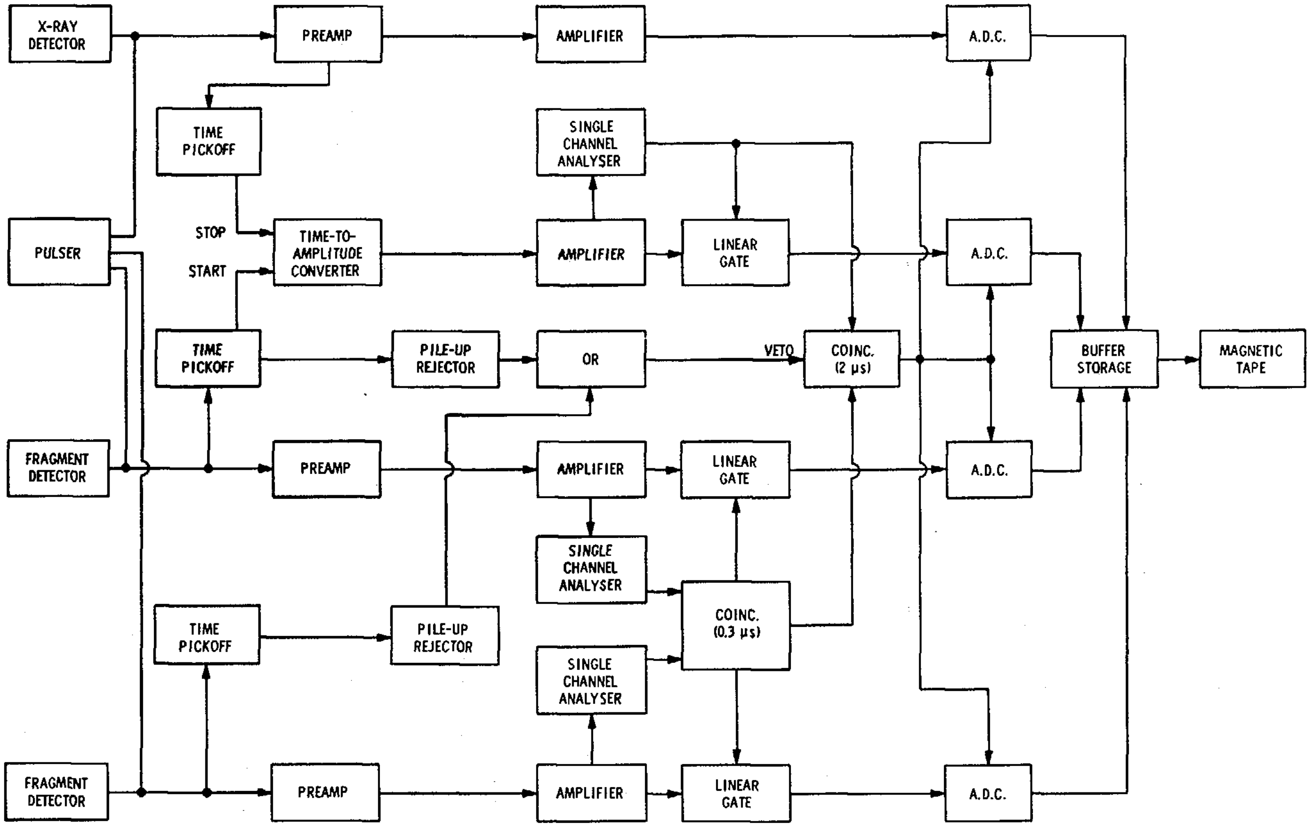

FIG. 2. Schematic diagram of the electronic system for processing and recording multiparameter data.

DATA ANALYSIS AND RESULTS

Fragment mass and kinetic energy analysis

The masses of the primary fragments were computed from their pulse heights in the fission fragment detectors using calibration methods reported in [13-15] and correcting for prompt neutron emission [16,17]. The neutron emission data were normalized where necessary to give the values 2.50 (^{233}U), 2.42 (^{235}U) and 2.89 (^{239}Pu) for $\bar{\nu}$ [18], the total number of prompt neutrons emitted per fission. The K x-ray data for ^{239}Pu were also analyzed in terms of their dependence on both the masses and the total kinetic energy (TKE) of the fragments. The TKE dependence of the neutron emission ν for a given mass M was taken into account assuming the relationship

$$\nu(M, TKE) = \bar{\nu}(M) + \frac{\bar{\nu}(M)}{\bar{\nu}(M) + \bar{\nu}(A_F - M)} \; \frac{\overline{TKE}(M) - TKE}{\bar{E}_n^*} \tag{1}$$

where $\bar{\nu}(M)$ is the average ν at mass M, $\overline{TKE}(M)$ is the average TKE at mass M, and $\bar{E}_n^*$ is the average of the sum of the binding energy and the center-of-mass kinetic energy of the neutrons [19]. In Table I are shown the results obtained for the average light primary masses $\bar{M}_L$, the standard deviations σ_M of the mass-yield distributions uncorrected for mass resolution, the average total kinetic energies $\overline{TKE}$, and the estimated standard deviations σ_{res} for the mass resolution. These values are in good agreement with [13-15]. The mass resolution was calculated taking into account the fluctuations in neutron emission [18], the energy resolution of the fission detectors (~1.5 MeV), and the finite thickness of the targets. The folding function $F_M(A)$ describing the finite mass resolution was chosen to be

$$F_M(A) = N \cdot \int_{A-0.5}^{A+0.5} \exp\left\{-\frac{(M-A)^2}{2\sigma^2}\right\} dA \tag{2}$$

where N and σ were determined to give, at a constant experimental (nominal) mass M, a normalized distribution of actual masses A with the estimated standard deviation (Table I). The unfolded mass yields $Y_A(A)$, related to the experimental mass yields $Y_M(M)$ by

$$Y_M(M) = \sum_{A-5}^{A+5} F_M(A) \quad Y_A(A) \tag{3}$$

were obtained by solving Eq. (3) with an approximate iterative procedure.

TABLE I. Results of mass and kinetic energy analysis

	^{233}U	^{235}U	^{239}Pu
$\bar{M}_L$ (amu)	94.92	96.48	100.41
σ_M (amu)	5.61	5.76	6.29
σ_{res} (amu)	1.59	1.49	1.66
$\overline{TKE}$ (MeV)	171.57	171.33	177.07

Analysis of K x-ray spectra

Some of the features of K x-ray emission in fission can be seen in energy spectra of the K x rays emitted by the ensemble of fission fragments (unsorted with respect to mass) as shown in Fig. 3. The pronounced

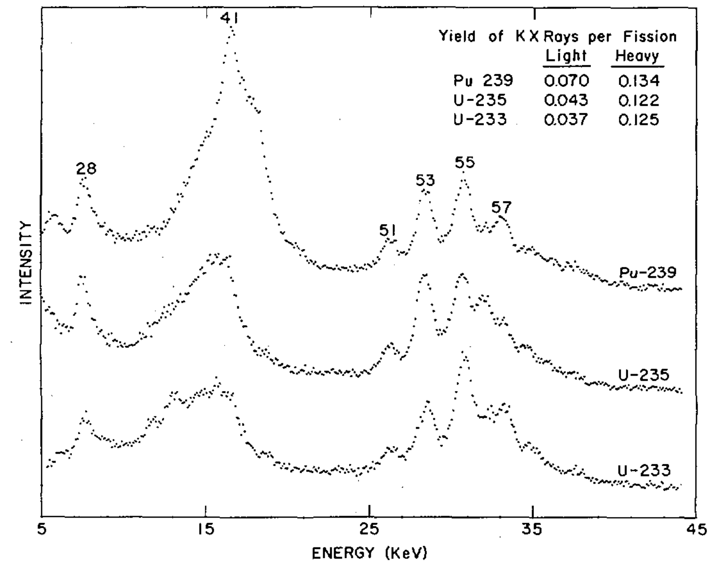

FIG. 3. Energy spectra of K X-rays emitted by fission fragments of all masses within 1 ns after fission of ^{233}U, ^{235}U and ^{239}Pu induced by thermal neutrons. Prominent peaks in the spectra are identified by atomic numbers. The peak at Z = 28 results from fluorescence by fission fragments of the nickel foils supporting the targets.

odd-even dependence on Z, which has also been observed in unsorted spectra for ^{252}Cf fission [4], is clearly evident in the heavy group from Z = 50 to 58. The total yields of K x rays (within ~1 nsec of fission) obtained from these spectra for the light and heavy groups are tabulated at upper right in the figure. The relative error in these values is about 5%, and the absolute error is estimated at 20%. The observed trend in light-group K x-ray yields reflects the strong variation of K x-ray yield with fragment mass and the known shifts in the light-group mass-yield curve for the three fissioning nuclei. The slightly larger yield for the heavy group in ^{239}Pu is consistent with the higher fission yields in the heavy wing of its mass-yield curve. The K x-ray peaks observed at 7.5 keV (Z = 28) result from fluorescence by fission fragments of the nickel foils supporting the targets. The observed intensities are in excellent agreement with calculated values based on reported cross sections [20] for K-shell ionization by fission fragments.

The primary interest in this investigation, however, was centered on mass-sorted K x-ray spectra, examples of which are given for ^{239}Pu in Fig. 4. These spectra, obtained for nominal mass intervals of 2 amu, were submitted to a least-squares computer fit, the results of which are shown

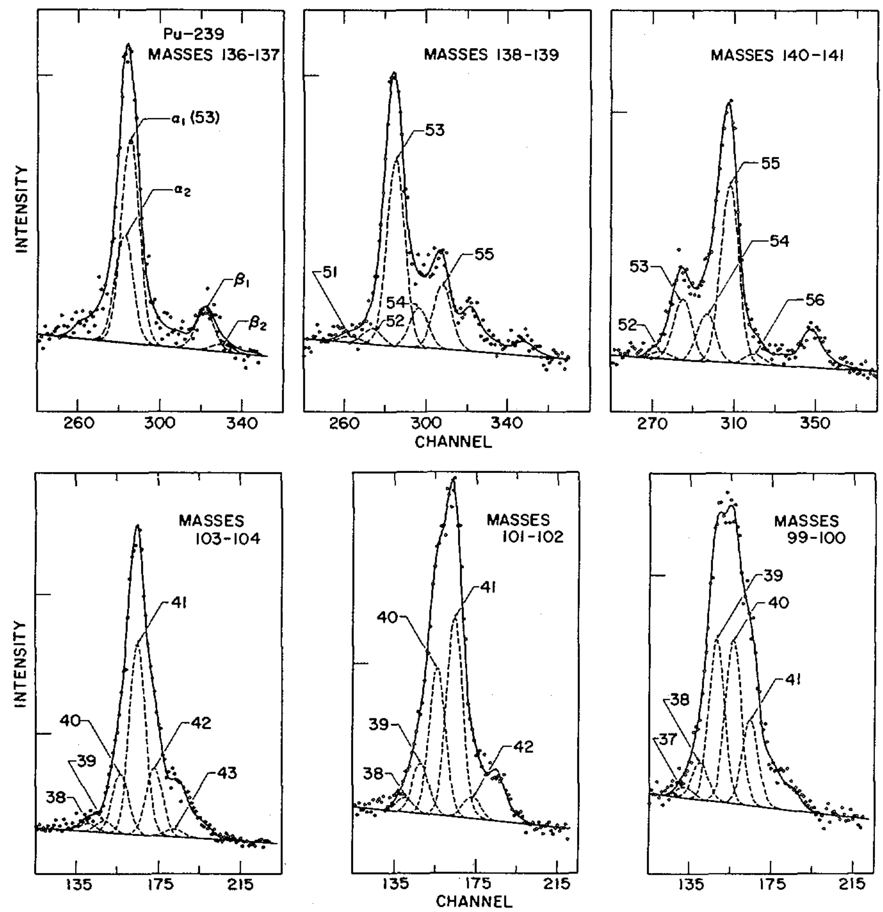

FIG. 4. Mass-sorted K X-ray spectra for some adjacent complementary fragment mass intervals in thermal neutron fission of ^{239}Pu. The relative contributions from the various elements were determined by computer fit (solid curves) to the observed data based on the known relative intensities of the K X-ray components (α_1, α_2, β_1 and β_2) for each element as shown for Z = 53 (dashed curves) in the mass interval 136-137. For visual clarity only the α_1 component for each element is shown in the other mass intervals. The ordinates are marked at intensity intervals of 500 events per channel. The channel-to-energy conversion is 100 eV/ channel.

as the solid curves. The purpose of the fitting technique was to resolve the complex experimental pulse-height distributions into the individual contributions from elemental K x-ray groups originating from fragments of different (adjacent) atomic numbers. The components (α_1, α_2, β_1, β_2) of each characteristic K x-ray group were represented by Gaussian distributions, and the known [12] relative areas and positions (centroids) of these components were kept fixed in the fitting procedure. Similarly, the relative positions of different K x-ray groups [12] were kept fixed. As an example, the components of the iodine K x-ray group (Z = 53) are shown (dashed lines) in the upper-left spectrum (mass interval 136-137) in Fig. 4. In this particular spectrum small contributions from K x-ray groups of adjacent

Z (51,52,54,55) are also present and have been taken into account, but have not been plotted for the sake of clarity. In all the other spectra (upper parts and lower parts of the figure give spectra for complementary mass intervals) only the $K\alpha_1$ components for each K x-ray group are given (dashed lines) to show relative contributions from various elements. The absolute positions (energy vs. channel number relationship) and the line widths were determined directly by the fitting procedure in the heavy group only, where the Z resolution is better than in the light group (as can be clearly seen in Fig. 4). There was no indication that K x-ray energies for the highly ionized heavy fragments are different (within 100 eV) from the values for neutral atoms [12]. However, the spectra for the moving fragments were found to be Doppler broadened. For the heavy fragments a Doppler width of about 500 eV (FWHM) was determined by comparison with standard sources. The line widths for the light-fragment group were given values in the fitting procedure calculated from those found in the heavy group, taking into account the experimentally determined response function of the Si(Li) detector with energy, and assuming for the Doppler width σ_{Dop} the relation

$$\sigma_{Dop} = \text{constant} \cdot \overline{V}_F(Z) \cdot \overline{E}_x(Z) \tag{4}$$

where $\overline{V}_F(Z)$ and $\overline{E}_x(Z)$ are the average fragment velocity and K x-ray energy as a function of Z. Small contributions to the line widths from instabilities in the electronic system were also taken into account.

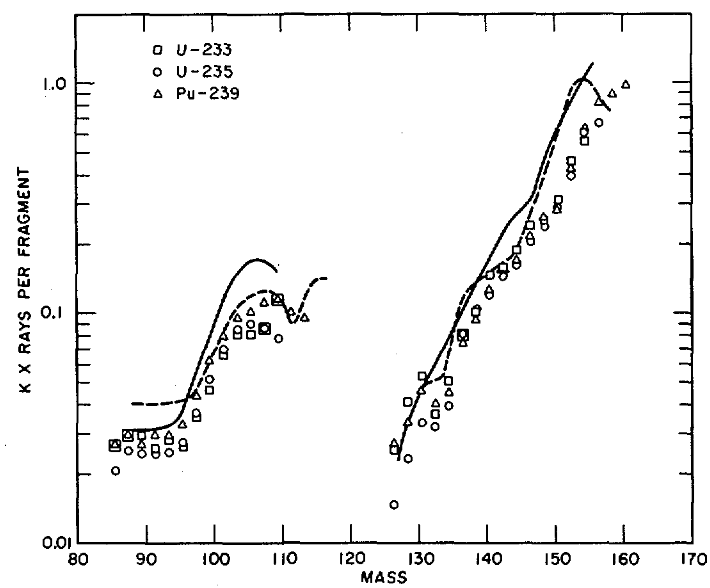

FIG. 5. Yields of K X-rays emitted by fission fragments within 1 ns after thermal neutron fission of ^{233}U, ^{235}U and ^{239}Pu as a function of fragment mass. Observed yields are plotted for primary fragment mass intervals of 2 amu. The solid curve represents the average yield for the three target nuclei corrected for mass resolution and plotted as a function of the average secondary fragment mass (after neutron emission). Previously reported results for spontaneous fission of ^{252}Cf [2] are shown for comparison (dashed curve).

By adding up the results obtained for the contributions from all the elements in a given mass interval and dividing by the experimental fragment yield for this interval, K x-ray yields per fragment (for ≤ 1 nsec after fission) as a function of primary mass (uncorrected for resolution) are obtained (data points in Fig. 5). The statistical error is less than 2% for most of the data points, increasing to as much as 20% at the extremes toward symmetric and far-asymmetric mass divisions. As can be seen, the K x-ray yields are essentially the same for the three target nuclei. The continuous curve in Fig. 5 represents an average for the three fissioning nuclei obtained from all the data points after conversion from primary masses to secondary masses (since K x rays are emitted from the fragments after prompt-neutron emission) and correction for mass resolution. Within the experimental errors these results are consistent with those obtained for ^{252}Cf fission [2] indicated by the dashed curve.

K x-ray emission and its application to charge distribution

The functions of main interest in this paper are P(Z,A), the mass-dependent charge distribution probability, and K(Z,A), the average probability that K x-ray emission will follow the formation of a fragment (Z,A). The measured K x-ray yields $Y_K(Z,M)$ in different nominal mass intervals are essentially products of these two unknown functions as seen in Eq. (5).

$$Y_K(Z,M) = \sum_A Y_A(A) \quad F_M(A) \quad P(Z,A) \cdot K(Z,A) \tag{5}$$

An attempt to break up these products into the two terms obviously depends on the availability of equations other than Eq. (5) with additional independent information on K and/or P.

A strong restriction on P(Z,A) is supplied by the principle of charge and mass complementarity in fission which can be stated as follows:

$$Y_A(A) = Y_A(A_F - A) \tag{6a}$$

and

$$P(Z,A) = P(Z_F - Z, A_F - A) \tag{6b}$$

where A_F and Z_F are the mass and charge, respectively, of the fissioning nucleus.

One difficulty in the K x-ray method lies in the fact that the number of new equations supplied by the complementarity restrictions is still insufficient to allow a complete and detailed description of both P(Z,A) and K(Z,A) for all the individual nuclei involved. Furthermore, the mass resolution obtained in semiconductor detector measurements is at best 3 or 4 amu (FWHM). As a consequence, mass-dependent quantities like K(Z,A) are averaged over mass intervals of this width. Attempts to describe this finite resolution by introducing folding functions such as $F_M(A)$ (Eqs. (2) and (3)) can be done only in an approximate way and, in those mass intervals where the true unfolded yields are changing rapidly with mass, are essentially confined to correction for differences between true average masses and nominal (experimental) masses. Unfolding procedures cannot bring out with reasonable accuracy the fluctuations of any mass-dependent observable in mass intervals narrower than the experimental mass resolution, and in particular odd-even mass (neutron number) effects remain essentially unobservable. As mentioned previously, however, odd-even Z effects are clearly observed.

These considerations suggest that a description of general trends in the quantities P(Z,A) and K(Z,A) with a strongly limited number of suitably chosen parameters in terms of discrete and well defined atomic numbers, but averaged over several adjacent isotopes (with odd and even mass numbers), is appropriate. The upper limit on the number of parameters is given by the number of equations of both type (5) and (6). For practical purposes the limit on this number is substantially lower because the experimental uncertainties in the observed K x-ray yields Y_K for different mass intervals are sufficient to give spurious solutions for the values of the unknown parameters if too many such parameters are introduced.

For the distribution function P(Z,A) the following parametric description was chosen:

$$P(Z,A) = N \exp\left\{\frac{[A_P(Z) - A]^2}{2\sigma_A^2}\right\} \tag{7}$$

with N determined by

$$\sum_Z P(Z,A) = 1 \tag{8}$$

For a given element Z with varying mass A, P is a Gaussian distribution with its center at $A_P(Z)$ and with a variance σ_A^2. Instead of the parameter $A_P(Z)$ it is convenient to use $\Delta_Z(Z)$ ("charge division parameter") defined by

$$\Delta_Z(Z) = Z - \rho_F \quad A_P(Z) \tag{9}$$

where ρ_F is the charge density Z_F/A_F of the fissioning nucleus. Note that the distribution of A for a given Z ("isotopic" distribution) is not given by P(Z,A) but by the product $Y_A(A) \cdot P(Z,A)$, so that in the wings of the mass-yield curve the isotopic distribution is not Gaussian. In radiochemical studies of charge distribution WAHL et al. [21] used a somewhat different parametric description:

$$P(Z,A) = N \exp\left\{-\frac{[Z_P(A) - Z]^2}{2\sigma_Z^2}\right\} \tag{10}$$

where

$$Z_P(A) = \rho_F \quad A + \Delta_A(A) \tag{11}$$

which described P by a Gaussian "isobaric" distribution in terms of Z

(A constant) rather than in terms of A (Z constant). If $\Delta_Z(Z)$ is not dependent on Z, both descriptions can be linked by

$$\sigma_Z = \sigma_A \ \rho_F \tag{12a}$$

$$\Delta_A(A) = \Delta_Z(Z) \left(\text{for } A = A_P(Z)\right) \tag{12b}$$

If $\Delta_Z(Z)$ is slowly varying with Z, equation (12b) remains a good approximation although P(Z,A) defined in Eq. (7) is, strictly speaking, non-Gaussian for varying Z, and its dispersion in Z is somewhat larger than that given by Eq. (12a).

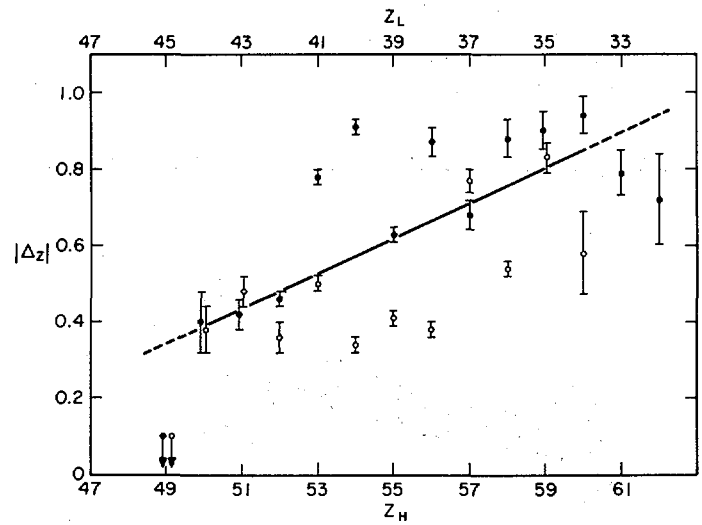

FIG. 6. "Effective" charge division parameters Δ_Z for thermal neutron fission of ^{239}Pu as a function of fragment atomic number. Heavy-group data are plotted as solid circles, complementary light-group data as open circles. The straight line is a least-squares fit to the data.

For the K x-ray emission K(Z,A) the analysis of the data was performed in two steps. In the first step the isotopic (mass) dependence of K for element Z was ignored, and the emission probability was simply described by $\overline{K}(Z)$, an average of K(Z,A) for all isotopes of element Z. Thus three parameters $\overline{K}(Z)$, $\Delta_Z(Z)$ and $\sigma_A(Z)$ (or $\sigma_Z = \sigma_A \ \rho_F$) were used to describe the observed intensities $Y_K(Z,M)$ for various mass intervals M and were determined by a least-squares fitting procedure. Values of Δ_Z determined with these assumptions are called "effective" because the isotopic dependence of K(Z,A) is neglected.

The effective Δ_Z values for ^{239}Pu are shown in Fig. 6 as a function of Z for the light group (open circles) and the heavy group (solid circles). A χ^2 analysis shows that the goodness-of-fit is sensitively dependent on the values of the charge division parameters but relatively insensitive to changes in $\sigma_A(Z)$. As a consequence, the purely statistical uncertainty of Δ_Z is quite small (of the order of 0.02) but relatively large (~0.4 amu) for σ_A (or ~0.15 charge units for σ_Z). As no systematic trend of σ_A with Z was found within its large error limit, the Δ_Z values plotted in Fig. 6 were determined with σ_A fixed at a value $\overline{\sigma}_A$, a weighted average for all the elements analyzed. Since the Δ_Z values giving the best fit were found to be slightly dependent on the actual value of σ_A, the statistical uncertainty in σ_A is reflected in an uncertainty in Δ_Z. The error bars in Fig. 6 refer mainly to this source of error. For the actual charge division parameters, equation (6b) requires that

$$\Delta_Z(Z) = \Delta_Z(Z_F - Z). \tag{6c}$$

It is seen that this condition is not fulfilled by the effective Δ_Z values for some elements. Assuming that the actual function $\Delta_Z(Z)$ is smooth, a straight line was least-squares fitted to all the data points as shown in Fig. 6. This implies that over intervals of several Z units there are no systematic deviations of the effective from the actual division parameters.

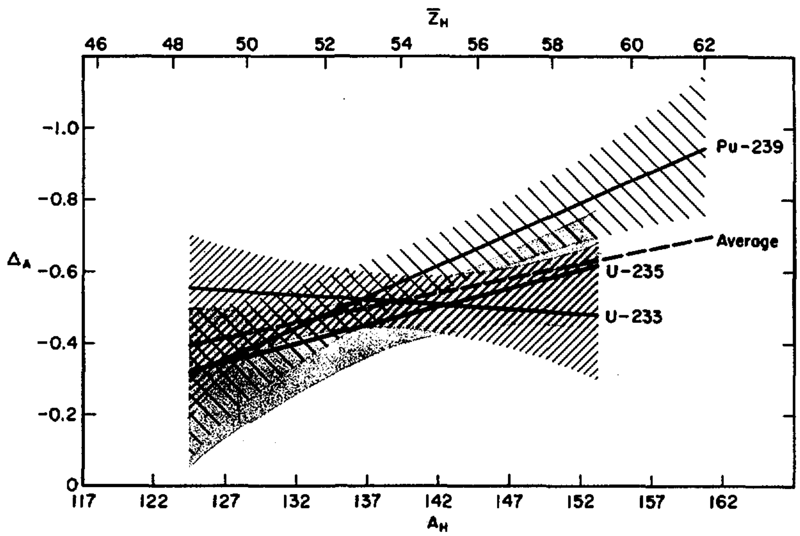

FIG. 7. Charge division diagrams for thermal neutron fission of ^{233}U, ^{235}U and ^{239}Pu. The solid lines (with their associated error bands) are linear least-squares fits to the data for "effective" charge division parameters Δ_A as a function of primary fragment mass. A_H refers to the heavy-group mass (or its light-group complement) in each case. The scale for the mean primary charge $\overline{Z}_H$ is an approximate average for the three fissioning nuclei and is intended for orientation only.

The data for ^{233}U and ^{235}U were treated in a similar way and a conversion from the Δ_Z vs. Z diagram to the more traditional Δ_A vs. A diagram was made using Eqs. (9) and (12b). Figure 7 shows Δ_A as a function of A (with the associated error bands) for all three target nuclei. The values found for the average $\overline{\sigma}_Z = \overline{\sigma}_A \ \rho_F$ are 0.42 (^{233}U), 0.44 (^{235}U), and 0.52 (^{239}Pu), with an estimated error of about 0.07, corresponding to an average FWHM of 1.10 ± 0.15 Z units.

In the case of ^{239}Pu the K x-ray events in each mass interval were also sorted into two bins of total kinetic energy (TKE): a "low TKE"- and "high TKE"-bin below and above the average TKE associated with the given mass interval. The first moments of the TKE distributions in these two intervals differ by an amount approximately equal to typical neutron binding energies (4 to 7 MeV) for fission fragments. The K x-ray spectra for low and high TKE were found to differ slightly, higher TKE favoring lower Z in the heavy-fragment group and higher Z in the light-fragment group. An effect in this direction is to be expected simply as a result of the strong correlation existing between the TKE release and the mass split in the fission process. In order to eliminate the influence of this known correlation on the TKE-sorted data, the mass distribution $Y_A(A)$ in Eq. (5) was replaced by $Y_A(A) \cdot P_{LO}(A)$ and $Y_A(A) \cdot P_{HI}(A)$, with $P_{LO}(A) + P_{HI}(A) = 1$, where P_{LO} and P_{HI} are the probabilities that fragments with masses A (and $A_F - A$) have a total kinetic energy lower (P_{LO}) or higher (P_{HI}) than the average TKE. Values for P_{LO} and P_{HI} were obtained for a first approximation from distributions of fission events in the two-dimensional plane of mass and TKE, uncorrected for finite energy- and mass-resolution effects. The charge division parameters Δ_Z obtained from the TKE-sorted data were found to deviate by less than 0.05 Z units from the data unsorted with respect to TKE. Since the neglect of resolution corrections in the mass- and TKE-dependent fragment yields amounts to an undercorrection of the effects due to TKE-mass split correlations, it is concluded that no evidence of a strong influence of TKE (for changes of 4 to 7 MeV) on the charge distribution parameters was found in this investigation. The influence of the TKE release on K x-ray intensities was found, however, to be consistent with the isotopic dependence of K(Z,A) as described in the discussion section.

In the second step of the data analysis a semi-quantitative explanation in terms of an isotopic dependence of the K x-ray emission was sought for the large scattering observed for some of the effective Δ_Z values. A comparison of the effective Δ_Z values found for the three target nuclei in the heavy fragment group is shown in Fig. 8. The data points have been joined by straight lines in order to emphasize the striking correlation in the values for a given atomic number. This correlation strongly suggests that the deviation of the effective Δ_Z from the actual Δ_Z is a characteristic determined by the specific isotopic dependence of K(Z,A) for each Z, and that this dependence is similar (possibly identical) for fragments irrespective of the fissioning nucleus from which they originate. It is reasonable to assume that mass-to-mass variations of K(Z,A) will tend to change the effective charge division parameters only when they "bias" the charge distribution in a fairly correlated manner over mass intervals approximately equal to the mass dispersion width. The most simple such correlational behavior of K(Z,A) for a given Z may be taken as an overall tendency for K to decrease or increase with mass. This is described as an "isotopic slope" $\overline{K}_1$ defined by

$$\overline{K}(Z,A) = \overline{K}_0(Z) + \overline{K}_1(Z) \quad A \tag{13}$$

The bars over the K-functions are a reminder that only major tendencies of the actual K(Z,A) are described. As mentioned earlier, odd-even correlations in A (Z constant) are washed out by the experimental mass dispersion and are therefore ignored.

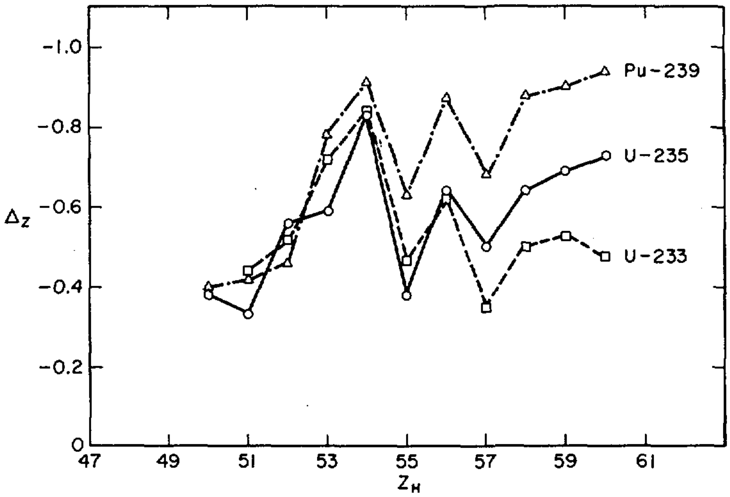

FIG. 8. "Effective" charge parameters Δ_Z for heavy-group fragments in thermal neutron fission of ^{233}U, ^{235}U and ^{239}Pu as a function of fragment atomic number.

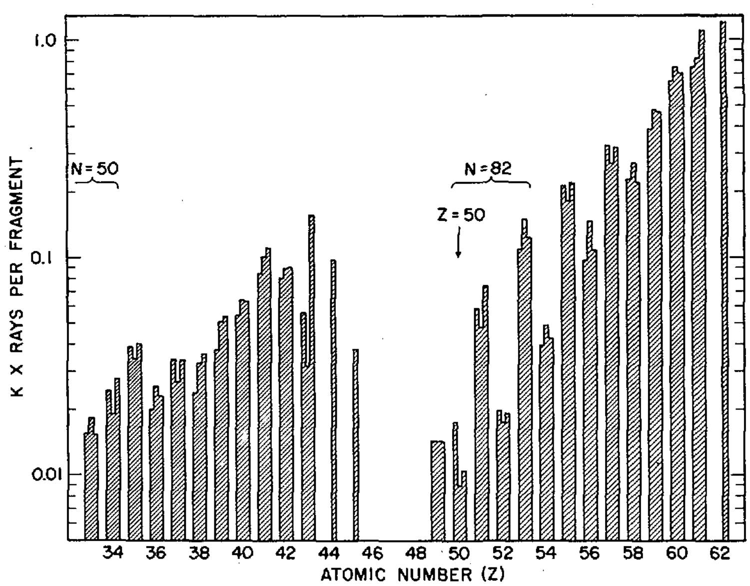

FIG. 9. K X-ray yields as a function of fragment atomic number (nuclear charge Z) for thermal neutron fission of ^{233}U, ^{235}U and ^{239}Pu. Yields are shown at each value of Z for the three target nuclei in order of increasing target mass number from left to right with the exceptions of Z = 44, 45 and 62 for which only the ^{239}Pu yields could be measured. The locations of closed nuclear shells are indicated.

The results of the data analysis based on the isotopic dependence (Eq. (13)) and smoothed Δ_Z parameters (Fig. 7) are presented in Table II. The average yields of K x rays per fragment $\overline{K}_Z$ as a function of fragment atomic number are also shown in Fig. 9. The errors in parentheses asso-

TABLE II. AVERAGE K X-RAY YIELD PER FRAGMENT $\overline{K}_Z$, AVERAGE PRIMARY MASS $\bar{A}_Z$, AND ISOTOPIC SLOPE $\overline{K}_1(Z)$ AS A FUNCTION OF ATOMIC NUMBER Z

$_Z$Element	^{233}U		^{235}U		^{239}Pu		$\overline{K}_1(Z)$ (%)
	$\bar{A}_Z$	$\overline{K}_Z$ (x 10^4)	$\bar{A}_Z$	$\overline{K}_Z$ (x 10^4)	$\bar{A}_Z$	$\overline{K}_Z$ (x 10^4)	
$_{33}$As	83.52	155±60 (48)	83.91	182±76 (67)	82.51	153±48 (46)	-
$_{34}$Se	85.61	243±33 (25)	86.11	195±35 (32)	85.26	276±39 (30)	25
$_{35}$Br	88.21	396±44 (16)	88.73	340±34 (21)	87.76	402±34 (20)	-5
$_{36}$Kr	90.45	199±15 (8)	91.17	255±15 (11)	90.42	230±20 (14)	25
$_{37}$Rb	92.80	339±20 (9)	93.68	265±13 (10)	93.01	339±22 (9)	-10
$_{38}$Sr	95.33	237±13 (8)	96.25	328±19 (10)	95.53	361±21 (7)	35
$_{39}$Y	97.77	388±18 (9)	98.90	506±22 (9)	98.11	539±18 (7)	25
$_{40}$Zr	100.30	544±27 (9)	101.47	640±31 (9)	100.75	626±28 (8)	30
$_{41}$Nb	102.56	843±68 (13)	103.78	1011±86 (13)	103.33	1107±41 (8)	±1
$_{42}$Mo	104.88	805±106 (29)	106.09	888±150 (25)	105.78	898±47 (9)	5
$_{43}$Tc	106.93	559±190	107.90	316±260 (170)	108.04	1541±152 (17)	-
$_{44}$Ru	-	-	-	-	110.62	976±118 (39)	-
$_{45}$Rh	-	-	-	-	112.84	379±92 (53)	-
$_{49}$In	127.16	183±68 (46)	128.10	90±70 (60)	127.29	203±96 (81)	-
$_{50}$Sn	129.12	176±32 (25)	129.88	88±25 (22)	129.38	104±28 (25)	-
$_{51}$Sb	131.46	584±55 (17)	132.22	477±40 (12)	131.96	741±76 (15)	-15
$_{52}$Te	133.74	190±16 (10)	134.55	173±15 (9)	134.22	192±16 (9)	5
$_{53}$I	136.24	1080±32 (14)	137.12	1488±45 (12)	136.67	1240±45 (11)	35
$_{54}$Xe	138.68	393±26 (12)	139.76	488±32 (13)	139.30	424±25 (12)	60
$_{55}$Cs	141.19	2120±48 (17)	142.33	1804±63 (15)	141.90	2190±90 (20)	-10
$_{56}$Ba	143.56	970±68 (17)	144.84	1466±96 (18)	144.49	1070±60 (20)	25
$_{57}$La	145.79	3280±280 (33)	147.24	2690±220 (33)	146.99	3200±100 (30)	-15
$_{58}$Ce	148.46	2260±180 (60)	149.91	2700±220 (60)	149.65	2200±160 (50)	10
$_{59}$Pr	150.64	3685±540 (120)	152.29	4680±600 (110)	152.28	4650±320 (75)	15
$_{60}$Nd	153.20	6410±1000 (385)	154.97	7460±950 (220)	154.89	7020±540 (160)	15
$_{61}$Pm	155.18	7470±2300 (1350)	156.78	8220±3600 (1300)	157.43	11100±950 (290)	-
$_{62}$Sm	-	-	-	-	159.53	12000±2000 (850)	-

ciated with the $\overline{K}_Z$ values in Table II are due only to counting statistics; the overall errors include uncertainties of 0.1 Z unit in Δ_Z and 0.3 amu in σ_A. Relative errors in comparison of $\overline{K}_Z$ values among the three target nuclei are estimated at about 5%. All values have an absolute error of about 20% owing mainly to uncertainty in the actual geometrical efficiency of x-ray detection. Also given in the table for each element (Z) are the average masses $\bar{A}_Z$ based on the observed mass-yield distributions and the parameters Δ_Z and σ_A. The observed average isotopic slope $\overline{K}_1(Z)$ for the three target nuclei is given in the table as a percentage change in the average K x-ray emission $\overline{K}(Z)$ per unit of mass for each element. Since $\overline{K}_1(Z)$ is strongly dependent on Δ_Z, the $\overline{K}_1(Z)$ values listed in the table are to be considered only as rough guide lines in the interpretation of the data discussed in the next section.

DISCUSSION

K x-ray emission

In both fragment groups the K x-ray yields per fragment increase with increasing mass (Fig. 5) and increasing Z (Fig. 9). Since the K x rays arise predominantly from internal conversion of the prompt γ rays [2], this saw-tooth dependence is expected to be correlated with similar trends observed for the total γ-ray energy as a function of mass [22] and for the mass dependence of the average number and energy of quanta emitted by fission fragments [22,23]. Previously reported leveling off or decrease in the K x-ray yield curves for A $\gtrsim$ 153 in ^{252}Cf fission [2,3] and A $\gtrsim$ 144 for ^{235}U [7] is not observed in this work.

The odd-even Z dependence can be explained as follows: As a consequence of the nuclear pairing forces, even-even nuclei do not have intrinsic states below ~1 MeV. Thus the lower states for spherical nuclei (around closed nucleon shells) are of collective vibrational type with relatively high energies (up to 1.5 MeV at the N = 82 shell) and therefore with extremely low conversion coefficients. As Z and N differ more and more from closed-shell values, the energies of the first two vibrational levels decrease, and the corresponding increase of the conversion coefficients will de-emphasize the odd-even Z effect. This tendency is reinforced by the fact that the excitation energy of the secondary fragments increases away from closed shells [22] thus making possible larger yield contributions from higher regions of the level schemes (above 1 MeV). Figure 9 shows clearly that the odd-even Z fluctuations in the heavy-fragment group tend to diminish as Z (and A) increases.

Odd-even Z effects are also present in the light group, especially for ^{233}U (see Table II), but the fluctuations are not as striking as those in the heavy group.

The relatively simple systematic trends of the K x-ray yields as a function of Z are an indication that collective states of vibrational and rotational nature, rather than specific intrinsic states involving one or few given particle and hole-states, determine the yields observed and dominate the de-excitation of the fission fragments.

The average isotopic slopes $\overline{K}_1$ (Z), defined in Eq. (13) and listed in Table II, may be given the following quantitative interpretation. Positive $\overline{K}_1$ (Z) indicates that for a given atomic number more K x rays tend to be emitted by the more neutron-rich isotopes and vice versa for negative $\overline{K}_1$ (Z). The (very approximate) values found are necessary to account for the scattering of the effective division parameters Δ_Z from the smooth Δ_Z line (see Fig. 6) assumed to represent the actual Δ_Z function. A comparison of the average K x-ray yields $\overline{K}$ (Z) for ^{233}U and ^{235}U shows that they differ by amounts qualitatively in agreement with the interpretation of the isotopic slopes, that is, the first moments $\overline{A}_Z$ of the primary mass distributions at given Z (Table II) suggest that the secondary fragments are on the average less neutron rich in ^{233}U than in ^{235}U (the neutron emission characteristics are very much alike for both target nuclei). Since most of the isotopic slopes are found to be positive, ^{235}U has slightly higher K x-ray yields for most atomic numbers, except for Z = 35,37,51,55 and 57 where $\overline{K}_1$ (Z) has a negative sign (Table II). This striking qualitative correlation shows that the interpretation of the observed scattering in effective Δ_Z values is essentially correct, and that the yield K (Z,A) for a fragment of given composition must be very nearly the same in the fission of both uranium isotopes.

^{239}Pu is an intermediate case between ^{233}U and ^{235}U which does not fit quite as well the simple interpretation given above for differences in the average $\overline{K}$ (Z). Because of the higher total proton number involved (94 vs. 92) certain features, such as the (unknown) Z dependence of the neutron emission, may be slightly different in the case of plutonium as compared with uranium. Small differences in $\overline{K}$ (Z) may be correlated with small differences in the neutron emission characteristics. Further investigations of this point may be interesting.

At given primary fragment masses fission events with a low TKE release involve high fragment excitations leading to a higher neutron emission probability. In these events the secondary fragment will be less neutron rich. This means that for positive $\overline{K}_1$ (Z) the fragment will emit on the average less K x rays and vice versa for negative $\overline{K}_1$ (Z). The TKE dependence of $\overline{K}$ (Z) (analyzed for ^{239}Pu) was found to be explainable in these terms. It is concluded that total kinetic energy has little or no influence on the yield of K x rays emitted by secondary fragments of given nuclear composition (Z,A).

Charge division

At present the major source of error in the determination of charge division probably lies in the strong variation in K X-ray emission; however, the ultimate limitation in this method may well be due to uncertainties in the fragment mass determination (calibration of the fission detectors and possible errors in the neutron emission data). The high degree of internal consistency in the K x-ray yield data enhances the confidence in the charge division data (Fig. 7) obtained with the K x-ray method because of the interdependence of the yield and charge division data.

The average Δ_Z line in Fig. 7 for all three target nuclei is only slightly outside the common error bands making any discussion of the observed differences speculative. The results of this investigation for charge division in thermal neutron fission of ^{235}U are compared in Fig. 10 with other reported results based on the K x-ray method [5] and on beta counting of mass-separated fission products [24]. Good agreement is found.

From systematic trends in the K x-ray yields (Fig. 9) it can be deduced that the yields from fragments with Z=49 and their light complements (43 for U and 45 for Pu) are surprisingly low. A possible explanation is that the fragment yields for these nuclei have been overestimated by a factor of two to three. In terms of the charge division parameter, this means that the actual value of Δ_Z for these elements is lower (near zero)

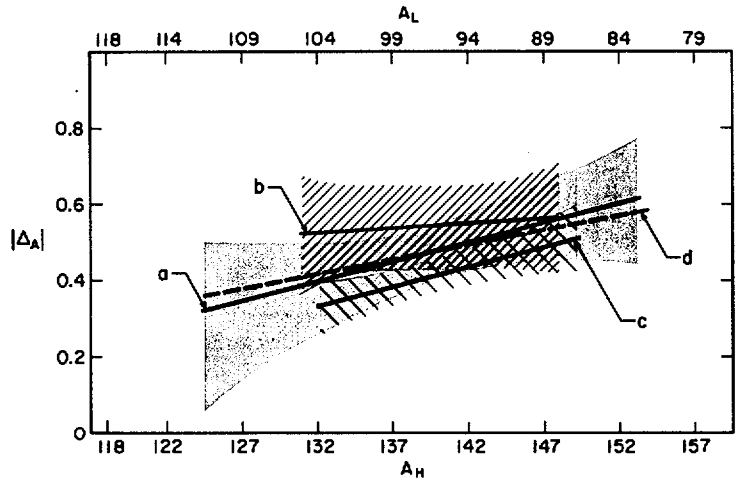

FIG. 10. Comparison of reported results for charge division in thermal neutron fission of ^{235}U. Curve (a): results of this investigation; curve (b): results for light-group fragments based on the K X-ray method using Argon-filled proportional detector [5]; curve (c): results based on beta counting of mass-separated fission products [24]; curve (d): average of curves (a), (b) and (c).

than suggested by the smooth lines in Figs. 6 and 7. This effect would be expected if a strong preferential formation of nuclei with Z=50 takes place during fission. Recent evaluation of radiochemical data [25] also suggests this "closed-shell effect."

Charge dispersion

The values found for the primary charge dispersion σ_Z are somewhat smaller than those determined for secondary fragments by radiochemical methods. A more detailed interpretation of this observation in terms of a dispersive effect by the prompt neutron emission will be attempted after a critical investigation of possible systematic errors underlying the specific assumptions made in the analysis of the present data.

The data analysis now in progress for a similar investigation of the spontaneous fission of ^{252}Cf, with a substantial increase in statistical accuracy over the presently reported data, is expected to clarify some of the features (isotopic- and TKE-dependence of the K x-ray yields and Z=50 shell effect on the fragment yields) outlined in this paper.

ACKNOWLEDGEMENTS

The authors wish to thank S. M. Fried for preparation of the target material $^{233}UF_4$, A. J. Gorski for his invaluable aid in preparation of the targets, and C. Chamot for the development of the K x-ray spectra-fitting program.

REFERENCES

[1] WAHL, A. C., in Physics and Chemistry of Fission 1, IAEA, Vienna (1965) 317.
[2] GLENDENIN, L. E., GRIFFIN, H. C., Physics Lett. 15 (1965) 153. Bull. Amer. Phys. Soc. 10 (1965) 13; GLENDENIN, L. E., UNIK, J. P., GRIFFIN, H. C., in Physics and Chemistry of Fission 1, IAEA, Vienna (1965) 369; GLENDENIN, L. E., UNIK, J. P., Phys. Rev. 140 (1965) B1301.
[3] BOWMAN, H. R., THOMPSON, S. G., WATSON, R. L., KAPOOR, S. S., RASMUSSEN, J. O., in Physics and Chemistry of Fission 2, IAEA, Vienna (1965) 125; KAPOOR, S. S., BOWMAN, H. R., THOMPSON, S. G., Phys. Rev. 140 (1965) B1310.
[4] WATSON, R. L., BOWMAN, H. R., THOMPSON, S. G., Phys. Rev. 162 (1967) 1169.
[5] REISDORF, W., Z. Physik 209 (1968) 77.
[6] BOHN, E. M., WEHRING, B. W., WYMAN, M. E., Appl. Phys. Letters 12 (1968) 199.
[7] KAPOOR, S. S., RAMAMURTHY, V. S., ZAGHLOUL, R., Phys. Rev. 177 (1969) 1776.
[8] LAFLEUR, P. D., GRIFFIN, H. C., Inorg. Nucl. Chem. Letters, in press.
[9] EISMONT, V. P., YURGENSON, V. A., Yadern. Fiz. 5 (1967) 1192 [English Transl.: Soviet J. Nucl. Phys. 5 (1967) 852.]
[10] KLEMA, E. D., PLEASONTON, F., SCHMITT, H. W., UNIK, J., IEEE Transactions on Nucl. Sci. NS-13, No. 1 (1966) 43; SCHMITT, H. W., PLEASONTON, F., Nuclear Instr. Meth. 40 (1966) 204.
[11] SHIRAISHI, F., Nuclear Instr. Meth. 69 (1969) 316.
[12] WAPSTRA, A. H., NIJGH, G. J., VAN LIESHOUT, R., Nuclear Spectroscopy Tables, North-Holland Publishing Co., Amsterdam (1959) 81.
[13] SCHMITT, H. W., NEILER, J. H., WALTER, F. J., Phys. Rev. 141 (1966) 1146.
[14] NEILER, J. H., WALTER, F. J., SCHMITT, H. W., Phys. Rev. 149 (1966) 894.
[15] PLEASONTON, F., Phys. Rev. 174 (1968) 1500.
[16] MILTON, J. C. D., FRASER, J. S., in Physics and Chemistry of Fission 2, IAEA, Vienna (1965) 39.
[17] APALIN, V. F., GRITSYUK, Yu. N., KUTIKOV, I. E., LEBEDEV, V. I., MIKAELIAN, L. A., Nucl. Phys. 71 (1965) 553.
[18] TERRELL, J., Phys. Rev. 127 (1962) 880.
[19] BOWMAN, H. R., MILTON, J. C. D., THOMPSON, S. G., SWIATECKI, W. J., Phys. Rev. 129 (1963) 2133.
[20] SPECHT, H. J., Z. Physik 185 (1965) 301.
[21] WAHL, A. C., FERGUSON, R. L., NETHAWAY, D. R., TROUTNER, D. E., WOLFSBERG, K., Phys. Rev. 126 (1962) 1112.
[22] MAIER-LEIBNITZ, H., SCHMITT, H. W., ARMBRUSTER, P., in Physics and Chemistry of Fission 2, IAEA, Vienna (1965) 143.
[23] JOHANSSON, S. A. E., Nucl. Phys. 60 (1964) 378.
[24] SISTEMICH, K., thesis, Nuclear Research Institute, Jülich, No. 574 (1969); private communication from P. ARMBRUSTER (1969).
[25] WAHL, A. C., private communication (1969).

DISCUSSION

S.S. KAPOOR : In Trombay we have carried out measurements to determine the K X-ray yield per fragment in the time range from 0 to about 1.0 μs; the results are shown in Fig. 1. Comparison of our results with

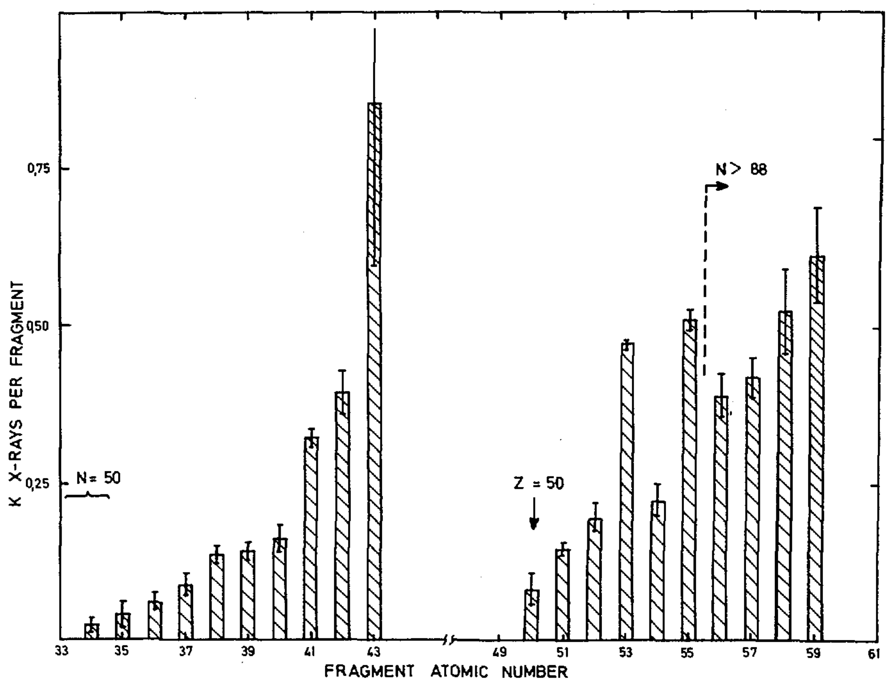

FIG. 1. K X-ray yield per fragment versus fragment atomic number.

those of Glendenin, which are in the time range up to 1 ns, leads to some interesting observations, which I would like to bring to your attention: (1) Our results for X-ray yield for Z = 52 are not lower than those for Z = 51; (2) *Increase in X-ray yield after Z = 56 (N > 88, deformed nuclei)* is not as rapid for our time range as for 0-1 ns. For example, Glendenin's results show $Y^X{}_{59}/Y^X{}_{56} = 4$ (0-1 ns), while ours show $Y^X{}_{59}/Y^X{}_{56} = 1.6$ (0-1 μs); (3) The yield for X-rays in the time range 0-1 μs when Z = 43 is significantly higher than when Z = 42 (our results), which is not observed in the time range 0-1 ns (Glendenin's results).

These comparisons show a significantly long half-life component for Z = 52 and Z = 43, and a decreasing half-life for Z > 56 (N > 88). The measurements of X-ray half-life versus Z performed by Bowman, Thompson and myself at Berkeley confirm this observation.

It appears, therefore, that in the time range 0-1 μs the X-ray intensity variation with Z is less erratic, that is, shows a less rapid variation for Z > 56, and also less even-odd effect for heavy fragments, as compared to the X-ray intensities in the time range 0-1 ns. It may therefore be better to measure Z_p versus mass by looking at the total number of X-rays emitted, say, up to 1 μsec.

J. P. UNIK: We have measured the time distribution for K X-ray emission from each element in the fission of ^{252}Cf from 0 to 1 μs after fission. We find that there are many elements which emit sizeable yields of K X-rays over this time range, as speculated by Dr. Kapoor.

T. P. DOAN: We have calculated the deformation of fragments and the stiffness parameter after alpha-particle emission. We have shown that when a fragment is magic it shares its properties (namely, the magic properties) with the fragment of complementary mass. This phenomenon is perhaps similar to the X-ray yield anomaly pointed out by Dr. Glendenin.

We find this phenomenon of complementariness (or transfer of magic properties) in a large number of fissioning nuclei.

L. E. GLENDENIN: We do not observe such similarity of behaviour for "magic" and "complementary-to-magic" fragments as far as K X-ray emission is concerned.

H. NIFENECKER: We have measured a long lifetime for K X-ray emission of fragments with Z = 52 (about 30 nsec, but not guaranteed).

At the Bordeaux meeting of the French Physical Society in March 1967 we reported on the variation of K X-ray yields due to an even-odd effect. We did not publish our results on the variation of $\bar{M}(Z)$ because of the non-complementarity of these variations. Attempts to correct our results for the variation in K X-ray yields did not significantly improve the situation. In our view, some of the non-complementarity may possibly be due to the Doppler shift of the X-rays.

L. E. GLENDENIN: We find a component with a half-life of approximately 200 nsec for K X-ray emission at Z = 52.

The Doppler effect causes a broadening in our K X-ray lines of about 300 eV and a slight negative energy shift of about 100 eV, but it is not the cause of the non-complementarity in nuclear charge. We think that the latter is due to strong mass dependences in K X-ray emission at given Z values.

S. AMIEL: I find it difficult to understand how you carry the K X-ray results into charge division without knowing the real distributions of the nuclear charge in fission. In other words, we are well aware that the even charge or mass yields are relatively higher than the odd ones. This means that we cannot deduce, on the basis of the X-ray data, what is the K X-ray yield per fragment, unless we know the odd-even fragment relationships. If averaging is done, the odd-even effects are masked. This may be very critical near closed shells, where for even masses or charges the X-ray yield is rather low and yet the independent fission yield is considerably enhanced.

P. ARMBRUSTER: The width of charge distribution before neutron emission that you found (1.1 charge units) is smaller than the value found by other methods (1.35 ± 0.08 charge units). Will you please comment on the errors in the width of distribution? Large variations in X-ray yields in an isobaric chain may lead to a value of charge distribution seemingly smaller than it actually is.

L. E. GLENDENIN: It is quite possible that the difference between our value of 1.10 ± 0.15 charge units (FWHM) for the primary charge dispersion and the somewhat larger values obtained for the secondary dispersion may in point of fact be small in view of all the experimental uncertainties.

P. FONG: I wish to refer once again to my doctoral dissertation 16 years ago, in which I concluded from the statistical theory that the width of the charge distribution curve is 1.2 charge units (FWHM). The experimental value at that time was about 2.0 and this was considered a serious disagreement. The value of 1.1 reported in this paper is very close to the prediction; the same is observed in other works on charge distribution (Ferguson and Reed, Wahl et al.). Incidentally, that dissertation contains many predictions which a wary scientist would not put down in print for fear of being refuted by experiment. Indeed, most of the predictions were refuted at that time. It is interesting to note that many of them have finally found experimental confirmation after 16 years.

APPLICATION DE NOUVELLES SEPARATIONS CHIMIQUES RAPIDES A LA DETERMINATION DE LA DISTRIBUTION EN CHARGES DANS LA FISSION A BASSE ENERGIE

J. BLACHOT, L.C. CARRAZ, P. CAVALLINI, A. GADELLE,
A. MOUSSA
Centre d'études nucléaires de Grenoble et
Institut des sciences nucléaires de Grenoble,
France

Abstract — Résumé

APPLICATION OF NEW FAST CHEMICAL SEPARATIONS TO THE DETERMINATION OF CHARGE DISTRIBUTION IN LOW-ENERGY FISSION. Methods of fast chemical separation have been developed. The first method is based on the recoil of fission products in $RuCl_3$; the mixture is then heated up to 600°C in a tube with a temperature gradient in less than one minute. The elements Te, Nb, Zr, Mo, Sb, I can thus be separated, the radiochemical purity being good and the yield excellent. The second method makes use of the recoil in naphthalene; sublimation takes place in a tube with a temperature gradient; this method permits the isolation of I and Br. To separate Sb, a method based on the formation of hydrides by treating zinc with an acid solution has also been employed.

These three fast methods have been used to determine the independent fractional or cumulative yields of the following fission products: ^{96}Nb, ^{97}Nb, ^{98}Nb, ^{99}Nb, ^{100}Nb, ^{128}Sb, ^{130}Sb, ^{131}Sb, ^{134}I, ^{136}I.

APPLICATION DE NOUVELLES SEPARATIONS CHIMIQUES RAPIDES A LA DETERMINATION DE LA DISTRIBUTION EN CHARGES DANS LA FISSION A BASSE ENERGIE. On a élaboré des méthodes de séparation chimique rapide. La première est fondée sur le recul des produits de fission dans du $RuCl_3$; puis chauffage à 600°C du mélange dans un tube dans lequel existe un gradient de température. On peut ainsi séparer, en moins d'une minute, avec un très bon rendement et une bonne pureté radiochimique, les éléments suivants: Te, Nb, Zr, Mo, Sb, I. La seconde est basée sur le recul dans le naphtalène et sublimation dans un tube à gradient de température; cette méthode permet d'isoler I et Br. On a appliqué également à la séparation de Sb la méthode basée sur la formation des hydrures par action d'une solution acide sur le zinc.

Ces trois méthodes rapides ont été utilisées pour la détermination des rendements indépendants fractionnels ou cumulatifs des produits de fission suivants: ^{96}Nb, ^{97}Nb, ^{98}Nb, ^{99}Nb, ^{100}Nb, ^{128}Sb, ^{130}Sb, ^{131}Sb, ^{134}I, ^{136}I.

1. INTRODUCTION

La distribution en charge dans la fission à basse énergie a déjà fait l'objet de nombreux travaux par les techniques radiochimiques [1]. Cependant les résultats obtenus sont encore fragmentaires, et l'accord avec les autres méthodes n'est pas toujours parfait. Dans certains cas le désaccord a pu être attribué à l'existence d'isomères encore inconnus, par exemple pour ^{98}Nb [2]. Les progrès de la spectroscopie nucléaire et l'emploi de détecteurs Ge(Li) pour le rayonnement gamma, combiné avec des séparations chimiques rapides, permettent d'étendre le champ des mesures.

Dans la fission de l'uranium les éléments des couples 51 - 41 et 49 - 43 présentent un intérêt particulier, car il a été suggéré par

TABLEAU I. CHAINES DES PRODUITS DE FISSION
(Les valeurs sans référence sont tirées de [4]

A	Chaînes	Rendement de chaîne [5]
96	Rb 0,2 s → Sr 4 s → Y 2,3 min → Zr stable → Nb 23,4 h → Mo stable	6,41
97	Rb 0,1 s → Sr 0,4 s → Y 1,1 s → Zr 17 h ↗ Nb 60 s ↓ Zr 17 h ↘ Nb 74 min ↗ Mo stable	6,33
98	Zr 31 s ↘ Nb 51 min ↘ Mo stable Zr 31 s ↘ Nb 2,8 s [6] ↗ Mo stable	5,93
99	Y 0,8 s → Zr 2,4 s ↗ Nb 2,4 min ↘ Mo 67 h → Zr 2,4 s ↘ Nb 14 s [7] ↗ Mo 67 h	6,25
100	Zr 1 s [7] ↘ Nb 3 min ↘ Mo stable Zr 1 s [7] ↘ Nb 6,6 s [7] ↗ Mo stable	6,58
127	Sn 4 min ↘ Sb 3,9 j ↗ Te 105 j ↘ I stable ↓ Sn 2,1 h ↗ Sb 3,9 j ↘ Te 9,3 h ↗ I stable	
128	Sn 60 min ↗ Sb [8] 10,5 min ↘ Te stable Sn 60 min ↘ Sb 9,6 h ↗ Te stable	
129	Sn 2 min ↘ Sb 4,35 h ↗ Te 37 j ↘ I 10^7 a → Xe stable ↓ Sn 7 min ↗ Sb 4,35 h ↘ Te 72 min ↗ I 10^7 a	
130	Sn 2,6 min ↗ Sb 5,7 min [8] ↘ Te stable Sn 2,6 min ↘ Sb 38 min ↗ Te stable	

TABLEAU I (suite)

A	Chaînes	*Rendement* de chaîne [5]
131	Te 30 h ↓ Te 25 min ; Xe 12 j / Xe stable Sn 1,32 min [9] → Sb 25 min ↗ Te 30 h ↘ I 8,05 j → Xe 12 j Sb 25 min ↘ Te 25 min ↗ I 8,05 j → Xe stable	2,93
134	Sb 1,5 s ↘ Te 42 min → I 53 min → Xe stable Sb 10 s [10] ↗ Te 42 min	8,06
135	Te 18 s [11] → I 6,7 h → Xe 9 h →	6,45
136	Te ? ↗ I 40 s [12] ↘ Xe stable Te ? ↘ I 82 s ↗ Xe stable	6,47

Wahl [3] que la scission 50 – 42 pourrait être favorisée à cause de la couche fermée à 50 protons. Le tableau I rassemble les données de la littérature relatives aux chaînes isobariques dont certains membres ont été étudiés ici.

2. TECHNIQUES EXPERIMENTALES

2.1. Irradiations

De l'uranium naturel a été soumis, dans le réacteur Mélusine, à un flux thermique de $6 \cdot 10^{12}$ n $\cdot$ cm^{-2}s^{-1} (flux rapide E> 1 MeV : 10^{11} n $\cdot$ cm^{-2}s^{-1}). Le transfert au laboratoire est fait par un tube pneumatique pour les irradiations courtes.

2.2. Mesures d'activité

Les mesures d'activité ont été faites par spectrométrie γ. Nous avons disposé de deux détecteurs Ge(Li), l'un de forme plane (4, 8 cm^2 $\times$ 1, 05 cm), l'autre de forme coaxiale (40 cm^3). La chaîne de mesure comprend un amplificateur Tennelec (Tc 130, Tc 200), un convertisseur (CA 13) et un bloc-mémoire (BM 96) Intertechnique. L'efficacité relative des détecteurs en fonction de l'énergie a été mesurée à l'aide des étalons classiques. Nous avons rassemblé dans le tableau II les données de spectroscopie nucléaire utilisées dans les calculs.

TABLEAU II. PROPRIETES NUCLEAIRES DES ISOTOPES UTILISES

Isotope	Transition (keV)	γ par désintégration	Réf.
^{96}Nb	778,2	0,97	[13]
^{97}Zr	743,2	0,912	[14]
^{97g}Nb (72 min)	658,1	0,983	[15]
^{98m}Nb (51 min)	787	1	[6]
^{100}Nb (3 min)	535	1	[16]
^{99}Mo	778,2	0,048	[4]
^{135}I	1260	0,28	[17]

2.3. Séparations chimiques

Des séparations très rapides peuvent être obtenues au moyen du marquage par recul des produits de fission dans une matrice convenable. Après divers essais, nous avons choisi $RuCl_3$ pour former des chlorures volatils, Φ_4Sn ou le naphtalène pour former les halogénures organiques.

2.3.1. Chlorures volatils [16]

On mélange du carbure d'uranium en poudre (grains de 0,7 à 5 μm) avec $RuCl_3$ anhydre, dans la proportion en masses $RuCl_3/UC = 3$. Le mélange bien homogénéisé est introduit dans une ampoule de silice (diamètre intérieur 4 mm), fermée par un tampon de laine de silice. Après irradiation, cette ampoule est introduite dans le tube à gradient de température, en un point où t = 600°C. La pression dans le tube est de l'ordre de 0,02 mmHg. La sublimation est rapide, et 40 s après l'introduction de l'ampoule on découpe le tube en sections de 1 à 3 cm de longueur. La répartition des activités le long du tube est représentée à la figure 1. Les mesures de rayonnement γ sont faites, soit section par section, soit sur l'ensemble des sections contenant un élément donné. Cette technique a été utilisée ici pour les isotopes du niobium. La figure 2 montre deux spectres de la fraction niobium.

2.3.2. Recul dans le naphtalène [18]

La méthode est très voisine, le rapport des masses de naphtalène et de carbure d'uranium est égal à 4. Après irradiation, on peut utiliser la sublimation ou la dissolution dans l'hexane. Dans ce cas, on verse la solution sur une colonne d'alumine, qui ne laisse passer que les composés organiques d'iode et de brome.

2.3.3. Séparation de l'iode par voie humide

Pour les mesures quantitatives, on peut critiquer les méthodes précédentes si l'on suppose que le rendement de marquage pour les fragments de fission reculant directement dans la matrice est différent de celui réalisé après filiation bêta. Nous avons donc utilisé également la méthode classique d'extraction par CCl_4, après un cycle d'oxydo-réduction de l'iode.

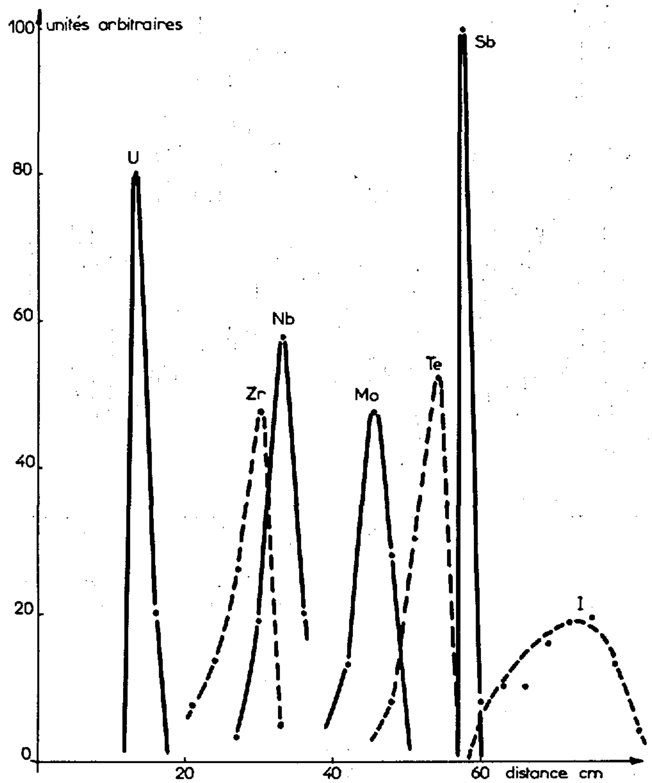

FIG.1. Répartition des éléments le long du tube à gradient de température (activité normalisée à 100 pour chaque élément).

2.3.4. Séparation de l'antimoine

Greendale et Love [19] ont décrit la technique qui consiste à mettre en contact une solution acide (H_2SO_4) d'uranium contenant 1 mg de Sb avec de la poudre de Zn chauffée à 100°C et à déposer un anneau métallique de Sb après passage de SbH_3 dans un four à 500°C. La méthode est très rapide, et les facteurs de décontamination pour les autres produits de fission sont élevés. Cette technique a été utilisée pour les isotopes ^{128}Sb, ^{130}Sb, ^{131}Sb.

2.4. Méthodes de calcul

Les activités des isotopes du niobium, à l'exception de ^{99}Nb, dont le schéma de désintégration est mal connu, ont été mesurées par rapport à celle de ^{97}Zr. Le rendement cumulatif de ^{97}Zr a été pris égal au rendement total de chaîne. Les rendements chimiques ont été déterminés au moyen de la chaîne $^{95}Zr - ^{95}Nb$.

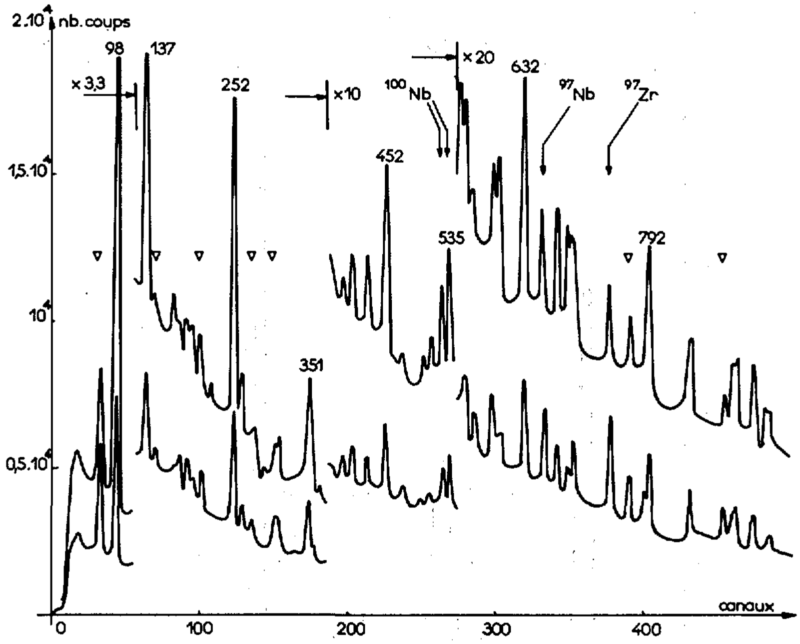

FIG.2. Spectre des isotopes du niobium de courte période ^{99}Nb et ^{100}Nb, 1° spectre supérieur t = 150 s à 270 s après l'irradiation, 2° spectre inférieur t = 390 s à 510 s, ▽ pics attribuables à ^{239}U, ^{134}Te, ^{133}Te.

TABLEAU III. RENDEMENTS, VALEURS OBTENUES
Rendements fractionnels indépendants
Rendements fractionnels cumulatifs†

^{96}Nb	$(8 \pm 2) \cdot 10^{-4}$	^{99}Nb (2,4 min)	0,3 †*
^{97}Nb (72 min)	$(1,3 \pm 0,2) \cdot 10^{-2}$ *	^{100}Nb (3 min)	$(3 \pm 1) \cdot 10^{-3}$ *
^{98}Nb (51 min)	$(8,1 \pm 0,4) \cdot 10^{-3}$ *		

Chaîne	Sn	Sb		Te
128	0,71†	$0,29 \pm 0,04$	0,07 (10 min) 0,22 (9 h)	négligé
130	0,50†	0,46	0,37 (5,7 min) 0,09 (38 min)	0,03
131	0,35†	0,52		0,121
	Te	I		Xe
134	0,90†	$0,1 \pm 0,013$		négligé

* Existence d'un isomère.

Pour ^{99}Nb (2, 4 min) on a mesuré l'activité de ^{99}Mo présente au bout d'un temps t_s = 2 min entre irradiation et séparation, et celle de ^{99}Mo formé ensuite par ^{99}Nb (2, 4 min). On a ainsi le rendement cumulatif fractionnel partiel pour cet isomère, en remarquant que ^{99}Nb (14 s) a pratiquement disparu au temps t_s.

Pour les autres isotopes de Sb et pour ^{134}I on a employé la méthode qui consiste à mesurer l'évolution de l'activité de l'isotope étudié en fonction du délai entre irradiation et séparation. On a alors les rendements fractionnels. La normalisation des conditions d'irradiation et du rendement chimique est faite, soit par référence à un autre isotope produit de fission (^{135}I), soit au moyen d'un entraîneur (Sb) qui est ensuite dosé par analyse par activation. On a admis pour ^{128}Sb et ^{130}Sb que la transition isomérique était négligeable [8]. Enfin, pour ^{136}I l'activité a été comparée à celle de ^{135}I.

3. RESULTATS ET DISCUSSION

Les valeurs obtenues sont rassemblées dans le tableau III.

^{96}Nb - Les valeurs antérieures du rendement étaient assez dispersées [1], et trop faibles [3]. La valeur que nous obtenons, avec Z_p = 38, 2, donne c = 1, 22 ± 0, 06, donc une valeur normale. Ainsi il n'est pas nécessaire de supposer l'existence d'un isomère. D'ailleurs Wogman et al. [20] trouvent également un rendement normal pour ^{96}Nb dans la fission à moyenne énergie.

^{97g}Nb - La situation antérieure était analogue [1]. Notre valeur, avec Z_p = 38, 65, donne c = 1, 56 ± 0, 08.

^{98m}Nb (51 min) - Cet isomère, de spin élevé, n'est probablement pas alimenté par filiation bêta. La valeur que nous obtenons pour le rendement est donc une limite supérieure pour le rendement indépendant. En supposant nulle la filiation bêta on obtient, avec Z_p = 39, 14, c = 0, 79 ± 0, 01.

^{99}Nb (2, 4 min) et ^{100}Nb (3 min) - L'existence d'isomères ne permet pas de conclusion certaine. Il semble que la chaîne Zr-Nb-Mo soit analogue pour les masses 98 et 100 (alimentation bêta quasi nulle de l'isomère de spin élevé).

^{128}Sb - La valeur obtenue est compatible avec Z_p = 50, 16 et c = 1, 10, ce qui semble confirmer l'anomalie déjà observée pour le rendement de ^{128}I déduit de la mesure de ^{128}Xe par spectrométrie de masse [21].

^{130}Sb et ^{131}Sb - Pour calculer les rendements fractionnels, on doit tenir compte de celui du tellure, que l'on détermine par tâtonnements successifs en ajustant Z_p et c. Pour la chaîne 130 on obtient Z_p = 50, 45 et c = 1, 10. Pour la chaîne 131 on obtient Z_p = 50, 72 et c = 1, 10. Ces valeurs confirment, dans la limite des erreurs, celles données par Wahl et al. [3] et par Strom et al. [9].

^{134}I et ^{136}I - La valeur donnée pour ^{134}I suppose l'absence d'isomère. Elle est compatible avec les anciennes mesures [1]. Cependant l'existence d'un isomère est possible [10] et des travaux sont en cours à ce sujet. Pour ^{136}I les mesures anciennes conduisaient à un rendement trop élevé pour ^{136}Xe. Nous avons constaté en réalité l'existence d'un isomère de période voisine de 40 s [12] (fig. 3)[1] et le schéma de désintégration est en cours d'élaboration. L'anomalie signalée pour ^{136}Xe sera donc sûrement réduite.

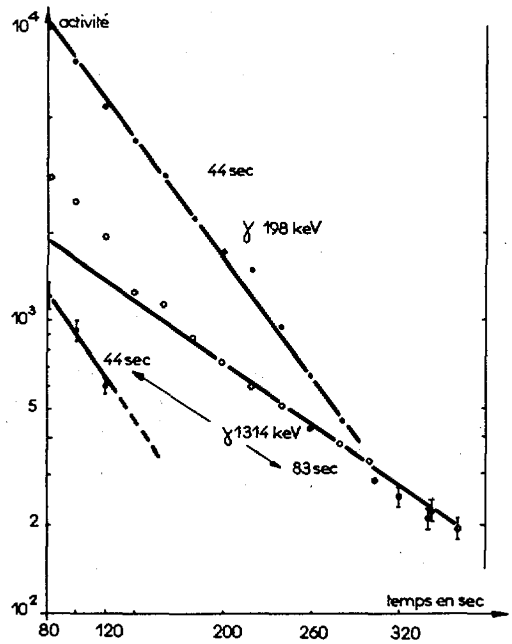

FIG. 3. Courbe de décroissance des γ de 198 keV et 1314 MeV de ^{136}I (origine des temps: fin d'irradiation).

En conclusion il nous semble que les anomalies de la distribution en charges au voisinage de la couche fermée Z = 50 ne sont pas confirmées pour les isotopes du niobium. Au voisinage de la masse 128 par contre, l'anomalie semble bien exister mais de nouvelles mesures sont souhaitables. Enfin l'existence d'isomères encore non décelés est toujours à prendre en considération.

REFERENCES

[1] HYDE, E.K., The Nuclear Properties of the Heavy Elements 3, Prentice Hall (1964) 141-56.
[2] HÜBENTHAL, K., C.r. hebd. Séanc. Acad. Sci. Paris 264B (1967) 468.
[3] WAHL, A.C., FERGUSON, R.L., NETHAWAY, D.R., TROUTNER, D.E., WOLFSBERG, K., Phys. Rev. 126 (1962) 1112.

[1] Après rédaction de ce mémoire nous avons pris connaissance du travail de Lundán et Siivola [22], qui confirme l'existence de cet isomère.

[4] LEDERER, C.M., HOLLANDER, J.M., PERLMAN, I., Table of isotopes, Sixth edition, Wiley J. and Sons, New York (1967).
[5] FARRAR, H., TOMLINSON, R.H., Nucl. Phys. 34 (1962) 367.
[6] HÜBENTHAL, K., MONNAND, E., MOUSSA, A., Nucl. Phys. A 128 (1969) 577.
[7] EIDENS, J., ROECKL, E., ARMBRUSTER, P., Nucl. Phys., A paraître.
[8] HERMANN, G., Communication privée.
[9] STROM, P.O., LOVE, D.L., GREENDALE, A.E., DELUCCHI, A., SAM, D., BALLOU, N.E., Phys. Rev. 144 (1966) 984.
[10] DELUCCHI, A.A., GREENDALE, A.E., STROM, P.O., Phys. Rev. 173 (1968) 1159.
[11] DENSCHLAG, H.O., A paraître.
[12] CARRAZ, L.C., BLACHOT, J., MONNAND, E., MOUSSA, A., A paraître.
[13] MONARO, S., BARRETTE, J., BOUTARD, A., Can. J. Phys. 46 (1968) 2375.
[14] SIIVOLA, A., GRAEFFE, G., Nucl. Phys. A 109 (1968) 369.
[15] GRAEFFE, G., SIIVOLA, A., Nucl. Phys. A 109 (1968) 380.
[16] CAVALLINI, P., Thèse 3e cycle, Grenoble, A paraître.
[17] OP DE BEECK, J.P., WALTERS, W.B., MIT-905-108 (1967) 10.
[18] CARRAZ, L.C., Thèse 3e cycle, Grenoble, A paraître.
[19] GREENDALE, A.E., LOVE, D.L., Analyt. Chem. 35 (1963) 632.
[20] WOGMAN, N.A., POWERS, J.A., COBBLE, J.W., Phys. Rev. 152 (1966) 1088.
[21] KENNETT, T.J., THODE, H.G., Phys. Rev. 103 (1956) 323.
[22] LUNDÁN, A., SIIVOLA, A., Annls Acad. Sci. fennicae A VI Physica (1968) 1288.

DISCUSSION

P. POLAK: We irradiated ^{238}U with 24-MeV deuterons and extracted Sb by an ion-exchange method. In the Sb fraction we observed, among others, gamma lines belonging to ^{126}Sb (12 d) and ^{126m}Sb (20 min) nuclides that could be considered to be shielded, as its parent is too long-lived to be observed. The 12-day ^{126}Sb was observed even in the untreated irradiated material. Even when irradiated with thermal neutrons, one would expect the strongest of the ^{126m}Sb gamma rays to be more intense by two orders of magnitude than, for example, the 685 keV ray from ^{127}Sb observed by Dr. Blachot (mainly because of its short half-life). We subjected our mixture of Sb isotopes to a mass-spectrometric separation (off-line) and were able to identify each gamma. We think Dr. Blachot's experiment should likewise have yielded a set of gamma rays (of 415, 667 and 695 keV respectively), and would like to know if he has observed these. We noticed that ^{126}Sb and ^{126m}Sb are formed in equal quantities, but we concede that in thermal neutron irradiation this may no longer be true.

J. BLACHOT: We, too, observed the gamma transitions to which you refer. Unfortunately, we do not yet have the values for gammas per decay event, but we hope to determine them. It is also true that the yield of ^{126}Sb is much smaller in low-energy fission than in fission with 26 MeV deuterons.

G. HERRMANN: I would like to comment on the isomerism of ^{136}I, which is an interesting case, since ^{136}I contains 53 protons and 83 neutrons. The existence of two isomers of ^{136}I having 86 sec and 35 sec half-life was confirmed by R. Denig and N. Trautmann at Mainz University by the ^{136}Xe(n, p)^{136}I reaction, using enriched ^{136}Xe. The observed gamma-ray spectra are in agreement with those reported by the speaker and by Lundán and Siivola (Ann. Acad. Sci. Fennícae A6 (1968) 287).

PRODUCTS FROM THERMAL-NEUTRON-INDUCED FISSION OF ^{235}U: A CORRELATION OF RADIOCHEMICAL CHARGE AND MASS DISTRIBUTION DATA *

A.C. WAHL, A.E. NORRIS†, R.A. ROUSE**, J.C. WILLIAMS††
Washington University, St. Louis, Missouri,
United States of America

Abstract

PRODUCTS FROM THERMAL-NEUTRON-INDUCED FISSION OF ^{235}U: A CORRELATION OF RADIOCHEMICAL CHARGE AND MASS DISTRIBUTION DATA. Mass and charge distribution data for fission products after prompt neutron emission have been compiled and used to determine ν_t, the average number of prompt neutrons emitted in forming products with complementary mass numbers ($A_\ell + A_h = 236 - \nu_t$), and also Z_p and σ, parameters in a new charge-distribution formulation. The compilation includes both new data and older data, some of it re-evaluated using current values for fission-product half-lives and delayed-neutron yields. The values of ν_t determined using Terrell's method with normalized chain yields are generally consistent with results derived from direct physical measurements. The Z_P values, the most probable (or average) charge for isobars derived from radiochemical data are also consistent with those determined by physical methods involving measurement of X-rays or beta-decay chain lengths. The new Gaussian width parameter σ has a value of 0.56 ± 0.06, which corresponds to a full-width at half-maximum, of 1.50 ± 0.12 charge units. The new charge-distribution formulation has been used with the normalized chain yields to estimate "normal" independent yields for all fission products, for elements, and for isotones. The estimated "normal" yields for complementary elements ($Z_\ell + Z_h = 92$) are essentially equal, as they should be. Comparison of estimated "normal" yields for elements with sums of independent experimental yields for the isotopes shows, where sufficient data exist, that even-Z elements have higher yields than odd-Z elements. The maximum in the "normal" isotone-yield curve occurs at N = 82, and the sum of the measured independent yields for the N = 82 isotones is ~30% higher. It is shown that the probable modes of fission (those giving asymmetric mass and charge division) occur only when the heavy fragment has 50 or more protons.

INTRODUCTION

A number of new yields for products of thermal-neutron induced fission of ^{235}U have been reported recently; in addition, new accurately determined half-life values for many short-lived fission products have made possible the re-evaluation of some older yield data. It seemed desirable, therefore, to summarize the yield data now available and to examine it for evidence of possible effects of nuclear structure on yields, i.e., enhanced probability for mass and charge divisions giving nuclei with even, odd, and/or magic numbers of protons or neutrons.

Although more yield data are available for thermal-neutron induced fission of ^{235}U than for other fission processes, the data are far from complete, and it is usually not possible to

* Work supported by the United States Atomic Energy Commission.
† Present address: Group J-11, Los Alamos Scientific Laboratory, Los Alamos, N.M.
** Present address: Department of Chemistry, Harvard University, Cambridge, Mass.
†† Present address: Department of Chemistry, Memphis State University, Memphis, Tenn.

compare many measured yields in a region of interest. It is useful, therefore, to have estimated yields for reference, derived either theoretically or empirically. We have estimated yields empirically using measured chain yields and estimated fractional independent yields derived from empirically determined Zp and charge-dispersion curves.

In deriving the empirical curves and in discussing the results it is convenient to identify atomic and mass numbers of complementary products. Since light charged particles, e.g., alpha particles, are emitted only rarely in fission, the sum of the atomic numbers of essentially all complementary products is 92, $Z_\ell + Z_h = 92$. The relationship between complementary mass numbers is less exact since varying numbers of neutrons are emitted; we adopt the approximate relationship, $A_\ell + A_h \approx 236 - \nu_t$, where ν_t is the average number of prompt neutrons emitted in forming products with mass numbers A_ℓ and A_h.

NEUTRON EMISSION

The variation of ν_t with A was derived from the chain yields listed in Table II in the Appendix using Terrell's summation method [1].[1] Most of the chain yields listed were derived from measured yields by normalizing them so that the sum of yields in each mass-yield peak was 100.00% and by correcting for delayed-neutron emission (see Table III in the Appendix). Some chain yields were estimated from a smooth mass-yield curve and are so designated in Table II. Normalization decreased measured yield values in the light-mass peak ($A \leqslant 116$) by 0.98%; those in the heavy-mass peak were increased by 1.22%, changes that are within the uncertainties of the experimental measurements.

The derived ν_t values are shown in Fig. 1, where they are compared with values derived from data from physical measurements [2, 3, 4]. Terrell's method gives no information about ν_t for symmetric fission since the value is affected directly by the arbitrary but necessary selection of the point of division between light and heavy mass-yield peaks. Three curves are shown which are in the range of the ν_t values derived from physical measurements; the curves converge rapidly near A_h = 125, where yields increase rapidly, so for $A_h \geqslant 127$ ($A_\ell \leqslant 107$) the selection of the point of division between peaks has no appreciable effect on the results.

Correction of the yields for delayed-neutron emission decreases ν_t values only slightly ($\leqslant 0.05$) in the range A_h = 136 - 150 (A_ℓ = 83 - 98) so the considerable uncertainty in the correction affects the results very little. Also, use of another compilation of chain yields [5] gave similar results, except the dip at A_h = 130 was not as deep.

---

[1]The computation was programmed for the IBM 7072 and 360 computers, and the results were checked graphically for a typical set of data.

The deep dip at $A_h = 130$ is due to the relatively small yields for $A = 127$ and $A = 129$ recently measured [6] and the 1.5% yield estimated for $A = 130$. (Assumption of a 2.0% yield for $A = 130$ increases ν_t at $A_h = 130$ by 0.15.) The difference in the results derived from physical and radiochemical measurements near $A = 130$ may be due in part to uncertainties in the chain yields and in the use of Terrell's method in regions of rapidly changing yields [7] and in part to the limited mass resolution inherent in the physical measurements.

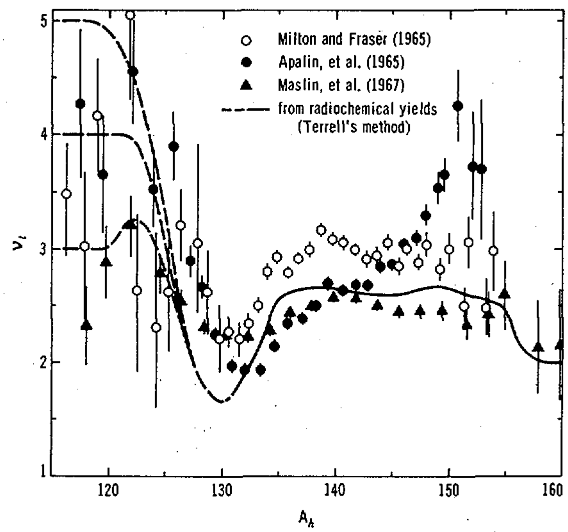

FIG. 1. Variation of ν_t, the number of neutrons emitted in forming products of complementary mass numbers, with A_h, the mass number of the heavy product.

There is no support for the large increase in ν_t for large mass numbers derived from one set of data [3] either from the results of other physical measurements or from the radiochemical data.

Since $\nu_t = 4$ gives a satisfactory energy balance[2] for symmetric mass division, the central curve has been used in the treatment that follows; values of ν_t are listed in Table II in the Appendix. The average number of prompt neutrons calculated from the curve and chain-yield values is 2.48, in agreement with the experimental value of 2.43±0.03 [11].

The average number of neutrons ν_p emitted in forming products of a given mass number was derived by multiplying ν_t by the fraction of neutrons (ν_h/ν_t) or ($1 - \nu_h/\nu_t$) emitted in forming the products of interest. The fraction was derived from a smooth curve drawn through points calculated from the

[2]The method of calculation of Schmitt, Neiler, and Walter [8] was used with data from Myers and Swiatecki's mass tables [9] and Signarbieux, Ribrag, and Nifenecker's [10] kinetic-energy measurements.

data obtained from the physical measurements [2, 3, 4]. (Above $A = 140$ the data from [3] were not used.) The curve drops from 0.50 at $A = 116$ to 0.17 at $A = 128$ and rises irregularly to 0.70 at $A \geqslant 155$. The ν_p values are listed in Table II in the Appendix; a plot (not shown) of ν_p vs. $A' = A + \nu_p$ shows an irregular saw-tooth curve with a maximum value of $\nu_p = 2.7$ at $A' = 112$ and a minimum value of $\nu_p = 0.3$ at $A' = 129$.

The uncertainties in the ν_t and ν_p values listed are estimated to be 0.2 to 0.3 mass units for $A_h > 130$ and $A_\ell < 104$. The uncertainty is due in part to inherent uncertainties in the method ($\pm$0.1 to 0.2 mass units in ν_t [7]) and in part to uncertainties in the yield values. For intermediate mass numbers the uncertainties may be considerably larger because of uncertainties in estimated yield values and because of the uncertainty in the point of division of the light and heavy mass-yield peaks.

CHARGE DISTRIBUTION

The fractional independent and cumulative yields presently known from radiochemical and mass-spectrometric measurements are summarized in the last column of Table II in the Appendix. The values were derived from data given in the listed reference using new half-life and yield values for re-evaluation of some of the data and taking averages where appropriate. All known data have been considered, but a few have been omitted because they were in disagreement with other data and were judged to be in error.

Fractional cumulative yields that are significantly less than unity are now known for two or more products for 19 mass numbers; these yields (except for $A = 84$) are plotted in Fig. 2 on a probability scale against atomic number. The straight lines fitted visually to the points show that the charge disperions are represented reasonably well for most mass numbers by Gaussian distributions [12], although the representation is certainly not exact. For some mass numbers the odd Z isobars have lower yields than the even Z isobars, an effect reported previously by Runnalls, Troutner, and Ferguson [13] and which will be discussed in more detail later. This effect may cause "abnormal" Z_P and σ values for mass numbers with yields for only two adjacent isobars [13].[3] In addition, the enhancement or depletion of yields by shell closures, an effect to be discussed later, can lead to "abnormal" Z_P and σ values or non-Gaussian charge dispersion.

Figs. 3 and 4 show, respectively, the plots of σ and a function of Z_P, both determined from the lines in Fig. 2, against $A' = A + \nu_p$. Although there is considerable scatter when all values are considered, the grouping is reasonably close when only data are considered for mass numbers with

[3] Z_P is the atomic number, not necessarily integral, for which the fractional independent yield for isobars is a maximum; σ is the width parameter for Gaussian charge dispersion in cumulative form [12].

yields for three or more isobars not having 50±1 or 82±1 neutrons or protons or being complementary to such nuclides (filled circles and squares in Figs. 3 and 4).

The average of the selected σ values (for A = 92 - 95 and 141 - 144) is 0.56, the same as the average derived from the yields of only the even Z nuclides with these mass numbers [13].

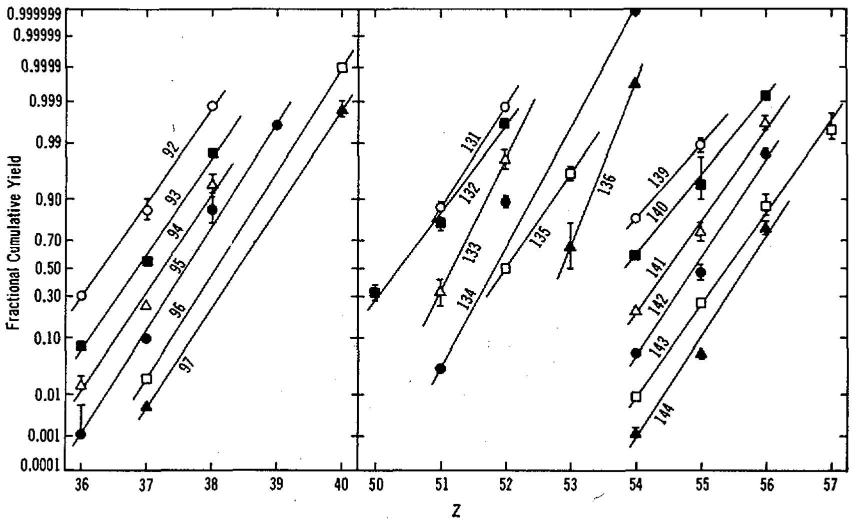

FIG. 2. Probability-scale plots of measured fractional cumulative-yield against atomic number. Mass numbers are given near the lines fitted visually to the data.

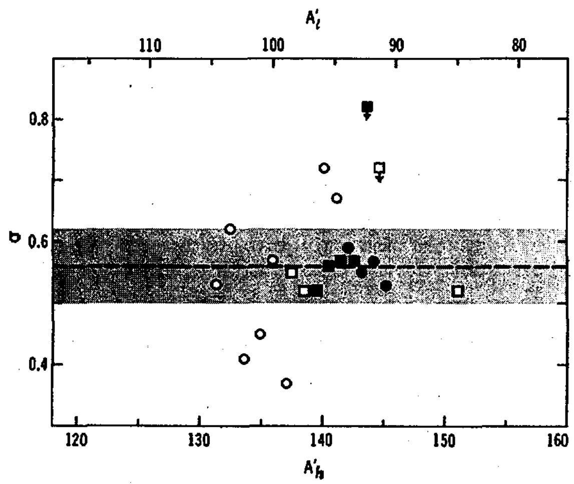

FIG. 3. Plot of the Gaussian charge-dispersion width-parameter σ against average mass number A' of primary fragment precursors. ○, heavy A; □, light A; ●, ■, A's with yields for 3 or more isobars not having 50±1 or 82±1 neutrons or protons or being complementary to such nuclides. Dashed line, with shaded area indicating estimated uncertainty, was used for estimating "normal" independent yields.

(The average of all 19 σ values is 0.55.) It can be seen from Fig. 3 that all of the selected values and a number of the others fall within the range σ = 0.50 to 0.62. The average σ value with its estimated uncertainty, 0.56±0.06, corresponds to a value of $c \approx 2\ (\sigma^2 + 1/12) = 0.80 \pm 0.14$ and to a full-width at half-maximum (f.w.h.m.) value of 1.50±0.12; the width is somewhat smaller than those previously derived from less complete data [12, 17], but it is within the uncertainties that were estimated.

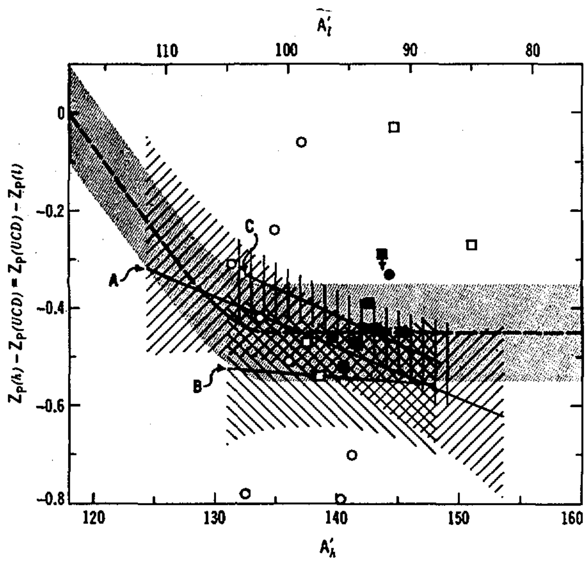

FIG. 4. Plot of the difference between Z_P and Z_P(UCD) = 92(A'/236) against A'. Results of radiochemical measurements: symbols have the same meaning as those in Fig. 3. Results of physical measurements: A [14], B [15], C [16]; cross hatching indicates the reported uncertainty in the Z_P function and the range of mass numbers investigated. Dashed line, with shaded area indicating estimated uncertainty, was used for estimating "normal" independent yields.

The charge dispersion width for products after prompt-neutron emission is appreciably greater than the width for primary fragments before neutron emission (f.w.h.m. = 1.04±0.12) recently determined by Glendenin, Unik, Griffin, and Reisdorf [14]. The difference is most probably due to the increase in charge dispersion from dispersion in the number of prompt neutrons emitted.

Fig. 4 shows the difference between experimental Zp values and those for unchanged charge distribution, Zp(UCD) = 92 x (A'/236). The figure shows that there is agreement between most radiochemical values and the results of various physical measurements. The average value of Zp(h) - Zp(UCD) is -0.44 for mass numbers 92 - 95 and 141 - 144 and is -0.45 for all 19 mass numbers for which Zp was determined radiochemically.

For reasons already discussed, we believe it is more informative to discuss yields of individual fission products than the obvious "abnormal" σ and Zp values plotted in Figs. 3 and

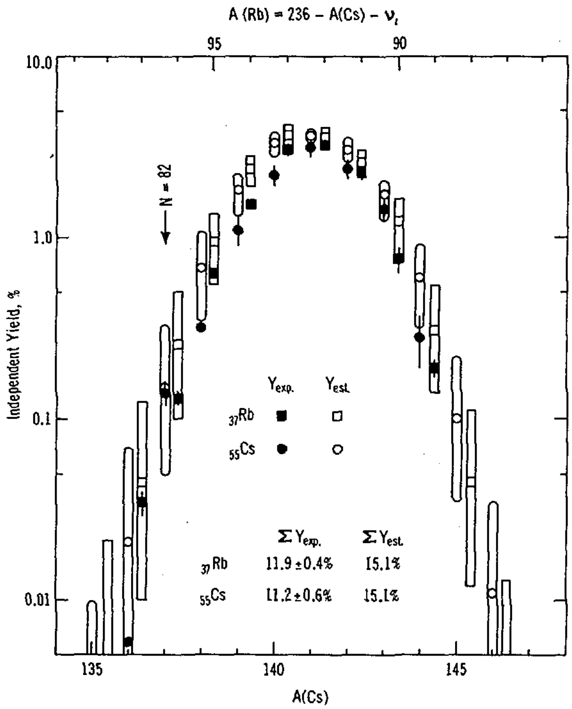

FIG. 5. Independent yields of Rb and Cs isotopes. Elongated areas indicate range of estimated values.

4. It is useful for this discussion to estimate "normal" independent yields by multiplying fractional independent yields, derived from average or assumed "normal" σ and Z_P values, by the experimental chain yields (listed in Table II in the Appendix).[4] The value of σ = 0.56±0.06 was used and was assumed to be independent of A. Values of Z_P were derived from $Z_P(h) - Z_P(UCD) = -0.45\pm0.1$ for $A'_h > 134$ ($A'_\ell < 102$), and since it is reasonable that for symmetric mass division there is also symmetric charge division, and the large fractional cumulative yields of ^{115}Pd [18] and ^{117}Pd [19] show that this assumption is at least approximately correct, the $Z_P(h) - Z_P(UCD)$ function was extrapolated to zero at A'=118 as shown by the dashed line in Fig. 4. The values of Z_P used are listed in column 5 of Table II in the Appendix.

Calculations were made to determine the "best" estimate of a "normal" independent yield using σ = 0.56 and the listed Z_P value and also, since these values are not known precisely, a range of reasonable estimated values was determined by taking the highest and lowest value calculated from the four combinations of σ = 0.50 or 0.62 with Z_P - 0.1 or Z_P + 0.1. Both the "best" estimated values and the ranges of estimated values are

[4]The computation was programmed for the IBM 7072 and 360 computers.

plotted as open areas in Figs. 5 and 6, which show estimated and measured independent yields for isotopes of the complementary elements $_{37}$Rb - $_{55}$Cs, and $_{38}$Sr - $_{54}$Xe, respectively. It is clear that with realistic uncertainties in σ and Z_P, independent yields which are a small fraction of a chain yield can be estimated only approximately.

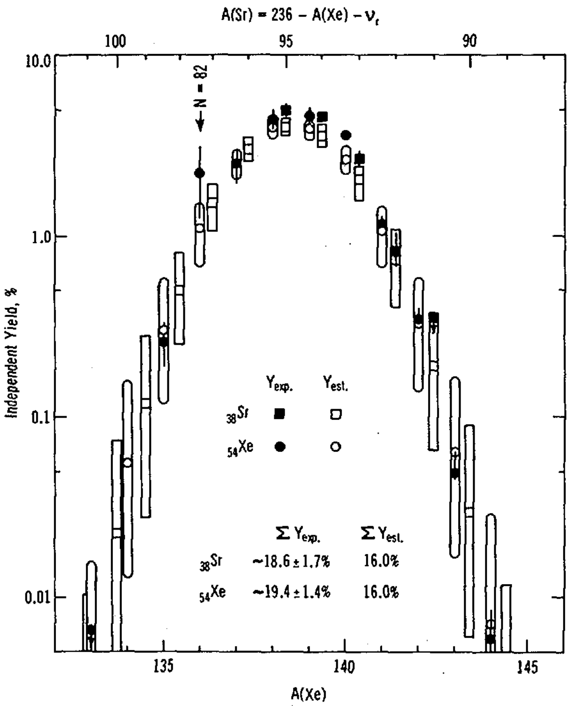

FIG. 6. Independent yields of Sr and Xe isotopes. Elongated areas indicate range of estimated values. The estimated cumulative yield of the I isobar has been subtracted from the measured cumulative yield of a Xe isotope; the estimation of the uncertainty in the resulting Xe independent yield is discussed in the text.

Also given in Figs. 5 and 6 are the sums of the "best" estimated independent yield values, and it can be seen that the sums for complementary elements are the same within 1%, as they should be. This is true for all complementary elements from $_{30}$Zn through $_{62}$Sm, except the estimated yields for $_{43}$Tc, $_{44}$Ru, and $_{45}$Rh are 1 to 4% higher than those of their complements. The condition of nearly equal yields for complementary elements is a necessary one for any satisfactory charge-distribution formulation, but the fulfillment of this condition does not prove that the formulation is correct.

Examination of Figs. 5 and 6 shows that most measured independent yields fall in or near the ranges of estimated yields, indicating that the charge-distribution formulation used is a reasonably good one for isotopes of Rb, Sr, Xe, and Cs. Comparison of estimated and measured independent yields

TABLE I. MAJOR DISCREPANCIES BETWEEN MEASURED AND ESTIMATED FRACTIONAL YIELDS

Fission product	Fractional independent {cumulative} yield		Comments
	Measured	Estimated (range)	
^{77}Ga	{0.57±0.02}	{0.92(0.87-0.96)}	Z odd
^{84}As	{0.17±0.02}	{0.45(0.36-0.52)}	Z odd, N = 51
^{105}Tc	<0.05	0.13(0.08-0.19)	Z odd, $_{49}$In complement
^{106}Tc	<0.11	0.34(0.26-0.39)	Z odd, $_{49}$In complement
^{123}Sn	~0.13±0.06	0.01(<0.04)	Z = 50
^{125}Sn	~0.35±0.15	0.08(0.04-0.13)	Z = 50
^{128}I	$(4\pm1)10^{-5}$	$0.02(<0.5)10^{-5}$	
^{132}Sn	{0.33±0.05}[a]	{0.10(0.05-0.16)}	Z = 50, N = 82
^{133}Sn	{<0.002}	{0.020(0.006-0.045)}	N = 83
^{134}Sb	{0.03±0.01}	{0.13(0.08-0.19)}	Z = 51, N = 83[b]
^{134}Te	0.86±0.08	0.62(0.55-0.71)	Z even, N = 82[b]
^{134}I	0.11±0.01	0.24(0.17-0.31)	Z odd, N = 81
^{136}Xe	~0.35±0.15	0.19(0.11-0.24)	Z even, N = 82[b]
^{140}Xe	{0.60±0.01}	{0.44(0.36-0.51)}	Z even
^{140}Cs	0.34±0.03	0.51(0.44-0.60)	Z odd
^{146}Pm	$(4.2\pm1.2)10^{-7}$	$0.002(<0.2)10^{-7}$	
^{148}Pm	$(7\pm2)10^{-5}$	$0.14(<2.4)10^{-5}$	

[a] Both a lower value of 0.14±0.04 [20] and a higher value of ~0.85 [21] have been reported; these are discussed later.

[b] Short-lived beta-decaying isomers of ^{134}Sb and ^{136}I that were not detected in the yield measurement but have been proposed [22, 23] could also cause the large discrepancies.

for all of the 88 fission products for which data exist indicates that the formulation is reasonably good in general. The 17 fission products for which the discrepancies between measured and estimated fractional yields are greatest are listed in Table I with yields and with brief comments concerning possible causes for the differences, most of which are probably associated with nuclear-structure effects discussed in a later section.

The discrepancies between the measured and estimated yields for ^{128}I, ^{146}Pm, and ^{148}Pm could be due to errors, such as contamination, in the measurement of very small yields. They could also reflect our uncertainty about the Zp and σ functions for near symmetric and for very asymmetric mass division. The values used for estimation are extrapolated, since there has been no direct determination of either Zp or σ for fission products in these mass regions. A value of σ could be assumed and Zp calculated from a single fractional yield, as was done previously [12], or Zp could be assumed and σ calculated from a single yield as Crouch has done [24], but it is not clear that either procedure is superior to extrapolation.

The estimation of Zp values from single yields of odd-Z nuclides (^{134}I, ^{136}Cs, and ^{138}Cs, in particular), yields that are now believed to be low because of their nuclear structures, as will be discussed later, contributed to the dip to -0.7 at $A'_h \approx 135$ in the Zp(h) - Zp(UCD) function proposed previously [12]. Also contributing to the dip were the "abnormal" Zp values determined for A = 139 and A = 140 from yields of adjacent isobars and/or yields of nuclides with 83 neutrons.

The value of σ might be expected to vary with A since a portion of the charge dispersion for products is due to dispersion in the number of neutrons emitted and since the average number of neutrons emitted varies with A. A difficulty that we found in investigating this effect is that varying σ (and using the same Zp function) results in unequal yields of complementary elements. Another potential difficulty with deriving σ from a single fractional yield is that an incorrect or correct but "abnormal" yield results in poor estimates of the yields for all other products with the same mass number.

DELAYED NEUTRON PRECURSORS

Table III in the Appendix is a summary of the delayed-neutron yields presently known or estimated. The table was compiled primarily to allow correction of measured chain-yields, but comparison of measured and estimated delayed-neutron emission probabilities, P_n, gives additional information about how well the proposed charge-distribution formulation correlates fission-product yield data. The agreement is satisfactory except for ^{134}Sb, ^{137}I, and ^{138}I, and the discrepancy between the estimated and measured yields of ^{134}Sb has already been noted in Table I and will be discussed in the next section.

Division of the ^{137}I and ^{138}I delayed-neutron yields by the measured P_n values gives $7.3 \pm 1.8\%$ and $5.0 \pm 1.8\%$, respectively, for the ^{137}I and ^{138}I cumulative yields. These values are large fractions of the total chain yield and would require much lower independent yields for ^{137}Xe and ^{138}Xe than those shown in Fig. 6. We consider this unlikely and suggest that uncertainties in the P_n values and/or delayed-neutron yields are probably larger than indicated.

NUCLEAR STRUCTURE EFFECTS ON YIELDS

Careful examination of Figs. 5 and 6 reveals that there is a general tendency for measured yields for the odd-Z elements, Rb and Cs, to fall below and for the measured yields for the even-Z elements, Sr and Xe, to fall above the "best" estimated yields. This tendency is substantiated by comparing the sums of the "experimental" and estimated yields given in the figures. These values, along with those for Kr, Sb, Te, I, and Ba, are plotted in Fig. 7, which also shows ranges of estimated yields for other elements. It is clear that yields for even-Z elements are higher than those of odd-Z elements.

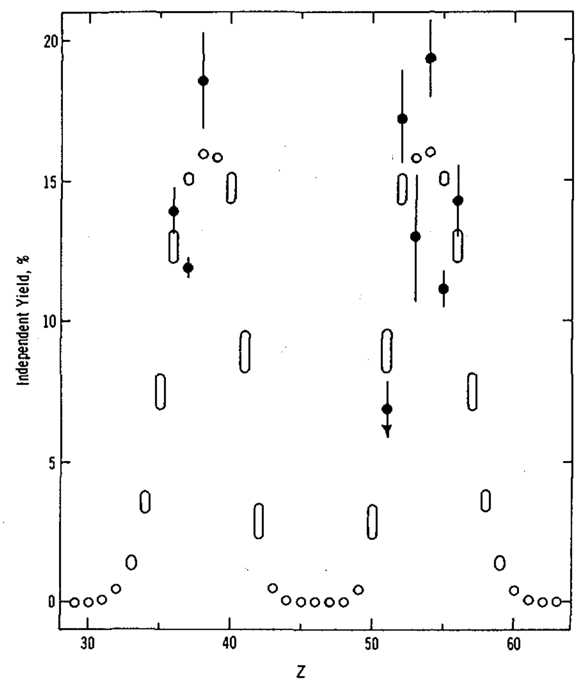

FIG. 7. Isotopic yield plot. ●, "experimental" value; ▯, range of estimated values (a circle indicates range < the diameter).

Included in the "experimental"-yield sums are some estimated yield values for nuclides for which measurements have not been made. Also, estimated cumulative yields of Br and I isobars have been subtracted from measured cumulative yields of Kr and Xe isotopes to give independent yields. The estimated yield contribution and/or correction expressed as percentage of the total yield of each element is: Kr (32%), Rb (0.5%), Sr (30%), Sb (13%), Te (10%), I (48%), Xe (34%), Cs (1.5%), Ba (16%). The uncertainty in the sums of "experimental" yields shown has been estimated by adding to the lower (upper) "limit" of a measured sum (value - (+) uncertainty) the low (high) end of the range of sums of estimated yields used. Since the estimated yield contribution is quite large for some elements,

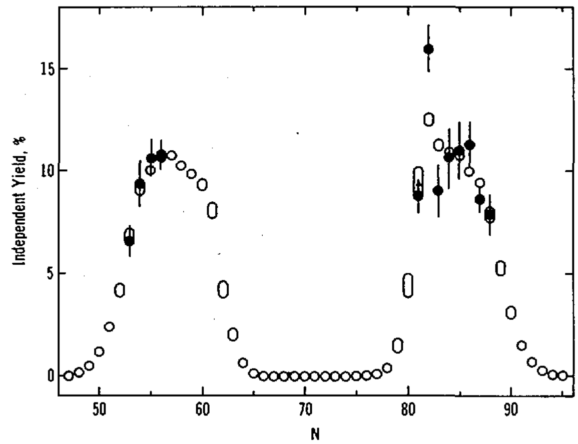

FIG. 8. Isotonic yield plot. ●, "experimental" value; ( ), range of estimated values (a circle indicates range < the diameter).

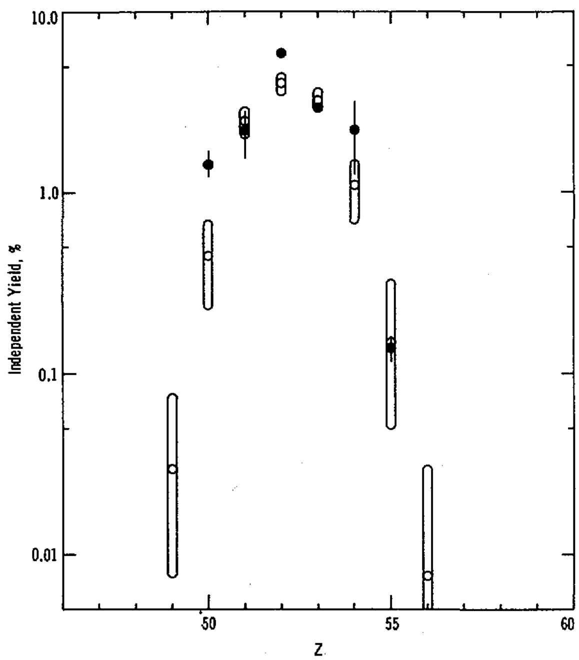

FIG. 9. Independent yields for 82-neutron species. Symbols have the same meaning as those used in Figs 5 and 6.

agreement between sums of "experimental" and estimated yields for these could not be considered significant; however, the differences observed are probably significant since inclusion of estimated yields only reduces the differences (to zero if the estimated yield contribution were 100%), provided the odd-even Z effect is real as is so strongly indicated.

The odd-even Z effect on yield reflects a preference for scission into even-Z fragments; thus proton pairing does enhance the probability of certain fission modes. A similar effect would be expected from neutron pairing, but as shown in Fig. 8 there is little evidence for it, except near the 82-neutron shell, probably because neutron emission disperses the effect so that it is not observed.

The yields for 82-neutron species are shown in Fig. 9, where the oscillation in yield for even- and odd-Z nuclides is seen again. The yields of even-Z nuclides are considerably larger than estimated, and the yields of odd-Z nuclides are about equal to the estimated values, rather than being lower as are those for most other odd-Z nuclides. The sum of yields for 82-neutron species is ~30% larger than the estimated sum, which, as seen in Fig. 8, is the highest of the estimated isotonic yields.

The low cumulative yield of ^{84}As (Table I) indicates that the 50-neutron species ^{84}Se has a high independent yield [25]. There is also evidence that 50-proton species have high independent yields (see Table I). The low yields of ^{133}Sn and ^{134}Sb, both 83-neutron species, may result from the ease of neutron loss due to low neutron binding energies. Conversely, the low yield of ^{134}I, an 81-neutron species, may result from high neutron binding energy of the 82-neutron precursor, ^{135}I.

It is interesting to note that the principal cause of "fine structure" in the mass-yield curve at A = 134 (yield = 8.1%) is the large independent yield of $^{134}_{52}Te_{82}$ (6.9%). Since $^{135}_{52}Te_{83}$ has a "normal" yield of 3.1%, compared to the estimated value of 2.8(2.4 - 3.3)%, it seems unlikely that the large ^{134}Te yield can be due mainly to neutron evaporation. Structural effects at scission probably contribute.

The yield of the doubly magic nuclide $^{132}_{50}Sn_{82}$ is of considerable interest. A large fractional cumulative yield of ~0.85 has been determined [21] by counting beta tracks in photographic emulsions exposed to one of the charge peaks for A = 132 separated with an Ewald-type mass spectrometer. This large yield has been used to support several theoretical models of nuclear-charge distribution [26, 27]. Two lower values of 0.14±0.03 [20] and 0.33±0.05 [28] have been determined by radiochemical methods. Possible causes of the discrepancies are complex and probably not well understood at present. The central and most recently determined value has been selected for discussion in this paper, and it may be noted that this value, corrected for a small estimated ^{132}In cumulative yield, fits in well with the odd-even Z effect for 82-neutron species shown in Fig. 9.

The causes of the high probability of fission modes giving asymmetric mass and charge divisions is, of course, of greatest interest. It will be noted in Fig. 7 that asymmetric charge division becomes probable only when the heavy fragment has 50 or more protons. The same conclusion can be drawn for many other fission processes, almost regardless of the charge-distribution formulation assumed, since the light sides of the heavy mass-yield peaks fall in the same narrow mass-number

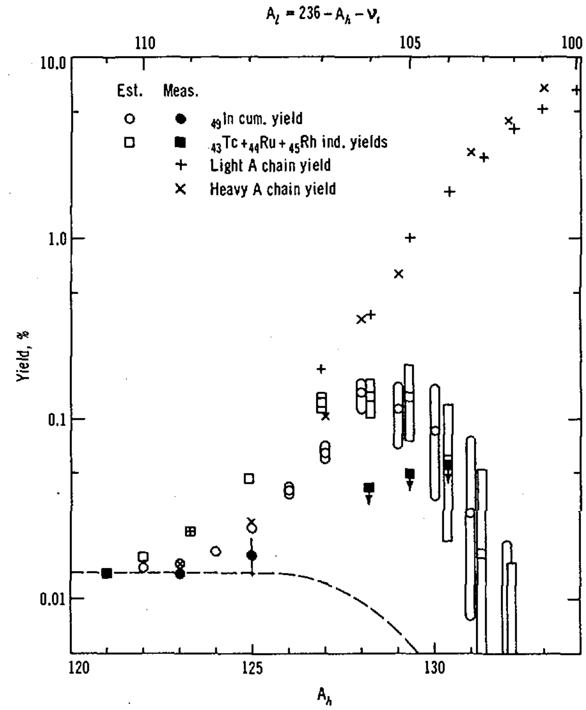

FIG. 10. Mass-yield curves for the mass-number regions in which chain yields increase rapidly from the small yields for symmetric mass division. Dashed line illustrates possible mass-yield curves for near symmetric charge division (Z = 43-49).

region (e.g., see Fig. 4 in [29]). The objection may be raised that the yields being compared — those of elements $_{43}$Tc through $_{49}$In with those of $_{42}$Mo and $_{50}$Sn — are only estimated. However, the estimates are much more dependent on the known chain yields than on the charge-distribution formulation assumed, at least for the reasonable ones that have been investigated, and in addition the data available indicate that the estimated yields used in this paper for $_{50}$Sn isotopes are low (see Table I) and those for the elements between $_{42}$Mo and $_{50}$Sn are high (see Fig. 10). It may be that the mass-yield curve for near symmetric charge division (Z = 43 - 49) is essentially flat topped as illustrated by the dashed line in Fig. 10.

Although the probability for fission increases sharply at Z = 50 for the heavy fragment, the maximum is reached only when N = 82, as shown in Fig. 8. Thus both shell-closure and pairing effects, as shown in Fig. 7, enhance the probability of some modes of fission.

ACKNOWLEDGEMENTS

It is a pleasure to thank J. Terrell for helpful advice concerning the calculation of ν_t and B. R. Erdal, M. M. Fowler, and R. G. Strickert for their assistance in modifying programs for use on the IBM 360 computer. The authors are indebted to P. Armbruster, E. A. C. Crouch, H. O. Denschlag, L. E. Glendenin, G. P. Ford, G. Herrmann, R. Klapisch, E. E. Maslin, G. D. O'Kelley, H. G. Thode, and D. E. Troutner for making their unpublished results available to us.

REFERENCES

[1] TERRELL, J., Phys. Rev. 127 (1962) 880.
[2] MILTON, J.C.D., FRASER, J.S., Physics and Chemistry of Fission, Vol. II, IAEA, Vienna (1965) 39.
[3] APALIN, V.F., GRITSYUK, Yu.N., KUTIKOV, I.E., LEBEDEV, V.I., MIKAELIAN, L.A., Nucl. Phys. 71 (1965) 553.
[4] MASLIN, E.E., RODGERS, A.L., CORE, W.G.F., Phys. Rev. 164 (1967) 1520.
[5] MEEK, M.E., RIDER, B.F., USAEC Rep. APED-5398-A (1968).
[6] ERDAL, B.R., WILLIAMS, J.C., WAHL, A.C., J. inorg. nucl. Chem. (in press).
[7] TERRELL, J., private communication (1965).
[8] SCHMITT, H.W., NEILER, J.H., WALTER, F.J., Phys. Rev. 141 (1965) 1146.
[9] MYERS, W.D., SWIATECKI, W.J., Nuclear Masses and Deformation, USAEC Rep. UCRL-11980 (1965).
[10] SIGNARBIEUX, C., RIBRAG, M., NIFENECKER, H., Nucl. Phys. A99 (1967) 41.
[11] HOPKINS, J.C., DIVEN, B.C., Nucl. Phys. 48 (1963) 433.
[12] WAHL, A.C., FERGUSON, R.L., NETHAWAY, D.R., TROUTNER, D.E., WOLFSBERG, K., Phys. Rev. 126 (1962) 1112.
[13] RUNNALLS, N.G., TROUTNER, D.E., FERGUSON, R.L., Phys. Rev. 179 (1969) 1188.
[14] GLENDENIN, L.E., UNIK, J.P., GRIFFIN, H.C., REISDORF, W., Second Symposium on the Physics and Chemistry of Fission, IAEA (1969) paper SM 122/114.
[15] REISDORF, W., Z. Physik 209 (1968) 77.
[16] SISTEMICH, K., ARMBRUSTER, P., private communication (1969); SISTEMICH, K., Ph.D. Thesis, Nuclear Research Institute, Jülich, No. 574 (1969).
[17] NORRIS, A.E., WAHL, A.C., Phys. Rev. 146 (1966) 926.
[18] ROACH, M.F., FERGUSON, R.L., TROUTNER, D.E., private communication (1967).
[19] WEISS, H.V., ELZIE, J.L., FRESCO, J.M., USNRDL Rep. TR-68-25 (1968).
[20] STROM, P.O., LOVE, D.L., GREENDALE, A.E., DELUCCHI, A.A., SAM, D., BALLOU, N.E., Phys. Rev. 144 (1966) 984.
[21] KONECNY, E., OPOWER, H., GÜNTHER, H., GÖBEL, H., Physics and Chemistry of Fission, Vol. I, IAEA, Vienna (1965) 401; more recent data from theses of GÖBEL, H., RÖSLER, H., quoted in [16, 26].
[22] DELUCCHI, A.A., GREENDALE, A.E., STROM, P.O., Phys. Rev. 173 (1968) 1159.

[23] LUNDÁN, A., SIIVOLA, A., Ann. Acad. Scientiarum Fennicae, AVI (1968) 287.

[24] CROUCH, E.A.C., UKAEA Rep. AERE-R 6056 (1969).

[25] del MARMOL, P., J. inorg. nucl. Chem. 30 (1968) 2873.

[26] NÖRENBERG, W., Z. Physik 197 (1966) 246.

[27] FRAISSNER, H., Z. Naturforschung 21a (1966) 1021.

[28] LIN, C-C., WAHL, A.C., preliminary results, unpublished (1969).

[29] WAHL, A.C., Physics and Chemistry of Fission, Vol. I, IAEA, Vienna (1965) 317.

[30] HERRMANN, G., Habilitationsschrift, Mainz, 1961, Table I, a compilation of fission yield data.

[31] WISH, L., USNRDL Rep. TR-68-35 (1968).

[32] KJELBERG, A., PAPPAS, A.C., J. inorg. nucl. Chem. 11 (1959) 173.

[33] TRACEY, B.L., THODE, H.G., private communication (1969); TRACEY, B.L., Ph.D. Thesis, McMaster University (1969).

[34] CROALL, I.F., WILLIS, H.H., J. inorg. nucl. Chem. 24 (1962) 221.

[35] FARRAR, H., FICKEL, H.R., TOMLINSON, R.H., Can. J. Phys. 40 (1962) 1017.

[36] FLYNN, F.F., GLENDENIN, L.E., private communication (1966).

[37] McHUGH, J.A., J. inorg. nucl. Chem., 28 (1966) 1787.

[38] TOMLINSON, L., HURDUS, M.H., J. inorg. nucl. Chem. 30 (1968) 1995.

[39] WAHL, A.C., J. inorg. nucl. Chem. 6 (1958) 263.

[40] CHAUMONT, J., ROECKL, E., NIR-EL, Y., KLAPISCH, R., private communication (1969).

[41] GRUMMITT, W.E., Milton, G.M., J. inorg. nucl. Chem. 5 (1957) 93.

[42] REED, G.W., Phys. Rev. 98 (1955) 1327.

[43] CARLSON, G.C., SCHICK, W.C., Jr., TALBERT, W.L., Jr., WOHN, F.K., Nucl. Phys. A125 (1969) 267.

[44] PATZELT, P., HERRMANN, G., Physics and Chemistry of Fission, Vol. II, IAEA, Vienna (1965) 243.

[45] AMAREL, I., BERNAS, R., FOUCHER, R., JASTRZEBSKI, J., JOHNSON, A., TEILLAC, J., GAUVIN, H., Phys. Letters 24B (1967) 402.

[46] TALBERT, W.L., Jr., TUCKER, A.B., DAY, G.M., Phys. Rev. 177 (1969) 1805.

[47] AMIEL, S., GILAT, J., NOTEA, A., YELLIN, E., Delayed Fission Neutrons, IAEA, Vienna (1968) 115.

[48] FRITZE, K., KENNETT, T.J., PRESTWICH, W.V., Can. J. Chem. 39 (1961) 675.

[49] ARCHER, N.P., KEECH, G.L., Can. J. Phys. 44 (1966) 1823.

[50] PERLOW, G.J., STEHNEY, A.F., Phys. Rev. 113 (1959) 1269.

[51] AMAREL, I., GAUVIN, H., JOHNSON, A., J. inorg. nucl. Chem. 31 (1969) 577.

[52] CLARKE, W.B., THODE, H.G., Can. J. Phys. 42 (1964) 213.
[53] ALVÄGER, T., NAUMANN, R.A., PETRY, R.F., SIDENIUS, G., THOMAS, T.D., Phys. Rev. 167 (1968) 1105.
[54] FRITZE, K., Can. J. Chem. 40 (1962) 1344.
[55] WAHL, A.C., NORRIS, A.E., FERGUSON, R.L., Phys. Rev. 146 (1966) 931.
[56] NIECE, L.H., USAEC Rep. ORNL-TM-1333 (1965).
[57] CROALL, I.F., J. inorg. nucl. Chem. 16 (1961) 358.
[58] GOEKING, C.F., O'KELLEY, G.D., private communication (1966).
[59] TROUTNER, D.E., FERGUSON, R.L., O'KELLEY, G.D., Phys. Rev. 130 (1963) 1466.
[60] SWARTOUT, J.A., SULLIVAN, W.H., Radiochemical Studies: The Fission Products (CORYELL, C.D., SUGARMAN, N., Eds.), McGraw Hill, New York (1951) 856.
[61] HASTINGS, J.D., TROUTNER, D.E., FERGUSON, R.L., Radiochimica Acta 11 (1969) 51.
[62] FORD, G.P., LEACHMAN, R.B., private communication (1965).
[63] WEISS, H.V., Phys. Rev. 139 (1965) B304.
[64] WAHL, A.C., NETHAWAY, D.R., Phys. Rev. 131 (1963) 830.
[65] ERDAL, B.R., WAHL, A.C., FERGUSON, R.L., preliminary results, unpublished; ERDAL, B.R., Ph.D. Thesis, Washington University, St. Louis, (1966).
[66] STROM, P.O., GRANT, G.R., PAPPAS, A.C., Can. J. Chem. 43 (1965) 2493.
[67] HERRMANN, G., private communication (1969).
[68] ARAS, N.K., GORDON, G.E., J. inorg. nucl. Chem. 28 (1966) 763.
[69] TROUTNER, D.E., WAHL, A.C., FERGUSON, R.L., Phys. Rev. 134 (1964) B1027.
[70] FOWLER, M.M., WAHL, A.C., preliminary results, unpublished (1969).
[71] KENNETT, T.J., THODE, H.G., Phys. Rev. 103 (1956) 323.
[72] FARRAR, H., TOMLINSON, R.H., Nucl. Phys. 34 (1962) 367.
[73] SARANTITES, D.G., GORDON, G.E., CORYELL, C.D., Phys. Rev. 138 (1965) B353.
[74] GREENDALE, A.E., DELUCCHI, A.A., USNRDL Rep. TR-69-11 (1968).
[75] PARSA, B., GORDON, G.E., WENZEL, A., J. inorg. nucl. Chem. 31 (1969) 585.
[76] KATCOFF, S., RUBINSON, W., Phys. Rev. 91 (1953) 1458.
[77] WAHL, A.C., Phys. Rev. 99 (1955) 730.
[78] DENSCHLAG, H.O., J. inorg. nucl. Chem. (in press).
[79] OKAZAKI, A., WALKER, W.G., BIGHAM, C.B., Can. J. Phys. 44 (1966) 237.
[80] BROWN, F., YAFFE, L., Can. J. Chem. 31 (1953) 242.
[81] HOAGLAND, E.J., SUGARMAN, N., Radiochemical Studies: The Fission Products (CORYELL, C.D., SUGARMAN, N., Eds.), McGraw Hill, New York (1951) 1031.
[82] DENIG, R., WAHL, A.C., preliminary results, unpublished (1969).

[83] STANLEY, C.W., KATCOFF, S., J. Chem. Phys. 17 (1949) 653.

[84] BAERG, A.P., BARTHOLOMEW, R.M., BETTS, R.H., Can. J. Chem. 38 (1960) 2147.

[85] WOLFSBERG, K., NETHAWAY, D.R., MALAN, H.P., WAHL, A.C., J. inorg. nucl. Chem. 12 (1960) 201.

[86] ROBERTS, F.P., WHEELWRIGHT, E.J., VAN TOYL, H.H., J. inorg. nucl. Chem. 25 (1963) 1298.

[87] RUNNALLS, N.V., TROUTNER, D.E., private communication (1966); RUNNALLS, N.V., Ph.D. Thesis, U. of Mo., Columbia (1966).

[88] BÄCHMANN, K., Radiochimica Acta 9 (1968) 27.

[89] CHU, Y.Y., Ph.D. Thesis, U. of Calif., Berkeley (1959).

[90] DANIELS, W.R., HOFFMAN, D.C., Phys. Rev. 145 (1966) 911.

[91] BUNNEY, L.R., SCADDEN, E.M., J. inorg. nucl. Chem. 27 (1965) 273.

[92] KEEPIN, G.R., WIMETT, T.F., ZEIGLER, R.K., J. Nucl. Energy 6 (1957) 1; Phys. Rev. 107 (1957) 1044.

[93] ARON, P.M., KOSTOCHKIN, O.I., PETRZHAK, K.A., SHPAKOV, V.I., Soviet Atomic Energy 16 (1964) 447.

[94] TOMLINSON, L., HURDUS, M.H., J. inorg. nucl. Chem. 30 (1968) 1649.

[95] del MARMOL, P., NEVE DE MEVERGNIES, M., J. inorg. nucl. Chem. 29 (1967) 273.

[96] ROECKL, E., EIDENS, J., ARMBRUSTER, P., Z. Physik 220 (1968) 101.

APPENDIX

TABLE II. SUMMARY OF FISSION YIELD DATA[a]

A	Chain yield, %	ν_t	ν_p	Z_P	Element, fractional independent (cumulative) yield
72	(2.0±0.3)10^{-5}[30]	2.00	0.60	28.75	
73	(1.0±0.2)10^{-4}[30]	2.00	0.60	29.14	
74	(3.4±0.5)10^{-4}[30]	2.00	0.60	29.53	
75	~1x10^{-3}[b]	2.00	0.60	29.92	
76	~3x10^{-3}[b]	2.00	0.60	30.31	
77	(7±1)10^{-3}[30]	2.06	0.62	30.71	Ga, (0.573±0.014)[31]
78	(2.1±0.3)10^{-2}[30]	2.25	0.68	31.12	As, (8.5±2.5)10^{-3}[32]
79	(5.3±0.8)10^{-2}[30]	2.50	0.78	31.55	
80	~0.11[b]	2.54	0.79	31.94	Br, ~(6±1)10^{-6}[33]
81	0.22±0.02[34]	2.57	0.82	32.35	
82	~0.35[b]	2.60	0.86	32.75	Br, ~(1.3±0.2)10^{-4} [30,33]
83	0.543±0.011[35]	2.64	0.90	33.16	As, (0.80±0.08)[25]
84	0.96±0.02[35]	2.67	0.96	33.57	As, (0.17±0.02)[25] Rb, (2.4±0.2)10^{-9}]36][c]
85	1.30±0.03[35]	2.67	1.01	33.98	
86	2.00±0.04[35]	2.64	1.08	34.40	Rb, (1.4±0.2)10^{-5}[30,37]
87	2.37±0.05[35]	2.61	1.17	34.82	Se, (0.48±0.10)[38]
88	3.56±0.07[35]	2.60	1.27	35.25	
89	4.71±0.09[35]	2.59	1.32	35.66	Kr, (0.960±0.004)[39] Rb, 0.047±0.016[40][d]
90	5.84±0.12[35]	2.59	1.35	36.06	Kr, (0.86±0.02)[39] Rb, 0.13±0.02[40][d] Y, <8x10^{-5}[41,42]

TABLE II. SUMMARY OF FISSION YIELD DATA[a] (cont'd)

A	Chain yield, %	ν_t	ν_p	Z_P	Element, fractional independent {cumulative} yield
91	5.91±0.12[35]	2.60	1.38	36.46	Kr, {0.59±0.01}[39] Rb, 0.40±0.02[40] Sr, 0.03±0.03[12][e] Y, <0.01[41,42]
92	5.91±0.12[35]	2.62	1.41	36.86	Kr, {0.31±0.01}[39] Rb, 0.55±0.03[40,55][d,e] Y, $(1.3\pm0.2)10^{-3}$[17][d]
93	6.35±0.13[35]	2.65	1.46	37.27	Kr, {$(7.8^{+1.2}_{-0.2})10^{-2}$}[12][e] Rb, 0.48±0.03[40,55][d,e] Y, $(1.6\pm0.2)10^{-2}$[17][d]
94	6.60±0.13[35]	2.66	1.49	37.67	Kr, {$(1.5^{+0.9}_{-0.2})10^{-2}$}[12][e] Rb, 0.23±0.01[40][d] Y, $(6\pm2)10^{-2}$[17][e]
95	6.52±0.13[35]	2.66	1.52	38.08	Kr, {$(1.1^{+5.0}_{-0.1})10^{-3}$}[12][e] Rb, $(9.8\pm0.5)10^{-2}$[40][d] Y, 0.13±0.06[17][e] Zr, $(4.0\pm0.6)10^{-3}$[56]
96	6.36±0.13[35]	2.65	1.54	38.47	Rb, $(2.06\pm0.12)10^{-2}$[40][d] Nb, $(1.0\pm0.2)10^{-4}$[12,57]
97	6.26±0.13[35]	2.62	1.55	38.87	Kr, {$<10^{-5}$}[12] Rb, $(5.6\pm0.7)10^{-3}$[40] Nb, $(1.7\pm0.8)10^{-3}$[12]
98	5.79±0.12[35]	2.58	1.55	39.26	Tc, $(1.5\pm0.2)10^{-7}$[58]
99	6.20±0.12[35]	2.48	1.54	39.65	Nb, {>0.83}[59]
100	6.52±0.13[35]	2.27	1.48	40.01	
101	5.1±0.3[30]	2.07	1.43	40.38	
102	4.1±0.2[30]	1.92	1.40	40.75	Rh, $<2\times10^{-7}$[60]

TABLE II. SUMMARY OF FISSION YIELD DATA[a] (cont'd)

A	Chain yield, %	ν_t	ν_p	Z_P	Element, fractional independent {cumulative} yield
103	2.8±0.2[30]	1.76	1.36	41.11	Mo, {>0.98}[61]
104	1.8±0.1[30]	1.65	1.32	41.47	
105	1.0±0.1[30]	1.69	1.42	41.88	Mo, {>0.95}[61]
106	0.38±0.02[30]	1.82	1.55	42.29	Mo, {>0.89}[61]
107	0.19±0.02[30]	2.10	1.67	42.72	
108	~0.05[b]	3.10	2.45	43.32	
109	0.024±0.003[62][c]	3.71	2.67	43.75	
110	~0.017[b]	3.94	2.60	44.08	
111	0.014±0.002[62][c]	4.00	2.48	44.40	
112	0.012±0.001[62][c]	4.00	2.32	44.70	Ag, $(6\pm3)10^{-5}$[18]
113	~0.011[b]	4.00	2.20	45.01	
114	~0.011[b]	4.00	2.08	45.31	
115	0.011±0.001[30]	4.00	2.04	45.66	Pd, {0.89±0.01}[18]
116	~0.011[b]	4.00	2.00	46.00	
117	~0.011[b]	4.00	1.96	46.34	Pd, {0.68±0.07}[19][c]
118	~0.011[b]	4.00	1.92	46.69	
119	~0.011[b]	4.00	1.80	46.99	
120	~0.012[b]	4.00	1.68	47.30	
121	0.014±0.001[6]	4.00	1.52	47.60	Cd, {≥0.53±0.06}[63][f] Sn, <0.23[64][e]
122	~0.015[b]	3.95	1.34	47.90	
123	0.016±0.001[6]	3.80	1.10	48.27	Sn, ~0.13±0.06[65]
124	~0.019[b]	3.48	0.84	48.43	Sb, $\sim(6\pm2)10^{-4}$[66,67]
125	0.027±0.003[6]	3.06	0.61	48.71	Sn, ~0.35±0.15[65]

TABLE II. SUMMARY OF FISSION YIELD DATA[a] (cont'd)

A	Chain yield, %	ν_t	ν_p	Z_P	Element, fractional independent {cumulative} yield
126	~0.05[b]	2.55	0.46	49.01	Sb, $\gtrsim$~(1.7±0.5)10^{-2} [66,67,68][f] I, <~2x10^{-4}[33]
127	0.104±0.004[6]	2.10	0.34	49.32	Sb, 0.057±0.010[69]
128	0.36±0.06[6]	1.84	0.28	49.66	I, (4±1)10^{-5}[33]
129	0.64±0.04[6]	1.72	0.28	50.02	Sb, ~0.12±0.07[70]
130	~1.5[b]	1.64	0.30	50.39	I, ~(1.6±0.2)10^{-4}[33, 71]
131	2.97±0.06[72]	1.73	0.38	50.80	Sn, $\gtrsim$0.39±0.08[20][f] Te, 0.124±0.014[73] I, (1.4±0.2)10^{-3}[74]
132	4.43±0.09[72]	1.90	0.49	51.21	Sn, {0.33±0.05}[28] Te, 0.20±0.03[20] I, (3.9±0.3)10^{-3}[74] Cs, <4x10^{-8}[37]
133	6.70±0.13[72]	2.10	0.65	51.65	Sn, <0.002[20] Sb, 0.33±0.10[20,75] I, 0.025±0.003[20,74] Xe, <10^{-3}[76]
134	8.13±0.16[72]	2.35	0.85	52.12	Sb, {0.03±0.01}[22,75] I, 0.11±0.01[74,77] Cs, (1.1±0.1)10^{-6}[37][c]
135	6.56±0.13[72]	2.55	0.99	52.56	I, 0.46±0.03[74,78] Xe, 0.04±0.01[76,79, 80,81]
136	6.33±0.13[72]	2.61	1.07	52.98	I, {0.65±0.15}[82,83] Cs, (9.3±0.5)10^{-4} [30,37,84]

TABLE II. SUMMARY OF FISSION YIELD DATA[a] (cont'd)

A	Chain yield, %	ν_t	ν_p	Z_P	Element, fractional independent {cumulative} yield
137	6.37±0.13[72]	2.64	1.11	53.39	Xe, {0.978±0.003}[12]
138	6.75±0.14[72]	2.66	1.14	53.79	Cs, 0.047±0.002[12][e]
139	6.51±0.13[72]	2.66	1.17	54.19	Xe, {0.82±0.02}[39]
					Cs, 0.24±0.04[40][d]
					Ba, $(1.1^{+0.5}_{-0.3})10^{-2}$[12][e]
140	6.43±0.13[72]	2.65	1.19	54.59	Xe, {0.596±0.010}[39]
					Cs, 0.31±0.04[40][d]
					Ba, $(4.6\pm3.0)10^{-2}$[12][e]
					La, $(7\pm1)10^{-4}$[41]
141	5.79±0.12[72]	2.63	1.21	54.99	Xe, $\{0.205^{+0.019}_{-0.004}\}$[85]
					Cs, 0.55±0.07[40][d]
					Ba, 0.26±0.05[12][e]
					La, $(3.7\pm1.3)10^{-3}$[12][e]
142	5.86±0.12[72]	2.61	1.23	55.39	Xe, $\{5.9^{+0.8}_{-0.3})10^{-2}\}$[85][e]
					Cs, 0.41±0.05[40][d]
					La, $(1.7\pm0.4)10^{-2}$[12][e]
143	5.80±0.12[72]	2.60	1.25	55.78	Xe, $\{(8.5^{+0.7}_{-0.5})10^{-3}\}$[39][e]
					Cs, 0.25±0.03[40][d]
					Ba, {0.88±0.06}[13]
					Ce, $(5.3\pm2.6)10^{-3}$[12][e]
144	5.37±0.11[72]	2.59	1.27	56.18	Xe, $\{(1.1^{+0.5}_{-0.1})10^{-3}\}$[39][e]
					Cs, $(5.2\pm1.6)10^{-2}$[40][d]
					Ba, {0.78±0.04}[13]
145	3.85±0.08[72]	2.59	1.30	56.58	
146	2.93±0.06[72]	2.60	1.38	57.00	Pm, $(4.2\pm1.2)10^{-7}$[86]
147	2.19±0.04[72]	2.63	1.55	57.46	Ce, $\{0.963^{+0.037}_{-0.063}\}$[87]

TABLE II. SUMMARY OF FISSION YIELD DATA[a] (cont'd)

A	Chain yield, %	ν_t	ν_p	Z_p	Element, fractional independent {cumulative} yield
148	1.63±0.03[72]	2.66	1.62	57.88	Pm, (7±2)10^{-5}[88]
149	1.03±0.02[72]	2.67	1.68	58.29	
150	0.636±0.013[72]	2.65	1.72	58.70	Pm, (2.1±0.1)10^{-3}[89]
151	0.404±0.008[72]	2.62	1.73	59.09	
152	0.263±0.005[72]	2.58	1.75	59.49	
153	0.150±0.003[72]	2.55	1.76	59.88	
154	0.073±0.002[72]	2.53	1.75	60.27	
155	(2.95±0.06)10^{-2}[72]	2.45	1.69	60.63	
156	(1.3±0.1)10^{-2}[90, 91]	2.18	1.53	60.96	
157	(6.1±0.5)10^{-3}[90, 91]	2.06	1.44	61.31	
158	(3.1±0.6)10^{-3}[90]	2.01	1.41	61.69	
159	(1.05±0.09)10^{-3}[90, 91]	2.00	1.40	62.08	
160	~4x10^{-4}[b]	2.00	1.40	62.47	Tb, <1.3x10^{-3}[67]
161	(9±1)10^{-5}[91]	2.00	1.40	62.86	

[a]Yield values are corrected for delayed neutron emission (see Table III) and are normalized so the sum of yields for each peak (A ⩽ 116 or ⩾ 117) is 100.00%. References are to sources of yield data from which listed values were derived. Uncertainties are for the yield measurements; some small additional, but generally unknown, uncertainty is introduced by the correction for delayed-neutron emission.

[b]Estimated from smooth mass-yield curve.

[c]Uncertainty of ~10% of value assumed.

[d]Relative independent cross sections for ^{89}Rb, ^{90}Rb, ^{91}Rb, ^{92}Rb, and ^{93}Rb and for ^{139}Cs, ^{140}Cs, and ^{141}Cs measured with a mass-spectrometer [40] were normalized to the independent yields determined radiochemically; the normalization factors were used to calculate independent yields for these and the

other Rb and Cs fission products measured. The radiochemical yields were measured or determined from differences between measured Kr or Xe cumulative yields and the Sr or Ba independent yields.

[e] Fractional yield data were re-evaluated using the following new half-life values ^{91}Kr (8.4±0.2 s), ^{91}Rb (58±2 s), ^{92}Kr (1.88±0.04 s), ^{92}Rb (4.5±0.1 s), ^{93}Kr (1.24±0.06 s), ^{93}Rb (5.9±0.3 s), ^{94}Kr (0.4±0.1 s), ^{94}Rb (2.7±0.2 s), ^{94}Sr (78±2 s), ^{95}Rb (0.4±0.1 s), ^{95}Sr (26±1 s), ^{138}I (6.3±0.7 s), ^{138}Xe (14.0±0.2 m), ^{139}Xe (40±1 s), ^{139}Cs (9.2±0.2 m), ^{140}Xe (13.5±0.2 s), ^{140}Cs (64±1 s), ^{141}Xe (1.72±0.02 s), ^{141}Cs (25±1 s), ^{142}Xe (1.25±0.15 s), ^{142}Cs (2.0±0.1 s), and ^{143}Xe (0.96±0.02 s) [43, 44, 45, 46, 47, 48, 49, 50, 51, 52, 53, 54]. The fractional cumulative yield of ^{143}Ba [13] and the yields of the ^{121}Sn isomers [6] were also used.

[f] Measured yield was taken as a lower limit because isomerism is known or appears probable from analogy with neighboring nuclides with similar structures and from consideration of simple shell-model states.

TABLE III. DELAYED-NEUTRON YIELDS

Delayed-neutron precursor	Delayed-neutron yield, %[a]	P_n, %	
		Measured	Estimated[b]
55-s ^{87}Br	0.055±0.005[67]	3.1±0.6[93]	2.6(2.2-3.1)
Sum	0.055±0.005		
55-s period yield	0.052±0.005[92]		
16-s ^{88}Br	0.12±0.03[67]	6.0±1.6[93]	5.1(3.4-7.3)
24-s ^{137}I	0.22±0.04[67]	3.0±0.5[93][g]	6.0(4.3-8.1)
25-s ^{141}Cs	0.0032±0.0006[c]	0.073±0.011[46]	0.07(0.05-0.09)
Sum	0.343±0.050		
22.7-s period yield	0.346±0.018[92]		
5.9-s ^{87}Se	0.005±0.002[67]	0.44±0.20[d]	0.7(0.3-1.5)
4.4-s ^{89}Br	0.16±0.06[67]	7±2[93]	9(4-15)
4.5-s ^{92}Rb	$(6±2)10^{-4}$[c]	0.012±0.004[46]	0.012(0.007-0.017)
5.9-s ^{93}Rb	0.05±0.01[c]	1.5±0.2[46,51]	1.2(0.8-1.6)
11-s ^{134}Sb	$(2.8±0.4)10^{-4}$ [94]	0.11±0.02[d]	0.03(0.01-0.05)
6.5-s ^{138}I	0.10±0.02[67]	2.0±0.6[93]	5(3-8)
Sum	0.316±0.064		
6.2-s period yield	0.310±0.036[92]		
2.0-s ^{85}As[e]	0.04±0.04 } 0.08±0.02 [94,95]		1.3(<5.0)
2.0-s ^{86}As[e]	0.04±0.04 }		4(<18)

TABLE III. DELAYED-NEUTRON YIELDS (cont'd)

Delayed-neutron precursor	Delayed-neutron yield, %[a]	P_n, %	
		Measured	Estimated[b]
2.2-s ^{88}Se	0.05±0.02[67][g]		1.6(0.6-4.4)
1.6-s ^{90}Br	0.13±0.05[67]		14(6-33)
1.9-s ^{92}Kr	$(7.4\pm1.3)10^{-4}$[c]	0.040±0.007[46]	0.05(0.03-0.08)
1.3-s ^{93}Kr	0.013±0.003[c]	2.6±0.5[46]	2.5(1.1-6.2)
2.7-s ^{94}Rb	0.16±0.04[c]	11.0±1.5[51]	6.4(4.0-10)
~2-s ^{98}Y[e]	0.02±0.01[67]		0.5(0.2-0.9)
1.7-s ^{135}Sb	0.035±0.003[94]		18(8-95)
2.0-s ^{139}I	0.11±0.04[67]		16(6-40)
1.7-s ^{141}Xe	$(6.4\pm1.2)10^{-4}$[c]	0.054±0.009[46]	0.06(0.03-0.11)
1.3-s ^{142}Xe	$(1.6\pm0.4)10^{-3}$[c]	0.45±0.08[46]	0.5(0.2-1.5)
2.0-s ^{142}Cs	$(7.4\pm2.1)10^{-3}$[c]	0.27±0.07[46]	0.22(0.14-0.32)
1.6-s ^{143}Cs	0.017±0.004[c]	1.13±0.25[51]	0.9(0.6-1.6)
1.1-s ^{144}Cs	$(3.1\pm1.1)10^{-3}$[c]	1.10±0.25[51]	0.5(0.2-1.3)
Sum	0.628±0.081		
2.3-s period yield	0.624±0.026[92]		
≈0.8-s ^{99}Y[e]	0.10±0.10[96]		4(<11)
≈0.8-s ^{140}I[e]	0.10±0.06[67]		60(>10)[f]
Sum	0.20±0.12		
0.61-s period yield	0.182±0.015[92]		

TABLE III. DELAYED-NEUTRON YIELDS (cont'd)

Delayed-neutron precursor	Delayed-neutron yield, %[a]	P_n, %	
		Measured	Estimated[b]
0.36-s ^{95}Rb	0.046±0.007[c]	7.1±0.9 [51]	5(3-9)
0.23-s ^{96}Rb	0.017±0.003[c]	12.7±1.5 [51]	6(3-19)
0.14-s ^{97}Rb	~0.010±0.005[c]	>20 [51]	~22(>4)[f]
Sum	0.073±0.009		
0.23-s period yield	0.066±0.008 [92]		
Total	1.62±0.18		
	1.58±0.05 [92]		

[a] Some values have been adjusted within the experimental uncertainty to bring the sum of yields from precursors with similar half-lives into agreement with period yields measured by Keepin [92].

[b] Estimated P_n values were calculated by dividing a delayed-neutron yield by the "best" estimate of the precursor cumulative yield. Ranges of P_n values, in (), were calculated by dividing the lower or upper "limits" of delayed-neutron yields, respectively, by upper or lower ends of the ranges of estimated cumulative yields.

[c] Product of P_n value and measured cumulative yield obtained from data in Table II.

[d] Ratio of measured delayed-neutron yield listed and measured cumulative yield obtained from data in Table II.

[e] Assignment uncertain.

[f] The upper end of the estimated range was >100%.

[g] Paper SM-122/22 of these Proceedings gives several new values and a number of values somewhat revised from those obtained from Ref. [67]. The major changes are: a measured P_n value of 4.7± 1.0% for ^{137}I and a yield of 0.003 ± 0.002% for ^{88}Br.

DISCUSSION

E. KONECNY: I am quite pleased to see that your new results on the $A = 132$ chain indicate a well-established shell effect in $Z_p(A)$ as a consequence of the $N = 82$, $Z = 50$ closed shells. As you may recall, we reported in Salzburg an (even more strongly) pronounced shell effect at $A = 132$ by using high-resolution mass spectrometer techniques combined with counting the number of beta decays in a nuclear emulsion. This method, we think, is very simple and clear. Because of the serious discrepancy with earlier radiochemical work, especially by Strom et al. (Phys. Rev. 144 (1966) 984), we have tried to look carefully for systematical errors in our method, but so far we have not found any serious ones. The most important objection to our method was that we might falsely include conversion electrons in our analysis by counting them as beta decays. We have ruled out this possibility by measuring the decay chains with a proportional counter in 4π-geometry, so that the conversion electrons are counted together with the preceding beta particle as one single event. The results were essentially not different from those reported at Salzburg. Thus, your new data are much closer to ours. The rest of the discrepancy may perhaps be explained by the fact that our method, in which selected fragment kinetic energies are used, and a radiochemical study measure, in fact, two different things: if, for instance, the shell effect is fully established at the average kinetic energy for the fragments of mass 132, at which energy we measured, we may quite possibly obtain a less pronounced shell effect in a radiochemical measurement, in which we integrate over all fragments with all kinetic energies, including events with low kinetic energies corresponding to high fragment excitation (where shell effects may be washed out).

I am also very glad that in your new results you do see an odd-even effect, whose presence we demonstrated some years ago.

H. O. DENSCHLAG: I have a comment on the authors' charge distribution curve. In the work summarized in abstract SM-122/26, we have plotted the charge distribution using essentially the fractional yield and prompt neutron evaporation data from your present compilation. The resulting points (Fig. 1) in the mass range $A = 140$-152, undisturbed by shell effects, lie on a smooth line. This shows, as we believe, that the Z_p curve is less sensitive to odd-even effects than the independent yields.

I would like to compare the experimental points to a prediction based on the dumb-bell model - a picture that has often been referred to in this symposium. We assume a dumb-bell configuration with 50 protons and 82 neutrons in the heavy sphere and 32 protons and 50 neutrons in the light one (Fig. 2). This picture leads to a clear-cut prediction in regard to Z_p for two mass splits, namely between the neck and the heavy and light spheres respectively (along the dotted lines in Fig. 2). The two resulting Z_p values are given as the end points of the bold straight line in Fig. 1. The line itself is a linear interpolation representing "knife cuts" through the neck at different positions. "Knife cuts" are probably a poor assumption, because the neutron-rich heavy sphere will probably collect preferentially protons from the neck. Taking this into account, the prediction can be brought into full agreement with the experimental results in this area representing the asymmetric mode of fission, except for the fine structure around $N = 82$ described in abstract SM-122/26.

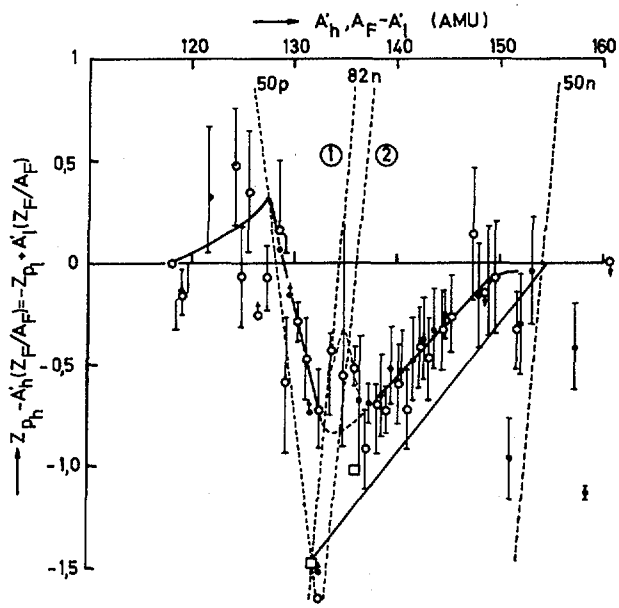

FIG. 1. Charge distribution plotted using essentially the fractional yield and prompt neutron evaporation data from the present paper by Wahl.

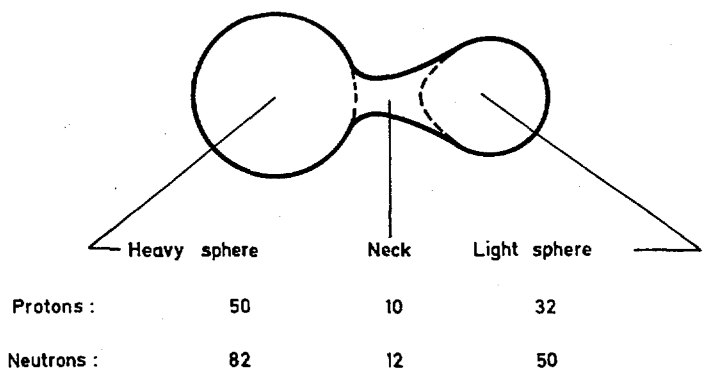

FIG. 2. Dumb-bell configuration.

J. UNIK: We have tried using the neutron yield-fragment mass correlations for ^{235}U given by Milton and Fraser (Ref. [2] of the paper) and also that of Maslin et al. (Ref. [4] of the paper). In our experiment, both the neutron functions gave very similar results. However, we have chosen to use the data of Milton and Fraser, since the data of Maslin et al. have not been corrected for the mass resolution inherent in their experiment.

G. HERRMANN: If the primary charge dispersion curve is considerably narrower than the dispersion curve observed in radiochemical measurements, as is indicated by the data reported by Dr. Glendenin (SM-122/114), then neutron evaporation has a strong effect on charge dispersion. However, since neutron evaporation changes considerably with fragment mass, a mass-dependent secondary dispersion should result if the primary dispersion is constant over the whole mass range. Have you, Dr. Wahl, or has Dr. Glendenin, estimated what the effect would be, especially whether this effect could be brought into agreement with the constant width of the secondary dispersion curve you report in your paper?

A. C. WAHL: We made a very rough estimate of a possible variation of ν_p with A due to neutron evaporation. It seemed reasonable but gave no better correlation with the independent yield data than did a constant ν_p. Therefore, it was not reported.

L. E. GLENDENIN: In reply to Dr. Herrmann, I would like to say that we find no appreciable mass dependence in the charge dispersion width over the mass range investigated. Calculations of the difference to be expected between primary and secondary charge dispersion widths are difficult to make, since no data are available for neutron emission by individual fragments (Z, A) but only average values.

THE EFFECTS OF NUCLEAR EXCITATION OF PROMPT FRAGMENTS ON THE INDEPENDENT YIELDS AND NEUTRON YIELDS IN FISSION

K.S. THIND, B.L. TRACY, H.G. THODE, R.H. TOMLINSON
McMaster University,
Hamilton, Ontario, Canada

Abstract

THE EFFECTS OF NUCLEAR EXCITATION OF PROMPT FRAGMENTS ON THE INDEPENDENT YIELDS AND NEUTRON YIELDS IN FISSION. It has been found possible to account for the fine structure in the neutron yield versus mass distribution. The prediction is based on the assumption of a prompt independent curve obtained from the equal-charge-displacement (ECD) postulate and a linear dependence of fission-fragment excitation energy with mass. The method adopted for calculating neutron yields has been used to investigate the effect of neutron emission on independent yields. Independent yields after neutron emission have been calculated using ECD and a "transition-state" method to describe the prompt charge distribution. The calculated independent yields have been compared with some recent data.

1. Introduction

When binary fission occurs two fragments are formed with identical independent yields. Depending on their excitation each fragment emits neutrons, thus contributing to several separate mass chains. The sum of all the contributions at a given mass and charge is the independent yield after neutron emission and is the quantity normally measured. For example the measured independent yield $Y(^{136}Cs)$ may be expressed as:

$$Y(^{136}Cs) = P_{(o)}y(^{136}Cs) + P_{(1)}y(^{137}Cs) + P_{(2)}y(^{138}Cs) + \ldots \quad (1)$$

where $P_{(o)}$ = probability of emitting zero neutrons from ^{136}Cs.
$P_{(1)}$ = probability of emitting 1 neutron from ^{137}Cs etc.
y = prompt independent yields (before neutron emission).

Several postulates have been proposed to describe the distribution of charge in fission: for example, the unchanged charge distribution (UCD), maximum energy release (MER) and equal charge displacement (ECD). At the present time the ECD postulate appears to give the best description of charge distribution in low-energy fission.

In the ECD postulate there are two empirical relationships:

$$(Z_A - Z_P)_1 = (Z_A - Z_P)_2 \quad (2)$$

and

$$p(Z) = \frac{1}{\sqrt{c\pi}}\, e^{-\frac{(Z - Z_P)^2}{c}} \quad (3)$$

where c is a constant; p(Z) = probability of formation of a nuclide with charge Z; Z_P = most probable charge; Z_A = most stable charge.

As there is no theory which accounts for either the equal charge displacement of equation (2) or the distribution of charge in equation (3), ECD must be considered a purely empirical concept.

Whereas ECD gives the best current representation of independent yields after neutron emission certain independent yields appear to be abnormally high or low when it is attempted to plot them on a smooth Gaussian plot. [1] Wahl [1] has used equation (3) with a value of c characteristic of each mass chain and taken Z_P as a measured quantity. Thus ECD, using equations (2) and (3) may be used to estimate any independent yield for any fissionable nuclide, with a precision usually within an order of magnitude. Wahl's representation merely allows the estimation of independent yields for those mass chains where some of the yields are known experimentally.

Since the neutron separation energies are in general different for each nuclide, particularly in the 82 neutron shell region, it is unlikely that any simple charge distribution could describe the independent yields after neutron emission, even if the independent yields for a given mass chain before neutron emission could be represented by a simple function of charge.

In this paper the independent yields after neutron emission are evaluated assuming two distributions of independent yields before neutron emission. To achieve this it is also necessary to assume the nuclear excitation of the prompt fragments and the neutron evaporation theory of Jackson [2]. The most consistent agreement between the measured independent yields and those calculated has been obtained from a "transition state" model.

In addition to the independent yields, the neutron yields from each mass have been calculated. Terrell [3] has suggested a "universal-neutron yield-curves" which for the heavy fragments is

$$\nu_2 = 0.10(A_2 - 126) \tag{4}$$

where ν_2 = neutron yield for heavy fragments. In fact the neutron yield vs mass is not a linear function and Tomlinson and Gorman [4] have shown that the non-linear character of the neutron yield vs mass could be explained in terms of differences in neutron binding energies. In the present work we have shown that for each fissile nuclide two related linear excitation energy vs mass functions will account for the non-linear neutron emission vs mass relationship. The calculated curves are compared with the experimental data of Apalin et al. [5], Fraser and Milton [6], Terrell [3] and Farrar and Tomlinson [7].

2. 1 Assumptions

The following assumptions have been used in order to calculate the neutron yields as a function of the mass number of the prompt fission fragments.

1) The ECD postulate for the most probable charge Z_p of the prompt fragments and a distribution of charge about Z_p represented by equation (2) using c = 1.4

On such a normalized charge distribution curve about 3 or 4 isobars comprise more than 90% of the chain yield. The neutron yield for this mass chain is mainly due to contributions from these isobars. Although different methods of obtaining Z_p or different distributions of yield could be used, neither the value of Z_p or the nature of the normalized distribution of yields about Z_p critically alters the result of the neutron yield calculation.

2) The sum of the excitation energies of the light and heavy prompt fragments is constant for mass ratios greater than about 1.2. This has been shown to be approximately true by Fraser and Milton [8], and may be represented by equation (5)

$$E_1 + E_2 = E \tag{5}$$

where E_1 and E_2 are the excitation energies including distortion for the prompt fragments and E is the average total excitation energy.

3) The average excitation energy of the prompt fragments is linearly related to their mass number according to equations (6) and (7).

$$E_1 = K' (A_1 - A_1^*) \tag{6}$$

$$E_2 = K' (A_2 - A_2^*) \tag{7}$$

where A is the mass number of the prompt fission fragment and the subscripts 1 and 2 refer to light and heavy fragments respectively. K' is a constant for a given fissile nuclide having the units of energy per nucleon and A_1^* and A_2^* are the intercepts of the linear functions on the mass co-ordinate. Since $A_1 + A_2 = A_f$, where A_f is the mass of the fissioning nuclide equations (5), (6) and (7) give equation (8).

$$A_1^* + A_2^* = A_f - \frac{E}{K'} \tag{8}$$

Equations (6) and (7) imply that the average excitation energy including distortion of the prompt fragments is independent of the nuclear charge for a given mass chain. The recent range measurements of Gordon et al. [9] have shown that the kinetic energy for shielded nuclides such as ^{86}Rb and ^{136}Cs are less than the average for the mass chains as found by Fraser and Milton [8]. This difference in the kinetic energies was found to be approximately equal to the difference in mass between the sum of the masses of the independent products and the sum of the masses of the pair of fragments having the most probable charge. Equations (6) and (7) together with the neutron binding energies are the most critical input to the calculation of the neutron yields. The validity of these functions must be assessed in terms of their success in predicting the neutron yields.

4) The average excitation energy of the prompt fragments has a Gaussian distribution with a full width at half maximum of about 5 MeV. This assumption is important only for low excitation energy. Without such a condition there would be a sharp cut off in the neutron yield when the average excitation energy is less than the neutron binding energy. For nuclear excitations considerably in excess of the neutron binding energy the calculated neutron emission probability is not materially affected by the width of such a distribution.

5) The prompt fragments evaporate neutrons as predicted from the theory of Jackson [2] using a nuclear temperature of 1.4 MeV.

2. 2 Calculations

The number of neutrons emitted by a prompt fragment is evaluated from the excitation energy and a set of neutron emission probability curves for this fragment. The excitation energy is obtained from equations (6) and (7) and the neutron emission probability curves are derived from Jackson's theory using binding energies of neutrons from Seeger's [10] mass formula.

Equation (9) was used for evaluating the number of neutrons emitted by the prompt fragments

$$\nu(A,Z) = \frac{\Sigma P_{(\nu)} \times \nu}{\Sigma P_{(\nu)}} \tag{9}$$

where $P_{(\nu)}$ is the probability of emitting ν neutrons; $\nu = 0, 1, 2, 3, \ldots$

The neutron yield $\bar{\nu}(A)$ is obtained by averaging the number of neutrons emitted, $\nu(A,Z)$, over the prompt independent yields as given by equation (10).

$$\bar{\nu}(A) = \frac{\Sigma[y(A,Z) \cdot X(A)] \cdot \nu(A,Z)}{\Sigma[y(A,Z) \cdot X(A)]} \tag{10}$$

where $y(A,Z)$ = prompt independent yields before neutron emission as determined from a Gaussian charge distribution (assumption 1).

$X(A)$ = prompt mass yields (taken from data of Milton and Fraser .... [8])

Neutron yields $\bar{\nu}(A)$ have been calculated for the thermal neutron fission of ^{233}U, ^{235}U and ^{239}Pu over a region of mass where considerable variation in both the cumulative mass yields and the neutron yields has been observed.

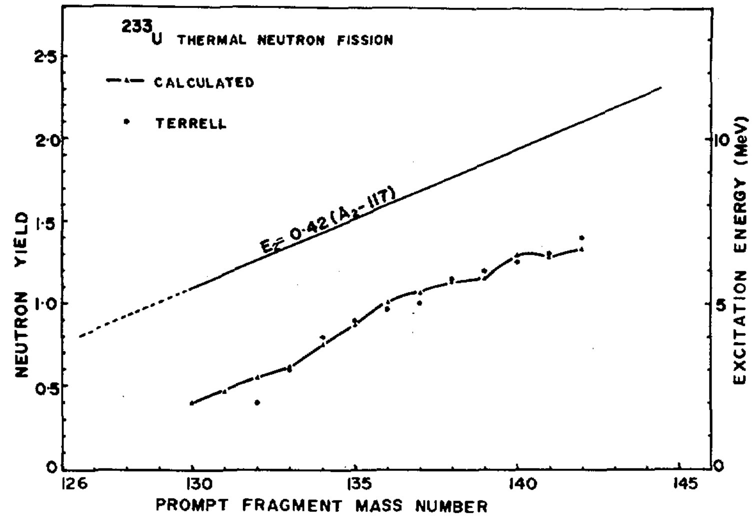

FIG. 1. Mass dependence of neutron yields and excitation energy.

The parameters K' and A_2^* in equation (6) were adjusted until the excitation energy function so obtained gave a reasonable fit of the neutron yields with the experimental values. Figures 1, 2 and 3 show the excitation energy functions, the calculated neutron yields and the experimental neutron yields for the prompt heavy fragments formed in the thermal neutron fission of ^{233}U, ^{235}U and ^{239}Pu. Error bars cannot be realistically shown on either the experimental or the theoretical curves but it must be considered that they are in good agreement with each other. Several groups, [3], [5], [6], [7], have obtained rather similar neutron yields for the heavy mass fragments of ^{235}U, and in this case the calculated curve corresponds most closely to the experimental data as shown in Fig. 2. Figures 4, 5 and 6 show the calculated neutron yields and the experimental values for the

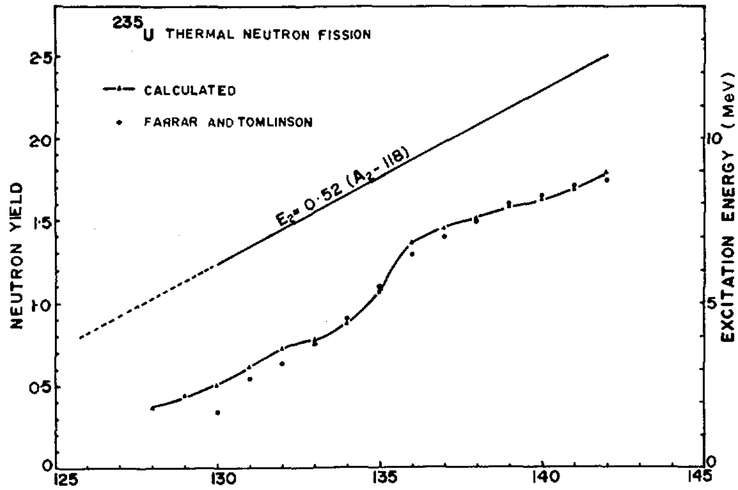

FIG. 2. Mass dependence of neutron yields and excitation energy.

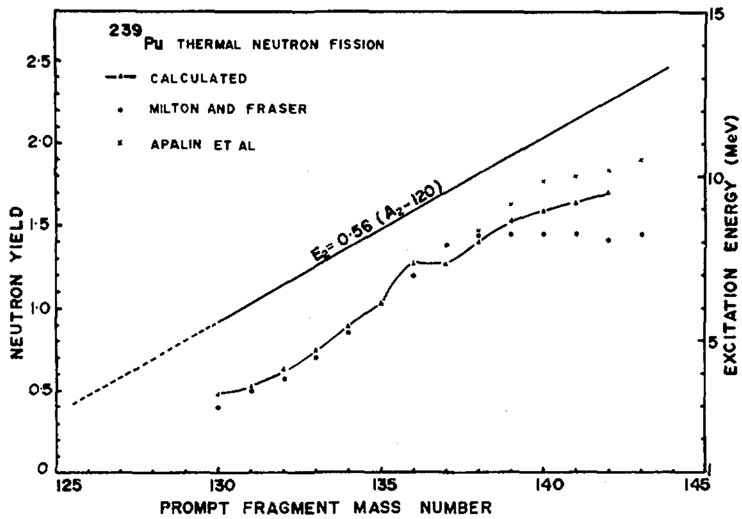

FIG. 3. Mass dependence of neutron yields and excitation energy.

complementary light fragments using equation (6) for the excitation energies and A_1^* fixed by the values of K' and A_2^* found for the heavy mass fragments and the use of equation (8). The value of E in each case was calculated from the difference in the total energy release, as calculated by Milton [11], and the average total kinetic energy, using the Cameron [12] and Seeger [10] mass formulae. The mass intercept of the calculated neutrons yields is directly dependent on differences in E calculated by these two mass formulae.

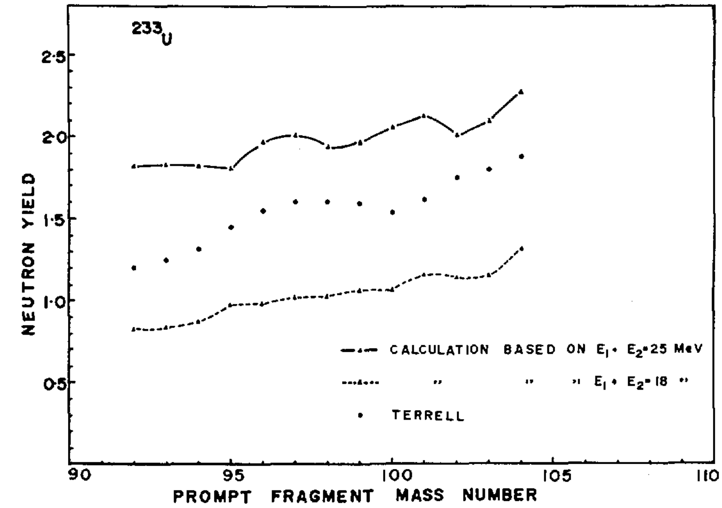

FIG. 4. Mass dependence of neutron yields.

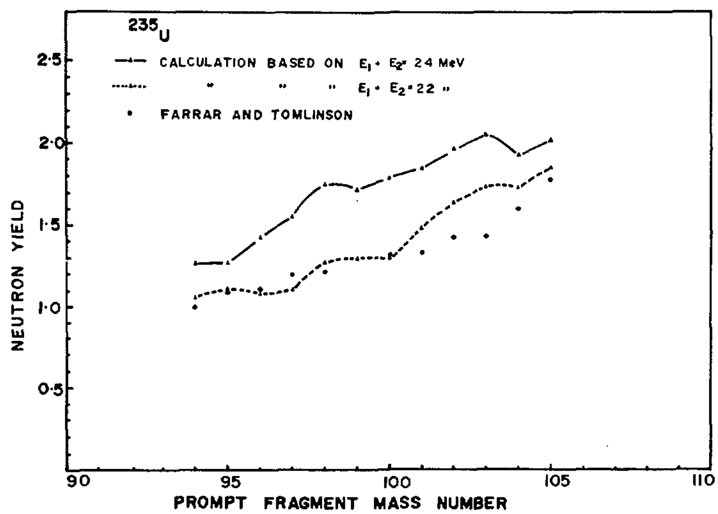

FIG. 5. Mass dependence of neutron yields.

If the value of E was a free parameter, the values which would account for the neutron yields of ^{233}U, ^{235}U and ^{239}Pu would be 21.0 MeV, 22.0 MeV and 24.0 MeV. These values compare with the values 25.0 MeV, 22 MeV and 27 MeV obtained by Milton and Fraser [8] using Cameron's mass formula and 19.0 MeV, 24 MeV and 21.0 MeV using Seeger's mass formula.

The intercept of the extrapolated excitation energy vs mass of the heavy fragment corresponds to one-half the mass of the

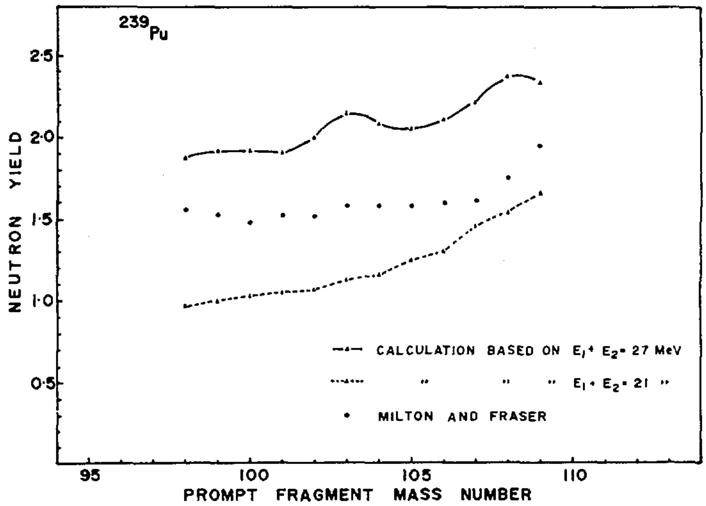

FIG. 6. Mass dependence of neutron yields.

fissioning nuclides reported here. No reason for this apparent coincidence can be provided at this time. It is obvious that in adjusting this constant, values differing by about ± 2 mass units would have been indistinguishable with respect to the curve fitting.

The excitation given by equation (6) and (7) refer to a level not including pairing as discussed in section 3. 1 . That the excitation energy vs mass curve extrapolates to mass 118 in the fission of ^{235}U, does not imply that the excitation is zero at that mass. The neutron yield data used to obtain this curve is not accurately known for the mass region between symmetry and mass 130. The kinetic energy data would imply that the excitation energy might vary significantly from the straight line extrapolation in this mass region and certainly the curve for the light fragments must connect to that for the heavy fragments in some manner which we are not as yet prepared to consider. The slope of the excitation curves implies that each additional proton or neutron associated with a fragment having mass greater than symmetry adds a constant amount of nuclear excitation and deformation energy.

It is felt that the present success in predicting the neutron yields justify the use of the simple equations (6) and (7).

3.1 Independent Yield Calculations

In column 3, Table I, are shown some calculated independent yields using the ECD postulate and c = 1.0 in equation (3). The method adopted for calculating neutron yields makes it possible to examine the

TABLE I

INDEPENDENT YIELDS

Fission Product	Fissile Nuclide	E C D Conventional	E C D After Neutron Emission	Transition State Method	Experimental Values	References
^{46}Nb	^{235}U	7.0×10^{-5}	3.8×10^{-4}	1.7×10^{-4}	$(1.0 \pm 0.2) \times 10^{-4}$	[1]
^{97}Nb	^{235}U	3.8×10^{-4}	3.7×10^{-3}	5.8×10^{-3}	$(1.7 \pm 0.8) \times 10^{-3}$	[1]
^{135}Xe	^{235}U	0.0104	0.0282	0.0591	0.0345 ±0.0019	[13]
^{135}Xe	^{239}Pu	0.0224	0.0548	0.1234	0.1513 ±0.0023	[13]
^{135}Xe	^{233}U	0.0600	0.0730	0.1193	0.2181 ±0.0069	[13]
^{134}Cs	^{235}U	1.1×10^{-5}	1.5×10^{-5}	2.12×10^{-6}	1.1×10^{-6}	[1]
^{136}Cs	^{235}U	6.9×10^{-3}	9.8×10^{-3}	1.9×10^{-3}	$(9.4 \pm 0.4) \times 10^{-4}$	[14]
^{138}Cs	^{235}U	0.110	0.192	0.111	0.045 ± 0.005	[1]
^{140}La	^{235}U	8.0×10^{-3}	1.2×10^{-2}	2.8×10^{-3}	7.0×10^{-4}	[15]
^{128}I	^{235}U	5.5×10^{-7}	1.9×10^{-6}	2.50×10^{-7}	$(3.7 \pm 0.8) \times 10^{-5}$	[16]
^{128}I	^{239}Pu	4.70×10^{-6}	6.17×10^{-5}	4.77×10^{-7}	$(1.23 \pm 0.14) \times 10^{-4}$	[16]
^{128}I	^{233}U	1.05×10^{-5}	1.2×10^{-5}	6.6×10^{-7}	$(3.0 \pm 0.5) \times 10^{-5}$	[16]
^{130}I	^{235}U	1.05×10^{-4}	1.58×10^{-4}	1.57×10^{-5}	$(1.15 \pm 0.15) \times 10^{-4}$	[16]
^{130}I	^{239}Pu	5.59×10^{-4}	2.88×10^{-3}	8.99×10^{-5}	$(1.87 \pm 0.06) \times 10^{-3}$	[16]
^{130}I	^{233}U	1.04×10^{-3}	1.12×10^{-3}	1.10×10^{-4}	$(1.12 \pm 0.07) \times 10^{-3}$	[16]

effect of prompt neutron emission. In column 4 the independent yields are calculated assuming ECD with c = 1.0 before neutron emission and the yields after neutron emission are determined with equation (1). The $P_{(\nu)}$ values have been calculated as discussed in section 2.2. In a typical independent yield such as ^{140}La from the thermal neutron fission of ^{235}U we find that 84% of it comes from the prompt yield of ^{142}La after loss of 2 neutrons and 16% from ^{141}La after loss of 1 neutron. It will be seen that the yields in column 4 are in better correspondence with the experimental yields than those in column 3. The yields after neutron emission are higher than those calculated by the normal ECD method. Apart from neutron binding energy effects which lead to variable changes, Z_P shifts towards Z_A in these calculations. Whereas there are many other reliable independent yields, the group selected represents all the ones on which the ideas of the present paper have been tested. There has been no attempt to plot the calculated independent yields after neutron emission in Table I, as there is no two parameter representation which would give a straight line or smooth curve except for the simple ECD method. It is already well known that all the experimental yields do not fit the simple ECD plots [1].

In column 5 of Table I, the independent yields have been calculated by an entirely different approach which we call the "Transition state" method. This is an adaptation of a method first developed by Eyring [17] to describe the rates of chemical reactions. Hyde [18] has also noted the similarity of chemical reactions to the fission process but has not reported the use of the chemical expression for detailed calculations. Using the approach of Eyring as applied to fission, it may be postulated that the fissioning species is in thermodynamic equilibrium with a transition state which then undergoes scission when an internal vibration becomes a translation along the reaction co-ordinate. In chemical notation Eyring has shown that the rate constant k of a reaction is given by

$$k = \frac{RT}{Nh} e^{-\Delta G^{\ddagger}/RT} \tag{11}$$

where R is the gas constant, T is the absolute temperature, N is Avogadro's number, h is Planck's constant, $\Delta G^{\ddagger}$ is the molar free energy of activation.

Applied to the fission process, assuming a constant volume system (liquid drop approximation), it is possible to write the following expression for two competing reactions involving the same initial species:

$$\frac{k(Z_1 \pm n,\ Z_2 \mp n;\ A_1,\ A_2)}{k(Z_1,\ Z_2;\ A_1,\ A_2)} = e^{-\frac{[\Delta U^{\ddagger}(Z_1 \pm n,\ Z_2 \mp n) - \Delta U^{\ddagger}(Z_1,\ Z_2)]}{\Theta}} \tag{12}$$

where $\Delta U^{\ddagger}$ is the internal energy of activation per fissioning nucleus and Θ is the nuclear temperature. This expression can be evaluated for the relative independent yields of a given mass chain, providing we are prepared to assume that the transition state is the divided but fully excited and deformed nuclei. This is comparable to the activated complex "looking like" the products in chemical notation.

The thermodynamic expression of the first law relating to the transition state for the fission process is:

$$M_f = M_1(Z_1) + M_2(Z_2) + C + K + D + E \tag{13}$$

where M_f = mass of the fissioning nuclide

$M_1(Z_1)$ and $M_2(Z_2)$ are the masses of the fission fragments

C = Coulomb energy

D = deformation energy

E = excitation energy

K = translational or kinetic energy

The energy release at the transition state may be written as:

$$M_f - M_1(Z_1) - M_2(Z_2) - C - D = K + E \tag{14}$$

Since it appears that D and E depend only on the fragment masses and not their charge (section 2. 2), the difference in the energy release for two pairs of fragments differing only in nuclear charge is given by

$$[M_1(Z_1) + M_2(Z_2)] - [M_1(Z_1 \pm n) + M_2(Z_2 \mp n)] - \Delta C = \Delta K \tag{15}$$

where ΔC = the difference in the Coulomb energy and ΔK = the difference in the kinetic energy.

Typical values of ΔM, range from 2 to 20 MeV for variations of one to three charge units from the fragment pair having the lowest mass. Even if all the Coulomb energy were present at the instant of scission, the difference in Coulomb repulsion for any reasonable shape for the pairs of fission fragments would only range up to about 2 MeV for such charge differences. We must conclude therefore that the differences in kinetic energy at the instant of scission are large. In other words the division into two fragments occurs after a considerable fraction of the Coulomb energy is converted into kinetic energy. This implies that the decision concerning mass and charge division is made after the fission barrier has been crossed.

To a first approximation, $\Delta U^{\ddagger}$ in equation (12) may be represented by ΔM, since the differences in entropy for such divisions will be approximately zero (excitation energies are the same). Thus the relative yields of two pairs of fission fragments differing only in charge is given by equation (16).

$$\frac{y(Z_1 \pm n,\ Z_2 \mp n;\ A_1,\ A_2)}{y(Z_1,\ Z_2;\ A_1,\ A_2)} \approx e^{-\frac{\Delta M}{\Theta}}, \tag{16}$$

where rate constants have been replaced by yields. The present ideas differ substantially from the theory of Fong [19]. In Fong's analysis the kinetic energy at the scission point is small. At the top of the fission barrier this is most certainly the case, but apparently a considerable portion of the Coulomb energy has been converted into kinetic energy when the fragments are formed at scission. Halpern [20] on the basis of α particle emission and Swiatecki [21] from the liquid drop model have drawn a similar conclusion.

Equation (16) ignores all parameters describing the fission barrier. This is possible since it is not concerned with the rate of transmission over the barrier but rather with the relative rates of formation of particular products coming from a nucleus which has already reached the barrier. The equation represents in a statistical way the relative probabilities of forming nuclides differing only in nuclear charge. This probability can be expressed in terms of a Boltzman expression involving momentum states only, as we believe that such products have very similar internal excitation. The transition state model has been important primarily in focussing attention on large differences in kinetic energy which must exist at the scission point. The assumption that the portion of the Coulomb energy still available at the instant of Scission is small may be judged on the basis of the success of equation (16) in predicting independent yields. It is obvious that this equation cannot be used to estimate relative yields for division to different masses without taking account of the appropriate differences in internal excitation.

For the nuclides listed in Table I, ΔM have been calculated using the Seeger mass formula without the pairing term as discussed below. Using a nuclear temperature of 1.4 MeV, the relative isobaric yields have been calculated. These relative yields have then been normalized to unity thus giving the fractional independent chain yields before neutron emission. In column 5 Table I are given the independent yields after neutron emission using the method discussed in section 3. 1.

The use of the semi-empirical mass formula without terms for nucleon pairing requires some justification. This is related to the use of a constant nuclear excitation for each nuclide of a given mass number no matter what its nuclear charge. Nuclides having the same number of nucleons and behaving as Fermi gases will have the same level density for a given excitation if this energy is measured from a level not including the pairing of the most loosely bound nucleons. The masses of the nuclides in this state may be computed by ignoring the pairing term in the semi-emperical mass formula. Not only is this easier, for computational procedures, than using the pairing term in the mass formula and then using appropriately different constants and energies in the level density relationship, but is also more reasonable on physical grounds. These nuclides are formed in their excited state and de-excite by neutron emission without ever discovering their ability to pair or not pair in the ground state.

With the exception of the calculated yields for masses 128 and 130, the calculated yields and experimental yields are within a factor of 3. For the Seeger mass formula the masses of nuclides near stability may usually be estimated to within an MeV or ΔM in equation (16) to within about 2 MeV. Apart from the uncertainties in calculating neutron emission effects which are also dependent on the semi-empirical mass formula, this would lead to an approximately 3 fold uncertainty in the estimated yields. It would appear therefore that the calculated yields are satisfactory within the limitation of the semi-empirical mass formula, for all except the 128 and 130 mass chains. In view of the uncertainty in assigning excitation energy to fragments between symmetry and mass number 130, judgement must be reserved on this approach for the calculation of independent yields in the symmetric mass region. The only free parameter in these calculations other than those brought about the semi-empirical mass formula is the nuclear temperature. The value of 1.4 MeV which has been used is the same value found appropriate by Leachman [22] and Jackson [2].

3.2 ECD in Terms of the Transition State Method

It is of some interest to examine the ECD postulate in terms of the "transition state" method. ECD may be justified provided a number of special conditions prevail, all of which can be more or less true. Firstly the variation of independent yields vs charge difference is not greatly altered by the emission of neutrons from the fission fragments providing the neutron binding energies and excitations are the same. We believe that the excitation is constant for a given

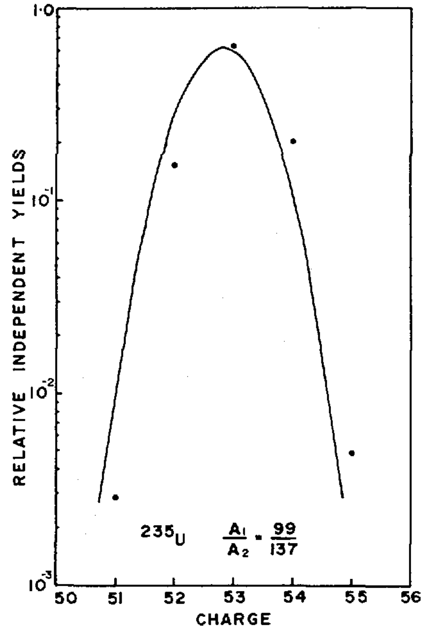

FIG. 7. Solid line shows prompt charge distribution based on ECD with C = 0.79. Solid circles are yields calculated by the transition state method.

mass and except for shell-effects on neutron binding a given independent yield tends to gain from other chains by neutron emission. There is of course a slight shift in Z_P associated with neutron emission. Z_P from the simple ECD would be nearly equivalent to a value corresponding to a minimum value of ΔM in the transition state method providing that the mass vs charge parabolas for the light and heavy fragment isobars are the same. Besides the shell effects, these parabolas are in general wider for the heavy masses than for the light, but since ΔM is calculated for pairs of fragments, this difference is minimized. The Gaussian character of the independent yields when plotted against $Z - Z_P$ may be understood in terms of the Boltzman expression $e^{-\Delta M/\Theta}$, since ΔM increases with each difference in charge from the most probable. For example, in the fission events leading to fragments of mass numbers 137 and 99 the calculated independent yields before neutron emission are plotted against charge as shown in Figure 7. In this figure the solid curve is the calculated ECD Gaussian with c = 0.79 and Z_P calculated from ECD before neutron emission. Similar comparisons may be obtained for even mass chains if the pairing terms in the semi-empirical mass formula is omitted.

REFERENCES

[1] WAHL, A. C., FURGUSON, D. R., NETHAWAY, D. E. and WOLFSBERG, K., Phys. Rev. 126 (1962) 1112.

[2] JACKSON, J. D., Can. J. Phys. 34 (1956) 767.

[3] TERRELL, J., Phys. Rev. 127 (1962) 880.

[4] GORMAN, D. J. and TOMLINSON, R. H., Can. J. Phys. 46 (1968) 1137.

[5] APALIN, V.F., GRITSYUK, N. Y., KUTIKOV, E. E., LEBEDEV, V. I., and MIKAELIAN, L. A., Nucl. Phys. 71 (1965) 553.

[6] MILTON, J. C. and FRASER, J. S., Annual Review of Nuclear Science, 16 (1966) 379.

[7] FARRAR, H. and TOMLINSON, R. H., Can. J. Phys. 40 (1962) 943.

[8] MILTON, J. C. D. and FRASER, J. S., Can. J. Phys. 40 (1962) 1626.

[9] NAKAHARA, H., HARVEY, J. W., GORDON, G. E., submitted to Can. J. Phys., June 1969.

[10] SEEGER, P. A., Nucl. Phys. 25 (1961) 1.

[11] MILTON, J. C. D., UCRL - 9883 Rev. (1962).

[12] CAMERON, A. G. W., CRP - 690, A.E.C.L. No 433 (1957).

[13] HAWKINGS, R. C., EDWARDS, W. J. and OLMSTEAD, W. J., Unpublished data.

[14] KATCOFF, S. and RUBINSON, W., Phys.Rev. 91 (1953) 1458.

[15] GRUMMITT, W. E. and MILTON, G. M., J. Inorg. & Nucl. Chem. 5 (1957) 93.

[16] TRACY, B. L. and THODE, H. G., Private communication - to be published.

[17] EYRING, H., J. Chem. Phys. 3 (1935) 107.

[18] HYDE, E. K., "The Nuclear Properties of Heavy Elements", III (1964).

[19] FONG, P., Phys. Rev. 102 (1956) 434.

[20] HALPERN, I., Unpublished report. See "Nuclear Chemistry", Vol. II, editted by L. Yaffe (1968).

[21] COHEN, S. and SWIATECKI, W. J., Annals of Phys. 22 (1963) 406.

[22] LEACHMAN, R. B., Phys. Rev. 101 (1956) 1005.

DISCUSSION

F. DICKMANN: You mentioned that the kinetic energy of the fission fragments of the scission point should be rather large. To make this statement plausible, you argued that a change of the mass-to-charge ratio of the fragments would affect the energy set free in the fission process much more than their Coulomb interaction at the scission point.

In my view, this will be so only if the shape of the scission configuration is insensitive to the mass-to-charge ratio of the fragments, which may not be true.

R. H. TOMLINSON: I agree completely with this point and, as indicated in my oral presentation, attempts to introduce a correction for this will be made in future studies.

USE OF ANGULAR-DISTRIBUTION MEASUREMENTS OF FISSION FRAGMENTS EMITTED FROM SINGLE CRYSTALS FOR DETERMINING THE LIFETIMES OF EXCITED COMPOUND NUCLEI

W.M. GIBSON
Bell Telephone Laboratories, Murray Hill, N.J.,
United States of America
and
K.O. NIELSEN
Institute of Physics, University of Aarhus,
Denmark

Abstract

USE OF ANGULAR-DISTRIBUTION MEASUREMENTS OF FISSION FRAGMENTS EMITTED FROM SINGLE CRYSTALS FOR DETERMINING THE LIFETIMES OF EXCITED COMPOUND NUCLEI. The angular distribution of fission fragments emitted from uranium oxide crystals bombarded with protons in the energy range 9-12 MeV has been measured by using plastic fission-track detectors. The protein energies, and with these the compound-nuclei excitation energies, were selected to give second-chance fission ^{238}Np compound nuclei with life-times in the range detectable by this technique. An upper limit of $\leq 7 \times 10^{-17}$ s has been established for the "effective lifetime" of compound nuclei formed by 12-MeV proton bombardment of ^{238}U. A value of $1.4 \pm 0.6 \times 10^{-16}$ s has been measured for the total lifetime and $2.5 \pm 1.2 \times 10^{-16}$ s for the partial fission lifetime of ^{238}Np compound nuclei at an average excitation energy of ~7.3 MeV. The measurements were found to be sensitive to random scattering effects. Experimental determination and analytical treatment of such effects are discussed.

INTRODUCTION

Measurements of the lifetime for spontaneous fission isotopes and fission isomers give important information on the properties of the fission barrier [1,2]. However, until now, attempts to measure the very short lifetimes of nuclei excited to energies above the fission barrier have only yielded lower limits [3-5]. This is, of course, because the lifetimes are very short. From neutron-induced fission widths, lifetimes of $\sim 10^{-14}$ sec are estimated for excitation near the barrier [6] and are expected to become rapidly shorter with increasing excitation energy. This report describes a technique based on directional effects connected with the penetration of charged particles in single crystals, which can be used for lifetime measurements in the 10^{-14} - 10^{-18} sec range and describes a measurement of the lifetime of a compound nucleus formed by 10-MeV proton bombardment of U^{238}. Emphasis will be placed on the experimental and analytical techniques.

BASIC PRINCIPLES OF MEASUREMENTS

When positively charged particles are emitted from a normal lattice position in a single crystal, they are almost completely restricted from moving in directions parallel to the low-index atomic planes or axes of the crystal. The angular distribution of such particles emerging from a single crystal shows a regular pattern of minima corresponding to emergence along the low-index axial or planar directions. This effect has been observed for positrons [7], protons [8], alpha particles [9], and fission fragments [5] and is described by the detailed theory of Lindhard [10].

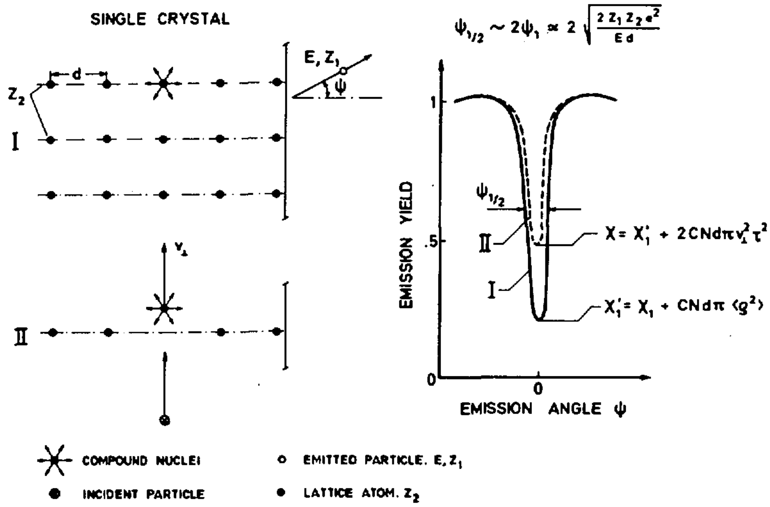

FIG. 1. A schematic representation of the angular distribution on emergence from a single crystal of charged particles emitted (I) from crystalline lattice positions and (II) from a recoiling compound nucleus formed by interaction of an incident particle with a lattice atom. The emission angle $\psi = 0$ is parallel to a row of lattice atoms of spacing d and proton number Z_2. The expressions shown for the width $\psi_{\frac{1}{2}}$ and minimum yield χ are derived from the Lindhard theory [10].

Figure 1 illustrates this effect. Curve I is the angular distribution of positively charged particles emitted from a normal lattice position. The dip can be described by the full width at half maximum, $\psi_{1/2}$, and by the minimum yield χ. If the point of origin of emitted particles is displaced from the atomic rows, the emergent yield distribution is changed as shown qualitatively by curve II of Fig. 1. The displacement affects both the angular width $\psi_{1/2}$ and the minimum yield χ. Both of these effects can be used to determine the mean displacement.

If the displacement arises from recoil of a compound nucleus formed by a nuclear reaction between a lattice atom and a particle incident on the crystal, it is possible from the known recoil velocity perpendicular to the atomic row to measure the mean lifetime τ for the decay of the recoiling compound nucleus.

The possibility of utilizing angular distribution measurements in this way for lifetime measurements was suggested several years ago* [8,12,13]. Recently, Brown et al. [5] have reported on the use of this technique to set a limit on the lifetime of compound nuclei formed by bombardment of U^{238} with 12-MeV protons.

* It is interesting that the first attempt to use emergent particle distribution measurements to measure a compound nuclear lifetime was reported in 1960 [11], even prior to the recognition of the correlated scattering effects upon which the present study is based.

Following the theoretical development and notation given by Lindhard [10], the interatomic potential normal to a row of atoms can be approximated by a screened Thomas-Fermi potential which decreases rapidly in the region of the Thomas-Fermi screening radius a and has an effective cutoff at a distance r_c, which is a few times larger than a. Positively charged particles emitted within a distance r_c in a direction parallel to the row are restricted from moving along the row direction because of deflection by the row potential amd this leads to the minima in the emergent particle angular distributions shown schematically in Fig. 1. The probability that such particles will contribute to the minimum yield in the angular distribution depends on their displacement from the equilibrium lattice position at the time of emission. For a continuum approximation to the row potential and for small displacements, Lindhard has derived a relation between the minimum yield and the mean square displacement $\langle r^2 \rangle$:

$$\chi_2 = \frac{\langle r^2 \rangle}{r_o^2} \qquad (1)$$

The effective area of the row in a plane perpendicular to the row is given by $\pi r_o^2 = 1/Nd$, where N is the atomic density in the crystal and d the atomic spacing along the row. The continuum approximation results in underestimation of the minimum yield by this relationship. This effect has been investigated experimentally for planar [14] and theoretically for axial [15] channeling. On the basis of Monte Carlo calculations of particle trajectories, Barrett [15] has proposed the form:

$$\chi_2 = C \frac{\langle r^2 \rangle}{r_o^2}$$

and has found for 400 keV - 5 MeV protons in a variety of crystals over a wide temperature range that $C \approx 2$-3. C is only approximately constant for small values of the displacement and must approach unity for large displacements. This will be discussed below.

In the normal emission from lattice atoms, $\langle r^2 \rangle$ can be replaced by the mean square thermal vibrational amplitude, ρ^2, but in the present case, an additional displacement x, due to the recoil of the compound nucleus, must be considered. This leads to:

$$\chi_2 = C\frac{\rho^2}{r_o^2} + C\int_0^{r_c} \frac{x^2}{r_o^2}\, e^{-\frac{x}{v_\perp \tau}} \frac{dx}{v_\perp \tau}$$

$$= C\frac{\rho^2}{r_o^2} + \frac{2Cv_\perp^2\tau^2}{r_o^2}\left[1 - \left(1 + \frac{r_c}{v_\perp \tau}\right)e^{-\frac{r_c}{v_\perp \tau}} - \frac{1}{2}\left(\frac{r_c}{v_\perp \tau}\right)^2 e^{-\frac{r_c}{v_\perp \tau}}\right] \qquad (2)$$

if exponential decayis assumed and $v_\perp \tau$ is the mean recoil distance given by the recoil velocity $v_\perp$ perpendicular to the atomic row and the mean lifetime τ. The term in brackets includes a correction for those particles which are emitted on the long tail of the exponential distribution at distances larger than r_c. The contribution of such particles to the minimum yield is very important and is discussed below. A similar correction for the thermal vibration term is not necessary because of the sharper cutoff in the gaussian distribution of the thermal vibration.

Particles emitted at distances larger than r_c are not blocked by the row potential and are therefore able to move in the direction of the row.

The contribution of such particles to the minimum yield is determined by their fractional probability, which is

$$\chi_3 = e^{-\frac{r_c}{v_\perp \tau}} \tag{3}$$

As discussed by Lindhard [10], in addition to contributions to the minimum yield from displacement effects, it is necessary to consider also a contribution, χ_1, arising from random scattering effects in the crystal or at the crystal surface. The observed minimum yield is then $\chi = \chi_1 + \chi_2 + \chi_3$. Treatment of the scattering effect as an additive term, in this way, neglects the dependence of random scattering on the particle trajectory distributions. Since random scattering into the string direction is expected to be only weakly dependent on $\langle r^2 \rangle$, this approximation should not introduce serious error. Furthermore, as will be shown later, comparison of results in which the scattering contribution is drastically changed, supports this conclusion.

The resulting relationship between a measured minimum yield and the mean lifetime for decay of a recoiling compound nucleus is

$$\chi - \chi_1' = \overbrace{\frac{2Cv_\perp^2\tau^2}{r_o^2}\left[1-\left(1+\frac{r_c}{v_\perp\tau}\right)e^{-\frac{r_c}{v_\perp\tau}} - \frac{1}{2}\left(\frac{r_c}{v_\perp\tau}\right)^2 e^{-\frac{r_c}{v_\perp\tau}}\right]}^{\mathrm{I}} + \overbrace{e^{-\frac{r_c}{v_\perp\tau}}}^{\mathrm{II}} \tag{4}$$

The term χ_1' now contains thermal vibration as well as random scattering effects. It should be pointed out that the energy loss of the recoil is not taken into account in eq. (4); however, for the small distances involved (i.e. $v_\perp\tau < r_o$), the energy loss is negligible.

Evaluation of the random scattering term χ_1' is very important in any lifetime determination. This will be considered in detail later. For the moment we will assume that the corrected value $\chi - \chi_1'$ can be determined. It still remains to determine the proper values of the constant C and the cutoff distance r_c. Actually, C is not independent of the mean displacement $v_\perp\tau$. Barrett [15] has found approximate independence for small values of the displacement, but it is apparent that C must approach unity at large values. In the absence of information on the functional dependence of C, we will assume a constant value of 2.5 ± 0.5 (as found for 400 keV - 5 MeV protons channeling in aluminum and tungsten). As we will show, the resulting lifetimes are relatively insensitive to the value of C or the details of displacement dependence over most of the range of interest. A more serious question concerns choice of the cutoff distance r_c. Andersen's [17] calculations and measurements of the effects of thermal vibration on the angular distribution of emitted particles suggest that the cutoff should be somewhat larger than a, the Thomas-Fermi screening distance. The proper value may depend on the multiple scattering and angular resolution for each particular case. We estimate that a value between $3a$ and $5a$ ($a \sim 0.1$Å) is probably appropriate in the present case. The two displacement terms of eq. (4) are plotted as a function of the mean recoil displacement in Fig. 2. The "cutoff term" (term II) is shown for $r_c = 0.3$, 0.4, and 0.5 Å. Term I is shown only for $r_c = 0.4$ Å. Figure 3 shows these two terms and their sum on an expanded scale for $r_c = 0.4$ Å. It is clear that for minimum yield changes of more than a few percent, the last term of eq. (4) will dominate.

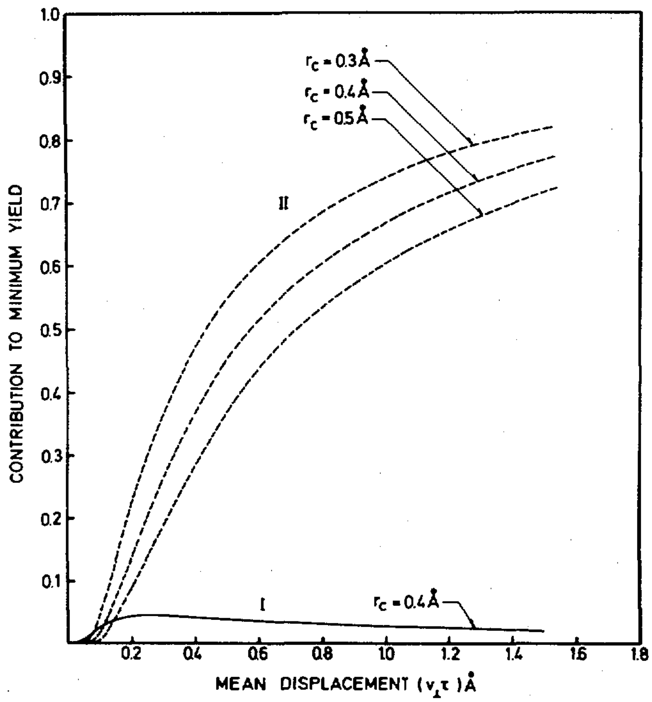

FIG. 2. The displacement terms of Eq. (4) plotted separately for values of the cut-off parameter, r_c, indicated.

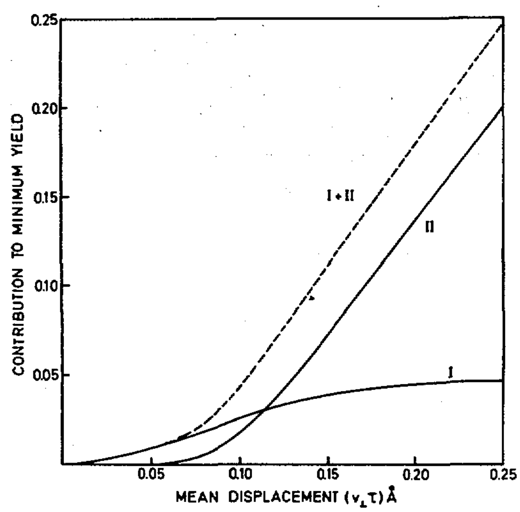

FIG. 3. An expanded plot of the terms of Eq. (4) for small values of the mean displacement. A cut-off distance $r_c + 0.4$ Å was used and a value of the constant C, as discussed in the text.

An alternative method of analysis of emitted particle angular distributions can also be considered. A comprehensive investigation of the influence of emission displacement on emitted particle angular distributions has been reported by Andersen [17]. Figure 4, showing angular distributions, calculated for the emission of 500 keV protons from a ⟨100⟩ string in a tungsten crystal for different values of the thermal vibrational amplitude, is reproduced from Andersen's paper.

It is possible, by means of the technique outlined by Andersen, to calculate the shape of the angular distribution, or alternatively the area [18] or volume of the yield minimum for different values of the mean square displacement of the emission point from equilibrium lattice positions. Such a calculation, however, does not consider random scattering effects. Furthermore, this calculation involves numerical integration of complicated integral expressions, thus complicating inclusion or investigation of the role of random scattering. For this reason, the analytical approach outlined above was used in the present work.

It was noted by Andersen [17] that the width of the angular distribution curve is perhaps less sensitive to random scattering effects than are some of the other features, e.g. the minimum yield. It will therefore be instructive to compare the calculated width variation to width changes expected from the final lifetime determinations. This can be done by using the tabulated values for the width as a function of thermal vibrational amplitude shown in Fig. 4*.

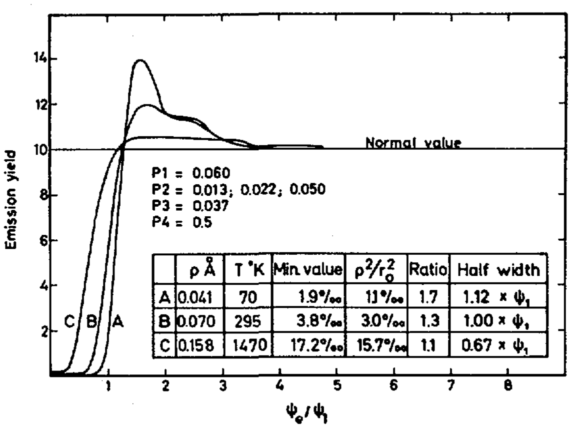

	ρ Å	T °K	Min. value	ρ^2/r_0^2	Ratio	Half width
A	0.041	70	1.9‰	1.1‰	1.7	1.12 × ψ_1
B	0.070	295	3.8‰	3.0‰	1.3	1.00 × ψ_1
C	0.158	1470	17.2‰	15.7‰	1.1	0.67 × ψ_1

FIG. 4. Influence of the vibrational amplitude ρ on the angular distribution of 500 keV protons emitted from a <100> string in tungsten calculated by Andersen [17]. P1, P2, P3, and P4 indicated on the figure are defined and discussed [17]. The unit ‰ stands for 'parts per thousand'.

EXPERIMENTAL PROCEDURE

The experimental arrangement is shown in Fig. 5. Uranium dioxide crystals were bombarded with protons in the energy range from 9.0 to 12.0 MeV at the Bell Laboratories - Rutgers University Tandem Van de Graaff. The cry-

---

* Normalization of the widths to ψ_1 makes the values shown in Fig. 4 applicable to other particle energies and types and to other crystals. Also, only a few percent error is introduced because a gaussian (instead of an exponential) emission distribution is used.

stals used* were cleaved from larger crystals with the ⟨111⟩ axis normal to the crystal surface. They were investigated thoroughly by Laue x-ray diffraction and by proton and helium ion scattering before the measurements to check for twinning, surface disorder, or other crystal imperfections and, after the measurements, to investigate for possible radiation damage or formation of surface films during the bombardment.

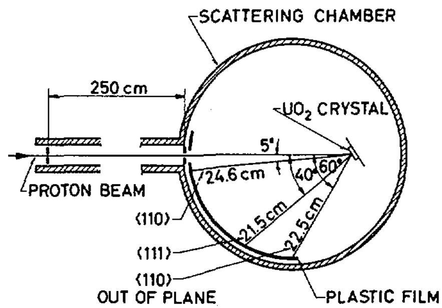

FIG. 5. Experimental arrangement. The beam collimators used were 1-mm diameter. The crystal orientation was determined and adjusted before the fission fragment measurements were started by using the sharp and well-defined angular distribution patterns [8] of 5-MeV protons measured in X-ray films.

Figure 6b shows the yield of 2-MeV helium ions scattered at ~ 160° from the uranium dioxide crystal as a function of the incidence direction relative to a ⟨110⟩ string. The observed minimum yield of 0.04 for scattering at a mean depth of ~ 4000 Å establishes an upper limit of a few percent twinning or disorder in the crystal and shows that any mosaic spread must be significantly less than the observed 0.83° half-width of the measured yield curve. Measurements of crystals vibratory-polished [19] or chemically etched for 5 min in a solution of 10 vol% H_2SO_4 in H_2O_2 (30%) showed consistently worse x-ray diffraction and helium ion channeling patterns than did the cleaved crystals.

Figure 6a shows the energy spectra of Rutherford-scattered, 2-MeV helium ions incident on the crystal in a random direction and parallel to a ⟨110⟩ direction before and after a series of three fission-fragment angular distribution measurements, in which a total of ~ 100 nA·hr of 12-MeV protons were incident on the crystal. Agreement of the two aligned spectra indicates that the crystals were not seriously damaged, at least not in the first few microns, during the fission fragment measurements.

The crystal was held in a goniometer and oriented as shown in Fig. 5 with the ⟨111⟩ axis (normal to the crystal surface) at 40° ± 2° to the incident beam and with a ⟨110⟩ axis in the same plane at an angle of 5° ± 2° to the incident beam and two other ⟨110⟩ axes, one above and one below the horizontal plane at an angle of 60° ± 2° to the incident beam. All of the ⟨110⟩ axes have an angle of 35°.2 to the crystal surface.

The integrated proton current was ~ 30 nA·hr for the 12-MeV, ~ 100 nA·hr for the 10-MeV, and ~ 150 nA·hr for the 9-MeV bombardments. Evidence of crystal heating could sometimes be detected on the 9=MeV runs. The tem-

* We are indebted to Mr. J.J. Scott of the Norton Co., Ontario, Canada, for making the crystals available to us.

perature was monitored with low-melting wax in contact with the sample and did not exceed ~ 80°C during the 9-MeV bombardments and 50°C during the 10- and 12-MeV bombardments.

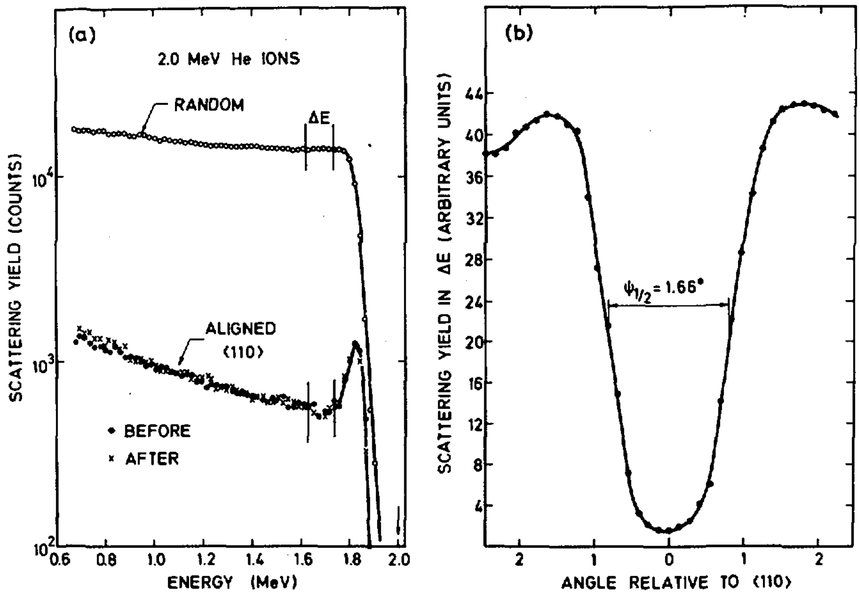

FIG. 6. (a): *Energy spectrum of 2.0-MeV helium ions scattered at ~160° from an uranium oxide crystal with incidence in a random direction and a <110> direction before (•) and after (x) a series of fission-fragment measurements.* (b): Yield of backscattered helium ions in the energy interval ΔE (corresponding to ~4000 Å mean scattering depth) as a function of the ion incidence relative to a <110> axis.

The fission fragments were detected with plastic films of the polycarbonate polymer of 4,4-dihydroxydiphenyl-2,2 propane*. A variety of film thicknesses from 8 μ to 0.5 mm were used. These were etched in 6N NaOH at 70°C for periods of 20 min to 1 hr to make the fission tracks visible under an optical microscope, but not tracks due to scattered protons or other light particles. Occasionally, thick films of cellulose nitrate or cellulose acetate were used. These were etched in 6N NaOH at room temperature for 6 hrs for the cellulose nitrate and ~ 10 hrs for the cellulose acetate. In some cases, an absorber film of 3 μ polycarbonate plastic was used over the detector film to discriminate against fission fragments which originated in the crystal at depths corresponding to a large fraction of the fragment range. Under similar irradiation conditions, the same results, within experimental uncertainty, were obtained, independent of the type of film used or the presence or absence of the 3 μ absorber film. Consequently, no distinction will be made in showing and discussing the results. The films were arranged to intercept all of the various emergent particle directions of interest at the same time, and the crystal-to-film distance was ~ 21 to 25 cm, as shown in Fig. 5.

---

* In the present study we have used only Makrofol, which is the Bayer AG tradename for this plastic. Similar plastics are available under the tradenames Plestar and Lexan polycarbonate.

LIFETIME MEASUREMENTS

In the present experiments, the observed fission fragments came from decay of both the primary Np^{239} and the secondary Np^{238} compound nuclei. The reaction sequence can be represented schematically:

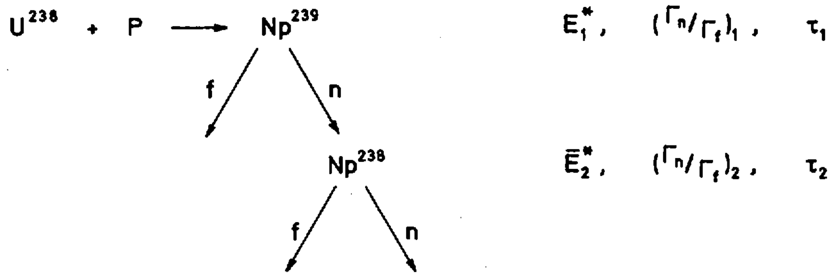

Here, the neutron-to-proton branching ratios $(\Gamma_n/\Gamma_f)_1$ and $(\Gamma_n/\Gamma_f)_2$ and the total decay times τ_1 and τ_2 are in general different for each of the compound nuclei and are dependent on the excitation energy E_1^* and E_2^* in each case. The excitation energy of the first-chance fission (Np^{239}) compound nucleus is given by:

$$E_1^* = E_p + 5.3 \text{ MeV}$$

where E_p is the incident proton energy. The excitation energy of the second-chance fission compound nucleus (Np^{238}) will have a range of values because of the variation energy of the neutron evaporated from Np^{239}, but will have an average energy about 8.0 MeV lower than E_1^*. The average recoil velocity of the Np^{238} compound nuclei will be the same as that computed for the primary Np^{239} compound nuclei from the incident proton energy because the neutron emission is essentially isotropic in the center of the mass system.

Because of the sequential decay, analysis of the observed minimum yield is:

$$\chi - \chi_1' = \left[\frac{1+(\Gamma_n/\Gamma_f)_2}{1+(\Gamma_n/\Gamma_f)_1+(\Gamma_n/\Gamma_f)_2}\right] \chi(v_\perp\tau_1) + \left[\frac{(\Gamma_n/\Gamma_f)_1}{1+(\Gamma_n/\Gamma_f)_1+(\Gamma_n/\Gamma_f)_2}\right] \chi(v_\perp\tau_2) \qquad (5)$$

where the functions $\chi(v_\perp\tau)$ refer to the right-hand side of eq. (4), and effects of neutron emission on the mean square recoil velocity have been neglected. The expressions in brackets indicate the fraction of the total number of fissions coming from the primary and secondary compound nuclei, respectively.

From the fission and neutron level width analysis of Huizenga and Vandenbosch [20], very short mean decay times ($< 10^{-17}$ sec) are expected for proton energies of 12 MeV and higher (up to 15 MeV) since both the primary Np^{239} and the secondary Np^{238} compound nuclei have high excitation energies (relative to the estimated fission threshold energy of ~ 6.0 MeV). Fast decay is also expected for proton energies of 9.0 MeV and lower since all of the fission fragments come from highly excited Np^{239} compound nuclei.

Figure 7 shows the results of the scan of a ⟨111⟩ axial direction for a 12-MeV bombardment. Similar results with somewhat poorer statistical accuracy were obtained for 9-MeV bombardment.

The width at half-height in the observed dip is slightly less than $2\psi_1$, calculated from the expression:

$$\psi_1 = \left(\frac{2\bar{Z}_1\bar{Z}_2 e^2}{\bar{E}\,\bar{d}}\right)^{1/2} \tag{6}$$

where $\bar{Z}_1$ and $\bar{E}$ are the mean atomic number and energy of the fission fragments and $\bar{Z}_2$ and $\bar{d}$ the mean values of the atomic number and atomic spacing along the $\langle 111\rangle$ row in UO_2, respectively. ψ_1 is related to the critical angle by $\psi_{1/2} = \alpha\psi_1$ [10], where α depends weakly on the mean vibrational amplitude ρ of the lattice atoms. As discussed by Eriksson and Davies [21], α is close to 1.0 for the $\langle 111\rangle$ axis in UO_2 if the steering is assumed to be due to the uranium atoms. The difference between the observed and the calculated widths is not considered significant. In fact, it is consistent with the observation that the particle channeling widths measured for helium-ion and deuteron scattering in uranium dioxide [21] and a large number of other crystals [22] are 20-30% lower than the calculated values. On the other hand, the difference could arise from the averaging technique used in the calculation or could be due to scattering effects. In any case, it is clear that random scattering is not producing a large change in width for this measurement.

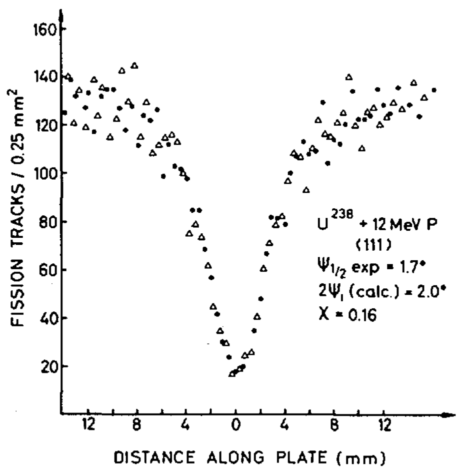

FIG. 7. Fission-track density on a plastic detector film across a position corresponding to fragment emission parallel to a <111> axis. The symbols △ and ● indicate scans in two orthogonal directions on the film. The ψ_1 value was calculated from Eq. (6) by using an average fission-fragment proton number of 46.5 and an average energy of 60 MeV. The axial direction was 40° ± 8° from the incident proton beam.

If it is assumed that the observed minimum yield comes entirely from the lifetime term of eq. (5) (i.e. if the contribution χ_1' due to scattering and thermal vibration effects is neglected), it is possible to set an upper limit on the "effective lifetime" for decay of compound nuclei formed by 12-MeV proton bombardment of U^{238}. The minimum yield of 0.16 from Fig. 7 gives $\tau_{eff} \leq 1.3 \times 10^{-16}$ sec*. This is a higher limit than the limit of

* For sequential decay, as in the present case, the "effective lifetime" is a complicated function of the branching ratios and lifetimes of the members of the decay chain.

$< 2 \times 10^{-17}$ sec reported by Brown et al. [5]. The difference is principally due to the smaller value of the cutoff distance $r_c = 0.1$ Å, which they used. Evaluation of their reported χ value by the method outlined here gives an upper limit of $\leq 9 \times 10^{-17}$ sec.

A better value for the lifetime can be obtained by evaluating the χ_1' term of eq. (5). Information on the magnitude of the scattering effects was obtained by helium-ion scattering measurements, which gave a value of $\chi = 0.12$ for the ⟨111⟩ "channeling dip" (directly related to the "blocking dip" through reversibility [10,26]) for 2-MeV helium ions scattered from a depth range corresponding to about one-half of the fission-fragment range. This value should represent a lower limit χ_1' in eq. (5) since multiple scattering effects are more pronounced for the heavy fission fragments than for helium ions. Based on this limit for χ_1', a more precise upper limit of $\leq 7 \times 10^{-17}$ sec is computed for the "effective lifetime" decay of Np^{238} and Np^{239} compound nuclei formed by 12-MeV proton bombardment of U^{238}.

For any real determination of the lifetime, it is necessary to determine χ and χ_1' of (eq. (5) under as nearly the same conditions as possible. Two methods have been investigated in the present study. In the first, the proton energy was chosen such that both τ_1 and τ_2 in eq. (5) were so short that determination of the minimum yield gives $\chi = \chi_1'$. At other proton energies, where τ_2 is not negligible, this value of χ_1' was then used to determine τ_2. As noted previously, only very fast fission ($< 10^{-17}$ sec) occurs at proton energies above 12 MeV and below 9 MeV. We therefore assume that under such conditions, contributions from the "lifetime terms" of eq. (5) are negligible compared to the scattering term χ_1'. At proton energies around 10 MeV, however, the excitation energy of the second-chance fission compound nucleus (Np^{238}) is so low that a significant contribution from the last term of eq. (5) is expected.

A series of experiments were carried out in which 10-MeV bombardments were followed and, in some cases, preceded by 12-MeV or 9-MeV bombardments. Care was taken to ensure that the particle beam was incident on the same spot in each series and that all conditions of beam alignment and crystal orientation were kept constant. Figure 8 shows the results of a scan for a 10-MeV proton bombardment compared to those of a 12-MeV bombardment normalized at large emission angles. Three separate 12-MeV bombardments and one 9-MeV bombardment were carried out and agreed within statistical uncertainty. Two separate 10-MeV bombardments bracketed by the 12-MeV and the 9-MeV bombardments were also in good agrement. The minimum yield values in Fig. 8 are the averages of various determinations weighted by their respective statistical uncertainty. The difference in the minimum yield value gives:

$$\left[\frac{(\Gamma_n/\Gamma_f)_1}{1+(\Gamma_n/\Gamma_f)_1+(\Gamma_n/\Gamma_f)_2}\right] \chi(v_\perp\tau_2) = 0.066 \pm 0.021$$

Estimates [20] of $(\Gamma_n/\Gamma_f)_1 \simeq 1.0$ and $(\Gamma_n/\Gamma_f)_2 = 0.8$ for Np^{239} and Np^{238} compound nuclei at excitation energies of 15.3 MeV and 7.3 MeV, respectively, yield

$$\chi(v_\perp\tau_2) = 0.183$$

From Fig. 3 this corresponds to $v_\perp\tau_2 = 0.20$ Å for the mean recoil distance giving the total lifetime

$$\tau_2 = 1.4 \pm 0.6 \times 10^{-16} \text{ sec}$$

and the partial fission lifetime

$$(\tau_f)_2 = 2.5 \pm 1.2 \times 10^{-16} \text{ sec}$$

for decay of the Np^{238} compound nucleus.

The mean recoil distance of the Np^{238} compound nucleus of 0.20 Å can be compared to the thermal vibrational amplitide of 0.07 Å for uranium atoms in the UO_2 [23]. From Andersen's analysis [17] of the dependence of the width of the emitted particle angular distribution on the thermal vibrational amplitude shown in Fig. 4, the width at 0.20 Å mean displacement should be 0.5 times the width at 0.07 Å. This is consistent with the width change of 0.4 ± 0.2 estimated for the angular distribution of the fission

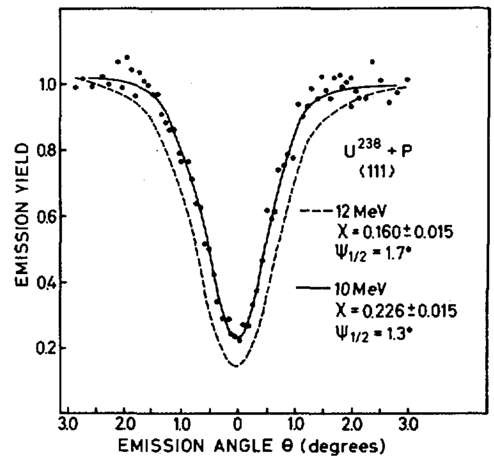

FIG. 8. Measured angular distributions, normalized at large emission angles, of fission fragments emitted parallel to a <111> axis for bombardment of UO_2 crystals with 10-MeV protons (-●-) and with 12- and 9-MeV protons (----). The values indicated for the minimum yield for the 12-MeV curve are the averages, weighted by their statistical uncertainty, of three runs at 12 MeV and one at 9 MeV. For the 10-MeV case, the minimum yield is the average of two runs at 10 MeV. The axial direction was 40° ± 2° from the incident proton beam in both cases.

fragments arising from decay of Np^{238} compound nuclei in going from the 12-MeV to the 10-MeV proton bombardments as obtained from the two curves of Fig. 8. The fraction of fissions from Np^{238} of 0.36 was used as obtained from the branching ratios given above. This estimate neglects random scattering effects and is meant only to indicate consistency, but, as pointed out previously, the absolute width measurements are in fair agreement with the expected value.

The second method used for evaluation of the scattering term χ_1' in eq. (5) makes use of a simultaneous measurement of the emission distribution along different ⟨110⟩ axes in the crystal. As shown in Fig. 5, the proton beam was incident at an angle of 5° ± 2° from a ⟨110⟩ axial direction. The compound nucleus recoil, since it follows the same direction as the incident proton, will have only a small velocity component, $v_\perp$, perpendidular to that particular ⟨110⟩ direction. Therefore, for fragment emission along that specific ⟨110⟩ direction, $\chi \approx \chi_1'$. There are, however, other ⟨110⟩ axial directions in the crystal at 60° ± 2° to the incident proton beam.

The velocity component of the recoil nuclei perpendicular to these axial directions is not small, so the emission yield measured along these directions is given by all the terms in eq. (5). (The first term is expected from the arguments and measurements discussed previously to be negligible since τ_1 is always very small under the experimental conditions used in the present experiment.) It is important to note that since all ⟨110⟩ axes have the same angle (35°2) relative to the crystal surface, and since the emission measurements for the different directions are made simultaneously, all depth, surface, radiation damage, crystal impurity, or other scattering effects should be completely equivalent in the two measurements.

Actually, recoil from neutrons emitted from Np^{239} broadens the displacement distribution of the decaying Np^{238} compound nuclei. Analogous to increasing the thermal vibrations, this will increase the minimum yield. This is especially serious for the aligned measurement and should be corrected for in applying this two-directional technique.

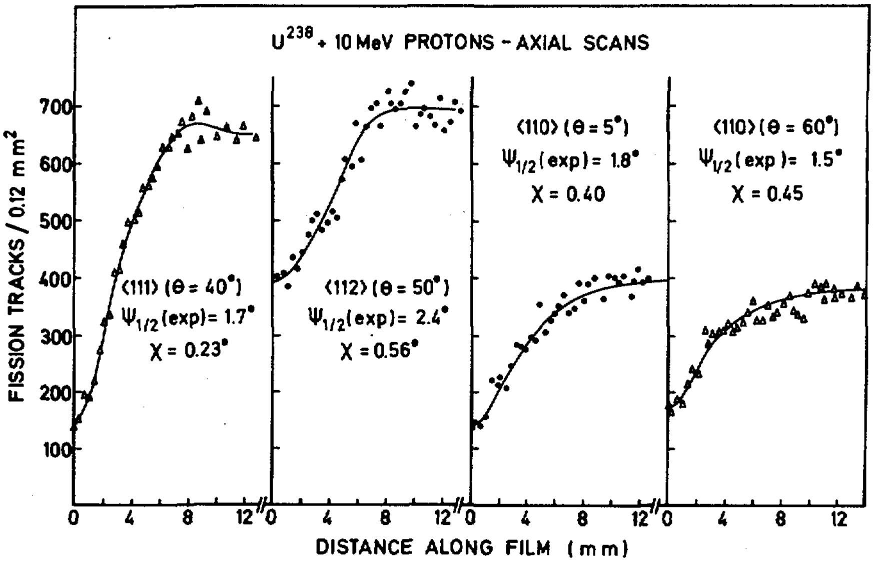

FIG. 9. Fission-fragment track density on the plastic detector film scanned across positions corresponding to fragment emission parallel to various axial directions. Only half of the symmetric yield minima are shown. θ is the angle of the axial direction relative to the incident proton beam. All curves are from the same proton bombardment.

Figure 9 shows the results of scanning a number of different axial directions from the same 10-MeV proton bombardment. All distributions were found to be symmetric in the directions scanned. The yield minima for ⟨110⟩ axes with recoil at different angles to the crystallographic axes are shown by curves 9c and 9d. As discussed in the following section, scattering effects are enhanced for ⟨110⟩ axes in UO_2. This makes the difference in minimum yield and therefore the derived lifetime less precise than that obtained for the ⟨111⟩ axial measurements. However, the difference between the angular distributions for the two recoil directions is significant and the lifetime derived from eq. (5) after correcting for the neutron recoil effect mentioned above is consistent with the value obtained previously.

For the ⟨110⟩ axial measurements, the lifetime term contributed ~ 10% to the measured minimum yield whereas for the ⟨111⟩ axial measurements, the contribution was ~ 30%. The consistency of the derived lifetimes for these two cases supports the approximation that the scattering effect can be combined additively to the lifetime and thermal vibration effects.

A difference in the width of the yield minima was also observed for the ⟨110⟩ axial measurements corresponding to different recoil directions, and the difference is in the same direction and of the same order of magnitude as that observed for the ⟨111⟩ measurements. However, scattering effects are apparently contributing significantly in this case since both curves are much narrower than $2\psi_1 = 3.^\circ 2$, calculated from eq. (6), so no lifetime estimate is felt to be justified.

SCATTERING EFFECTS

In almost all cases, random scattering effects are important in determining compound-nucleus lifetimes from observed emitted particle angular distributions. In this section, we will sonsider some of the factors which influence random scattering.

The random scattering effect includes multiple scattering in disordered or impurity surface layers and in the crystal itself as well as single (Rutherford) scattering in surface layers or from impurities or imperfections in the crystal. It is therefore clear that the quality of the crystal, as well as the absence of surface disorder or impurities, is important. However, even in perfect crystals with clean and ordered surfaces, multiple scattering will occur as the particle penetrates the crystal. This is the same effect that leads to the particle escape from channels in particle channeling experiments [24].

In a binary crystal with constituents as different in proton number as in the UO_2 crystals used in these experiments, special scattering effects exist. These arise because of the presence of non-equivalent atomic rows or planes in the crystal. A representation of a {110} plane for UO_2 is shown in Fig. 10. This plane contains the three major low-index axial directions which are also indicated in the figure. Because of the high proton number of uranium, the inter-atomic potentials are determined almost entirely by the uranium atoms and the rows and planes of the uranium sub-lattice should dominate the correlated particle scattering. It should then be expected that the small spacing of uranium atoms along the ⟨110⟩ direction would lead to a smaller minimum yield χ (according to eq. (4)) and an increased width $\psi_{1/2}$ (according to eq. (6)) for particle emission along that direction compared to the ⟨111⟩ direction. However, comparison of the angular distributions observed for these two directions in the same experiment, as shown in Fig. 9, indicates just the opposite trend. The ⟨110⟩ minima have a much higher χ value than has the ⟨111⟩ minimum.The reason for this apparent anomaly can be seen by referring to Fig. 10. The anomalously shallow minima for the ⟨110⟩ directions arise from scattering of the emitted fragments by rows of oxygen atoms, which lie between the uranium rows. Since all particles emitted from the uranium sites can penetrate the lower interatomic potential due to the oxygen rows, the oxygen acts very much the same as interstitial impurity atoms in scattering the emitted particles. On the other hand, in the ⟨111⟩ direction, all rows are the same and the anomalous scattering due to oxygen rows is not present. The same effect is observed for emission along planes. Figure 11 shows angular distributions for fragment emission along a {111} plane and a {110} for the same 10-MeV bombardment shown in Fig. 9. Again, the {111}, which contains intermediate oxygen planes, shows a greatly increased scattering effect. This phenomenon appears to be much more extreme for emitted fission fragments than for the protons or helium ions scattered at an equivalent depth. The light ions, however, show a considerably larger depth dependence along the ⟨110⟩ axis than along the ⟨111⟩ axis because of the same scattering effect. This has been studied extensively for scattered deuterons and helium ions by Erissson and Davies [21].

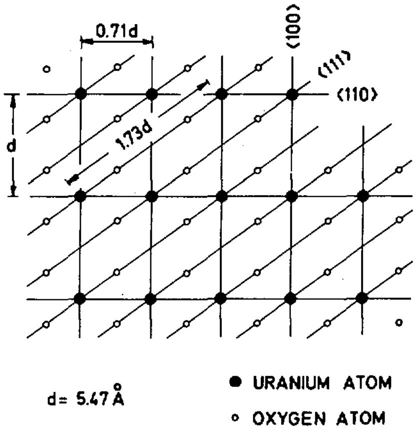

FIG. 10. The atomic arrangement of UO_2 projected onto the {110} plane.

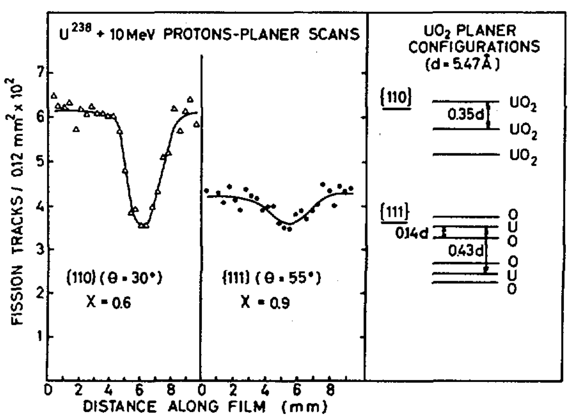

FIG. 11. Fission-fragment track density on the plastic detector film scanned across positions corresponding to fragment emission parallel to low-index planes. θ is the angle of the center of each scan relative to the incident proton beam. These data are from the same proton bombardment as those on Fig. 9.

POSSIBLE IMPROVEMENTS

The measurement reported above is an "effective lifetime", which is influenced by fission and neutron emission of both the primary Np^{239} compound nucleus and the secondary Np^{238} compound nucleus. To relate this quantity to any of the total or partial lifetimes involved requires knowledge of the neutron and fission branching ratios, Γ_n/Γ_f . This relationship is especially uncertain for the second-chance fission Np^{238}

compound nuclei because the excitation energy is not accurately known or well-defined. For charged-particle-induced fission of heavy elements, this situation is necessary since only by working with second- or third-chance fission is it possible to reduce the excitation energy enough to get suitable control over the lifetime. However, by using monoenergetic neutrons in the energy range from ~ 1 to ~ 5 MeV to induce the fission, this uncertainty can be removed since the observed fission fragments all arise from the primary compound nucleus at an appropriate, well-defined and controlled excitation energy. Measurements of the fission of U^{238} and Th^{232} with monoenergetic neutrons are in progress.

For some materials, the crystal temperature has been found to have a large influence on the random scattering in particle channeling experiments [25]. Therefore, dependence of emitted fragment angular distributions on the temperature is being investigated. In any case, it should be remembered that the χ_1' term of eq. (5) contains both thermal vibration and random scattering effects (see eq. (2)). As the scattering effects are reduced or more accurately determined, the thermal vibrations will become increasingly important. When the mean square recoil displacement becomes smaller than the mean square thermal vibrational amplitude, the measurement becomes insensitive to changes in the lifetime, so this will represent the ultimate lifetime limit that can be achieved. By cooling the crystal to very low temperatures, the thermal vibrations can be reduced to ~ 0.01 Å, so for a recoil velocity $v_\perp$ of 10^8 cm/sec, it appears that if the scattering effects can be well enough measured or reduced, lifetime measurements as short as ~ 10^{-18} sec might be possible.

ACKNOWLEDGEMENTS

We would like to acknowledge the assistance of P. Ambrosius-Olesen in scanning the plastic detector films and members of the Niels Bohr Institute Tandem Laboratory for their help in furnishing detector films and providing information on development and scanning. We also wish to thank J.U. Andersen, J.A. Davies, and J. Lindhard for discussions and guidance in analyzing the angular distributions. Mrs. Alice Grandjean is thanked for her help with the typing of the manuscript.

REFERENCES

[1] HALPERN, I., Ann.Rev.Nucl.Sci. 9 (1959) 245

[2] VANDENBOSCH, R., and WOLF, K.L., Proc.II Int.Conf. on the Physics and Chemistry of Fission, Vienna, July 1969

[3] FEATHER, N., Nature 143 (1939) 597

[4] STEIN, W.E., Los Alamos Scientific Laboratory Report No LADC-5367 (1960) (Unpublished)

[5] BROWN, F., MARSDEN, D.A., and WERNER, R.D., Phys.Rev.Letters 20 (1968) 1449

[6] A value of ~ 0.1 was used, cf. Table III of ref. [1]

[7] UGGERHØJ, E., Phys.Letters 22 (1966) 382

[8] GEMMEL, D.S., and HOLLAND, R.E., Phys.Rev.Letters 14 (1965) 945

[9] DOMEIJ, B., and BJÖRKQUIST, K., Phys.Letters 14 (1965) 127

[10] LINDHARD, J., Kgl.Danske Videnskab.Selskab, Mat.-Fys.Medd. 34 No 14 (1965)

[11] TREACY, P.B., Australian J.of Sci. 22 (1960) 334

[12] LINDHARD, J. private communication (1964)

[13] TULINOV, A.F., Dokl.Akad.Nauk.SSR 162 (1965) 546 [English translation: Soviet Phys.-Dokl. 10 (1965) 463]

[14] ALTMAN, M.R., FELDMAN, L.C., and GIBSON, W.M., Phys.Rev.Letters (to be published). See also: Bull.Am.Phys.Soc. 14 (1969) 372 (abstract)

[15] BARRETT, J.H., Bull.Am.Phys.Soc. 14 (1969) 372 (abstract)

[16] LINDHARD, J., SCHARFF, M., and SCHIØTT, H.E., Kgl.Danske Videnskab. Selskab, Mat.-Fys.Medd. 33 No 14 (1963)

[17] ANDERSEN, J.U., Kgl.Danske Videnskab.Selskab, Mat.-Fys.Medd. 36 No 7 (1967)

[18] KOMAKI, K., and FUJIMOTO, F, Phys.Letters 29A (1969) 544

[19] WHITTON, J.L., J.Appl.Phys. 36 (1965) 3917

[20] HUIZENGA, J.R., and VANDENBOSCH, R., in Nuclear Reactions, Vol. II, ed. by ENDT, P.M., and SMITH, P.B., North-Holland Publishing Co., Amsterdam (1962) p. 42, and VANDENBOSCH, R. (private communication, 1969)

[21] ERIKSSON, L., DAVIES, J.A., Arkiv Fysik 39 (1969) 439

[22] PICRAUX, S.T., DAVIES, J.A., ERIKSSON, L., JOHANSSON, N.G.E., and MAYER, J.W., Phys.Rev. 180 (1969) 873

[23] Derived from the Debye-Waller Factors for UO_2, given by DOLLING, G., COWLEY, R.A., and WOODS, A.D.B., Can.J.Phys. 43 (1965) 1397

[24] FELDMAN, L.C., APPLETON, B.R., and BROWN, W.L., Proc.Int.Conf. on Solid State Physics Research With Accelerators, September 1967, Brookhaven Nat.Lab. Report BNL 50083 (1967) 58

[25] WHITTON, J.L., Can.J.Phys. 46 (1968) 581

[26] BØGH, E., and WHITTON, J.L., Phys.Rev.Letters 19 (1967) 553

DISCUSSION

P. ARMBRUSTER: Could you detect alpha particles by your technique and the fission products by solid-state detectors? If so, your technique could be used to prove that alpha particles in ternary fission are emitted at scission.

W.M. GIBSON: Yes, in principle. Therefore, the life-times of any charged particles emitted from a recoiling compound nucleus can be measured.

F. RUSTICHELLI: What is the dependence of the precision and sensibility of your method on the quality, i.e. on the mosaic spread of the crystal used?

W.M. GIBSON: The quality of the crystal plays a very important role, as you might expect. This was investigated in great detail by X-ray measurements. The latter measurements, for example, indicated minimum yields, which set a very low limit on the presence of mosaic spread in these crystals. I think that it may be possible to improve the crystals that were made but I do not expect an improvement in the bulk properties of the uranium oxide crystals to lead to a very large change, because bulk properties of these crystals were very good. However, the scattering due to oxygen in these uranium oxide crystals is very pronounced and a significant improvement can be expected if we use for example, pure uranium crystals.

SUMMARY OF THE SYMPOSIUM

J. C. D. MILTON
Atomic Energy of Canada Ltd,
Chalk River, Ontario,
Canada

I am acutely embarrassed standing up here before you, and I am wondering, in fact I have been wondering for five days, how I ever got into this position. Not only am I keeping you all from catching your trains or having your dinner but you no doubt are expecting me to say something important. Now, this Symposium, I feel, has been momentous in the history of fission and naturally a summary speaker should say something momentous. I feel, infact, a little bit the way Neil Armstrong must have felt when he stepped on to the moon. I know I do not have 500 million people watching me; nevertheless I have a substantial fraction of the world of fission listening to me and they all are expecting to hear something memorable. So I thought about doing a little jump and saying: it is a little leap for me but a tremendous leap for fission, — but that had been done before. So I began to ask how one might symbolize this Symposium. Symbols are very important in this world, and one can never underestimate the importance of them, as any French physicist can tell you who has tried to think of a subscript for the light fragment (l = leger), and then tries to think of a subscript for the heavy fragment (l = lourd); he has to do something different. So, symbols are very important and I tried to think of something that would symbolize this Symposium, and, of course, I am sure, it will come as no great surprise to you that the symbol of the Symposium should look as is shown in Fig. 1. Not only has nearly every speaker felt compelled to refer to it but those who have not, have felt compelled to apologize for not doing so. So it seemed to me that this symbol was appropriate in another way too, because if you look at it in the right way, it certainly looks like an S on its side and of course, the man who is responsible more than any other for the tone of this Symposium is Strutinsky. Of course, I am going to ignore the fact that in the cyrillic alphabet his initial would better symbolize a single-humped barrier. Anyway, it seemed to me that this symbol is important for another reason too, because it indicates how different this Symposium has been from all other conferences and Symposia on fission because at other fission conferences the symbol has been like that of Fig. 2. I show this to remind you that although there has not been too much said about it, the double-humped mass yield is still something that has to be explained in fission.

I mentioned the fact that I thought this conference had been different from all others in fission but in fact, I think there really has only been one other symposium of this caliber. That, of course, was the Salzburg Symposium in 1965. It is true, there were the two great Geneva Conferences which were somehow related to fission but I think I would exclude them because they were attended mostly by the chiefs and very few of us Indians got to them. There were also semiprivate conferences on

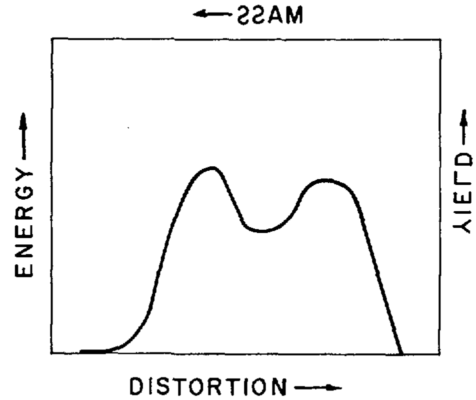

FIG. 1.

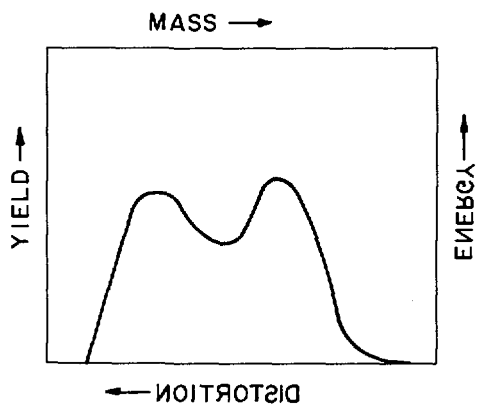

FIG. 2.

fission in Chalk River in 1956 and in Los Alamos in 1958, but you had to be either Canadian, American or British to go to them and so they were in no way a substitute for the great Symposia in Salzburg and here. So I think it is instructive to compare this Symposium with Salzburg. I think, it was true there, as it is here, that the Symposium ended on a note of great optimism. Griffin, I remember, was somewhat apprehensive but nevertheless happy about the thought of a great flood of data, when the experimenters, with the help of on-line computers measured everything about fission, and the poor theorist would then have to explain it. I think he is probably resting easier now because the great flood has not developed. Swiatecki, for his part, with his large calculations on statics behind him, was looking forward to some rigorous, but still model-dependent dynamical calculations from Nix and others, but especially he was looking forward to a concerted attack on fundamental theories of fission. I do not think that we have got really very much nearer to a concerted attack on a fundamental theory of fission than we were then, but I think there is very good reason to hope that we might, because I think one of the most important features of this Symposium has been the fact that we now have for the first time a large number of nuclear theorists interested in fission. Put in another way, the marriage of fission to nuclear physics after an engagement of nearly 30 years may finally be taking place.

There were solid achievements at Salzburg, and in some cases we have not learned very much since that time. For example, Terrell's masterful summary of the prompt neutrons still stands as almost the last word on the subject. In all this euphoria we probably partially overlooked one fact and one problem. The problem was the recent discovery of isomeric fission by Flerov, Polikanov et al. in Dubna. The fact was the new mass formula of Swiatecki, which for the first time, produced a simple, but soundly based and effective, shell-correction term to the liquid-drop masses. Already Swiatecki was talking privately about shells in deformed nuclei and using for his authority the old testament itself, that is Hill and Wheeler wherein, suitably interpreted, almost anything can be found. It has remained for Strutinsky to put some flesh and blood on these ideas. I think, there is another type of difference between this Symposium and the one at Salzburg; at Salzburg, there were about the same number of delegates as here, 200 from 29 countries whereas here, by my count there are 235 from 28 countries. But the atmosphere here seemed to be more conducive of discussion, of which I think there has been a good deal. Perhaps this is the result of the fact that although there were more delegates here there were fewer papers. Only about 50 papers were presented and this of course caused a certain amount of anguish because 160 were submitted, whereas at Salzburg 75 papers were given, which I presume was the number submitted.

Let me go on now to say that I think many people will agree that this Symposium has been a turning point in the fortunes of fission. Perhaps those people whose papers were guillotined will only agree rather ruefully. Many people will also agree that had there been no Strutinsky, this would have been a very different symposium and many people will agree that the prevalent mood at this conference has been one of optimism. But it is undoubtedly true, as is usually the case, that this Symposium has provided more good questions than good answers. Nevertheless, I think that the hopeful mood is justified.

As I mentioned before, a large number of nuclear theorists are working on the solid liquid-drop base (if that is not a contradiction) provided by Swiatecki and Nix. It appears that the time is ripe for some real nuclear theory to be applied to fission. Already at this Symposium we have heard the results of a dynamical calculation from Hasse and Hilf (SM-122/28) which included shell-effects, admittedly in a crude and surely incorrect way, but nevertheless a start. Then we have heard the beginnings of some calculations of mass and inertia coefficients from the Copenhagen group (SM-122/62) and it will be interesting to see if the tremendous amount of structure they find is substantiated by later work. In addition to these semi-classical problems, I think, there are many other interesting ones for theorists, and it would certainly be very nice to see an attack on the multi-dimensional barrier penetration problem. Of course, we all await with great interest to see if and how more rigorous calculations of the potential energy versus deformation differ from Strutinsky's.

Experimentally, the list of problems is very large. Despite the immense amount of work by Muga (SM-122/99) we still do not know very much about ternary fission. The situation with "non-honest-to-God" ternary fission (to modify Muga's phrase), that is, fission accompanied by scission neutrons or charged particles is quite different. We have a tremendous amount of data available. While we can glibly repeat all the old clichés about what we expect to learn about the scission configuration from these data, the fact is that the numerous trajectory calculations that are now going on are only beginning to show us how to interpret these data.

Turning now to the case of the fission isomers, it seems again that we have an embarrassment of riches, nearly everything has an isomer or two, and everything means all the way down to the rare earths according to the recent work of Alexander and Ruddy (submitted to ACS Meeting, New York, September 1969). Accurate life-times and cross-sections for these isomers are, however, another matter and we desperately need to consolidate our gains. While more isomers will be, and I am sure should be found, what we really need are more accurate measurements. And then, if it turns out that these lifetimes have a highly non-statistical distribution it will be time to worry. Particularly interesting are those cases where two isomers are observed in a single nucleus, and we eagerly await the confirmation of the 5-nanosecond and the 29-nanosecond isomers observed by Elwyn and Ferguson in ^{240}Pu (Sm-122/54). If we had the measurements I mentioned above for those cases in which there is more than one isomer in a given nucleus, then we could start to learn something about the spectroscopy of the class-two states, the states in the intermediate well, and something about the relative shapes of the barrier for the different types of excitation. These measurements together with, for example, (d, pf) prompt fission studies can also tell us how the class two states are mixed with the class-one states. There certainly can be no doubt that we need to know more about the class two states: we need to know their spacings, their spins, their transition properties and we would like to know their structure.

Following on now, according to the program, we come next to the vexing problem of the variation of the properties from resonance to resonance in neutron fission. Many people believe that there are significant differences in the properties from resonance to resonance but sometimes even the sign of the effect is not known. The situation seemed to me to be pretty bad, but it is not quite as bad as I thought it was before I sat down last night and prepared Table I.

I am certainly not an expert in this field, but I thought it might be interesting to take all the resonances that were reported by Weinstein, the 13 shown in column 1, to see how people agreed on the determination of spins. To my surprise it turned out that they agreed rather well. In the second column of the table I have put the number of determinations. It ranges from 3 to 5. In the third column, I have given the spin as determined by the wishes of the majority. The table looks mostly blank. I did that on purpose, because blank means agreement with the majority. A dash means no opinion and crosses mean disagreement with the majority. And, as you can see, in no case does more than one experimentalist disagree with the majority. This may be somewhat illusory because I am sure there is an unknown phase factor and people tend to choose the phase

TABLE I. ^{235}U RESONANCE SPIN ASSIGNMENTS

E (eV)	Number of determinations	Spin (preference of majority)	Weinstein	Ashgar	Weigman	Bowman	Cowan	Melkonian
6.39	3	4				-	-	-
7.08	4	3					-	-
8.79	4	3			-		-	x
11.67	3	4			-	x		
12.39	4	4				x	-	-
15.45	5	3	-					
16.10	5	3	x	-				
16.67	5	3	x					
18.05	3	3	x		-		-	-
19.30	3	4				-	-	-
21.10	4	3		-		-		
22.95	5	3						-
23.65	3	3	-	-	x			

Weinstein, Reed, Block, F1 SM-122/113 (1969).
Ashgar, Michaudon, Payce, Phys. Lett. 26B (1964) 664.
Weigman, Winter, Heske, as quoted by Weinstein.
Bowman, Berman, Bagham, Wash-1127.
Cowan, Bayhurst, Prestwood, Phys. Rev. 130 (1963) 2380.
Melkonian, Mehta, in Physics and Chemistry of Fission (Proc. Symp. Salzburg, 1965) 1, IAEA, Vienna (1965).

factor that minimizes the disagreement. But nevertheless, I was impressed to see that perhaps we are coming close to getting some real insight from these measurements. However, I would certainly caution those people who think for example that $\bar{\nu}$ ought to be anticorrelated with the total kinetic energy, because I think that it is clear that it is not so simple. For example, as was mentioned in Session F, changes in the gamma-ray energy or the neutron kinetic energy or perhaps even different Q-values for the reaction may play a rôle. The observed effects are very small and hence very small influences must be considered.

I think, passing on now to another topic, one of the most exciting experimental techniques to come out at this Symposium was the advent of the ^3He, ^4He dilution refrigerator into the low-temperature alignment field. We have all had high hopes for results on the angular distributions of the fragments from aligned nuclei, but as you all know the results have been slow in coming. So we look forward, or at least I do, with great interest to see whether there really are states with K = J as indicated by Dabbs et al. (SM-122/123) and also to see if there are really no states with K = 0 as suggested by Pattenden and Postma for ^{235}U (SM-122/57) (Dabbs et al. had previously found that K = 0 was surprisingly infrequent).

In fact, the whole question of the behaviour of K throughout the various stages of the fission process is a puzzling one, but one we hope will be elucidated before the next fission symposium.

Now I would like to say a word about photofission. I think it is particularly important to have more photofission results, especially near the threshold. As stressed by the chairman of Session E, photofission results are relatively simple to interpret, that is much simpler to interpret than (d, p) results. So far most photofission experiments have been done using bremsstrahlung spectra, although there was some earlier work with reaction gamma rays. But reaction gamma rays do not always occur with the right energy and it is never very clear to me what the accuracy of unfolding a bremsstrahlung process is. And for this reason we await further results on photofission and, in particular, I think we would all like to see the results from the Compton monochrometer of Knowles at Chalk River.

I do not plan to say anything about neutrons and gamma rays, delayed or prompt, except that it is unfortunate that Armbruster's experiment at Jülich (SM-122/23) did not get results on the fragment spin distribution before the conference. I think that there is no doubt that the availability of on-line mass separators and large Ge(Li) gamma detectors is going to result in a good deal of high-quality data in the near future. But as Amiel pointed out in his review talk in Session G, these data are going to tell us much about the spectroscopy of neutron-rich nuclei, but not very much about fission.

ADDITIONAL ABSTRACTS AND SHORT CONTRIBUTIONS

Owing to limitations in the time available at the Symposium, and the need to keep the Proceedings down to a reasonable size, a considerable amount of work originally submitted for possible inclusion in the Symposium could not be presented orally. Abstracts of this work are printed in this Section.

Readers interested in the work summarized in these Abstracts should apply to the individual authors for further details.

SESSION A

ASYMMETRIC INSTABILITIES IN THE LIQUID-DROP MODEL OF NUCLEAR FISSION (SM-122/17)

S. Gallone, S. Garribba, G. Ghilardotti,
SNAM Progetti S. p. A. - LRSR,
Politecnico di Milano, Milano, Italy

In a previous paper, which is briefly summarized, a method was described to evaluate the potential energy of a deformed nucleus and to discuss the instabilities of the fission shapes with respect to asymmetric deformations. The object of this communication is to report the numerical results which have been obtained on the basis of the theory mentioned. According to our scheme of calculation, the deformation energy is given as a quadratic form of suitable deformation parameters, describing the nuclear shape in terms of small deformations of a reference ellipsoid. The first part of the work gives a brief account of the methods used for the calculations, and of the criteria applied to determine the equilibrium shapes. The saddle shapes and the related critical energies have been calculated first. Graphs of the critical energies are given and compared with the results of other authors. The next step was to study the stability of the saddle shape with respect to asymmetric of deformations. The results obtained show that for values of the Bohr parameter lower than some critical value, which has been estimated, the saddle shape is actually unstable with respect to these deformations. Figures show the deformations associated with this type of asymmetric instabilities.

A STATISTICAL MODEL OF FISSION (SM-122/19)

U. Facchini, E. Gadioli-Erba, E. Saetta-Menichella,
Laboratories CISE (Segrate) and University of Milano, Italy

A statistical model of the fission process of heavy nuclei is presented. In this model the number of final states in which the fragments may be excited and a suitable fission barrier between the two fragments are taken into account. The barrier is described by means of the inverse process, i. e. the fission of two excited fragments, and shows a greater repulsion than the usual Coulomb forces. The fission of ^{235}U induced by slow and fast neutrons is analysed with the help of this model. The most recent experimental results for the average kinetic energies and for the excitation energies are utilized for the fitting. The level density parameters that enter in the theory are obtained from the recent collection of data on nuclear levels. By means of this model, the kinetic energy spectra and the excitation energy of the fission fragments are reproduced. The number of neutrons emitted by the fragments is also calculated and good agreement with the well-known saw-tooth shapes is obtained. When mass spectra are analysed the possible existence of shell effects in the fission process is evidenced. It is also possible to study the average fission widths and their trend as a function of incident neutron energy.

THE MECHANISMS OF PLUTONIUM-239 FISSION BY MUONS (SM-122/52)

A. Buta, D. Dorcioman, N. Grama, V. Hulubei,
L. Marinescu, M. Petraşcu, Gh. Voiculescu,
Institute for Atomic Physics Bucharest, Romania,
and
M. Omelianenco,
JINR, Dubna, USSR

In a recent experiment performed at the Dubna synchrocyclotron, the authors measured the time distribution of fission fragments when a ^{239}Pu target was bombarded with slow negative muons. These measurements were based on a two-parameter analysis (time and pulse height) of the recorded events, the zero time being given by the stopping of the muon within the target. The time distribution obtained is consistent with the distribution obtained in 1966 in a measurement based on a single-parameter analysis. The characteristic feature of this time distribution is the appreciable excess of events at zero time compared with the events related to the exponential decay law of muons in Pu. The events following the exponential decay law are due to the nuclear muon capture through the reaction $\mu^- + p \rightarrow n + \nu$. The muon life-time in ^{239}Pu as measured by us in the present work is 67 ± 8 ns. The excess of events at zero time is related to the mechanism suggested by Zaretsky, consisting in the direct transfer of the 2p-1s transition energy to the nucleus. This process of direct energy transfer in a series of heavy mesic atoms was experimentally proved by Pontecorvo and coworkers. However, in elements like uranium and thorium the contribution of this mechanism in the excitation of fission was much less than expected. Theoretically, this disagreement was interpreted by Zaretsky and Novikov by assuming a modification of the fission barrier due to the presence of the muon on the K-shell. It follows from the present results on plutonium that the ratio between the events related to the direct energy transfer and the events related to muon capture is 0.28 ± 0.04, i.e. essentially larger than the corresponding value for uranium and thorium. This value supports the calculation of Zaretsky and Novikov concerning the modification of the fission barrier in the presence of muons.

POSSIBLE CORRELATION OF THE GERADE-UNGERADE CHARACTER OF INDEPENDENT PARTICLE LEVELS WITH FISSION ASYMMETRY (SM-122/120)

G.P. Ford, D.C. Hoffmann,
University of California, Los Alamos Scientific Laboratory,
Los Alamos, N.M., USA

It has been suggested that the ratio of the most probable masses, M_H and M_L, of the heavy and light groups, respectively, in fission is given by N_g/N_u, the ratio of the number of nucleons in gerade orbits to the number in ungerade orbits. Gerade orbits are symmetric under reflection of the spatial co-ordinates in the plane perpendicular to the symmetry axis. We

have calculated the expectation value of the reflection operator for individual particle orbits in deformed Woods-Saxon potentials for β = 0, 0.3, 0.6, 0.75, and 0.9, because these levels are neither completely gerade or ungerade. Values of N_g and N_u were calculated by equating N_g - N_u to the sum of these expectation values over the occupied levels.

Values of N_g/N_u for β closest to the ground-state equilibrium deformation are given for several nuclei: ^{210}Po, 1.56; ^{226}Ra, 1.47; ^{230}Th, 1.47; ^{236}U, 1.48; ^{245}Cm, 1.46; ^{252}Cf, 144. When these values of N_g/N_u are plotted versus A they lie close to a line whose slope is - 0.001. Experimental values for M_H/M_L in the mass region from 227 to 236 also fall fairly close to the same line, but at higher masses values of M_H/M_L are considerably below the line. The mass region from 227 to 236 is characterized by triple-peaked fission yield curves, but since the middle peak is associated with symmetric fission, we have obtained M_H/M_L from the other two peaks which are associated with asymmetric fission. The ratio of 1.56 calculated for ^{210}Po does not agree with the observed symmetric fission in this mass region. Since N_g/N_u only decreases 6 - 10% as β is increased from 0 to 0.9, it appears that asymmetric fission would be predicted at either the ground-state or saddle-point deformation.

Perhaps the correlation of N_g/N_u with M_H/M_L is only applicable to low-energy (asymmetric) fission and that for the higher energies where symmetric fission is observed, this theory based on the independent-particle model is not valid. Even if the independent-particle model is appropriate, a different set of levels must be occupied, and our values of N_g/N_u for the lowest levels would not apply. Efforts are being made to extend this treatment to higher excitation energies.

ANGULAR ANISOTROPY OF FRAGMENTS FROM TERNARY FISSION OF ^{235}U AND ^{238}U (SM-122/8)

I. Kovács, L. Nagy, T. Nagy, I. Vinnay,
Central Research Institute for Physics
of Hungarian Academy of Sciences,
Budapest, Hungary

The angular anisotropy of fragments from ternary fission of ^{238}U and ^{235}U induced in both nuclides by 14 MeV and in the latter also by 2.5 MeV energy neutrons was measured by semiconductor detectors. The experimental setup was the following. The targets of about 2 mg/cm^2 thickness, 18 mm diameter, on 9.7 mg/cm^2 thick stainless-steel backing, were mounted on the detector of long-range α-particles. The fragments were detected by semiconductor detectors one of which was mounted by 0°, the other at 90° to the flight path of neutrons. The ternary-fission events were singled out by counting the coincidences between the α-detector and one of the fragment detectors at 2 cm distance from the other one. The neutron source of 1.4 cm diameter was placed 2.5 cm from the target. The ratio of the relative probabilities of ternary fission was determined, i.e. the value of p_0/p_{90} where the indices stand for directions of fragment flight path relative to that of the neutrons.

The ratio p_0/p_{90} was obtained for ^{235}U at 2.5 MeV neutron energy, to be 1.06 ± 0.13, while for ^{235}U and ^{238}U at 14 MeV neutron energy, the ratio was 1.30 ± 0.11 and 1.45 ± 0.12, respectively. This shows that, at 14 MeV neutron energy, the anisotropy is higher for ternary-fission fission fragments than for binary-fission ones. Since the long-range α-particles are emitted with high probability nearly normal to the fragment flight path, they are expected to have a sidewise-peaked angular distribution.

At high excitation energies the angular anisotropy is predicted in terms of the statistical model as $W(0°)/W(90°) = 1 + I_m^2/8K_0^2$, where K_0 is the average value of the angular momentum projection on the nuclear axis and I_m is the maximum possible angular momentum of the fissioning nucleus. The higher value of the anisotropy of ternary fission fragments obtained in the present measurement at 14-MeV bombarding energy suggests a higher probability of ternary fission for states with lower values of K_0.

THE ANGULAR AND ENERGY DISTRIBUTION OF ALPHA PARTICLES EMITTED IN THERMAL NEUTRON FISSION OF ^{235}U (SM-122/12)

Y. Gazit, A. Katase, G. Ben-David, R. Moreh,
Israel Atomic Energy Commission,
Soreq Nuclear Research Centre, Israel

The angular and energy distribution of α-particles emitted in the thermal neutron fission of ^{235}U have been measured in a three-parameter correlation experiment. The total angular and energy distributions as well as the angular distribution as a function of fragment mass ratio are given. The results were used in trajectory calculations to find the initial conditions of the fission fragment mass ratio of 1.44; the following initial conditions are obtained: fission-fragment separation d=23 fm., average initial fragment kinetic-energy 25.5 MeV, average α-particle energy at scission 2 MeV, and the distance of the α-particle from the fission axis 1 fm.

EMISSION PROBABILITIES OF LIGHT NUCLEI IN FISSION (SM-122/14)

Y. Boneh,
Nuclear Research Center, Negev, Israel,
Z. Fraenkel,
Weizmann Institute of Science, Rehovot, Israel,
and
E. Nardi,
Israel Atomic Energy Commission, Soreq Nuclear Research Centre
and Weizmann Institute of Science, Rehovot, Israel

The emission probabilities of the various light nuclei emitted in fission were investigated on the basis of a model in which particle-emission results from a rapid change of potential energy in the "neck" region of the fissioning nucleus. The nucleus was treated by means of a one-dimensional potential well of infinite depth. The relative emission probabilities and kinetic energies of the neutrons, protons and the other light nuclei emitted in fission were investigated as a function of the rise time and shape of the rising potential.

EMISSION OF LIGHT CHARGED NUCLEI IN THE n-THERMAL FISSION OF $^{239}Pu^*$ (SM-122/16)

F. Cavallari, M. Cambiaghi, F. Fossati, T. Pinelli
Istituto di Fisica Nucleare dell'Università Pavia,
and
Istituto Nazionale di Fisica Nucleare, Gruppo di Pavia, Italy

Various charged nuclei in the n-thermal fission of ^{239}Pu have been detected by using a telescope consisting of two semiconductor detectors.

The identified particles with the relative features are reported:
Long-range alpha particles. During three independent runs 14330 particles have been detected. To evidence the low part of the energetic spectrum no absorber has been interposed between the target and the telescope: nevertheless a triple fast coincidence has been realized with the fragment and telescope detectors pulses to allow the particles to be revealed. The observed energetic interval is from 7 to 28 MeV. The most probable energy is 16 ± 1 MeV with a FWHM. of 9 MeV. The given resolution is due to the continuous damage induced on the DE detector by the fission fragments and natural alphas of ^{239}Pu. The energy spectrum is symmetrically distributed around the peak energy spectrum of Gaussian shape.
Helium-six. 250 of these events have been identified. The observed energy spectrum extends from 8 to 18 MeV with the most probable energy at 12 ± 1 MeV and an FWHM. of 7 MeV. The yield relative to 100 alphas is 1.7 ± 0.2.
Helium-three. These particles have been detected during two runs with a Ni absorber interposed between the telescope and the target. The yield relative to 100 alphas is 0,9. Owing to overlapping of the alpha-particle tail, this yield is to be considered as an upper limit. The peak energy is 16 ± 1 MeV but probably the energy spectrum is influenced by the alpha tail.
Tritons. The observed energy interval is from 5.5 to 11 MeV. The peak energy is 8.2 ± 0.7 MeV with an FWHM. of 6 ± 1 MeV. The yield relative to 100 alphas is 5.5 ± 0.5.
Deuterons. Evidence has been obtained of such particles in the energy range from 4 to 7 MeV. The lower limit of the yield relative to 100 alphas is 0.3.

INVESTIGATION OF PROMPT NEUTRONS ACCOMPANYING SPONTANEOUS TERNARY FISSION OF ^{252}Cf *

(SM-122/64)

H. Piekarz, J. Błocki, T. Krogulski, E. Piasecki,
Institute of Nuclear Research, Świerk, Poland

The properties of prompt neutrons accompanying the spontaneous ^{252}Cf ternary fission with alpha-particle as a third fragment have been examined. The angular distributions of neutrons with respect to the direction of fission-fragment flight were measured for ternary and binary fission. The average number of neutrons and the relative yield of neutrons emitted from the light and heavy fragments in the ternary fission were determined by comparison with those observed in binary fission. The neutron yield as a function of the alpha-particle kinetic energy was also found. The kinetic energy of the single fission fragment was measured in coincidence with neutrons and the alpha-particle. The neutron counter consisted of a stilbene crystal 40 × 40 mm and a 56 AVP photomultiplier. A pulse-shape discriminator allowed a separation of the neutrons from the gamma-rays. Silicon surface-barrier detectors registered fission fragments and alpha-particles from tripartition (the latter in the energy interval of 10-30 MeV).

* The measurements were taken by the Nuclear Chemistry Group of CERN in Geneva.

A typical fast-slow coincidence system was applied. We can conclude that:

1. The angular distribution of neutrons with respect to the fission fragments is quite similar in the binary and ternary fissions.
2. $\langle \nu \rangle_{ternary} = 3.10 \pm 0.08$.
3. The ratio of the number of neutrons emitted from the light fragment to that emitted from the heavy one is similar in the binary and ternary fissions.
4. The neutron yield decreases with increasing alpha-particle energy: $\langle \delta\nu/\delta E_{\alpha} \rangle = -0.042 \pm 0.01$ MeV^{-1}.
5. The total kinetic energy released in ternary fission is by a value of 3.8 ± 1.3 MeV higher than that released in binary fission.

EMISSION OF LIGHT NUCLEI IN THERMAL NEUTRON FISSION OF ^{239}Pu (SM-122/65)

T. Krogulski, J. Chwaszczewska, M. Dakowski, E. Piasecki, M. Sowiński, J. Tys,
Institute of Nuclear Research, Świerk, Poland

The relative intensities and energy spectra of ^1H, ^2H, ^3H, ^4He, ^6He, and ^8He particles from the thermal neutron fission of ^{239}Pu have been measured. The 6 mg/cm^2 thick ^{239}Pu target was irradiated in thermal neutron flux of 6×10^8 cm^{-2}s^{-1}. The semiconductor counter telescope permitted distinguishing between the registered particles so that the energy spectra of hydrogen and helium isotopes could be measured.

A Gaussian distribution was fitted to the spectra by the least-squares method. We conclude that all the spectra are sufficiently well-described by a Gaussian distribution although there are small deviations from it. The most striking feature of the measured spectra is the fact that the energy distribution for all isotopes of hydrogen is almost the same, and the maximum of distribution which decreases regularly with the isotope mass in the case of helium.

The intensities relative to the emission of 100 alphas have been calculated by assuming that the low-energy part of the spectrum which is not registered is symmetrical to the corresponding high-energy part.

The results are presented in Table I.

TABLE I. RESULTS OF MEASUREMENTS

Particle	Energy range of undistorted spectra (MeV)	Relative intensity (extrapolated)	E_{peak} (MeV)	FWHM (MeV)
p	4 - 18	1.9 ± 0.1	8.40 ± 0.15	7.2 ± 0.3
d	4.5 - 19	0.5 ± 0.1	8.2 ± 0.3	7.2 ± 0.5
t	5.5 - 20	6.8 ± 0.3	8.20 ± 0.15	7.6 ± 0.4
^4He	10 - 29	100	16.0 ± 0.1	10.6 ± 0.2
^6He	11 - 28	1.9 ± 0.2	11.8 ± 0.1	10.6 ± 0.6
^8He	12 - 23	0.08 ± 0.02	< 12	> 9

MODEL CALCULATIONS OF THE ENERGY AND ANGULAR DISTRIBUTIONS OF LIGHT NUCLEI ACCOMPANYING FISSION (SM-122/66)

J. Błocki, T. Krogulski,
Institute of Nuclear Research, Świerk, Poland

The Geilikman model dealing with the emission of α-particles in the fission of ^{236}U was modified and extended to other particles. This model treats classically the motion of the third particle in the mutual Coulomb field of the two fragments. The system of these three bodies is parametrized in terms of the initial dynamic variables. Among these, the initial distances between three bodies and the initial energy of the light nucleus were found to influence most markedly the final energy and angular distributions of the light nucleus investigated. Thus, the model calculations were performed with the remaining initial conditions as follows: (i) isotropic spatial distribution of the light-nuclei initial velocity; (ii) the deformed fragments are replaced by point charges; (iii) the total Coulomb potential and kinetic energy of the system is equal to the most probable kinetic energy released in the alpha-tripartition; (iv) the mass distribution of fragments is replaced by the definite mass ratio equal to the most probable ratio in the alpha-tripartition.

If the experimental results are compared with the calculated ones it is seen that 1. the energy distributions of helium and hydrogen isotopes are sufficiently well described by the model of three Coulomb-interacting bodies in close as well as in elongated configurations of the scissioning nuclei when the initial energy distribution of the light particles with two adjustable parameters is used; 2. to understand the observed angular distributions of inevitable hydrogen and helium isotopes in terms of the model presented, it seems to assume an elongated configuration of the scissioning nuclei and a fairly wide distribution of the initial position of light nuclei between the fragments.

PARAMETRES RELATIFS A LA DEFORMATION DES FRAGMENTS DANS LA FISSION TERNAIRE (SM-122/81)

T.P. Doan, M. Asghar, C. Carles, R. Chastel,
Laboratoire de Physique Nucléaire de la Faculté des Sciences de Bordeaux,
Le Haut Vigneau, France

Nous avons calculé la déformation de gros fragments de tripartition, D(M), leur énergie de déformation, $E_D(M)$, et d'autres quantités reliées à celles-ci. Nous avons supposé que les fragments sont des ellipsoïdes de révolution uniformément chargés et que la particule légère est placée sur la ligne joignant leurs centres, celle-ci coïncidant avec leurs grands axes. Les résultats sont consistants, dans les limites de 10 à 15%, avec nos calculs antérieurs, dans lesquels nous supposons que les ellipsoïdes de révolution étaient chargés en surface.

Nous utilisons les résultats pour déterminer les quantités suivantes:
1. Nombre de neutrons prompts en fission ternaire en fonction de la masse des fragments $\nu_T(M)$. Les valeurs calculées de $\nu_T(M)$ en fonction de la

masse pour ^{252}Cf sont en bon accord avec les valeurs expérimentales. La valeur moyenne $\langle \nu_T(M) \rangle$ pour ^{235}U est en accord avec la valeur expérimentale;
2. Probabilité intrinsèque de l'émission de la particule alpha $P_\alpha(M)$ en fonction de la masse des fragments. Nos résultats concordent très bien avec les données expérimentales de Schmitt et al. sur le ^{235}U;
3. Quelques paramètres de physique nucléaire: paramètres de déformation $\beta_2(M)$, coefficients de déformation de Nilsson $\delta(M)$, moment quadrupôlaire des fragments de tripartition $Q_0(M)$ et le paramètre $C_2(M)$ qui représente la résistance à la déformation.

Nous comparons quantitativement ces résultats avec les données expérimentales et théoriques. Par example, nos valeurs de $C_2(M)$ concordent bien avec celles trouvées par Fong par extrapolation aux fragments de fission binaire riches en neutrons des valeurs de C_2 trouvées pour les noyaux stables. Nos valeurs de β_2 sont en très bon accord avec celles calculées par Ignatyuk en utilisant le modèle en couche à particule indépendante et elles s'accordent assez bien avec les résultats expérimentaux obtenus par excitation coulombienne.

English translation of the preceding Abstract (SM-122/81):

PARAMETERS RELATING TO THE DEFORMATION OF FRAGMENTS IN TERNARY FISSION

We have calculated the deformation of the large tripartition fragments D(M), their deformation energy $E_D(M)$ and other associated quantities. We assumed that the fragments were uniformly charged ellipsiods of revolution, and that the light particle was located on the line joining their centres, this line coinciding with their major axes. The results are consistent, within 10-15%, with our previous calculations, in which we assumed that the ellipsoids of revolution were charged on the surface.

We use the results to determine the following quantities:
1. The number of ternary-fission prompt neutrons as a function of the mass of the fragments $\nu_T(M)$. The values of $\nu_T(M)$ calculated as a function of mass for ^{252}Cf are in good agreement with the experimental values. The mean values $\langle \nu_T(M) \rangle$ for ^{235}U agrees with the experimental value;
2. The intrinsic probability of emission of the alpha particle $P_\alpha(M)$ as a function of the mass of the fragments. Our results agree very satisfactorily with the experimental data of Schmitt et al. for ^{235}U;
3. Certain parameters of nuclear physics: parameters of deformation $\beta_2(M)$, Nilsson deformation co-efficients $\delta(M)$, quadrupole moment of tripartition fragments $Q_0(M)$, and the parameter $C_2(M)$, representing resistance to deformation.

We quantitatively compared these results with the existing experimental and theoretical data. For example, our values for $C_2(M)$ agree well with those which Fong found by extrapolation of the values of C_2 for stable nuclei to neutron-rich binary fission fragments. Our values for β_2 are in very good agreement with those calculated by Ignatyuk, who used the independent-particle shell model, and agree fairly well with the experimental results obtained by Coulomb excitation.

MESURE CORRELEE DANS LA TRIPARTITION DE ^{235}U PAR NEUTRONS THERMIQUES (SM-122/82)

C. Carles, M. Asghar, T. P. Doan, R. Chastel, M. Ribrag,
Laboratoire de Physique Nucléaire de la Faculté des Sciences de Bordeaux
and
Centre d'Etudes Nucléaires de Saclay,
Gif-sur-Yvette, France

Nous avons utilisé un système d'analyse multiparamétrique avec des détecteurs à semi-conducteur pour mesurer les masses et les énergies des fragments de fission binaire et de tripartition (émission de particules α de long parcours) de l'U^{235} par neutrons thermiques. Nous avons analysé environ 27 000 événements de tripartition et plusieurs centaines de milliers d'événements de fission binaire. L'utilisation d'une mesure de différence de temps de vol entre les deux gros fragments nous a permis de minimiser les événements parasites dans les régions de masses symmétriques et très asymmétriques.

Les principaux résultats que nous obtenons sont les suivants:

1) la probabilité d'émission de particules α en fonction de la masse des fragments de fission binaire suivant la définition de Schmitt et al. Nos résultats sont en accord avec ceux donnés par Schmitt et al. mais notre méthode nous permet en outre d'obtenir des résultats dans les zones de faible taux de production (masses symmétriques et très asymmétriques);

2) les pics de distribution de masse des fragments sont plus étroits pour la tripartition que pour la fission binaire;

3) nous étudions la variation de l'énergie cinétique totale en fonction du rapport des masses en fission binaire et en tripartition.

English translation of the preceding Abstract (SM-122/82):

CORRELATED MEASUREMENT IN TERNARY FISSION OF ^{235}U BY THERMAL NEUTRONS

We used a system of multiparameter analysis with semi-conductor detectors in order to measure the masses and energies of the fragments emitted during the binary fission and tripartition (emission of long-range α-particles) of ^{235}U by thermal neutrons. We analysed about 27 000 tripartition events and several hundreds of thousands of binary fission events. By using the measurement of the difference between the times-of-flight of the two large fragments, we were able to minimize parasitic events in the regions of symmetric and highly asymmetric masses.

We obtained the following principal results:

1) Regarding the probability of α-particle emission as a function of the mass of the binary fission fragments according to the definition of Schmitt et al., our results agree with those of Schmitt et al., but our method gives, in addition, results in the zones of low production rates (symmetric and highly asymmetric masses);

2) The mass distribution peaks of the fragments are narrower in the case of tripartition than in that of binary fission;

3) We study the variation of the total kinetic energy as a function of the ratio of the masses involved in binary fission and tripartition.

ETUDE DE LA FISSION TERNAIRE INDUITE PAR DE PROTONS DE HAUTE ENERGIE. VISUALISATION A

L'AIDE DE DETECTEURS SOLIDES (SM-122/87)

R. Stein, J. Ralarosy, G. Remy, J. Tripier, M. Debeauvais,
Laboratoire de Physique Corpusculaire, Strasbourg-Cronenbourg, France

La mise au point de relations parcours-énergie précises dans des nouveaux détecteurs, nous a permis une étude cinématique de certaines interactions ternaires visualisées dans les détecteurs solides.

Nous avons en particulier calculé, grâce à certaines hypothèses, la distribution en masse et en moment des fragments émis et cela pour plusieurs centaines d'événements ternaires.

Le cas des cibles U, Pb et Th pour des protons incident de 3, 18 et 24 GeV/c est examiné.

English translation of the preceding Abstract (SM-122/87):

STUDY OF TERNARY FISSION INDUCED BY HIGH-ENERGY PROTONS. RECORDING BY MEANS OF SOLID DETECTORS

The kinematic study of some ternary interactions recorded by means of solid detectors has been made possible by the development of accurate range-energy relations in these new detectors.

Using certain hypotheses, we have calculated, in particular, the mass and momentum distribution of the fragments emitted, and have done this for several hundred ternary events.

The case of U, Pb and Th targets for 3, 18 and 24 GeV/c incident protons is considered.

TERNARY FISSION OF ^{232}Th, ^{238}U and ^{239}Pu (SM-122/95)

L. Medveczky, G. Somogyi,
Institute of Nuclear Research of the Hungarian Academy of Sciences,
Debrecen, Hungary
and
G. Götz,
Fachbereich Angewandte Physik der Friedrich Schiller Universität Jena,
German Democratic Republic

The purpose of the present study is to report the data of the ternary photofission of ^{232}Th, ^{238}U and ^{239}Pu. The fissions were induced with the bremsstrahlung of a 27.5 MeV electron beam, and were detected simultaneously with track-detectors of different threshold (muscovite mica, plastic Melinex O) for the discrimination of the tracks of the binary and ternary events the sandwich technique was used. During this investigation altogether about 1.5 million binary fission events were scanned. With all the three nuclei the three-prong events showed a higher frequency in the plastic detectors than in the mica ones. A number of two-prong events with a space angle smaller than 180° were also found. In both of the above events the angular and range distributions were measured. The range distribution of

the three-prong events indicates the presence of a symmetric and an asymmetric group. Comparing the results achieved with the two-track detectors of different threshold, and considering the interfering fission-fragment scattering effect, the conclusion could be drawn that a significant part of the three-prong events could not originate from scattering processes. On the basis of the results it seems that in the case of Th and U the frequency of the ternary fission having third fragment of a mass number $10 \leq m \leq 30$ is higher than those of a mass number >30. It has been established that the ratios of the symmetrical ternary-fission events (the mass of each fragment being >30) to the binary fission events, in the case of ^{232}Th, ^{238}U and ^{239}Pu are $\sim 8 \times 10^{-6}$, $\sim 11 \times 10^{-6}$ and $< 3 \times 10^{-6}$, respectively.

VARIATION OF THE BINARY-TO-TERNARY FISSION RATIO FOR ^{235}U IN THE RESONANCE REGION (SM-122/139)

A.J. Deruytter,
Central Bureau for Nuclear Measurements, Euratom Geel, Belgium,
and
C. Wagemans,
NFWO, Rijksuniversiteit te Gent and SCK-CEN, Mol, Belgium

Precise measurements were performed of the ratio of binary-to-ternary fission in the neutron energy region below 23 eV.

The neutron source was the uranium target of the linear electron accelerator of the C.B.N.M. at Geel (Belgium). The neutron energy-selection was made by time-of-flight at a short (8 metre) well-collimated flight-path. The high neutron intensity allowed good collimation of the neutron beam onto the target and good resolution of the time-of-flight spectra in the considered energy-range since only two deposits of highly enriched ^{235}U (on both sides of an aluminium disk) of about 2 mg/cm^2 were used.

Large gold-silicon surface-barrier detectors on both sides of the back-to-back target were used for the consecutive measurements of long-range α-particles (absorbers in) and fission fragments (absorbers out). These detectors show a well-resolved energy spectrum for the detected particles. Time-of-flight spectra were recorded in both conditions.

The ratios of the surfaces in counting-rate versus neutron energy spectra for binary and ternary fission in the strongest isolated resonances were calculated and compared with previously published contradictory data (Table I). These ratios are also compared with the variation of other fission characteristics in these resonances and with the few known resonance spins (Table II).

TABLE I. COMPARISON OF T/B VALUES

E (eV)	Mehta et al. [1]	Michaudon et al. [2]		These measurements		
		I	II	I	II	Average
21.1	96 ± 5	92.5 ± 5	105.5 ± 3.5	122 ± 6	118 ± 8	120 ± 5
19.3	97.5 ± 3	90 ± 2.5	105 ± 2	114 ± 3.5	116 ± 5	115 ± 3
12.39	99 ± 3	92.5 ± 2.5	100 ± 2	105.5 ± 4	99 ± 6	102 ± 3.5
8.78*	100 ± 2	100 ± 1.5	100 ± 1.5	100 ± 3	100 ± 4	100 ± 2.5
Detection level	9 MeV	7.3 MeV	10.9 MeV	10 MeV		
Detector	Si(Au)	ionization chamber		Si(Au)		

* All the ratios are normalized at this energy

TABLE II. COMPARISON WITH OTHER FISSION CHARACTERISTICS AND RESONANCE SPINS

Energy (eV)	T/B normalized at 8.79 eV	Spin assignments			Cowan et al. [6] mass distribution
		Direct	Indirect (normalized at 8.79 eV)		
		Poortmans et al. [3] (scattering)	Melkonian et al. [4] (kinetic energy)	Asghar et al. [5] (γ-ray multipl.)	
21.1	120 ± 5		4^-		A
19.3	115 ± 3	4^-	4^-	4^-	A
12.39	102 ± 3.5	3^-		4^-	
8.79	100 ± 2.5	3^-	3^-	3^-	(A)

REFERENCES

[1] MEHTA, G., Ph.D. Thesis, Columbia University (1963).
[2] MICHAUDON, A., Rapport CEA-R. 2552 (1964).
[3] POORTMANS, F. et al., this Conference SM-122/70.
[4] MELKONIAN, E. et al., in Physics and Chem. of Fission (Proc. Symp. Salzburg, 1955 2, IAEA, Vienna 1966).
[5] ASHGAR, M. et al., Phys. Lett. 26B (1968) 664.
[6] COWAN, G. et al., Phys. Rev. 130 (1963) 2380.

ДЛИННОПРОБЕЖНЫЕ ЧАСТИЦЫ ДЕЛЕНИЯ (IAEA-SM-122/146)

В.М. Адамов, С.С. Коваленко, К.А. Петржак, И.И. Тютюгин
Физико-технический институт им. А.Ф.Иоффе, Ленинград,
Союз Советских Социалистических Республик

В настоящей работе определены отношения вероятностей деления с вылетом длиннопробежных частиц (ДПЧ-деление) ^{232}Th, ^{233}U, ^{238}U, ^{237}Np нейтронами с энергией 14 Мэв к вероятности ДПЧ-деления ^{235}U медленными нейтронами. Эти величины равны соответственно 0,3 ± 0,2; 1,2 ± 0,1; 0,64 ± 0,06; 1,3 ± 0,1. Измерены выходы протонов и тритонов при делении вышеуказанных ядер (кроме ^{232}Th) нейтронами с энергией 14 Мэв, а также при делении ^{233}U, ^{235}U медленными нейтронами и при спонтанном делении ^{244}Cm. Во всех случаях (кроме ^{232}Th) измерялись спектры альфа-частиц и тритонов; при делении ^{235}U медленными нейтронами и при спонтанном делении ^{244}Cm измерены спектры протонов. В опыте регистрировались совпадения между осколком и длиннопробежной частицей. Осколки регистрировались мелкой ионизационной камерой, длиннопробежные частицы – кристаллом CsI (Tl). Разделение частиц по массам производилось методом анализа времени высвечивания в кристалле при регистрации частиц. Полученные данные позволили установить, что: 1) вероятность ДПЧ-деления возрастает с увеличеснием параметра Z^2/A; 2) выходы протонов и тритонов на 100 альфа-частиц лежат в пределах 2 ÷ 4% и 7 ÷ 10%, соответственно, и не зависят от энергии возбуждения; 3) максимумы энергетических распределений альфа-частиц лежат при энергии 16 ± 1 Мэв для всех ядер; соответствующая величина для протонов и тритонов равна 8 ÷ 9 Мэв. Обсуждаются возможные причины изменения вероятности ДПЧ-деления при изменении Z^2/A и энергии возбуждения.

English translation of the preceding abstract (SM-122/146):

LONG-RANGE PARTICLES IN FISSION

The authors determined the relative probabilities of 14-MeV neutron-induced fission of ^{232}Th, ^{233}U, ^{238}U and ^{237}Np involving the emission of long-range particles ("long-range particle" fission) and of "long-range particle" fission of ^{235}U induced by slow neutrons. The ratios are, respectively, 0.3 ± 0.2, 1.2 ± 0.1, 0.64 ± 0.06 and 1.3 ± 0.1. Then they measured proton and triton yields in the 14-MeV neutron-induced fission of the above-mentioned nuclei (other than ^{232}Th) and in the fission of ^{233}U and ^{235}U by slow neutrons and the spontaneous fission of ^{244}Cm. The alpha-particle and triton spectra were measured in all cases (except for ^{232}Th) and the proton spectra were also measured for the fission of ^{235}U by slow neutrons and the spontaneous fission of ^{244}Cm. Coincidences between the fragment and the long-range particle were recorded experimentally, fragments being recorded by a small ionization chamber and long-range particles by a CsI(Tl) crystal. The mass distribution of the particles was determined by analysing the duration of fluorescence in the crystal when particles were recorded. The data obtained show that: (1) The probability of "long-range particle" fission increases as

Z^2/A increases; (2) Proton and triton yields per 100 alpha particles are between 2 and 4% and 7 and 10%, respectively, and are independent of the excitation energy; (3) The alpha particle energy distribution peaks are at 16 ± 1 MeV for all nuclei, the corresponding value for protons and tritons being between 8 and 9 MeV. The authors discuss the possible reasons for the variation in the probability of "long-range particle" fission with changes in Z^2/A and the excitation energy.

ТРОЙНОЕ ДЕЛЕНИЕ ^{235}U МЕДЛЕННЫМИ НЕЙТРОНАМИ

(IAEA-SM-122/151)

В.М. Адамов, Л.В. Драпчинский, С.С. Коваленко, К.А. Петржак, И.И. Тютюгин
Физико-технический институт им. А.Ф.Иоффе, Ленинград,
Союз Советских Социалистических Республик

С помощью поверхностно-барьерных детекторов одновременно измерялись кинетические энергии осколков и длиннопробежных α-частиц при делении ^{235}U медленными нейтронами. Работа проводилась на реакторе Физико-технического института им А.Ф.Иоффе. Определено, что средняя суммарная кинетическая энергия осколков тройного деления на 15 Мэв меньше, чем в случае двойного деления. Это значение хорошо согласуется с ранее полученными результатами. Полуширина распределения суммарной кинетической энергии осколков тройного деления на 4,7 Мэв меньше, чем двойного. Получена зависимость средней кинетической энергии и дисперии кинетической энергии осколков от энергии α-частиц. Средняя кинетическая энергия осколков линейно уменьшается с ростом энергии α-частиц с наклоном $\frac{\Delta E_к}{\Delta E_\alpha} = 0{,}35$. Дисперсия энергии в пределах ошибок опыта не зависит от энергии α-частицы. Средняя энергия α-частиц линейно уменьшается от 16,0 Мэв до 14,5 Мэв с ростом суммарной кинетической энергии осколков от 140 Мэв до 170 Мэв. Определена также зависимость кинетической энергии легкой и тяжелой групп осколков от энергии α-частицы. Эти данные позволяют предполагать, что α-частица формируется в основном из нуклонов тяжелого осколка.

English translation of the preceding Abstract (SM-122/151):

TERNARY FISSION OF ^{235}U BY THERMAL NEUTRONS

Surface barrier detectors were used to measure simultaneously the kinetic energies of fragments and long-range alpha particles in the fission of ^{235}U by thermal neutrons. The work was done on the reactor at the Ioffe Physico-technical Institute. It was found that the mean total kinetic energy of ternary-fission fragments is 15 MeV less than in the case of binary fission. This value is in good agreement with earlier results. The distribution half-width for the total kinetic energy of ternary-fission fragments is 4.7 MeV less than for binary-fission fragments. The authors determined the mean kinetic energy and the spread in the kinetic energy of fragments as functions of alpha-particle energy. The mean kinetic energy of the fragments decreases linearly as the alpha particle energy increases, the angle of dip $\Delta E_k/\Delta E_\alpha$ being 0.35. Within the limits of experimental error the energy spread does not depend on the alpha particle energy. The mean alpha particle energy decreases linearly from 16.0 MeV to 14.5 MeV as the total kinetic energy of the fragments increases from 140 MeV to 170 MeV. The authors determined the kinetic energy of the light and heavy groups of fragments as a function of alpha particle energy. These data point to the fact that alpha particles are formed mainly from nuclei of a heavy fragment.

SESSION C

AN EMPIRICAL CORRELATION FORMULA OF SPONTANEOUS FISSION HALF-LIVES (SM-122/4)

Eiko Takekoshi
Japan Atomic Energy Research Institute, Tokai Research Establishment,
Tokai-mura, Naka-gun, Ibaraki-ken, Japan

A simple empirical correlation formula has been proposed separately for the spontaneous fission half-lives data with the nuclides in the range of Pu ~ Fm and in the wider range of Th ~ 104. Its functional form was derived on the basis of Swiatecki's correlation formula [1], in which the spontaneous fission half-lives were expressed as a function of the usual fissionability parameter (Z^2/A) and the mass deviation (δM) of the experimental mass from Green's mass formula [2]. The correlation functions proposed in the present work are of the form $\log_{10}\tau = c_1 + c_2(1-X)\,\delta M + c_3 + \Delta$ for the nuclides in the wider range of Th ~ 104. Here τ, δM and X are the spontaneous fission half-lives measured in years, the mass deviation in MeV, and the fissionability parameter, respectively. The values of δM and X are calculated by using the original [3] and the revised [4] Myers-Swiatecki mass formulas and also by using the Seeger-Perisho mass law [5]. The parameters of c_1, c_2, c_3, and Δ were determined by following an iterative least-square procedure. For 19 even-even, 7 odd-A, 2 odd-odd nuclides in the range of Pu ~ Fm, the correlation formula with the best fitness was found to be $\log_{10}\tau = -347.032X - 19.020(1-X)\,\delta M + 288.894 + \Delta$ (4.451 for odd-A nuclides and 3.520 for odd-odd nuclides) with the weighted variance of 0.796, by using the original Myers-Swiatecki mass formula. For 26 even-even, 8 odd-A, 2 odd-odd nuclides in the wider range of Th ~ 104, the correlation formula with the best fitness was found to be $\log_{10}\tau = 2821.608(1-X)^3 - 25.285(1-X)\,\delta M - 18.949 + \Delta$ (3.725 for odd-A nuclides and 3.363 for odd-odd nuclides) with the weighted variance of 0.604, by using the revised Myers-Swiatecki mass formula. Both correlation function forms do not seem to be very successful, when the X- and δM-values are calculated by using the Seeger-Perisho mass law. In their mass law the fissionability parameters (X) are extremely close together for a given element.

REFERENCES

[1] SWIATECKI, W.J., Phys. Rev. 100 (1955) 973.
[2] GREEN, A.E.S., Phys. Rev. 95 (1954) 1006.
[3] MYERS, W.B., SWIATECKI, W.J., Nucl. Phys. 81 (1966) 1 and University of California Lawrence Radiation Laboratory Report UCRL-11980, 1965.
[4] MYERS, W.D., SWIATECKI, W.J., Arkiv for Fysik 36 No.43 (1967) 343.
[5] SEEGER, P.A., PERISHO, R.C., University of California Los Alamos Scientific Laboratory Report LA-3751, 1967.

NUCLEAR SINGLE-PARTICLE HAMILTONIAN FOR ADIABATIC FISSION THEORY (SM-122/47)

H. Meldner
Institut für Theoretische Physik, Freie Universität Berlin,
Berlin

A simple shell-model Hamiltonian is discussed that allows self-consistent solutions in the case of axial symmetry. This is an extension of earlier work where a realistic nuclear single-particle Hamiltonian was successfully applied to spherical nuclei [1]. The proposed Hamiltonian is basically non-local and reads in "local energy approximation"

$$H_{m_i} = (\vec{p}^{\,2}/2m) + v(\epsilon_{\nu,m_i})\{1 - [\rho_{m_i}(z,b)/\rho_1]^{2/3}\}\,[1 - (\sigma/\hbar)(\vec{p}\times\vec{s})\vec{\nabla}]\rho_{m_i}(z,b)$$
$$+ (\tfrac{1}{2} - m_i)V_c(z,b)$$

The subscript ν stands for all quantum numbers specifying a bound nucleon except for its iso-spin 3-component m_i. V_c is the static Coulomb potential and (z, b) are cylinder co-ordinates; v is essentially the Fourier transform of the non-locality function that contains two parameters; ρ_1 and σ are the critical density and spin-orbit splitting parameters. The fifth parameter of this model is given by the iso-spin weighting constant τ in the effective nuclear density

$$\rho_{m_i} = [\rho_{(-m_i)} + \tau\rho_{m_i}]\,(1+\tau)^{-1}$$

where

$$\rho_{m_i} = \sum_{\nu}^{\nu_{\mathrm{Fermi}}} |\varphi_{\nu,m_i}|^2$$

i.e. the sum of the squares of the wave functions which are calculated self-consistently this way. The problematic boundary condition of "volume conservation" in equipotential contours, for example, is completely avoided here. In fact, most of the classical difficulties [2] of the Nilsson-type models for deformed nuclei and adiabatic fission computations do not arise.

REFERENCES

[1] MELDNER, H., UCRL-17801 and Phys. Rev. 178 4.
[2] WILETS, L., Theories of Nuclear Fission (Clarendon Press, Oxford, England, 1964), Chapter 4,3.

NUCLEAR CURVATURE TENSION AND THE POSSIBILITY OF SHAPE ISOMERS FOR NUCLEI NEAR Ra (SM-122/48)

E. Hilf, H. von Groote
Physikalisches Institut der Universität Würzburg,
Federal Republic of Germany

The shape dependence of nuclear masses is discussed. The saddle-point area of the potential energy surface has been studied. We used a semi-empiric mass formula containing a volume-, a surface-, a curvature-, a Coulomb-term as well as the shell correction term of Myers and Swiatecki (version II), the shape-dependent pairing energy as suggested by Moretto and Noerenberg and the asymmetry and compressibility terms of the droplet model of Myers and Swiatecki. The nuclear shape at the saddle-point and the "flatness" (the width of the inverse fission oscillator) of its vicinity is calculated as a function of charge Z, atomic weight A, and the fissility parameter κ, respectively. The well-known change at the κ-area of Ra from constricted saddle-point shapes for light nuclei to sausage-like ones for heavy nuclei has been studied. This change is emphasized by a curvature tension and simultaneously the saddle-point area becomes very flat. For sufficiently large values of the curvature tension a small second minimum occurs, which means a small double-hump fission barrier. This is due to the different ways in which surface tension and curvature tension act on deformed nuclei. The formation of a Strutinsky minimum in a small area of nuclei near Ra is fostered to the same degree as the value of the curvature tension is increased. The Strutinsky shell correction term, however (which led to the shape isomers of very heavy nuclei predicted), is still unknown for the strongly deformed and constricted saddle-point shapes in question. Some simple other shell terms have been tried. The numerical values of the surface and curvature tensions are estimated by fitting simultaneously the fission barriers of light and heavy nuclei and using the estimate of the nuclear particle density of Seeger, $\rho = 1.46\ \mathrm{fm}^{-3}$.

ON THE POTENTIAL SURFACE OF HEAVY NUCLEI (SM-122/63)

H.C. Pauli*, V.M. Strutinsky**
The Niels Bohr Institute, University of Copenhagen, Denmark

The potential energy is split up into a smoothly behaving background and a rapidly varying contribution due to the nuclear shell structure of which the latter has been computed by the shell correction method. These shell corrections are presented and discussed for P_2-P_4- and different P_3-like deformations. To check the sensitivity of the results on the different shell models, the calculations have been performed for the Nilsson model - the $\vec{\ell}\cdot\vec{s}$-term has been replaced by the more correct $\vec{s}\cdot[\vec{p}\times \mathrm{grad}V]$ term in the Hamiltonian - and a deformed generalized Saxon-Woods potential with a constant and deformation-independent surface thickness.

---

* On leave from the University of Basel, Switzerland.

** On leave from the I.V. Kurchatov Institute, Moscow, USSR.

VALIDITY OF NUCLEAR DEFORMATION ENERGIES OBTAINED FROM SINGLE-PARTICLE LEVELS (SM-122/112)

L. Wilets
Department of Physics, University of Washington, Seattle, USA
and
W.H. Bassichis
Department of Physics, MIT, Cambridge, Mass., USA.

A detailed description of the fission process relies upon a knowledge of the deformation energy surface. Several extensive theoretical investigations of the surface are currently being conducted at various institutions. They differ in such details as the shape of the shell model potential, inclusion of higher moments of deformation, handling of saturation, etc., or in the method of normalization of empirical data, such as Strutinsky's statistical averaging. They all do contain the common feature that they utilize IPM energies and wave functions of some generalized Nilsson form in order to simulate the results of an idealized (perhaps modified) Hartree-Fock calculation. Aside from practical ambiguities in such procedures, there remain fundamental difficulties in the programs: it is not possible to deduce total energies, as a function of deformation, from single particle energies and wave functions alone, without further knowledge of the two-body interaction.

To test the degree of validity or failure of various energy summation prescriptions, Hartree-Fock calculations were performed on light nuclei using an effective interaction which had already proved successful in reproducing a number of nuclear properties. The Hartree-Fock energies and wave functions were then also utilized as input for the various summation procedures and the results compared with Hartree-Fock. Our conclusions do not depend upon how accurate or realistic the assumed interaction is (so long as it is "reasonable"). The calculation is a numerical experiment, a comparison of an internally consistent model with various approximations to the model.

We find that most prescriptions give qualitatively erroneous results. The simple summation of eigenvalues (which cannot yield absolute energies) appears to be qualitatively reasonable although quantitatively in error. In the case of ^{20}Ne, for example, it yields an equilibrium quadrupole moment which is 28% too small and a curvature which is too stiff.

We conclude that a quantitative calculation of the deformation surface requires a model which incorporates further information about the two-body interaction, such as Hartree-Fock.

MICROSCOPIC INERTIAL MASS PARAMETER FOR SUPER-HEAVY NUCLEI (SM-122/153)

A. Sobiczewski, Z. Szymański, S. Wycech
Institute for Nuclear Research and Warsaw University, Warsaw, Poland.

The inertial mass parameter B characterizing the kinetic energy of a collective motion of a nucleus is calculated for nuclei in the neighbourhood of the hypothetical doubly-closed-shell nucleus $^{298}(114)$. The collective motion considered consists of the change of the quadrupole, axially symmetric deformation of the nucleus. The parameter B is obtained under the assumption that the collective motion is adiabatic with respect to the intrinsic motions. The numerical calculations are performed with help of the recent version of the Nilsson potential (with the $\langle \vec{l}^2 \rangle$, term). The pairing correlations are taken into account. It appears that the microscopic values of B calculated for an even-even nucleus is about 10 times larger than the corresponding hydrodynamical values. It appears also that the parameter B is a sensitive function of the quadrupole and the hexadecapole deformations of the single-particle potential, as well as of the pairing forces strength G. For example the ±5% change in G gives crudely ±20% change in B. Rough estimates of the coupling between the quadrupole ($\lambda = 2$) and hexadecapole ($\lambda = 4$) oscillations show that it may change the B value considerably. The addition of an odd nucleon to an even-even system increases the B values by about 30%. It is mainly due to the decrease in the pairing correlations caused by the presence of the odd, not paired, particle. Such a large growth of B alone (i.e. even with no effect of the odd particle on the fission barrier) may increase the spontaneous fission half-lives by a few orders.

SINGLE-PARTICLE ENERGIES IN A DEFORMED POTENTIAL (SM-122/155)

T. Johansson
Lund Institute of Technology,
Department of Mathematical Physics,
Lund, Sweden

A nuclear single-particle Hamiltonian $H = T + V + k\vec{s} \cdot (\vec{p} \times \mathrm{grad}\, V)$, where k is a constant, is investigated. The potential V is a sum of three terms i.e. a deformed harmonic oscillator (h.o.), another deformed h.o. squared, and a Gaussian. The squared h.o. is added instead of Nilsson's $\vec{l}^2$-term in order to interpolate between a h.o. and a square well. The Gaussian tends to divide the nucleus into two separated parts, and to produce a neck in the shape of the nucleus. To investigate the average macroscopic properties of this potential we use the Thomas-Fermi method and write the mass density as $\rho \sim (\lambda - V)^{3/2}$ where the Fermi energy λ is determined from the number of particles. In this way, it is, e.g. possible to keep the volume of the nucleus constant during deformation. By giving the h.o. and the squared h.o. different deformations the diffuseness can be varied to some extent. To calculate the single-particle energies we use the method of diagonalization of the Hamiltonian in a representation. As a basis we use the asymptotic wave functions. They are characterized by the quantum numbers N, n_z, Λ and Ω and by the frequencies $\omega_\perp$ and ω_z of the generating h.o.. These quantities are determined in such a way that the single-particle energies are obtained with desired accuracy using as few basis wave functions as possible. It turns out that the squared h.o. is the main term in the potential and that the h.o.-term is a correction that has to be given a negative sign in order to reproduce the levels in ^{208}Pb as well as possible. Consistently with this, one obtains a radius of about $1.2A^{1/3}$ and a diffuseness of about 2.6 fm from the Thomas-Fermi distribution.

ON THE THEORY OF NUCLEAR FISSION (SM-122/162)

C. Syros
European Atomic Energy Community,
Brussels, Belgium

Starting from two-body interactions and imposing the restrictions implied by the exclusion principle on the four- and two-body nucleon correlations a potential energy function is deduced. It consists of two parts - the short-range microscopic and the long-range collective one. The excess neutrons (N - Z) show correlations related to the interaction between the intrinsic ($\vec{R}_i$) and the collective ($\vec{R}_c$) degrees of freedom of the system.

By assuming a particular form of this interaction and writing the wave function of the nucleus at the scissioning point as a bilinear rotationally invariant combination of intrinsic and collective wave functions the separated equations

$$\left[T_i + V_i(\vec{R}_i) + \frac{D_f - d_f}{D_f} (\mathscr{E} + V(\vec{R}_i)(\vec{J} \cdot \vec{L})) \right] \psi_i(\vec{R}_i) = E_i \psi_i(\vec{R}_i)$$

and

$$\left[T_c + V_c(\vec{R}_c) + \frac{d_f}{D_f} (\mathscr{E} + \overline{V} \cdot \langle \vec{J} \cdot \vec{L} \rangle) \right] \varphi_c(\vec{R}_c) = E_c \varphi_c(\vec{R}_c)$$

are obtained, where $(D_f - d_f)$, d_f are the numbers of intrinsic and collective degrees of freedom, and $\mathscr{E}$ the total energy available during the reaction. As a preliminary application the second Strutinsky minimum has been represented by the Morse potential. Rotational states are more easily populated than vibrational ones leading to the reported multipolarity of gamma emission. The calculated mass distributions show binding-energy structure and agree qualitatively with the experimental data.

POTENTIAL BARRIER EFFECTS IN THE POPULATION OF $^{242mf}Am$ AND $^{244mf}Am$ SPONTANEOUSLY FISSIONING ISOMERIC STATES (SM-122/18)

N. Vîlcov
Institute for Atomic Physics,
Bucharest, Romania

In the case of certain transuranium nuclei, by taking into account the shell-effects, energy-deformation curves characterized by a secondary minimum (the Strutinsky's two-humped potential barrier) are obtained. This secondary minimum corresponds to an excitation energy of 2.5-3 MeV in the $^{242,244}Am$ isotopes. The sub-threshold fission resonances in ^{237}Np, ^{241}Pu, ^{241}Am etc. provided an excellent confirmation of the two-humped potential barrier hypothesis. Considering the experimental difficulties met in the study of sub-threshold fission resonances, information about the two-humped potential barrier obtained in other ways, is extremely useful. This is why the study of spontaneously fissioning isomers is now of great interest. The paper deals with the study of the potential-barrier shape effects on the population of the isomeric states $^{242mf}Am$ and $^{244mf}Am$ by fast neutron capture. The Flerov-Druin shape-isomerism hypothesis, the only one able to justify the appearance of spontaneously fissioning isomeric states, was simply put into a concrete form on the basis of the two-humped potential barrier model, by identifying the secondary minimum with the isomeric state. The shape of the excitation function in the case of $T_{\frac{1}{2}}$ = 14 ms $^{242mf}Am$ isomeric state population through fast neutron capture is shown to be directly connected with the shape of the potential barrier of the nucleus resulting from capture. The combination of experimental data on induced fission and spontaneously fissioning isomeric states population provides us with the possibility of determining the potential barrier parameters. At the same time, recent experimental data on the $^{244mf}Am$ spontaneously fissioning isomer ($T_{\frac{1}{2}}$ = 0.6 ms) obtained through fast neutron capture cannot be explained in terms of the two-humped potential barrier model.

The necessity of taking into account three-dimensional deformations for explaining both induced fission and isomeric state population processes is analysed. However, the shape of the excitation function of the reaction $^{243}Am\,(n,\gamma)\,^{244mf}Am$ does not exclude the possibility of angular momentum effects which are able to explain the existing experimental data in terms of the one-dimensional potential barrier model.

ANGULAR ANISOTROPY OF FISSION FRAGMENTS IN THE NEUTRON-INDUCED FISSION OF ^{235}U (SM-122/43)

D.M. Nadkarni, S.S. Kapoor
Bhabha Atomic Research Centre, Trombay, Bombay, India

Recent studies of the angular distribution of fission fragments in the fission of heavy nuclei following direct reactions have indicated some evidence for a rather large pairing energy gap in the transition state spectra of even-even fissioning nuclei. In the present work the transition-state nucleus ^{236}U has been investigated by measuring the angular distributions of fission fragments in the fission of ^{235}U induced by monoenergetic neutrons of 20 different neutron energies ranging from 0.1 to 3.1 MeV. These measurements were made with a set-up consisting of three semiconductor detectors which recorded the energy spectra of fission fragments emitted at the average angles of 0°, 45° and 90° with respect to the incident neutron direction. The relative solid angles of detection for the three detectors were experimentally determined using isotropic fragment distributions in the case of thermal-neutron-induced fission of ^{235}U. For each neutron energy the angular anisotropy was obtained by a least-square fit to the measured angular distributions taking into account the angular-resolution effects due to the finite size of the target and the detectors. The parameter K_0^2 of the assumed Gaussian distribution of the K-states at the transition-state nucleus was then determined for each neutron bombarding energy using the theoretical expression for the angular anisotropy which includes the effects of target spin and nuclear deformation. The average orbital angular momenta of the fissioning nucleus for different bombarding energies were evaluated using optical-model neutron-transmission coefficients. The observed variation of K_0^2 with excitation energy shows a steep increase in the value of K_0^2 at an excitation energy of 2.0 ± 0.1 MeV above the fission threshold. This increase in the value of K_0^2 has been interpreted as the onset of two quasi-particle excitations of the highly deformed transition state nucleus ^{236}U. At excitation energies below the two-quasi-particle excitation low values of K_0^2 are expected whereas fairly high values of K_0^2 were observed in the present work. This suggests that the statistical assumption of a Gaussian distribution of K-states below the two-quasi-particle excitation energy may not be valid because only a restricted number of vibrational K-states are available.

SPONTANEOUS FISSION IN THE NEUTRON BOMBARDMENT OF URANIUM ISOTOPES (SM-122/54)

A.J. Elwyn*, A.T.C. Ferguson
Nuclear Physics Division, AERE, Harwell, United Kingdom

A search is being made for spontaneously fissioning isomers with half-lives in the range of 10-1000 ns from the neutron bombardment of the various isotopes of uranium. The time distribution of the pulses due to the detection of fission fragments are studied after bombardment by 0.1-77 MeV neutrons produced in reactions initiated by the pulsed proton

* On leave from Argonne National Laboratory, USA.

and deuteron beams from the IBIS electrostatic accelerator. With the present technique the intensity of the residual beam between beam bursts is less than 10^{-5} of the main beam intensity so that the time distribution of the pulses in any delayed fission process can be observed quite cleanly. Preliminary results obtained with solid-state detectors indicate the existence of weakly excited events having a half-life of about 100 ns in the bombardment of ^{235}U by 2 MeV neutrons. Further studies are in progress to determine the half-life more accurately, as well as to obtain a measure of the cross-section for the formation of a possible spontaneously fissioning mode.

FISSION-FRAGMENT ANGULAR DISTRIBUTIONS FROM RESONANCE FISSION WITH ORIENTED NUCLEI (SM-122/57)

N.J. Pattenden
AERE, Harwell, Didcot, Berks, United Kingdom
and
H. Postma
FOM, University of Leiden, Holland

The angular distribution of fission fragments from oriented ^{235}U nuclei has been measured as a function of incident neutron energy from 0.04 eV to about 2000 eV, using the Harwell electron linear accelerator time-of-flight spectrometer with an electron pulse width of 0.23 μs and a flight path of 10 m. The ^{235}U nuclei were aligned using the electric hyperfine structure method, suggested by Pound (Phys. Rev. 76 (1949) 1410), in the rubidium-uranylnitrate single crystal. Thirty-six crystals with surfaces enriched with ^{235}U were attached to a copper plate with their c-axes parallel. They were mounted in a cryostat in the neutron beam and cooled to about 0.1K with a He-3/He-4 dilution refrigerator. Fission fragments in directions both parallel and perpendicular to the c-axis were detected by silicon diffused-junction semi-conductor detectors operating at a temperature of 1°K. Separate measurements were made to determine the detector background and the unoriented fission rate.

The fission-fragment anisotropy follows a relation of the form $W(\theta) = 1 + A_2 f_2 P_2 (\cos\theta)$ + higher terms, where A_2 is a nuclear parameter depending essentially on K and J, and f_2 is an orientation parameter. The variation of the effect with temperature at particular neutron energies has been studied down to about 0.08°K. The effect tends to saturation and little advantage is obtained from working below $\sim$ 0.1°K. The variation of f_2 with temperature must be considered carefully, but the higher terms may be largely neglected. The parameter A_2 shows significant fluctuations as a function of neutron energy, for example, changing from about -1.1 to -0.5 from 0.2 to 0.5 eV, in qualitative agreement with the work of Dabbs et al., reported at the Salzburg Conference (Proc. Conf. Salzburg, 1965 1, 39). The A_2 values for individual resonances below about 70 eV, and its average values over groups of resonances at higher energies are being obtained.

Later the work will be extended to cover the nuclei ^{233}U and ^{237}Np.

THE ^{230}Th FISSION CROSS-SECTION NEAR 715 KeV (SM-122/61)

L.G. Earwaker, G.D. James
AERE, Harwell, Didcot, Berks, United Kingdom

A measurement of the ^{230}Th fission cross-section from 675 keV to 1.4 MeV has been made with an energy resolution of 5 keV on the IBIS accelerator using the ^{7}Li(p, n) reaction to generate neutrons and a Si-Au surface barrier fission-fragment detector. This cross-section was first measured by Gokhberg et al. [1] and later measured by Evans and Jones [2] and by Vorotnikov et al. [3] at an energy resolution of about 50 keV. These authors observed a decrease in the fission cross-section with increasing neutron energy from the peak at 715 keV to the valley at 780 keV of a factor of 3. It has been shown by Lynn [4] that it is very difficult to explain this decrease on the theory of inelastic neutron competition [5]. The present results, normalized to 0.37b at 1.4 MeV give a cross-section of 0.16b at 715 keV decreasing to 0.017b at 780 keV. This larger decrease is even harder to explain in terms of inelastic competition, but is readily explained if the resonance is due to a level in the second fission potential-barrier minimum. The observed width of the resonance is 35 keV.

REFERENCES

[1] GOKHBERG, B.M., OSTROSHENENKO, G.A., SHIGIN, V.A., Dokl. Akad. Nauk SSR 128 (1959) 1157; Soviet Phys. Doklady 4 (1960) 1074.
[2] EVANS, J.E., JONES, E.A., unpublished, see Ref. [4].
[3] VOROTNIKOV, P.E., DUBROVINA, S.M., OSTROSHENENKO, G.A., SHIGIN, V.A., Soviet. J. nucl. Physics 5 (1967) 207.
[4] LYNN, J.E., in Nuclear Data for Reactors 2, IAEA, Vienna (1967) 89.
[5] WHEELER, J.A., Physica 22 (1956) 1103; Fast Neutron Physics, New York, Interscience (1963) 2051.

SPIN DETERMINATIONS OF ^{235}U RESONANCES BELOW 100 eV (SM-122/70)

F. Poortmans, H. Ceulemans
SCK - CEN Mol,
and
E. Migneco, J. Theobald
CBNM, Euratom, Geel,
Belgium

Accurate and direct spin determinations of resonances in fissile nuclides have become necessary to achieve better insight into the physics of nuclear fission. Except for experiments with polarized neutrons and polarized targets, which are difficult to perform, the most direct and reliable method is to measure the ratio of scattering to total cross-section. To this end a scattering chamber with very low background, surrounded by nine ^{3}He detectors of 6'' long, 1'' diameter, 10 atm.

pressure and short jittertime has been tested and installed at a 30 m flight path of the Linac at CBNM, Euratom, Geel. The main advantages of the detectors are their good discrimination properties against gamma rays and fission neutrons. With this system it is possible to measure resonances which have $\Gamma_n^0/\Gamma \geqq 3 \times 10^{-3}$ and $\Gamma_n^0/\Gamma_f \geqq 5 \times 10^{-3}$.

Scattering measurements on ^{235}U resonances below 100 eV are in progress and although many are too weak, a statistically meaningful sample lies within the capabilities of our instrumentation.

DETERMINATION DU SPIN DES RESONANCES INDUITES PAR DES NEUTRONS LENTS DANS LE ^{239}Pu (SM-122/76)

J. Trochon, B. Lucas
Centre d'Etudes Nucléaires de Saclay, France

Une mesure de diffusion élastique de neutrons lents par le ^{239}Pu a été réalisée de 16 eV à 300 eV par la méthode du temps de vol auprès de l'accélérateur linéaire de 45 MeV de Saclay, utilisé comme source pulsée de neutrons. Placé à une distance de vol de 32 m, le détecteur est constitué de six photomultiplicateurs équipés de scintillateurs liquides chargés au bore-10, du type Jackson et Thomas. L'élimination des rayons γ se fait par discrimination de forme. Mais ce détecteur, formé de composés organiques hydrogénés est également sensible aux neutrons rapides. Afin d'évaluer la contribution des neutrons de fission, les auteurs ont inclus dans le détecteur deux photomultiplicateurs équipés de scintillateurs liquides Ne 213 détectant les neutrons rapides par l'intermédiaire des protons de recul. A l'aide d'une source Cf les auteurs ont mesuré l'efficacité relative des deux types de scintillateurs. La courbe de diffusion élastique est alors obtenue par différence et la normalisation est faite par comparaison avec un échantillon de plomb. Les résultats ont été corrigés de l'effet de diffusion multiple et d'auto-absorption. L'échantillon de ^{239}Pu est constitué d'une plaque métallique de 5 cm de diamètre, recouvert de deux feuilles d'aluminium, chacune d'épaisseur 0,012 mm. Les auteurs ont utilisé deux épaisseurs, 0,08 mm et 0,13 mm afin de vérifier la qualité des corrections apportées. Les valeurs obtenues sont présentées et comparées avec celles publiées par les autres laboratoires.

English translation of the preceding Abstract (SM-122/76):

DETERMINATION OF THE SPIN OF RESONANCES INDUCED BY SLOW NEUTRONS IN ^{239}Pu

The elastic scattering of slow neutrons by ^{239}Pu was measured in the range 16 eV-300 eV by the time-of-flight method in the 45 MeV Saclay linear accelerator used as a pulsed-neutron source. The detector, which was placed at 32 m flight distance, consisted of six photomultipliers equipped with liquid scintillators filled with boron-10, of the Jackson and Thomas type. The γ-rays were eliminated by form discriminators. Constituted as it is of hydrogenated organic compounds, this detector is also sensitive to fast neutrons. To determine the contribution of the

fission neutrons, the authors included in the detector two photomultipliers equipped with NE 213 liquid scintillators to detect fast neutrons through the intermediary of recoil protons. Using a Cf source the relative efficiency of the two types of scintillator was measured. The elastic scattering curve was then obtained from the difference, and normalization was effected by comparison with a lead sample. The results were corrected for the effect of multiple scattering and self-absorption. The ^{239}Pu sample consisted of a metal plate 5 cm in diameter covered with two aluminium foils, each 0.012 mm thick. Two thicknesses, 0.08 mm and 0.13 mm, were used in order to check the quality of the corrections. The values obtained are presented and the results are compared with those published by other laboratories.

MESURES CORRELEES DES ENERGIES CINETIQUES DES FRAGMENTS DE FISSION DANS LE DOMAINE DES RESONANCES NEUTRONIQUES DE ^{235}U (SM-122/77)

C. Signarbieux, M. Ribrag
Centre d'Etudes Nucléaires de Saclay, France

Ces mesures ont été entreprises dans le but d' étudier l' influence éventuelle de l' état de spin sur le processus de fission et corrélativement de tenter de classer les niveaux de résonance en 2 groupes correspondants aux 2 états de spin possibles. L' expérience a été realisée à l' accélérateur linéaire de Saclay sur une base de vol de 8 m de longueur; le détecteur était une chambre à grille double, qui contenait un dépôt mince de 100 cm^2 ^{235}U (100 mg/cm^2) sur support mince (40 mg/cm^2 de VYNS). Pour chaque événement, 4 paramètres ont été enregistrés: les temps de vol du neutron incident, les énergies cinétiques (e_1 et e_2) des 2 fragments de fission, un paramètre supplémentaire relié à l' angle d' émission des fragments par rapport au dépôt (ce paramètre permet au dépouillement, d' éliminar les trajectoires très inclinées et de diminuer beaucoup les effets de queue sur les spectres d' énergie). Au total $1,8 \times 10^7$ événements ont été stockés sur bande magnétique. Les résultats concernent 11 résonances suivantes: 1,14 - 3,14 - 3,6 - 6,4 - 7,07 - 8,8 - 12,4 - 19,3 - 21,06 - 32,1 - 35,2 eV. Dans chacune de ces résonances le nombre d' événements était supérieur à 10^5. La comparaison détaillée des distributions de probabilité P (e_1, e_2), des distributions des masses et d' énergie cinétique totale n' a montré aucune variation significative de résonance à résonance. Cette conclusion est en désaccord avec des résultats précédemment publiés.

English translation of the preceding Abstract (SM-122/77):

CORRELATED MEASUREMENTS OF THE KINETIC ENERGIES OF FISSION FRAGMENTS IN THE REGION OF NEUTRON RESONANCES OF ^{235}U

These measurements were made with a view to studying the possible effect of the spin state on the fission process and also to making a tentative classification of the resonance levels into two groups corresponding to the two possible spin states. The experiment was performed on the Saclay linear accelerator using a flight path of 8 m. The detector was a double-grid chamber containing a thin layer of ^{235}U (100 cm^2, 100 mg/cm^2) on a thin backing (40 mg/cm^2 of VYNS). Four parameters were recorded for each event: the time-of-flight of the incident neutron, the kinetic energies (e_1 and e_2) of two fission fragments, a supplementary parameter connected with the emission angle of the fragments with respect to the deposit (during analysis, this parameter makes it possible to eliminate the highly inclined trajectories and diminish, to a great extent, the tail effects on the energy spectra). In all, 1.8×10^7 events were stored on magnetic tape. The results deal with the following 11 resonances: 1.14, 3.14, 3.6, 6.4, 7.07, 8.8, 12.4, 19.3, 21.06, 32.1 and 35.2 eV. In each of these resonances the number of events was greater than 10^5. The detailed comparison of the distributions of probability P (e_1 and e_2) and the distributions of masses and total kinetic energy did not show any significant variation from one resonance to another. This conclusion does not agree with the results published earlier.

DISTRIBUTIONS ANGULAIRES DE PHOTOFISSION PRES DU SEUIL DES ELEMENTS ^{232}Th, ^{238}U, ^{226}Ra (SM-122/84)

B. Tamain, M. Monnin
Laboratoire de Physique Nucléaire,
Faculté des Sciences,
Clermont-Ferrand,
France

Les distributions angulaires de photofission des éléments ^{232}Th et ^{238}U sont mesurées au voisinage du seuil pour toute une série d' énergies maximales de rayonnement de freinage. On se propose ainsi d' étudier avec soin la modification de la distribution angulaire de photofission liée à la variation de l' énergie d' excitation. La distribution angulaire de photofission du ^{226}Ra est déterminée pour quelques valeurs de l' énergie maximale du rayonnement de freinage de l' ordre de 10 MeV. Cette mesure a pour but d' étendre les connaissances des distributions angulaires de photofission des éléments pair-pair à d' autres noyaux que ceux de ^{232}Th et ^{238}U. Les électrons utilisés sont accélérés dans un accélérateur linéaire puis déviés par deux électro-aimants. L' avantage d' un tel dispositif réside dans la grande précision avec laquelle il permet de définir l' énergie des électrons (3 à 5%). Les fragments de fission sont détectés dans des détecteurs solides de traces (polycarbonates et polyimides) disposés sur la paroi interne d' une enceinte à vide tronconique. Les flux parasites (essentiellement de neutrons) sont évalués ainsi que les incertitudes correspondantes. Les résultats sont interprétés à la lumière de la théorie des «canaux de fission» de A. Bohr.

English translation of the preceding Abstract (SM-122/84):

ANGULAR DISTRIBUTIONS IN PHOTOFISSION OF ^{232}Th, ^{238}U AND ^{226}Ra NEAR THE THRESHOLD

The angular distributions in the photofission of elements ^{232}Th and ^{238}U are measured in the neighbourhood of the threshold for a series of maximum bremsstrahlung energies. In this way it is proposed to carefully study the modification in the angular distribution of photofission linked with the variation in excitation energy. The angular distribution of the photofission of ^{226}Ra is determined for some values of the maximum bremsstrahlung energy of the order of 10 MeV. The aim of this measurement is to extend the knowledge of the angular distributions of the photofission of even-even elements to nuclei other than those of ^{232}Th and ^{238}U. The electrons used are accelerated in a linear accelerator and are then deflected by two electromagnets. The advantage of this device lies in the high precision with which the electron energy can be determined (3 - 5%). The fission fragments are detected in the solid track detectors (polycarbonates and polyimides) arranged on the inner wall of a vacuum chamber having the shape of a truncated cone. The parasitic fluxes (mainly neutrons) as well as the corresponding indeterminacies are evaluated. The results are interpreted in the light of the "fission channels" theory of A. Bohr.

MESURE A HAUTE RESOLUTION ET ANALYSE DE LA SECTION EFFICACE DE FISSION DE ^{239}Pu (SM-122/91)

J. Blons, H. Derrien, A. Michaudon
Centre d'Etudes Nucléaires de Saclay, France

La section efficace de fission de ^{239}Pu a été mesurée en-dessous de 35 keV en utilisant l' accélérateur linéaire de 45 MeV comme source pulsée de neutrons. La résolution nominale était de 1 ns/m environ et les dépôts de ^{239}Pu étaient portés à la température de l' azote liquide dans un scintillateur gazeux. L' analyse de cette section efficace, conjuguée avec celle de la section efficace totale, a été faite par une méthode de moindres carrés avec le formalisme de Breit-Wigner à un niveau. La résolution de cette mesure a permis d' étendre à 450 eV l' analyse détaillée des résonances. Dans un grand nombre de cas, l' analyse de forme conduit à la détermination du spin des résonances.

Les résultats confirment et précisent l'existence de deux familles de résonances, ayant des valeurs moyennes de la largeur de fission qui sont très différentes et qui correspondent aux deux états de spin $J = 0^+$ et $J = 1^+$. L'étude du coefficient d'autocorrélation de la section efficace de fission jusqu'à une énergie de 2 keV, montre qu'il est incompatible avec un modèle statistique où les propriétés des paramètres sont indépendantes de l'énergie. Cette étude montre l'existence d'une structure intermédiaire dont l'espacement moyen est d'environ 450 eV. Elle est interprétée comme étant due à la fission en-dessous du seuil de la voie 1^+ pour laquelle le couplage à la fission plus intense à certaines énergies correspond à des états intermédiaires 1^+ situés dans le puits de potentiel de la barrière de fission à deux bosses calculée par Strutinsky. Cette interprétation est confirmée par le fait que les résonances étroites (donc probablement de spin $J = 1^+$) ont une largeur de fission beaucoup plus faible entre 450 eV et 650 eV (environ 10 MeV) qu'en dessous de 400 eV (environ 40 MeV). Cet effet explique donc la décroissance de la section efficace de fission vers 500 eV. Il est discuté, notamment du point de vue des propriétés de l'état de transition 1^+ et de la réaction $(n, \gamma f)$. Des résultats obtenus sur d'autres noyaux fissiles (^{235}U et ^{241}Pu) sont également présentés.

English translation of the preceding Abstract (SM-122/91):

HIGH-RESOLUTION MEASUREMENT AND ANALYSIS OF THE FISSION CROSS-SECTION OF ^{239}Pu

The fission cross-section of ^{239}Pu was measured below 35 keV, using the 45-MeV linear accelerator as pulsed neutron source. The nominal resolution was approximately 1 ns/m and the ^{239}Pu deposits were brought to the temperature of liquid nitrogen in a gaseous scintillator. This cross-section was analysed together with the total cross-section by the mean-squares method with the single-level Breit-Wigner formalism. The resolution of this measurement enabled us to extend the detailed resonance analysis to 450 eV. In a large number of cases, the analysis of shape leads to the determination of the resonance spin. The results confirm and refine the existence of two resonance families, having very different mean values of fission width corresponding to two spin states $J = 0^+$ and $J = 1^+$. The study of the autocorrelation coefficient of the fission cross-section up to 2 keV energy shows that this coefficient is incompatible with a statistical model.in which the properties of the parameters are independent of energy. The present study shows that there exists an intermediate structure whose mean spacing is about 450 eV. It is interpreted as being due to fission below the threshold of the 1^+ channel for which the coupling with more intense fission at some energies corresponds to the 1^+ intermediate states situated in the potential well of the two-hump fission barrier calculated by Strutinsky. This interpretation is confirmed by the fact that the narrow resonances (hence probably of spin $J = 1^+$) have a much smaller fission width between 450 eV and 650 eV (about 10 MeV) than below 400 eV (about 40 MeV). This effect thus explains the diminution of the fission cross-section towards 500 eV.

It is discussed particularly from the point of view of the properties of the 1^+ transition state and the $(n, \gamma f)$ reaction. The results obtained with other fissile nuclei (^{235}U and ^{241}Pu) are also presented.

ANALYSE, A L'AIDE DE FORMALISMES A PLUSIEURS NIVEAUX ET DE 7 eV A 100 eV, DES SECTIONS EFFICACES TOTALE ET DE FISSION DE ^{239}Pu (SM-122/92)

H. Derrien, J. Blons, A. Michaudon
Centre d'Etudes Nucléaires de Saclay, France

Les sections efficaces totale et de fission ont été mesurées à Saclay en utilisant l'accélérateur linéaire de 45 MeV comme source pulsée de neutrons. Les deux mesures ont été faites avec une résolution nominale voisine de 1 ns/m et avec des échantillons portés à la température de l'azote liquide. L'analyse de forme des résonances à l'aide de formalisme de Breit-Wigner à un niveau permet d'obtenir dans la majorité des cas une bonne valeur des paramètres. Cependant, ce formalisme ne peut pas toujours reproduire la forme des sections efficaces telles qu'elles sont mesurées. En particulier, certaines différences entre les courbes théoriques et expérimentales peuvent être nettement diminuées en ajoutant des résonances dont l'existence n'est pas établie d'une façon certaine. C'est pour pouvoir reproduire le plus fidèlement possible la forme des sections efficaces que l'analyse a été poursuivie avec deux formalismes à plusieurs niveaux qui tient compte de l'interférence entre résonances de mêmes spin et parité. Les deux formalismes étudiés sont ceux de D.B. Adler et F.T. Adler d'une part, et de Reich et Moore d'autre part. Dans les deux cas l'ajustement des courbes théoriques aux résultats expérimentaux se fait par la méthode des moindres carrés.

Les résultats de l'analyse sont présentés, notamment: (a) la comparaison des courbes théoriques aux résultats expérimentaux; (b) les cas où l'interférence entre résonances permet de supprimer quelques résonances qui avaient dû être introduites avec le formalisme à un niveau (par example à 11,5 eV; 58,84 eV; 83,52 eV); (c) le nombre de voies de sortie pour les spins 0^+ et 1^+.

Ces résultats sont obtenus dans la gamme d'énergie située en-dessous de 100 eV. Ils ne peuvent pas être extrapolés à une gamme d'énergie beaucoup plus élevée à cause du phénomène de structure intermédiaire qui a été récemment mis en évidence et qui peut être expliqué par la fission au-dessous du seuil de la (des) voie(s) 1^+ et donc par le couplage à des états intermédiaires de mêmes spin et parité situés dans le puits de la barrière de fission à deux bosses calculée par Strutinsky.

English translation of the preceding Abstract (SM-122/92):

MULTILEVEL ANALYSIS OF TOTAL AND FISSION CROSS-SECTIONS OF ^{239}Pu IN REGION BETWEEN 7 eV AND 100 eV

The total and fission cross-sections were measured at Saclay using the 45 MeV linear accelerator as a pulsed neutron source. The two measurements were made with a nominal resolution of around 1 ns/m using samples at the temperature of liquid nitrogen. Analysis of resonance shape using the single-level Breit-Wigner formalism shows a good fit to the parameters in the majority of cases. This formalism, however, cannot always reproduce the shape of the cross-sections as measured. In particular, certain differences between the theoretical and the experimental curves can be considerably reduced by adding resonances whose existence has not been firmly established. In order to reproduce the form of the cross-sections as accurately as possible, the analysis was conducted using two multi-level formalisms, thus taking into account interference between resonances with the same spin and parity. The two formalisms studied were those of D.B. Adler and F.T. Adler and of Reich and Moore. In both cases the fitting of the theoretical curves to the experimental results is effected by the least-squares method.

The results of analysis are given and include: (a) A comparison of theoretical curves with experimental results; (b) Cases in which interference between resonances made it possible to exclude some resonances which had had to be introduced with the single-level formalism (for instance at 11.5 eV, 58.84 eV and 83.52 eV); (c) The number of exit channels for 0^+ and 1^+ spins.

These results are obtained in the energy range below 100 eV. They cannot be extrapolated to any much higher energy range because of the intermediate structure phenomenon established recently, which can be explained by the sub-threshold fission of the 1^+ channel(s) and consequently by the pairing at intermediate states of the same spin and parity in the well of the double-humped fission barrier calculated by Strutinsky.

DIRECT-REACTION FISSION OF ODD-A URANIUM AND PLUTONIUM ISOTOPES (SM-122/101)

H.C. Britt, J.D. Cramer
Los Alamos Scientific Laboratory,
Los Alamos, New Mexico, USA

Fission-fragment angular correlations and fission probabilities have been measured for a series of odd-A uranium and plutonium isotopes excited by (d,p), (t,p), and (t,d) reactions. The following fissioning

nuclei have been studied using the indicated direct reactions: 1. ^{235}U: from (d,pf), (t,pf); 2. ^{237}U: from (d,pf), (t,pf); 3. ^{239}U: from (d,pf); 4. ^{241}Pu: from (d,pf), (t,pf), (t,df); 5. ^{243}Pu: from (d,pf), (t,df). Deuteron or triton beams with an energy of 18 MeV were used and the outgoing charged particles from the direct reaction were detected at angles of 130° of 150° with an experimental energy resolution of ~150 keV. Fragment angular correlations were obtained at 7 angles for the (d,pf) and (t,pf) experiments and at 24 angles for the (t,df) measurements. The results of the angular correlations were fitted to a series of even Legendre polynomials and fission probabilities as a function of excitation energy were obtained for each case.

Fission probabilities and angular correlation coefficients were compared for each case to previously reported (n,f) results. For the (n,f) reaction fission probabilities are obtained by dividing reported (n,f) cross-sections by calculated total reaction cross-sections. The direct reaction experiments show fission thresholds at excitation energies equal to or less than threshold energies observed in (n,f) experiments. This result is consistent with the fact that the direct reactions are not limited to angular momentum transfers of ℓ = 0 or 1 that are predominant at low energy in the neutron-capture reactions. Thus, the direct reaction results can show fission through low-lying transition states that have spins and parities that are inaccessible to neutron capture reactions. The direct reaction results show thresholds equal to the thresholds measured in neutron experiments (to within ± 50 keV) for ^{239}U and ^{243}Pu. For ^{241}Pu the threshold measured in the direct reaction experiments is ~ 200 keV lower than the threshold from (n,f) experiments. Qualitative characteristics of the transition state spectra for the nuclei studied are determined from detailed comparisons of the results obtained using the various reactions.

AN EXACT CALCULATION OF THE PENETRABILITY THROUGH TWO-PEAKED FISSION BARRIERS* (SM-122/103)

J.D. Cramer, J.R. Nix
University of California,
Los Alamos Scientific Laboratory,
Los Alamos, New Mexico, USA

Several recently observed fission phenomena have been interpreted qualitatively in terms of a two-peaked potential energy of deformation in the fission direction. The intermediate well in such a potential provides a source for the short-lived spontaneously fissioning isomers now observed in over a dozen nuclei. The presence of discrete energy levels in the intermediate well may explain anomalous effects which have long been apparent in neutron-induced fission cross-sections for several of the even-even target nuclei, such as the structure observed in the cross-sections of ^{234}U and ^{230}Th targets, and most recently the systematic clustering of sub-threshold fission resonances in several compound

* Work performed under the auspices of the US Atomic Energy Commission.

nuclear systems. Theoretical predictions of single-particle effects on the potential energy of deformation support this interpretation.

These recent developments require a fresh examination of the penetration of the fission barrier. In particular, it is important to consider more complicated shapes than the inverted harmonic-oscillator potential introduced by Hill and Wheeler. For this reason we have performed an exact calculation of the penetrability through fission barriers $V(\epsilon)$ defined in terms of two parabolic peaks connected smoothly with a third parabola forming the intermediate well. The potential is specified by the peak energies E_1 and E_2 and the minimum energy E_0 of the connecting curve, along with the constants $\hbar\omega_1$, $\hbar\omega_2$ and $\hbar\omega_0$ related to the curvatures of the three parabolas. For a wave of unit amplitude impinging on the barrier, the amplitude of the transmitted wave is determined by requiring that the wave functions (expressed exactly in terms of parabolic cylinder functions) and their first derivatives match at the connecting points ϵ_1 and ϵ_2. This leads to a closed expression for the amplitude of the transmitted wave, from which the penetrability is obtained. At energies well below the barrier tops, the exact penetrabilities agree with those calculated by use of the WKB approximation. The penetrability is essentially an increasing exponential function, but exhibits narrow resonances at the positions of the quasi-bound vibrational states in the intermediate well. The width Γ of these resonances is extremely small (~ 0.1 eV) for the levels near the bottom of the well, but increases as the energy increases. This trend continues in some cases above the top of the barrier, producing broad peaks in the penetrability function. Results are presented for various classes of two-peaked barriers and compared to recent experimental data.

FISSION BARRIER DETERMINATIONS AND FRAGMENT ANGULAR CORRELATIONS FOR THE ^{244}Pu, ^{242}Pu, ^{240}U, ^{238}U, ^{234}Th, and ^{232}Th COMPOUND NUCLEI FROM (t, pf) REACTIONS (SM-122/104)

J.D. Cramer, H.C. Britt
University of California,
Los Alamos Scientific Laboratory,
New Mexico, USA

Fission probabilities and the angular distribution of the fission fragments have been measured for six even-even compound nuclear systems using the (t, pf) reaction. Angular correlations of fission fragments obtained in these experiments provide information about the low-lying collective excitations or transition states at the fission barrier. The (t, p) reaction in particular leads to neutron-rich residual nuclei un obtainable by other methods. The absence of spin coupling for (t, p) reactions on even-even targets provides angular distributions with well defined structure in the region of the fission barrier.

The experimental data were obtained using an 18-MeV triton beam on targets of ^{242}Pu, ^{240}Pu, ^{238}U, ^{236}U, ^{232}Th and ^{230}Th at Los Alamos Van-de-Graaff accelerator facility. Outgoing protons were detected at

140° relative to the incident triton beam. Excitation energies ranging from 3.0 to 9.0 MeV were obtained in these experiments. Fission fragment angular distributions were measured at 24 angles from 0° to 140° relative to the kinematic recoil angle.

The data were fitted to a series of even Legendre polynomials

$$W(\theta) = A_0 \left[1 + \sum_L g_L P_L (\cos \theta)\right]$$

and the coefficients g_2 through g_{12} and A_0 were determined as a function of excitation energy. The fission probability P_f was obtained from the ratio of A_0 to the (t, p) cross-section for the target nucleus. The results exhibit well defined structure in the angular coefficients which correlates with structure in the fission probability for most of the nuclei studied.

In an attempt to interpret this observed structure the experimentally determined fitting parameters P_f and g are compared with calculated results of a microscopic model. This model takes into consideration the penetrability and angular dependence of fission through each member of the various transition bands at the saddle point and appropriately sums the results for comparison with the data. The effects of barrier penetration through a two-peaked deformation potential are explored in this analysis.

This survey of the fission properties of several nuclei indicates some general trends relating the saddle point deformation to the character of the transition level structure.

INTERMEDIATE STRUCTURE IN THE NEUTRON-INDUCED-FISSION CROSS-SECTION OF ^{232}U (SM-122/105)

J.A. Farrell
University of California,
Los Alamos, New Mexico, USA

The fission cross-section of ^{232}U has been measured from a neutron energy of 65 eV to 6 keV with a resolution of approximately 12 ns/m using an underground nuclear explosion as a pulsed neutron source. ^{232}U is the only even-even target nucleus with an appreciable low energy fission cross-section and therefore furnishes an opportunity to study the resonance parameters of a fissionable nucleus without the complications introduced by the presence of two spin states. The data have been fitted with a multilevel cross-section formula from 65 to 220 eV. It was necessary to assume the existence of two $\frac{1}{2}^+$ fission channels to fit adequately the valleys between resonances. The average fission width of the 14 resonances between 80 and 150 eV is only 1/4 of the average fission width of the next 14 resonances between 150 and 220 eV. The interference between each of the resonances between 80 and 150 eV was found to be destructive in the dominant fission channel and mostly constructive in the second. Since the interference would be expected to be random, this suggests the presence of one or more resonances with small neutron widths and very large fission widths of 30 eV or more in this region. Such a resonance, which would be nearly invisible in the fission cross-section but would interfere strongly with the neighbouring resonances, can be interpreted as due to a state in the second minimum of the fission potential barrier where the excitation energy is near the second maximum and the coupling between states in the two wells is relatively weak.

To test this hypothesis, several sets of mock data were generated assuming a single fission channel and a very wide resonance with a negligible neutron width. It was possible to fit the mock data without including a wide resonance if a second fission channel was introduced. The resulting parameters display interference properties and small apparent widths similar to those obtained from the ^{232}U analysis. Based on these results, we interprete the small fission widths, two fission channels, and apparent correlation in interference between resonances obtained in the ^{232}U fit as probably spurious, being due to the fact that one or more wide levels have been missed.

CHANNEL EFFECTS IN THE INTERACTIONS OF RESONANCE ENERGY NEUTRONS WITH ^{233}U (SM-122/117)

E. Melkonian, J. Felvinci
Columbia University,
New York, USA

Difficulties have arisen in the past in the interpretation of the fission cross section of ^{233}U arising from the large ratio of level width to spacing of the resonances. Recently, using the Nevis synchrocyclotron as a pulsed neutron source, a time-of-flight experiment was performed on ^{233}U to search for measurable differences between resonances. These measurements consist of event-by-event recording of the neutron time-of-flight together with the energy of (a) one fission fragment, or (b) a gamma-ray above 3 MeV.

The following observations, suggestive of underlying physical phenomena, were made:

1. Average fission-fragment energies were calculated as a function of neutron time-of-flight. Across several of the resonances, there was observed a small but distinct decrease toward longer flight times of this average fission-fragment energy. This could be explained on the assumption that some of the fissions take place through an intermediate state leading to delays of the order of 100 nsec and to lower average energy.
2. Gamma-ray yields from the 4.8 eV, 11.5 eV and 16.3 eV resonances were considerably higher than would be expected on the basis of fission and capture cross-section data. The 4.8 eV resonance has been identified by multilevel analysis as 2+, which is consistent with the higher gamma yield. This would imply that the 11.5 eV and 16.3 eV resonances are also 2+.

3. Neutron time-of-flight spectra for various sections of the fission fragment energy distribution were obtained. Some of the resonances showed statistically significant differences in yield. These particular resonances are tought to be of the same J value (probably 3+). The results could be interpreted as arising from fission through different channels of the same spin state.

Futher analyses of these results are in progress.

PENETRATION OF A DOUBLE BARRIER (SM-122/119)

C.Y. Wong, J. Bang
University of Copenhagen,
Niels Bohr Institute,
Denmark

The Hill-Wheeler formula for penetration through a single barrier is generalized to the cases where the potential is

1. a parabola joined at each end by two inverted parabolas and
2. two inverted parabolas joined together.

The transmission function can be obtained exactly and can be expressed analytically in terms of parabolic cylinder functions. It is found that at appropriate energies, when the Bohr quantization rule is satisfied at the second minimum, a resonance structure shows up at the transmission function. The result of the calculation is applied to analyse the experimental data of (d, pf) and (n, pf)reactions with targets of ^{239}Pu, ^{241}Pu, ^{233}U, and ^{235}U. It is found that the resonances in the (d, pf) reaction can be explained quite well by penetration through a double barrier. The fission barriers for these nuclei, defined in this case as the highest point of the double barrier, are found to be considerably higher than those assumed in the past by various investigators.

РАСПРЕДЕЛЕНИЯ ОСКОЛКОВ ПО МАССАМ И КИНЕТИЧЕСКИМ ЭНЕРГИЯМ ПРИ ДЕЛЕНИИ ЯДЕР БЫСТРЫМИ НЕЙТРОНАМИ (IAEA-SM-122/133)

В.Г. Воробьева, П.П. Дьяченко, Б.Д. Кузьминов,
А.И. Сергачев, Л.Д. Смиренкина
Физико-энергетический институт, Обнинск,
Союз Советских Социалистических Республик
А. Лайтаи
Центральный институт физических исследований, Будапешт,
Венгерская Народная Республика

В работе исследовалось влияние энергии возбуждения делящихся ядер (четно-четного ^{236}U, четно-нечетных ^{233}Th, ^{239}U и нечетно-нечетного ^{238}Np) на распределения осколков по массам и кинетическим энергиям. Деления вызывались моноэнергетическими нейтронами с энергией от тепловых до $E_n \approx 6$ Мэв с шагом $100 + 300$ кэв и нейтронами с $E_n = 15,5$ Мэв. Обсуждаются следующие явления:

1. Влияние переходных состояний делящихся ядер на выходы γ и кинетические энергии $E_к$ осколков. Для самого легкого ядра – ^{232}Th обнаружены резкие изменения γ и $E_к$ при делении вблизи порога, что можно приписать влиянию отдельных каналов деления. Для других ядер γ и $E_к$ сохраняются неизменными при превышении энергии над барьером на 1-1,5 Мэв. Наблюдавшиеся в работе других авторов вариации $E_к$ при $E_n < 600$ кэв для ^{235}U в настоящей работе не проявились. Эти результаты истолковываются в пользу представлений о двугорбой структуре барьера деления. Измерена зависимость угловой анизотропии от масс осколков при делении ^{235}U и ^{238}U нейтронами с $E_n = 3$ Мэв и $E_n = 1,6$ Мэв, соответственно. В пределах ошибок опыта ($\pm 2\%$) корреляция масс и угловой анизотропии отсутствует.

2. Совокупность результатов по γ и $E_к$ анализируется в рамках статистической модели. Получены параметры плотности уровней осколков α и энергии возбуждения E_0 для ядра в точке разрыва, которые наилучшим образом описывают совокупность экспериментальных данных. Отмечается, что результаты эксперимента могут быть качественно поняты в рамках теоретических представлений А.В.Игнатюка, основанных на вычислении плотности состояний ядра перед разрывом, с привлечением метода оболочечных поправок В.М.Струтинского.

3. Тонкая структура кривой выходов осколков проявляется только для четно-четных и четно-нечетных делящихся ядер. При делении ^{237}Np нейтронами тонкая структура отсутствует. Обсуждается корреляция тонкой структуры выходов осколков и кривой зависимости энергии деления от нуклонного состава пар осколков.

English translation of the preceding Abstract (SM-122/133):

MASS AND KINETIC ENERGY DISTRIBUTIONS OF FAST-FISSION FRAGMENTS

The authors investigate the influence of the excitation energy of fissionable nuclei (even-even ^{236}U, even-odd ^{233}Th and ^{239}U, and odd-odd ^{238}Np) on the mass and kinetic energy distributions of the fission fragments. Fissions were induced by monoenergetic neutrons with energies ranging from thermal to $E_n \approx 6$ MeV (increasing in steps of 100-300 keV) and by 15.5-MeV neutrons.

The following phenomena are discussed:

1. The influence of the transition states of fissionable nuclei on the yields and kinetic energies of the fission fragments. For the lightest nucleus considered (^{232}Th) abrupt variations in yield and kinetic energy are observed in fission near the threshold, possibly due to the influence of the individual fission channels. For the other nuclei the kinetic energies also remain unchanged when the energy exceeds the barrier and reaches 1-1.5 MeV. The kinetic energy variations at $E_n < 600$ keV observed by other authors in the case of ^{235}U did not appear in the present work. These results are interpreted as supporting the idea of a double-humped fission barrier structure. The authors measured the dependence of angular anisotropy on fission fragment mass in ^{235}U and ^{238}U fission by 3-MeV and 1.6-MeV neutrons respectively. Within the limits of the experimental error ($\pm$ 2%), there is no correlation between fission fragment mass and angular anisotropy;
2. The yield and kinetic energy results are analysed within the framework of a statistical model. Those parameters are found which best describe the experimental data as a whole (level density of the fission fragments and excitation energy for a nucleus at the scission point). It is noted that the experimental results can be understood qualitatively within the framework of A.V. Ignatyuk's theoretical concepts based on calculation of the density of nuclear states before scission with the help of V.M. Strutinsky's shell correction method;

3. Fine structure of the fragment yield curve was found only in the case of even-even and even-odd fissionable nuclei. There was no fine structure in ^{237}Np fission by neutrons. The correlation between the fine structure of the fission fragment yields and the curve showing the dependence of fission energy on the nucleonic composition of fission fragment pairs is discussed.

ФОТОДЕЛЕНИЯ ^{232}Th, ^{238}U, ^{238}Pu, ^{240}Pu, ^{242}Pu ВБЛИЗИ ПОРОГА (IAEA-SM-122/135)

С.П. Капица, Ю.М. Ципенюк
Институт физических проблем им. С.И.Вавилова, Москва
Н.С. Работнов, Г.Н. Смиренкин, А.С. Солдатов, Л.Н. Усачев
Физико-энергетический институт, Обнинск,
Союз Советских Социалистических Республик

Приводятся экспериментальные данные по сечениям и угловым распределениям осколков фотоделения, частично опубликованные ранее. Измерения проводились на тормозном спектре, производилось восстановление энергетических зависимостей парциальных сечений фотоделения в пересчете на монохроматические кванты. Угловые распределения анализировались по формуле

$$W(\theta) = a + b \sin^2 \theta + c \sin^2 2\theta$$

Максимальное наблюденное значение анизотропии (в/а) достигает ~ 100 (^{232}Th, $E_{max} = 5{,}2$ Мэв), а квадрупольной (с/в) ~ 3 (^{240}Pu, $E_{max} = 5{,}2$ Мэв). Данные анализируются в связи с гипотезой двугорбого барьера, которая, по-видимому, объясняет некоторые экспериментальные факты, резко выпадающие из традиционной картины.

English translation of the preceding Abstract (SM-122/135):

PHOTOFISSION OF ^{232}Th, ^{238}U, ^{238}Pu, ^{240}Pu AND ^{242}Pu NEAR THE THRESHOLD

The authors present experimental data (some of which have been published previously) regarding the cross-sections and angular distribution of photofission fragments. They carried out measurements on the bremsstrahlung spectrum and reconstructed the energy dependences of the partial cross-sections of photofission as a function of monochromatic quanta. The angular distributions were analysed using the formula

$$W(\vartheta) = a + b \sin^2 \vartheta + c \sin^2 2\vartheta$$

The maximum observed value of anisotropy (b/a) is ~ 100 (^{232}Th, $E_{max} = 5.4$ MeV) and of the quadrupole component (c/b) ~ 3 (^{240}Pu, $E_{max} = 5.2$ MeV). The data are analysed in relation to the double-humped barrier hypothesis, which evidently explains certain experimental findings which are clearly inconsistent with the traditional picture.

SUB-THRESHOLD FISSION OF ^{241}Am (SM-122/140)

E. Migneco, J. Theobald, J. Wartena
Central Bureau for Nuclear Measurements,
EURATOM, Geel, Belgium

The neutron-induced sub-threshold fission cross-section of ^{241}Am is measured in the energy range between 1 eV and 3 keV with nominal time-of-flight resolution of 20 ns/m and 2 ns/m using the CBNM linear accelerator as pulsed neutron source and a liquid scintillator for the detection of the fission neutrons. This detector is equipped with pulse shape discriminators and pile up rejectors against the high γ-radiation from the sample. This experiment has been motivated by our sub-threshold fission cross-section data on ^{240}Pu showing the groupwise resonance enhancement due to intermediate states in the fission exit channel and by the fission cross-section display of ^{241}Am (n, f) in the Petrel report of P.A. Seeger et al. where intermediate structures of different types are slightly indicated. With our high resolution experiment we try to investigate further the existence of intermediate levels of the type found in sub-threshold fission of ^{240}Pu. The presence of intermediate states as well as the existence of a spontaneously fissioning shape isomer in ^{242}Am found by Flerov et al. have been interpreted by Bjørnholm, Lynn and Weigmann on the basis of the theory of Strutinsky. It has been pointed out by J.R. Nix that a quantitative analysis of the experimental results on the ratio of the half-lives of the ground state and the isomeric spontaneous fission of ^{242}Am is not in agreement with the value for the energy of a secondary potential minimum deduced from the isomer excitation function and from fission cross-section resonance spacings. With our experiment we have tried to investigate carefully the latter point. Our result is that between 1 and 3 keV no narrow cross-section structures greater than 1 barn are observed, while we clearly confirm the resonances at low energy up to 150 eV, which have been already measured by C. Bowman as well as P.A. Seeger et al. This result agrees with the discussion of E. Lynn at the Dubna Conference on Nuclear Structure, in which he mentioned that the general behaviour of the ^{241}Am sub-threshold fission cross-section does not fit with the size of the narrow intermediate structures indicated in the Petrel data between 1 and 3 keV.

SESSION F

DELAYED GAMMA-RAYS FROM SPONTANEOUS FISSION OF ^{252}Cf (SM-122/2)

K. Skarsvåg
Institutt for Atomenergi, Kjeller, Norway

The main difficulty in experiments with delayed gamma-rays is the elimination of the fission neutrons. In recent years fast neutron diffusion and moderation in small assemblies has been studied by the pulsed-neutron technique. These studies have made it clear that it can be difficult to eliminate the fission neutrons by shielding only, a fact which has not been fully appreciated in early measurements of the number, energy spectrum and time distribution of delayed gamma-rays from fission.

In the present experiment the relative number and the time distribution of delayed gamma-rays from spontaneous fission of ^{252}Cf has been measured for gamma-ray energies greater than 100 keV. The gamma-rays were detected by a NaI(Tl) crystal, 3 inch in diameter and 3 inch thick, in coincidence with a semi-conductor detector for the fission fragments. The fission neutrons have been eliminated by the method of time-of-flight, a method which can be used for times shorter than the flight time of the fastest fission neutrons over the direct distance from source to gamma-ray detector. For measurements in the nanosecond time range the NaI(Tl) had a 8 mm wide collimator in front of it, and the time distribution was measured by scanning the flight path of the fission fragments. In the time ranges 5 to 30 ns and 30 to 120 ns the time distribution was measured electronically with a time resolution of 6 ns and with the NaI(Tl) detector at a distance of several metres from the source. In the time range 5 to 30 ns the measurements were made with a shield between the ^{252}Cf source and the NaI(Tl) detector.

CALCULATION OF ANGULAR AND ENERGY DISTRIBUTION OF PROMPT NEUTRONS FROM FISSION (SM-122/9)

G. Y. Kluge
Central Research Institute for Physics
of the Hungarian Academy of Sciences,
Budapest, Hungary

Calculations of angular and energy distributions of prompt neutrons from fission are reported. The purpose of the calculations was to account for the deviations of the experimental from the predicted energy and for the angular distributions in terms of a more adequate evaporation theory. In this way we hope to clarify the existence of that small fraction of neutrons which is assumed to be emitted isotropically in the laboratory system and not from moving fragments.

In the present calculation the total neutron spectrum from fission is described as a sum of contributions from individual fragments weighted by their frequency of occurrence and the number of neutrons emitted. The emission of neutrons from individual fragments is evaluated by assuming isotropic evaporation in a frame of reference moving with the fragment. Two types of emission spectra are considered. The simplified type characterized by the number and average energy of the neutrons emitted per fragment is given as $\varphi(\epsilon) = C\epsilon_n \exp(-\epsilon/T)$. The parameters T, n and the average energy $\bar{\epsilon}$ are related as $\bar{\epsilon} = (n-1)T$ and C is a constant normalizing the spectra to the number of emitted neutrons $\nu = \int_0^\infty \varphi(\epsilon)d\epsilon$. The other type is based on the original Weisskopf formula and describes a neutron cascade consisting of maximum three successive emissions. The parameters of the spectrum of first type can be obtained in terms of a statistical theory with the assumption of thermal equilibrium at the moment of scission. For the second type, using the same assumption of thermal equilibrium, the inverse neutron cross-sections and the level densities of nuclei are included as calculated from the results of Dostrovsky et al., Cameron and Gilbert, respectively.

With the knowledge of the initial excitation energies of the individual fragment pairs, the above calculations permit the formulation of a complete theory of prompt fission neutron emission from which all characteristic parameters of neutron emission and their dependence on the excitation energy can be predicted. Numerical results for the spontaneous fission of ^{252}Cf and for the slow-neutron-induced fission of ^{235}U are given.

PROMPT $\bar{\nu}$ IN SPONTANEOUS AND NEUTRON-INDUCED FISSION OF ^{236}U (SM-122/20)

M. Holmberg, H. Condé
Research Institute of National Defence,
Stockholm, Sweden

This paper gives the average number of prompt neutrons per fission, $\bar{\nu}$, for the neutron-induced fission of ^{236}U in the energy region 0.8 - 6.5 MeV. The $\bar{\nu}$-value for the spontaneous fission of ^{236}U is also reported. It should be noted that the spontaneous value may be compared with the measurements of ^{235}U + n since this reaction gives the same compound nucleus. There are indications that the spontaneous $\bar{\nu}$-values for various isotopes are higher than the ones expected from extrapolations from the induced fission for the same compound nuclei. No earlier measurement exists of the spontaneous $\bar{\nu}$-value of ^{236}U.

The prompt $\bar{\nu}$-value of the neutron-induced fission of ^{236}U is of interest since the fission cross-section shows a structure in the threshold region. This structure gives valuable information about the fission channels since the various K bands are separated. For another fissionable nucleus having a similar structure, ^{232}Th, a relatively high $\bar{\nu}$-value has been reported in the vicinity of the threshold. Since no data of prompt $\bar{\nu}$ for ^{236}U + n have been reported previously, this measurement also gives a comparison with the $\bar{\nu}$-values for other uranium isotopes. In general, the $\bar{\nu}$-values are roughly the same for isotopes having the same atomic number Z.

The accuracy of the neutron-induced data is about 5%, whereas the spontaneous $\bar{\nu}$-value has an error of 4%.

PROMPT GAMMA-RAYS FROM $^{235}U(n, f)$, $^{239}Pu(n, f)$ AND ^{252}Cf (SPONTANEOUS FISSION) (SM-122/33)

V. V. Verbinski, H. Weber, R. E. Sund
Gulf General Atomic Incorporated,
San Diego, California, USA

The spectra of prompt gamma-rays from the fission of ^{235}U, ^{239}Pu and ^{252}Cf were measured with the same gamma-ray spectrometer and geometrical arrangement, making it possible to determine with good accuracy any small differences in spectral shape and in total gamma-ray yield. The gamma-ray spectrometer utilized a 5.85 cm diameter by 15 cm long NaI(Tl) detector surrounded by a 20 cm OD by 30 cm long NaI(Tl) anti-Compton sheath. The response to monoenergetic gamma-rays consisted of a total-energy peak with a small residue at lower pulse heights, making it possible to obtain the entire spectrum from 0.14 to 10 MeV with good accuracy. The fission events were detected with a surface barrier type detector. Gamma ray emitted within 10^{-8} s of the fragments were identified by means of a coincidence circuit, and the fission neutrons were eliminated by locating the gamma-ray detector 70 cm away from the fission foil. Practically all of the fission neutrons require more than 10^{-8} s to travel this distance.

The gamma-ray pulse height distributions and the detector efficiencies were determined with various gamma-ray sources, and a response matrix generated from these data was used to unfold the spectra with a smoothing technique. The prompt gamma-rays from spontaneous fission of ^{252}Cf produce the softest spectrum and the largest total gamma-ray energy yield E_γ(TOT) from 0.14 to 10 MeV of 6.84 MeV per fission, with an average gamma-ray energy $\bar{E}_\gamma$ of 0.88 MeV. For ^{239}Pu, the corresponding values were E (TOT9 = 6.82 MeV, and E = 0.94 MeV. For ^{235}U, E_γ(TOT) = 6.51 MeV, and $\bar{E}_\gamma$ = 0.97 MeV. The relation of these trends to nuclear properties is discussed. The relative values of E_γ(TOT) are known to about 0.1 MeV, while the overall systematic error is approximately 0.3 MeV.

PROMPT NEUTRON AND K X-RAY EMISSION FROM ^{236}U FISSION FRAGMENTS (SM-122/34)

J. W. Bolgman†, V. S. Ramamurthy*, R. L. Walsh
AAEC Research Establishment,
Lucas Heights, N. S. W., Australia

A four-parameter investigation of neutron emission from individual ^{236}U fission fragments is in progress. Prompt fission neutrons are detected in a large liquid scintillator operated in quadruple coincidence with three other detectors. Two surface barrier detectors determine the complementary fission-fragment kinetic energies and a third detector, a high-resolution lithium-drifted silicon detector, is used to measure the characteristic K X-rays emitted from one of the primary fission products. The

† On attachment from University of N. S. W., Wollongong College.

* On attachment from the Bhabha Atomic Research Centre, Trombay, India.

four-parameter data have been analysed to yield the average number of neutrons emitted from ^{236}U fission fragments of specific mass and charge. In addition, data from a preliminary investigation of the charge distribution for the thermal neutron fission of ^{235}U are presented.

PROMPT GAMMA-RAYS FROM THERMAL NEUTRON-INDUCED FISSION OF ^{235}U (SM-122/40)

H. Albinsson, L. Lindow
AB Atomenergi, Studsvik, Nyköping, Sweden

Measurements have been made on the gamma radiation from fission fragments in slow-neutron-induced fission of ^{235}U. The fragments were detected with solid-state detectors of the surface-barrier type and the gamma radiation with a NaI scintillator. The fragment energies were used to determine the masses, and the gamma radiation was measured as a function of fragment mass. Time discrimination between the fission gammas and the prompt neutrons released in the fission process was employed to reduce the background. The gamma radiation emitted during different time intervals after the fission event was studied with a recoil distance technique, i.e. by changing the position of a collimator along the path of the fission fragments. In this way, an estimate of the life-times of the gamma-emitting states was made. The relative yield of the gamma-rays was determined as a function of mass, gamma-ray energy and time after the fission event.

Comparisons are made with data obtained from ^{252}Cf fission. Attention is drawn to features which seem to be the same in ^{235}U and ^{252}Cf fission.

The photon-yield curve as a function of mass resembles that of the prompt-neutron yield although more structure was found in the former case. This structure may be related to long-lived states in deformed nuclei and relatively low excitations in spherical nuclei.

The following tentative half-lives of the gamma radiation have been found: 7×10^{-12}, 2×10^{-11}, and 5×10^{-11} s. These values concern the integral radiation without respect to energy and mass selection because so far a careful analysis of the corrections could not be made.

THE PRESENT STATUS OF $\bar{\nu}$ (SM-122/55)

D.W. Colvin
Atomic Energy Research Establishment, Harwell, United Kingdom

Renewed interest in fission-neutron multiplicity from both fission- and reactor-physics points of view has led to a careful evaluation of all the experimental information available to the spring of 1969. Where possible and necessary, all data have been normalized to currently accepted cross-sections and weight adjusted on the basis of present-day experience in the difficulties of making measurements. Recommended values are presented for thermal and spontaneous fission in ^{233}U, ^{235}U, ^{239}Pu, ^{241}Pu, and ^{240}Pu and ^{252}Cf. Least-squares fits are given to all available data on the dependence of $\bar{\nu}$ on incident neutron energy, and the reliability of the information discussed in the light of present-day reactor requirements as well as its relevance to current theories in fission physics. Results are presented initially as ratios to ^{252}Cf to allow future absolute adjustments; however, absolute values are included based on an up-to-date evaluation of $\bar{\nu}_{spon.}$ for ^{252}Cf.

Reliable precise values of $\bar{\nu}$, perhaps the most fundamental parameter in an Atomic Energy Programme, are still unavailable from an understanding of the fission process, and only a series of painstaking measurements, carefully analysed, can form the basis for reliable input to the corpus of information known as evaluated nuclear data files, which provide the basic physics information for reactor design. Discrepancies and gaps in the data revealed by analysis, as well as experiments using the evaluated files point the way to the most proper fresh experiments required to improve our knowledge. That information of this accuracy presents a challenge to the theoretician is not an incidental benefit.

MESURE DU NOMBRE MOYEN DE NEUTRONS PROMPTS DE FISSION ET DES PROBABILITES ASSOCIEES POUR LA FISSION DE ^{235}U, ^{238}U ET ^{239}Pu INDUITE PAR DES NEUTRONS D'ENERGIE COMPRISE ENTRE 1,5 ET 15 MeV (SM-122/93)

M. Soleilhac, J. Fréhaut, J. Gauriau
CEA, France

Le nombre de neutrons instantanés ($\bar{\nu}$) émis dans la fission de ^{235}U, ^{238}U et ^{239}Pu par des neutrons d'énergie comprise entre 1,5 et 15 MeV a été mesuré simultanément sur ces trois corps en utilisant la technique du gros scintillateur liquide. Les mesures ont été effectuées par rapport au $\bar{\nu}$ pour la fission spontanée du ^{252}Cf.

Nous avons utilisé une chambre à fission rapide contenant l'étalon et les trois corps à mesurer. Les neutrons ont été produits en utilisant le faisceau pulsé d'un accélérateur Van de Graaff 12 MeV et une cible gazeuse. L'énergie des neutrons incidents a été mesurée pour les 29 points expérimentaux en utilisant la technique du temps de vol.

La précision relative de 1% obtenue a permis de mettre en évidence pour ^{235}U une augmentation de pente de 46% de la courbe $\bar{\nu}$ (E) entre 5 et 7,5 MeV, correspondant au phénomène (n,n'f). Aucune discontinuité comparable n'apparaît vers 12 MeV. Pour ^{238}U la variation de $\bar{\nu}$ en fonction de l'énergie est linéaire. Pour ^{239}Pu la loi ν (E) est pratiquement linéaire; des discontinuités de l'ordre de 1% peuvent toutefois exister vers 6 et 12 MeV. Des résultats obtenus nous avons pu déduire les valeurs des probabilités associées P (ν).

Les résultats sont en accord avec l'ensemble des mesures publiées.

English translation of the preceding Abstract (SM-122/93):

MEASUREMENT OF THE AVERAGE NUMBER OF PROMPT FISSION NEUTRONS AND ASSOCIATED PROBABILITIES FOR THE FISSION OF ^{235}U, ^{238}U and ^{239}Pu INDUCED BY NEUTRONS IN THE ENERGY RANGE 1.5-15 MeV

The number of prompt neutrons ($\bar{\nu}$) emitted in the fission of ^{235}U, ^{238}U and ^{239}Pu by neutrons in the energy range 1.5-15 MeV was simultaneously

measured on these three substances with the large liquid scintillator technique. The measurements were made relative to $\bar{\nu}$ for the spontaneous fission of ^{252}Cf.

We used a fast fission chamber containing the standard and the three substances to be measured. The neutrons were produced with the pulsed beam from a 12 MeV Van-de-Graaff accelerator and a gaseous target. Incident neutron energy was measured for the 29 experimental points by using the time-of-flight method.

The achieved relative precision of 1% revealed, for ^{235}U, a 46% increase in the slope of the curve $\bar{\nu}(E)$ between 5 and 7.5 MeV, corresponding to the process (n, n'f). No comparable discontinuity appears towards 12 MeV. For ^{238}U, the energy dependence of $\bar{\nu}$ is linear. For ^{239}Pu, the law $\nu(E)$ is practically linear, but discontinuities of about 1% may occur in the region of 6 and 12 MeV. We were able to deduce the values of the associated probabilities $P(\nu)$ from the results obtained.

The results are in agreement with all the measurements published.

ИССЛЕДОВАНИЕ РЕНТГЕНОВСКОГО ИЗЛУЧЕНИЯ ПРИ ДЕЛЕНИИ ТЯЖЕЛЫХ ЯДЕР ТЕПЛОВЫМИ НЕЙТРОНАМИ (IAEA-SM-122/152)

А.Н. Смирнов, С.М. Соловьев, Л.И. Тывин, В.П. Эйсмонт
Союз Советских Социалистических Республик

На современной, по существу, начальной стадии экспериментов более или менее полные и непротиворечивые данные о свойствах характеристического излучения получены только для спонтанного деления ^{252}Cf, когда не возникает проблемы фона от вызывающих деление частиц (квантов). В настоящей работе описывается ряд опытов по измерению выходов и энергетического распределения рентгеновских лучей при делении, индуцированном тепловыми нейтронами.

С целью лучшего понимания как вопросов эмиссии самого характеристического излучения, так и свойств распределения заряда, вслед за ранее исследованными случаями (деление ^{235}U и ^{239}Pu) изучены рентгеновские лучи осколков ^{233}U. В сравнительных (к ^{235}U) измерениях определены спектры и интенсивность характеристических К-лучей. Для ^{233}U энергия квантов, испускаемых легким осколком, меньше, а тяжелым – больше, чем для ^{235}U. Разница в энергии приписана разнице в зарядах, которая сравнивается с существующими гипотезами. Сделаны некоторые заключения о влиянии на распределение зарядов оболочечных эффектов. Интенсивность излучения обоих ядер найдена одинаковой (в пределах 10%).

Уникальная возможность измерения мгновенного заряда осколков в корреляции с другими параметрами деления, предоставляемая методом характеристических лучей, использована для определения зарядов осколков в актах деления (^{235}U) с вылетом длиннопробежных α-частиц (в дальнейшем для краткости именуемого тройным делением). Для этого в одинаковых условиях измерены энергетические спектры, а также выходы, К-излучения в двойном и тройном делении. Отмечено, что спектры излучения двойного и тройного деления весьма схожи: оба имеют по два пика, почти одинаковых по положению и величине, что, несомненно, отражает большое подобие зарядовых свойств осколков, образующихся в этих процессах. Вместе с тем, в спектрах наблюдены некоторые отличия, заключающиеся в сдвигах правых склонов пиков излучения легкого и тяжелого осколков тройного деления в сторону меньших энергий. Найдено, что величина сдвигов соответствует вылету α-частиц. Для отношения выходов излучения (тройного к двойному) получено значение, близкое к единице: $0{,}9 \pm 0{,}2$. Отсутствие заметных различий в выходах, по-видимому, указывает на отсутствие больших различий в спинах осколков двойного и тройного деления.

Ввиду противоречивости литературных данных по выходам К-излучения при делении ^{235}U (результаты отдельных работ отличаются в 2-3 раза), проведены измерения интенсивности рентгеновских лучей осколков ^{235}U относительно осколков спонтанного деления ^{252}Cf, выход для которых известен с наибольшей достоверностью. Сравнение проведено при максимально возможной идентичности условий.

English translation of the preceding Abstract (SM-122/152):

INVESTIGATION OF X-RAY EMISSION IN FISSION OF HEAVY NUCLEI BY THERMAL NEUTRONS

At present, essentially preliminary stage of the experiments, more or less complete and consistent data on the properties of characteristic radiation have been obtained only for spontaneous fission (^{252}Cf), where there is no problem of a background from fission-inducing particles (quanta). The paper describes a series of experiments to measure the X-ray yields and energy distribution in fission induced by thermal neutrons.

With a view to gaining a better understanding both of questions of the emission of characteristic radiation itself and of the properties of its charge distribution, following on earlier investigations into the fission of ^{235}U and ^{239}Pu, the authors studied X-rays from fragments of ^{233}U. They measured the spectra and intensity of characteristic K-radiation relative to ^{235}U and found that the energy of the quanta emitted by light fragments is less in the case of ^{233}U than for ^{235}U, while for heavy fragments it is greater. They attribute this difference in energy to a difference in charge, and compare this latter difference with current hypotheses. Certain conclusions are drawn regarding the influence of shell effects on charge distribution. The radiation intensity is found to be identical (to within $\pm$ 10%) for both nuclei.

The unique possibility of measuring the prompt charge of fragments simultaneously with other fission parameters that is offered by the characteristic rays method was used to determine fragment charges in ^{235}U fission events involving the ejection of long-range alpha particles (subsequently called ternary fission for short). For this purpose the energy spectra and yields of K-radiation in binary and ternary fission were measured under identical conditions. It was found that the radiation spectra for binary and ternary fission are very similar: they both have two peaks that are almost identical in respect of position and magnitude, which doubtless reflects the close similarity between the charge properties of the fragments formed by this process. Some differences, however, were observed in the spectra, in that the right-hand slopes of the radiation peaks for the light and heavy fragments from ternary fission are shifted in the direction of lower energies. It was found that the magnitude of the shifts corresponds to the ejection of alpha particles. The ratio of radiation yields (ternary to binary) was found to be close to unity: 0.9 ± 0.2. The fact that there are no appreciable differences in yield obviously points to there being no major differences in the spins of binary and ternary fission fragments.

In view of the inconsistent data in the literature on K-radiation yields in the fission of ^{235}U (the results obtained by individual authors differ by a factor of 2 to 3), the intensity of X-radiation from ^{235}U fragments was measured relative to that obtained with fragments from the spontaneous fission of ^{252}Cf, the yield for which is known most reliably. The comparison was made under conditions which were as identical as possible.

О ВАРИАЦИИ КИНЕТИЧЕСКОЙ ЭНЕРГИИ ОСКОЛКОВ ПРИ ДЕЛЕНИИ ^{235}U НЕЙТРОНАМИ С ЭНЕРГИЕЙ 0,15-1,68 Мэв (IAEA-SM-122/161)

Е. Дерменджиев, Н. Кашукеев, Ц. Пантелеев, И.В. Сизов, Тян Сан Хак
Объединенный институт ядерных исследований, Дубна (СССР)

На электростатическом генераторе ЭГ-5 Лаборатории нейтронной физики Объединенного института ядерных исследований методом измерения относительного выхода W осколков из двух урановых мишеней исследовалась вариация кинетической энергии $E_к$ осколков деления ^{235}U. Зависимость $W(E_n)$ изучалась в интервале энергий нейтронов E_n = 0,15 - 1,68 Мэв. Найдено, что при $E_n \sim 0{,}77$ Мэв и $E_n \sim 1 - 1{,}68$ Мэв $\bar{E}_к > \bar{E}_{к_{тепл.}}$ на ~0,4 Мэв.

English translation of the preceding Abstract (SM-122/161):

ON THE VARIATION OF FRAGMENT KINETIC ENERGY IN THE FISSION OF ^{235}U INDUCED BY 0.15 TO 1.68 MeV NEUTRONS

The variation of the kinetic energy E_k of fission fragments of ^{235}U was studied on the electrostatic EG-5 LNF OIYaI generator by measuring the relative yield of fragments W from two uranium targets. The function $W(E_H)$ was studied in the neutron energy interval E_H = 0.15 - 1.68 MeV. It is found that for $E_H \sim 0.77$ MeV and $E_H \sim 1 - 1.68$ MeV $\bar{E}_k > \bar{E}_{k\ thermal}$ by about 0.4 MeV.

ON THE PERIODICAL STRUCTURE IN THE RESONANCE NEUTRON FISSION CROSS-SECTIONS OF ^{235}U AND ^{239}Pu (SM-122/160)

Yu. V. Ryabov, N. Janeva
JINR, Institute for Neutron Physics,
Dubna, USSR

The method of investigating the periodical behaviour of the fission cross-sections was suggested by P. Egelstaff [1]. In the present paper this method is applied in the analysis of the fission cross-sections of ^{235}U and ^{239}Pu in the energy range between 50 eV and 3 keV [2].

The calculated serial correlation coefficient is defined by

$$r_k = \frac{C_{0v}[a_j(W);\ a_{j+k}(W)]}{\{\mathrm{var}\, a_j(W);\ \mathrm{var}\, a_{j+k}(W)\}^{\frac{1}{2}}}$$

with j = 1, 2, ...n, where k = 1, 2, ... n/2,

$$a_j = A(jW) - A[(j+1)W]; \quad A(E) = \sum_{0}^{E} \left[\frac{\sigma_r(E')\sqrt{E'}}{\langle \sigma_r(E')\sqrt{E'} \rangle} - 1 \right] \Delta E'$$

ΔE is the distance between consecutive points, W is the averaging interval.

The correlograms for ^{235}U and ^{239}Pu are obtained for different values of W ranging from 40 to 150 eV. The correlograms show the oscillations with a period of 200 eV for ^{235}U and 400 eV for ^{239}Pu.

This effect may be explained by the existence of the set of gross structure resonances in the second minimum [4] of the potential energy curve of fissioning nuclei.

REFERENCES

[1] EGELSTAFF, P., J. nucl. Energy 7 (1958) 35.
[2] RYABOV, Yu.V. et al., Atomn. Energ. 24 (1968) 351.
[3] LYNN, J.E., "Neutron Resonance Reactions" (Clarendon Press, Oxford (1968)).
[4] STRUTINSKY, V.M., Nucl. Phys. A95 (1-67) 420.

SESSION G

DELAYED-NEUTRON ENERGY SPECTRA (SM-122/37)

S. Shalev, J.M. Cuttler, G. Ben-Yaakov
Department of Nuclear Science,
TECHNION, Israel Institute of Technology,
Haifa, Israel

The need for measurements of delayed-fission-neutron energies is discussed, and the sparse data previously available are reviewed. Some suggestions are made regarding the possible form of delayed-neutron spectra, using information obtained from fission-yield data, identified neutron precursors, level-density calculations and delayed-proton emitters.

The development of high-efficiency, high-resolution ^{3}He proportional and ionization spectrometers is discussed in some detail, including the results obtained with thermal and monoenergetic fast-neutron irradiations using a Van-de-Graaff accelerator. Spectrometer optimization is described for optimum energy resolution, while maintaining high fast-neutron-detection efficiency, low gamma-ray sensitivity, and negligible pile-up and base-line shift distortions.

The analysis of a complex pulse-height distribution is carried out by a non-linear least-squares method. The energy-dependent response function of the spectrometer is expressed as an analytical function, the parameters of which have been determined experimentally by a series of highly monoenergetic fast-neutron irradiations. The experimental and computational techniques are described in detail, with particular emphasis on their application to the analysis of delayed-neutron energy spectra.

The energy spectra of delayed neutrons are presented for the fission of ^{235}U, ^{238}U and ^{232}Th. Individual spectra are given for each of the longer-lived groups. Energy calibration is carried out by determining the delayed-neutron energy spectrum of ^{17}N obtained from the reaction ^{18}O(t, α)^{17}N. The experimental arrangements are described in detail, and a complete analysis is presented of possible sources of error in each stage: neutron emission from the sample, scattering in the laboratory, detector response, electronic pulse analysis and calibration techniques. The experimental results are compared with previous measurements and conclusions drawn with respect to reactor control and basic research into the decay of fission products.

GAMMA-SPECTROSCOPIC STUDIES OF SHORT-LIVED FISSION PRODUCT HALOGENS (SM-122/41)

A. Lundán, A. Siivola
Department of Technical Physics,
Technical University of Helsinki,
Otaniemi, Helsinki, Finland

Gamma rays associated with short-lived fission product iodine and bromine isotopes have been investigated using Ge(Li) and NaI(Tl) detectors and a 4096-channel two-parameter spectrometer. Both manual and auto-

mated techniques have been used to separate iodine and bromine chemically from other fission products of uranium.

In the first experiments, the decay of the 83s ^{136}I was investigated [1]. Irradiated samples of uranyl nitrate were dissolved in hot 1-M HNO_3 and iodine was then extracted into CCl_4. The organic phase was separated, purified by washing with HNO_3, and measured. The separation procedure, which was done manually, took about 2 min and measurement was started 2.5 min after the end of irradiation.

A total of 21 gamma-rays were assigned to the decay of ^{136}I. According to the proposed level scheme these depopulate 14 levels in ^{136}Xe. Some of these transitions also have a shorter-lived component with a half-life of 40 ± 5 s. This is thought to be due to an isomeric state in ^{136}I that decays be beta emission to the energy levels of ^{136}Xe.

In February 1969, the construction of an apparatus for continuous production and fast transfer of fission product halogens and rare gases was concluded in our laboratory. The working principle of this device is to bring iodine and bromine in gaseous form through hot-atom reactions with methane, as first suggested by Denschlag et al. [2]. The operation of the apparatus is completely automatized. Gas transfer times shorter than 1 s can be achieved.

In the gamma spectra of the fission product isotopes produced with the aid of this device four short-lived gamma-rays have been found, whose energies and half-lives are 1223.0 ± 3.9 keV (2.2 ± 0.3 s), 144.5 ± 3.2 keV (2.7 ± 0.3 s), 808.3 ± 6.4 keV (15.7 ± 1.6 s) and 776.8 ± 0.3 keV (17.5 ± 1.1 s). The last one probably belongs to the isotopes ^{88}Br, as suggested by Denschlag and Gordus [3]. The origin of the three other gamma-rays is not clear yet. Preliminary experiments have shown that they may be associated with rare-gase activities rather than halogens. Furthermore, the 144.5-keV transition seems to follow the xenon fraction and the 808.3 keV transition the krypton fraction in the chemical separation procedure.

REFERENCES

[1] LUNDÁN, A., SIIVOLA, A., On the decay of ^{136}I, Ann. Acad. Sci. Fenn. A. 6 (1968) 288.

[2] DENSCHLAG, H.O., HENZEL, N., HERRMANN, G., Reaktion von Spaltrückstoß-Kernen mit Methan und Benzol, Radiochim. Acta 1 (1963) 172.

[3] DENSCHLAG, H.O., GORDUS, A., Gas-chromatographic technique for rapid isolation of uranium fission products, Z. analyt. Chem. 226 (1967) 62.

IMPROVEMENTS IN THE SEMITHEORETICAL APPROACH TO DELAYED NEUTRON EMISSION (SM-122/51)

A.C. Pappas, T. Sverdrup
University of Oslo,
Blindern, Norway

Delayed-neutron emission probabilities and expected spectra of the emitted neutrons are considered in a semitheoretical approach, but along the lines of improvement previously suggested by Jahnsen, T., Pappas, A.C., Tunaal, T.,(in Delayed Fission Neutrons(Proc. Panel Vienna, 1967), IAEA, Vienna (1968) 35). In the present study probabilities are estimated for a number of precursors on the basis of recent knowledge to the parameters involved. The obtained results with respect to P(n) are compared with available experimental information and correlated to spin and angular momentum effects caused by excitation energy in the emitter nucleus. The energy influence found on the spin distribution is introduced and spectra of the emitted neutrons estimated. These show a much smaller contribution from energetic neutrons than expected from all previous treatments, thus in much better agreement with the one or two measured spectra. The results may, therefore, be useful in analysing neutron spectra as measured from the complex mixture of delayed-neutron precursors always observed under experimental conditions.

STUDY OF SHORT-LIVED SELENIUM FISSION PRODUCTS (SM-122/69)

P. del Marmol, D. C. Perricos *
Centre d'Etude Nucléaire, CEN - SCK, Mol, Belgium

By means of a fast pneumatic rabbit coupled to an automatic radiochemical separation system, ^{87}Se and ^{88}Se are separated in a few seconds as hydrides from the thermal neutron fission products of ^{235}U. After recovery in water, selenium was further purified from Br, I and Rb by passing it through a mixed precipitate of AgCl and Cs-phosphomolybdate and its delayed-neutron activity was followed by means of ^{3}He counters. The half-lives were measured through the neutron activities of their bromine daughters as 5.9 ± 0.2 s for ^{87}Se and 1.3 ± 0.3 s for ^{88}Se.

From a delayed neutron activity consistent with the ^{87}Se half-life and in constant ratio with the ^{87}Br activity, a P_n value of $0.23 \pm 0.07\%$ was evaluated for ^{87}Se. A shorter-lived neutron activity was observed and could be due to ^{88}Se, but the evidence was too weak so that an upper limit of $P_n \leq 1\%$ is estimated for this isotope.

BETA-DECAY ENERGY FOLLOWING FISSION (SM-122/131)

T. D. MacMahon, J. Scobie, H. W. Wilson
The Scottish Research Reactor Centre, East Kilbride, Scotland

A considerable uncertainty exists in the energy released following fission in the form of beta radiation from the fission products. Work supported in part by the UKAEA has been carried out at the Scottish Research Reactor Centre to measure the rate of decay of beta energy for times up to 10^5 s following irradiation of ^{235}U for periods of 10 to 10^5 s. From the data it is possible to derive the total beta energy release and this is calculated to be 6.3 ± 0.5 MeV per fission. It is hoped to present data for ^{233}U and ^{239}Pu fission.

* IAEA fellow from Nuclear Research Center Democritos, Athens, Greece.

ЗАПАЗДЫВАЮЩИЕ НЕЙТРОНЫ ^{232}Th И РАСПРЕДЕЛЕНИЕ ЗАРЯДА В ДЕЛЕНИИ (IAEA-SM-122/136)

Б.П. Максютенко, М.З. Тараско
Физико-энергетический институт, Обнинск,
Союз Советских Социалистических Республик

Измерены относительные выходы запаздывающих нейтронов ^{232}Th при делении нейтронами с энергией в диапазоне 5,0-7,2 Мэв: реакция Д (α, n) ^{3}He, мишень толщиной 200 кэв. Полученные изменения отношения выходов групп значительно больше ранее измеренных на толстой мишени (1-2,5 Мэв).

Разработан новый математический метод разложения кривых распада. Он позволяет выделить значительно большее число вкладчиков экспонент, чем метод наименьших квадратов. С помощью этого метода получено 11 групп, из которых 7 соответствуют чистым изотопам-предшественникам запаздывающих нейтронов. Наблюдается корреляция в изменениях выходов различных групп. На примере изотопов брома показывается возможность изучить изменения соответствующего распределения заряда в делении с изменением энергии.

English translation of the preceding Abstract (SM-122/136):

DELAYED NEUTRONS OF THORIUM-232 AND CHARGE DISTRIBUTION IN FISSION

The authors measured the relative fission yields of delayed neutrons of ^{232}Th following fission by neutrons in the 5.0-7.2 MeV energy range (D(d, p)^{3}He reaction, target thickness 200 keV). The resulting variations in the ratio of group yields are considerably greater than those previously measured on a thick target (1-2.5 MeV).

A new mathematical method of analysing the decay curves was developed, making it possible to isolate an appreciably larger number of contributors to the exponents than the least-squares method. Using this method eleven groups were obtained, seven of which correspond to the pure isotopes which are precursors of the delayed neutrons. A correlation is noted in respect of the variations in yield between the different groups. Taking the isotopes of bromine as an example, the authors show that it is possible to study changes in charge distribution in fission as a function of energy changes.

PROMPT NEUTRON EMISSION FROM FISSION FRAGMENTS IN 14-MeV NEUTRON- AND PHOTO-FISSION OF ^{232}Th AND ^{238}U (SM-122/142)

H. D. Sharma
University of Waterloo,
Waterloo, Ont.
and
L. H. Gevaert, R. E. Jervis
University of Toronto,
Toronto, Ont., Canada

The radiochemical yields, Y(A), for selected nuclides in the mass region from 99 to 125, have been determined in the fission of ^{232}Th and ^{238}U with 14.7 MeV neutrons and with photons from 25-MeV bremsstrahlung.

The compilation of radiochemical and mass-spectrometric yields by Gevaert [1] has provided a set of Y(A) values for comparison with the prompt mass yields, y(A), obtained by Gönnenwein and Pfeiffer [2]. The method requires normalization of Y(A), such that $\Sigma_{A_L} Y(A_L) = \Sigma_{A_C - A_L - \tilde{\nu}} Y(A_H) = 100$ where A_C is the mass number of fissioning nuclides. $\tilde{\nu}$ (A), the average number of prompt neutrons emitted by a fission fragment A, was calculated from an analysis of the difference of $\Sigma y(A)$ and $\Sigma Y(A)$ curves [3], thus enabling calculation of $\bar{\nu}_T$, the mean total number of prompt neutrons emitted from both fragments. The normalization of Y(A) at A = 117 for ^{238}U with 14 MeV neutrons, and average $A_C = 238$, gave a value of $\bar{\nu}_T = 3.8$ which is in agreement with the value of 3.75 obtained by Gönnenwein and Pfeiffer (or $\bar{\nu} = 4.7$ which includes pre-fission neutrons). The $\tilde{\nu}$ (A) curve shows that in the asymmetric region up to $A \leqq 108$ and $A \geqq 132$, the curve has a somewhat similar shape as the one observed in thermal neutron fission (saw-tooth curve) whereas in the symmetric region $\tilde{\nu}$ (A) = 0.5 ± 0.5 at A = 110 and gradually increases to 4.0 ± 0.5 at A = 129. The radiochemical yields in the asymmetric region in ^{232}Th fission with 14 MeV neutrons are not yet well established. However, if it is assumed that $\sum_{A_L}^{114} Y(A) = 100$, the $\tilde{\nu}$ (A) curve in the symmetric region again shows that $\tilde{\nu}$ (A) = 0.3 ± 0.5 at A = 105 and increases to 4 ± 0.5 at A = 129. From these curves, it can be speculated that one of the shapes of fissioning nucleus at the scission point has two equal volumes separated by a neck which leads to fission fragments in the symmetric region in fission at moderate excitation energy. The neck is perhaps a little longer in the case of ^{232}Th. The results do not either support or refute the two-mode hypothesis. Perhaps, some mass-spectrometric yields in the symmetric region and time-of-flight measurements of fission fragments will be helpful in determining the precise shape of $\tilde{\nu}$ (A) curve for these fissioning nuclides and thus support the validity of two-mode hypothesis or fragment shell theory.

In the photofission of ^{232}Th and ^{238}U, Y(A) curves do not resemble the respective ones obtained in 14 MeV neutron fission. Calculations of $\tilde{\nu}$ (A) for ^{238}U from a comparison of an assumed y(A) curve based on the values of y(A) obtained with photons from 33 MeV bremsstrahlung [4], show that the $\tilde{\nu}$ (A) curve has discontinuities in the symmetric region. It is also of some importance to determine accurate mass-spectrometric and prompt mass yields to calculate $\tilde{\nu}$ (A) in photo-fission. Alternatively, measurements of neutron emission as a function of mass along with prompt yields may perhaps be helpful in explaining the differences in the radiochemical yields in these fissioning systems.

REFERENCES

[1] GEVAERT, L.H.T., Thesis, University of Toronto, Toronto, Ontario, Canada (1968).

[2] GÖNNENWEIN, F., PFEIFFER, E., Z. Physik 207 (1967) 209.

[3] TERRELL, J., Phys. Rev. 127 (1962) 880.

[4] HOGG, G.R., Nucl. Phys. 72 (1965) 167.

HIGH-ENERGY PHOTOFISSION IN ^{238}U, ^{232}Th AND ^{209}Bi (SM-122/156)

B. Schröder, G. Nydahl, B. Forkman
Department of Nuclear Physics,
Lund Institute of Technology and Department of Physics,
University of Lund, Sweden

The mass-yield distributions from photofission of ^{238}U and ^{232}Th at 300 - 1100 MeV and of ^{209}Bi at 700 MeV have been measured by using catcher-foil techniques combined with gamma-ray spectroscopy. By means of a subtraction method the high-energy single-humped mass distributions of uranium and thorium were calculated; they show a half-width (FWHM) between 17 and 22 mass units, similar to that obtained in the bismuth case. The cross-sections of symmetric and asymmetric photofission in uranium and thorium have been calculated from the peak-to-valley ratios obtained. The cross-sections showed resonances around 350 MeV which was interpreted as a pion-effect.

SESSION H

THE MOST PROBABLE CHARGE IN FISSION OF URANIUM INDUCED BY 12-55 MeV PROTONS (SM-122/5)

H. Umezawa
Japan Atomic Energy Research Institute,
Tokai Research Establishment, Japan

The behaviour of the most probable charge, Z_p, has been investigated through radiochemical measurements of the fission yields of several shielded nuclides in ^{238}U fission induced by 12-55 MeV protons. A stacked-foil target assembly containing twelve uranium targets (20-70 mg U_3O_8/cm^2, ^{238}U 99.3%, ^{235}U 0.68%) accompanied with aluminum absorbers was irradiated with a 55 MeV proton beam for 9-18 hours by a synchrocyclotron of the Institute for Nuclear Study, University of Tokyo. One of the uranium targets was placed out of the range of the proton beam and worked as the monitor target for background neutrons. After the irradiation, each target was analysed by systematic radiochemical analysis mainly based on ion-exchange technique.

Determined were the independent yields of the shielded nuclides, ^{86}Rb, ^{134}Cs, and ^{160}Tb, and the cumulative yields of ^{72}Zn, ^{89}Sr, ^{97}Y, ^{99}Mo, ^{112}Pd, ^{115}Cd, ^{132}Te, ^{140}Ba, ^{141}Ce, ^{144}Ce, ^{143}Pr, ^{147}Nd, ^{149}Pm, ^{153}Sm, ^{156}Eu, and ^{161}Tb. Assuming a Gaussian charge dispersion curve with $2\sigma^2 = 0.95$, ECD rule, and that the number of emitted neutrons in fission is given by $2.7 + Ex/8$ as a function of the excitation energy Ex of the compound nucleus, the total chain yields were calculated from the measured cumulative yields, and the yield-mass curves were constructed for each of the eleven proton energies. The absolute yield of a shielded nuclide was converted to the fractional independent yield by dividing by the total chain yield for the given mass chain read off from the yield-mass curve; the Z_p-value in the corresponding mass chain was then determined by using the above-mentioned charge-dispersion curve.

The Z_p-values obtained follow neither the ECD nor the UCD rule. They are located between the values predicted by the ECD and UCD rules, which are close to the ECD-values at low energies and gradually approach the UCD-values as the proton energy increases. The intermediate-energy fission mechanism is to be discussed in terms of a systematic behaviour of the Z_p-values found in this way.

RANGE DISPERSION OF $^{235}U(n, f)$ RECOILS IN ALUMINIUM (SM-122/6)

T. Ishimori, M. Saeki
Nuclear Physics Laboratory, Tokai Research Establishment,
JAERI, Tokai-mura, Ibaraki-ken, Japan

According to the experiments with collimated recoils, it is reasonable to assume that the fission recoils of definite mass number show a range dispersion of normal distribution type. The values of average ranges in aluminium are also available from other studies. Therefore, in the present work, range dispersion of recoil nuclides is studied (mass number 95, 97, 99, 103, 131, 132, 133, 135 and 141) in aluminum using no collimation.

Experimental:

The target assembly consisted of very thin ^{235}U target and several thin aluminium catchers (1.4 - 3.4 mg Al/mg). After neutron irradiation, the radioactivity caught by each catcher was determined by using both γ-spectrometry and decay tracing of photopeaks. Thus, the average concentration of a given nuclide was obtained for each catcher.

In the present work, no collimator is used. Therefore, resoils of a given mass number should distribute according to the area function of the normal distribution in the catcher medium. If the standard deviation of the original normal distribution is given, the shape of the above function is determined. For a given value of standard deviation, the distance depth from the target, which should stand for the average concentration obtained experimentally, can be calculated.

On a probability paper, the relationship between the recoil concentration and depth of aluminium should give a straight line passing through the point corresponding to the average range for one half of the original.

For a given value of standard deviation (σ_g), the straight line mentioned above is drawn. From the inclination of the line the standard deviation (σ_f) is obtained.

For a series of σ_g, the above operation was repeated and the most probable value of the standard deviation was obtained from the σ value which satisfied the relation

$$\sigma_f/\sigma_g = 1$$

Results obtained

Mass number	95	97	99	103	131	132	133	135	141
% Half-width	14.2	16.0	17.1	17.9	25.2	29.2	26.4	30.6	34.6

THE AVERAGE PRIMARY CHARGE VALUES IN ^{235}U THERMAL FISSION (SM-122/24)

K. Sistemich, P. Armbruster, J. Eidens, E. Roeckl
Institut für Festkörper- und Neutronenphysik KFA Jülich, Federal Republic of Germany

The average primary charge in ^{235}U thermal fission has been determined from the total number of beta decays. The gas-filled mass separator at the Research Reactor Jülich 2 produces a beam of fission products in separation times of 1 μs. Long-lived fission products have been used for a mass calibration within the light and heavy fission product group. The total number of β decays between time zero and 3000 s after fission is measured by a 4π-β-counter using an acitvity build-up technique. Average charge values in the mass regions of high fission yields have been determined with an accuracy of ± 0.08 charge units. A Wahl-diagram for ^{235}U thermal fission is presented. Besides, the average variance of the charge distribution is determined by making use of the nuclear charge dispersion of the gas-filled separator. A value of $\bar{\sigma}$ = (0.59 ± 0.03) charge units has been obtained in agreement with radiochemical measurements.

The measurement is compared with former results obtained by radiochemical and physical methods. The standard deviations between the different measurements amount to 0.08 - 0.10 charge units.

A calculation of the average charge values, assuming a two-spheroid model of the scission configuration, is presented. The potential energy of the fission configuration has been minimized. The charge values are calculated either by an approach using measured kinetic and excitation energies of the primary fragments or by the mass formula of Myers and Swiatecki. Standard deviations between calculation and measurement of 0.12 charge units have been obtained. The general importance of nuclear charge measurements for fission theory is stressed in a final discussion.

MASS AND ENERGY DISTRIBUTIONS OF FISSION FRAGMENTS FROM ^{232}Th (n, f) BY MeV NEUTRONS (SM-122/25)

F. Gönnenwein, W. Holubarsch, E. Pfeiffer
Physikalisches Institut der Universität Tübingen, Federal Republic of Germany

The fission of ^{232}Th induced by MeV neutrons has been analysed in a two-parameter experiment. The coincident fission fragments were detected in semi-conductor counters and the resulting pulse heights gathered into a 64 × 64 matrix. From these data mass and energy of the primary fragments have been calculated. The neutron bombarding energies were 1.92, 2.97 and 4.81 MeV with an energy spread of typically 150 keV. This means, that the fragments observed virtually stem from first-chance fission. At least 2×10^4 events were collected for each energy. The mass distributions obtained compare quite favourably with those from radiochemical studies. The peak-to-valley ratios found for the double-humped mass yield curves vary from 560/1, 122/1 to 45/1 for neutron energies 1.92, 2.97 and 4.81 MeV respectively. All mass distributions show a structure at fragment mass numbers A ≈ 135 and A ≈ 141. The mean total fragment kinetic energy $\bar{E}_k$ = (169.0 ± 2.0), (169.7 ± 2.0) and (170.5 ± 2.0) MeV, whereas the dip in kinetic energy (i.e. the difference between maximum kinetic energy in the energy-vs-mass plot and the kinetic energy at symmetric mass division) is 22.5, 20.3 and 18.7 MeV for neutron projectile energies of 1.92, 2.97 and 4.81 MeV, respectively. When the bombarding energy is increased, the fragment kinetic energy is raised for all mass divisions, except perhaps for extremely asymmetric mass ratios. However, this raise is more pronounced for near-symmetric fission than for high-yield asymmetric fragments: whereas the kinetic energy in the former mass region changed by nearly 5 MeV, this change is less than 1 MeV in the asymmetric region for the span of excitation energies studied.

CHARGE DISTRIBUTION IN LOW-ENERGY FISSION REACTIONS (SM-122/26)

H.O. Denschlag, S.M. Qaim *, W. Eckhardt, G. Herrmann
Institut für Anorganische Chemie und Kernchemie der Universität Mainz,
Federal Republic of Germany

Charge dispersion in spontaneous fission of ^{252}Cf was determined for the fission chains with mass numbers 139 and 140 and was found to be σ = 0.62 ± 0.05 and 0.7 ± 0.2, respectively, comparable with the average dispersion observed in thermal-neutron-induced fission (σ = 0.59 ±0.06 [1]).

The fractional independent yield values of ^{133}I, ^{134}I and ^{135}I were determined in four different fission reactions using a rapid technique for the separation of iodine from precursors [2]. Results are given in the following Table I.

TABLE I. FRACTIONAL INDEPENDENT YIELDS (%)

Reaction	^{133}I	^{134}I	^{135}I
$^{235}U(n_{th}, F)$	≤ 4	12 ± 2	47 ± 2
$^{233}U(n_{th}, F)$	14 ± 3	33 ± 4	61 ± 5
$^{239}Pu(n_{th}, F)$	15 ± 5	33 ± 5	61 ± 5
$^{232}Th(n_R, F)$	≤ 5	≥ 3	12 ± 6

n_R Reactor neutrons screened by Cd

The yields of ^{135}I listed above and independent yields of ^{135}Xe in the thermal-neutron fission of ^{235}U, ^{233}U and ^{239}Pu (3) were used to calculate the width parameters of the Gaussian charge dispersion curve resulting in a value of σ = 0.58 ± 0.11 for all three fission reactions.

The most probable charges (Z_P-values) of the fission chains 133 and 134, calculated using the experimental yields and σ = 0.59 lie on the (updated) charge distribution curve of Wahl [1, 4] for all three fission reactions.

The Z_P-values of chain 135, on the other hand, fall off the line by about 1/4 unit towards Z = 53. We interpret this behaviour as a tendency to realize the closed neutron shell N = 82 in the fission chain 135.

The Z_p-values of chains 96 and 97 [4], complementary to 135 in the fission of ^{233}U deviate from the Z_P-curve by the same amount as that of chain 135, but fall on the smooth line in the absence of magic complementary products as in fission of ^{239}Pu.

We conclude that both scission of the nucleus into fragments, and subsequent evaporation of prompt neutrons are affected by the closed 82-neutron shell.

Experiments with 14 MeV neutrons are under way.

---

* Alexander von Humboldt Fellow, on leave from Pakistan Atomic Energy Commission.

REFERENCES

[1] WAHL, A.C., in Physics and Chemistry of Fission (Proc. Symp. Salzburg, 1965) 1, IAEA, Vienna (1965) 317.
[2] DENSCHLAG, H.O., J. inorg. nucl. Chem. 31 (1969) 1873.
[3] OKAZAKI, A., WALKER, W.H., BIGHAM, C.B., Can. J. Phys. 44 (1966) 237.
[4] WAHL, A.C., FERGUSON, R.L., NETHAWAY, D.R., TROUTNER, D.E., WOLFSBERG, K., Phys. Rev. 126 (1962) 1112.

FRAGMENT ENERGY CORRELATION MEASUREMENTS FOR THE PROTON-INDUCED FISSION OF ^{226}Ra (SM-122/27)

E. Konecny
Technische Hochschule, München, Federal Republic of Germany
and
W. Nörenberg
Universität Heidelberg, Federal Republic of Germany
and
H.W. Schmitt
Oak Ridge National Laboratory, Oak Ridge, Tenn., USA

The yield, the average total fragment kinetic energy and the width of the total fragment kinetic energy distribution have been determined as functions of fragment mass from two-parameter fragment-energy-correlation experiments for the proton-induced fission of ^{226}Ra. Results were obtained for proton energies E_p = 9, 11 and 13 MeV. The average total fragment kinetic energy is found to decrease slowly with increasing compound-nucleus excitation energy. The observed rate of decrease is generally largest for fragment pairs in which one fragment is near doubly magic, i.e. for heavy fragment mass $\approx$ 132 amu. Increase in relative yield of the symmetric peak of the mass distribution with increasing excitation energy is once again observed. These and other observations are interpreted in terms of the previously proposed two-component hypothesis together with molecular model considerations including the assumption that the number of quasi-particle excitations at scission is determined by the excitation energy at the saddle point.

RADIOCHEMICAL STUDIES OF RECOIL PRODUCTS IN THE INTERACTION OF 28 GeV AND 2.2 GeV PROTONS WITH URANIUM, BISMUTH AND GOLD (SM-122/32)

K. Baechmann, J.B. Cumming
Brookhaven National Laboratory, Upton, N.Y.
and
Technische Hochschule Darmstadt, Federal Republic of Germany

The recoil properties of a number of products (lanthanides, barium, palladium and strontium) formed by the interaction of 28 GeV and 2.2 GeV protons with uranium, gold and bismuth were measured by a radiochemical

method, using a thick target-thick catcher arrangement as well as a thin target - thin catcher arrangement. The ranges of neutron-deficient products are considerably lower than the ranges of neutron-excess products. There is a strong decreasing tendency for the kinetic energies of neutron-deficient isotopes if the bombarding energy is increased. The momentum spectra of neutron-deficient products are split up in a spallation-like and a fission-like contribution assuming that $\langle P \rangle / \sqrt{\Delta A}$ (mean momentum divided by the mass difference between target and product nucleus) is constant. The contribution of spallation is decreasing with increasing ΔA. The forward-to-backward ratio was used to calculate the average deposition energies of the fissioning nuclei. There is a strong dependence of the deposition energy on the N/Z value of the product with a slope of about - 750 MeV per unit change of N/Z.

MASS DISTRIBUTION IN LOW-ENERGY FISSION BY GAMMA ANALYSIS (SM-122/36)

A. Notea, D. Nir
Department of Nuclear Science,
TECHNION- Israel Institute of Technology, Haifa, Israel

Cumulative chain yields following low-energy fission have been determined by gamma-ray analysis using a calibrated Ge(Li) spectrometer. Gamma-ray spectra in the energy range 25 to 2200 keV were obtained from two days to one year after end of irradiation, and analysed to identify the gamma-ray emitters and determine their absolute intensities.

Relative chain yields were determined and confirmed for those chains in which two or more fission products were detectable, such as ^{95}Zr - ^{95}Nb, ^{135}I - ^{135}Xe, ^{140}Ba - ^{140}La, ^{144}Ce - ^{144}Pr. In these cases, and for nuclei emitting several gamma-rays, the relative intensities were determined and compared with other published data. In many cases our values show the smallest uncertainty and provide a better fit to the decay schemes.

The relative mass distributions are presented for thermal neutron fission of ^{233}U, ^{235}U and ^{239}Pu and reactor neutron fission of ^{232}Th. The yields are compared with suitably normalized radiochemical measurements. Agreement is good, with the exception of ^{103}Ru which is higher than the radiochemical yield value. The anomaly does not appear to be due to errors in either the measured data or the decay scheme.

The results obtained indicate the reliability and accuracy of the method for fission-product mass-distribution measurements. The method will be used for measurements of yield changes with fissionable nuclei excitation energy.

INDEPENDENT YIELDS AND DISTRIBUTIONS OF ISOTOPES OF Br, Kr, I AND Xe IN THERMAL NEUTRON FISSION OF ^{235}U STUDIED WITH AN ON-LINE SEPARATOR (SM-122/38)

S. Amiel, Ch. Braun, B. Ehrenberg, H. Feldstein, Y. Nir-El, M. Oron, E. Yellin
Nuclear Chemistry Department,
Soreq Nuclear Research Center, Yavne, Israel

The determination of yields of individual nuclides formed in fission and the measurement of their nuclear properties is being carried out with the aid of an electromagnetic mass separator. The separator is connected in an on-line mode with a target placed at an external neutron beam of a nuclear reactor. The measurements are performed by controlled neutron irradiations, very rapid chemical separations and transfer of a specific element for subsequent isotopic separation. Overall times of transfer and separation are of the order of one second. The experimental arrangement permits direct measurements of separated isotopes over a wide range of masses, on both sides of the Z_p line. Of great advantage is the possibility provided by this technique of obtaining in a single time-controlled irradiation a simultaneous determination of independent and fractional yields of an isotopic series.

The elements Br, I, Kr and Xe have been studied. Yields were determined by the assay of the individual isotopes or their descendents collected at various positions on an aluminium strip. These measurements were supplemented by direct on-line measurements of very short-lived activities to determine the halflives of the isotopes in question, their daughters and their precursors, and to evaluate the corrections required to compensate for decay and build-up during extraction, chemical separation, transfer and ion-source residence time. Selective recoil labelling was also employed in the determination of the independent yields.

The results for the independent fission yields of isotopes of elements at the asymmetric mass yield peaks in the thermal neutron fission of ^{235}U are presented. The shape of the independent isotopic distribution curves obtained in the present experiments points to the importance of nuclear structure effects in the yields from low-energy fission. The results are discussed in the light of the available experimental data on isobaric charge dispersions at various masses and the existing models of mass and charge distributions in fission.

Data relevant to the fission yields and nuclear properties of some nuclides for which little or no information has been published are given as well.

EMISSION OF K X-RAYS IN THE THERMAL FISSION OF ^{235}U (SM-122/42)

S.S. Kapoor, S.K. Kataria, S.R.S. Murthy, P.N. Rama Rao
Bhabha Atomic Research Centre, Trombay, Bombay, India

The yields of K X-rays emitted by fragments of specified nuclear charges have been determined in the thermal fission of ^{235}U. The X-ray energies were measured with a cooled lithium-drifted silicon detector having

an energy resolution equal to 0.88 keV FWHM at 26.25 keV. The fragments were detected in nearly 2π geometry by a semiconductor detector placed at a separation of 0.5 mm from the ^{235}U source coated on 7 mg/cm^2 aluminum backing. This arrangement was chosen to eliminate Doppler broadening of X-ray lines and uncertainties associated with solid angle of detection if X-rays were emitted from flying fragments. The spectrum of K X-rays in coincidence with fission were recorded on a 1024 channel analyser The solid angle of detection was experimentally determined by measuring the number of L X-rays per alpha in the decay of ^{234}U present in the source. The observed spectra were analysed by a least-square fitting code to determine the total number of K X-rays emitted per fission from fragments of different atomic numbers. In general, the X-ray yield per fragment is found to increase as one moves away from the closed shell regions of N = 50, Z = 50 and N = 82. A striking feature observed in the systematics of the X-ray yields is a significantly lower yield for xenon (even Z) as compared to the neighbouring odd Z products, and the absence of a spectacular increase in the yield beyond N = 88, as found earlier for ^{252}Cf case. The present results are discussed with regard to the characteristics of transitions leading to internal conversion and the possible effects of the initial spin of the fragments.

Experiments are in progress to determine also the K X-ray yields as a function of fragment mass. For this work, the foil-fragment detector assembly consists of two thin silicon semi-conductor detectors placed very close on either side of a thin ^{235}U foil. The kinetic energies of the pairs of fragments and the coincident K X-rays are recorded event by event using a multiparameter analyser. These results on the variation of K X-ray yield with mass will also be reported and discussed.

RANGES OF FISSION PRODUCTS IN SOLID MATERIALS (SM-122/46)

H. Muenzel
Institut für Radiochemie, Kernforschungszentrum Karlsruhe,
Federal Republic of Germany

The different empirical range-energy relations for fission products used in recoil work are compared with each other. In general, the standard deviations of the constants used are rather large and their dependence on the mass number A and atomic number Z of the ion are quite uncertain. Therefore a new range-energy relation was derived. First, the constants in an approximated theoretical expression for the specific energy loss due to ionisation were calculated by a least fit of known experimental data. Then using this equation and an expression for nuclear stopping given by Lindhard the dependence of the range (R) on energy (E), A and Z was calculated by numerical integration. The results were approximated by the formulas

$$R = \alpha E^{\beta} \qquad E < 2 \text{ MeV}$$
$$R = \alpha E^{\beta} + \gamma \qquad 2 < E < 40 \text{ MeV}$$
$$R = \alpha E^{\beta} \qquad 300 < E < 100 \text{ MeV}$$

for light absorber materials, e.g. Al, the new range-energy relation agrees very well with experimental data. However, in the case of heavy absorber materials, e.g. U, there is a systematic deviation of several per cent.

THE RANGES AND ENERGIES OF FRAGMENTS FROM SPONTANEOUS FISSION OF ^{252}Cf (SM-122/49)

N.K. Aras, E.N. Caner, O. Birgül
Department of Chemistry,
Middle East Technical University, Ankara, Turkey *

The ranges and energies of fragments from spontaneous fission of ^{252}Cf. The average ranges of fragments from spontaneous fission of ^{252}Cf were measured in aluminium by stopping the fission fragments in foils. Specific fission products were chemically separated from the various foils and their radiations counted. The following range values were obtained in mg Al/cm^2:

^{99}Mo : 3.83 ± 0.07	^{115}Cd : 3.61 ± 0.02
^{111}Ag : 3.66 ± 0.04	^{131}I : 3.42 ± 0.12
^{113}Ag : 3.62 ± 0.07	^{140}Ba : 3.03 ± 0.04

The fragment ranges were converted to energies using range-energy relations of Lindhard, Scharff and Schiott. This conversion takes into account contributions from both electronic and nuclear stopping of the fragments in aluminium.

Modifications were made in the electronic stopping part of the equation, in order to obtain an agreement with the experimentally measured kinetic energies of Schmitt et al. For some fragments, the most probable charge, Z_p, and number of neutron emitted, ν_A, for a given mass number, A, are not well known and there are large differences between values determined by different workers. Therefore, in this calculation different sets of Z_p and ν_A values were used and comparisons made.

The agreement between experimentally measured and calculated kinetic energies was good. However, the prediction of specific energy loss in aluminium as a function of energy by Lindhard et al. is not accurate in the electronic-stopping region.

* This work was supported in part by the Turkish Atomic Energy Commission.

DETERMINATION OF THE NEUTRON FISSION MASS-YIELD-CURVES FOR 241 AND 242m AMERICIUM (SM-122/72)

W. Weinlaender
Institut für Radiochemie der Technischen Hochschule München, Garching bei München, Federal Republic of Germany

For the americium isotopes ^{241} and ^{242}m the mass yield curve for thermal neutron fission is determined. The yield of the main fission products is measured by direct gamma spectroscopy with lithium-drifted germanium detectors of the irradiated sample and compared with the yields of these elements from ^{239}Pu neutron fission. Some of the elements with lower yield are separated by ion-exchange methods before measurement. The mass-yield-curves found for 241 and 242m americium are compared with those of the neighbouring nuclides.

MESURE SIMULTANEE DE L'ENERGIE CINETIQUE ET DE LA CHARGE DES FRAGMENTS DE FISSION DE ^{235}U (SM-122/79)

H. Nifenecker, J. Poitou, M. Ribrag
Service de la Métrologie et de la Physique Neutroniques Fondamentales, Centre d'Etudes Nucléaires de Saclay, France

Une étude approfondie de la méthode de détermination des distributions de charge des produits de fission par la mesure de leur émission de rayonnement X a été entreprise. On a mesuré la constance de temps de décroissance de l'émission X en fonction de la charge des fragments. On peut ainsi tenir compte exactement des modifications des fonctions de réponse du détecteur du rayon X dues à l'effet Doppler. Compte tenu de ces améliorations dans l'analyse des résultats expérimentaux, on détermine la distribution de charge des fragments de masse donnée. Les résultats sont discutés. On étudie également cette distribution de charge pour diverses valeurs de l'énergie cinétique totale des fragments et on discute les effets d'appariement dans les distributions de charge.

English translation of the preceding Abstract (SM-122/79):

THE SIMULTANEOUS MEASUREMENT OF THE KINETIC ENERGY AND CHARGE OF ^{235}U FISSION FRAGMENTS

A detailed study of the method of determining charge distributions in fission products by measuring their X-ray emission was undertaken. The time constant of the decrease of X-ray emission was measured as a function of the fragment charge. The changes in the X-ray detector's response function due to the Doppler effect could thus be accurately taken into account. With these improvements in the analysis of experimental results, the authors determine the charge distribution in fragments of a given mass, and discuss the results. A study is also made of this charge distribution for various values of the total kinetic energy of the fragments, and the pairing effects in charge distribution are discussed.

ETUDE DE LA FISSION SPONTANEE DE QUELQUES NOYAUX LOURDS (SM-122/83)

M. Monnin, B. Tamain
Laboratoire de Physique Nucléaire,
Faculté des Sciences, Clermont-Ferrand, France

Les périodes de fission spontanée des éléments ^{232}U, ^{233}U, ^{235}U, ^{238}U, ^{232}Th sont mesurées ou majorées à l'aide des détecteurs solides de traces.

Dans le cas des isotopes de masses 232 et 238 de l'uranium, les longueurs des traces des deux fragments émis en corrélation permettent une détermination de la distribution en masse.

English translation of the preceding Abstract (SM-122/83):

STUDY OF THE SPONTANEOUS FISSION OF SOME HEAVY NUCLEI

The spontaneous fission half-lives of the elements ^{232}U, ^{233}U, ^{235}U, ^{238}U and ^{232}Th have been measured or increased with the help of solid track detectors.

In the case of uranium isotopes of mass 232 and 238, the track lengths of the two fragments emitted in correlation make it possible to determine the mass distribution.

FISSION DE ^{238}U ET DE ^{239}PU A MOYENNE ENERGIE. DETERMINATION SEMI-EXPERIMENTALE DE LA DISTRIBUTION EN MASSES (SM-122/94)

F. Communeau, A. Moussá
Commissariat à l'Energie Atomique,
C.E. Bruyéres-le-Châtel et C.E.N. Grenoble, France

Des cibles d'uranium et de plutonium ont été soumises à un flux de neutrons de moyenne énergie issus de réactions (D, T). Plusieurs irradiations ont été effectuées correspondant à des temps de quelque 10 heures et à des flux intégrés de neutrons de 1, 5 à 3×10^{15} environ en 4n. Le nombre de fissions obtenues dans l'échantillon variait de 1 à 4×10^{12}. Chaque cible est mise en solution et les éléments suivants sont séparés: strontium, yttrium, zirconium, molybdène, palladium, argent, cadmium, baryum, lanthane, cèrium, praséodyme, néodyme, europium, samarium. Le rendement de la séparation chimique est mesuré. Les mesures effectuées par spectroscopie gamma et beta portent sur un (ou deux) éléments des chaînes 89, 91, 93, 95, 97, 99, 109, 111, 112, 115, 140, 141, 143, 144, 147, 153, 156. Diverses corrections sont apportées aux résultats bruts pour tenir compte notamment des facteurs de géométrie, de l'épaisseur des sources, des décroissances entre irradiation et séparation chimique et entre séparations et mesures. Pour une irradiation, les différents nombres d'atomes trouvés sont rapportés à l'un d'eux (^{95}Zr ou ^{147}Nd). Ensuite, et pour chaque masse, les divers résultats donnent lieu à une pondération tenant compte des sources d'erreurs recensées. Pour les masses dont les rendements relatifs ont été ainsi mesurés, les masses "complémentaires" sont calculées à partir de courbes $\nu = f(A)$; la contribution des divers processus de

fission est évaluée à partir de considérations semi-expérimentales. La courbe d'ensemble sinsi déterminée est ajustée de façon à normaliser à 200 l'aire délimitée par le tracé. Les résultats ainsi obtenus, affectés d'une erreur calculée et d'une erreur estimée sont comparés aux valeurs publiées.

English translation of the preceding Abstract (SM-122/94):

MEDIUM-ENERGY NEUTRON-INDUCED FISSION OF ^{238}U AND ^{239}Pu. SEMI-EXPERIMENTAL DETERMINATION OF MASS DISTRIBUTION

Uranium and plutonium targets were subjected to a flux of neutrons of average energy from (D, T) reactions. Several irradiations were made, representing times of some 10 hours, at integrated neutron fluxes of about 1.5 to 3×10^{15} in 4π geometry. The number of fissions obtained in the sample varied from 1 to 4×10^{12}. Each target is immersed in solution and the following elements are separated: strontium, yttrium, zirconium, molybdenum, palladium, silver, cadmium, barium, lanthanum, cerium, praseodymium, neodymium, europium and samarium. The chemical separation yield is measured. The measurements made by gamma- and beta-spectroscopy are for 1 (or 2) elements in the chains 89, 91, 93, 95, 97, 99, 109, 111, 112, 115, 140, 141, 143, 144, 147, 153, 156. Various corrections are applied to the crude results in order to take account, inter alia, of geometrical factors, source thickness, and decay between irradiation and chemical separation and between separation and measurements. For a particular irradiation, the different numbers of atoms found are elated to one of them (^{95}Zr or ^{147}Nd). A weighting factor for each mass is then applied in respect of the various results obtained, account being taken of the sources of errors recorded. For the masses whose relative yields have thus been measured, the "complementary" masses are calculated from $\nu = f(A)$ curves; the contribution of the various fission processes is evaluated from semi-experimental considerations. The overall curve thus determined is adjusted so as to standardize the area plotted to 200. The results obtained, which bear a calculated error and an estimated error, are compared with the published values.

RADIOCHEMICAL STUDIES IN THE SYMMETRIC REGION OF ^{235}U FISSION (SM-122/115)

H. V. Weiss, N. E. Ballou, J. L. Elzie, J. M. Fresco
Naval Radiological Defense Laboratory,
San Francisco, California, USA

As part of a study on the distribution of nuclear charge in the region of symmetric fission of ^{235}U with thermal neutrons, ^{118}Pd was identified and its cumulative fractional chain yield was determined. The Pd was isolated free from Ag and Cd at different times after fission, and the quantity of descendant ^{118}Cd activity produced was measured. A half-life of 3.1 ± 0.3 s was derived from these data. Through a comparison of the ^{118}Cd activity produced by ^{118}Pd with the total ^{118}Cd activity produced by all isobars, a cumulative fractional chain yield of 0.29 ± 0.03 was computed for ^{118}Pd.

By the rapid separation of Ag after irradiation and subsequent measurement of the respective Cd daughter activity, the fractional independent yields of ^{117}Ag and ^{118}Ag were also measured. These values are 0.35 ± 0.05 and 0.55 ± 0.10, respectively. The width-parameter, σ, for the Gaussian distribution of nuclear charge was computed to be 0.65 for the 118-mass chain. The most probably nuclear charge (Z_p) was estimated to be 46.22 ± 0.17 and 46.88 ± 0.12 for mass 117 and 118, respectively.

Also a procedure was developed to determine the half-life of ^{115m}Ag. Ag was separated from the Pd precursor and Cd descendant within 1 s after neutron irradiation of ^{235}U. The separation was accomplished by the deposition of fission-formed Ag from solution onto finely divided copper powder; the interfering elements passed through the copper bed. At various times after the Ag separation, the Cd daughter products formed were quantitatively stripped from the Ag parent. The various fractions collected were radiochemically purified and analysed for 2.3 - d ^{115m}Cd. The contribution of each of two ^{115}Ag isomers to the ^{115m}Cd activity was resolved. From these data the half-life derived for ^{115m}Ag was $55.0 \left({+2.4 \atop -1.5} \right)$ s.

MASS-ENERGY CORRELATIONS IN THE 7-to 13-MeV PROTON-INDUCED FISSION OF Th, U, AND Pu ISOTOPES* (SM-122/126)

R.L. Ferguson, S.C. Burnett, F. Plasil, F. Pleasonton, H.W. Schmitt
Oak Ridge National Laboratory, Oak Ridge, Tenn. USA

Measurements have been made of correlated fragment kinetic energies for proton-induced fission of ^{232}Th, ^{233}U, ^{235}U, ^{238}U and ^{239}Pu. In the proton energy range 7 - 13 MeV, results were obtained for ^{238}U at fifteen bombarding energies, for ^{235}U at seven, for ^{233}U at five, for ^{232}Th at four, and for ^{239}Pu at three energies. Fifty thousand to one hundred thousand events were analysed in most of the experiments.

Silicon surface barrier detectors were used to determine the kinetic energies of correlated pairs of fission fragments from thin deposits of fissile materials which were bombarded by protons at the ORNL tandem accelerator. Since one of the objectives of this work was to compile a set of self-consistent results for a wide range of fissioning systems, experimental conditions and procedures were as nearly uniform as practicable for all cases. The data were transformed to give fragment mass and kinetic energy distributions and their correlations. In the three cases for which information on fragment neutron emission was available, the average mass and kinetic energy distribution were corrected for the effects of neutron emission.

General characteristics of all the distributions obtained were observed to be qualitatively similar, but striking differences were found in certain quantitative aspects. Although asymmetric fission was observed to predominate in all the systems investigated, the contribution from symmetric

* Research sponsored by the US Atomic Energy Commission under contract with the Union Carbide Corporation.

mass division was found to become more important as bombarding energies were increased. For ^{232}Th a third peak, corresponding to symmetric mass division, was observed at proton energies of 0.25 MeV and greater. Despite a careful search in the case of ^{238}U, no evidence was found for steps in the mass distribution peak-to-valley ratio as a function of proton energy. Overall widths of the mass distributions were little affected by changes in bombarding energy. In general, the average total fragment kinetic energy $\overline{E}_K$ was observed to decrease $\sim$1-2 MeV with increasing bombarding energy over the range studied. In every case the graph of $\overline{E}_K$ versus fragment mass exhibited a peak in the region of heavy fragment mass $\sim$132 and a dip of $\sim$10-20 MeV at symmetric mass division.

КИНЕТИЧЕСКАЯ ЭНЕРГИЯ ОСКОЛКОВ И ЭНЕРГЕТИЧЕСКИЙ БАЛАНС ПРИ ДЕЛЕНИИ ^{235}U НЕЙТРОНАМИ ЭНЕРГИЙ В ИНТЕРВАЛЕ 0-0,6 Мэв (IAEA-SM-122/137)

П.П. Дьяченко, Б.Д. Кузьминов
Физико-энергетический институт, Обнинск,
Союз Советских Социалистических Республик
А. Лайтаи
Центральный институт физических исследований, Будапешт,
Венгерская Народная Республика

В работе выполнены относительные измерения средней кинетической энергии осколков с точностью ± 100 кэв при делении ^{235}U нейтронами с энергией 0-0,6 Мэв.
Обсуждается влияние изменений распределения зарядов и масс осколков на кинетическую энергию и на среднее число нейтронов деления.

English translation of the preceding Abstract (SM-122/137):

FRAGMENT KINETIC ENERGY AND ENERGY BALANCE IN THE 0-0.6 MeV NEUTRON-INDUCED FISSION OF ^{235}U

The authors carried out relative measurements with an accuracy of 100 keV on the mean kinetic energy of 0-0.6 MeV neutron-induced fission fragments of ^{235}U.
They discuss the effect of variations in the charge and mass distribution of the fragments on the kinetic energy and the mean number of fission neutrons.

DETERMINATION PAR SPECTROMETRIE DE MASSE EN LIGNE DE LA DISTRIBUTION ISOTOPIQUE DU RUBIDIUM ET DU CESIUM PRODUITS AU COURS DE LA FISSION A BASSE, MOYENNE ET HAUTE ENERGIE (SM-122/141)

J. Chaumont, E. Roeckl, Y. Nir-El, R. Klapisch
CSNSM, Orsay et IPN Orsay, France

La méthode du spectromètre de masse en ligne que nous avions décrite par ailleurs a été appliquée à la détermination des rendements indépendants de produits de fission alcalins des systémes fissionants suivants: ^{235}U + n

thermiques, ^{238}U et Th par protons de 150 MeV, ^{238}U, Th et Ta par protons de 24 GeV.

La cible est constituée par une couche d'uranium ou de thorium de 1 à 2 mg cm^{-2} déposée sur une vingtaine de plaquettes de graphite de 70 à 80 μm. L'ensemble, enveloppé dans une nacelle en tantale mince est porté à une température de 1800°C. Les fragments de fission sont arrêtès dans le graphite et, comme nous le montrons, les éléments alcalins en ressortent très rapidement par diffusion. Sur la surface de tantale chaude, les isotopes de Rb et Cs sont ionisés sélectivement en raison de leur faible potentiel d'ionisation. L'analyse en masse des ions réaccélérés est effectuée par un spectromètre de masse à secteur magnétique de 90° d'un pouvoir de résolution $\Delta M/M = 1/200$ (à 1% du pic) assurant une résolution complète des isotopes du Rb et Cs. Le comptage des ions est effectué par un multiplicateur d'électrons et les spectres de masse enregistrés à l'aide d'un analyseur multiéchelle.

La méthode permet de mesurer aussi bien des isotopes stables que ceux de très courtes périodes (100 millisecondes pour ^{97}Rb). La limite de sensibilité dans les conditions usuelles est d'environ 10 μb.

A basse énergie, l'irradiation dans un flux de 10^8 n cm^{-2} s^{-1} au réacteur EL 3 de Saclay a permis de mesurer les Rb de (A= 89 à A=97) et les Cs de (A=139 à A=145). Les distributions sont approximativement gaussiennes et sont centrées respectivement sur A=92, pour Z=37 (Rb) et A=141 pour Z=55 (cs). On en déduit, pour ces fragments complémentaires, une valeur moyenne du nombre de neutrons émis qui confirme les résultats obtenus par d'autres méthodes.

Les distributions isotopiques qui s'élargissent à moyenne énergie (150 MeV), s'étendent à haute énergie (10 et 24 GeV) beaucoup plus loin du côté des isotopes déficients en neutrons qu'il n'avait pas été possible de le montrer expérimentalement jusqu'ici. La comparaison entre des cibles de Ta, Th et U permet de discuter les contributions respectives de fission à haute énergie et de spallation.

English translation of the preceding Abstract (SM-122/141):

DETERMINATION BY ON-LINE MASS SPECTROMETRY OF THE ISOTOPIC DISTRIBUTION OF RUBIDIUM AND CAESIUM PRODUCED DURING LOW, MEDIUM AND HIGH ENERGY FISSION

The on-line mass spectrometric method described by us elsewhere was used to determine the independent yields of alkaline fission products of the following fissioning systems: ^{235}U + thermal n, ^{238}U and Th by 150 MeV protons, ^{238}U, Th and Ta by 24 GeV protons.

The target consists of a 1 to 2 mg/cm^2 layer of uranium or thorium deposited on some 20 small graphite plates of 70-80 μm. The assembly, located in a thin tantalum container, is heated to a temperature of 1800°C. The fission fragments are stopped by the graphite and, as is shown in the paper, the alkaline elements escape very quickly by diffusion. On the surface of the hot tantalum the Rb and Cs isotopes are ionized selectively because of their weak ionization potential. Mass analysis of the re-accelerated ions is carried out with a mass spectrometer with an angle of 90° and a resolving power of $\Delta M/M = 1/200$ (at 1% of the peak), ensuring complete resolution of the Rb and Cs isotopes. The ions are counted with an electron multiplier and the mass spectra are recorded by means of a multi-channel analyser.

The method can be used for the measurement of both stable isotopes and very short-lived isotopes (100 ms for ^{97}Rb). The sensitivity limit under the usual conditions is about 10 μb.

At low energy, irradiation in a flux of 10^8 n cm^{-2} s^{-1} in the EL3 reactor at Saclay permitted measurements of A=89 to A=97 for Rb and A=139 to A=145 for Cs. The distributions are approximately Gaussian and are centred on A=92.3 for Z=37 (Rb) and A=141 for Z=55 (Cs).

For these complementary fragments an average value of the number of neutrons emitted has been deduced, confirming the results obtained by other methods.

The isotopic distributions, which broaden at medium energy (150 MeV), extend at high energy (10 and 24 GeV) much further in the neutron-deficient direction than could be shown experimentally hitherto. Comparison of Ta, Th and U targets makes it possible to discuss the respective contributions of high-energy fission and spallation.

CHARGE DISTRIBUTION IN THE SYMMETRIC REGION OF HIGH ENERGY PROTON INDUCED FISSION OF URANIUM (SM-122/143)

E. Hagebø
CERN, Geneva, Switzerland

As a continuation of the studies in high-energy proton-induced fission at CERN, some yields of indium and tin isotopes from the fission of uranium with 570 MeV and 18.2 GeV protons are reported. The yields have been determined by conventional radiochemical methods including the use of an electromagnetic isotope separator.

These yields are used together with published yields of isotopes of other elements in the same mass region to construct charge dispersion curves for A = 117. The charge dispersion curve at 18.2 GeV is double-humped, and one of the two parts is identical in form and position to the 570 MeV.

Also Z_p, the most probable charge for each mass number, as well as the width of the charge dispersion curve as a function of fission product mass and of proton energy has been established.

Although Z_p moves slightly with energy below 570 MeV, it seems that in the symmetric fission region the width of the charge dispersion curve is independent of mass number and proton energy.

О РАСПРЕДЕЛЕНИИ ЭНЕРГИИ ВОЗБУЖДЕНИЯ МЕЖДУ ОСКОЛКАМИ ДЕЛЕНИЯ (IAEA-SM-122/144)

М.В. Блинов, Н.М. Казаринов, И.Т. Крисюк, С.С. Коваленко
Институт атомной энергии им. И.В.Курчатова, Москва,
Союз Советских Социалистических Республик

Путем регистрации совпадений между нейтронами, испускаемыми легким и тяжелым осколками в случае деления ^{235}U тепловыми нейтронами, определена величина $<\nu_\lambda \nu_T>$, $\frac{M_1}{M_2}$, $E_к$. Эта же величина была рассчитана с использованием литературных

данных по зависимости $\nu(M)$, $\frac{\delta\nu}{\delta E^*}$ (M), W(E), W(M). Экспериментальное значение $<\nu_\lambda\ \nu_T>$ близко к рассчитанному, хотя и несколько меньше. Разница в этих величинах может быть связана с эффектом перераспределения энергии возбуждения между осколками при фиксированных значениях M и $E_к$.

English translation of the preceding Abstract (SM-122/144)

EXCITATION ENERGY DISTRIBUTION IN FISSION PRODUCTS

By recording coincidences between neutrons emitted by light and heavy fragments in the fission of ^{235}U by thermal neutrons, the authors determine the value of $\langle \nu_\lambda \nu_T \rangle$, M_1/M_2, E_k. This value is calculated using data from the literature regarding the functions of ν (M), $\delta\nu/\delta E^*$(M), W(E), W(M). The experimental value of $\langle \nu_\lambda \nu_T \rangle$ is close to the calculated value but somewhat lower. The difference between these two values may be due to the redistribution of excitation energy between fragments at fixed values of M and E_k.

ЗАВИСИМОСТЬ ВЕЛИЧИНЫ АНИЗОТРОПИИ ИСПУСКАНИЯ НЕЙТРОНОВ ДЕЛЕНИЯ ОТ ПОЛНОЙ КИНЕТИЧЕСКОЙ ЭНЕРГИИ ОСКОЛКОВ

(IAEA-SM-122/145)

М.В. Блинов, Н.М. Казаринов, И.Т. Крисюк, А.Н. Протопопов
Институт атомной энергии им. И.В.Курчатова, Москва,
Союз Советских Социалистических Республик

Измерена зависимость среднего числа нейтронов деления от полной кинетической энергии осколков для случая деления ^{235}U тепловыми нейтронами. Измерения проводились для двух углов вылета нейтрона (0° и 90°). Суммарная энергия осколков определялась двумя полупроводниковыми счетчиками, а нейтроны регистрировались сцинтилляционным счетчиком. Отделение нейтронов от γ-квантов производилось по времени пролета. Получена зависимость величины угловой анизотропии вылета нейтронов от полной кинетической энергии осколков. Проведены расчеты по модели испарения нейтронов из возбужденных осколков. Результаты работы обсуждаются с точки зрения возможности существования дополнительного механизма эмиссии нейтроиов деления.

English translation of the preceding Abstract (SM-122/145)

DEPENDENCE OF ANISOTROPY OF EMITTED NEUTRONS ON TOTAL KINETIC ENERGY OF FRAGMENTS

The authors measured the dependence of the mean number of fission neutrons on the total kinetic energy of the fragments in the thermal neutron-induced fission of ^{235}U. The measurements were performed for two neutron ejection angles (0° and 90°). The total fragment energy was determined by two semi-detector counters, while the neutrons were recorded by a scintillation counter. The neutrons were separated from the gamma quanta by the time-of-flight method. The authors determined the angular anisotropy of neutron ejection as a function of the total kinetic energy of the fragments. The calculations were performed according to the model which postulates the boiling-off of neutrons from excited fragments. The results obtained are discussed with special reference to the question whether there can be an additional mechanism for the emission of fission neutrons.

О ТОНКОЙ СТРУКТУРЕ ВЫХОДОВ ОСКОЛКОВ ПРИ ДЕЛЕНИИ ТЯЖЕЛЫХ ЯДЕР (IAEA-SM-122/147)

И.А. Баранов, А.Н. Протопопов, Б.М. Ширяев
Союз Советских Социалистических Республик

С помощью полупроводниковых кремниевых счетчиков измерены спектры кинетической энергии осколков, совпадающих с парными осколками определенной заданной энергии $E_к$. Величина $E_к$ бралась различной в интервале от 60 до 112 Мэв.

Для случаев, когда $E_к > 100$ Мэв, полученные спектры обнаруживают тонкую структуру величины выходов осколков в зависимости от энергии (или массового числа) осколка. Для малых $E_к$ спектры представляют собой одиночные пики, что не согласуется с данными работы [1].

Анализ данных по тонкой структуре выходов показывает, что для больших $E_к$ имеет место корреляция между величиной выходов осколков и конечной энергией возбуждения осколков, в то время как для малых $E_к$ такая корреляция отсутствует. С точки зрения статистической модели Эриксона [2] качественно это может быть объяснено влиянием проницаемости потенциального барьера для осколков на величину выхода. Однако подсчеты выходов осколков по упомянутой модели с учетом влияния проницаемости барьера параболической формы для распределений с некоторыми фиксированными $E_к$ дают результаты, не согласующиеся с экспериментальными распределениями.

Подсчет конечной энергии возбуждения осколков при делении составных ядер различной четности показывает, что структура в энергии возбуждения осколков наиболее четко проявляется для четно-нечетных составных ядер и отсутствует у нечетно-нечетных ядер. Из анализа энергии возбуждения для различных ядер и экспериментальных данных по тонкой структуре делается предположение о преимущественном влиянии на структуру характера разделения заряда между осколками.

ЛИТЕРАТУРА

[1] ANDRITSOPOLOUS, G., Nucl.Phys. A 94 (1967) 537.
[2] ERICSON, T., Advan.Phys. 9 (1960) 36.

English translation of the preceding Abstract (SM-122/147)

FINE-STRUCTURE OF FRAGMENT YIELDS IN FISSION OF HEAVY NUCLEI

Semi-conductor silicon counters were used to measure the kinetic-energy spectra of fragments coinciding with pairs of fragments of a given fixed energy E_k. Different values of E_k were selected between 60 and 112 MeV. Where E_k is greater than 100 MeV the spectra obtained reveal fine-structure of fragment yields depending on the energy (or mass number) of the fragment. At low E_k-values the spectra are separate peaks, which does not agree with the findings of Andritsopolous.

Analysis of the data on the fine-structure of yields shows that at high E_k-values there is correlation between the fragment yields and the final excitation of the fragments, while at low E_k-values no such correlation is found. From the viewpoint of Ericson's statistical model this could be explained qualitatively by the fact that yield is influenced by the extent to which the potential barrier is penetrable by fragments. However, rough calculations made of fragment yields using this model and taking into account the effect of penetrability of a barrier of parabolic shape for distributions with certain fixed values of E_k give results which do not accord with the experimental distribution.

Calculation of the final excitation energy of fragments in the fission of compound nuclei differing in parity shows that the fragment excitation energy displays structure most clearly in the case of even-odd nuclei while no structure is to be seen in the case of odd-odd nuclei. From an analysis of the excitation energy for different nuclei and the experimental data on fine-structure the authors suggest that structure depends primarily on the character of charge dispersion between the fragments.

АНОМАЛЬНОЕ УГЛОВОЕ РАСПРЕДЕЛЕНИЕ ОСКОЛКОВ ДЕЛЕНИЯ ^{226}Ra НЕЙТРОНАМИ С ЭНЕРГИЕЙ 14÷16 Мэв (IAEA-SM-122/148)

Ю.А. Бабенко, Ю.А. Немилов, Ю.А. Селицкий, Л.А. Плескачевский, В.Б. Фунштейн
Союз Советских Социалистических Республик

Деление ядер тяжелее тория в случае возбуждений, превышающих барьер деления на несколько Мэв, обычно характеризовалось угловыми распределениями типа $\sigma(\theta) = a + b\cos^2\theta$. В работе [1] был обнаружен случай отклонения от этой закономерности, когда ^{226}Ra делился нейтронами с энергией 14,6 Мэв. С целью исследования причины увеличенного выхода осколков под углом 60° к направлению облучающих радий нейтронов были сняты угловые распределения и сечения деления при больших энергиях нейтронов, до $E_n = 20$ Мэв. Оказалось, что аномальное распределение с дополнительным максимумом под углом 60° исчезает при $E_n > 16$ Мэв. Одновременно с этим анизотропия уменьшается до значений ~1,1. Сечение деления в области $E_n = 13 \div 20$ Мэв в пределах точности ±7% не проявляет отклонений от плавного роста. По-видимому, аномальность в угловом распределении осколков возникает только при нейтронном облучении, т.к. проверка деления ^{226}Ra дейтронами с аналогичным возбуждением привела к обычным распределениям.

ЛИТЕРАТУРА

[1] БАБЕНКО, Ю.А., НЕМИЛОВ, Ю.А., СЕЛИЦКИЙ, Ю.А., ФУНШТЕЙН, В.Б., Ядерная физика 4 (1968) 269.

English translation of the preceding Abstract (SM-122/148)

ANOMALOUS ANGULAR DISTRIBUTION OF FRAGMENTS IN FISSION OF ^{226}Ra BY NEUTRONS IN ENERGY REGION 14-16 MeV

The fission of nuclei heavier than thorium in the event of excitations several MeV above the fission barrier has normally been characterized by angular distributions of the type $\sigma(\theta) = a + b\cos^2\theta$. Babenko et al. (1968) found a case of divergence from this law, in the 14-MeV neutron-induced fission of ^{226}Ra. To study the reason for the increased fragment yield at an angle of 60° to the direction of bombarding-neutron incidence, the authors took the angular distributions and fission cross-sections for higher neutron energies, up to 20 MeV. It was found that the anomalous distribution with an additional peak at an angle of 60° disappears when the neutron energy exceeds 16 MeV. At the same time the anisotropy drops to a value of about 1.1. The fission cross-section in the neutron energy range from 13 to 20 MeV does not, to within ± 7%, show any deviations from a smooth growth curve. The anomaly in the angular distribution of fragments evidently arises only in the case of neutron irradiation, since a cross-check with the deuteron-induced fission of ^{226}Ra at similar excitation levels resulted in the normal distribution patterns.

УГЛОВАЯ АНИЗОТРОПИЯ ОСКОЛКОВ ПРИ ДЕЛЕНИИ ^{226}Ra НЕЙТРОНАМИ С ЭНЕРГИЕЙ 4÷9 Мэв (IAEA-SM-122/149)

Ю.А. Бабенко, В.Т. Ипполитов, Ю.А. Немилов, Ю.А. Селицкий, В.Б. Фунштейн
Союз Советских Социалистических Республик

Измерены угловые распределения осколков делений ^{226}Ra нейтронами с энергией 4÷9 Мэв. Форма распределений во всех случаях согласуется с предсказаниями статистической теории Халперна-Струтинского. Интересен тот факт, что при E_n = 4,7÷7,1 Мэв анизотропия постоянна и имеет весьма большую величину (A = 1,5). Вычисление дисперсии(K_0^2) проекции углового момента на приближенную ось симметрии ядра дает при E_n = 6,2÷7,1 Мэв значение K_0^2 = 8 - 10. Это приблизительно в два раза меньше значений K_0^2 для более тяжелых ядер при соответствующей энергии возбуждения над порогом [1] и в точности соответствует значению Гриффина [2] для дисперсии, определяемой лишь моментом неспаренной частицы. Делается вывод о значительном увеличении энергии спаривания в седловой точке ^{227}Ra.

ЛИТЕРАТУРА

[1] LO-NIGRO, S., MILONE, C., N.Phys. A 96 (1967) 617.
[2] GRIFFIN, J., Phys. Rev. 132 (1963) 2204.

English translation of the preceding Abstract (SM-122/149)

ANGULAR ANISOTROPY OF FRAGMENTS IN FISSION OF ^{226}Ra BY NEUTRONS IN ENERGY REGION 4-9 MeV

The authors measured the angular distributions of fission fragments from 4-9 MeV neutron-induced fission of ^{226}Ra. The shape of the distributions in all cases agrees with the predictions of the Halpern-Strutinsky statistical theory. It is interesting that when E_n is between 4.7 and 7.1 MeV the anisotropy is constant and has a very high value (A = 1.5). Calculations of the dispersion (K_0^2) of the projection of the angular momentum on the approximate symmetry axis of the nucleus gives a K_0^2 value of between 8 and 10 when E_n is between 6.2 and 7.1 MeV. This is approximately half the K_0^2 values for heavier nuclei at a corresponding excitation energy above the threshold, and corresponds exactly to Griffin's value for dispersion determined solely by the momentum of the unpaired particle. These results seem to point to a considerable increase in the pairing energy at the saddle point of ^{227}Ra.

ТРЕХПАРАМЕТРОВЫЕ ИЗМЕРЕНИЯ СПОНТАННОГО ДЕЛЕНИЯ ^{244}Cm (IAEA-SM-122/150)

И.Д. Алхазов, С.С. Коваленко, О.И. Косточкин, Л.З. Малкин, К.А. Петржак, В.И. Шпаков
Союз Советских Социалистических Республик

С помощью полупроводниковых детекторов и нейтронного жидкостного сцинтилляционного счетчика выполнены измерения кинетических энергий двух осколков и числа мгновенных нейтронов в одном акте деления ^{244}Cm.

Рассчитаны с помощью ЭВМ Минск-22 контурные диаграммы в системе координат энергий обоих осколков, контурные диаграммы в координатах отношение масс—суммариая кинетическая энергия как для случаев испускания различного числа нейтронов, так и для

суммы всех случаев. На их основе построены спектры суммарной кинетической энергии и кинетической энергии одного из осколков, массовое распределение осколков деления ^{244}Cm. Для средней суммарной кинетической энергии получена величина, равная (188,6 ± 1,6) Мэв. Средние массы легкого и тяжелого осколков равны 104,6 ± 1,0 и 139,0 ± 1,4 массовых единиц.

Получены также контурная диаграмма распределения среднего числа мгновенных нейтронов и контурная диаграмма энергии возбуждения (с точностью до энергии γ - квантов) в системах координат кинетических энергий осколков и отношение масс—суммарная кинетическая энергия.

Построены зависимости суммарной кинетической энергии и кинетической энергии одного осколка от отношения масс, средних масс от суммарной кинетической энергии, зависимости числа мгновенных нейтронов от суммарной кинетической энергии для различных отношений масс и от отношения масс для различных значений суммарной кинетической энергии, зависимость средней энергии, затрачиваемой на испускание одного нейтрона, от отношения масс и другие.

Производилось определение величины аппаратурной дисперсии, получена зависимость ядерной дисперсии от отношения масс.

English translation of the preceding Abstract (SM-122/150)

THREE-PARAMETER MEASUREMENTS OF SPONTANEOUS FISSION OF ^{244}Cm

The authors used semi-conductor detectors and a neutron liquid scintillation counter to measure the kinetic energies of two fragments and the number of prompt neutrons in fission of a single ^{244}Cm nucleus.

A Minsk-22 digital computer was used to compute the contour diagrams in a system of co-ordinates representing the energies of both fragments and in co-ordinates representing the mass ratio and the total kinetic energy both for cases where various numbers of neutrons were emitted and for the sum of all cases. These diagrams were used to obtain the spectra for the total kinetic energy and the kinetic energy of one of the fragments and the mass distribution of ^{244}Cm fission fragments. The mean total kinetic energy was found to be equal to 188.6 ± 1.6 MeV. The average masses of the light and heavy fragments are 104.6 ± 1.0 and 139.0 ± 1.4 mass units, respectively.

The authors also obtained contour diagrams showing the distribution of the mean number of prompt neutrons and the excitation energy (accurate to within the energy of the gamma quanta) in co-ordinate systems representing the kinetic energies of the fragments and the mass ratio and total kinetic energy.

They then plotted the total kinetic energy and the kinetic energy of one fragment as a function of mass ratio, the average masses as a function of total kinetic energy, the number of prompt neutrons as a function of total kinetic energy for various ratios and as a function of mass ratio for various total kinetic energy values, the mean energy consumed per neutron emitted as a function of mass ratio and so on.

They also determined the extent of dispersion due to the apparatus and calculated the dependence of nuclear dispersion on mass ratio.

TRANSMISSION MEASUREMENTS OF ^{235}U FISSION FRAGMENTS IN Mg, Al, Fe, Ni, Ag (SM-122/154)

V. Aiello, G. Maracci, F. Rustichelli
EURATOM, ISPRA, Italy.

Transmission measurements of the fission fragments arising in ^{235}U thermal-neutron-induced fission were performed by irradiating a back-to-back fission chamber in the thermal column of the RB-2 reactor of Montecuccolino (Bologna) Italy. The back-to-back fission chamber is a gas-flow counter utilizing argon containing 2 per cent nitrogen. The electrode spacing was 10 mm and the gas pressure was adjusted slightly above ambient pressure. The operating voltage was 100 V positive applied to each anode. The source of fission fragments consists of a thin layer of natural uranium ($\sim 0.2 mg/cm^2$) evaporated under vacuum on a Pt disc. This uranium deposit is located in one of the two fission chambers of the counter. Irradiations were made in a neutron flux of $\sim 10^9$ cm^{-2} s^{-1}. During irradiation the fission fragments, which are able to penetrate a thin sheet of variable thickness (1-10 mg/cm^2) of the element investigated, are directly counted. By repeating the measurements with different thickness of the sheets, one obtains a transmission curve of the ^{235}U fission fragments for each element investigated. Another natural uranium deposit located in the second fission chamber acts as a monitor for the neutron flux for the different sorts of irradiation.

From the transmission curves it is possible to derive the relative effective stopping power of the different targets, and the ranges of the fission fragments in the different elements investigated. Actually the ranges are obtained by coupling the measured relative stopping powers with the absolute value of the range of ^{235}U fission fragment in Al, measured by Segré and Wiegand, by an independent experiment using the activation technique. The results obtained are compared with theoretical calculations concerning the loss of energy of fission fragments in material.

ORGANIZING COMMITTEE

J. J. GRIFFIN	United States of America
G. HERRMANN	Federal Republic of Germany
V. STRUTINSKY	Union of Soviet Socialist Republics

CHAIRMEN OF SESSIONS

Session A	E. R. RAE	United Kingdom
Session B	M. NEVE DE MEVERGNIES	Belgium
Session C	L. WILETS	United States of America
Session D	J. RYABOV	Union of Soviet Socialist Republics
Session E	S. BJØRNHOLM	Denmark
Session F	G. C. HANNA	Canada
Session G	P. ARMBRUSTER	Federal Republic of Germany
Session H	A. MICHAUDON	France

SECRETARIAT OF THE SYMPOSIUM

Scientific Secretary	J. DOLNIČAR	Division of Research and Laboratories, IAEA
Editor	J. W. WEIL	Division of Publications, IAEA
Records Officer	S. K. DATTA	Division of Languages, IAEA
Administrative Secretary	H. H. STORHAUG	Division of Scientific and Technical Information, IAEA

LIST OF PARTICIPANTS

AUSTRALIA

Boldeman, J.W.	Australian Atomic Energy Commission, Lucas Heights, Sydney

AUSTRIA

Fleck, C.M.	Atominstitut der Österreichischen Hochschulen, Schüttelstrasse 115, 1020 Vienna
Fritz, K.	Waagner-Biro AG, Margarethenstrasse 70, 1050 Vienna
Jagersberger, H.	Atominstitut der Österreichischen Hochschulen, Schüttelstrasse 115, 1020 Vienna
Lurf, G.	Waagner-Biro AG, Margarethenstrasse 70, 1050 Vienna
Rumpold, K.	Österreichische Studiengesellschaft für Atomenergie, Reaktorzentrum Seibersdorf, 2444 Seibersdorf
Schreinlechner, I.	Österreichische Studiengesellschaft für Atomenergie, Lenaugasse 10, 1080 Vienna
Semturs, F.	Österreichische Studiengesellschaft für Atomenergie, Reaktorzentrum Seibersdorf, 2444 Seibersdorf
Warhanek, H.	Institut für Radiumforschung und Kernphysik, Universität Wien, 1090 Vienna

BELGIUM

Demildt, A.	Nuclear Energy Centre, SCK-CEN, Mol
Marmol, P. Del	Nuclear Energy Centre, SCK-CEN, Mol
Nève de Mevergnies, M.	Nuclear Energy Centre, SCK-CEN, Mol
Poortmans, F.	Nuclear Energy Centre, SCK-CEN, Mol.
Wagemans, C.	Nuclear Energy Centre, SCK-CEN, Mol

BULGARIA

Kashukeev, N.T.	Institute of Physics, Bul. Lenin 72, Sofia 13

CANADA

Fraser, J.S.	Atomic Energy of Canada Ltd., Chalk River, Ont.
Hanna, G.C.	Atomic Energy of Canada Ltd., Chalk River, Ont.
Milton, J.C.D.	Chalk River Nuclear Laboratories, Chalk River, Ont.
Sharma, H.D.	University of Waterloo, Waterloo, Ont.
Tomlinson, R.H.	McMaster University, Hamilton, Ont.
Tracy, B.L.	McMaster University, Hamilton, Ont.
Yaffe, L.	Department of Chemistry, McGill University, Montreal, Que.

CZECHOSLOVAKIA

Dlouhý, Z.	Nuclear Research Institute, Řež

DENMARK

Bjørnholm, S.	Niels Bohr Institute, University of Copenhagen, Risø pr. 4000 Roskilde
Bondorf, J.P.	Niels Bohr Institute, Blegdamsvej 17, 2100 Copenhagen
Brack, M.	Niels Bohr Institute, Blegdamsvej 17, 2100 Copenhagen
Christensen, C.J.	DAEC, Research Establishment Risø, 4000 Roskilde
Damgaard, J.	Niels Bohr Institute, Blegdamsvej 17, 2100 Copenhagen
Gibson, W.M.	Institute of Physics, Aarhus University, 8000 Aarhus
Myers, W.D.	Niels Bohr Institute, Blegdamsvej 17, 2100 Copenhagen

Nielsen, K.O.	Institute of Physics, Aarhus University, 8000 Aarhus
Otroshenko, G.	Niels Bohr Institute, Blegdamsvej 17, 2100 Copenhagen
Pauli, H. Ch.	Niels Bohr Institute, Blegdamsvej 17, 2100 Copenhagen
Pedersen, J.	Niels Bohr Institute, University of Copenhagen, Risø pr. 4000 Roskilde
Polikanov, S.M.	Niels Bohr Institute, Blegdamsvej 17, 2100 Copenhagen
Ravn, H.	Institute of Physics, Aarhus University, 8000 Aarhus
Sletten, G.	Niels Bohr Institute, Blegdamsvej 17, 2100 Copenhagen
Wandel, C.F.	Institute of Physics, Aarhus University, 8000 Aarhus
Wong, C.Y.	Niels Bohr Institute, Blegdamsvej 17, 2100 Copenhagen and Oak Ridge National Laboratory, USA

FINLAND

Lundán, A.I.	Department of Technical Physics, Technical University of Helsinki, Otaniemi, Helsinki

FRANCE

Asghar, M.	Laboratoire de Physique Nucléaire, Université de Bordeaux, Le Haut Vigneau, 33-Gradignan
Barjon, R.	Institut des Sciences Nucléaires, CEDEX 257, 38-Grenoble
Blachot, J.	Commissariat à l'Energie Atomique, Centre d'Etudes Nucléaires de Grenoble, 38-Grenoble
Blons, J.	SPMNF., CEN de Saclay, B.P. No.2, 91-Gif-sur-Yvette
Carles, C.	Laboratoire de Physique Nucléaire, Université de Bordeaux, Le Haut Vigneau, 33-Gradignan
Chastel, R.	Laboratoire de Physique Nucléaire, Le Haut Vigneau, 33-Gradignan

Communeau, F.	CEA, B.P. No.63, 92-Montrouge
Crançon, J.	CEN de Grenoble, B.P. No.269, 38-Grenoble
Doan, T.P.	Laboratoire de Physique Nucléaire, Le Haut Vigneau, 33-Gradignan
Engelhardt, H.-D.	Institut des Sciences Nucléaires, Laboratoire du Génie Atomique, 53, rue des Martyrs, 38-Grenoble
Frehaut, J.E.	CEA, B.P. No.61, 92-Montrouge
Gaudin, M.	CEA-CEN de Saclay B.P. No.2, 91-Gif-sur Yvette
Gauvin, H.	Institut de Physique Nucléaire, Laboratoire de Chimie Nucléaire, B.P. No.1, 91-Orsay
Joly, R.L.	SMNF/DRP, CEN de Saclay, B.P. No.2, 91-Gif-sur-Yvette
Klapisch, R.	Centre de Spectrométrie Nucléaire et de Spectrométrie de Masse, 91-Campus-Orsay
Michaudon, A.F.	CEN de Saclay, B.P. No.2, 91-Gif-sur-Yvette
Monnin, M.	Laboratoire de Physique Nucléaire, 34, Avenue Carnot, 63-Clermont-Ferrand
Nifenecker, H.A.	DRP/SMPNF, CEN de Saclay, B.P. No.2, 91-Gif-sur-Yvette
Péter, J.	Institut de Physique Nucléaire, B.P. No.1, 91-Orsay
Pinston, J.A.	CEN de Grenoble, 53-rue des Martyrs, 38-Grenoble
Poitou, J.	CEN de Saclay, B.P. No.2, 91-Gif-sur-Yvette
Quentin, P.	DRP/SMPNF, CEA-CEN de Saclay, B.P. No.2, 91-Gif-sur-Yvette
Signarbieux, G.	CEA, rue de Varennes, Paris 7e
Soleilhac, M.	CEA, B.P. No.61, 92-Montrouge
Stein, R.	Laboratoire de physique corpusculaire, 2, rue du Loess, Strasbourg

Szabo, I.	CEA-CEN de Cadarache, B.P. No. 1, 13-St. Paul-lez-Durance
Tamain, B.L.M.	Laboratoire de Physique Nucléaire, 34, Avenue Carnot, 63-Clermont-Ferrand

GERMANY, Federal Republic of

Albrecht, K.	Institut für Theoretische Physik der Universität Frankfurt, Robert-Mayer-Str. 8-10, 6000 Frankfurt
Armbruster, P.	Kernforschungsanlage Jülich, Postfach 365, 5170 Jülich
Aumann, D.C.	Institut für Radiochemie der Technischen Hochschule München, 8046 Garching
Bächmann, K.	Lehrstuhl für Kernchemie, Technische Hochschule, 6100 Darmstadt
Bock, R.	Institut für Anorganische Chemie und Kernchemie, Johannes-Gutenberg-Universität, Postf. 3980, 6500 Mainz
Brentano, P. von	*Max-Planck-Institut für Kernphysik, Saupfercheckweg, 6900 Heidelberg
Denschlag, H.O.	Institut für Anorganische Chemie und Kernchemie, Universität, Postf. 3980, 6500 Mainz
Dickmann, F.W.J.	Gesellschaft für Kernforschung mbH, Postfach 3640, 7500 Karlsruhe
Dietrich, K.M.	Institut für Theoretische Physik, Universität, Philosophenweg 16, 6900 Heidelberg
Droste, G. von	Physikalisch-Technische Bundesanstalt, Bundesallee 100, 3300 Braunschweig
Eidens, J.	Kernforschungsanlage Jülich, Postfach 365, 5170 Jülich
Ewald, H.	Universität Giessen, II. Physikalisches Institut, Arndtstrasse 2, 6300 Giessen
Fiebig, R.	Gesellschaft für Kernenergieverwertung in Schiffbau und Schiffahrt mbH, Reaktorstation, 2057 Geesthacht-Tesperhude
Fiedler, G.	Universität Giessen, II. Physikalisches Institut, Arndtstrasse 2, 6300 Giessen
Folger, H.A.	Institut für Anorganische Chemie und Kernchemie, Johannes-Gutenberg-Universität, 6500 Mainz

Gasteiger, R.	Institut für Radiochemie der Technischen Hochschule München, 8000 München
Gönnenwein, F.J.	Physikalisches Institut, Universität,Gmelinstrasse 6, 7400 Tübingen
Grimm, W.	Institut für Anorganische Chemie und Kernchemie, Johannes-Gutenberg-Universität, Postf. 3980, 6500 Mainz
Groote, H.H. von	Physikalisches Institut der Universität Würzburg, Röntgenring 8, 8700 Würzburg
Grosse, E.A.	Max-Planck-Institut für Kernphysik Postfach 1248, 6900 Heidelberg
Gunther, H.	Universität Giessen, II. Physikalisches Institut, Arndtstrasse 2, 6300 Giessen
Herrmann, G.	Universität Mainz, Postfach 3980 Kernreaktor, 6500 Mainz
Hilf, E.R.H.	Physikalisches Institut der Universität Würzburg, Röntgenring 8, 8700 Würzburg
Hofmann, D.	Institut für Kernphysik, August-Euler-Strasse 6, 6000 Frankfurt/Main
Hofmann, H.	Kernforschungszentrum, Institut für Angewandte Kernphysik, Weberstrasse 5, 7500 Karlsruhe
Holm, H.	Institut für Theoretische Physik, Universität, Robert-Mayer-Strasse 8-10, 6000 Frankfurt
Horsch, F.	Gesellschaft für Kernforschung, Weberstrasse 5, 7500 Karlsruhe
Hübenthal, K.	IFN, Kernforschungsanlage, Postfach 365, 5170 Jülich
Kluge, H.	Physikalisch-Technische Bundesanstalt, Bundesallee 100, 3300 Braunschweig
Konecny, E.	Technische Hochschule München, Arcisstrasse 15, 8000 München
Krappe, H.-J.	Hahn-Meitner-Institut für Kernforschung, Glienickerstrasse 100, 1000 Berlin 39
Kratz, K.-L.	Institut für Anorganische Chemie und Kernchemie, Johannes-Gutenberg-Universität, Postf. 3980, 6500 Mainz
Labus, H.	Kernforschungsanlage Jülich, Postfach 365, 5170 Jülich
Lawin, H.	Kernforschunganlage Jülich, Postfach 365, 5170 Jülich
Metag, V.	Max-Planck-Institut für Kernphysik, Postfach 1248, 6900 Heidelberg

Mosel, U.	Institut für Theoretische Physik, Universität, Robert-Mayer-Str. 8-10, 6000 Frankfurt
Müller, W.	Gesellschaft für Strahlenforschung mbH, 8043 Neuherberg b. München
Münzel, H.	Institut für Radiochemie, Kernforschungszentrum, Weberstr. 5, 7500 Karlsruhe
Neidhart, B.	Lehrstuhl für Kernchemie, Technische Hochschule, 6100 Darmstadt
Nörenberg, W.	Institut für Theoretische Physik, Universität, Philosophenweg 16, 6900 Heidelberg
Repnow, R.	Max-Planck-Institut für Kernphysik, Postfach 1248, 6900 Heidelberg
Roeckl, E.	Kernforschungsanlage Jülich, Postfach 365, 5170 Jülich
Rösler, H.	Technische Hochschule München, Physik-Department, Arcisstrasse 21, 8000 München 2
Schmidt, J.J.	Gesellschaft für Kernforschung, Postfach 3640, 7500 Karlsruhe
Schüssler, H.D.	Institut für Anorganische Chemie und Kernchemie, Universität, Postfach 3980, 6500 Mainz
Siegert, G.E.	Universität Giessen, II. Physikalisches Institut, Arndtstrasse 2, 6300 Giessen
Sistemich, K.	Kernforschungsanlage Jülich, Postfach 365, 5170 Jülich
Specht, H.J.	Sektion Physik der Universität München, Amalienstrasse 54/I, 8000 München 13
Weinreich, R.J.	Institut für Anorganische Chemie und Kernchemie, Universität, Postfach 3980, 6500 Mainz
Wurm, J.P.	Max-Planck-Institut für Kernphysik, Saupfercheckweg, 6900 Heidelberg

GREECE

Papadopoulos, N.	Greek Atomic Energy Commission, Nuclear Research Centre Democritos, Aghia Paraskevi Attikis, Athens
Perricos, D.C.	Greek Atomic Energy Commission, Nuclear Research Centre Democritos, Aghia Paraskevi Attikis, Athens

HUNGARY

Csikai, G.	Institute of Experimental Physics, Bem tér 18/a, Debrecen
Kluge, G.	Central Research Institute for Physics, P.O. B. 49, Budapest 114
Kovács, I.	Central Research Institute for Physics, P.O. B.49, Budapest 114
Lajtai, A.	Central Research Institute for Physics, P.O.B.49, Budapest 114
Medveczky, L.	Institute of Nuclear Research of the Hungarian Academy of Sciences, P.O. B.51, Debrecen 1
Nagy, L.	Central Research Institute for Physics, P.O. B. 49, Budapest 114
Vinnay, I.	Central Research Institute for Physics, P.O. B. 49, Budapest 114

INDIA

Kapoor, S.S.	Nuclear Physics Division, Bhabha Atomic Research Centre, Trombay, Bombay 74
Ramamurthy, V.S.	Nuclear Physics Division, Bhabha Atomic Research Centre, Trombay, Bombay 74
Ramaniah, M.V.	Radiochemistry Division, Bhabha Atomic Research Centre, Trombay, Bombay 74

ISRAEL

Amiel, S.	Soreq Nuclear Research Centre, Yavne
Ben-David, G.	Soreq Nuclear Research Centre, Yavne
Boazy, M.	Soreq Nuclear Research Centre, Yavne
Gazit, Y.	Soreq Nuclear Research Centre, Yavne
Nardi, E.	Soreq Nuclear Research Centre, Yavne and Weizmann Institute of Sciences, Rehovoth
Rosner, B.	Department of Physics, Technion, Israel Institute of Technology, Haifa

ITALY

Benzi, V.	Comitato Nazionale per l'Energia Nucleare, Via Mazzini 2, Bologna
Cavallari, F.	Istituto Nazionale di Fisica Nucleare, Gruppo di Pavia Università, Viale Taramelli 4, Pavia
Criscuolo, L.	FIAT, Sezione Energia Nucleare, Via Settembrini 235, Turin
Fubini, A.	Centro Studi Nucleari della Casaccia, Via Anguillarese, Rome
Moretto, L.G.	Università di Pavia, Viale Taramelli 12, Pavia
Pinelli, T.	Istituto Nazionale di Fisica Nucleare, Gruppo di Pavia, Università, Viale Taramelli, Pavia
Rollier, M.A.	Laboratorio di Radiochimica, Università, Pavia
Saetta Menichella, E.	CISE, C.P. 3986, 20100 Milan
Stella, R.	Laboratorio di Radiochimica, Viale Taramelli 12, 27100 Pavia
Zifferero, M.	National Committee for Nuclear Energy (CNEN), Viale Regina Margherita 125, Rome

JAPAN

Matsuura, T.	Institute for Atomic Energy, Rikkyo University, Sajima, Yokosuka
Takekoshi, E.	Japan Atomic Energy Research Institute, Tokai-mura, Naka-gun, Ibaraki-ken

MOROCCO

El-Hammami-Sordo, K.	Faculté des Sciences, Université Mohammed V, Rabat

NETHERLANDS

Aten, A.H.W.	Instituut voor Kernphysisch Onderzoek, Oosterringdijk 18, Amsterdam
Polak, P.	Instituut voor Kernphysisch Onderzoek, Oosterringdijk 18, Amsterdam

NORWAY

Alstad, J.	Nuclear Chemistry, Institute of Chemistry, University of Oslo, Oslo 3
Pappas, A.C.	Nuclear Chemistry Division, Dept. of Chemistry, University of Oslo, Oslo 3
Skarsvåg, K.	Institutt for Atomenergi, P.O. B. 40, 2007 Kjeller

PAKISTAN

Qaim, S.M.	Pakistan Atomic Energy Commission, Karachi At present: Institut für Anorganische Chemie and Kernchemie, Universität, 6500 Mainz, Federal Republic of Germany

POLAND

Krogulski, T.	Institute of Nuclear Research, Świerk k. Otwocka
Piasecki, E.	Institute of Nuclear Research, Świerk k. Otwocka
Sobiszewski, A.	Institute for Nuclear Research, Hoza 69, Warsaw
Wołczek, O.	Palac Kultury i Nauki, XVIII. p., Warsaw

ROMANIA

Muscalu, S.	Faculty of Physics, University, Academy Street 14, Bucharest
Vîlcov, N.	Institute of Atomic Physics, P.O.B. 35, Bucharest

SWEDEN

Albinsson, H.	AB Atomenergi, Studsvik, 61101 Nyköping
Condé, P.H.L.	Research Institute of National Defence, 10450 Stockholm 80
Holmberg, M.	Research Institute of National Defence, 10450 Stockholm 80
Jägara, S.V.	Research Institute for Physics, Roslagsvägen 100, 10405 Stockholm 50
Johansson, K.T.A.	Department of Mathematical Physics, Lund Institute of Technology, Box 725, Lund 7

Prawitz, J.	Stockholm International Peace Research Institute, Sveavägen 166, 11346 Stockholm
Schröder, B.	Institute of Nuclear Physics, Lund University, Professorsgatan 3, Lund
Wallin, L. B.	Research Institute of National Defence, 10450 Stockholm 80

SWITZERLAND

Gunten, H.R. von	Eidgenössisches Institut für Reaktorforschung, 5303 Würenlingen
Jordan, P.A.	Eidgenössische Technische Hochschule, Laboratorium für Organische Chemie, Universitätsstrasse 6, 8006 Zürich

TURKEY

Aras, N.K.	Chemistry Department, Middle East Technical University, Ankara

UNION OF SOVIET SOCIALIST REPUBLICS

Nesterov, V.G.	Institute of Physics and Power Engineering, Obninsk, Moscow

UNITED KINGDOM

Colvin, D.W.	UKAEA, AERE, Harwell, Didcot, Berks
Cuninghame, J.G.	UKAEA, AERE, Harwell, Didcot, Berks
Earwaker, L.G.	The University of Birmingham, Birmingham 29
Feather, N.	University of Edinburgh, Old College, South Bridge, Edinburgh 8
Ferguson, A.T.G.	UKAEA, AERE, Harwell, Didcot, Berks
Galloway, R.B.	Department of Natural Philosophy, The University, Drummond Street, Edinburgh 8
Grant, I.S.	The Schuster Laboratories, Manchester University, Manchester 13
Gregory, K.	The Schuster Laboratories, Manchester University, Manchester 13
James, G.D.	UKAEA, AERE, Harwell, Didcot, Berks
Large, N.R.	UKAEA, AERE, Harwell, Didcot, Berks

Lynn, J.E.	UKAEA, AERE, Harwell, Didcot, Berks
Pattenden, N.J.	UKAEA, AERE, Harwell, Didcot, Berks
Rae, E.R.	UKAEA, AERE, Harwell, Didcot, Berks
Scobie, J.	Scottish Research Reactor Centre, East Kilbride, Glasgow
Tomlinson, L.	UKAEA, AERE, Harwell, Didcot, Berks
Vass, D.G.	Department of Natural Philosophy, University of Edinburgh, Drummond Street, Edinburgh 8
Williams, R.J.	The Schuster Laboratories, Manchester University, Manchester 13

UNITED STATES OF AMERICA

Block, R.	Rensselaer Polytechnic Institute, Troy, N.Y.
Britt, H.C.	Los Alamos Scientific Laboratory, P.O.B. 1663, Los Alamos, N. Mex. 87544
Davis, R.H.	Physics Department, Florida State University, Tallahassee, Fla. 32306
Deutsch, R.W.	Department of Nuclear Science and Engineering, Catholic University, Washington, D.C. 20017
East, L.V.	Los Alamos Scientific Laboratory, P.O.B. 1663, Los Alamos, N.Mex. 87544
Elwyn, A.J.	Argonne National Laboratory, Argonne, Ill. 60439
Ferguson, R.	Oak Ridge National Laboratory, P.O.B.X, Oak Ridge, Tenn. 37830
Fong, P.	Emory University, Atlanta, Ga. 30322
Glendenin, L.	Argonne National Laboratory, 9700 S. Cass Avenue, Argonne, Ill. 60439
Goldberg, A.	Lawrence Radiation Laboratory, Livermore, Calif.
Gollobin, P.L.	Presearch, Inc., 8720 Georgia Ave., Silver Spring, Md. 20910
Griffin, J.	University of Maryland, Physics Department, College Park, Md. 20742
Holmgren, H.D.	University of Maryland, Physics Department, College Park, Md. 20742
Huizenga, J.P.	University of Rochester, Rochester, N.Y. 14627

John, W.	Lawrence Radiation Laboratory, Box 808, Livermore, Calif. 94550
Matuszek, J.	*Isotopes, A Teledyne Company, 50, Van Buren Avenue,* Westwood, N.J. 07675
Meyer, E., Jr.	Lewis College, Lockport, Ill. 60441
Muga, L.	University of Florida, 406 Science Building, Gainesville, Fla. 32601
Nix, J.R.	Los Alamos Scientific Laboratory, University of California, Los Alamos, N. Mex. 87544
Perez, R.	Oak Ridge National Laboratory, Oak Ridge, P.O.B.X., Tenn. 37830
Plasil, F.	Oak Ridge National Laboratory, Oak Ridge, P.O.B.X., Tenn. 37830
Rogosa, G.L.	Division of Research, US Atomic Energy Commission, Washington, D.C. 20545
Schmitt, H.W.	Oak Ridge National Laboratory, Oak Ridge, Tenn. 37830
Sperber, D.	Rensselaer Polytechnic Institute, Troy, N.Y. 12181
Talbert, W.L., Jr.	Physics Department, Iowa State University, Ames, Iowa 50010
Unik, J.	Argonne National Laboratory, Building 200, 9700 S. Cass Avenue, Argonne, Ill. 60439
Vandenbosch, R.	University of Washington, Seattle, Wash. 98105
Verbinski, V.	Gulf General Atomic, P.O.B. 608, San Diego, Calif. 92112
Wahl, A.C.	Washington University, St. Louis, Mo.
Weinstein, H.S.	Rensselaer Polytechnic Institute, Troy, N.Y. 12181
Wilets, L.	Department of Physics, University of Washington, Seattle, Wash. 98105

ORGANIZATIONS

CHAMBRE DE COMMERCE INTERNATIONALE

Staudinger, W.	Danubia, A.G., Krottenbachstrasse 82-88, 1190 Vienna, Austria

CERN

Hagebø, E.	European Organization for Nuclear Research, 1211 Geneva 23, Switzerland

EURATOM

Deruytter, A.J.	Central Bureau of Nuclear Measurements, Steenweg naar Retie, Geel, Belgium
Migneco, E.	Central Bureau of Nuclear Measurements, Steenweg naar Retie, Geel, Belgium
Rustichelli, F.	C.C.R. Ispra (Varese), C.P. 1, Italy
Syros, C.	Commission des Communautés européennes, 51-53, rue Belliard, Bruxelles, Belgique
Theobald, J.P.	Central Bureau for Nuclear Measurements, Steenweg naar Retie, Geel, Belgium

EUROCHEMIC

Berg, R.	Société Européenne pour le Traitement, Chimique des Combustibles Irradiés, Mol-Donk, Belgium

JINR

Dermendzhiev, E.	Joint Institute for Nuclear Research, Dubna
Karamyan, S.A.	Joint Institute for Nuclear Research, Dubna
Nagy, T.	Joint Institute for Nuclear Research, Dubna
Ryabov, J.	Joint Institute for Nuclear Research, Dubna
Zvára, I.	Joint Institute for Nuclear Research, Dubna

WORLD ENERGY CONFERENCE

Rumpold, K.	see under Austria

AUTHOR INDEX

Numerals underlined refer to the first page of a paper.
Other numerals refer to a contribution to the discussion.

TRANSLITERATION INDEX

IAEA SALES AGENTS AND BOOKSELLERS

Orders for Agency publications can be placed with your bookseller or any of the addresses listed below:

ARGENTINA
Comisión Nacional de
Energía Atómica
Avenida del Libertador 8250
Buenos Aires

AUSTRALIA
Hunter Publications
23 McKillop Street
Melbourne, C.1

AUSTRIA
Publishing Section
International Atomic Energy Agency
Kärntner Ring 11
P.O. Box 590
A-1011 Vienna

BELGIUM
Office International
de Librairie
30, Avenue Marnix
Brussels 5

CANADA
Canadian Government Printing Bureau,
International Publications Main Stores,
Room 2738, Second Floor,
Sacred Heart Boulevard,
Hull, Québec

C.S.S.R.
S.N.T.L.
Spolena 51
Nové Mesto
Prague 1

DENMARK
Ejnar Munksgaard Ltd.
6 Norregade
DK-1165 Copenhagen K

FRANCE
Office International de
Documentation et Librairie
48, Rue Gay-Lussac
F-75 Paris 5e

GERMANY, Fed. Rep.
R. Oldenbourg Verlag
Rosenheimer Strasse 145
D-8 Munich 80

HUNGARY
Kultura
Hungarian Trading Company
for Books and Newspapers
P.O. Box 149
Budapest 62

ISRAEL
Heiliger & Co.
3, Nathan Strauss Str.
Jerusalem

ITALY
Agenzia Editoriale Commissionaria
A.E.I.O.U.
Via Meravigli 16
I-20123 Milan

JAPAN
Maruzen Company, Ltd.
P.O. Box 5050,
100-31 Tokyo International

MEXICO
Librería Internacional, S.A.
Av. Sonora 206
México 11, D.F.

NETHERLANDS
Martinus Nijhoff N.V.
Lange Voorhout 9
P.O. Box 269
The Hague

PAKISTAN
Mirza Book Agency
65, Shahrah Quaid-E-Azam
P.O. Box 729
Lahore - 3

POLAND
Ars Polona
Centrala Handlu Zagranicznego
Krakowskie Przedmiescie 7
Warsaw

ROMANIA
Cartimex
3-5 13 Decembrie Street
P.O. Box 134-135
Bucarest

SPAIN
Librería Bosch
Ronda Universidad 11
Barcelona - 7

SWEDEN
C.E. Fritzes Kungl. Hovbokhandel
Fredsgatan 2
Stockholm 16

SWITZERLAND
Librairie Payot
Rue Grenus 6
CH-1211 Geneva 11

U.S.S.R.
Mezhdunarodnaya Kniga
Smolenskaya-Sennaya 32-34
Moscow G-200

U.K.
Her Majesty's Stationery Office
P.O. Box 569
London S.E.1

U.S.A.
UNIPUB, Inc.
P.O. Box 433
New York, N.Y. 10016

YUGOSLAVIA
Jugoslovenska Knjiga
Terazije 27
Belgrade

IAEA Publications can also be purchased retail at the United Nations Bookshop at United Nations Headquarters, New York, from the news-stand at the Agency's Headquarters, Vienna, and at most conferences, symposia and seminars organized by the Agency.

In order to facilitate the distribution of its publications, the Agency is prepared to accept payment in UNESCO coupons or in local currencies.

Orders and inquiries from countries not listed above may be sent to:

Publishing Section
International Atomic Energy Agency
Kärntner Ring 11
P.O. Box 590
A-1011 Vienna, Austria

INTERNATIONAL
ATOMIC ENERGY AGENCY
VIENNA, 1969

PRICE: US $25.00
Austrian Schillings 646,-
(£10.8.4; F.Fr. 138,80 DM 91,50)

SUBJECT GROUP: III
Physics/Nuclear Physics,
Reactor Physics, Fission